Lecture Notes in Civil Engineering

Volume 4

Lecture Notes in Civil Engineering (LNCE) publishes the latest developments in Civil Engineering - quickly, informally and in top quality. Though original research reported in proceedings and post-proceedings represents the core of LNCE, edited volumes of exceptionally high quality and interest may also be considered for publication. Volumes published in LNCE embrace all aspects and subfields of, as well as new challenges in, Civil Engineering. Topics in the series include:

– Construction and Structural Mechanics
– Building Materials
– Concrete, Steel and Timber Structures
– Geotechnical Engineering
– Earthquake Engineering
– Coastal Engineering
– Hydraulics, Hydrology and Water Resources Engineering
– Environmental Engineering and Sustainability
– Structural Health and Monitoring
– Surveying and Geographical Information Systems
– Heating, Ventilation and Air Conditioning (HVAC)
– Transportation and Traffic
– Risk Analysis
– Safety and Security

More information about this series at http://www.springer.com/series/15087

Giorgio Mannina
Editor

Frontiers in Wastewater Treatment and Modelling

FICWTM 2017

Springer

Editor
Giorgio Mannina
University of Palermo
Palermo
Italy

To Sergio, Eleonora, Marcella and Carlo.
Thank you God for this achievement bless
all of us.

Preface

Today, multidisciplinary is a key to solving issues in the water field. The works in several International Water Association (IWA) Specialist Groups have demonstrated the importance of both innovative technologies and mathematical modelling, and that the exchange of scientific and technical information among researchers and practitioners involved in these fields is crucial for effectively advancing knowledge.

Mathematical modelling has the advantage of allowing scenario analysis before designing the real plant in order to ensure an optimized system.

To foster the multidisciplinary collaboration among different water specialists, the dialogue is a must in order to better share specific knowledge.

With this final aim with the support of the International Water Association (IWA) and the University of Palermo, Italy it was organized the FICWTM 2017, Frontiers International Conference on Wastewater Treatment from 21 to 24 of May 2017.

The FICWTM final aim was to create a forum for promoting the discussion among scientists, professionals, and academia in different areas of the broader theme of environmental engineering and sciences. To facilitate discussion, no parallel sessions were organized and the number of participants was limited to highly motivated professionals.

The conference was organized in nine sessions, and for each of them, a keynote by a referral researcher was presented. Specifically, the keynotes were held by the following professors, whose contributions were highly inspiring: Damien Batstone, George A. Ekama, B. Jefferson, Ulf Jeppsson, Piet Lens, Ingmar Nopens, Hallvard Ødegaard, Gustaf Olsson, and Mark C.M van Loosdrecht.

The wealth of information exchanged during FICWTM was of great benefit to all involved in challenging environmental issues caused by the increase of pollutants loads discharged into natural environment ecosystems. Those challenges require the building of a regulatory framework as well as control strategies. This framework needs to be based on scientific evidence associated with exposure and health risk for pollution prevention and remediation strategies. The application of innovative remedial techniques and new scientific methods is a key in order to reach sustainable development. It is therefore crucial to address the existing pollution

problems, and protect public health as well as preserve the welfare of the environment.

The application of cost-effective technologies for waste treatment and controls is much needed in order to make possible the implementation of appropriate regulatory measures that insure success of broader policy in pollution prevention.

Engineers and scientists working in water sector area need to be familiar with a wide range of issues including the physical processes of mixing and dispersion, biological developments, and mathematical modelling. Hence, a continuous exchange of information between water professionals in different parts of the world is essential.

Protection of the environment, one of the pillars of sustainable development, is an absolute priority for the international community. In this context, the FICWTM conference aimed to focus on relevant experiences, up-to-date scientific research, and findings carried out all over the world to protect and preserve the environment.

FICWTM 2017 is also a part of the three-year research project PRIN-GHG which was about the reduction of greenhouse gas from wastewater treatment plants. The financial support by the Italian Ministry of Education, University and Research is acknowledged. The research project had also an educational goal which aim was to train through seminars and advanced course young researchers involved in the project. In particular, three editions of the advanced course on wastewater treatment and mathematical modelling were organized at Palermo University, Italy, and four international seminars on the binomial between water and energy.

During the project, both experimental and mathematical activities were carried out on pilot plant and real wastewater treatment plants with the final aim to wide and strengthen the knowledge on energy optimization and emission reduction from wastewater treatment plants. This book contains also several contributions of the project researches.

This book contains contributions presented at Frontiers International Conference on Wastewater Treatment which was held at the University of Palermo, Italy, from 21 to 24 of May.

Overall, this book is organized into nine parts. Each part deals with a specific topic of the frontier in wastewater treatment and modelling. Specifically, the following parts are present: Part A—Carbon nutrient removal and recovery, Part B—Instrumentation and control and automation (ICA) & benchmarking, Part C—Membrane bioreactors, Part D—Anaerobic digestion, Part E—New frontiers in wastewater treatment, Part F—Greenhouse gases from wastewater treatment plants, Part G—Moving bed biofilm reactors and hybrid systems, Part H—Anaerobic digestion and modelling, and Part I—Computational fluid dynamic (CFD) in wastewater treatment.

Each contribution of the conference has been peer-reviewed by at least three members of the scientific committee*. Their efforts have contributed to the high quality of the final book contributions, and therefore, their reviewing activity is acknowledged and appreciated.

This book and the conference would have never been organized without the support and great input of professors and friends: George A Ekama (University of Cape Town, South Africa), Hallvard Ødegaard (Norwegian Institute of Technology, Norway), Gustaf Olsson (Lund University, Sweden), Peter Vanrolleghem (Laval University, Canada) and Gaspare Viviani (Palermo University, Italy).

Finally, I express my thanks to Mr. Pierpaolo Riva, publishing editor at Springer, for his support during the preparation of the final book.

I do hope that the reader will find the book a source of inspiration for both research and professional life.

<div align="right">Giorgio Mannina</div>

---

* Giorgio Mannina, Italy-Conference Chair; Norhayati Abdullah, Malaysia; Eduardo Ayesa, Spain; Dan Ames, USA; Juan Antonio Baeza Labat, Spain; Damien Batstone, Australia; Evangelina Belia, Canada; Joshua P. Boltz, USA; Christoph Brepols, Germany; David Butler, UK; Donatella Caniani, Italy; Marco Capodici, Italy; Roberto Canziani, Italy; Joaquim Comas, Spain; Alida Cosenza, Italy; Mauro De Marchis, Italy; Daniele Di Trapani, Italy; George A. Ekama, South Africa; Giovanni Esposito, Italy; Francesco Fatone, Italy; Krist Gernaey, Denmark; Sylvie Gillot, France; Riccardo Gori, Italy; Xia Huang, China; Bruce Jefferson, UK; Ulf Jeppsson, Sweden; Katsuki Kimura, Japan; Piet Lens, Netherlands; Zifu Li, China; Yanchen Liu, China; Jacek Makinia, Poland; Simos Malamis, Greece; Ingmar Nopens, Belgium; Hallvard Ødegaard, Norway; Jan Oleszkiewicz, Canada; Gustaf Olsson, Sweden; Diego Rosso, USA; Ilse Smets, Belgium; Michael Stenstrom, USA; Mathieu Sperandio, France; Michele Torregrossa, Italy; Marcos von Sperling, Brasil; Jiri Wanner, Czech Republic; Mark C. M van Loosdrecht, Netherlands; Peter Vanrolleghem, Canada; Gaspare Viviani, Italy; Eveline I.P. Volcke, Belgium; Zhiguo Yuan, Australia

Contents

Contents

Membrane Bioreactors

Carbon Nutrient Removal and Recovery

The Impact of High Mixed Liquor Concentration (3-13 gVSS/ℓ) on the Kinetic Rates of the N and P Removal Bioprocesses in Membrane Biological Nutrient Removal Activated Sludge Systems

V. Parco, G.J.G. du Toit, and G.A. Ekama[✉]

Water Research Group, Department of Civil Engineering,
University of Cape Town, Rondebosch 7701, South Africa
george.ekama@uct.ac.za

Abstract. The impact of including membranes for solid liquid separation and high volatile suspended solids (VSS) concentration (3-12 gVSS/ℓ) on the kinetics of biological nitrogen and phosphorus removal (BNR) was investigated. To achieve this, a membrane bioreactor (MBR) biological nutrient removal (BNR) activated sludge (AS) system was operated for 450 days in parallel with a conventional BNR system with a settling tank (CAS). The influence of high VSS concentration (up to 12 gVSS/ℓ) in the MBR system on the system performance and the nitrification, denitrification and phosphorus release and uptake kinetic rates were measured with aerobic, anoxic and anaerobic batch tests on mixed liquor (ML) harvested from the MBR system, diluted to different VSS concentrations, and from the CAS system. Also, the limitation of ammonia, oxygen, nitrate and acetate on the kinetic rates was investigated with batch tests. The results show that the BNRAS steady state and kinetic models developed for low VSS concentration BNRAS systems with secondary settling tanks can be applied with reasonable confidence to predict the performance of high VSS concentration BNRAS systems with membranes, except for the maximum specific growth rate of the nitrifiers, which was observed to be significantly lower in the MBR system.

Keywords: Membrane · Settling tanks · Nitrification · Denitrification · Biological phosphorus removal · Kinetics

1   Introduction

For conventional (with settling tanks) activated sludge (CAS) systems for biological nutrient removal (BNR), considerable knowledge has been accumulated on their performance, design and operation. Design procedures and performance simulation models have been developed based on well structured and researched stoichiometric and kinetic principles of the underlying fundamental biologically mediated processes. It is not certain whether this knowledge developed for CAS BNR systems can be applied directly to membrane bioreactor (MBR) BNR systems, given the significant differences

that may arise when membranes are included such as (i) floc structure (Zhang et al. 1997; Cicek et al. 1999; Huang et al. 2001; Yamamoto 2002; Gao et al. 2004; Manser et al. 2005), (ii) bacterial communities (Ghyoot et al. 1999; Luxmy et al. 2000; Liebig et al. 2001; Smith et al. 2002; Manser et al. 2005), (iii) metabolic activities (Lee et al. 2003; Han et al. 2005; Sperandio et al. 2005; Li et al. 2005) and (iv) sludge production (Cicek et al. 1999; Smith et al. 2002; Holbrook et al. 2005; Monti et al. 2005).

Ramphao et al. (2005) concluded that incorporating membranes in BNR AS systems makes a profound difference not only to the design of the BNR system itself, but also to the approach to design of the whole wastewater treatment plant. This paper presents research that investigates whether the steady state and kinetic models developed for CAS BNR systems can be applied also with reasonable accuracy to model MBR BNR systems.

Accordingly, the kinetic rates of nitrification, denitrification, anaerobic acetate uptake and P release, anoxic P release/uptake and aerobic P uptake were measured in batch tests over a range of volatile suspended solids (VSS) concentrations (3-12 gVSS/ℓ) on sludge harvested from an MBR-BNR system and compared with the corresponding rates measured in a parallel CAS BNR system at 3 gVSS/ℓ. Also, the influence of the limitation of substrate (ammonia, oxygen, nitrate, phosphorus, acetic acid) concentrations on the kinetic rates was investigated in the batch tests. To provide additional information on the anoxic behaviour of phosphate accumulating organisms (PAO), the ability of the AS in MBR BNR systems to denitrify under anoxic conditions with simultaneous phosphate uptake was investigated and quantified.

2   Material and Methods

Two parallel lab-scale membrane (MBR) and conventional (CAS) activated sludge systems were operated for 450 days at 20°C allowing their behaviour to be monitored and their performance compared. Both systems were UCT configurations (Figs. 1 and 2, Table 1) so that denitrification and biological excess phosphorus removal (BEPR) could function independently, provided the recycles do not overload the anoxic reactor with nitrate. System design and operational parameters such as zone mass fractions, inter-reactor recycles and sludge ages were kept the same in both systems (Table 1). Five A4 size Kubota® membrane panels submerged in the aerobic reactor of the MBR system replaced the function of the SST.
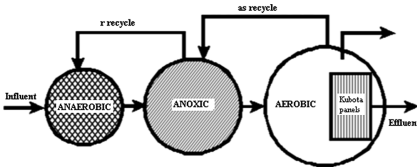
Fig. 1. Schematic layout of MBR UCT system
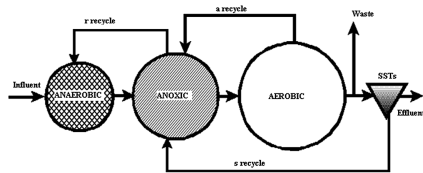
Fig. 2. Schematic layout of CAS UCT system

Table 1. MBR and CAS UCT systems' design and operating parameters

System parameters	MBR UCT	CAS UCT
Sludge age (d)	20	20
Anaerobic (R1) mass fraction (%), Volume (ℓ)	12.6[a]/19	12.6[a]/5.6
Anoxic (R2) mass fraction (%), Volume (ℓ)	27.9[a]/21	27.9[a]/6.2
Aerobic (R3) mass fraction (%), Volume (ℓ)	59.5[a]/35	59.5[a]/13.2
a-recycle (R3 to R2)	3:1	2:1
r-recycle (R2 to R1)	1:1	1:1
s-sludge Return Recycle (SST to R2)	-	1:1
Hydraulic retention time (d)	0.53	1.67
MLVSS concentration (mg/ℓ)	12 500	3 600
MLTSS concentration (mg/ℓ)	18 000	5 000
Influent flow (ℓ/d)	140	15
Feed COD concentration (mg/ℓ)	1000	1000
Membrane flux (m^3/m^2/d)	0.239	-

[a] For the given a- and r-recycle ratios.

The systems were fed screened (1 mm mesh) raw unsettled municipal wastewater from the Mitchell's Plain Wastewater Treatment Plant (Cape Town, South Africa), augmented with sodium acetate (200 mgCOD/ℓ to accentuate BEPR), ammonia (20 mgN/ℓ to increase TKN/COD), phosphorus (to ensure > 5 mgP/ℓ in effluent) and sodium bicarbonate (to provide some alkalinity for pH buffering). The wastewater was collected in 2 m^3 batches, macerated and stored in stainless steel tanks at 4°C and served as feed for both systems for 15 to 20d. Daily, after thorough mixing, the required volume of wastewater was withdrawn from the stainless tanks and diluted with tap water to the target COD concentration (800 mgCOD/ℓ). After adding the supplements, a sample is taken and the required volume for 1 days feed transferred into the systems' refrigerated (8°C) feed drums. The feed drums were gently stirred (1–2 rpm) to keep settleable solids in suspension and covered with a floating lid to minimize oxygen entrainment. The influent was pumped into each system with a multi-channel peristaltic pump, which also pumped the recycle flows. The influent tube was passed through a water bath at 20°C to avoid temperature decrease in the anaerobic reactor, in particular the MBR system with the very short hydraulic retention time.

The two systems were monitored daily via the parameters listed in Table 2. Additionally, recycle flow rates and trans-membrane pressure (TMP, constant flux) were monitored daily. Once monthly mixed liquor samples were analysed by a microbiologist for filament identification and floc morphology. Also mixed liquor samples were sent fortnightly for FISH analysis (Maharaj et al. 2007). The influent readily biodegradable organics (RBO) COD) concentration (before supplement addition) was measured daily in a fully aerobic square wave fed (12 h feed on, 12 h feed off) AS system at 2.5 days sludge age according to Ekama et al. (1986).

For each wastewater batch (which was accepted to represent a steady-state period), the daily results were averaged (after analysis for outliers). These steady-state averages were used to assess the performance of the systems and the following process

Table 2. Sampling position and parameter measurement

Test	COD	TKN	FSA	NO$_3$	NO$_2$	T-P	TSS	VSS	OUR	DSVI	pH
Influent	F; UF	UF	F			UF					
Anaerobic				F	F	F	UF	UF			
Anoxic				F	F	F	UF	UF			
Aerobic	UF	UF		F	F	F	UF	UF	D	D^a	D
Final effluent	F; UF	F; UF	F	F	F	F; UF					

F = 0.45 µm filtered; UF = Unfiltered samples; D = Direct measurement taken. COD; TKN; FSA (Free and Saline Ammonia); T-P (Total Phosphorus); TSS; VSS (Standard Methods 1985). DSVI = Dilute Sludge Volume Index; (Ekama and Marais 1984); OUR = Oxygen Utilization Rate (Randall et al. 1991).

[a] For the MBR system, the unfiltered COD was measured at the 800 mℓ mark of the 1000 mℓ measuring cylinder after 30 min settling.

characteristics were calculated: System COD and N mass balances; influent unbiodegradable soluble and particulate COD fractions (f$_{S'us}$ and f$_{S'up}$ respectively, Ekama and Wentzel 1999); mixed liquor VSS/TSS, COD/VSS and TKN/VSS ratios; nitrate and P mass changes across each reactor, sludge production and the influent readily biodegradable (RB) COD from the OUR measured in the square-wave fed 2.5d sludge age AS system (du Toit et al. 2007).

To determine the kinetics rates, aerobic, anoxic-aerobic and anaerobic-aerobic and anaerobic-anoxic-aerobic batch tests on the mixed liquor harvested from the different reactors of the two BNR systems were conducted (Parco 2006; Parco et al. 2006, 2007). Particularly on the MBR system the influence of the VSS concentration and of the limitation of ammonia, oxygen, nitrate and acetate concentrations on the kinetic rates was examined. Moreover, to provide additional information on the anoxic behaviour of phosphate accumulating organisms (PAO), the ability of AS in MBR and CAS systems to denitrify under anoxic conditions with simultaneous phosphate uptake was investigated and quantified to check the extent of anoxic P uptake BEPR in the systems. This is important to accurately separate OHO and PAO denitrification behaviour. Detailed results of the whole investigation summarised here are given by Parco (2006) or du Toit et al. (2010).

3 Batch Test Inventory

Three groups of aerobic nitrification batch tests (37 in all) were conducted to evaluate the effect of VSS, ammonia and dissolved oxygen (DO) concentration on the nitrification kinetics in the MBR system: 29 Group (1), i.e. 10 with 10-20 mgN-NH$_4$/ℓ, 12 with 30-40 mgN-NH$_4$/ℓ and 7 with 50 mgN-NH$_4$/ℓ on MBR system ML diluted (with effluent) to different VSS concentrations between 2 and 14 gVSS/ℓ, i.e. 8 with 2-3 gVSS/ℓ, 2 with ∼4 gVSS/ℓ, 6 with ∼5-6 gVSS/ℓ, 5 with 7-10 gVSS/ℓ, 2 with 10-11 gVSS/ℓ and 5 with 12-14 gVSS/ℓ on MBR system ML, 2 Group (2), i.e. 2 on MBR system ML at the same VSS concentration (∼9 gVSS/ℓ) but at different DO concentrations 2-5 and 10-15 mgO/ℓ) and 6 Group (3), i.e. in parallel, 3 on each of MBR

and CAS system ML with MBR ML diluted to the same low VSS concentration as that from the CAS system (2-3 gVSS/ℓ) to determine the effect of the membranes.

Five groups of anoxic batch tests for denitrification (33 in all) were conducted, viz. Group (1): On MBR system ML at different VSS concentrations between 2.5 and 12 gVSS/ℓ with ML from the anaerobic and aerobic reactors mixed in proportion to the recycles entering the anoxic reactor; Group (2): like Group (1) but at different nitrate concentrations; Group (3): like Groups (1) and (2) but with different proportions of anaerobic and aerobic ML (Set I - 50/50 by VSS mass, Set II - 100% anaerobic and Set III - 100% aerobic); Group (4) on MBR and CAS system ML in parallel with the MBR ML diluted to the same low VSS concentration as that from the CAS system (2-3 gVSS/ℓ) and with ML from the anaerobic and aerobic reactors mixed in proportion to the recycles entering the anoxic reactor and Group (5): like Group (4) but with wastewater added.

Altogether fifteen anaerobic batch tests were conducted, 13 (BTs 1 to 13) with low to moderate acetate dosages varying from 0.009 to 0.043 mgHAcCOD/mgVSS and VSS concentrations ranging from 2.7 to 11.2 gVSS/ℓ, one (BT14) with excess acetate addition at 0.166 gHAcCOD/gVSS at 6.37 gVSS/ℓ and one (BT15) with wastewater addition at 5.52 gVSS/ℓ.

4   Calculating the Bioprocess Specific Kinetic Rates

In the steady-state design procedures and dynamic models, the increased sludge production in MBR systems can be accommodated by increasing the influent unbiodegradable particulate COD fraction ($f_{S'up}$). This was done in this investigation. Fixing the unbiodegradable soluble COD fraction ($f_{S'us}$) for the MBR and CAS systems at the values found above, i.e. 0.045 and 0.066 respectively, the $f_{S'up}$ fraction for the MBR and CAS systems were calculated to be 0.241 and 0.084 mgCOD/mgCOD respectively to match the measured average mass of VSS in the systems (Ekama and Wentzel 1999). Noting that the model takes account of the different masses of PAOs in the two systems, it is a concern that for two systems with the same design and operating parameters fed the same wastewater, different $f_{S'up}$ fractions are obtained. If $f_{S'up}$ is really a wastewater characteristic, $f_{S'up}$ should be the same for both systems. The problem of obtaining different $f_{S'up}$ fractions for the MBR and CAS systems, is that they result in different OHO (f_{avOHO}) and PAO (f_{avPAO}) biomass fractions of the VSS in the systems, where $f_{avOHO} = X_{BH}/X_v$ and $f_{avPAO} = X_{BG}/X_v$ and X_{BH}, X_{BG} and X_v are the OHO, PAO and total VSS concentrations respectively. However, the method of calculating $f_{S'up}$ by matching the calculated mass of VSS in the system with that measured has always has been applied in the past to determine the f_{avOHO} and f_{avPAO} active fractions and the OHO and PAO specific kinetic rates (van Haandel et al. 1981; Wentzel et al. 1990; Clayton et al. 1991; Ekama and Wentzel 1999) and these specific rates have been adopted as default values in the ASM1 and ASM2 kinetic models. So because there is no other way of determining biomass specific kinetic rates from experimental systems fed real wastewater, the uncertainty that different $f_{S'up}$ fractions will have on the kinetic rates, while not ideal, has to be accepted as it has been in the past (Ekama and Wentzel 1999) because expressing kinetic rates in terms of VSS

makes the rates incomparable between different BNR systems. In the end, steady state models aligned with and based on the same but simplified principles as kinetic models are the only interface between experimental systems and the kinetic models.

Because the kinetic rates determined from the batch tests results were assigned to the biomass population mediating the particular bioprocess, and the steady state NDBEPR model (Wentzel et al. 1990) was used to determine the OHO (f_{avOHO}) and PAO (f_{avPAO}) active fractions from the measured data on the MBR and CAS systems, it was important for the OHO specific denitrification rate and the PAO specific P release and P uptake rates that the observed and predicted P removal of the systems matched well. This ensured that the OHO and PAO specific kinetic rates were consistent with estimates of the OHO (f_{avOHO}) and PAO (f_{avOHO}) active fractions determined in the past. The wastewater batch average calculated P removal of the MBR system based on the known system operating parameters, dosed acetate (200 mg/ℓ) and measured wastewater RBO concentration was > 2 mgP/l below that measure P removal but thereafter matched well. The nitrification batch tests, for which a close correlation between predicted and measured P removal was not important, were conducted at the beginning of the investigation when the predicted and measured P removal did not match well. The denitrification (anoxic) and P release and P uptake (anaerobic-anoxic/aerobic) batch tests were conducted during wastewater batches 10 to 25, when the predicted and measured P removal did match well. The measured kinetic rates in the MBR and CAS systems can therefore be legitimately compared with rates measured in previous investigations.

5 Conclusions

To assess the impact of high VSS concentration in membrane bioreactor biological nutrient removal (BNR) activated sludge (AS) systems on the bioprocess kinetic rates that mediate biological N and P removal, two identical (except for the hydraulic retention time) parallel laboratory scale University of Cape Town (UCT) nitrification denitrification (ND) biological excess phosphorus removal (BEPR) systems fed the same real wastewater were operated for 450 days, one at a low VSS concentration (3 gVSS/ℓ) and solid liquid separation with a secondary settling tank (CAS system), the other at a high VSS concentration (13 gVSS/ℓ) and solid liquid separation with submerged panel membranes (MBR system). From the BNR performance of these two systems and from aerobic, anoxic-aerobic and anaerobic-anoxic-aerobic batch tests on sludge harvested from the two systems the following conclusions were drawn.

The MBR system achieved a higher COD removal (effluent COD 41 mgCOD/ℓ) compared with the CAS system (unfiltered 74 mgCOD/ℓ, 0.45 µm filtered 51 mgCOD/ℓ) due to the complete retention of particulate organics and some colloidal organics considered soluble in CAS systems. However, the "unfiltered effluent" COD concentration from the MBR system (measured at the 800 ml mark in the 1000 ml measuring cylinder after 30 min settling in the diluted sludge volume index test) was much higher (139 mgCOD/ℓ) than the unfiltered COD from the CAS system (73 mgCOD/ℓ). Both systems achieved similar in N removals (MBR 83%, CAS 81%). Nitrification was complete in both systems - effluent free and saline ammonia

(FSA) concentration from the MBR system was 0.7 mgFSA-N/ℓ and from the CAS system 0.9 mgFSA-N/ℓ. Denitrification was better in the MBR system (effluent nitrate MBR 18.0 mgNO$_3$-N/ℓ and CAS 20.0 mgNO$_3$-N/ℓ) due to the negligible impact of the dissolved oxygen in the recycle to the anoxic reactor at the high VSS concentration of the MBR system. The P removal in the MBR system (22.5 mgP/ℓ) was higher than that in the CAS system (17.4 mgP/ℓ). This was due to the recycle of nitrate from the anoxic reactor to the anaerobic reactor and greater anoxic P uptake in the CAS system due to the non-zero nitrate concentration in the anoxic reactor. This made the kinetic rates associated with BEPR measured in the batch tests incomparable between the two systems. Due to the higher sludge production by the MBR system [0.31 (gVSS/d)/(gCOD/d)] than by the CAS system [0.20 (gVSS/d)/(gCOD/d)], the influent unbiodegradable particulate COD fraction (f$_{S'up}$) of the MBR system was higher (0.241) than that of the CAS system (0.084). This affected the fractionation of the VSS into the ordinary heterotrophic organism (OHO) and phosphate accumulating organism (PAO) active fractions in the two systems with the steady state BNR models, which also affected the observed OHO and PAO VSS specific kinetic rates calculated from the results of the batch tests on sludge harvested from two systems. This affect was unavoidable because kinetic rates expressed in terms of VSS are not comparable between different BNR systems. This effect was unaviodable because steady state models aligned with and based on the same but simplified principles as kinetic models are the only interface between experimental systems and the kinetic models.

From the aerobic nitrification batch tests: (1) At the same low VSS concentration, the MBR system exhibited lower VSS specific ammonia utilization rate (SAUR) and autotrophic nitrifier organism (ANO) maximum specific growth rates (μ$_A$) than the parallel CAS system, apparently due to different selection pressures imposed by membranes and SSTs. (2) For the MBR system, as the VSS concentration increased, the SAUR and μ$_A$ decreased, apparently due to ammonia and/or oxygen transfer limitations. (3) For the MBR system at the VSS concentration, as the initial ammonia concentration increased, the SAUR and μ$_A$ increased, indicating possible ammonia transport limitation at increasing VSS concentration.

From the above, it was evident that the ANOs in the MBR and CAS systems exhibited different behaviour, apparently induced by different environments under which the ANOs develop. The reasons for this possibly are: (1) In CAS systems with SSTs, organism loss via the effluent occurs including ANOs. Therefore CAS system may select ANOs with higher maximum specific growth rates (μ$_A$) than MBR systems. In the MBR system all the ANOs are retained, including slow growing ones. (2) At the high VSS concentrations in the MBR system, oxygen and ammonia transport limitations decrease the observed SAUR and μ$_A$.

From the anoxic-aerobic batch tests, the OHOVSS specific denitrification rate by OHOs (K$_{2OHO}$) utilizing slowly biodegradable organics (SBO) obtained at different MBR system VSS concentrations (2.5-12 gVSS/ℓ) and different initial nitrate concentrations ranging from 30 to 90 mgN/ℓ showed no effect to initial nitrate concentration, in agreement with past work (van Haandel et al. 1981, Clayton et al. 1991; Ekama and Wentzel 1999) and no effect to VSS concentration. From all the anoxic batch tests, the average K$_{2OHO}$ was 0.264 mgNO$_3$-N/(mgOHOVSS.d), which is very

close to the average K_{2OHO} rate reported in the literature for conventional (low VSS) BNR systems with SSTs, i.e. 0.255 from Ekama and Wentzel (1999).

From the anaerobic-anoxic-aerobic batch tests, the specific VSS and specific PAOVSS anaerobic acetate (as COD) uptake and P release rates showed no effect of VSS or initial acetate concentration. Also, the results obtained with different concentrations of acetate added showed the acetate uptake rate to be zero order with respect to acetate concentration, which is in agreement with literature studies (Wentzel et al. 1985, 1989). The P release to acetate uptake ratio also showed no effect with acetate dose and VSS concentration. The specific VSS and specific PAOVSS aerobic and anoxic P uptake rates also showed no effect of VSS concentration. The average PAOVSS specific anaerobic acetate uptake and P release rates and the aerobic P uptake rate obtained over the VSS concentration range were within the range of literature rates observed on enhanced PAO culture systems, confirming that within experimental variation, high VSS concentration does not affect the rates.

In the anaerobic-anoxic/aerobic batch tests with acetate uptake, the PAOs showed significantly higher anoxic P uptake and denitrification rates than in the MBR system itself, where high acetate and excess nitrate did not occur. In the former the PAOs denitrified 22% of the nitrate whereas in the MBR system only 11%. The OHOVSS specific denitrification rates were within the same 0.2 to 0.3 mgNO$_3$-N/(mgOHOVSS. d) range in all the batch with an anoxic phase. While the PAOVSS specific denitrification rate in the anaerobic-anoxic/aerobic batch tests was about half of the OHOVSS specific denitrification rate, in the MBR system, the PAOVSS specific denitrification rate was only 1/14th of the OHOVSS specific denitrification rate because the conditions in the anaerobic-anoxic/aerobic batch tests (high acetate and nitrate) were not prevalent in continuous flow BNR systems fed real wastewater. The large reduction in P removal resulting from significant anoxic P uptake BEPR seems counter-productive for the very small PAO contribution to denitrification.

The results from this investigation show that the BNRAS steady state and kinetic models developed for low VSS concentration BNRAS systems with secondary settling tanks can be applied with reasonable confidence to predict the performance of high VSS concentration BNRAS systems with membranes, except for the maximum specific growth rate of the nitrifiers, which was observed to be significantly lower in the MBR system.

Specific denitrification rates are zero order with respect to nitrate concentration and HAc consumption rates are zero order respect to HAc concentration in agreement with previous observations on conventional BNR systems. Anoxic P uptake has been consistently observed and the existence of 2 groups of PAO bacteria has been demonstrated. Anoxic P uptake is detrimental to the BEPR performance in a BNR system. However, quantitative links between design and operational parameters and the extent of anoxic P uptake have not been established. This has hindered incorporation of anoxic P uptake in the design and simulation models for BNR systems, with or without membranes, and requires resolution. The specific denitrification rates of OHOs are significantly higher than those of PAOs, to confirm the greater affinity of OHOs than PAOs for nitrate.

References

Cicek N, Franco JP, Suidan MT, Urbain V, Manem J (1999) Characterization and comparison of membrane bioreactor and a conventional activated sludge system in the treatment of wastewater containing high molecular weight compounds. Wat Environ Res 71(1):64–70

Clayton JA, Ekama GA, Wentzel MC, Marais GVR (1991) Denitrification kinetics in biological N and P removal activated sludge systems treating municipal wastewaters. Wat Sci Tech 23:1025–1035

du Toit GJG, Parco V, Ramphao MC, Wentzel MC, Ekama GA (2007) Design and performance of BNR activated sludge systems with flat sheet membranes for solid liquid separation. Wat Sci Tech 56(6):105–113

du Toit GJG, Parco V, Ramphao MC, Wentzel MC, Lakay MT, Mafungwa HZ, Ekama GA (2010) The performance and kinetics of biological nitrogen and phosphorus removal with ultra-filtration membranes for solid-liquid separation. Final WRC Report for Projects K8/814 and K5/1537, Water Research Commission, Private Bag X03, Gezina 0031, Pretoria, South Africa

Ekama GA, Marais GVR (1984) Two improved activated sludge settleability parameters. IMIESA 9(6):20–27

Ekama GA, Dold PL, Marais GVR (1986) Procedures for determining influent COD fractions and the maximum specific growth of the heterotrophs in activated sludge systems. Wat Sci Tech 18(6):91–114

Ekama GA, Wentzel MC (1999) Denitrification kinetics in biological N and P removal activated sludge systems treating municipal wastewaters. Wat Sci Tech 39(6):69–77

Gao M, Yang M, Li H, Yang H, Zhang Y (2004) Comparison between a submerged bioreactor and a conventional activated sludge on treating ammonia-bearing inorganic wastewater. J Biotech 108:265–268

Ghyoot W, Vandale S, Verstraete W (1999) Nitrogen removal from sludge reject water with a membrane assisted bioreactor. Wat Res 33(1):23–32

Han SS, Bae TH, Jang GG, Tak TM (2005) Influence of sludge retention time on membrane fouling and bioactivities in membrane bioreactor system. Proc Biochem **40**:2393–2400

Holbrook RD, Massie KA, Novak JT (2005) A comparison of membrane bioreactor and a conventional activated sludge mixed liquor and biosolids characteristics. Wat Environ Res 77 (4):323–360

Huang X, Gui P, Qiuan Y (2001) Influence of sludge retention time on microbial behaviour in a submerged membrane bioreactor. Proc Biochem 36(10):1001–1006

Lee W, Kang S, Shin H (2003) Sludge characteristics and their contribution to microfiltration in submerged membrane bioreactors. J Membr Sci 216:217–227

Li H, Gao M, Yang H, Zhang Y, Kamagata Y (2005) Comparison of nitrification performance and microbial community between a submerged bioreactor and a conventional activated sludge. Wat Sci Tech 51(6–7):193–200

Liebig T, Wagner M, Bjerrum L, Denecke M (2001) Nitrification performance and nitrifier community composition of a cheostat and a membrane-assisted bioreactor for the nitrification of sludge reject water. Bio Biosyst Eng 24:203–210

Luxmy BS, Nakajima F, Yamamoto K (2000) Analysis of bacterial community in a membrane separation bioreactors by fluorescent in situ hybridization and DGGE techniques. Wat Sci Tech 41(10–11):259–268

Maharaj S, du Toit GJG, Wentzel MC, Bux F (2007) Molecular approaches to study the dynamics of nitrifying bacteria in a conventional activated sludge system and membrane bioreactor. 4th International Water Association Leading-Edge Conference and Exhibition on Water & Wastewater Technology, Singapore, 3–6 June (Poster)

Manser J, Gujer W, Siegrist H (2005) Consequence of mass transfer effects on the kinetics of nitrifiers. Wat Res 39:4633–4642

Monti A, Hall ER, Dawsin RN, Husain H, Kelly HG (2005) Comparative study of biological nutrient removal (BNR) processes with sedimentation and membrane based separation. Biotech Bioeng 94(4):740–752

Parco V (2006) Bioreattori a membrana per la rimozione biologica dei nutrienti: cinetiche di processo ed efficienze. PhD thesis. University of Palermo, Palermo, Sicily (in Italian)

Parco V, Wentzel MC, Ekama GA (2006) Kinetics of nitrogen removal in a MBR nutrient removal activated sludge system. Desalination 199(1–3):89–91

Parco V, du Toit GJG, Wentzel MC, Ekama GA (2007) Biological nutrient removal in membrane bioreactors: denitrification and phosphorus removal kinetics. Wat Sci Tech 56(6):125–134

Ramphao MC, Wentzel MC, Ekama GA, Alexander WV (2005) The impact of membrane solid-liquid separation on the design of biological nutrient removal activated sludge systems. Biotech Bioeng 89(6):630–646

Randall EW, Wilkinson A, Ekama GA (1991) An instrument for the direct determination of oxygen utilization rate. Water SA 17(1):11–18

Smith S, Jefferson B, Judd SJ (2002) Membrane bioreactors: hybrid activated sludge or a new process? CHISA, Prague, August 2002

Sperandio M, Mass M, Espinoza Bouchot C, Cadassud C (2005) Characterization of sludge structure and activity on submerged membrane bioreactor. Wat Sci Tech 52(10–11):401–408

Standard Methods (1985) Standard methods for the examination of water and wastewater, 16th edn., APHA, WEF, AWWA, Washington DC USA

Van Haandel AC, Ekama GA, Marais GVR (1981) The activated sludge process Part 3 - single sludge denitrification. Water Res 15(10):1135–1152

Wentzel MC, Dold PL, Ekama GA, Marais GVR (1985) Kinetics of biological phosphorus release. Wat Sci Tech 17:57–71

Wentzel MC, Dold PL, Ekama GA, Marais GVR (1989) Enhanced polyphosphate organism cultures in activated sludge systems Part III - kinetic model. Water SA 15(2):89–102

Wentzel MC, Ekama GA, Dold PL, Marais GVR (1990) Biological excess phosphorus removal - steady state process design. Water SA 16(1):29–48

Yamamoto K (2002) Membrane bioreactor: an advanced wastewater treatment/reclamation technology and its function in excess sludge minimization. In: Advances in water and wastewater treatment technology, Amsterdam, pp 229–237

Zhang B, Yamamoto K, Ohgaki S, Kamiko N (1997) Floc size distribution and bacterial activities in membrane separation activated sludge processes for small scale wastewater treatment reclamation. Wat Sci Tech 35(6):37–44

Recovery of Ammonia and Production of High-Grade Phosphates from Side-Stream Digester Effluents Using Gas-Permeable Membranes

M.B. Vanotti[(✉)], P.J. Dube, and A.A. Szogi

United States Department of Agriculture, Agricultural Research Service,
Coastal Plains Soil, Water and Plant Research Center,
2611 W. Lucas Street, Florence, SC 29501, USA
Matias.Vanotti@ars.usda.gov

Abstract. Phosphorus recovery was combined with ammonia recovery using gas-permeable membranes. In a first step, the ammonia and alkalinity were removed from municipal side-stream wastewater using low-rate aeration and a gas-permeable membrane manifold. In a second step, the phosphorus was removed using magnesium chloride (MgCl2) and reduced amounts of alkali. The side-stream wastewater contained 730 mg N/L, 140 mg P/L and 2900 mg/L alkalinity. The process recovered approximately 79–93% of the ammonia and 80–100% of the phosphorus. Surprisingly, the phosphates produced were very-high grade (42–44% P_2O_5) with a composition similar to the bio-mineral newberyite. However, lower grade phosphate products (27–29% P_2O_5) were produced whenever the N recovery step was bypassed or carbonate alkalinity was added. Therefore, removal of ammonia and alkalinity are important considerations for production of very-high grade phosphate product.

Keywords: Ammonia recovery · Phosphorus recovery · Newberyite

1 Introduction

Conservation and recovery of nitrogen (N) and phosphorus (P) from municipal, industrial and agricultural effluents using anaerobic digesters (AD) is important because of economic and environmental reasons.

A promising new method to recover ammonia (NH_3) from wastewater is the use of gas-permeable membranes (Vanotti and Szogi 2015). The gas-permeable membrane manifolds are submerged in the liquid manure, and the gaseous NH_3 is removed from the liquid matrix before it escapes into the atmosphere. The N removal is done with low-rate aeration in the reactors that naturally increases the pH of the liquid and accelerates the rate of passage of NH_3 (>96%) through the submerged gas-permeable membrane manifold and further concentration in an acid stripping solution reservoir (Garcia-Gonzalez et al. 2015; Dube et al. 2016). The effluent after ammonia treatment is low in ammonia and carbonates. In turn, these conditions improve precipitation of phosphate minerals of high-grade.

The objective of this work was to develop new technology for simultaneous N and P recovery suitable for municipal digester effluents (Vanotti et al. 2016). It combines a gas-permeable membrane technology (N recovery) with P recovery of solid products by precipitation of phosphates. Phosphorus precipitating compounds such as for example, magnesium chloride ($MgCl_2$), are added to the system after the N removal. The new system was first tested using livestock wastewater (Vanotti et al. 2017). In this work, municipal side-stream wastewater was used. Results of this study and others were used to file a US Patent on the new process.

2 Materials and Methods

In this case study, the wastewater was side stream collected from James River municipal plant, Hampton Roads Sanitation District, Virginia. The side stream wastewater was a centrate effluent from waste sludge that was subjected to anaerobic digestion and solids separation and contained about 140 mg/L P and 730 mg N/L. Ammonia was substantially removed in a first treatment step (Fig. 1). In a second step, $MgCl_2$ was added to the N treated effluent in the phosphorus recovery tank. The gas permeable membrane module was connected with a stripping solution reservoir containing diluted acid as described in Dube et al. (2016) and Garcia-Gonzalez et al. (2015). Low rate aeration was delivered to the bottom of tank. Gas-permeable membrane was tubular and made of e-PTFE material. Nitrification inhibitor (22 ppm) was
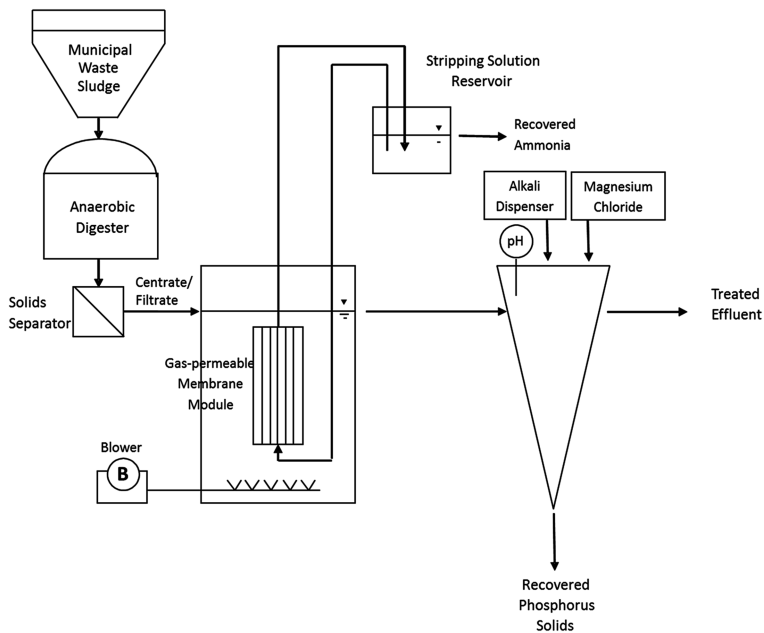
Fig. 1. Schematic diagram of nitrogen (N) and phosphorus (P) recovery system using ammonia separation tank and P recovery tank

added to ensure nitrification inhibition. Concentrated acid was added to the stripping solution to an end-point pH of 1 when the pH increased above about 2 as result of active ammonia capture. In a second step, the treated effluent from the N recovery tank was transferred to phosphorus separation tank where it was mixed with $MgCl_2$ and NaOH to obtain a phosphorus precipitate and an effluent without phosphorus or ammonia. $MgCl_2$ was applied to obtain a Mg:P ratio 1.2:1. Alkali NaOH was applied to pH 9.2. The chemicals were mixed for about one minute. After about a 0.5 h gravity sedimentation period, the phosphorus precipitate was dewatered using glass fiber filters, and characterized for total N, P, Mg, Ca, and K and plant available phosphorus.

3 Results and Discussions

Phosphorus recovery of anaerobically digested municipal wastewater via $MgCl_2$ precipitation was enhanced by combining it with the recovery of NH_3 through gas-permeable membranes and low-rate aeration. The low-rate aeration stripped the carbonates in the wastewater and increased pH, which accelerated NH_3 uptake by the gas-permeable membrane system (Fig. 2). The ammonia capture process substantially reduced carbonate alkalinity, from 2990 mg/L to 130 mg/L, and ammonia concentration, from 730 mg N/L to 50 mg/L. These conditions benefited subsequent P recovery. The combined process provided quantitative (ca 100%) P recovery efficiency (Table 1).
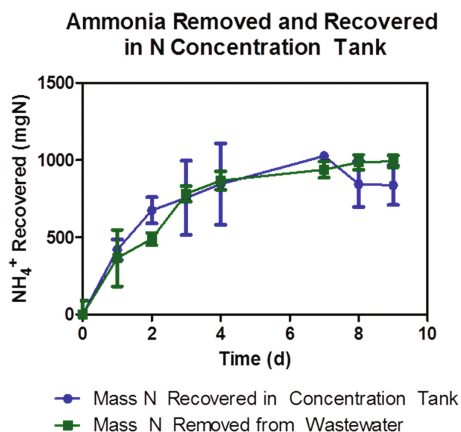
Fig. 2. Mass removal and recovery of nitrogen (N) from municipal wastewater using gas-permeable membranes and aeration

With active NH_3 extraction, the magnesium phosphates that were produced contained high P_2O_5 grade (42%) and high plant availability (Table 2). The phosphorus product was similar to the composition of newberyite ($MgHPO_4.3H2O$), a biomineral found in guano deposits, which has approximately 40.8% P_2O_5 and 13.9% Mg composition and 1:1 P:Mg molar ratio.

Table 1. Changes in concentration and mass balances for nitrogen (N) and phosphorus (P) using side-stream municipal wastewater

	Influent concentration	Effluent concentration	Mass inflow	Mass outflow				Total recovery
			Initial manure	Recovered solid	Recovered by membrane	Effluent	
	mg/L		mg (% of initial)					
N	733	60	1100 (100%)	30 (2.73%)	837 (76.09%)	90 (8.18%)	867 (78.82%)
P	133	20	200 (100%)	212 (106.00%)	0 (0%)	30 (15.00%)	212 (106.00%)

Table 2. Composition of recovered phosphate mineral solid in the system of Fig. 1 using approximately 5.42 mmol/L MgCl2 and approximately 10 mmol/L NaOH

Composition of recovered solid					
N	P (P_2O_5)	Mg	Ca	K	Plant available P (Citrate soluble)
%					
2.56	18.30 (42.0)	14.6	1.4	1.9	98.4

However, in other tests conducted with the same municipal wastewater, whenever the N recovery step was bypassed or carbonate alkalinity was added, the phosphate minerals obtained had lower grade (27–29% P_2O_5) (Vanotti et al. 2016). Therefore, removal of ammonia and carbonates are important considerations for production of very-high grade phosphate products.

4   Conclusions

These results showed that it is possible to produce Mg phosphates with high P_2O_5 content by removing the NH_3 from the liquid with the gas-permeable membrane process. In a first step, the ammonia and alkalinity were removed from municipal side-stream wastewater using low-rate aeration and a gas-permeable membrane manifold. In a second step, the phosphorus was removed using magnesium chloride (MgCl2) and reduced amounts of alkali. The phosphates produced were very-high grade (42–44% P_2O_5) with a composition similar to the bio-mineral newberyite. This is an important finding because recovered phosphates with high P_2O_5 content are more in line with mineral commercial fertilizers and favored by the fertilizer industry.

References

Dube PJ, Vanotti MB, Szogi AA, García-González MC (2016) Enhancing recovery of ammonia from swine manure anaerobic digester effluent using gas-permeable membrane technology. Waste Manag 49:372–377

García-González MC, Vanotti MB, Szogi AA (2015) Recovery of ammonia from swine manure using gas-permeable membranes: effect of aeration. J Environ Manag 152:19–26

Vanotti MB, Szogi AA (2015) Systems and methods for reducing ammonia emissions from liquid effluents and for recovering ammonia. U.S. Patent 9,005,333 B1. U.S. Patent and Trademark Office

Vanotti MB, Szogi AA, Dube PJ (2016) Systems and methods for recovering ammonium and phosphorus from liquid effluents. U.S. Patent Application 15/170,129. U.S. Patent and Trademark Office

Vanotti MB, Dube PJ, Szogi AA (2017) Recovery of ammonia and phosphate minerals from swine wastewater using gas-permeable membranes. Water Res. doi:10.1016/j.watres.2017.01.045

The Start-up of Mainstream Anammox Process Is Limited Only by Nitrite Supply

Y. Law[1(✉)], S. Swa Thi[1], X.M. Chen[2], T.Q.N. Nguyen[1], T.W. Seviour[1], R.B.H. Williams[3], B. Ni[2], and S. Wuertz[1]

[1] Singapore Centre for Environmental Life Sciences Engineering, Nanyang Technological University, Singapore 637551, Singapore
[2] Advanced Water Management Centre, The University of Queensland, St Lucia 4072, Australia
[3] Singapore Centre for Environmental Life Sciences Engineering, National University of Singapore, Singapore 119077, Singapore

Abstract. In this study, we investigated start-up of an Anammox bioprocess from a secondary activated sludge seed fed primary effluent from a domestic used water reclamation plant (WRP). To test the hypothesis that an anammox-enriched sludge could still be achieved under such conditions given enough nitrite and ammonium, nitrite was supplemented at a molar ratio of 2:1 to ammonium. Anammox activity was observed within 50 d of operation and the relative abundance of Anammox bacteria increased from <0.1% gradually up to 4% after 100 d of operation, concomitant with complete ammonium removal. Despite consumption of chemical oxygen demand (COD) by heterotrophic denitrifiers, the Anammox biomass continued to accumulate up to 20% of relative abundance, contributing to biofilm and granule formation in the reactor. Thus, a high influent COD concentration is not inhibitory to the start-up of an Anammox system as long as sufficient nitrite is provided.

Keywords: Nitrogen removal · Denitrification · Biofilm

1 Introduction

Full-scale nitritation-anammox has thus far been limited to used waters with a high ammonia concentration and a low chemical oxygen demand (COD) to total nitrogen (N) ratio (Lackner et al. 2014). Domestic used water typically has a COD:N of 10-14 (Henze and Comeau 2008) which favours the proliferation of fast growing heterotrophic denitrifying organisms, that in turn present as competitors of the Anammox bacteria for nitrite utilisation. Nonetheless, fully functioning Anammox bacteria have been observed in activated sludge systems treating municipal used water, even in the presence of COD, albeit at low relative abundance. This suggests that an alternative strategy to achieve full scale partial nitration/anammox for domestic used water treatment is possible, by enhancing the activity of pre-existing Anammox populations in conventional nitrification-denitrification activated sludges.

To date, all studies on the effect of COD in raw and pretreated municipal used waters on Anammox activity have been conducted on systems with high

Anammox-bacteria enrichments (Jenni et al. 2014). The extent to which COD inhibits the establishment of a stable and functioning Anammox enrichment for used water treatment has not been described. The aim of this work was therefore to investigate whether Anammox can be achieved in activated sludge treating settled used water without additional pre-treatment to remove organic carbon. We hypothesized that the presence of organic carbon will not compromise the growth of Anammox bacteria conditional on the provision of sufficient nitrite.

2   Materials and Methods

A sequencing batch reactor (SBR) with a working volume of 4 L was seeded with returned activated sludge (RAS) from a domestic water reclamation plant (WRP) in Singapore and fed primary effluent. Primary effluent was collected from the WRP once a week. The nitrite concentration was then adjusted to a molar ratio of 2:1 relative to ammonium and stored at 4°C to prevent degradation. A heating jacket was connected to maintain the SBR temperature at 33 ± 1°C, higher than the typical temperature of domestic wastewater in Singapore of 31°C to encourage Anammox activity. For enrichment purpose, the sludge retention time (SRT) was not controlled whereby sludge loss only occurred through sampling for nutrient and solids analyses. Once a stable co-culture of Anammox and heterotrophic denitrifier was established, individual batch experiments with nitrite was conducted in the SBR to assess the contribution of Anammox and denitrifiers under varying nitrite concentrations. Data from the batch experiments were used to model the Anammox and heterotrophic denitrifier substrate kinetics.

Mixed liquor samples were collected periodically for DNA extraction. With the gDNA extract, sequencing libraries were prepared and run on an Illumina HiSeq2500 sequencer using 250 bp paired-end sequencing. The metagenome data was used for community analysis based on Ribotagger method using reads annotated to 16S V4-regions.

3   Results and Discussion

Anaerobic ammonium removal activity was observed after 50 d of operation. The effluent ammonium concentration dropped continuously from day 58 to day 75 even at a relatively low abundance of Anammox bacteria of less than 2% (Fig. 1A–B). *Brocadia* was the only Anammox taxa detected in the whole community shotgun metagenome data throughout reactor operation. Despite the presence of heterotrophic denitrification, the nitrite supply was sufficient to support Anammox activity as indicated by the residual nitrite detected in the effluent. The reactor displayed stable ammonium removal activity after 80 days of operation in line with an increase in relative abundance of Anammox bacteria (Fig. 1B).

Red biofilms were visible on the wall and surface of the stirrer and suspended red granules were also observed providing further evidence for the existence of Anammox bacteria (Kartal et al. 2013). Biofilm formation was also indicated by a decrease in mixed
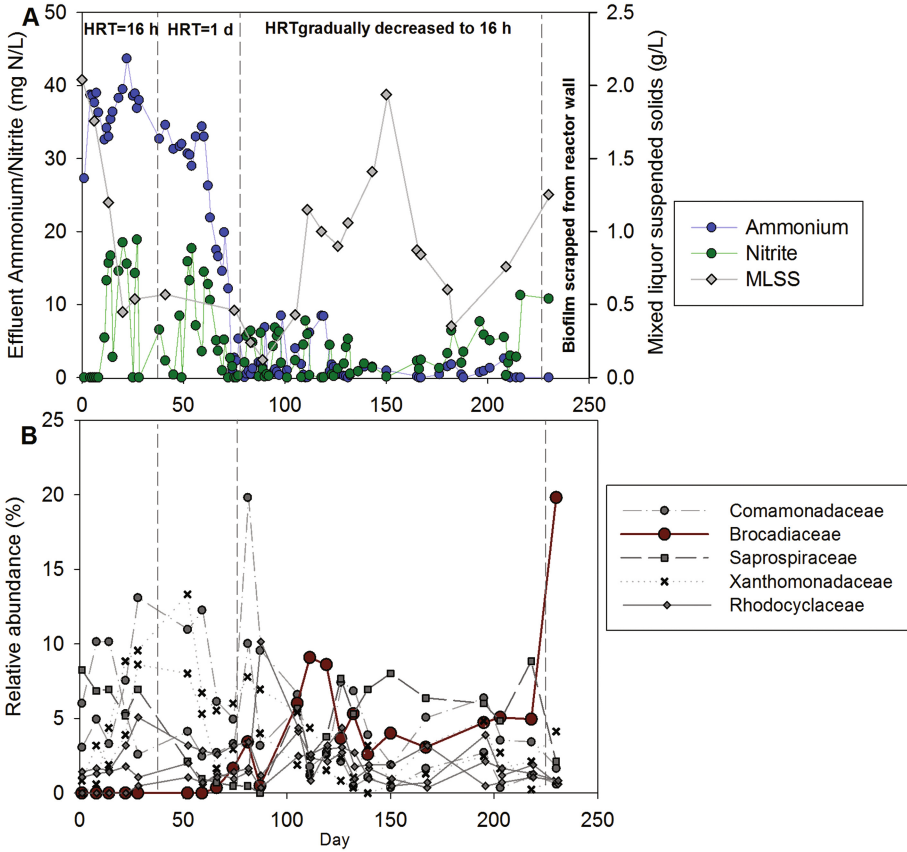
Fig. 1. The effluent ammonium, nitrite and suspended solids concentration (top) of an Anammox- heterotrophic denitrifying reactor fed with primary effluent augmented with nitrite and the corresponding relative abundance of the top ten most abundant annotated taxa detected in the suspended biomass based on Ribotagger results (bottom) (Color figure online)

liquor suspended solids (MLSS) concentration and a decrease in Anammox relative abundance in suspension after day 110 of reactor operation (Fig. 1). When the biofilm was removed from the wall of the reactor, Brocadia was the most dominant taxon in the suspended biomass suggesting preferential attached growth of the Anammox bacteria (Fig. 1). Using qPCR data within the first 120 day of operation, the doubling time of the Anammox bacteria was estimated to be approximately 11.9 ± 1.7 days.

Batch experiments conducted with varying nitrite concentration showed that both specific ammonium oxidation rate (AOR) and nitrite reduction rate (NRR) increased commensurate with nitrite concentration from 5 to 60 mg N/L. However, the AOR: NRR decreased by 50% at a nitrite concentration of 60 mg N/L versus 5 mg N/L suggesting that high nitrite concentrations favour Anammox over heterotrophic denitrification activity. Indeed, modelling analysis of the data obtained from the batch

experiments estimated the nitrite affinity constant of Anammox to be 16.8 ± 0.9 mg/L which is significantly higher than that of the heterotrophic denitrifier (i.e. 1.4 ± 0.5 mg/L).

4   Conclusions

This study demonstrated that an Anammox biomass can be built up from activated sludge without bioaugmentation with an Anammox enrichment within 3 months of operation. The activity of Anammox bacteria was not compromised despite the presence of complex organic carbon source in primary effluent of a domestic used water reclamation plant as long as sufficient nitrite is supplied.

References

Henze M, Comeau Y (2008) Biological wastewater treatment: principles, modelling and design. In: Henze M, van Loosdrecht M, Ekama GA, Brdjanovic D (eds.) Biological Wastewater Treatment Principles, Modelling and Design. IWA Publishing, London

Jenni S, Vlaeminck SE, Morgenroth E, Udert KM (2014) Successful application of nitritation/anammox to wastewater with elevated organic carbon to ammonia ratios. Water Res 49:316–326

Kartal B, De Almeida NM, Maalcke WJ, Op den Camp HJM, Jetten MSM, Keltjens JT (2013) How to make a living from anaerobic ammonium oxidation. FEMS Microbiol Rev 37 (3):428–461

Lackner S, Gilbert EM, Vlaeminck SE, Joss A, Horn H, van Loosdrecht MCM (2014) Full-scale partial nitrition/anammox experiences - an application survey. Water Res 55:292–303

Phosphorus Recovery from Sewage
in a Pilot-Scale UASB-DHS System

A. Nurmiyanto[1,2(✉)], H. Kodera[1], T. Kindaichi[1], N. Ozaki[1],
and A. Ohashi[1]

[1] Graduate School of Engineering, Hiroshima University, 1-4-1 Kagamiyama,
Higasihiroshima 739-8527, Japan
[2] Department of Environmental Engineering, Islamic University of Indonesia,
Yogyakarta 55581, Indonesia

Abstract. The operation of a pilot-scale plant for the demonstration of phosphate (P) recovery from actual sewage was investigated for more than 5-years. The pilot plant consisted of a 500 L up flow anaerobic sludge blanket (UASB) and 540 L down flow hanging sponge (F-DHS) reactor as pre-treatment unit, subsequently a 66 L of P-DHS reactor operation was modified to enhance recovery of P. The combined UASB-DHS system could achieve good organic removal efficiencies accounted for 87%, 84% and 90% for BOD, COD, and SS respectively. Under the optimum operational condition, the P-DHS reactor was able to concentrate P up to 120 mg P L-1 in the recovery solution. Nevertheless, high P concentration could not be easily maintained over the years. It started to worsen when the pH in F-DHS effluent dropped until below 6, but then slightly increased when the pH is being controlled in a range of 7-8. Interestingly, a cyclic pattern was observed in the P concentration of the recovery solution in response to the temperature, regardless of whether the pH was controlled or not. High P concentration only achieved temporally in spring ($16 < T < 20°C$) and further become deteriorated as temperature rise in summer ($T > 30°C$). Therefore, in order to achieve a high P concentration in the recovery solution the F-DHS effluent temperature should be controlled in a range of 15–20°C.

Keywords: Down-flow hanging sponge · Phosphorus recovery · Polyphosphate accumulating organisms · Up-flow anaerobic sludge blanket · Wastewater treatment

1 Introduction

The development of wastewater treatment technology for P removal also offers the opportunity for P recycling for maintaining resources sustainability. The most common configuration used for biological P recovery in wastewater treatment plant (WWTP) is by integrating activated sludge (AS) process with enhanced biological phosphorus removal (EBPR) (Oehmen et al. 2007). Nevertheless, the extraction of rich P containing in the produced sludge is rather expensive. Campos et al. (2009) pointed out that sludge handling costs could account for 50–60% from total operational costs of ASP itself. However, a combination of up-flow anaerobic sludge blanket (UASB) and down-flow hanging sponge (DHS) reactor has emerged as an interesting alternative

wastewater treatment process (Tandukar et al. 2007). Furthermore, the volume of excess sludge produced from a UASB-DHS reactor was 15-times lower compared than in the conventional AS process.

Thereby to increasing the economical benefit of P recovery in EBPR process, a combination with UASB-DHS system emphasizing on its low excess sludge production is necessary to be developed. It has been previously reported that a laboratory scale DHS system could demonstrated that a synthetic sewage (5 mg P L^{-1}) was concentrated to a recovery solution of 125 mg P L^{-1} in a bench scale experiment without any excess sludge produced (Kodera et al. 2013). The present study shows P recovery performance of UASB-DHS system in a pilot scale operated in extended time to investigate whether the novel system can be applicable to real sewage.

2   Materials and Methods

2.1   Pilot Scale Operation

A combination of UASB and DHS system was installed in WWTP facility of Higashihiroshima City, Japan. Total 1 m^3 day^{-1} of actual sewage was treated in a pilot scale reactor (Fig. 1). Initially, the biodegradable organic content in wastewater was degraded anaerobically inside the UASB reactor. UASB effluent was then uniformly distributed from the top of DHS reactor and the water gravitationally flowed-down through the biofilm carrier inside the DHS reactor under aerobic condition. Finally, the treated water from the DHS reactor was introduced in to P-DHS reactor for P recovery purposes in a specific operation cycle. The pilot-scale system were operated continuously for 5 year at an ambient temperature which varied from 9°C during winter to 35°C during summer.
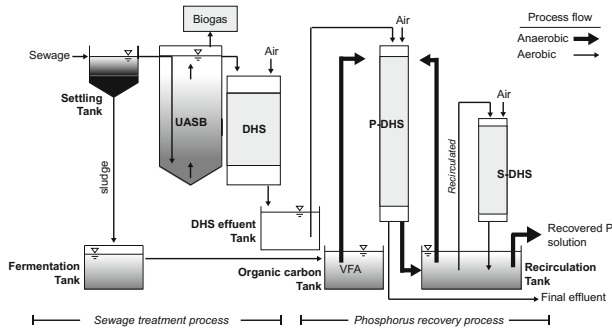
Fig. 1. The conceptual of UASB-DHS system for sewage treatment and phosphorus recovery process

2.2   Principle of Phosphorus Recovery as Concentration Solution in P-DHS Reactor

To establish phosphorus recovery process using DHS reactor, the DHS biofilm carrier should be enriched with polyphosphate accumulating organism (PAOs), by alternatingly exposed to anaerobic and aerobic conditions. The alternating operation is a sequence of three steps (Fig. 1) as follows: *(1) Aerobic period*: P-containing water from F-DHS effluent is supplied to the reactor, while air is continuously ventilated to facilitate aerobic environment. P is being up take by PAOs residing in the DHS biofilm, and after aerobic period is finished the treated water is discharged. *(2) Anaerobic period*: The reactor is filled with a recirculation solution and an organic substrate (e.g. VFA), air supply was stopped to keep anaerobic environment in the reactor. In this stage PAOs store the organic substrate and release the accumulated P into the recirculation solution. *(3) Recovery period*: The solution is drained into the recirculation tank, and the overflow water was collected in recovery tank. By repeating the sequence period, PAOs are enriched within the reactor and at the same time, P concentration in the recirculation tank continually increased until a plateau is reached. As a result, a high P contained in the solution could be recovered from the system and could be easily utilized as a liquid fertilizer.

3   Results and Discussion

3.1   Performance of UASB and F-DHS Reactors

Organic substances were insufficiently removed in the UASB for all 5 years of the operation (Table 1). The average t-COD concentration was 201 ± 41 mg L^{-1} in the UASB effluent, corresponding to approximately 28% removal efficiency. In contrast, the high sulfate was consumed to 198 mg SO_4^{2-} L^{-1}, which means approximately 80% of t-COD removal was reduced to hydrogen sulfur. This produced high hydrogen sulfur probably inhibited methanogenic activity and COD removal (Choi and Rim 1991; Harada et al. 1994). As a result, the biogas production was very little impossible to collect the biogas from the UASB. The t-BOD substance of 140 ± 68 mg L^{-1} was also remained in UASB effluent at a high concentration.

On the other hand, in the F-DHS reactor installed as post-treatment unit of UASB, the sewage treatment was successfully performed. Even after Day 745, when we reduced the air-supply rate from 400 to 30 L hr^{-1} for preventing pH drop, which is described below in detail. The average t-COD concentration in the DHS effluent was 31 ± 21 mg L^{-1} until Day 744 and then became a little bit worse to 51 ± 16 mg L^{-1}. The similar phenomenon was observed for t-BOD (22 ± 17 to 45 ± 21 mg L^{-1}). This deterioration would be caused by DO depression from 5.2 ± 2.1 to 2.4 ± 1.8 mg L^{-1} in the F-DHS effluent along with decreased air-supply. In the whole UASB-F-DHS system, the sewage removal efficiencies reached approximately 90% for both BOD and COD. In regards to P, the concentration was consistent throughout the UASB and F-DHS system. This result of no P removal was reasonable because sludge withdrawing was never carried out from the UASB and F-DHS reactors in the entire operational period of 5 years.

Table 1. Summary of water quality and performances of up-flow anaerobic sludge blanket (UASB) reactor, down-flow hanging sponge (F-DHS) reactors, and phosphorus DHS (P-DHS) reactor in the entire pilot scale system

Parameters	Periods					
	All periods		Phase 1 (day 1 to 744)		Phase 2 (day 745 to 1850)	
	Sewage	UASB eff	DHS eff	P.DHS eff	DHS eff	P.DHS eff
pH	7.3 (0.3)	7.2 (0.3)	6.6 (0.7)	7.1 (0.8)	7.3 (0.5)	7.5 (0.5)
DO (mgO$_2$ L^{-1})	1.3 (1.8)	0.4 (0.4)	5.2 (2.1)	6.1 (2.3)	2.4 (1.8)	6.2 (2.2)
t-BOD (mg L^{-1})	172 (45)	140 (68)	22 (17)	16 (11)	45 (21)	18 (8)
t-COD (mg L^{-1})	278 (57)	201 (41)	37 (15)	31 (21)	51 (16)	24 (10)
SS (mg L^{-1})	61 (24)	38 (20)	6 (4)	4 (5)	10 (4)	7 (4)
PO$_4^{3-}$(mg-P L^{-1})	1.7 (0.4)	1.7 (0.2)	1.6 (0.3)	1.4 (0.4)	1.6 (0.4)	1.3 (1.5)
NH$_4^+$ (mg-N L^{-1})	33 (5)	36 (6)	22 (8)	17 (7)	27 (5)	22 (7)
NO$_2^-$ (mg-N L^{-1})	0	0	1.5 (2.2)	0.6 (0.8)	1.0 (2.1)	0.2 (0.2)
NO$_3^-$ (mg-N L^{-1})	0.4 (0.8)	0.5 (0.9)	10 (8)	10 (7)	3 (3)	9 (8)
SO$_4^{2-}$ (mg L^{-1})	291 (116)	198 (112)	278 (93)	284 (87)	251 (96)	235 (70)
Removal		UASB	UASB+DHS	ALL	UASB+DHS	ALL
BOD (%)		19 (23)	87 (7)	91 (10)	72 (11)	89 (10)
COD (%)		28 (24)	87 (22)	89 (6)	84 (13)	92 (6)
SS (%)		38 (32)	90 (10)	94 (9)	83 (17)	88 (9)
PO$_4$-P (%)		3 (7)	6 (3)	18 (21)	6 (4)	24 (11)
NH$_4$-N (%)		-	33 (22)	49 (28)	18 (19)	33 (16)

3.2 Performance of P-DHS Reactors

The P-DHS reactor was set to concentrate the P concentration of the effluent discharged from the F-DHS reactor for phosphorus removal and recovering as a concentrated solution. However, The P-DHS reactor did not easily work well. Therefore, the operational condition was changed four times, then it took a very long time of 5 years to achieve the objective of this study. Eventually, we demonstrated that phosphorus could be recovered for the actual sewage as a high P solution of approximately 120 mg P L-1 (Fig. 2D), which is comparable to a recovered solution in a similar study using an artificial wastewater (Kodera et al. 2013). It is also important to note that besides no sludge withdrawal was carried out during the operation, a high P concentration obtained in this study also considered as economically feasible for fertilizer production according to the minimum requirement value from Cornel and Schaum (2009). Through the long-term pilot-scale treatment, however, it was found that this P recovery process could be applied under restricted operational environments as described below.

3.2.1 Performance Without S-DHS Reactor (The First Year)

In the start-up of P-DHS operation, the P concentration of recovery solution gradually increased (Fig. 2D), which means the proposed P concentrating process by P-DHS would be applicable for municipal sewages, and enrichment of PAOs was expected. However, after P concentration arrived at approximately 30 mg P L^{-1} on day 50, the
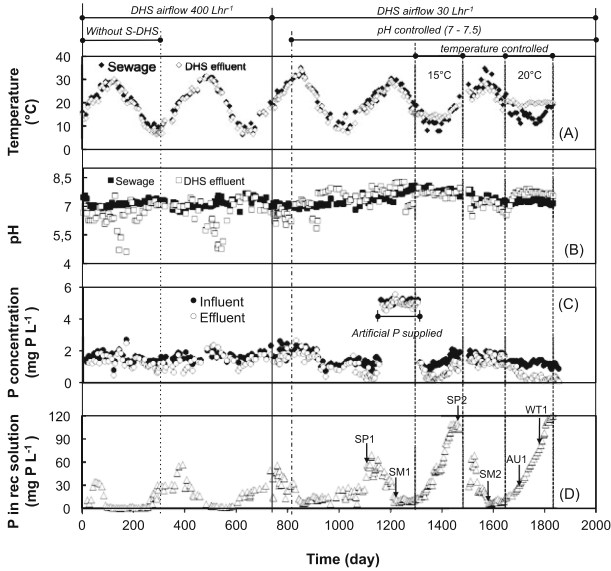
Fig. 2. Timeline of P-DHS reactor performances with certain operating condition changes. Time course of: temperature (A); pH (B); phosphate concentration (C); and amount of P recovered in the recovery solution (D). Arrow line labelled with SP1 until WT1 indicate biomass-sampling time on P-DHS reactor

concentration declined before reaching the target concentration of over 100 mg P L^{-1}. We waited an increase of P concentration for a long time, but no recovery and no removal were observed. It was though that this disruption of the P concentrating process was caused by hydrogen sulfide, which inhibits PAOs activity (Rubio-Rincon et al. 2016), because a high hydrogen sulfide was detected in the recirculation tank (data not shown). The hydrogen sulfide would be produced by sulfate reducing bacteria (SRB) detected in the recirculation tank, where some of volatile fatty acids provided to P-DHS in the anaerobic phase was remained, and the SRB grew on the organic substances and sulfate from the F-DHS effluent. The SRB would be also enriched in the P-DHS reactor.

3.2.2   Performance with S-DHS Reactor (The Second Year)

To prevent the hydrogen sulfide production, the S-DHS reactor was installed in the P recovery process on day 280. The S-DHS reactor successfully worked at once to make the solution in the recirculation tank aerobic and keep it low COD concentrations. As a result, SRB disappeared and no hydrogen sulfide was detected ever since then (data not shown). As soon as installing the S-DHS reactor, P concentration of recovery solution had a tendency to increase again (Fig. 2D). P was gradually concentrated and reached 55 mg P L^{-1} on day 370. However, it turned to decrease again until day 570. Even though the hydrogen sulfide inhibition had been solved, the worsening of performance happened. We noticed the pH of F-DHS effluent became lower during this period (Fig. 2B). The pH drop was derived from nitrification as mentioned above. The low pH

perhaps caused the deterioration of performance because P concentration of recovery solution increased again just when the pH of F-DHS effluent returned back to around 7.

3.2.3 pH Controlled Period (The Third and Fourth Years)

Many researchers reported that a favorable environment for PAOs was neutral or higher pH in EBPR processes (Filipe et al. 1997; Oehmen et al. 2007). It would be essential for phosphorus recovery to prevent pH drop derived from nitrification in our proposing system. The airflow rate is one of operational parameters to weaken nitrification in the F-DHS reactor and can be easily controlled. With hope for stopping unfavorable pH decrease, the airflow rate was reduced to 30 L h^{-1} less than one-tenth on day 745. As expected, a weaker nitrification was successfully performed in the summer (data not shown), resulting in prevention of the severe pH drop keeping over pH 6.0 (Fig. 3B). Unfortunately, however, the phosphorus recovery was not improved in comparison with the performance of second year, which suggests that the pH control by airflow rate might be insufficient.
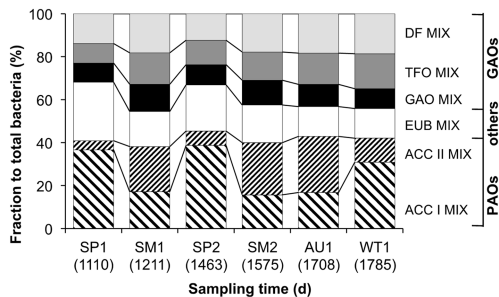
Fig. 3. Microbial community structure in the P-DHS reactor taken from different season

We, therefore, installed a pH controller with 1N NaOH solution in the F-DHS effluent reserving tank on day 800. As a result, the pH in the tank was maintained in a range of 7–8. Despite the preferable pH, after P concentration in the recovery solution increased up to 70 mg P L^{-1} around day 1120, the recovery performance was deteriorated. Since P concentration of sewage supply was relatively low. We thought low P concentration might negatively affect PAOs activity, then P concentration in the P-DHS influent was artificially increased to 5 mg P L^{-1} by adding sodium P during day 1160–1300. Nevertheless, no improvement of the recovery performance was observed.

The increase of recovery P concentration occurred at low temperatures in every season from winter to middle of spring. On the other hand, the degradation happened when the temperature became higher in summer. The observed cyclical phenomenon (Figs. 2B and C) strongly suggests that temperature would be one of the key factors to govern the phosphorus recovery performance.

3.2.4 Temperature Controlled Period (The Fourth and Fifth Years)

To confirm an effect of temperature on the P-DHS performance, the water temperature control was tried using a heater of 1 kWh and a cooler of 1 kWh, which were installed in the F-DHS effluent reserving tank on day 1290, with a thermostat. As soon as the F-DHS effluent was provided at 15°C, which was set and successfully controlled, the P concentration in the recovery solution steadily increased and eventually achieved approximately 110 mg P L-1 on day 1420 (Fig. 2D). However, unfortunately, the control was failed and the water temperature increased in the summer because the cooling power was insufficient. Consequently, the P concentrated solution was not kept, and the concentration felt down little by little, resulting in almost no phosphorus recovery on day 1580.

However, with the coming of autumn, the air temperature dropped then the water temperature control became possible. By controlling the water temperature at 20°C instead of 15°C because a P removal was observed even 20°C around, the P-DHS performance completely rebounded. Finally, P concentration reached 120 mg P L-1 (Fig. 2D) and the F-DHS effluent of around 1.2 mg P L-1 was removed to less than 0.2 mg P L-1 in the P-DHS reactor, corresponding to nearly 83% phosphorus removal (Fig. 2C). As just described, the long-term pilot-scale experiment demonstrated that phosphorus recovery was possible for the actual sewage as a concentrated solution under the temperature-controlled condition.

3.3 Microbial Population Dynamic in the P-DHS Reactor

The stability of EBPR system relies on the existence and activity of PAOs within the microbial population. Therefore, to further explore the microbial community in the P-DHS reactor, total 6 biomass samples were collected from the P-DHS carrier media throughout the operational periods (Fig. 2D). The composition of the microbial population on each sample was then characterized by using FISH, as depicted in Fig. 3. It can be seen that most dominant GAOs was observed as *Defluvicoccus* related group, they could stably maintained their population over the 13% of total bacteria in all sampling periods. PAOs Type I was dominated up to 36.6% of total bacteria in the spring (day 1110) but then decreased until 17.2% in the summer (day 1211), again a similar PAOs composition trend was observed on the next season of spring (day 1463) and summer (day 1575). PAO Type I population was then increased significantly from 16.8% in the autumn (day 1708) to approximately 30.8% of the total bacteria in the winter (day 1785). Concomitantly, the PAOs Type II populations showed inverted trends. Interestingly, the changes within the PAOs community appear to indirectly relate to the phosphorus recovery performance. It seems that PAO Type I might play an important role in the phosphorus recovery process rather than PAO Type II. Therefore, future investigation on different PAO types metabolism is necessary, which should become a key research area for the establishment of a stable EBPR technology.

4 Conclusions

The present study demonstrated that the proposed system to recover P as concentrated solution could be applicable to real sewage through the four years operation of a pilot scale P-DHS plant. However, it is found that the temperature is a crucial factor for the success of high phosphorus recovery.

References

Campos JL, Otero L, Franco A, Mosquera-Corral A, Roca E (2009) Ozonation strategies to reduce sludge production of a seafood industry WWTP. Biores Tech 100:1069–1073

Cornel P, Schaum C (2009) Phosphorus recovery from wastewater: needs, technologies and costs. Water Sci Tech 59:1069–1076

Choi E, Rim JM (1991) Competition and inhibition of sulfate reducers and methane producers in anaerobic treatment. Wat Sci Tech 23:1259–1264

Filipe CD, Daigger GT, Grady CP (1997) Effects of pH on the rates of aerobic metabolism of phosphate-accumulating and glycogen-accumulating organisms. Water Environ Res 73:213–222

Harada H, Uemura S, Momonoi K (1994) Interaction between sulfate reducing bacteria and methane producing bacteria in UASB reactors fed with low strength wastes containing different levels of sulfate. Water Res 28:355–367

Kodera H, Hatamoto M, Abe K, Kindaichi T, Ozaki N, Ohashi A (2013) Phosphate recovery as concentrated solution from treated wastewater by a PAO-enriched biofilm reactor. Water Res 47:2025–2032

Oehmen A, Lemos PC, Carvalho G, Yuan Z, Blackall LL, Reis MAM (2007) Advances in enhanced biological phosphorus removal: from micro to macro scale. Water Res 41:2271–2300

Rubio-Rincon FJ, Lopez-Vazquez CM, Welles L, van Loosdrecht MCM, Brdjanovic D (2016) Sulphide effects on the physiology of Candidatus Accumulibacter phosphatis type I. Appl Microbiol Biotechnol: 12:1–12

Tandukar M, Ohashi A, Harada H (2007) Performance comparison of a pilot-scale UASB and DHS system and activated sludge process for the treatment of municipal wastewater. Water Res 41:2697–2705

An Empirical Model for Carbon Recovery in a Rotating Belt Filter and Its Application in the Frame of Plantwide Evaluation

Chitta Ranjan Behera[1], Farnaz Daynouri-Pancino[2],
Domenico Santoro[2], Krist V. Gernaey[1], and Gürkan Sin[1(✉)]

[1] Department of Chemical and Biochemical Engineering,
Technical University of Denmark, 2800 Kongens Lyngby, Denmark
gsi@kt.dtu.dk
[2] Trojan Technologies, 3020 Gore Road, London, ON N5V 4T7, Canada

Abstract. The rotating belt filter (RBF) is an emerging and enabling technology for carbon recovery and also an alternative to the primary clarifier (PC), sludge thickening and dewatering. A recent study indicates that the RBF has the potential to reduce capital cost, footprint and improve energy and nutrient recovery in comparison to a conventional PC. Moreover, it is also believed that the RBF can fractionate carbon (enrichment of cellulose, namely toilet paper) based on particulate size, more efficiently than a PC. It is, therefore, necessary to understand and quantify the uniqueness of the RBF performance to maximize plant-wide benefits when retrofitted in existing wastewater treatment plants (WWTPs). Thus, a rigorous plant-wide study is required to interpret the deeper influence of an RBF on the major downstream units (such as activated sludge tanks, sludge digester, etc.). This study emphasizes the development of a simplified empirical model for describing carbon recovery in an RBF and the impact of the RBF implementation on plant-wide evaluation.

Keywords: Rotating belt filter · Carbon recovery · Empirical model · Plant-wide evaluation

1 Introduction

Primary treatment in a wastewater treatment plant (WWTP) is crucial, and its role in fostering the performance of anaerobic digestion (AD) by diverting more carbon to AD is gaining more and more attraction. In a traditional WWTP, the primary clarifier (PC) is one of the unit operations (for primary treatment) which works based on gravity separation to remove total suspended solids (TSS) and lower the biological oxygen demand. However, the footprint and capital cost associated with it are not competitive enough to meet the modern plant design philosophies (such as higher carbon recovery, compact size, etc.).

On the other hand, a new emerging cake filtration based technology called RBF has several advantages (Franchi et al. 2015) compared to a primary clarifier such as: (i) it requires 1/10th of the PC space; (ii) installation is convenient; and (iii) the technique can handle a sudden peak load. In addition to that, Paulsrud et al. (2014) also found that

the percentage of volatile solids and the biochemical methane potential of the sludge is higher for a plant operating with an RBF in comparison to a PC. So this observation further motivates to use the RBF for boosting the AD performance and subsequently cut down the energy consumption demand by the activated sludge process. However, the increased carbon removal in primary treatment when operating an RBF raises some concerns over the pre-denitrification performance efficiency (Paulsrud et al. 2014). Recent studies (Razafimanantsoa et al. 2014; Rusten et al. 2016) have indicated that the RBF has no impact on the denitrification rate in a moving bed biofilm reactor (MBBR), and a minimal impact on activated sludge process (AS). Razafimanantsoa et al. (2014) also suggested carrying out additional studies as denitrification depends on multiple factors. This study further motivates to perform a rigorous dynamic plant-wide evaluation to assess the impact of the RBF (on the widely used model SF 2000 as shown in Fig. 1) on the plant-wide scale. Chakraborty (2015) and DeGroot et al. (2016) have presented mechanistic models for dynamic simulation and design exploration of the RBF. However, due to the complexity of the model and the higher number of measurements that is required to calibrate such a model before using it in a simulation, this further complicates the plant-wide simulation of a WWTP.
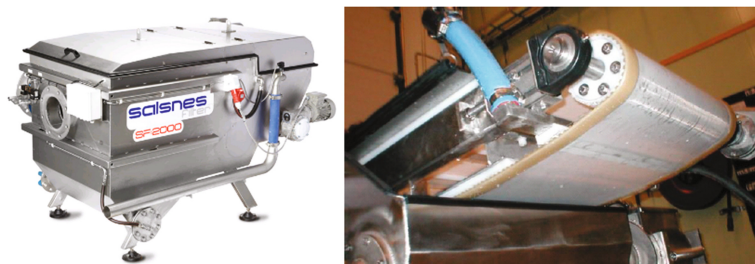
Fig. 1. **(a)** RBF unit (model SF-2000) **(b)** Inclined filtration screen (Franchi et al. 2015)

To allow plant-wide simulation in a relatively easy way, this study is focused on developing a new simplified empirical model to estimate the suspended carbon recovery from the RBF. Furthermore, the model is extended to carry out an impact assessment of the RBF on the plant-wide scale.

2   Materials and Methods

2.1   Working Principle

The RBF (as shown in Fig. 1) works based on cake filtration which removes suspended solids from waste water by using a polyester screen (as shown in the Fig. 1b). The RBF is operated by continuously moving the belt on which the waste water passes, and during this process, solids are retained on the filter mat and form a layer which is then further separated by the air knife. The mat is periodically cleaned by compressed air and a water spray. The sludge collected in this process can be further thickened based

on the application (such as direct feed to a sludge stabilization unit), without adding any external dewatering equipment. The mesh size for the RBF screen varies from 50 to 500 micron which increases the application domain. In this study, the SF 2000 model (with screen size 350 micron) is considered for empirical model development as it is widely used for sewage water treatment.

2.2   Theory of Operation

In cake filtration, the flow through porous media is governed by Darcy's law which is given as

$$\frac{q}{A} = -\frac{k}{\mu} \cdot \frac{dp}{dx} \tag{1}$$

Where the flux (q/A) is proportional to the pressure gradient (dp/dx) and k is the permeability of the filter and μ is the dynamic viscosity of the water. Using Eq. 1 as a basis, Chakraborty (2015) has developed a mechanistic model (Eq. 2) to estimate the effluent total suspended solids (TSS) concentration. This model captures the underlying mechanism very well. However, the usage of this model always depends on several parameters (such as specific cake resistance, water level, etc.) as inputs which require additional effort before the model can be applied.

$$TSS_{out} = TSS_{in} - \frac{\omega.B}{Q_{in}.\alpha}\left(\frac{B.g.\rho_w.(H - H_{ref}).H_o}{Q_{in}.\mu.\sin\theta} - R_m\right) \tag{2}$$

Where,

Q_{in} = influent flow rate [m3/h]	ω = rotational speed of the screen [rpm]
R_m = resistance by the screen [m/kg]	μ = viscosity of the effluent [kg/(s·m)]
α = specific cake resistance [m/kg]	H = average water level [m]
H_o = initial water level [m]	H_{ref} = water level in the effluent tank [m]
ρ_W = density of water [kg/m3]	B = width of the screen [m]

Likewise, (DeGroot et al. 2016) have proposed a CFD based dynamic model (Eq. 3) for design exploration and sizing of the RBF.

$$\frac{\partial \overline{m_c}}{\partial t} + c.\frac{\partial \overline{m_c}}{\partial x} = C_{TSS_{in}}.\eta.v \tag{3}$$

Where,

$$\eta = \frac{a_\eta}{a_\eta + \exp(-b_\eta.\overline{m_c})} \quad v = \frac{\Delta p}{\mu.a_R.\exp(b_R.\overline{m_c})}$$

a_R, a_η, b_R, b_η are parameter constants, m_c represents the cake mass per unit area and C is the belt speed.

This model (as depicted in Eq. 3) presented by DeGroot et al. is helpful when executing a hydrodynamics study. However, using this model to perform plant-wide simulation may slow down the computations considerably, and moreover, additional measurements and appropriate initial conditions are required.

3   Results and Discussion

3.1   Carbon Recovery Model Development and Evaluation

Experimental data reported in Franchi et al. (2015) were generated using the SF-2000 RBF unit whose belt screen size is 350 microns. The data were collected under different flow rate conditions, ranging from 120 to 370 gpm and for a range of TSS value, ranging from 10 mg/L to 1400 mg/L. As these experimental data represent the wide variability of TSS concentration at the inlet and the corresponding RBF removal efficiency, the data were selected for developing the simplified empirical model for estimating suspended carbon recovery from the RBF. Figure 2 represents the pattern (model prediction is presented in red line) that exists between TSS removal efficiency and the TSS at the inlet. The empirical model (as depicted in Eq. 4) for carbon recovery is developed by framing it as a nonlinear least square problem. This empirical model
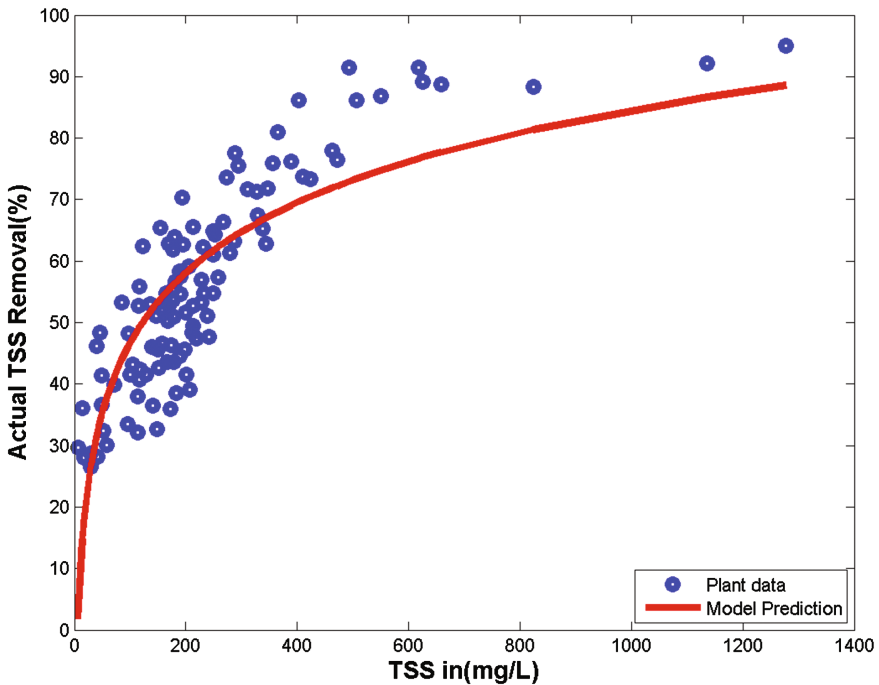
Fig. 2. Development of empirical based model for carbon recovery (Color figure online)

has two model parameters (namely K_1-16.45 and K_2-29.1) with adjusted regression coefficient (R^2_{adj}) value 0.67. The uniqueness of this model is that it has only two model parameters (compared to Eqs. 2 and 3) and it needs only TSS measurement, which is widely measured at plant side. Therefore, it is decided to use the developed model for plant-wide impact assessment analysis.

$$\eta_{TSS} = K_1 Log(TSS_{in}) - K_2 \tag{4}$$

Where,

K_1, K_2 are empirical model parameters, η_{TSS} is TSS removal efficiency (%) and TSS_{in} is the concentration of suspended solid at influent.

It is also observed that as the TSS at the inlet of the RBF increases, the removal efficiency also rises and this is because in the belt filter the deposited particulates form additional layer apart from the screen. Therefore, in total, there are in fact two layer screens, which help to retain a higher number of suspended particles on the filter.

3.2   Plant-Wide Steady State Simulation Analysis

The plant-wide steady state simulation for an RBF is performed using the modified BSM2 framework (as depicted in Fig. 3) and the plant-wide overall mass balance for COD, TN, TSS, etc. are summarized. The developed empirical model along with mass balance concept is implemented to build the rotating belt filter model for steady state plant-wide analysis. The wastewater influent defined in Gernaey et al. (2011) is used for the impact assessment. Around 68% of influent TSS (estimated by developed empirical model) is removed from the RBF which further translated to 1385 kg CH_4/d methane production from AD and below effluent COD limit (i.e. 44.8 mg COD/l). It is also observed that the C/N ratio is significantly reduced from 11.6 to 5.2, which is more
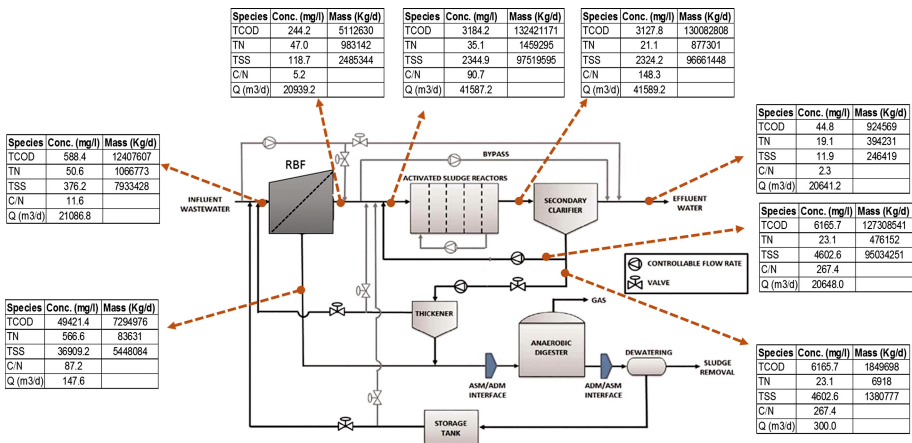
Fig. 3. Steady state plant-wide analysis for a rotating belt filter

than 50%. As a result, the effluent TN concentration (21.1 mg N/l) is slightly higher than the discharge limit (18 mg N/l).

4   Conclusions

A new simplified empirical model is proposed for the estimation of suspended carbon recovery from wastewater by using an RBF. The developed empirical RBF model has a lower number of model parameters (only two) and a reduced requirement for measurements (only TSS influent concentration) compared to the models retrieved from literature (Eqs. 2 and 3). Further, this simplified empirical model is extended to perform a steady state plant-wide analysis where the influence of an RBF on downstream is observed and quantified. It is noticed that the RBF has higher TSS removal efficiency (around 68%) compared to PC (around 50%). This higher removal efficiency further facilitates to higher methane production (1385 kg CH4/d for RBF and 1065 kg CH4/d for PC) low effluent COD concentration (44.8 mg COD/l for RBF and 47.8 mg COD/l for PC). On the other hand, the effluent TN concentration is 19.1 mg-N/l for RBF, which is just above the effluent discharge, limit (18 mg-N/l). This difference may fall in the prediction uncertainty, as there is a scope to enhance the model prediction further. It is important to mention that in this study only one operating condition for an RBF (with thick mat formation) is analyzed. Therefore additional research required to extend the verification of RBF impact at different operating procedure namely without thick mat formation.

References

Chakraborty T (2015) Evaluation of filtration performance of a rotating belt filter for different primary wastewater influents. Doctoral dissertation, The University of Western Ontario

DeGroot CT, Sheikholeslamzadeh E, Santoro D, Sarathy S, Lyng TO, Wen Y, Rosso D (2016) Dynamic modeling of rotating belt filters enables design exploration and advanced sizing with varying influent conditions. Proc Water Environ Fed 14:1158–1168

Franchi A, Williams K, Lyng TO, Lem W, Santoro D (2015) Rotating belt filters as enabling technology for energy-neutral wastewater treatment plants: current status and applications. Proc Water Environ Fed 2015(13):1743–1749

Gernaey KV et al (2011) Dynamic influent pollutant disturbance scenario generation using a phenomenological modelling approach. Environ Model Softw 26(11):1255–1267

Paulsrud B, Rusten B, Aas B (2014) Increasing the sludge energy potential of wastewater treatment plants by introducing fine mesh sieves for primary treatment. Water Sci Technol 69 (3):560–565

Rusten B, Razafimanantsoa VA, Andriamiarinjaka MA, Otis CL, Sahu AK, Bilstad T (2016) Impact of fine mesh sieve primary treatment on nitrogen removal in moving bed biofilm reactors. Water Sci Technol 73(2):337–344

Razafimanantsoa VA, Ydstebø L, Bilstad T, Sahu AK, Rusten B (2014) Effect of selective organic fractions on denitrification rates using Salsnes filter as primary treatment. Water Sci Technol 69(9):1942–1948

Thermodynamic Modelling Is Needed to Describe the Effect of High Temperature on Microbial Nitrogen Removal Processes

K.A. Ismail, M. Patón, and J. Rodríguez[(✉)]

Department of Chemical and Environmental Engineering (CEE),
Masdar Institute of Science and Technology,
PO Box 54224, Abu Dhabi, United Arab Emirates
`jrodriguez@masdar.ac.ae`

Abstract. Existing models of nitrogen removal and related microbial reactions in conventional wastewater treatment plants are capable of describing most of the relevant behaviour of these plants. These models may however fall short on describing the effects of temperature on the microbial activity including the inhibition of nitrite oxidation. In this work a detailed model is presented incorporating the most and also some of the less commonly observed microbial nitrogen reaction pathways. The model calculates thermodynamic variables dynamically based on the dynamic concentrations. This allows for a detailed dynamic analysis of the thermodynamic feasibility of all reactions and of the effects of temperature. The results indicate that the well-known inhibition of nitrite oxidation at high temperature is caused by thermodynamic limitations.

Keywords: Nitrogen removal · Thermodynamics · Temperature effect · Sewage treatment

1 Introduction

Nitrogen removal process in conventional wastewater treatment plants is an essential treatment step catalysed by different types of microorganisms. The conventional process of nitrogen removal involves a two-step oxidation of ammonium into nitrate followed by a step of reduction of nitrate into nitrogen gas. There is a lack of literature on the comprehensive high temperature microbial bio-kinetics modelling that includes complete physicochemistry and thermodynamic elements. The IWA Activated sludge models (ASM) have been developed and implemented to study the behaviour of the processes involved in the activated sludge systems in wastewater treatment plants (Henze et al. 1987). The ASM1 is mainly developed to predict the nitrification and denitrification performance under steady state and dynamic conditions (Henze et al. 2000). Activated sludge models have been extensively applied and calibrated primarily for temperatures of 10 °C and 20 °C, much lower than those observed in regions where the temperatures can reach as high as 38 °C. The microbial cells maintenance and maximum substrate uptake rates are known to be the main parameters affected by temperature, together with physicochemical variables such as acid-base constants.

However, for reactions running close to equilibrium the temperature effect on their Gibbs energy may bring them thermodynamically unfeasible. Methods have been developed to adjust parameters of great influence on the removal of nitrogen processes at different temperatures (Heijnen 1999), however they are limited to specific kinetic parameters and not under an integrated bio-kinetic-thermodynamic perspective.

The aim of this work is to develop a mathematical model that integrates the temperature effects occurring in the nitrogen microbial metabolism reactions including the thermodynamics to assess the impact of high temperature on the overall nitrogen removal.

2   Model Description

Microbial reactions. The modelling approach is based on the ASM models structure with additional nitrogen conversion pathways included as well as sulphur oxidation-reduction reactions. Calculation of thermodynamic feasibility is performed for all the reactions included. A complete acid base speciation is also described based on temperature dependent thermodynamic properties.

The complete stoichiometry of all the bio-kinetic reactions modelled is presented in Fig. 1.

Variables (mol/L)		AOB	NOB	DNO2	DNO3	AMX	DRNO2	DRNO3	Het	SRB	SOB_O2	SOB_NO2	SOB_NO3	Decay	Hydrolysis
Total Ammonia-N	Samn	-1				-1	0.86	0.80	-0.24	-0.04	-0.04			0.16	
Nitrite	Sno2	0.99	-1	-1		-1.14	-1					-1			
Nitrate	Sno3		1.00		-1	0.16		-1					-1		
Nitrogen	Sn2			0.49	0.47	0.99						0.49	0.49		
Oxygen	So2	-1.42	-0.48						-0.74		-1.80				
Inorganic carbon	Sic	-0.06	-0.02	0.77	1.30	-0.07	1.54	2.05	0.80	1.82	-0.19	-0.12	-0.15	0.04	
Soluble BOD	Ss			-0.43	-0.78		-1.13	-1.52	-1	-1				0.42	1
Hydrogen sulfide	Sh2s									0.91	-1	-0.45	-0.71		
Sulfate	Sso4									-0.91	1	0.45	0.71		
Inert soluble	Si														
Ammonia oxidizers	Xaob	0.06												-1	
Nitrite oxidizers	Xnob		0.02											(-1)	
Heterotrophic denitrifiers	Xdn			0.10	0.26									(-1)	
Anaerobic nitrifiers	Xamx					0.07								(-1)	
Dissimilatory NOX	Xdnra						0.72	0.99						(-1)	
Aerobic heterotrophs	Xhet								1.20					(-1)	
Sulfate reducers	Xsrb									0.18				(-1)	
Sulfide oxidizers	Xsob										0.19	0.12	0.15	(-1)	
Inert suspended	Xi													0.2	
Slowly biodegradable substrate	Xs														-1

– **Autotrophic nitrification**
– **Dissimilatory NO2/NO3 reduction**
– **Anammox**
– **Aerobic oxidation of COD**
– **Heterotrophic denitrification**
– **Autotrophic denitrification**
– **Sulfate reduction**

Fig. 1. Detailed stoichiometry of the microbial reactions (left). Overview of the microbial pathways included in the model (right). Aerobic autotrophic nitrification process is carried out in a two-step process: ammonium and nitrite oxidation respectively. Nitrate reduction is either via heterotrophic denitrification with the oxidation of soluble BOD or autotrophic denitrification using hydrogen sulphide as an electron donor. Sulphate reduction uses BOD as electron donor. Anaerobic ammonium oxidation by anammox as well as dissimilatory nitrite/nitrate reduction are included. Soluble BOD is also oxidized aerobically by heterotrophs

The stoichiometric biomass yields of some of the reactions have been set from literature while others have been estimated based on the Gibbs energy dissipation method (Kleerebezem and van Loosdrecht 2010) for a constant temperature.

$$Y_{\frac{X}{S}}^{Met} = \left(\left(\frac{Y_s^{cat}(\Delta G_{Diss} + \Delta G_{An})}{-\Delta G_{cat}} \right) + Y_S^{An} \right)^{-1}; \quad \Delta G_{Diss} = -\Delta G_{cat} \frac{\frac{1}{Y_X^{Met}} - Y_S^{An}}{Y_S^{Cat}} - \Delta G_{An}$$

where the dissipated Gibbs energy ΔG_{Diss} depends on the type of carbon source used in the biosynthesis. Values for ΔG_{Diss} are 3500 kJ/C-mol for autotrophic growth on CO_2 with reverse electron transport and 457.1 kJ/C-mol for acetate in the heterotrophic growth reactions.

The model biomass yields and therefore the stoichiometric parameters are not modified with temperature and kept at their original estimated values. This is due to the observation of a very small effect and to the large complexity associated to incorporating a dynamic stoichiometry matrix in the model function of the dynamic Gibbs energy values.

2.1 Temperature Effects on Kinetics

The microbial reactions follow conventional Monod type kinetics while biomass decay rates follow first order kinetics (Henze et al. 2000). The model kinetic parameters such as maximum growth rate and decay constants are highly dependent on temperature and this dependency is modeled by the modified Arrhenius correlation.

The following equations represent the maintenance and the maximum uptake rate as functions of temperature respectively (Heijnen 1999).

$$m_G = 4.5 \exp[\frac{-69,000}{R}\left(\frac{1}{T} - \frac{1}{298}\right)] \quad q^{max} = q_{T^0}^{max} \exp[\frac{-69,000}{R}\left(\frac{1}{T} - \frac{1}{298}\right)]$$

m_G and q^{max} are corrected by temperature using an Arrhenius correlation with an activation energy (E_a) of 69 kJ/mol for all reactions except for ammonium and nitrite oxidizers 65 kJ/mol and 45 kJ/mol have been used respectively (Hellinga et al. 1999). The E_a values are typically obtained empirically by measuring the effect of temperature on maximum growth rates of microorganisms.

2.2 Temperature Effects on Thermodynamics

It is known that most microbial conversion reactions occurring in activated sludge systems run far from thermodynamic equilibrium and therefore no temperature effects on reaction feasibility are observed. However some reactions (e.g. nitrite oxidation and sulphate reduction) may indeed run close to thermodynamic equilibrium and ultimately be affected by temperature to the point of approaching thermodynamic equilibrium. In order to capture this, a thermodynamic based inhibition of the reaction rates is implemented as suggested in (Kleerebezem and Stams 2000), (Kleerebezem and van Loosdrecht 2006) such that when the ΔG crosses a threshold minimum value (ΔG_{min}) the rate of reaction decreases according to $\left(1 - e^{Kth*\frac{\Delta G - \Delta G_{min}}{T*Rth}}\right)$.

Model simulation case study. The above model was implemented for an activated sludge WWTP similar to that in the Al-Wathba 2 plant in Abu-Dhabi. The model was implemented into three plant compartments, namely a small anoxic pre-chamber, aerated tank and secondary settler (see Fig. 2).
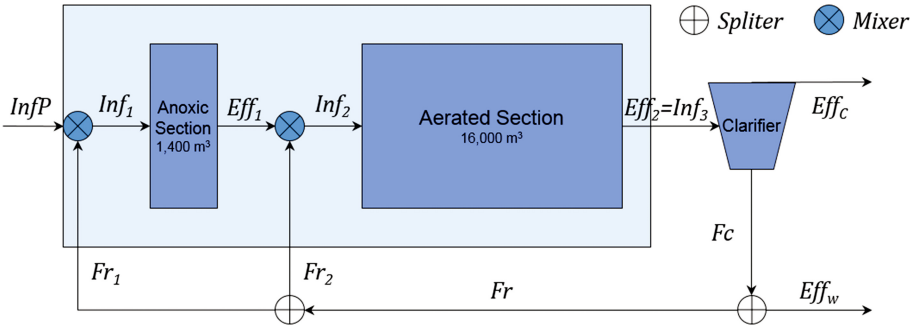
Fig. 2. An overview of the activated sludge system as modelled. InfP is the wastewater influent, Inf1 and Inf2 are the input streams that are mixed with the recycled streams Fr1 to form the input Fd1 to the anoxic zone and Fr2 to form the input Fd2 to the aerobic tank respectively. Eff1 and Eff2 are the effluent streams of the anoxic zone and the aerobic tank respectively. The streams generated in the clarifier are the clarified effluent Effc, concentrated flow Fc and the wastage flow Effw. Both tanks (anoxic and aerobic) are connected to the settler through the recycle streams

3   Model Implementation

An existing model implementation framework (Rodríguez et al. 2009) for simulation of bioprocess models that uses a combined Matlab-Simulink – Ms Excel interface with the thermodynamic extension has been used (Fig. 3).
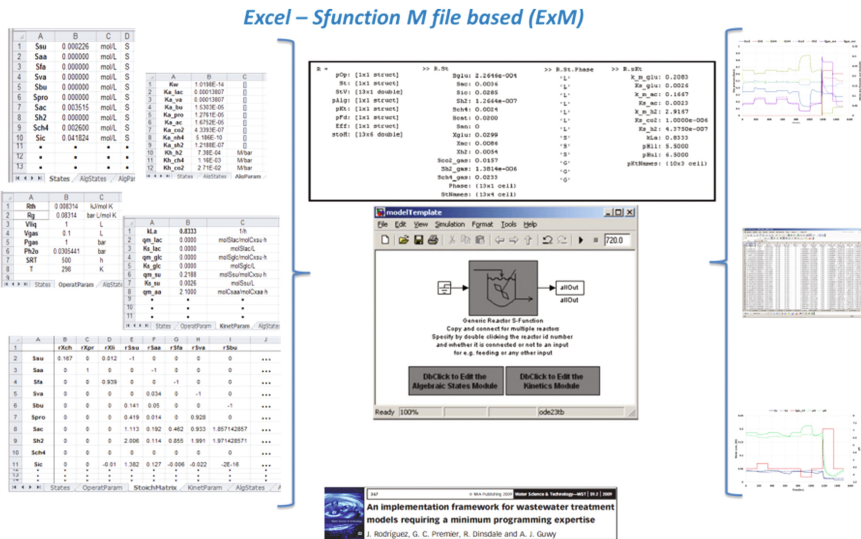
Fig. 3. Overview of modelling implementation architecture as per (Rodríguez et al. 2009)

4 Results and Discussion

A steady state simulation of the WWTP model was obtained at six different temperatures. The model simulations describe the thermodynamic impact of temperature on the microbial processes for which only the SRB and NOB appears as close to equilibrium. Among these the NOB appears to be impacted to the point of themrodynamic inhibition.

The parameter ΔG_{min} is proposed as the one to be adjusted to capture the exact temperature at which NOB reaction stops. In this study a ΔG_{min} of -20 kJ/mol is used to stop NOB at T = 38 °C as it has been experimentally observed in WWT plants in Abu Dhabi.

The following graphs clearly illustrate the effect of temperature on the nitrogen removal processes, especially NOB, and suggest a more detailed explanation needed for nitrite oxidation inhibition. Biomass concentration and nitrogen removal efficiency appear impacted by temperature. As temperature increases the maintenance needs increase which is directly proportional to the decay of biomass and this illustrates the reduction of biomass at higher temperatures (see Figs. 4 and 5).
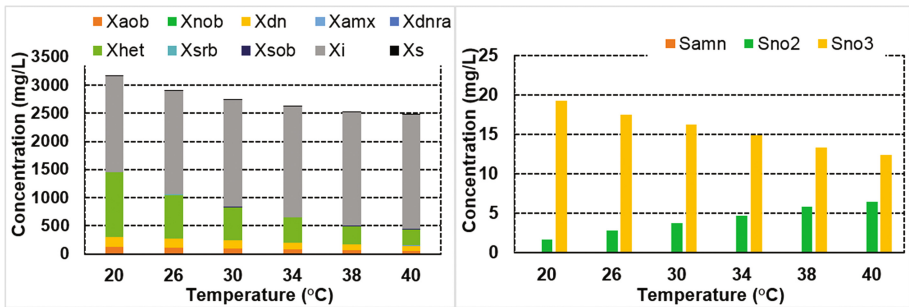
Fig. 4. Steady state concentrations of biomass (left) & nitrogen soluble components (right)
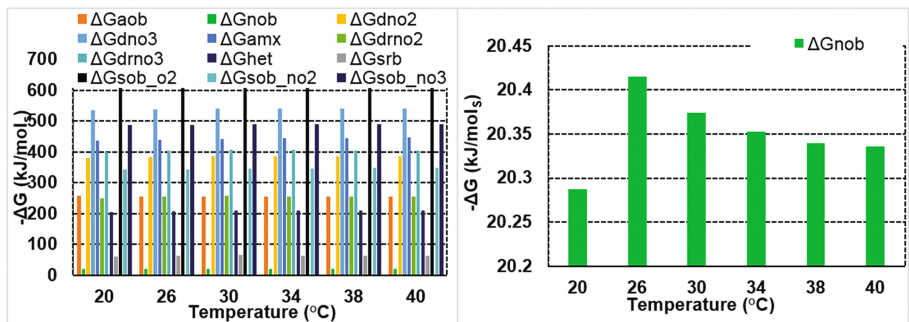
Fig. 5. Gibbs free energies of all the microbial reactions (left). Gibbs energy for the key components NOB

5   Conclusions

These preliminary results suggest that a detailed thermodynamic modelling of the nitrite oxidation process is required to capture properly the effect of temperature and for a better understanding and description of microbial nitrogen removal processes, in particualr for nitrite oxidation which appears to occur very close to thermodynamic equlibrium.

References

Heijnen JJ (1999) Bioenergetics of microbial growth. In: The encyclopedia of bioprocess technology: fermentation, biocatalysis, and bioseparation, pp 267–291. Wiley, New York

Hellinga C, van Loosdrecht MCM, Heijnen JJ (1999) Model based design of a novel process for nitrogen removal from concentrated flows. Math Comput Model Dyn Syst 5(4):351–371

Henze M, Gujer W, Mino T, van Loosdrecht MCM (2000) Activated sludge models ASM1, ASM2, ASM2d and ASM3. IWA Publishing, London

Kleerebezem R, van Loosdrecht MCM (2010) A generalized method for thermodynamic state analysis of environmental systems. Crit Rev Environ Sci Technol 40(1):1–54

Henze M, Grady CPL Jr, Gujer W, Marais GR, Matsuo T (1987) Activated sludge model no. 1. Scientific and Technical report no. 1. IAWPRC, London

Kleerebezem R, Stams AJM (2000) Kinetics of syntrophic cultures: a theoretical treatise on butyrate fermentation. Biotechnol Bioeng 67(5):529–543

Kleerebezem R, van Loosdrecht MCM (2006) Critical analysis of some concepts proposed in ADM1. Water Sci Technol 54(4):51–57

Rodríguez J, Premier GC, Dinsdale R, Guwy AJ (2009) An implementation framework for wastewater treatment models requiring a minimum programming expertise. Water Sci Technol 59(2):367–380

Application of DHS-USB System and Ozone in Recirculating Freshwater Aquaria Towards Zero Water Exchange Aquaria

N. Adlin[1(✉)], M. Hatamoto[2], Y. Hirakata[1], T. Watari[2],
N. Matsuura[2,3], and T. Yamaguchi[1]

[1] Science of Technology Innovation, Nagaoka University of Technology,
Nagaoka, Japan
[2] Environmental Systems Engineering, Nagaoka University of Technology,
Nagaoka, Japan
[3] Faculty of Environmental Design, Institute of Science and Engineering,
Kanazawa University, Kanazawa, Japan

Abstract. In recirculating aquaria system (RAS), partial water exchange was performed regularly as a part of aquaria maintenance for maintaining water quality and aesthetic beauty. To reduce large consumption of water during maintenance, this study proposed a biological nitrogen removal system consisted of down-flow hanging sponge (DHS) and an up-flow sludge blanket (USB) system with combination of ozone (O_3) to simultaneously maintain nitrogen compounds concentration and remove yellow substances that implicate color in aquaria without performing water exchange. The performance of the system was evaluated using on site freshwater aquaria at ambient temperature (20–34 °C). NH_3, NO_2^-, and NO_3^- concentration detected was 0.10 ± 0.12, 0.03 ± 0.13 and 6.40 ± 7.46 mg N L^{-1} respectively. Color were maintained at 6 color units at phase 2 and 4 when O_3 was applied continuously for 8 h per day. In addition, 16S rRNA gene of microorganisms from the bioreactors were sequenced to identify the microbial communities present. The analysis revealed that ammonia oxidizing archaea (AOA) such as *Ca. Nitrososphaera* played important role in nitrification and *Thauera* played important role in denitrification. Fish survived throughout the study despite no water exchange was performed for 425 days. The application of O_3 in combination with DHS-USB system appeared to be a promising technology towards less-maintenance aquaria.

Keywords: Recirculating aquaria system · Biological nitrogen removal · Ozone

1 Introduction

Nitrogenous wastes released from fish respiration, excrement, and feed waste are highly toxic and harmful for fish in aquaria (Thorarensen et al. 2010). Continual exposure to high NH_3 concentration can lead fish towards physical impairment, inhibition of growth, and fatality (Weinstein et al. 1998). Generally, conventional methods such as the use of sand filter and exchanging 10–20% of water from tank capacity was performed per week

to maintain water quality and aesthetic beauty in aquaria. However, regular water exchange stress the fish, and filtration methods use substantial amounts of water during backwashing to clear filter that became clogged over time (Losordo et al. 1999). As water is becoming scarce, an effective way to control water quality in aquaria is crucial to reduce large amount of water usage for maintenance (Asano et al. 2003). Our research group developed a biological nitrogen removal system consisted of down-flow hanging sponge (DHS) and up-flow sludge blanket (USB) system for marine aquaria (Furukawa et al. 2016). The system maintained nitrogenous compounds concentration at low level. Thus, reduced the necessity to perform water exchange. DHS-USB system achieved target water quality standard for aquaria by maintaining Total Ammonia Nitrogen (TAN) and NO_2^- concentration less than 0.1 mg-N L^{-1} and NO_3^- concentration less than 40 mg-N L^{-1} during the study. However, it was still problematic to maintain aesthetic beauty in aquaria. Accumulation of yellow substances was observed over time, making water exchange obligatory despite color was innocuous and cause no fatality threat to aquatic animals. In this study, we considered the application of O_3 in combination with DHS-USB system to eliminate water exchange for aquaria. O_3 has capability to prevent accumulation of yellow substances (Otte et al. 1977, Colberg and Lingg 1978; Rosenthal and Otte 1979; Schroeder et al. 2011). However, removal of yellow substances was often hampered in presence of NO_2^-. In addition, competition in NO_2^- removal between NO_2^- oxidation process and biological nitrogen removal system often resulted to reduction of biological nitrogen removal system performance (Summerfelt 2003, Schroeder et al. 2011). The focus of this study will be on demonstrating the suitability of Ozone-DHS-USB system in maintaining aquaria's water quality within freshwater breeding standard, NH_3: 0.1, NO_2^-: 0.1 and NO_3^-: 10 (mg N L^{-1}) and aesthetic beauty as much as performing 50% water exchange that were usually performed to reduce color of aquaria water. This study attempts to investigate the potential of Ozone-DHS-USB system as zero-water exchange system for on-site aquaria at ambient temperature and long-term operation.

2   Materials and Methods

This study was conducted in five phases (Table 1). The aquaria had 600 L top tank and 100 L bottom tank. Ornamental carp (*Cyprinus carpio var. Koi*) was bred in top tank. The DHS-USB system was placed at bottom tank. DHS reactor's volume was 12 L, based on sponge volume and USB reactor was 8 L. HRT of DHS and USB was 0.01 and 2.7, respectively. External carbon source was connected to USB reactor to facilitate denitrification in the reactor. C/N ratio was 1.2 throughout the study. Quantity of additional carbon source was calculated with Eq. (1) (Hamaguchi et al. 2010). Target level of nitrogenous compounds are as follows: $NH_3 < 0.1$, $NO_2^- < 0.1$, and $NO_3^- < 10$ (mg N L^{-1}).

$$\text{Additional organic matter quantity} \left(\text{mg C L}^{-1} \right)$$
$$= (\text{g C})/(\text{g N}) \text{ ratio} \times \text{inflow NO}_3^- \text{ - N conc.} + 0.375 \times \text{inflow DO conc.} \tag{1}$$

Table 1. Fish and system details

	Start-up	Phase 1	Phase 2	Phase 3	Phase 4
Operational day	0–14	15–248	249–494	495–557	558–600
Fish type	*Cyprinus carpio var. koi*				
Fish density (kg m^{-3})	4.5 (2)[a]	N.D.[b]	3	3.6	N.D.[b]
Feed volume (kg food kg fish weight^{-1} day^{-1})			0.01		
Ozone exposure (h)	-	-	8	-	8
HRT in DHS (h)			0.01		
HRT in USB (h)			2.7		
C/N ratio			1.2		
External organic matter		NaAc[c]			
	-	HAc[d]		HAc[d]	

[a]Fish density was decreased from 4.5 kg m^{-3} to 2.0 kg m^{-3}
[b]No data
[c]Sodium acetate
[d]Acetic acid

Dissolved oxygen (DO) concentration was maintained above 5 mg L^{-1}. Short-term continuous ozonation was operated at Phase 2 and 4 over a period of 8 h at constant O_3 concentration of 70 mg-O_3 h^{-1}. During the time of study, DHS-USB system remained on operation and carps were not removed from the aquaria. Yellow substance and nitrogenous components in aquaria was monitored by routine analysis of samples taken from aquaria tank. Microbial DNA from sponge and sludge sample at day 370 were extracted using FastDNA SPIN Kit for Soil (MP Biomedicals, Santa Ana, CA) followed the manufacturer protocols. PCR amplification was performed using the 515F and 806R primer set and Premix Ex Taq Hot Start Version (Takara Bio Inc., Shiga, Japan) at conditions as follows: 1 cycle of initial complete denaturation at 94 °C (3 min), 25 cycles of 94 °CC (45 s), 50 °CC (60 s), 72 °CC (90 s), and final extension at 72 °CC (10 min). PCR products were sequenced using a MiSeq Reagent Kit v2 with MiSeq System (Illumina Inc., San Diego, CA, USA) and sequences were analyzed using Quantitative Insights into Microbial Ecology (QIIME v.1.9.1).

3   Results and Discussions

NH_3, NO_2^-, and NO_3^- concentration in aquaria was maintained within standard level for fish breeding (Fig. 1). NH_3 and NO_2^- removal in aquaria was steady throughout the study with average concentration at 0.10 ± 0.12 and 0.03 ± 0.13 mg N L^{-1} respectively. Fluctuation of NO_3^- concentration was observed at early phase 2 and during phase 3 but average NO_3^- concentration was still maintained below attainment level for freshwater breeding at 6.40 ± 7.46 mg N L^{-1}. The fluctuation was due to improper management of the reactor such as absence of carbon source in the organic matter tank. USB reactor's performance recovered when carbon source was restored. Changes in
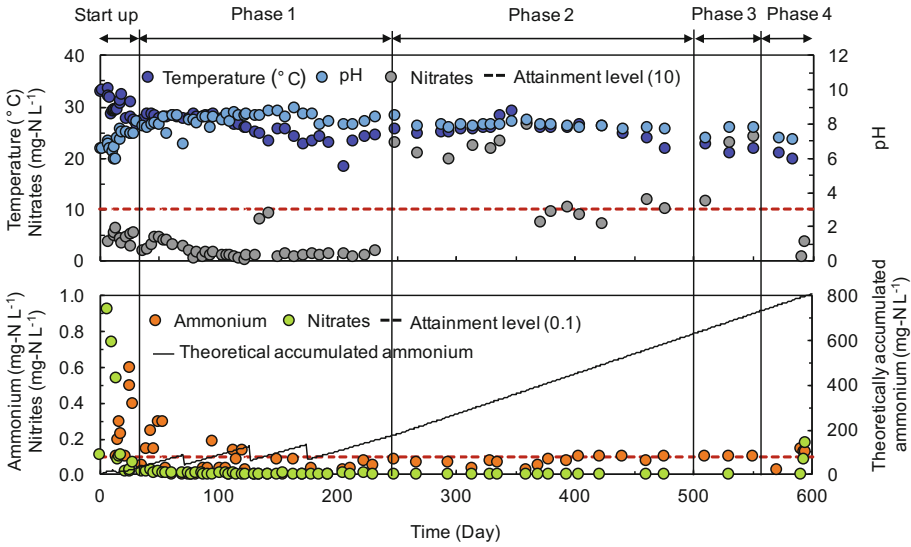
Fig. 1. Temperature (°C), pH and nitrogenous compounds versus time

color and turbidity in aquaria water was observed from ending of phase 2 to phase 4 (Fig. 2). Average color obtained in aquaria water was 7.3 ± 0.5, 9.3 ± 2.18 and 5.5 ± 0.6 (color units) for phase 2, 3 and 4 respectively. Phase 3 (no ozonation) has the highest color unit among all phases. Maximum color reading of 13 NTU was obtained at the end of the phase. After seven days of O_3 re-application (phase 4) in the aquaria, color dropped to 6, equivalent to reduction about 50% from maximum color reading obtained at the end of phase 3. The result demonstrated that O_3 can reduced and maintained color as much as performing water exchange. In addition, water exchange was not performed for 425 days since ozonation was applied in aquaria. O_3 is harmful to humans and highly toxic to aquatic organisms. It is important to maintain low O_3 concentration in aquaria. 0.01 mg O_3 L^{-1} was reported lethal to fish (Summerfelt and Hochheimer 1997). In this study, no abnormal behavior and health effect on carps were observed at 0.03 mg O_3 L^{-1}. This suggested that carp might have higher tolerance to ozone toxicity.

To further understand the nitrogen removal process in the reactor, microbial community in the reactor was analyzed based on the 16S rRNA gene sequence. The most abundant phyla detected in the DHS and USB reactor was *Proteobacteria* with average total sequence reads of 27% and 49.8% respectively (Fig. 3). AOB was not detected, even though high ratio of *Proteobacteria* was detected in DHS reactor. Interestingly, ammonia oxidizing archaea (AOA) from genera *Ca. Nitrososphaera* seems to play the important role in ammonia removal in DHS reactor. Nitrite oxidizing bacteria (NOB) such as *Nitrospira moscoviensis* was also detected. This species favor low salinity water and grow best at temperatures between 28–30 °C (Off et al. 2010). Therefore, they were frequently detected in breeding systems associated with carp and goldfish (Sugita et al. 2005). Heterotrophic denitrifier, *Thauera* was the most dominant
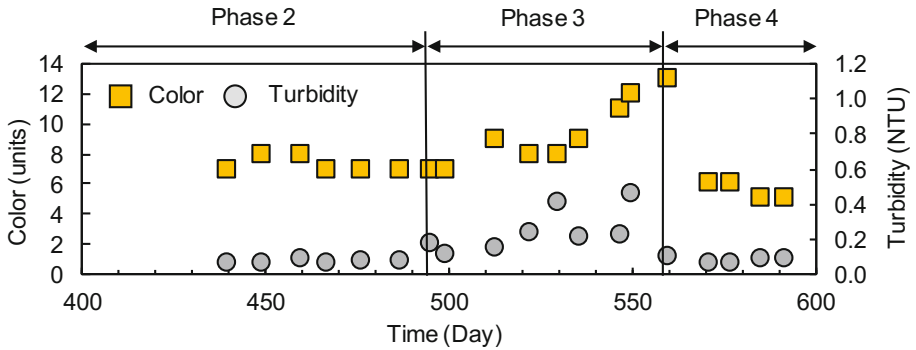
Fig. 2. Color (color units) and turbidity (NTU) of aquaria water versus time
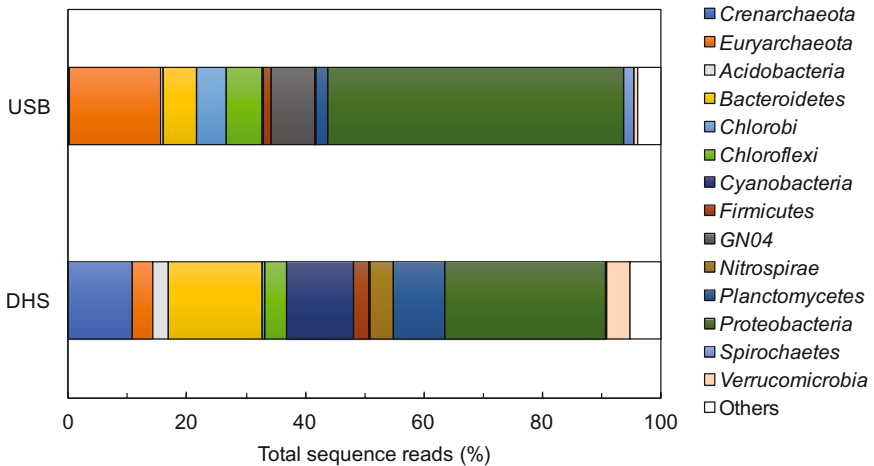
Fig. 3. Predominant microbial community detected in DHS and USB reactor at phyla level

genera with denitrification abilities detected in USB reactor. *Thauera* also favor low salinity condition. In addition, *Thauera* has capability to utilize acetate in anoxic condition (Liu et al. 2015, Ginige et al. 2005, Furukawa et al. 2016). The use of sodium acetate as carbon source and freshwater condition in aquaria might explained high detection of *Thauera* in USB reactor.

4 Conclusions

The presence of beneficial AOA, NOB and denitrifying bacteria seemed to play major role in nitrogen removal process in DHS-USB system. NH_3, NO_2^-, and NO_3^- concentration was maintained within the attainment level at 0.10 ± 0.12, 0.03 ± 0.13 and 6.40 ± 7.46 mg N L^{-1} respectively at on-site aquaria influenced by ambient

temperature during long-term operation. Continuous O_3 exposure for 8 h per day was sufficient to maintain clear water in aquaria below 10 color unit. Re-application of O_3 reduced about 50% color unit from previous reading. This showed that O_3 can reduce color as much as performing water exchange. Reduction in DHS reactor performance was not observed despite competition for NO_2^- were reported often impacted the system performance. 0.03 mg L^{-1} dissolved O_3 was detected in the water but fish survived without performing water exchange for 425 days. Ozone-DHS-USB system was suggested to have high potential towards zero-water exchange system for aquaria. Aquaria and fish breeding industry will benefit greatly from Ozone-DHS-USB system. Elimination of water exchange necessity on regular basis, can reduce maintenance cost, provide water security and lead to maintenance-free system for aquaria.

References

Thorarensen H, Farrell AP (2010) Comparative analysis of the biological requirements for salmonid production at a range of densities in closed-containment systems. In: Chadwick EMP, Parsons GJ, Sayavong B (eds) Evaluation of closed-containment technologies for saltwater Salmon aquaculture. National Research Council of Canada, Ottawa, pp 46–48

Weinstein DI, Kimmel E (1998) Behavioral response of carp (Cyprinus carpio) to ammonia stress. Aquaculture 165:81–93

Losordo TM, Masser MP, Rakocy JE (1999) Recirculating aquaculture tank production systems a review of component options, p 12. http://darc.cms.udel.edu/AquaPrimer/recircoptions.pdf

Asano L, Ako H, Shimizu E (2003) Limited water exchange production systems for freshwater ornamental fish. Aquacult Res 34:937–941

Furukawa A, Matsuura N, Mori M et al (2016) Development of a DHS-USB recirculating system to remove nitrogen from a marine fish aquarium. Aquacult Eng 74:174–179

Otte G, Hilge V, Rosenthal H (1977) Effect of ozone on yellow substances accumulated in a recycling system for fish culture. International council for the exploration of the sea, Fisheries improvement committee, C.M-E:27, Copenhagen

Colberg PJ, Lingg AJ (1978) Effect of ozonation on microbial fish pathogens, ammonia, nitrate, nitrite and BOD in simulated reuse hatchery water. J Fish Res Board Can 25:1290–1296

Otte G, Rosenthal H (1979) Management of a closed brackish water system for high density fish culture by biological and chemical treatment. Aquaculture 18:169–181

Schroeder JP, Croot PL, Von Dewitz B et al (2011) Potential and limitations of ozone for the removal of ammonia, nitrite, and yellow substances in marine recirculating aquaculture systems. Aquacult Eng 45(1):35–41

Summerfelt ST (2003) Ozonation and UV irradiation an introduction and examples of current applications. Aquacult Eng 28:21–36

Hamaguchi T, Ono S, Kurabe M et al (2010) Development of the Recirculating nitrogen removal system for a marine aquarium water. Environ Eng Res 47:297–303 Japanese with English abstract

Summerfelt ST, Hochheimer JH (1997) Review of ozone process and applications as an oxidizing agent in aquaculture. Progressive Fish Culturist 59:94–105

Off S, Alawi M, Spieck E (2010) Enrichment and physiological characterization of a novel Nitrospira-like bacterium obtained from a marine sponge. Appl Environ Microbiol 7 (14):4640–4646

Sugita H, Nakamura H, Shimada T (2005) Microbial communities associated with filter material in recirculating aquaculture systems f freshwater fish. Aquaculture 243:403–409

Liu C, Zhao C, Wang A et al (2015) Denitrifying sulfide removal process on high-salinity wastewaters. Appl Microbiol Biotechnol 99(15):6463–6469

Ginige MP, Keller J, Blackall LL (2005) Investigation of an acetate-fed denitrifying microbial community by stable isotope probing, full-cycle rRNA analysis, and fluorescent in situ hybridization-microautoradiography. Appl Environ Microb 71(12):8683–8691

Short and Long Term Effect of Decreasing Temperature on Anammox Activity and Enrichment in Mainstream Granular Sludge Process

P. De Cocker[1,2,4]([✉]), Y. Bessiere[1], G. Hernandez-Raquet[1], S. Dubos[1],
M. Mercade[1], X.Y. Sun[4], I. Mozo[2], B. Barillon[2], G. Gaval[2],
M. Caligaris[3], S. Martin Ruel[2], S.E. Vlaeminck[4,5], and M. Sperandio[1]

[1] Laboratoire d'Ingénierie des Systèmes Biologiques et des Procédés - CNRS,
UMR5504, Université de Toulouse, INSA, UPS, INP, LISBP - INRA,
UMR792, Toulouse, France
[2] SUEZ, CIRSEE, Le Pecq, France
[3] SUEZ, Treatment Solutions, Rueil Malmaison, France
[4] Center of Microbial Ecology and Technology (CMET),
Ghent University, Ghent, Belgium
[5] Research Group of Sustainable Energy, Air and Water Technology,
University of Antwerp, Antwerp, Belgium

Abstract. This study investigates the impact of lower temperature on short term and long term (down to 10 °C) on a completely anoxic anammox granular sludge process. This is the first time granular sludge Anammox is operated in pure anoxic condition in SBR and at low temperature. Conversion performance, kinetic parameters, sludge characteristics and microbial community were analyzed.

Keywords: Mainstream anammox · Low temperature · Granular sludge

1 Introduction

Partial nitritation/anammox (PN/A) is an autotrophic biological nitrogen removal process which allows to reduce oxygen consumption, remove the need for organic carbon and reduce sludge production. It can thus present a more energy-, carbon- and cost-efficient treatment compared to the conventional nitrification/denitrification process (Vlaeminck et al. 2014). The main roadblocks for PN/A implementation on pre-treated sewage, so-called mainstream PN/A, are robust tools to suppress nitrite oxidizing bacteria (NOB) and promote anammox bacteria (AnAOB) under relatively low influent nitrogen concentrations (40–80 mg NH_4^+-N/L), non-negligible amounts of biodegradable organic carbon and relatively low temperatures (10–30 °C). Due to the various potential economic and ecologic advantages to come from applications of anammox in mainstream N-removal processes, increasingly more research is being conducted to adapt anammox biomass to lower temperatures in various set-ups (SBR/MBBR) with flocs, granules or carriers, fed with synthetic or real wastewater.

2 Materials and Methods

2.1 Short Term Batch Experiments

For the short-term temperature effects, the specific anammox activity (SAA) was determined in 500 mL Schott bottles at five different temperatures (10–30 °C). Four different types (referred to as LISBP, CDA, LSD and LRO) of biomass from anammox-based processes were tested using a synthetic medium with 30 mg N/L (NH_4^+-N/NO_2^--N ratio was 1/1.32), without added COD and incubated under anoxic conditions. The NH_4^+, NO_2^- and NO_3^- concentrations were measured throughout the experiment (which lasted between 9 and 150 h depending on the imposed temperature).

2.2 Long Term Experiments with SBR Reactors

Two anoxic lab-scale SBR reactors have been operated on synthetic influent for over ten months. Both reactors were inoculated with the same biomass and operated identically for the first two months. After this, operating conditions in the reference reactor (SBR_{ref}) were kept constant throughout the entire experiment while in the test reactor (SBR_{test}) operating conditions (temperature and corresponding loading rate) were gradually changed to examine the long term effect of decreasing temperature on its performance. The respective anammox kinetics were determined for each reactor by monitoring the *in situ* NH_4^+, NO_2^- and NO_3^- concentrations all along one reaction phase.

3 Results

3.1 Batch Tests

In the short-term temperature effect experiments, a decrease in temperature resulted in a decrease in specific anammox activity (SAA; expressed in mg NH_4^+-N/g VSS/d) for all four types of biomass, results are shown in Fig. 1. This response was variable depending on the initial biomass and variability was stronger for lower temperatures (15 °C–10 °C). One single temperature coefficient (Arrhenius θ-value) was not sufficient to accurately describe the SAA response for the entire temperature range (30 °C–10 °C). To see if the difference in temperature dependency could be explained by physical or microbiological factors, assays were performed after specific disaggregation and the microbial community composition was analyzed.

3.2 Reactor Performance

For the long-term reactor tests, the volumetric activity of the control reactor SBR_{ref} has continuously increased upon inoculation and reached about six times its initial value up to 11 mg NH_4^+/L/h. In SBR_{test}, the decrease in temperature resulted in a decrease of volumetric activity. This effect was most pronounced when temperature decreased from 30 to 20 °C, resulting in a 3-fold drop in activity (due to biomass
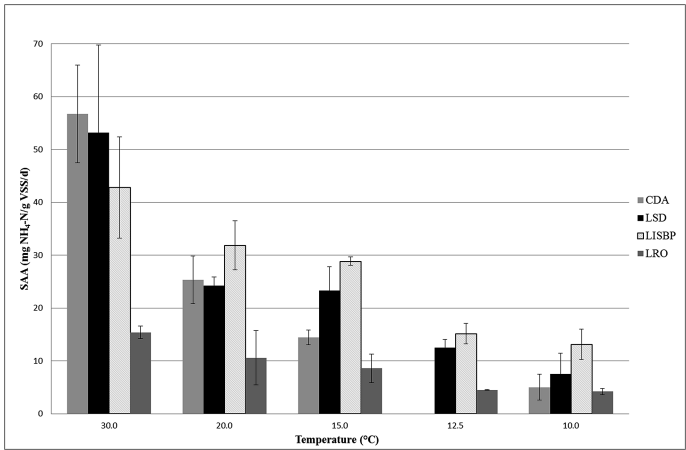
Fig. 1. Specific anammox activities for the different biomasses at different temperatures

selection and sludge loss). Activity recovered throughout the next two months; the temperature was then further decreased. The impact of these decreases in temperature was smaller, the relative loss in activity was lower (20 and 35% for 15 °C and 12.5 °C respectively) and each time activity recovered within the month, even when operated at 10 ° (after a 75% drop in activity). Results from FISH analyses and 16S rRNA amplicon sequencing will be used to compare the evolution in microbial diversity in both reactors and get an indication of the level of anammox enrichment (Fig. 2).
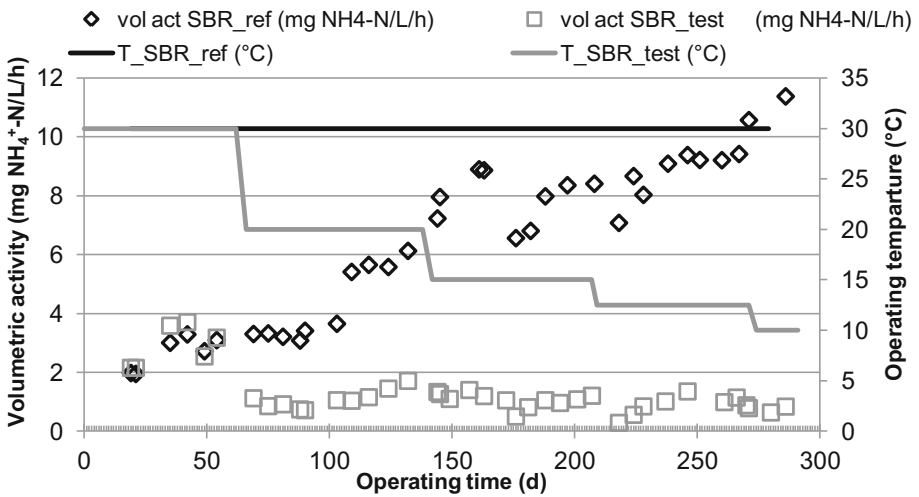
Fig. 2. Volumetric activities related to operating temperature for SBR_ref (black, diamonds) and SBR_test (grey, squares) throughout the experiment

During reactor operation, the biomass evolved from a dark brownish and very heterogeneous, hybrid sludge (the inoculum) containing flocs, granules and suspended biomass to a bright red, predominantly granular sludge. Even at 10 °C, the granules demonstrated very good settling properties due to their size and density. Larger granules seem to be observed (2–6 mm diameter) which could show that lowering the specific growth rate can even improve the granulation process. Analyses of the particle size distribution (PSD) and image analysis are being completed for confirming or informing that observation.

3.3 Long Term vs. Short Term Temperature Effect

The SAA observed at start of the reactor operation (30 °C) was 51.6 mg NH_4^+-N/gVSS/d which was comparable to the activities observed during most of the batch tests at the same temperature (Table 1). Throughout the experiment, SAA increased in both SBR_{ref} (30 °C) and SBR_{test} (10 °C), reaching values of 824.8 and 99.8 mg NH_4^+-N/gVSS/d respectively at day 286. The SAA observed in SBR_{test} at 10 °C was around seven to ten times higher than the values obtained during the short term test at the same temperature. After 286 days, SAA observed at 10 °C was 12% of the activity observed at 30 °C which is comparable to the results found for the CDA and LSD sludge (9 and 14% respectively). The SAA found at 10 °C is the highest value ever reported at that temperature. The observed increases in specific anammox activity during the long term experiment can be correlated to an enrichment and/or adaptation of the anammox sludge. FISH analyses and 16S rRNA amplicon sequencing results will provide more insight. These findings will be useful for the design of future low temperature applications.

Table 1. Comparison of specific anammox activities (expressed in mg NH_4^+-N/gVSS/d) for short and long term experiments

	Short term				Long term		
	CDA	LSD	LRO	LISBP	SBR_{ref} d1	SBR_{ref} d286	SBR_{test} d286
SAA 30 °C	56.8 ± 13.9	53.2 ± 16.5	15.4 ± 1.2	42.8 ± 9.6	51.6	824.8	-
SAA 10 °C	5 ± 2.4	7.5 ± 3.9	4.2 ± 0.6	13.1 ± 2.9	-	-	99.8
Ratio 10 °C/30 °C	9%	14%	27%	31%	-	-	12%[a]

[a]ratio SBR_test/SBR_ref on d286

The SAA values obtained in this study at 10 °C under optimal conditions (purely anoxic, no substrate limitation) are considerably higher than values previously reported in literature, this is illustrated in Table 2.

Table 2. List of specific anammox activities in other low temperature studies

Set-up	Temperature	Specific anammox activity (mg NH_4^+-N/gVSS/d)	Reference
Anoxic batch test (short term)	10 °C	0–11	Lotti et al. 2013
PN/A SBAR	10 °C	22	Lotti et al. 2014
PN/A SBR	10 °C	16	Hu et al. 2013
PN/A gaslift SBR	10 °C	13–19	Hendrickx et al. 2014
Anoxic SBR	10 °C	99.8	This study

4   Conclusions

This study gives new insights concerning Anammox operation at low temperature:

- Long term compared to short term experiments allows much higher SAA at 10 °C, but the decrease in SAA due to temperature reduction was finally in the same order of magnitude.
- Reactor was successfully operated for over 300 days, activity was maintained even at 10 °C
- Long term adaptation/enrichment increased SAA at 10 °C by 7–10 fold compared to batch tests. This is the highest SAA reported at 10 °C for granular sludge corresponding to the optimal conditions for Anammox growth: purely Anoxic and no substrate limitation.
- Granular sludge with excellent settling properties and large granules was formed and maintained at 10 °C indicating that lowering the growth rate can even improve the granulation process

References

Hendrickx TLG, Kampman C, Zeeman G, Temmink H, Hu Z, Kartal B, Buisman CJN (2014) High specific activity for anammox bacteria enriched from activated sludge at 10 °C. Bioresour Technol 163:214–221

Hu Z, Lotti T, de Kreuk M, Kleerebezem R, van Loosdrecht M, Kruit J, Jetten MS, Kartal B (2013) Nitrogen removal by a nitritation-anammox bioreactor at low temperature. Appl Environ Microbiol 79:2807–2812

Lotti T, Kleerebezem R, van Erp Taalman Kip C, Hendrickx T, Kruit J, Van Loosdrecht M (2014) Anammox growth on pretreated municipal wastewater. Environ Sci Technol 48 (14):7874–7880

Lotti T, Kleerebezem R, van Loosdrecht M (2013) Effect of temperature on anammox bacteria cultivated under different conditions. In: Nutrient removal and recovery 2013: Trends in Resource Recovery and use

Vlaeminck SE, De Clippeleir H, Verstraete W (2012) Microbial resource management of one-stage partial nitrition/anammox. Microb Biotechnol 5(3):433–448

Phosphorus Recovery from Waste Activated Sludge: Microwave Treatment and Ozonation with Acid & Alkaline Pre-treatments

S. Cosgun[1(✉)] and N. Semerci[2]

[1] Environmental Engineering and Bioengineering, Marmara University, Istanbul, Turkey
[2] Environmental Engineering, Marmara University, Istanbul, Turkey

Abstract. This study investigated phosphorus recovery from activated sludge through ozonation and microwave treatment with acid and alkali pre-treatments. Three main groups (pH treatment & ozonation, pH treatment & microwave, pH treatment & ozonation & microwave) were studied for COD and P release. Results of batch experiments have shown that, optimum pH for sludge disintegration and phosphorus release is 10 according to •OH radical formation. Also studying at low pH levels gives an advantage due to effect of acidic condition on cell lysis. Besides, according to results of phosphorus fraction experiments in raw sludge, the other advantage of low pH levels is releasing of apatite (bound to calcium) phosphorus. Both ozonation and microwave treatments were effective for sludge disintegration, the highest COD release was observed after microwave treatment of ozonated samples. However, microwave was much more effective than ozonation on phosphorus, significant amount of phosphorus released into the bulk solution in both ozonation and microwave treatments. Despite of COD release, microwave and ozonation & microwave have similar efficiencies on phosphorus release, ozonation might be negligible before microwave due to high production cost. On the other hand, after analyses of struvite samples, pH = 8.5 and 2 days reaction time was determined as the optimum conditions for struvite purity.

Keywords: Phosphorus recovery · Sludge ozonation · Microwave treatment

1 Introduction

Activated sludge process has been employed to treat a wide variety of wastewater. Activated sludge has a content rich in phosphorus which is an essential element for living organisms. Recovery of phosphorus from waste activated sludge as struvite ($NH_4MgPO_4.6H_2O$) or calcium phosphate ($Ca_3(PO_4)_2$) is a good alternative while considering the phosphorus depletion. However, disintegration of bacterial cell for the release of phosphorus is the most challenging step. It should be efficient, economical and applicable. In this study, ozonation and microwave treatment with acid or alkaline pre-treatments were applied to enhance phosphorus recovery from excess sludge and the results were compared to reach most efficient process.

2   Materials and Methods

Batch experiments were carried out to study the relationship between treatment and phosphorus recovery. Before sludge disintegration studies, soluble and solid phosphorus fractions in different pH levels were determined according to Xu et al. (2015) to obtain phosphorus potential of the sludge.

Three main groups (pH treatment & ozonation, pH treatment & microwave, pH treatment & ozonation & microwave) were studied for COD and P release. Before ozonation and microwave treatment, pH of sludge was adjusted to 2, 4 or 10 and mixed at 100 rpm for 30 min. Ozone gas was given for 30 and 60 min of contact time to the sludge for ozonation. The microwave treatment was applied to the sludge samples from pre-treatment and each contact time of ozonation for 45 min at 95°C and supplied power of 1600 W. PO_4^{3-}, NH_4, COD, TSS and VSS were determined on Standard Methods (APHA, 20th edition). Mg and Ca were measured by atomic absorption spectrophotometry. Results of experiments were analysed with SPSS 23 software. Sludge solubilisation degree was calculated in terms of COD release;

$$\text{COD Release}(\%) = \frac{(\text{solubleCOD} - \text{solubleCOD}_{\text{initial}})}{\text{particulateCOD}_{\text{initial}}} \times 100 \qquad (1)$$

After sludge disintegration, supernatant had been taken from sludge and if it is necessary $MgCl_2.6H_2O$ and $(NH_4)_2SO_4$ solutions were added to achieve Mg: PO_4^{3-}: NH_4 molar ratio as 1:1.4:1 as mentioned in Bi et al. (2014). Different alkaline pH conditions in the range of 8.5–11.5 were chosen to check Mg and Ca amounts in struvite precipitates. Struvite samples were analysed by SEM and XRD.

3   Results

Sludge disintegration results in terms of COD release are given in Fig. 1. In ozonation experiments, the highest sludge solubilisation was observed at pH = 10 samples as 19% with a significant difference (p = 0.037), this might be related to oxidation effect of hydroxyl radicals which were formed during ozonation as represented in Eq. 2 (Gunten 2003);

$$O_3 + OH^- \rightarrow HO_2^- + O_2 \quad O_3 + HO_2^- \rightarrow {}^{\bullet}OH + O_2^{\bullet-} + O_2 \qquad (2)$$
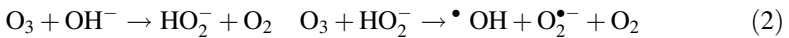
Beside this, ozonation at pH = 2 experiments resulted in slightly higher sludge solubilisation than pH = 4 as 12.3 and 10.9% (p = 0.051). COD releases after microwave treatment of pre-treated sludge samples had shown a similar distribution with ozonation (Fig. 2). These results have shown the effect of acidic and alkaline conditions on cell lysis in addition to ozonation and microwave. As shown in Fig. 3, higher sludge solubilisations were obtained by microwave treatment of ozonated sludge samples as 36, 32 and 41.3% for pH = 2, pH = 4 and pH = 10 samples (p = 0.05, p = 0.061 and p = 0.037). As an interesting result; a slight increase in total COD concentration was observed after microwave treatment (Fig. 4). A similar situation was

1.
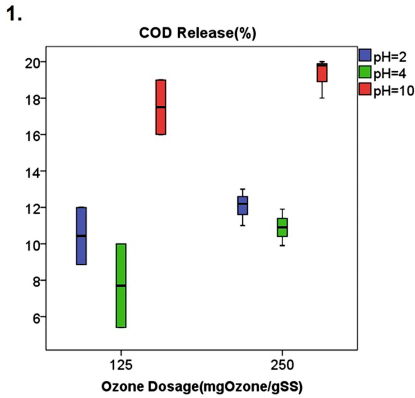
Fig. 1. COD releases after ozonation with $125(\pm\ 30)$ and $250(\pm\ 30)$ mgO$_3$/gSS dosages after different pH pre-treatments

2.
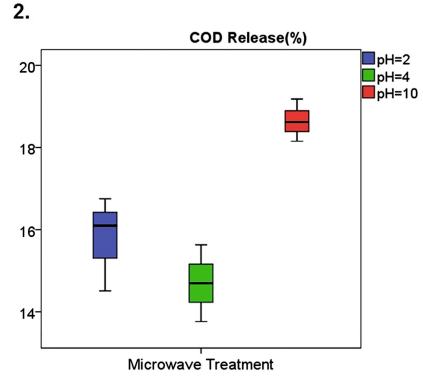
Fig. 2. COD release after microwave treatment of sludge samples with different pH pre-treatments

1.
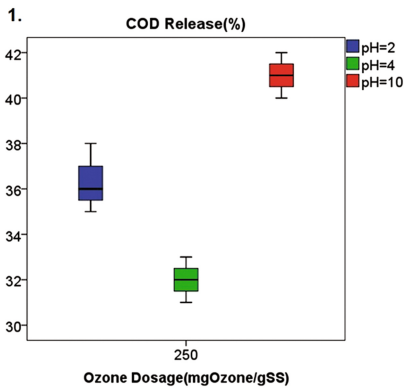
Fig. 3. COD release after microwave treatment of ozonated sludge samples

2.
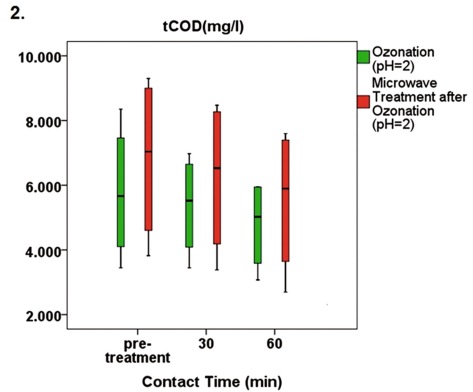
Fig. 4. tCOD increase after microwave treatment of pre-treated and ozonated sludge samples (pH = 2)

reported by Wang et al. (2016) too. This might be caused by the release of materials such as intracellular substances like proteins and sugars and extracellular polysaccharides. Also a high mineralization occurred during ozonation due to oxidation of soluble COD.

As shown in Fig. 5, the highest increase in phosphorus concentration in terms of mgPO$_4$-P/gSS$_{initial}$ was observed in pH = 10 samples for ozonation (p = 0.042, p = 0.016, p = 0.018). Microwave treatment was much more effective for phosphorus release than ozonation. 5.4 mgPO$_4$-P/gSS$_{in}$ phosphorus was obtained by ozonation of pH = 10 samples, this concentration has reached to 11.5 in microwave treatment after

1.
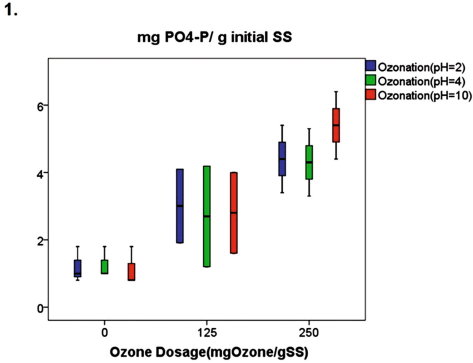
Fig. 5. Increase in orthophosphate concentration after ozonation with 125(± 30) and 250 (± 30) mgO₃/gSS dosages at different pH levels

2.
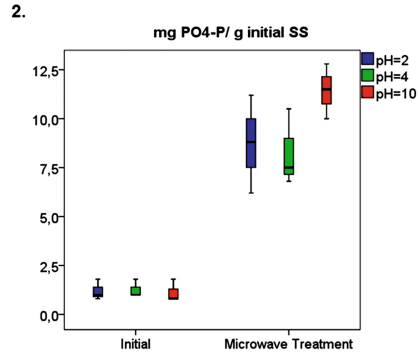
Fig. 6. Increase in orthophosphate concentration after microwave treatment of sludge samples with different pH pre-treatments

1.
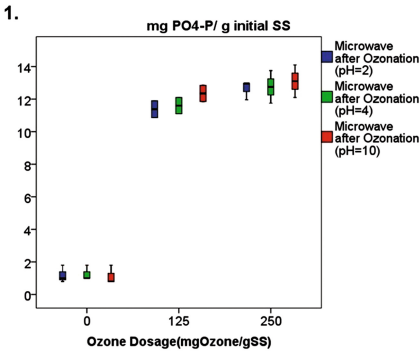
Fig. 7. Increase in orthophosphate concentration after microwave treatment of ozonated sludge samples

2.
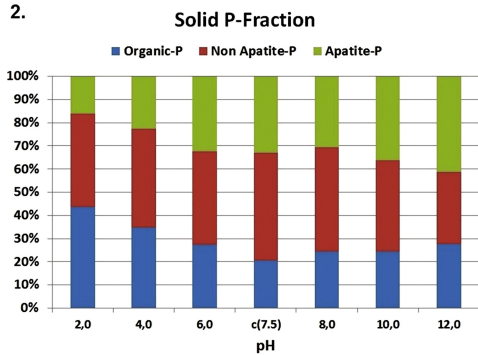
Fig. 8. Organic, apatite (bound to Ca) and non-apatite (bound to Al, Fe and Mn oxyhydrates) phosphorus fraction of raw sludge at different pH levels in solid phase

pH = 10 pre-treatment experiments while initial concentration of phosphorus was 1.6 mgPO$_4$-P/gSS$_{in}$ (Fig. 6).

After microwave treatment of ozonated sludge samples, all experiments were resulted with the similar results around 12 mgPO$_4$-P/gSS$_{in}$ (Fig. 7). Ozonation can be commented as unnecessary according to these results by considering the cost analysis. According to solid phosphorus fraction (Fig. 8), this might be commented that solubilisation of apatite phosphorus at low pH levels is another reason of phosphorus release beside the cell lysis.

Phosphorus, which got into reactive phase by sludge disintegration experiments was obtained as struvite as shown in Fig. 9. The optimum pH for struvite purity was
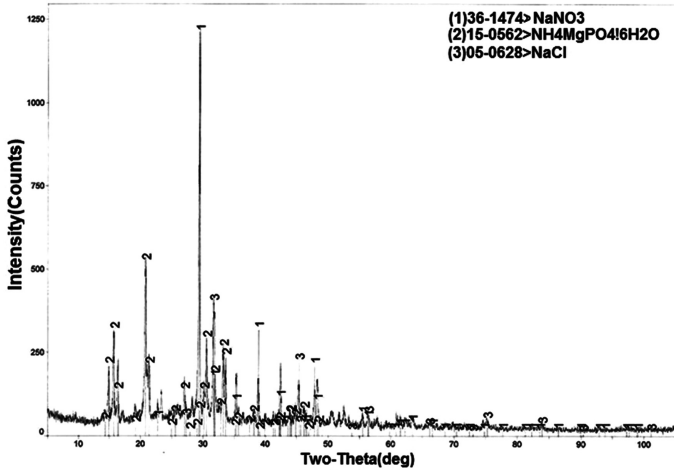
Fig. 9. XRD analysis of a struvite sample

determined as 8.5 with a low mixing rate as 30 rpm and long reaction time as 2 days, but still there is a need for studying for purification according to $NaNO_3$ and $NaCl$ contaminations.

References

Bi W, Li Y, Hu Y (2014) Recovery of phosphorus and nitrogen from alkaline hydrolysis supernatant of excess sludge by magnesium ammonium phosphate. Bio Tech 166:1–8

Gunten U (2003) Ozonation of drinking water: Part I. Oxidation kinetics and product formation. Wat Res 37:1443–1467

Xu Y, Liu HJ, Luo J, Qian G, Wang A (2015) pH dependent phosphorus release from waste activated sludge: contributions of phosphorus speciation. Chem Eng J 267:260–265

Wang Y, Xiao Q, Zhong H, Zheng X, Wei Y (2016) Effect of organic matter on phosphorus recovery from sewage sludge subjected to microwave hybrid pretreatment. J Env Sci 39:29–36

Respirometric Evaluation of Toxicity of 2,4-Dichlorophenol Towards Activated Sludge and the Ability of Biomass Acclimation

P. Van Aken[1(✉)], N. Lambert[1], R. Van den Broeck[1], J. Degrève[2], and R. Dewil[1]

[1] PETLab, Department of Chemical Engineering, KU Leuven,
Sint-Katelijne-Waver, Belgium
[2] Biological and Chemical Systems Technology, Reactor Engineering
and Safety Section, Department of Engineering, KU Leuven, Heverlee, Belgium

Abstract. In the present research, both direct and co-metabolic biodegradation of 2,4-dichlorophenol by mixed activated sludge cultures are investigated by performing respirometric experiments. Firstly, the biomass inhibition due to the toxic pollutant is studied by performing a respirometric toxicity detection experiment. A lag phase for the activity of the biomass showed up because of 2,4-dichlorophenol. The length of the lag phase increased by increasing the concentration of 2,4-dichlorophenol. At higher concentrations, the micro-organisms required more adaption time to the presence of the toxic pollutant. Remarkably, the biomass restored its activity partially. Furthermore, respirometric experiments are performed for several days to investigate biomass acclimation towards the repeated addition of 2,4-dichlorophenol. A significant decrease of the reaction time needed was obtained by biomass acclimation. Immediately after the second addition, an increase of the biomass activity combined with both COD and 2,4-dichlorophenol degradation were observed. The biomass was able to adapt and even to degrade the toxic pollutant. At the second addition, this acclimation period was not necessary.

Keywords: Chlorophenol · Cometabolic biodegradation · Respirometry

1 Introduction

The presence of recalcitrant organic matter in industrial wastewaters is regarded as a serious threat to the environment. Increased knowledge on the consequences of water pollution and diminishing water resources have created the need for regulations to prevent pollution, to promote sustainable water usage and to protect the environment (Tabrizi and Mehrvar 2004). Hence, the European commission and US Environmental Protection Agency published a list of priority substances, including chlorophenols.

Hence, the proper treatment of chlorophenolic wastewaters is critical and applicability depends on its effectiveness, profitability and side effects. Several technologies are already investigated for their removal from wastewater (Armenante et al. 1999; Jung et al. 2001; Al Momani et al. 2004). Some of these techniques are based on the phase transfer, which requires further treatment. Furthermore, chemical oxidation

methods are usually not economically feasible and biological processes do not always achieve satisfactory results. However, biological degradation often occurs after bio-mass acclimation. Micro-organisms adapt to such pollutants and obtain the degradation capacity as time proceeds.

Pomiès et al. (2013) described two biodegradation pathways, i.e., direct biodegra-dation by a fraction of the total biomass and co-metabolism. Direct biodegradation implies the development and maintenance of specific biomass by using the pollutants as carbon and energy source, while co-metabolism is based on the simultaneous degra-dation of a co-substrate and the pollutant. The co-substrate is necessarily present because it serves as growth-substrate while non-specific enzymes of bacteria transforms the non-growth-substrate. The synthesis of these enzymes is only induced by the growth-substrate (Aktas 2012).

Major topics in the biodegradation of these pollutants are the use of specific cul-tures, co-metabolic degradation and novel biological processes such as biomass immobilization. Conversely, only a few studies report the use of mixed cultures and biomass acclimation (Aktas 2012). Also, the treatment feasibility is most frequently evaluated based on global and specific degradation efficiencies only. In this study, both direct and cometabolic biodegradation of 2,4-dichlorophenol (2,4-DCP) by mixed activated sludge cultures are investigated by performing respirometric experiments. Respirometry is a useful method to measure the activity and viability of micro-organisms present in aerobic activated sludge (Oller et al. 2011).

2 Materials and Methods

2.1 Materials

2,4-DCP (99%) and phenol ($\geq$99%, unstabilized) were obtained from Alfa Aesar and Sigma Aldrich, respectively. Sodium Acetate (99+%, extra pure, anhydrous) and methanol (HPLC grade) were purchased from Acros organics. Activated sludge was obtained from a municipal treatment plant (Aquafin, Mechelen-Noord, Belgium). The sludge sample was taken at the sludge recycle, located between the secondary settler and the aeration basin. Prior to the respirometric measurements, the activated sludge is continuously aerated for 12 h to degrade remaining biodegradable products and to assure endogenous respiration of the biomass.

2.2 Respiration Procedure

The apparatus consists of six glass batch reactors (1.0 L) at constant temperature (20 °C). Each reactor consists of a static liquid phase and a static gas phase, both thoroughly stirred by a magnetic mixer. The oxygen concentration is monitored by dissolved oxygen sensors (Visiferm LDO, Hamilton) and controlled between 3 mgO_2/L and 5 mgO_2/L. The danger of oxygen shortage (below 2 mgO_2/L) in the system is solved by repeated aeration for a short period of time. The oxygen concentration in the system will decrease during the un-aerated periods because of the biodegradation of organic compounds and the endogenous respiration of the activated sludge. From each obtained decrease in

oxygen concentration, the Oxygen Uptake Rate (OUR) is calculated with Least Squares Fitting. When dividing the obtained OUR values by the MLVSS concentration, Specific Oxygen Uptake Rates (SOUR), expressed as $mgO_2/(gMLVSS.h)$, can be calculated. In each reactor, the biomass concentration was 3.00 gMLSS/L (MLVSS = $\pm$2.04 g/L). At the start of each experiment, the biomass is aerated in the absence of substrate such that the endogenous respiration rate can be determined.

2.3 Toxicity Assessment

A respirometric toxicity detection method is used based on the OECD method 209. Instead of the synthetic sewage, sodium acetate (NaAc) is utilized as the reference substrate (Ricco et al. 2004). The respiration rate of the biomass under specific conditions is evaluated by the oxygen concentration profile in the liquid phase. The respirometric reactor, described in the previous paragraph, is used. The NaAc concentration in each experiment was 500 mg/L. This excess concentration is necessary to reach the maximum respiration rate.

2.4 Analytical Techniques

The COD measurements are carried out by using LCK test tubes (Hach, conform ISO 6060:1989). The 2,4-DCP and phenol concentration in the samples is analyzed by HPLC using an Agilent 1100 HPLC system equipped with an Agilent G1314A UV detector at a wavelength of 240 nm and an Agilent Eclipse Plus C18 column at 30 °C. The mobile phase is composed of a methanol–water mixture (60/40 in volume) and has a flow rate of 1 mL/min.

3 Results and Discussion

3.1 Determination of Toxicity Effects

The SOUR profiles obtained by adding NaAc and different 2,4-DCP concentrations to the biomass are presented in Fig. 1. The mentioned concentrations are the ones in the respirometric reactor and the vertical grey line represents the time at which NaAc and 2,4-DCP were added. At the left of the vertical line, the endogenous respiration rate is shown. Because the same biomass was used in each experiment, similar endogenous SOUR-values were observed.

For the 2,4-DCP concentrations of 40 mg/L and 50 mg/L, the SOUR-values remained approximately at the endogenous SOUR-value for almost 24.2 h and 27.1 h, respectively. A first significant SOUR-increase was observed after these periods and, furthermore, the maximum SOUR-value was only reached after 31.2 h and 34.2 h, respectively. In contrast, when only NaAc ([2,4-DCP] = 0 mg/L) was dosed to the activated sludge, an immediately increase of the biomass activity occurred. A lag phase for the biological activity of the biomass showed up as a consequence of the addition of 2,4-DCP. The lag phase was defined as the time between the dosing of the wastewater
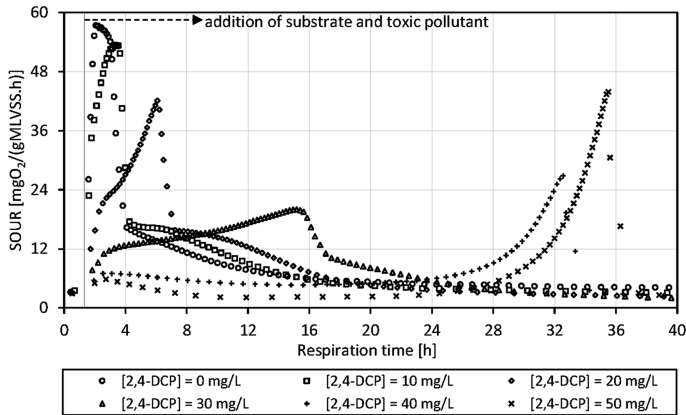
Fig. 1. SOUR profiles of non-acclimated SBR biomass with NaAc and 2,4-DCP

and the observation of the maximum SOUR-value. The length of the lag phase increased when the concentration of 2,4-DCP was increased. At higher 2,4-DCP concentrations, the micro-organisms required more time to adapt to the presence of the toxic pollutant. This behavior of the biomass was the first observed toxic effect. Remarkably, the biomass was able to restore its activity partially, as is evidenced by the activity peak arising at 32.6 h and 35.5 h in Fig. 1 for 2,4-DCP concentration of 40 mg/L and 50 mg/L, respectively. The increase in biomass activity in each SOUR profile was due to the biodegradation of NaAc only. 2,4-DCP was not degraded and this observation was confirmed by both COD and 2,4-DCP analyses. Also, a decrease of the maximum SOUR-value was observed by increasing the 2,4-DCP concentration, except for the 2,4-DCP concentrations of 40 mg/L and 50 mg/L. The decrease of the maximum SOUR-value indicated a decrease in biomass activity caused by the presence of the toxic pollutant. In case of the exceptions, the maximum SOUR-value again increased.

3.2   Direct Biodegradation of 2,4-DCP

The biomass activity during the biodegradation of 50 mg/L, 100 mg/L and 200 mg/L 2,4-DCP was observed. The results obtained at 100 mg/L 2,4-DCP are represented in Fig. 2. The moment at which a solution was added to the reactor, is indicated by the vertical grey line. As observed before, the biomass activity decreased just after the first addition of 2,4-DCP. The extent of the decrease depended on the 2,4-DCP concentration.

Remarkably, at the same time the biomass activity decreased, the COD-value increased and, moreover, the increase was related to the 2,4-DCP concentration. For example, at 2,4-DCP concentrations of 50 mg/L, 100 mg/L and 200 mg/L, COD increases of 14 mgO$_2$/L, 41 mgO$_2$/L and 190 mgO$_2$/L were observed, respectively. Due to cell lysis, less active biomass was present in the reactor, causing a lower endogenous level. After the biodegradation of 2,4-DCP, COD values of 46 mgO$_2$/L, 73 mgO$_2$/L and
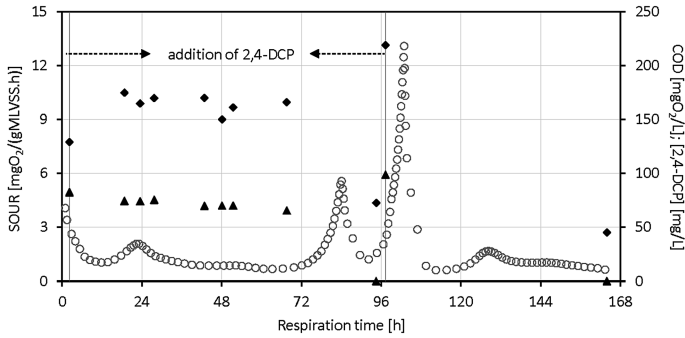
Fig. 2. The evolution of respiration rate (○), COD (♦) and 2,4-DCP (▲) concentration during the biodegradation of 100 mg/L 2,4-DCP

286 mgO$_2$/L were measured at initial 2,4-DCP concentrations of 50 mg/L, 100 mg/L and 200 mg/L, respectively. Apparently, the inert organic matter was increased and the released COD fraction was only partially degraded. The complete degradation of 2,4-DCP was observed after a respiration time of 60.7 h, 81.9 h and 154.5 h for 2,4-DCP concentrations of 50 mg/L, 100 mg/L and 200 mg/L, respectively. Higher concentrations of the inhibitory substrate cause a decrease in biomass growth rate, and thereby the oxygen consumption as well. Furthermore, the maximum SOUR-values of 1.79 mgO$_2$/(MLVSS.h), 5.57 mgO$_2$/(MLVSS.h) and 7.67 mgO$_2$/(MLVSS.h) observed during biodegradation of 50 mg/L 2,4-DCP, 100 mg/L 2,4-DCP and 200 mg/L 2,4-DCP, respectively, indicate that the height of the SOUR-peak is related to the concentration of 2,4-DCP as well. Finally, the biodegradation of the second added chlorophenolic solution occurred within a shorter respiration time. For example, at a 2,4-DCP concentration of 100 mg/L, the maximum SOUR-value due to the degradation of the toxic pollutant was observed at 5.6 h after the second addition of the chlorophenolic solution. Compared to the first addition, the respiration time needed was reduced with approximately 93%. Moreover, the maximum SOUR-value due to the degradation of 2,4-DCP increased from 5.57 mgO$_2$/(MLVSS.h) to 13.09 mgO$_2$/(MLVSS.h). Similar trends were observed at 50 mg/L 2,4-DCP. Hence, the second time the chlorophenolic pollutant was added, the activated sludge was adapted to the toxic pollutant.

3.3   Cometabolic Biodegradation of 2,4-DCP

The use of phenol as primary metabolite for biomass growth was investigated. Different concentrations of 2,4-DCP were investigated, i.e. 50 mg/L, 100 mg/L and 200 mg/L. Unfortunately, it was not possible to determine reliable SOUR-values during the experiment of 200 mg/L 2,4-DCP. After the addition of both phenol and 2,4-DCP to the biomass, a constant DO concentration was observed during 16.0 h. None biomass activity was observed and the concentration of 2,4-DCP remained constant. Hence, further results concerning this experiment are not discussed.

Figure 3 illustrates the results of the cometabolic biodegradation of 50 mg/L 2,4-DCP. Again, the vertical grey line indicates the addition of new substrate. After the first addition, the SOUR-value decreased to a new endogenous respiration rate, i.e., 0.91 mgO$_2$/(gMLVSS.h) and 0.44 mgO$_2$/(gMLVSS.h) for 50 mg/L 2,4-DCP and 100 mg/L 2,4-DCP, respectively. At 100 mg/L 2,4-DCP, the inhibition was higher, resulting in a lower SOUR-value. This was in accordance with the previous results. After a lag phase, the biomass activity increased and a first SOUR-peak was observed. The lag phases observed after the first addition were 29.6 h and 37.2 h for 50 mg/L 2,4-DCP and 100 mg/L 2,4-DCP, respectively. At higher concentrations of the toxic pollutant, the biomass needed more time to adapt to the presence of the toxic pollutant. COD, 2,4-DCP and phenol concentration of the supernatant liquid were determined after this SOUR-peak. For the 2,4-DCP concentration of 50 mg/L, COD and phenol concentrations showed a significant reduction by approximately 67% and 100%, while the 2,4-DCP concentration only decreased by 24%. Knowing that a part of the decrease of 2,4-DCP concentration was caused by stripping, mainly phenol was oxidized, resulting in this first SOUR-peak. In Fig. 3, a second smaller increase of the biomass activity occurred after the first SOUR-peak. After this second SOUR-peak, a 2,4-DCP concentration of 0 mg/L was measured. Hence, this increase in biomass activity was caused by the degradation of the toxic pollutant. A maximum SOUR-value of 2.04 mgO$_2$/(gMLVSS.h) was measured at 54.0 h respiration time after the addition of both phenol and 2,4-DCP. Similar results were observed at 100 mg/L 2,4-DCP. After the second addition of phenol and 2,4-DCP, the activated sludge immediately showed an increase in activity. At 50 mg/L 2,4-DCP and 100 mg/L 2,4-DCP, the lag phase decreased to 11.7 h and 24.34, respectively. The activated sludge was able to adapt to the presence of both pollutants. Furthermore, also 2,4-DCP was degraded during this SOUR-peak. Phenol and 2,4-DCP were added to the reactor for a third time. For both pollutants, the biomass activity immediately increased and only one SOUR-peak was observed due to the degradation of both phenol and 2,4-DCP. A degradation efficiency of 100% for both pollutants was noticed at the different 2,4-DCP concentrations, resulting in a COD reduction of almost 98%. At 50 mg/L 2,4-DCP, a change in maximum SOUR-value (17.59 mgO$_2$/(gMLVSS.h)) and lag
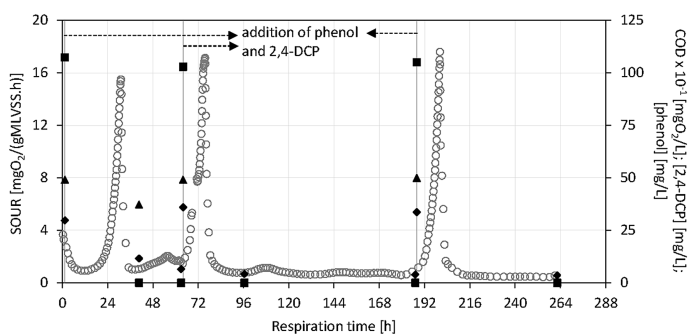
Fig. 3. The evolution of the respiration rate (○), COD (◆), 2,4-DCP (▲) and phenol (■) concentration during the cometabolic biodegradation of 50 mg/L 2,4-DCP

phase (12.2 h) was not observed. However, at 100 mg/L 2,4-DCP the maximum SOUR-value increased to a value of 14.57 mgO_2/(gMLVSS.h) and the lag phase decreased to 14 h.

4   Conclusions

Firstly, the toxicity effects of 2,4-DCP on activated sludge were determined. At high concentrations of 2,4-DCP, a time difference between the addition of the pollutant to the biomass and the maximum increase of biomass activity due to substrate degradation was observed and called the lag phase. This lag phase was related to the concentration of the pollutant. Hence, at increasing chlorophenol concentrations the micro-organisms present in activated sludge needed more time to adapt to the presence of the toxic pollutant. Eventually, the biomass was able to restore its activity. Since the pollutant concentration remained approximately constant while a significant COD decrease was observed, it was concluded that the increased activity was due to the degradation of NaAc. The maximum observed SOUR-value decreased by increasing the concentration of 2,4-DCP. Moreover, at high pollutant concentrations an SOUR-profile of a typical growth phase of biomass was observed.

Secondly, the biodegradation of different concentrations of 2,4-DCP as single carbon source and in the presence of a cometabolite was investigated. For the single carbon source experiments, a clear release of organic matter was observed due to the disintegration of the activated sludge, resulting in an increasing COD-value of the supernatant liquid. The extent of the COD release depended on the initial concentration of 2,4-DCP. Moreover, the concentration of 2,4-DCP remained approximately constant during this period. Furthermore, a second smaller SOUR-peak was observed and caused by the degradation of 2,4-DCP. The long respiration time, needed for the biodegradation of 2,4-DCP, is related to the pollutant concentration and the nature of the cometabolite. A significant decrease of the reaction time, needed for the degradation of 2,4-DCP, was obtained by acclimation of the biomass. Despite these promising results, the effects on biomass structure and degradation efficiencies of the nitrification process over a longer period of time, e.g. weeks, were not experimentally observed.

References

Aktas Ö (2012) Effect of S_0/X_0 ratio and acclimation on respirometry of activated sludge in the cometabolic biodegradation of phenolic compounds. Bioresource Technol 111:98–104

Al Momani F, Sans C, Esplugas S (2004) A comparative study of the advanced oxidation of 2,4-dichlorophenol. J Hazard Mater 107(3):123–129

Armenante PM, Kafkewitz D, Lewandowski GA, Jou CJ (1999) Anaerobic–aerobic treatment of halogenated phenolic compounds. Water Res 33(3):681–692

Jung MW, Ahn KH, Lee Y, Kim KP, Rhee JS, Park JT, Paeng KJ (2001) Adsorption characteristics of phenol and chlorophenols on granular-activated carbons (GAC). Microchem J 70(2):123–131

Oller I, Malato S, Sánchez-Pérez JA (2011) Combination of advanced oxidation processes and biological treatments for wastewater decontamination - a review. Sci Total Environ 409 (20):4141–4166

Pomiès M, Choubert JM, Wisniewski C, Coquery M (2013) Modelling of micropollutant removal in biological wastewater treatments: a review. Sci Total Environ 443:733–748

Ricco G, Tomei MC, Ramadori R, Laera G (2004) Toxicity assessment of common xenobiotic compounds on municipal activated sludge: comparison between respirometry and Microtox®. Water Res 38(8):2103–2110

Tabrizi GB, Mehrvar M (2004) Integration of advanced oxidation technologies and biological processes: recent developments, trends, and advances. J Environ Sci Heal A 39(11–12): 3029–3081

Differential Expression of Genes Involved in Utilization of Benzo(a)Pyrene in *Burkholderia vietnamiensis* G4 Strain

G.P. Cauduro[1(✉)], T. Falcon[1], A.L. Leal[2], and V.H. Valiati[1]

[1] Universidade do Vale do Rio dos Sinos, Biology Graduate Program, São Leopoldo, Brazil
[2] Companhia Riograndense de Saneamento, Biology Laboratory, Triunfo, Brazil

Abstract. Polyaromatic Hydrocarbons (PAH) are recalcitrant pollutants that are among the major Petroleum by-products. Among them, benzo(a)pyrene receives special attention as it is carcinogenic and highly insoluble, being really difficult to decompose with conventional treatments. Wastewater treatment plants (WWTP), often use biological techniques such as activated sludge, that rely on microorganisms to degrade organic compounds. *Burkholderia* genus is known for its biodegradation ability and have been used as study model. Using transcripts and mRNA analyses, one can find out genomic regions and functions involved in this aptitude. In this work we used the model strain *B. vietnamiensis* G4 aiming to find genes that are differentially expressed in the presence of benzo (a)pyrene. Six transcriptomes where generated from each experimental unit in order to compare gene expression and infer which genes are involved in benzo (a)pyrene degradation pathways. Thirty-six genes were differentially expressed in the group exposed to benzo(a)pyrene, most of them involved in catalytic activity. The most significant genomic regions are: *phenylacetic acid degradation protein paaN* involved in degradation of organic compounds to obtain energy, *oxidoreductase FAD-binding subunit* in the regulation of electrons within groups of dioxygenase enzymes, with potential to break benzene rings, and *glutamic semialdehyde dehydrogenase*, a region described as responsible for the ability of phenol degradation. These candidate genes are now target to new studies aiming optimization of treatment processes.

Keywords: Polyaromatic hydrocarbons · Organic pollution · Persistent pollutants · Transcriptome

1 Introduction

The use of petroleum is constant in the world, as this is the major energy matrix and an important industrial feedstock. However, refining petroleum generates a waste full of chemical by-products that may damage human and environmental health. Among this waste we found Polyaromatic Hydrocarbons (PAH), classified as some of the most persistent pollutants in nature due to their chemical structure that make their degradation very complex, either by natural or artificial processes (Haritash and

Kaushik 2009). Sixteen of these compounds are listed as priority for remediation, among them, benzo(a)pyrene (Yan 2004).

Several techniques are known for both treatment of the wastewater produced by petroleum industry and remediation of contaminated areas. One of the most used is bioremediation, which uses living organisms (especially microorganisms) to transform/treat the pollutants. In wastewater treatment plants (WWTP), activated sludge is a common choice for the treatment of this kind of waste (Daims et al. 2006; Valentin-Vargas et al. 2012). Among the microorganisms known for being able to degrade persistent compounds such as PAHs, the *Burkholderia* genus stands out, and strains from this genus have been used as model to study the processes involved in this ability (O'Sullivan and Mahenthiralingam 2005). High throughput sequencing is nowadays allowing researches to reach a wider knowledge about biodegradation by bacteria. Using transcripts and mRNA analyses, one can find out genomic regions and functions involved in this aptitude (Martin and Wang 2011).

2   Materials and Methods

In order to better understand biodegradation processes, in this work we used the model strain *B. vietnamiensis* G4 in two experimental units, where one group was exposed to benzo(a)pyrene and a control group was not. Six transcriptomes where generated from each experimental unit in order to compare gene expression and infer which genes are involved in benzo(a)pyrene degradation pathways.

The data where analysed with the bioinformatics tools TopHat, Bowtie, cufflinks, cummeRbund and PvClust, implemented in the platforms R and Rstudio.

Sequences were compared to the complete genome of *B. vietnamiensis* G4.

3   Results and Discussion

The results allowed us to select genes that are differentially expressed when the bacteria are in contact with this PAH. With this analysis, we found 7,840 genes, representing 99% genome coverage. Clustering analysis reveal two well supported groups (bootstrap > 95%), one with differentially expressed genes in the presence of benzo(a) pyrene and the control with genes expressed in absence of this compound (Fig. 1). Most of the differentially expressed genes had a higher Fragments per Kilobase Million (fpkm) in the group exposed to benzo(a)pyrene, indicating a higher expression of this genes in the experimental group, as shown in the heatmap (Fig. 2).

Thirty-six genes were differentially expressed in the group exposed to benzo(a) pyrene, most of them involved in catalytic activity (main activities in Fig. 3). Among these candidate genes, the most significant genomic regions are: *phenylacetic acid degradation protein paaN* involved in degradation of organic compounds to obtain energy, *oxidoreductase FAD-binding subunit* in the regulation of electrons within groups of dioxygenase enzymes, with potential to break benzene rings, and *glutamic semialdehyde dehydrogenase*, a region described as responsible for the ability of phenol degradation (Table 1).
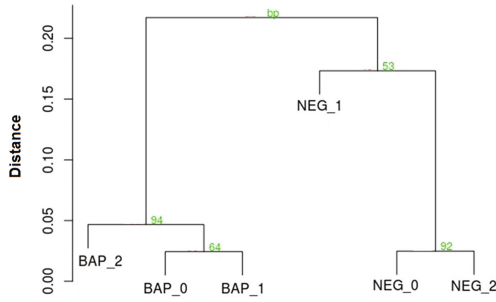
Fig. 1. Correlation dendrogram of experimental and control groups using genes. Numbers in the branches indicate bootstrap support. Bap represents experimental group exposed to benzo(a) pyrene and neg represents control group (not exposed)
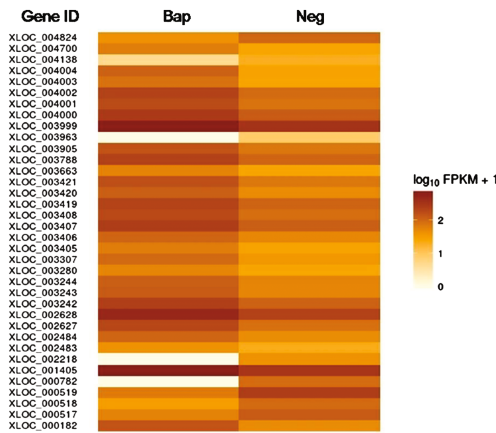
Fig. 2. Heatmap where darker colors represent higher expression. Bap represents experimental group exposed to benzo(a)pyrene and neg represents control group (not exposed). fpkm = Fragments per kilobase million
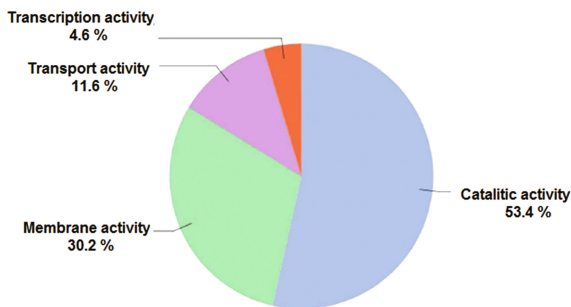
Fig. 3. Functional groups of the identified genes

Table 1. List of the 36 differentially expressed genes and their proteins

Genes	gene_id	Proteins
Bcep1808_0385	XLOC_000182	Glutamate synthase subunit beta
Bcep1808_0516 to_0520	XLOC_001405	Phenylacetic acid degradation protein paaN
Bcep1808_1100, Bcep1808_1101	XLOC_000517	Arginine succinyltransferase
Bcep1808_1102	XLOC_000518	Succinylglutamic semialdehyde dehydrogenase
Bcep1808_1103, Bcep1808_1104	XLOC_000519	Succinylglutamate desuccinylase
Bcep1808_1880	XLOC_000782	Hypothetical protein
Bcep1808_2727	XLOC_002218	Hypothetical protein
Bcep1808_3332 to_3334	XLOC_003242	3-hydroxyisobutyrate dehydrogenase
Bcep1808_3335	XLOC_003243	Methylmalonate-semialdehyde dehydrogenase
Bcep1808_3336	XLOC_003244	AMP-dependent synthetase/ligase
Bcep1808_3412	XLOC_002483	Formyltetrahydrofolate deformylase
Bcep1808_3415	XLOC_003280	Oxidoreductase FAD-binding subunit
Bcep1808_3424	XLOC_002484	Transcriptional regulator
Bcep1808_3471, Bcep1808_3472	XLOC_003307	Glycine betaine/L-proline ABC transporter ATPase
Bcep1808_3677	XLOC_003405	Methylitaconate delta2-delta3-isomerase
Bcep1808_3678	XLOC_003406	Aconitate hydratase
Bcep1808_3679	XLOC_003407	Methylcitrate synthase
Bcep1808_3680	XLOC_003408	2-methylisocitrate lyase
Bcep1808_3702, Bcep1808_3703	XLOC_003419	Oligopeptide/dipeptide ABC transporter ATPase
Bcep1808_3704	XLOC_003420	Binding-protein-dependent transport system inner membrane protein
Bcep1808_3705	XLOC_003421	Binding-protein-dependent transport system inner membrane protein
Bcep1808_3754	XLOC_002627	Lysine exporter protein LysE/YggA
Bcep1808_3755, Bcep1808_3756	XLOC_002628	Aldo/Keto reductase
Bcep1808_4620 to_4622	XLOC_003663	Major facilitator transporter
Bcep1808_5065 to_5069	XLOC_003788	3-hydroxy-acyl-CoA dehydrogenase
Bcep1808_5376	XLOC_003905	XRE family transcriptional regulator
Bcep1808_5569	XLOC_003999	Extracellular solute-binding protein
Bcep1808_5570	XLOC_004000	Polar amino acid ABC transporter, inner membrane subunit
Bcep1808_5571	XLOC_004001	Polar amino acid ABC transporter, inner membrane subunit

Table 1. (*continued*)

Genes	gene_id	Proteins
Bcep1808_5572	XLOC_004002	ABC transporter related
Bcep1808_5573	XLOC_004003	Histidine ammonia-lyase
Bcep1808_5574	XLOC_004004	Histidine utilization repressor
Bcep1808_6015 to_6018	XLOC_004138	nitrogenase molybdenum-iron protein beta chain
Bcep1808_6619	XLOC_004700	FAD linked oxidase domain-containing protein
Bcep1808_6947, Bcep1808_6948	XLOC_004824	Hypothetical protein
Bcep1808_R0084	XLOC_003963	16S ribosomal RNA

4   Conclusion

These candidate genes are now target to new studies to improve the understanding of biodegradation ability, allowing optimization of treatment processes, increasing the natural degradation ability of these bacteria and so, reducing the impacts generated by PAH to the environment.

References

Daims H, Taylor MW, Wagner M (2006) Wastewater treatment: a model system for microbial ecology. Trends Biotechnol 24:483–489

Haritash AK, Kaushik CP (2009) Biodegradation aspects of Polycyclic Hydrocarbons (PAH): a review. J Hazard Mater 169:1–15

Martin JA, Wang Z (2011) Next-generation transcriptome assembly: review. Nat Rev Genet 12:671–682

O'Sullivan LA, Mahenthiranlingan E (2005) Biotechnological potential within the genus Burkholderia. Lett Appl Microbiol 41:8–11

Valentin-Vargas A, Toro-Labrador G, Massol-Deyá AA (2012) Bacterial community dynamics in full-scale activated sludge bioreactors: operational and ecological factors driving community assembly and performance. PLoS One 7:1–12

Yan J, Wanga L, Fub PP, Yua H (2004) Photomutagenicity of 16 polycyclic aromatic hydrocarbons from the US EPA priority pollutant list. Mutat Res 557(1):99–108

Biokinetic Behaviour of Autochthonous Halophilic Biomass at Different Salinity: Comparison Between Activated Sludge and Granular Sludge Systems

S.F. Corsino[✉], M. Capodici, M. Torregrossa, and G. Viviani

Department of Civil, Environmental, Aerospatial Engineering and Material,
University of Palermo, Viale delle Scienze building 8, 90128 Palermo, Italy

Abstract. The main goal of this study was the evaluation of the impact of increasing salinity on halophilic biomass in forms of flocculent and granular sludge for the treatment of hypersaline fish-canning wastewater, focusing on the metabolic behavior of autotrophic biomass. For this purpose, two sequencing batch reactors, one with aerobic granular sludge (GSBR) and the other with flocculent activated sludge (SBR) were monitored. In both reactors, a halophilic biomass was cultivated from a real saline wastewater collected from a fish-canning industry. The salt concentration was stepwise increased (2 gNaCl L-1) from 30 gNaCl L-1 to 50 gNaCl L-1. Therefore, ammonia and nitrite uptake rates for granular and flocculent biomass were evaluated at each salinity increase. Both AUR and NUR tests revealed a high metabolic activity despite the extreme salinity environment. AUR ranged between 4.6 mgNH$_4$-N gVSS-1 h-1 and 3.10 mgNH$_4$-N gVSS-1 h-1 in the GSBR showing, on the whole, a decreasing trend with salinity increasing. In the SBR instead, AUR was mainly affected by the biomass ageing, while a slight dependency of salinity was observed only above 46 gNaCl L-1 when it started in decreasing. The nitrite uptake rate did not show any significant connection with the increasing salinity.

Keywords: Autochthonous-halophilic biomass · Kinetic · Salinity

1 Introduction

Nowadays, several industries including petroleum, chemical and fish-canning produce a large amount of wastewater which contains organic pollutants, high nutrient concentrations and high salinity (chloride). The treatment methods generally used for these wastewaters are chemical and physical ones, like membrane separation, ion exchange or electrodialysis (Fan et al. 2011). If on the one hand, these methods are highly performing, on the other hand lead to some problems such as high costs, secondary pollution, and therefore, these technologies are only applied in certain conditions (He et al. 2016). Contrarily, although biological treatments offer better economic performance, their implementation is rare because high salinity can raise osmotic separate microbial cell plasma, reduce the metabolic enzyme activity, destroy the structure of microbial enzymes and inhibit the growth of microorganisms, affecting in such a way

the bacterial metabolism and then biological performances. Some researches focused on saline and hypersaline wastewater treatment processes and nutrient removal efficiency by means of halo-tolerant biomass (Corsino et al. 2016; Ferrer-Polonio et al. 2016). However, results showed that both halo-tolerant activated sludge and granular sludge lost effectiveness over a certain salinity, especially in terms of nitrogen removal. These studies emphasize the need to use specialized bacteria, particularly for the treatment of real high salt wastewater. In the literature, there is a lack of knowledge concerning the development of halophilic biomass and its implementation for hypersaline wastewater treatment. Additionally, although it is known that halophilic bacteria are more resistant to extreme saline environments rather than halo-tolerant, there is no information about how increasing salinity affects their metabolic kinetics.

Moreover, based on researches about the treatment of industrial/saline wastewater, many related papers stressed the advantage to operate with aerobic granular sludge instead of conventional activated sludge. Therefore, halophilic bacteria bio-aggregation could be a further advantage, allowing operating at higher salinity, or with faster kinetics, compared with halophilic activated sludge.

The aim of this study was to evaluate the impact of increasing salinity on halophilic biomass in forms of flocculent and granular sludge for the treatment of hypersaline fish-canning wastewater, focusing on the metabolic behaviour of autotrophic biomass.

2   Materials and Methods

Two sequencing batch reactors, one with aerobic granular sludge (GSBR) and the other with flocculent activated sludge (SBR) were monitored. In both reactors, halophilic biomass was cultivated from a real saline wastewater collected from a fish-canning industry. The chemical oxygen demand (COD) fractionation tests carried out in the raw wastewater (salinity equal to 150 $gNaCl\ L^{-1}$) revealed the presence of a significant amount of active biomass, suggesting the presence of halophilic bacteria strains. On the basis of this observation, it was decided to cultivate this biomass in forms of flocculent activated sludge in the SBR (8 L volume) at 30 $gNaCl\ L^{-1}$, and subsequently the same was seeded in the GSBR (4 L volume) where it grew in forms of aerobic granules. During the cultivation phase, the raw wastewater was diluted with tap water to obtain a salinity equal to 30 $gNaCl\ L^{-1}$. When steady state conditions were reached in both the reactors, salt concentration was gradually increased (2 $gNaCl\ L^{-1}$ in each sub-period) by adding sodium chloride to the diluted wastewater. In this way, the BOD_5 and total nitrogen concentration of the feed remained unchanged for the whole experiment. Then, salinity was step-wise increased up to 50 $gNaCl\ L^{-1}$. Until the sub-period corresponding to salinity equal to 40 $gNaCl\ L^{-1}$, sludge retention time (SRT) was not imposed, and mixed liquor was purged in accordance with the biomass growth. In this period SRT resulted close to 27 days in both reactors. However, due to the excessive increase of inert material within the aerobic granules and the ageing of the flocculent biomass, from the sub-period corresponding to salinity equal to 40 $gNaCl\ L^{-1}$until the end of the experiment, SRT was maintained close to 14 days by daily purging a known volume of mixed liquor. In Table 1 the main operating parameters and the influent wastewater characteristics are reported.

Table 1 Operational parameters for GSBR and SBR and wastewater influent characteristics

	GSBR	SBR	Unit
Cycle length	12	24	(h)
Volume	4	8	(L)
VER	50	50	(%)
SRT (I)	27 ± 3	26 ± 2	(d)
SRT (II)	14 ± 2	13 ± 3	(d)
BOD_5	786 ± 91	786 ± 91	$(mg\ L^{-1})$
TN	146 ± 18	146 ± 18	$(mg\ L^{-1})$
Salinity	$30 \div 50$	$30 \div 50$	$(gNaCl\ L^{-1})$

VER = Volumetric Exchange Ratio; SRT = Sludge Retention Time; BOD_5 = Biochemical Oxygen Demand; TOC = Total Organic Carbon; TN = Total Nitrogen.

The oxygen concentration in the liquid bulk was maintained close to the saturation value according to the environment temperature. However, it gradually decreased with the increase in salinity.

The reaction cycle included 60 min of feeding (not-aerated) in both the reactors, 5 and 20 min of settling in the GSBR and GSBR respectively and 5 of effluent discharges. The reaction phase instead was fully aerated in the GSBR (650 min), whereas in the SBR it was divided into 675 min of aeration, 675 min of anoxic mixing followed by 5 min of aeration to favour nitrogen stripping. The cycle length and the distribution of aerated/not-aerated periods were fixed to maximize the nitrogen removal.

In this study, kinetic tests referred to autotrophic bacteria metabolism and in general to nitrogen removal were run. Accordingly, in each sub-period ammonium uptake rate (AUR) and nitrite uptake rate (NUR) tests were run, in order to evaluate the impact of increasing salinity on the nitrogen removal kinetics. Kinetic tests were run only when analyses revealed that steady-state in terms of nitrogen removal efficiency was reached.

Kinetic tests were carried out in a 1.5 L reactor (3 gTSS L^{-1}) at controlled temperature (20 °C). Ammonium chloride and sodium nitrite were used as ammonia and nitrite sources respectively. Kinetic tests were run for 2 h (each) during which, at regular time interval (10 min), 10 ml of sample was withdrawn and filtered through a 0.45 μm membrane for the NH_4-N and NO_2-N analyses. During AUR tests the dissolved oxygen concentration was maintained close to the saturation value (in accordance with the temperature and salinity), while during NUR tests, a magnetic stirrer continuously mixed the reactor. Although anoxic conditions generally occur within the inner layers of granules even in the presence of dissolved oxygen in the bulk, it was decided to carry out the tests under the same conditions for both the biomasses. Sodium acetate was added as a carbon source to evaluate the maximum nitrite uptake rate. AUR and NUR values were calculated as the slope of the linear regression line and then referred to the volatile suspended solids concentration of the kinetic test reactor.

3   Results and Discussions

In both the reactors nitrogen was removed via nitritation and denitritation processes. Nitrite was the only catabolic product of ammonia oxidation process, suggesting the absence, or inhibition, of nitrite oxidizing bacteria. Nitrites were then reduced to molecular nitrogen within the anoxic phase in the SBR and within the anoxic layers of the granules, simultaneously with the nitritation process, in the GSBR.

Both kinetic parameters revealed a high metabolic activity despite the extreme salinity environment and the results were comparable with those referred to conventional activated sludge (Capodici et al. 2016). AUR and NUR values at the salinity levels tested during the experiments are reported in Fig. 1.
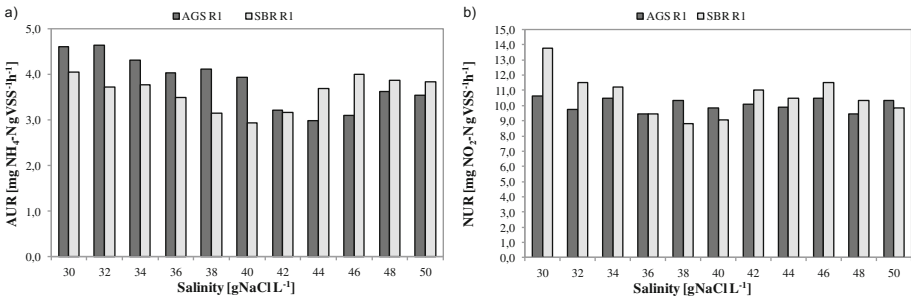
Fig. 1. Ammonium (a) and nitrite (b) uptake rates throughout the experiment at different salinity

When the salinity increased from 30 gNaCl L^{-1} to 40 gNaCl L^{-1}, the removal rate of ammonia slightly reduced in the GSBR (7% reduction) (Fig. 1a). The steady value at 30 gNaCl was 4.27 mgNH$_4$-N gVSS^{-1}h^{-1}, and it slightly decreased to 3.97 mgNH$_4$-N gVSS^{-1}h^{-1} at 40 gNaCl L^{-1}. Therefore, the increase in salinity had no significant effect on the ammonia oxidizing bacteria in the aerobic granules within this salinity range. In contrast, in the SBR the AUR reduction (28%) was more clear, indeed it decreased from 4.05 mgNH$_4$-N gVSS^{-1}h^{-1} to 2.93 mgNH$_4$-N gVSS^{-1}h^{-1} within the same range of salinity above stated.

After the sub-period VI (salinity equal to 40 gNaCl L^{-1}) nitrogen removal efficiency started to decrease in both the reactors. Currently, the best explanation of this occurrence was the biomass ageing, especially in the GSBR. In fact, at the end of this period, the VSS/TSS ratio was close to 50% and 65%, respectively in the aerobic granules and in the flocculent biomass, suggesting the advanced ageing state of the biomass, especially in the GSBR. Moreover, due to the inclusions of inert material (salt) within the granules' structure, their size exceeded 4 mm. This inevitably caused limitation to the oxygen diffusion within the inner layers, endangering the ammonia oxidation process. Therefore, it was decided to reduce the SRT to 14 days by daily purging a known volume of mixed liquor from both the reactors. Particularly, the GSBR was purged from the bottom, after the granules were settled, to withdraw the heaviest ones and so those with the highest VSS/TSS ratio.

The new operating conditions had an immediate effect on the SBR kinetics. Indeed, the ammonia removal rate increased and then stabilized close to 3.85 $mgNH_4$-N $gVSS^{-1}h^{-1}$, a value close to that one of the experiment beginning. In contrast, from 40 $gNaCl\,L^{-1}$ to 46 $gNaCl\,L^{-1}$ the ammonia removal rate in the GSBR steadily declined from 3.98 $mgNH_4$-N $gVSS^{-1}h^{-1}$ to 3.10 $mgNH_4$-N $gVSS^{-1}h^{-1}$. Subsequently, the reversal of the AUR trend occurred, as previously observed in the SBR, but slightly shifted in time, and in the last experimental phase the AUR value attested at $mgNH_4$-N $gVSS^{-1}h^{-1}$.

On the whole, the obtained results pointed out as up to 40 $gNaCl\,L^{-1}$ the metabolic activity of ammonia oxidizing bacteria was higher in the granular sludge reactor than the flocculent SBR. Autotrophic bacteria grow in the inner layers of aerobic granules and for this reason are less exposed to the salinity environment respect to those in the activated flocculent sludge. Because of the smaller and less compact structure of the activated sludge than the granular one, autotrophic bacteria in the flocs are more susceptible to the osmotic pressure. Currently, this could be the best explanation for the obtained results. However, exceeding a certain value of salinity, the oxygen diffusion within the liquid bulk starts to be salt-limited. The compact structure of the granules, if on the one side represent a kind of protecting shield for bacteria, on the other side is a further barrier to oxygen diffusion through their inner layers. Consequently, at high salinity, the ammonia oxidation was likely oxygen limiting and this effect was more marked in the GSBR. The sludge renewing had a quick effect on the biomass metabolism in the SBR, while it took more time in the GSBR. Moreover, it is likely that, at low salinity, halo-tolerant and halophilic bacteria coexist within the activated sludge, whereas at higher salinity (likely over 40 $gNaCl\,L^{-1}$), the halophilic strains became the dominant bacteria in the biomass. Their acclimation in the GSBR required more time, probably due to the higher hydraulic selection pressure than the SBR that caused their washout in the early stages.

The removal rate of nitrite did not show any significant connection with the increasing salinity (Fig. 1b). The nitrite uptake rate in both the reactors ranged between 9 $mgNO_2$-N $gVSS^{-1}h^{-1}$ and 10.5 $mgNO_2$-N $gVSS^{-1}h^{-1}$ and no significant different between granular and flocculent sludge was observed. The obtained results indicated that the halophilic heterotrophic bacteria are less sensitive to salinity than autotrophic. However, it was observed that the specific observed heterotrophic yield (Y_{obs}) reduced with the salinity (0.2 ÷ 0.13 $gVSS\ gBOD^{-1}$), suggesting that high salt concentration limit the heterotrophic bacteria growth, even if, a lower SRT is helpful to promote the biomass growth.

It has to be stressed that the obtained results cannot be compared with others in similar conditions because of the lack of knowledge in the literature. Although the acclimation to the salinity of conventional activated sludge is possible (Lefebvre and Moletta 2006; Wang et al. 2015), this is limited within a small range. Therefore, over a certain value of salinity the cultivation of halophilic strain could be a valuable solution for the treatment of hypersaline wastewater.

4   Conclusions

In this study, ammonia and nitrite uptake rates for granular and flocculent biomass were investigated under different salinity from 30 $gNaCl\ L^{-1}$ to 50 $gNaCl\ L^{-1}$.

Both AUR and NUR tests revealed a high metabolic activity despite the extreme salinity environment. AUR ranged between 4.6 mgNH$_4$-N gVSS^{-1}h^{-1} and 3.10 mgNH$_4$-N gVSS^{-1}h^{-1} in the GSBR showing, on the whole, a decreasing trend with salinity increasing. In the SBR instead, AUR was mainly affected by the biomass ageing, while a slight dependency of salinity was observed only above 46 gNaCl L^{-1} when it started in decreasing. The nitrite uptake rate did not show any significant connection with the increasing salinity and ranged between 9 mgNO$_2$-N gVSS^{-1}h^{-1} and 10.5 mgNO$_2$-N gVSS^{-1}h^{-1} in both the reactors.

References

Capodici M, Corsino SF, Di Pippo F, Di Trapani D, Torregrossa M (2016) An innovative respirometric method to assess the autotrophic active fraction: application to an alternate oxic–anoxic MBR pilot plant. Chem Eng J 300:367–375

Corsino SF, Capodici M, Morici C, Torregrossa M, Viviani G (2016) Simultaneous nitritation–denitritation for the treatment of high-strength nitrogen in hypersaline wastewater by aerobic granular sludge. Water Res 88:329–336

Fan JL, Zhang J, Zhang CL, Ren L, Shi QQ (2011) Adsorption of 2, 4, 6-trichlorophenol from aqueous solution onto activated carbon derived from loosestrife. Desalination 267:139–146

Ferrer-Polonio E, Mendoza-Roca JA, Iborra-Clar A, Alonso-Molina JL, PastorAlcaniz L (2016) Biological treatment performance of hypersaline wastewaters with high phenols concentration from table olive packaging industry using sequencing batch reactors. J Ind Eng Chem 43:44–52

He H, Chen Y, Li X, Cheng Y, Yang C, Zeng G (2016) Influence of salinity on microorganisms in activated sludge processes: a review. Int Biodeterior Biodegradation (in Press). http://dx.doi.org/10.1016/j.ibiod.2016.10.007

Lefebvre O, Moletta R (2006) Treatment of organic pollution in industrial saline wastewater: a literature review. Water Res 40:3671–3682

Wang ZC, Gao MC, She ZL, Wang S, Jin CJ, Zhao YG, Yang SY, Guo L (2015) Effects of salinity on performance, extracellular polymeric substances and microbial community of an aerobic granular sequencing batch reactor. Sep Purif Technol 144:223–231

The Benchmark Simulation Modelling Platform – Areas of Recent Development and Extension

U. Jeppsson[(✉)]

Division of Industrial Electrical Engineering ad Automation (IEA),
Department of Biomedical Engineering,
Lund University, Box 118, 22100 Lund, Sweden
`ulf.jeppsson@iea.lth.se`

Abstract. As the formal work of the IWA Task Group on Benchmarking of Control Strategies for Wastewater treatment Plants (WWTPs) has come to an end, it is essential to continue to disseminate the intense research in this field that is still carried out. In 2013 and 2014, all authors of the IWA Scientific and Technical Report on benchmarking came together to provide their insights, highlighting areas where knowledge was still deficient and where new opportunities were emerging, as well as to propose potential avenues for future development and application of the general benchmarking framework and its associated tools. The focus was on the topics of temporal and spatial extensions, process modifications within the WWTP, improved realism of models, control strategy extensions, the potential for new evaluation tools within the existing benchmark system and the need for full-scale validation. Four years later, it is clear that many of these goals have already been accomplished and the toolbox of Benchmark Simulations Models has been greatly extended and enhanced. The focus of this paper is to provide a number of examples of these recent extensions. As always, the different BSM softwares are freely available for the benefit of the global research community.

Keywords: Benchmark · BSM · Control · Modelling · Simulation · Wastewater treatment

1 Introduction

Over the past 20 years, considerable investments have been made in acquiring knowledge as how to best perform objective benchmarking of control and monitoring strategies for wastewater treatment plants (WWTPs) and how to evaluate the results using a detailed simulation protocol. The success of the COST/IWA benchmark simulation models BSM1, BSM1_LT and BSM2 (*e.g.* Spanjers et al. 1998; Copp 2002; Rosen et al. 2004; Jeppsson et al. 2007; Nopens et al. 2010; Corominas et al. 2011; Gernaey et al. 2014; http://www.benchmarkwwpt.org) for control strategy and monitoring system development and evaluation clearly illustrates the usefulness of such tools for the wastewater research community. More than 500 papers, conference presentations and theses on work based on/related to the benchmark systems have been

published to date. The freely available simulation models are used by numerous research groups around the world for various purposes and are available as predefined software tools in several commercial WWTP simulator packages (*e.g.* GPS-X^{TM}, SIMBA$^{®}$, WEST$^{®}$) – as well as in a stand-alone FORTRAN implementation and for the general MATLAB$^{®}$/SIMULINK$^{®}$ platform. Implementations (and ring-testing) with varying success have also been achieved in STOAT^{TM}, BioWin^{TM}, AQUASIM, JASS, SciLab and EFOR^{TM}.

Efforts have focussed on providing tools for analysing and solving real problems for real WWTPs and establishing a general platform and simulation protocol that can be further extended in the future. As the IWA Task Group on Benchmarking of Control Strategies published the official Scientific and Technical Report (STR) in 2014 (Gernaey et al. 2014), it is important to take advantage of the experience gained by the researchers that have been involved in the BSM development over the years. The focus of this paper is to provide a number of examples of the main areas for recent extensions and enhancements of the BSM family.

Jeppsson et al. (2013); Vanrolleghem et al. (2014) discuss a number of potential avenues for extensions of the BSMs. Based on those defined needs, recent developments related to five areas: (1) Spatial extensions; (2) Process extensions within the WWTP; (3) Improved realism of the models used in the BSMs; (4) Control strategy extensions; and (5) Extended evaluation tools, are presented and discussed.

2 Area 1: Spatial Extensions

The family of benchmark systems were traditionally defined as 'within-the-fence' systems, *i.e.* model descriptions and simulations did not extend outside the borders of the WWTP. However, the catchment, sewer system, WWTP and receiving water body are strongly interlinked and therefore it is essential to understand the interactions between the sub-systems in order to improve the performance of both the individual sub-systems but also the system as a whole as well as to protect the receiving waters in a holistic manner. Modelling is a valuable tool for not only understanding the sub-systems and their interactions but also serves as an engineering tool to explore the potential for improvement in the performance using different approaches (e.g. process control, upgrading of the existing infrastructure).

The urban wastewater system (UWS) consists of different sub-systems that are interconnected. These sub-systems include: (1) catchment – generating the wastewater during dry weather and rain events; (2) sewer system – transporting the generated wastewater for treatment; (3) WWTP – where physico-chemical and biological processes are used to remove pollutants from the wastewater; and finally, (4) receiving water system – where all the treated wastewater as well as excess flow from the sewer network (overflows) are discharged.

Traditionally, these sub-systems are operated and optimized individually. For example, sewer systems are optimized to reduce the overflow volumes and pollutant discharges to the receiving water whereas WWTPs are optimized to reduce the concentration of pollutants that are released as effluent. However, it is well established that

strong interactions exist and all the sub-systems in the UWS should be operated in a holistic manner in order to improve the receiving water quality.

For the above reasons the BSM–UWS has been developed. It is an integrated model library that can be used to simulate the dynamics of flow rate and pollutant loads in all the sub-systems of an UWS on a single simulation platform. It defines a hypothetical UWS using the model library, so that future users can use the pre-defined layout to study multiple control strategies and system modifications. In order to facilitate an objective evaluation of the results, evaluation criteria for river water quality as well as sewer system and WWTP performance have been added.

The existing dynamic influent pollutant disturbance generator (DIPDSG) presented by Gernaey et al. (2011) is extended with several new model blocks to describe the catchment (Flores-Alsina et al. 2014b). An upgraded BSM2 WWTP is used (currently only the water line) with minor modifications is used to simulate the WWTP. Model blocks for the sewer network (includes transportation and storage) have been developed (Saagi et al. 2016) and the river water system model is based on the River Water Quality Model no. 1 (Reichert et al. 2001). In addition, extensions to the sewer models to describe the transport and transformation of micropollutants have been developed (Lindblom 2009; Snip et al. 2014). New evaluation criteria for sewer performance and river water quality are included.

Using the model library, a hypothetical UWS for an urban catchment with 80 000 population equivalents and an area of 540 hectares is available (Saagi et al. 2017). The developed UWS layout can be used to develop different integrated control strategies and analyse system modifications.

3 Area 2: Process Extensions

Apart from the necessary new process modules to describe the UWS (see above), much focus has been directed towards recovery processes. As problems associated with shortage in resource supply arise, wastewater treatment plants turn to innovation to transform themselves into resource recovery facilities. Water groups worldwide recognize that wastewater treatment plants are no longer disposal facilities but rather sources of clean water, energy and nutrients. Process models for stripping units, crystallisers and biogas upgrading units (to vehicle gas quality) have been included in some BSM versions (Arnell 2016; Solon et al. 2017). However, more process extensions are needed to fully describe the different possibilities for nutrient recovery.

To better describe and analyse the aeration system and how to best control it, the BSM has been extended with a blower module and an adequate description of the oxygen transfer efficiency for different membrane diffuser discs (Arnell 2016).

Currently, additional process extensions related to fixed-film and integrated fixed-film activated sludge (IFAS) processes, granular sludge (Feldman et al. 2016, 2017) and membrane bioreactor systems are also being developed.

4   Area 3: Improved Realism of Existing Models

As the traditional BSMs were based on the Activated Sludge Model no. 1 (Henze et al. 1987) and the Anaerobic Digestion model no. 1 (Batstone et al. 2002), they only allowed for detailed analysis and evaluation of COD and nitrogen removal systems. This was a major drawback and significant work has been devoted to enhance the BSMs in this respect.

One of the most important resources that can be recovered from wastewater treatment plants is phosphorus. Mathematical modelling can be utilised to analyse various operational strategies to recover phosphorus from the wastewater. However, incorporating phosphorus transformation processes in plant-wide models is complex. Firstly, the tri-valence of phosphates suggests non-ideality which requires the use of a physico-chemical model to account for this non-ideality. Secondly, phosphorus has strong interlinks with sulfur and iron which necessitates inclusion of their transformations into biological and physico-chemical models. Lastly, consolidating a plant-wide model aimed at describing phosphorus removal and/or recovery requires interfacing, modifications to the plant layout, addition of recovery unit processes and development of new control and operational strategies.

A physico-chemical model has been developed to take into account ion activity corrections, ion pairing effects, aqueous phase chemical equilibria, multiple mineral precipitation and gas stripping/adsorption allowing also for full pH prediction (Solon et al. 2015a, b; Flores-Alsina et al. 2015). This model is then linked with standard approaches used in wastewater engineering, such as the Activated Sludge Models no. 1, 2d and 3 (ASM1, 2d, 3) and Anaerobic Digestion Model no. 1 (ADM1) (Solon et al. 2015b). The extension of the ASM2d and the ADM1 with phosphorus, sulfur and iron-related conversions followed (Flores-Alsina et al. 2016). Finally, the extended models and the physico-chemical model have been consolidated into a plant-wide model provided by the Benchmark Simulation Model No. 2 (Solon et al. 2017). The resulting model is used for simulation-based scenario analysis aiming at finding ways to improve the operation of a wastewater treatment plant aimed at phosphorus removal and recovery. For users not requiring the high complexity of the above model, special versions of BSM1 and BSM2 exist, which are based on the traditional ASM2d, ASM3 and ASM3-bioP (Rieger et al. 2001) models.

The Takács secondary settler model (Takács et al. 1991) has previously been the standard choice in the BSM systems. It uses a modified Vesilind settling function (Vesilind 1968) to describe the hindered settling. Although widely used, the approach has issues related to numerical robustness and also limitations in its ability to predict wet weather operation of the settler. The Bürger-Diehl settler model (Bürger et al. 2011, 2012, 2013) overcomes many of these limitations. Three principal processes included in the BD-model are: (1) bulk flow; (2) hindered settling; and (3) compression. Without a significant increase in simulation time, the model has been able to improve the description of the secondary settler behaviour. Gradually, the Bürger-Diehl model is becoming the standard settler model used in the BSMs. In many cases, the settler is now also modelled as a reactive settler based on any of the standard ASM models. The inclusion of inorganic dissolved and particulate fractions in all models are

becoming standard as well as applying different settling efficiencies for different particulate fractions in the primary clarifier.

It has been shown in numerous studies that aeration is one of the most energy consuming processes at WWTPs, commonly accounting for 40–60% of the total electrical power demand (Olsson 2012; Lingsten et al. 2013). Therefore, aeration comprises one of the major operational costs for any WWTP with secondary biological treatment facilitating nitrification. Because of its importance, the aeration system models in BSM have been improved in terms of oxygen transfer and blower models rather than applying the BSM default volumetric mass transfer coefficient of oxygen supply.

The importance of predicting greenhouse gas emissions has increased dramatically since the BSMs were first conceived. For this reason a special version of the BSM2 named Benchmark Simulation Model no. 2 Greenhouse gas (BSM2G) has been developed. The principles described by Hiatt and Grady (2008) with two-step nitrification and four-step denitrification have been included, featuring heterotrophic N_2O production. As a complement, denitrification by ammonia oxidizing bacteria (AOB) has been included following Mampaey et al. (2013) where AOB have the capability of reducing NO_2^- to NO and N_2O. Fundamental contributions to this development was done by Flores-Alsina et al. (2011) and Guo and Vanrolleghem (2014) and finalised by Arnell (2016). Apart from the CO_2 from biological respiration of COD in the activated sludge unit, anaerobic digester and biological side-stream treatment and N_2O from nitrogen conversion processes in activated sludge and side-stream reactors, several direct and indirect emissions are also included:

- fugitive emissions of CO_2 and CH_4 from the anaerobic digester and co-generation unit. Dissolved CH_4 in the digester effluent is stripped and a CO_2 credit is included for power production from biomethane;
- CO_2, N_2O and CH_4 from sludge storage;
- CO_2 from off-site heat and power generation;
- CO_2 from production of external carbon source;
- N_2O from conversion of effluent nitrogen in recipient;
- CO_2 for transport of sludge for disposal;
- CO_2, N_2O and CH_4 from disposal of sludge.

5 Area 4: Control Strategy Extensions

Due to the spatial extension, new processes and enhanced models a large number of new control possibilities have become possible and have therefore been added to the BSM family. Many of these are directly related to system-wide control strategies, i.e. including the sewer system and (limited number) the receiving water body. However, also the addition of a complete physico-chemical description and phosphorus, sulfur and iron-related conversions implies new control possibilities within the WWTP itself, especially related to addition of different chemicals. Examples can be found in Flores-Alsina et al. (2014a); Saagi et al. (2016); Saagi et al. (2017); Solon et al. (2017). More details related to this area will be provided in the final paper.

6   Area 5: Extension of Evaluation Tools

The basic premise on which benchmarking is based are the metrics used in the evaluation phase. The availability and reliability of the evaluation tools to effectively 'score' the process under study is essential for the success of any benchmark system. Hence, the evaluation criteria (the metrics) must efficiently simplify a complex comparison into a few meaningful index values that capture the relative strengths and weaknesses of the items being compared.

The standard BSM platform was, and still is, based on three main types of evaluation criteria (effluent quality, operational cost issues and risk). Effluent quality is considered through an Effluent Quality Index (*EQI*), which has been defined to quantify into a single term the effluent pollution load to a receiving water body. This combined with an effluent violation metric gives a reasonable overview of the ability of the benchmarked system to meet a particular effluent requirement whatever that might be. Energy 'costs' are considered through pumping, mixing and aeration energy calculations. Sludge 'costs' are considered through sludge production and disposal calculations and costs related to chemical additions are also included (external carbon source). Together these 'costs' form an Operational Cost Index (*OCI*) using empirical factors. Finally, process risk is considered through a fuzzy logic calculation of microbiology-related operational problems to create a Risk Index (has not been modified).

To assess the performance of the now possible combined C, N and P control strategies, an updated set of evaluation criteria is necessary. The *EQI* has been updated to include the additional P load, both organic and inorganic. Because of the modifications to the plant layout and operation, additional costs are also considered, such as those relating to the additional recycles (anoxic, anaerobic), aerators (CO_2 stripping) and several chemicals (for chemical P precipitation and/or recovery) (Solon et al. 2017).

Sewer system performance during rain events is generally assessed by the amount of flow rate and pollution that is discharged into the river system (the lower, the better). As part of the new BSM–UWS the following new set of evaluation criteria are computed:

1. Overflow duration ($d.yr^{-1}$): the total overflow duration for a given year/evaluation period.
2. Overflow frequency ($events.yr^{-1}$): represents the number of overflow events annually. Two overflow events are separated if there is at least one hour difference in time between these events.
3. Overflow volume ($m^3.yr^{-1}$): the total volume of overflow from all overflow locations that reaches the receiving water system in a year.
4. Overflow quality index (*OQI*, kg pollutant $units.d^{-1}$): an aggregated pollution index similar to the *EQI* used for the wastewater treatment plant. It considers the pollutant load from different pollutants (chemical oxygen demand (COD), biological oxygen demand (BOD), total suspended solids (TSS), total Kjeldahl nitrogen (TKN), nitrate (NO_3^-) and phosphate (PO_4^{3-})) and assigns weights to each one. The *OQI* is the sum of the total load for each pollutant multiplied with its individual weight. The weights for individual pollutants are similar to those used in the BSM1 and BSM2 models.

5. Hourly maximum concentration $(g.m^{-3})$: the concentration that is continuously exceeded for a period of at least 1 h. Calculated for TSS, TKN and PO_4^{3-}.
6. Exceedance duration $(d.yr^{-1})$: the total duration for which the pollutant concentration exceeds a pre-defined threshold limit. It represents the duration of acute pollutant discharge to the receiving water system. Pollutants considered are TSS, TKN and PO_4^{3-}.

All the above criteria are described for the entire sewer system but can also be computed for each overflow location individually.

Three new evaluation criteria have been defined to assess the chemical quality of the river in BSM–UWS, mainly in terms of un-ionized ammonia (NH_3) and dissolved oxygen (DO). They are:

1. Exceedance duration $(d.yr^{-1})$: represent the total duration in a year for which the concentrations of DO and NH_3 exceed threshold values. The threshold values used are: NH_3 – 0.018 $g.m^{-3}$ and DO – 6 $g.m^{-3}$.
2. Hourly minimum oxygen concentration $(g.m^{-3})$: minimum dissolved oxygen concentration that is continuously reached for a duration of at least 1 h.
3. Hourly maximum ammonia concentration $(g.m^{-3})$: un-ionized ammonia concentration that is continuously exceeded for a period of at least 1 h.

More information on BSM–UWS evaluation criteria is available in Saagi et al. (2016, 2017).

As the BSM platform has been extended with greenhouse gas emissions (in BSM1G and BSM2G), a criterion to evaluate the impact of control strategies on this has also been added, offering more knowledge about the overall "sustainability" of the plant (Flores-Alsina et al. 2011, 2014a; Arnell 2016). The calculated greenhouse gas emissions are converted to CO_2 equivalents using GWP factors for a 100-year time horizon from IPCC (2013): 34 for methane and 298 for nitrous oxide, including climate-carbon feedbacks. The various emissions are reported separately and a selection of which emissions to report can be made case-by-case (for example in total or excluding biogenic emissions).

However, along with on-site effects the plant operations at the same time have global environmental impacts due to production of input goods, discharge of residues and discarding of wastes. These impacts are only covered to a limited extent in the dynamic process models. Greenhouse gas emissions from production of power and some chemicals, residual effluent nitrogen and disposal of sludge are for example included in the BSM2G. Other impacts are not considered but may very well be crucial for the overall environmental impact of the operations. Global environmental impacts of products and processes are commonly assessed by life cycle analysis (LCA). In LCA, the object under study is evaluated for the environmental impacts that the inputs and outputs give rise to over the course of the entire life cycle. For these reasons, an LCA model was constructed following ISO 14040 (2006) using the Gabi software tool (Gabi software 6.3, Thinkstep, Leinfelden-Echterdingen, Germany, 2013) for the BSM2G describing the same unit operations but extended with up-stream processes for production of input goods and downstream impact of residuals and wastes. The exported results from the BSM2G were imported to the LCA model.

When combining the BSM2G with the LCA model two exceptions from the default evaluation procedure were made. The offsite processes, production of power and chemicals, together with the downstream ones in recipient and from sludge disposal, are excluded from the evaluation procedure of BSM2G. Instead the impacts from these processes are included in the LCA. The six most important impact categories were selected based on previous studies (Corominas et al. 2013) for which impacts were calculated: abiotic depletion potential of elemental and fossil resources, eutrophication potential, acidification potential, global warming potential and ozone depletion potential.

The above extension of combining BSM and LCA for a more holistic evaluation has been successful and more information is available in Arnell (2016) and Arnell et al. (2017). However, it cannot be considered as a standard way of evaluating BSM systems as it requires access to special LCA software. But for cases when an extra thorough evaluation is required, it has been shown that the principle works well.

7   Conclusions

The BSM systems serve as a highly useful and freely available software platform and simulation protocol for research groups all over the world. Whether used for their initially intended purpose of objective benchmarking of control strategies and monitoring algorithms or as a starting point for other types of investigations, is of minor importance. As the IWA Task Group has come to an end, it is the group's obligation and responsibility to promote potential avenues for future development and disseminate information about the latest developments. A significant number of the extensions and improvements suggested in 2013/2014 have now been accomplished and were briefly described in this paper. It is the sincere hope of the Task Group that this will inspire other research groups to continue the development of the BSM platform, thereby allowing it to flourish and remain a state-of-the-art tool for research, development and practical application within the fascinating field of modelling, control, monitoring and simulation of urban wastewater systems.

References

Arnell M (2016) Performance assessment of wastewater treatment plants – multi-objective analysis using plant-wide models. PhD thesis, Division of Industrial Electrical Engineering and Automation, Lund University, Sweden

Arnell M, Rahmberg M, Oliveira F, Jeppsson U (2017) Multi-objective performance assessment of wastewater treatment plants combining plant-wide process models and life cycle assessment. J Water Clim (submitted)

Batstone DJ, Keller J, Angelidaki RI, Kalyuzhnyi SV, Pavlostathis SG, Rozzi A, Sanders WTM, Siegrist H, Vavilin VA (2002) Anaerobic digestion model no. 1. IWA scientific and technical report no. 13. IWA Publishing, London

Bürger R, Diehl S, Farås S, Nopens I (2012) On reliable and unreliable numerical methods for the simulation of secondary settling tanks in wastewater treatment. Comput Chem Eng 41:93–105

Bürger R, Diehl S, Farås S, Nopens I, Torfs E (2013) A consistent modelling methodology for secondary settling tanks: a reliable numerical method. Water Sci Technol 68(1):192–208

Bürger R, Diehl S, Nopens I (2011) A consistent modelling methodology for secondary settling tanks in wastewater treatment. Water Res 45(6):2247–2260

Copp JB (ed.) (2002) The COST simulation benchmark – description and simulator manual. Office for official publications of the European communities, Luxembourg. ISBN 92–894-1658-0

Corominas L, Foley J, Guest JS, Hospido A, Larsen HF, Morera S, Shaw A (2013) Life cycle assessment applied to wastewater treatment: state of the art. Water Res 47(15):5480–5492

Corominas L, Villez K, Aguado D, Rieger L, Rosen C, Vanrolleghem PA (2011) Performance evaluation of fault detection methods for wastewater treatment processes. Biotechnol Bioeng 108(2):333–334

Feldman H, Faraghi Parapari N, Bendix Larsen S, Kjellberg K, Flores-Alsina X, Sin G, Jeppsson U, Gernaey KV (2016) Model-based optimization of an industrial wastewater treatment plant combining a full-scale granular sludge reactor and autotrophic nitrogen removal. In: IWA 10th world water congress and exhibition (IWA 2016), Brisbane, Australia, 9–13 October 2016

Feldman H, Flores-Alsina X, Ramin P, Kjellberg K, Jeppsson U, Batstone DJ, Gernaey KV (2017) Optimizing the operational/control conditions of a full-scale industrial granular anaerobic digester. In: 12th IWA conference on instrumentation, control and automation (ICA 2017), Quebec, Canada, 11–14 June 2017

Flores-Alsina X, Arnell M, Amerlinck Y, Corominas Ll, Gernaey KV, Guo L, Lindblom E, Nopens I, Porro J, Shaw A, Snip L, Vanrolleghem PA, Jeppsson U (2014a) Balancing effluent quality, economic cost and greenhouse gas emissions during the evaluation of (plant-wide) control/operational strategies in WWTPs. Sci Total Environ 466–467:616–624

Flores-Alsina X, Corominas L, Snip L, Vanrolleghem PA (2011) Including greenhouse gas emissions during benchmarking of wastewater treatment plant control strategies. Water Res 45(16):4700–4710

Flores-Alsina X, Kazadi-Mbamba C, Solon K, Vrecko D, Tait S, Batstone D, Jeppsson U, Gernaey KV (2015) A plant-wide aqueous phase chemistry module describing pH variations and ion speciation/pairing in wastewater treatment process models. Water Res 85:255–265

Flores-Alsina X, Saagi R, Lindblom E, Thirsing C, Thornberg D, Gernaey KV, Jeppsson U (2014b) Calibration and validation of a phenomenological influent pollutant disturbance scenario generator using full-scale data. Water Res 51:172–185

Flores-Alsina X, Solon K, Kazadi-Mbamba C, Tait S, Gernaey KV, Jeppsson U, Batstone DJ (2016) Modelling phosphorus (P), sulfur (S) and iron (Fe) interactions for dynamic simulations of anaerobic digestion processes. Water Res 95:370–382

Gernaey KV, Flores-Alsina X, Rosen C, Benedetti L, Jeppsson U (2011) Dynamic influent pollutant disturbance scenario generation using a phenomenological modelling approach. Environ Model Softw 26(11):1255–1267

Gernaey KV, Jeppsson U, Vanrolleghem PA, Copp JB (eds.) (2014) Benchmarking of control strategies for wastewater treatment plants. IWA scientific and technical report no. 23. IWA Publishing, London. ISBN 9781843391463

Guo LS, Vanrolleghem PA (2014) Calibration and validation of an activated sludge model for greenhouse gases no. 1 (ASMG1): prediction of temperature-dependent N_2O emission dynamics. Bioprocess Biosyst Eng 37(2):151–163

Henze M, Grady Jr, CPL, Gujer W, Marais GVR, Matsuo T (1987) Activated sludge model no. 1. IWA scientific and technical report no. 1. IWA Publishing, London

Hiatt WC, Grady CPL (2008) An updated process model for carbon oxidation, nitrification, and denitrification. Water Environ Res 80(11):2145–2156

IPCC (2013) Climate change 2013: the physical science basis. Contribution of working group I to the 5th assessment report of the intergovernmental panel on climate change. Cambridge University Press, Cambridge, United Kingdom and New York, NY, USA

ISO 14040 (2006) Environmental management – Life cycle assessment – Principles and framework. International Organization for Standardization, Geneva, Switzerland

Jeppsson U, Alex J, Batstone D, Benedetti L, Comas J, Copp JB, Corominas L, Flores-Alsina X, Gernaey KV, Nopens I, Pons M-N, Rodriguez-Roda I, Rosen C, Steyer J-P, Vanrolleghem PA, Volcke EIP, Vrecko D (2013) Benchmark simulation models, quo vadis? Water Sci Technol 68(1):1–15

Jeppsson U, Pons M-N, Nopens I, Alex J, Copp JB, Gernaey KV, Rosen C, Steyer J-P, Vanrolleghem PA (2007) Benchmark simulation model no 2 – general protocol and exploratory case studies. Water Sci Technol 56(8):67–78

Lindblom E (2009) Dynamic modelling of micropollutants in the integrated urban wastewater system. PhD thesis, DTU Environment, Technical University of Denmark

Lingsten A, Lundkvist M, Hellström D (2013) Swedish water and wastewater utilities use of energy in 2011. Technical report SVU 2013–17, The Swedish Water and Wastewater Association, Stockholm, Sweden

Mampaey KE, Beuckels B, Kampschreur MJ, Kleerebezem R, van Loosdrecht MCM, Volcke EIP (2013) Modelling nitrous and nitric oxide emissions by autotrophic ammonia-oxidizing bacteria. Environ Technol 34(12):1555–1566

Nopens I, Benedetti L, Jeppsson U, Pons M-N, Alex J, Copp JB, Gernaey KV, Rosen C, Steyer J-P, Vanrolleghem PA (2010) Benchmark simulation model no 2 – finalisation of plant layout and default control strategy. Water Sci Technol 62(9):1967–1974

Olsson G (2012) Water and energy – threats and opportunities. IWA Publishing, London

Reichert P, Borchardt D, Henze M, Rauch W, Shanahan P, Somlyódy L, Vanrolleghem PA (2001) River water quality model no. 1. IWA scientific and technical report no. 12. IWA Publishing, London. ISBN 9781900222822

Rieger L, Koch G, Kühni M, Gujer W, Siegrist H (2001) The EAWAG Bio-P module for activated sludge model no. 3. Water Res 35(16):3887–3903

Rosen C, Jeppsson U, Vanrolleghem PA (2004) Towards a common benchmark for long-term process control and monitoring performance evaluation. Water Sci Technol 50(11):41–49

Saagi R, Flores-Alsina X, Fu G, Butler D, Gernaey KV, Jeppsson U (2016) Catchment & sewer network simulation model to benchmark control strategies within urban wastewater systems. Environ Model Softw 78:16–30

Saagi R, Flores-Alsina X, Kroll S, Gernaey KV, Jeppsson U (2017) A model library for simulation and benchmarking of integrated urban wastewater systems. Environ Model Softw 93:282–295

Snip LJP, Flores-Alsina X, Plósz BG, Jeppsson U, Gernaey KV (2014) Modelling the occurrence, transport and fate of pharmaceuticals in wastewater systems. Environ Model Softw 62:112–127

Spanjers H, Vanrolleghem PA, Nguyen K, Vanhooren H, Patry GG (1998) Towards a simulation-benchmark for evaluating respirometry-based control strategies. Water Sci Technol 37(12):219–226

Solon K, Flores-Alsina X, Gernaey KV, Jeppsson U (2015a) Effects of influent fractionation, kinetics, stoichiometry and mass transfer on CH_4, H_2 and CO_2 production for (plant-wide) modelling of anaerobic digesters. Water Sci Technol 71(6):870–877

Solon K, Flores-Alsina X, Kazadi-Mbamba C, Ikumi D, Volcke EIP, Vaneeckhaute C, Ekama G, Vanrolleghem PA, Batstone DJ, Gernaey KV, Jeppsson U (2017) Plant-wide modelling of phosphorus transformations in wastewater treatment systems: impacts of control and operational strategies. Water Res 113:97–110

Solon K, Flores-Alsina X, Kazadi-Mbamba C, Volcke EIP, Tait S, Batstone D, Gernaey KV, Jeppsson U (2015b) Effects of ion strength and ion pairing on (plant-wide) modelling of anaerobic digestion processes. Water Res 70:235–245

Takács I, Patry GG, Nolasco D (1991) A dynamic model of the clarification-thickening process. Water Res 25(10):1263–1271

Vanrolleghem PA, Flores-Alsina X, Guo L, Solon K, Ikumi D, Batstone D, Brouckaert C, Takács I, Grau P, Ekama G, Jeppsson U, Gernaey KV (2014) Towards BSM2-GPS-X: a plant-wide benchmark simulation model not only for carbon and nitrogen, but also for greenhouse gases (G), phosphorus (P), sulphur (S) and micropollutants (X), all within the fence of WWTPs/WRRFs. In: 4th IWA/WEF wastewater treatment modelling seminar (WWTmod 2014), Spa, Belgium, 30 March–2 April 2014

Vesilind PA (1968) Design of prototype thickeners from batch settling tests. Water Sewage Works 115(7):302–307

Automating the Raw Data to Model Input Process Using Flexible Open Source Tools

C. De Mulder[1(✉)], T. Flameling[2], J. Langeveld[3], Y. Amerlinck[1],
S. Weijers[2], and I. Nopens[1]

[1] BIOMATH, Department of Mathematical Modelling,
Statistics and Bioinformatics, Faculty of Bioscience Engineering,
Ghent University, Coupure Links 653, 9000 Ghent, Belgium
[2] Waterschap De Dommel, PO Box 10.001, 5280 DA Boxtel, The Netherlands
[3] Delft University of Technology, Stevinweg 1, 2628 CN Delft, The Netherlands

Abstract. The availability of dynamic influent data is of crucial importance for model development, as it provides the model input needed realistic dynamic simulations. Data analysis and reconciliation of such data are however often very time-consuming tasks, making that, even when some online influent data is indeed available, the option is often chosen to generate influent data in one way or the other. A lot of information contained in the available data is lost in that way. This contribution showcases a python package that allows for a streamlined data analysis workflow and provides possibilities for data analysis, validation and gap filling, with as main goal to recover and use as much (influent) data as possible. In the end, this provides a means towards more scientifically sound dynamic simulations and model calibration and validation, while limiting the time spent on data reconciliation.

Keywords: Data analysis · Modelling · Python package

1 Introduction

Data collection and analysis is one of the most time-consuming aspects of any modelling effort (Hauduc et al. 2009). Data can provide input to the model and is used for its calibration and validation, thereby being an inherent part of the way towards a reliable model with good predictive power. In the case of Water Resource Recovery Facility (WRRF) models, where influent data is necessary as an input, an additional issue is the need for relatively high-frequency data if the model is to capture the true dynamic nature of the installation (Cierkens et al. 2012; Martin and Vanrolleghem 2014). In most cases, this kind of data is not sufficiently available, and influent data is generated based on lower-frequency data or other available knowledge (Langergraber et al. 2008; Gernaey et al. 2011). In other cases, high-frequency data are indeed available, but are subject to classic data acquisition characteristics, such as noise or sensor failure (Rieger et al. 2010). Often, this leads researchers and practitioners to still opt for the generation of artificial influent data, leaving a lot of information unused.

This contribution attempts to optimally make use of the available high-frequency data, while reducing the time invested in data reconciliation. Currently emphasising the

usage of online data, the presented package allows to standardize the workflow of generating a useable influent dataset from online, high-frequency data.

2   Materials and Methods

The data used throughout this work was acquired at the WRRF of Eindhoven, The Netherlands, operated by Waterboard De Dommel. A year-long dataset for 2013 was received, containing online sensor data for the three sewer flows entering the plant, as well as data from the combined flows. Data acquisition frequency was 5 min.

The code used for data analysis was written in Python^{TM} (freely available, Python Software Foundation, Oregon, USA) in the form of a package, implying that package functionalities become available upon loading it. The Jupyter Notebook environment (Project Jupyter, jupyter.org) was used to ensure a clear and reproducible workflow. Package functionalities and the envisioned workflow can be summarized as follows:

1. **Formatting**: Formatting functions include simple data-type conversions, conversion of absolute to relative time and usage of a column of choice as index.
2. **Data exploration**: Before any operations are executed on the data, the matplotlib and pandas packages (Hunter 2007; McKinney 2010) are used to make plots and look for possible anomalies or correlations.
3. **Data filtering**: Functions are provided to do a couple of reliability checks on the data. This mostly includes noise filtering, e.g. based on a constant signal or on the slope between data points.
4. **Data filling**: Once the non-reliable data-points are tagged, they can be replaced in several ways, including interpolation, correlation with other measured values and modeled influent data.

In the described case, gaps present in the provided dataset and detected through data filtering, are semi-automatically filled by either linear interpolation or influent model predictions, depending on the size of the data gap; small gaps of up to one hour are filled by interpolation, larger ones with influent model output. This influent model output is the output of an empirical model, developed earlier by Langeveld et al. (2014) and implemented in WEST (MIKEbyDHI, Denmark). The reader is referred to the above reference for a thorough description of this model. Calibration and validation of the influent model were done using data from different periods in 2013. The entire automated workflow for the analysis and gap filling is then demonstrated for a 3-week period.

3   Results and Discussion

Example calibration and validation results for one of the three incoming influent flows are shown in Figs. 1 and 2. Other calibration and validation plots look similar. Next to showing a good fit for both calibration (after adjusting average influent flow and concentrations) and validation, both figures also give an insight in the quality of the data, in this case COD and TSS data. Although no very large gaps can be seen on the graphs (this would also defeat the calibration and validation purpose), quite some noise is present in the datasets.
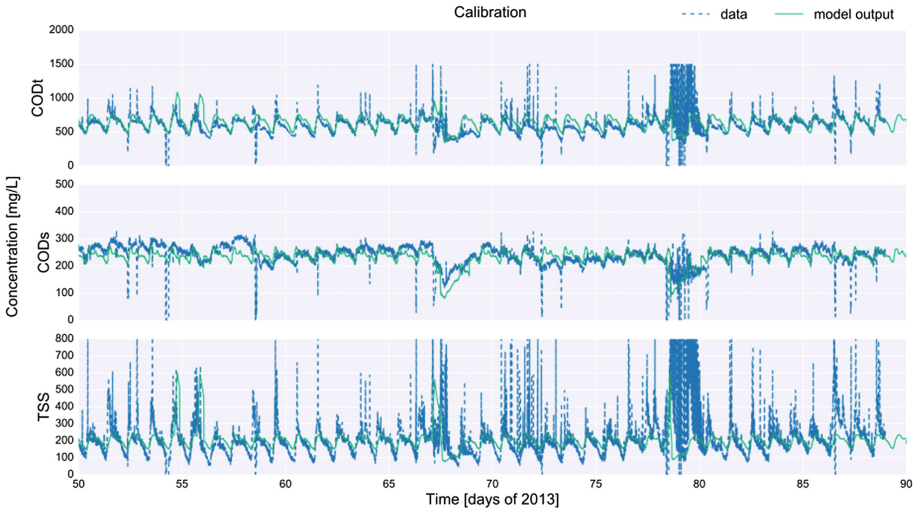
Fig. 1. Calibration results for the influent model used to predict influent concentrations. From top to bottom: Total COD, Soluble COD and Total Suspended Solids concentrations. This calibration happened on data from February 19th to March 31st, 2013

Fig. 2. Validation results for the influent model used to predict influent concentrations. From top to bottom: Total COD, Soluble COD and Total Suspended Solids concentrations. Validation happened on data from September 7th to October 17th, 2013
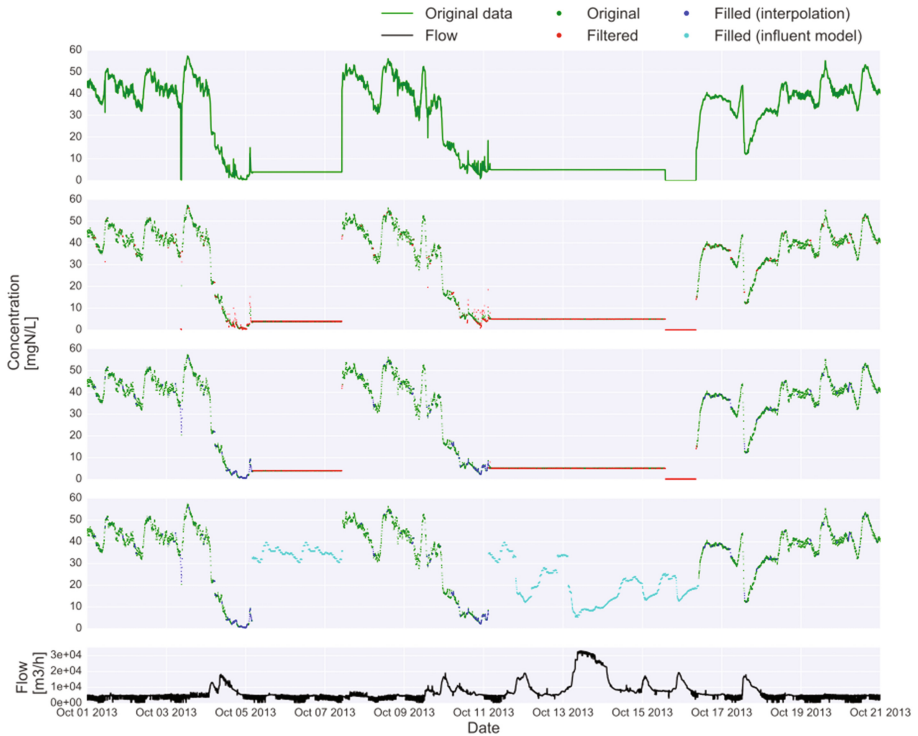
Fig. 3. Plots of the complete filtering and filling procedure, example-wise shown for 20 days of ammonia measurements. From top to bottom: original data; original data-points and data-points filtered out by noise filtering and sensor failure detection; original and filtered data-points, along with data-points replaced by interpolation; original data-points and data-points filled by interpolation or by filling with modeled values; the influent flow at the WWTP

Figure 3 shows the aggregated result of the data analysis functionalities and workflow developed, here for ammonia measurements in the combined influent. Starting out with the data as shown in the upper plot, data are subsequently (1) filtered based on noise and sensor failure detection, (2) filled using linear interpolation, where the period of missing data is no longer than 1 h (12 data points) and (3) filled using the influent model values within periods as defined by the user. The flexibility of this last part is emphasised by Fig. 4, showing the same dataset, but an increased range of the time periods within which measurements are replaced with modelled values. This custom change of time periods has of course the disadvantage of not being automated, but does yield a smoother dataset, avoiding possible numerical problems during simulation.
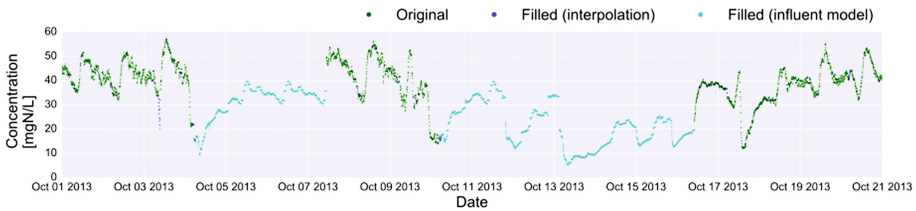
Fig. 4. The filled dataset for ammonia measurements, making use of an extended range within which to use modeled values for replacement

4   Conclusions and Perspectives

The described procedure was found very useful in obtaining an influent dataset to be used to feed the WRRF model of Eindhoven. In contrast with current methods as referred to in the introduction, the proposed work flow ensures that as much as possible of the information contained in the online data is used. The object-oriented implementation as a package and the use of the Jupyter Notebook environment provide both flexibility and a means of easy communication between researchers and operators from the Waterboard, making the data analysis process reproducible, reliable and transparent.

In the future, the goal is to extend this data analysis package with additional functionalities, to provide more automation possibilities through improved detection of false data points and to make the package openly accessible in a repository under a suitable license.

References

Cierkens K, Plano S, Benedetti L, Weijers S, de Jonge J, Nopens I (2012) Impact of influent data frequency and model structure on the quality of WWTP model calibration and uncertainty. Water Sci Technol 65(2):233–242

Gernaey KV, Flores-Alsina X, Rosen C, Benedetti L, Jeppsson U (2011) Dynamic influent pollutant disturbance scenario generation using a phenomenological modelling approach. Environ Model Softw 26:1255–1267

Hauduc H, Gillot S, Rieger L, Winkler S (2009) Activated sludge modelling in practice: an international survey. Water Sci Technol 60(8):1943–1951

Hunter JD (2007) Matplotlib: a 2d graphics environment. Comput Sci Eng 9(3):90–95

Langergraber G, Alex J, Weissenbacher N, Woerner D, Ahnert M, Frehmann T, Halft N, Hobus I, Plattes M, Spering V, Winkler S (2008) Generation of diunral variation for influent data for dynamic simulation. Water Sci Technol 57(9):1483–1486

Langeveld J, Schilperoort R, Van Daal P, Benedetti L, Amerlinck Y, de Jonge J, Flameling T, Nopens I, Weijers S (2014) A new empirical sewer water quality model for the prediction of WWTP influent quality. In: Proceedings of the 13th conference on urban drainage

Martin C, Vanrolleghem PA (2014) Analysing, completing, and generating influent data for WWTP modelling: a critical review. Environ Model Softw 60:188–201

McKinney W (2010) Data structures for statistical computing in python. In: van der Walt S, Millman J (eds) Proceedings of the 9th Python in science conference, pp 51–56

Rieger L, Takacs I, Villez K, Siegrist H, Lessard P, Vanrolleghem PA, Comeau Y (2010) Data reconciliation for wastewater treatment plant simulation studies - planning for high-quality data and typical sources of errors. Water Environ Res 82(5):426–438

Modeling of N$_2$O Emissions in a Full-Scale Activated Sludge Sequencing Batch Reactor

T.M. Massara[1(✉)], E. Katsou[1], A. Guisasola[2],
A. Rodriguez-Caballero[3], M. Pijuan[3], and J.A. Baeza[2]

[1] Department of Mechanical, Aerospace and Civil Engineering,
Institute of Environment, Health and Societies, Brunel University London,
Uxbridge Campus, Middlesex, Uxbridge UB8 3PH, UK
`{Theoni.Massara,evina.katsou}@brunel.ac.uk`
[2] GENOCOV. Departament d'Enginyeria Química,
Biològica i Ambiental, Escola d'Enginyeria, Universitat Autònoma de Barcelona,
Cerdanyola del Vallès (Barcelona), 08193 Barcelona, Spain
`{Albert.Guisasola,JuanAntonio.Baeza}@uab.cat`
[3] Catalan Institute for Water Research (ICRA), Emili Grahit Street, 101,
H2O Building, Scientific and Technological Park of the University
of Girona, 17003 Girona, Spain
`rodriguez.caballero.adrian@gmail.com,`
`mpijuan@icra.cat`

Abstract. Nitrous oxide (N$_2$O) is a greenhouse gas with a significant global warming potential. A dynamic model was developed to estimate the N$_2$O production and emission in a full-scale sequencing batch reactor (SBR) municipal wastewater treatment plant (WWTP). Based on the Activated Sludge Model 1 (ASM1), the model considered all known biological and abiotic N$_2$O production pathways along with the application of a 'stripping effectivity' (SE) coefficient for reflecting the non-ideality of the stripping model. N$_2$O data of two different cycles (types B and C) were used for the model calibration. Cycle B involved the alternation amongst aerated and non-aerated phases, whereas cycle C included a unique long aerobic phase. Optimizing the dissolved oxygen (DO) and SE parameters for both cycles provided a good fit of the model (DO = 1.6 mg L^{-1} and SE = 0.11 for cycle B, and DO = 1.66 mg L^{-1} and SE = 0.11 for cycle C). In both cases, N$_2$O emission peaks were related to high nitrite concentration in the liquid phase. Nitrifier denitrification was identified as the predominant biological pathway for N$_2$O generation. Although SBR operation occurred at similar DO and SE values for both cycles, the emission factor was significantly different; 0.8% for cycle B and 1.5% for cycle C, indicating the impact of cycle configuration on the N$_2$O emission. Thus, optimized SBR operation is essential in order to achieve a low overall carbon footprint through the avoidance of high N$_2$O emissions and energy requirements.

Keywords: N$_2$O emissions · Sequencing batch reactor · Full-scale modeling

1 Introduction

Nitrous oxide (N$_2$O) is a greenhouse gas (GHG) with a global warming potential 265 times higher than carbon dioxide in a 100-year period (IPCC 2013). During wastewater treatment, N$_2$O production and emission is mostly observed during the biological nutrient removal (Pan et al. 2016). With such a significant greenhouse effect, the development of mathematical models estimating N$_2$O dynamics emerges as an effective way to study the effect of operational conditions to decrease the carbon footprint in WWTPs. The implementation of these models will enable the establishment of mitigation strategies and, subsequently, optimal plant design and process control (Mannina et al. 2016; Pocquet et al. 2016; Massara et al. in press).

Three different biological pathways have been suggested for N$_2$O production during the biological nitrogen (N) removal in wastewater treatment plants (WWTPs): nitrifier denitrification, incomplete hydroxylamine (NH$_2$OH) oxidation and heterotrophic denitrification. The first two occur through the activity of Ammonia Oxidizing

Table 1 List of the 20 processes considered in our ASM-type model for 4-step nitrification-denitrification combined with a 2-pathway model for N$_2$O production by AOB and two abiotic processes.

Process Number	Process	
1	Hydrolysis	Aerobic Hydrolysis
2		Anoxic Hydrolysis (NO$_3^-$ → NO$_2^-$)
3		Anoxic Hydrolysis (NO$_2^-$ → N$_2$)
4		Anaerobic Hydrolysis
5	Heterotrophic organisms	Aerobic Growth on Ss
6		Anoxic Growth of Heterotrophs on Ss (NO$_3^-$ → NO$_2^-$)
7		Anoxic Growth of Heterotrophs on Ss (NO$_2^-$ → NO)
8		Anoxic Growth of Heterotrophs on Ss (NO → N$_2$O)
9		Anoxic Growth of Heterotrophs on Ss (N$_2$O → N$_2$)
10		Lysis
11	Nitrifying organisms	NH$_3$ oxidation to NH$_2$OH with oxygen consumption
12		NH$_2$OH oxidation to NO coupled with oxygen reduction (AOB growth here)
13		NO oxidation to NO$_2^-$ coupled with oxygen reduction
14		NO reduction to N$_2$O coupled with the NH$_2$OH oxidation to NO$_2^-$ (N$_2$O from NH$_2$OH oxidation pathway)
15		HNO$_2$ reduction to N$_2$O coupled with NH$_2$OH oxidation to NO$_2^-$ (N$_2$O from nitrifier denitrification pathway)
16		Aerobic Growth of NOB
17		Lysis of AOB
18		Lysis of NOB
19	Abiotic N$_2$O production	NH$_2$OH decomposition to N$_2$O
20		N-nitrosation of NH$_2$OH (HNO$_2$ as nitrosating agent)

Bacteria (AOB) (Wunderlin et al. 2012). It is common practice to apply the IWA Activated Sludge Models (ASM) (Henze et al. 2000) for the description of biological chemical oxygen demand (COD) and nutrient removal in WWTPs. However, the original ASM models take no account of the N_2O production and quantification. Hence, the aims of this work were: (i) to create an ASM-type model integrating the N_2O dynamics for a full-scale municipal sequencing batch reactor (SBR) plant, and (ii) calibrate the developed model with real N_2O emission data from the previous relevant study of Rodriguez-Caballero et al. (2015) (Table 1).

2   Materials and Methods

The model presented in this paper was based on the ASM1 (Henze et al. 2000) and was modified to include phosphate consumption by nitrifiers and heterotrophs. Afterwards, it was coupled with the two-pathway model of Pocquet et al. (2016) for N_2O production by AOB. Moreover, the heterotrophic denitrification steps were imported from Hiatt and Grady (2008). Furthermore, recent studies have revealed that abiotic N_2O production pathways can have a non-negligible contribution to the emissions during wastewater treatment (Harper et al. 2015; Soler-Jofra et al. 2016). For that reason, abiotic N_2O production (i.e. NH_2OH decomposition to N_2O, and N-nitrosation of NH_2OH with nitrous acid as nitrosating agent) (Domingo-Félez and Smets 2016) was also considered. Thus, the final model incorporated all the currently known pathways for N_2O production.

The kinetic model was developed in MATLAB and implemented for an existing full-scale SBR performing COD and N removal in the municipal WWTP of La Roca del Valles (Barcelona, Spain) (48,000 population equivalents). Rodriguez-Caballero et al. (2015) examined different operational cycles to evaluate the effects on N_2O production. They continuously monitored both gaseous and dissolved N_2O using a gas analyzer and a microsensor, respectively, for 33 days between February and March 2014 corresponding to a total number of 143 cycles. Those measurements served for the calibration of the model presented in the current study.

Two different cycle types (type B and C) applied by Rodriguez-Caballero et al. (2015) for the same influent are presented in this abstract. They both began with a 10-min lag phase during which the mixed liquor was stirred before feeding started. Cycle B involved the alternation amongst two aerated (13–40 min) and two non-aerated phases ($\sim$25 min). The reaction phase for Cycle C included the sequence of two shorter non-aerated phases ($\sim$25 min) with a long aerated one (66 min) between them. Feeding was continuous. Details on the operational parameters and influent characteristics used in this work can be found in Rodriguez-Caballero et al. (2015).

N_2O stripping was modeled by using the dissolved N_2O concentration and the volumetric mass transfer coefficient (k_La) for N_2O. We also included a 'stripping effectivity' (SE) coefficient expressing the non-ideality of this typical simplified model.

3   Results and Discussion

The total N$_2$O emission (in g N-N$_2$O d^{-1}) for a cycle was an additional simulated variable. The evolution of this variable in time was used for calculating the instantaneous N$_2$O emission. The results are given in Figs. 1 and 2 for cycle B and cycle C, respectively.
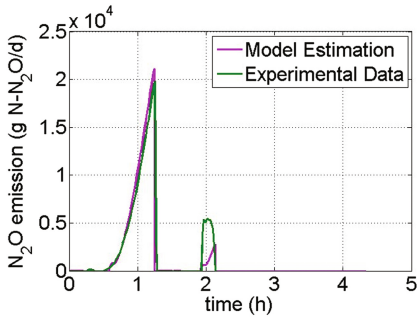
Fig. 1. *Optimized Cycle type B:* The N$_2$O instantaneous emission estimated by the model compared to the experimental data. Optimized DO setpoint during the aerated phases = 1.6 mg L^{-1}.
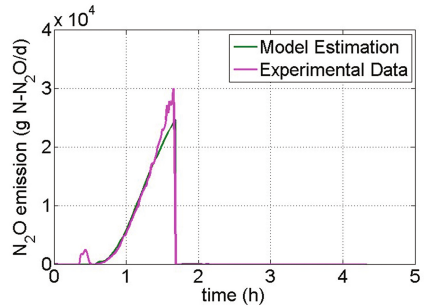
Fig. 2. *Optimized Cycle type C:* The N$_2$O instantaneous emission estimated by the model compared to the experimental data. Optimized DO setpoint during the aerated phases = 1.66 mg L^{-1}.

N$_2$O emissions are expected to be negligible in the non-aerated phases due to the negligible stripping (Ahn et al. 2010). In accordance with this idea, both the experimental data and our model linked the emissions with air flow or, equivalently, with the aerated phases. Within the attempt to calibrate the model, the SE parameter was firstly evaluated. For both cycle types, a rather satisfactory fitting to the experimental N$_2$O emission occurred under the same k_La modelling approach and SE value. It was noted that a SE equal to 0.11 contributed to a quite successful description of the experimental data in both cases, thus suggesting a clear influence of the stripping modeling on the final results.

According to the Global Water Research Coalition, the nitrification-related microbial routes (i.e. the two AOB pathways) are considered as major hotspots for N$_2$O emissions in full-scale domestic WWTPs (GWRC et al. 2011). During nitrification, insufficient aeration has an inhibitory effect (Kampschreur et al. 2009), and can therefore lead to increased emissions through the AOB pathways. After the SE study, we explored the DO setpoint during the aerobic phases of each cycle as an important operational parameter. The results after the DO setpoint and SE optimization for cycles B and C are shown in Figs. 1 and 2, respectively. First, it can be seen that the simulation results are fitted well on the experimental ones. However, this version of the model with default kinetic parameters was unable to precisely capture the emission peak at the beginning of the 2nd aerated phase of Cycle B (Fig. 1); especially the part of
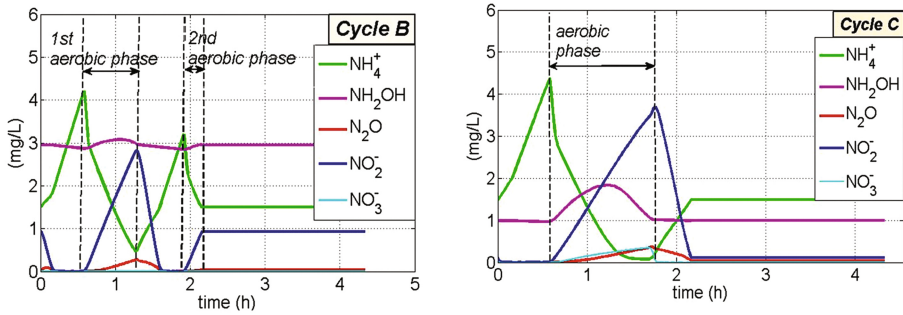
Fig. 3. *Optimized Cycles type B & C:* The evolution of the NH_4^+, NH_2OH, N_2O, NO_2^- and NO_3^- concentrations.

the emissions noted at the very beginning of the peak. It can be hypothesized that these emissions were rapidly recorded as a result of the stripping of the N_2O produced during the previous anoxic phase. This effect could be related to a N_2O denitrification rate during the anoxic phase lower than the value predicted by the model, which could lead to a higher final N_2O concentration at the end of the anoxic phase that would be stripped at the beginning of the aerobic phase. This divergence was not observed in cycle C because in this case only one aerobic phase existed. Specific experiments to evaluate N_2O denitrification rate would help to improve the model fitting. Secondly, we received the following output of the optimization process: optimal DO = 1.6 mg L^{-1} and SE = 0.11 (cycle B), optimal DO = 1.66 mg L^{-1} and SE = 0.11 (cycle C). Both cycle types were applied for the same influent. The optimal fit occurred at similar DO setpoint and SE. However, the emission factor differed significantly, being 0.8% for cycle B and 1.5% for cycle C. This is probably attributed to the long aerated phase of cycle C which can be connected with the higher N_2O emissions. As shown in Fig. 3 for both cycles, the N_2O concentration peaks coincided with the nitrite (NO_2^-) peaks in the liquid phase. This was observed for both the long aerobic phase of cycle C as well as for the 1st aerobic phase of cycle B; as mentioned above, the 2nd aerobic phase of cycle B was less successfully depicted in our simulations. Consequently, it can be deduced that nitrifier denitrification was the predominant AOB pathway for N_2O generation. The optimal fit was obtained for a rather low DO setpoint (1.6 mg L^{-1} for cycle B and 1.66 mg L^{-1} for cycle C). This observation is in agreement with past studies regarding the AOB pathways relative contribution; compared to incomplete NH_2OH oxidation, nitrifier denitrification has been suggested as increasingly contributing with the DO decrease (Anderson et al. 1993; Sutka et al. 2006; Kampschreur et al. 2008).

4 Conclusions

It can be concluded that the cycle configuration influences the emission magnitude. Long aerobic phases can increase the plant's carbon footprint due to the following: (i) higher energy requirements, (ii) higher N_2O production through the

nitrification-related pathways, and (iii) subsequent N$_2$O emission because of stripping. In this frame, process optimization is important. Optimal SBR operation includes the application of an optimal DO setpoint during aerobic phases of medium length. Under optimized SBR operation, satisfying nitrification along with moderate N$_2$O emissions and reasonable energy requirements are more likely to be achieved. In that sense, the implementation of cycles with multiple (shorter) aerated phases (e.g. cycle B in this work) instead of cycle configurations with few and relatively long aeration periods (e.g. cycle C in this work) seems more suitable.

This work will hopefully constitute a flexible model for the prediction and mitigation of N$_2$O emissions in full-scale SBR WWTPs with the added value of easily adapting to different cycle types.

References

Ahn JH, Kim S, Park H, Rahm B, Pagilla K, Chandran K (2010) N$_2$O emissions from activated sludge processes, 2008–2009: results of a national monitoring survey in the United States. Environ Sci Technol 44:4505–4511

Anderson I, Poth M, Homstead J, Burdige D (1993) A comparison of NO and N$_2$O nitrifier Alcaligenes faecalis. Appl Environ Microbiol 59:3525–3533

Domingo-Félez C, Smets BF (2016) A consilience model to describe N$_2$O production during biological N removal. Environ. Sci. Water Res. Technol. 2:923–930

GWRC, Foley J, Yuan Z, Keller J, Senante E, Chandran K, Willis J, et al. (2011) N$_2$O and CH$_4$ emission from wastewater collection and treatment systems. Technical report, London, United Kingdom

Harper WF, Takeuchi Y, Riya S, Hosomi M, Terada A (2015) Novel abiotic reactions increase nitrous oxide production during partial nitrification: Modeling and experiments. Chem Eng J 281:1017–1023

Henze M, Gujer W, Mino T, van Loosdrecht M (2000) Activated Sludge Models ASM1, ASM2, ASM2d and ASM3. IWA Publishing, London

Hiatt WC, Grady CPL (2008) An updated process model for carbon oxidation, nitrification, and denitrification. Water Environ Res 80(11):2145–2156

Kampschreur MJ, Tan NCG, Kleerebezem R, Picioreanu C, Jetten MSM, van Loosdrecht MCM (2008) Effect of dynamic process conditions on nitrogen oxide emission from a nitrifying culture. Environ Sci Technol 42:429–435

Kampschreur MJ, Temmink H, Kleerebezem R, Jetten MSM, van Loosdrecht MCM (2009) Nitrous oxide emission during wastewater treatment. Water Res 43:4093–4103

IPCC (2013) The final draft report, dated 7th June 2013, of the Working Group I contribution to the IPCC 5th Assessment Report. In: Climate change 2013: the physical science basis. www.climatechange2013.org/report/review-drafts/

Mannina G, Ekama G, Caniani D, Cosenza A, Esposito G, Gori R, Garrido-baserba M, Rosso D, Olsson G (2016) Greenhouse gases from wastewater treatment - a review of modelling tools. Sci Total Environ 551–552:254–270

Massara TM, Malamis S, Guisasola A, Baeza JA, Noutsopoulos C, Katsou E (in press) A review on nitrous oxide (N_2O) emissions during biological nutrient removal from municipal wastewater and sludge reject water. Sci Total Environ

Pan Y, van den Akker B, Ye L, Ni B-J, Watts S, Reid K, Yuan Z (2016) Unravelling the spatial variation of nitrous oxide emissions from a step-feed plug-flow full scale wastewater treatment plant. Sci Rep 6:20792

Pocquet M, Wu Z, Queinnec I, Sperandio M (2016) A two pathway model for N_2O emissions by ammonium oxidizing bacteria supported by the NO/N_2O variation. Water Res 88:948–959

Rodriguez-Caballero A, Aymerich I, Marques R, Poch M, Pijuan M (2015) Minimizing N_2O emissions and carbon footprint on a full-scale activated sludge sequencing batch reactor. Water Res 71:1–10

Soler-Jofra A, Stevens B, Hoekstra M, Picioreanu C, Sorokin D, van Loosdrecht MCM, Perez J (2016) Importance of abiotic hydroxylamine conversion on nitrous oxide emissions during nitritation of reject water. Chem Eng J 287:720–726

Sutka RL, Ostrom NE, Ostrom PH, Breznak JA, Gandhi H, Pitt AJ, Li F (2006) Distinguishing nitrous oxide production from nitrification and denitrification on the basis of isotopomer abundances. Appl Environ Microbiol 72:638–644

Wunderlin P, Mohn J, Joss A, Emmenegger L, Siegrist H (2012) Mechanisms of N_2O production in biological wastewater treatment under nitrifying and denitrifying conditions. Water Res 46:1027–1037

Comprehensive Evaluation of a Sewage Treatment Plant as a Base for Recirculation of Materials and Energy in the Region

T. Fukushima[✉]

METAWATER Co., Ltd., JR Kanda Manseibashi Bldg, 1-25, Kandasudacho, Chiyoda-ku, Tokyo 101-0041, Japan

Abstract. Based on the concept that a sewage treatment plant should serve as a base for the circulation of materials and energy in a region, a combined electric power generation system using both digestion gas and sludge incineration for power generation was studied in the use of organics in influent. To function as a base for the circulation of materials, the plant was assumed to employ phosphorus recovery, which was estimated individually for an ash alkali process and a MAP process. Using a model treatment plant with a capacity of 48,000 m^3/day, it was found that introducing high-efficiency solid-liquid separation to recover solid organics proved effective in increasing the electric-power self-supply ratio attained in normal power generation. With digestion gas this ratio was raised from 6.2% to 13.0%, and with combined power generation, the ratio was raised three times higher to 18.6%. Phosphorus recovery was increased by 10% to 30% over the conventional process in an ash alkali process by introducing an AO process using the transfer of phosphorus to sludge as part of the wastewater treatment process. When various measures are evaluated in terms of water eco-efficiency from a viewpoint of environmental performance in the sewage treatment plants, power generation using sludge incineration was 1.96 kg/kWh, compared to the benchmark, which was 1.62 kg/kWh of power generation with digestion gas, and phosphorus recovery was 2.08 kg/kWh. The target for water eco-efficiency may be set to 3 kg/kW/h when various measures are combined.

Keywords: Power self-supply ratio · Phosphorus recovery · Water eco-efficiency

1 Introduction

In Japan, the government issued a new Sewerage Vision in July 2014. It highlights "the use of sewage treatment plants as bases for integration, self-sustainability, and the supply of water, resources, and energy" as a way toward the "Full Development of Sewerage Systems, as a Path for Recycling." Similar activities can be observed elsewhere in the world. China has announced a new concept for sewage treatment plants focusing on energy self-supply and expanding reclaimed water utilization by recovering nutrients and organics in influent. (Chen 2014) Reports have been published in Europe about efforts being made in development methods for recovering organics,

energy, and nutrients from wastewater (viewed as "used water") through thickening. (Veratrate et al. 2009) In some cases almost complete energy self-supply has been achieved.

Toward establishing sewage treatment plants as bases for the recirculation of materials and energy in the region, gas power generation using digestion gas, power generation through sludge incineration are being studied as measures to utilize organics in influent.

2   Materials and Methods

Along with a study of water quality and power consumption, a study was conducted of measures adopted to achieve enhanced energy and material recovery. A sewage treatment plant simulator, the Performance Evaluation System (PES), was used to grasp the actions of the sewage treatment plant systems for the model plant shown in Table 1.

Table 1. Conditions at the model plant

Operating condition	Capacity	48,000 m^3/day
	Treatment method	Conventional activated sludge process
	Water temperature	20 °C
	Return sludge ratio	20% constant
	Primary sludge	2% of treated water drawn
	Excess sludge	MLSS drawn at a given rate of 1500 mg/L
Detention time	Primary settling tank	1.5 h
	Reactor	8.0 h
	Secondary settling tank	2.0 h
Influent quality	COD	360 mg/L (soluble: 35%)
	SS	160 mg/L (VSS: 60%)
	T-N	35 mg/L (NH$_4$-N: 20 mg/L)
	T-P	4.0 mg/L (PO$_4$-P: 2.0 mg/L)
Sludge treatment	Thickening	Separation thickening (Gravity; GT & centrifugal; CT)
	Digestion	Anaerobic digestion (Gravity thickened sludge only)
	Dehydrator	Centrifugal dewatering equipment
	Incinerator	Fluidized bed incinerator

The energy potential (EP) of the organics in the influent sewage was converted to energy (electric power) based on 3.49 Wh/kg COD (Cornel et al. 2012). Variations in the energy potential and power consumption (negative expressions) in each treatment process are shown in Fig. 1 (Fukushima 2015). Most of the power was consumed in the aeration tank and incinerator where the EP of the organics in the sewage was lost to a
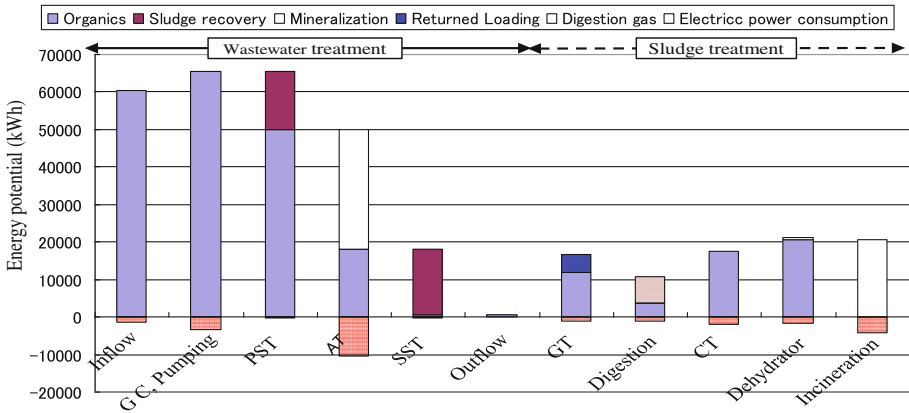
Fig. 1. Energy flows at the model plant

substantial degree. For sewage treatments plant to function as facilities for energy circulation in a watershed, it is essential that electrical energy self-supply be established through maximum utilization of the EP in sewage organics.

3   Results and Discussion

Including the B-DASH project of the Sewerage and Wastewater Management Department of the Ministry of Land, Infrastructure, Transport and Tourism (MLIT), many attempts are being made to improve energy saving and energy creation in sewage treatment plants. (B-DASH project HP). This paper deals with digestion gas power generation and power generation with sludge incineration. These systems are increasingly being introduced in sewage treatment plants and their performance is being verified. An evaluation of the energy recovery technology used in these systems in terms of energy self-supply rates will be presented, along with a comparison of the two systems with cases in which intensive solid-liquid separation with improved solid recovery (solid recovery rate raised to 66%) in primary settling is introduced.

The two energy recovery technologies shown below were studied.

(1) Digestion gas power generation (Miyata et al. 2015)
     Anaerobic digestion is done only for primary sludge (gravity thickened sludge), with the generated digestion gas used for power generation with a highly efficient fuel cell.
(2) Power generation with sludge incineration (Moriya et al. 2015)
     The "high-efficiency waste-heat generation" (with a power generation capacity of 250 kWh/h at 100 t/day) that proved highly effective for dewatered sludge in the 25B-DASH project was selected because it is easy to introduce into existing facilities.

The power self-supply rates attained respectively by power generation with digestion gas, power generation with sludge incineration, and their combination are

shown together with the power consumption rates and treated water quality levels in Table 2. The benchmarks, or basic pattern, (for primary settling) are a solid recovery rate of 34%, power generation of 1,580 kWh/day, and a power self-supply rate of 6.2% (with a power consumption rate of 0.53 kWh/m^3). This power consumption rate is the value that is standard in the world (Olsson 2012).

Aggressive recovery of solids, which is the essential point of this study, proved to be highly effective. Introducing high-efficiency solid-liquid separation resulted approximately in a two-fold increase in power generation, which rose to 3,100 kWh/day, and a power self-supply rate of 13.0%. Intensification of the solid recovery function in the primary treatment process as an alternative to primary settling resulted in a decreased amount of air due to the decrease in the organic inflow load into the aeration tank, which led to a decrease in power consumption. (The power consumption rate was 0.50 kWh/m^3).

In cases in which only power generation with sludge incineration was introduced (without anaerobic digestion), power generation was 1,780 kWh/day, which was equivalent to cases in which primary sludge digestion gas generation was introduced. Introducing intensive solid-liquid separation proved not to be effective, with power generation remaining at 1,780 kWh/day.

Combined power generation was greatest, power generation and the self-supply rate increased to 3,170 kWh/day and 12.3%, respectively. The further introduction of high-efficiency solid-liquid separation resulted in power generation and the self-supply rate, to 4,460 kWh/day and 18.6%, respectively.

Two processes were employed in trial calculations of phosphorus recovery. Records of the application of these processes were taken into account, and these processes were set as indicated below on the basis of numerical values in the Guidebook on the subject. (Japan MILT 2010)

(1) MAP process: This process was employed for dewatered filtrate, including digested sludge supernatant, with phosphorus recovery efficiency targeted at 85%.
(2) Ash alkaline process: This process was employed for incineration ash, with phosphorus recovery efficiency targeted at 50%.

The results of the calculation of phosphorus recovery are shown in Fig. 2. The amount recovered was high when only sewage sludge was treated and the ash alkali process was applied to the incineration ash. Specifically, the anaerobic-oxic(AO) process that transforms phosphorus positively into sludge (excess sludge) in the water treatment process can lead to recovery of 65 kg of phosphorus, which is equivalent to 30% or more of the phosphorus in influent sewage.

Evidently, sewage treatment plants have a great deal of potential as facilities for circulating materials and energy in a given region. Water eco-efficiency is proposed here as an index for comprehensive evaluation of phosphorus recovery and energy recovery. Water eco-efficiency is determined using the following Eq. (1):

$$\text{Water eco} - \text{efficiency (kg/kWh)} = (\text{Water environmental load removed} + \text{Resources recovered})/\text{Power consumption}$$

$$(1)$$

Table 2. Summary of measures used to improve power self-supply rate

Features	Power generation with digestion gas		Power generation with sludge incineration		Power generation with digestion gas & power generation with sludge incineration	
	Primary settling	High-efficiency solid-liquid separation	Primary settling	High-efficiency solid-liquid separation	Primary settling	High-efficiency solid-liquid separation
	Recovery in primary settling: 34%	Recovery ratio improved to 66%	Incineration of dewatered sludge		Sludge from primary settling to be used for digestion gas power generation Dewatered sludge to be incinerated for power generation	
Electric consumption rate	0.53	0.50	0.51	0.47	0.54	0.50
Electric consumption	25390	23910	24510	22670	25680	23980
Power generation (kWh), digestion gas	1580	3100	–	–	1600	3120
Power generation (kWh), sludge incineration	–	–	1780	1780	1570	1340
Total power generation	**1580**	**3100**	**1780**	**1780**	**3170**	**4460**
Power self-supply ratio	6.2%	13.0%	7.3%	7.9%	12.3%	18.6%
MLSS	1490	1510	1490	1510	1490	1510
Treated water quality COD (mg/L)	3.9	3.5	4.0	3.5	4.0	3.5
SS (mg/L)	15.7	15.4	15.7	15.4	15.7	15.4
T-N (mg/L)	22.6	24.7	20.8	21.4	22.5	24.6
T-P (mg/L)	2.2	2.6	1.8	1.9	2.2	2.6
Source	–	23B-DASH	25B-DASH		23 & 25B-DASH	

* Excess sludge withdrawal adjusted so that MLSS becomes 1500 mg/L.
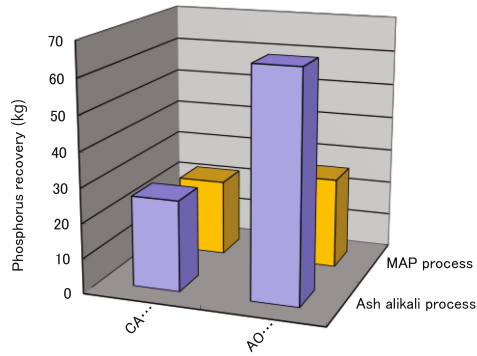
Fig. 2. Phosphorus recovery results

To calculate the water environmental load, T-N and T-P are integrated into COD by using a conversion factor. The conversion factor is: T- N: 19.7; T-P: 142.5. (Ishida et al. 2005)

Figure 3 illustrates the variation in water eco-efficiency in terms of power consumption and water environmental load removed. When compared with the benchmark (x), energy recovery measures (◆) show increased water eco-efficiency and a decrease in power consumption due to power generation. Introducing high-efficiency solid-liquid separation results in increased power generation, and a slight decrease in water environmental load removal due to the influence of the rejected water.
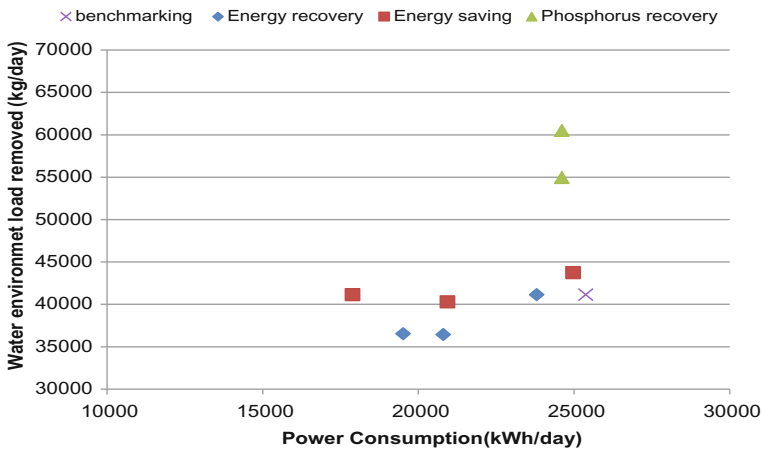
Fig. 3. Power consumption and water environmental load removed

Although power consumption did not change with the phosphorus recovery measure (▲), water eco-efficiency improved due to an increase in the water environmental load removed in line with the phosphorus recovery.

Also energy saving measures decrease power consumption, leading to increased water eco-efficiency. Therefore, the three measures (■) that facilitate introduction were examined. They are (1) pseudo recycled nitrification/denitrification pattern, (2) nitrification suppression operation, and (3) non-aeration recirculation sewage treatment with highly effective energy conservation.

When the reactor is operated in the pseudo recycled nitrification/denitrification pattern by partially reducing aeration (1/4) of its front half, organics in the influent are used partially as a carbon source for denitrification of NO_3-N in the return sludge. This in turn enables energy saving while leading to improved treated water quality. With the power consumption decreasing to 24,970 kWh and the water environmental load removal increasing to 43,728 kg, the water eco-efficiency was 1.75 kg/kWh. The process employed this time was the conventional one with complete nitrification. This meant its operation, while suppressing nitrification, could reduce aeration for nitrification. Power consumption could be reduced to 20,940 kWh, and water eco-efficiency was 1.92 kg/kWh. In addition, the non-aeration recirculation sewage treatment process, which is currently being demonstrated in the 26B-DASH project, is expected to achieve a 70% reduction of power consumption in the sewage treatment process, 23 with water eco-efficiency estimated to be at 2.30 kg/kWh.

It should be noted that the anaerobic-anoxic-oxic process (A2O process), which is one of the advanced treatment processes, can achieve a substantial removal of water environmental load by removing nitrogen and phosphorus while offering high environmental performance, with an eco-efficiency rate of 2.70 kg/kWh.

In all cases, the challenge is to develop technology that will enable reaching a water eco-efficiency rate of about 3 kg/kWh for sewage treatment plants. Demonstrations of combinations are also considered necessary.

4   Conclusions

(1) The power self-supply rate approximately doubled to 13.0% when high-efficiency solid-liquid separation was introduced into a digestion gas electric power generation system used. With the addition of power generation from sludge incineration, the power self-supply rate approximately tripled to 18.6% when combined power generation expected to generate 4,460 kWh/day was adopted.
(2) When the material and energy recovery functions were evaluated using a "water eco-efficiency index". It increased to 1.75 kg/kWh when digestion-gas electric power generation incorporating high-efficiency solid-liquid separation was implemented. The phosphorus recovery process achieved higher water eco-efficiency than the energy recovery process.
(3) The eco-efficiency of functions was estimated for the water, material and energy circulation base through the combination of technologies. Remaining challenges include technology development aiming at an eco-efficiency rate of about 3 kg/kWh for sewage treatment plants. Demonstrations of combinations are also considered necessary.

References

Chen J (2014) Improving China's wastewater treatment with new concept, Water21, 53–54, August

Cornel P, Choo KH, Lazarova V (2012) Water-energy interactions in water reuse. IWA Publishing, London

Fukushima T (2015) The basic study on the energy potential flow analysis of a sewage treatment plant. Mod Environ Sci Eng 1(2):72–78

Ishida S, Hanaki K, Aramaki T (2005) Introduction of tradable permit system among sewage treatment plants in tokyo bay watershed and its effect. J Jan Soc Civ Eng 804 (VII-37):804_73–804_81 (in Japanese)

Japan Ministry of Land, Infrastructure, Transport and Tourism (2010) Guide of the phosphorus exploitation of resources in the sewerage (in Japanese)

Miyata A, Matsui Y, Yamashita H, Shimada M (2015) Energy management system utilizing intensive solid liquid separation, Water and Energy 2015

Moriya Y, Yanase T, Yoshimura H, Tajima A (2015) Saving and generation in an innovative sewage sludge incineration system, Water and Energy 2015

Olsson G (2012) Water and energy threats and opportunities. IWA Publishing, London

Veratrate W, Caveye PV, Diamantis V (2009) Maximum use of resources present in domestic "used water". Bioresour Technol 100:5537–5545

Development of an in-House Lattice-Boltzmann Simulator Towards Bioreactors for Wastewater Treatment: Underlying Concepts

V.A. Fortunato[✉], F.L. Caneppele, R. Ribeiro, and J.A. Rabi

Faculty of Animal Science and Food Engineering, University of São Paulo,
Av. Duque de Caxias Norte 225, Pirassununga, SP 13635-900, Brazil

Abstract. Lattice Boltzmann method (LBM) has become a powerful technique to simulate bioprocesses in porous media. Based on a relatively simple dynamic 1-D model, the present work is a first step towards a comprehensive LBM simulator of bioreactor for vinasse treatment, taken as case study. Species concentrations were LBM-simulated at appropriate order of magnitude.

Keywords: Mathematical modelling · Numerical simulation · Lattice boltzmann method

1 Introduction

Comprehensive knowledge of bioprocesses is prone to rely on equations whose complexity invokes numerical methods. This is the case of bioreactors for wastewater treatment where bioprocesses are combined with transport phenomena (Głuszcz et al. 2011). Besides the variability in terms of chemical kinetics and composition, mathematical hurdles arise due to the mutual interference between fluid flow velocity and species concentrations (Parco et al. 2007). Computational fluid dynamics (CFD) arises as helpful tool (Brannock et al. 2010) and the importance of computational modelling towards bioprocesses has been recognized while innovative methods have been developed and applied (Datta and Sablani 2007).

Envisaged in (McNamara and Zanetti 1988), lattice Boltzmann method (LBM) has become a powerful technique to numerically simulate bioprocesses (van der Sman 2007). As it does not directly solve Navier-Stokes equations (Succi 2001), LBM renders relatively simpler computer codes (Mohamad 2011). LBM can quite straightforwardly deal with single-phase or multiphase flow, whether or not coupled to transport phenomena and/or chemical reactions (Sukop and Thorne Jr. 2006). Bearing in mind the computational modelling of continuous-flow bioreactors via LBM, one may numerically simulate biofilm formation and detachment (Picioreanu et al. 2001) as well as biogas bubbles generation and transport (Chen 2010).

This work is part of ongoing research whose goal is to develop in-house LBM simulators of food and bioprocesses (Durán et al. 2015; Okiyama et al. 2015; Rabi and Kamimura 2016; Rosa et al. 2016). While there is no doubt about the efficiency of

classic numerical methods (and off-the-shelf software) to perform analogous simulations, LBM is herein pointed as an alternative route to computationally model bioreactors for wastewater treatment.

2 Material and Methos

2.1 Theory: Bioreactor Modelling and Lattice-Boltzmann Simulation

This work is a preliminary step towards the development of an in-house LBM simulator of continuous-flow bioreactors for wastewater treatment. In view of that, an existing cylindrical laboratory-scale APBR (anaerobic packed bed reactor) for sugarcane vinasse treatment is taken as case study (Ferraz Jr. 2013). Resulting from sugarcane juice distillation, vinasse is an effluent from sugar-ethanol industries, whose large-scale use has pointed to fertirrigation in sugarcane crops after it undergoes anaerobic treatment (Vlissidis and Zouboulis 1993).

Figure 1(a) depicts the aforementioned experimental APBR. As sketched in Fig. 1 (b), it comprises feeding module (FM), bed section (BS), effluent collection area (EC) and biogas collection area (BC). Low-density polyethylene cylinders randomly fill up BS module (as the supporting medium), thus yielding porosity ε. Let $\dot{V}$ be the volumetric flow rate of vinasse so that interstitial fluid velocity in BS becomes $v = 4\dot{V}/(\varepsilon \pi d^2)$, where d is bed diameter.
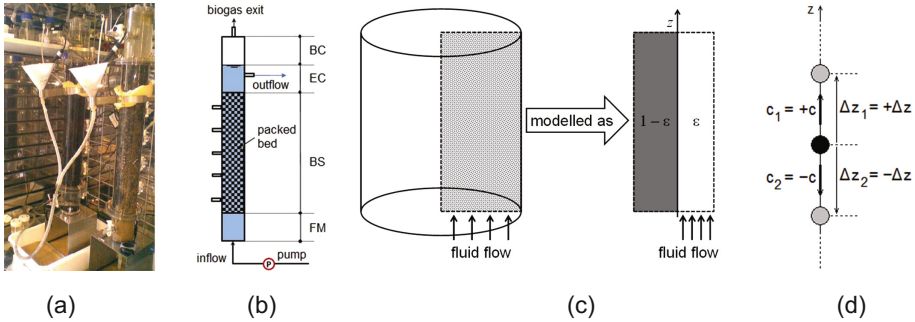
Fig. 1. LBM simulation of APBR for vinasse treatment: (a) picture of experimental bioreactors; (b) APBR sketch comprising feeding module (FM), bed section (BS), effluent collection area (EC) and biogas collection area (BC); (c) dynamic 1-D approach for BS with porosity ε; (d) basic and repetitive linear structure of D1Q2 LBM lattice

In line with LBM simulators implemented in our research (Durán et al. 2015; Okiyama et al. 2015; Rabi and Kamimura 2016; Rosa et al. 2016), a dynamic 1-D model is herein put forward. Coordinate axis z is oriented along with vinasse up-flow so that inlet is at $z = 0$ while exit is at $z = L$, where L is the total length. After considering an axisymmetric plane as shown in Fig. 1(d), stratification is assumed so that chemical species concentrations (or any other quantity) become functions of time t and coordinate z., i.e. $y_i = y_i(z, t)$.

In view of comprehensiveness and scale-up towards large equipment, convective-diffusive transport in the fluid phase has been considered since early versions of our LBM simulators, which can cope with concentrations y_i modelled by partial differential equations of the form:

$$\frac{\partial y_i}{\partial t} + v\frac{\partial y_i}{\partial z} = D_i\frac{\partial^2 y_i}{\partial z^2} + \dot{r}_i \tag{1}$$

where v is interstitial flow velocity (which is the same for all species), D_i is species diffusivity in the fluid phase, and rate $\dot{r}_i$ includes source and/or sink terms related to species generation and/or consumption via chemical reactions. Inspired by ADM1 - IWA Anaerobic Digestion Model No 1 (Batstone et al. 2002), Table 1 lists chemical species concentrations intended to be accounted for in the LBM simulator of continuous-flow APBR for vinasse treatment.

Table 1. Species to be accounted for in the LBM simulator of continuous-flow APBR for vinasse treatment.

y_i	Concentration of	Units	ρ_n	Concentration of	Units
y_1	chemical oxygen demand (COD)	kg-COD/m^3	y_8	acetate (ethanoate) ion	M = kmol/m^3
y_2	acetic (ethanoic) acid	kg-COD/m^3	y_9	propionate (propanoate) ion	M = kmol/m^3
y_3	propionic (propanoic) acid	kg-COD/m^3	y_{10}	butyrate (butanoate) ion	M = kmol/m^3
y_4	butyric (butanoic) acid	kg-COD/m^3	y_{11}	hydrogen ion (H$^+$)	M = kmol/m^3
y_5	dissolved hydrogen gas (H$_2$)	kg-COD/m^3	y_{12}	inorganic carbon	kmol-C/m^3
y_6	ethanol (ethyl alcohol)	kg-COD/m^3	y_{13}	dissolved carbon dioxide	kmol-C/m^3
y_{71}	biomass for sugar degradation	kg-COD/m^3	y_{14}	bicarbonate ion	kmol-C/m^3
y_{72}	biomass for H$_2$ degradation	kg-COD/m^3	y_{15}	carbon dioxide in the biogas	kmol-C/m^3
y_{73}	biomass for propionic acid degradation	kg-COD/m^3	y_{16}	hydrogen gas (H$_2$) in the biogas	M = kmol/m^3
y_{74}	biomass for butyric acid degradation	kg-COD/m^3			

LBM considers any medium (whether solid or fluid) as comprised by fictitious constituent particles following a sequence of synchronised streaming and collision steps in a discrete space, namely a fictitious lattice. During streaming, particles travel from one site to another through links defined by the fictitious lattice. As particles simultaneously arrive at sites, they mutually collide so that their velocities become rearranged for subsequent streaming-collision steps. By imposing conservation

principles (e.g. mass and momentum) to such repetitive particle dynamics, macroscopic medium can be numerically simulated (Succi 2001).

LBM mathematically relies on the so-called particle distribution function $f(\vec{r}, \vec{c}, t)$ giving, at time t and about position $\vec{r}$, the number of particles per unit volume with velocities between $\vec{c}$ and $\vec{c} + d\vec{c}$. One may then retrieve observable properties (e.g. species concentration) by taking suitable moments of function f, which is governed by Boltzmann's transport equation. In the absence of external forces while invoking BGK approach (after Bhatnagar, Gross and Krook) for the collision operator, Boltzmann's transport equation is written as:

$$\frac{\partial f}{\partial t} + \vec{c} \cdot \vec{\nabla} f = \frac{1}{\Delta t_{\text{relax}}} (f^{\text{eq}} - f) \tag{2}$$

where Δt_{relax} and f^{eq} are relaxation time and equilibrium distribution function respectively.

LBM is implemented to solve Eq. (2) as written in terms of the fictitious lattice assigned to the true medium, when it becomes known as lattice Boltzmann equation (LBE). Functions f_k are allocated to each streaming velocity c_k in the lattice. LBM lattices are identified as $DnQm$, being n the dimension of the problem (e.g. $n = 1$ for 1-D problem) whereas m refers to the number of particle distribution functions f_k to be solved for each observable property.

As this work proposes a dynamic 1-D model, D1Q2 lattice is employed, whose basic and repetitive linear structure comprises a central lattice site linked to two neighbouring sites, one at each side. As shown in Fig. 1(d), let $k = 1$ and $k = 2$ respectively refer to forward (i.e. upward) and backward (i.e. downward) streaming directions. LBE-BGK is written for each particle distribution function f_k (related to each streaming link k) at position z and time t:

$$\frac{\partial f_k(z,t)}{\partial t} + c_k \frac{\partial f_k(z,t)}{\partial z} = \frac{f_k^{\text{eq}}(z,t) - f_k(z,t)}{\Delta t_{\text{relax}}} \tag{3}$$

If Δt is the advancing time step then $c_1 = +\Delta z / \Delta t$ and $c_2 = -\Delta z / \Delta t$ are upward and downward streaming speeds respectively. The numerical solution method of Eq. (3) is addressed next.

2.2   Numerical Solution Method

There are two approaches to simulate species transport in multicomponent systems via LBM. Species can be simulated either as an active component (so that an increase of its local concentration leads to a local decrease in background fluid concentration) or as a passive solute carried by the solvent (Sukop and Thorne Jr. 2006). In this work we follow the latter approach as it has been adopted in LBM simulators previously implemented in our research.

Accordingly, particle distribution functions $f_{i,k}$ are assigned to each concentration y_i invoked in the model. At time t and position z, functions $f_{i,k} = f_{i,k}(z, t)$ become known by numerically solving Eq. (3) and the corresponding species concentration can be

retrieved simply as:

$$y_i(z,t) = \sum_k f_{i,k}(z,t) \xrightarrow{\text{D1Q2 lattice}} y_i(z,t) = f_{i,1}(z,t) + f_{i,2}(z,t) \tag{4}$$

Space-time discretisation of Eq. (3) renders an algebraic equation whose computational evolution is implemented in two separate iterative steps. Time evolution is accomplished in the collision step where particle distribution functions $f_{i,k}$ are updated from instant t to $t + \Delta t$ for all lattice links k and lattice sites at positions z in the solution domain. Eventual source or sink terms $\dot{r}_i$ (e.g. species generation or consumption by means of chemical reactions) are included at this LBM step so that the following algebraic expression holds:

$$f_{i,k}(z,t+\Delta t) = (1-\omega_i)f_{i,k}(z,t) + \omega_i f_{i,k}^{\text{eq}}(z,t) + w_k \,\Delta t \,\dot{r}_i \tag{5}$$

where $\omega_i = \Delta t_{\text{relax},i}/\Delta t$ is known as relaxation parameter and w_k are weighting factors, namely $w_1 = w_2 = 1/2$ for D1Q2 lattice. Space evolution is achieved in streaming step as collision outcomes are transmitted to adjacent lattice sites in all streaming directions simply as:

$$f_{i,k}(z+\Delta z_k, t+\Delta t) = f_{i,k}(z,t+\Delta t) \tag{6}$$

Collision and streaming steps, Eqs. (5) and (6), are repeated until final simulation instant is reached. Besides Eq. (4), LBM simulation becomes connected to macroscopic medium via relaxation parameters and equilibrium distribution functions. In a dynamic 1-D model (which is the present case), the latter refer to the bulk fluid (i.e. effluent) velocity v as:

$$f_{i,k}^{\text{eq}}(z,t) = w_k \, y_i(z,t) \, (1 \pm \text{Ma}) \tag{7}$$

while the former are related to individual species diffusivities D_n according to:

$$\frac{1}{\omega_i} = \frac{D_i \,\Delta t}{(\Delta z)^2} + \frac{1}{2} \quad \Rightarrow \quad \frac{1}{\omega_i} = \frac{\text{Ma}}{\text{Pe}_i} + \frac{1}{2}, \quad \text{Ma} = \frac{v \,\Delta t}{\Delta z} \quad \text{and} \quad \text{Pe}_i = \frac{v \,\Delta t}{D_i} \tag{8}$$

where Ma and Pe_i are lattice-based Mach number and lattice-based mass-transfer Péclet number, respectively. In Eq. (7), the sign before Ma is positive for forward (i.e. upward, $k = 1$) streaming and negative for backward (i.e. downward, $k = 2$) streaming.

With regard to inlet boundary conditions, one obtains $f_{i,2}(0,t) = f_{i,2}(0+\Delta z, t)$ via backward streaming from adjacent lattice site while $f_{i,1}(0,t)$ is the unknown. One may impose Dirichlet condition by combining first-order finite-differences estimate of $\partial \rho_i / \partial z$ with Eq. (4) to obtain:

$$\text{At } z = 0: \quad f_{i,1}(0,t) = y_{i,\text{in}} - f_{i,2}(0,t) \tag{9}$$

where $y_{i,\text{in}}$ is the species concentration in the feeding effluent. Danckwerts inlet condition is addressed in (Rabi and Kamimura 2016). At exit, $f_{i,1}(L, t) = f_{i,1}(L - \Delta z, t)$ is obtained from forward streaming while $f_{i,2}(L, t)$ is the unknown. Null Neumann condition is imposed by again combining first-order finite-differences estimate of $\partial y_i/\partial z$ with Eq. (4) and the final result is:

$$\text{At } z = L: \quad f_{i,2}(L, t) = f_{i,2}(L - \Delta z, t) \tag{10}$$

Last but not least, if $y_i(z, 0)$ is the initial condition imposed to species concentration, initial conditions for corresponding particle distribution functions are implemented as:

$$\text{At } t = 0: \quad f_{i,k}(z, 0) = w_k \, y_i(z, 0) \tag{11}$$

3   Results and Discussions

A first-round LBM simulator was implemented to numerically solve Eq. (1) for species $i = 1$ to 5 in Table 1, together with single (i.e. "unified") biomass species y_7 (instead of using species y_{71} to y_{74}). For such rather simplified scenario, Table 2 shows generation and consumption rates $\dot{r}_i$, which are expressed in terms of the common auxiliary parameter A defined as:

$$A = k_{\text{m,su}} \frac{y_1(z, t)}{K_{\text{S,su}} + y_1(z, t)} y_7(z, t), \quad \text{with} \quad k_{\text{m,su}} = 30 \text{ day}^{-1} \quad \text{and} \\ K_{\text{S,su}} = 0.5 \, \frac{\text{kg - COD}}{\text{m}^3} \tag{12}$$

Null Neumann boundary condition ($\partial y_i/\partial z = 0$) was imposed to all species at the exit while the feeding values $y_{i,\text{in}}$ for Dirichlet inlet condition are shown in Table 2. Initial conditions $y_i(z, 0) = 0$ were set to species $i = 1$ to 5 while $y_7(z, 0) = 0.1$ kg-COD/m^3 was set to species $i = 7$. Further APBR and LBM parameters used in simulations comprise: $L = 1$ m, $v = 2$ m/s, $k_{\text{d1}} = 0.02$ day^{-1}, $Y_{\text{su}} = 0.1$, $f_{\text{C2,su}} = 0.41$, $f_{\text{C3,su}} = 0.27$, $f_{\text{C4,su}} = 0.13$, $f_{\text{H2,su}} = 0.19$, $D_i = 0.02$ m^2/day^{-1} (small diffusivity arbitrarily set for all species), $\Delta z = 0.01$ m, and $\Delta t = 0.0005$ day.

Table 2. Reaction rates and inlet concentrations for species considered in the preliminary LBM simulator

Chemical species	$i = 1$	$i = 2$	$i = 3$	$i = 4$	$i = 5$	$i = 7$
Reaction rate $\dot{r}_i$	A	$(1 - Y_{\text{su}}) \cdot f_{\text{C2,su}} \cdot A$	$(1 - Y_{\text{su}}) \cdot f_{\text{C3,su}} \cdot A$	$(1 - Y_{\text{su}}) \cdot f_{\text{C4,su}} \cdot A$	$(1 - Y_{\text{su}}) \cdot f_{\text{H2,su}} \cdot A$	$Y_{\text{su}} \cdot A - k_{\text{d1}} \cdot y_7$
Inlet $y_{i,\text{in}}$ (kg-COD/m^3)	24.7	0.5013	0.0801	0.5266	0.0001	0.1

   While the LBM simulator can provide concentrations $y_i(z, t)$ at any position z and time t, for brevity and grouping results with similar order of magnitude, Fig. 2 shows time-dependent concentrations at the exit $y_i(L, t)$ for (a) $i = 1$ (COD) and (b) $i = 2$ to 5 and 7 (further species). As far as the experimental APBR is concerned, COD was measured as 26.1 kg-COD/m^3 at $t = 1$ day, which is consistent with simulations shown in Fig. 2(a). Figure 2(b) suggests that acidogenesis, H$_2$ and biomass generation were successfully simulated via as well.
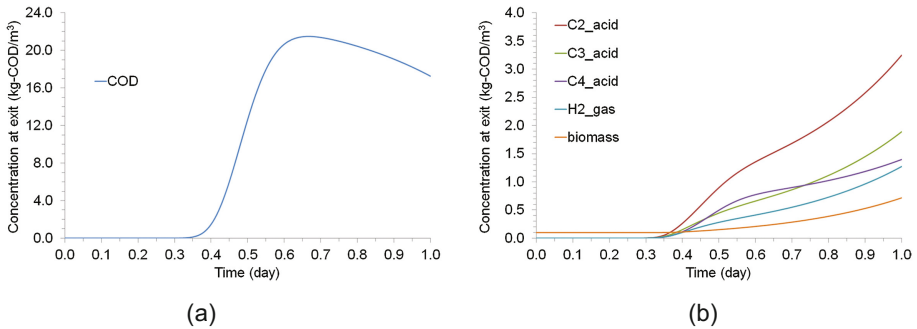
Fig. 2. LBM-simulated time-dependent species concentrations at the exit $y_i(L, t)$: (a) $i = 1$, (b) $i = 2$ to 5 and 7

4   Conclusions

Although relatively simple at its current development, the dynamic 1-D model for continuous-flow APBR was successfully implemented via LBM. Species concentrations were numerically simulated at suitable order of magnitude. Future developments of the LBM simulator point to the inclusion of further chemical species as well as fine-tuning model parameters.

References

Batstone DJ, Keller J, Angelidaki I, Kalyuzhnyi SV, Pavlostathis SG, Rozzi A, Sanders WT, Siegrist H, Vavilin VA (2002) The IWA anaerobic digestion model no 1 (ADM1). Water Sci Technol 45(10):65–73

Brannock M, Leslie G, Wang Y, Buetehorn S (2010) Optimising mixing and nutrient removal in membrane bioreactors: CFD modelling and experimental validation. Desalination 250 (2):815–818

Chen X (2010) Simulation of 2D cavitation bubble growth under shear flow by lattice Boltzmann model. Commun. Comput. Phys. 7(1):212–223

Datta AK, Sablani SS (2007) Mathematical modeling techniques in food and bioprocess: an overview. In: Sablani SS, Rahman MS, Datta AK, Mujumdar AR (eds) Handbook of food and bioprocess modeling techniques. CRC Press, Boca Raton, pp 1–11

Durán R, Villa AL, Ribeiro R, Rabi JA (2015) Pectin extraction from mango peels in batch reactor: dynamic one-dimensional modeling and lattice Boltzmann simulation. Chem Prod Process Model 10(3):203–210

Ferraz ADN Jr (2013) Anaerobic digestion of sugar cane vinasse in acidogenic fixed bed reactor followed by methanogenic reactor sludge blanket type. PhD thesis (in Portuguese), São Carlos School of Engineering, University of São Paulo, São Carlos, Brazil

Głuszcz P, Petera J, Ledakowicz S (2011) Mathematical modeling of the integrated process of mercury bioremediation in the industrial bioreactor. Bioproc Biosyst Eng 34(3):275–285

McNamara GR, Zanetti G (1988) Use of the Boltzmann equation to simulate lattice-gas automata. Phys Rev Lett 61(20):2332–2335

Mohamad AA (2011) Lattice Boltzmann method: fundamentals and engineering applications with computer codes. Springer, London

Okiyama DCG, Kamimura ES, Rabi JA (2015) Biospecific affinity chromatography: computational modelling via lattice Boltzmann method and influence of lattice-based dimensionless parameters. Int J Biotech Wellness Ind 4:40–50

Parco V, Du Toit G, Wentzel M, Ekama G (2007) Biological nutrient removal in membrane bioreactors: denitrification and phosphorus removal kinetics. Water Sci Technol 56(6):125–134

Picioreanu C, van Loosdrecht MCM, Heijnen JJ (2001) Two-dimensional model of biofilm detachment caused by internal stress from liquid flow. Biotech Bioeng 72(2):205–218

Rabi JA, Kamimura ES (2016) Lattice-Boltzmann simulation of lipase separation via bioaffinity chromatography: imposing Dirichlet or Danckwerts inlet condition. Procedia Eng 157:238–245

Rosa RH, von Atzingen GV, Belandria V, Oliveira AL, Bostyn S, Rabi JA (2016) Lattice Boltzmann simulation of cafestol and kahweol extraction from green coffee beans in high-pressure system. J Food Eng 176:88–96

Succi S (2001) The lattice Boltzmann equation for fluid dynamics and beyond. Oxford University Press Inc., New York

Sukop MC, Thorne DT Jr (2006) Lattice Boltzmann modeling - an introduction for geoscientists and engineers. Springer, Berlin

van der Sman RGM (2007) Lattice Boltzmann simulation of microstructures. In: Sablani SS, Rahman MS, Datta AK, Mujumdar AR (eds) Handbook of food and bioprocess modeling techniques. CRC Press, Boca Raton, pp 15–39

Vlissidis A, Zouboulis AI (1993) Themophilic anaerobic digestion of alcohol distillery wastewaters. Biores Technol 43(2):131–140

Differential Titrimeter for Nitrification Process Control and Energetic Optimization in a Large WRRF

C. Caretti[1(✉)], A. Mannucci[1], G. Munz[1], I. Ducci[1], and D. Fibbi[2]

[1] Civil and Environmental Engineering Department, University of Florence, via S. Marta 3, 50139 Florence, Italy
[2] G.I.D.A. S.p.A., Via Baciacavallo 36, Prato, Italy

Abstract. The objective of this study was to validate an innovative monitoring technique suitable for online control of nitrification rates for aeration control system and to use it to replace or integrate conventional batch tests for the estimation of nitrifying biomass kinetic parameters. For this purpose, a continuously-fed online differential titrimeter was designed and installed in a large industrial WRRF (Calice, Italy). The possibility to use the output of the titrimeter for the calibration of AOB (Ammonia Oxidation Bacteria) kinetic parameters was assessed by comparing the accuracy of the model using kinetic parameters calibrated on titrimeter output result and that of the model using kinetic parameters estimated on the results of conventional kinetic batch tests. The titrimeter is a robust tool to replace or integrate conventional batch tests for the estimation of nitrifying biomass kinetic parameters. Having validated the values obtained with the titrimeter, a new aeration control system was implemented full scale within Calice WRRF, which is no longer based on DO measurements and measurements of the effluent characteristics, but rather, on the values of the nitrification rate calculated continuously and in real time, thus allowing to adopt timely intervention measures in the case of malfunctioning of the process associated with changes in the plant operating conditions, eventual inhibition phenomena or other external factors.

Keywords: Nitrification · Process control · Titrimetry

1 Introduction

The oxidation and nitrification process is characterized by a high energy demand for the aeration system. This causes a significant environmental impact and represents one of the main budget items of wastewater treatment plants. In order to ensure high effluent quality, process management often involves high dissolved oxygen concentration and sludge retention time, thus causing an increase of both operational costs and carbon footprint of the whole treatment process (Rosso and Stenstrom 2005). Aeration process management is therefore a key aspect, and its optimization using alternative technologies and protocols allows significant advantages, both in terms of economic and environmental costs. This study is part of the Biocloc project (BIOprocess ControL through Online titrimetry to reduce Carbon footprint in wastewater treatment),

co-funded by the EC within the Life + Programme. The aim of the research is to demonstrate the suitability of an innovative monitoring instrument for activated sludge process control, based on the online measurement of the nitrification rate (Hong et al. 2012).

2   Materials and Methods

For this purpose, a continuously fed online differential titrimeter has been designed, manufactured and installed within the Calice WRRF, which treats about 39,000 m^3/d of effluents coming from sewage (domestic and textile wastewaters in coming from the district of Prato, one of the main textile area Europe) and about 700 m^3/d of truck-transported liquid wastes.

The titrimeter consists of two identical CSTRs (Continuous Stirred-Tank Reactors) each with a volume of 2 L, equipped with four identical pumping systems for mixed liquor input, substrate dosing, hydrogen peroxide and sodium hydroxide dosing for the control of DO and pH. The titrimeter is continuously fed (2 L/h) with the mixed liquor from one of the Calice WRRF oxidation tanks and kept in non-limited conditions. The output of the system is therefore the maximum nitrification rate in the operating condition of the Calice oxidation tanks (DO, T, pH, SST). The estimation of the nitrification rate through titrimetry relies on the possibility of using nitrification inhibitors to compare the alkalinity consumption in both the presence and the absence of the inhibitor. In the differential titrimeter, the maximum ammonia oxidation rate is calculated by comparing the NaOH dosing rate in the control reactor and the reactor where nitrification is inhibited (Caretti et al. 2015). The difference between alkalinity consumption rates of inhibited and non-inhibited identical reactors enables identification of the alkalinity consumption due to nitrification, which is proportional to the oxidized substrate as a function of the stoichiometry of the nitrification process (Fig. 1).
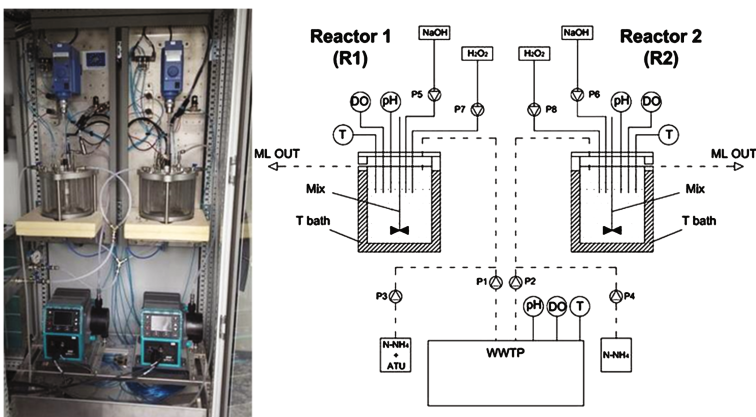
Fig. 1. Schematic of the titrimeter

The Calice WRRF process was modelled in order to describe the WRRF behaviour in the actual operating conditions and the implemented model proved to be a useful tool for monitoring the plant and predicting the behaviour of the processes. Kinetic parameters can vary as a function of load quality and environmental conditions especially in industrial wastewater treatment and a long term estimation of kinetic parameters requires an intensive modelling activity, data collection and off-line bench scale tests. All the above information (when half saturation for oxygen is known) can be substituted and/or integrated, by the continuous measurement of actual maximum nitrification rate that depends on several variables including maximum specific growth rate and active biomass nitrifying concentration (depending in turn on SRT, decay coefficient, load, temperature, etc.).

The continuous and online titrimeter capable of monitoring actual maximum nitrification rate was used as a tool to improve the estimation of nitrification kinetic parameters.

The output of the titrimeter (year 2015) have been used in order to calibrate some AOB biomass kinetic parameters: an endogenous decay coefficient for AOB biomass ($b_{AOB} = 0.2$ d^{-1}) similar to that obtained by Munz et al. (2011) in anoxic conditions and a maximum growth rate ($\mu max, _{AOB} = 0.34$ d^{-1}) in accordance with literature data were estimated.

3   Results and Conclusions

The nitrification rate obtained through the titrimeter and the output of the model are reported in Fig. 2.
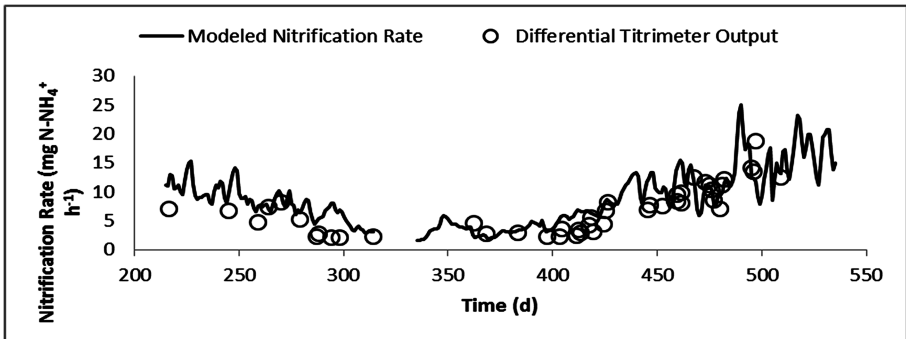
Fig. 2. Modeled nitrification rate and differential titrimeter output

As reported in Fig. 3, Temperature strongly influences AOB activity; during the experimentation the temperature varies according to seasonal variation and reaches values around 14 °C and 25 °C in winter and summer season, respectively. Influent ammonia loadings vary between 200 and 500 kg N-NH$_4^+$ d^{-1}. Influent loads and temperature variation caused a variation of AOB concentration in the mixed liquor that
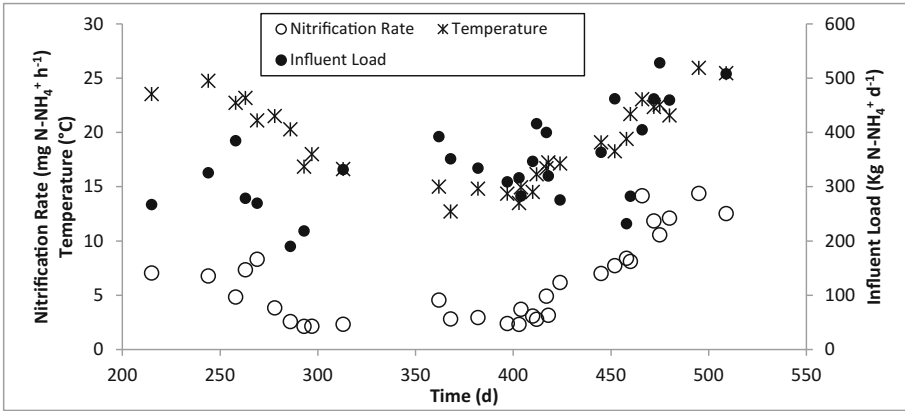
Fig. 3. Differential titrimeter output, Influent ammonia load and temperature vs. time

was around 40 mg(COD)$_{AOB}$ L^{-1} and 100 mg(COD)$_{AOB}$ L^{-1} in the winter and summer season, respectively.

The K$_{N-NH3}$ value and temperature correction factor for AOB growth were then calibrated on the results of the 2015 WRRF monitoring campaign and validated on the results of the 2014 WRRF monitoring campaign. A value of 0.009 mg N-NH$_3$/L and 1.105 were estimated for K$_N$_NH3 and $\theta_{\mu max, AOB}$, respectively. Figure 4 shows the results of the validation.
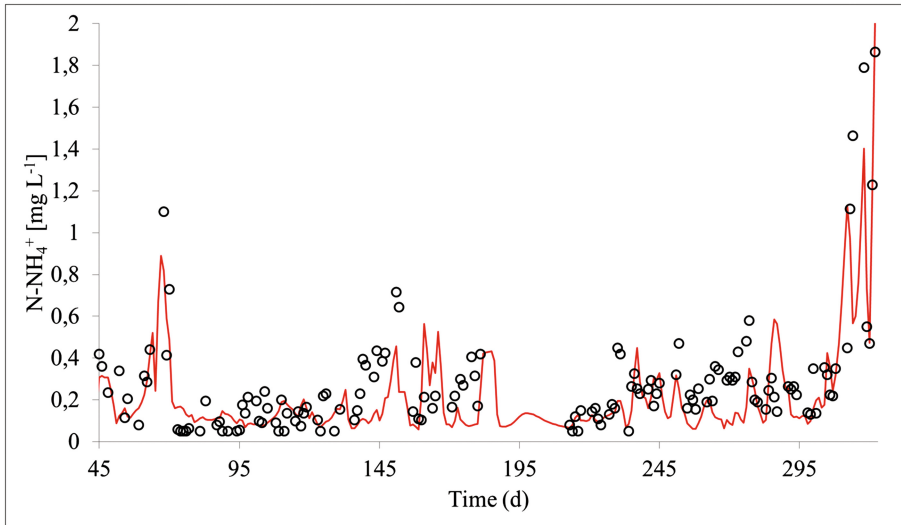
Fig. 4. Experimental (dots) and modeled effluent ammonia concentration (red line). (Color figure online)

Having validated the obtained values of the nitrification rate, and therefore also the procedure for obtaining them, it is therefore possible to consider a monitoring of the aeration system in the Calice oxidation tanks which is no longer based on DO measurements and measurements of the effluent characteristics, but rather, on the values of the nitrification rate calculated continuously and in real time, thus allowing to adopt timely intervention measures in the case of malfunctioning of the process associated with changes in the plant operating conditions, eventual inhibition phenomena or other external factors. A simplified algorithm was defined to use the output of the titrimeter as a new input for the supervision system in order to optimize the entire aeration system operation. Starting from influent ammonia load, required ammonia removal efficiency and estimated nitrification rate, the DO concentration that needs to be maintained in the aerobic tank for nitrification is evaluated according to the following equation:

$$\frac{dN}{dt}_{\text{titrimeter}} \frac{DO_{AER}}{DO_{AER} + K_0} \frac{N}{N + K_N} = (N_{in} - N)\, Q_{in}$$

where:

- $dN/dt_{\text{titrimeter}}$: maximum nitrification rate (the output of the prototype, mgN-NH_4^+ h^{-1});
- DO_{AER}: dissolved oxygen concentration in the aerobic tank, mg O_2 L^{-1};
- K_O and K_N: semisaturation constants for oxygen and ammonia, mg O_2 L^{-1} and mg N-NH_4^+ L^{-1};
- N_{in} and N: influent and effluent ammonia concentration, mgN-NH_4^+ L^{-1};
- Q_{in}: influent flow, L h^{-1}.

The algorithm have been used to simulate the DO concentration to be applied as set point in Calice WRRF nitrification tank.

The final algorithm that consider the contribution of the ammonia uptake is reported in the following equation:

$$d\frac{(N - NH_4^+)}{dt}\Bigg|_{\substack{\text{titrimetro} \\ \text{"massimo"}}} \cdot \frac{DO_v}{DO_v + K_O} \cdot \frac{N_{out}}{N_{out} + K_N} = \left(\left(N_{in} - N(f(T))_{up-take}\right) - N_{out}\right) \cdot Q_{in}$$

Where

$$K_N = 0,016 \frac{MM_N}{MM_{NH_4^+}} \left(\frac{e^{\frac{6334}{(273+T)}} + 10^{pH}}{10^{pH}}\right)$$

and the ammonia uptake was estimated as a function of the temperature (strictly related to the solid concentration) according to the following empirical equation:

$$N_{up-take} = -0,0299 * T + 2,59525$$

References

Caretti C, Mannucci A, Munz G, Neri S, Daddi D (2015) A continuous online titrimeter prototype for biological nitrification control in an urban wastewater treatment plant. In: Proceedings of nutrient removal and recovery 2015, Gdanks, Poland, May 2015

Munz G, Lubello C, Oleszkiewicz JA (2011) Factors affecting the growth rates of ammonium and nitrite oxidizing bacteria. Chemosphere 83(5):720–725

Rosso D, Stenstrom MK (2005) Comparative economic analysis of the impacts of mean cell retention time and denitrification on aeration systems. Wat Res 39(16):3773–3780

Hong S, Choi I, Lim BJ, Kim H (2012) A DO- and pH-based early warning system of nitrification inhibition for biological nitrogen removal processes. Sensors 12:16334–16352

Assessing Potential Savings at WWTP Using Dynamic Simulation

E. Remigi[1(✉)], A. Lynggaard-Jensen[2,3], P. Andreasen[2], E. Fontenot[4], and J. Christensen[5]

[1] DHI, Agern Allé 5, 2970 Hørsholm, Denmark
[2] DHI, Finlandsgade 10, 8200 Århus, Denmark
[3] Aarhus Vand A/S, Bautavej 1, 8210 Århus, Denmark
[4] DHI, 141 Union Blvd Ste 250, Lakewood, CO 80228, USA
[5] Urbana Champaign Sanitary District, Urbana, IL 61803, USA

Abstract. This work illustrates the first phase of this collaboration which focused on a model-based approach to assess the feasibility and plan level outcomes for control of the nitrification tower pumping station and chemical feed rates for disinfection (identified as the plant operations with the biggest potential for cost saving).

Keywords: Modelling · Simulation · Cost · Saving · Scenarios

1 Introduction

Urbana & Champaign Sanitary District (UCSD) and DHI Water & Environment, Inc. (DHI) initiated a collaborative effort aimed at overcoming current evident bottlenecks in operations and ideally implementing a DIMS.CORE Real-Time-Control for the Urbana wastewater treatment facility, characterized by a monthly average influent flow rate ranging from 45,000 to 70,000 m^3/d (12.0 to 18.5 MGD) and an average BOD load of 12,210 kg/d (data of 2014).

University of Illinois students in the area result in abrupt variations of the load: the lowest (157,000 PE) and the highest organic load (275,000 PE) occurred in June and in September respectively.

2 Materials and Methods

Operational data for the trickling filter, activated sludge and disinfection stages were used to identify possible bottlenecks and to set up and calibrate a WEST (MIKE Powered by DHI) model of the entire plant (Fig. 1).

For the baseline scenario, current operations and control strategy employed at the plant were inputted into the model and aeration, pumping and chemical yearly costs evaluated.

The main bottleneck identified upon an initial survey of the facility (and confirmed by the dynamic simulations) was the large volumes of trickling filter (TF) effluent that
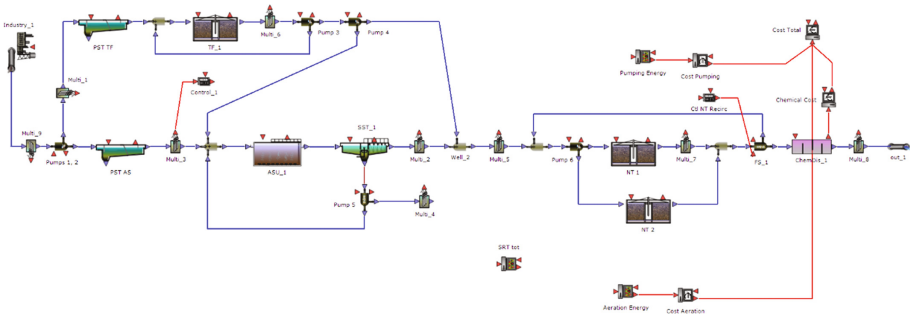
Fig. 1. WEST layout for the Urbana WWTP

are pumped to the activated sludge (AS) tanks – which in turns result in high loads on the clarifiers and sludge carry-over to the nitrification towers (NT).

Three scenarios were tested:

1. "Nitrification towers operation and control": to replace the fixed-rate pumps currently utilized, by a flow paced pumping logic based on VFDs and control of recycle;
2. "Disinfection operation and control": to regulate the dosage of hypochlorite based on the target bacterial count in the effluent;
3. "Change of aeration control, return sludge control and operation of activated sludge plant": to divert the TF effluent directly to the NT (by-passing the AS stage); to control aeration based on combined nitrate and ammonia concentrations measurements in the effluent.

3   Results and Discussion

Selected results of the model calibration for year 2014 (baseline scenario) are shown in Figs. 2, 3 and 4: given the primary goal of designing a WEST model that served as desktop calculator, the fit between measured dataset and simulated outputs was considered satisfactory.
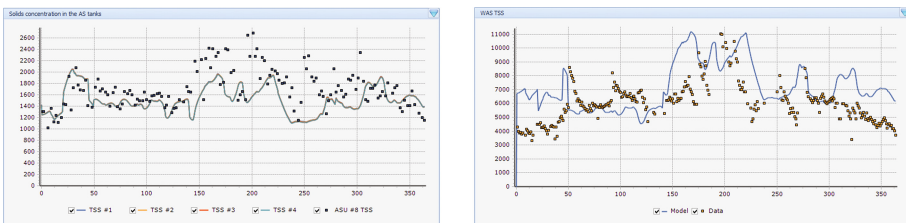
Fig. 2. Solids concentration (g/m3) in the AS tanks (left) and in the waste activated sludge (right): simulation vs. year 2014 dataset
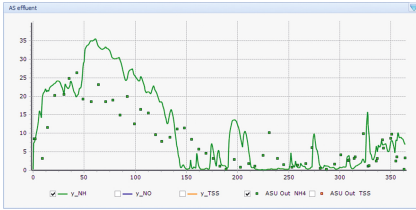
Fig. 3. Ammonia concentration (g/m3) in the AS effluent: simulation vs. year 2014 dataset
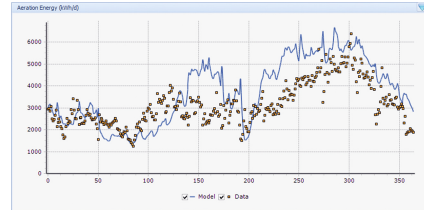
Fig. 4. Aeration energy (kWh/d): simulation vs. year 2014 dataset

A control strategy was developed for scenario 1 and simulated in WEST to reduce the recycle rates and pumping volume to the NT process units, whereby the four pumps currently in operation would each be equipped with VFDs, capable of operating the pumps between turndown ratios of 0.8 and 1.0.

In order to evaluate the change in energy consumption at the NT pumping station, rather than using an average daily flow rate, a more resolved representation of the flows at the treatment plant was used by applying typical diurnal patterns for dry- and wet weather flow.

In the scope of scenario 2, it was proposed that the sodium hypochlorite dosing rate be based on the combination of retention time and chlorine concentration rather than just on a fixed concentration.

Due to the relatively high dosage which is currently applied, results show that a 20–30% reduction in sodium hypochlorite and sodium bisulphite dosage could be achieved. The implementation of active control to adjust the chemical feed rates for disinfection could be controlled by DIMS.CORE. a software platform which can be integrated with sensor equipment and SCADA Systems to achieve integrated control.

The scenario 3 analysis focused on alternate operational strategies for the control of aeration in the activated sludge process units, return activated sludge handling, and recycle of effluent from the tricking filter to the activated sludge process unit – the latter to be completely inactivated so that all effluent from the trickling filters is directed to the nitrification towers, thereby reducing energy for this pumping as well as for the return sludge pumping from the secondary clarifiers.

The aeration control in the AS process is altered: while the first (no. 1) and last (no. 4) sections of the tanks are controlled in the same manner as in the baseline status model, the DO set-point in the two middle sections (no. 2 and 3) is controlled to reduce nitrate and to minimize ammonia concentration respectively.

Next to the reduction in energy consumption for pumping, this scenario could achieve a reduced demand for the blower operation as well.

Results for the baseline operation and proposed scenarios are summarised in Table 1.

Table 1. Simulated yearly costs (USD) for aeration, dosage of sodium hypochlorite for disinfection and for pumping

	Aeration	Chemicals	Pumping	Total
Baseline	$ 100,200	$ 66,100	$ 376,700	$ 543,000
Scenario #1	$ 100,200	$ 66,100	$ 239,700	$ 406,000
Scenario #2	$ 100,200	$ 53,100	$ 376,700	$ 530,000
Scenario #3	$ 108,600	$ 66,100	$ 319,500	$ 494,200
Composite	$ 108,600	$ 53,100	$ 182,500	$ 344,200

4   Conclusions

The desktop study and results from the WEST simulations show a significant potential to achieve reductions in energy consumption and chemical usage at the WWTP.

From the tested combination of scenarios, energy consumption and costs associated with aeration and pumping were predicted to be increased by 8% and reduced by almost 52% respectively; while costs associated with chemical usage for disinfection to be reduced by 20%.

The slight increase in aeration cost is primarily the result of the higher loading to the AS process units; the remarkable reduction in pumping cost is due to the effect of using VFD logic and limiting the recycle over the NT, combined to the reduction in RAS sludge pumping and pumping of the TF effluent to the AS process unit.

Effect of Sludge Retention Time on the Efficiency of Excess Sludge Reduction by Ultrasonic Disintegration

N. Lambert[1(✉)], P. Van Aken[1], I. Smets[2], and R. Dewil[1]

[1] Department of Chemical Engineering,
Process and Environmental Technology Lab, KU Leuven,
J. de Nayerlaan 5, 2860 Sint-Katelijne-Waver, Belgium
[2] Department of Chemical Engineering, Bio- & Chemical Systems Technology,
Reactor Engineering and Safety, KU Leuven Chem&Tech, KU Leuven,
Celestijnenlaan 200F Bus 2424, 3001 Heverlee, Belgium

Abstract. Excess sludge reduction in activated sludge plants can, inter alia, be achieved by the integration of sludge disintegration technology in the recycle stream of activated sludge treatment plants. In previous research by Lambert et al. (2016), a long-term experimental study of 120 days at a biodiesel production plant demonstrated that ultrasonic sludge disintegration can result in a substantial reduction of waste sludge of about 45%, and this at a relatively low specific energy. Moreover, it was revealed from this pilot experiment that the efficiency of the excess sludge reduction, indicated as SRE (Sludge Reduction Efficiency), increases when the activated sludge plant is operated at a higher sludge retention time (SRT). This is an important finding, because this would mean that the ultrasonic technology can be operated more cost efficiently at a higher sludge retention time. To confirm this finding and to give a deeper insight into the underlying mechanisms and long-term effects that promote the excess sludge reduction, lab-scale aerobic digestion experiments were performed. Both the endogenous respiration rate and the VSS concentration were monitored during the 30 days' experimental period, and could give more information about the fate and the biodegradation of the particulate COD in activated sludge. Modeling the batch tests indicated a higher endogenous residue decay rate (b_{XE}) and a clear instantaneous change in the active biomass concentration, of nearly 50%, which can be directly assigned to the ultrasonic pre-treatment. This has ultimately led to a more thorough VSS reduction at the end of the digestion period.

Keywords: Ultrasonic disintegration · Activated sludge · Aerobic digestion · Endogenous residue

1 Introduction

Activated sludge systems are widely used for the treatment of industrial and municipal wastewater worldwide. They combine a high purification efficiency and robustness with relatively low treatment costs (Mohammadi et al. 2011; Tamis et al. 2011; Yang et al. 2011). One drawback, however, is the high production of excess sludge

(Mohammadi et al. 2011; Lee et al. 2009; Zhang et al. 2012). It is generally accepted that in activated sludge processes an increased sludge age (SRT) is associated with a decreased net sludge production. This phenomenon is generally interpreted as a result of endogenous respiration processes (Van Loosdrecht and Henze 1999). Another approach that is currently under investigation is the application of sludge disintegration methods to effectively decrease the excess sludge production at the source by the integration of sludge disintegration technology in the recycle stream of activated sludge treatment plants. Different sludge disintegration techniques were described and thoroughly investigated in the scientific literature of the last decennia, including ozonation and ultrasonic sludge disintegration (US) (Wei et al. 2003; Mahmood and Elliott 2006). Still there are some key questions unanswered and moreover there is a lack of knowledge about the link between the energy input or chemical dosage and the resulting excess sludge reduction. To investigate these unanswered questions, long-term pilot experiments on a relevant scale could give a deeper insight into the underlying mechanisms and long-term effects that promote the excess sludge reduction.

In previous research by Lambert et al. (2016), a long-term experimental study of 120 days was carried out at a biodiesel production plant and demonstrated that ultrasonic sludge disintegration can result in a substantial reduction of waste sludge. The pilot scale installation consists of two fully automated sequencing batch reactors (SBRs), operated in parallel (BIO1 and BIO2), and each with a total active volume of 1 m^3. BIO1 is a regular SBR reactor, whereas BIO2 is equipped with a recirculation system to enable ultrasonic (US) treatment of (a part of) the thickened sludge. The wastewater at this plant contains a high concentration of organics (tCOD = 9284 − 10402 mg O$_2$/L = sum of the soluble and particulate COD), but almost no particulate matter. The latter ensured that there was no or only limited build-up of inert particulate COD (X_U) in the activated sludge. The long-term pilot experiment at the biodiesel production plant showed that a significant reduction in the excess sludge production could be realized, as shown in Table 1. Moreover, it was also revealed that the efficiency of the excess sludge reduction, indicated as SRE (Sludge Reduction Efficiency) in Table 1, increases at higher sludge retention time values (SRT). This is an important finding, because this would mean that the ultrasonic treatment can be operated more cost efficiently at higher sludge retention times. The reason for this increased efficiency is probably linked to the underlying mechanism of the ultrasonic treatment. In our hypothesis, the ultrasonic disintegration and solubilization induce not only the instantaneous formation of soluble biodegradable and inert COD, but also an extensive disintegration of the active biomass, causing the formation of non-active particulate/colloidal COD. Consequently, a shift of active biomass (X_{BH} and X_{BA}) into an endogenous residue (X_E) and slowly biodegradable particulate material (X_S) will occur, as proposed in the death regeneration model of Dold et al. (1980). In addition, there is also the suspicion that the inert particulate fraction of the activated sludge (X_E and X_U), will become partially more biodegradable by the ultrasonic treatment. After the ultrasonic pre-treatment, this shift in particulate COD fractions will probably result in a faster and more extensive Volatile Suspended Solids (VSS) reduction, in comparison with untreated activated sludge samples.

Table 1. Overview of the most important operational parameters of the pilot experiments at the Biodiesel production plant

Case studies	SRT (d)	$P_{X,VSS}$ (g VSS/d)	F/M (g COD/g DS)	Y_{obs} measured (g COD/g COD)	SRE[a] (%)
BIO1 biodiesel (Run1)	11.0	161	0.26	0.537	
BIO2 + US biodiesel (Run1)	11.0	175	0.20	0.457	**15%**
BIO1 biodiesel (Run2)	20.6	120	0.26	0.395	
BIO2 + US biodiesel (Run2)	21.8	123	0.20	0.284	**28%**
BIO1 biodiesel (Run3)	42.2	33	0.09	0.366	
BIO2 + US biodiesel (Run3)	43.7	35	0.10	0.202	**45%**

[a]$SRE(\%) = \left(1 - \frac{Y_{obs,treated}}{Y_{obs,control}}\right).100$

2 Materials and Methods

To substantiate the suspicions mentioned above, long-term experiments on laboratory scale can provide a decisive answer. During these long-term respirometric digestion experiments the biodegradility of the inert fraction which is present in the activated sludge can be monitored by means of a follow-up of the MLSS and VSS concentration and the endogenous respiration rate (b_{XB}) as a function of the time. In our research two identical 2 L samples of activated sludge, of which one was treated via ultrasonic disintegration at a specific energy of 16667 kJ/kg DS, are monitored during a 30-day experimental period. Aerobic conditions are maintained during the whole experimental period by controlling the air flow based on the oxygen concentration in the respiration vessel. At an upper limit of 4 mg O_2/L the air pump was switched off and at the lower limit of 2 mg O_2/L the air pump was switched back on. On a regular basis, both the ML (V)SS concentration and the total COD (tCOD) concentration were analyzed. In this way, the decrease of de VSS concentration can be monitored in time. For the determination of the endogenous decay rate from the experimental data of the aerobic digestion experiments, two analysis methods can be used, based on monitoring the change of either the VSS or the oxygen uptake rate (OUR) with time (Ramdani et al. 2010). In both analysis methods, there should be made an estimate of the biomass concentration $X_B = X_{BH} + X_{BA}$. However, the X_B determination requires an assumption of the endogenous residue fraction, f_P. In our experimental setup, we set the inert endogenous fraction equal to 0.20 as was determined by Marais and Ekama (1976). The procedure of both analysis methods is derived from the work of Ramdani et al. (2010).

For the VSS based method the following equation can be used to determine the decay rate of the active biomass (b_{XB}) and the decay rate of the endogenous residue (b_{XE}) during the aerobic digestion and to estimate the initial active biomass concentration ($X_{B(0)}$). The units of $X_{B(0)}$ in the next equation are expressed in mg VSS/L.

$$VSS_{(t)} = VSS_u + \left(1 - f_p\right).X_{B(0)}.e^{-b_{XB}.t} + \left(f_p\right).X_{B(0)}.e^{-b_{XE}.t} \tag{1}$$

with,

VSS$_{(t)}$ VSS concentration at aerobic digestion time t (g/L).

VSS$_u$ Ultimate value of VSS concentration of the digested sludge (g/L). The ultimate VSS concentration will be reached when the active biomass concentration is negligibly small.

t   Aerobic digestion time (days).

In the OUR-based method, derived from the work of van Haandel et al. (1998), a distinction is made between the oxygen uptake of the heterotrophs (OUR$_H$) and autotrophs (OUR$_A$). Indeed, it is true that during the endogenous aerobic digestion process, besides the COD release in the form of slowly biodegradable substrate (X$_S$), also nitrogen is released. Therefore, it must also be taken into consideration that autotrophic biomass activity will occur. Oxygen will be consumed for the execution of the nitrification of ammonium (S$_{NH}$) to nitrate (S$_{NO}$). The autotrophic oxygen uptake rate linked to biomass decay can be easily calculated when the nitrogen content of the biomass is known. It is assumed that biomass contains approximately 0.07 to 0.1 mg N/mg COD (Marais and Ekama 1976). This constant will be further abbreviated in the text as f$_N$. In our calculations, we use a f$_N$ value of 0.07. Knowing that there is a stoichiometric demand of 4.57 mg oxygen per mg nitrogen that is converted during the nitrification process (Courchaine 1968), the following OUR equations can be written:

$$OUR_{H+A(t)} = (1 + 4.57 f_N) \cdot \left(\left[(1 - f_p - \boldsymbol{f_{XS}}) \cdot b_{XB} \cdot X_{B(0)} \cdot e^{-b_{XB} \cdot t} \right] + \left[(f_p) \cdot b_{XE} \cdot X_{B(0)} \cdot e^{-b_{XE} \cdot t} \right] \right) \quad (2)$$

with,

f$_{XS}$ Fraction of slowly degradable COD. To calculate the fraction of active biomass (f$_{XB}$) after ultrasonic disintegration, the solubilization of X$_B$ into X$_S$ should also be taken into account, making f$_{XB}$ = (1−f$_p$−f$_{XS}$).

3   Results and Discussions

The VSS-based and OUR-based method were applied to the experimental data that were gathered during the 30-days aerobic digestion trial to calculate both the decay rate of the active biomass (b$_{XB}$) and endogenous residue (b$_{XE}$) and to estimate the initial biomass concentration (X$_{B(0)}$). This was done for both the pre-treated and non-treated reactor, by fitting the simulated volatile suspended solids and oxygen uptake rate to measured data. The experimental and modelled results of both aerobic digestion reactors can be seen in Fig. 1. Modeling the batch tests indicated first-order endogenous residue decay rates of 0.012 d^{-1} and 0.021 d^{-1} for the untreated batch test and the pre-treated batch aerobic digestion, respectively. The latter then also confirmed the fact that the efficiency of the excess sludge reduction, as a result of the ultrasonic disintegration, is served by a longer sludge retention time in the activated sludge system. In addition, a clear change in the active biomass concentration, X$_B$, could be established, wherein the ultrasonic pre-treatment leads to an instantaneous decrease of the biomass
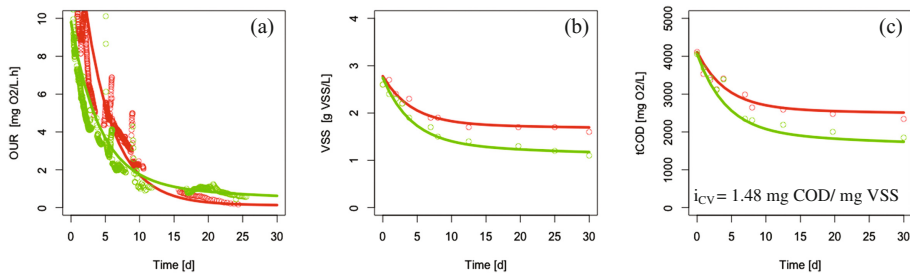
Fig. 1. Experimental and modelled OUR (a) VSS (b) and total COD (tCOD) data (c) during the aerobic digestion of activated sludge without any pre-treatment of the activated sludge (marked in red) and with ultrasonic pretreatment at a specific energy level of 16667 kJ/kg DS (marked in green) (Color figure online)

concentration of nearly 50%. Eventually it was also demonstrated that further VSS-reduction can be achieved by the ultrasonic pre-treatment of the activated sludge, which translates into a lower ultimate VSS concentration (VSS_u), of 1.1 g VSS/L instead of 1.7 g VSS/L in the untreated digestion reactor.

When the experimental endogenous OUR levels of both digestion reactors are compared (Fig. 1(a)), it can be concluded that in the initial phase of the digestion period, the endogenous OUR of the ultrasonic treated activated sludge is significantly lower than that of the non-treated reactor. This finding is related to the lower active biomass concentration at the start of the aerobic digestion, as a direct result of the instantaneous ultrasonic degradation. After a period of 10 days of aerobic treatment, there is a clear shift in OUR level between both digestion reactors. The endogenous OUR level of the treated reactor was becoming higher than that of the non-treated reference reactor. This phenomenon can be explained by the increased biodegradability of the inert/endogenous fraction of the ultrasonic treated activated sludge sample in comparison with that of the non-treated sludge. As a result of the ultrasonic treatment, more biodegradable material is available in the second phase of the digestion experiment, with an increased OUR as an obvious consequence.

4   Conclusions

In the past, several researchers have demonstrated that the inert particulate fraction of activated sludge is nevertheless biodegradable, but is characterized by a very slow degradation rate. Based on our own experimental data of long-term aerobic digestion experiments, the suspicion is confirmed that the inert particulate COD contained in activated sludge (e.g. endogenous residue, X_E) becomes more/faster biodegradable by carrying out an ultrasonic pre-treatment of the activated sludge. The net decay rate of the endogenous residue will double by the use of an ultrasonic pre-treatment at a relatively low specific energy level (<20000 kJ/kg DS). From the performed scientific research it can also be presumed that combining biological wastewater treatment with ultrasonic sludge disintegration of a part of the return activated sludge, will benefit from a longer

SRT. From previous research on pilot scale at a biodiesel production plant by Lambert et al. (2016), it could be demonstrated that the efficiency of the excess sludge reduction by ultrasonic pre-treatment (expressed in terms of SRE) increases with an increasing SRT, although this was not expected in advance. Initially it was thought that only the instant changes due to the ultrasonic pre-treatment had an effect on the excess sludge reduction. Instant degradation caused by the ultrasonic treatment ensures solubilization and disintegration of a part of the volatile suspended solids. During this process, active biomass (X_B) is converted into readily, slowly biodegradable and inert COD (S_S, X_S and S_i). With the present knowledge it appears that not only the instantaneous effects of the ultrasonic treatment should be taken into account. Also the rather slow processes, such as the degradation of the inert particulate fraction, are affected by the ultrasonic pre-treatment, and have a non-negligible effect on the final waste sludge reduction. The experimental results of the aerobic digestion experiments on laboratory scale, performed in the context of this paper, confirm this assertion and provide more insight into the underlying mechanism of ultrasonic pre-treatment. This knowledge is invaluable for developing a mechanistically inspired model for ultrasonic sludge disintegration that is compatible with existing Activated Sludge Models (ASM's).

References

Courchaine RJ (1968) Significance of nitrification in stream analysis: effects on the oxygen balance. J Water Pollut Control Fed 40(5):835–847

Dold PL, Ekama GA, Marais G (1980) A general model for the activated sludge process. Prog Water Technol 12(6):47–77

Lambert N, Van Eyck K, Feremans J, Van den Broeck R, Smets I, Dewil R (2016) Ultrasonic sludge disintegration in nutrient deficient activated sludge wastewater treatment plants. In: 2nd IWA conference on holistic sludge management, Malmö, Sweden, 7–9 June 2016

Lee SH, Chung CW, Yu YJ, Rhee YH (2009) Effect of alkaline protease-producing Exiguobacterium sp. YS1 inoculation on the solubilization and bacterial community of waste activated sludge. Biores Technol 100(20):4597–4603

Mahmood T, Elliott A (2006) A review of secondary sludge reduction technologies for the pulp and paper industry. Water Res 40(11):2093–2112

Marais G, Ekama GA (1976) The activated sludge process part I-steady state behaviour. Water SA 2(4):164–200

Mohammadi AR, Mehrdadi N, Bidhendi GN, Torabian A (2011) Excess sludge reduction using ultrasonic waves in biological wastewater treatment. Desalination 275(1):67–73

Ramdani A, Dold P, Déléris S, Lamarre D, Gadbois A, Comeau Y (2010) Biodegradation of the endogenous residue of activated sludge. Water Res 44(7):2179–2188

Tamis J, Van Schouwenburg G, Kleerebezem R, van Loosdrecht MCM (2011) A full scale worm reactor for efficient sludge reduction by predation in a wastewater treatment plant. Water Res 45(18):5916–5924

van Haandel AC, Catunda PF, Araujo LDS (1998) Biological sludge stabilisation Part 1: Kinetics of aerobic sludge digestion. Water SA 24(3):223–230

Van Loosdrecht MC, Henze M (1999) Maintenance, endogeneous respiration, lysis, decay and predation. Water Sci Technol 39(1):107–117

Wei Y, Van Houten RT, Borger AR, Eikelboom DH, Fan Y (2003) Minimization of excess sludge production for biological wastewater treatment. Water Res 37(18):4453–4467

Yang SS, Guo WQ, Zhou XJ, Meng ZH, Liu B, Ren NQ (2011) Optimization of operating parameters for sludge process reduction under alternating aerobic/oxygen-limited conditions by response surface methodology. Biores Technol 102(21):9843–9851

Zhang X, Tian Y, Wang Q, Chen L, Wang X (2012) Heavy metal distribution and speciation during sludge reduction using aquatic worms. Biores Technol 126:41–47

Performance Investigation of the Primary Clarifier- Case Study of Castiglione Torinese

S. Borzooei[1(✉)], M.C. Zanetti[1], E. Lorenzi[2], and G. Scibilia[2]

[1] DIATI, Politecnico di Torino, Torino, Italy
[2] SMAT (Turin Metropolitan Water Society), Torino, Italy

Abstract. In this study, to investigate removal efficiency of the primary clarifier at Castiglione Torinese water resource recovery facility (WRRF), 20 consecutive day sampling campaign was conducted. The data are partitioned per weather conditions and relations between influent total chemical oxygen demand (COD_T), soluble chemical oxygen demand (COD_s), total suspended solids (TSS), ammonium (NH_4) and phosphate (PO_4) concentrations and their corresponding removal efficiencies are investigated. Significant differences in removal efficiencies between various parameters and unexpected increasing of concentrations of COD_s, NH_4, PO_4 are observed. The analysis revealed the possibility of establishment of empirical relations between influent concentrations and their corresponding removal efficiencies of the primary clarifier in Castiglione Torinese in case of availability of high frequency data. To reason out increasing of COD_s, NH_4, PO_4 concentrations, initially the impact of surface overflow on removal efficiencies are studied. The results show that removal efficiencies are not notably influenced by changing of the surface overflow. Secondly, manipulating the sludge pumping patterns, the effect of primary sludge blanket height (SBH) on removal efficiencies are analysed and considering the available data frequency, conclusions were drawn. Finally, according to findings and detail specifications of sewer system and the treatment plant, hypotheses were proposed for justification of increasing concentrations.

Keywords: Primary clarifier · Removal efficiency · Sludge blanket height

1 Introduction

Considering highly dynamic performance and complex mechanisms involved in primary clarifiers functionality, limited operational control strategies, optimization techniques and quantitative performance measures are available about these important treatment units (Lessard and Beck 1988). In this study, to evaluate the performance of the primary clarifier at the Castiglione Torinese WRRF, data collected in sampling campaign conducted from September 26, 2016 till October 21, 2016 were investigated. Using the data partitioning methodology proposed in Borzooei et al. (2016), the primary clarifier data were partitioned per weather conditions and correlations between influent total chemical oxygen demand (COD_T), soluble chemical oxygen demand (COD_s), TSS, ammonium (NH_4) and phosphate (PO_4) concentrations and their corresponding removal efficiencies were investigated. Considering the wet weather events

during sampling period, the impact of surface overflow rate on primary clarifier's performance was scrutinized and conclusions were drawn accordingly. Further, the impact of sludge blanket height (SBH) and specifications of sewer system and Castiglione plant on removal efficiencies of increasing concentrations were considered and two main hypotheses were proposed for reasoning of increasing concentrations.

2   Materials and Methods

2.1   Castiglione Torinese Water Resource Recovery Facility

Castiglione Torinese WRRF is in about 11 km Northeast of Turin, capital of Piemonte, Northwest of Italy. The plant is operating to treat 590,000 m^3/d of combined municipal and industrial wastewater, corresponding to organic load of 2.1 M of equivalent inhabitants. The water line is made of four major modules each consists of two primary clarifiers and anoxic tanks, following by six aeration tanks and secondary clarifiers which is the typical Modified Ludzack-Ettinger (MLE) activated sludge systems with primary clarifier, as can be seen in Fig. 1. In this study, since the specifications of primary clarifiers in different modules are the same, one of the sloping bottom circular primary clarifiers (CA3006) located in third module of the plant was considered (Fig. 1). CA3006 clarifier physical specifications are tabulated in Table 1.

Fig. 1. Castiglione Torinese WRRF and CA3006 primary clarifier (Adopted from SMAT)

Table 1. Detail physical Properties of CA3006 primary clarifiers

Name	Unit	value
Diameter	m	52
Surface area	m^2	2123
Water depth at center	m	5
Water depth at sidewall	m	2.6
Volume	m^3	8067

2.2   Data Collection and Sampling Campaign

In order to investigate removal efficiency of primary clarifier, sampling campaign was organized on 20 consecutive days excluding weekends from September 26, 2016 till October 21, 2016. During the sampling campaign period, grab samples were collected from the influent of the CA3006 primary clarifier at 9:00 am and accounting for the average hydraulic retention time of the clarifier which is about 2.5 h. during dry weather flow condition, grab samples were taken from effluent of the clarifier at 11:30 am. The samples were analyzed by an accredited lab to measure COD_T, COD_S, PO_4, NH_4 and TSS in accordance with IRSA methodology (Istituto di ricerca sulle acque). Influent flowrate of the primary clarifier was continuously measured with 5 min interval, by ultrasonic flowmeters installed in the entrance of each module of the plant. For calculation of the actual hydraulic retention time, average of the online flowrate measurements within the 3 h. period of the sampling (From 9:00 am to 12:00 pm) was considered for each day. The amount of primary sludge collected from the clarifier was also measured by monitoring the sludge pumping pattern.

2.3   Precipitation Rate

For the comprehensive description of methods implemented for obtaining the precipitation rates and data partitioning for Castiglione Torinese plant, Borzooei et al. (2016) should be consulted. Average influent concentrations of primary clarifiers in different weather condition are tabulated in Table 2.

Table 2. Average concentrations of influent of the primary clarifier during sampling campaign in different weather conditions

	COD_T	TSS	COD_S	NH_4	PO_4
All data	295.35	175.33	41.45	27.73	1.43
Dry weather	247.29	129.75	41.57	27.06	1.35
Wet weather	407.50	274.10	41.17	29.30	1.65

3   Results and Discussions

The data collected from sampling campaign were analyzed and removal efficiency of primary clarifier was calculated from Eq. 1:

$$\text{Removal efficiency}(\%) = (\frac{C_{in} - C_{out}}{C_{in}}) \cdot 100 \tag{1}$$

Where C_{in} and C_{out} are, the concentrations measured in influent and effluent of the clarifier respectively.

3.1   Descriptive Statistics of Removal Efficiencies

Descriptive statistical analysis was conducted on the data set consisting of 20 daily grab samples, of which 14 dry weather and 6 wet weather days. Maximum (Max), Minimum (Min) and mean of the removal efficiencies were determined as tabulated in Table 3.

Table 3. Descriptive statistics of removal efficiencies for the primary clarifier in Castiglione Torinese from September till October 2016

		COD_T removal	TSS removal	CODs removal	NH_4 removal	PO_4* removal
All days	Min	14.83	17.91	−21.62	−39.15	−75.21
	Mean	36.38	56.58	−4.84	−12.82	−25.17
	Max	75.49	85.49	14.00	11.62	15.17
Dry weather	Min	13.11	17.91	−21.62	−39.15	−75.2
	Mean	28.09	41.89	−7.66	−17.02	−25.95
	Max	53.95	68.74	14.00	5.14	−9.32
Wet weather	Min	41.69	56.58	4.65	−20.99	−29.73
	Mean	52.90	77.18	5.00	−0.68	−14.58
	Max	75.50	85.49	5.71	11.62	15.17

*The −179.1% removal efficiency recorded on 06/10/2016 was recognized as the outlier.

3.2   Investigation the Relations Between Removal Efficiencies and Influent Concentrations

To study the impact of influent concentrations on primary clarifier removal efficiencies, scatter plots of influent concentration of COD_T, TSS, CODs, NH_4 and PO_4 versus corresponding removal efficiencies were prepared. Linear regression analyses were performed to generate the line of best fit and R^2 values were estimated. Table 4 demonstrates the linear regression results considering total data set, dry and wet weather data. These observations can highlight the possibility of establishment of empirical relations between influent concentrations and their corresponding removal efficiency for primary clarifier in Castiglione Torinese in case of availability of high frequency data.

3.3   Study the Impact of Surface Overflow Rate on Removal Efficiencies

For studying the impact of surface overflow rate on removal efficiencies of the primary clarifier in Castiglione Torinese, scatter plots of COD_T, TSS, COD_s, NH_4 and PO_4 removal efficiencies, versus surface over flowrates were prepared (Fig. 2a and b). As can be seen in Fig. 2a and b, surface over flowrates of primary clarifier were frequently recorded between 1.5 to 1.8 and for the 3 heavy rain periods between 2.1 to 2.5. Demonstrated in Fig. 2a, most of the recorded removal efficiencies are between 10–80%. For increasing concentrations (COD_s, NH_4 and PO_4), most of the recorded removal efficiencies are between −45 to15% as can be seen in Fig. 2b. Although due to

Table 4. The linear regression coefficients (Y = a.X + b) for the correlations encounter between influent concentrations and corresponding removal efficiencies for the primary clarifier in Castiglione Torinese from September till October 2016

	Y	X	a	b	R^2
Total data	COD_T removal	Influent COD_T	0.16	−10.03	0.8
	TSS removal	Influent TSS	0.22	14.82	0.75
	NH_4 removal	Influent NH_4	2.73	−89.14	0.58
	COD_s removal	Influent CODs	0.39	−20.37	0.07
	PO_4 removal	Influent PO_4	110	−190.25	0.68
Dry data	COD_T removal	Influent COD_T	0.25	−32.74	0.7
	TSS removal	Influent TSS	0.4	−8.65	0.74
	NH_4 removal	Influent NH_4	2.67	−89.78	0.57
	COD_s removal	Influent CODs	0.51	−27.46	0.15
	PO_4 removal	Influent PO_4	53.45	−105.48	0.38
Wet data	COD_T removal	Influent COD_T	0.11	11.3	0.79
	TSS removal	Influent TSS	0.12	41.63	0.68
	NH_4 removal	Influent NH_4	2.73	−89.14	0.58
	COD_s removal	Influent CODs	−0.13	10.4	0.98
	PO_4 removal	Influent PO_4	2.07	−64.8	0.56

scattered nature of the points in both Fig. 2a and b, drawing a solid conclusion about how changes in the surface overflow rates are associated with changes in the removal efficiencies is not possible, surprisingly higher removal efficiencies can be observed in days with higher surface overflows.

3.4 Studying the Impact of Sludge Blanket Height (SBH) on Removal Efficiency of Increasing Parameters

With the assumption that primary sludge blanket retention time (SBRT) may influence the removal efficiencies of different parameters and in particular increasing parameters (COD_s, NH_4 and PO_4) in primary clarifier, for a short period of time, changing the primary sludge pumping rates, SBH was measured and the results were studied with removal efficiencies recorded in corresponding days. It is assumed also that an average SBH in a day can be positively correlated with SBRT.

Daily SBH was calculated by averaging two readings in the day. Recorded data on days with transition condition from one pumping pattern to another were not considered. The zero SBH values recorded on 06/10/2016 were recognized as the outlier. The results can be seen in Table 5. It is expected that only two times measurements in a day impose high inaccuracies on the obtained results; however, regardless of recorded SBH values increasing of the pumping time from scenario I to III decreases SBRT.
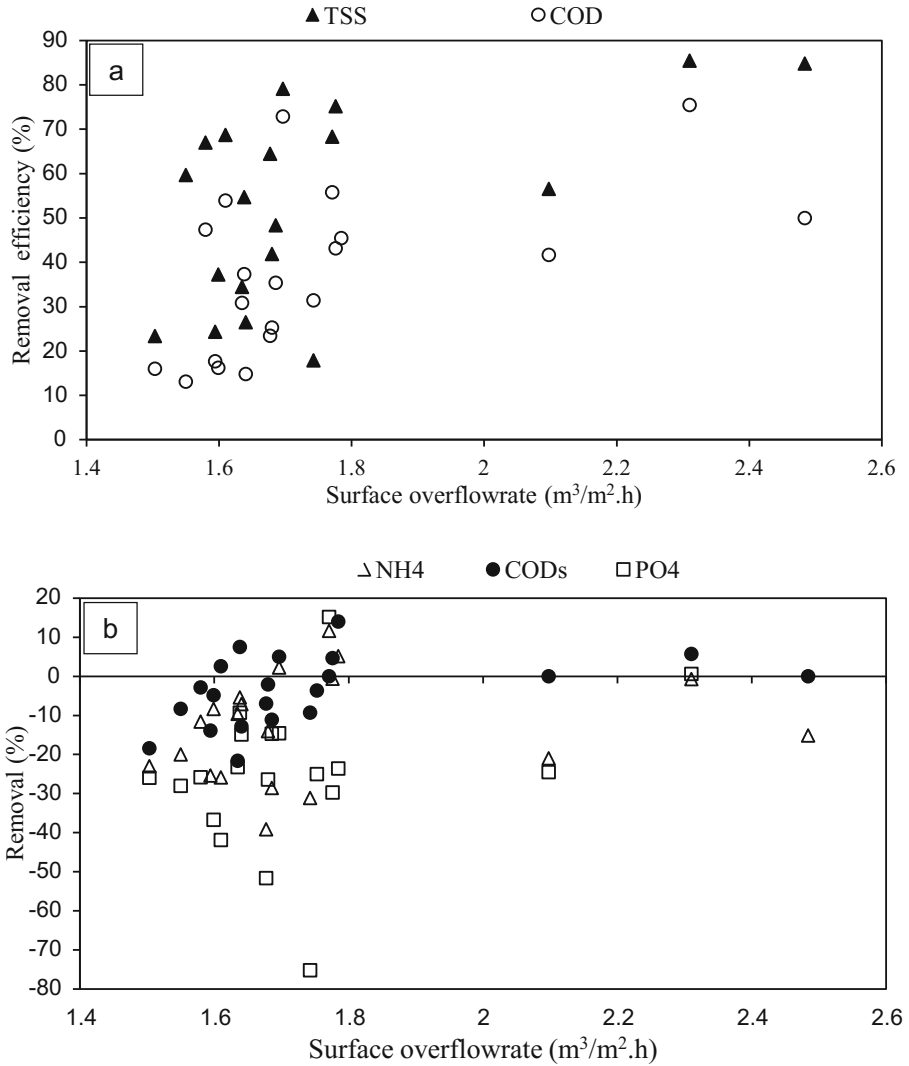
Fig. 2. Removal efficiencies versus surface overflow rates

Table 5. Pumping patterns, daily average SBH and increasing concentrations removal efficiencies

Scenario	Average SBH (cm)	NH$_4$ removal (%)	CODs removal (%)	PO$_4$ removal (%)
I	27.5	−23.3	–	−45.5
II	36.25	−40.1	−61.8	−50.83
III	28.75	−16.8	−48.1	−13.8

3.5   Reasoning of Increasing Concentrations

In Castiglione Torinese plant, the reject water from the sludge treatment line is collected in equalization basin and sent to grit and sand removal section where it is mixed with the screened influent wastewater. Since the reject water is collected from pre-thickeners, anaerobic digesters, post-thickeners, dewatering and sludge conditioning units, it is the source of very high amount of NH_4, PO_4 and organic matters. It is also possible that heterotrophic biomass and PAO organisms are present in portion of reject water which comes from nondestructive sludge treatment units. The mixture of reject water and screened influent wastewater is further treated by using of four sets of settling rectangular tanks with "To and fro" scraper bridge in addition to pre-aeration systems with centrifugal fans and sand, grit material (material with higher specific gravity), oil and grease are removed from it. The possible hypothesis about the increase of NH_4 can be that particulate organic nitrogen is aerobically hydrolyzed to soluble organic nitrogen in parallel with hydrolysis of the slowly biodegradable organic matter. The soluble organic nitrogen is converted to ammonia nitrogen via ammonification. The hydrolysis and ammonification processes should occur during the hydraulic retention time of the primary clarifier (2.5 h). Hydrolysis reactions depend on availability of electron acceptors and aerobic hydrolysis is typically faster that two other types of hydrolysis. Consequently, it is believed that increasing of the dissolved oxygen (DO) by pre-aeration units leads to higher rate of hydrolysis and it makes it possible that both process happen in HRT of primary clarifier.

Increasing of the PO_4 might be contributed to high concentration of PO_4 and possible presence of PAOs in reject water. Also, presence of pressure mains and free flow zones in sewer system can make alternating aerobic and anaerobic conditions which are favourable for the present PAOs.

4   Conclusions

In this study, removal efficiency the primary clarifier at Castiglione Torinese WRRF was investigated. The collected data in sampling campaign were partitioned according to weather conditions and relations between influent total chemical oxygen demand (COD_T), soluble chemical oxygen demand (COD_s), total suspended solids (TSS), ammonium (NH_4) and Phosphate (PO_4) and their corresponding removal efficiencies were studied. Significant differences in removal efficiencies between various parameters and unexpected increasing in concentrations of soluble COD_s, NH_4, PO_4 were observed. The analysis revealed highly predictive relations between the majority of influent concentrations and removal efficiencies. The impact of surface overflow rate and sludge blanket height (SBH) on PO_4, COD_s and NH_4 removal efficiencies were studied. Two main hypotheses were proposed for justification of increasing of PO_4 and NH_4 concentrations according to detail specifications of sewer system and Castiglione plant.

References

Borzooei S. Teegavarapu R, Abolfathi S, Zanetti MC (2016) Application of data partitioning method for analysis of plant influent flow and loading–case study of castiglione Torinese, Italy. Submitted unpublished manuscript

Lessard P, Beck MB (1988) Dynamic modeling of primary sedimentation. J Environ Eng 114:753–769

Membrane Bioreactors

Future Perspectives for MBR Applications at the Erftverband

C. Brepols[(⊠)], K. Drensla, A. Janot, L. Beyerle, and H. Schäfer

Erftverband, Am Erftverband 6, 50126 Bergheim, Germany

Abstract. The river water association Erftverband looks back on two decades of experience in Membrane bioreactor (MBR) operations in the Erft river catchment in Germany. MBR operations have been monitored scientifically during that period and process optimisations have taken place leading to new key figures for MBR operations. Membrane lifetime and energy consumption of the treatment process are cornerstones of MBRs economic feasibility. In both fields the Erftverband has demonstrated that initial expectations are exceeded. With that background Erftverband sees a promising potential for MBR in the future development of wastewater treatment in the Erft river catchment.

Keywords: Membrane bioreactor · Energy · Micropollutants

1 Introduction

Between 1999 and 2008 the water association Erftverband commissioned three membrane bioreactor plants (MBR) for municipal wastewater treatment with capacities between 3,000 and 80,000 population equivalents (PE). The hydrological situation in the Erft river catchment requires a high quality of wastewater treatment. The original interest in MBR technology thus was driven by high regulative demands on nutrient removal and also pathogen removal (Brepols 2010). Before the last MBR was completed in 2008 Erftverband had already installed full biological nutrient removal on all conventional activated sludge plants. As a consequence there was then no further demand for new MBR applications in the association area.

In 2013 Erftverband has started a programme of consolidation and refurbishment of existing wastewater treatment plants (WWTP) in the Erft river catchment. Small and inefficient wastewater treatment plant will be decommissioned with their sewage transferred to larger facilities. Erftverband plans to reduce the number of WWTPs from originally 40 to about 20 WWTPs after the year 2025 (Brepols et al. 2013; Schäfer et al. 2013). Within this process also future treatment goals like micropollutant and microplastics removal are considered for at least some of the remaining larger WWTP.

2 Materials and Methods

Since their start-up intensive plant optimisations have taken place to improve membrane cleaning and operations (e.g. Lyko et al. 2008; Drensla 2011; Drensla 2015) and to reduce the energy consumption for the filtration process. The results and conclusions

Table 1. Technical data of MBRs at Erftverband

	Rödingen, 3,000 PE	Glessen, 9,000 PE	Nordkanal, 80,000 PE
Year of commissioning	1999	2008	2004
Bioreactor volume	400 m^3 + 80 m^3 in 2 filtration tanks	1600 m^3 + 320 m^3 in 4 filtration tanks	9300 m^3 with 8 integrated filtration lines
Membrane surface	5,280 m^2	12,100 m^2	84,480 m^2
Membrane type	Immersed hollow fibre modules		

presented in the following have been retrieved from practical design and operations of MBR and scientific studies which are carried out at the Erftverband MBRs. Technical data on the three MBRs are given in Table 1.

3   Results and Discussions

Between 2010 and 2015 the specific energy consumption of the Nordkanal MBR was cut down from 0.94 kWh/m^3 to 0.63 kWh/m^3 wastewater treated due to improvements on inflow management, process automation and membrane and bioprocess aeration (see Fig. 1). Further energy reductions are planned: Construction works to refurbish Nordkanal MBR with primary clarification and anaerobic sludge treatment have begun in February 2017. It is expected that energy consumption for the biological treatment will thus be reduced while roughly 30% of the required electrical energy can be produced by co-generation (Brepols 2013).
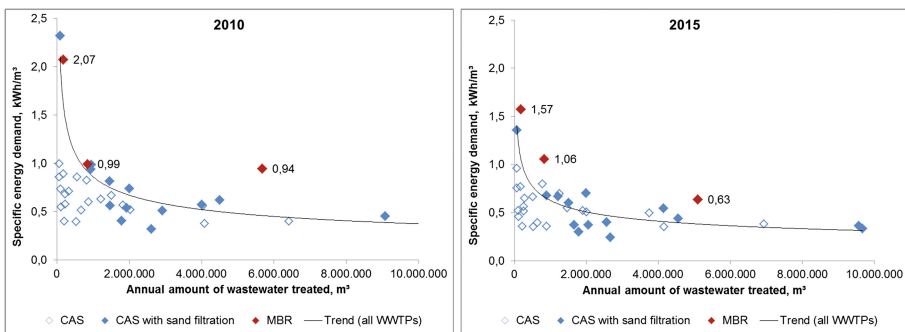
Fig. 1. Specific energy demand of wastewater treatment plants (WWTPs) with different capacities and conventional activated sludge (CAS) treatment, CAS with tertiary sand filtration and MBR for the years 2010 (left) and 2015 (right)

Improved membrane cleaning and handling (Drensla 2015) a technical lifetime of the membrane filtration modules of more than 12 years could be achieved at Nordkanal MBR so far, with most of the membrane units in continued operation since 2004. A comparison of key figures from the original design of Nordkanal MBR, which date back to the year 2000, and data retrieved from current operations show substantial changes (Table 2) which can be taken into account for the design of new MBRs.

Table 2. Comparison of key operational parameters of Nordkanal MBR

Parameter	Unit	Original value	Current value
Filtration time	s	400	900
Backwash/Relaxation time	s	50	50
Operational net flux	L/(m^2 h bar)	< 28	< 45
Biomass concentration	gMLSS/L	12	<8

It has been discussed to facilitate micropollutant removal at Nordkanal MBR by dosing powdered activated carbon (PAC) to the bioreactor. First qualitative assessments showed that no noticeable negative effects on membrane filtration could be monitored However economic feasibility and technical side effects of the PAC dosage need further evaluation.

Another pilot study on micropollutant removal is planned at Glessen MBR using full-scale granular activated carbon (GAC) filters on the MBR effluent. Erftverband currently applies for a regulators permit to begin the building phase. Meanwhile, comparable lab-scale tests by Knopp et al. (2016) have shown positive effects of membrane filtration on the efficiency of a down-stream GAC filtration (Knopp et al. 2016). By reducing background DOC and suspended solids load on the GAC, a relevant increase in filtration bed volumes is expected.

Similar to pathogens removal membrane filtration shows benefits as a defined physical barrier when in comes to microplastics removal. A comparative study on microplastics removal in selected WWTPs has shown that the average number of particles in MBR effluent is by a factor 5 to 14 lower than in conventional tertiary treatment by sand filtration or secondary clarifier effluent (Joost 2014; Mintenig et al. 2014).

4 Conclusions

The Erftverband has gained long-term operational experience with its MBR applications. It can be seen that membrane filtration is still reliable and effective after more than 10 years. Process improvements have yielded lower energy requirements which make MBR even more comparable to energy demand of conventional treatment processes. MBRs' capabilities to reduce pathogens and microplastics are obvious. Possible process combinations with MBR to remove soluble micropollutants are at least promising.

The Erftverband currently runs a programme to consolidate the number of small WWTPs in operation by the year 2025 (Brepols et al. 2013; Schäfer et al. 2013). Feasibility studies for retrofitting remaining WWTPs will also include MBR technology as a viable alternative to conventional retrofits because of the required high standards in wastewater treatment.

References

Brepols C (2010) Operating large scale membrane bioreactors for municipal wastewater treatment. Iwa Publishing, London

Brepols C (2013) Nachrüstung einer Faulungsanlage auf der MBA Nordkanal - Zwischenergebnisse. In: 10. Aachener Tagung Wasser und Membranen, AMW2013. Aachen: Aachener Verfahrenstechnik, RWTH Aachen

Brepols C, Schäfer H, Engelhardt N (2013) A new regional strategy for wastewater and sludge treatment. In: Conference proceedings IWA HSM 2013, IWA holistic sludge management 2013, Västeras, Sweden

Drensla K (2011) Fouling mechanisms and cleaning strategies in membrane bioreactors for municipal wastewater treatment. In: Conference proceedings, IWA-membrane technology conference, Aachen

Drensla K (2015) Chemische Reinigung von getauchten Niederdruck-Hohlfasermembranen auf großtechnischen kommunalen MBR-Anlagen. kassel university press, (Reihe Wasser - Abwasser - Umwelt 37). Universität Kassel, Kassel. urn:nbn:de:0002-400394

Joost L (2014) Mikroplastik- Stichprobenhafte Untersuchungen zum Vorkommen in ausgewählten Kläranlagen-Abflüssen. Report to Erftverband

Knopp G, Yang F, Cornel P (2016) Elimination von Mikroverunreinigungen aus biologisch gereinigtem Kommunalabwasser mittels kombinierter Membran- und Aktivkohleadsorptionsverfahren. GWF Wasser – Abwasser, pp 46–59

Lyko S et al (2008) Long-term monitoring of a full-scale municipal membrane bioreactor—characterisation of foulants and operational performance. J Membr Sc 317(1–2):78–87. http://www.sciencedirect.com/science/article/pii/S0376738807004814

Mintenig S, Int-Veen I, Löder M, Gerdts G (2014) Mikroplastik in ausgewählten Kläranlagen des Oldenburgisch- Ostfriesischen Wasserverbandes (OOWV) in Niedersachsen Probenanalyse mittels Mikro-FTIR Spektroskopie (Abschlussbericht). Alfred-Wegener-Institut, Helmholtz-Zentrum für Polar- und Meeresforschung (AWI) Biologische Anstalt Helgoland, Helgoland

Schäfer H, Brepols C, Engelhardt N (2013) Innovative Energiekonzepte für die Kläranlagen des Erftverbandes. wasserwirtschaft - wassertechnik WWT, Modernisierungs Report (2013/14), pp 31–35

Performance of a Baffled Membrane Bioreactor (BMBR) Operated with Sponge Biomass Carriers: Substantial Reduction in Operational Energy

K. Kimura[(⊠)] and S. Yamamoto

Division of Environmental Engineering, Hokkaido University,
N13W8, Kita-Ku, Sapporo 060-8628, Japan

Abstract. The authors have proposed a baffled membrane bioreactor (BMBR) that can eliminate the energy needed for the mixed liquor circulation. A combination of the BMBR concept and use of biomass carriers is promising, and a substantial reduction in energy consumption should be possible. In this study, a pilot-scale BMBR treating municipal wastewater was operated with sponge biomass carriers and its performance was investigated in terms of treated water quality and energy consumption (aeration intensity). Long-term operation of the BMBR revealed that aeration demand for the BMBR was substantially reduced with minimal membrane fouling and excellent nitrogen removal being achieved. The expected energy consumption (aeration intensity) in a full-scale BMBR operated with sponge carriers is very low, definitely lower than the values in "normal" MBRs. With the proposed modification of the MBR, processes using MBRs will no longer be considered to be energy-intensive processes.

Keywords: Wastewater treatment · Nitrogen removal · Membrane fouling

1 Introduction

The quality of water after treatment of wastewater using membrane bioreactors (MBRs) is much better than that after conventional wastewater treatments. However, large energy consumption in operations of MBRs has been an obstacle for wider application of MBRs. Many studies have focused on energy consumption in MBRs, and several key components in energy consumption have been identified. One of the main energy consumers in the operation of MBRs is circulation of the mixed liquor suspension between an aerobic MBR and an anoxic tank. MBRs are usually intensively aerated and are therefore aerobic. For removal of nitrogen, an anoxic tank must be separately installed and mixed liquor must be circulated between the anoxic tank and the MBR. This circulation of the mixed liquor suspension accounts for 10-15% of total energy consumption of MBRs (Fenu et al. 2010). We have proposed a baffled membrane bioreactor (BMBR) that can eliminate the energy needed for the mixed liquor circulation (Kimura et al. 2008). Figure 1 shows the concept of the BMBR.

In the BMBR, a baffle box is inserted in a submerged MBR, and aeration is carried out inside the baffles. In the operation of the BMBR, the water level is intentionally

changed by control of raw wastew-
ater feeding. When the water level is
high and above the top of the baffles
(Fig. 1(a)), complete mixing in the
BMBR is assumed due to aeration
and the whole reactor is aerobic.
When the water level reaches the
predetermined highest level, the
addition of wastewater is stopped
with membrane filtration being

Fig. 1. Schematic concept of the BMBR

continued. As a result of membrane filtration, the water level gradually goes down and
eventually reaches the top of the inserted baffles. From this stage, the BMBR is divided
into two parts: the part outside the baffles becomes anoxic due to the absence of oxygen
supply (Fig. 1(b), no mixing between the interior and the exterior) and the interior of
the baffles remains aerobic. The water level continues to decrease and finally reaches
the predetermined bottom level. The addition of raw wastewater is then restarted. An
important point in the addition of raw wastewater is that it must be carried out in the
part outside the baffles. Denitrification should occur outside the baffles by using organic
matter in the wastewater and nitrate under an anoxic condition, whereas aerobic
nitrification is carried out inside the baffles. When the water level exceeds the top of the
baffles, the reactor is completely mixed again. Thus, by using a BMBR, simultaneous
nitrification/denitrification is carried out without recirculation of the mixed liquor
suspension using external energy input, and substantial energy saving is possible.

The largest fraction of energy consumption in the operation of an MBR is intensive
aeration required for membrane cleaning (Fenu et al. 2010), and the BMBR is not an
exception. Aeration intensity in a submerged MBR can be reduced by introducing
biomass carriers with membrane fouling being effectively controlled (Kurita et al. 2014).
Biomass carriers scratch the membrane surface, and cake formation on the membrane
surface can be controlled. A combination of the BMBR concept and use of biomass
carriers is promising, and a substantial reduction in energy consumption should be
possible. In this study, a pilot-scale BMBR treating municipal wastewater was operated
with sponge biomass carriers and its performance was investigated in terms of treated
water quality and energy consumption (aeration intensity). Long-term operation of the
BMBR revealed that aeration demand for the BMBR was substantially reduced with
minimal membrane fouling and excellent nitrogen removal being achieved.

2   Materials and Methods

A pilot-scale BMBR installed at Soseigawa wastewater treatment plant (Sapporo,
Japan) was used in this study. The effective volume of the reactor was 650 L. Flat-sheet
membranes made from PVDF polymer were inserted in the BMBR. Nominal pore size
of the membrane was 0.1 μm. The maximum membrane surface area in the BMBR was
9 m^2. To change the flow rate of the reactor (hydraulic retention time (HRT) of the
reactor), the number of the membrane plates inserted (i.e., available membrane area)
was varied. The clearances between the membrane plates were 9 mm. Sludge retention
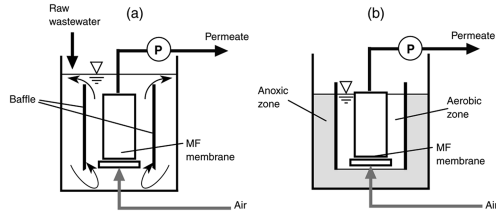
time (SRT) of the reactor was fixed at 20 days, resulting in MLSS concentration in the reactor in the range between 7,500 and 13,500 mg/L. Continuous operation was initiated in May 2016 after observing sufficient acclimatization of biomass. In the long-term operation, as described later, water temperature was significantly lowered.

The sponge biomass carriers used in this study were made from polyester. They were dice-shaped and each dimension was 4 mm. The sponge carriers exhibited excellent membrane cleaning performance in the bench-scale experiment (Kurita et al. 2016). Based on the results obtained in the bench-scale test, sponge carriers corresponding to 5% of the reactor volume were placed in the BMBR. Separation of the sponge carriers from the biomass suspension was easily achieved by using sieves.

In the long-term operation of the BMBR, various operational conditions were examined. Table 1 shows the operational conditions examined in this study. Membrane flux of 12.8–25.0 LMH was examined. In a preliminary test conducted without the sponge carriers, it was found that aeration intensity of 150 L/min was necessary to operate the pilot-scale BMBR with those fluxes. That aeration intensity is considered to be normal for an MBR of this scale. In this study, we tried to substantially reduce the aeration intensity by using sponge carriers. In a separate preliminary study, the movement of sponge carriers in the BMBR was carefully checked by digital image analysis. We tried to mimic the movement of sponge carriers observed in the bench-scale study (Kurita et al. 2016), in which the carriers exhibited excellent membrane cleaning, and we tried to reproduce the movement in the pilot-scale BMBR. It was found that aeration intensity of 150 L/min was not necessary in the preliminary test. It was also found that coarse bubble aeration, which is generally preferred for membrane cleaning, was not adequate for mimicking the movement of sponge carriers. In this study, to mimic the movement of sponge carriers observed in the bench-scale study, a new aerator that could produce micro-bubbles was fabricated and installed in the BMBR. It was found that a low aeration intensity of 30–50 L/min was sufficient for moving the sponge carriers with the new aerator (data not shown). Thus, it was expected that the BMBR could be operated with a low aeration intensity without fouling.

Table 1. Operational conditions examined in the pilot-scale study

	Run 1-1	Run 1-2	Run 2	Run 3-1	Run 3-2	Run 3-3	Run 3-4
Aeration intensity (L/min)	50	30	50	50	50	50	50
Membrane flux (LMH)	25.0	25.0	25.0	12.8	14.0	15.4	17.1
HRT (h)	6.2	6.2	6.2	6.0	5.5	5.0	4.5

3 Results and Conclusions

Figure 2 shows the increase in TMP in the pilot-scale BMBR. Despite the fact that aeration intensity was substantially lowered in this study, the rate of increase in TMP was very slow. The effectiveness of introducing sponge carriers was obvious.
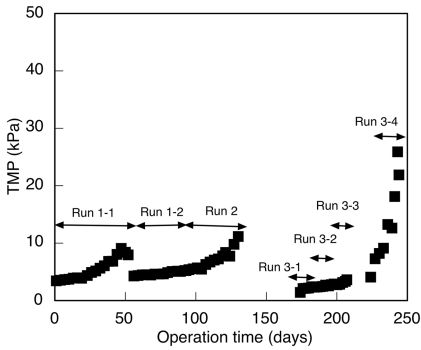
Fig. 2. Increase in TMP in the pilot-scale study (left)
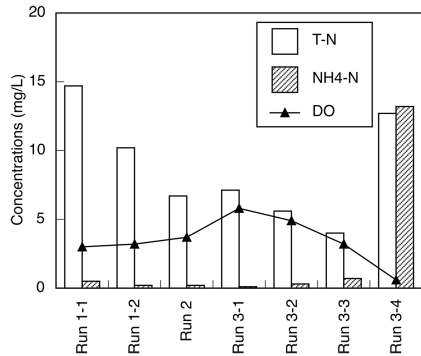
Fig. 3. Average concentrations of T-N/NH4-N in the permeate and DO concentrations in the interior in each run (right)

The sponge carriers adequately moved in the BMBR without accumulating in the clearances, and they continuously cleaned the membrane surface. However, the performance of the BMBR was not good for nitrogen removal. The degree of denitrification was limited in Run 1-1 as shown in Fig. 3. The poor denitrification in Run 1-1 was due to insufficient creation of an anoxic condition in the exterior zone. Figure 4 shows representative variations of DO concentration in the interior and exterior zones in the BMBR observed in Run 1-1. As shown in Fig. 4, the length of the anoxic period created in the exterior zone in Run 1-1 was too short to facilitate denitrification. To improve this situation, an extra water level in the operation cycle (designated middle-level hereafter) was introduced in Run 1-2.

When the water level reached the middle-level after restarting wastewater addition, the addition of wastewater was stopped and the water level was allowed to go down. When wastewater feeding was restarted and the wastewater level reached the middle-level again, the water level was allowed to rise to the highest set level. The effect of this modification was obvious and resulted in improvement of nitrogen removal efficiency in Run 1-2 (see Fig. 3). In Run 2, aeration intensity was reduced to promote denitirication by lowering the DO concentration in the interior zone. The total nitrogen concentration in the treated water was lowered to about 6 mg/L in Run 2 with complete nitrification being maintained. Specific aeration demands based on membrane
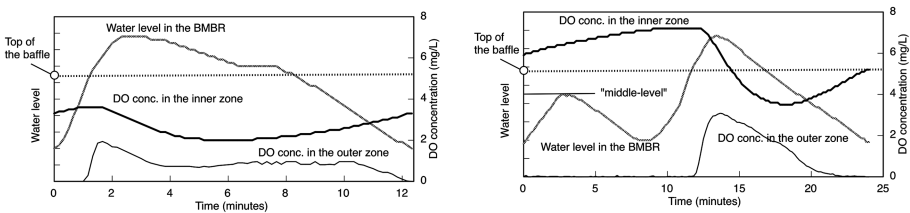
Fig. 4. Variations of DO concentrations in the BMBR in Run 1-1 (left) and Run 1-2 (right)

area (SADm) in Run 2 was very small, 0.2 m^3/m^2/h. The value of SADm achieved in Run 2 in this study was comparable to those reported for full-scale MBRs (0.2–0.6 m^3/m^2/h, (Krzeminski et al. 2012)). Even with the aeration intensity tested in Run 1 (50 L/min), SADm was 0.3 m^3/m^2/h. Aeration efficiency is increased in a large-scale facility. The BMBR with sponge carriers can therefore be operated with a very low aeration intensity (i.e., a very small energy consumption) when it is operated in full-scale. As shown in Fig. 2, the increase in TMP in Run 2 was minimal, reflecting high cleaning efficiency of the sponge carriers under the condition of low aeration intensity of 30 L/min. At the last stage of Run 2, a mechanical trouble in the apparatus happened, which then caused acceleration of TMP increase. Operation of Run 3 was initiated after addressing the problem and acclimatization of biomass.

In Run 3, reduction in HRT was attempted by gradually changing the applied membrane flux. The BMBR exhibited good performances under the condition of short HRTs: excellent treated water quality without an increase in TMP was achieved. It should be noted that this high performance in Run 3 was observed under the condition of a low water temperature of <10 C°. When HRT was decreased to 4.5 h (Run 3-4), however, DO concentration in the inner zone of the BMBR was low (about 0.5 mg/L). In Run 3-4, loading to the reactor exceeded the capacity of oxygen supply of the aerator. As a result of the low DO concentration, biomass conditions became totally different. Under the condition of such low DO concentrations, biomass was significantly damaged: release of a large amount of soluble microbial products (SMP) and break-up of microbial flocs were observed (data not shown). Both of these were thought to cause severe membrane fouling. To reduce HRT further and allow the BMBR to be used under the condition of a high loading, improvement in oxygen supply efficiency in the reactor is necessary. However, this is not difficult. There is still a plenty of room for improvement in the performance of the BMBR, although the performance observed in the present study was good.

4 Conclusions

In this study, reduction of energy consumption in MBRs was examined by using the BMBR with sponge biomass carriers. Experimental results obtained in a long-term pilot-scale test using municipal wastewater are summarized as follows:

- Aeration intensity in MBRs can be substantially reduced without experiencing severe membrane fouling by using sponge carriers
- Excellent nitrogen removal can be carried out with the BMBR without external energy input for mixed liquor circulation
- Low DO concentrations in aerobic part of the reactor causes severe membrane fouling

References

Fenu A, Roels J, Wambecq T, De Gussem K, Thoeye C, De Gueldre G, Van De Steene B (2010) Energy audit of a full scale MBR system. Desalination 262:121–128

Kimura K, Nishisako R, Miyoshi T, Shimada R, Watanabe Y (2008) Baffled membrane bioreactor (BMBR) for efficient removal from municipal wastewater. Water Res 42:625–632

Krzeminski P, van der Graaf JHJM, van Lier JB (2012) Specific energy consumption of membrane bioreactor (MBR) for sewage treatment. Water Sci Technol 65(2):380–392

Kurita T, Kimura K, Watanabe Y (2014) The influence of granular materials on the operation and membrane foling characteristics of submerged MBRs. J Membr Sci 469:292–299

Kurita T, Mogi T, Kimura K (2016) Influence of different biofilm carriers on the operation and membrane fouling of submerged membrane bioreactors. Sep Purif Technol 169:43–49

An Electro Moving Bed Membrane Bioreactor (eMB-MBR) as a Novel Technology for Wastewater Treatment and Reuse

L. Borea[✉], V. Naddeo, and V. Belgiorno

Sanitary Environmental Engineering Division (SEED),
Department of Civil Engineering, University of Salerno,
via Giovanni Paolo II 132, 84084 Fisciano, SA, Italy

Abstract. Membrane bioreactor (MBR) is a reliable and promising technology for wastewater treatment and reuse. However, since membrane fouling and energy consumption still remain operational obstacles and challenges for the widespread application of the MBR technology, research studies for fouling control are still underway. Recently, among different integrated approaches for membrane fouling mitigation, the combinations of MBRs with electrochemical processes (eMBR/electro MBR) or with moving bed biofilm reactor (MBBR) have been adopted as alternative technological methods. In the present study, the performance of an electro moving bed membrane bioreactor (eMB-MBR), in terms of treatment efficiency and fouling formation, was investigated as a novel integrated process which combines an electro MBR with a moving bed membrane bioreactor (MB-MBR). An intermittent voltage gradient of 3 V/cm was applied between two electrodes immersed around a membrane module inside the bioreactor filled with carriers at 30% filling ratio. A MB-MBR was operated as a control test. The integration of electrochemical processes into the MB-MBR improved the treatment performance especially in terms of nutrient removal, with an enhancement of orthophosphate (PO_4-P) and ammonia nitrogen (NH_4-N) removal efficiencies up to 55.0% and 98.7%. The filtration cycles were extended in the eMB-MBR with a reduction of membrane fouling rate of around 60% and of membrane fouling precursors respect to the control test. The results obtained showed the synergic effect of the combined process. Hence, the eMB-MBR process represents a novel exciting technology which is deemed possible for wastewater treatment.

Keywords: Electro MBR · Electric field · Fouling · Membrane bioreactor (MBR) · Moving bed biofilm reactor (MBBR)

1 Introduction

The population growth, urbanization, climate change and environmental pollution represent a challenge to the sustainable development of the society that requires the progress and the improvement of technology able to allow wastewater reuse as alternative water source in order to lessen water shortage (Luo et al. 2017).

Membrane bioreactors (MBRs) have attracted increasing interest in the last decades due to their potential applications and advantages such as high effluent quality and disinfection capability, small plant footprint, reduced sludge production and elimination of the need of tertiary treatment for wastewater reuse (Stephenson et al. 2000; Chen et al. 2016; Villamil et al. 2016). However, membrane fouling still limits the widespread application of the MBRs due to the high energy demand and operational costs associated to this phenomenon.

In the last years, among innovative strategies for membrane fouling control, the combinations of MBRs with electrochemical processes (Ensano et al. 2016; Ibeid et al. 2015) or with moving bed biofilm reactor (MBBR) (Di Trapani et al. 2014; Leyva-Díaz et al. 2015) have been proposed.

Recent studies have proven that the integration of electrochemical processes into MBRs represents an alternative technological approach for membrane fouling control and the enhancement of treatment efficiencies due to the different electrochemical mechanisms produced inside the electro MBR (eMBR) such as electrocoagulation, electro-osmosis, electro-oxidation and electrophoresis (Borea et al. 2017; Hasan et al. 2014).

The addition of a freely moving carrier media inside the MBR, realizing a moving bed membrane bioreactor (MB-MBR), also increases the performance of the MBR treatment and reduces membrane fouling since the immobilized microbial cells on the carriers offer an additional advantage of seamlessly integrated simultaneous nitrification and denitrification and there is also a lower concentration of suspended solids in the system due to the attachment of biomass to the media (Duan et al. 2013; Leyva-Díaz et al. 2015).

The present study aimed to assess the performance, in terms of treatment efficiency and fouling formation, of a novel integrated process which combines an eMBR with a MB-MBR in the same bioreactor (electro moving bed membrane bioreactor – eMB-MBR). The result were compared with those of a MB-MBR, operated as a control test.

The eMB-MBR is the first attempt to combine electrochemical processes with MBBR and MBR technology in one reactor.

2   Materials and Methods

A laboratory scale experimental setup was designed according to Fig. 1. The eMB-MBR reactor, characterized by a working volume of 13 L, was continuously fed with a synthetic solution, simulating real municipal wastewater, whose composition and characteristics are reported in a previous study (Borea et al. 2017).

A ZeeWeed®-1 (ZW-1) submerged PVDF hollow fibre ultrafiltration membrane module (GE/Zenon Membrane Solution) with a nominal pore diameter of 0.04 μm and an effective membrane surface area of 0.047 m^2 was placed vertically in the centre of the eMB-MBR. A perforated cylindrical aluminium anode and stainless steel cathode were immersed around the membrane module at a distance between them of 6 cm. The eMB-MBR was also filled with BIOMASTER BCN 012 KLS Amitec® carriers, with a 30% filling ratio (FR) and a net surface area in the reactor of 500 m^2/m^3. Air diffusers
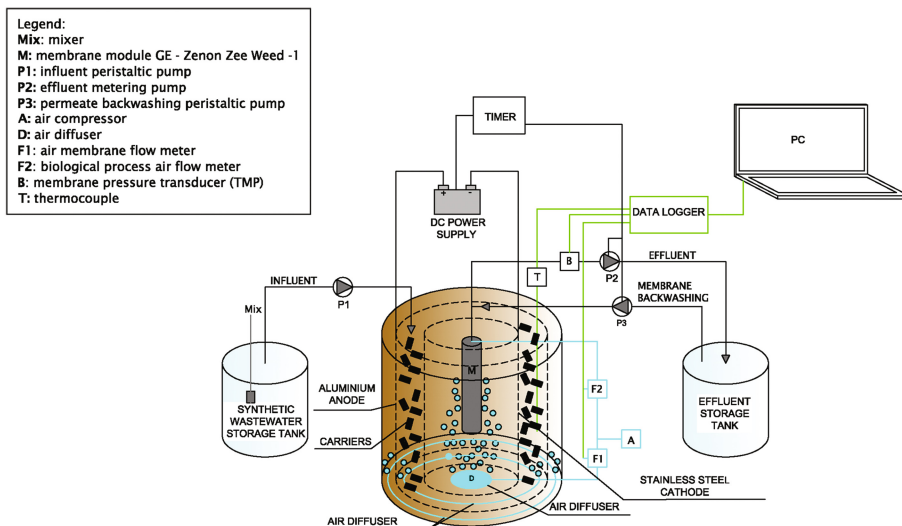
Fig. 1. Experimental setup of the eMB-MBR system

were located below and around the membrane module for maintaining the required oxygen and providing good mixing of suspended sludge flocs and carriers inside the bioreactor. The effluent was withdrawn via metering pump operated at a constant flux of 15 L/m^2 h.

The reactor operated in two phases: in the first it worked as a MB-MBR with the electrodes disconnected from the power supply (control test), in second it worked as an eMB-MBR with the electrodes connected to a digital external DC power supply (CPX400, TTi, 0-60 V, 0-20 A) with an intermittent operation mode of 5 min ON and 20 min OFF, by a programmable electronic controller, at voltage gradients of 3 V/cm according to a previous study (Borea et al. 2017). Influent, effluent and supernatant were sampled and analysed for COD, ammonia nitrogen (NH$_4$-N), nitrate nitrogen (NO$_3$-N), nitrite nitrogen (NO$_2$-N) and orthophosphate (PO$_4$-P) according to the Standard methods (APAT and CNR-IRSA, 2003). Mixed liquor suspended solids (MLSS) and mixed liquor volatile suspended solids (MLVSS) were measured in agreement with the Standard methods (APAT and CNR-IRSA, 2003). Biofilm solids (BS) were determined according to the procedure described by Plattes et al. (2006). The pH, dissolved oxygen concentration (DO), the temperature and the redox potential were also analysed using a multiparametric probe (Hanna Instruments, HI2838). The extracellular polymeric substances (EPS) and soluble microbial products (SMP) in terms of proteins (Frølund et al. 1995) and carbohydrates (DuBois et al. 1956) and transparent exopolymer particles (TEP) (De la Torre et al. 2008) were measured for evaluating membrane fouling formation along with the trans-membrane pressure (TMP) variation over time through a pressure transducer (PX409-0-15VI, Omega) connected to a datalogger (34972A LXI Data Acquisition/Switch unit, Agilent).

3   Results and Discussions

The integration of electrochemical processes into the MB-MBR improved the treatment performance especially in terms of nutrient removal. NH_4-N and PO_4-P removal efficiencies increased, respectively, from 49.8% and 76.7% in the MB-MBR up to 55.0% and 98.7% in the eMB-MBR, due to synergic effect of the combined processes.

The electric field applied led to different electrochemical mechanisms such as electrocoagulation, electroosmosis and electrophoresis, which influence the sludge properties in the bioreactor and, thus, the removal performances. In the eMB-MBR the anoxic conditions, beyond inside the carriers, were also produced, when the electric field was ON, by the reductive reactions at the cathode side that consumed the dissolved oxygen leading to a decrease of redox potential and dissolved oxygen values. The alternation of anoxic and aerobic conditions enhanced the performance of the nitrification process allowing, beyond it, the denitrification.

This improvement of orthophosphate removal results from electrocoagulation and precipitation of $AlPO_4$ and $Al(OH)_3$.

The filtration cycles were extended in the eMB-MBR, as shown in Fig. 2, with a 60% reduction of membrane fouling rate respect to the control test.
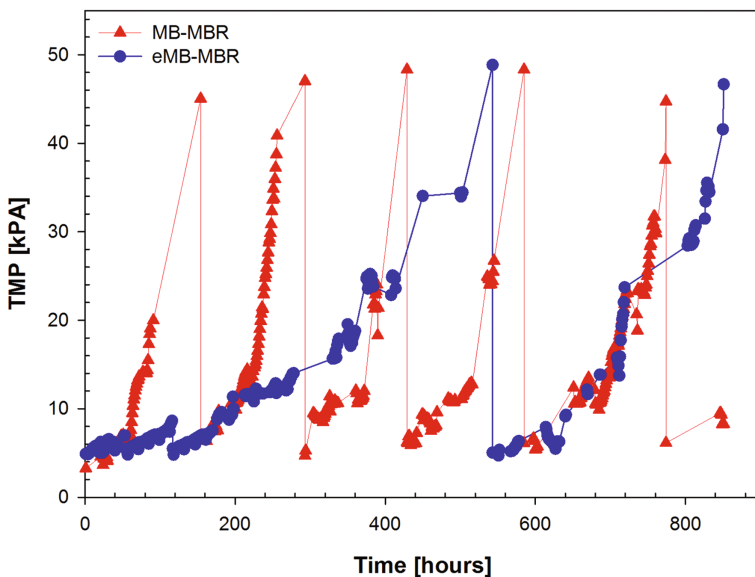
Fig. 2. TMP rise up in the MB-MBR and in the eMB-MBR experimental runs

This reduction, observed in the eMB-MBR, corresponded to a decrease of fouling precursors. The decrease of membrane fouling precursors, the increase of particle size diameter due to electrocoagulation process along with electrophoresis mechanism minimized membrane fouling rate in the eMB-MBR. The different behaviour observed in the Fig. 2 between the first and the second cycle of the eMB-MBR run could be attributed to

the formation, due to different mechanisms, of irreversible fouling which was not recovered after the chemical cleaning and with the application of the electric field.

In the eMB-MBR, a small fraction of the energy, equal to 0.6 kWh per m^3 of wastewater treated, was consumed for the application of the electric field respect to the amount of energy saved due to the reduction of membrane fouling. However, an overall energy balance and costs analysis of the systems studied was not performed due to the laboratory scale of the reactors which could have given results not plausible or applicable to full scale plants.

4 Conclusions

In this work, a novel integrated process, eMB-MBR, which combines electrochemical processes with MBBR and MBR technology, was investigated. The results found showed that the synergic effect of the combined processes led to an enhancement of the effluent quality and a reduction of membrane fouling. Hence, the eMB-MBR process represents an exciting technology which is deemed possible for the treatment of wastewater. Further studies should be focused on the scale up of the system with a more complete energy balance and a cost analysis which take into account the overall energy consumptions and operational costs.

References

APAT and CNR-IRSA (2003). Metodi analitici per le acque. Manuali e Linee Guida 29/2003

Borea L, Naddeo V, Belgiorno V (2017) Application of electrochemical processes to membrane bioreactors for improving nutrient removal and fouling control. Environ Sci Pollut Res 24:321–333. doi:10.1007/s11356-016-7786-7

Chen J, Zhang M, Li F, Qian L, Lin H, Yang L, Wu X, Zhou X, He Y, Liao B-Q (2016) Membrane fouling in a membrane bioreactor: high filtration resistance of gel layer and its underlying mechanism. Water Res 102:82–89. doi:10.1016/j.watres.2016.06.028

De la Torre T, Lesjean B, Drews A, Kraume M (2008) Monitoring of transparent exopolymer particles (TEP) in a membrane bioreactor (MBR) and correlation with other fouling indicators. Water Sci Technol 58:1903–1909

Di Trapani D, Di Bella G, Mannina G, Torregrossa M, Viviani G (2014) Comparison between moving bed-membrane bioreactor (MB-MBR) and membrane bioreactor (MBR) systems: influence of wastewater salinity variation. Bioresour Technol 162:60–69. doi:10.1016/j.biortech.2014.03.126

Duan L, Jiang W, Song Y, Xia S, Hermanowicz SW (2013) The characteristics of extracellular polymeric substances and soluble microbial products in moving bed biofilm reactor-membrane bioreactor. Bioresour Technol 148:436–442. doi:10.1016/j.biortech.2013.08.147

DuBois M, Gilles KA, Hamilton JK, Rebers PA, Smith F (1956) Colorimetric method for determination of sugars and related substances. Anal Chem 28:350–356. doi:10.1021/ac60111a017

Ensano BMB, Borea L, Naddeo V, Belgiorno V, de Luna MDG, Ballesteros FC (2016) Combination of electrochemical processes with membrane bioreactors for wastewater treatment and fouling control: a review. Front Environ Sci 4. doi:10.3389/fenvs.2016.00057

Frølund B, Griebe T, Nielsen PH (1995) Enzymatic activity in the activated-sludge floc matrix. Appl Microbiol Biotechnol 43:755–761

Hasan SW, Elektorowicz M, Oleszkiewicz JA (2014) Start-up period investigation of pilot-scale submerged membrane electro-bioreactor (SMEBR) treating raw municipal wastewater. Chemosphere 97:71–77. doi:10.1016/j.chemosphere.2013.11.009

Ibeid S, Elektorowicz M, Oleszkiewicz JA (2015) Electro-conditioning of activated sludge in a membrane electro-bioreactor for improved dewatering and reduced membrane fouling. J Membr Sci 494:136–142. doi:10.1016/j.memsci.2015.07.051

Leyva-Díaz JC, González-Martínez A, González-López J, Muñío MM, Poyatos JM (2015) Kinetic modeling and microbiological study of two-step nitrification in a membrane bioreactor and hybrid moving bed biofilm reactor–membrane bioreactor for wastewater treatment. Chem Eng J 259:692–702. doi:10.1016/j.cej.2014.07.136

Luo W, Phan HV, Xie M, Hai FI, Price WE, Elimelech M, Nghiem LD (2017) Osmotic versus conventional membrane bioreactors integrated with reverse osmosis for water reuse: biological stability, membrane fouling, and contaminant removal. Water Res 109:122–134. doi:10.1016/j.watres.2016.11.036

Stephenson T, Brindle K, Judd S, Jefferson B (2000) Membrane Bioreactors for Wastewater Treatment. Intl Water Assn, London, UK

Plattes M, Henry E, Schosseler PM, Weidenhaupt A (2006) Modelling and dynamic simulation of a moving bed bioreactor for the treatment of municipal wastewater. Biochem Eng J 32:61–68. doi:10.1016/j.bej.2006.07.009

Villamil JA, Monsalvo VM, Lopez J, Mohedano AF, Rodriguez JJ (2016) Fouling control in membrane bioreactors with sewage-sludge based adsorbents. Water Res 105:65–75. doi:10.1016/j.watres.2016.08.059

Influence of Temperature on the Start-up of Membrane Bioreactor: Kinetic Study

J.C. Leyva-Díaz[1,2(✉)], J. Martín-Pascual[1,2], G. Calero-Díaz[3], J.C. Torres[3], and J.M. Poyatos[1,2]

[1] Department of Civil Engineering, University of Granada, Granada, Spain
[2] Institute of Water Research, University of Granada, Granada, Spain
[3] Department of I+D+I of HiDRALiA, HiDRALiA, Málaga, Spain

Abstract. The start-up phase of a membrane bioreactor (MBR) for municipal wastewater treatment was studied to determine the effect of temperature on the organic matter removal and heterotrophic kinetics. The MBR system was analyzed at hydraulic retention times (HRTs) of 6 h and 10 h and temperature values varying between 11.5 °C and 30.1 °C. Arrhenius and Monod models were used to evaluate the effect of temperature on the biological process of organic matter removal. At the most favorable conditions of HRT (10 h) and MLSS (6,000 mg L^{-1}) corresponding to phase 4, the effect of these variables dominated over the temperature. Heterotrophic biomass from phase 2 (HRT = 10 h, MLSS = 4,000 mg L^{-1} and T = 30.1 °C) had the highest values of COD degradation rate ($r_{su,H}$).

Keywords: Membrane bioreactor · Heterotrophic kinetics · Temperature

1 Introduction

Membrane bioreactor (MBR) systems have been widely used for the treatment of municipal and industrial wastewater (Wintgens et al. 2005). These systems improve the conventional activated sludge processes due to their higher effluent quality, smaller space and reactor requirements, increased volumetric loadings and lower sludge production rates (Oppenheimer et al. 2001; Poyatos et al. 2008; Wang et al. 2009).

Temperature is one of the most important operational factors affecting MBR process (Judd 2011). Temperature of mixed liquor varies due to seasonal and diurnal temperature changes (Arévalo et al. 2014). In light of this, microbial activity, reaction rate of the biological process occurring in MBR and other physicochemical properties could be influenced by temperature conditions (Calderón et al. 2012; Grandclément et al. 2017). The influence of temperature on the heterotrophic bacteria kinetics was evaluated through the Monod and Arrhenius models (Monod 1949; Grandclément et al. 2017).

The aim of this study was to assess the effect of temperature variations on the performance of a pilot-scale MBR concerning its heterotrophic kinetics in the start-up phase at hydraulic retention time (HRT) values of 6 h and 10 h, and mixed liquor suspended solids (MLSS) concentrations for the steady state of 4,000 mg L^{-1} and 6,000 mg L^{-1}.

2 Materials and Methods

A pilot-scale MBR was analyzed during the start-up periods corresponding to four operation phases (Table 1). Bioreactor was fed with municipal wastewater coming from the primary settler of Wastewater Treatment Plant of Puente de los Vados, located in Granada (Spain). MBR system was designed as an aerated cylindrical bioreactor of 272 L, as well as an external rectangular unit of 78 L which contained four vertically oriented submerged modules of hollow-fiber ultrafiltration membrane (ZW-10, ZENON®). The membrane was flowing from the outside to the inner side by sucking. The total membrane area was 3.72 m^2.

Table 1. Operation conditions and heterotrophic kinetic parameters, $\mu_{m,H}$, $K_{M,H}$, Y_H, b_H, for the different phases of start-up of MBR system. Y_H (yield coefficient for heterotrophic biomass), $\mu_{m,H}$ (maximum specific growth rate for heterotrophic biomass), $K_{M,H}$ (half-saturation coefficient for organic matter), b_H (decay coefficient for heterotrophic biomass).

Phase	HRT (h)	MLSS (mg L^{-1})	T (°C)	Y_H (mgVSS mgCOD^{-1})	$\mu_{m,H}$ (h^{-1})	$K_{M,H}$ (mgO$_2$ L^{-1})	b_H (day^{-1})
1	6	4,000	14.2	0.4100 ± 0.0502	0.0101 ± 0.0024	8.0652 ± 0.7662	0.0494 ± 0.0074
2	10	4,000	30.1	0.9076 ± 0.0976	0.1075 ± 0.0205	30.7323 ± 3.3806	0.2361 ± 0.0307
3	6	6,000	22.9	0.6216 ± 0.0784	0.0182 ± 0.0020	13.6928 ± 1.4377	0.1405 ± 0.0139
4	10	6,000	11.5	0.4356 ± 0.0314	0.0336 ± 0.0040	24.5231 ± 2.8202	0.0828 ± 0.0091

Heterotrophic kinetic parameters and chemical oxygen demand (COD) degradation rate ($r_{su,H}$) were evaluated through a respirometric method according to Leyva-Díaz et al. (2013). The evolution of the dynamic oxygen uptake rate (R_s) was registered in dynamic respirometric experiments. Furthermore, an endogenous respiration test was also performed (Leyva-Díaz et al. 2013).

Thus, both respirometric tests facilitated the estimation of the maximum specific growth rate ($\mu_{m,H}$), substrate half-saturation coefficient ($K_{M,H}$), yield coefficient (Y_H) and decay coefficient (b_H) for heterotrophic biomass. The assessment of these parameters was carried out in six steps:

(1) Determination of the oxygen consumption (OC) through the integration of R_s, as shown in Eq. (1):

$$OC = \int_{t_0}^{t} R_s dt \quad (mgO_2 L^{-1}) \tag{1}$$

(2) Estimation of Y_H according to Eq. (2) described by Helle (1999):

$$Y_H = \frac{S - OC}{S \cdot f_{cv}} \quad (mgVSS \; mgCOD^{-1}) \tag{2}$$

where S is the substrate concentration (mgO_2 L^{-1}) and f_{cv} is a conversion factor (1.48 $mgCOD$ $mgVSS^{-1}$).

(3) Evaluation of the substrate degradation rate (r_{su}) from R_s:

$$r_{su} = \frac{R_s}{1 - Y_H \cdot f_{cv}} \quad (mgO_2 L^{-1} h^{-1}) \tag{3}$$

(4) Assessment of the empirical specific growth rate (μ_{emp}) from the relation between the cell growth rate and r_{su}:

$$\mu_{emp} = \frac{Y_H \cdot R_s}{(1 - Y_H \cdot f_{cv}) \cdot X_H} \quad (h^{-1}) \tag{4}$$

where X_H is the concentration of heterotrophic biomass ($mgVSS$ L^{-1})

(5) Estimation of $\mu_{m,H}$ and $K_{M,H}$ through the linearization of the Monod model:

$$\frac{1}{\mu_{emp}} = \frac{1}{\mu_{m,H}} + \frac{K_{M,H}}{\mu_{m,H}} \cdot \frac{1}{S} \quad (h) \tag{5}$$

(6) Estimation of b_H according to Eq. (6) described by Ekama et al. (1986):

$$b_H = \frac{OUR_{end}}{1.42 \cdot X_T \cdot [1 - Y_H(1 - f_p)]} \quad (day^{-1}) \tag{6}$$

where OUR_{end} is the endogenous oxygen uptake rate (mgO_2 L^{-1} h^{-1}), X_T is the total biomass concentration ($mgTSS$ L^{-1}) and $(1-f_p)$ is the fraction of volatile biomass ($mgVSS$ $mgTSS^{-1}$).

The conversion of kinetic parameters to working temperature was carried out following Eq. (7) proposed by Metcalf & Eddy (2003):

$$r_T = r_{20} \cdot \theta^{(T-20)} \tag{7}$$

where r_T and r_{20} symbolize the kinetic parameters at working temperature and 20°C, respectively, θ is a fitting parameter with a value of 1.04 for MBR and T is the working temperature.

Furthermore, Arrhenius equation was used to fit the heterotrophic kinetic parameters as a function of temperature, as shown in Eq. (8):

$$\ln(r_T) = \ln(A) - \frac{E_a}{R} \cdot \frac{1}{T} \qquad (8)$$

where A is the pre-exponential factor, R is the gas constant and E_a is the activation energy of the biological process.

Therefore, the $r_{su,H}$ can be expressed depending on the temperature through the heterotrophic kinetic parameters, as well as the substrate and biomass concentrations, as indicated in Eq. (9):

$$r_{su,H} = \frac{\mu_{m,H} \cdot S \cdot X_H}{Y_H \cdot (K_{M,H} + S)} \qquad (9)$$

3 Results and Discussion

Table 1 shows the values of Y_H, $\mu_{m,H}$, $K_{M,H}$ and b_H. As observed in Table 1, the values of Y_H and b_H increased with temperature due to maintenance energy requirements for biomass and increase of microbial activity (Pollice et al. 2007).

Figure 1 shows that the napierian logarithm of the heterotrophic kinetic parameters was correlated with the inverse of temperature, except for the values of phase 4, characterized by the lowest temperature (11.5°C). The deviation of the values corresponding to phase 4 was probably due to the more favorable operation conditions of HRT and MLSS that characterized this phase (HRT = 10 h and MLSS = 6,000 mg L^{-1}),
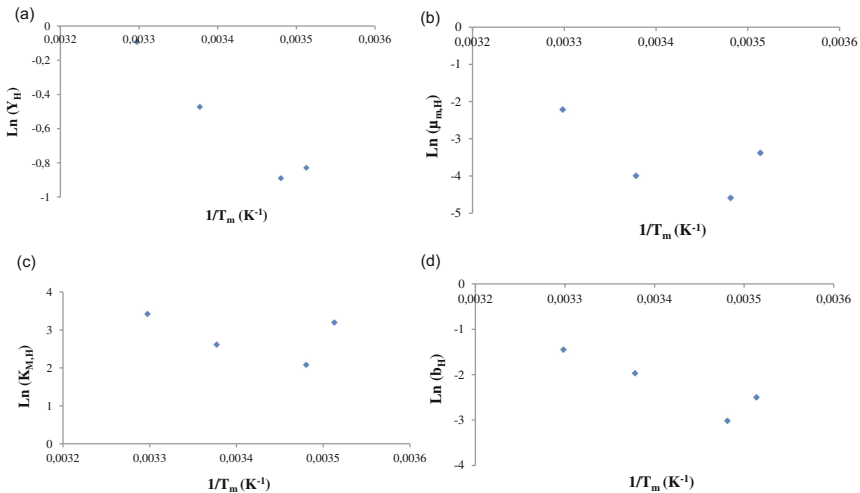
Fig. 1. Linear regression of the napierian logarithm of heterotrophic kinetic parameters, (a) Y_H, (b) $\mu_{m,H}$, (c) $K_{M,H}$, and (d) b_H, depending on the inverse of temperature using Arrhenius equation. Y_H (yield coefficient for heterotrophic biomass), $\mu_{m,H}$ (maximum specific growth rate for heterotrophic biomass), $K_{M,H}$ (half-saturation coefficient for organic matter), b_H (decay coefficient for heterotrophic biomass).
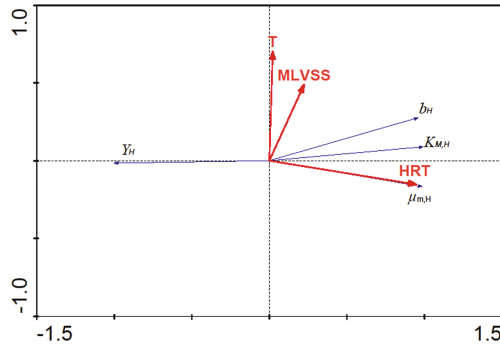
Fig. 2. Triplot diagram for RDA of the heterotrophic kinetic parameters, $\mu_{m,H}$, $K_{M,H}$, Y_H, b_H, in relation to the variables HRT, MLVSS and T. RDA (redundancy analysis), $\mu_{m,H}$ (maximum specific growth rate for heterotrophic biomass), $K_{M,H}$ (half-saturation coefficient for organic matter), Y_H (yield coefficient for heterotrophic biomass), b_H (decay coefficient for heterotrophic biomass), HRT (hydraulic retention time), MLVSS (mixed liquor volatile suspended solids), T (temperature).

cancelling out the effect of temperature. This is supported by Fig. 2 as $\mu_{m,H}$, $K_{M,H}$, b_H are more positively correlated with HRT and mixed liquor volatile suspended solids (MLVSS) than temperature.

This effect was also observed when the $r_{su,H}$ was analyzed (Fig. 3). Equation (10) was obtained to explain the evolution of $r_{su,H}$ depending on temperature, substrate concentration and heterotrophic biomass concentration:

$$r_{su,H} = \frac{1.16 \cdot 10^3 \cdot e^{\frac{-2939}{T}} \cdot S \cdot X_H}{1.08 \cdot 10^5 \cdot e^{\frac{-2563}{T}} + S} \tag{10}$$

As observed in Fig. 3a, heterotrophic biomasses from phase 2 and phase 3, which were characterized by the highest temperatures showed the highest values for $r_{su,H}$. However, heterotrophic biomass corresponding to phase 4 had higher values of $r_{su,H}$ than heterotrophic bacteria from phase 1 in spite of its lower value of temperature (11.5 °C). This is explained as a consequence of the higher influence of HRT and MLSS compared with temperature. Furthermore, it should be noted that heterotrophic biomass required less time for organic matter oxidation during the start-up of phase 2 due to its higher $r_{su,H}$ (Fig. 3a).

This was in accordance with the COD removal efficiencies obtained in the four phases (Fig. 3b). Heterotrophic biomass from phase 2 showed the highest COD removal, followed by the biomass from phases 3 and 4.
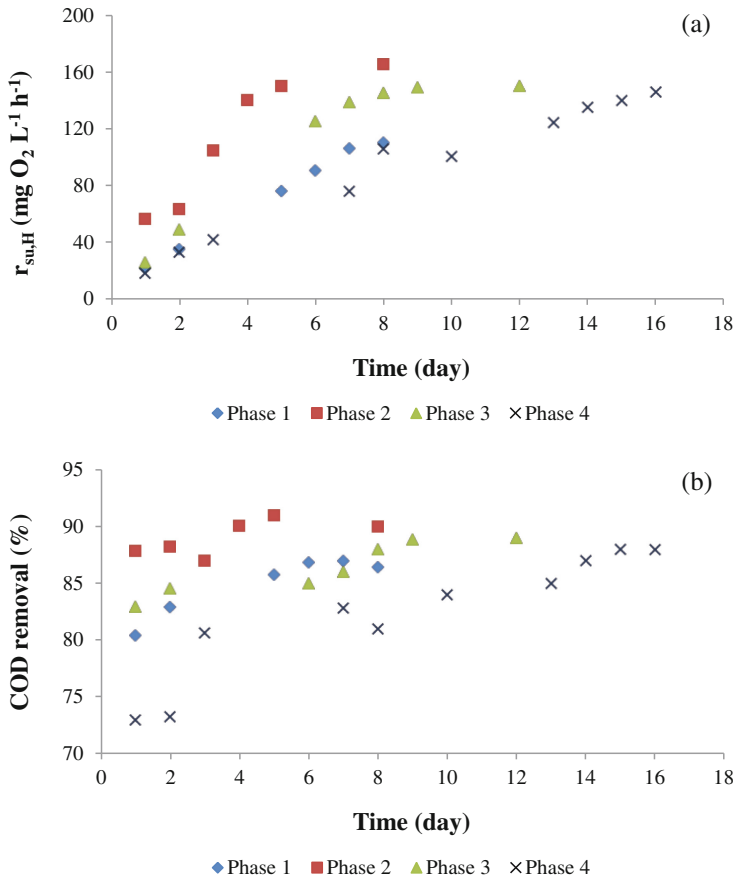
Fig. 3. (a) Evolution of COD degradation rate ($r_{su,H}$) obtained for heterotrophic biomass from MBR, and (b) COD removal during the four start-up phases. Phase 1: HRT = 6 h and MLSS = 4,000 mg L^{-1}; Phase 2: HRT = 10 h and MLSS = 4,000 mg L^{-1}; Phase 3: HRT = 6 h and MLSS = 6,000 mg L^{-1}; Phase 4: HRT = 10 h and MLSS = 6,000 mg L^{-1}. COD (chemical oxygen demand), HRT (hydraulic retention time), MLSS (mixed liquor suspended solids).

4   Conclusions

The kinetic behavior of heterotrophic biomass corresponding to phase 4 did not fit the Arrhenius model. This was probably due to the fact that the MBR worked at the most favorable operation conditions of HRT (10 h) and MLSS (6,000 mg L^{-1}), and the effect of temperature (11.5°C) was cancelled out. This was confirmed by the higher values of $r_{su,H}$ and COD removal for phase 4 compared with those from phase 1 (HRT = 6 h, MLSS = 4,000 mg L^{-1} and T = 14.2°C). Under the operation conditions of HRT = 10 h, MLSS = 4,000 mg L^{-1} and T = 30.1°C that characterized phase 2, heterotrophic biomass showed the highest $r_{su,H}$, which implied less time to oxidize organic matter during the start-up.

References

Arévalo J, Ruiz LM, Pérez J, Gómez MA (2014) Effect of temperature on membrane bioreactor performance working with high hydraulic and sludge retention time. Biochem Eng J 88:42–49

Calderón K, González-Martínez A, Montero-Puente C, Reboleiro-Rivas P, Poyatos JM, Juarez-Jiménez B, Martínez-Toledo MV, Rodelas B (2012) Bacterial com-munity structure and enzyme activities in a membrane bioreactor (MBR) using pure oxygen as an aeration source. Bioresour Technol 103:87–94

Ekama GA, Dold PL, Marais GVR (1986) Procedures for determining influent COD fractions and the maximum specific growth rate of heterotrophs in activated sludge systems. Water Sci Technol 18(6):91–114

Grandclément C, Seyssiecq I, Piram A, Wong-Wah-Chung P, Vanot G, Tiliacos N, Roche N, Doumenq P (2017) From the conventional biological wastewater treatment to hybrid processes, the evaluation of organic micropollutant removal: a review. Water Res 111:297–317

Helle S (1999) A respirometric investigation of the activated sludge treatment of BKME during steady state and transient operating conditions, Thesis. University of British Columbia, Vancouver

Judd, S. (2011) The MBR Book. Principles and Applications of Membrane Bioreactors for Water and Wastewater Treatment. 2nd edn. Elsevier, London

Leyva-Díaz JC, Calderón K, Rodríguez FA, González-López J, Hontoria E, Poyatos JM (2013) Comparative kinetic study between moving bed biofilm reactor-membrane bioreactor and membrane bioreactor systems and their influence on organic matter and nutrients removal. Biochem Eng J 77:28–40

Metcalf & Eddy (2003) Wastewater engineering treatment and reuse. Mc Graw Hill, New York

Monod J (1949) The growth of bacterial cultures. Annu Rev Microbiol 3:371–394

Oppenheimer J, Trussell R, Boulos L, Adham S, Gagliardo P (2001) Feasibility of the membrane bioreactor process for water reclamation. Water Sci Technol 43(10):203–209

Pollice A, Giordano C, Laera G, Saturno D, Mininni G (2007) Physical characteristics of the sludge in a complete retention membrane bioreactor. Water Res 41:1832–1840

Poyatos JM, Molina-Muñoz M, González-López J, Hontoria E (2008) Effects of hydraulic retention time, temperature, and MLSS concentration on the effluent quality of a membrane bioreactor. Environ. Toxicol. II 110:109–116

Wang Z, Chu J, Song Y, Cui Y, Zhang H, Zhao X, Li Z, Yao J (2009) Influence of operating conditions on the efficiency of domestic wastewater treatment in membrane bioreactors. Desalination 245:73–81

Wintgens T, Melin T, Schafer A, Khan S, Muston M, Bixio D, Thoeye C (2005) The role of membrane processes in municipal wastewater reclamation and reuse. Desalination 178:1–11

On-Line Monitoring of NDMA Precursors in MBR-NF Pilot Plant by Using Fluorescence EEM

R. Finocchiaro[1(✉)], M.J. Farré[2], J. Mamo[3], and P. Roccaro[1]

[1] Department of Civil Engineering and Architecture,
University of Catania, Viale A. Doria 6, Catania, Italy
[2] ICRA, Catalan Institute for Water Research,
Scientific and Technological Park of the University of Girona,
H2O Building, Emili Grahit 101, 17003 Girona, Spain
[3] Chemical and Environmental Engineering Laboratory (LEQUIA),
Institut de Medi Ambient, University of Girona,
Campus Montilivi s/n, 17071 Girona, Catalonia, Spain

Abstract. This study examined the applicability of fluorescence excitation/emission matrices (EEM) as online monitoring tool of N-Nitrosodimethylamine (NDMA) precursors throughout a pilot-scale advanced wastewater treatment train, which included a membrane biological reactor (MBR) followed by nanofiltration (NF). The data were generated using samples of the raw wastewater, MBR effluent, NF feed, NF permeate and NF concentrate collected over a four months period and at varying operating conditions (SRT, etc.). Examination of selected fluorescence and absorbance indices obtained by the weekly plant samples combined with the data of NDMA precursors calculated with the formation potential test showed strong relationships between the NDMAFP and the intensity of specific fluorescence components. In particular, the fluorescence region of the EEM associated with aromatic proteins and tyrosine-like substances was strongly correlated with the NDMA precursors. This result gives insight on the type of NDMA precursors that can be found in domestic wastewater and demonstrate that fluorescence EEM can be used to monitor the concentration of NDMA precursors in situ and in real time during advance wastewater treatment processes such as MBR and NF.

Keywords: N-Nitrosodimethylamine · MBR · NF · Disinfection byproducts

1 Introduction

N-nitrosamines constitute an emerging group of disinfection by-products (DBPs), with a cancer risk of 10^{-6} for a concentration of 0.7 ng/L for N-nitrosodimethylamine (NDMA) in drinking water (USEPA 1993).

Several studies have focused on NDMA precursor removal by different water and wastewater processes. Conventional processes could not control nitrosamines because of the hydrophilic and low molecular weight properties of nitrosamine precursors. The most employed mitigation strategy to remove nitrosamines is photolysis, which is only

partially effective at destruction of nitrosamines precursors (Krasner et al. 2013). Activated sludge and also granular activated carbon (GAC) are both effective treatments for NDMA precursor removal, as well as membrane processes. However, even reverse osmosis (RO) remove partially NDMA and its precursors (Sgroi et al. 2015).

Developing tools to monitor NDMA precursors is important to optimize target treatment strategies that might be more cost effective or less energy intensive. This study examined the applicability of fluorescence excitation/emission matrices (EEM) as online monitoring tool of NDMA precursors using treated wastewater from a pilot-scale treatment train, which included a membrane biological reactor (MBR) followed by nanofiltration (NF).

2 Materials and Methods

The data were generated using samples of the raw wastewater, MBR effluent, NF feed, NF permeate and NF concentrate collected over a four months period and at varying operating conditions (SRT, etc.).

The MBR-NF pilot plant was installed at the full-scale WWTP of Quart, Girona (Spain) and thus treating real wastewater with a capacity of 3.4 m^3 day^{-1}. The plant shown in Fig. 1 consists of pre-screening followed by a bioreactor having a total volume of 2.26 m^3 divided into four compartments according to the UCT configuration for nutrient removal. The submerged flat sheet membrane from Kubota had a total surface area of 8 m^2 and a pore size of 0.4 μm. The operating conditions of the MBR system are given in Table 1.
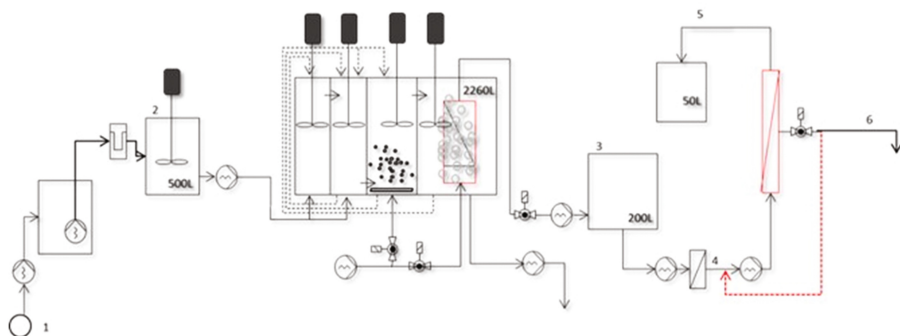
Fig. 1. MBR-NF pilot plant. Sampling points: (1) sewer, (2) influent tank, (3) MBR permeate tank, (4) NF feed, (5) NF permeate and (6) NF concentrate (Mamo et al. 2016)

The NF system consisted of variable frequency drive (VFD) controlled high-pressure pump and a single 4" × 40" membrane element. The membranes tested was a Filmtec NF90 4040 membrane. The tight NF membrane tested had a negative surface charge and was hydrophobic. Internal concentrate recirculation was employed to increase the system recovery while remaining within membrane supplier's

Table 1. MBR process conditions and membrane properties

Parameter	Unit	Value
Membrane area	m^2	8
System flow (Q)	Lh^{-1}	180
Permeate flow	Lh^{-1}	200
System flux	$Lm^{-2}h^{-1}$	25
Solids concentration (MBR tank)	$g\ L^{-1}$	7
SRT	Days	30
Filtration: relaxation cycles	Min	9:1
Air scour flow rate	$m^3 \cdot h^{-1}$	10

Table 2. NF process conditions and membrane properties

Parameter	Unit	Value
Membrane surface area	m^2	7.62
Permeate flux (average)	$Lm^{-2}h^{-1}$	18
Permeate flow	Lh^{-1}	135
Feed pressure	bar	3.3
System recovery	%	75
Material		Polyamide
NaCl rejection	%	85–95
Surface charge		Negative
MWCO estimate	Da	≈ 200
Surface roughness	nm	63.9

specifications. The VFD and the actuated concentrate valve allowed the system to be operated at a constant average permeate flux based on a fixed permeate flow set point of 135 L•h^{-1}. Both membranes were operated at system recovery (Qp/Qf) of 75% and a flux (Qp/Membrane surface area) of 18 L m^{-2} h^{-1} which may be considered within the average system flux of operating installations surveyed by Raffin et al. (2013) which ranged between 16.8 and 21 L m^{-2} h^{-1}. The recovery of the membrane element (Qp/Qs) which includes concentrate recirculation was set at 12.5% within the manufacturer's guidelines and similar to those used by the operating plants surveyed by Raffin et al. (2013) which ranged between 8.6 and 12.7%. The operating conditions and membrane properties of the NF membrane system are given in Table 2.

Total NDMA precursors were quantified by first carrying out an NDMA formation potential (FP) test on the water samples and then analyzing the generated NDMA by solid-phase microextraction (SPME) followed by gas chromatography coupled to a triple quadrupole mass spectrometer (GC-QqQ). For the NDMA FP test, the protocol published by Mitch et al. (2003) was followed.

EEM spectra were recorded using a Hitachi F-7000 fluorescence spectrophotometer. The spectrometer used a xenon excitation source and the slits of excitation and emission were set at 5 nm. The EEM were collected with corresponding scanning emission (EM) spectra from 250 to 580 nm at 5-nm increments by varying the

excitation (EX) wavelength from 220 to 450 nm at 5-nm sampling intervals. Fluorescence regional integration (FRI) was performed according to published literature (Chen et al. 2003; Sgroi et al. 2017) to calculate the total fluorescence intensities integrating the volume under the whole EEM surface for each sample. Other conventional water quality parameters (e.g. BOD_5, COD, N, P, TSS) were analysed following APHA standard methods (APHA 2012).

3   Results and Discussions

Both MBR and NF removed a large part of NDMA precursors (measured as NDMA FP). For instance, Fig. 2 shows the concentration of NDMA FP at each treatment step in different sampling days. The removal of NDMA precursors by the MBR pilot system was affected by the MBR conditions, resulting in a range from 72% (conditions of nitrification minimization) to above 94% (fully nitrifying condition). Considering the system MBR-NF pilot plant, the removal of NDMA precursors was above 90% confirming the high capacity of NF in removing NDMA precursors (Mamo et al. 2016).
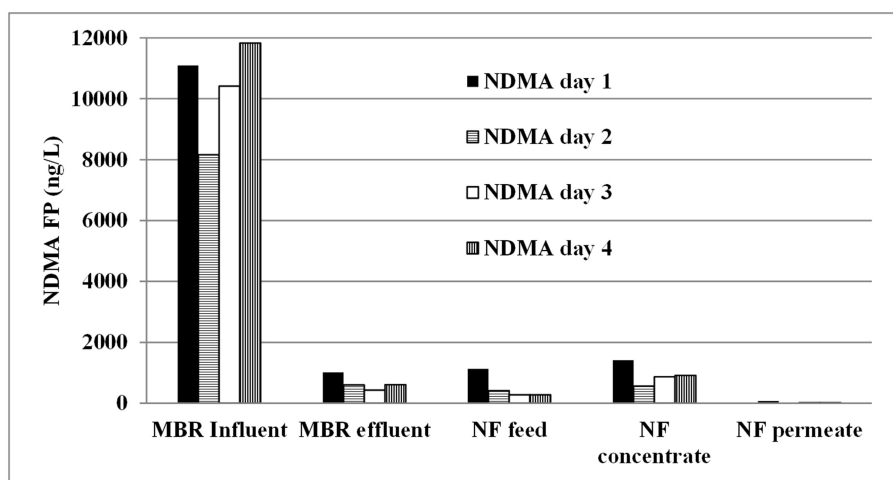
Fig. 2. Concentration of NDMA precursors (NDMA FP) throughout the NBR-NF treatment train

A strong relationship was observed between fluorescence EEMs and the concentration of NDMA precursors calculated with the formation potential test. For instance, Fig. 3 shows a very good correlation between NDMAFP and a fluorescence index indicative of the presence of aromatic proteins in the wastewater samples. Indeed, the acquisition of 3-dimensional excitation-emission matrices (EEMs) provides a "fingerprint" of contributions of different component classes comprising dissolved organic matter (DOM) (Sgroi et al. 2017). Prior research has explored the development and application of fluorescence indexes for specific water quality monitoring. For instance,
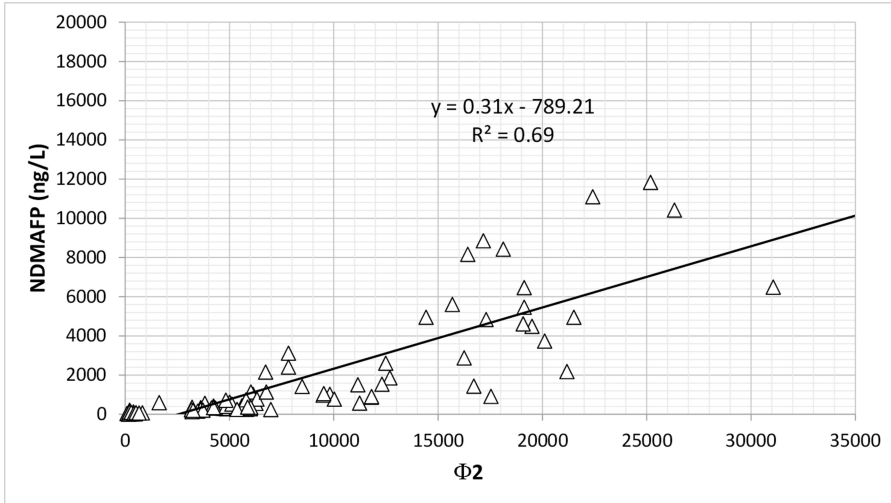
Fig. 3. Correlation between the concentration of NDMA precursors (NDMA FP) and a selected fluorescence index

selected fluorescence indexes have been demonstrated to be useful surrogate parameters for controlling the formation of trace organic compounds (Roccaro et al. 2009, 2010 and 2011; Sgroi et al. 2014) during disinfection/oxidation processes, and for monitoring the removal of emerging contaminants during full-scale conventional and advanced wastewater treatment processes (Anumol et al. 2015; Sgroi et al. 2017).

Results obtained in this study pones more weight on the application of fluorescence for controlling the removal of NDMA precursors in membrane-based processes. In particular, it was observed that the removal of the fluorescence region of the EEM associated with aromatic proteins and tyrosine-like substances was strongly correlated with the removal of NDMA precursors. This result gives more insight also on the identification of the characteristics of the NDMA precursors.

4   Conclusions

Fluorescence spectroscopy is a rapid, cost-effective, reagentless technique that requires little or no sample preparation prior to analysis. In this study, it was shown that selected fluorescence indexes are correlated with NDMA precursors in membrane based-processes. In particular, the obtained results give insight on the type of NDMA precursors that can be found in domestic wastewater and demonstrate that fluorescence EEM can be used to monitor the concentration of NDMA precursors in-situ and in real time during advanced wastewater treatment processes based on membranes, such as MBR and NF.

References

Anumol T, Sgroi M, Park M, Roccaro P, Snyder SA (2015) Predicting trace organic compound breakthrough in granular activated carbon using fluorescence and UV absorbance as surrogates. Water Res 76:76–87

APHA (2012) Standard Methods for the Examination of Water and Wastewater, 22th edn. American Public Health Association, American Water Works Association, and the Water Environment Federation, Washington, DC

Chen W, Westerhoff P, Leenheer JA, Booksh K (2003) Fluorescence excitation-emission matrix regional integration to quantify spectra for dissolved organic matter. Environ Sci Technol 37 (24):5701–5710

Krasner SW, Mitch WA, McCurry DL, Hanigan D, Westerhoff P (2013) Formation, precursors, control, and occurrence of nitrosamines in drinking water: a review. Water Res 47:4433–4450

Mamo J, Insa S, Monclús H, Rodríguez-Roda I, Comas J, Barceló D, Farré MJ (2016) Fate of NDMA precursors through an MBR-NF pilot plant for urban wastewater reclamation and the effect of changing aeration conditions. Water Res 102:383–393

Mitch WA, Gerecke AC, Sedlak DL (2003) A N-Nitrosodimethylamine (NDMA) precursor analysis for chlorination of water and wastewater. Water Res 37(15):3733–3741

Raffin M, Germain E, Judd S (2013) Wastewater polishing using membrane technology: a review of existing installations. Environ Technol 34(5):617–627

Roccaro P, Vagliasindi FGA, Korshin GV (2009) Changes in NOM fluorescence caused by chlorination and their associations with disinfection by-products formation. Environ Sci Technol 43(3):724–729

Roccaro P, Vagliasindi FGA (2010) Monitoring emerging chlorination by-products in drinking water using UVabsorbance and fluorescence indexes. Desalin. Water Treat. 23(1–3):118–122

Roccaro P, Vagliasindi FGA, Korshin GV (2011) Quantifying the formation of nitrogen-containing disinfection by-products in chlorinated water using absorbance and fluorescence indexes. Water Sci Technol 63(1):40–44

Sgroi M, Roccaro P, Oelker GL, Snyder SA (2014) N-Nitrosodimethylamine formation upon ozonation and identification of precursor source in a municipal wastewater treatment plant. Environ Sci Technol 48(17):10308–10315

Sgroi M, Roccaro P, Oelker GL, Snyder SA (2015) N-nitrosodimethylamine (NDMA) formation at an indirect potable reuse facility. Water Res 70:174–183

Sgroi M, Roccaro P, Korshin GV, Greco V, Sciuto S, Anumol T, Snyder SA, Vagliasindi FGA (2017) Use of fluorescence EEM to monitor the removal of emerging contaminants in full scale wastewater treatment plants. J Hazard Mater 323:367–376

USEPA (United States Environmental Protection Agency) (1993). IRIS Database. http://www.epa.gov/ncea/iris/

Self-forming Dynamic Membrane as a Sustainable Alternative to Synthetic Membranes for MBR

P. Vergine[✉], C. Salerno, G. Berardi, and A. Pollice

IRSA CNR, Viale F. De Blasio, 5, 70132 Bari, Italy
{pompilio.vergine, carlo.salerno, giovanni.berardi,
alfieri.pollice}@ba.irsa.cnr.it

Keywords: Dynamic membrane · MBR · Mesh · Wastewater

1 Introduction

The Membrane BioReactor (MBR) is a well-known technology for wastewater treatment that integrates bioprocesses with membrane filtration. The MBR has been widely applied for the treatment of both urban and industrial wastewater and it can be considered a reliable process in order to produce high quality effluents (Judd 2011). However, synthetic membranes are relatively expensive and delicate. Changes in the influent characteristics or in the operating conditions of the bioprocess may rapidly cause irreversible fouling of the membranes, so reducing their lifespan.

In this context, a possible evolution towards systems having potentially lower installation and operating costs is the Self Forming Dynamic Membrane BioReactor (SFD MBR). The main characteristic of this technology is the self-formation of a biological filtering layer on a support (mesh) of inert material, having pore size generally between 20 and 100 µm (Ersahin et al. 2012). The biological layer, also called "dynamic membrane", has a lower porosity than the mesh itself, so acting as the key player in the filtration processes (Kiso et al. 2000; Xiong et al. 2016).

The state of the art for this technology indicates that the process is promising, but still under development in terms of both supporting materials and operating conditions. Before a possible scale-up to real applications, it is necessary to optimize the operating conditions at bench scale. In this perspective, the influence of mesh pore size and air scouring intensity on the performance of the bioreactor was investigated in a previous study (Salerno et al. 2017). The corresponding findings suggest that a continuous, but moderate, air scouring is a key factor for ensuring effective operation. The 50 µm mesh operated with low air scouring intensity (150 mL/min) resulted as the optimal compromise between high effluent quality and limited cleaning frequency, so this configuration was applied in the present study. The aim of this work is to verify the reliability of a SFD MBR operated at solids retention times (SRT) typical of conventional MBR and during a medium-term experimentation (5 months).

2   Materials and Methods

A bench-scale aerobic SFD MBR was operated for the treatment of real municipal wastewater. The system was equipped with a 50 μm nylon mesh, which was continuously air scoured at a flow rate of 150 mL/min (corresponding to 1.25 m^3/h per m^2 of mesh surface). The reactor was started up with a biomass inoculum of 1.5 g/L as TSS (total suspended solids) and operated under constant temperature of 20°C with an organic volumetric loading rate (VLR) of 1.05 KgCOD m^3/d and an SRT of 30 days. The flow rate was maintained at approximately 12 L/d, corresponding to a membrane flux of 70 L/m^2/h and an HRT of 9 h. The feed consisted in pre-settled municipal wastewater, collected weekly at a local wastewater treatment plant, stored at 4° C (continuously stirred) and diluted with tap water in order to maintain the VLR value constant. The transmembrane pressure (TMP, expressed in mbar as absolute value) was monitored by direct reading every two hours during the day, i.e. from 9 a.m. to 5 p.m., Monday to Friday. Mesh cleaning was performed when the TMP observed was higher than 100 mbar. Cleaning consisted in removing the module from the reactor and jet rinsing the mesh surface with tap water. No chemicals were used for cleaning, in order to evaluate possible persistent clogging of the mesh. The analyses of COD (Chemical Oxygen Demand), TSS, total phosphorus (TP), total nitrogen (TN), and NH_4^+ were performed according to Standard Methods (APHA, AWWA, and WEF 2005). The effluent turbidity was measured in triplicate through a 2100P turbidimeter (HACH).

3   Results and Discussion

Under the operating conditions maintained for the biological processes (SRT of 30 d, VLR of 1.05 KgCOD m^3/d), the bioreactor reached and maintained a steady state concentration of solids in the mixed liquor of 7.1 ± 1.2 gTSS/L.

The main water quality parameters were measured in both the influent and the effluent of the bioreactor, and the results are reported in Table 1. The SFD MBR removed 93% of the COD and achieved complete nitrification (NH_4^+ always lower than 1 mgN/L). The average values of TSS concentration and turbidity in the effluent indicate that the dynamic membrane had a very good filtration performance. Moreover, the maximum values of COD and TSS concentration measured in the effluent were 32.4 mg/L and 5.4 mg/L, respectively.

Table 1. Physicochemical characteristics of influent and effluent of the bioreactor. Average values (± standard deviations) at steady state

	COD (mg/L)	TSS (mg/L)	TN (mg/L)	TP (mg/L)
Influent	411,9 ± 33,1	173,0 ± 32,0	49,5 ± 7,9	10,6 ± 1,9
Effluent	26,3 ± 3,4	3,4 ± 1,3	35,0 ± 4,8	8,1 ± 1,6

The performance of the system was also evaluated in terms of mesh clogging and consequent cleaning requirements. Indeed, the cake layer causes partial clogging of the mesh itself, which can be noticed through TMP measurements. When clogging becomes relevant, decrease of the system's productivity may occur. Moreover, partial clogging causes the increase of the suction pressure. This higher pressure destabilizes the cake layer (promoting channelling) and, consequently, causes a worsening of the effluent quality. When cleaning was executed at TMP values close to 100 mbar, these two phenomena were prevented and the SFD MBR maintained a good filtration performance in terms of effluent quality even after 5 months of operation. As a matter of fact, during the entire experimentation the flow rate of the effluent produced was stable at approximately 12 L/d and its turbidity was always lower than 5 NTU.

In Fig. 1, the evolution of TMP and effluent turbidity during the period included between two consecutive cleaning events is displayed. This example confirms that during the stage of its formation, the dynamic membrane has a lower filtration capacity than in its maturity stage. However, effluents with higher turbidity are produced only during the first two hours after each cleaning. Therefore, considering a daily average, the quality of the effluent produced was not considerably affected by the loss of the cake layer due to cleaning operations.
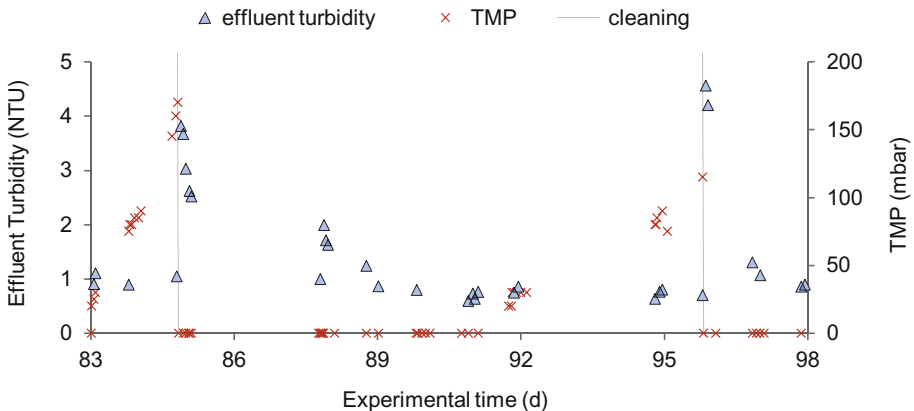
Fig. 1. Evolution of transmembrane pressure (TMP) and effluent turbidity between two subsequent cleaning events

Figure 2 reports the evolution of the mesh cleaning frequency over time. Under steady state conditions (reached after 2 months of operation), the mesh required less than one cleaning per week. In a previous study performed under similar conditions (except a higher flux and a lower SRT), the authors observed a persistent fouling of the mesh which caused an increase of cleaning frequency (Salerno et al. 2017). In this study the cleaning frequency did not increase over time suggesting more efficient operation under the conditions proposed here.
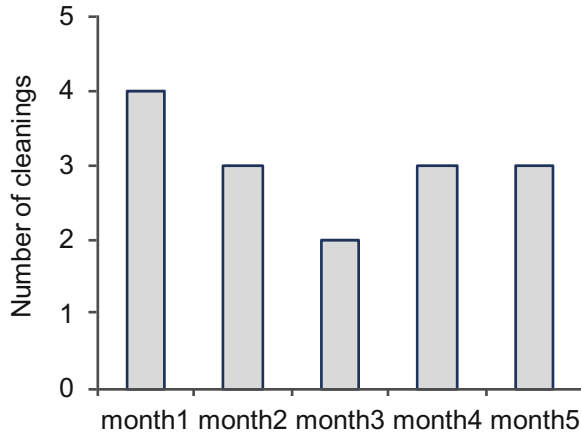
Fig. 2. Evolution of the mesh cleaning frequency along the experimental period

4 Conclusions

The results here presented in terms of effluent quality (maximum TSS of 5.4 mg/L) and concentration of TSS in the mixed liquor (stably around 7 gTSS/L), allow to consider the reliability of this system as comparable to that of a MBR equipped with synthetic micro/ultrafiltration membranes. The lower investment costs and the limited maintenance required indicate the SFD MBR as a sustainable alternative to conventional MBR.

References

American Public Health Association (APHA), American Water Works Association (AWWA), Water Environment Federation (WEF) (2005) Standard Methods for the Examination of Water and Wastewater. APHA, Washington

Ersahin ME, Ozgun H, Dereli RK, Ozturk I, Roest K, van Lier JB (2012) A review on dynamic membrane filtration: Materials, applications and future perspectives. Bioresour Technol 122:196–206

Judd S (2011) The MBR book, 2nd edn. Elsevier Ltd., Amsterdam

Kiso Y, Jung Y-J, Ichinari T, Park M, Kitao T, Nishimura K, Min K (2000) Wastewater treatment performance of a filtration bio-reactor equipped with a mesh as a filter material. Water Res 34(17):4143–4150

Xiong J, Dafang F, Rajendra PS, Ducoste JJ (2016) Structural characteristics and development of the cake layer in a dynamic membrane bioreactor. Sep Purif Technol 167:88–96

Salerno C, Vergine P, Berardi G, Pollice A (2017) Influence of air scouring on the performance of a Self Forming Dynamic Membrane BioReactor (SFD MBR) for municipal wastewater treatment. Bioresour Technol 223:301–306

Membrane Electro-Bioreactor for Small Wastewater Treatment Systems

M. Elektorowicz[1](✉), S. Ibeid[1], A. Belanger[1], and J.A. Oleszkiewicz[2]

[1] Department of Building, Civil and Environmental Engineering,
Concordia University, Montreal, QC, Canada
[2] Department of Civil Engineering, University of Manitoba,
Winnipeg, MB, Canada

Abstract. Membrane electro-bioreactor (MEBR) was tested in pilot scale to evaluate its suitability to treat low wastewater flowrates in remote locations. The system treated municipal wastewater with highly variable, continuously changing concentrations of COD, ammonia and phosphorous. The MEBR combining biological, electrokinetic and membrane filtration processes allowed achievement of 90-99% of phosphorous, COD, and nitrogen. The results confirmed that MEBR could be applied to self–sustained building, separate dwellings, and in remote locations. It would be capable in substituting septic tanks, and used for mobile septage pre-treatment. It can be implemented in small and medium size municipalities, villages, mining or military camps as well as remote aboriginal population reserves.

Keywords: Wastewater treatment · Electro-bioreactor · Nutrient removal

1 Introduction

It is a necessity to improve methods of treatment of wastewater with a low daily flowrate, particularly in remote locations. The population in Quebec (as well as most other Canadian provinces) is dispersed due to the type of industrial activities (mining, agriculture and pulp and paper, etc.) or due to the lifestyle of aboriginal communities. For example, around 1/6 of Quebec inhabitants live in regions where population density is less than 7 inhabitants/km^2, hence, collection of sewage present major problems. Moreover, 20% of Quebec population does not have access to sewage collection system, and 15% use private septic tanks, which do not remove nutrients. Around 40% of wastewater treatment facilities have a flowrate less than 500 m^3/d and many even less than 10 m^3/d (Mamrot 2016).

To resolve the problems a novel membrane electro-bioreactor (MEBR) system was proposed (Elektorowicz, et al. 2011). The system works based on a combination of membrane filtration with biological and electrokinetic processes taking place in a single vessel. The vessel consists of a series of ultra-, micro- or nano-filtration membranes, and couples of Al-Fe electrodes submerged in a continuous flow complete mixed bioreactor filled with raw wastewater (Ibeid et al. 2013a). The system does not require primary treatment and its functioning can be automatically controlled. Once the direct current (DC) is activated in the electro-bioreactor, various electrochemical phenomena

take place; for example, by varying redox potential and controlling dissolved oxygen (DO), aerobic and anoxic conditions are created alternately (Elektorowicz et al. 2011). Subsequently, nitrifying and denitrifying organisms can grow in the same bioreactor and facilitate the biotransformation of ammonium into nitrogen gas through nitrification/denitrification process. Phosphorous is removed due to simultaneous electro-coagulation process (Ibeid et al. 2016, Wei et al. 2011). The electric field changes properties of the mix liquor suspended solids, affects foulants and produces more manageable biosolids and decreases membrane fouling (Ibeid et al. 2016, 2015, and 2013b, Hasan et al. 2012). Our previous work (Ibeid et al. 2013a, Wei et al. 2011, Hasan et al. 2012, Bani-Melhem and Elektorowicz 2010) showed that intermittent exposure mode and low current density are necessary to maintain high microbial activity. Previous small scale studies, which were carried out using microfiltration and ultrafiltration hollow fiber membranes, permitted assess adequate operation parameters with respect to electrical mode operation, SRT, HRT, the MLSS concentration and transmembrane pressure (Hasan et al. 2012, Ibeid et al. 2013a). The results showed possibility to remove more than 99% of COD, phosphorous and total nitrogen from wastewater (Bani-Melhem and Elektorowicz 2010; Ibeid 2013a; Elektorowicz et al. 2011). The first pilot scale test reached the removal efficiencies up to 99% for phosphorus, 90% for organic carbon and up to 82%–97% for total nitrogen without any additives (Hasan et al. 2014). Since MEBR has a small footprint and can be built as a modular system, it is ideally suited to be used in remote locations where a deficiency of labor and energy are common problems.

The main objective of the project, was to build a prototype of the membrane electro-bioreactor and show that it was able to produce an excellent quality effluent from raw wastewater in a single vessel. More specifically, it should be demonstrated that: (i) the treatment process functioning in real conditions (subjected to fluctuation of dilute raw wastewater characteristics) can produce an effluent superior the local regulations; and (ii) can be applied to small size treatment facilities.

2   Materials and Methods

To achieve the above mentioned objectives, self-standing facilities were installed in an isolated cabin (Fig. 1) in l'Assomption, QC (Canada). The membrane electro-bioreactor (MEBR) system has been treating 2 m^3/day of municipal wastewater for last 7 months. The wastewater was supplied directly from sewer, after initial 6 mm screening. The tests were, therefore, conducted under real pilot scale conditions, and moreover with real raw wastewater whose characteristics with respect to carbon, nitrogen and phosphorous fluctuated continually. Due to combined sewage system, the fluctuations were more visible during the rainy periods. Overall, the initial concentration of COD, total nitrogen, and phosphorous fluctuated between: 170 to 49 mg O_2/L, 34 to 11.7 mg N/L, and 6.5 to 0.5 mg P/L, respectively.

An external membrane module was chosen for the electro-bioreactor to enable automatic membrane cleaning. Such solution would require minimal maintenance important for remote locations. A series of Fe-Al electrodes were submerged in
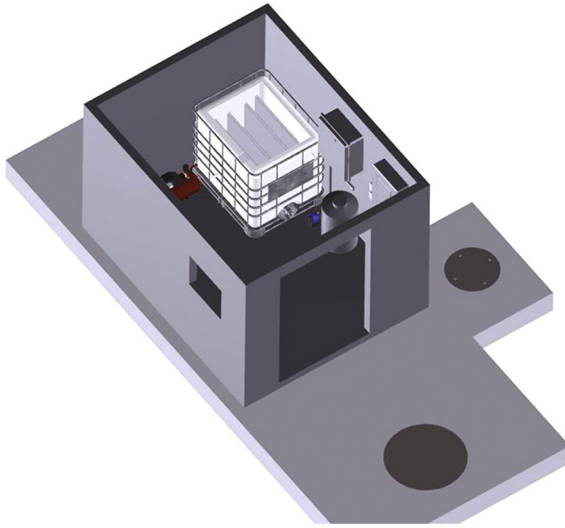
Fig. 1. Pilot MEBR system in a self-standing cabin (after Elektorowicz et al. 2011)

1 m^3 bioreactor. An intermittent current were applied, while 7 V was measured. An SRT of 20 d was selected.

Since the second objective of the project was to optimize the MEBR so that it may be used in self-standing buildings as well as in remote locations, the study addressed: (i) implementation of the system control and automation, and (ii) using Wi-Fi. Successful wastewater treatment depends on an adequate combination of the electrical strength (current density), dissolved oxygen concentration and biological activity. Since temperature, carbon, nitrogen and phosphorous fluctuate over time, adjustments were required. A smart control system with an automatic adjustment of power supply, pumps and compressor was designed to maintain high efficiency of the treatment. Application of WiFi would also allow to control several electro-bioreactors dispersed in remote locations from one central control room.

There are two approaches to saving operation costs: (i) through the type of energy used and (ii) optimization (acceleration) of the treatment process, while ensuring optimal performance, reducing energy consumption, allowing remote connectivity, and collecting all relevant information with data log-system. Subsequently, water levels within the feed reservoir and bioreactor were measured using an ultrasonic transducer. Desired dissolved oxygen (DO) concentration was controlled inside the bioreactor using a PID controller algorithm with a DO probe as feedback, and a mass flow controller was used to inject air into the fine bubble diffusers located at the bottom of the electro-bioreactor. The air was supplied by an air compressor. Current density (CD) was controlled using another PID controller with a current transducer as feedback and a programmable power supply as an electrical energy source. The algorithms were implemented using a programmable controller. The system's processes were locally monitored and modified via a touch-screen panel, or via the programming software.

Remote connectivity was realized using a wireless router, which allowed the system to be monitored and updated remotely, along with accessing data logs.

3   Results and Discussion

The analyses of the treated water showed excellent removal (over 99%) of COD, total nitrogen and phosphates over the treated period of time. The system has run for last seven months, where optimization of the installations (including the control system, size of reactor, feeding system, diffusors and electrodes configuration) and measurements were conducted. The final installations allowed for optimal treatment of the dilute municipal sewage despite its fluctuations. Indeed, the last set of results showed that ammonia, nitrates, and COD might achieve the concentrations of 0.1 mg NH_3/L, 1.1 mg NO_3/L, and 1-5 mg COD mg/L, respectively in the effluent (Fig. 2). Phosphorous was simultaneously almost completely removed reaching an average level of 0.03 mg/L (Fig. 3). When compared to the Quebec standards for effluent, where BOD_5 and phosphorous should have maximal values of 15 mg/L (22 mg/L as COD) and 1 mg/L, respectively, the generated water can be safely used for irrigation purposes; respectively, the results we obtained from our effluent were superior and hence conform to the standards. Some guidelines also focus on pathogen content where a maximum of 200 to 50000 fecal coliforms/100 mL should be found in the effluent after its treatment. Since membrane ultrafiltration was applied into the MEBR system, no such bacteria was expected in the effluent. The concentrations of nitrates/nitrites (as N) in the effluent were also below the allowable concentration of 10 mg/L for drinking water. When compared to the norms required by Agriculture and Agri-Food Canada as per their guidelines, the generated effluent can already be used for primary food production, food retailing and some food processing. Overall, the obtained effluent quality were better than the Quebec guidelines with respect to BOD, nitrogen and phosphorus concentrations, which are 5–25 mg O_2/L, 10 TN mg/L, 1-0.1 TP mg/L, respectively.
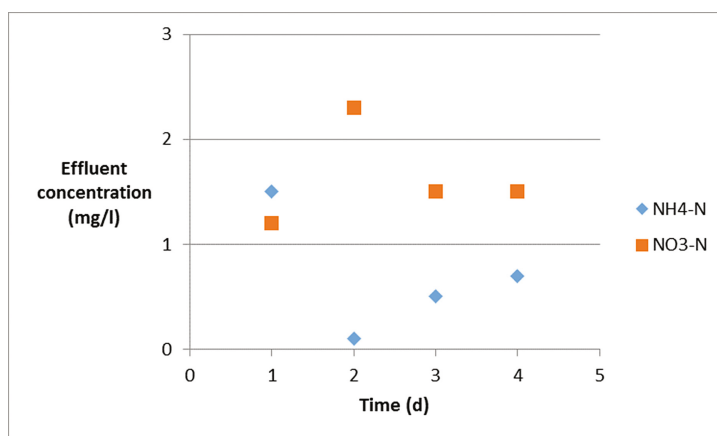
Fig. 2. Nitrate and ammonia concentrations in MEBR effluent
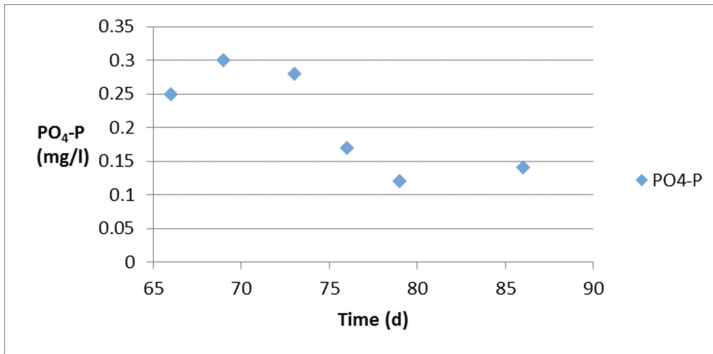
Fig. 3. Phosphorous concentration in MEBR effluent

The above results showed the production of an exceptional quality effluent in a compact MEBR system exposed to raw dilute sewage. Northern locations Such results suggested a number of applications of the MEBR. Due to its small foot print and low voltage used, it can be applied as a sole method not only for wastewater treatment but also for water recovery. Due to an efficient methodological approach can substitute septic tanks, can be installed in decentralized wastewater treatment plants or on mobile platform to carry rescue during catastrophic events. It would be particularly recommended for new developments without a sewage network or for remote locations. This study showed that such application can be facilitate by the application of the Wi-Fi control and automation system.

Since the electro-bioreactor being a modular system, the MEBR can be easy adapted to the fluctuated number of users which any other system does.

4   Conclusion

The study showed the feasibility of the MEBR system to achieve over 90% removal of contaminants from wastewater, considerable higher quality than the regulations required for effluents in Quebec. The results from the pilot installation of the membrane electro-bioreactor under real continuous conditions confirmed the feasibility of simultaneous treatment of C, N, and P in a sole vessel, which is adequate for decentralized wastewater treatment facilities. The study confirmed that MEBR could be applied to small size wastewater treatment facilities particularly to self–sustained building, separate dwellings, and in remote locations. It could substitute septic tanks, and even be used for mobile septage pre-treatment. Due to optimization of MEBR operation conditions automation and control, it potentially might be ideal for remote locations characterized by deficiency of water, energy and qualified labor.

Overall, the final outcome of the project confirmed adequacy of operating parameters for a cost-effective MEBR treating raw wastewater and allowing recovery of water for further usage. Due to low energy consumption (0.3 kWh/m^3), there is also the possibility to run the MEBR using a solar system or other alternative energy.

Such solution would allow the system to be cost-effective and independent, and hence, making it even more advantageous in remote areas. This solution would additionally decrease operation costs of the system.

References

Mamrot (2016) Ministère des Affaires municipales et de l'Occupation du Direction de l'infrastructure, Stations d'épuration. www.mamrot.gouv.qc.ca

Bani Melhem K, Elektorowicz M (2010) Development of a novel submerged membrane electoro-bioreactor (SMEBR): performance for fouling reduction. Env. Sci. and Techn. 44 (9):3298–3304

Elektorowicz M, Ibeid S, Oleszkiewicz J (2011) Simultaneous Removal of C, P and N in a single electro-bioreactor. App patent EFS ID: 12030689, Int. App 61596471

Hasan SW, Elektorowicz M, Oleszkiewicz J (2014) Start-up period investigation of pilot-scale submerged membrane electro-bioreactor (SMEBR) treating raw municipal wastewater. Chemosphere 97:71–77

Ibeid S, Elektorowicz M, Oleszkiewicz J (2013a) Novel electrokinetic approach reduces membrane fouling. Water Res 47:6358–6366

Ibeid S, Elektorowicz M, Oleszkiewicz J (2016) Impact of electrocoagulation of soluble microbial products (SMP) on membrane fouling at different volatile suspended solids (VSS) concentrations. Environ Techn 38(4):385–393

Ibeid S, Elektorowicz M, Oleszkiewicz J (2015) Electro-conditioning of activated sludge in a membrane electro-bioreactor for improved dewatering and reduced membrane fouling. J Membrane Sci 494:136–142

Ibeid S, Elektorowicz M, Oleszkiewicz J (2013b) Modification of activated sludge characteristics caused by application of continuous and intermittent current. Water Res 47(2):903–910

Wei V, Elektorowicz M, Oleszkiewicz J (2011) Influence of electric current on bacterial viability in wastewater treatment. Water Res 45:5058–5062

Hasan SW, Elektorowicz M, Oleszkiewicz J (2012) Correlations between trans-membrane pressure (TMP) and sludge properties in submerged membrane electro-bioreactor (SMEBR) and conventional membrane bioreactor (MBR). Bioresource Techn 120:199–205

Potential and Challenges of Osmotic Membrane Bioreactor (OMBR) for (Potable) Water Reuse: A Pilot Scale Study

Gaetan Blandin[1(✉)], Joaquim Comas[1,2],
and Ignasi Rodriguez-Roda[1,2]

[1] LEQUIA, Institute of the Environment, University of Girona, Girona, Spain
[2] ICRA, Catalan Institute for Water Research, Girona, Spain

Abstract. Recently, forward osmosis (FO) has been applied to the context of membrane bioreactor (MBR) and is called osmotic MBR (OMBR). This promising process relying on a dense FO membrane and osmotic gradient demonstrated higher rejections of all contaminants and lower fouling propensity than for MBR. The concept that we developed aims at (partially) retrofit existing MBR into OMBR. In addition to the use of existing MBR installation, such process also allows for combined operation of MBR and OMBR to avoid salinity build-up and to be flexible/reversible in term of operation in MBR/OMBR modes to fit with (seasonal) water quality needs. The study presented aimed at validating the proof of concept of such retrofitting which includes also the development of OMBR/FO module with similar performance than MBR/UF ones. As such, OMBR plate were designed based on Kubota MF cartridge 203 design and using new generation of thin film composite FO membrane. Then, pilot tests were conducted using a 50L MBR/OMBR pilot for two months. Stable operation was obtained in terms of depuration efficiency and water flux. Salinity build up occurred in the reactor, but conductivity was maintained below 3 mS.cm-1 thanks to the salt purge via the MBR permeate. Fouling was observed both for MBR and OMBR operation; however, for OMBR, osmotic backwash every 3 days allowed for complete removal of the fouling layer. Finally, 90% rejection of all pharmaceuticals compounds tested was observed in OMBR operation as a result of combined biological degradation and high rejection of FO membranes.

Keywords: Membrane bioreactor · Forward osmosis · Water reuse

1   Introduction

Forward osmosis (FO) is an emerging and very promising membrane technology relying on an osmotic gradient driving force and a dense membrane (Klaysom et al. 2013). Thanks to this particular configuration, FO allows for high rejection of all contaminants while having low fouling propensity and does not require energy for water extraction. Recently, this concept has been extended to the context of membrane bioreactor (MBR) and is called osmotic MBR (OMBR) (Holloway et al. 2015a). As such, instead of using a porous ultrafiltration (UF) or microfiltration (MF) membrane,
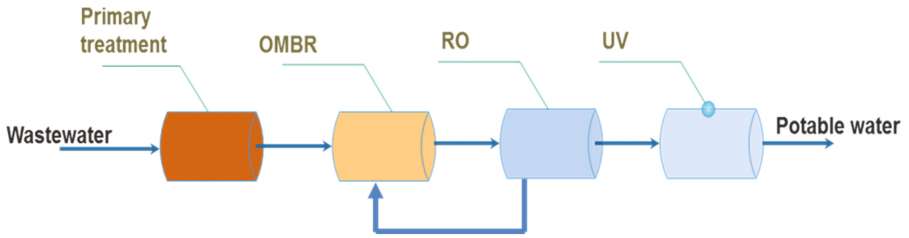
Fig. 1. OMBR-RO integration in water reuse

a dense FO membrane is submerged in a bioreactor and a saline (draw) solution is circulated on the other side of the membrane to extract the purified wastewater. In the context of water reuse OMBR can be combined with reverse osmosis (RO, for draw recovery in a closed loop) that offers water safety thanks to the double dense barrier protection and avoid the production of brine, which is a major economic advantage over MBR-RO (Fig. 1).

To date, one major technical OMBR limitation is the salinity build-up occurring in the submerged OMBR tank affecting the biodegradation efficiency due to (1) the accumulation of salts coming from the influent and (2) the reverse diffusion from the draw solution. To overcome these challenges, reducing sludge retention time, improving FO membranes, optimising the draw solution were all tested but none of them can offer an economically competitive solution. Another option investigated was to operate both a FO (OMBR) and UF/MF (MBR) systems in parallel, UF/MF acting as a salt purge. Long term operation of such system was demonstrated (Holloway et al. 2015b; Luo et al. 2015) but it mains drawback is the need to invest in novel and extended membrane filtration units and MBR/OMBR facilities. As an alternative, our study aims to evaluate the opportunity to (partially) retrofit existing MBR into OMBR. In addition to the use of existing MBR installation, such process also allows for combined operation of MBR and OMBR to avoid salinity build-up and to be
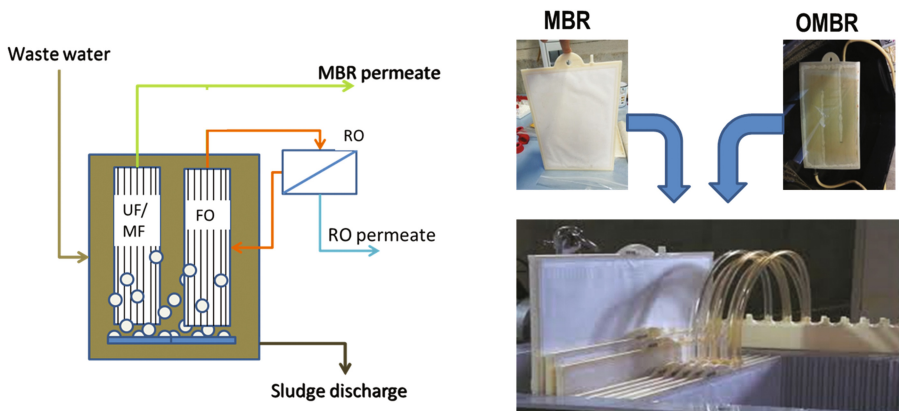
Fig. 2. Combined MBR-OMBR operation

flexible/reversible in term of operation in MBR/OMBR modes to fit with (seasonal) water quality needs (Fig. 2). Our study aimed at validating such retrofitting which also includes the development of OMBR/FO module with similar performance than MBR/UF ones.

2   Materials and Methods

OMBR plate design was developed based on Kubota MF cartridge 203 design and using new generation of thin film composite (TFC) FO membranes. Systematic assessment and validation of optimized OMBR plates were first realized (draw channel spacers, cross flow velocity, pumping mode, draw solution concentration) and compared to cross flow cell tests (optimum hydraulics).

Then, pilot tests were conducted using a 50L MBR/OMBR pilot for two months. The system was inoculated with sludge from a wastewater treatment plant and fed with synthetic wastewater. Concentration of the mixed liquor was maintained at 8 g.L^{-1}. The system was operated with 3 membrane plates, either KUBOTA MF plate or combination of MF and FO plates. Several short term tests were conducted over the two months of operation and after reactor stabilisation. Finally, pilot scale proof of concept was performed during two weeks in continuous operation with one MBR plate and two FO plates (TFC1 and TFC2).

3   Results and Discussion

First tests with tap water as feed demonstrated that thanks to new membranes and the developed design it was possible to operate OMBR plates at similar water flux than MF one (10-15 L.m^{-2}.h^{-1}) when using synthetic seawater (35 g.L^{-1}) as draw solution for the two tested TFC membranes (Fig. 3a). This represents already a strong water flux improvement in comparison with those commonly observed in the literature, i.e. typically much lower than 10 L.m^{-2}.h^{-1} and/or obtained with much higher draw concentration (Luo et al., 2017; Wang et al. 2017). Moreover, some important improvements are still possible and desirable so to operate the system at much lower draw concentration and to decrease RO operating pressure. Typically, based on our cross flow setup tests with optimised hydraulics, draw solution concentration as low as 10 g.L^{-1} can be sufficient to operate OMBR system (Fig. 3b).

During pilot scale testing, stable operation was obtained in terms of depuration efficiency with removal of COD above 95 and 98% and NH4+ above 90 and 97% for MF and FO membrane respectively. Water flux was maintained around 10 ± 2 L.m-2.h-1 for all tested membranes (Fig. 4).

Salinity build up occurred in the reactor, but conductivity was maintained below 4 mS.cm^{-1} thanks to the salt purge via the MBR permeate. Significant fouling was observed both for MBR and OMBR operation, probably amplified by imperfect aeration and continuous permeation (no relaxation nor backwashing cycle). Cleaning protocol was applied every three days, i.e. osmotic backwashing for OMBR membranes, chemical cleaning with NaOCl for MF membrane. Interestingly, for OMBR,
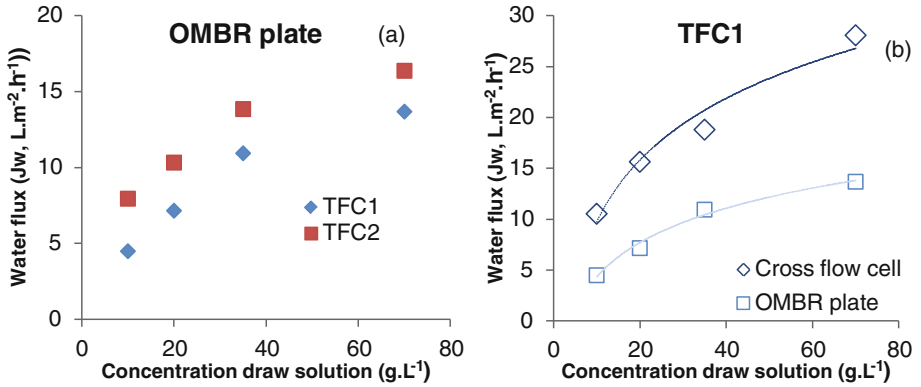
Fig. 3. Comparison of water permeation flux as function of draw concentration (seawater) for (a) OMBR plates and two different TFC FO membranes and (b) for cross flow cell (perfect hydraulics) and OMBR plates
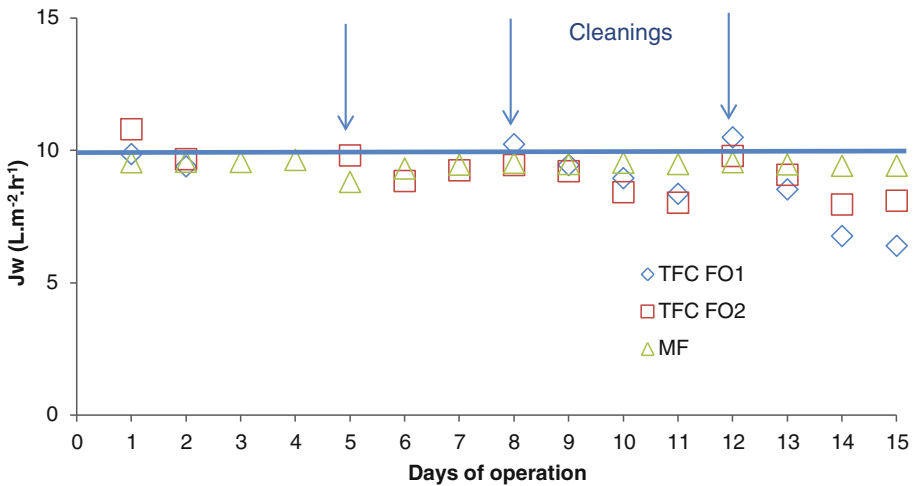
Fig. 4. Average daily water permeation flux during 2 weeks of operation of OMBR-MBR

osmotic backwash every 3 days allowed for complete removal of the fouling layer while chemical cleaning did not allow for complete recovery for MBR plate. Also, 90% rejection of all pharmaceuticals compounds tested was observed in OMBR operation as a result of combined biological degradation and high rejection of FO membranes. Reversely for MBR membrane, rejection of pharmaceuticals was solely driven by the biological degradation, the membrane itself not acting as a physical barrier.

4 Conclusions

Ultimately, the proof of concept of retrofitting and upgrading MBR into OMBR was performed and demonstrated the positive impact of OMBR in term of moderate fouling and high rejection of all contaminants to support water reuse scheme. Further work is required to further develop and assess OMBR on a longer term operation.

References

Holloway RW, Achilli A, Cath TY (2015a) The osmotic membrane bioreactor: a critical review. Environ Sci Water Res Technol 1:581–605

Holloway RW, Wait AS, Fernandes da Silva A, Herron J, Schutter MD, Lampi K, Cath TY (2015b) Long-term pilot scale investigation of novel hybrid ultrafiltration-osmotic membrane bioreactors. Desalination 363:64–74

Klaysom C, Cath TY, Depuydt T, Vankelecom IFJ (2013) Forward and pressure retarded osmosis: potential solutions for global challenges in energy and water supply. Chem Soc Rev

Luo W, Hai FI, Kang J, Price WE, Nghiem LD, Elimelech M (2015) The role of forward osmosis and microfiltration in an integrated osmotic-microfiltration membrane bioreactor system. Chemosphere 136:125–132

Luo W, Phan HV, Xie M, Hai FI, Price WE, Elimelech M, Nghiem LD (2017) Osmotic versus conventional membrane bioreactors integrated with reverse osmosis for water reuse: biological stability, membrane fouling, and contaminant removal. Water Res 109:122–134

Wang X, Zhao Y, Li X, Ren Y (2017) Performance evaluation of a microfiltration-osmotic membrane bioreactor (MF-OMBR) during removing silver nanoparticles from simulated wastewater. Chem Eng J 313:171–178

Low-Cost Ceramic Membranes Manufacture for MBR: Comparison of Pilot and Industrial Scale

E. Zuriaga[1(✉)], I. Pastor[1], B. Hernández[1], L. Basiero[1],
M.-M. Lorente-Ayza[2], M.C. Bordes[2], E. Sanchez[2], and M. Abellán[3]

[1] Sociedad de Fomento Agrícola Castellonense S.A. (FACSA), Castellón, Spain
ezuriaga@facsa.com
[2] Departamento Ingenieria Química,
Instituto Universitario Tecnología Cerámica,
University Jaume I, Castellón, Spain
[3] Enstidad de Saneamiento y Depuración de la Región de Murcia (ESAMUR),
Murcia, Spain

Abstract. The objective of this study is to manufacture ceramic membranes with lower cost than the commercial ceramic ones, more sustainable and competitive. Tewari et al. (2010) evaluated the efficiency of low cost ceramic membranes at laboratory scale. The membranes developed are made from agricultural and industrial wastes, such as olive stones (from olive oil production) used as a pore former, marble powder and chamotte (from fired tile scrap). Different formulations have been compared to achieve the adequate plasticity of the mixture and permeability of the membrane. The properties of the ceramic membrane are mainly determined by their composition, particle size of the pore former and sintering temperature. The membranes are being validated at pilot scale in the university and at industrial scale in an MBR located in Aledo WWTP (Murcia, Spain).

Keywords: Membrane bioreactor · Ceramic membrane · Water reuse

1 Introduction

Water reclamation and reuse in the Mediterranean region has become more important in recent years due to water scarcity. Membrane technology allows the reuse of the treated water for irrigation or other issues. One of these technologies applied in the wastewater treatment plants (WWTP) is the membrane bioreactor (MBR), which combines the biological treatment with membrane processes. The advantage that the membrane bioreactor offers is that it is a compact system, which allows working with high concentration of mixed liquor suspended solids (MLSS), low production of excess sludge and better quality of treated water. The disadvantage is the membrane fouling, which decreases permeability and requires cleaning procedures and membrane replacement.

MBRs can operate with organic and inorganic membranes. Through this work ceramic flat-sheet membranes been developed. The advantage of these membranes

is that they are more robust and they have better chemical, thermal and mechanical properties, which facilitates their operation under severe conditions and also to apply harsh cleaning procedures (high temperature and strong cleaning reagents). Regarding the fouling of ceramic membranes in comparison with the polymeric ones, similar trends were obtained by Lee and Kim (2014). The drawback of conventional ceramic membranes is that they are more expensive, due to the cost of the materials used in their manufacture (alumina, titania or zirconia oxides) and the difficulty of processing them.

2   Materials and Methods

The ceramic membranes developed in this project are based on raw materials normally used in the ceramic tile industry (basically clay, quartz and feldspar), mixed with agro-industrial wastes in elevated proportions (higher than 40% wt), such as marble dust (from the marble working industry), chamotte from fired scrap (from ceramic tile industry) and olive stones (from the olive oil industry).

Ceramic flat-sheet membranes can be manufactured by both, extrusion and dry pressing. The membrane's properties (pore size, permeability, etc.) are directly affected by the shaping method, as Lorente-Ayza et al. (2015) pointed out. Nevertheless, extrusion allows the manufacture of a wide range of configuration and shapes and, consequently, has been chosen as the support's method of manufacture. In Fig. 1, a layout of the support manufacturing process is provided. First, raw materials and wastes are mixed in the suitable proportions with water, to obtain a paste with enough plasticity to be extruded. Next, the material is forced to pass through a shredder into a vacuum chamber; finally, an auger is used to consolidate the material and extrude it through the die. After a slow drying, the membranes are sintered; the sintering cycle should be defined to avoid the incidence of defects and ensure the mechanical strength of the membrane; nevertheless, the maximum sintering temperature and dwelling time influences directly over the permeability and pore size of the obtained membrane.
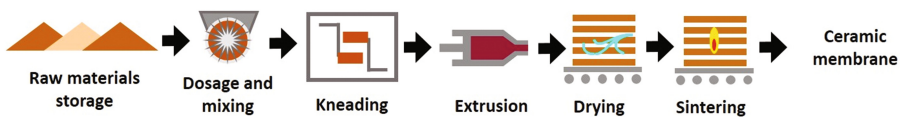
Fig. 1. Scheme of membrane manufacture by extrusion

It has to be highlighted that the scaling up of the pilot membrane manufacturing process to industrial scale is a very complex stage, since although the equipments are similar, they have different characteristics. For example, the extruder device used at industrial scale can apply higher pressure to the material and obtains higher vacuum pressures, and, as a consequence, the extruded membranes present higher bulk density (lower porosity) and higher mechanical resistance. On the other hand, the industrial kilns used to sinter the membranes show higher gradients of temperature, so the properties of the sintered membranes could present more dispersion.

3   Results

In the present work, the characteristics of recycled ceramic membranes obtained at pilot and industrial scale have been compared, in terms of water absorption, water permeability and mean pore size, being water absorption representative of the open porosity.

The membrane area of the industrial and pilot membranes is 0.2 m^2 and 0.09 m^2, respectively. Both membranes are manufactured with inner channels to facilitate the permeate collection and plastic caps have been designed to collect the effluent.

Figures 2 and 3 show how the membranes obtained at pilot scale present higher permeability and porosity than the industrial ones. Moreover, the evolution when the
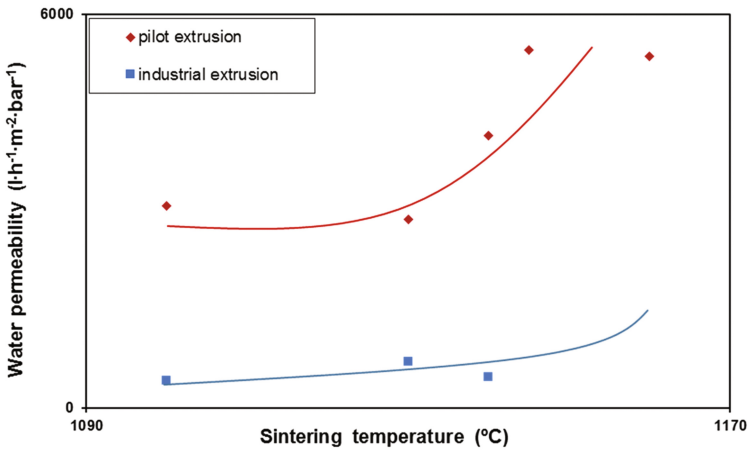
Fig. 2. Evolution of water permeability at increasing sintering temperature
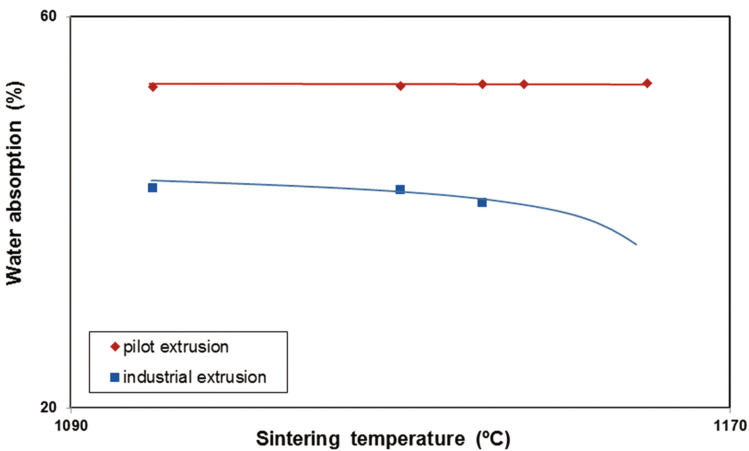
Fig. 3. Evolution of water absorption at increasing sintering temperature

sintering temperature is increased is also different at both scales. Finally, the mean pore size varies from values of 6 μm for the pilot membranes to 2 μm for the industrial membranes.

4   Conclusions

Ceramic membranes based on agro-industrial wastes have been manufactured at pilot and industrial scale. Comparing both membranes it has to be concluded that the properties of the ones manufactured at industrial scale (in a conventional ceramic tile industry) have better properties than the pilot membranes, achieving lower pore size, porosity and water permeability. This is due to pressure that the extruder can apply. In order to adapt the industrial process to the manufacture of membranes the raw materials pretreatment were adapted to the real scale and the sintering process.

Due to the differences found between the two manufacturing processes tested, the validation in the wastewater treatment plant is being developed with the membrane manufactured at industrial scale and it has been discarded the pilot scale one. The concentration of MLSS in the pilot MBR is between 5–8 g/L and the COD in the permeate is being analyzed and transmembrane pressure is being monitored.

References

Lee SJ, Kim JH (2014) Differential natural organic matter fouling of ceramic versus polymeric ultrafiltration membranes. Water Res 48:43–51

Tewari PK, Singh RK, Batra VS, Balakrishnan M (2010) Membrane bioreactor (MBR) for wastewater treatment: filtration performance evaluation of low cost polymeric and ceramic membranes. Sep Purif Technol 71(2010):200–204

Lorente-Ayza M-M, Mestre S, Menéndez M, Sánchez E (2015) Comparison of extruded and pressed low cost ceramic supports for microfiltration membranes. J Eur Ceram Soc 35:3681–3691

The Sludge Dewaterability in Advanced Wastewater Treatment: A Survey of Four Different Membrane BioReactor Pilot Plants

G. Mannina$^{(\boxtimes)}$, M. Capodici, and G. Viviani

Dipartimento di Ingegneria Civile, Ambientale, Aerospaziale,
dei Materiali, Università degli Studi di Palermo, Palermo, Italy

Abstract. The wasted activated sludge dewaterability represents a major concern for Wastewater Treatment Plants (WWTPs) managers. Indeed, whereas the dewatered sludge could represents a re-usable matrix, the principal drawback related to the wasted sludge dewaterability is the high water content due to the presence of extracellular polymeric substances (EPS) that allow the trapping of water molecules within the bio sludge flocs. In order to provide an outlook of the dewaterability features of activated sludge derived from advanced WWTP, the present research reports a long term survey (over two years) aimed at assessing the principal dewaterability parameters of the sludge wasted from different Membrane BioReactor pilot plants.

Keywords: Sludge dewaterability · MBR · EPS · CST · SRF

1 Introduction

The wasted activated sludge dewaterability represents a major concern for Wastewater Treatment Plants (WWTPs) managers. Indeed, whereas the dewatered sludge could represents a re-usable matrix (e.g., as a supplement to composting or as a feedstock to energy production, Skinner et al. 2015), the re-use results limited by the high cost involved in transport and drying.

Furthermore, when sludge features avoid the re-use, the disposal costs significantly affect the WWTP economical management, up to 60% (Chen et al. 2016; Low et al. 2000). As the cost for sludge treatment and disposal ranges around 280–470 €/t and since 1t of fresh sludge to be disposed is composed on average by 0.25–0.30 t of suspended solids (SS), the correct understanding of dewaterability phenomenon represents a key factor in order to improve the effectiveness of water separation process (Capodici et al. 2016; Ginestet 2007).

In order to cope with the needing of reduce sludge impact on the economic management of WWTP, researcher and designer interest moved in developing and refining treatment technologies such as membrane bioreactors (MBR), capable to reduce the specific sludge production. However, despite such efforts mechanical dewatering represents up to nowadays a crucial step in reducing the amount of sludge to be disposed (Marinetti et al. 2009).

Several studies have been carried out in order to identify the most effective dewatering strategy (among others, Bonilla et al. 2015; Chen et al. 2016; Liu et al. 2016; Rao et al. 2017). The principal drawback related to the wasted sludge dewaterability is the high water content due to the presence of extracellular polymeric substances (EPS) that allow the trapping of water molecules within the bio sludge flocs (Mowla et al. 2013).

In details, four different types of water contained in sludge have been defined: free water, interstitial water, vicinal water and water of hydratation.

More in details, gravitational settling can easily separate free water. Mechanical dewatering devices, such as centrifugation or vacuum filtration, can achieve interstitial water separation. Any mechanical device cannot separate vicinal water, physically bound to solid particles surface. Water of hydratation, chemically bound to solid particles surface, can be separated only by heating at temperature above 105°C (Mowla et al. 2013).

However, it is worth noticing that also the WWTP layout, affecting the metabolic reactions that may occur, play a role in the complex dewaterability phenomenon. Indeed, the sludge origin is recognized as one of the key factor involved in sludge dewaterability (Capodici et al. 2016; Jin et al. 2004; Wang et al. 2014).

In order to provide an outlook of the dewaterability features of activated sludge derived from advanced WWTP, the present research reports a long term survey (over two years) during which the principal dewaterability parameters of the wasted sludge were investigated.

In details, four different WWTPs layout were investigated: System batch reactor (SBR), pre denitrification scheme, University of Cape Town (UCT) scheme and Integrated Fixed Film Activated Sludge (IFAS) operated in UCT scheme.

Furthermore, it was applied also a variation of the influent wastewater features and the operational parameters, such as sludge retention time (SRT) and hydraulic retention time (HRT). During the aforementioned layout the solid liquid separation was achieved by means of an hollow fibres ultrafiltration (UF) unit, thus applying the Membrane Bio Reactor (MBR) technology.

2 Materials and Methods

The sludge investigated in the present study were collected from 4 different MBR pilot plant, realized at the Laboratory of Sanitary and Environmental Engineering of Palermo University, fed with wastewater taken from the sewer system of the Palermo University and operated in 7 different conditions (see Table 1).

During the configuration I, II and III, solid–liquid separation was performed via UF membrane module Zenon Zeeweed, ZW 10, with specific area equal to 0.98 m^2 and a nominal porosity of 0.04 μm. During configurations IV, V, VI, and VII the solid–liquid separation phase was carried out by means of an UF module Koch PURON® 3 bundle with specific area equal to 1.40 m^2 and a nominal porosity of 0.03 μm.

The dewaterability was investigated by measuring, in accordance with literature (Capodici et al. 2016), in mixed liquor samples collected from each biological reactor, the Capillary Suction Time (CST) and the Specific Resistance to Filtration (SRF) in void conditions (–50 kPa).

Table 1. Layout and operative condition of the investigated MBR systems

Phase	WWTP Layout	MBR module	Operative condition	Reference
I	SBR-DN-MBR	ZW10	Stepwise salinity (0–10 gNaCl L^{-1})	(Mannina et al. 2016a)
II	DN-MBR	ZW10	Stepwise salinity (10–20 gNaCl L^{-1})	(Mannina et al. 2016b)
III	DN-MBR	ZW10	20 gNaCl L^{-1} and diesel fuel	(Mannina et al. 2016b)
IV	UCT-MBR	PURON	Influent C/N variation	(Mannina et al. 2016c)
V	UCT-IFAS-MBR	PURON	SRT variation	
VI	UCT-IFAS-MBR	PURON	Influent C/N variation	
VII	UCT-IFAS-MBR	PURON	HRT/SRT variation	

Furthermore, in order to highlight the influence exerted by the biological behaviour of biomass on the dewaterability features, the main chemical parameters were measured in accordance with standard methods (APHA 2005): among others, Chemical Oxygen Demand (COD), Total Nitrogen (TN), and nitrogen forms (NH4-N, NO2-N, NO3-N), Total Suspended Solid (TSS). Moreover, since the EPS content of mixed liquor is recognized as a key factor related to sludge dewaterability features, the total EPS content and the Soluble Microbial Product (SMP) were measured in accordance with literature (Capodici et al. 2014; Cosenza et al. 2013).

3   Results

A correspondence between the sludge dewaterability features and the different lay out configurations was noticed.

In Fig. 1, the mean values of CST measured in the aerobic reactor during each experimental Phase are depicted.

Reported data allow to observe that during the Phases I, II and III (salinity stepwise phase and diesel fuel addition, see Table 1), the CST increased with the salinity increase. Thus, when diesel fuel was treated, the CST (as well as SRF) sharply increased (142 s as maximum CST measured during Phase III).

The SRF measurements provided similar results, thus corroborating the CST findings with respect to the progressive decrease of sludge filterability during Phase III. The worsening in the sludge filterability was also noticed by filtering the sample collected for the chemical analysis. Indeed, a longer duration of the vacuum pump operations needed to collect significant volumes of filtered sample was required during Phase III.

Furthermore, after filtration, the filtration media resulted covered by a homogeneous jelly layer. Such result is likely ascribable to a progressive increase in sludge viscosity due both to the salinity increase and to the hydrocarbon presence.
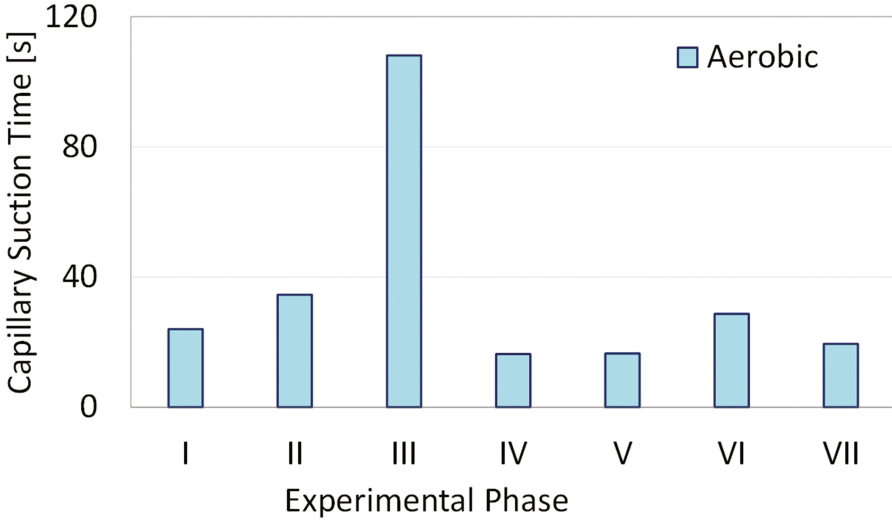
Fig. 1. Mean values of Capillary Suction Time measured on sludge collected from aerobic reactor during the experimentation

Furthermore, during the experimentation it was noticed the influence exerted by EPS and SMP content. In Fig. 2 some correlations involving EPS, SMP, CST and SRF during Phase V are depicted.
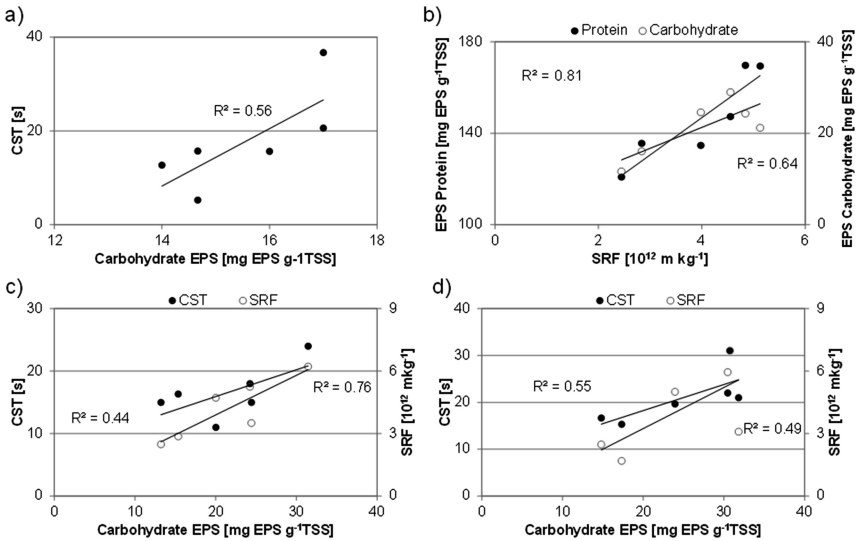
Fig. 2. Correlation during Phase V: CST vs specific bound carbohydrates EPS in anaerobic reactor (a); specific bound proteins and carbohydrates EPS vs SRF in anoxic reactor(b); CST and SRF vs specific bound carbohydrates EPS in aerobic reactor (c); CST and SRF vs specific bound carbohydrates EPS in MBR reactor (d)

Results reported in Fig. 2 highlight that the carbohydrate fraction of EPS significantly affected the dewaterability during Phase II. In details sludge derived from aerobic and MBR reactors (Fig. 2c and d) resulted affected from carbohydrate in terms of CST as well as SRF. Conversely, in the anoxic reactor the influence exerted by the protein fraction resulted evident ($R2 = 0.81$).

The anaerobic reactor resulted less affected by the EPS content likely due to the lowest TSS concentration.

4 Conclusion

The hardest sludge to be dewatered was found during the phases I, II and III. Such result points out the importance played by influent features in affecting dewaterability. Indeed, during the stepwise salinity increase, the CST as well as the SRF grew up. Moreover, when hydrocarbon was treated (Phase III), the dewatering operations resulted extremely difficult to accomplish. Moreover, this finding allows affirming that further study aimed at improving the dewaterability of sludge originated from industrial wastewater treatment are needed.

References

APHA (2005) Standard methods for the examination of water and wastewater. Stand Methods 541. doi:10.2105/AJPH.51.6.940-a

Bonilla S, Tran H, Allen DG (2015) Enhancing pulp and paper mill biosludge dewaterability using enzymes. Water Res 68:692–700. doi:10.1016/j.watres.2014.10.057

Capodici M, Di Bella G, Nicosia S, Torregrossa M (2014) Effect of chemical and biological surfactants on activated sludge of MBR system: microscopic analysis and foam test. Bioresour Technol 177. doi:10.1016/j.biortech.2014.11.064

Capodici M, Mannina G, Torregrossa M (2016) Waste activated sludge dewaterability: comparative evaluation of sludge derived from CAS and MBR systems. Desalin Water Treat 57. doi:10.1080/19443994.2016.1180478

Chen Z, Zhang W, Wang D, Ma T, Bai R, Yu D (2016) Enhancement of waste activated sludge dewaterability using calcium peroxide pre-oxidation and chemical re-flocculation. Water Res 103:170–181. doi:10.1016/j.watres.2016.07.018

Cosenza A, Di Bella G, Mannina G, Torregrossa M (2013) The role of EPS in fouling and foaming phenomena for a membrane bioreactor. Bioresour Technol 147:184–192. doi:10.1016/j.biortech.2013.08.026

Ginestet P (2007) Comparative evaluation of sludge reduction routes. Eur Water Res Ser. doi:10.1017/CBO9781107415324.004

Jin B, Wilén BM, Lant P (2004) Impacts of morphological, physical and chemical properties of sludge flocs on dewaterability of activated sludge. Chem Eng J 98:115–126. doi:10.1016/j.cej.2003.05.002

Liu H, Xiao H, Fu B, Liu H (2016) Feasibility of sludge deep-dewatering with sawdust conditioning for incineration disposal without energy input. Chem Eng J 313:655–662. doi:10.1016/j.cej.2016.09.107

Low EW, Chase HA, Milner MG, Curtis TP (2000) Uncoupling of metabolism to reduce biomass production in the activated sludge process. Water Res 34:3204–3212. doi:10.1016/s0043-1354(99)00364-4

Marinetti M, Malpei F, Bonomo L (2009) Relevance of expression phase in dewatering of sludge with chamber filter presses. J Environ Eng ASCE 135(12):1380–1387

Mannina G, Capodici M, Cosenza A, Di Trapani D (2016a) Carbon and nutrient biological removal in a University of Cape Town membrane bioreactor: Analysis of a pilot plant operated under two different C/N ratios. Chem Eng J 296:289–299. doi:10.1016/j.cej.2016.03.114

Mannina G, Capodici M, Cosenza A, Di Trapani D, Viviani G (2016b) Sequential batch membrane bio-reactor for wastewater treatment: the effect of increased salinity. Bioresour Technol 209:205–212. doi:10.1016/j.biortech.2016.02.122

Mannina G, Cosenza A, Di Trapani D, Capodici M, Viviani G (2016) Membrane bioreactors for treatment of saline wastewater contaminated by hydrocarbons (diesel fuel): an experimental pilot plant case study. Chem Eng J 291. doi:10.1016/j.cej.2016.01.107

Mowla D, Tran HN, Allen DG (2013) A review of the properties of biosludge and its relevance to enhanced dewatering processes. Biomass Bioenerg 58:365–378. doi:10.1016/j.biombioe.2013.09.002

Rao B, Huang G, Lu X, Wan Y, Jiang Z, Chen D, Liu X, Liang A (2017) An ultrahigh-pressure filtration and device design and optimiz study on high dry dewatering of sludge. Process Saf Environ Prot 106:129–137. doi:10.1016/j.psep.2017.01.001

Skinner SJ, Studer LJ, Dixon DR, Hillis P, Rees CA, Wall RC, Cavalida RG, Usher SP, Stickland AD, Scales PJ (2015) Quantification of wastewater sludge dewatering. Water Res 82:2–13. doi:10.1016/j.watres.2015.04.045

Wang LF, He DQ, Tong ZH, Li WW, Yu HQ (2014) Characterization of dewatering process of activated sludge assisted by cationic surfactants. Biochem Eng J 91:174–178. doi:10.1016/j.bej.2014.08.008

Application of the Oxic-Settling-Anaerobic Process in a Membrane Bioreactor for Excess Sludge Reduction

T. Silva de Oliveira[✉], S.F. Corsino, D. Di Trapani,
and M. Torregrossa

Department of Civil, Environmental, Aerospatial Engineering and Material,
University of Palermo, Viale delle Scienze Building 8, 90128 Palermo, Italy

Abstract. The main goal of this study was the evaluation of the excess sludge reduction in a MBR for biological nitrogen removal (BNR) through the implementation of the Oxic-Settling-Anaerobic (OSA) process. For this purpose, a MBR pilot plant (42 L volume) was realized according to a pre-denitrification scheme. The whole experimentation was divided into two periods, named Period 1 and Period 2, respectively. In Period 1 the pilot plant was started-up and the excess sludge production was evaluated. In Period 2 the plant configuration was partially modified by inserting an anaerobic reactor into the return activated sludge (RAS) line to realize an OSA configuration. In Period 1, the Y_{obs} resulted equal to 0.39 gVSS $g^{-1}COD_{removed}$, in accordance with the reference values for MBR plants reported in the literature (Wang et al. 2013). Similarly, all the kinetic and stoichiometric parameters, for both autotrophic and heterotrophic biomass, resulted in line with those reported in a MBR with a pre-denitrification scheme (Lubello et al. 2009). In contrast, in Period 2 the Yobs showed a significant decrease, reaching a pseudo steady-state value of 0.17 gVSS $g^{-1}COD_{removed}$ at the end of the experiments, highlighting a reduction of 55% compared to Period 1.

Keywords: Membrane bioreactor · Excess sludge minimization · OSA

1 Introduction

In the last years, biological treatment has become one of the most adopted alternatives for wastewater treatment. Nevertheless, besides its good performances, there are some issues that still deserve attention, i.e. the operating costs that concern mainly the disposal of the excess sludge production. According to the literature, the European Union annually produces over 10 million tons of waste activated sludge (WAS) and the United States currently generates about 8.2 million tons of dry WAS per year (Wang et al. 2012). The European Waste Framework Directive (2008/98 CE) highlighted that the minimization at the source must be a priority.

Nevertheless, the treatment and disposal of excess sludge is expensive. Usually, it accounts about 30–60% of the total operating cost in a conventional activated sludge (CAS) treatment plant (Saby et al. 2003). Some authors have explored in the last years different solutions to reduce the excess sludge production, but most of the known alternatives imply high energy consumption that raises the costs, thus making them difficultly applicable (Foladori et al. 2010).

Among these alternatives, the use of the Oxic-Settling-Anaerobic (OSA) process have been widely studied, mainly in CAS systems (Torregrossa et al. 2012). However, few authors have combined the OSA system with Membrane-Bioreactors (MBRs). Therefore, there are still several challenges to identify the optimal plant configuration, since it is not trivial to find a good balance between the necessary sludge production and the reduction of the excess production.

Semplante et al. (2014) in a review paper highlighted that a plant configuration with anoxic, aerobic and anaerobic alternation can achieve 50% of excess sludge reduction, even in CAS configuration. By including the use of MBR for the liquid-solid separation, this rate could improve. MBRs have four mechanisms for sludge minimization: biological maintenance metabolism, lysis-cryptic growth, predation of bacteria and uncoupling metabolism, also MBRs are operated under long sludge retention time (SRT) resulting in low food/microorganisms (F/M) ratio and a high mixed liquor suspended solids (MLSS) concentration (Wang et al. 2013).

Bearing in mind the above considerations, the main goal of this study was the evaluation of the excess sludge reduction in a MBR for biological nutrients removal by means of implementation of the OSA process.

2   Materials and Methods

In this study, the excess sludge production in a submerged MBR pilot plant for biological nutrients removal was monitored. The MBR pilot plant (42 L) was realized according to a pre-denitrification scheme. Particularly, the pilot plant consisted of an anoxic (18 L) and an aerobic tank (24 L). The solid-liquid separation phase was achieved by an ultrafiltration hollow-fiber membrane module (PURON® Single bundle Demo, nominal pore size 0.03 μm, membrane area 0.47 m^2) located within the aerobic tank (thus, in a submerged configuration). The filtration cycle had a duration of 6 min, divided into 5 min of permeate suction and 1 min of backwashing. The membrane backwashing was performed by pumping a volume of permeate back through the membrane fibers from the Clean In Place (CIP) tank.

The MBR was seeded with activated sludge collected from a wastewater treatment plant with a conventional activated sludge scheme (inoculum TSS equal to 3 gTSS L^{-1}).

The whole experimentation was divided into two periods, named Period 1 and Period 2, respectively. In Period 1, the pilot plant was started-up and the excess sludge production was evaluated. The MBR was fed with synthetic wastewater through a peristaltic pump from a feeding tank to the anoxic reactor, with a flow rate approximately equal to 2.3 Lh^{-1}. Then, the mixed liquor flowed by gravity to the aerobic/membrane reactor where a net permeate flow rate close to 2.3 Lh^{-1} was extracted through the membrane module. The mixed liquor was pumped to the anoxic tank via an internal recycling with a flow rate equal to 11.5 Lh^{-1}, corresponding to a nitrate recycling ratio of 5:1. This period lasted about 4 weeks, until steady-state conditions were reached.

In Period 2, the plant configuration was partially modified by inserting an anaerobic reactor into the return activated sludge (RAS) line to realize an OSA configuration. Particularly, in addition to the configuration above described, a fraction of the mixed liquor was pumped from the aerobic tank to the OSA reactor (13.8 L) with a flow rate

equal to 2.3 Lh^{-1} and then it was recycled to the anoxic reactor. The hydraulic retention time (HRT) in the OSA reactor was imposed equal to 6 h (about one third of the HRT of the entire pilot plant).

The anoxic and the OSA reactors were continuously mixed by a vertical axis mixer. In the aerobic/membrane reactor, the oxygen was supplied by a blower connected to a diffuser porous stone placed at the bottom of the reactor.

The synthetic wastewater was composed of (in 100 L): 35 g of potato starch, 4.5 g of peptone, 15 g of sodium acetate (CH_3COONa), 4 g of urea (CH_4N_2O), 14.5 g of ammonium chloride (NH_4Cl) and 6 g of dipotassium phosphate (K_2HPO_4). The main influent wastewater characteristics are summarized in Table 1.

The influent wastewater, the mixed liquor inside the anoxic, aerobic, OSA tanks and the permeate were sampled three times a week for the physical-chemical analyses.

Table 1. Summary of the main wastewater influent characteristics

	MBR	Unit
Total COD	580 ± 15	(mg L^{-1})
Soluble COD	435 ± 23	(mg L^{-1})
Total Nitrogen	63 ± 8	(mg L^{-1})
NH_4-N	57 ± 4	(mg L^{-1})
PO_4-P	12 ± 2	(mg L^{-1})
BOD_5	386 ± 12	(mg L^{-1})

In particular, the biological performances were monitored through the total chemical oxygen demand (tCOD), soluble COD (sCOD), ammonium nitrogen (NH_4-N), nitrate nitrogen (NO_3-N), total nitrogen (TN), Biochemical Oxygen Demand (BOD) analyses in the influent wastewater, in the anoxic and aerobic supernatant and in the permeate. Moreover, total suspended solids (TSS), volatile suspended solids (VSS) and sludge features (granulometry, viscosity, hydrophobicity, sludge volume index (SVI), extracellular polymeric substances (EPS) and dewaterability) were performed once a week in all the reactors. All the chemical-physical analyses were carried out according to the Standard Methods (APHA 2005). In order to evaluate the effect of the OSA process implementation on the biomass biological diversity, microscopic observations were carried out for the identification of filamentous bacteria and other microorganisms.

The observed heterotrophic yield coefficient (Y_{obs}), referred to the whole system, was evaluated through mass balances between sludge withdrawn, sludge production and solids in the effluent, dividing by the cumulated TCOD removed, according to the procedure reported by Torregrossa et al. (2012).

In addition, respirometric batch experiments were performed to evaluate both the autotrophic and heterotrophic kinetic parameters. Furthermore, pH, dissolved oxygen (DO), oxidation-reduction potential (ORP) and temperature were also monitored in each tank by means of specific probes. Lastly, in order to estimate the excess sludge production, the specific observed heterotrophic yield coefficient (Yobs), referred to the whole system, was calculated on the basis of mass balances between sludge withdrawn and sludge production, dividing by the cumulated sCOD removed.

3   Results and Discussion

The achieved results highlighted excellent performances in terms of organic matter removal. Indeed, the total COD removals (average values) were 95 and 98% in Period 1 and Period 2, respectively. Even the biological COD removal (i.e. evaluated upstream membrane filtration) was particularly high, with an average value approximately equal to 94% throughout the experiments. The observed data confirmed the high robustness of MBRs systems towards the removal of the organic substrates.
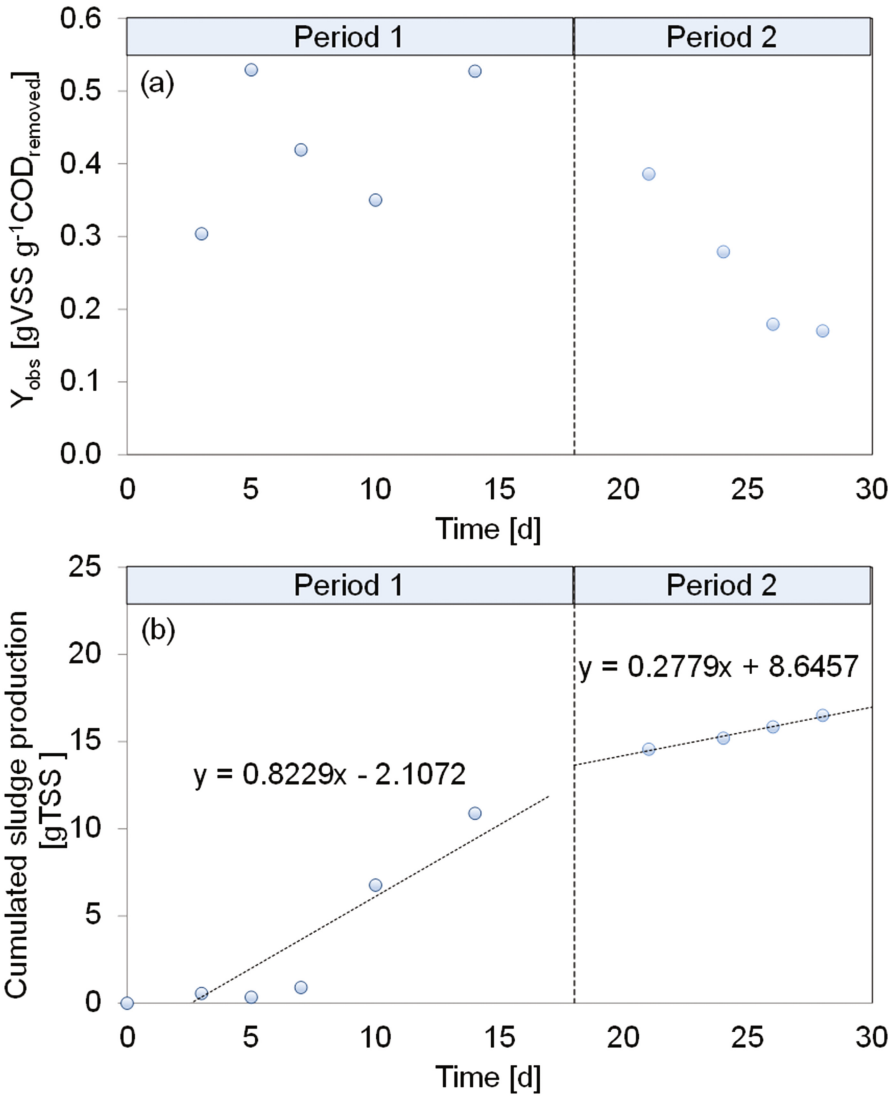
Fig. 1. Profiles of Y_{obs} (a) and cumulated excess sludge production (b) throughout experiments

Concerning the reduction of sludge production, Fig. 1a depicts the assessed Y_{obs} values, whilst Fig. 1b reports the cumulated sludge produced throughout the experiments.

From the observation of data reported in Fig. 1a, the Yobs decreased from an average value of 0.39 gVSS g^{-1}COD$_{removed}$ in Period 1 to a steady state value of 0.17 gVSS g^{-1}COD$_{removed}$ at the end of Period 2, corresponding to a 55% net reduction. It is worth noting that such a reduction was achieved with a HRT of the OSA reactor of 6 h only; a further increase of the HRT would likely increase this reduction, thus enhancing to reach a potential "zero net growth".

As shown in Fig. 1b, after the change of the pilot plant configuration, characterized by the introduction of the OSA reactor, the net sludge production significantly decreased compared to what observed in Period 1. Indeed, in Period 1 the sludge production was 0.83 gTSS d^{-1}, while in Period 2 it decreased down to 0.28 gTSS d^{-1}, thus confirming the effectiveness of the OSA configuration.

In terms of biomass biokinetic activity, evaluated through respirometry, Table 2 summarizes the main kinetic/stoichiometric values achieved throughout the experiments.

Table 2. Average values of the main kinetic and stoichiometric parameters measured during experiments

Plant configuration	MBR	MBR-OSA
Heterotrophic		
Y_H [g VSS g^{-1} COD]	0.54	0.44
Y_H [mg COD mg^{-1} COD]	0.78	0.63
$\mu_{H,max}$ [d^{-1}]	2.58	2.10
K_S [mg COD L^{-1}]	2.74	4.58
SOUR$_{max}$ [mg O$_2$ g^{-1}VSS h^{-1}]	26.69	29.57
Autotrophic		
Y_A [g VSS g^{-1}NH$_4$-N]	0.19	0.21
$\mu_{A,max}$ [d^{-1}]	0.28	0.29
K_{NH} [mg NH$_4$-N L^{-1}]	3.22	2.88
SOUR$_{max}$ [mg O$_2$ g^{-1}VSS h^{-1}]	15.96	19.64

From the observation of Table 2, it is worth noting that the Y_H values achieved through respirometry were slightly higher compared to the Y_{obs} ones. This discrepancy is only apparent: indeed, the Yobs values were evaluated on the basis of mass balances, that took into account the biomass decay, differently from a respirometric batch test which duration is much more limited.

4   Conclusions

The present study explored the performance of an OSA-MBR pilot plant for the reduction of sludge production. The achieved results highlighted the high potentiality of this configuration, enhancing the reduction of the observed sludge yield up to 55%. Moreover, the performances of the system in terms of organic matter removal

efficiency were not significantly affected by the change in configuration, with a total COD removal of 98% in Period 2 (OSA configuration). Since the HRT of the OSA reactor was imposed at 6 h only, it is possible to assume that future research activities characterized by higher HRT values might enhance a further decrease of the excess sludge production.

References

Foladori P, Andreotolla G, Ziglio G (2010) Sludge reduction technologies in wastewater treatment plants. IWA Publishing. 380 p. ISBN 13: 9781843392781

Lubello C, Caffaz S, Gori R, Munz G (2009) A modified Activated Sludge Model to estimate solids production at low and high solids retention time. Water Res 43(18):4539–4548

Saby S, Djafer M, Chen G (2003) Effect of low ORP in anoxic sludge zone on excess sludge production in oxic-settling-anoxic activated sludge process. Water Res 37:11–20

Semblante G, Hai F, Ngo H, Guo W, You S, Price W (2014) Sludge cycling between aerobic, anoxic and anaerobic regimes to reduce sludge production during wastewater treatment: Performance, mechanisms, and implications. Biores Technol 155:395–409

Torregrossa M, Di Bella G, Di Trapani D (2012) Comparison between ozonation and the OSA process: analysis of excess sludge reduction and biomass activity in two different pilot plants. Water Sci Technol 66:185–192

Wang Z, Yu H, Ma J, Zheng X, Wu Z (2013) Recent advances in membrane bio-technologies for sludge reduction and treatment. Biotechnol Adv 31:1187–1199

Wang ZW, Mei XJ, Ma JX, Wu ZC (2012) Recent advances in microbial fuel cells integrated with sludge treatment. Chem Eng Technol 35(10):1733–1743

Anaerobic Digestion

ZVI Addition in Continuous Anaerobic Digestion Systems Dramatically Decreases P Recovery Potential: Dynamic Modelling

D. Puyol[1(✉)], X. Flores-Alsina[2], Y. Segura[1(✉)], R. Molina[1],
S. Jerez[1], K.V. Gernaey[2], J.A. Melero[1], and F. Martinez[1]

[1] Universidad Rey Juan Carlos, Madrid, Spain
[2] Technical University of Denmark, Kongens Lyngby, Denmark

Abstract. The objective of this study is to show the preliminary results of a (dynamic) mathematical model describing the effects of zero valent iron (ZVI) addition during the anaerobic digestion of waste activated sludge from wastewater treatment systems. A modified version of the Anaerobic Digestion Model No. 1 (ADM1) upgraded with an improved physico-chemical description, ZVI corrosion, propionate uptake enhancement and multiple mineral precipitation is used as a modelling platform. The proposed approach is tested against two case studies which correspond to two lab scale anaerobic digesters (AD2, AD1), with and without adding ZVI, respectively, and running in parallel for a period of 87 days. Experimental results show that ZVI enhances methane production. However, the P recovery potential is dramatically reduced as soluble P decreased by one order of magnitude in AD2 with respect to AD1. Simulations demonstrate that the model is capable to satisfactorily reproduce the dynamics of hydrolysis, acetogenesis, acidogenesis, nutrient release, pH and methanogenesis in the control anaerobic digester (AD1). This study also evidences the enhancement of methane production by the influence of ZVI on the acidogenesis and methanogenesis processes in AD2. In addition, it also identifies saturation conditions for siderite ($FeCO_3$) and vivianite ($Fe_3(PO_4)_2$), which causes changes in the biogas composition (% CH_4 versus % CO_2) and P release (lower values). This is the first study analysing the decrease of P recovery potential due to the addition of ZVI into AD systems.

Keywords: ADM1 · Multiple mineral precipitation · Activated sludge · Zero valent iron · P recovery potential

1 Introduction

Anaerobic digestion (AD) is a mature technology for bioenergy production (through biogas) that is mostly implemented as waste sludge stabilization method in wastewater treatment plants, as well as direct bioenergy production from energy crops. The economic feasibility of AD is generally related to the methane yields and current research in AD is directed to intensification techniques to enhance biogas production through different approaches (Segura et al. 2016). Beside the obvious initial choice of improvement of reactor configuration and operation conditions, great advances are made in the use of alternative feedstocks to expand its application within the bioenergy sector.

Novel feedstocks include hardly-biodegradable microbial biomass as microalgae, phototrophic bacteria and high-loaded adsorption sludge (A-stage sludge), and solid organic waste as the organic fraction of the municipal solid waste (OFMSW), ligno-cellulosic biomass or petroleum hydrocarbons (Holm-Nielsen et al. 2009). In this way, co-digestion of substrates is a good alternative to increase the digester organic loading rate (OLR) and improving the economic viability of AD plants due to higher methane production (Mata-Alvarez et al. 2014). During AD, organic biodegradable material is biologically degraded in absence of oxygen following four different steps, and producing biogas. Among the different steps involved in AD (hydrolysis, acidogenesis, acetogenesis and methanogenesis), enzymatic reduction of complex organic compounds to simpler and soluble molecules during hydrolysis is usually the limiting step of the process. Therefore, multiple methods have been explored to improve the hydrolysis, both thermal as well as physic-chemical (Carlsson et al. 2012).

Pre-treatments of the sludge (hydrothermal treatments, oxidative processes, etc.) have been proposed as alternative to increase biodegradability and overall kinetics of the biomethanation processes occurring during AD (Segura et al. 2016). Among these alternatives, the use of zero-valent iron (ZVI) has become a promising option due to its low cost. ZVI is (generally) a waste product, it is easy to apply (direct contact with the waste sludge) and it has the capacity to decrease oxidative–reductive potential (ORP) of the anaerobic digestion media. Hence, ZVI provides a more favourable environment for anaerobic digestion (Liu et al. 2011). Moreover, iron is a cofactor of several enzymatic activities occurring in the fermentation stage during acidogenesis (Liu et al. 2012). Actually, ZVI accelerates the hydrolysis and fermentation stages of AD due to its action as electron donor by corrosion (reaction 1), generating H_2 that can be used by hydrogenotrophic methanogens, sulfate reducing bacteria or dechorinating bacteria. This reduces the overall redox state of the system, thereby significantly improving the hydrolysis of the hardly-biodegradable fraction of the organic waste (Feng et al. 2014). Additionally, the process acts a buffer of the acid produced by acidogens, which is crucial to maintain a stable and favourable condition for methanogenesis, and consequently improving the biochemical methane potential in the AD system (Zhen et al. 2015).

$$Fe^0 + 2H_2O \rightarrow Fe^{2+} + H_2 + 2OH^- \qquad (1)$$
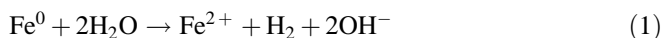
However, the Fe^{2+} released during this process modifies the physico-chemical structure of the system. Fe^{2+} can reduce the biogenic sulphide by pyrite (FeS_2) precipitation, but can also interact with other anions, notably bicarbonate and phosphate, to form siderite ($FeCO_3$) and vivianite ($Fe_3(PO_4)_2 \cdot 8H_2O$) (An et al. 2014). $Fe_3(PO_4)_2 \cdot 8H_2O$ precipitation entraps the soluble phosphorus (P) released upon AD. Though this reduces P contamination in the main line, most importantly it also reduces the P recovery potential due to accumulation of $Fe_3(PO_4)_2 \cdot 8H_2O$ in the stabilized sludge, from where subsequent recovery is difficult and costly. This theoretical process has never been considered as a problem in the use of ZVI for AD enhancement, even though occurrence of a similar reaction system between $Fe^{3+}-Fe^{2+}-P$ has been widely demonstrated occurring in anoxic soils (Heiberg et al. 2012; Rother et al. 2014). Typically, around 90% of the influent P at sewage treatment plants with enhanced P

removal ends up in biosolids. This is a low-value product due to the its reduced bioavailability as part of iron and aluminum precipitates, and even its application as soil conditioner is restricted (Latif et al. 2015). Uncontrolled P precipitation is a common problem in anaerobic digestors, where the formation of deposits cause reduced working volume of reactors and scale downstream AD system, such as pipelines, pump heads, etc. (Latif et al. 2017). This P thereby remains inaccesible to further recovery efforts and it is difficult to justify losses of P recovery potential in return for some increase of the methane production. P is an essential nutrient in the agricultural sector, and its demand is highly increasing. It is also a limited resource that cannot be replaced by any other element (Cordell et al. 2009).

Thus, the aim of this work is to analyse the effects of ZVI on the methane and P recovery potentials from activated sludge upon AD. A continuous AD reactor will be started-up and run to steady-state conditions, while following the methane production and P released to the digestate in presence and absence of ZVI.

2 Materials and Methods

Two identical 2 L continuously fed anaerobic digesters were used under mesophilic conditions ($37 \pm 0.5^{\circ}$C) to treat domestic secondary sludge. AD1 was used as control avoiding addition of ZVI at any time. On the other hand, the effect of ZVI addition was explored in AD2. Model predictions were calibrated using two data sets comprised of 87 days. Table 1 and Fig. 1, summarize the operational conditions and characterization of the inlet streams for the two set-ups, respectively.

Table 1. Experimental design of the operational conditions for AD1 & AD2

	Time (d)	HRT (d)	AD1		AD2	
			ZVI (g L^{-1})	Extra P* (mg L^{-1})	ZVI (g L^{-1})	Extra P (mg L^{-1})
1	20	20	–	–	2.5	–
2	14	10	–	–	2.5	–
3	13	10	–	10	2.5	10
4	12	20	–	10	2.5	10

*Extra P source was added to enhance the range of dynamic conditions of the experiment

Influent characterization was based on the model interface for the Benchmark Simulation Model No. 2 (BSM2) and the Anaerobic Digester Model (ADM1) designed by Nopens et al. (2009). Thus, from COD_{sol}, the fractions of S_{su} (40%) and S_{fa} (60%) are assumed. Influent S_I is estimated from COD_{sol} in the effluent. A similar procedure (from effluent COD_{part}) is used to characterize the unbiodegrabable fraction (X_I) and to distinguish it from the biodegrabale (X_{ch}, X_{pr} and X_{li}) fraction. S_{iC}, S_{iN} and S_{iP} values are obtained from alkalinity, NH_4^+ and PO_4^{-3} measurements, respectively. ADM1 parameter values are adjusted using the first data set (AD1) (hydrolysis, acidogensis, aceogensis, methanogensis and nutrient release). This parameter set is used in AD2 to further adjustment of corrosion, enhanced acidogenesis and multiple mineral precipitation.
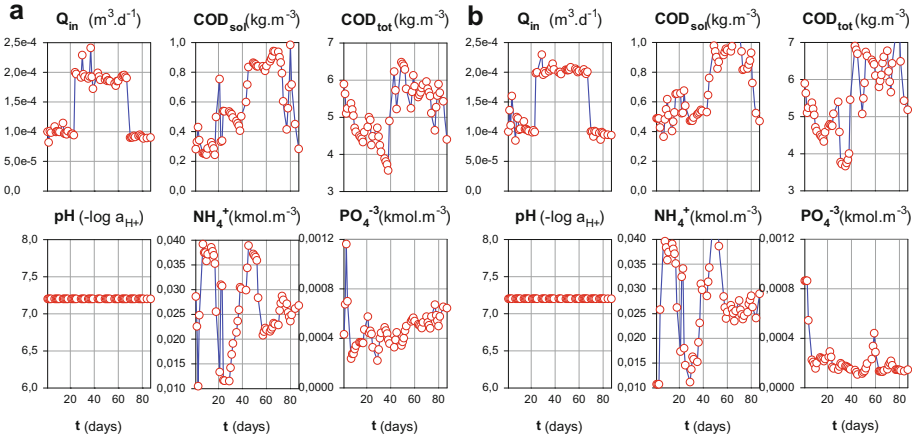
Fig. 1. Influent dynamic conditions for AD1 (a) and AD2 (b)

Total and soluble COD, alkalinity and TS/VS were measured according to Standard Methods. NH_4^+ and PO_4^{3-} were quantified by using Merck kits. Biogas production was measured by Ritter Milligascounters, whereas biogas composition was analyzed by GC-TCD. Soluble Fe^{2+}, Ca^{2+}, Mg^{2+}, K^+ and Na^+ were quantified by ICP-OES. Elemental composition, chemical and electronic state of the elements in the dry solid fraction of the digestate were analysed by X-ray photoelectron spectroscopy (XPS) following the method described elsewhere (Segura et al. 2015).

A modified version of the Anaerobic Digestion Model No 1 (ADM1) (Batstone et al. 2002) upgraded with an improved physico-chemical description (Flores-Alsina et al. 2016) was used as a testing platform. As it has been previously mentioned, the model also includes ZVI corrosion (Xiao et al. 2013), propionate uptake enhancement (Liu et al. 2015) and multiple mineral precipitation (Kazadi Mbamba et al. 2015).

3 Results

Figure 1 shows the time course of selected variables along the treatment in AD1 (a) and AD2 (b). The main results from the continuous experiment are: (i) methane production was statistically slightly improved in AD2 with respect to AD1 (*p-value* < 0.05), which confirms that ZVI enhances methane production; (ii) CO_2 production decreased in AD2 with respect to AD1, supporting the proposed mechanism of $FeCO_3$ formationdue to the interaction of released Fe^{2+} with bicarbonate; (iii) both inlet as well as outlet P concentrations were much lower (one order of magnitude) in AD2 with respect to AD1. In addition, binding energies for iron were assigned to low dispersed Fe^{2+} ions, which is consequent with precipitation of Fe and P as $Fe_3(PO_4)_2 \cdot 8H_2O$, and therefore the mechanism of P precipitation as $Fe_3(PO_4)_2 \cdot 8H_2O$ due to Fe^{2+} release is experimentally supported.

Simulation results show that the model is able to predict the main processes taking place during anaerobic digestion. The parameter set used for reactor AD1 was also successfully used to simulate operational conditions of reactor AD2. Parameter values for ZVI corrosion, propionate uptake enhancement and multiple mineral precipitation were adjusted to match $COD_{soluble}$, biogas production (and composition) and nutrient release (in that case N and P). ZVI corrosion was formulated to be a fast process and occurs chemically. Propionate uptake was assumed to be reinforced. Default parameters reported in Liu et al. (2015) were used for that purpose since a good match for COD_{sol} and CH_4 was achieved. Saturation index (SI) values provided by the speciation model were positive for $FeCO_3$ and $Fe_3(PO_4)_2 \cdot 8H_2O$, whereas precipitation constants (K_{FeCO3} and $K_{Fe3(PO3)2}$) were adjusted to match CO_2 and PO_4^{-3} measurements. Uptake rates for acidogenic and acetogenic bacteria had to be increased (double) in order to match S_{su}, S_{aa}, S_{fa} and VFA (= $S_{va} + S_{bu} + S_{pro}, + S_{ac}$) profiles with the measured COD_{sol} and biogas (CH_4 and CO_2) values. The N content in X_{pr}/S_{aa} and the P content in X_{li} were used to adjust N and P release. The good correlation between experimental and simulated
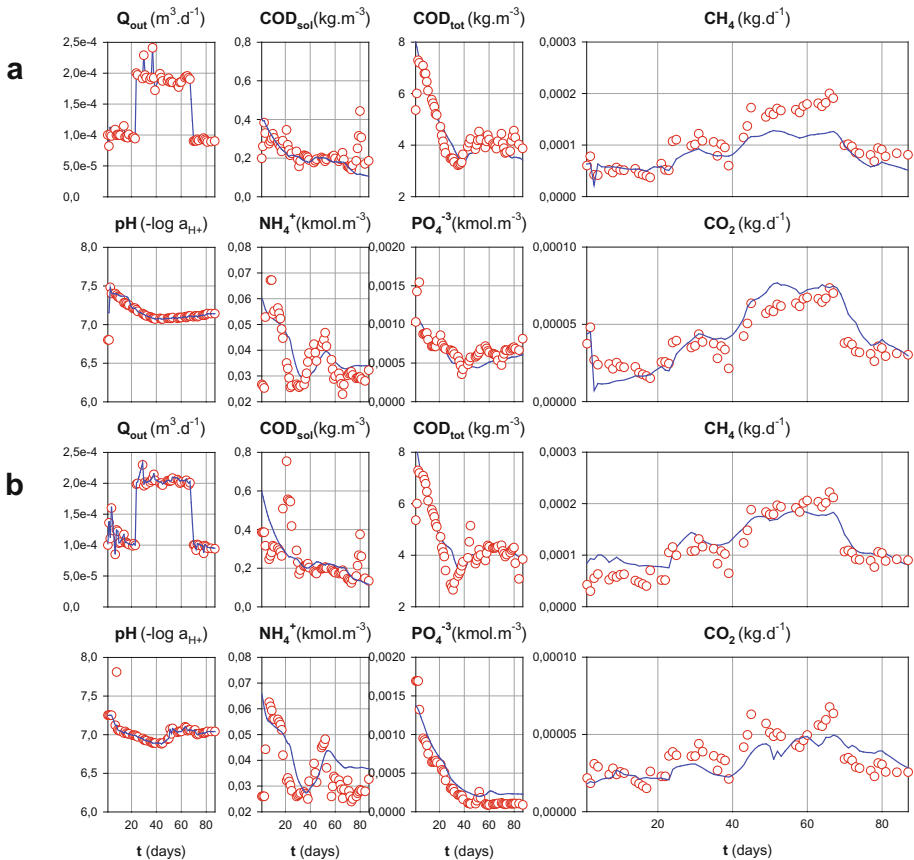
Fig. 2. Experimental results (symbols) and dynamic simulation results (lines) of the AD perfomance without (AD1, (a) and with (AD2, (b) ZVI addition

$COD_{particulate}$ (= COD_{total} − COD_{sol}) indicates a correct estimation of particulates (X_{ch}, X_{pro}, X_{ii}) hydrolysis and biomass (X_{biomas}) growth decay by the model (Fig. 2).

4   Conclusions

This study shows experimentally that ZVI addition into anaerobic digesters enhances methane potential but clearly decreases P recovery potential due to P immobilization, presumably as $Fe_3(PO_4)_2 \cdot 8H_2O$. The preliminary modelling results reported in this study indicate the potential capabilities of the proposed modelling approach when describing iron mediated processes. The implementation of a proper physico-chemical framework is crucial to correctly predict pH and ion speciation/pairing. The latter has a crucial effect on multiple mineral precipitation which ends up affecting biogas composition and nutrient release. Finally, it should be remark that a thorough cost/benefits analysis should be addressed to establish the actual benefit of ZVI as treatment to increase CH_4 production in AD, due to the potential loss of P recovery by $Fe_3(PO_4)_2 \cdot 8H_2O$ precipitation.

References

An J-S, Back Y-J, Kim K-C, Cha R, Jeong T-J (2014) Optimization for the removal of orthophosphate from aqueous solution by chemical precipitation using ferrous chloride. Environ Technol 35:1668–1675

Batstone DJ, Keller J, Angelidaki I, Kalyuzhnyi SV, Pavlostathis SG, Rozzi A, Sanders WT, Siegrist H, Vavilin VA (2002) The IWA anaerobic digestion model no 1 (ADM1). Water Sci Technol 45(10):65–73

Carlsson M, Lagerkvist A, Morgan-Sagastume F (2012) The effects of substrate pre-treatment on anaerobic digestion systems: a review. Waste Manag 32(9):1634–1650

Cordell D, Drangert J-O, White S (2009) The story of phosphorus: global food security and food for thought. Global Environ Change 19(2):292–305

Feng Y, Zhang Y, Quan X, Chen S (2014) Enhanced anaerobic digestion of waste activated sludge digestion by the addition of zero valent iron. Water Res 52:242–250

Flores-Alsina X, Solon K, Kazadi Mbamba C, Tait S, Gernaey KV, Jeppsson U, Batstone DJ (2016) Modelling phosphorus (P), sulfur (S) and iron (Fe) interactions for dynamic simulations of anaerobic digestion processes. Water Res 95:370–382

Heiberg L, Koch CB, Kjaergaard C, Jensen HS, Hans Christian BH (2012) Vivianite precipitation and phosphate sorption following iron reduction in anoxic soils. J Environ Qual 41:938–949

Holm-Nielsen JB, Al Seadi T, Oleskowicz-Popiel P (2009) The future of anaerobic digestion and biogas utilization. Bioresour Technol 100(22):5478–5484

Kazadi Mbamba C, Tait S, Flores-Alsina X, Batstone DJ (2015) A systematic study of multiple minerals precipitation modelling in wastewater treatment. Water Res 85:359–370

Latif MA, Mehta CM, Batstone DJ (2015) Low pH anaerobic digestion of waste activated sludge for enhanced phosphorous release. Water Res 81:288–293

Latif MA, Mehta CM, Batstone DJ (2017) Influence of low pH on continuous anaerobic digestion of waste activated sludge. Water Res. 113:42–49

Liu Y, Zhang Y, Quan X, Chen S, Zhao H (2011) Applying an electric field in a built-in zero valent iron—anaerobic reactor for enhancement of sludge granulation. Water Res 45:1258–1266

Liu Y, Zhang Y, Quan X, Li Y, Zhao Z, Meng X, Chen S (2012) Optimization of anaerobic acidogenesis by adding FeO powder to enhance anaerobic wastewater treatment. Chem Eng J 192:179–185

Liu Y, Zhang Y, Ni BJ (2015) Zero valent iron simultaneously enhances methane production and sulfate reduction in anaerobic granular sludge reactors. Water Res 75:292–300

Mata-Alvarez J, Dosta J, Romero-Güiza MS, Fonoll X, Peces M, Astals S (2014) A critical review on anaerobic co-digestion achievements between 2010 and 2013. Renew Sust Energ Rev 36:412–427

Noeps I, Batstone D, Copp J, Jeppsson U, Volcke E, Alex J, Vanrolleghem PA (2009) An ASM/ADM model interface for dynamic plant-wide simulation. Water Res 43(7):1913–1923

Rothe M, Frederichs T, Eder M, Kleeberg A, Hupfe M (2014) Evidence for vivianite formation and its contribution to long-term phosphorus retention in a recent lake sediment: a novel analytical approach. Biogeosciences 11:5169–5180

Segura Y, Puyol D, Ballesteros L, Martínez F, Melero JA (2016) Wastewater sludges pretreated by different oxidation systems at mild conditions to promote the biogas formation in anaerobic processes. Eviron Sci Pollut R 23:24393–24401

Segura Y, Martinez F, Melero JA, Fierro JLG (2015) Zero valent iron mediated Fenton degradation of industrial wastewater: Treatment performance and characterization of final composites. Chem Eng J 269:298–305

Xiao X, Sheng GP, Mu Y, Yu HQ (2013) A modeling approach to describe ZVI-based anaerobic system. Water Res 47(16):6007–6013

Zhen G, Lu X, Li YY, Liu Y, Zhao Y (2015) Influence of zero valent scrap iron (ZVSI) supply on methane production from waste activated sludge. Chem Eng J 263:461–470

Eukaryotic Community in UASB Reactor Treating Domestic Sewage Based on 18S rRNA Gene Sequencing

Y. Hirakata[1(✉)], M. Hatamoto[2], M. Oshiki[3], N. Araki[3],
and T. Yamaguchi[1,2]

[1] Department of Science of Technology Innovation,
Nagaoka University of Technology, Nagaoka, Japan
[2] Department of Environmental Systems Engineering,
Nagaoka University of Technology, Nagaoka, Japan
[3] Department of Civil Engineering, National Institute of Technology,
Nagaoka College, Nagaoka, Japan

Abstract. Microbial eukaryotes play important roles in sewage treatment systems. In an up-flow anaerobic sludge blanket (UASB) reactor fed with domestic sewage, anaerobic bacteria, archaea, and microbial eukaryotes (protist and fungi) coexist. To date, bacterial and archaeal communities in the UASB reactor have been widely studied. However, little is known about the eukaryotic community structure and function in most of anaerobic treatment systems. In this study, we analyzed eukaryotic community in the UASB reactor treating domestic sewage over 2 years operational period based on 18S rRNA gene sequences. In addition, multivariate statistics were applied to elucidate the correlation between eukaryotic community and operational conditions of the UASB reactor. The dominant protist groups observed were from phylum *Ciliophora*, *Apicomplexa*, *Perkisea* and *Amoebozoa* in the UASB reactor. Followings were flagellate protist such as *Cercozoa*, *Sulcozoa*, *Bicosoecida*, *Choanomonada*, *Dinoflagellata* and *Metamonada*. The result showed protist phylum and water temperature were not correlated. Only phylum *Sulcozoa* positively correlated with COD and suspended solid (SS), whereas other protist showed low correlation. The dominant fungi groups were LKM11, LKM15 and phylum *Ascomycota*. Uncultured LKM15 correlated with sulfide whereas phylum *Discicristoidea* and *Chytridiomycota* showed negative correlation. Phylum *Ascomycota* seemed most abundant when sulfide was low, but their association with environmental variables remained unclear. These results suggested that some protist and fungi groups could be used as indicator of environmental parameters in the UASB reactor.

Keywords: Eukaryotic community · Anaerobic treatment · Domestic sewage

1 Introduction

Microbial eukaryotes play important roles in sewage treatment systems. Protists are often used as indicators of treatment performance in activated sludge process treating domestic sewage. The reduction of sludge production by protist bacterivory is well known in aerobic treatment systems. Some of fungi are also known to contribute to

denitrification and cellulose degradation. In an up-flow anaerobic sludge blanket (UASB) reactor fed with domestic sewage, anaerobic bacteria, archaea, and microbial eukaryotes (protist and fungi) coexist. To date, bacterial and archaeal communities in the UASB reactor have been widely studied. However, little is known about the eukaryotic community structure and function in most of anaerobic treatment systems.

The eukaryotes have been commonly identified morphologically by microscopic observation. However, identifying anaerobic protist by microscopic observation is prone to error because some protist species are fast-moving protozoa and indiscernibly small. Furthermore, most fungi are difficult to identify by microscopic observation. Recently, molecular biological techniques have been applied to analyze a greater diversity of eukaryotes in wastewater treatment systems and environments (Miyaoka et al. 2016; Simon et al. 2015). Molecular techniques can detect eukaryotes that cannot be observed by microscopic observation. In this study, we analyzed eukaryotic community in UASB reactor treating domestic sewage over 2 years of operational period using 18S rRNA gene sequencing. In addition, multivariate statistics were applied to elucidate correlation between eukaryotic community and operational condition of the UASB reactor.

2 Materials and Methods

An UASB reactor with total volume of 1,178 L and 4.7 m height was operated in domestic sewage treatment center at Nagaoka City, Japan. The hydraulic retention time of the system was set at 8 h. To activate the microorganisms responsible for sulfur redox cycles, the system was fed with raw sewage that was supplemented with 50–150 mg-S L^{-1} sodium sulfate. Additional details on the UASB reactor were described previously (Aida et al. 2015). Sludge samples were collected from sampling port at 1.278 m above from the bottom of the reactor. The collected samples were then immediately stored at $-20°$ C until DNA extraction was performed.

The genomic DNA was extracted from collected samples using a FastDNA SPIN Kit for Soil (MP Biomedicals, Carlsbad, CA, USA). The DNA concentration was determined using a NanoDrop Spectrophotometer ND-1000 (Thermo Fisher Scientific, Waltham, MA, USA).

General eukaryotic primers V4_1F and TAReukREV3 were used to amplify the V4 region of the eukaryotic 18S rRNA gene (Bass et al. 2016). The PCR was performed using a thermal cycler (Applied Biosystems, Foster City, CA, USA) under the following cycling conditions: 5 min at $94°$ C; 15 cycles of 30 s at $94°$ C, 45 s at $53°$ C, and 1 min at $72°$ C; 20 cycles of 30 s at $94°$ C, 45 s at $48°$ C, and 1 min at $72°$ C; and the final extension step 10 min at $72°$ C. The amplification of the 18S rRNA gene region was ascertained by agarose gel electrophoresis using 100 bp DNA ladder (NIPPON Genetics, Tokyo, Japan). The amplicon was purified using an Agencourt AMPure XP Kit (Beckman Coulter, Brea, CA, USA) and used for preparation of a library by means of the MiSeq Reagent Kit v2 nano (Illumina, San Diego, CA, USA) for sequencing on Illumina MiSeq. Amplicon library concentrations were measured using BioAnalyzer DNA 1000 (Agilent Technologies, Santa Clara, CA, USA).

Sequence reads were processed using Quantitative Insights Into Microbial Ecology (QIIME) version 1.8.0 (Caporaso et al. 2012). Sequence reads with a low quality score

(Phred quality score $\leq$ 30) were eliminated using the Trimmomatic v0.33 (Bolger et al. 2014), and paired-end sequence reads were then assembled in the paired-end assembler for the Illumina sequence software package (PANDAseq) (Masella et al. 2012). Operational taxonomic units (OTUs) clustering at 97% sequences identity were conducted with the UCLUST algorithm (Edgar et al. 2010). The taxonomic classification was determined using SILVA database 123 (Quast et al. 2012). Chimeric sequences were identified with ChimeraSlayer (Haas et al. 2011). After detrended correspondence analysis (DCA) was performed to determine the appropriate type of model for direct gradient analysis, canonical correspondence analysis (CCA) and redundancy analysis (RDA) were performed to investigate correlations between eukaryotic communities and environmental factors with R software (Oksanen et al. 2007). These analyses include operational condition of the UASB reactor and protist or fungi OTUs representing at least 0.3% reads per sample, on average.

3   Results and Discussions

In this study, we analyzed the protist community structures in 10 sludge samples collected from UASB reactor treating domestic sewage based on 18S rRNA gene sequencing. A total of 168,317 sequences were obtained. Fungi were predominantly detected with relative abundance of 84% from total sequences. Relative protist abundance was very low (4% of the total number of sequences). In addition, metazoa and algae were also detected (8% and 4% respectively). Metazoa and algae most probably had flowed into the UASB reactor with sewage.

Taxonomic classification of the protist and fungi community structures was shown in Fig. 1. The dominant protist groups detected were from phylum *Ciliophora*, *Apicomplexa*, *Perkisea* and *Amoebozoa*, with average relative abundance of 30%, 21%, 12%, and 12% of all protist sequences, respectively. Followings were flagellate protist such as phylum *Cercozoa*, *Sulcozoa*, *Bicosoecida*, *Choanomonada*, *Dinoflagellata* and *Metamonada* (>1%, on average). *Ciliophora*, *Amoebozoa* and most heterotrophic flagellate protists are major bacterial consumer in anaerobic environment. On the other hand, phylum *Apicomplexa* and *Perkisea* are well known as parasitic protists. These parasitic protists present in wastewater were reported capable of forming cyst (Ajonina et al. 2012). Phylum *Ciliophora* was also dominantly observed microscopically in the UASB reactor. On the other hands, phylum *Amoebozoa* and flagellate protist cannot be observed by microscopic observation (Hirakata et al. 2016). 18S rRNA gene analysis showed that existing larger protist diversity, which was recognized by microscopic observation previously was uncovered in UASB reactor. In particular, phylum *Ciliophora* and *Amoebozoa* were found frequently from both aerobic and anaerobic environment. It is possible that some species of *Ciliophora* and *Amoebozoa* present in effluent sewage.

The dominant fungi groups were LKM11, LKM15 and phylum *Ascomycota* with average relative abundance of 39%, 31%, and 19% of all fungi sequences, respectively (Fig. 2). The member of phylum *Ascomycota* was capable of degrading cellulose. Organisms in LKM11 and LKM15 group were detected from anoxic environment such as lake or pond sediments (Wurzbacher et al. 2016). Additionally, LKM11 group was
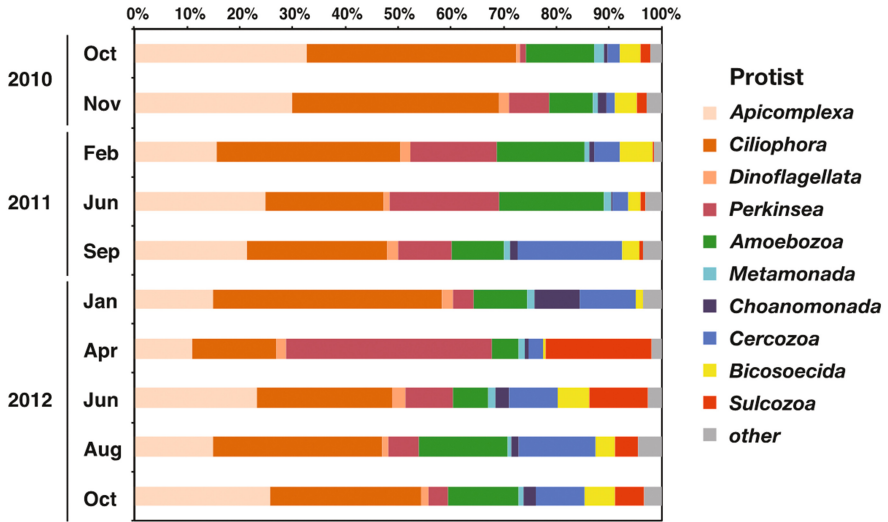
Fig. 1. Phylum level taxonomic classification of the protist community structures based on 18S rRNA gene in the UASB reactor treating domestic sewage over 2 years of operation
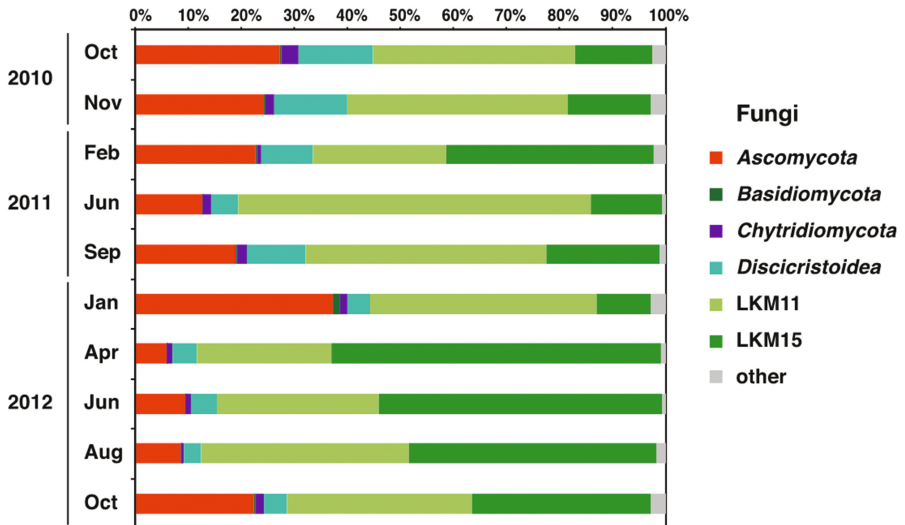
Fig. 2. Phylum level taxonomic classification of the fungi community structures based on 18S rRNA gene in the UASB reactor treating domestic sewage over 2 years of operation
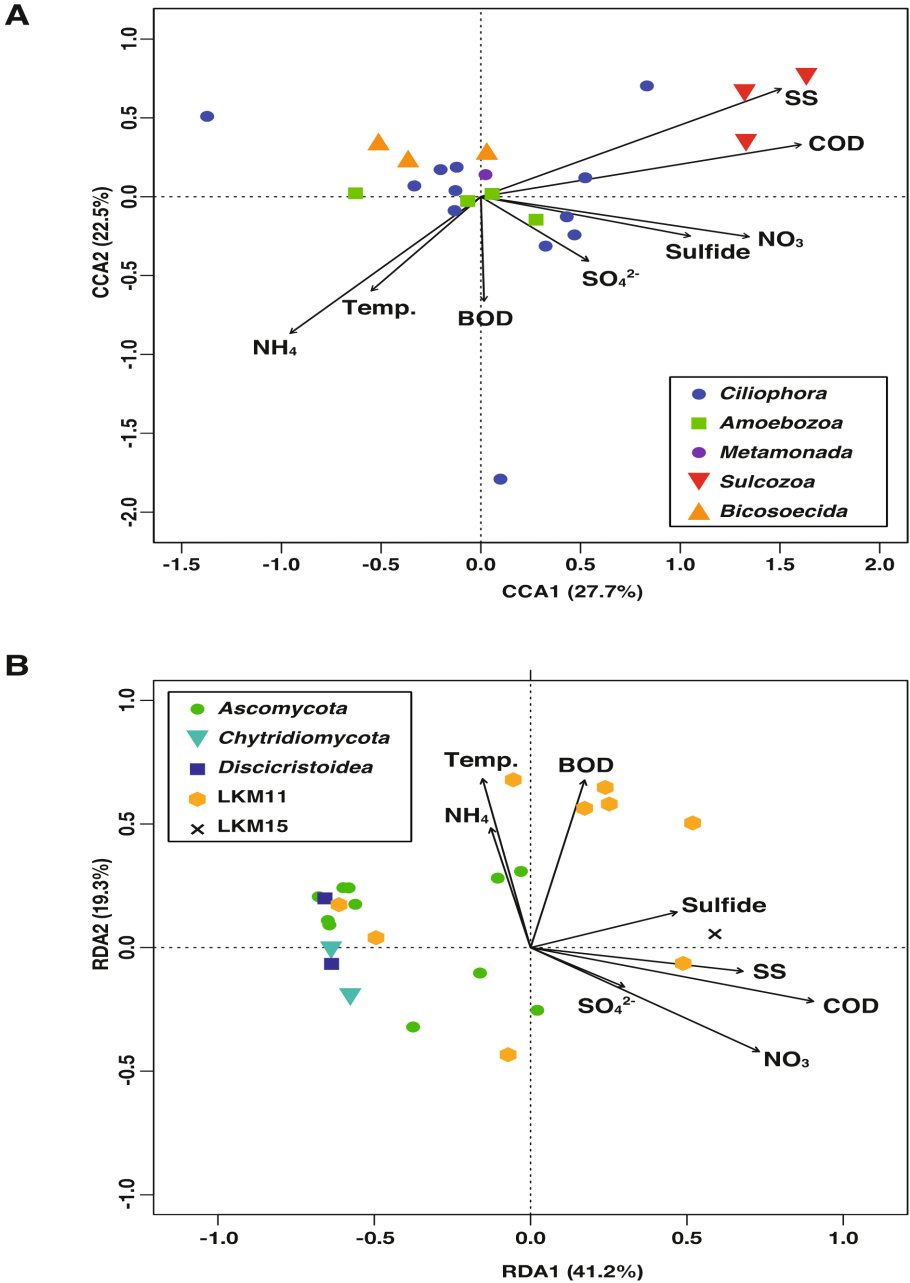
Fig. 3. Multivariate statistics. CCA plot based on operational condition of the UASB reactor and protist OTU abundance (A). RDA plot based on operational condition and fungi OTU abundance (B)

also detected from activated sludge treating domestic sewage (Matsunaga et al. 2014). Thus, their functions of LKM11 and LKM15 group in sewage treatment process are still largely unknown. Their functions need to be examined in more detail in future study.

Multivariate statistics were performed to see correlations between eukaryotic communities and environmental parameters. The CCA analysis showed that *Sulcozoa* OTUs positively correlated with COD and suspended solid (SS), whereas most OTUs showed a low correlation (Fig. 3A). Most OTUs and water temperature were not correlated too. This result suggested that *Sulcozoa* protist grow under high organic loading lates while other protists that had low correlation with COD and SS were not influenced by organic loading lates in the UASB reactor. As shown by RDA analysis, OTU related uncultured LKM15 correlated with sulfide, whereas *Discicristoidea* and *Chytridiomycota* showed a negative correlation (Fig. 3B). Phylum *Ascomycota* seemed most abundant when sulfide was lower, but their association with environmental variables remained unclear. Therefore, effect of sulfide could be important for these fungi phylum. These results suggested that some protist and fungi groups could be used as indicator of environmental parameters such as COD, SS and sulfide.

4 Conclusions

The eukaryotic community analysis based on 18S rRNA gene sequencing revealed larger diversity in the UASB reactor. The dominant protist groups were phylum *Ciliophora* and *Amoebozoa* in the UASB reactor. In addition, uncultured LKM11 and LKM15 groups were also dominated in the UASB reactor. The multivariate statistics showed that some protist and fungi groups could be used as indicator of environmental parameters in the UASB reactor. The physiological role of these uncultured eukaryotes groups should be examined to understand relationship between eukaryotes and environmental parameters in the future studies.

References

Aida AA, Kuroda K, Yamamoto M, Nakamura A, Hatamoto M, Yamaguchi T (2015) Diversity profile of microbes associated with anaerobic sulfur oxidation in an upflow anaerobic sludge blanket reactor treating municipal sewage. Microbes Environ 30(2):157–163

Ajonina C, Buzie C, Ajonina IU, Basner A, Reinhardt H, Gulyas H, Liebau E, Otterpohl R (2012) Occurrence of Cryptosporidium in a wastewater treatment plant in North Germany. J Toxicol Environ Health Part A 75(22–23):1351–1358

Bass D, Silberman JD, Brown MW, Tice AK, Jousset A, Geisen S, Hartikainen H (2016) Coprophilic amoebae and flagellates, including Guttulinopsis, Rosculus and Helkesimastix, characterise a divergent and diverse rhizarian radiation and contribute to a large diversity of faecal-associated protists. Environ Microbiol 18(5):1604–1619

Bolger AM, Lohse M, Usadel B (2014) Trimmomatic: a flexible trimmer for Illumina sequence data. Bioinformatics 30(15):2114–2120

Caporaso JG, Lauber CL, Walters WA, Berg-Lyons D, Huntley J, Fierer N, Owens SM, Betley J, Fraser L, Bauer M, Gormley N, Gilbert JA, Smith G, Knight R (2012) Ultra-high-throughput microbial community analysis on the Illumina HiSeq and MiSeq platforms. ISME J 6 (8):1621–1624

Edgar RC (2010) Search and clustering orders of magnitude faster than BLAST. Bioinformatics 26:2460–2461

Haas BJ, Gevers D, Earl AM, Feldgarden M, Ward DV, Giannoukos G, Ciulla D, Tabbasa D, Highlander SK, Sodergren E, Methe B, DeSantis TZ, Petrosino JF, Knight R, Methé B (2011) Chimeric 16S rRNA sequence formation and detection in Sanger and 454-pyrosequenced PCR amplicons. Genome Res 21(3):494–504

Hirakata Y, Oshiki M, Kuroda K, Hatamoto M, Kubota K, Yamaguchi T, Harada H, Araki N (2016) Effects of predation by protists on prokaryotic community function, structure, and diversity in anaerobic granular sludge. Microbes Environ 31(3):279–287

Masella AP, Bartram AK, Truszkowski JM, Brown DG, Neufeld JD (2012) PANDAseq: paired-end assembler for illumina sequences. BMC Bioinf 13:31

Matsunaga K, Kubota K, Harada H (2014) Molecular diversity of eukaryotes in municipal wastewater treatment processes as revealed by 18S rRNA gene analysis. Microbes Environ 29 (4):401–407

Miyaoka Y, Hatamoto M, Yamaguchi T, Syutsubo K (2016) Eukaryotic community shift in response to organic loading rate of an aerobic trickling filter (down-flow hanging sponge reactor) treating domestic sewage. Microb Ecol 73:1–14

Oksanen J, Kindt R, Legendre P, O'Hara B, Stevens MHH, Oksanen MJ (2007) The vegan package. Commun Ecol Package 10:631–637 Suggests MASS

Simon M, López-García P, Deschamps P, Moreira D, Restoux G, Bertolino P, Jardillier L (2015) Marked seasonality and high spatial variability of protist communities in shallow freshwater systems. ISME J 9:1941–1953

Quast C, Pruesse E, Yilmaz P, Gerken J, Schweer T, Yarza P, Peplies J, Glöckner FO (2012) The SILVA ribosomal RNA gene database project: improved data processing and web-based tools. Nucleic Acids Res 41:590–596

Wurzbacher C, Warthmann N, Bourne E, Attermeyer K, Allgaier M, Powell JR, Detering H, Mbedi S, Grossart HP, Monaghan MT (2016) High habitat-specificity in fungal communities in oligo-mesotrophic, temperate Lake Stechlin (North-East Germany). MycoKeys 16:17–44

Performance and Kinetic Analysis of a Static Granular Bed Reactor Treating Poultry Slaughterhouse Wastewater

M. Basitere[1(✉)], M. Njoya[1], M.S. Sheldon[1], S.K.O. Ntwampe[2], and Z. Rinquest[1]

[1] Department of Chemical Engineering,
Cape Peninsula University of Technology, Cape Town, South Africa
[2] Bioresource Engineering Research Group (BioERG),
Department of Biotechnology, Cape Peninsula University of Technology,
Cape Town, South Africa

Abstract. Poultry slaughterhouses consume a substantial quantity of clean water during processing of live birds. Subsequently, high strength poultry slaughterhouse wastewater (PSW) is generated at different stages during poultry product processing. In this study, Static Granular Bed Reactor (SGBR) was used to treat the PSW from a poultry product processing facility in the Western Cape, South Africa. The performance of the SGBR was primarily evaluated for chemical oxygen demand (COD) removal with the kinetics of the treatment process of the PSW being evaluated using the modified Stover-Kincannon and the Grau second order models. Overall, the treatment efficiency averaged >90% when the SGBR were operated at steady state for a 68 days experimental trial. Furthermore, both the Grau second-order and the modified Stover-Kincannon models were used to develop a kinetic model which sufficiently described the COD removal. The Grau second-order model produced a better fit ($R^2 > 0.99$) when compared to the Stover-Kincannon model ($R^2 > 0.80$). The kinetic relationship derived from the lab-scale SGBRs can thus be used to predict the performance of the pilot scale SGBRs treating the PSW under mesophilic conditions.

Keywords: Static granular bed reactor · Poultry slaughterhouse wastewater · Grau-second order model · Stover-Kincannon model

1 Introduction

In South Africa, the poultry slaughterhouse industry consumes a significant quantity of drinking water for the slaughtering and processing of birds, cleaning and sanitising of equipment (Park et al. 2012). This results in the generation of high volumes of wastewater which contains high levels of organic matter quantifiable as Biochemical Oxygen Demand (BOD) and/or Chemical Oxygen Demand (COD). The wastewater will also have Phosphorous and Nitrogenous compounds including blood, Fats, Oil, Grease (FOG) and proteins (Debik and Coskun 2009). To circumvent severe environmental pollution and subsequent municipal charges, the poultry slaughterhouse wastewater (PSW) must be efficiently treated prior to discharge into the local municipal sewage system.

Anaerobic digestion is one of the most favourably methods utilised for the treatment of high strength PSW due its environmentally benignity (Jijai et al. 2016). Static Granular Bed Reactors (SGBRs), which is a novel bioreactor developed by Ellis and Mach (2004) at the Iowa State University Environmental Laboratory, was used to treat the PSW. The SGBR design incorporates highly active dense microbial granules in a simple downflow configuration. The design enables kinetic modelling, a characteristic which facilitates process performance efficiency quantification and the ability to assess the impact of fundamental bioprocess phenomena under different enviromental conditions. It is important to analyse the process kinetics of the SGBR under different enviromental conditions as to provide a rational basis for process analysis, control and optimisation (Yu et al. 1998). The kinetics of a process such as those observed in SGBRs, involves a variety of bioremediation steps such: (a) hydrolysis, acidogenesis, acetogenesis and methanogenesis, which are involved in the biodegradation of organic substrates.

Kinetic models that have been successfully used for anaerobic digesters include: (a) second order Grau and (b) the modified Stover-Kincannon models, for the prediction of effluent substrate concentrations as an output process variable for anaerobic wastewater treatment processes, with known input data at steady state conditions. Debik and Coskun (2009) reported that the Grau second-order and Stover-Kincannon models were successfully employed to develop a kinetic model for a SGBR treating PSW at ambient temperature.

This study uses an analytical approach to develop a kinetic model which describes the operation of an anaerobic digestion process (SGBR) at mesophilic conditions, in order to effectively model and thus evaluate process efficiency in order to formulate design relationships for the treatment of PSW in South Africa.

2   Materials and Methods

2.1   Reactor set-up and equipment

A laboratory bench-scale polyvinyl chloride (PVC) SGBR anaerobic digester was used for this study. The reactors had a total working volume of 1.53 L with an inner diameter and height of 0.071 and 0.5867 m, respectively. Grit sieves (2 mm) and pea gravel (average size of 5 mm) were used at the bottom of each bioreactor to prevent granular sludge backflow due to the peristaltic (pulsating) movement of the PSW influent. The reactor was inoculated with 0.95 L of anaerobic granular sludge collected from a industrial-scale up-flow anaerobic sludge bed (UASB) reactor operated at a local brewery (SABMiller Plc, Newlands Brewery, South Africa) to which 0.43 L of PSW was added. The PSW was collected from a poultry slaughterhouse located in the Western Cape, South Africa. A multi-head Gilson (Germany) peristalic pump was used to pump the influent to the top of the bioreactors. A similar pump was also used to pump effluent at the bottom of the reactor. The reactor was operated under mesophilic temperature (35 to 37 °C) with the temperature being regulated using a heated water jacket connected to a thermostatic water bath. The HRT of the reactor was kept at 55 h over a period 50 days and steped down to 40 h over a period of 18 days. All values reported, are averaged values for the bioreactor used.

3   Results and Discussion

3.1   COD removal rates

During the start up period which was 19 days long, the influent was diluted using a 50% (v/v) dilution with the observed COD removal efficiency being greater than 90%. With a further reduction in the dilution, i.e. at 33% (v/v), the COD reduction efficiency was maintained in excess of 90% for over a period of 5 days. Subsequently, the undiluted PSW was supplied to the SGBRs from days 25 to 68, maintaining COD reduction at similar rates as those observed during the start-up periods. Although, the SGBRs experienced headloses and clogging after the initiation of the start-up periods, the utilisation of a backwash between 50 to 60 days elleviated such operational deficiencies. This culminated in the reduction in COD reduction to below 90%, with a further stabilisation being required after the use of the backwash line. Generally, the overall COD reduction for the designed system over the evaluation period was greater than 90%, with the treated effluent quality characteristics being within the municipality (City of Cape Town municipality) discharge standards/by-laws for disposal into the municipal/domestic wastewater treatment plants.

3.2   Evaluation of kinetic parameters: Grau second order model

The kinetic parameters used in the Grau second order model, i.e. a and b in equation

$$\frac{S_0\theta_H}{S_0 - S} = a + b\theta_H,$$ (1)

can be determined using a linear trendline in order to quantify the intercept (a) and the slope (b) by assessing the interrelatedness between HRT/E, and HRT as shown in Fig. 1.

The obtained values for a, and b, were 0.1793 and 0.93, respectively, with a correlation co-efficient of $R^2 > 0,989$. These values, i.e. for a and b, can be used to predict process efficiency, with the COD effluent concentration from the SGBRs being adequately described by (Eq. 2):

$$S = S_0\left(1 - \frac{\theta}{0,1793 + 0,93\theta}\right)$$ (2)

3.3   Evaluation of kinetic parameters: Stover-Kincannon model

Accordingly, other kinetic parameters depicting the relation between the inverse substrate utilization rate and the inverse of the loading rate as described by the Stover-Kincannon model, - see Fig. 2, can be used to further describe the SGBRs performance. Such an evaluation, can be linearly associated with the maximum removal rate constant, U_{max} including the saturation constant, K_B as depicted in this equation
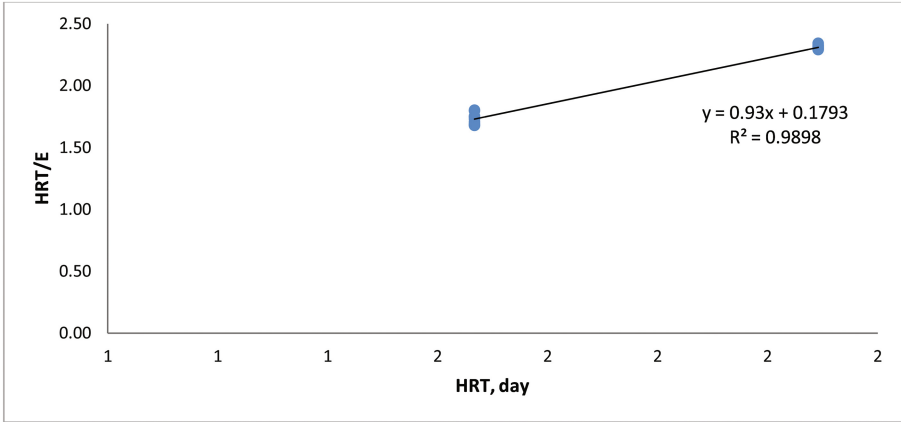
Fig. 1. Evaluation of Grau second-order model kinetic parameters
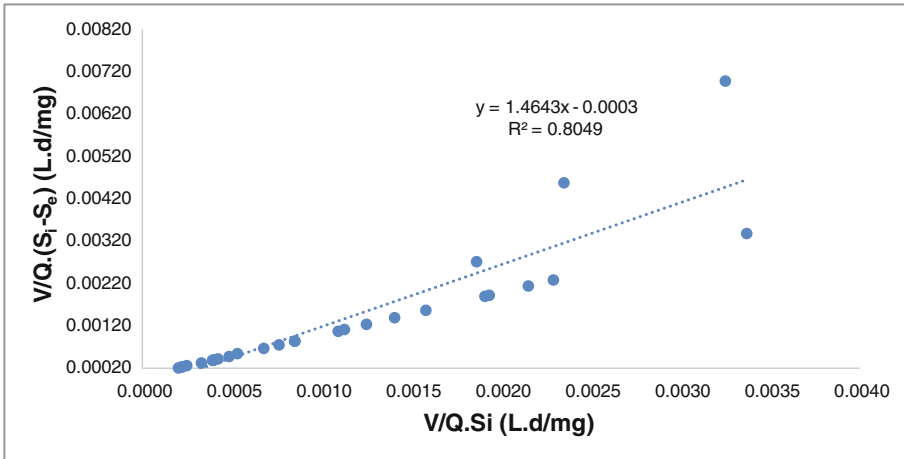
Fig. 2. Evaluation of modified Stover-Kincannon model kinetic parameters

$$\left(\frac{dS}{dt}\right)^{-1} = \frac{V}{Q(S_0 - S_e)} = \frac{K_B}{U_{max}}\left(\frac{V}{QS_0}\right) + \frac{1}{U_{max}}. \tag{3}$$

The U_{max} and K_B values were estimated as 3,333 g COD/L.day and 4,881 g COD/L.day, respectively, with a correlation coefficient (R^2) of 0.80, between modelled and experimental values, being achieved.

The predicted values of U_{max} was below the observed maximum OLR (6,529 mg COD/L.day) applied to the SGBRs during this study, indicating the incapacity of the SGBRs to treat high strength PSW, which suggested that a pretreatment system might be required. This was further illustrated by clogging by suspended solids on pea gravel

resulting in COD entrapment. Overall, the residual COD from the SGBRs, defined as the prevalence of organic substrate concentration, was modelled using Eq. 4.

$$S_e(\frac{g}{L}) = S_0 - \frac{3,333S_0}{4,881 + (\frac{QS_0}{V})} \tag{4}$$

4   Conclusions

The bench-scale SGBRs operated at mesophilic conditions exhibited admirable process performance over a period of 68 days. The overall COD reduction rate was greater than 90% at an OLR rate ranging from 0.56 to 3,14 g COD/L.day. A positive correlation between actual (residual) and modelled COD in the effluent from the SGBRs was found using both the Grau second order ($R^2 > 0.99$) and modified Stover Kincannon models ($R^2 > 0.80$). The SGBRs designed maitained high COD reduction which was maintained regardless of changes in organic loading rates. SGBRs inefficiencies were attributed clogging caused by buildup of total suspended solids (TSS) with backwashing further reducing treatment efficiencies.

References

Debik E, Coskun T (2009) Use of the Static Granular Bed Reactor (SGBR) with anaerobic sludge to treat poultry slaughterhouse wastewater and kinetic modeling. Biores Technol 100:2777–2782

Ellis TG, Mach KF (2004). U.S. Patent No. 6,709,591. U.S. Patent and Trademark Office, Washington, DC

Jijai S, Siripatana C, Sompong O, Ismail N (2016) Kinetic models for prediction of COD effluent from upflow anaerobic sludge blanket (UASB) reactor for cannery seafood wastewater treatment. Jurnal Teknologi 78(5–6):93–99

Park J, Oh JH, Ellis TG (2012) Evaluation of an on-site pilot static granular bed reactor (SGBR) for the treatment of slaughterhouse wastewater. Bioprocess Biosyst Eng 35(3):459–468

Yu H, Wilson F, Tay JH (1998) Kinetic analysis of an anaerobic filter treating soybean wastewater. Water Res 32(11):3341–3352

Thermophilic Hydrolysis and Fermentation to Produce Short-Chain Fatty Acids from Waste Sludge

Z.Q. Zuo[(✉)], M. Zheng, H.L. Xiong, Y.C. Liu, and H.C. Shi

State Key Joint Laboratory of Environment Simulation and Pollution Control, School of Environment, Tsinghua University, Beijing 100084, China

Abstract. Thermophilic conditions for waste sludge fermentation have been reported to produce more SCFAs than mesophilic conditions. In this study, A series of SCFAs production experiments were carried out under different sludge sources and conditions to calibrate and validate the proposed model. A kinetic model had been developed to understand the production of SCFAs from waste sludge via thermophilic fermentation. Good agreement was obtained between the measured SCFAs, soluble chemical oxygen demand and volatile suspended solids data and the model output results.

Keywords: Short-chain fatty acids production · Thermophilic · Hydrolysis · Fermentation · Kinetic modelling

1 Introduction

The production of short-chain fatty acids (SCFAs) from waste sludge has attracted growing attention in wastewater treatment plants (WWTPs) because SCFAs can be used as raw substrates for the production of biodegradable plastics or as the preferred carbon source to enhance biological nutrient removal. Conventionally, anaerobic fermentation for organic degradation included three procedures: hydrolysis, acidogenensis and methanogenesis. SCFAs are produced in the acidogenensis process and utilized in the methanogenesis process. Therefore, reducing methanogenesis during anaerobic sludge treatment is critical for the production of SCFAs.

Short-chain fatty acids (SCFAs) production from waste sludge has been attracted growing attention in wastewater treatment plant (WWTP) because the SCFAs could be used as raw substrates for biodegradable plastic production (Mengmeng et al. 2009) or preferred carbon source to enhance biological nutrient removal (Chen et al. 2007). Inhibiting activity of methanogens was a direct way to promote SCFAs production while some extreme conditions were often needed, such as pH = 10 (Chen et al. 2007; Zhang et al. 2010). The other way was using hydrolytic-acidogenic (H-A) reactor with short retention time, when SCFAs production rate can exceed the utilization kinetically under blank pH condition (Sahm 1984; Siegert and Banks 2005). The short retention time was also benefit to washing out the methanogenic microorganisms in the H-A reactor (De La Rubia et al. 2009). However, currently, improvement of SCFAs production is still critical for waste sludge treatment.

2   Materials and Methods

The used waste sludge in the experiments was from Xiao Hongmen plant for municipal wastewater treatment in Beijing, China. Thermophilic hydrolysis and fermentation assays were conducted in anaerobic reactors with effective volume of 3.6 L. The reactor was equipped with mechanical stirring with a rotate speed at 150 rpm. Thermostatically magnetic stirrer was fixed at the bottom of the reactor with a rotate speed at 1200 rpm to control the reaction temperatures as set initially. Generally, we conducted 2-days batch assays to obtain the SCFAs production data. MLSS, MLVSS, COD, carbohydrate, protein, humic acid and SCFAs were measured in the tests.

Kinetic model
The thermophilic hydrolysis and fermentation kinetic model is structured with six components, including total particulate organic matter (X_P), degradable particulate organic matter (X_S), non-degradable particulate organic matter (X_U), fermentable hydrolysate (S_F), non-fermentable hydrolysate (S_I), produced SCFAs (S_V), and acidogenic bacteria (X_h). A new hydrolysis components ratio parameter ε is defined to represent the percentage of degradable particulate organic matter X_S in the X_P. Another new hydrolysate fermentability parameter β is also involved in the model. The mathematical matrix form of the kinetic model is shown in Table 1. In this method, the generation or utilization rate of a model component for a given biochemical process can be obtained by multiplying related stoichiometric and kinetic processes.

Table 1. Kinetic model of sludge hydrolysis and fermentation process

Dynamic process	X_S	S_F	S_I	S_V	X_h	Rate
Hydrolysis of X_S	-1	β	$1-\beta$			$k\,X_S$
Fermentation		-1		1	Y_h	$\dfrac{k_{m,h}}{1+\frac{K_{S,h}}{S_F}+\frac{S_V}{K_{i,h}}}.X_h$
Decay of X_h	1				-1	$k_{d,h}.X_h$

3   Results and Discussion

Thermophilic hydrolysis and fermentation experimental results shows that the particulate organic matters decreases to 16.01 g COD/L during two days' fermentation with an initial MLVSS concentration as high as 21.62 g COD/L. The soluble COD gradually increases from 0.56 to 6.07 g COD/L (Fig. 1A). The soluble organic matters includes carbohydrate, protein, humic acids, SCFAs, and other uncertain types (Fig. 1B). The SCFAs concentration reaches a maximum level of 2.16 g COD/L on 1.5 days, accounting for 37.5% of SCOD. The maximum concentrations of carbohydrate, protein, humic acids and uncertain organic matters are obtained on 0.5 days. Then, they are basically unchanged in the experiments. The concentration of uncertain organic matters rapidly decreased with the observed SCFAs concentration increasing after 0.5 days. The result indicates that the hydrolysates as part of the uncertain organic matters will convert to the SCFAs, and the produced carbohydrate, protein and humic acids will be non-fermentable.
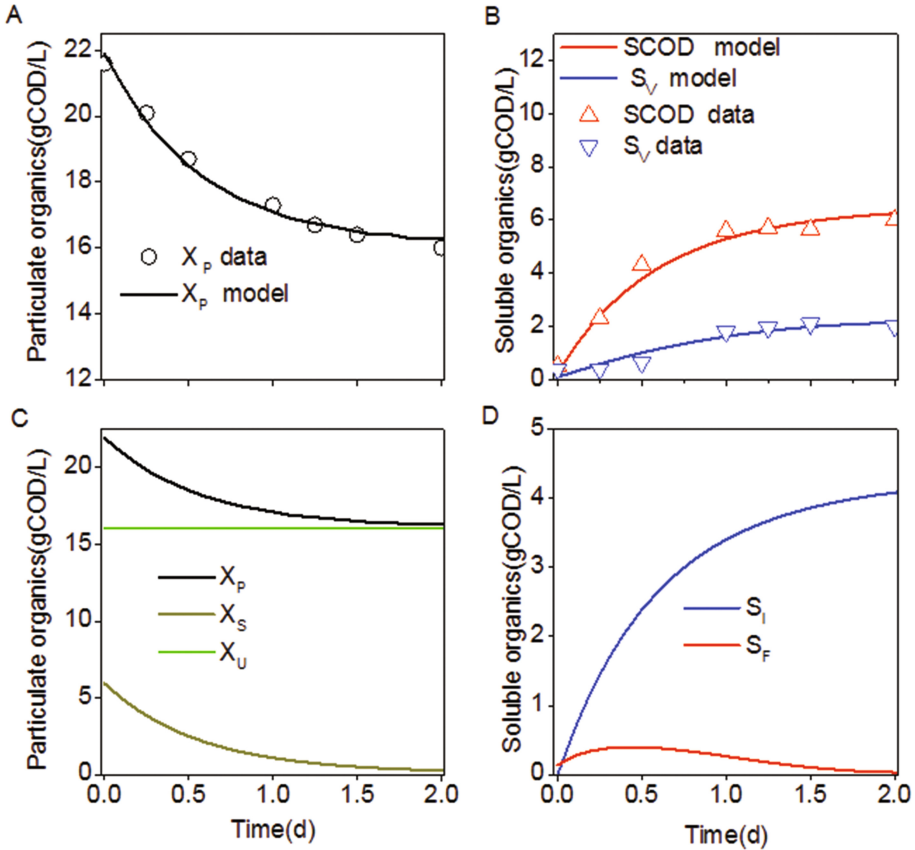
Fig. 1. Verification comparison of two models with experiment data. *A* showed prediction of particulate COD with two models. *B* showed fitting results of SCOD and SCFAs with two models. *C* showed X_P components based on the proposed model prediction. *D* showed hydrolysate components based on the proposed model predictions

Knowledge about sludge hydrolysis and fermentation kinetics is essential toward the optimum design and operation for producing the SCFAs. Furthermore, we propose a kinetic approach to describe the hydrolysis of degradable particulate organic matters and SCFAs production in a dynamic model. The new kinetic approach is able to determine the actual concentration of the degradable particulate organic matters in the waste sludge and predict the SCFAs production in the H-A reactor. The established model is calibrated and validated with thermophilic hydrolysis and fermentation experimental results (Fig. 1). By modeling calibration, a preliminary range of key parameters under thermophilic condition is obtained (k: $2.27–10d^{-1}$, ε: $0.13–0.37$, β: $0.34–0.86$, $k_{m,h}$: $6.05–11.98d^{-1}$). It is expected that this model is useful for better understanding the behavior of SCFAs production from the waste sludge.

4 Conclusions

We developed a kinetic model to describe hydrolysis of degradable particulate organic matters and acidification of fermentable hydrolysate for SCFAs production. Sensitivity analysis verified the reliability of parameter estimation. Series of measured thermophilic fermentation data were conducted to calibrate and validate the kinetic model. The established kinetic model could match the experimental data adequately.

References

Chen Y, Jiang S, Yuan H, Zhou Q, Gu G (2007) Hydrolysis and acidification of waste activated sludge at different pHs. Water Res 41:683–689

De La Rubia MA, Raposo F, Borja R (2009) Evaluation of the hydrolytic-acidogenic step of a two-stage mesophilic anaerobic digestion process of sunflower oil cake. Bioresour Technol 100:4133–4138

Mengmeng C, Hong C, Qingliang Z, Shirley SN, Jie R (2009) Optimal production of polyhydroxyalkanoates (PHA) in activated sludge fed by volatile fatty acids (VFAs) generated from alkaline excess sludge fermentation. Bioresour Technol 100:1399–1405

Sahm H (1984) Anaerobic wastewater treatment. Adv Biochem Eng Biotechnol 29:83–115

Siegert I, Banks C (2005) The effect of volatile fatty acid additions on the anaerobic digestion of cellulose and glucose in batch reactors. Process Biochem 40:3412–3418

Zhang P, Chen Y, Zhou Q, Zheng X, Zhu X, Zhao Y (2010) Understanding short-chain fatty acids accumulation enhanced in waste activated sludge alkaline fermentation: kinetics and microbiology. Environ Sci Technol 44:9343–9348

How Does the Mass Transfer Restriction Change the Reaction's Kinetic Order for Acid Mine Drainage Treatment in an Anaerobic Bioreactor?

P.T. Couto[1(✉)], R.P. Rodriguez[2], R. Ribeiro[3], and G.A. Valdiviesso[2]

[1] Department of Hydraulics and Sanitation, University of São Paulo (USP), São Carlos, SP, Brazil
[2] Science and Technology Institute, Federal University of Alfenas, Poços de Caldas, MG, Brazil
[3] Laboratory of Environmental Biotechnology, University of São Paulo (USP), Pirassununga, SP, Brazil

Abstract. In this work was described the acid mine drainage treatment in an anaerobic bioreactor, where was evaluated the mass transfer resistance's effects on appearance of the reaction's kinetic order using a mathematical model, Malthus-Monod-Fick model.

Keywords: Modeling · Anaerobic bioreactor · Acid mine drainage

1 Introduction

The acid mine drainage (AMD) is a wastewater of the mining industry. In the biological treatment, the AMD is treat in anaerobic bioreactor using sulfate reducing bacteria (SRB), where the sulfate is reduced to sulfide, that reacts with the heavy metal dissolved in solution and form the metal sulfide, that precipitate and there is increase of the pH in this process (Akcil and Koldas 2006).

In addition to knowing how the biological treatment process, it is important to model the data in order to extract new results that only the graphical verification does not present. Therefore, the goal of this work was to assume a mathematical model, Malthus-Monod-Fick model, capable of describing the AMD treatment in anaerobic reactor and evaluate the mass transfer resistance's effects on appearance of the reaction's kinetic order (Couto 2016).

2 Methodology

In the experimental phase of this biological process in a batch reactor with a consortium of microorganisms, ethanol was used as source of energy and source of carbon by SRB and the following biochemical reaction occurred, due to SRB (Vieira et al. 2016):

$$\frac{3}{2}SO_4^{2-} + CH_3CH_2OH + H^+ \rightarrow \frac{3}{2}H_2S + 2HCO_3^- + H_2O \tag{1}$$
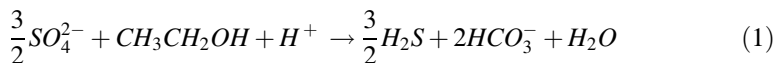
For the modeling, the ethanol, substrate and electron donor was identified by S and the sulfate, electron acceptor, was identified by A. Thus, it was possible to evaluate the consumption of sulfate and ethanol by SRB along the time, $S(t)$ and $A(t)$. By Eq. 1 there is a stoichiometric relation of $DQO/SO_4^{2-} = 2/3$, but we assumed experimentally a relation $DQO/SO_4^{2-} = 1$, to favor SRB (Couto 2016; Silva et al. 2002).

To describe the treatment process, we adopted the Malthus growth model $(dX/dt = rX)$, but as the microbial population does not grow infinitely, the population growth rate (r) was replaced by the specific growth rate of the Monod model $(\mu = \mu_{max}S/(K_S + S))$. Moreover, since the substrate consumption over time is determined by $\left(-\frac{dS}{dt} = (a_i/Y_i)dX/dt\right)$, we have the Malthus-Monod equation (Eq. 2), which describes the substrate consumption resulting from the biochemical reaction, presented in Eq. 1.

$$-\left(\frac{dS}{dt}\right)_{Rea} = \frac{\hat{\mu}^{SRB}}{Y^{SRB}} \frac{S}{K_S + S} \frac{A}{K_A + A} X^{SRB} \tag{2}$$

However, SRB does not act alone in the reactor and there is others bacterial groups disputing the electron donor, for example fermentative bacteria (FB). This way, Malthus-Monod equation became:

$$-\left(\frac{dS}{dt}\right)_{Rea} = \frac{\hat{\mu}^{SRB}}{Y^{SRB}} \frac{S}{K_S + S} \frac{A}{K_A + A} X^{SRB} + \frac{\hat{\mu}^{FB}}{Y^{FB}} \frac{S}{K_S + S} X^{FB} \tag{3}$$

It should be noted that the consumption of substrate over time does not occur only as a result of the biochemical reaction, but also by the mass transfer in the biofilm, determined by Fick's Law Equation for spherical coordinates in the case of self-immobilized granules:

$$-\left(\frac{\partial S}{\partial t}\right)_{Dif} = D\left[\frac{2}{r}\frac{\partial S}{\partial r} + \frac{\partial^2 S}{\partial r^2}\right] \tag{4}$$

Therefore, the consumption of substrate over time is obtained by Eq. 5, a model called Malthus-Monod-Fick (Couto 2016):

$$-\left(\frac{\partial S}{\partial t}\right)_{Total} = \left(\frac{\partial S}{\partial t}\right)_{Dif} + \left(\frac{\partial S}{\partial t}\right)_{Rea} \tag{5}$$

If there is no mass transfer restriction, the term referring to diffusion does not affect the substrate consumption rate and the reaction is the limiting step. On the other hand, if there is a mass transfer restriction both terms must be taken into account.

For the mathematical simulation in the C++ ROOT library, the finite difference method was used to discretize the Malthus-Monod-Fick model. In this model the initial

Table 1 Values of the parameters used in the modeling process (Rittmann and McCarty 2001)

Parameters	SRB	FB
$\hat{\mu}(h^{-1})$	0.013	0.05
$Y(mgSSVmgCOD^{-1})$	0.10	0.13
$K_S(mgCODl^{-1})$	<0.001	<0.001
$K_A(mgSO_4^{2-}l^{-1})$	<0.001	–

concentrations of sulfate and ethanol were the same $(S_0 = A_0 = 500 \text{ mg } l^{-1})$ and the parameters used are presented in Table 1. It was observed that the values of the Monod's parameters for anaerobic metabolism were very small $(K < 0.001)$, typical of zero-order kinetics, but these values may be variable and little predictable, because they are affect by the mass transfer resistance and the affinity for the substrate (Rittmann and McCarty 2001).

3   Results and Discussions

The simulation was performed for four different scenarios, which were Fig. 1:

- Prediction 1: Only SRB acting in the reactor, without mass transfer restriction;
- Prediction 2: SRB and FB acting in the reactor, without mass transfer restriction;
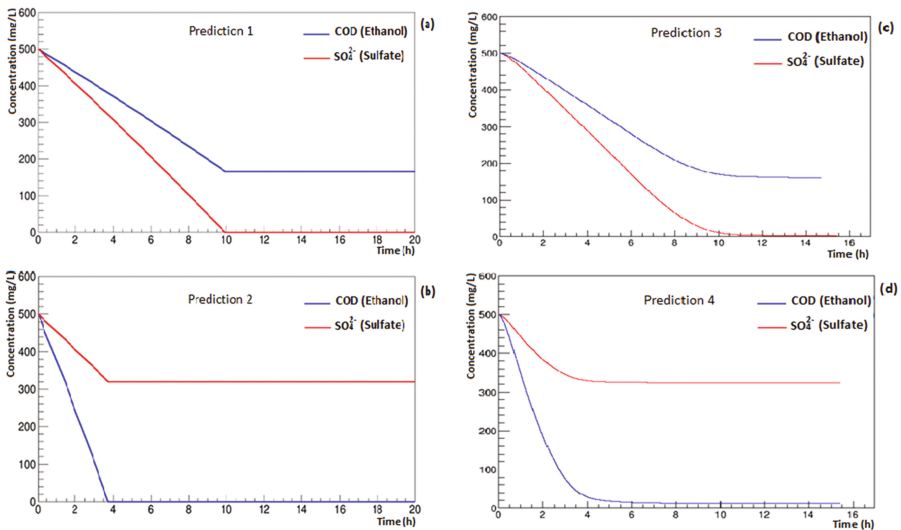
Fig. 1 Malthus-Monod-Fick model predictions: (a) Only SRB acting in the reactor, without mass transfer restriction; (b) SRB and FB acting in the reactor, without mass transfer restriction; (c) Only SRB acting in the reactor, with mass transfer restriction; (d) SRB and FB acting in the reactor, with mass transfer restriction

- Prediction 3: Only SRB acting in the reactor, with mass transfer restriction;
- Prediction 4: SRB and FB acting in the reactor, with mass transfer restriction.

The diffusion of substrate in the water ($D_{water} = 5,4\,\text{mm}^2\text{h}^{-1}$) (Flora et al. 1995 and Gonzalez-Gil et al. 2001) is always greater than the diffusion of substrate in the granule (D), for this reason it was assumed that $D < D_{water}$ the internal mass transfer restriction occurs in the granule, however when $D = D_{water}$ there is no mass transfer restriction.

From the model predictions shown in Fig. 1, it is possible to observe that when only SRB are acting in the process (Fig. 1(a) and (c)) there is a total consumption of sulfate and an excess of ethanol, since this was added in quantities larger than that required by stoichiometric. However, when SRB and FB compete for the substrate (Fig. 1(b) and (d)), ethanol is rapidly consumed and there is an excess of sulfate, since only SRB consumes it. Furthermore, when there is no mass transfer resistance (Fig. 1(a) and (b)), substrates consumption over time is constant, characteristic of zero-order kinetics. Nevertheless, when there is mass transfer restriction (Fig. 1(c) and (d)), even using negligible Monod coefficients ($K < 0.001$, Table 1), the kinetics presents a first order behavior.

4   Conclusions

It is concluded with this research that for anaerobic processes the Monod coefficients are small and that the behavior of first order kinetics results from an increase of the mass transfer restriction in the granule. This work, even being used in this specific case of AMD treatment using SRB, may contribute to other researchers in other scenarios using anaerobic processes, proving even more that the reaction's kinetic order is directly linked to the mass transfer restriction. The next step of this work is to adjust the model with the real data and do the statistical analysis to know if the model describes adequately the reality.

References

Akcil A, Koldas S (2006) Acid Mine Drainage (AMD): causes, treatment and case studies. J Cleaner Prod 14:1139–1145

Couto PT (2016) Métodos numéricos e estatísticos aplicados à modelagem de um reator em batelada anaeróbio, no tratamento de drenagem ácida de mina. M.Sc. thesis, Department of Science and Technology, Univ. Fed. of Alfenas, Poços de Caldas, Brazil, 93 p.

Flora J et al (1995) A modeling study of anaerobic biofilm systems: I. Detailed biofilm modeling. Biotech Bioeng 46:43–53

Gonzalez-Gil G, et al. (2001) Kinetics and mass-transfer phenomena in anaerobic granular sludge. Biotech Bioeng 73:125–134

Rittmann BE, McCarty PL (2001) Environmental biotechnology: principles and applications. McGraw-Hill, US

Silva AJ et al (2002) Sulphate removal from industrial wastewater using a packed-bed anaerobic reactor. Proc Biochem 37:927–935

Vieira BF, Couto PT, Sancinetti, GP, Klein B, Zyl D, van Rodriguez RP (2016) Acidic pH and presence of metals as important parameters to establish a sulfidogenic process in anaerobic reactor. J Environ Sci Health Part A: Toxic Hazard Subst Environ Eng 51:793–797

Optimal Scheduling and Fouling Control in Membrane Bioreactor

N. Kalboussi[1,2]($\boxtimes$), J. Harmand[3], F. Ellouze[1,2], and N. Ben Amar[1,2]

[1] Institut National des Sciences Appliquée et de Technologie,
Université de Carthage, Tunis, Tunisia
[2] Ecole Nationale d'Ingénieurs de Tunis, LAMSIN,
Université de Tunis El Manar, Tunis, Tunisia
[3] LBE, INRA, 11100 Narbonne, France

Abstract. This paper deals with the optimal control of membrane fouling allowing the maximization of the total water production of a MBR system over a given period of time. The main objective is to find the optimal switching sequence of filtration and backwash cycles that mitigates membrane fouling and maintains a good performance of the process. The key contribution of our work is in the synthesis of a generic and robust optimal control that can be applied in practice to a large number of different MBR processes.

Keywords: Membrane bioreactor · Fouling · Optimal control

1 Introduction

Membrane bioreactor technology (MBR) is the combination of a bioreactor process and a membrane filtration system. The membrane maintains the microorganisms and the solid particles in the biological tank. Thus, there is no need to recirculate the microorganisms as in the conventional systems and the quality of the effluent is better. However, membranes are inevitably subject to fouling due to the retention of particles onto and in the membrane pores. Membrane fouling leads to productivity reduction, increase in the cleaning downtime and membrane life span shortness. Therefore, it is essential to control membrane fouling in order to ensure an optimized MBR system functioning. Over the last decades, one of the main interests of research in MBR was finding sustainable membrane fouling control strategies [1]. In a recent work by Cogan et al. [2, 3], an analytical approach applying Pontryagin's maximum principle has been presented to predict the optimal instants of switching between backwash and filtration periods that maximize the overall water production of a specific model of a microfiltration process over a given period of time. However, the optimal control analysis of Cogan *et al*. is questionable because the transversality condition of the Maximum Principle is not verified. In the present work, we revisit this problem and we give the optimal control strategy for a large class of MBR systems.

2   Modeling of Membrane Fouling

To capture the dynamic behavior of the membrane fouling, we use a mathematical model that has been proved, in a previous work [4], to be generic enough to be used for optimization and control purposes. Care was taken to use a generic fouling model subject to general applicable hypotheses in order to obtain a generic optimal control synthesis. In the present work, it is assumed that the membrane fouling is only due to the particle deposition onto the membrane surface. Let m be the mass of the cake layer formed during the water filtration. The dynamic of m during filtration follows:

$$\dot{m} = b/(e+m) = f_1(m) > 0 \tag{1}$$

During backwash, the dynamic of the mass due to detachment can be written as follows:

$$\dot{m} = -a * m = -f_2(m) \leq 0 \tag{2}$$

The water flow rate that passes through the membrane is modeled by a function which only depends on the accumulated mass onto the membrane surface:

$$g(m) = d/(e+m) > 0 \tag{3}$$

3   The Optimal Control Synthesis and Numerical Results

The MBR is a switching process between two functioning modes: filtration and backwash. For this reason, by convention, we consider a control u that takes values 1 during filtration period and -1 during backwash. Then, the dynamic of the fouling layer formed by the attachment of a mass m onto the membrane surface can be written as follows:

$$\dot{m} = \frac{1+u}{2} * f_1(m) - \frac{1-u}{2} * f_2(m) \tag{4}$$

The aim of this work is to determine the optimal switching between the two functioning modes that maximize the water production of the MBR process over a time interval $[0;T]$. Then, the objective function of the optimal control problem can be expressed as:

$$J_T(m0, u(.)) = \int_0^T u(t)g(m(t))dt \tag{5}$$

Using the Pontryagin Maximum Principle [5], we established that the optimal control sequence is defined as:

$$u^* = \begin{cases} 1, & \text{if } m(t) < \bar{m} \text{ or } t \geq \bar{T} \\ \bar{u}, & \text{if } m(t) = \bar{m} \text{ and } t < \bar{T} \\ -1, & \text{if } m(t) > \bar{m} \end{cases} \tag{6}$$

with $\bar{m}$, $\bar{T}$ and $\bar{u}$ some values which are derived from the optimal synthesis (whose expressions are not presented here, cf. [6] for detailed calculations). To summarize, according to the position of $m(t)$ with respect to $\bar{m}$, the membrane filtration process operates as follows: The process operates in filtration ($u = 1$, if the membrane is still poorly fouled ($m(t) < \bar{m}$)) or in Backwash ($u = -1$, if the membrane is considered quite fouled ($m(t) > \bar{m}$)) until it reaches the singular arc (defined by $\bar{u}$ and $\bar{m}$) and stay on it ($m(t) = \bar{m}$) by applying the constant control ($u = \bar{u}$) until the switching time $\bar{T}$ is reached. After the time $\bar{T}$, it is optimal to filtrate until the terminal time T. Note, however, that the singular control, $\bar{u}$, has no physical meaning in practice (the process must operate either in filtration or in backwash). Therefore, we have to find the optimal switching between filtration and backwash to approximate the singular control $\bar{u}$ such that $m(t)$ remains close to $\bar{m}$. To do so, a first strategy consists in considering that $\bar{u}$ is the percentage of filtration time (T_f) over an operating cycle (T_p), such that:

$$\bar{u} = \frac{T_f}{T_p} \quad \text{with} \quad T_p = \frac{T_{SA}}{N} = T_f + T_{BW} \tag{7}$$

and where T_{SA} is the total time for which it is optimal to apply the constant control $\bar{u}$ and N the number of cycles fixed by the user over the time-period T_{SA}. Notice that in our original work (cf. [6]), we proposed an optimal control for a completely general model where functions f_1, f_2, g are only defined by their qualitative properties. In the present paper, we restrict our attention to specific functions f_1, f_2, g defined in Sect. 2 with parameters values reported in Table 1 and a prediction horizon of 10 h. Figure 1 shows the theoretical optimal control $u(t)$ over T for a given initial condition ($m_0 = 10^{-3}$g). Since, m_0 is lower than $\bar{m} = 4$ g, the optimal strategy is to filtrate until $m(t)$ reaches $\bar{m}$. Then the singular control $\bar{u} = 0,86$ is applied until $\bar{T} = 9.96$ h, before finally switching back to filtration until T is reached. The total water produced over T is then about 650.36 litres (see Fig. 1). However, a classical strategy recommended by the membrane suppliers (9 mn filtration, 1 mn Backwash) can produce only 506 litres. Because it has no physical meaning to apply controls that are different than -1 or $+1$, we investigate the degradation of the optimal strategy when we take into account such

Table 1. Values of the model parameters considered in the numerical simulations

	a	b	d	e
Parameters	400	2.7530e+03	1800	20
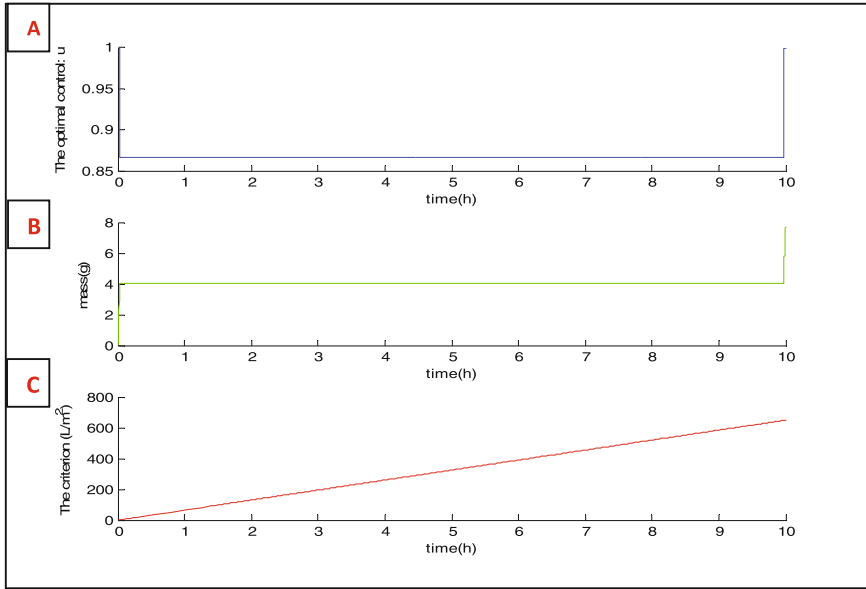
Fig. 1. **(A)** The theoretical optimal control sequence over T. **(B)** The corresponding mass accumulated. **(C)** The corresponding water production
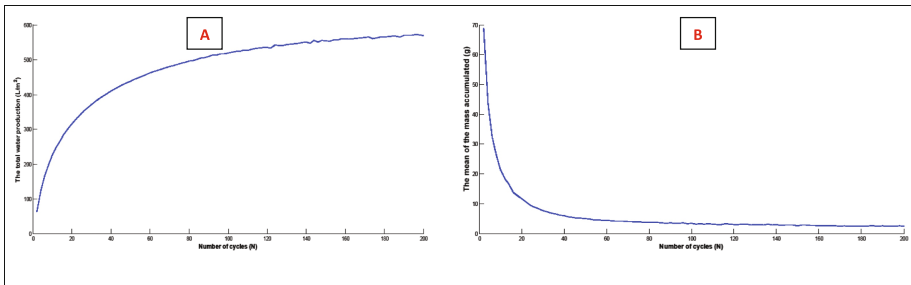
Fig. 2. **(A)** The total water production of the MBR process as a function of N (the number of filtration/backwash sequence). **(B)** The mean mass accumulated as a function of N (the number of filtration/backwash sequence)

practical considerations. For that, we plotted in Fig. 2 the total water production (J) of the MBR process as a function of the number N of backwash/filtration cycles. As expected, for large N, J is enhanced and get closer to the optimal solution and the mean of the mass accumulated onto the membrane surface decreases and tends to $\bar{m}$. An example of control when N = 20 is represented in the Fig. 3.
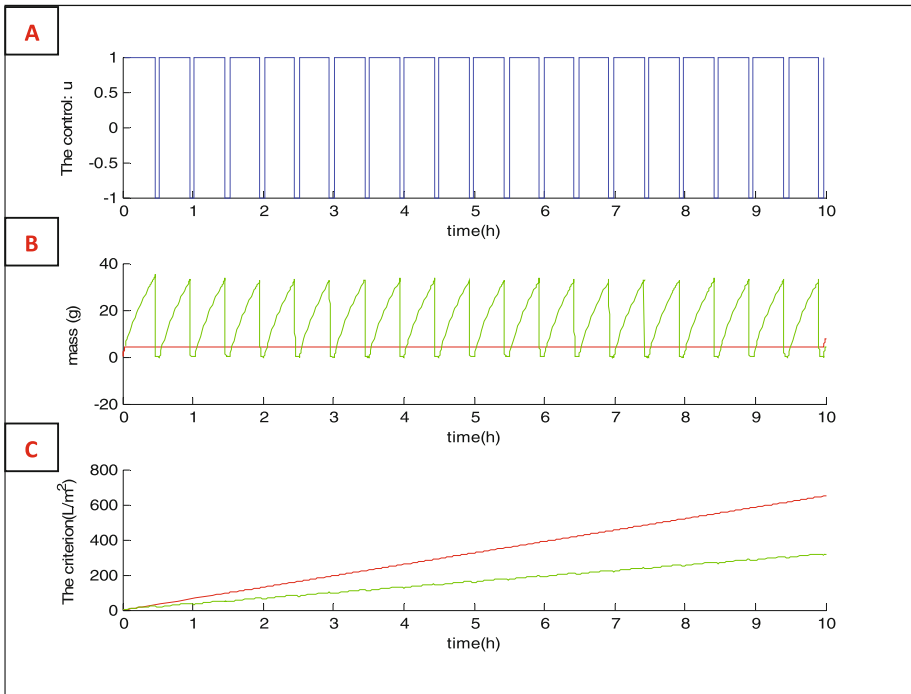
Fig. 3. (A) The control sequence for N = 20. **(B)** The green line is the corresponding mass accumulated; the red line is the optimal mass accumulated. **(C)** The green line is the corresponding water production; the red line is the optimal water production (Color figure online)

4 Conclusion

The optimal strategy obtained using the Pontryagin Maximum Principle improves the water production of the MBR process compared to a classical operating strategy recommended by the membrane suppliers. The main advantage of the optimal control approach proposed here is that it has been synthesized for a very large class of models, essentially defined by qualitative properties of the fouling model functions.

References

1. Iorhemen OT, Hamza RA, Tay JH (2016) Membrane Bioreactor (MBR) technology for wastewater treatment and reclamation: membrane fouling. Membranes 6(2):33
2. Cogan N, Chellam S (2014) A method for determining the optimal back-washing frequency and duration for dead-end microfiltration. J Membr Sci 469:410–417

3. Cogan N et al (2016) Optimal backwashing in dead-end bacterial microfiltration with irreversible attachment mediated by extracellular polymeric substances production. J Membr Sci 520:337–344
4. Kalboussi N, Harmand J, Ben Amar N, Ellouze F (2016) A comparative study of three membrane fouling models - towards a generic model for optimization purposes. In: CARI 2016, Tunis, Tunisia
5. Gamkrelidze R, Pontrjagin LS, Boltjanskij VG (1964) The mathematical theory of optimal processes. Macmillan Company, New York
6. Kalbussi N, et al (2016) Optimal control of filtration and back wash under membrane clogging. https://hal.archives-ouvertes.fr/hal-01393233

Process Performance and Microbial Community Structure of an Anaerobic Baffled Reactor for Natural Rubber Processing Wastewater Treatment

T. Watari[1,3,4,9(✉)], P.T. Thao[2,9], Y. Hirakata[5,9], M. Hatamoto[1,6,9], D. Tanikawa[7,9], K. Syutsubo[8,9], N.L. Huong[2,9], N.M. Tan[3,9], M. Fukuda[8,9], and T. Yamaguchi[1,6,9]

[1] Department of Environmental Systems Engineering, Nagaoka University of Technology, Nagaoka, Japan
[2] Department of Biotechnology, Hanoi University of Science and Technology, Hanoi, Vietnam
[3] Department of Chemical Engineering, Hanoi University of Science and Technology, Hanoi, Vietnam
[4] Environmental Engineering and Water Technology Department, UNESCO-IHE, Delft, The Netherlands
[5] Department of Science of Technology Innovation, Nagaoka University of Technology, Nagaoka, Japan
[6] Top Runner Incubation Center for Academia-Industry Fusion, Nagaoka University of Technology, Nagaoka, Japan
[7] Department Civil and Environmental Engineering, National Institute of Technology, Kure College, Kure, Japan
[8] Center for Regional Environmental Research Tsukuba, National Institute for Environmental Studies, Tsukuba, Japan
[9] Department of Bioengineering, Nagaoka University of Technology, Nagaoka, Japan

Abstract. Natural rubber processing wastewater contains high concentration of organic compounds mainly acids and ammonia. This wastewater also contains large amount of residual rubber particles. In this study, a laboratory-scale experiment was conducted to evaluate process performance of anaerobic baffled reactor (ABR) treating this wastewater. In addition, microbial community structure in different compartments of ABR was characterized. The highest COD removal efficiency of $92.3 \pm 6.3\%$ was observed when operated under organic loading rate of 1.4 ± 0.3 kg-COD$\cdot$m$^{-3}\cdot$day^{-1}. Maximum methane gas production of 29.8 NL$\cdot$day^{-1} was observed on day 177. Massively parallel next generation sequencing showed the difference of acetogen community could be caused by the difference in pH of these compartments. Acetate utilizing methanogen *Methanosaeta* was predominantly detected in the 3rd and 4th compartments with abundance of 9.8% to 16.4%. This result indicated that the ABR is considered as a novel applicable treatment system for this wastewater.

Keywords: Anaerobic treatment · Microbial community analysis · Natural rubber processing wastewater

1 Introduction

Currently, rubber is one of major export items that contributes to gross domestic production growth in Vietnam economy. According to the latest statistics of Vietnam Rubber Association, Vietnam is the world's third largest rubber producer and the fifth largest exporter in 2014. A part from the profits, natural rubber processing wastewater which contained high concentration of ammonia and organic pollutants that were mainly acids is an urgent environmental problem. Vietnam conventional technical processes for natural rubber processing wastewater mentioned in the study of Nguyen and Luong (2012) were series of decantation, anaerobic digestion and aerobic reactor followed by polishing tank. However, large amount of residual rubber particles in this wastewater has become an obstacle for stable operation in modern reactors because they can easily clog the reactors. An anaerobic baffled reactor (ABR) is a single reactor configuration divided into a few compartments by vertical baffles allowing liquid flow under and over them. The risk of clogging and excessive bed expansion were minimized, moreover, a high void volume is maintained without the need of expensive and operationally work for intensive gas collection systems or sludge separation systems. In addition, the compartmentalization with different microbial community within may provide the opportunity to separate hydrolysis, acidogenesis and methanogenesis with their optimum conditions longitudinally down the reactor. There are various types of ABR with wide range of applications, particularly for high-strength wastewater, described in previous studies (Barber and Stuckey 1999). Therefore, ABR is the most feasible and efficient alternative for conventional treatment systems. The specific configuration of ABR could prevent the negative effects of acid condition and high level of suspended solid in the wastewater on anaerobic digestion without pre-treatment process. Natural rubber processing wastewater treatment using ABR has been investigated by Saritpongteeraka et al. (2008), Tanikawa et al. (2016a) and Watari et al. (2017). The coagulation process of rubber latex uses sulfuric acid (Saritpongteeraka and Chaiprapat 2008) or organic acids (Tanikawa et al. 2016a) in Thailand and Vietnam, respectively. Differences in wastewater profile resulted to performance and characteristics difference of ABR treating natural rubber processing wastewater in each country. So far, only few investigations about ABR treating natural rubber processing wastewater in Vietnam (Tanikawa et al. 2016a and Watari et al. 2017) was performed and information about microbial consortia in retained sludge in individual compartments of the ABR was scarce. Therefore, this research focuses on investigation of the microbial community structure in different compartments of the ABR using metagenomic technology, as well as evaluation the tolerance of ABR to high organic loading rate by increasing stepwise chemical oxygen demand (COD) concentration of influent.

2 Materials and Methods

The natural rubber processing wastewater was made from coagulation process of concentrated rubber latex following the rubber sheet coagulate method used in an actual natural rubber processing factory in the North Vietnam. The characteristics of raw natural rubber processing wastewater was pH 4.9 ± 0.1; total COD of $19{,}170 \pm 1{,}100$ mg·L^{-1};

total biochemical oxygen demand (BOD) of 12,590 $\pm$ 2,020 mg·L^{-1} and total nitrogen (TN) of 1,960 $\pm$ 490 mg-N·L^{-1}. The raw wastewater was diluted to the appropriate COD concentration by tap water and used as the influent.

Figure 1 show schematic diagram of ABR used in this study. The ABR was operated in Hanoi University of Science and Technology, Vietnam. The ABR made up of polyvinyl chloride pipes (diameter: 110 mm, height: 1000 mm) had 10 compartments and working volume of 68 L. Compartments 2 to 9 were covered by plastic polyvinyl chloride caps in order to keep anaerobic condition. The operation temperature was maintained ambient temperature of 27.1 $\pm$ 4.7 °C. The anaerobic sludge collected from anaerobic digester treating livestock manure was inoculated in compartment 3rd to 10th. The hydraulic retention time (HRT) was calculated based on working volume and flow rate.
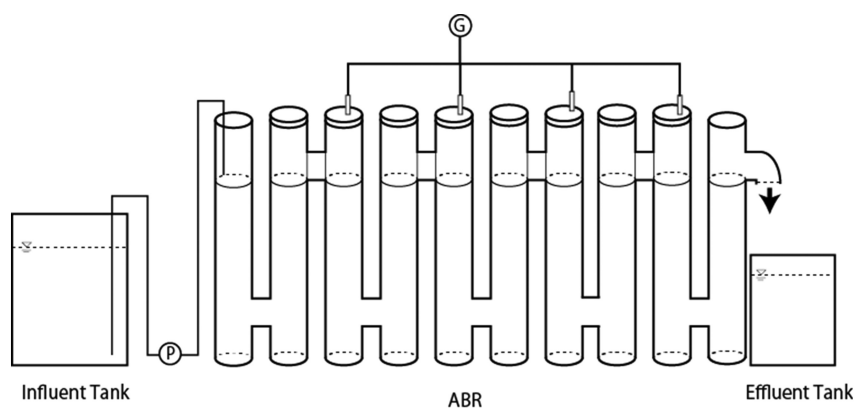
Fig. 1. Schematic diagram of anaerobic baffled reactor

Table 1 shows operational condition of ABR. The performance of the ABR was evaluated by determination of parameters COD, total suspended solids (TSS) and TN of influent and effluent. COD and TN were measured by multiple water quality checker (DR-2800, HACH). Biogas production was measured using wet gas meter (WS-1A, Shinagawa), and biogas composition was analyzed using a gas chromatograph equipped with a thermal conductivity detector (GC-8A, Shimadzu). The sludge samples were collected from the bottom of the ABR reactor in each compartment on day 143. The PCR primers used in the amplification were the universal forward primer Univ515F and the universal reverse primer Univ806R with annealing temperature of 50 °C. Massively parallel 16S rRNA sequencing and data analysis were performed based on the methods of Caporaso et al. (2012). Representative genera were selected on the basis of the >2% maximum abundance rate in each ABR comportment microbial community.

Table 1. Operational conditions for anaerobic baffled reactor.

Phase	Day	Flow rate L/day	HRT day	OLR kg-COD/(m3 ·day)
1	1–83	20.3 ± 5.2	3.2 ± 1.0	1.1 ± 0.3
2	84–143	19.4 ± 3.3	3.2 ± 0.7	1.4 ± 0.3
3	143–224	15.9 ± 2.2	3.9 ± 0.6	2.1 ± 0.1

3 Results and Discussions

The ABR was started up with an influent COD of 3,000 mg·L^{-1} and operated for 224 days. The OLR of ABR was increased stepwise by increasing the influent COD concentration. The total COD, TSS and TN concentrations and removal efficiencies of ABR were shown in Fig. 2. The COD removal efficiency of ABR was gradually improved and reached 92.4% on day 72. The COD concentrations of influent and effluent were 3,420 ± 660 mg·L^{-1} and 1,500 ± 620 mg·L^{-1}. During phase 1, the ABR performed 56.2 ± 18.5% of COD removal efficiency with OLR of 1.1 ± 0.3 kg-COD·m^{-3}·day^{-1}. The highest COD removal efficiency of 92.3 ± 6.3% was observed during phase 2 when operated under OLR of 1.4 ± 0.3 kg-COD·m^{-3}·day^{-1}. This removal efficiency was higher than previous study that applied ABR to this wastewater (Saritpongteeraka and Chaiprapat 2008). The high removal efficiency in this study could be related to the high level of acetate from coagulation as the major COD pollutant in Vietnam natural rubber processing wastewater. An upflow anaerobic sludge blanket (UASB) reactor is most promising system for this wastewater; some laboratory scale UASB reactor achieved high organic removal efficiency together with high methane recovery rate (Watari et al. 2016). However, the pilot scale UASB reactor could operate at low OLR condition due to influent containing high sulfate or suspend solids (Tanikawa et al. 2016b; Watari et al. 2017). Tanikawa et al. (2016b) reported that the pilot scale UASB reactor treating natural rubber processing wastewater containing high sulfate performed 95.7 ± 1.3% of total COD removal efficiency with OLR of 0.8 kg-COD·m^{-3}·day^{-1} in Thailand. Also, the pilot scale UASB reactor treating natural rubber discharged from ribbed smoked sheet performed 55.6 ± 16.6% for total COD removal efficiency and 77.8 ± 10.3% for BOD with OLR of 1.7 kg-COD·m^{-3}·day^{-1} (Watari et al. 2017). There are several limitations for application of UASB reactor to this wastewater. Thus, ABR which have different compartments could be a strong point for its application in treatment of natural rubber processing wastewater

The composition of biogas during phase 2 was 73.7 ± 5.1% of methane, 23.8 ± 5.5 of carbon dioxide and 2.5 ± 2.4% of nitrogen. The maximum methane gas production of 29.8 NL·day^{-1} was observed on day 177. The methane recovery ratio based on removed total COD was 52.4 ± 33.6% during phase 2. The ABR performed good TSS removal of 91.0 ± 0.6% during phase 2. The accumulated natural rubber particulars were never removed from the ABR. These results suggested that the ABR trapped suspend solids from natural rubber processing wastewater and could degrade it to soluble organics. The total COD, TSS and TN of effluent were 311 ± 218 mg·L^{-1}, 27 ± 12 mg·L^{-1} and 460 ± 44 mg-N·L^{-1}, respectively during phase 2. This result shows most of the organic compounds were removed in ABR. This result indicated that
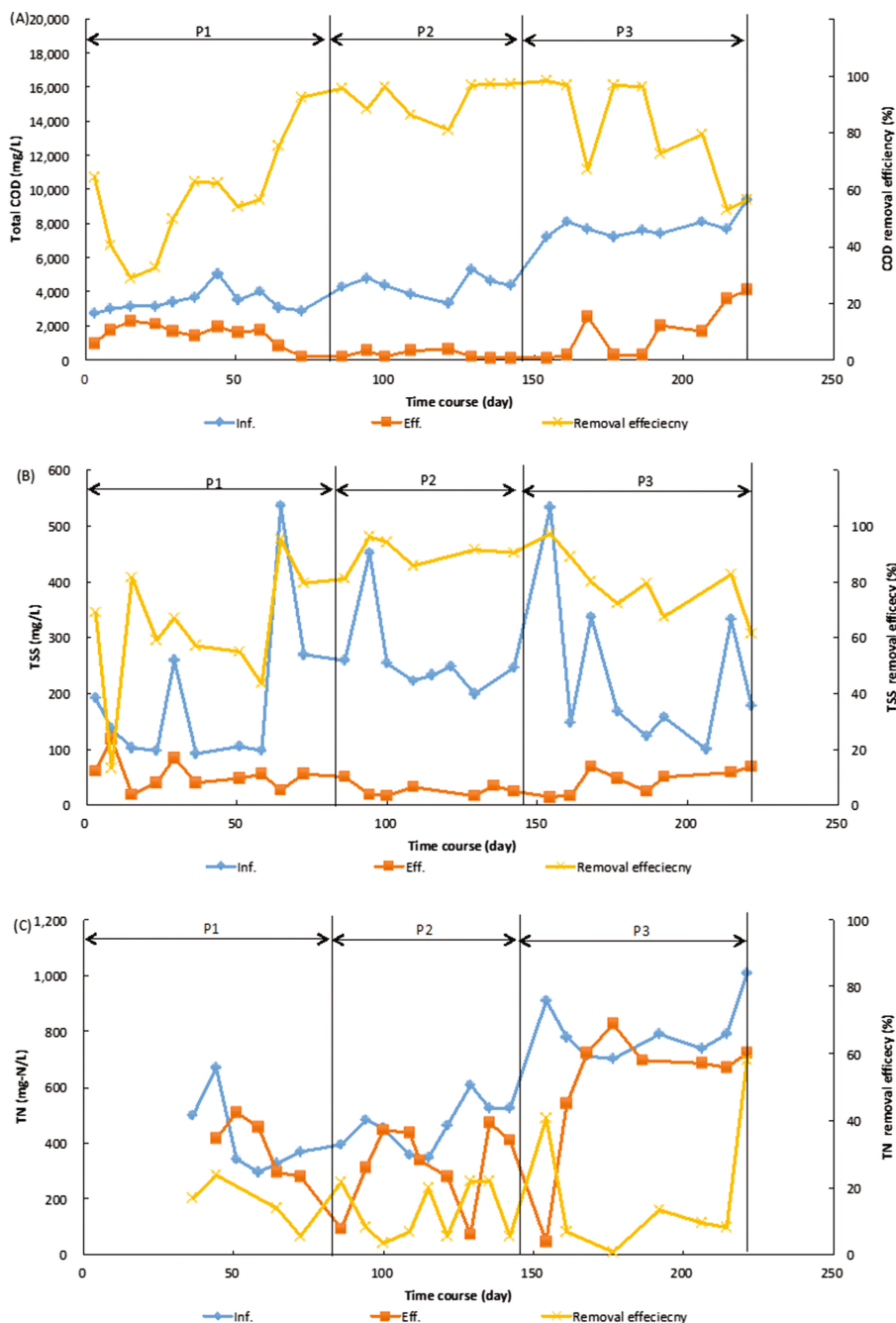
Fig. 2. Time course of (A) Total COD, (B) TSS and (C) TN concentrations during the entire experimental periods

the ABR is considered as a novel applicable treatment system for this wastewater. However, it requires further post-treatment to achieve industrial standards.

After increasing OLR up to 2.1 ± 0.1 kg-COD·m^{-3}·day^{-1}, the process performance of ABR deteriorated. The influent and effluent COD of ABR were $7,890 \pm 680$ mg-COD·L^{-1} and $1,840 \pm 1,520$ mg-COD·L^{-1}, respectively during phase 3. At the end of experiment, the foam was observed on the water surface of the reactor. Previous study reported that accumulation of acetate could be caused a foaming (Ganidi et al. 2009). Therefore, the optimal OLR for this wastewater should be approximately 1.5 kg-COD·m^{-3}·day^{-1} in this study.

The microbial community structure of ABR retained sludge in each compartments were analyzed by using 16S rRNA gene sequence. The principle microbial groups in the ABR retained sludges were the phyla *Bacteroidetes*, *Firmicutes*, *Proteobacteria*,
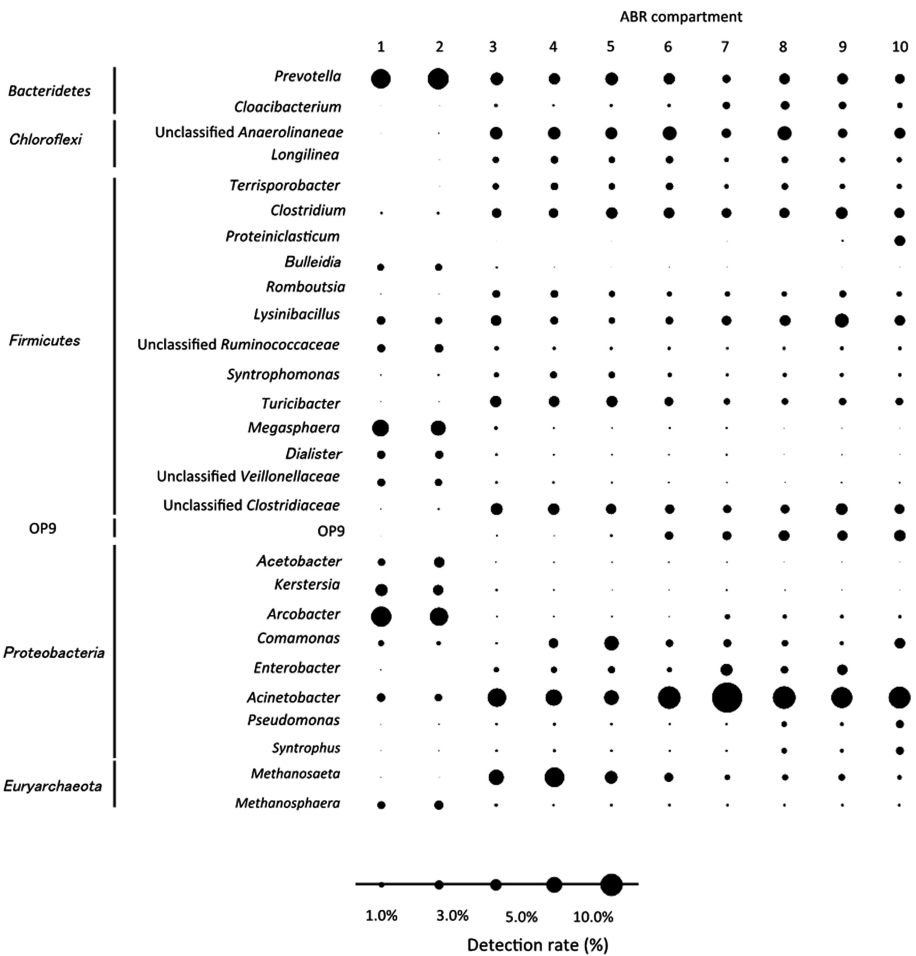
Fig. 3. Microbial community composition of the anaerobic baffled reactor. Circles sizes correspond to abundance rates, as shown at the bottom of the figure

Chloroflexi, and *Euryarchaeota*. These microbial groups have been frequently and commonly encountered in mesophile methanogenic sludges (Narihiro et al. 2008). Figure 3 shows the predominant genera of the ABR retained sludge on day 143. In compartment 1st and 2nd, *Arcobacter*, *Megasphaera* and *Prevotella* were highly detected. *Arcobacter* was found in the raw sewage and reported nitrate-reducing bacteria. Sequence related to *Nitrosomonadaceae* was also detected in the 1st compartment. Therefore, ammonia in the wastewater could be oxidized or contained in the influent and utilized by *Arcobacter*. *Megasphera* and *Prevotella* were known as acetogen that can grow in low pH condition. Thus, these bacteria could degrade organic compound in first step of degradation process for this wastewater. *Terrisporobacter* and *Clostridum* known as acetogen were dominated in 3rd and 4th compartments. *Actinetobacter* highly found in the downstream degraded organic under high pH condition. Therefore, this difference of acetogen community could be caused by the difference in pH of these compartments. In addition, volatile fatty acid oxidizing bacteria, *Syntrophomonas* and *Syntrophus* were highly detected in the 3rd to 6th compartments. In archaea, acetate utilizing methanogen *Methanosaeta* was predominantly detected in the 3rd and 4th compartments with abundance of 9.8% to 16.4%. These results demonstrated the necessity of maintaining favorable environments for syntrophic association in ABR.

4 Conclusions

The ABR was applied to natural rubber processing wastewater treatment in Vietnam. The ABR performed good process performance of $92.3 \pm 0.3\%$ COD removal efficiency with OLR of 1.4 ± 0.3 kg-COD·m^{-3}·day^{-1}. In addition, $52.4 \pm 33.6\%$ of methane recovery ratio was achieved. However, further post-treatment system is required to achieve the industrial standards. Microbial community analysis showed that several acetogens were detected and these bacteria could degrade organic compound in first step of degradation process for this wastewater. This finding suggested that these bacteria may have a role in organic matter degradation. These results demonstrate the great potential of the ABR for natural rubber processing wastewater treatment.

References

Caporaso JG, Lauber CL, Walters WA, Berg-Lyons D, Huntley J, Fierer N, Owens SM, Betley J, Fraser L, Bauer M, Gormley N, Gilbert JA, Smith G, Knight R (2012) Ultra-high-throughput microbial community analysis on the Illumina HiSeq and MiSeq platforms. ISME J 6 (8):1621–1624

Ganidi N, Tyrrel S, Cartmell E (2009) Anaerobic digestion foaming causes – a review. Bioresour Technol 100(23):5546–5554

Narihiro T, Terada T, Kikuchi K, Iguchi A, Ikeda M, Yamauchi T, Shiraishi K, Kamagata Y, Nakamura K, Sekiguchi Y (2008) Comparative analysis of bacterial and archaeal communities in methanogenic sludge granules from upflow anaerobic sludge blanket reactors treating various food-processing, high-strength organic wastewaters. Microb Environ 24 (2):88–96

Nguyen HN, Luong TT (2012) Situation of wastewater treatment of natural rubber latex processing in the Southeastern region. Vietnam J Viet Environ 2:58–64

Saritpongteeraka K, Chaiprapat S (2008) Effects of pH adjustment by parawood ash and effluent recycle ratio on the performance of anaerobic baffled reactors treating high sulfate wastewater. Bioresour Technol 99:8987–8994

Tanikawa D, Syutsubo K, Watari T, Miyaoka Y, Hatamoto M, Iijima S, Fukuda M, Nguyen NB, Yamaguchi T (2016a) Greenhouse gas emissions from open-type anaerobic wastewater treatment system in natural rubber processing factory. J Clean Prod 119:32–37

Tanikawa D, Syutsubo K, Hatamoto M, Fukuda M, Takahashi M, Choeisai PK, Yamaguchi T (2016b) Treatment of natural rubber processing wastewater using a combination system of a two-stage up-flow anaerobic sludge blanket and down-flow hanging sponge system. Water Sci Technol 73(8):1777–1784

Watari T, Thanh NT, Tsuruoka N, Tanikawa D, Kuroda K, Huong NL, Tan NM, Hai HT, Hatamoto M, Syutsubo K, Fukuda M, Yamaguchi T (2016) Development of a BR–UASB– DHS system for natural rubber processing wastewater treatment. Environ Technol 37(4): 459–465

Watari T, Mai TC, Tanikawa D, Hirakata Y, Hatamoto M, Syutsubo K, Nguyen NB, Fukuda M, Yamaguchi T (2017, in press) Performance evaluation of the pilot scale upflow anaerobic sludge blanket - downflow hanging sponge system for natural rubber processing wastewater treatment in South Vietnam. Bioresour Technol

Barber WP, Stuckey DC (1999) The use of the anaerobic baffled reactor (ABR) for wastewater treatment: a review. Water Res 33:2423–2432

Contribution of Modeling in the Understanding of the Anaerobic Digestion: Application to the Digestion of Protein-Rich Substrates

Z. Khedim[1(✉)], B. Benyahia[1], and J. Harmand[2]

[1] Laboratoire d'Automatique de Tlemcen, Université de Tlemcen,
Tlemcen, Algérie
{zeyneb.khedim,boumediene.benyahia}@univ-tlemcen.dz
[2] Laboratoire de Biotechnologie et de l'Environnement, INRA,
Narbonne, France
jerome.Harmand@inra.fr

Abstract. This paper deals with the analysis of a Microalgae Anaerobic Digestion model (MAD model), to study the influence of the ammonia on the fermentation of such protein- rich substrate. Using the operating diagram of the model, we show the key role of the operating parameters: Dilution rate (**D**) and the nitrogen input concentration (**N$_{in}$**), on the process performances. To investigate the ammonia toxicity phenomenon and its subsequent impact, we focus on the variation Free ammoniacal Nitrogen (FAN) concentration and the biogas yield with respect to the changes of **D** and **N$_{in}$**. Numerical simulations provide the FAN critical concentration leading to bacteria inhibition as well as the ideal values of the control parameters allowing to maximize biogas production, on the one hand, and to avoid any process failure, on the other hand. Our study highlights the effectiveness of the modeling to detect ammonia inhibition risk, that can then be used for control and optimization purposes of such anaerobic digestion process.

Keywords: Anaerobic digestion · MAD model · FAN threshold inhibition

1 Introduction

The Anaerobic Digestion (AD) process is sensible to various instabilities affecting its performance, which could even lead to its failure (Kafle et al. 2014). Total ammoniacal nitrogen (TAN) is one of the inorganic compounds that greatly affects the chemical environment of AD (Rajagopal et al. 2013) because of its decomposition into ammonium (NH_4^+) and Free Ammoniacal Nitrogen (FAN) that are toxic for methanogenic microorganisms at high concentration (Yenigün and Demirel 2013; Kovács et al. 2013). This risk of inhibition/toxicity may significantly increase in the case of protein rich substrates as Slaughterhouse waste (Ek et al. 2011), Casein and Pig Blood (Kovács et al. 2013), Microalgae (Becker 2007), since the breakdown of such substrates yields an important amount of FAN. Several papers are dedicated to the study of ammonia

toxicity. In particular, attempts have been made to define the limits for ammonia inhibition and the practical strategies for recovering process damage, via fermentation experiments of various substrates at different pH and temperature values (Rajagopal et al. 2013; Ek et al. 2011; Kovács et al. 2013). In our investigation, we try to early detect a risk of inhibition using modeling. In particular, based on the Microalgae Anaerobic Digestion model (MAD) (Mairet et al. 2012), we try to deduce the impact of the ammonia input concentration (N_{in}) on model equilibria. TAN and FAN critical concentrations are reported at a pH of 7 and at a temperature of 35 °C. In addition, biogas yield is evaluated according to changes of hydraulic loading (D) and N_{in}.

2 MAD Model

The MAD model is a two steps-three reactions model proposed by (Mairet et al. 2012). It considers four substrates S_1 (lipids-sugars), S_2 (proteins), S_3 (Volatile Fatty Acids) and S_I (inert), and three bacterial consortia X_1, X_2 and X_3. X_1 and X_2 degrade S_1 and S_2 respectively to produce S_3, which is converted by X_3 into biogas. Model equations are given by:

$$\dot{S}_1 = D(\beta_1 S_{in} - S_1) - \alpha_1 \mu_1 X_1 \tag{1}$$

$$\dot{S}_2 = D(\beta_2 S_{in} - S_2) - \alpha_5 \mu_2 X_2 \tag{2}$$

$$\dot{S}_3 = -DS_3 + \alpha_3 \mu_1 X_1 + \alpha_6 \mu_2 X_2 - \alpha_9 \mu_3 X_3 \tag{3}$$

$$\dot{X}_1 = (\mu_1 - D)X_1 \tag{4}$$

$$\dot{X}_2 = (\mu_2 - D)X_2 \tag{5}$$

$$\dot{X}_3 = (\mu_3 - D)X_3 \tag{6}$$

$$\dot{N} = D(N_{in} - N) - \alpha_2 \mu_1 X_1 + \alpha_7 \mu_2 X_2 - \alpha_{10} \mu_3 X_3 \tag{7}$$

$$\dot{C} = D(C_{in} - C) + \alpha_4 \mu_1 X_1 + \alpha_8 \mu_2 X_2 + \alpha_{12} \mu_3 X_3 - \rho_{CO2} \tag{8}$$

where D is the dilution rate, $\alpha_i (i = 1, \ldots, 12)$ are the stoichiometric parameters, S_{in}, N_{in} and C_{in}, are the input concentration of organic matters S_1, inorganic nitrogen N and inorganic carbon C, respectively. The biogas dynamics are characterized by the following equations:

$$\dot{P}_{CO2} = -P_{CO2}\frac{q_{gas}}{V_{gas}} + \rho_{CO2}\frac{V_{liq}RT_{op}}{V_{gas}} \tag{9}$$

$$\dot{P}_{CH4} = -P_{CH4}\frac{q_{gas}}{V_{gas}} + \rho_{CH4}\frac{V_{liq}RT_{op}}{V_{gas}} \tag{10}$$

with P_{CO2} and P_{CH4} the partial pressures of CO_2 and CH_4, ρ_{CO2} and ρ_{CH4} their liquid-gas transfer rates, $V_{liq}, V_{gas}, R, T_{op}, P_{atm}, q_{gas}$ the liquid volume, gas volume, gas law constant, temperature, atmospheric pressure and biogas flow rate, respectively. The model is completed by the following algebraic equations:

$$\rho_{CO2} = k_L a \left(\frac{h}{K_C + h} C - K_{H,CO_2} P_{CO2} \right) \tag{11}$$

$$\rho_{CH4} = \alpha_{11} \mu_3 X_3 \tag{12}$$

$$\left[NH_4^+ \right] = \frac{h}{K_N + h} N \tag{13}$$

$$K_N = \frac{h[NH_3]}{[NH_4^+]} \tag{14}$$

$$q_{gas} = k_p (P_{CH_4} + P_{CO_2} - P_{atm}) \tag{15}$$

where K_C, K_{H,CO_2} and K_N are chemical constants. $k_L a$ is a physico-chemical coefficient. $\left[NH_4^+ \right], [NH_3]$, h are the concentrations of ammonium, FAN and bicarbonate, respectively.

The kinetics $\mu_i(.)$ are represented by the following functions

$$\mu_i(S_i, X_i) = \bar{\mu}_i \frac{S_i}{S_i + K_{Si} X_i}, \ i = 1, 2, \ \mu_3(S_3, N) = \bar{\mu}_3 \frac{S_3}{S_3 + K_{S3} + S_3^2/K_{I3}} \frac{K_{I,NH_3}}{K_{I,NH_3} + \lambda N},$$
$$\lambda = \frac{K_N}{K_N + h} \tag{16}$$

3 Results and Discussions

We consider $\xi^T = [S_1, S_2, S_3, X_1, X_2, X_3, N, C, \ P_{CO2}, P_{CH4}]^T$, the vguector of the state variables of the MAD model. pH is considered as a model's input. It is assumed to be constant equal to 7. The model was first calibrated using the high nitrogen content of the chlorella vulgaris microalgae (Becker 2007). To study the consequence of a further increase in the TAN concentration, we fixed substrate inputs at the maximum value taken in the experiments S_{in0} = 6 g COD/l (Mairet et al. 2012), and we varied values of the operating parameters D and N_{in}.

According to these parameters, the Operating Diagram (OD) of the MAD model is then numerically deduced. It shows how the system (the set of equilibria) behaves when the values of the model control parameters change. To calculate model equilibrium, we set the right hand of Eqs. (1)–(10) equal to zero. MAD has at most 13 equilibrium points. These equilibria are obtained from seven cases matching to the washout/not washout of each bacteria (Fig. 1). For each value of D and N_{in}, the nature of the 13 equilibria is evaluated according to the condition of the existence and the sign
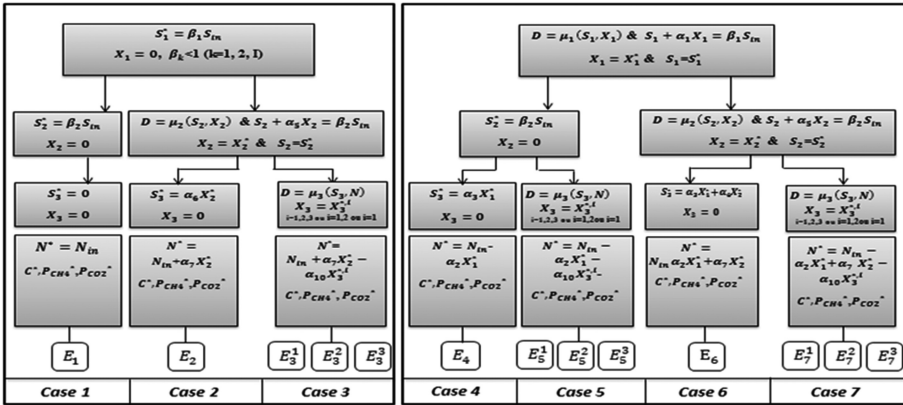
Fig. 1. Diagram summarizing the equilibria of system (1)–(10)
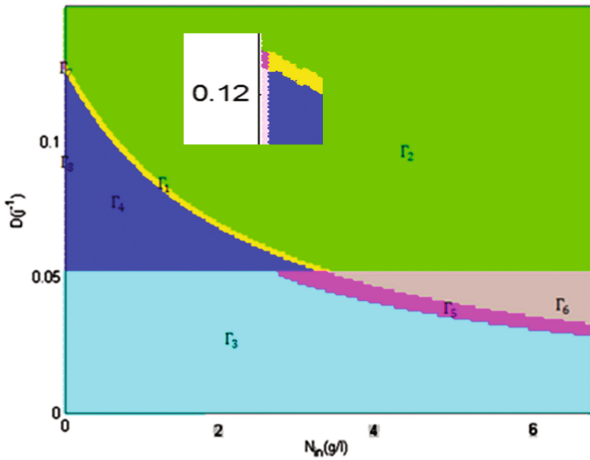
Fig. 2. Operating diagram according to (D, N_{in}) of the MAD

of the jacobian eigenvalues. The resulted set of equilibria forms a combination (Γ) presented by a color on the OD (cf. Fig. 2).

Table 1 illustrates the 8 possible combinations shown in Fig. 2, where only the fields Γ_3 and Γ_4 guarantee stability when the others present either bistability or washout. Notice that, the number and size of the OD areas are strongly dependent of the pH of the system. A low or high pH values induce a narrowing of stability areas and the spreading of the washout ones.

To define the FAN critical/ideal concentrations during the AD of chlorella vulgaris in a CSTR, we perform numerical simulation of FAN concentration within the previous range of D and N_{in}.

Table 1. Equilibria existence and stability according to N_{in} and D, (I: unstable, S: stable, Any sign: equilibrium does not exist, X: unstable or does not exist)

Area	E_1	E_2	E_3^1	E_3^2	E_3^3	E_4	E_5^1	E_5^2	E_5^3	E_6	E_7^1	E_7^2	E_7^3
Γ_1	I					S	I	S					
Γ_2	I					S							
Γ_3	I	I		I		I		X		I		S	
Γ_4	I					I		S					
Γ_5	I	I	X	X				I		S	I	S	
Γ_6	I	I				I	X	X		S			
Γ_7	I					S	I						
$\Gamma_8.$	I					I							

From Fig. 3, it is shown that FAN depends mainly on N_{in}. It can be slightly alleviated by increasing D (Hejnfelt and Angelidaki 2009) but with only 0.002 g FA/l. However, FAN takes small values for small values of N_{in} (blue range) that correspond to all the left hand of Γ_3 and Γ_4 areas. When N_{in} increase, a severe stress of ammonia is observed (threshold inhibition level: cyan to red), which may lead to the failure of the process (Γ_6 and Γ_2). Thus, N_{in} value must be carefully chosen to prevent toxicity.
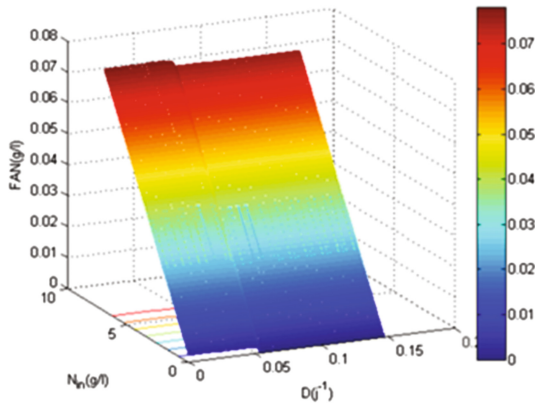
Fig. 3. Changes of FAN concentration according to D and N_{in} changes (Color figure online)

Aiming to maximize process efficiency, we calculate, for each area Γ of Fig. 2, biogas yield at the stable equilibrium. In the case of bistability (Γ_5 or Γ_1), we represent the interior point (positive equilibrium excluding washout).

Figure 4 shows that the maximum biogas yield is obtained when D and N_{in} belong to the red ranges. This refers to the upper of the area Γ_3 of Fig. 2. However this yield decreases with N_{in} (Γ_5, Γ_6) or when the bacteria are washed out (Γ_4). It implies that beside the judicious choice of N_{in}, D must take a high value in area Γ_3 enabling an optimum biogas production. Thus, the compromise between an optimum biogas production and a suitable N_{in} concentration must be satisfied.
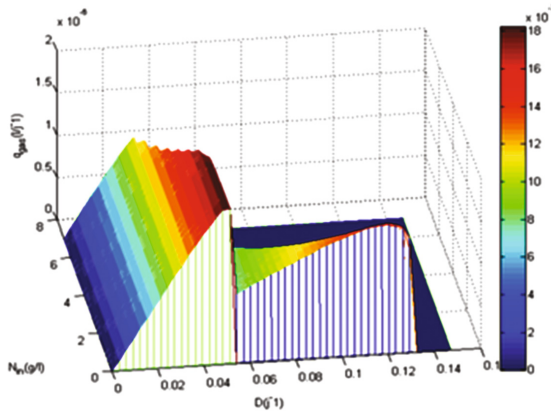
Fig. 4. Biogas yield of the MAD model (Color figure online)

In our study, we report the operating conditions preventing the ammonia stress while ensuring a maximal biogas production in the case of digestion of chlorella vulgaris microalgae at pH7. The analysis of the MAD qualitative properties with various operating conditions favors the understanding of its behavior to monitor such undesirable phenomena.

In the area Γ_3 of Fig. 2, none population is washed out (E_7^2 stable): this reveal that $0.001 - 0.05j^{-1}$ and $0 - 6.8g/l$ are the ideal ranges for D and N_{in}, respectively, to guarantee a stability of process, except when D and N_{in} belong to Γ_5 and Γ_6, in which case ammonia becomes inhibitory ($N_{in} = 3.44g/l$).

Figure 3 allows us to deduce FAN inhibition levels. It infers to the beginning of light green color with a numerical value 0.0317g FAN/l (2.340g TAN/l). This agrees with the commonly known TAN toxicity, ranging from 1.5 to 3g/l (Parkin and Owen 1986). Because of TAN and FAN concentration are strongly dependent on pH and temperature, the deduced values agree very well with the relationship proposed by (Hansen et al. 1998) as well as with the study by (Fernandes et al. 2012) suggesting that FAN must represent less than 1% of TAN under such conditions.

Even if these threshold does not cause the inhibition in stable area (Γ_3), they result in a low biogas production (Fig. 4). Beside, Fig. 4 shows that under this threshold, D must take high values (ideal about $0.051j^{-1}$) to guarantee a maximum production of biogas. In practice, by maintaining D at the ideal value without exceeding N_{in} inhibitory concentration, we can ensure process efficiency during *chlorella vulgaris* AD.

These results are useful when we operate the system at pH = 7. A small change of the value of this parameter involves a significant change on the OD, and thus the variation of the FAN threshold inhibition level and the biogas yield.

4   Conclusions

This paper presents the influence of ammonia input concentration on the fermentation of Protein-rich substrates using a Microalgae Anaerobic Digestion (MAD) model. Based on the mathematical analysis of MAD, we will be able to predict the process behavior in the presence of an increased source of nitrogen. The numerical simulations provide the FAN critical concentration to be avoided as well as the ideal values of operating parameters for the optimum biogas production. These results will be very helpful in the case of digestion of chlorella vulgaris microalgae mainly for process monitoring.

References

Becker EW (2007) Micro-algae as a source of protein. Biotechnol Adv 25:207–210

Kafle GK, Bhattarai S, Kim SH, Chen L (2014) Effect of feed to microbe ratios on anaerobic digestion of Chinese cabbage waste under mesophilic and thermophilic conditions: Biogas potential and kinetic study. J Environ Manage 133:293–301

Ek A, Hallin S, Vallin L, Schnurer A, Karlsson M (2011) Slaughterhouse waste co-digestion-experiences from 15 years of full-scale operation. In: World renewable energy congress 2011, Sweden, 8–13 May 2011. Linköping, Sweden

Kovács E, Wirth R, Maróti G, Bagi Z, Rákhely G, Kovács KL (2013) Biogas production from protein-rich biomass: fed-batch anaerobic fermentation of casein and of pig blood and, associated changes in microbial community composition. PLoS ONE. 8(10):e77265

Fernandes TV, Keesman KJ, Zeeman G, van Lier JB (2012) Effect of ammonia on the anaerobic hydrolysis of cellulose and tributyrin. Biomass Bioenerg 47:316–323

Hansen HK, Angelidaki I, Ahring BK (1998) Anaerobic digestion of swine manure: inhibition by ammonia. Water Res 32(1):5–12

Hejnfelt A, Angelidaki I (2009) Biomass bioenergy, anaerobic digestion of slaughterhouse by-products. Biomass Bioenerg 33(8):1046–1054

Mairet F, Bernard O, Cameron E, Ras M, Lardon L, Steyer JP, Chachuat B (2012) Three-reaction model for the anaerobic digestion of microalgae. Biotechnol Bioeng 109:415–425

Parkin GF, Owen WF (1986) Fundamentals of anaerobic digestion of wastewater sludges. J Environ Eng (United States) 112(8):867–920

Rajagopal R, Massé DI, Singh G (2013) A critical review on inhibition of anaerobic digestion process by excess ammonia. Bioresour Technol 143(632):641

Yenigün O, Demirel B (2013) Ammonia inhibition in anaerobic digestion: a review. Process Biochem 48(5–6):901–911

Dynamic Thermodynamic Simulation of ADM1 Validates the Hydrogen Inhibition Approach and Suggests an Unfeasible Butyrate Degradation Pathway

M. Patón and J. Rodríguez[✉]

Department of Chemical and Environmental Engineering, Masdar Institute
of Science and Technology, P.O. Box 54224, Abu Dhabi, United Arab Emirates
jrodriguez@masdar.ac.ae

Abstract. In this work, a dynamic calculation of the thermodynamics of the considered reactions in ADM1 highlighted the role of hydrogen on VFA degradation. In ADM1, a hydrogen inhibition factor based on its concentration is used to represent the same effect. Our comparison of a thermodynamic-based against the simpler concentration-based inhibition factor during dynamic simulations validates the ADM1 approach. Our results also show the need to correct the VFAs Gibbs energies with temperature if a thermodynamic-based inhibition is to be used. The thermodynamics of butyrate degradation under both experimental and simulated conditions suggest the unfeasibility of the reaction and the need for a revision of the current pathway biochemistry.

Keywords: Thermodynamic inhibition · Temperature correction · Bioenergetics

1 Introduction

The most widely used model for anaerobic digestion is the ADM1 (Batstone et al. 2002). In the model, the maximum uptake rate (q_{max}) is limited by different factors: Monod and inhibition functions for pH, free ammonia and/or hydrogen.

The so-called hydrogen inhibition factor was incorporated in ADM1 to capture the impact of dissolved hydrogen concentration on the energetics of volatile fatty acids (VFA) degradation reactions. An empirical function was used for simplicity (Batstone et al. 2002).

The above approach had however its limitations including the fact that it allows for reactions to run even when they are not energetically favourable (Kleerebezem and van Loosdrecht 2006). It also increased the already significant number of parameters in the model with questionable mechanistic interpretation (Rodríguez et al. 2006).

The use of the available free energy can explain the same inhibition as shown in literature (Hoh and Cord-Ruwisch 1996; Kleerebezem and Stams 2000). In this work, an alternative to the hydrogen inhibition function used in ADM1 is presented. The approach consists of an inhibition function based on the free energy available for each reaction.

2   Materials and Methods

ADM1 was simulated using an Excel-MATLAB/Simulink framework (Rodríguez et al. 2009). States variables are defined in molar concentrations for more accuracy (Kleerebezem and van Loosdrecht 2006) and to facilitate pH and thermodynamic calculations. All the parameters used for the ADM1 simulations were obtained from BSM2 (Rosen and Jeppsson 2006).

Due to the stiff nature of the ADM1 the steady state assumption for dissolved hydrogen is used and solved algebraically as described by Rosen et al. (2006).

The activity coefficients of all chemical species were also considered for increased accuracy and energetics calculation following the approach described in González-Cabaleiro (2015).

Gibbs free energy for each reaction (ΔG_R) in ADM1 was calculated as:

$$\mu_i = \Delta G_i^0 + R_{th} \cdot T \cdot \ln a_i \tag{1}$$

$$\Delta G_R = \sum_{i=1}^{N} \upsilon_i \cdot \mu_i \tag{2}$$

where μ_i is the chemical potential of each individual species, ΔG_i^0 is the Gibbs energy formation (in kJ/mol) for each of the components in the reaction, R_{th} is the universal gas law (bar L/mol K), T is temperature (in K) a_i is the activity for the species (for solids is 1) involved in the reaction and υ_i the stoichiometric coefficient of the component i.

In order to restrict the reaction rate to the thermodynamically feasible range, each kinetic rate is multiplied by a factor based on the free energy available. In this work, the empirical function proposed in (Kleerebezem and Stams 2000; Kleerebezem and van Loosdrecht 2006) was used:

$$if\ \Delta G_r < 0, \quad I_{th} = 1 - \frac{\Delta G_R}{R_{th} \cdot T}, \quad else\ I_{th} = 0 \tag{3}$$

On the other hand, inhibition for VFA reactions in ADM1 is modelled as:

$$I_{h2,i} = \frac{K_{I,h2,i}}{K_{I,h2,i} + S_{h2}} \tag{4}$$

where $K_{i,h2,i}$ is the inhibition parameter (in mol/L) for species i.

An example of a reaction between the two approaches is shown in Table 1:

Table 1. Resulting kinetic using hydrogen inhibition (ADM1) and a thermodynamic-based inhibition (this work)

Hydrogen-based inhibition	Thermodynamic-based inhibition
$q_{Spro} = q_{\max,pro} \cdot \frac{S_{pro}}{K_{S,pro} + S_{pro}} \cdot I_{pH} \cdot I_{IN} \cdot I_{h2,pro}$	$q_{Spro} = q_{\max,pro} \cdot \frac{S_{pro}}{K_{S,pro} + S_{pro}} \cdot I_{pH} \cdot I_{IN} \cdot I_{th,rspro}$

The difference between inhibition functions is shown in Fig. 1:
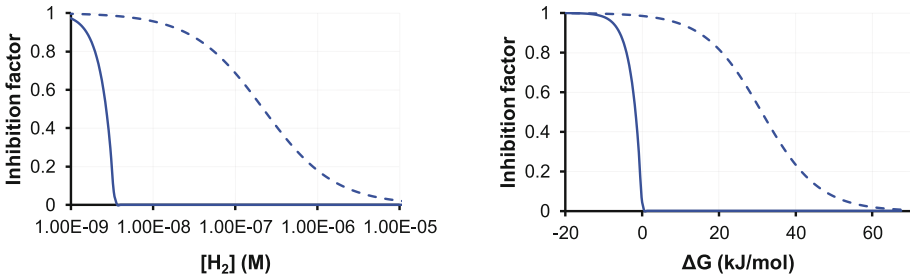
Fig. 1. Thermodynamic-based (solid line) and concentration-based (dashed lines) inhibition factors for propionate degradation for hydrogen concentration (left) and Gibbs free energy (right)

The advantage of using a thermodynamics-based inhibition approach such as the one described in Table 1 is that no extra parameter calibration is required. It also allows for a mechanistic interpretation of the results and additional accuracy as the model only allows for reactions that are energetically favourable to run.

To evaluate the proposed thermodynamic-based inhibition function against the original ADM1, a highly dynamic AD scenario was selected in which ADM1 was applied (Zaher et al. 2004). The simulated reactor consists of a 2 L lab-scale CSTR that was fed with wastewater from an alcoholic distillery plant.

3   Results and Discussion

Energetics of ADM1: The energetics for all ADM1 reactions are shown dynamically in Fig. 2. Sugars, aminoacids and acetate degradation are reactions that run far from equilibrium (with values below than −250, −80 and −20 kJ/mol respectively) and therefore are unlikely to be ever limited thermodynamically. However, the rest of the reactions show values closer to equilibrium and even become unfavourable at some stages during the simulation (e.g. at t = 3000 h). Those reactions that run close to equilibrium have hydrogen either as a substrate (methanogenesis) or as a product (LCFA and VFA degradation). Through this energetic study of the model, the key role of the hydrogen concentration on the thermodynamic limitation of the reactions is clearly highlighted.

Comparison of inhibition models. The key simulation results for the proposed case study are presented in Fig. 3 comparatively: Two thermodynamic inhibition variations were evaluated: *ADM1_Ith0,* which does not correct by temperature Gibbs formation of VFAs (valerate, butyrate and propionate) and *ADM1_Ith,* which takes temperature corrections into account. Those two were compared against the standard ADM1 (with the hydrogen inhibition function).
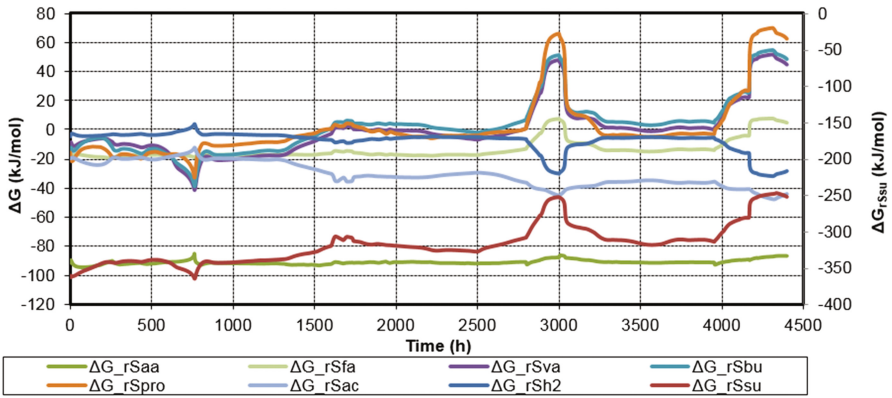
Fig. 2. Energetics of the uptake reactions considered in ADM1
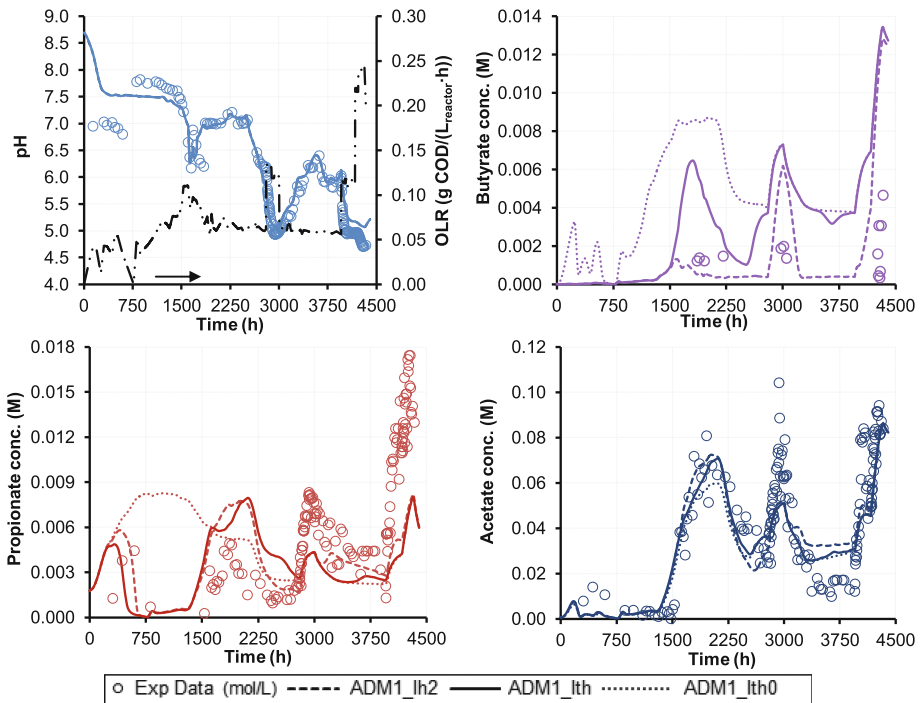
Fig. 3. Results of the simulation for VFA and pH for ADM1 with hydrogen and with thermodynamic inhibition

No major differences were observed in gas flow (data not shown) or pH simulation between the three models. However, differences appeared to be more significant for VFA concentrations. The simulation that considered a thermodynamic inhibition without correction for temperature did overpredict the concentration of both butyrate

and propionate in the reactor. The reason was that butyrate and propionate degradation reactions are unfavourable if no temperature correction is considered. When temperature correction was incorporated, the model was indeed able to capture in a similar way to ADM1 the concentration of propionate, although still overestimating to a lower degree the butyrate concentrations. The need for those accurate calculations with temperature effect makes sense thermodynamically considering the substrate to products molarities of the reactions involved. It therefore becomes clear that if thermodynamic calculations are to be used to inhibit reactions, the effect of temperature needs to be included.

An additional observation is that ADM1 predicted the degradation of butyrate at thermodynamic values that render the reaction as not feasible (at t = 1700–2500 and 3100–4000 h). Both looking at the thermodynamics of the simulated and the experimental data, it appears that butyrate degradation is not feasible under the current pathway used. These observations suggest that a reconsideration and evaluation of the butyrate degradation pathway may be necessary.

4   Conclusions

The main conclusions of this work are:

– Hydrogen is confirmed as a key inhibitor-like component in VFA degradation due to thermodynamics.
– The hydrogen inhibition factor approach used in ADM1 is validated as it reproduces the actual thermodynamic inhibition quite accurately at typical AD process concentrations in a simple manner that does not require dynamic computation of thermodynamics.

  Future work may include:

– Revision of the current biochemistry of the butyrate degradation pathways as they appear thermodynamically unfeasible at reactor concentrations.

References

Batstone DJ, Keller J, Angelidaki I, Kalyuzhnyi SV, Pavlostathis SG, Rozzi A, Sanders WTM, Siegrist H, Vavilin VA (2002) The IWA anaerobic digestion model no 1 (ADM1). Water Sci Technol 45(10):65–73
González-Cabaleiro R (2015) Bioenergetics-based modelling of microbial ecosystems for biotechnological applications. PhD, Grupo de Ingeniería Ambiental y Bioprocesos, Universidade de Santiago de Compostela

Hoh CY, Cord-Ruwisch R (1996) A practical kinetic model that considers endproduct inhibition in anaerobic digestion processes by including the equilibrium constant. Biotechnol Bioeng 51 (5):597–604

Kleerebezem R, Stams AJ (2000) Kinetics of syntrophic cultures: a theoretical treatise on butyrate fermentation. Biotechnol Bioeng 67(5):529–543

Kleerebezem R, van Loosdrecht MC (2006) Critical analysis of some concepts proposed in ADM1. Water Sci Technol 54(4):51–57

Rodríguez J, Lema JM, van Loosdrecht MCM, Kleerebezem R (2006) Variable stoichiometry with thermodynamic control in ADM1. Water Sci Technol 54(4):101–110

Rodríguez J, Premier GC, Dinsdale R, Guwy AJ (2009) An implementation framework for wastewater treatment models requiring a minimum programming expertise. Water Sci Technol 59(2):367–380

Rosen C, Jeppsson U (2006) Aspects on ADM1 implementation within the BSM2 framework. Department of Industrial Electrical Engineering and Automation, Lund University, Lund, Sweden, pp 1–35

Rosen C, Vrecko D, Gernaey KV, Pons MN, Jeppsson U (2006) Implementing ADM1 for plant-wide benchmark simulations in Matlab/Simulink. Water Sci Technol 54(4):11–19

Zaher U, Rodríguez J, Franco A, Vanrolleghem P (2004) Application of the IWA ADM1 model to simulate anaerobic digester dynamics using a concise set of practical measurements. In: Selected proceedings of the IWA international conference. Water and Environment Management Series (WEMS), Kuala Lumpur, Malaysia, pp 249–58

Energy Recovery from Immobilised Cells of *Scenedesmus obliquus* after Wastewater Treatment

M. Gomez San Juan[1], F. Ometto[2], R. Whitton[1], M. Pidou[1,2],
B. Jefferson[1], and R. Villa[1(✉)]

[1] Cranfield University, CWSI, Cranfield, UK
[2] Scandinavian Biogas Fuels AB, Linköping, SE, Sweden

Abstract. Biomethane batch test of alginate beads and beads with algae at different stages of utilisation in the wastewater treatment plants showed that immobilised *S. obliquus* yield similar biogas and biomethane than freely suspended algae (between 60.51 ± 4.19 and 82.32 ± 2.17 mL g-1 VSadd) and that a pre-treatment stage was not necessary for the digestion process.

Keywords: Anaerobic digestion · Biogas · Wastewater treatment

1 Introduction

Microalgae have shown to be able to remediate nutrients effectively from secondary wastewater, their use in WWT processes and biogas production by anaerobic digestion (AD) was first reported by Golueke et al. (1957) and Oswald and Golueke (1960). At the time, the authors' main conclusion was that, although the algae removed nutrients to satisfactory levels, the overall process was not economically and energetically viable, and regrettably this is still the case today (Ometto 2014b). Process intensification can be achieved using cells entrapped into a resin or gelatinous media, such as alginate or synthetic polymers (3.3 g·L-1 DW). Ruiz-Marín et al. (2010, 2011) and Whitton et al. (2016) all demonstrated good nutrient removals with immobilised algae. However, even when immobilised, the inclusion of microalgae in the WWT process for nutrients absorption could only be justified if biomass is processed to recover energy.

Of the currently available biomass-to-energy technologies, gasification, thermochemical liquefaction, direct combustion and anaerobic digestion (AD), AD provides the most feasible process for large scale application which, depending on the chemical composition, has the potential to yield up to 800 mlCH$_4$ gVS^{-1} (Heaven et al. 2011). However, microalgae species have the ability to resist microbial degradation, their structure and chemical composition identified the cell wall as the main limiting factor to microbial degradation (Atkinson et al. 1972; Burczyk et al. 1999). High energy (thermal

and ultrasound) and low energy (mechanical and biological) pre-treatments can be used to: (1) degrade the cell wall, (2) release AOM and hence (3) enhance methane production (Alzate et al. 2012; González-Fernández et al. 2012; Cho et al. 2013).

Batch anaerobic digestion experiments were used to assess the effect of thermal and biological pre-treatment on the methane production of immobilised *Scenedesmus obliquus*, after nutrients removal process.

2 Materials and Methods

2.1 Algae Culture and Immobilisation

The *S. obliquus* (276/42) culture was obtained from the Culture Collection for Algae and Protozoa (CCAP), (Oban, UK). Microalgae was cultured in batch in 100 L tanks containing 50 L Jaworski media as reported in Ometto et al. (2014b,c). Immobilisation conditions were reported in Whitton et al. (2016).

2.2 Batch Anaerobic Digesters

Five different substrates were analysed in this work. Four types of algal beads; (1) Blank Beads with no algal biomass, with only the alginate matrix (BB), (2) Clean Algal Beads (CA), fresh beads containing microalgae cells imbedded in the alginate matrix that have not been used for wastewater remediation, (3) Beads after 6 days of wastewater treatment (6-d UA), (4) Beads at 10 days usage (10-d UA), and (5) the residual algal sludge at the end of the columns experiment (AS). All substrates were characterised in terms of TS and VS before and after anaerobic digestion. The four types of beads were pre-treated and the degradation of their structure was analysed. The biomethane test was carried out on both untreated and enzymatically treated substrates. The batch tests were done as reported (Ometto et al. 2014b).

2.3 Pre-treatments (Thermal and Biological)

Thermal pre-treatment of the beads biomass was achieved using an autoclave at 121°C and 1.06 bar for 30 min. The solid content (VS and TS) and the sCOD were measured

Table 1. List of enzyme used for the biomass pre-treatment

Enzyme	Commercial name	Composition	Conditions tested
E1	DepolTM 40L	Cellulase 1,200 U g^{-1} + Endogalactouronase 800 U g^{-1}	25, 50, 150, 250, and 350 U mL^{-1}
E2	LipomodTM 957	Esterase 3,600 U g^{-1} + Protease 90 U g^{-1}	150 and 250 U mL^{-1} (7.5 U kg^{-1}TS)
E3	LipomodTM 166P	Esterase 5,220 U g^{-1}	150 and 250 U mL^{-1} (7.5 U kg^{-1}TS)
E4	Lipase LT	Lipase 100,000 U g^{-1}	150 and 250 U mL^{-1} 7.5 U kg^{-1}TS
E5	Accelerase 1500	Endoglucanase 2200 U g^{-1} + β-Glucosidase 450 U g^{-1}	150 and 250 U mL^{-1} (7.5 U kg^{-1}TS)

in duplicate before and after treatment (Ometto 2014c). Only beads pre-treated with E1 and E2 at 150 U mL^{-1} (equivalent to 7.5 U kg^{-1} TS) were used for the biomethane test.

The enzymes used in the study experiments are summarised in Table 1.

3   Results and Discussion

The calculation of the biogas yield for the untreated beads were 29.73 $\pm$ 2.17 mL for DS; 160.12 $\pm$ 6.66 mL for Blank Beads (BB); 124.27 $\pm$ 15.56 mL for (Clean algae beads) CA; 179.54 $\pm$ 12.43 mL for 6-d (Untreated Algae Beads) UA; 254.17 $\pm$ 6.71 mL for 10-d UA; 175.51 $\pm$ 32 mL for AS; and 217.82 $\pm$ 24 mL for control with cellulose. Ometto et al. (2014c) obtained a biogas yield of 265.28 $\pm$ 10 mL g-1 VSadd, which is similar to the 10-d UA value.. 10-d UA beads demonstrated a similar behaviour to suspended *S. obliquus* microalgae for biogas and biomethane production. The 10-d beads were weak and misshapen due to degradation of the alginate matrix hence exposing the immobilised cells, this is likely to be the reason for the similarity to suspended calls. The lower performance of 6-d UA, and the even lower of CA, was likely due to the lower biomass concentration as a result of the reduced contact time with wastewater and reduced growth (105 microalgae cells in CA beads, 5.3 $\times$ 105 cells in 6-d UA, and 7 $\times$ 105 cells in 10-d UA). Results are reported in Fig. 1.

Biogas yield of enzymatically pre-treated beads, resulted in enzymes and dosage: 1316.3   121.60 $\pm$ 32.18 mL   (for   BB+E1);   125.27 $\pm$ 24.01 mL   (for   CA+E1); 142.41 $\pm$ 3.44 mL (for 6-d UA+E1); 271.16 $\pm$ 3.04 mL (for 6-d UA+E2); 20 and 135.83 $\pm$ 9.72 mL (for 10-d UA+E1). The cumulative biogas values are lower than those reported by Ometto (2014c) for suspended *S. obliquus* with the same $\pm$ 224 mL g^{-1}
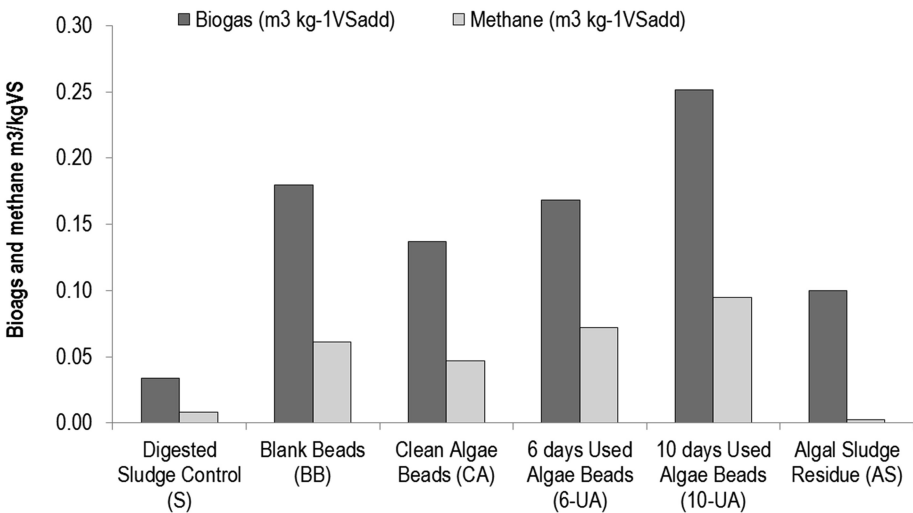
Fig. 1. Biogas and biomethane production in batch tests of untreated exhausted algae beads after nutrient removal

VSadd with E1 at 150 U mL^{-1} and 986.34 $\pm$ 201 mL g^{-1} VSadd with E2 at 150 U mL^{-1}. About the CH$_4$ production, excepting BB, all substrates yielded a very similar amount of biomethane after 33 days. Results are reported in Fig. 2.

ESEM pictures (Fig. 3) of the untreated and treated beads showed that higher biodegradability was observed after enzymatic pre-treatment in terms of alginate structure damage. The granules visible on the outside of the treated beads are likely to be non-dissolved enzymes.
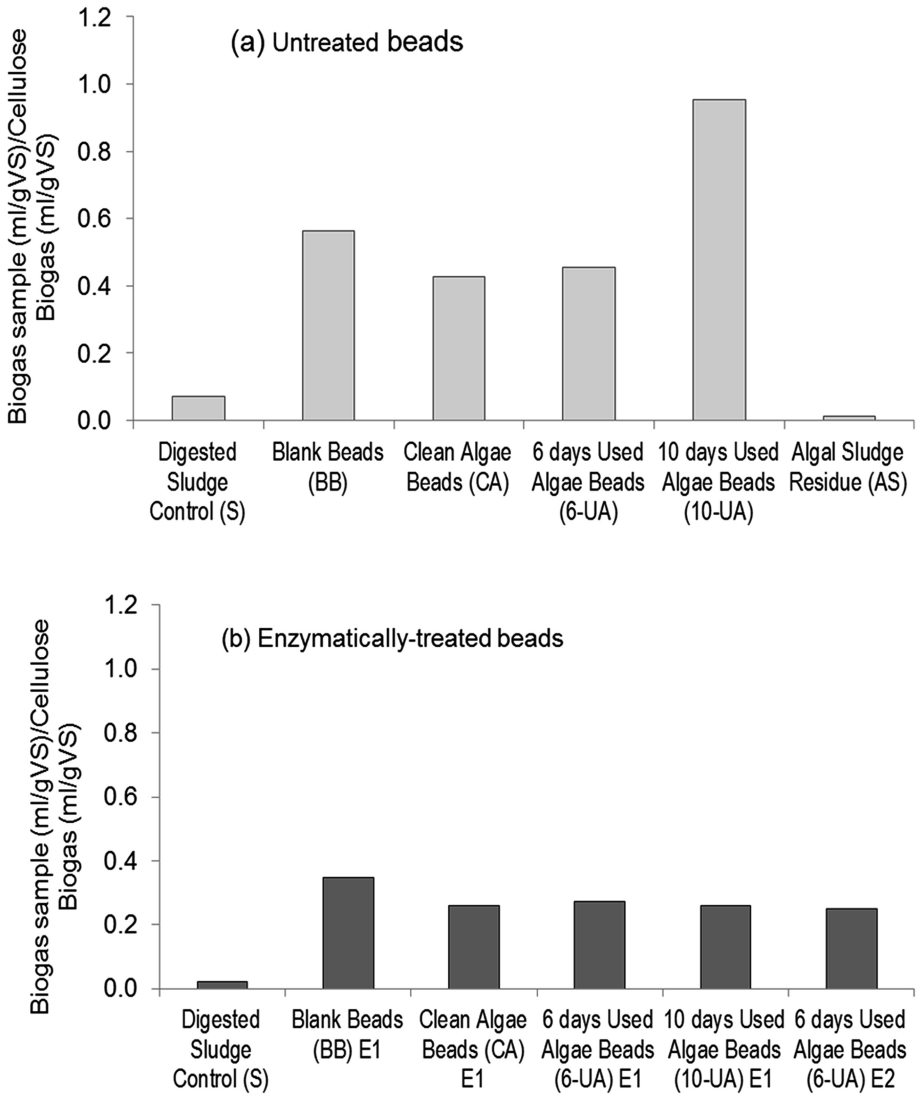
Fig. 2. Comparison of biogas production of treated (enzymatically) and untreated algae beads in batch tests. Biogas values have been normalised using the value obtained for cellulose (reference material) to allow comparison amongst different batches

BB untreated

BB enzymatically pre-treated

CA untreated

CA enzymatically pre-treated

6-d UA untreate

6-d UA enzymatically pre-treated.

10-d UA untreated

10-d UA enzymatically pre-treated
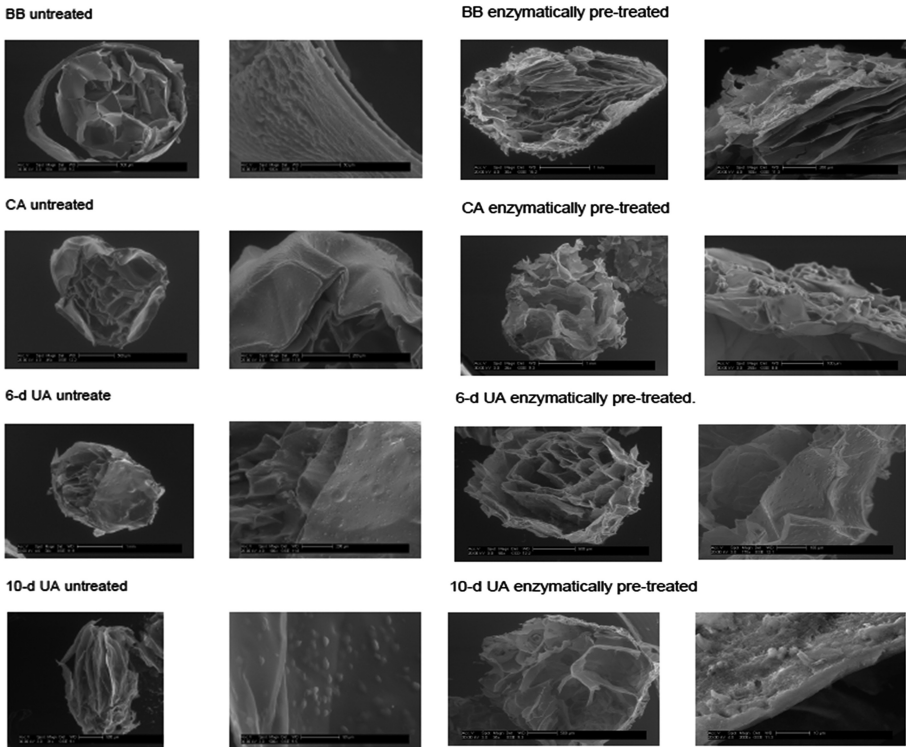
Fig. 3. ESEM pictures of treated (enzymatically) and untreated algae beads

4   Conclusions

- Biogas can be produced from microalgae (*S. obliquus*) after wastewater treatment process.
- Immobilised *S. obliquus* used for wastewater treatment can produce similar biogas and biomethane yields compared to freely suspended *S.obliquus*.
- Specific biogas and methane values of microalgae beads gave industry-acceptable values (up to 80%).
- Pre-treatment of the algae beads to increase biogas production did not give positive results. This indicates an inhibition during AD, probably caused by the released of calcium alginate (bead matrix).

References

Alzate ME, Muñoz R, Rogalla F, Fdz-Polanco F, Perez-Elvira SI (2012) Biochemical methane potential of microalgae: influence of substrate to inoculum ratio, biomass concentration and pretreatment. Bioresour Technol 123:488–494

Atkinson AWJ, Gunning BES, John PCL (1972) Sporopollenin in the cell wall of Chlorella and other algae: ultrastructure, chemistry, and incorporation of 14C-acetate, studied in synchronous cultures. Planta 107:1–32

Burczyk J, Śmietana B, Termińska-Pabis K, Zych M, Kowaloski P (1999) Comparison of nitrogen content amino acid composition and glucosamine content of cell walls of various chlorococcales algae. Phytochemistry 51:491–497

Cho S, Park S, Seon J, Yu J, Lee T (2013) Evaluation of thermal, ultrasonic and alkali pretreatments on mixed-microalgal biomass to enhance anaerobic methane production. Bioresour Technol 143:330–336

Golueke CG, Oswald WJ, Gotaas HB (1957) Anaerobic digestion of algae. Appl Biotechnol 5:47–55

González-Fernández C, Sialve B, Bernet N, Steyer JP (2012) Thermal pretreatment to improve methane production of Scenedesmus biomass. Biomass Bioenergy 40:105–111

Heaven S, Milledge J, Zhang Y (2011) Comments on Anaerobic digestion of microalgae as a necessary step to make microalgal biodiesel sustainable. Biotechnol Adv 29(1):164–167

Ometto F, Whitton R, Coulon F, Jefferson B, Villa R (2014b) Improving the Energy Balance of an Integrated Microalgal Wastewater Treatment Process. Waste Biomass Valor 5:245–253

Ometto F (2014c) Microalgae to energy: biomass recovery and pre-treatments optimization for biogas production integrated with wastewater nutrients removal. Ph.D. thesis. Cranfield University

Ometto F, Quiroga G, Pseničkǎ P, Whitton R, Jefferson B, Villa R (2014d) Impacts of microalgae pre-treatments for improved anaerobic digestion: thermal treatment, thermal hydrolysis, ultrasound and enzymatic hydrolysis. Wat Res 65:350–361

Oswald WJ, Golueke CG (1960) Biological transformation of solar energy. Adv Appl Microbiol 2:223–262

Ruiz-Marin A, Mendoza-Espinosa LG, Stephenson T (2010) Growth and nutrient removal in free and immobilized green algae in batch and semicontinuous cultures treating real wastewater. Bioresour Technol 101:58–64

Ruiz-Marín A, Mendoza-Espinosa LG, Sánchez-Saavedra M (2011) Photosynthetic characteristics and growth of alginate-immobilized Scenedesmus obliquus. Agrociencia 45:303–313

Whitton R, Le Mevel A, Pidou M, Ometto F, Villa R, Jefferson B (2016) Influence of microalgal N and P composition on wastewater nutrient remediation. Wat Res 91:371–378

Fault Diagnosis of Anaerobic Digester System Using Nonlinear State Estimator: Application to India's Largest Dairy Unit

Mallavarappu Deepika Rani[1]([✉]), Laya Das[2], and Babji Srinivasan[1]

[1] Department of Chemical Engineering,
Indian Institute of Technology Gandhinagar, Gandhinagar, India
[2] Department of Electrical Engineering,
Indian Institute of Technology Gandhinagar, Gandhinagar, India

Abstract. The complex biochemical processes along with uncertain load disturbances in anaerobic digesters (AD) lead to frequent upsets and poor performance of the overall system. Several techniques have been proposed in the literature to address fault detection and isolation in the anaerobic digester. However, these methods do not provide information about the internal states of the system and use expert and heuristics for fault isolation. In this work, we first developed a first principle based model of the AD unit at one of India's largest dairy and validated using experimental results. Subsequently, we used this model to demonstrate the applicability of nonlinear state estimation approaches for fault diagnosis.

Keywords: Anaerobic digestion · State estimation · Fault diagnosis

1 Introduction

Anaerobic digester employs multiple bacterial species to break biodegradable material in the feedstock under anaerobic conditions. Due to highly nonlinear, complicated and interacting nature, AD unit is prone to faults that can lead to instabilities and upsets in the digester resulting in deterioration of the quality of biogas and other effluents. In order to maintain and control the operation of the unit, it is necessary to understand the different processes involved in the digestion and continuously monitor important internal variables of these processes. However, typical measurements from the AD unit such as pH, alkalinity and chemical oxygen demand (COD) do not contain sufficient information regarding the internal variables of the system, thereby hindering reliable fault diagnosis of the unit.

State estimation is a technique that allows estimating the internal state variables of a system from knowledge of the process and available measurements. State estimation is used for soft sensing, wherein information is derived from actual sensor measurements along with the process model and provides "sensed" values of internal state variables. It serves as an on line health monitoring tool (Spindler and Vanrolleghem 2015) and is closely coupled with model based control strategies, which has been proposed for waste water treatment systems (Bernard et al. 2001, Alcaraz et al. 2002, Busch et al.

2013, Rodriguez et al. 2015, Haugen et al. 2014). The Kalman filter was proposed in 1960 as a recursive state estimator for linear systems, which was proved to be the best optimal filter for linear systems. The idea of recursive state estimation technique was then extended to non-linear systems resulting in the extended Kalman filter. Though suboptimal, this is the most widely used state estimator for nonlinear systesm. Apart from estimation approaches, Fuzzy logic based approaches (Gaida et al. 2012) have also been used for monitoring and diagnosis of AD. However, most of these existing works employ a linear or a highly simplified non-linear model for estimation (including as few as four state variables), limiting their applicability in extracting information about internal state of the system, and affecting the reliability of results. The anaerobic digester model 1 (ADM1) (Batstone et al. 2002) which is a fairly detailed model has been used (Gaida et al. 2012). However, the technique relies entirely on pattern recognition based approaches with the reliability of the estimate highly dependent on the training datasets. One of the recent works attempt to evaluate two different state estimation techniques for its utility in activated sludge systems (Busch et al. 2013). This work concludes that for the activated sludge process, both the estimators provide fairly good results based on the mean squared error values between the true and estimated states. However, the work also points out clearly that a detailed comparison based on a common benchmark needs to be performed.

In this work, a model for the AD based on the Seigrist model has been developed and validated using experimental studies in one of India's largest dairy unit. Nonlinear state estimation is performed with the above model with 24 differential equations using Extended Kalman filter to estimate important internal variables of the system. Results highlight that the proposed method reveals information about internal states of the system, adding value to fault diagnosis of the AD units.

2   Materials and Methods

In this work, we use a model developed for the anaerobic digester units of Amul dairy plant. The ETP at Amul Dairy contains anaerobic digesters and activated sludge systems to treat the waste water (layout shown in Fig. 1). The measurements obtained from the plant for modeling include pH, total COD, filtered COD, total suspended solids (TSS) and total Kjeldalh Nitrogen (TKN). The model considered in this work is based on the original Siegrist model for anaerobic digester and contains 24 coupled nonlinear ordinary differential equations (Siegriest et al. 2002). The data is collected for a duration of six months (September–February) out of which initial two months data (seasonal effect is neglected) is used to tune the model parameters. The parameters of the model are estimated from data obtained from Amul dairy plant and the output of the developed model as shown in Fig. 2 matches closely (only average values are provided) with that of the plant.

The model developed for the anaerobic digester can be expressed as:

$$\dot{x}(t) = f(x(t), u(t)) + \omega(t)$$
$$y(t) = Cx(t) + v(t)$$
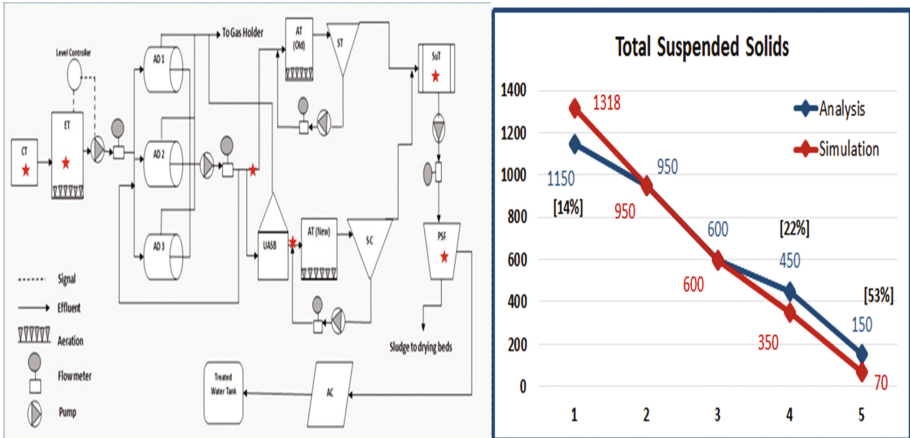
Fig. 1. Layout of the Effluent Treatment plant at Amul Diary (Left Pane), Comparison of simulated data with results of analysis of the samples collected from ETP (Right Pane)
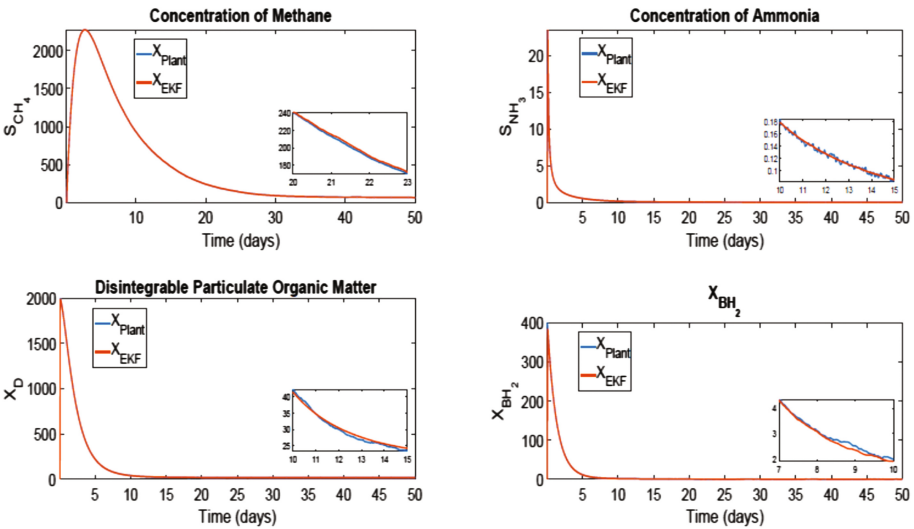
Fig. 2. True and Estimated states for AD with Extended Kalman Filter (only four representative state variables are shown)

where x(t) represent the state variables, y(t) represent the measured variables and u(t) represent the input to the process. The variables w(t) and v(t) are independently and identically distributed (IID) noise sequences with zero mean and covariances Q and R respectively. In the above equations, f(.) includes the set of 24 ordinary differential equations and C is the measurement matrix that relates the measurements at discrete instants of time (approximately 15 min) to the internal states of the system.

The Extended Kalman filter, a nonlinear estimation technique used in this work for state estimation, combines the states predicted using the model and the information provided by measurements to obtain state estimates at all sampling instants in a recursive predictor-corrector framework as follows:

Prediction:

$$\hat{x}_{k+1|k} = f(\hat{x}_{k|k}, u_k)$$
$$P_{k+1|k} = A_k P_{k|k} A_k^T + Q$$

where A_K is the Jacobian matrix that is used to propagate the state error covariance (P) using a first order approximation of its Taylor series expansion. The correction step proceeds as follows:

Correction:

$$K_{k+1} = P_{k+1|k} C^T (C P_{k+1|k} C^T + R)^{-1}$$
$$\hat{x}_{k+1|k+1} = \hat{x}_{k+1|k} + K_{k+1}(Y_k - C\hat{x}_{k+1|k})$$
$$P_{k+1|k+1} = P_{k+1|k} - K_{k+1} C P_{k+1|k}$$

3 Results and Discussion

Results from this approach indicate that the proposed approach can estimate the internal states of the system. For instance, as shown in Fig. 2, EKF output closely matches closely that of the model and is found to have good performance in estimating the internal states of the system with the available measurements. Further, it can help monitor the anaerobic system by identifying: (i) inhibition of the process due to excess ammonia, (ii) inhibition due to accumulation of long chain fatty acids and (iii) inhibition of the process due to poor growth of methanogens.

For instance, in one of the simulations, fault is introduced such that only methanogenesis part of the overall process is disturbed. As a result growth rate of methanogens is affected due to which methane and CO2 production decreased. As methanogens are disturbed their intake of VFA decreased, resulting in VFA accumulation, decrease of pH and low alkalinity. As shown in Fig. 3, the estimator output under normal conditions (with legend as original), this process behavior is accurately estimated by EKF. As shown in Fig. 3, the internal states of the process estimated during normal and faulty case are different from the above faults. Thus, the state estimation approach could be used to identify the faults in the AD units. As seen from Fig. 3, the estimator output differs significantly from that of the normal operating conditions, indicating an abnormal behaviour in the plant.
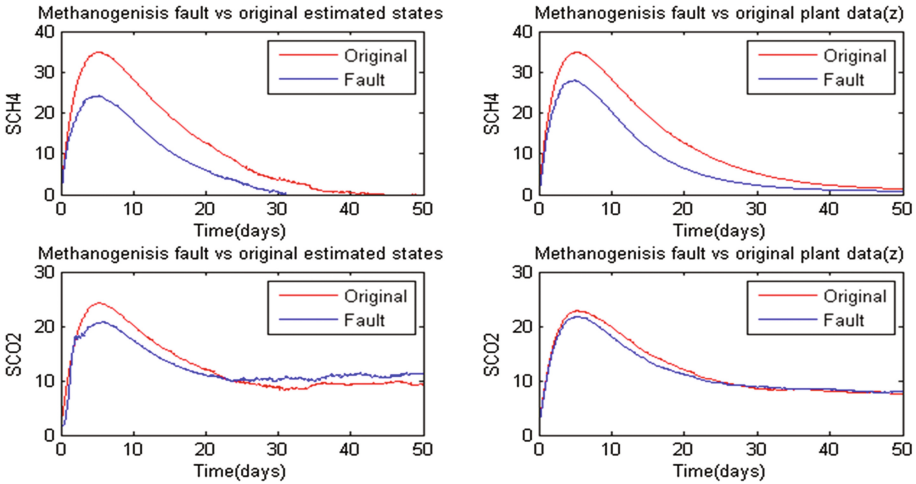
Fig. 3. Inhibition of methanogens was the fault introduced. Various states estimated during the non-faulty (original) case and faulty case are shown. Deviation of the estimated states under non-faulty and faulty conditions provide clues for identification of the root cause for the fault

4   Conclusions

An Extended Kalman Filter (EKF) is used to estimate the internal state of the anaerobic digester. It is also shown that the estimator could help identify the faults in the process. This approach is demonstrated using the first principles model of the AD unit at Amul Dairy. The model is validated using experiments at the dairy unit which is then used in EKF for state estimation and fault diagnosis. Results obtained from this work are promising and indicate that internal states of the system could be used in monitoring and control of the anaerobic digester.

Our future work is directed towards implementation of the proposed estimation work in the dairy plant. Also, it is important to understand the performance of various estimators when there is a mismatch between the developed model and the plant. We are currently focussing on development of algorithms (based on solution to full information problem, the ideal second order nonlinear state estimator) to quantify the performances of nonlinear state estimators.

References

Spindler A, Vanrolleghem P (2015) Continuous measurement quality control of wrrf operational data. In: Proceedings of the 88th annual water environment federation technical exhibition and conference, pp 26–30

Bernard O, Polit M, Hadj-Sadok Z, Pengov M, Dochain D, Estaben M, Labat P (2001) Advanced monitoring and control of anaerobic wastewater treatment plants: software sensors and controllers for an anaerobic digester. Water Sci Technol 43(7):175–182

Alcaraz-Gonalez V, Harmand J, Rapaport A, Steyer J, Gonzalez-Alvarez V, Pelayo-Ortiz C (2002) Software sensors for highly uncertain wwtps: a new approach based on interval observers. Water Res 36(10):2515–2524

Busch J, Elixmann D, Kuhl P, Gerkens C, Schloder JP, Bock HG, Marquardt W (2013) State estimation for large-scale wastewater treatment plants. Water Res 47(13):4774–4787

Haugen F, Bakke R, Lie B (2014) State estimation and model-based control of a pilot anaerobic digestion reactor. J Control Sci Eng 2014:19

Rodriguez A, Quiroz G, Femat R, Mendez-Acosta H, de Leon J (2015) An adaptive observer for operation monitoring of anaerobic digestion wastewater treatment. Chem Eng J 269:186–193

Gaida D, Wolf C, Meyer C, Stuhlsatz A, Lippel J, Back T, Bongards M, McLoone S (2012) State estimation for anaerobic digesters using the adm1. Water Sci Technol 66(5):1088–1095

Siegrist H, Vogt D, Garcia-Heras JL, Gujer W (2002) Mathematical model for meso-and thermophilic anaerobic sewage sludge digestion. Environ Sci Technol 36(5):1113–1123

Batstone DJ, Keller J, Angelidaki I, Kalyuzhnyi S, Pavlostathis S, Rozzi A, Sanders W, Siegrist H, Vavilin V (2002) The iwa anaerobic digestion model no 1 (adm1). Water Sci Technol 45(10):65–73

New Frontiers in Wastewater Treatment

Removal of Pharmaceuticals from WWTP Secondary Effluent with Biofilters

L. Sbardella[1,2(✉)], A. Fenu[2], J. Comas[1], I. Rodriguez Roda[1], and M. Weemaes[2]

[1] Catalan Institute for Water Research (ICRA),
C/Emili Grahit 101, 17003 Girona, Spain
[2] Aquafin NV, Dijkstraat 8, 2630 Aartselaar, Belgium

Abstract. In this study the performances of a biological activated carbon filter (BAC) followed by an ultrafiltration step have been evaluated with specific regard to pharmaceutical active compounds removal (PhACs) from secondary effluent of wastewater treatment plant. The long-term operation of this technology resulted in overall removal (>75%) of the studied compounds. Aiming at understanding the mechanisms ruling the removal of the investigated PhACs, together with the BAC pilot plant, a lab-scale column set-up was operated. The column set-up was composed by two biotic columns and by an abiotic one. This scheme allowed to highlight the capability of biofilters to remove via biodegradation compounds which are classified as recalcitrant to biological process. On the same time, the column characterized by the combined effect of adsorption and biological activity, showed removal percentages which were not obtained neither in the standard biofilter (sand) nor in the standard granular activated carbon (abiotic) filter. In conclusion, both the results from the pilot and the lab-scale, suggested biofiltration as a viable option to improve secondary effluent quality and to efficiently remove PhACS.

Keywords: Biofiltration · Pharmaceutical active compounds · Biological activated carbon · Ultrafiltration

1 Introduction

Wastewater treatment plants (WWTPs) and conventional activated sludge (CAS) processes are ineffective in removing emerging micropollutants which are then discharged into water bodies (Verlicchi et al. 2012). Although there is a lack of regulation in terms of discharging limits, the awareness and therefore the concern about the risks associated to these compounds has arisen. To date, five pharmaceutical active compounds (PhACs) have been included in the list of priority substances from the EU. The two most promising technologies proposed to remove these emerging contaminants from the effluent of WWTPs are oxidation via ozone and adsorption onto activated carbon (AC). Although the high removal efficiencies obtained with these two techniques, they exhibit drawbacks which have led the scientific community to investigate how to improve them. Among the proposed technologies, the use of biological activated carbon filter may overcome the limits of standard AC filtration.

Biofilters have been widely applied for the removal of organic matter in drinking water facilities Only recently biofiltration has shown also the potential to be an effective process for the control of many trace organic contaminants including PhACs (Zearley et al. 2012) in drinking water process, while few is known about the implementation of biofilters as a tertiary treatment for wastewater.

The aim of this study is (i) to assess the performances of BAC filter followed by an ultrafiltration (UF) step over one year period, (ii) to examine adsorption and biodegradation behaviour of PhACs mixture and (iii) to evaluate the role of the filtering material, by comparing sand and granular activated carbon (GAC), in terms of removal.

2   Material and Methods

A BAC pilot scale with an operating volume of 1.5 m^3 is continuously fed with 2 m^3/h of secondary effluent, thus resulting in an empty bed contact time (EBCT) of 45 min. The biofilter is followed by an ultrafiltration (UF) step. The concentrate of the UF is recirculated on top of the pilot ensuring oxic conditions throughout the biofilter. The performances of the BAC pilot + UF, as a suitable tertiary treatment, have been monitored along 1 year.

To enlighten the inner mechanism ruling the removal processes, three different lab-scale columns were operated in parallel to the pilot. Two columns were biotic (active biomass) and one was abiotic (inactive biomass due to sodium azide spiking). Sand was used as filtering material in one biotic column (C1), while granular activated carbon were used both in the biotic (C2) and abiotic columns (C3) (Fig. 1). The columns are operated with an EBCT of 45 min; same as the pilot plant. Aiming at analysing bulk parameters and PhACs concentrations, sampling events have been carried out for both the set-up every 2 weeks and every month respectively for bulk parameters and PhACs.
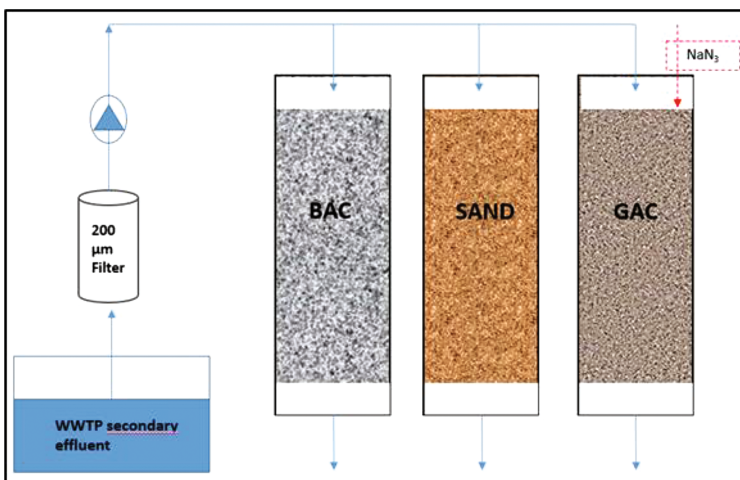
Fig. 1. Columns set-up layout, from lef to right C2, C1, C3

3   Results and Discussion

With regard to conventional parameters, both the pilot and the columns showed biological activity (Table 1) confirming significant active biomass kinetics in terms of N and COD removal. The COD removal in C3 may be attributed to adsorption onto GAC, as well as for the N removal since no NO3 formation has been detected in this column.

Table 1. Removal of conventional parameters and formation of nitrate (a).

	Sand	Biotic	Abiotic	Pilot
	(%)	(%)	(%)	(%)
NH4	85 ± 10	66 ± 13	20 ± 7	86 ± 6
NO3 (a)	11 ± 5	17 ± 10	(−)	47 ± 29
COD	19 ± 11	40 ± 5	13 ± 1	37 ± 6
DOC	26 ± 18	37 ± 6	20 ± 9	15 ± 8

PhACs removal on the BAC + UF pilot was characterized by different trends over the monitoring period. Although after the first months of operation the pilot achieved high removal efficiency (>75% for all the studied compounds), the increase of the treated bed volumes, resulted in a clear decrease of its performances in terms of PhACs removal (Fig. 2). For example carbamazepine was removed up to 86% after 2 months of operation, while this value dropped to 61% and 25% respectively after 8 and 11 months of operation. Only azithromycin removal displayed a different behaviour, showing indeed the same value (55%) after 2 and 11 months. Nevertheless, this result can be considered satisfying since in a previous study from Gobel et al. (2007) biofilters showed no removal of azithromycin. UF step (i) achieved a reduction of TOC, COD and SS, (ii) facilitate the inactivation of microbial regrowth and (iii) played a crucial role in the removal of some PhACs, although the size exclusion mechanism with UF has been reported as ineffective for PhACs removal.

Focusing on the lab-scale study for mechanisms identification, both the biologically inhibited and the biotic column filled with AC, reached a complete removal for metoprolol, atenolol, trimethoprim, propanolol (Table 2). For 9 compounds was possible to identify the improvement obtained due to the presence of active biomass in the BAC column when compared to the abiotic one (only GAC). Interesting to be pointed out is that this trend occurred for compounds which are classified as moderately $(1 < Kbio \ L/gVSS/d < 0.5)$, but also as hardly $(Kbio < 0.5 \ L/gVSS/d)$ biodegradable. Although for carbamazepine and venlafaxine this phenomena was moderate, since they are commonly well removed from GAC, in other cases such as irbesartan and diclofenac, the role of biomass was more relevant, almost doubling the removal efficiencies with respect to only GAC, for diclofenac and irbersartan. Since the 17 chosen compounds are known to be hardly removed during CAS, the enhanced performances obtained from C2 suggest that biofiltration can –partially- overcome the limits of
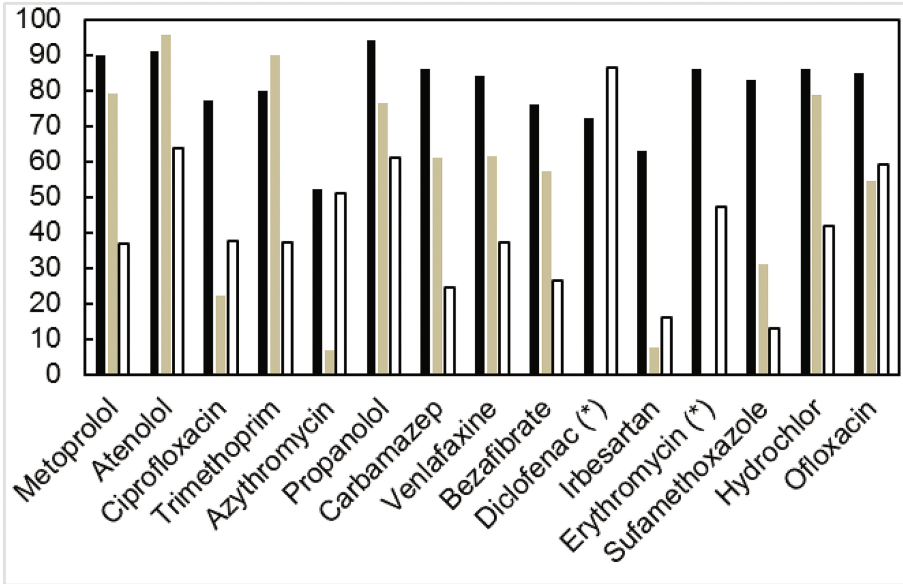
Fig. 2. Removal of PhACs from the pilot plant after 2 (■), 8 (▦) and 11 (□) months of operation. (*) Compounds not detected during the second sampling campaign.

Table 2. Comparison between the columns: SAND (C1), BAC (C2), ABIOTIC (C3). In the first two columns of this table, values into brackets refer to mean removal from C2 (first number in order of appearance) and C3.

BAC > ABIOTIC	BAC = ABIOTIC	RELEASED from BAC	RELEASED from SAND	REMOVED from SAND
Azytrhomycin (58; 56), Carbamazepine (94; 89), Venlafaxine (95; 92), Bezafibrate (37; 31), Irbesartan (43; 24), Diclofenac (75; 39), Sulfamethoxazole (54; 48), Ofloxacin (85; 53), Hydrochlorothiazide (96; 91)	Metropolol (100; 100), Atenolol (100; 100), Trimethoprim (100; 100), Propanolol (100; 100)	Iopromide, Salycilic acid, Erythromicin, Ciprofloxacin	Azytrhomycin, Carbamazepine, Venlafaxine, Bezafibrate, Irbesartan, Diclofenac, Sulfamethoxazole, Hydrochlorothiazide, Metropolol Trimethoprim, Propanolol, Iopromide, Salycilic acid, Erythromicin, Ciprofloxacin	Ofloxacin (36)

conventional biological processes. In all likelihood this is due to the high sludge retention time (SRT) inside the biofilters. Higher values of SRT have been shown to contribute to a wider microbial population and, with regard to organic micropollutants, this increase the metabolic and cometabolic pathways (Clara et al. 2005). From the comparison between C2 and C3 the biofilm contribution to PhACs removal can be quantified in about 13%.

Out of the 17 studied PhACs, only ofloxacin was partially removed from the sand column (36%). Low biomass degradation capacity could be explained by the low EBCT value of 45 min which may not be enough for proper biofilm development on sand granules. Besides the poor biomass activity toward the target compounds, the scarce removal may be attributed to the release of PhACs from the sand column as it is shown in Table 2. The origin of this release is most likely due to the solids which accumulate inside the column, despite the 200 µm pre-filtration of the influent. This aspect may result in underestimating the real influent load of PhACs (by measuring only the liquid phase) and thus underestimating the real removal capacity of the biofilter itself. This phenomenon can take place also in the column C2 and in the pilot plant.

4   Conclusion

Only biological activity from biofilm, albeit improves the performances of conventional GAC, is insufficient to ensure adequate elimination of the majority of the studied PhACs. However, the combination of biofilm activity with adsorption onto granular activated carbon, coupled with a subsequent polishing stage such as the UF, seemed to be a viable solution to improve the quality of WWTPs secondary effluent. In contrast with many other studies, we found a significant contribution of the UF step in the removal of some PhACs. Finally, the role played by the solids stocked in the reactors is not negligible and could affect the real quantification of the removal values. Therefore further studies including mass balances of PhACs in both liquid and solid phase, as well as calculation of releasing kinetics from suspended solids, need to be undertaken.

References

Clara M, Kreuzinger N, Strenn B, Gans O, Kroiss H (2005) The solids retention time—a suitable design parameter to evaluate the capacity of wastewater treatment plants to remove micropollutants. Water Res 39:97–106

Gobel A, McArdell CS, Joss A, Siegrist H, Giger W (2007) Fate of sulphonamides, macrolides, and trimethoprim in different wastewater treatment technologies. Sci Total Environ 372: 361–371

Verlicchi P, Al Aukidy M, Zambello E (2012) Occurence of pharmaceutical compounds in urban wastewater: removal mass load and environmental risk after secondary treatment – a review. Sci Total Environ 429:123–155

Zearley TL, Summers RS (2012) Removal of trace organic micropollutants by drinking water biological filters. Environ Sci Technol 46:9412–9419

Study of the Competition Between Complete Nitrification by a Single Organism and Ammonia- and Nitrite-Oxidizing Bacteria

R. González-Cabaleiro[1]([✉]), T.P. Curtis[2], and I.D. Ofiţeru[1]

[1] School of Chemical Engineering and Advanced Materials,
Newcastle University, Merz Court, Newcastle upon Tyne NE1 7RU, UK
{rebeca.gonzalez-cabaleiro,dana.ofiteru}@ncl.ac.uk
[2] School of Civil Engineering and Geosciences, Newcastle University,
Cassie Building, Newcastle upon Tyne NE1 7RU, UK
tom.curtis@ncl.ac.uk

Abstract. Complete nitrification by only one microorganism has been recently experimentally discovered. However, it was theoretically predicted almost 10 years ago by hypothesizing that complete nitrifiers are yield strategist that have a metabolic advantage to survive in biofilms. In this work, we study the competition for ammonia between complete nitrifiers and the canonical division of labour between ammonia and nitrite oxidizing bacteria in biofilms by using an individual based model. The model calculates the maximum growth yield using thermodynamics to evaluate the limitation in growth for each functional group in each position of the computational domain. Our results suggest that the trade-off between growth yield and growth rate in ammonia oxidizing bacteria and in complete nitrifiers is not significant as to observe a clear advantage for complete nitrifiers existence in biofilms.

Keywords: Individual-based model · Nitrification · Thermodynamics · Division of labour

1 Introduction

Since nitrification was discovered by Winogradsky in 1890, it was considered a product of an efficient division of labour between two microbial functional groups. Firstly, ammonia-oxidizing bacteria (AOB), that oxidizes ammonia to nitrite and secondly, nitrite-oxidizing bacteria, NOB, that converts the product of AOB to nitrate. Our understanding of the nitrification process changed when in 2015 was proven the existence of a single microorganism *Nitrospira commamox (Commamox)*, able to do the whole nitrification (Daims et al. 2015, van Kessel et al. 2015).

Using ammonia as a substrate, AOB catalyses its oxidation only until NO_2. This implies a reduction on the number of catabolic steps for AOB catabolism versus a microorganism doing the complete nitrification (ammonia to nitrate). Due to the longer metabolic pathway, *Commamox* is assumed to be slower substrate consumer than any AOB (Kreft 2004). On the other hand, the complete nitrification releases more energy

that can be used for anabolism and therefore, the theoretical growth yield of *Commamox* is higher.

One-step nitrification was theoretically predicted by Costa et al. (2006) before its experimental discovery. An analysis of its metabolism showed that a microorganism able to do the whole nitrification process is energetically feasible. The *Commamox* was assumed to be a yield strategist versus the AOB considered a rate strategist. Therefore, it was hypothesised its dominance in biofilms, in which is considered that yield strategists will always have a metabolic advantage (Kreft 2004).

In this work, the competition of the two strategists is analysed in detail using an individual-based model (IbM). We repeat the analysis of Kreft (2004) in which we are calculating the maximum growth yield for each functional group using thermodynamics. Our simulations predict the dominance of AOB against *Commamox* in biofilm, showing that an accurate evaluation of the yields is essential for concluding on the competition between yield and rate strategists.

2   Materials and Methods

A 2D IbM is used to analyse the competition for the NH_3 available in the system between *Commamox* and the AOB in syntrophic relation with NOB. The model assumes a pH 7 and speciation of all the chemical forms. It is considered that AOB and *Commamox* are mainly consuming ammonia in the NH_3 form (Suzuki et al. 1974) whereas NOB is assumed to consume NO_2^- and produce NO_3^-. The diffusion equation for substrates and products is solved in all the computational domain, considering the activity of the bacteria and the concentrations in the bulk of the liquid (Kreft et al. 2001). The model has been previously validated repeating the simulations presented by Kreft (2004) where the dominance of yield strategists in biofilms was proposed.

The growth of each bacteria is described calculating the amount of energy available for its metabolism in each position of the reactor (Eqs. (1–3)) (Gonzalez-Cabaleiro et al. 2015). The maximum growth yield is calculated using the Energy Dissipation Method $\left(Y_{XS}^{max}\right)$ (Kleerebezem and van Loosdrecht 2010). An average maintenance requirement of 4.5 kJ/C-mol·h (Tijhuis et al. 1993) is also assumed. Therefore the energy harvested is calculated knowing the kinetics of substrate uptake of each functional group according to Kreft et al. (2001). Then, growth is considered only if the cell is harvesting more energy than the necessary to maintain (Eq. (1)). Otherwise, bacteria will maintain (Eq. (2)) or decay linearly with the lack of energy with a constant $k_d = 0.01$ h^{-1} (Eq. (3)).

$$\mu = Y_{XS}^{max} \cdot \left(q_S^{met} - m_S^{req}\right) \quad if \quad q_s > m_s \tag{1}$$

$$\mu = 0 \quad if \quad q_s = m_s \tag{2}$$

$$\mu = -k_d \cdot \frac{m_S^{req} - q_S^{cat}}{m_S^{req}} \quad if \quad q_s < m_s \tag{3}$$

The growth parameters for AOB and NOB are the same as presented in Kreft et al. (2001). For the *Commamox* group the kinetic parameters are assumed equal to the AOB but the q^{max} is reduced proportionally to the number of the extra electrons that are released from the NH_3 to reduce the O_2 to H_2O ($q_s^{max}{}_{Comm} = q_s^{max}{}_{AOB} \cdot 6/8$), following the hypothesis presented by Heijnen and Kleerebezem (2010) (Gonzalez-Cabaleiro et al. 2015).

3 Results and Discussion

Considering that *Commamox* is a yield strategist competing for ammonia against AOB, it has been hypothesised that it could be isolated from biofilms where substrate transport by diffusion limits the process (Kreft 2004, Costa et al. 2006). This work studies three systems that have constant concentrations in the liquid bulk (Table 1). Transfer to the gas phase is not considered.

The results show that *Commmamox* do not outcompete AOB bacteria in most of the conditions, being the division of labour, the dominant strategy in all the three cases. The energy difference between AOB and *Commamox* does not imply an important advantage for *Commamox* to outcompete AOB in these simulations. However, the

Table 1. Concentrations in the liquid bulk for the three cases studied

	Case 1	Case 2	Case 3
NH_3	2 mM	$1 \cdot 10^{-3}$ mM	2 mM
NO_2^-	0	0	0
NO_3^-	0	0	0
O_2	$3.13 \cdot 10^{-3}$ mM	0.281 mM	0.281 mM
CO_2	5 mM	5 mM	5 mM

Case 1: O_2 limitation after 24 days

ammonia-oxidizing bacteria (red): 325 bacteria
nitrite-oxidizing bacteria (green): 12 bacteria
complete ammonia oxidizers, *commamox* (blue): 275 bacteria
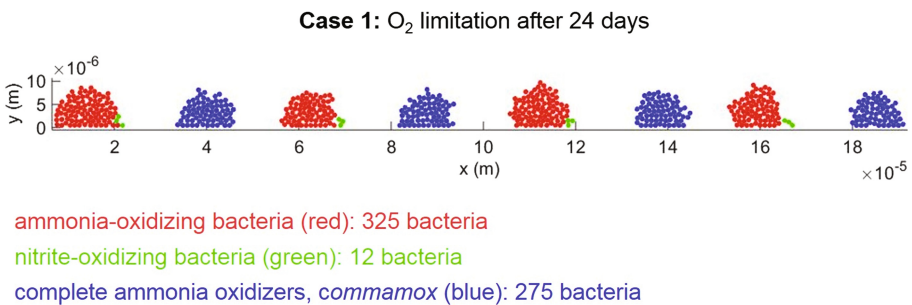
Fig. 1. Biofilm growth after 24 days for Case 1 with 2 mM of NH_3 and O_2 limitation (1 mg/L) in the liquid bulk

Case 2: NH$_3$ limitation after 24 days

ammonia-oxidizing bacteria (red): 181 bacteria

nitrite-oxidizing bacteria (green): 251 bacteria

complete ammonia oxidizers, *commamox* (blue): 257 bacteria
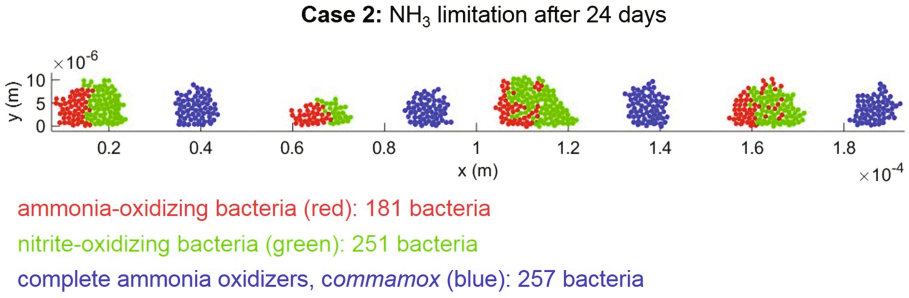
Fig. 2. Biofilm growth after 24 days for the case with NH$_3$ limitation (1 µM) and saturation of O$_2$ (9 mg/L) in the liquid bulk

Case 3: No limitation after 100 hours

ammonia-oxidizing bacteria (red): 7697 bacteria

nitrite-oxidizing bacteria (green): 130 bacteria

complete ammonia oxidizers, *commamox* (blue): 4854 bacteria
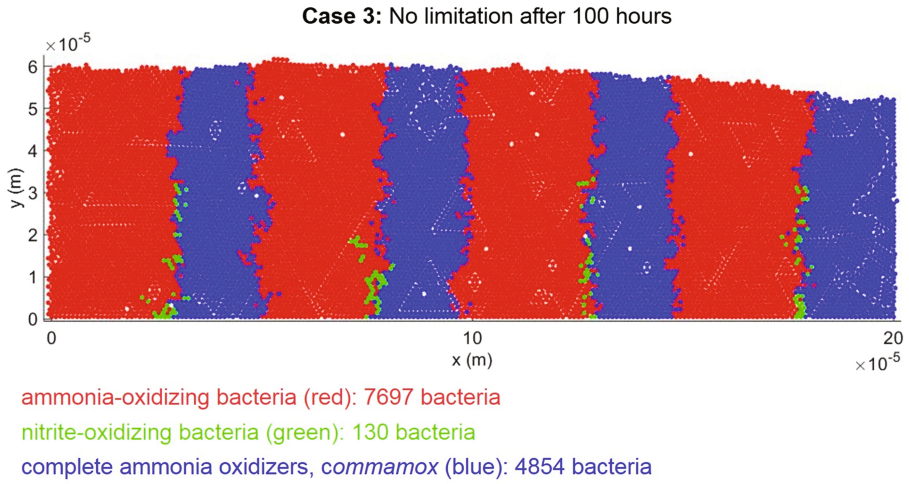
Fig. 3. Biofilm after 100 h with 2 mM of NH$_3$ and saturation of O$_2$ (9 mg/L) in the liquid bulk
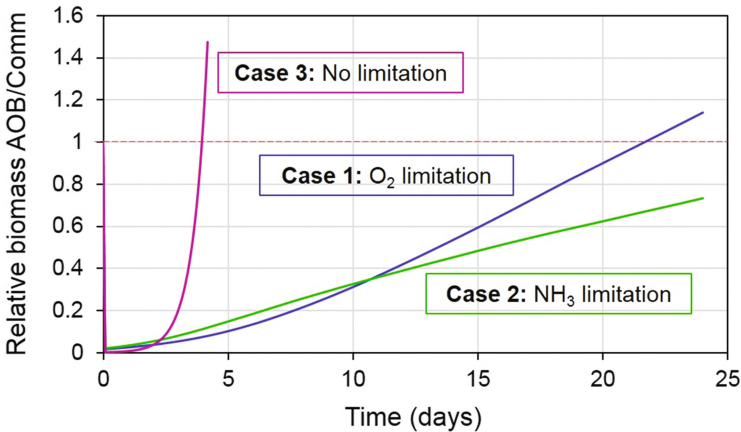
Fig. 4. Relative abundance of AOB and *Commamox* for the three cases studied

reduction of the metabolic process for AOB compared with *Commamox* could be of advantage as they become faster degraders of NH_3 (Figs. 1, 2 and 3).

The relative abundance of AOB against *Commamox* is shown in Fig. 4. For each of the three cases a clear tendency towards AOB dominance is observed.

4 Conclusions

- The discovery of complete nitrification performed by one microorganism could be explained by the similar energy harvesting per amount of electron in both *Commamox* and AOB (Gonzalez-Cabaleiro et al. 2015).
- It remains unclear if complete nitrification could be a metabolic advantage in biofilm competition. Although *Commamox* are able to grow more per mole of NH_3 consumed, the energetic advantage could not be enough to justify its dominance in any niche. Our simulations do not show a clear dominance of *Commamox* in any of the cases presented.
- Only in niches where the substrate limitation is extreme, we could observe an advantage of *Commamox* strategy versus AOB.

References

Costa E, Pérez J, Kreft J-U (2006) Why is metabolic labour divided in nitrification? Trends Microbiol 14:213–219

Daims H, Lebedeva EV, Pjevac P, Han P, Herbold C, Albertsen M et al (2015) Complete nitrification by Nitrospira bacteria. Nature 528:504–509

Gonzalez-Cabaleiro R, Ofiteru ID, Lema JM, Rodriguez J (2015) Microbial catabolic activities are naturally selected by metabolic energy harvest rate. ISME J 9:2630–2641

Heijnen JJ, Kleerebezem R (2010) Bioenergetics of microbial growth. In: Flickinger MC (ed) Encyclopedia of industrial biotechnology, bioprocess, bioseparation, and cell technology. John Wiley & Sons, Inc., pp 1–24

Kleerebezem R, van Loosdrecht MCM (2010) A generalized method for thermodynamic state analysis of environmental systems. Crit Rev Env Sci 40:1–54

Kreft J-U, Picioreanu C, Wimpenny JWT, van Loosdrecht MCM (2001) Individual-based modelling of biofilms. Microbiology 147:2897–2912

Kreft JU (2004) Biofilms promote altruism. Microbiology 150:2751–2760

Suzuki I, Dular U, Kwok SC (1974) Ammonia or ammonium ion as substrate for oxidation by Nitrosomonas europaea cells and extracts. J Bacteriol 120:556–558

Tijhuis L, van Loosdrecht MC, Heijnen JJ (1993) A thermodynamically based correlation for maintenance gibbs energy requirements in aerobic and anaerobic chemotrophic growth. Biotechnol Bioeng 42:509–519

van Kessel MAHJ, Speth DR, Albertsen M, Nielsen PH, Op den Camp HJM, Kartal B et al (2015) Complete nitrification by a single microorganism. Nature 528:555–559

Maximising Energy Harvest from Constructed Wetland-Microbial Fuel Cell Using Capacitor Engaged Duty Cycling Strategy

L. Xu[1(✉)], Y.Q. Zhao[1,2], C. Fan[2], Z.R. Fan[2], and F.C. Zhao[2]

[1] UCD Dooge Centre for Water Resources Research,
School of Civil Engineering, University College Dublin,
Belfield, Dublin 4, Ireland
[2] Key Laboratory of Subsurface Hydrology and Ecological Effects
in Arid Region (Ministry of Education),
School of Environmental Science and Engineering,
Chang'an University, Xi'an 710054, People's Republic of China

Abstract. Although the newly established constructed wetland-microbial fuel cell (CW-MFC) has attracted considerable attention for wastewater treatment and electricity generation. However, the integration of MFC into CWs always faces a large portion of energy losses due to the existence of higher internal resistances. Here, a novel working strategy for energy harvesting from CW-MFC system, named as capacitor engaged duty cycling (CDC) strategy, was proposed and tested. Results showed that with duty cycle (D) value of 31.58% (D = 31.58%), the effective charge obtained from CDC strategy is 11.9% higher than the conventional continuous loading (CL) mode. Further lower D value to 18.75%, the total charge harvested increased about 17.57%. In addition, CDC operation mode also shows advantages over higher internal resistance system. This operation strategy has the potential to minimize the energy losses with a suitable D value. Overall, this method showed a simple but effectively way to maximize the energy harvesting from CW-MFC system.

Keywords: Constructed wetland-microbial fuel cell · Energy harvesting · Capacitor · Duty cycling

1 Introduction

Based on the 2020 energy strategy released by European Commission, the EU aims to reduce its greenhouse gas emissions by at least 20% before 2020 and to increase the share of renewable energy to at least 20% of consumption as well as to achieve energy savings of 20% or more (European Union 2011). To reach this ambitious target, more efficient and sustainable energy sources should be explored for future utilizations. As one of the substitutions, microbial fuel cell (MFC) and its derivations have attracted massive attentions among scientists from different fields due to their unique merit of extracting energy directly from waste streams into electricity (Logan 2008). Though MFC shows a promising development, it still confronted a series of challenges before it can be finally applied into full/practical operation (Xu et al. 2016).

Constructed wetland-microbial fuel cell (CW-MFC), as a kind of newly emerged platform to embed MFC into constructed wetland for wastewater treatment and electricity generation, presented an alternative solution to alleviate the energy stress (Doherty et al. 2015). However, due to its large dimension and complex environmental conditions, the internal resistances of CW-MFCs are usually significantly higher than those in pure MFC systems. This means a large proportion of the energy generated will be lost through the internal resistances and thus causes a lower energy output. Several studies showed that the capacitor engaged systems have positive influence on energy capture (Kim et al. 2011; Liang et al. 2011), while the advantages of duty cycling strategy were also realised by some other researchers (Gardel et al. 2012). However, to the best of our knowledge, none was explored in CW-MFC system.

2   Experimental Set-up

A capacitor engaged duty cycling was proposed in this study (Fig. 1). The CW-MFC system consists of an air-cathode on the top of the CW and an embedded anode underneath to form the MFC, while dewatered alum sludge was used as substrate for the CW (Zhao et al. 2011). A capacitor array was built to storage and discharge the energy gainned from the CW-MFC system and a programmable micro-controller was used to control the circuit operating under a setted circumstance (i.e. Continuously loading-CL, Duty cycling-DC or Capacitor engaged duty cycling-CDC). For continuous loading/operation, the cathode and anode were connected with a constant external resistance of 1000 Ω, while duty cycling means an intermitted loading mode. A capacitor engaged mode was to use the capacitors to storage the energy then discharged
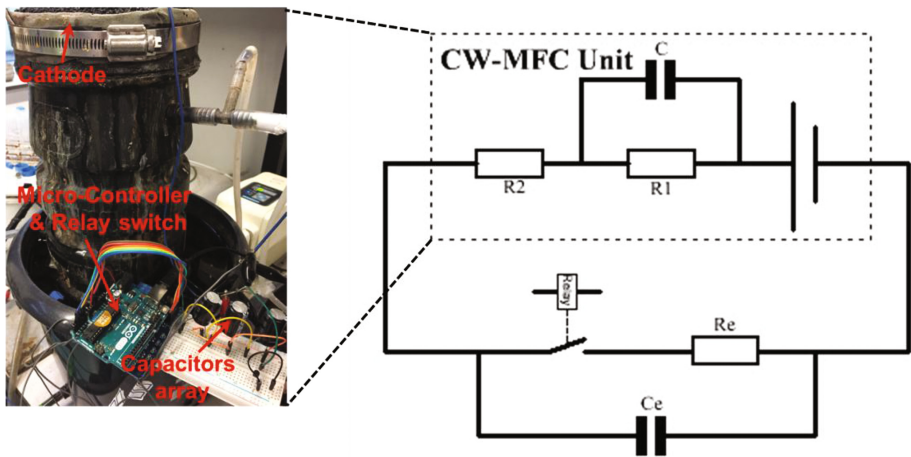
Fig. 1. Schematic circuit diagram of capacitor engaged duty cycling strategy (R1 and R2 represent the charge transfer resistance and electrolyte resistance; C means internal capacitance; Re means external resistance; Ce is the capacitors array)

through the external resistance under DC mode. During the CW-MFC operation, the synthetic wastewater with COD and NH4+-N of 500 mg/L and 30 mg/L, respectively, was employed for wastewater treatment and electricity generation.

3   Main Results

Results showed that with duty cycle value (discharge time/one full cycle time) of 32.17% (D = 32.17%), the overall charge obtained from CDC strategy is 11.9% higher than the conventional continuous loading mode. Further lower the D value to 21.63%, the total charge harvested increased about 17.57% (Fig. 2). The CDC operation strategy has the potential to work infinitely close to open circuit voltage (OCV) with further lower D value. Overall, this novel approach showed a simple but effectively way to maximize the energy harvest from MFC based CW system, especially for those with comparative higher internal resistance.
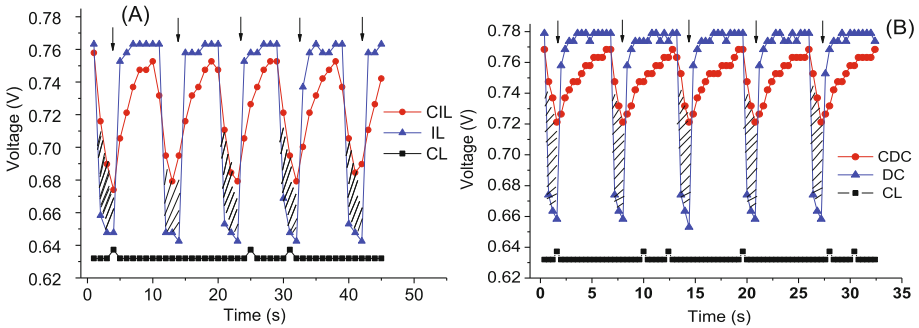
Fig. 2. Differences of the output voltage among three different working strategies with different D value (A) D = 32.17%, (B) D = 21.63% (CL: Continuous loading strategy; DC: Duty cycling strategy; CDC: Capacitor engaged duty cycling strategy)

4   Perspective

This system under trial in this study only has one anode electrode, which means that during the duty cycling mode or capacitor engaged duty cycling mode, the charging period actually did not contribute to the overall charge recovery. The solution to this is to use multi anodes MFC system, which is similar as described in Gardel et al. (2012). As such, during the charging period of one anode, other anodes can be alternatively connected to the circuit for continuous output (Fig. 3). It has been proved that the microbial community of anode biofilms would not be influenced by the duty cycling operation mode Gardel et al. (2012). It should be no problem to use multi anodes system in the capacitor engaged system either. However, further studies are needed to verify this concept. In terms of the number of anode electrodes (n) required during the operation, it can be calculated based on the D value via $n = \max\{n \in Z \mid n \leq (1-D)/D + 1\}$.
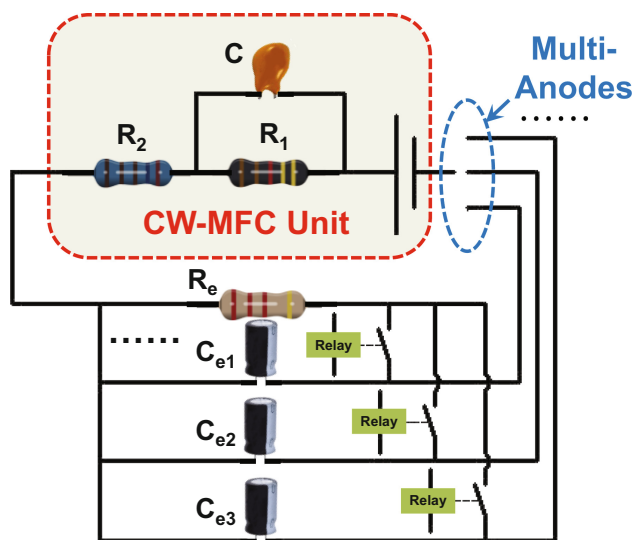
Fig. 3. Schematic circuit diagram of capacitor engaged duty cycling strategy with multi anodes

The advantage of the capacitors engaged system is that most of the energy lost through the internal resistance can be minimized. In the normal operation mode, i.e. the continuous loading mode, energy loss through the internal resistance can account for a large amount of the overall energy produced in the MFC system. This directly depends on the internal resistance. The high internal resistance will result into a correspondent high energy loss, which is reflected as the lower voltage output. This is especially significant in CW-MFC system, as the internal resistance in such system is usually higher than the traditional pure MFCs, which represents a more efficient operation regime for electrons harvesting. Furthermore, the amount of electrons extracted from the system directly influenced the coulombic efficiency of the system, which also pointed out a potential approach to improve the organic removal efficiency within CWs system, since the electrons released were directly related to the amount of organics oxidation through the anode exoelectrogens.

It is important to mention that some relevant parameters in this circuit are worth further investigation. For example, how will the capacitance of the capacitor influence the overall output or how can the external resistance influence the optimization of D values during the operation? Overall, the capacitor engaged duty cycling strategy proposed in this study owns a promising position for the energy extraction within CW-MFC system.

5   Conclusions

A novel operation strategy of capacitor engaged duty cycling for energy harvesting from CW-MFC system was presented and tested in this study. Through which, the electrons harvested from the system is higher than traditional continuous loading mode

and is also higher than later developed duty cycling mode with the same effective discharging time. By adjusting suitable D value (say 18.8%), the total charge harvested from the system can be considerably increased (say 17.6%). This novel operation strategy has the ability to minimize the system internal energy losses and thus owns the potential to maximize the energy harvesting from the CW-MFC system. However, further work on dealing with the multi-anode system and parameters optimization is needed prior to the final application in energy harvesting.

References

European Union (2011) Energy 2020, A strategy for competitive, sustainable and secure energy

Doherty L, Zhao Y, Zhao X, Hu Y, Hao X, Xu L, Liu R (2015) A review of a recently emerged technology: Constructed wetland - microbial fuel cells. Water Res 85:38–45

Gardel EJ, Nielsen ME, Grisdela PT Jr, Girguis PR (2012) Duty cycling influences current generation in multi-anode environmental microbial fuel cells. Environ Sci Technol 46 (9):5222–5229

Kim Y, Hatzell MC, Hutchinson AJ, Logan BE (2011) Capturing power at higher voltages from arrays of microbial fuel cells without voltage reversal. Energy Environ Sci 4(11):4662

Liang P, Wu W, Wei J, Yuan L, Xia X, Huang X (2011) Alternate charging and discharging of capacitor to enhance the electron production of bioelectrochemical systems. Environ Sci Technol 45(15):6647–6653

Logan BE (2008) Microbial fuel cells. John Wiley & Sons, Chichester

Xu L, Zhao Y, Doherty L, Hu Y, Hao X (2016) The integrated processes for wastewater treatment based on the principle of microbial fuel cells: a review. Crit Rev Environ Sci Technol 46(1):60–91

Zhao Y, Babatunde AO, Hu YS, Kumar JLG, Zhao XH (2011) Pilot field-scale demonstration of a novel alum sludge-based constructed wetland system for enhanced wastewater treatment. Process Biochem 46(1):278–283

Release of Organics by Conventional Activated Sludge with Appropriate Ultrasonic Treatment for Nitritation

M. Zheng[✉], S. Wu, Y.C. Liu, and Q. Dong

State Key Joint Laboratory of Environment Simulation and Pollution Control,
School of Environment, Tsinghua University, Beijing 100084, China

Abstract. Achievement of nitritation that oxidizes ammonia to nitrite but not further to nitrate is still critical in wastewater treatment. Recently, it has been reported that controlled ultrasonic treatment would be a promising approach for nitritation process because nitrite-oxidizing bacteria is more sensitive to the ultrasonic treatment than ammonia-oxidizing bacteria. In this study, batch assays were performed to investigate the effects of appropriate ultrasonic treatment with energy density less than 0.8–1.2 kJ/mL for the nitritation on the organics release. The organics release with the increase in the energy density could be described by the monod kinetic model with a maximum increase in SCOD of 0.14 mg COD/mg VS. The ultrasonic treatment would induce at most 60% decrease in heterotrophic activity. The results should be useful to evaluate feasibility of ultrasonic technique for full-scale implementation.

Keywords: Ultrasound · Energy density · Conventional activated sludge · Organics release · Nitritation

1   Introduction

Nitrogen removal from wastewater via nitrite i.e. ammonia oxidation to nitrite (or nitritation) followed by shortcut denitrification or anaerobic ammonia oxidation (ANAMMOX) processes has been attractive for years because of saving energy and carbon source required as well as smaller foot print than conventional nitrification followed by denitrification process (Gao et al. 2010). This reaction requires conversion of ammonium to nitrite but not further to nitrate by controlling microbial nitrogen metabolic pathway as

$$NH_4^+ + 1.5O_2 \rightarrow NO_2^- + 2H^+ + H_2O \tag{1}$$
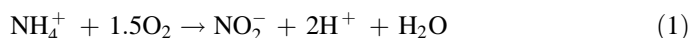
Achievement of the nitritation basically depends on selection of microbial population in which nitrite-oxidizing bacteria (NOB) is suppressed or eliminated and ammonia-oxidizing bacteria (AOB) is predominated. To date, researchers have proposed several approaches to the selection of AOB and suppression of NOB. In 1998, the SHARON process was firstly proposed, which employed mesophilic temperature ranging between 30 and 40°C and short sludge retention time (SRT) of about 1.5 days

to enhance Nitritation (Hellinga et al. 1998). In recent years there has been development of new technologies that use additional chemical dosing sludge treatment to exclude the NOB. For example, Wang et al. (2014) found that free nitrous acid (FNA) in the concentration range of 0.24–1.35 mg HNO_2–N/L inactivates NOB to a larger extent than it does on AOB. A combined FNA-based sludge treatment and oxygen limitation strategy successfully washed out the NOB from the activated sludge (Wang et al. 2016). It is now known that FNA is substantially more biocidal to NOB than to AOB.

Until recently, our group had found that nitrifying bacteria, AOB and NOB together, were sensitive to a common oscillating sound pressure wave at a frequency above 20 kHz, called ultrasound (Zheng et al. 2013; Zheng et al. 2016). Ultrasonic treatment is considered a "green" technology owing to its high efficiency, low instrumental requirement, and significantly reduced process time. Batch activity assays indicated that when ultrasound was applied, AOB activity reached a peak level and then declined but NOB activity deteriorated continuously as the power intensity of ultrasound increased (Zheng et al. 2016). Sequencing batch reactors had been operated to confirm the positive effect of ultrasound on partial nitrification, enhancement of AOB activity, and excluding the NOB in activated sludge (Table 1). However, no information on organics release has been reported by conventional activated sludge with appropriate ultrasonic treatment for nitritation so far.

Table 1. Achievement of the nitritation in three reactors at full aeration (DO > 1.0 mg/L) by using the ultrasonic sludge treatment

No.	Influent		Ultrasonic treatment conditions				Effluent
	NH_4^+-N (mg/L)	COD (mg/L)	P (W)	E_S (kJ/mL)	Interval time (h)	Treated sludge	Nitrite accumulation ratio (%)[c]
I	50	750	100	0.3	8	Mixed liquor	Up to 74%
II[a]	685	587	100	0.1–0.2	8	Mixed liquor	99%
III[b]	620	0	200	0.6–1.2	12	Densed sludge	Up to 81%

[a] Urine wastewater containing high free ammonia as Influent at a pH of 8.8; [b] pH was auto-controlled to be 7.5 ± 0.2 in the reactor; and [c] Nitrite accumulation ratio (NAR) was calculated as a ratio of nitrite to sum of nitrite and nitrate in the effluent.

This study aims to investigate the effects of ultrasonic treatment conditions on the organics release. Batch assays by using ultrasonic treatment on conventional activated sludge were performed. The obtained ultrasonic intensity for enhancing AOB activity indicated appropriate ultrasonic treatment for nitritation, and then used for the investigation on the organic release as well as heterotrophic activity.

2   Materials and Methods

Conventional activated sludge source. Conventional activated sludge was from a full-scale municipal wastewater treatment plant in the campus of Tsinghua University (Tsinghua Water Reuse, Beijing). The plant had stable performance of nitrogen removal via nitrification and denitrification, indicating that AOB and NOB were both enriched in the activated sludge.

Ultrasonic treatment experiment. Batch assays were conducted in volumetric flasks in duplicate. The sludge was added to the flask, stirred and then continuously treated by an ultrasound generator (SCIENTZ–II D, Ningbo Xinzhi Co., Ltd., variable parameters in ranges of 9.5–950 W, 0–999 min, 20–25 kHz). The mixed liquor samples were taken periodically for microbial activity and released organic concentration analyses. The released soluble COD per mg VS (volatile solid) of the sludge under various ultrasonic intensities, powers, active volumes, and biomass concentrations were investigated in groups of batch assays.

Chemical analysis and calculation. Measurements of COD and VS concentrations were performed in the accordance with Standard Methods. The intensity of ultrasonic treatment expressed as energy density (E_S, kJ/mL) was calculated in Eq. 1:

$$E_s = \frac{P \cdot t}{1000V} \tag{1}$$

where P is the ultrasonic active power (W); t is the irradiation time (s); and V is the effective volume of the ultrasonic treatment unit (mL).

The relative activity represented by the ratio of activity with ultrasound energy density to initial activity (without ultrasound) was normalized by the activity in the presence of ultrasonic treatment versus that without ultrasound.

3   Results and Discussions

Appropriate ultrasonic treatment for the nitritation. Figure 1 shows that the ultrasonic energy density E_S below 0.8 kJ/mL had a positive effect on the relative AOB activity and the extensive ultrasonic treatment with E_S up to 2.0 kJ/mL declined the AOB activity. The result is comparable with the ultrasonic bidirectional effect i.e. the AOB activity was enhanced, reached a peak level, and then declined while the NOB activity declined as ultrasonic intensity increased (Zheng et al. 2016). Table 1 summarizes achievement of the nitritation in three reactors at full aeration (DO > 1.0 mg/L) by using ultrasonic sludge treatment. The ultrasound generator started to work after fresh influent filled in the reactor during each operation cycle. The interval time between two ultrasonic treatment was set equal to the operational cycle time (8–12 h). The results clearly demonstrated that the obtained E_S range (less than 0.8–1.2 kJ/mL, depends on the ultrasonic conditions) for the enhancement of AOB activity in the batch assays was appropriate for achieving the nitritation in the bioreactors due to different response of AOB and NOB to the ultrasonic treatment. The ultrasonic approach is easier to be
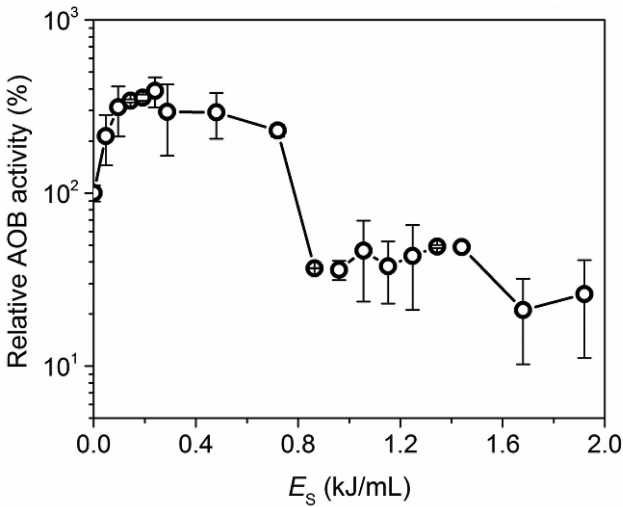
Fig. 1. Relative AOB activity at different ultrasonic energy density (E_S). The used ultrasonic power was 200 W

operated and controlled in comparison with previously proposed control methods for achieving nitrite accumulation by limiting oxygen level, high FA and FNA inhibition, short SRT as well as high temperature (up to 35°C). Appropriate ultrasonic treatment for the nitration is a breakthrough of selection of AOB population with depression of NOB.

Effect of ultrasonic energy density on organics release. Figure 2 shows a gradual increase in soluble COD with ultrasonic intensity increasing. The organics release resulted from the cell lysed ultrasonically. Thus, the contents and nutrients stored in the cell were released and entered in the mixed liquor. Using the results from batch assays described above, the increase in SCOD versus E_S was plotted by using nonlinear regression to fit a monod kinetic model. The tests results fit well the kinetic model by regression plotting with a R^2 value of 0.97 (Fig. 2). The estimated maximum increase in SCOD is 0.14 mg COD/mg VS, which is comparable with the maximum value approximately 0.16 mg COD/mg VS by FNA pre-treatment (Wang et al. 2013). The half-saturation constant of E_S is estimated to be 2.2 kJ/mL. The result indicated that the organics release kinetics in the E_S range of 0–1.2 kJ/mL for the nitration was still close to the first-order reaction kinetics.

Relationship between heterotrophic activity and organics release. Figure 3 shows that the organics release was enhanced with the relative heterotrophic activity decreased. As shown above, the Increase in SCOD was below 0.05 when the E_S was less than 1.2 kJ/mL. Therefore. The relative heterotrophic activity at set $E_S \leq$ 1.2 kJ/mL was calculated to be in the range of 40%–100%. In other words, the appropriate ultrasonic treatment for the nitration would induce at most 60% decrease in heterotrophic activity. This result should be critical to evaluate the effect of ultrasound on the overall bioprocess other than the nitration process.
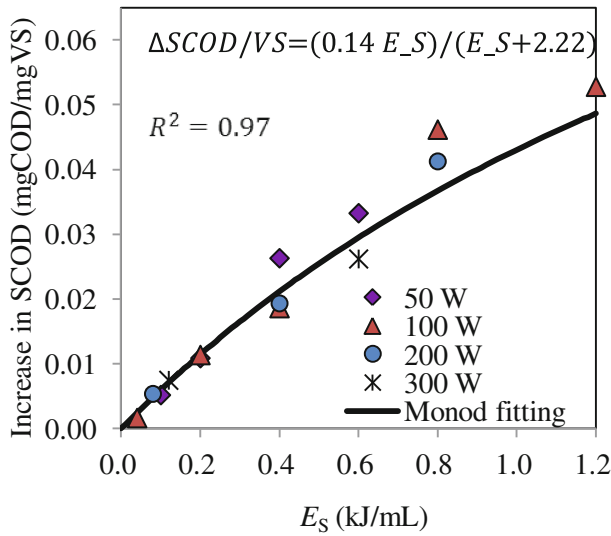
Fig. 2. Soluble COD release at different ultrasonic energy density (E_S) and monod fitting results
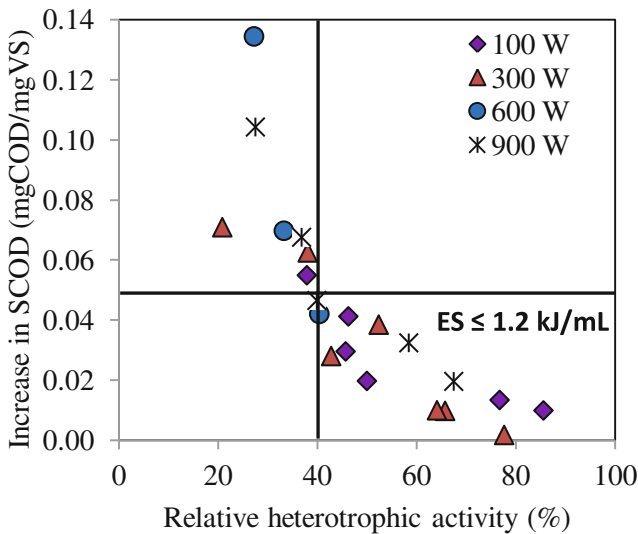
Fig. 3. Relationship between relative heterotrophic activity and increase in soluble COD.

Our previous studies indicated that a properly controlled ultrasonic intensity is essential to enhance the AOB and depress NOB activities. Although we identified a proper ultrasonic density level in these studies, due to scale effect, further research will be needed to test the various ultrasonic power density/intensity with at least pilot scale reactor to obtain sound operational parameters for full scale application. Currently, ultrasonic equipments for sludge treatment are commercially available with flow rates

from 0.02 to 200 m^3/h (Pilli et al. 2011), which can be selected or modified for the nitritation process. And, the results obtained in this work would be useful to evaluate feasibility of ultrasonic technique for full-scale implementation.

4 Conclusions

The ultrasonic energy density less than 0.8–1.2 kJ/mL was appropriate for achievement of the nitritation. The organics release with the increase in the energy density could be described by the monod kinetic model with a maximum increase in SCOD of 0.14 mg COD/mg VS. The appropriate ultrasonic treatment for nitritation would induce at most 60% decrease in heterotrophic activity.

References

Gao DW, Peng YZ, Wu WM (2010) Kinetic model for biological nitrogen removal using shortcut nitrification-denitrification process in sequencing batch reactor. Environ Sci Technol 44(13):5015–5021

Hellinga C, Schellen AAJC, Mulder JW, van Loosdrecht MCM, Heijnen JJ (1998) The SHARON process: an innovative method for nitrogen removal from ammonium-rich waste water. Water Sci Technol 37(9):135–142

Pilli S, Bhunia P, Yan S, LeBlanc RJ, Tyagi RD, Surampalli RY (2011) Ultrasonic pretreatment of sludge: a review. Ultrason Sonochem 18(1):1–18

Wang D, Wang Q, Laloo A, Xu Y, Bond PL, Yuan Z (2016) Achieving stable nitritation for mainstream deammonification by combining free nitrous acid-based sludge treatment and oxygen limitation. Sci Rep 6:25547

Wang Q, Ye L, Jiang G, Jensen PD, Batstone DJ, Yuan Z (2013) Free nitrous acid (FNA)-based pretreatment enhances methane production from waste activated sludge. Environ Sci Technol 47:11897–11904

Wang Q, Ye L, Jiang G, Hu S, Yuan Z (2014) Side-stream sludge treatment using free nitrous acid selectively eliminates nitrite oxidizing bacteria and achieves the nitrite pathway. Water Res 55:245–255

Zheng M, Liu YC, Xu KN, Wang CW, He H, Zhu W, Dong Q (2013) Use of low frequency and density ultrasound to stimulate partial nitrification and simultaneous nitrification and denitrification. Bioresour Technol 146:537–542

Zheng M, Liu YC, Xin J, Zuo H, Wang CW, Wu WM (2016) Ultrasonic treatment enhanced ammonia-oxidizing bacterial (AOB) activity for nitritation process. Environ Sci Technol 50:864–871

Microbial Fuel Cell Bioreactors for Treatment of Waters Contaminated by Naphthenic Acids

G. Valdes Labrada and M. Nemati[✉]

Department of Chemical and Biological Engineering,
University of Saskatchewan, Saskatoon, Canada
Mehdi.Nemati@usask.ca

Abstract. Aerobic biodegradation of surrogate NAs have been investigated in our earlier works using stirred tank, packed-bed, and circulating packed-bed bioreactors. We have also demonstrated the successful anoxic biodegradation of NAs coupled to reduction of nitrate or nitrite, with the biodegradation rates obtained under anoxic conditions being comparable to those achieved under aerobic conditions. Given the success in anoxic biodegradation of NAs and the recent developments in the field of microbial fuel cells as a promising technology for treatment of wastewaters, in the present work we report the results of an investigation on application of microbial fuel cell type bioreactors for the treatment of waters contaminated by NAs with concomitant generation of energy.

Keywords: Oil sand process water · Biodegradation · Microbial fuel cell

1 Introduction

Oil sands of Western Canada represent one of the largest global oil reserves. Extraction of bitumen from shallow oil sands through Clark hot water process generates tailings that are comprised of water, sand, clay, and unrecovered hydrocarbons. A major portion of water associated with these tailings is recovered and recycled back to the extraction process. The remaining part, referred to as oil sand process water (OSPW), is retained in the tailing ponds due to their toxicity and a zero discharge policy. Naphthenic acids (NAs) that are transferred from the bitumen to the aqueous phase during the extraction process are the main toxic constituents of these waters. Given the environmental challenges that are associated with OSPW and tailings and the need for the sustainable use of water, a large number of works aiming on physicochemical or biological treatments of OSPW have been conducted (Doll et al. 2005; Martin et al. 2010; Zubot et al. 2012; Hwang et al. 2013), with the biotreatment or an integrated physicochemical and biological process appear to be the most practical strategies for the treatment of OSPW.

2 Materials and Methods

Biodegradation of two surrogate naphthenic acids, a linear NA (octanoic acid referred to as OA) and a cyclic NA (trans- 4-methyl-1-cyclohexane carboxylic acid referred to as trans-4MCHCA) were investigated in this work. A mixed culture originated from

the soil of an industrial site contaminated with heavy hydrocarbons was used in all experiments.

H-type microbial fuel cell bioreactors with graphite rod or granular graphite electrodes (Fig. 1), operated batchwise or continuously were used in this study (Fig. 2). Effects of NA concentration and loading rate on the performance of MFCs in terms of biodegradation rate and electrochemical outputs were investigated in batch and continuous modes of operation.

Fig. 1. Graphite rods (left) and granules (right)
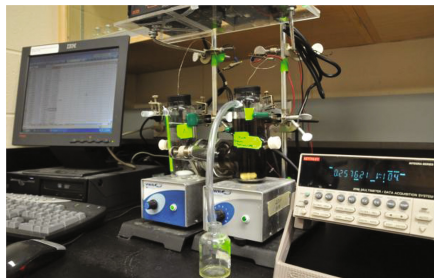
Fig. 2. A typical microbial fuel cell set-up

Optical density (OD) of the samples from MFC, measured by a Mini Shimadzu spectrophotometer (Model 1240), was used to determine the biomass concentration. A Varian-430 Gas Chromatograph with flame ionization detector (FID) was used to determine the concentration of NAs. Real time circuit potential was monitored using a Keithley 2700 multimeter, equipped with 7700 data logger (Keithley Instruments Inc., Cleveland, USA). Polarization and power curves were developed using Linear Sweep Voltammetry (LSV) and a Gamry R600 potentiostat (Gamry Instruments, Warminster, USA).

3   Results

Biodegradation of both NAs was successfully achieved in the MFC bioreactors. A typical set of data obtained with 500 ppm trans-4MCHCA and OA are presented in Fig. 3. Increase in NA concentration from 100 to 250 mg L^{-1} led to marked increase in biodegradation rates of both trans-4MCHCA and OA but biodegradation rates at initial concentration of 250 and 500 mg L^{-1} were close. Moreover, for all tested NAs concentrations, OA biodegradation proceeded at rates which were much faster than those of trans-4MCHCA, indicating that an NA with the linear structure was more amenable to biodegradation when compared to its cyclic counterpart.
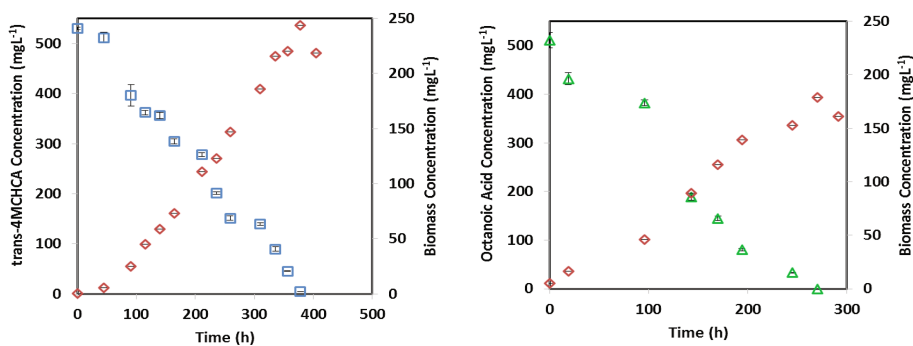
Fig. 3. Biodegradation of 500 ppm trans-4MCHCA (Left) and octanoic acid (right) in batchwise operated MFCs

Co-biodegradation of mixtures of trans-4MCHCA and OA in different combinations led to diauxic growth of bacterial culture, whereby OA was used first and only after complete exhaustion of OA, biodegradation of trans-4MCHCA occurred. This was clear in the biomass concentration profile by two exponential phases separated by a lag phase. Comparison of co-biodegradation rates and biodegradation rates obtained with individual NAs revealed that the presence of trans-4MCHCA did not impact the biodegradation of OA. However, trans-4MCHCA biodegradation rate was enhanced due to presence of OA. This indicated that the presence of a linear NA that is more amenable to biodegradation could have a positive impact on the biodegradation of the cyclic NA, the more recalcitrannt NA.

Conducting biodegradation of tarns-4MCHCA and OA in MFCs with granular graphite electrodes resulted in biodegradation rates that were significantly faster than those in the MFCs with single rod electrodes operated under similar conditions. This improved performance can be attributed to the extended surface area provided by the granular graphite that allowed formation of extensive biofilm (i.e. a suitable matrix for cell immobilization), as well as facilitating the transfer of electrons to the anode.

Typical set of results obtained in the continuous flow MFCs with granular graphite electrodes are presented in Fig. 4. This figure also includes the power curves that correspond to maximum biodegradation rates.
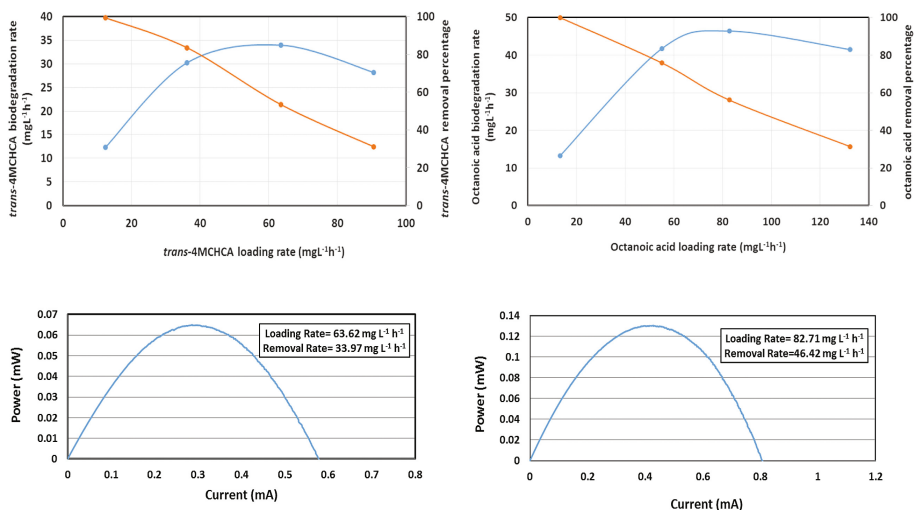
Fig. 4. Biodegradation of 500 ppm trans-4MCHCA (Left) and 500 ppm OA (right) in continuous flow MFCs. Power curves correspond to maximum biodegradation rates

As seen, with both trans-4MCHCA and OA increase in NA loading rate up to a certain level enhanced the biodegradation rate. Consistent with the results obtained in the batch operated MFCs, biodegradation rate of OA in general was higher than that of trans-4MCHCA. For instance the maximum biodegradation of OA was 46.2 mg $L^{-1} h^{-1}$ and obtained at a loading rate of 82.17 mg $L^{-1} h^{-1}$, while the corresponding values in case of trans-4MCHCA were 33.97 and 63.62 mg $L^{-1} h^{-1}$. The improved performance of MFC with OA was also evident in terms of power output, whereby the maximum current and power in case of OA (0.42 mA and 0.13 mW, respectively) were higher than those obtained with tran-4MCHCA (0.29 mA and 0.065 mW, respectively).

4   Conclusions

Biodegradation of both linear and cyclic NAs was successfully achieved in the MFC bioreactors. In the batchwise operated MFCs increase in NA concentration from 100 to 250 mg L^{-1} led to enhanced biodegradation rates but the biodegradation rates at of 250 and 500 mg L^{-1} were close. Regardless of NA initial concentration, OA biodegradation proceeded at rates which were much faster than those for trans-4MCHCA, indicating that an NA with the linear structure was more amenable to biodegradation when compared to its cyclic counterpart. Co-biodegradation of mixtures of NAs led to diauxic growth of bacterial culture, whereby the linear NA was used first and biodegradation of cyclic NA occurred once the linear NA was exhausted. Moreover, the presence of the linear NA had a positive impact on the biodegradation of the cyclic NA.

The extended surface area provided by the granular graphite allowed formation of an extensive biofilm and facilitated the transfer of electrons and thus led in substantial improvement of biodegradation process. In the continuous flow MFCs increase in NA

loading rate up to a certain level enhanced the biodegradation rate. Biodegradation rate of OA (linear structure) was higher than that of trans-4MCHCA (cyclic NA). The use of linear NA also led to improved electrochemical performance of MFC whereby the maximum current and power outputs in case of OA were higher than those obtained with tran-4MCHCA.

References

Doll TE, Frimmel FH (2005) Removal of selected persistent organic pollutants by heterogeneous photocatalysis in water. Catal Today 101:195–202

Hwang G, Dong T, Islam MS, Sheng Z, Pérez-Estrada LA, Liu Y (2013) The impacts of ozonation on oil sands process-affected water biodegradability and biofilm formation characteristics in bioreactors. Bioresour Technol 130:269–277

Martin JM, Barri T, Han X, Fedorak PM, El-Din M, Perez L (2010) Ozonation of oil sands process-affected water accelerates microbial bioremediation. Environ Sci Technol 44:8350–8356

Zubot W, MacKinnon MD, Chelme-Ayala P, Smith DW, Gamal El-Din M (2012) Petroleum coke adsorption as a water management option for oil sands process-affected water. Sci Total Environ 427–428:364–372

Pharmaceuticals in Wastewater Treatment Plants of Tuscany: Occurrence and Toxicity

L. Palli[1]([✉]), F. Spina[2], C. Varese[2], A. Romagnolo[2], A. Bonari[3],
C. Bossi[3], I. Pompilio[3], S. Dugheri[4], S. Tilli[5], A. Scozzafava[5],
D. Santianni[6], S. Caffaz[6], and R. Gori[1]

[1] Department of Civil and Environmental Engineering,
University of Florence, Via Santa Marta 3, 50139 Florence, Italy
[2] Department of Life Sciences and Systems Biology,
University of Turin, Viale P.A. Mattioli 25, 10125 Turin, Italy
[3] Department of Clinic and Experimental Medicine,
University of Florence, Largo Brambilla 3, 50134 Florence, Italy
[4] Laboratory of Industrial Hygiene and Toxicology,
Azienda Ospedaliero-Universitaria Careggi,
Largo Palagi 1, 50134 Florence, Italy
[5] Department of Chemistry "Ugo Schiff", University of Florence,
Via della Lastruccia 3, Sesto Fiorentino, 50019 Florence, Italy
[6] Publiacqua SpA, Via Villamagna 90/c, 50126 Florence, Italy

Abstract. A monitoring on the occurrence of nine different pharmaceutical active compounds at the inlet and outlet of three wastewater treatment plants in Tuscany has been made. Moreover, the overall toxicity of the wastewater was evaluated using two different bioassays.

Results show that few compounds were completely removed during the treatment processes (doxycycline and paracetamol), some others were only partially removed (such as ketoprofen, atenolol and amoxicillin) while most of them were not reduced after the treatment, as in the case of diclofenac, carbamazepine, clarithromycin and β-estradiol.

Keywords: Pharmaceuticals · Wastewater · Ecotoxicity

1 Introduction

Pollution from pharmaceuticals in surface- and ground-waters is recognized as an environmental issue in many countries, arousing the attention from both the public and scientific communities (Cruz Morató et al. 2013; Salgado et al. 2013). In particular, in the past 20 years many scientific papers have been addressed on their possible adverse effects (Vasquez et al. 2014). Pharmaceuticals are released into the environment due to human activities (i.e. patient excretion). Considering also that a strict legislation is not spread worldwide, data about the occurrence of these compounds into receiving waters are rare and scattered. Moreover once in the sewage system, they reach wastewater treatment plants (WWTPs), where they are not completely degraded (Cunningham et al. 2006). As a result, a significant portion of drugs and their metabolites are released

into the aquatic system and they might also reach drinking water treatment plants (Kümmerer 2009). It is therefore important to monitor the occurrence of pharmaceuticals in WWTP and the overall ecotoxicological effect to different organisms.

2 Materials and Methods

In the present study, we evaluated the concentration of nine pharmaceutical active compounds (PhACs) and the overall ecotoxicity of the influent and effluent of three WWTPs in Tuscany, managed by Publiacqua SpA and located in Figline Valdarno (WWTP1), Lastra a Signa (WWTP2) and Pistoia (WWTP3). The nine PhACs are belonging to different classes: non-steroidal anti-inflammatory drugs (NSAID) (diclofenac, ketoprofen, paracetamol), antibiotics (amoxicillin, clarithromycin, doxycycline), β-blocker (atenolol), antiepileptic drug (carbamazepine) and hormone (β-estradiol).

For all the pharmaceuticals except for β-estradiol the analytical determination has been achieved through sample purification (25 ml of raw wastewater) through off-line Solid Phase Extraction (SPE) (Oasis HLB 3 cc, 60 mg, 30 μm particle size, Waters Corporation) and then analysis in LC MS/MS Waters Xevo TQ-S, Acquity UPLC Column Manager. Analytical column: CORTECTS C18, 2.7 μm particle size, Waters Corporation. Mobile phase was a gradient (0,5 ml/min) with water with 0.1 acetic acid (A) and acetonitrile (B). Solvent B from 0% to 80% in 12 min. (Becerra-Herrera et al. 2015; López-Serna et al. 2010; Spina et al. 2015; Zuccato et al. 2010).

For the determination of β-estradiol, sample (1 mL) was derivatized with 1,2-Dimethylimidazole-4-sulfonyl Chloride (DMISC), purified with off-line SPE (SPEC C18 15 mg 3 ml), subsequently extracted with hexane and finally analyzed in LC MS/MS Waters Xevo TQ-S, Acquity UPLC Column Manager. Analytical column: Luna Phenyl-Hexyl 100 Å, 3,0 μm particle size. Mobile phase was a gradient (0,5 ml/min) with water with 0.1 acetic acid (A) and acetonitrile (B). Solvent B from 0% to 80% in 12 min. (Xu and Spink 2007).

Moreover, the overall ecotoxicity of the wastewater was evaluated using two bioassays evaluating the plant germination and elongation (*Lepidium sativus, Cucumis sativum, Sorghum commune*) and the algal growth inhibition (*Raphidocelis subcapitata*).

3 Results and Discussions

Table 1 shows the concentration of the nine PhAC in the effluents and influents of the three WWTPs. It is possible to see that some compounds are well-removed inside the WWTP (as in the case of doxycycline or paracetamol), some others are only partially removed (such as ketoprofen, atenolol and amoxicillin) while most of them are not reduced after the treatment, as in the case of diclofenac, carbamazepine, clarithromycin and β-estradiol. This is in line with already published data (inter alia Castiglioni et al. 2005; Hernando et al. 2006; Roberts and Thomas 2006).

It is interesting to consider that WWTP3 is the one that shows, on average, higher concentrations of pharmaceuticals. This was expected before WWTP3 treats, together with urban wastewater, a separate flux collected from a near hospital. WWTP1 and

Table 1. Pharmaceuticals concentration (ng/L) detected in the effluents and influents of the three WWTPs. Limit of detection: LoD

Sample	diclofenac	ketoprofen	paracetamol	carbamazepine	atenolol	amoxicillin	clarithromycin	doxycycline	17-β-estradiol
WWTP1 effluent	1564	72	< LoD	129	61	1000	173	< LoD	5
WWTP1 influent	1651	351	1181	143	540	1345	53	309	8
WWTP2 effluent	2364	182	< LoD	247	58	813	79	< LoD	5
WWTP2 influent	1957	819	741	205	561	518	180	176	5
WWTP3 effluent	2199	111	< LoD	726	359	436	146	< LoD	5
WWTP3 influent	2103	512	5264	333	1733	662	155	520	8

WWTP2 treat both only urban wastewater but differs mainly for the dimensions (37500 PE for WWTP1, 600000 PE WWTP2, and 120000 PE for WWTP3). All the three considered WWTPs use conventional activated sludge process with pre-denitrification.

As regards the ecotoxicity, the model organisms responded differently to the water samples: as expected, in order to have a precise risk assessment, a battery of bioassays gives more complete information than a single test. For instance, the influent of WWTP2 stimulated *S. commune* and *L. sativum* but inhibited *C. sativus*. Concerning the fitotoxicity, *C. sativum* was the most sensitive organism to the wastewaters. Data of the two most sensitive bioassays are reported in Table 2. As indicated by the strong algal inhibition, influents were quite toxic. With the only exception of WWTP1 where the effluent was not toxic anymore, the treatments performed in the other WWTPs were not efficient in the reduction of the environmental hazard. On the contrary, IG% indicates that the effluents of WWTP2 and WWTP3 were more toxic that the influents.

Table 2. Ecotoxicity of the influents and effluents of the three WWTPs: results of the algal test are expressed as algal growth inhibition percentage (I%); *C. sativum* test indicates the germination index percentage (IG%)

	Algal test		*C. sativum* test	
	influent	effluent	influent	effluent
WWTP1	44.7	−2.4	92.7	103.7
WWTP2	53.9	−7.7	83.7	49.5
WWTP3	44.7	14.6	92.4	85.6

4   Conclusions

In the present study the presence and the toxicity of nine PhAC in three WWTP in Tuscany has been presented. Obtaiend data clearly indicate that conventional treatment processes do not completely remove these micropollutants. Among them, analgesics, anti-inflamatories, psychiatric drugs, antibiotics and hormones. Selected pharmaceuticals could be divided into three groups according to their behavior in WWTPs: a few

compounds were completely removed during the treatment processes (doxycycline and paracetamol), some others are only partially removed (such as ketoprofen, atenolol and amoxicillin) while most of them are not reduced after the treatment, as in the case of diclofenac, carbamazepine, clarithromycin and β-estradiol.

From our study it can be concluded that the potential risk of pharmaceuticals should be monitored carefully, taking into account seasonal variability and using more bioassay data, because many uncertainties still exist in the determination and toxicity of metabolites in water environments.

References

Becerra-Herrera M, Honda L, Richter P (2015) Ultra-high-performance liquid chromatography-time-of-flight high resolution mass spectrometry to quantify acidic drugs in wastewater. J Chromatogr A 1423:96–103. doi:10.1016/j.chroma.2015.10.071

Castiglioni S, Bagnati R, Fanelli R, Pomati F, Calamari D, Zuccato E (2005) Removal of pharmaceuticals in sewage treatment plants in Italy. Environ Sci Technol 40:357–363. doi:10.1021/ES050991M

Cruz Morató C, Ferrando Climent L, Rodriguez Mozaz S, Barceló D, Marco-Urrea E, Vicent T, Sarrà M (2013) Degradation of pharmaceuticals in non-sterile urban wastewater by Trametes versicolor in a fluidized bed bioreactor. Water Res 47:5200–5210

Cunningham V, Buzby M, Hutchinson T, Mastrocco F, Parke N, Roden N (2006) Effects of human pharmaceuticals on aquatic life: next steps. Environ Sci Technol 40:3457–3461

Hernando MD, Mezcua M, Fernández-Alba AR, Barceló D (2006) Environmental risk assessment of pharmaceutical residues in wastewater effluents, surface waters and sediments. Talanta 69:334–342. doi:10.1016/j.talanta.2005.09.037

Kümmerer K (2009) The presence of pharmaceuticals in the environment due to human use–present knowledge and future challenges. J Environ Manag 90:2354–2366

López-Serna R, Pérez S, Ginebreda A, Petrović M, Barceló D (2010) Fully automated determination of 74 pharmaceuticals in environmental and waste waters by online solid phase extraction-liquid chromatography-electrospray-tandem mass spectrometry. Talanta 83:410–424. doi:10.1016/j.talanta.2010.09.046

Roberts PH, Thomas KV (2006) The occurrence of selected pharmaceuticals in wastewater effluent and surface waters of the lower Tyne catchment. Sci Total Environ 356:143–153. doi:10.1016/j.scitotenv.2005.04.031

Salgado R, Pereira VJ, Carvalho G, Soeiro R, Gaffney V, Almeida C, Vale Cardoso V, Ferreira E, Benoliel MJ, Ternes TA, Oehmen A, Reis MAM, Noronha JP (2013) Photodegradation kinetics and transformation products of ketoprofen, diclofenac and atenolol in pure water and treated wastewater. J Hazard Mater 244–245:516–527

Spina F, Cordero C, Schilirò T, Sgorbini B, Pignata C, Gilli G, Bicchi C, Varese GC (2015) Removal of micropollutants by fungal laccases in model solution and municipal wastewater: evaluation of estrogenic activity and ecotoxicity. J Clean Prod 100:185–194

Vasquez MI, Lambrianides A, Schneider M, Kümmerer K, Fatta-Kassinos D (2014) Environmental side effects of pharmaceutical cocktails: What we know and what we should know. J Hazard Mater 279:169–189

Xu L, Spink DC (2007) 1,2-Dimethylimidazole-4-sulfonyl chloride, a novel derivatization reagent for the analysis of phenolic compounds by liquid chromatography electrospray tandem mass spectrometry: application to 1-hydroxypyrene in human urine. J Chromatogr B 855:159–165. doi:10.1016/j.jchromb.2007.04.039

Zuccato E, Castiglioni S, Bagnati R, Melis M, Fanelli R (2010) Source, occurrence and fate of antibiotics in the Italian aquatic environment. J Hazard Mater 179:1042–1048. doi:10.1016/j.jhazmat.2010.03.110

Removal of Conventional Water Quality Parameters, Emerging Contaminants and Fluorescing Organic Matter in a Hybrid Constructed Wetland System

M. Sgroi[1(✉)], C. Pelissari[2], C. Ávila[3], P.H. Sezerino[2],
F.G.A. Vagliasindi[1], J. García[4], and P. Roccaro[1]

[1] Department of Civil Engineering and Architecture,
University of Catania, Catania, Italy
[2] Department of Sanitary and Environmental Engineering,
Federal University of Santa Catarina, Florianópolis, Brazil
[3] ICRA, Catalan Institute for Water Research,
Scientific and Technological Park of the University of Girona, Girona, Spain
[4] Department of Civil and Environmental Engineering,
Universitat Politècnica de Catalunya-BarcelonaTech, Barcelona, Spain

Abstract. Constructed wetlands (CWs) are nature-based wastewater treatment systems, which are often implemented in decentralized areas and small communities. In recent decades, the CW technology has rapidly evolved through the use of various designs and operational modes or other intensifications so as to improve effluent water quality with respect to various pollutants from wastewater. In the present study, the removal of conventional water quality parameters, emerging organic contaminants (EOCs) and fluorescence signature was investigated in a hybrid constructed wetland system comprising different CW configurations: (i) unsaturated vertical subsurface flow (VF), (ii) partial saturated vertical subsurface flow (VF sat), (iii) saturated horizontal flow (HF) and (iv) free water surface (FWS) wetlands. The obtained results showed higher removal of BOD_5, COD and fluorescing organic matter in the aerobic VF reactor, whereas the anoxic HF wetland was the most efficient unit for nitrogen removal. The partially saturated VF wetland showed a greater performance in the reduction of nitrogen and highly biodegradable EOCs than the unsaturated VF bed. Finally, linear regression analyses performed between removal of water quality parameters, EOCs and fluorescence measurements suggested the possibility to use fluorescence indexes as useful indicators of water treatment efficacy and/or surrogate parameters for EOCs monitoring.

Keywords: Pharmaceutical and personal care products · Real time monitoring · Treatment wetland · Wastewater treatment · Fluorescence spectroscopy

1 Introduction

Constructed wetlands (CWs) are nature-based wastewater treatment systems, which are often implemented in decentralized areas and small communities due to their advantages over conventional wastewater treatment plants (WWTPs), that include their

simple operation and maintenance and low to zero energy input. In recent decades, the CW technology has rapidly evolved through the use of various designs and operational modes or other intensifications so as to improve effluent water quality with respect to various pollutants from wastewater. Particularly, the occurrence and fate of emerging organic contaminants (EOCs) in CW systems have only recently come under scrutiny, and more studies are needed for a complete and thorough understanding of the behaviour of these contaminants in CWs systems operating under different conditions (Verlicchi and Zambello 2014; Avila et al. 2016, 2017).

Fluorescence spectroscopy is considered a useful tool for characterizing dissolved organic matter (DOM) in various natural and engineered aquatic systems. This spectroscopic technique has been investigated in previous studies for its use as an indicator of water treatment efficacy and treated water quality (Carstea et al. 2016). The acquisition of 3-dimensional excitation-emission matrices (EEMs) provides a "map" of contributions of different component classes comprising dissolved organic matter (DOM), and correlations have been determined between the fluorescence intensity of various EEM peaks and typical water quality parameters or EOCs in conventional WWTPs (Cohen et al. 2014; Carstea et al. 2016; Sgroi et al. 2017). However, to the best of our knowledge, there are no studies dwelling on the use of fluorescence measurements as indicator of water treatment efficacy as well as surrogate for EOCs monitoring in CW systems.

The objectives of this study were: (i) to investigate the removal of conventional water quality parameters, EOCs and fluorescing organic matter in two treatment lines comprising different CW configurations; (ii) to evaluate the use of fluorescence indexes as effective indicators of water treatment efficacy and/or surrogate parameters for EOCs monitoring in the two CW treatment lines.

2 Material and Methods

The study was conducted in an experimental hybrid constructed wetland system located at the Universitat Politècnica de Catalunya in Barcelona (Spain) (Mediterranean climate). Urban wastewater was settled in an Imhoff tank ($0.2 \ m^3$), which was followed by two vertical subsurface flow (VF) constructed wetlands ($1.5 \ m^2$ each) operating in parallel. They were intermittently fed, receiving a hydraulic loading rate of about $0.13 \ m \ d^{-1}$. One of them was partially saturated with 0.30 cm water (out of a total filter depth of 0.8 m) as a strategy to enhance total nitrogen removal, while the other one was typically unsaturated. The effluent of the partially saturated VF (VF sat) bed was discarded back to the sewerage system (treatment line 1). On the other hand, the effluent of the unsaturated typical VF (VF) was pumped into a horizontal subsurface flow (HF) and a free water surface (FWS) wetlands ($2 \ m^2$ each) working in series (treatment line 2). All beds were planted with *Phragmites australis* and the vegetation was well developed at the time of the experiment.

Samples (8h-composite) were collected from April to July 2016 (n = 12), and after the determination of onsite water quality parameters, samples were immediately taken to the laboratory, where analysis was carried out within 24 h. The determination of the selected EOCs followed Anumol et al. (2013) recommendations. Analysis of

conventional water quality parameters was conducted according to standard methods. Absorbance measurements were performed with a Shimadzu UV-1800 spectrophotometer (Kyoto, Japan). Fluorescence data acquired by a Shimadzu RF-5301PC fluorescence spectrophotometer (Kyoto, Japan) were corrected as described in Sgroi et al. (2017).

3 Results and Discussion

Removal efficiencies of water quality parameters, EOCs and fluorescence signature were different in each treatment unit. COD and BOD_5 were better removed in the unsaturated VF wetland (VF) than in the partially saturated VF bed (VFsat) due to better aeration conditions. The HF wetland, which operated under anoxic conditions, showed low removal of BOD_5 and unchanged concentrations for COD. Nevertheless, the HF bed was the most efficient unit for total nitrogen (TN) elimination (Table 1).

Table 1. Average ($\pm$sd) of relative COD, BOD_5 and TN concentrations normalized by the influent values in the Imhoff tank and the different CW units of treatment line 1 (VFsat) and 2 (VF+HF+FWS)

Parameter	Imhoff tank	VF Sat	VF	HF	FWS
BOD_5 (%)	72 $\pm$ 6	37 $\pm$ 7	15 $\pm$ 6	3 $\pm$ 1	6 $\pm$ 3
COD (%)	74 $\pm$ 19	48 $\pm$ 28	28 $\pm$ 12	32 $\pm$ 20	37 $\pm$ 27
TN (%)	92 $\pm$ 13	47 $\pm$ 8	57 $\pm$ 10	22 $\pm$ 6	9 $\pm$ 5

Highly biodegradable EOCs such as caffeine and trimethoprim were almost completely removed in both VF wetlands, showing a slightly higher removal in the VFsat than in the VF wetland, as opposed to DEET that showed superior removal in the unsaturated VF. Sucralose and sulfametoxazole were negligibly removed in all the CW units, except for the enhanced removal capacity of sulfamethoxazole in the VFsat (Table 2). These observed differences need further investigation.

Table 2. Average ($\pm$sd) of relative concentrations of target emerging organic contaminants normalized by the influent values in the Imhoff tank and the different CW units of treatment line 1 (VFsat) and 2 (VF+HF+FWS)

Emerging contaminant	Imhoff tank	VF Sat	VF	HF	FWS
Caffeine (%)	77 $\pm$ 20	3 $\pm$ 5	7 $\pm$ 5	1 $\pm$ 1	0 $\pm$ 0
Trimethoprim (%)	96 $\pm$ 11	1 $\pm$ 3	13 $\pm$ 24	0 $\pm$ 0	0 $\pm$ 0
DEET (%)	84 $\pm$ 16	60 $\pm$ 36	37 $\pm$ 28	23 $\pm$ 23	23 $\pm$ 15
Sulfamethoxazole (%)	93 $\pm$ 33	39 $\pm$ 39	108 $\pm$ 123	122 $\pm$ 106	76 $\pm$ 67
Sucralose (%)	111 $\pm$ 31	91 $\pm$ 28	94 $\pm$ 22	106 $\pm$ 34	98 $\pm$ 22

Fluorescing organic matter removal through the different treatment units had a similar behaviour to BOD_5 and COD, with the highest removal in the aerobic VF wetland (Fig. 1). Linear regression analysis reported significant correlations between fluorescence EEM peaks, BOD_5, COD and the more degradable EOCs, confirming the possibility to use fluorescence measurements as useful indicators of water treatment efficacy and/or surrogate parameters for EOCs monitoring in CWs systems.
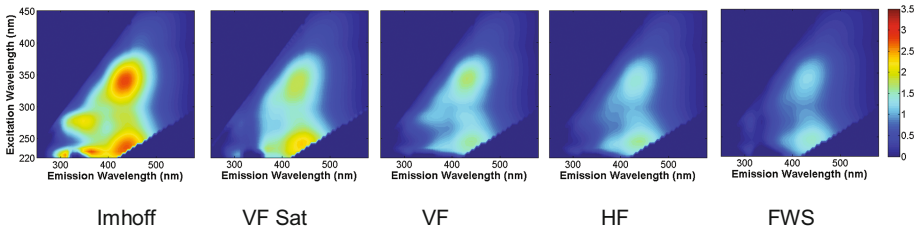
Fig. 1. Fluorescence EEMs in the Imhoff tank and the different CW units of treatment line 1 (VFsat) and 2 (VF+HF+FWS) collected on April 12th 2016

4   Conclusion

The present study investigated the removal of water quality parameters, EOCs and fluorescence signature along different units of a hybrid constructed wetland system. Water quality parameters such as BOD_5 and COD, and fluorescing organic matter showed a higher removal in the aerobic VF reactor, whereas the anoxic HF wetland was the most efficient unit for nitrogen removal. The partially saturated VF wetland showed a greater performance in the reduction of nitrogen and highly biodegradable EOCs than the unsaturated VF bed. Results of linear regression analyses performed between the removal of water quality parameters, EOCs and fluorescence signature suggest the possibility to use fluorescence measurements as useful indicators of water treatment efficacy and/or surrogate parameters for EOCs monitoring.

References

Anumol T, Merel S, Clarke B, Snyder SA (2013) Ultra high performance liquid chromatography tandem mass spectrometry for rapid analysis of trace organic contaminants in water. Chem Cent J 7:104

Ávila C, García J, Garfí M (2016) Influence of hydraulic loading rate, simulated storm events and seasonality on the treatment performance of an experimental three-stage hybrid constructed wetland system. Ecol Eng 87:324–332

Ávila C, Pelissari C, Sezerino PH, Sgroi M, Roccaro P, García J (2017) Enhancement of total nitrogen removal through effluent recirculation and fate of PPCPs in a hybrid constructed wetland system treating urban wastewater. Sci Total Environ 584–585:414–425. doi:10.1016/j.scitotenv.2017.01.024

Carstea EM, Bridgeman J, Baker A, Reynolds DM (2016) Fluorescence spectroscopy for wastewater monitoring: a review. Water Res 95:205–219

Cohen E, Levy GJ, Borisover M (2014) Fluorescent components of organic matter in wastewater: efficacy and selectivity of the water treatment. Water Res 55:323–334

Sgroi M, Roccaro P, Korshin GV, Greco V, Sciuto S, Anumol T, Snyder SA, Vagliasindi FGA (2017) Use of fluorescence EEM to monitor the removal of emerging contaminants in full scale wastewater treatment plants. J Hazard Mater 323:367–376

Verlicchi P, Zambello E (2014) How efficient are constructed wetlands in removing pharmaceuticals from untreated and treated urban wastewater? Rev Sci Total Environ 470–471:1281–1306

REWAQUA: An Advanced Technology for Water Purification in Sustainable Aquaculture Based on Photocatalytic Ozonation

F. Parrino[1(✉)], G. Camera Roda[2], V. Loddo[1], and L. Palmisano[1]

[1] Dipartimento di Energia, Ingegneria dell'Informazione
e Modelli Matematici (DEIM), University of Palermo,
Viale delle Scienze Ed. 6, 90128 Palermo, Italy
[2] Department of Civil, Chemical, Environmental, and Materials Engineering,
University of Bologna, via Terracini 28, 40131 Bologna, Italy

Abstract. The present study has been undertaken in order to test the real potential of photocatalytic ozonation in a bench-scale recirculating aquaculture system working on a 180 L reef coral aquarium. Notably, this choice may be considered representative. In fact, (i) the system is virtually closed so that fresh water turnover is practically negligible, (ii) the presence of living organisms is highly diversified (corals, fishes, molluscs, echinoderms and crustaceans) and some of them are particularly sensitive to water quality, (iii) high salinity strongly puts a strain on the purification system. The hereby presented purification method has been named REWAQUA, which stands for REcycling Water for AQUAculture and AQUAria. REWAQUA allows purification rates higher than the sum of the rates of the single technologies (photocatalysis and ozonation) operating in series. Furthermore the production of bromate ions, which are carcinogenic by-products of ozonation, is efficiently controlled. Two years observation of the reef coral aquarium reveals that photocatalytic ozonation is a good candidate for water purification in recirculating systems in view of a sustainable aquaculture.

Keywords: Photocatalysis · Ozonation · Integrated systems · Recirculating aquaculture systems

1 Introduction

Closed and relatively intensive systems are highly desirable for a sustainable aquaculture and are currently applied in order to limit water consumption and wastewater production. On the other hand, these systems require an efficient water treatment in order to ensure suitable living conditions to the aquatic target organisms (fishes, molluscs and crustaceans) and to provide high quality and food-safe final products. Advanced oxidation processes (AOPs) are promising tools to this task. Among them ozonation is already successfully applied in aquaculture [1], maintenance of aquariums, drinking water sterilization and purification. Other AOPs as e.g. heterogeneous

photocatalysis may present interesting features to overcome the problems related to ozonation. This technology is based on the ability of semiconductors, under light irradiation of suitable wavelength, to generate hydroxyl radicals or active oxygen species which in turn allow degradation of organic compounds [2] and water sterilization. Notably, it has been demonstrated [3] that photocatalysis and ozonation acting simultaneously (photocatalytic ozonation) afford purification rates higher than the sum of the rates of the single processes sequentially applied. This synergistic effect presents important consequences for practical applications in terms of global process efficiency and operative costs. The benefits of coupling photocatalysis and ozonation are not limited to the increase of the oxidation rate, but include also the control of bromate ions which are the ozonation by-products of main concern [4]. Indeed, as bromide ions are virtually omnipresent in every ground and surface water, carcinogenic bromate ions may be almost quantitatively produced if the sole ozonation is used for purification purposes. This aspect is of paramount importance for marine aquaculture applications as bromide concentration in seawater is ca. 67 mg$\cdot$L^{-1} and the high amount of bromate ions produced may be lethal for the living organisms (minimum lethal concentration equal to 10 µg$\cdot$L^{-1}) [5].

By taking into account the above mentioned considerations, the present study has been undertaken in order to test the real potential of photocatalytic ozonation in a bench-scale recycling aquaculture system (RAS) working on a 180 L reef coral aquarium. Notably, this choice may be considered representative. In fact, (i) the system is virtually closed so that fresh water turnover is practically negligible, (ii) the presence of living organisms is highly diversified (corals, fishes, molluscs, echinoderms and crustaceans) and some of them are particularly sensitive to water quality, (iii) the presence of organics and the organisms population density may be easily controlled, (iv) high salinity strongly puts a strain on the purification system. The hereby presented purification method has been named REWAQUA, which stands for REcycling Water for AQUAculture and AQUAria.

2 Materials and Methods

The 180 L reef coral aquarium (Fig. 1) used contained a dense population of small marine organisms. Simulated seawater has been prepared by dissolving a commercial mixture of sea salts (Reef Crystal ®) in demineralised water up to a concentration of 34 g$\cdot$L^{-1}.

Water was continuously discharged from the aquarium tank to a 25 L sump where it was treated and recycled to the tank by means of an immersed centrifugal pump (flow rate equal to ca. 900 L$\cdot$h^{-1}). An electric heater ensured a constant water temperature of ca. 26 °C. The following elements enabled water purification: skimmer, biological filter, phosphate trap (ion-exchange resins), photocatalytic reactor, ozonator.

The photocatalytic reactor consisted of two coaxials Pyrex glass tubes. The dimensions of the annular photoreactor were: inner diameter = 2.4 cm, outer diameter = 3.4 cm and length = 26.5 cm. A linear fluorescent blacklight lamp (Philips 8 W TL/08) was placed on the axis of the reactor emitting UVA radiation from 350 to 400 nm with 82% of the emitted radiant power concentrated from 360 to 380 nm and
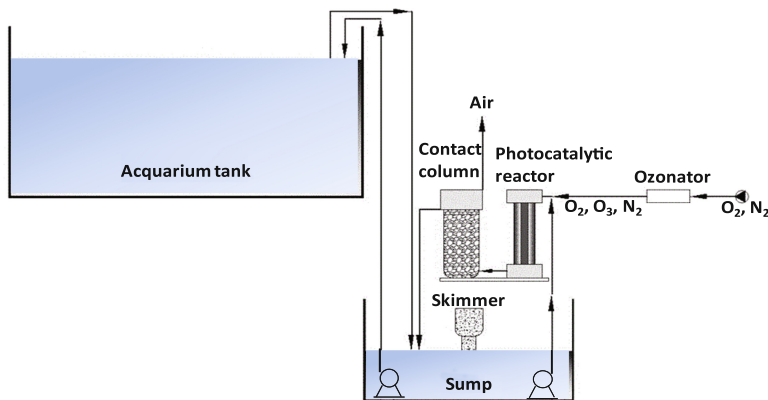
Fig. 1. Scheme of the system

with an emission peak at 365 nm. The radiation intensity was about 24 $W \cdot m^{-2}$. Glass beads (diameter 4 mm) covered with a TiO_2 film were packed into the annulus between the two tubes. The ozonator, fed with air and working on the basis of corona discharge effect, produced 10 $L \cdot h^{-1}$ of an ozone containing gaseous mixture. Water exiting the reactor circulated through a contact column in order to get rid of the residual ozone. Water quality was monitored by measuring different parameters as pH, water hardness, oxidation-reduction potential (ORP), concentration of phosphate, of ammonia, of nitrates and of nitrites. Ozone concentration in the liquid phase was estimated by measuring the absorbance at 421 nm by means of a UV-vis spectrophotometer. Bromate concentration was measured according to the method reported by Brookman et al. [6]. Total organic carbon (TOC) values were measured by means of a Shimadzu TOC analyzer. Finally, absorbance at 254 nm was regularly measured by means of an UV-vis spectrophotometer as an indication of the concentration of dissolved organic compounds (DOC).

3 Results and Discussion

The following procedure has been performed for a quite long period: photocatalysis alone has been applied during the day whereas photocatalytic ozonation was carried out for three hours during the night. In this way it was possible to virtually avoid bromate ion formation whilst maintaining significant purification rates. Indeed, photocatalysis working alone is able to reduce bromate ions, possibly formed in the presence of ozone, to innocuous bromide ions. On the other hand, as previously mentioned, photocatalytic ozonation affords purification yields higher than those obtained with the two processes working in series [3]. Results are reported in Fig. 2.

In the absence of photocatalysis and/or ozonation (see region A) it is observed the accumulation of organic compounds recalcitrant to biological (biological filter) or physical (skimmer) treatments. Indeed, the absorbance in the first period increased with a growing yellowish appearance. Conversely, when photocatalysis and/or ozonation
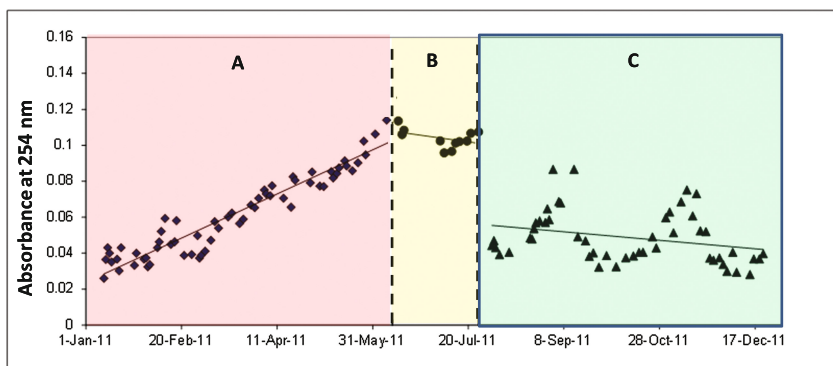
Fig. 2. Time evolution of the 254 nm absorbance of the water in the tank from January to December 2011. Ote that the values of the absorbance are representative the dissolved organic compounds concentration. Region A without photocatalysis and ozonation; region B with photocatalysis alone; region C with photocatalytic ozonation.

were applied water resulted clear and colourless. In fact, both photocatalysis or ozonation were able to limit the presence of dissolved organics as it can be noticed from the decrease of the absorbance in regions B and C. In particular, when photocatalysis and ozonation were simultaneously applied (region C) the purification efficiency looks to be highly efficient.

Notably, ozonation was able also to avoid any fouling of the photocatalytic fixed bed as ozone is able to oxidize the organic matter adsorbed or deposited on the TiO_2 film.

Figure 3 reports two representative tests. In the plot A the trend of ORP and of bromate ions concentration was monitored versus the reaction time. Samples were taken from the sump. Only ozonation was applied in the first 180 min, then the ozonator was turned off and the lamp of the photocatalytic reactor was switched on. In the presence of ozone, in the dark both the bromate concentration and the ORP values increased. On the other hand, when ozonator was switched off and photocatalysis was applied both values rapidly decreased. However, in the experiment carried out in the aquarium it cannot be excluded that the water flowing from the tank into the sump diluted both the bromate and the oxidizing species thus contributing to the decrease of their concentrations. In order to check this hypothesis some tests were performed in a separate configuration. In particular, 1 L seawater solution containing ca. 200 ppm of formic acid as a model organic compound and 18 ppm of bromate ions was recirculated in the photocatalytic reactor. The concentrations of formic acid and of bromate ions are reported in Fig. 3(B) versus reaction time. Results show that in presence of the sole photocatalysis an efficient bromate reduction take place together with a decrease of formic acid concentration. This demonstrates that alternating cycles of ozonation and photocatalysis enables efficient bromate control even in the real conditions of a reef coral aquarium. Furthermore, as demonstrated in the relevant literature [3], process intensification occurs for the degradation of organic compounds when photocatalysis is carried out in the presence of ozone.
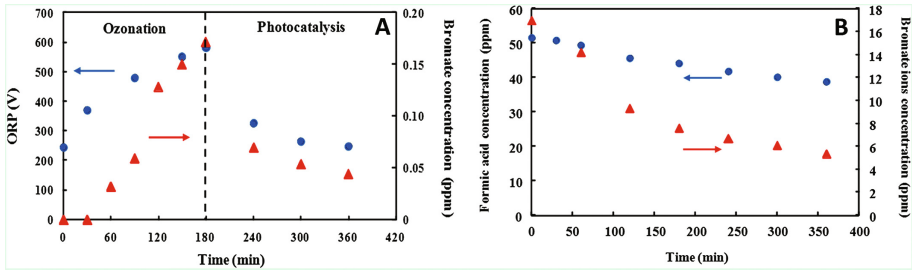
Fig. 3. (A) ORP values (V) and bromate concentration (ppm) versus reaction time for a run carried out in the reef coral aquarium where ozonation and photocatalysis were sequentially applied. (B) Formic acid and bromate ion concentrations (ppm) for a photocatalytic run carried out in 1 L seawater solution.

The durability of the photocatalytic bed was tested by comparing the degradation of formic acid versus reaction time. The activity of the photocatalytic bed was ca. 60% of the initial one after 18 months of use. Notably, the activity may be totally restored after washing with an acidic aqueous solution followed by 2 h ozonation in demineralized water. Last but not least, the living organisms present in the aquarium never showed any sign of sufferance during two years of experimentation. Further investigations are ongoing in order to check the capabilities of photocatalytic ozonation for the microbial disinfection of the aquarium water.

4   Conclusions

Photocatalytic ozonation was successfully applied for the purification of the water in a 180 L reef coral aquarium working as a closed system. The two year lasting investigation highlighted positive performances in view of future real applications in the field of sustainable aquaculture, water potabilization etc. The proposed advanced technology is simple and of easy automation. Other interesting features are: reasonable operative costs; possibility of using sunlight to activate the process; prompt start of the process without the lag which is typical of the biological treatments; minimal maintenance; limited aging of the photocatalytic material with possibility of its regeneration; optimal levels of oxygen and ORP for the living organisms; easy control of bromate formation.

References

1. Martins CIM, Eding EH, Verdegem MCJ, Heinsbroek LTN, Schneider O, Blancheton JP, Roque d'Orbcastel E, Verreth JAJ (2010) New developments in recirculating aquaculture systems in Europe: a perspective on environmental sustainability. Aquacu Eng 43:83–93
2. Pichat P (2013) Photocatalysis and water purification: from fundamentals to applications. Wiley, Weinheim

3. Parrino F, Camera-Roda G, Loddo V, Augugliaro V, Palmisano L (2015) Photocatalytic ozonation: maximization of the reaction rate and control of undesired by-products. Appl Catal B: Environ 178:37–43
4. Butler R, Godley A, Lytton L, Cartmell E (2005) Bromate environmental contamination: review of impact and possible treatment. Crit Rev Environ Sci Technol 35:193–217
5. Parrino F, Camera-Roda G, Loddo V, Palmisano G, Augugliaro V (2014) Combination of ozonation and photocatalysis for purification of aqueous effluents containing formic acid as probe pollutant and bromide ion. Water Res 50:189–199
6. Brookman RM, Mcclintock AM, Gagnon GA (2011) A method for the detection of bromate in brackish water. Aquac Eng 45:9–12

Efficient Treatment of Synthetic Wastewater Contaminated with Emerging Pollutants by Anaerobic Purple Phototrophic Bacteria

I. de las Heras[1,2], B. Padrino[1], R. Molina[1], Y. Segura[1], J.A. Melero[1], A.F. Mohedano[2], F. Martínez[1], and D. Puyol[1(✉)]

[1] Group of Chemical and Environmental Engineering,
University Rey Juan Carlos, Madrid, Spain
daniel.puyol@urjc.es
[2] Chemical Engineering Section,
University Autonoma of Madrid, Madrid, Spain

Abstract. This work investigates the biological treatment of synthetic wastewater contaminated with emerging pollutants (EPs) by anaerobic purple phototrophic bacteria (PPB) in a continuous photo-anaerobic membrane bioreactor. The effect of the hydraulic retention time (HRT) on the reactor performance has been analysed. Results indicate that the reactor performance is stable and the PPB can settle inside the reactor. A COD removal efficiency higher than 90% is achieved at a HRT of 24 h. Lowering the HRT to 12 h caused an initial drop of the COD efficiency that was subsequently recovered along the curse of the experiment. Biomass showed a high activity (close to 1 g COD/g COD d) and good settling characteristics when the attached growth was avoided, indicating a good link to downstream processes. Anaerobic digestion of PPB biomass was performed by dedicated BMP tests. Results indicate that lowering the HRT considerably improves the biogenic methane potential, presumably due to accumulation of organic compounds. A further analysis of EPs balances is being carried out and will show the fate of these compounds within the reactor.

Keywords: Anoxygenic purple phototrophic bacteria · Emerging pollutants · Novel wastewater treatment concept

1 Introduction

New concepts of wastewater treatment plants (WWTP) try to change the perspective of wastewater management from decontamination to opportunity by addressing energy neutrality (or even positivity) and maximizing resource recovery (Puyol et al. 2017). Purple phototrophic bacteria (PPB) are a novel biological vector to achieve these goals by assimilation (growth and accumulation) rather than dissipation (oxidation/reduction processes) of both organic and inorganic compounds. PPB have a very versatile metabolism and can use low-energy infrared light to perform all their biological activity. They have a high biomass growth yield (maximizing C and N assimilation), and can accumulate nutrients as P and K. Additionally, they can accumulate bioplastics and

produce H_2 as an electron acceptor to regulate their redox state. Therefore, they have been proposed to be a main actor in novel WWTPs concepts (Batstone et al. 2015).

PPB has been used for treating industrial wastewater of various nature in different engineered systems (Chitapornpan et al. 2012). Also, PPB have been recently used for domestic wastewater treatment with an infrared photo-anaerobic membrane bioreactor (PAnMBR) (Hülsen et al. 2016a), where major mechanisms for WW depuration involve assimilative (non-destructive) processes. This generates a high volume of sludge that can be used as feedstock for anaerobic digestion, or can be downstream processed to obtain raw matter to be used as organic fertilizers or food additives (Puyol et al. 2017). On the other hand, emerging pollutants (EPs) in wastewater (WW) are not commonly monitored because they are still not regulated and their concentration is extremely low. However, their continuous discharge, accumulation and synergistic combination can cause adverse effects to the environment and/or to the human being. Typical examples of EPs are pharmaceuticals, pesticides, surfactants, food additives or solvents, and once these compounds flow into domestic WWTPs their efficient removal is difficult and costly. Therefore, efforts are being driven towards controlling their propagation in the original sources of contamination (Deblonde et al. 2011). However, WWs containing EPs may suppose a problem since the concentration of these contaminants in the sludge may dramatically increase unless the biomass actively metabolize them. Currently there are no studies analysing the use of PPB for treating EPs-contaminated wastewater. Therefore, the aim of this study is to analyse the biological treatment of a synthetic wastewater (SWW) contaminated with EPs by means of a PPB-based PAnMBR.

2   Materials and Methods

Domestic wastewater (DWW) was used as inoculum, whose average composition (n = 5) was: 312 mg total COD (TCOD)/L, 123 mg soluble COD (SCOD)/L, 93 mg SST, 75 mg SSV, 39 mg NH_4^+-N/L and 4.2 mg PO_4^{3-}-P/L. SWW composition was based on a comprehensive analysis of a real vegetables processing wastewater, as follows (mg/L): F^- (0.25), Cl^- (280), Br^- (12), NO_3^- (50), SO_4^{2-} (50), PO_4^{3-} (16.8), Na^+ (165), NH_4^+ (0.7), K^+ (110), Mg^{2+} (10), Ca^{2+} (50), TOC (150). TOC was added as a mixture of acetate, propionate, butyrate, ethanol and yeast extract (1:1:1:1:0.1 by COD). Turbidity (100 NTU) was supplemented by adding 100 mg kaolin/L. Trace metals were also supplemented as follows (mg/L): H_2BO_3 (2.8), $MnCl_2 \cdot 4H_2O$ (2.03), $(NH_4)_6Mo_7O_{24} \cdot 4H_2O$ (0.55), $ZnCl_2$ (0.11), $CuCl_2 \cdot 2H_2O$ (0.028), EDTA (2). Resulting TCOD and SCOD values averaged (n = 19) 349 and 261 mgCOD/L, respectively. EPs were added at 50 ng/L from a 50 ug/L mixture of the following compounds: 4-acetamidoantipyrine, acesulfame K, amoxicillin, atenolol, atrazine, azithromycin, azoxystrobin, bisphenol A, caffeine, carbamazepine, ciprofloxacin, clofibric acid, cyclophosphamide, DEET, diclofenac, dimethoate, estron, gemfibrozil, HHCB (galaxolide), hydrochlorothiazide, ibuprofen, imidacloprid, iohexol, iopamidol, isoproturon, metamitron, metoprolol, metronidazole, progesterone, PFOA, ranitidine, simazine, sucralose, sulfamethoxazole, sulpirida, terbutryn, triclosan, tris-chloroethyl-phosphate (TCEP), methiocarb, procymidone, thiamethoxam, buprofezin and iprodione.

An automatized PAnMBR reactor was operated for 80 d. The reactor design is based on a previous work (Hülsen et al. 2016a). The reactor was covered with a UV/VIS filtering foil and was illuminated with two 150 W IR lamps. Temperature was not controlled, and varied between 33 and 36 °C. Anoxygenic conditions were ensured by flushing the reactor with N_2. The solid retention time was fixed after the acclimation period to a value of 4 d, maintaining a biomass concentration higher than 1 g VSS/L. The experimental design is summarized in Table 1.

Table 1. Experimental design of the PAnMBR operation. Values in brackets are standard deviations

Stage	Wastewater	Time (d)	HRT (d)	T (°C)	TCOD (mg/L)	pH
PPB Enrichment	DWW	8	1.0 (0.0)	33.4 (2.5)	312 (193)	7.5 (0.1)
Acclimation	SWW	31	1.0 (0.1)	34.4 (1.6)	305 (203)	6.5 (0.3)
Stage 1	SWW + EPs	14	1.1 (0.1)	35.2 (2.6)	328 (88)	6.9 (0.1)
Stage 2		23	0.5 (0.1)	33.4 (3.2)	345 (60)	6.9 (0.1)

Phototrophic activity experiments were performed by using a modified Ormerod medium described elsewhere (Hülsen et al. 2016b). 500 mg acetate-COD/L was used as substrate. Specific activities (k_M, gCOD/gCOD d) were estimated by using Aquasim 2.1d.

Biomethane potential (BMP) tests were performed following the recommendations of Angelidaki et al. (2009). An inoculum to substrate (I/S) ratio of 2:1 was chosen. Biomass was extracted from the PAnMBR, centrifuged and maintained at 4 °C before BMP tests, then used as sole substrate during the anaerobic digestion. Kinetic parameters (hydrolysis constant, k_H, in 1/d; and BMP, in mL CH_4/gVS), 95% confidence intervals and 95% confidence regions were estimated by using Aquasim 2.1d according to Batstone et al. (2003)

COD, TSS/VSS, TKN and SVI were measured following standard procedures. NH_4^+, PO_4^{3-} and TP were measured by Merck® kits. CH_4 and CO_2 were measured by GC/TCD. BMP overpressure was measured by a digital pressure-meter directly injected into the headspace. Irradiance was measured with a spectroradiometer. Biomass spectra was analysed by VIS-NIR spectrometry.

3   Results and Discussion

The PAnMBR reactor followed different operative stages. Figure 1 shows the time course of organic loading rate (OLR) and COD removal efficiency along the reactor operation. The PAnMBR needed 8 days to achieve a stable PPB biomass, and 30 d to achieve the steady state at a HRT of 1 d. Thereafter, EPs and turbidity (through kaolin) were supplemented into the system. Reactor performance remained invariable during the first stage, working at HRT of 1 d, averaging COD removal efficiencies of 86%. When the HRT was reduced to 0.5 d, the COD efficiency dropped dramatically down to 33% and was subsequently recovered until achieving efficiencies closed to 90%. This indicates that this anaerobic reactor is able to operate under a hydraulic regime similar to activated sludge. The PPB biomass development was key to achieve a stable operation.
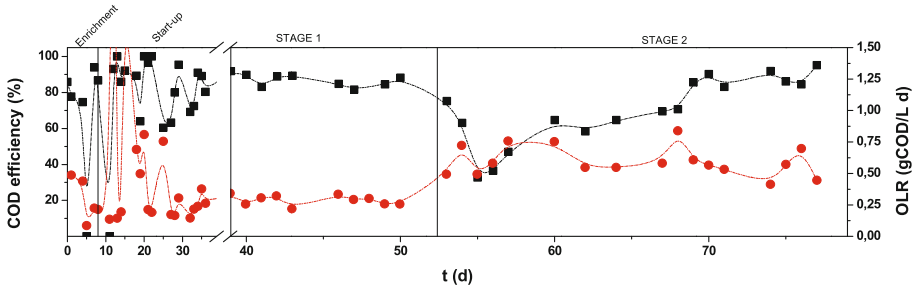
Fig. 1. Effect of the organic loading rate (OLR, circles) on the COD removal efficiency (squares)

The analysis of PPB biomass development was performed qualitatively by measuring the VIS-IR spectra of biomass samples from the reactor. Figure 2 illustrates a continuous settlement and consolidation of the PPB biomass. The original inoculum quickly changed to a PPB-based sludge as indicated by the appearance of two peaks in the NIR (Fig. 2a), at 805 and 850 nm. These wavelengths correspond to bacteriochlorophyll A (typically found in purple phototrophic bacteria), and are a clear sign of PPB enrichment. After switching from DWW to the SWW, the PPB biomass initially underwent a regression, but was gradually recovering until settling in the sludge community (Fig. 2b). There were few changes during the stage 1. Decreasing the HRT to around 0.5 d in the stage 2 caused a general decrease in biomass (the absorbance for any wavelength decreased). However, the two bacteriochlorophyll A peaks not only remained, but also their intensity was gradually increasing along the stage 2 (Fig. 2c). This confirms that the hydraulic regime (and possibly the increase of the substrate loading rate) caused a positive effect on the development of the PPB biomass. Under anaerobic conditions and lack of visible irradiation, PPB can settle and dominate organic environments due to their high growth rate and their metabolic versatility. Other anaerobes, especially the acetate consumers, cannot compete with PPB, and are ultimately washed out from the reactor due to the low SRT imposed (4 d).
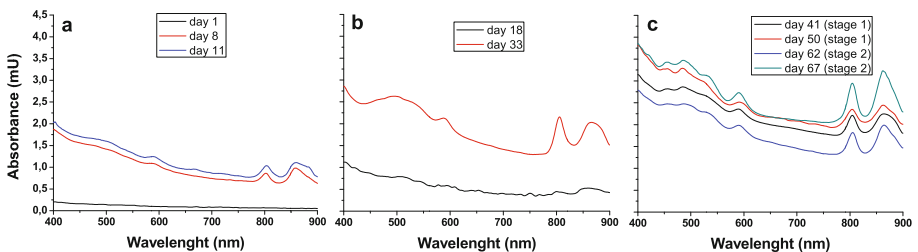
Fig. 2. VIS/NIR biomass spectra indicating PPB development (a), settlement (b) and consolidation (c) during the enrichment, the start-up and the designed operation of the PAnMBR, respectively

To assess biomass recovery for downstream processes, PPB growth was analysed. Figure 3 depicts the biomass distribution along the reactor (suspended sludge), and surface membrane and reactor walls (attached biomass). During the start-up (uncontrolled growth), the biomass was preferentially colonizing reactor walls due to maximum exposure to irradiation. During the stable operation of the reactor the biomass attached to the walls and those forming biofilms on the membrane were detached once per week. Thereafter, the VSS proportion inside the reactor vessel was completely inversed, and most of the biomass (above 70%) was growing inside the reactor. This also caused two effects in the PPB behaviour. The phototrophic specific activity of the biomass significantly increased from 0.59 to 0.97 g COD/gCOD d, and the biomass growth yield remained almost constant (0.91 vs 0.88 gCOD/gCOD). Also, the COD/N/P ratio of the biomass varied from 100/5.1/2.5 to 100/6.2/3.7. This indicates that limiting the biofilm formation enhances the biomass growth, and possibly the nutrients removal by accumulative processes linked to growth. Additionally, the SVI greatly enhanced up to achieving 6.9 mL/gVSS, may be due to increase in the hydraulic sheer force that obligates the biomass to nucleate and form bacterial aggregates that ease the sludge settleability. This obviously can also improve further downstream processes.
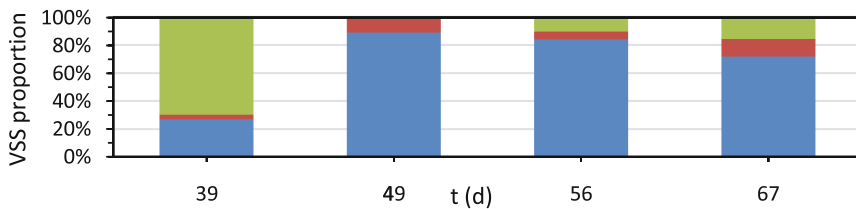
Fig. 3. VSS distribution between reactor (blue), membrane (red) and walls (green) in the PAnMBR before (day 39th) and after (day 49th, stage 1; days 56 and 67, stage 2) controlling the biofilms formation inside the reactor (Color figure online)

Energy recovery was assessed by dedicated BMP tests. Figure 4 shows the time course of BMP and simulation curves with optimized parameters values (Fig. 4a) and the confidence regions (at 95% threshold) for hydrolysis constants and maximum BMP calculated by t-tailed least-squares minimization. As shown, it is evident that lowering the HRT entailed an increase of the biomethane potential of the PPB sludge. Values of BMP varied from $136 \pm 4\,6$ mL CH_4/gSV at early stage of the start-up stage (with an average HRT of 1 d) to 227 ± 6 mL CH_4/gSV at the end of the second stage, after achieving steady-state with an HRT of 0.5 d. This basically means that the promotion of PPB biomass growth by HRT lowering (e.g. increasing the organic loading rate) while maintaining constant the biomass concentration inside the reactor considerably improved the digestibility of the PPB biomass. Kinetics of the AD process also were considerably enhanced, as can be deduced by the statistically significantly increase of the k_H parameter value from 0.22 ± 0.02 1/d at the beginning of the start-up process to 0.29 ± 0.03 1/d at the end of the stage 2. Hydrolysis of actively growing bacteria is suggested to be boosted since growing bacteria are more dedicated to replication and cell division rather than to
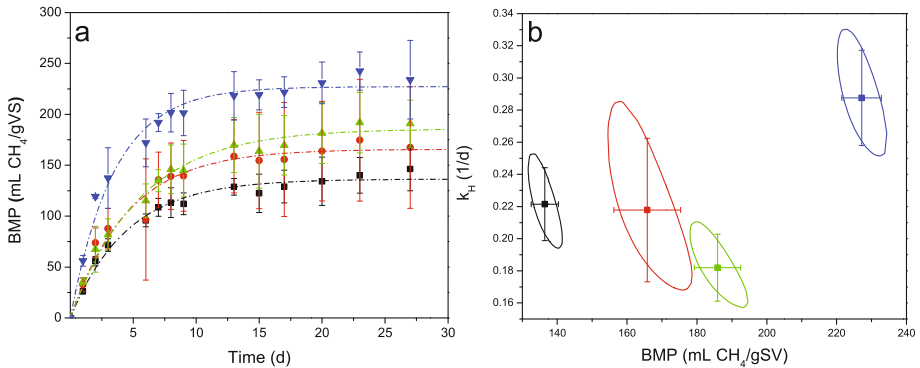
Fig. 4. Biochemical methane potential of PPB sludge at different experimental stages: start-up (days 27, 28, 29 and 39, black), stage 1 (days 42, 47 and 49, red), early stage 2 (days 57 and 67, green) and late stage 2 (days 69, 75 and 77, blue). Time course of BMP (symbols) and simulation curves (dash-dot lines), where error bars are 95% confidence intervals from triplicate measurements (a); and 95% confidence regions of k_H and BMP values, where error bars are uncorrelated, linear parameter 95% confidence regions (b) (Color figure online)

bacterial wall development. Also, a lower HRT may promote active accumulative processes in PPB bacteria like the production of biopolymers as PHA or glycogen, which are easier to be anaerobically digested and converted into biogas.

4 Conclusions and Future Work

This work shows that a PPB-based PAnMBR is a promising option to treat wastewater contaminated with EPs even at a HRT of 0.5 d. PPB biomass can settle and the reactor performance is stable. Energy recovery (through anaerobic digestion) can be considerably enhanced by lowering the HRT of the reactor. This has critical connotations on the applicability and energetic sustainability of PPB to treat low-strength wastewater (as domestic wastewater and some industrial as pharmaceutical or hospital wastewater).

Future analysis will show the fate of the EPs in the system. EPs contained in the influent, effluent and in the biomass (after bacterial lysis and extraction) are being analysed by HPLC-MS/MS, thereby a mass balance will indicate if the EPs are absorbed into the biomass, biodegraded, or retained in the reactor membrane. Preliminary analysis on batch tests showed that PPB biomass is a promising option to reduce the EPs contamination in low-strength wastewater, as this biomass could considerably reduce (elimination higher than 80%) the presence of up to 45 EPs typically found in hospital wastewater (data not shown). Also, the evolution of the biomass is currently being comprehensively characterized by DGGE by using the puF gene (targeting PPB), and by 16-S Illumina massive sequencing to analyse the biodiversity and the dominance of the bacterial groups.

References

Angelidaki I, Alves M, Bolzonella D, Borzacconi L, Campos JL, Guwy AJ, Kalyuzhnyi S, Jenicek P, Van Lier JB (2009) Defining the biomethane potential (BMP) of solid organic wastes and energy crops: a proposed protocol for batch assays. Water Sci Technol 59(5):927–934

Batstone DJ, Hülsen T, Mehta CM, Keller J (2015) Platforms for energy and nutrient recovery from domestic wastewater: a review. Chemosphere 140:2–11

Batstone DJ, Pind PF, Angelidaki I (2003) Kinetics of thermophilic, anaerobic oxidation of straight and branched chain butyrate and valerate. Biotechnol Bioeng 84(2):195–204

Chitapornpan S, Chiemchaisri C, Chiemchaisri W, Honda R, Yamamoto K (2012) Photosynthetic bacteria production from food processing wastewater in sequencing batch and membrane photo-bioreactors. Water Sci Technol 65(3):504–512

Deblonde T, Cossu-Leguille C, Hartemann P (2011) Emerging pollutants in wastewater: a review of the literature. Int J Hyg Environ Health 214(6):442–448

Hülsen T, Barry EM, Lu Y, Puyol D, Keller J, Batstone DJ (2016a) Domestic wastewater treatment with purple phototrophic bacteria using a novel continuous photo anaerobic membrane bioreactor. Water Res 100:486–495

Hülsen T, Barry EM, Lu Y, Puyol D, Batstone DJ (2016b) Low temperature treatment of domestic wastewater by purple phototrophic bacteria: Performance, activity, and community. Water Res 100:537–545

Puyol D, Batstone D, Hülsen T, Astals S, Peces M, Krömer J (2017) Resource recovery from wastewater by biological technologies: opportunities, challenges and prospects. Front Microbiol 7(2106)

Studies on Treatment of Bitumen Effluents by Means of Advanced Oxidation Processes (AOPs) in Basic pH Conditions

G. Boczkaj[1(✉)], A. Fernandes[1], and M. Gągol[2]

[1] Department of Chemical and Process Engineering, Chemical Faculty,
Gdansk University of Technology, Gdansk, Poland
[2] Department of Polymers, Chemical Faculty,
Gdansk University of Technology, Gdansk, Poland

Abstract. The paper presents the results of studies on chemical treatment of effluents from production of bitumen of petroleum origin. Due to the presence of sulfide ions, the pH of these effluents is strongly alkaline. Several Advanced Oxidation Processes (AOPs) were studied, including the use of hydroxyl and sulfate radicals oxidants, the hydrodynamic cavitation as well as sonocavitation. The best processes allow to obtain 45% reduction of chemical oxygen demand value (COD) along with effective degradation of the majority of the volatile organic compounds present in the effluents. Some of the studied processes, especially the one using sonocavitation revealed to produce high amounts of VOCs by-products.

Keywords: Wastewater treatment · AOP · Cavitation · VOC · Bitumen

1 Introduction

Petroleum or refinery effluents are well known to be highly polluted and to contain several groups of organic compounds, including a significant amount of volatile organic compounds (VOCs) [1, 2]. A particularly important group of refinery effluents are produced in an alkaline medium, like spent caustic [3] and post oxidative effluents [4]. This strong alkaline pH results from the need of quantitative absorption of hydrogen sulfide, present in the form of S^{2-}. The pH correction to neutral or acidic values is not preferred due to the production of hydrogen sulfide which can be emitted to the atmosphere. Such effluents have also a high total load of organic pollutants and can't be purified directly by biological wastewater treatment processes. Therefore effective, alternative, easy and cheap technologies are needed to treat these sewages at their natural pH in order to reduce their toxicity and even to increase the range of pH where such effluents can be treated.

This paper is focused on the comparison of a few alternative Advanced Oxidation Processes (AOPs) effectiveness in the treatment of effluents from production of bitumen (a post-oxidative effluents). The production of bitumens involves oxidation of residue from vacuum distillation of crude oil to obtain products with desired properties. During operations yielding the raw material for bitumen production (vacuum distillation) as

well as the process of oxidation with hot air, the bitumen mass deposited on heating elements undergoes partial thermal cracking, which results in the formation of unsaturated and aromatic compounds as well as hydrogen sulfide, water vapor, carbonyl sulfide, carbon disulfide and others. These compounds undergo further transformations yielding a variety of volatile compounds: ketones, aldehydes, organic acids, phenols and their derivatives, as well as organosulfur and organonitrogen compounds. A fraction of the resulting volatile compounds is removed from the reactor with hot air, yielding so-called exhaust gases, which undergo scrubbing in a basic aqueous solution or absorption in wash oil [4]. If the scrubbing of waste-gases is made using the aqueous solution (mainly of sodium hydroxide), a specific effluents from bitumen production are formed (a so-called post-oxidative effluents). Such effluents contain a condensed oil phase (removed by plate-separator), sulfide ions and organic compounds dissolved in the water phase. Such stream are an interesting subject of the research in the field of WWT but also on the chemical composition of the effluents as well as the pathways of oxidation of selected groups of compounds during chemical treatment.

The studied AOPs include non-catalytic and catalytic oxidation using hydrogen peroxide, ozone and sulfate based oxidants with connection of photooxidation processes as well as cavitation phenomena. The use of cavitation phenomena for wastewater treatment (WWT) is a promising approach and in this studies a two groups of such processes – hydrodynamic cavitation and sonocavitation were studied. A recent study revealed that classic AOPs using ozone were more effective than other processes in the treatment of model and real WW at basic conditions. In addition the sulfate radical based AOPs can include a wider pH range of treatment and further studies on real WW is suggested [3]. We are a first research team, that studies this type of industrial effluents. Surprisingly, such interesting industrial and environmental issue never earlier has been discussed in the scientific literature.

2   Materials and Methods

In this studies a real post oxidative sewages from bitumen production plant from Lotos Asfalt (Grupa Lotos, Poland) were used (COD - within the range of 18.000–22.000 mg/L; BOD within the range of 5000–6000 mg/L, pH 10.5.). Hydrogen Peroxide 30%, Sodium Sulfite nonahydrated ($Na_2S.9H_2O$), Sodium Persulfate ($Na_2S_2O_8$) and Potassium Peroxymonosulfate ($KHSO_5$) were purchased from POCH Poland.

2.1   AOP Apparatus

The studies were performed using a three large-laboratory scale installations, (1) a one using a tank reactor for classic AOPs (Fig. 1) (2) a second one for hydrodynamic based AOPs (Fig. 2) (3) a third one for sonocavitation based processes (kindly provided for this research by Bandelin company) (Fig. 3).

The equipment used for the process analytics is fully described in our previous papers [4–8].

Fig. 1. A batch reactor for classic AOPs. 1 - reactor, 2 - control panel (mixing and temperature), 3 - pump for oxidant, 4 - ozonator, 5 - pump for effluents

2.2 Sewage Treatment

In every procedure, a volume of 5 dm^3 was used. For reactor (1) the sewages were pumped to the reactor, working in a batch mode. The installations (2) and (3) were operated in batch mode with recirculation of the effluents through a sonocavitation or hydrodynamic cavitation chamber.

All procedures were done at an initial pH of 10.5. Regarding the oxidant dose, the flowrate was established depending on the ratio between the oxygen (O_2) added from the oxidant source and the COD in the sewages (r_{ox}). Samples with a total volume of 0.022 dm^3 were taken before the beginning of treatment, 15 min in the first hour of treatment, at 90 min, 120 min, and every hour after 120 min and at the end of the treatment. The treatment time depended on the r_{ox}. The pH was measured by pH strips in every sample taken.

Fig. 2. A hydrodynamic cavitation reactor. 1 - effluent tank, 2 - control panel (mixing, temperature, volumetric flow), 3 - pump for effluents, 4 - pressure control, 5 - Venturi tube, 6 - flow control
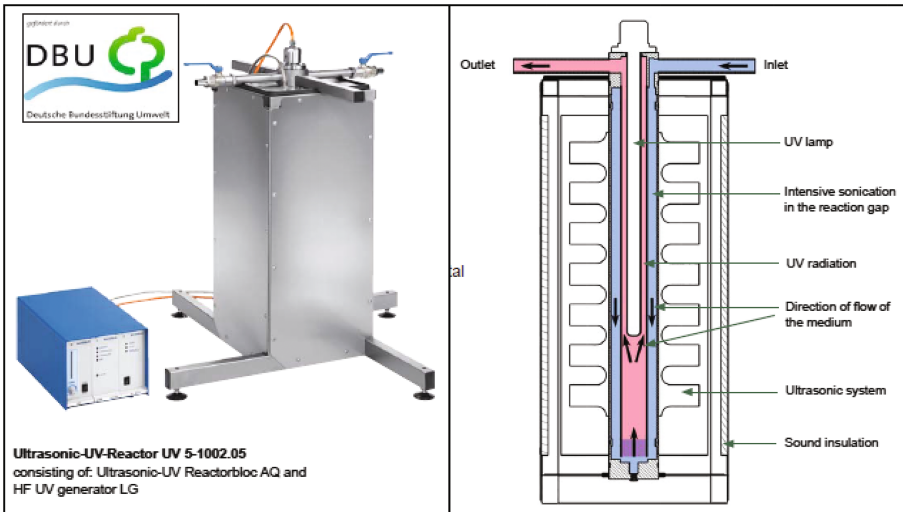

Fig. 3. A Sonocavitation reactor

2.3   Process Analytics

All analytical methods used in these studies are described in details in our previous papers [4–8]. Generally, the COD, BOD and Sulfides were controlled by standard test methods. VOCs were analysed by means of gas chromatography (GC) with selective detectors as well as mass spectrometry (MS).

3   Results and Discussions

The effluents from a bitumen production were submitted to treatment by various types of AOPs. The parameters under study were the influence of the oxidant to COD ratio (r_{ox}), the type of oxidant and the temperature of the process on the degradation effectiveness (for batch mode reactor). For hydrodynamic cavitation processes the results of treatment were also compared with cavitation number. The parameters used for determining the efficiency of the treatments were COD, BOD, $[S^{2-}]$ and selected groups of VOCs such as oxygen containing (O-VOCs), sulfur (VSCs) and nitrogen (VNCs) controlled by GC technique.

The studies revealed that in the case of "classic" AOP (non-cavitation assisted) peroxone (a H_2O_2 and O_3 introduced in the same time) at 40 °C achieved 43% and 36% of COD and BOD removal resulting to be the most effective studied AOP from this group. The used r_{ox} was 1.02. In all studied processes the sulfide ions were quantitatively oxidized in the first 15 min of treatment. Regarding the volatile sulfur compounds (VSCs), they achieved high degradation removals, with values after treatment bellow the limit of detection values of used analytical methods. In the case of O-VOCs and VNCs some compounds were identified as a secondary pollutants, which concentration was increasing during the treatment.

In the case of sulfate radicals AOPs (S-AOPs), peroxymonosulfate with a r_{ox} of 1.43 at 60 °C achieved 43% COD and BOD removal resulting to be the most effective AOP studied. These type of oxidants can be activated by the temperature of the medium, thus the amount of sulfate radicals available for reaction with pollutants is increased at elevated temperatures. Persulfate is more effective for studied purpose than peroxymonosulfate in terms of r_{ox} and temperature. This results mainly from higher E° value of persulfate. In comparison with classic AOPs persulfate and peroxymonsulfate achieved higher degradation but needed higher r_{ox}.

The sole use of cavitation phenomena (induced by flow or ultrasounds) for degradation of chemical compounds present in the effluents from bitumen production allows to lower the COD by 13%. The hydrodynamic cavitation allows to degrade more effectively VOCs, but what is more important – without production of new volatiles as by-products. Coupling cavitation with oxidation by external oxidants allows to lower the COD by approx. 44%.

In overall, in most of the studied processes a high degradation of VOCs was achieved. The studied AOPs effectively reduce the total load of pollutants but also allow to decrease the total content of volatile organic compounds. This is particularly important and have a practical value – it lowers the malodorness of the sewages. It is important in the case of next stages of treatment which are mainly the biological processes. The biological stage is often performed at open-air reservoirs, which causes emission of VOCs to the atmosphere. The decrease of content of VOCs as well as the decrease of total load of pollutants makes the studied processes have applicational value for real wastewater treatment plants.

4   Conclusions

Effluents from bitumen production are an interesting type of wastewater. They contain a wide variety of organic compounds sulfide, and from that reason the chemical treatment must be performed in strongly basic pH. The studies revealed, that it is possible to pre-treat this effluent with effectiveness up to 45% in respect to COD. Further increase of degradation is hard to obtain due to the presence of hydrocarbon type compounds which a persistent to degradation in the studied conditions. A comparison of processes revealed significant changes in respect to degradation of selected VOCs as well as possibility of by-products formation.

References

1. Saien J, Shahrezaei F (2012) Organic pollutants removal from petroleum refinery wastewater with nanotitania photocatalyst and uv light emission. Int J Photoenergy 2012:1–5
2. Shahrezaei F, Mansouri Y, Zinatizadeh AAL, Akhbari A (2012) Process modeling and kinetic evaluation of petroleum refinery wastewater treatment in a photocatalytic reactor using TiO2 nanoparticles. Powder Technol 221:203–212
3. Boczkaj G, Fernandes A (2017) Wastewater treatment by means of Advanced Oxidation Processes at basic pH conditions: a review. Chem Eng J (accepted manuscript). doi:10.1016/j. cej.2017.03.084
4. Boczkaj G, Kamiński M, Przyjazny A (2010) Process control and investigation of oxidation kinetics of postoxidative effluents using gas chromatography with pulsed flame photometric detection (GC-PFPD). Ind Eng Chem Res 49:12654–12662
5. Boczkaj G, Przyjazny A, Kamiński M (2014) New procedures for control of industrial effluents treatment processes. Ind Eng Chem Res 56:1503–1514
6. Boczkaj G, Makoś P, Fernandes A, Przyjazny A (2017) New procedure for the examination of the degradation of volatile organonitrogen compounds during the treatment of industrial effluents. J Sep Sci (accepted manuscript). doi:10.1002/jssc.201601237
7. Boczkaj G, Makoś P, Fernandes A, Przyjazny A (2017) New procedure for the control of the treatment of industrial effluents to remove volatile organosulfur compounds. J Sep Sci 39:3847–4052
8. Boczkaj G, Makoś P, Przyjazny A (2016) Application of dispersive liquid-liquid microextraction and gas chromatography-mass spectrometry (DLLME-GC-MS) for the determination of oxygenated volatile organic compounds in effluents from the production of petroleum bitumen. J Sep Sci 39:2604–2615

Emerging Contaminants Mineralization by a Photo-Electrochemical Method Based on WO₃

A. Molinari$^{(\boxtimes)}$, G. Longobucco, L. Pasti, V. Cristino, S. Caramori, and C.A. Bignozzi

Department of Chemical and Pharmaceutical Sciences, University of Ferrara, Via Fossato di Mortara 17, 44121 Ferrara, Italy

Abstract. WO₃ absorbs light up to 470 nm and when illuminated in the presence of water generates OH• radicals, which promote oxidation of organic pollutants, such as drugs. In the case of WO₃ photoanodes, a considerable acceleration (4–5 times) of degradation kinetics is obtained through the application of a 1.5 V potential bias, which is instrumental to optimize the charge separation within the films and to maximize holes transfer rate to the electrolyte. Moreover, after sufficiently long irradiation, complete mineralization of the organics is achieved. Photoelectrocatalysis is observed even in diluted supporting electrolyte conditions, representing the average salinity of natural freshwater samples, demonstrating the practical feasibility of this approach.

Keywords: Drug mineralization · Hydroxyl radicals · Photo-electrocatalysis

1 Introduction

Protection of water resources, of fresh and salt water ecosystems and of the water we drink and bathe in is certainly one of the cornerstones of environmental protection in the world. Moreover, rising world industrialization paralleled by the increment of world population, particularly in water scarce countries, make the reuse of wastewater a compulsory practice, which is not without drawbacks. In particular, potential health risks due to the presence of highly toxic organic pollutants and of contaminants of emerging concerns (CECs), which include pharmaceuticals, detergents, hormones, were proved challenging for conventional wastewater and recycled water treatments, which are only partially effective in their removal. Then, CECs are discharged into the environment and can have impacts on human health and aquatic organisms.

Among wide band gap semiconductors, WO₃ is able to capture visible photons up to 450–480 nm. WO₃ can be prepared as films on conductive glass (such as FTO). Moreover, band edge energy levels are suitable to drive demanding oxidation reactions (Bignozzi et al. 2013). Reaction of photo-holes with the aqueous medium followed by electron paramagnetic resonance pointed out that OH• radicals are the primary intermediates produced at the illuminated WO₃ surface (Cristino 2016). Thus, oxidation of organic and inorganic species (i.e. hole scavengers) at the WO₃ surface is likely to occur according to a OH• mediated mechanism rather than by direct reaction with

photo-holes. The possibility of carrying out a photoelectrolytic water decontamination in diluted aqueous solutions with respect to both electrolyte and contaminant target concentration has rarely been considered and to the best of our knowledge not in the case of WO_3.

In this contribution, we report on the photo-electrochemical degradation under visible light of pharmaceuticals. We show that photoelectrocatalytic process improves degradation rate with respect to the simple photocatalytic one. Conditions of visible light and of diluted supporting electrolyte show the practical feasibility of the proposed approach.

2   Materials and Methods

Transparent nanocrystalline photoanodes onto cleaned FTO glass were prepared by sequential spin coating deposition of a precursor containing H_2WO_4. Anodized WO_3 on W foils was prepared by anodization (40 V for 7 h at 40 °C). Final annealing in air at 550 °C gives photoanodes 2 mm thick.

The electrode was placed in a photoelectrochemical cell, immersed in aqueous solution (at known pH) containing the drug to be degraded (10 ppm) and the supporting electrolyte (0.1 M or 7×10^{-4} M) and irradiated both in the absence and in the presence of an applied bias. At the end of the experiment, the filtered solution was analysed by HPLC. Prolonged irradiation experiments were performed for HPLC-MS analysis.

EPR spin trapping experiments were carried out by using a Bruker ER200 MRD spectrometer and 5,5' dimethyl-pyrrolin N-oxide (DMPO, 5×10^{-2} M) as a spin trap.

3   Results and Discussion

Incident light (of suitable energy) is absorbed by the photoactive material (Fig. 1). $OH^{\bullet}$ radicals are produced independently by the excitation wavelength of the semiconductor by reaction of photogenerated holes with water. EPR spin trapping experiments point out the generation of $OH^{\bullet}$ (Cristino 2016). This photocatalytic process is still operating in the presence of a drug. Figure 2 (full symbols) reports the results obtained with atenolol (ATN) chosen as an example, but they can be successfully extended for carbamazepine, levofloxacine and others. It is seen that the two different electrodes (i.e. colloidal and anodized WO_3) display equivalent photocatalytic performances.

The application of a positive potential to WO_3 should increase exponentially the surface concentration of the photoholes (Fig. 1). This should lead to a parallel increase of the charge transfer rate reflecting the OH• production rate at the photoactive interface. Photo-electrochemical processes (applied bias of 1.5 V) in the case of ATN are reported in Fig. 2 (empty symbols) where it can be immediately appreciated the substantial acceleration of the CEC degradation rate. In fact, the degradation of ATN is almost complete after 5 h irradiation (Longobucco 2017).

HPLC–MS/MS analysis has been performed not only in the case of ATN but also for the other considered drugs in order to determine the intermediates and samples
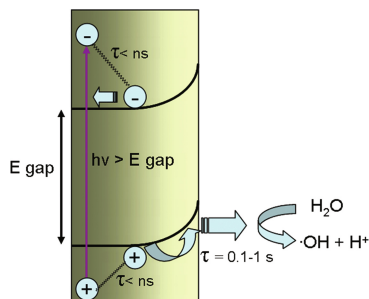
Fig. 1. Generation of charge carriers by illumination of WO_3 followed by interfacial electron transfer
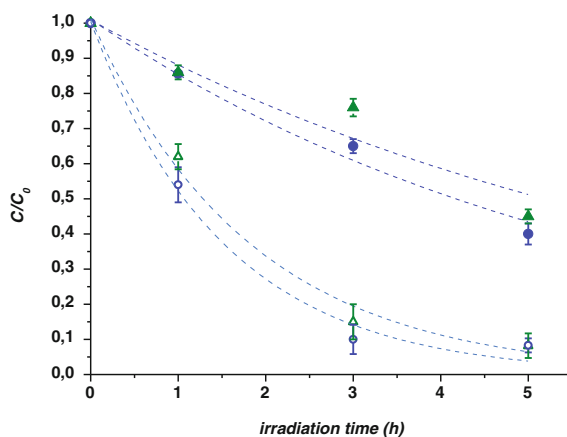
Fig. 2. Degradation of ATN (C_0 = 10 mg/L) dissolved in aqueous solution containing $NaClO_4$ (0.1 M) by irradiation (λ > 360 nm) of colloidal WO_3 deposited on FTO (▲ green) and of anodically grown WO_3 on W foils (● blue) without bias (full symbols) and with an applied bias of 1.5 V vs Pt to the photoanode (empty symbols) (Color figure online)

composed of aliquots withdrawn from photo-electrocatalytic processes, at different time intervals, were analysed. Figure 3 reports the results in the case of ATN and Table 1 collects the structures of intermediates classified according to their *m/z* ratio.

The formation of mono- and di-hydroxylated derivatives confirms that photo-electrodegradation process is mediated by OH•. Indeed, these results are also in agreement with the EPR spin trapping investigation, indicating the possible addition of OH˙ radical to the drug molecule. Since chemical standards were not available, the overall photo-oxidation process was monitored as peak intensity as a function of the irradiation time. It is seen that 90% of ATN disappeared after 5–8 h (depending on the working pH): prolonging irradiation, the peak intensities of all identified intermediates were observed to decrease as shown in the insert of Fig. 3 until no residual peaks were
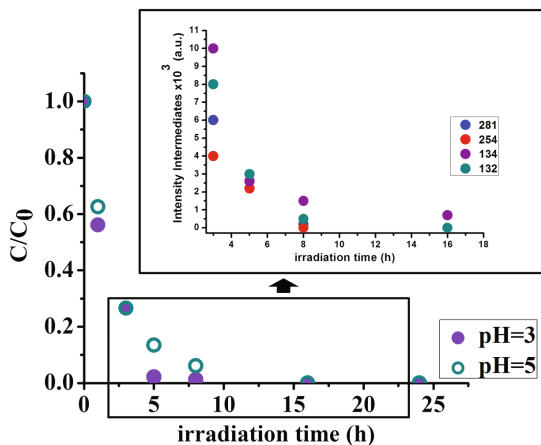
Fig. 3. Degradation of ATN (C_0 = 10 mg/L) in aqueous solutions containing $NaClO_4$ (0.1 M) at either pH 3 or 5 during irradiation (λ > 360 nm) of a WO_3 photoelectrode biased at 1.5 V vs Pt. The chromatographic peak intensity of the degradation intermediates as a function of irradiation time is reported in the inset (pH 5). See Table 1 for the structures of intermediates classified according to their *m/z* ratio
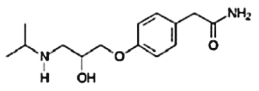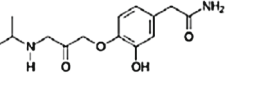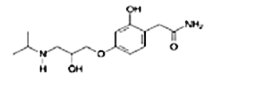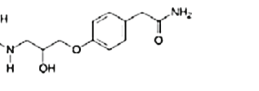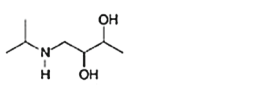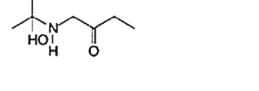
detected anymore after 15 h irradiation, indicating the occurrence of complete mineralization of the organics. This result is furthered confirmed by TOC measurement.

Since these starting experiments are promising and in order to investigate the applicability of the WO_3 based photo-electro oxidation process in conditions, which should be more representative of naturally occurring wastewaters, we consider to evaluate the process on solutions having compositions more compatible with naturally occurring environmental conditions.

Figure 4 shows the degradation kinetics of atenolol obtained in aqueous solutions at pH 6, which is the superior pH limit for the WO_3 stability, in the presence of high (0.1 M) and low (0.7 mM) Na_2SO_4 concentrations (almost universally present in natural waters). Although the first order kinetic constant for atenolol degradation decreases by increasing the pH (k = 0.65 h^{-1} at pH 3 and k = 0.41 h^{-1} at pH 6) a degradation of 85% of the starting atenolol is still observed. Moreover, the change of supporting electrolyte (from perchlorate to sulphate) has a negligible effect on atenolol photodegradation kinetic. The concentration of 0.7 mM is equivalent to the salinity of freshwaters. Interestingly, despite a ca. 5 fold reduction in the photocurrent flowing across the photo-electrochemical cell, the decay of atenolol concentration is not particularly affected by this factor, indicating that the applied bias is still effective in countering charge recombination by spatially separating photogenerated holes and electrons.

Finally, it is observed that atenolol degradation kinetic still occurs when WO_3 photoanode is illuminated with wavelengths higher than 420 nm. Interestingly, under these conditions no photocatalytic activity is usually obtained with undoped TiO_2.

Table 1. ATN degradation intermediates, retention times, fragment ions and proposed structures.

Precursor ion	t_r	MS^2	Structure
267.17	6.87	225.07 190.01 208.06	
281.15	8.39	116.19 121.08	
299.16	14.19 15.27	253.04	
254	12.5	236.20 245.15	
134	2.26	116.10	
132	1.98 2.23	86.06	
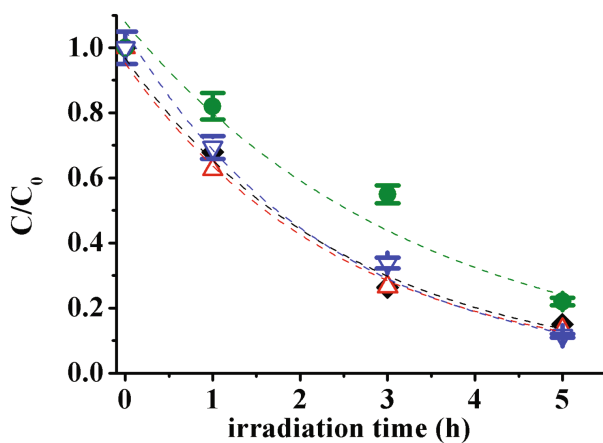
Fig. 4. Photo-electrocatalytic degradation ($\lambda > 360$ nm) of atenolol ($C_0 = 10$ mg/L) in aqueous solutions (pH 6) containing: $NaClO_4$ (0.1 M) (♦), Na_2SO_4 (0.1 M) △, Na_2SO_4 (0.7 mM) ▽, Na_2SO_4 (0.1 M) ($\lambda > 420$ nm) ● during irradiation of a WO_3 photoanode biased at 1.5 V vs Pt

4   Conclusions

In this work, we explore the possibility to carry out near UV-visible photodegradation experiments of environmentally relevant target molecules representing potentially hazardous recalcitrant CECs, by using WO_3 films. These films are able to absorb visible light up to 470 nm and to generate OH• radicals, promoting OH• mediated oxidation pathways. Even in conditions where the photocurrent generation was not optimized, like diluted supporting electrolyte (0.7 mM) that represents the average salinity of natural freshwater samples, the photo-electrochemical degradation process (applied bias condition) preserved its effectiveness, demonstrating the advantageous practical feasibility of the photo-electrochemical approach.

References

Bignozzi CA, Caramori S, Cristino V, Argazzi R, Meda L, Tacca A (2013) Nanostructured photoelectrodes based on WO_3: applications to photooxidation of aqueous electrolytes. Chem Soc Rev 42:2228–2246

Cristino V, Marinello S, Molinari A, Caramori S, Carli S, Boaretto R, Argazzi R, Meda L, Bignozzi CA (2016) Some aspects of the charge transfer dynamics in nanostructured WO_3 films. J Mater Chem A 4:2995–3006

Longobucco G, Pasti L, Molinari A, Marchetti N, Caramori S, Cristino V, Boaretto R, Bignozzi CA (2017, in press) Photoelectrochemical mineralization of emerging contaminants at porous WO3 interfaces. Appl Catal B: Environ

Effect of Increasing the Surface Area of the Graphite Electrodes on Electricity Production in a Microbial Fuel Cell (MFC) Fed with Domestic Wastewater

D. Villarreal-Martínez[1(✉)], G. Arzate-Martínez[1],
L. Reynoso-Cuevas[2], and A. Salinas-Martínez[1]

[1] Laboratorio de Biotecnología Ambiental, Avenida Universidad Sur 1001,
Universidad Politécnica de Guanajuato, Juan Alonso,
C.P. 38483, Cortázar, Gto, México
[2] S.C. Departamento de Ingeniería Sustentable,
Centro de Investigación en Materiales Avanzados,
Calle CIMAV #110, Ejido Arroyo Seco, C.P. 34147, Durango, Dgo, México

Abstract. Non-metallic carbon electrodes are widely used in the construction of Microbial Fuel Cells (MFCs) mainly due to their high conductivity and low cost. The objective of this work was to determine the effect of increasing the surface area of the electrodes (with values of R1 = 241 and R2 = 205 cm^2, achieved by making several spherical indentations on them) on the voltage generated in the MFC while treating residual wastewater. The MFC consisted of a chamber provided with four graphite electrodes connected each other by an electric circuit and a resistance of 10 Ω. The device was tested with three different initial organic matter concentrations in the wastewater (389.6, 428.6 and 453.6 mg L^{-1}) and a total process time of 8 days. The voltage generation rates were 0.29 and 0.25 mV·day^{-1} (between the 2nd and 5th day) and the maximum values of voltage registered (at 5th day) were 1.9 and 1.5 mV for R1 and R2 respectively. The organic matter removal rates were also dependent of the electrodes surface area; we obtained values of 49.6 mg.L^{-1}/day for R1 and 34.5 mg.L^{-1}/day for R2.

Keywords: Microbial fuel cells · Electrode surface area · Electricity production

1 Introduction

A Microbial Fuel Cell (MFC) is a biochemical reactor that generates electrical energy by the oxidation of organic matter in the presence of fermentative bacteria. There is a considerable quantity of reports in which the characterization of the performance of MFCs is made; in these reports, a wide variety of substrates, such as glucose, acetate, lactate or wastewater are employed (Baranitharan et al. 2014). The use of wastewater as a substrate for electricity generation is seen as a promising approach because it is a renewable energy source; nevertheless, this technology is currently in an early stage of research and development since its implementation on an industrial scale still faces technical and economic difficulties (Gonzalez et al. 2014).

As in a MFC, the microorganisms act as a catalyst in the transfer of electrons from the substrate to the anode; as a consequence, the selection of the microbial strain (either pure or in consortium) has a paramount importance in its performance. Also, the different aspects related to the design of a MFC, such as, the efficient assembly of electrodes, the use of a membrane to decrease the resistance associated with proton transfer, the effective interaction of the substrate with the microbial consortium, the surface area suitable for the microbial growth in the electrodes and the ideality of the catholyte, among others, are important parameters on which the generation of electricity in the MFC depends (Kim et al. 2015).

2   Materials and Methods

The experimental device consisted of a single chamber MFC built with 3 mm-thick acrylic walls. Four graphite electrodes (2.8 × 8 × 0.3 cm) were placed equidistant to each other inside the reactor. They were connected each other by an external circuit with copper wire (awg 16 gauge) and a resistance of 10 Ω. In order to increase the surface of the electrodes, spherical indentations were made.

The process was evaluated for 8 days, at a temperature of $35 \pm 0.5\,°C$, the cell volume was 1.6 L and a recirculation flow rate of $7.8\,L·h^{-1}$ was maintained with a peristaltic pump (MasterFlex L/S, Easy–Load II). Domestic wastewater was collected in the septic tank of the University, the MFC was filled using a residual water/sludge ratio of 2:1. Electricity production was monitored daily by a discrete 3-point sampling of the voltage generated, reporting a daily average, using a Fulgore® digital multimeter, model FU0233 for this measurement. Organic matter consumption was determined indirectly by measuring the Chemical Oxygen Demand (COD) (NMX-AA-030-SCFI 2001), every 24 h.

Statistical analysis was carried out using a complete factorial design of two factors (the total area of the electrodes and the initial concentration of organic matter present in the water samples). Two levels were tested to evaluate the influence of the electrode surface area (R1 = 241 and R2 = 205 cm^2) and three initial concentrations of organic matter (389.6, 428.6 and $453.6\ mg·L^{-1}$). The experiments were performed in triplicate and an analysis of variance with $\alpha < 0.05$ was performed using *Stats pad software version 2.0.2* to determine significant statistical differences among the experimental conditions.

3   Results and Discussions

The voltage generated in both reactors throughout the experiment showed a Gaussian behavior (Fig. 1a). In the first two days, the voltage increase observed remained essentially constant because the bacteria are adapting to the operating conditions of the reactor. From day 2, the rate of voltage production increased (R1 = 0.29 and R2 = $0.25\ mV·day^{-1}$) and the highest measured voltage was observed on day 5 in all the treatments tested (R1 = 1.9 mV and R2 = 1.5 mV). From day 5 until the end of the experiment, the voltages measured in the different treatments decreased and returned to their initial value, These results may be related to the consumption of organic matter during the process (Fig. 1b); the first two days, a lower rate of degradation was
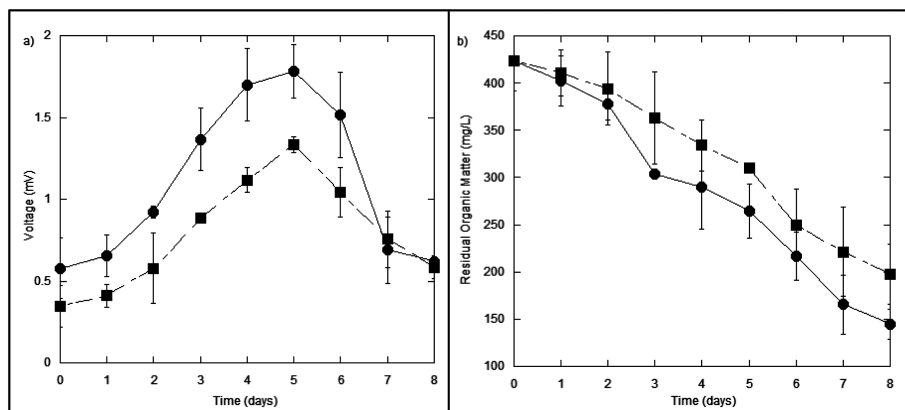
Fig. 1. Parameters evaluated in the MFC, where circle corresponds to R1 and square to R2: (a) electrical behavior of the system; and (b) degradation of organic matter during the treatment of the domestic wastewater

observed, 23.3 mg·L^{-1}/day for R1 and 15.23 mg·L^{-1}/day for R2; However, from day 3, the degradation rate doubled to 49.6 for R1 mg·L^{-1}/day and 34.5 mg·L^{-1}/day for R2.

According to the data presented in Fig. 2a, it is observed that there is a directly proportional relationship between the area of the electrodes and the rate of voltage production; it is noted that the initial concentration of organic matter of 428.6 mg·L^{-1} is the one that reaches a higher rate of voltage production. Figure 2b shows a directly proportional effect between the area of the electrodes and the maximum voltage value
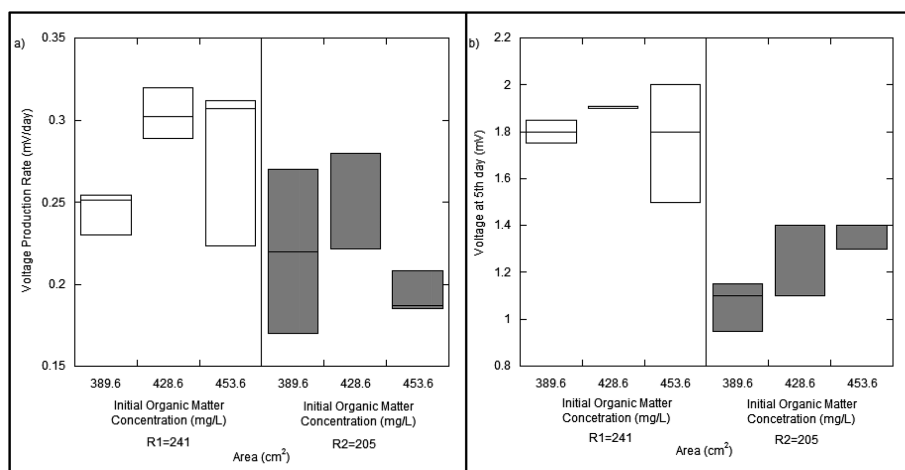
Fig. 2. Electricity production in a MFC. (a) Voltage production rate. (b) maximum value of voltage reached (at 5 days)

reached at day 5; however, the initial concentration of organic matter has not a statistically significant effect on this parameter.

The maximum voltage generated was 1.9 mV for R1 and 1.5 mV for R2 (day 5), with an initial organic matter concentration of 428.6 mg·L^{-1}; these results are similar to those obtained by Penteado et al. (2016), who recorded values ranging from 0.2 to 72 mV (day 9), using waste water from a winery with an initial organic matter concentration of 6,850 mg·L^{-1} and carbon paper and carbon fiber electrodes in a double chamber MFC. They concluded that the maximum amount of voltage generated depends on the material of the electrodes. Other authors have considered increasing the ratio of the electrode surface area to the reactor volume to improve the electrical efficiency of the cells. Kim et al. (2015), reported a production of 634 mV·m^{-3} in a 9-day process within 2.2 h using a 0.1 L cathode MFC with graphite fiber brush anodes (0.57 cm^2) and residual water with 400 mg·L^{-1} of initial organic matter. The results obtained were similar with those observed in this study, in which we produced a higher ratio 1,187 mV·m^{-3}, under the tested conditions. Likewise, Sciarria et al. (2013), reported that when using one-chamber reactors (0.028 L) with graphite fiber brush electrodes (0.22 m^2), they obtained 1,428.5 mV·m^{-3} at day 5 (12.5 total days), with an initial concentration of organic matter of 2,600 mg·L^{-1}; which exemplifies how the increase of the area, the use of different materials to build the electrodes in the anode chamber and the increase of the organic matter concentration, are intimately related to the amount of voltage generated in an MFC.

Zhao et al. (2016), analyzed the relationship between the electricity production and initial organic matter concentration in an MFC; in this work, they found that when the organic matter content was high (10–16% w/w), the rate and the maximum voltage
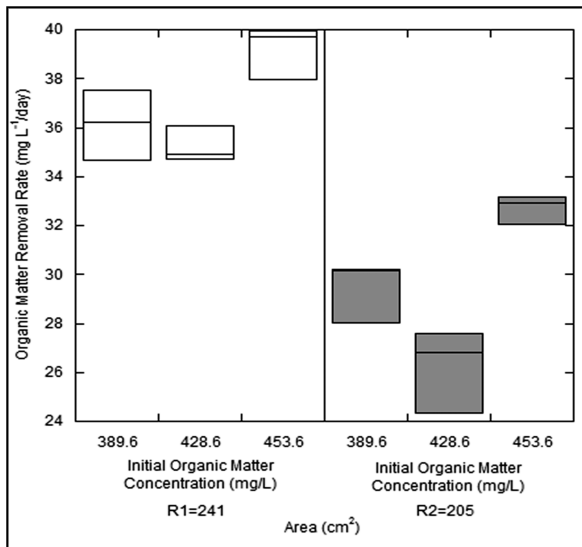
Fig. 3. Rate of removal of organic matter in MFCs

produced were higher; nevertheless, in this cases, voltage production tended to be unstable mainly due to the generation and accumulation of bubbles related to fermentation and methanogenesis processes. This was also observed in this work, in which the total organic matter inside the MFC (including the organic matter present in the water and the sludge) ranged from 8 to 21% w/w; for this reason, we implemented a gas purge at the top of the reactor.

In this work an average organic matter removal of 65 and 52% were obtained for R1 and R2, respectively. Increasing the electrode surface (an amount of 18%) had a statistically significant effect on the rate of removal of organic matter, which augmented by about 20% (Fig. 3), with an average removal rate of 36.86 mg·L^{-1}/day for R1 and 29.47 mg·L^{-1}/day for R2. In addition, it was observed that the initial concentration of organic matter in the wastewater has a directly proportional relation ($\alpha < 0.5$) with the organic matter removal rate; the higher initial organic matter concentration (453.66 mg·L^{-1}), the higher its removal rate.

4   Conclusions

It was determined that the surface of the electrode had a direct relationship with the amount of the generated voltage in the MFC; the higher voltage production corresponded to the reactor having greater surface area. Likewise, it was also observed that the initial concentration of organic matter present in the substrate has a directly proportional effect on the amount of voltage generated in the studied conditions.

References

Baranitharan E, Khan R, Prasad DMR, Teo W, Tan G, Jose R (2014) Effect of biofilm formation on the performance of microbial fuel. Bioproc Biosyst Eng 38:15–24

Gonzalez A, Perez J, Cañizares P, Rodrigo M, Fernandez F, Lobato J (2014) Study of a photosynthetic MFC for energy recovery from synthetic industrial fruit juice wastewater. Int J Hydrogen Energ 39:21828–21836

Kim K, Yang W, Logan B (2015) Impact of electrode configurations on retention time and domestic wastewater treatment efficiency using microbial fuel cells. Water Res 80:41–46

NMX-AA-030-SCFI, 2001 *Análisis de Agua. Determinación de la Demanda Química de Oxígeno en aguas naturales, residuales y residuales tratadas. Métodos de prueba,* México: Secretaría de Comercio y Fomento Industrial

Penteado E, Fernandez C, Zaiat M, Gonzalez E, Rodrigo M (2016) Influence of carbon electrode material on energy recovery from winery wastewater using a dual-chamber microbial fuel cell. Environ Technol 12:1–9

Sciarria T, Tenca A, D'Epifania A, Mecheri B, Merlino G, Barbato M, Borin S, Licoccia S, Garavaglia V, Adani F (2013) Using olive mill wastewater to improve performance in producing. Bioresour Technol 147:246–253

Zhao Q, Li R, Ji M, Ren J (2016) Organic content influences sediment microbial fuel cell performance and community structure. Bioresour Technol 220:549–556

Catalytic Wet Air Oxidation (CWAO) of Industrial Wastewaters: Mechanistic Evidences, Catalyst Development and Kinetic Modeling

F. Arena[1(✉)], R. Di Chio[1], C. Espro[1], A. Palella[2], and L. Spadaro[2]

[1] Department of Engineering, University of Messina, Messina, Italy
[2] Istituto CNR-ITAE "Nicola Giordano", Messina, Italy

Abstract. Huge water consumptions and pollutants releases in the environment urge effective water decontamination technologies, fostering extensive recycle and reuse of industrial process-water and wastewater. The heterogeneous catalytic wet air oxidation (CWAO) offers a practical solution to the problem of decontamination of industrial effluents characterised by high concentration of toxic-refractory compounds, which are also detrimental for the active sludge of biological systems. Therefore, this work shows the superior CWAO performance of a new class of *nanostructured* $MnCeO_x$ catalysts toward the mineralization of some common toxic and refractory industrial pollutants. Mechanistic and kinetic evidences are summarised into a Langmuir-Hinshelwood reaction mechanism, leading to a formal kinetic model predicting the CWAO performance of nanostructured $MnCeO_x$ catalysts and optimum reaction conditions.

Keywords: Catalytic wet air oxidation (CWAO) · Nanocomposite MnCeOx catalysts · Toxic-Refractory wastewaters

1 Introduction

Since more than two decades, wastewater detoxification has become a topic of major concern, pressed by a constantly increasing world population and the consequent growth of water needs for agricultural and industrial purposes, both accounting for more than 90% of current global freshwater consumption [1]. This implies continuous depletion and pollution of natural resources, while ca. 700 million people globally lack access to safe water supply and ca. 2.4 billion are without access to basic sanitation [1]. Hence, new water-management policies are required in order to accomplish drastic cuts of water consumption by systematic application of suitable decontamination-remediation technologies, nowadays accounting for a global business worthy of ca. $625 billion and with an estimated growth annual rate of 4% [2]. In this context, the heterogeneous catalytic wet air oxidation (CWAO) offers a versatile and economically viable solution to the large-scale depollution of concentrated industrial wastewaters (COD > 10 g/L), especially those containing refractory and/or toxic compounds for the conventional biological treatment [3]. Although the CWAO technology could foster systematic recycle and reuse of process-waters and wastewaters, yet, its exploitation is still hindered by the

lack of efficient, robust, and cost-effective catalysts alternative to supported noble-metals [4]. Therefore, this work is aimed at providing an outline of our most relevant research findings on the CWAO efficiency of *nanocomposite* MnCeO$_x$ catalysts in the range of 100–160 °C toward "probe" molecules (e.g., phenol and carboxylic acids), representative of some common classes of organic pollutants. Systematic kinetic studies highlight the mechanistic issues of the CWAO process, leading to a formal kinetic model accounting for catalyst performance and optimum reaction conditions.

2   Materials and Methods

Nanostructured MnCeO$_x$ catalysts (MxCy) with Ce/Mn (y/x) atomic ratios between 3/1 and 0 (MnO$_x$) were synthesised via the *redox-precipitation* route [5, 6]. A reference MnCeO$_x$ sample (Mn/Ce, 1) was prepared via co-precipitation of MnCl$_2$ and CeCl$_3$ (M1C1-P4) precursors [7], while a 5 wt% Pt/CeO$_2$ (Pt$_{at}$/Ce$_{at}$, 0.05) catalysts was obtained by incipient wetness impregnation of a high surface area ceria sample with a Pt(NH$_3$)$_4$(NO$_3$)$_2$ solution, and subsequent drying at 90 °C [8]. The list of the studied catalysts is given in Table 1.

Table 1. Physico-chemical properties of the studied catalysts

Catalyst	Bulk composition						SA (m^2/g)	PV (cm^3/g)	APD (nm)
	(wt%)^a			(at.%)		Ce$_{at}$/Mn$_{at}$			
	MnO$_x$	CeO$_x$	KO$_x$	Mn	Ce				
M1C3	14.1	85.8	0.1	24.2	75.5	3.00	204	0.55	24
M1C1	34.4	65.4	0.2	50.7	48.8	1.00	190	0.46	25
M3C1	59.9	36.8	3.2	70.8	22.0	0.33	184	0.57	27
M5C1	66.9	28.4	4.7	74.3	16.0	0.20	159	0.56	30
M9C1	77.0	17.6	5.4	80.3	9.3	0.10	136	0.49	31
M	93.5	–	6.5	88.6	0.0	0.00	94	0.34	31

^{a} Calculated as MnO$_2$, CeO$_2$ and K$_2$O.

CWAO tests in the range of 100–160 °C and total pressure of 1.0–1.8 MPa (P$_{O2}$, 0.9 MPa) were carried out in a PTFE-lined autoclave (0.25 L), equipped with a magnetic impeller ($\approx$800 rpm). The reactor was loaded with an aqueous suspension (0.14 L) of the catalyst (5 g/L) and fed with a continuous O$_2$ flow at the rate of 0.1 stp·L min^{-1}. After heating at the reaction temperature, a concentrated substrate solution (0.01 L) was injected by a pressurized loop to give an initial concentration of 1 g/L (R = w$_{cat}$/w$_{sub}$, 5), unless otherwise specified.

3   Results and Discussions

The activity data in the CWAO of phenol (373 K) of MnCeO$_x$ catalysts (Mn/Ce, 1), prepared via *redox-precipitation* (M1C1-R4) and co-precipitation (M1C1-P4) methods, are compared in Fig. 1 in terms of phenol and TOC concentration *vs.* reaction time during two consecutive runs.
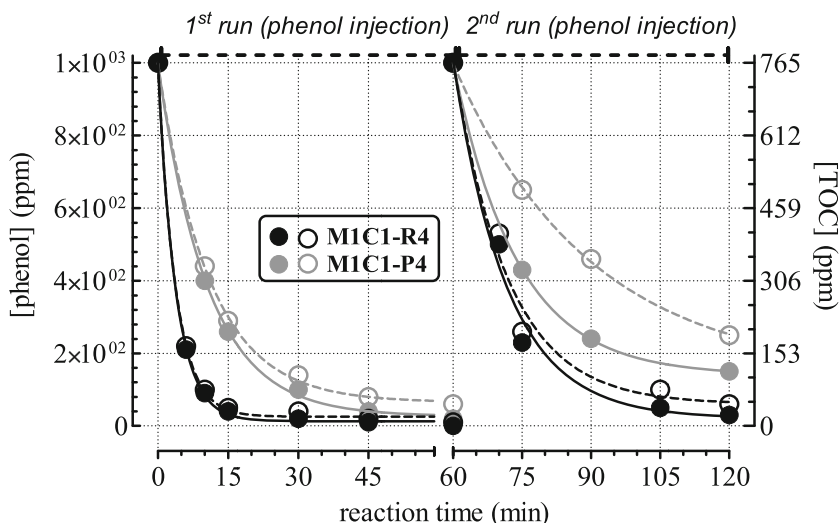
Fig. 1. CWAO activity data (T, 373 K; P, 1.0 MPa; R, 5) of the M1C1-R4 (black symbols) and M1C1-P4 catalysts (grey symbols); Phenol (full symbols) and TOC (open symbols) concentration *vs.* reaction time

The M1C1-R4 catalyst features a very high water purification efficiency probed by the complete (>95%) abatement of phenol and TOC in both first and second runs after 15 and 45 min, respectively. The M1C1-P4 system is considerably less active, since in the first run it attains a complete elimination of phenol and TOC after 1 h, and a partial removal of phenol (85%) and TOC (75%) in the 2nd run. Moreover, an almost instantaneous pH decrease to a value of 4.2 is recorded with the M1C1-R4 catalyst, while for the latter one a pH value of 4.9 is recorded after 30 min. This evidence is diagnostic of an incipient (partial) oxidation of the substrate and the consequent release of carboxylic acids (e.g., formic, oxalic, acetic) [4], being faster on the redox-precipitated system [5–7]. In spite of acidic pH, metal leaching is in both cases negligible, corresponding to less than 0.1% of manganese load.

The CWAO pattern of the M1C1-P4 catalyst is further compared with a typical Pt/CeO$_2$ system in Fig. 2 (T, 423 K; P, 1.4 MPa; R, 2), showing phenol and TOC conversion, CO$_2$ selectivity and pH during 6 h of reaction time. The Pt/CeO$_2$ system shows asymptotic growth of phenol and TOC conversion to final values of 55 and 45% respectively, along with CO$_2$ selectivity and pH values of 20 and 4%, respectively
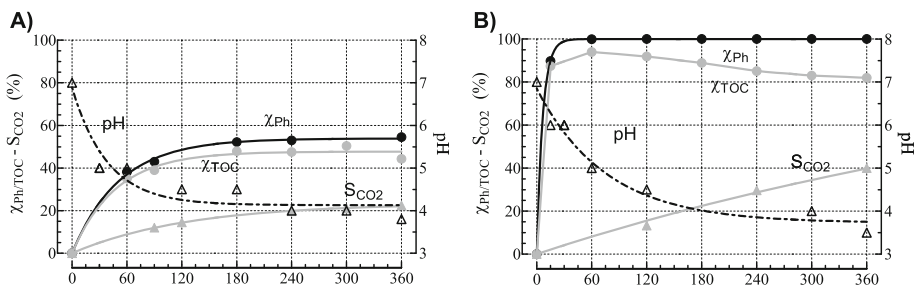
Fig. 2. CWAO activity data (T, 423 K; P, 1.4 MPa; R, 2) of Pt/CeO_2 (A) and M1C1-P4 catalysts (B)

(Fig. 2A). The M1C1-P4 catalyst has a considerably better performance, probed by the complete removal of phenol and a TOC abatement of 90% after 1 h; thereafter, the TOC conversion lowers slightly until a final value of 80%, when pH and CO_2 selectivity values of 3.5 and 40%, are recorded (Fig. 2B). Notably, in both cases experimental data signal significant gaps in C-mass balance (i.e., S_{CO2}-X_{TOC}), corresponding to 25 and 40% for Pt/CeO_2 and M1C1-P4 catalysts, respectively [4–8].

Thus, despite a different CWAO performance, the similar reactivity pattern of the studied catalysts is consistent with a *dual-site* Langmuir–Hinshelwood (L–H) reaction pathway, including a *fast* adsorption step, responsible for phenol and TOC conversion, following its *slow* surface oxidation (*r.d.s.*) on different surface sites (i.e., "α", "σ-O") [4, 7].

Indeed, the reaction scheme in Fig. 3 shows that both by-product release (e.g., C1-C2 acids) and catalyst fouling depend on side-reactions of the mineralization step (i.e., CO_2 formation), accounting for residual TOC and incipient catalyst deactivation [4, 7].
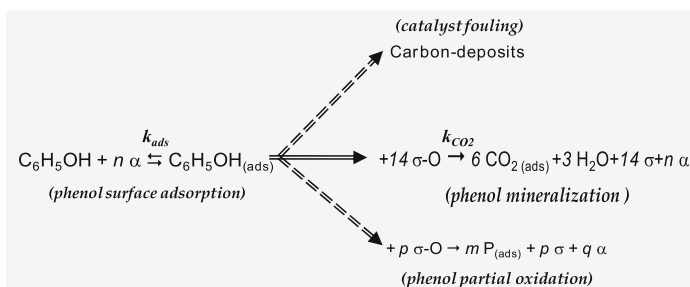
Fig. 3. Simplified reaction scheme of the heterogeneous CWAO of phenol

Furthermore, a thorough kinetic study of the CWAO of phenol has been devoted at ascertaining the influence of chemical composition on the reactivity pattern of the composite materials in view of catalyst optimization. Mechanistic evidences coming from the effects of catalyst load, oxygen pressure, temperature and substrate

concentration have been summarised in a formal L-H kinetic model predicting the reactivity of nanostructured $MnCeO_x$ catalysts in the CWAO of phenol in the range of 100–160 °C.

4 Conclusions

- The heterogeneous Catalytic Wet Air Oxidation (CWAO) represents the most promising technology for purification of industrial wastewater.
- Catalyst development is the main drawback to the large scale application of the CWAO technology.
- Systematic studies on reaction mechanism and kinetics lead to development of a new class of nanostructured $MnCeO_x$ catalyst very efficient in the CWAO of toxic and refractory pollutants.
- Low-cost catalyst formulations coupled to high water-purification efficiency are key-factors for the large scale application of the CWAO technology.

References

1. World Health Organization and UNICEF Joint Monitoring Programme (2015) Progress on Drinking Water and Sanitation, 2015 Update and MDG Assessment
2. Global Water and Wastewater Market Outlook, 2016, Frost & Sullivan
3. Levec J, Pintar A (2007) Catalytic wet-air oxidation processes: a review. Catal Today 124:172–184
4. Arena F, Di Chio R, Gumina B, Spadaro L, Trunfio G (2015) Recent advances on wet air oxidation catalysts for treatment of industrial wastewaters. Inorg Chim Acta 431:101–109
5. Arena F, Spadaro L, WO 2012168957 A1, 2012
6. Arena F, Trunfio G, Negro J, Fazio B, Spadaro L (2007) Basic evidence of the molecular dispersion of MnCeOx catalysts synthesized via a novel "redox-precipitation" route. Chem Mater 19:2269–2276
7. Arena F, Trunfio G, Negro J, Spadaro L (2008) Optimization of the MnCeOx system for the catalytic wet oxidation of phenol with oxygen (CWAO). Appl Catal B Environ 85:40–47
8. Arena F, Italiano C, Spadaro L (2012) Efficiency and reactivity pattern of ceria-based noble metal and transition metal-oxide catalysts in the wet air oxidation of phenol. Appl Catal B Environ 115–116:336–345

Treatment of Industrial Wastewater Containing Amides Using Novel Bacterium in Semi-continuous Reactor

M. Sogani[1]([✉]), A. Dongre[2], and K. Sonu[2]

[1] School of Civil and Chemical Engineering,
Manipal University Jaipur, Jaipur, India
[2] Department of Mechanical Engineering,
Arya Institute of Engineering and Technology Kukas, Jaipur, India

Abstract. The work initially isolates and identifies the bacteria from pharmaceutical industrial wastewaters having amidase activity and then immobilizes and optimizes the reaction conditions adopting variants of batch, fed batch and continuous reactor system for maximum bioconversion of acetamide to acetohydroxamic acid. The maximum acyltransferase activity was obtained in 100 mM potassium phosphate buffer (pH 7.5) with substrate concentration 0.850 mmoles of acetamide and 1.7 mmoles of hydroxylamine hydrochloride with resting cells 0.94 mg (cell dry weight) (0.322 Uml-1) for 20 min at 55 °C. It had showed broad substrate specificity. Acetamide was the best substrate followed by acetonitrile. Industrial wastewater contains a large number of metal ions thus in view of future application of this research for real pharmaceutical wastewater treatment, the effect of a various metal ions on the immobilized cells was studied. Among the various metal ions and inhibitors, $AgNO_3$ had only severely affected the enzyme activity. The short operation time of the proposed process, coupled with the possibility of an enzyme reuse during several cycles, are effective tools to implement this economically competitive semi-continuous reactor for amide biodegradation in pharmaceutical wastewaters.

Keywords: Industrial wastewater · Acetamide · Acetohydroxamic acid · Semi-continuous reactor

1 Introduction

Toxic nitrile and amides are extensively used in Pharmaceutical industrial operations due to which their occurrence in waste presents a major environmental and ecological hazard. Improperly handled and disposed industrial wastewaters imperil both human health and the environment. Among the nitrile degrading enzymes, amidases can play an important role in the detoxification of these compounds. This study makes use of microbial isolates with amidase acyl transferase activity in order to maximize the biodegradation of amides in industrial wastewaters. Moreover, it results in synthesis of pharmaceutically active hydroxamic acids, which have been reported as tumor inhibitors, anti-HIV, anti-malarial and anti-cancerous. Hydroxamic acids can also conjugate and eliminate containing metal ions and thus may be used for wastewater treatment and

in nuclear technology. The work initially isolates and identifies the bacteria from pharmaceutical wastewaters having amidase activity and then immobilizes and optimizes the reaction conditions for maximum acyl transferse activity adopting variants of batch, fed batch and continuous reactor system.

2 Materials and Methods

In this work the effect of various substrates (aliphatic and aromatic amides) on acyl transferase activity of both immobilized cells was studied. However, further work involved acetamide as both immobilized cells exhibited good substrate affinity for it. Industrial wastewater contains a large number of metal ions thus in view of future application of this research for real pharmaceutical wastewater treatment, the effect of a various metal ions on both immobilized cells was studied.

Batch, fed-batch and semi-continuous operational modes were studied under laboratory conditions. The operational stability of acyltransferase was studied by preincubating immobilized resting cells of *Bacillus* in 0.1 M potassium phosphate buffer (pH 7.5) at 45 °C and 50 °C for 250 min. Enzymatic acetohydroxamic acid production kinetics under previously optimized conditions was investigated. The rate of conversion was higher in semi-continuous mode then fed and batch modes with *Bacillus* immobilized cells. Thereafter, a semi-continuous reactor for acetohydroxamic acid production was operated under the optimal conditions established in kinetic trials. Effect of substrate on ATA was studied by varying the concentration of acetamide and hydroxylamine-HCl.

A semi-continuous reactor was designed for acetohydroxamic acid production. The reactor vessel was glass with 3.0 L reaction volume. The reaction mixture was continuously recirculated through the column. The reactor was used to carry out successive reactions of acetohydroxamic acid production. For the startup, Beads $\approx$ 15 ml RC 50 mg dcw, 50.0 ml of 2 M acetamide 62.5 ml of 8 M hydroxylamine – HCl and 387.5 ml of 100 mM potassium phosphate buffer were added to the reactor. The total volume of mixture inside the reactor was 500 ml. Each reaction was carried out at 45 °C with agitation at 200 rpm over 2.0 h reaction time. Recirculation of the mixture through the column was continuous during the reaction. After each reaction the mixture was transferred to the settler to separate the products. The reaction cycles followed were repeated maintaining acetamide: hydroxylamine – HCl ratio as 1:5. Cells were separated from the reaction mixture by centrifugation at 10000 g for 10 min at 30 °C. Supernatant was freeze dried. The amount of acetohydroxamic acid formed was determined by using spectrophotometry and by HPLC and the kinetic parameters were calculated by means of a Line Weaver Burk Plot (or double reciprocal plot). The HPLC analysis showed the yield of acetohydroxamic acid was 96% (mol mol^{-1}).

3   Results and Discussions

The enzyme of both immobilized cells efficiently hydrolyzed aliphatic amides in comparison to aromatic amides (Table 1). Propionamide was a very good substrate followed by butyramide, acetamide, and lactamide for *Rhodococcus* cells. Similarly, Acetamide was a very good substrate followed by Propionamide, butyramide, and acrylamide for *Bacillus* cells. It indicated that the amidase of both microorganisms is a broad-spectrum aliphatic amidase.

Table 1. Effect of substrates on acyltransferase activity of immobilized cells (Substrate affinity of acyl transferase of *Bacillus* and *Rhodococcus*)

Substrates	Relative enzyme activity (%)	Relative enzyme activity (%)
	Bacillus	Rhodococcus
Acetamide	100	77
Acrylamide	86	19
Nicotinamide	56	22
Benzamide	21	14
Caprolactam	35	1
Cyanoacetamide	19	14
Thioacetamide	7	5
Lactamide	7	57
Propionamide	91	100
Butyramide	89	84

In the presence of $AgNO_3$ (1 mM) 99% residual activity of amidase of *Rhodococcus* was recorded. However, at the same concentration of $AgNO_3$ inhibition of amidase is seen in *Bacillus* cells (Table 2).

Table 2. Effect of metal ions and inhibitors on acyltransferase activity of immobilized cells (Effect of Metal ions and inhibitors of acyl transferase of Bacillus *and* Rhodococcus)

Meta ions/Inhibitors (1 mM)	Relative enzyme activity (%)	Relative enzyme activity (%)
	Bacillus	Rhodococcus
None (Control)	100	100
FeCb	92	106
MgCh.6H.iO	105	104
$ZnS0_4.7H_20$	106	104
$CuS0_4.5H_20$	59	13
$AgN0_3$	12	99
HgCh	30	75
C0CI2	115	90
CaCh	103	105
Urea	99	105
EDTA	96	102

CuSO$_4$.5H$_2$O had inhibitory effect on enzyme of both cells. The metal ion chelators did not significantly altered the enzyme activity, which indicated either the complete absence of metal ions at the active site of enzyme or metal ions are tightly bound to the active site.

To get the optimum mole ratio of substrates (acetamide and hydroxylamine – HCl), the concentrations of acetamide was varied from 100 mM to 1000 mM at different hydroxylamine – HCl concentrations (200, 400, 600, 800, 1000, 1200, 1400, 1600, 1800 and 2000 mM) to determine the K$_m$ and V$_{max}$ of the immobilized amidase of *Bacillus* species. Initially acyltransferase activity of whole cells increased with an increase in acetamide concentration but just thereafter it remained constant or decreased with amide concentration for all hydroxylamine – HCl concentrations studied. The highest acyltransferase activity was obtained with 1000 mM hydroxylamine – HCl and 200 mM acetamide (Fig. 1 limited data shown for simplicity).
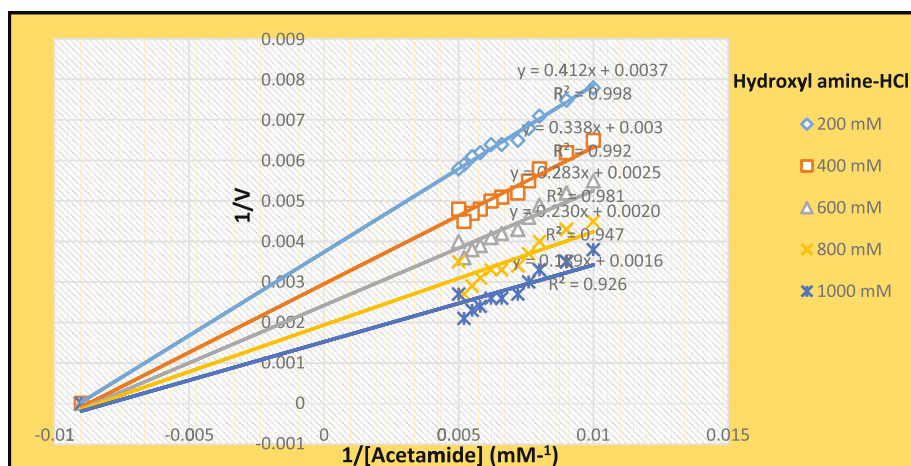
Fig. 1. A double reciprocal plot of 1/V and 1/[Acetamide]

Acetohydroxamic acid production showed no inhibition by acetamide and hydroxylamine-HCl under the conditions used. Therefore, the reaction was described by a ping-pong mechanism and non-competitive inhibition by hydroxylamine. The kinetic parameters determined were: for acetamide (K$_m$A 226 mM and V$_{max}$ = 71 μ mol/min/mg dcw) and hydroxylamine HCl (K$_m$B 995 mM and V$_{max}$ = 806 μ mol/min/mg dcw) (Figs. 2 and 3). The enzyme acyltransferase had a lesser affinity towards the hydroxylamine as compared to acetamide due to higher K$_m$ value. In this semi-continuous reactor, immobilized enzymes were successively reused remaining in the reactor during all reaction cycles. Under these conditions, it was possible to maintain acetohydroxamic acid production yields of greater than 90% over four reaction cycles. Both the kinetic study and reactor operation showed *Bacillus* immobilized acyltransferase didn't present any significant activity loss at high hydroxylamine concentrations.
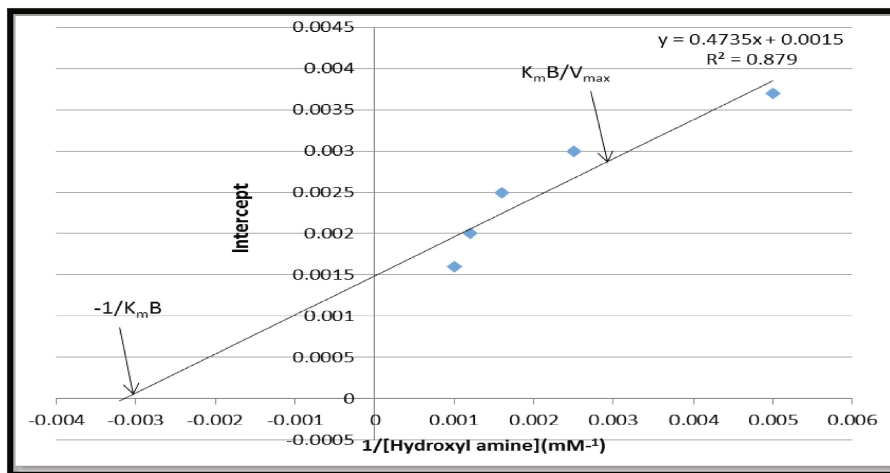
Fig. 2. Plot of intercept values ($1/V_{max}$) from double reciprocal plot against 1/[hydroxylamine-HCl]
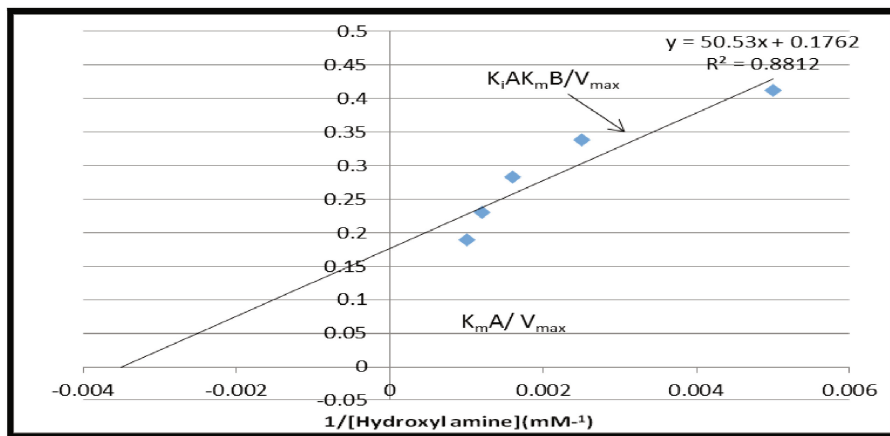
Fig. 3. Plot of slope values (K_m^{app}/V_{max}^{app}) from double reciprocal plot against 1/[hydroxylamine]

4   Conclusions

The present study resulted in substantial acetohydroxamic acid production using whole cell biocatalyst in short time course. Similar process can be scaled up for bioremediation of various amides and the synthesis of other pharmaceutically relevant hydroxamic acid which finds wide application in different industries. Further, investigations regarding scale up of this integrated process with immobilized microorganisms for elimination of toxic amides and nitriles will be focusing towards recovery of resources so as to make wastewater management energy positive and financially viable.

Methanogenic Activity and Growth at Low Temperature Anaerobic Wastewater Treatment (4, 15 °C) Using Cold Adapted Inocula

E. Petropoulos[(✉)], J. Dolfing, and T.P. Curtis

School of Civil Engineering and Geosciences,
Newcastle University, NE17RU Newcastle, UK

Abstract. We have developed an alternative cold-adapted (4, 8 °C), Arctic/Alpine inoculum to overcome the obstacle of limited hydrolysis and methanogenesis that is common in low temperature anaerobic wastewater (WW) treatment systems. This special WW-fuelled inoculum was employed here to study its activity and growth at low temperatures (4 and 15 °C) with real wastewater as substrate. Cell specific methanogenic activities (4–15 °C) were comparable with those observed for mesophiles at higher temperatures (37 °C) ($\approx$2.0 $gCOD_{methane} \cdot gVSS^{-1} \cdot day^{-1}$). Low temperature (4 °C) acclimation forms methanogenic communities that perform robustly at 4 °C and better than those pre-acclimated to higher temperatures (8 °C) when incubated at 15 °C. An evaluation of the inoculum resistance to migration of 'outsiders' at low (4–8 °C) and high (15 °C) temperatures showed that the lower the temperature the higher the probability for migration (archaeal migration rate at 4–8 °C 1.69×10^{-5} $death^{-1} > 6.44 \times 10^{-6}$ $death^{-1}$ at 15 °C). Limited cell growth at low temperature treatment systems is one of the main reasons. This limitation can be overcome as growth kinetics at low temperatures (4 °C) are comparable to those observed in mesophilic reactors ($\approx$20 days – growth coef.: 0.05 day^{-1}) depending on the substrate availability. Thus, continuous, rich in COD feeding regimes may assist cold adapted biomasses to not only grow at low temperatures but also to decrease the probability to be outpaced by of WW-originated 'invaders'.

Keywords: Anaerobic treatment · Low temperature · Specific activity · Migration rate · Growth

1 Introduction

Most attempts to acclimatize mesophilic sludge to lower temperatures for anaerobic wastewater treatment purposes failing to accomplish both hydrolysis and methanogenesis at <8 °C with real WW as substrate. A recent study by Petropoulos et al. (2017) has shown that the development of a cold-adapted biomass using inocula obtained from cold environments is a promising approach for successful anaerobic domestic WW treatment at low temperatures ($\geq$4 °C). The specific, WW-fuelled,

methanogenic activity of this inoculum is re-evaluated here (from/to 4 and 15 °C) and compared with activities obtained by mesophilic inocula at various temperatures.

It is under question whether the microbial structure of the seed would remain unchanged if and when exposed to non-sterile wastewater. A way to estimate the status of the biomass in such scenario is by estimating the 'migration rates', the probability of an individual from the 'inside' die and be replaced by an individual from the 'outside'. In this study the 'inside' is the sample out of the remaining reactor volume that stands for the 'outside'. The cells from the former represent the local community that needs to remain stable in the face of the latter, the potential invaders. A high probability of outsiders outpacing the insiders (migration rate) is likely at low temperatures due to low growth and consequently a taxon in the local community is more likely to be replaced by individuals from a source community (e.g. actual WW). Hence an inoculum at low temperatures may be more prone to migration than an inoculum at higher temperatures, where growth is more evident. Migration can be tackled by high growth (Curtis and Sloan 2004). Following a continuous feeding regime and by adding a UF membrane to minimize cell losses we show that growth at low temperatures is attainable and subsequently migration can be lowered.

2 Materials and Methods

Inocula. Eight reactors were seeded volumetrically with an equal mixture of putatively cold-adapted biomasses from reactors that were previously treating wastewater at low temperatures (4 and 8 °C). The nature and origin of this inoculum is sediments from Lake Geneva and soils from Svalbard, in the high Arctic (Petropoulos 2015).

Wastewater. Wastewater was collected from the Tudhoe Mill (County Durham, UK) wastewater treatment plant (WWTP), which treats domestic wastewater. Primary settled influent was used to ensure the absence of large solids that might block the pumps that were employed to feed the reactors. During the operation no pH adjustments were made (pH: 7.0 on day 1). The wastewater COD varied from 150 to 600 mg.L^{-1}.

Methanogenic activity tests. Methanogenic activity of inocula pre-acclimated to 4 and 8 °C was measured at 4 and 15 °C (operational temperatures, average high and average low for the region of Newcastle UK). The selected setup was similar with the one described by Bowen et al. 2014. The seed: total. vol. ratio was 1:4 based on Petropoulos, 2015. All mini-reactors (Wheaton vials) were prepared in duplicates. Controls with only inoculum and only wastewater were also prepared. The results display the activity of the inoculum after abstracting the activity from the two controls. The activity is expressed per methanogenic cell, the cell enumeration was carried out on day 18 and 27 via McrA gene qPCR. The qPCR was carried out according to Steinberg and Regan (2009). The conversion of the activity cell^{-1} to VSS^{-1} was based on Rittman and McCrarty 2001 (1 cell = 1 × 10^{-12} gVSS).

Migration rates. The rates were calculated based on OTU tables generated after pyro-sequencing DNA (5 µl DNA sample from 100 µl extracted) from 1 ml mixed liquor of 1L batch reactors (Petropoulos et al. 2017 setup;).The OTU tables between 4

and 8 °C were merged as low temperatures (n = 4), the rates from 15 °C were estimated separately (n = 4), warm temperature. The assumption that the 4 and 8 °C count as one was made since the calculation requires at least 3 replicates (n = 2 each) and previous MDS plots (Petropoulos et al. 2017) showed that the difference between the two community structures is minimal. The estimation involved neutral models (Sloan et al. 2006) on the sequencing pattern of long retention time batch reactors (4–8 and 15 °C after 1100 days).

Continuous reactor setup. Eight 1L reactors were seeded with a mixture of 4 and 8 °C (1:1 $^v/_v$) acclimated inocula (from par. 2.1), fed with UV sterilised primary settled domestic WW at a 1:1 $^v/_v$ ratio and set at 4 and 15 °C (n = 4). The reactors were equipped with hollow fibre membrane units to prevent biomass washout, allowing an operational flux (LMH) of 2.3 L.m^2.hr (HRT = 7 days$_{day34-present}$). Daily operation included a daily 4 h relaxation plus a 3 h backwash (after day 58). The operational OLR and SLR were 0.08 kgCOD.m^{-3}.day^{-1} and 6.13 ± 1.4 kgCOD.kgVSS$_{methamogens}$$^{-1}$.day^{-1} (based on mcrA qPCR enumeration and conversion of the cells to VSS assuming that 1 cell weighs 1×10^{-12} grams (Rittman 2001)).

Chemical analysis. COD, sCOD, TSS, VSS were measured based on APHA, 2005. VFAs were measured on DIONEX ICS-1000, Anions were measured on Dionex Anion Micro Membrane Suppressor (AMMS-ICE II); methane gas was measured onto a Carlo Erba HRGC S160 GC fitted with an FID detector and HP-PLOTQ column.

Methane production. The methane production rate is a sum of the gaseous, and dissolved in the aqueous phase (mixed liquor and effluent) CH$_4$ that was formed per HRT.

Cell enumeration and growth. Methane formation combined with average per temperature specific methanogenic activity was used to give an indication of the number of methanogens that are present in the reactor (Eq. 1). Knowing the cell abundance (N) at Δt for t$_1$ (N$_o$) and t$_2$ (N$_t$) and by using 1st order kinetics (Eq. 2) we can calculate the k (growth coefficient).

$$Cell\ abundance(N\ cells) = \frac{\Sigma\ methane\ production\ (mol/day)}{cell\ specific\ activity\ (\frac{mol}{cell}/day)} \tag{1}$$

$$Nt = No\ e^{kt} \tag{2}$$

3 Results and Discussion

3.1 Batch Setup

Methanogenic Activity. Activity tests (Bowen et al. 2014 setup) with inocula from permanently cold environments (Petropoulos 2015), that had been grown with UV-sterilized WW at 4 and 8 °C for >1100 days, showed that a biomass acclimated at low temperature (4oC) performs robustly at both cold and warmer temperature (15 °C) compared to a biomass that had been acclimated at higher temperature (8 °C) (Fig. 1a).
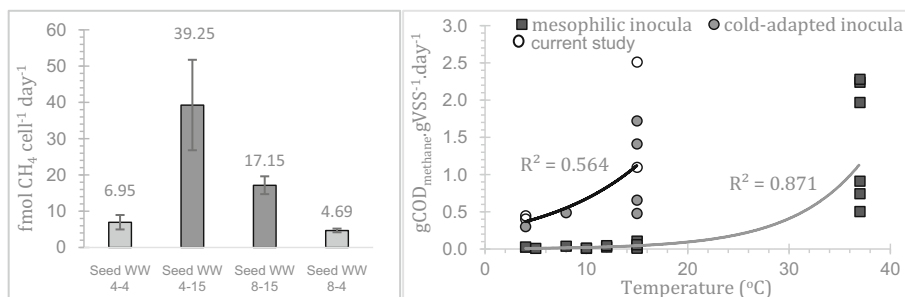
Fig. 1. (a) Specific methanogenic activity per methanogenic cell ('Seed WW' stands for arctic inoculum fed with domestic WW; 1st and 2nd number stands for the acclimation and the operational temperature respectively; (b) specific methanogenic activity by psychrophilic/cold-adapted and mesophilic inocula at various temperatures (Dolfing and Mulder 1985; Bowen et al. 2014; Keating et al. 2016; Luostarinen and Rintala 2005, 2007; McHugh et al. 2006 etc.)) (1 cell = 1×10^{-12} grams VSS (Rittman, 2001))

Cold adapted cells can convert COD: CH_4 at rates similar with those achieved by mesophilic inocula at warmer conditions (37 °C) (Fig. 1b). The activity at this study was found similar to the activity that was measured by previous putative psychrophilic populations in anaerobic reactors (Petropoulos et al. 2017; Collins et al. 2005 (Fig. 1 b)). The exponential trend on Fig. 1b points the different methanogenic capacity between psychrophilic/cold-adapted and mesophilic methanogens at various temperatures.

Microbial community stability. Inoculation of a bioreactor with cold-adapted cells is a strategy for the promotion of WW treatment at low temperature. Curtis and Sloan (2004) suggested that 'invasion' of WW cells may challenge an established microbial diversity since the community develops through a continuous cycle of immigration, births and death (Sloan et al. 2006). After pyro-sequencing DNA samples from the mixed liquor of 1L batch reactors (Petropoulos et al. 2017) the migration rates of the inoculum were estimated. The estimation involved application of neutral models (Sloan et al. 2006) on the sequencing pattern of long retention time batch reactors (4–8 and 15 °C after 1100 days). Whilst bacterial migration rates were similar at all temperatures (2.84×10^{-5} death^{-1}), the archaeal rates showed that the cells are more prone to migration at low temperatures (migration rate$_{4-8oC}$ of 1.69×10^{-5} death^{-1} > 6.44 10^{-6} death^{-1} at 15 °C). QPCR$_{McrA}$ showed that this is attributed to low growth at low temperatures caused by slow hydrolysis/limited feed. Continuous feed may promote growth and lower migration (Curtis and Sloan 2004).

3.2   Continuous Setup

Continuous feeding regime. During the continuous operation methane production was separated into two phases regardless the temperature, the lag phase (d.0-65) and the 'vigorous' phase (d.66-present) (Fig. 2).
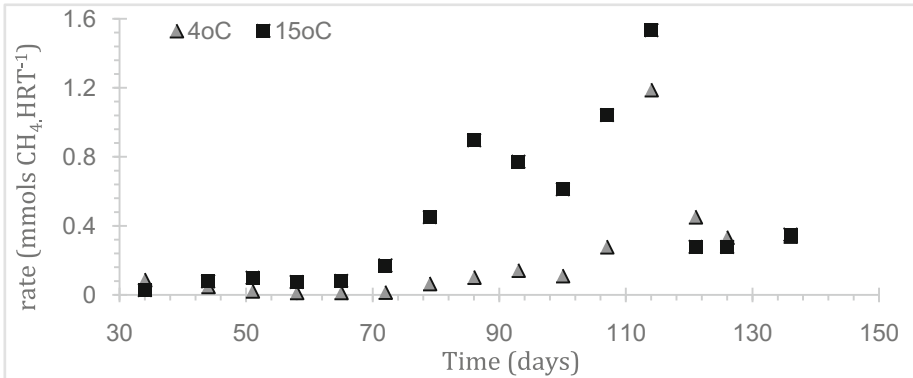
Fig. 2.   Methane production rate per HRT at both temperatures (4 and 15 °C)

Methane production. Methane production was poor over the lag phase with the methane at 15 °C only increasing linearly. At 4 °C a curve in the methane production rate was formed with the minimum reached on day 58 (Fig. 2). The curve may signify the acclimation screening mechanism (mixture of biomasses adapted at 4 and 8 °C as inoculum) where only the resilient/adapted cells would thrive at these operational conditions, most likely the pre-acclimated to 8 °C cells were outpaced by those pre-acclimated to 4 °C when both at 4 °C. Once the community is screened (d.65) growth becomes apparent. Methane production rate at 4 °C increased reaching an average of 30 ± 9.6% CH_4:COD (d.79-present) of the theoretical conversion; at the same period the conversion at 15 °C reached the 38 ± 14.6%.

COD sinks. High WW sulphate concentration led to low COD to methane conversions (average SO_4 influent concentration of 134 mg.L^{-1}) at both temperatures (43 and 97% sulphate reduction at 4 and 15 °C respectively). Hence, sulphate reduction played an important role in COD removal, especially at 15 °C. This explains why the methane rate at higher temperature was lower to at 4 °C. The sulphate reduction Q_{10} was estimated as 2.1. Sulphate reduction is unlikely to be observed using simulated wastewater as substrate. Plethora of research endeavours that use synthetic wastewater aiming to the degradation of the substrate mainly by methanogens. With actual wastewater this is partly the case.

Enumeration and Growth. The growth exponential trendline of the growth coefficients as a function of sCOD at Δt_{51-107} show that methanogenic cells from low and high temperature may achieve similar doubling times (Fig. 3a). This states that growth

(k $\sim$ 0.05 day^{-1}, doubling time $\sim$ 20 days) at low temperatures (≥ 4 °C) is attainable but requires high available COD (> 200 mg.L^{-1} for the cells to uptake (Fig. 3b). The positive growth coefficients were estimated and correlated with the sCOD in the mixed liquor. Negative coefficients were neglected since they do not signify growth. All negative coefficients appeared at sCOD lower to 116 and 38 mg.L^{-1} for 4 and 15 °C respectively. The 4 °C trend (Fig. 3b) is a rough estimation of the relationship between sCOD and growth since the R^2 is low and the data points limited. Further experimentation would give more information at the Relationship between growth and carbon availability at extremely low temperatures (4 °C). Regardless the weak correlation growth at 4 °C is attainable and subsequently migration at low temperatures can be reduced to levels that would possibly allow the application of such inocula to operate in the presence of WW-originated cells.
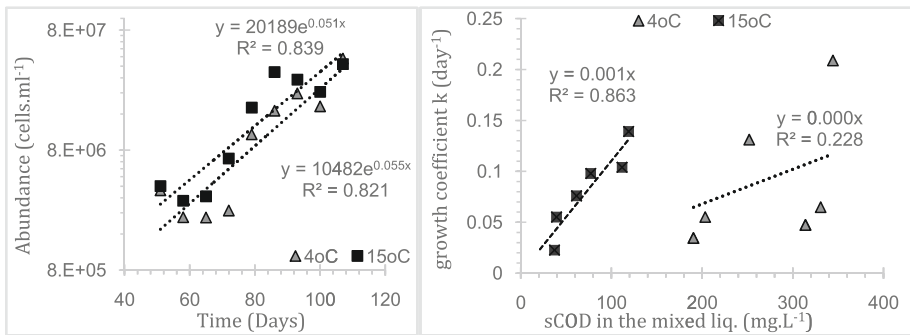
Fig. 3. (a) Abundance of the methanogenic cells based on the average specific activity at 4 and 15 °C; (b) methanogenic growth coefficient k as a function of the available sCOD present in the mixed liquor at 4 and 15 °C (negative coefficients based on Fig. 3a were excluded as they signify decay)

Wastewater Treatment Efficiency. Between the 1st and the 2nd phase no significant differences in the COD$_{effluent}$ pattern were observed at 15 °C. At 4 °C robust hydrolysis activity appeared on day 72 with a sCOD$_{ML}$ peak followed by a high effluent COD concentration that afterwards decreased to meet the UWWTD directive standard (COD < 125 mg/L) after day 121. The hypothesis of accumulation of organic material in the mixed liquor due to slow hydrolysis as a removal mechanism, especially at 4 °C, (Petropoulos et al., 2017) is plausible since sCOD$_{ML}$ > sCOD$_{inf}$ (d. 93 – Fig. 4). At the 1st phase the membrane biofilm contributed to treatment predominantly at 15 °C (further COD removal between the mixed liquor and the effluent of 22 ± 4% and 32 ± 5% at 4 and 15 °C respectively (Fig. 4)). From day 65 the membrane was a key component at low temperatures contributing to the sCOD removal by up to 45%. This may be attributed to the promotion of syntrophic interactions that is required at lower temperatures (Smith et al. 2015).
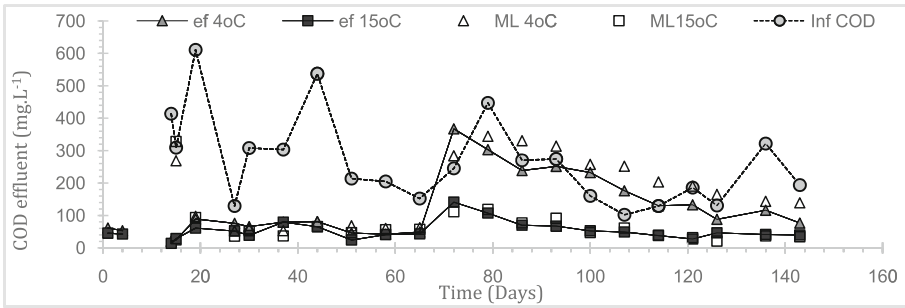
Fig. 4. Organic material in the influent (inf), effluent (ef) and in the mixed liquor (ML) at 4 and 15 °C

4 Conclusions

Cold adapted inocula may facilitate anaerobic treatment wastewater at low temperatures with specific methanogenic rates comparable with those attained by mesophiles at higher temperatures. Acclimation to low temperature (4 °C) forms communities that perform robustly at 4 °C and better than biomasses that were acclimated to higher ones when both at high temperatures (e.g. 15 °C). Cold-adapted methanogens are able to grow at 4 °C with realistic doubling times in the presence of adequate organic material. Thus, migration rates can be lowered and stability of the cold-adapted microbial community structure can be promoted.

References

Bowen EJ, Dolfing J, Davenport RJ, Read FL, Curtis TP (2014) Low temperature limitation of bioreactor sludge in anaerobic treatment of domestic wastewater. Wat Sci Tech 69(5):1004–1013

Collins G, Mahony T, O'Flaherty V (2005) Stability and reproducibility of low-temperature anaerobic biological wastewater treatment. FEMS Microbiol Ecol 55:449–458

Curtis TP, Sloan WT (2004) Prokaryotic diversity and its limits: microbial community structure in nature and implications for microbial ecology. Cur Opin Microbiol 7:221–226

Dolfing J, Mulder J-W (1985) Comparison of methane production rate and coenzyme F_{420} content of methanogenic consortia in anaerobic granular sludge. Appl Environ Microbiol 49(5):1142–1145

Keating C, Chin JP, Hughes D, Manesiotis P, Cysneiros D, Mahony T, O'Flaherty V (2016) Biological phosphorus removal during high-rate, low-temperature, anaerobic digestion of wastewater. Front Microbiol 7:226–240

Luostarinen SA, Rintala JA (2005) Anaerobic on-site treatment of black water and dairy parlour wastewater in UASB-septic tanks at low temperatures. Wat Res 39:436–448

Luostarinen SA, Rintala JA (2007) Anaerobic on-site treatment of kitchen waste in combination with black water in UASB-septic tanks at low temperatures. Biores Technol 98(9):1734–1740

McHugh S, Collins G, O'Flaherty V (2006) Long-term, high-rate anaerobic biological treatment of whey wastewaters at psychrophilic temperatures. Biores Technol 97:1669–1678

Petropoulos E, Dolfing J, Bowen E, Davenport R, Curtis T (2017) Developing cold-adapted biomass for the anaerobic treatment of domestic wastewater at low temperatures (4, 8 and 15 °C) with inocula from cold environments. Wat Res 112:100–109. doi:10.1016/j.watres.2016.12.009

Petropoulos E (2015) Investigating the true limits of anaerobic wastewater treatment of wastewater at low temperature using a cold-adapted inoculum, PhD thesis, Newcastle University, Newcastle, UK

Rittman BE, McCarty PL (2001) Environmental Biotechnology. McGraw-Hill, Singapore

Smith AL, Skerlos SJ, Raskin L (2015) Anaerobic membrane bioreactor treatment of domestic wastewater at psychrophilic temperatures ranging from 15 °C to 3 °C. Environ Sci Wat Res Technol 1:56–64

Sloan WT, Lunn M, Woodcock S, Head IM, Nee S, Curtis TP (2006) Quantifying the roles of immigration and chance in shaping prokaryote community structure. Environ Microbiol 8:732–740

Steinberg LM, Regan JM (2009) mcrA-Targeted real-time quantitative PCR method to examine methanogen communities. Appl Environ Microbiol 75(13):4435–4442

Biosorption of Cr (VI) from Aqueous Solutions by Dead Biomass of *Pleurotus Mutilus* in Torus Reactor

A. Alouache[1(✉)], A. Selatnia[1,2], and F. Halet[1,3]

[1] Laboratoire d'Etude et de Développement des Techniques de Traitement
et d'Epuration des Eaux et de Gestion Environnementale,
LEDTEGE Ecole Normale Supérieure Kouba, Bp 92,
16050 vieux Kouba Algiers, Algeria
[2] Département de Génie Chimique, Ecole Nationale Polytechnique,
10 Avenue Hassen Badi, BP 182, El Harrach, Algiers, Algeria
[3] Université M'HAMED BOUGARA de Boumerdes, Boumerdes, Algeria

Abstract. The removal of Cr(VI) from aqueous solutions by a *Pleurotus mutilus* macrofungal biomass was investigated in a torus reactor. The reactor experiments were performed in laboratory with biomass concentration of 2 g/l and particle size ranging between 160 and 200 µm. The effect of pH and initial concentration of hexavalent chromium on biosorption assays were determined after 3 h of treatment. The optimum conditions are: pH = 5.4 and initial concentration of Cr(VI) equal to 100 mg/l. This first application of a torus reactor in biosorption phenomena demonstrates interesting results. Indeed, a biosorption capacity of 29.46 mg/g was reached. Applying the Langumir and Freundlich isotherm modelling, the equilibrium data are fitted best by Langumir isotherm equation.

Keywords: Biosorption · Cr(VI) · Torus reactor · Pleurotus mutilus

1 Introduction

Heavy metals are widely used in surface treatment and industrial manufacturing processes. They are a major problem for disposal in wastewater, especially chromium, which has a widespread use in tanning, textile, leather processing and preservation of wood. According to the WHO, its authorized level in surface and drinking waters are 0.1 and 0.05 mg/l respectively (Khitous et al. 2016). Large quantities, up to 270 mg/l are released under the two most abundant forms: Cr (III) and Cr (VI). This last is the most toxic, causing environmental problems and affecting the public health (Ghosh 2009). Therefore, it is necessary to remove this pollutant in order to reach the permissible concentration level before discharging it in wastewater. Hence, numerous chemical and physical methods have been developed, namely: adsorption methods. However, the cost plays an important role in the choice of the appropriate one. Consequently, microbial biomass (algae, yeast, bacteria and fungi) and different lignocellulosic materials are selected and investigated among several types of adsorbents.

These natural materials, called biosorbents, are abundant in the nature and have a low price comparing to others (Razmovski and Šćiban 2008).

Similarly, different types of reactors were used and developed by authors for the heavy metals removal studies. Batch reactors and columns are the most used in Cr(VI) removal. However, very little attention has been devoted to loop reactor, which has been proposed for the first time by (Norwood 1962) in a slurry polymerization of olefins. It has potential applications in biochemical reaction and processing of highly viscous liquids. According to (Murakami et al. 1982; Nouri et al. 1997; Sato et al. 1979), the loop reactor presents several advantages, in this type of reactor, heterogeneous solution may be prevented under high Reynolds number; due to high agitation speed which keeps all solid particles in suspension. This reactor is also known for its easy scale up, and good mixing with the absence of the dead volume. These characteristics prevent the formation of the vortex phenomena and limitation of mass and heat transfer. According to the literature, it appear clearly that biosorption of hexavalent chromium was not carried out in loop (torus) reactor.

The overall objective of this work is to investigate the treatment of hexavalent chromium Cr(VI) from aqueous solutions using *Pleurotus mutilus* biomass in a torus reactor.

2 Materials and Methods

2.1 Biomass Preparation and Characterization

The industrial fungal waste, obtained after *Pleuromutilin* extraction from *P. mutilus* biomass, was provided by the SAIDAL antibiotic complex of Médéa (Algeria). This waste was thoroughly washed with distilled water and dried for 24 h at 50 °C in an oven. The dried residue was grounded manually in a mortar, sieved to yield particles of 160–200 μm size, and stored at room temperature before characterization and biosorption experiments. The physical and chemical properties of this biosorbent are shown in Table 3 according to (Khitous et al. 2015; Selatnia 2004).

2.2 Chromium Hexavalent Solutions Preparation and Analysis

A solution of Chromium hexavalent used for the experiments was prepared by dissolving required amount of Potassium dichromate salt, $K_2Cr_2O_7$ in distilled water to obtain a concentration of 1000 mg/L. Various solutions of Cr(VI) were prepared with concentrations ranging from 25 to 150 mg L^{-1}. The pH of solutions was adjusted by negligible volumes of 0.1 M of NaOH or HCl solutions. The residual concentration of Cr(VI) was measured by titration with 1,5-diphenylcarbazide (DPC) in acidic condition after filtration. The samples were then analyzed with UV-visible spectrophotometer (OPTIZEN 1412 V) as absorbance at 540 nm (Khitous et al. 2016; Rai et al. 2016; Rangabhashiyam and Selvaraju 2015).

2.3 Description of the Experimental Device

The torus reactor used in this study is presented in Fig. 1. The reactor was made from transparent pipe with an internal diameter (D_t) of 50 mm, a length of 1400 mm and total working volume of 2.9 l. The mixing was achieved by a marine screw impeller. The stirring is driven by a variable speed motor (IKA-WERK RW20) providing a stirring speed of 800 rpm (homogeneous solution) at which the torus biosorption experiments were realized. The geometrical characteristics of the reactor and the marine screw impeller are given in Tables 1 and 2 respectively. Note that this reactor is similar to those utilized by (Belleville et al. 1992; Nasrallah et al. 2008; Nouri et al. 2008).
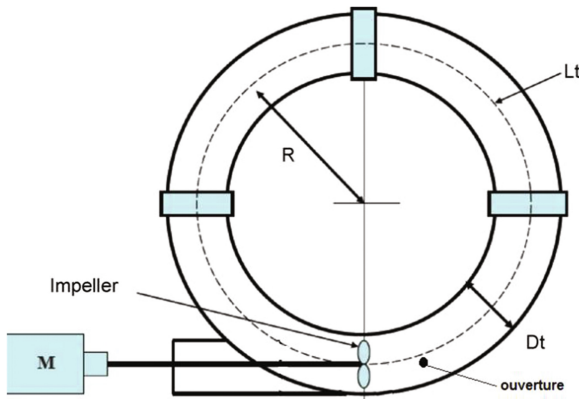
Fig. 1. Sketch of the torus reactor

Table 1. Characteristics of the reactor

V_R	D_t	L_t	R_t
(litre)	(mm)	(mm)	(mm)
2.9	50	1400	250

Table 2. Characteristics of the marine screw impeller.

r	d_t	φ
(mm)	(mm)	(rad)
20	5	$\pi/4$

Table 3. The physical and chemical characteristics of the biomass.

Particle size	d_p	ρ_{app}	S_p	Zeta potontiel
(µm)	(µm)	(g/cm^3)	(m^2/g)	(V)
160–200	180	0,43	0,13	−0,062

3   Results and Discussions

3.1   Effect of Initial Cr (VI) Concentration

The effect of initial concentration on the Cr(VI) removal by *Pleurotus mutilus* in torus reactor was carried out with various concentrations ranging from 25 to 150 mg/L. we can see clearly from Fig. 2 that Cr (VI) uptake increased as the initial Cr(VI) increases. Over 100 mg/L, a decline in the sorption capacity is revealed. This is mainly due to the saturation of the binding sites of the adsorbent surface. Finally an equilibrium dynamic form between Cr(VI) ions in solution and at surface of adsorbent was established (Rai et al. 2016; Rangabhashiyam and Selvaraju 2015). Consequently, the optimum initial concentration of chromium hexavalent of 100 mg/l was selected.
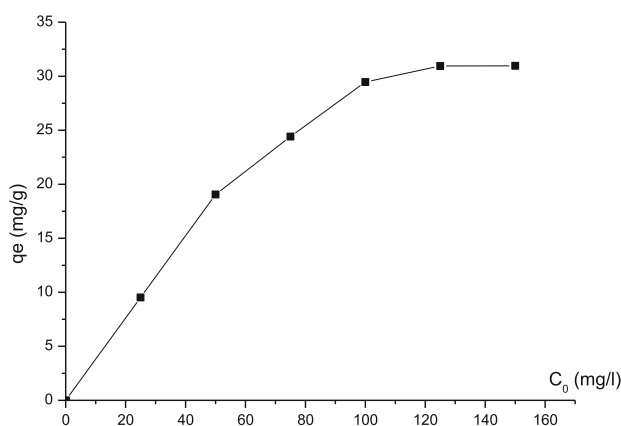
Fig. 2. Effect of initial concentration of chromium on the biosorption capacity of the *pieurotus mutilus* biomass: (pH = 5.4, C_b = 2 g/l, T = 20 °C,PS: 160–200 μm)

3.2   Effect of PH on Metal Ion Biosorption

The effect of pH on sorption capacity was studied by varying pH values from 3 to 10. The experiments were conducted at initial concentration of 100 mg/l of chromium, a sorbent dose of 2 g/l and an agitation speed of 800 rpm in homogeneous solution for a period of 03 h. Figure 3 shows an increase in the sorption capacity of Cr (VI) as the pH increases from 3 to 6. The increased binding of Cr (VI) ions at low value of pH (pH value less than 5) can be explained by the electrostatic attraction between the positive charge of the biomass and $HCrO_4^-$ ions present in solution. At pH>5, the positive charge of the biomass decreases. This last become negatively charged. In parallel, the dominant species of Cr ions in solution are $HCrO_4^-$ and CrO_4^{2-}. From pH value great than 8, a decrease in biosorption capacity is revealed. This decrease can be explained by the decrease of electrostatic attraction between the negative charge of the biomass and Cr ions. Consequently, the optimal pH value was selected around 5.4 for the
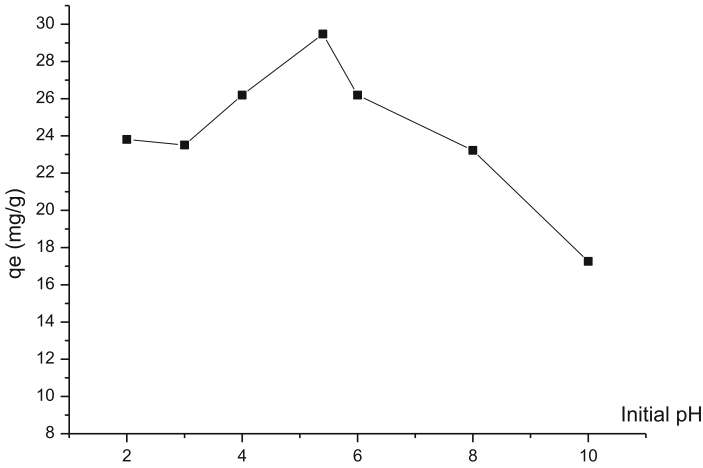
Fig. 3. Effect of initial pH of chromium solution on the biosorption capacity of the *Pleurotus mutilus* biomass: ($C_0 = 100$ mg/l, $C_b = 2$ g/l T = 20 °C, PS: 160–200 μm)

removal of Cr (VI) by *Pleurotus mutilus with* a sorption capacity around 29.46 mg/g. Similar results were previously reported by (Khitous et al. 2016).

3.3   Effect of Contact Time

The effect of contact time on the chromium hexavalent sorption is shown in Fig. 4. The uptake of Cr(VI) is highly increasing with increasing contact time until 60 min. After that, the sorption capacity reduces and tends to have a constant value. In the beginning
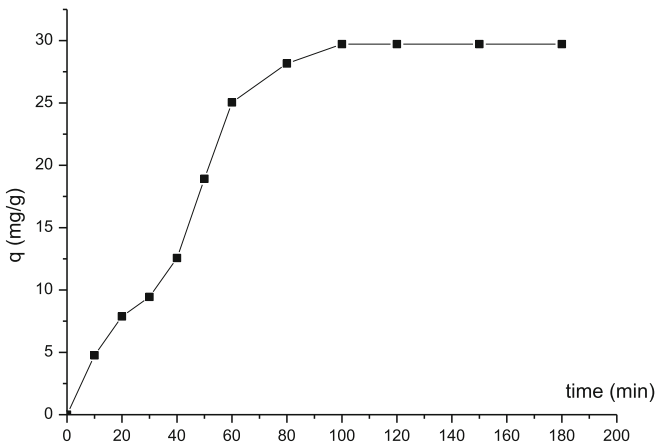
Fig. 4. Kenetic of chromium biosorption capacity by the Pleurotus mutilus biomass: (pH = 5.4, $C_0 = 100$ mg/l, $C_b = 2$ g/l T = 20 °C, PS: 160–200 μm)

of the process, all active sites of the adsorbent are available for the sorption of Cr(VI) ions. Consequently, the adsorption was faster rate. The adsorption rates decreases and becomes almost constant with increasing the contact time as the active sites were occupied, which means that the sorption equilibrium of Cr(VI) is reached. For the given situation, adsorption equilibrium time and stability are observed to be 150 min. These results are in full agreement with those found by (Khitous et al. 2016; Rai et al. 2016).

3.4 Sorption Isotherms

The metal uptake by dead biomass is characterized by two successive stages; the first is fast followed by a much slower process. Langmuir and Freundlich models were applied to study the equilibrium adsorption data for *Pleurotus mutilus*. The Freundlich constants, (K_f) and (n) are calculated by plotting (lnq_e) versus (lnC_e) The Langmuir constants are calculated by plotting (Ce/qe) versus (Ce). The adsorption isotherm parameters of both isotherms are shown in Table 4. A further analysis of Langmuir isotherm can be made. For R_L values varying between 0 and 1, a favorable adsorption process is dominant. While an unfavorable adsorption is for $R_L > 1$, when $R_L = 1$ adsorption is linear and if $R_L = 0$, it is irreversible (Rai et al. 2016). For our experiments, the dimensionless parameter, R_L is found to be between 0–1, which confirms the favorable adsorption process for Cr (VI) removal. The coefficient of correlation for Langmuir isotherm model is much greater than that of Freundlich isotherm model as shown in Table 4. Then, the Langmuir model feet the data more closely.

Table 4. Isotheme model parameters for Cr (VI) by *Pleurotus mutilis* biomass

Isotherm model	Parameter	Value
Langmuir $\frac{C_e}{q_e} = \frac{C_e}{q_m} + \frac{1}{bq_m}$ $R_L = \frac{1}{1+bC_0}$	q_m (mg/g)	23.25
	b	1.13
	R^2	0.916
	R_L	0.087
Freundlich $lnq_e = lnK_f + \frac{1}{n}lnC_e$	n	1.32
	K_f	1.29
	R^2	0.888

4 Conclusion

This first application of torus reactor in biosorption phenomena shows interesting results. The *Pleurotus mutilis* biomass displayed promising characteristics as a potential biosorbant for chromium recovery from contaminated water due to its low cost (waste material with no pretreatment needed). The maximum sorption capacity was reached at pH = 5.4 and initial concentration of 100 mg/l. The isotherme adsorption study showed that the equilibrium data are fitted best by Langumir isotherm equation.

Nomenclature

C_b: Biomass concentration (g/l)
C_0:   Initial metal ion concentration in the solution (mg/l)
C_e: Residual metal ion concentration at equilibrium (mg/l)
PS: Biomass particle size (μm)
b, q_m: Langmuir's adsorption constants
K_f, n :   Freundlich's adsorption constants
q: Amount of adsorbed metal ion on the biomass at time t (mg/g)
q_e: Adsorbed metal ion quantity per gram of biomass at equilibrium (mg/g)
t: Time for biosorption (min)
T: Temperature (°C)
d_p: Mean diameter of biosorbent particle (μm)
S_p: Specific surface area of the biosorbent (m^2/g)
R_L: Adimensional number
DPC   1.5-Diphenyl carbazide
D_t: Inner diameter of the torus reactor (mm)
L_t: Total mean length of the torus reactor (mm)
R_t: Radius of the torus reactor (mm)
r: Radius of impeller (mm)
d_t: Impeller axe diameter (mm)

Greek letter

ρ_{app} :   Apparent density of the sorbent (g/cm^3)
φ: Pitch angle of blade (rad)

References

Belleville P, Nouri L, Legrand J (1992) Mixing characteristics in the torus reactor. Chem Eng Technol 15(4):282–289

Ghosh PK (2009) Hexavalent chromium [Cr (VI)] removal by acid modified waste activated carbons. J Hazard Mater 171(1):116–122

Khitous M, Moussous S, Selatnia A, Kherat M (2015) Biosorption of Cd(II) by Pleurotus mutilusbiomass in fixed-bed column: experimental and breakthrough curves analysis. Desalin Water Treat 57(35):16559–16570

Khitous M, Salem Z, Halliche D (2016) Sorption of Cr (VI) by MgAl-NO3 hydrotalcite in fixed-bed column: experiments and prediction of breakthrough curves. Korean J Chem Eng 33(2):638–648

Murakami Y, Hirose T, Ono S, Eitoku H, Nishijima T (1982) Power consumption and pumping characteristics in a loop reactor. Indus Eng Chem Process Des Dev 21(2):273–276

Nasrallah N, Legrand J, Bensmaili A, Nouri L (2008) Effect of impeller type on the mixing in torus reactors. Chem Eng Process 47(12):2175–2183

Norwood D (1962) Japan patent. Shawa37-1 0 0, 87(1):962

Nouri L, Legrand J, Popineau Y, Belleville P (1997) Enzymatic hydrolysis of wheat proteins Part 2: comparison of performance of batch-stirred and torus reactors. Chem Eng J 65(3): 195–199

Nouri LH, Legrand J, Benmalek N, Imerzoukene F, Yeddou A-R, Halet F (2008) Character-isation and comparison of the micromixing efficiency in torus and batch stirred reactors. Chem Eng J 142(1):78–86

Rai MK, Shahi G, Meena V, Meena R, Chakraborty S, Singh RS, Rai BN (2016) Removal of hexavalent chromium Cr (VI) using activated carbon prepared from mango kernel activated with H3PO4. Resour Efficient Technol 2:S63–S70

Rangabhashiyam S, Selvaraju N (2015) Adsorptive remediation of hexavalent chromium from synthetic wastewater by a natural and ZnCl 2 activated Sterculia guttata shell. J Mol Liquids 207:39–49

Razmovski R, Šćiban M (2008) Biosorption of Cr(VI) and Cu(II) by waste tea fungal biomass. Ecol Eng 34(2):179–186

Sato Y, Murakami Y, Hirose T, Hashiguchi Y, Ono S, Ichikawa M (1979) Flow pattern, circulation velocity and pressure loss in loop reactor. J Chem Eng Jpn 12(6):448–453

Selatnia A, Boukazoula A, Kechid N, Bakhti MZ, Chergui A, Kerchich Y (2004) Biosorption of lead (II) from aqueous solution by a bacterial dead Streptomyces rimosus biomass. Biochem Eng J 19(2):127–135

Simultaneous Treatment of Wastewater and Direct Blue 2 Azo Dye in a Biological Aerated Filter Under Different Oxygen Concentrations

E. González-Gutiérrez-de-Lara[✉] and S. González-Martínez

Environmental Engineering Department, Institute of Engineering,
National University of Mexico (Universidad Nacional Autónoma de México),
Mexico City, Mexico
egonzalezg@iingen.unam.mx

Abstract. Wastewater discharges containing dyes are a compromising situation in many parts of the world. Azo dyes are the most widely used and contribute more than half of the total production of dyes. The mineralization of azo dyes is difficult due to its complex and recalcitrant structure. Biological treatment has proven to be a cost-effective and efficient alternative for dye degradation. An aerated biological filter fed with synthetic wastewater and dye, was strategically reduced it, the dissolved oxygen concentration (5 to 0 L/min). In this filter packed with porous material (lava stone) grows a biofilm, and presents simultaneous aerobic and anaerobic zones. This filter is able to remove organic matter and ammonia nitrogen efficiently. In general terms, as the air flow decreases and consequently the dissolved oxygen concentration, the removal of organic matter and ammonia nitrogen decreases, however, the removal of the Direct Blue 2 dye increases. In addition to this, the removal of ammonia nitrogen and phosphorus increases when dye is added to the wastewater. The Redox potential decreased along with the oxygen concentration and reflected reducing conditions from before stopping the aeration. The cell retention time decreased, but as the air supply was cut off, it increased. In the last stage of experimentation (DO at 0 mg/L) turbidity appeared, typical of fermentations, making it impossible to determine the majority of the biochemical parameters of the reactor.

Keywords: Wastewater treatment · BAF · Biological aerated filter · Azo dye · Oxygen control

1 Introduction

Although Azo dye Direct Blue 2 (DB2) is forbidden in many countries, others use it commonly to dye blue denim. It's estimated that approximately 50% of the dyes used in the textile industry ends up discharging to wastewater or receiving water bodies (Puvaneswari et al. 2006). Government authorities in developed countries are concerned about the escalation of dye concentrations in industrial effluents and have encouraged the innovation of novel technologies that are not only feasible and cost-competitive but also ecofriendly (Kong et al. 2015).

Generally, azo dyes are not considered to be toxic to humans. Chronic effects are associated with those who work in textile processing units. The cleavage of azo bonds in azo dyes results in formation of aromatic amines, which can act as mutagens. Azo dyes accidentally consumed by humans are biochemically reduced by microbes present in the gastrointestinal tract leading to formation of dye intermediates that act as carcinogens by forming acyl oxy amines via N-hydroxylation and can initiate bladder cancer (Popli et al. 2015), as well as being toxic to aquatic life (Puvaneswari et al. 2006).

Azo dyes are stable in light and resistant to microbial degradation or fading away due to washing. Therefore, azo dyes are not readily removed from waste water by conventional waste water treatment methods. It has been estimated that about 10% of the dyestuff in the dyeing process of textiles do not bind to fibers and are, therefore, released to the environment (Puvaneswari et al. 2006).

Different technologies are used for the treatment of dyes including chemical oxidation, flocculation, ozonation, photolysis, ion exchange, irradiation, precipitation, electrochemical treatment and adsorption (Wang et al. 2011). Removal of pollutants from the environment by biological methods has significant advantages over other methods because of the adaptability of various micro-organisms in degrading various compounds.

Contrary to the results of van der Zee and Villaverde (2005), Cobos-Becerra and González-Martínez (2013) showed that azo dye Direct Blue 2 can be removed from wastewater in both aerobic and anaerobic biological filters. It is still not clear if the removal reported by Cobos-Becerra and González-Martínez (2013) was caused by anaerobic niches in the porous carrier in the aerobic filter in combination with aerobic biochemical processes or the aerobic microorganisms were able to decompose the dye as substrate. The treatment in the anaerobic filter proved to remove the dye and to produce and simultaneously remove aromatic amines.

Fig. 1. Hypothetical behaviour of the transformations of substances in a pore of filter material based on the work of van der Zee and Villaverde (2005)

According to the work of van der Zee and Villaverde (2005) and Cobos-Becerra and González-Martínez (2013) Fig. 1 was built indicating that an aerobic biofilm growing on a porous surface will create an anaerobic region in the deeper parts of the pores. On the biofilm surface, aerobic processes will take part allowing the unchanged azo dye to diffuse to the anaerobic region where the azo bonds will be broken to form aromatic amines, which will diffuse to the aerobic region to be mineralized under aerobic conditions.
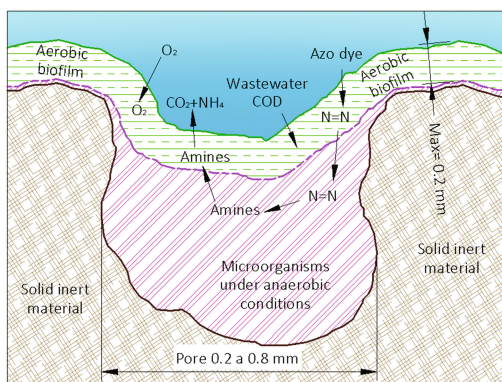
The main objective of this work was to demonstrate that azo dyes could be removed, simultaneously with organic matter, when the biofilm carrier has deeper pores.

2   Materials and Methods

The experimental filter was constructed using a PVC pipe placed vertically, 15 cm in diameter and 1.90 m height (Fig. 2). The filter material was lava stones, 12.7 mm average diameter, and one meter height. The feed was from the bottom (upflow) and the effluent was at the top of the bed. Sampling points were placed every 20 cm along the filter height. Air was supplied from the bottom of the filter continuously, adjusted with mass flow controller to deliver 5.0, 2.0, 1.0, 0.5 and 0.0 L/min. Dissolved oxygen (DO) was continuously monitored using a dissolved oxygen probe In the inner part of the reactor at the effluent height.

The experiment ran during 180 days. The wastewater was synthetically prepared in the lab and adjusted to a constant organic loading rate of 6 gCOD/m2·d (1.75 kgCOD/m3·d) using maltodextrin and vegetal hydrolysed protein (from soya) as organic matter and a complement of micronutrients. The synthetic wastewater was kept under refrigeration to prevent the additional entry of microorganisms into the system. When the system was stabilized at 2.0 mg/L of DO, Direct Blue 2 azo dye was added at a concentration of 30 mg/L. Parameters such as COD, Kjeldahl nitrogen, nitrate, nitrite, orthophosphates, total and volatile suspended solids, colour and redox potential were performed according to APHA (2012).

3   Results and Discussion

Table 1 shows the main operational characteristics (air flow, DO) and the removal rates for COD, ammonia nitrogen, PO_4-P, colour, and MCRT and redox. It can be observed that COD maximal removal rates was 83% at an air flow of 2.0 L/min without azo dye. With decreasing air flow, COD removal decreased to a minimum value of 46% with azo dye and the lowest air flow of 0.5 L/min (no detectable DO).

Without dye addition NH$_4$-N removal went from 79% under an air flow of 5.0 L/min to 16% under 2.0 L/min and, with dye addition NH$_4$-N removal decreased with decreasing DO concentration from
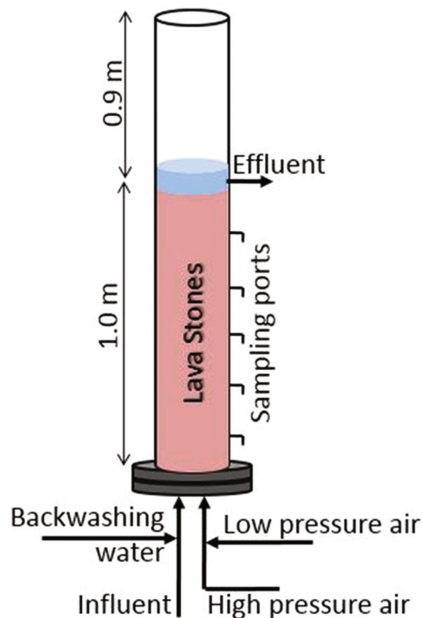
Fig. 2. The pilot biological aerated filter

Table 1. Biochemical behaviour of the experimental filter

	Q_{air}	Diss O_2	COD Rem	NH_4-N Rem	PO_4-P Rem	Colour Rem	MCRT	Redox
	(L/min)	(mg/L)	(%)	(%)	(%)	(%)	(d)	(mV)
Without dye	5.0	6.5–7.5	81	79	40	–	5.0	–
	2.0	3.0–4.5	83	16	17	–	4.5	123
With dye	2.0	3.0–4.2	69	38	23	30	3.5	97
	1.0	0.6–1.5	69	13	36	31	3.0	54
	0.5	0.0–0.5	46	8	7	40	2.5	−31
	0.0	0.0	44	NA	NA	NA	3.5	−439

Rem = removal; NA - not available, MCRT = mean cellular retention time

38 to 8%. Nitrite remained under 0.2 mg/L at all flow rates. The maximum phosphate removal rate of 40% was obtained under an air flow of 5.0 L/min (6.5 to 7.5 mgO$_2$/L) and the lowest of 7% under an air flow of 0.5 L/min with azo dye addition. Colour removal increased with decreasing dissolved oxygen and maximum colour removal (40%) was achieved with aeration of 0.5 L/min and almost a non-detectable DO concentration (Fig. 3).
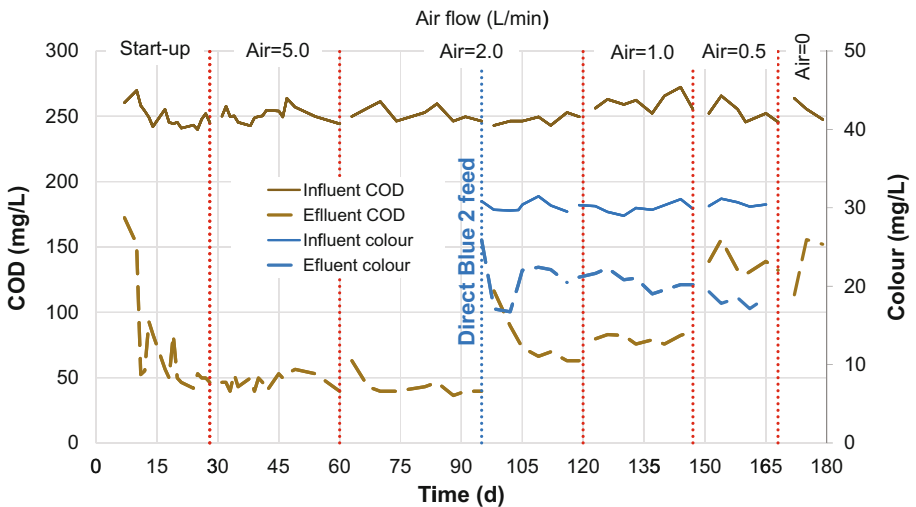

Fig. 3. Organic matter and dye concentrations over the completely experimental time

For the determinations of colour removal with no air supply, the filter effluent presented high turbidity; no filtration or centrifugation of the samples managed to reduce the turbidity causing photometric determinations to fail. As expected, redox potential decreased with decreasing air flow (oxygen concentration) from 123 mV with an air flow of 5.0 L/min to −439 mV without air supply at all. Mean cellular retention time decreased with decreasing DO concentration: Without dye addition the value varied between 4.5 and 5 days and, with dye addition, the values went from 3.5 days under air flow of 2.0 L/min to 2.5 days under air flow of 0.5 L/min.

It is important to note that future research should be geared to working with concentrations of OD below 0.5 mg/L, since evidently and according to the bibliography, the higher removal of dyes is increased as the dissolved oxygen decreases.

4   Conclusions

- COD removal rates decreased with decreasing DO concentrations. Dye addition affected negatively COD removal.
- Ammonia nitrogen concentration removal rates decreased with decreasing DO concentrations and it increases slightly when the dye was firstly added and then it decreased with decreasing air supply.
- Colour removal slightly increased with decreasing DO concentration from 30 to 40%. It is estimated that the color removal significantly increased at the beginning of the experiment period is due to adsorption processes in the biofilm, reflecting a false removal data.
- Mean cellular retention time decreased with decreasing DO concentration.
- Redox values and COD removal rates decreased when the azo dye was added to the filter.

References

APHA, AWWA (2012) Standard Methods for the Examination of Water and Wastewater, 18th edn. American Public Health Association/America Water Works Association

van der Zee FP, Villaverde S (2005) Combined anaerobic-aerobic treatment of azo dyes - a short review of bioreactor studies. Water Res 39:1425–1440

Cobos-Becerra YL, Gonzalez-Martinez S (2013) Influence of the organic loading rate on the hydraulic behaviour and the azo-dye removal in an anaerobic filter. J Chem Technol Biotechnol 90:566–572

Kong F, Wang A, Ren H-Y (2015) Improved azo dye decolorization in an advanced integrated system of bioelectrochemical module with surrounding electrode deployment and anaerobic sludge reactor. Bioresour Technol 175:624–628

Wang Z, Huang K, Xue M, Liu Z (2011) Textile Dyeing Wastewater Treatment. INTECH Open access Publisher, China

Popli S, Patel UD (2015) Destruction of azo dyes by anaerobic–aerobic sequential biological treatment. Int J Environ Sci Technol 12:405

Puvaneswari N, Muthukrishnan J, Gunasekkaren P (2006) Toxicity assessment and microbial degradation of azo dyes. Indian J Exper Biol. 44:618–626

Greenhouse Gas Emissions from Membrane Bioreactors

G. Mannina[1(✉)], M. Capodici[1], A. Cosenza[1], D. Di Trapani[1],
and Mark C.M. van Loosdrecht[2]

[1] Dipartimento di Ingegneria Civile, Ambientale, Aerospaziale, dei Materiali,
Università di Palermo, Viale delle Scienze, Ed. 8, 90128 Palermo, Italy
[2] Department of Biotechnology, Delft University of Technology, Julianalaan 67,
2628 BC Delft, Netherlands

Abstract. Nowadays, it is widely accepted that wastewater treatment plants (WWTPs) are significant sources of greenhouse gas (GHG) emission, contributing to the anthropogenic sources. Among the GHG emitted from WWTPs, nitrous oxide (N_2O) has been identified of having the major interest/concern, since its high global warming potential (GWP), is 298 times higher than that of CO_2 and also to its capability to react with stratospheric ozone causing the layer depletion. Up to now, most of the experimental investigations have been carried out on conventional activated sludge (CAS) processes. The knowledge of N_2O emission from advanced technologies such membrane bioreactors (MBRs) is still very limited. The present paper is aimed at providing a picture of the GHG emissions from MBR systems. In particular, data of N_2O acquired from pilot plant systems monitoring are here presented. The key aim of the study was to highlight the effect of wastewater features and operational conditions on N_2O production/emission from MBRs.

Keywords: Wastewater treatment · Global warming · Filtration · Nutrients

1 Introduction

During the last decade, the awareness that wastewater treatment plants (WWTPs) are responsible of greenhouse gas emissions has considerably increased. The hard work done by the Intergovernmental Panel on Climate Change, aimed at identifying the causes, impacts and possible response strategies for mitigating climate change, has allowed to recognize the sector of waste and wastewater as accounting for about 3% of global GHG emissions (Climate Change 2007; IPCC 2013). The US Environmental Protection Agency (2013) estimated that the wastewater treatment sector was responsible for over 5% of global non- carbon dioxide GHG emissions in 2005, and predicted that GHG emission would increase by 27% by 2030.

It is widely accepted in literature that WWTPs emit GHGs through three main sources, i.e., direct, indirect internal and indirect external (GWRC 2011). Direct GHG emissions are due to the biological processes occurring inside the WWTP and represent the catabolite or obligate intermediate of reaction. Indirect GHG internal emissions are mainly due to the consumption of electrical or thermal energy. Finally, indirect GHG

external emissions are mainly related to sources not directly controlled within the WWTP.

The acquired awareness of "WWTP as source of GHG" has contributed to broaden the traditional goal of WWTPs to the GHG matter. Indeed, the traditional aim of WWTPs to achieve very stringent effluent limit includes now the GHG emission issue (Flores-Alsina et al. 2011a).

Among the GHG emitted from WWTPs, N_2O has been identified of having the major interest. Despite the amount of N_2O emitted from WWTPs is considerably lower than CO_2 or CH_4, the major interest on its emission from WWTPs is due to its high global warming potential (GWP), 298 times higher than that of CO_2, and to its capability to react with stratospheric ozone causing the layer depletion (IPCC 2007).

N_2O is mainly produced in the biological nitrogen removal (BNR) processes via nitrification and denitrification both from autotrophic and heterotrophic bacteria (Kampschreur et al. 2009). The main part of the study on N_2O are related to conventional activated sludge systems (CAS) and the knowledge acquired may not be transferred into innovative systems such as membrane bioreactors (MBR). Indeed, MBRs are characterized by some specific peculiarities (biomass selection; absence of secondary clarifier which can contribute in N_2O production; intensive aeration for fouling mitigation in membrane compartment which can promote N2O stripping; etc.), which may hamper a direct transferability of the results derived for CAS systems.

The main goal of this paper is to summarize the key elements influencing the N_2O production/emission from MBR WWTPs.

2 Materials and Methods

During the Italian research project PRIN2012 entitled "Energy consumption and GreenHouse Gas (GHG) emissions in the wastewater treatment plants: a decision support system for planning and management" 2 years of experimental activities were carried out. The main aim was to assess the effect of different MBR configurations, influent wastewater (municipal or industrial), operational conditions (sludge retention time, SRT, carbon-to-nitrogen ratio, C/N, hydraulic retention time, HRT) and membrane modules on the N_2O production/emission. In Fig. 1 the experimental lay out investigated are depicted.

Briefly, pilot plant N.1 (SB-MBR) was designed according to a pre-denitrification scheme in a sequential feeding mode. It consisted of two in-series reactors anoxic-aerobic followed by a MBR compartment (Zenon, ZW 10). The experimental campaign was divided into six Phases during which the salt concentration was gradually increased from 0 to 10 g NaCl L^{-1}. Pilot plant N.2 (DN-MBR) consisted of two in-series reactors anoxic-aerobic fed in continuous followed by a MBR compartment. The experimental campaign was divided in two Phases: increasing salinity of the influent (from 10 g NaCl L^{-1} up to 20 g NaCl L^{-1}) during Phase I, while in Phase II the inlet wastewater was characterized by constant salinity (20 g NaCl L^{-1}) and hydrocarbons dosage. Anaerobic, anoxic and aerobic in-series reactors, according to the University of Cape Town (UCT) scheme (Ekama et al. 1983), characterized pilot plant N.3 (UCT-MBR). The MBR module was UF module Koch PURON® 3 bundle.
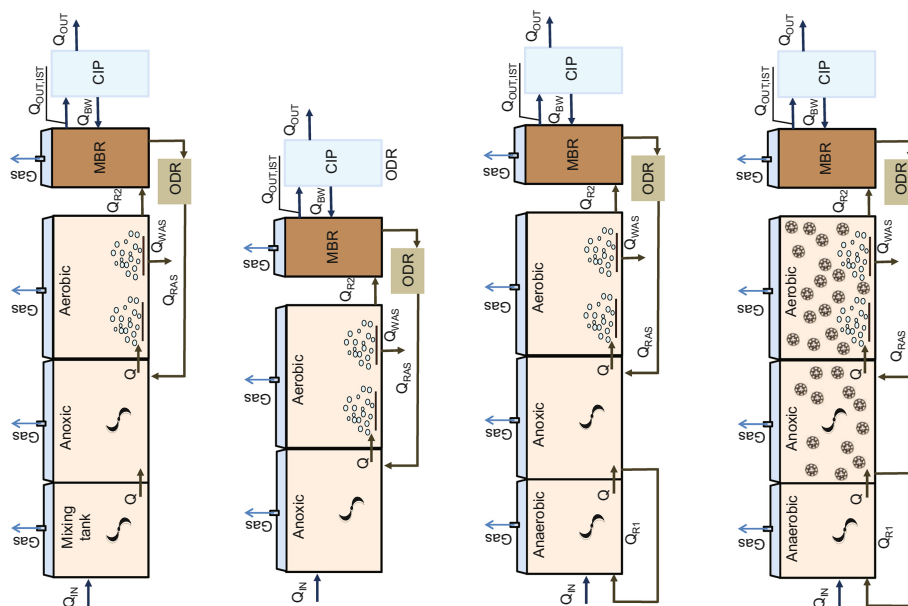
Fig. 1. Schematic layout of the investigated pilot plants: SB-MBR (a), pre-denitrification MBR (b), UCT-MBR (c) and UCT-MB-MBR (d)

The experimental campaign was divided in two Phases, each characterized by a different value of the inlet C/N ratio: C/N = 10 and C/N = 5 during Phase I and Phase II respectively. Pilot plant N.4, (UCT-MB-MBR), consisted of the same scheme of Pilot Plant N.3. Furthermore, suspended plastic carriers (Amitech) for biofilm growth have been added to the anoxic and the aerobic reactors, with filling fraction of 15 and 40. The experimental campaign was aimed at investigating the influence of operational variables (namely, SRT, C/N ratio and HRT-SRT) on N_2O production and emission.

For further details on pilot plant description as well as on experimental campaings the reader is addressed to literature (Mannina et al. 2016a, b, c; 2017a, b).

Samples from the liquid bulk of each reactor were collected and the dissolved nitrous oxide was extracted in accordance with procedure proposed by (Kimochi et al. 1998). Sample of the permeate flow were also collected in order to quantify the dissolved N_2O concentration discharged with the effluent flow rate. Both, dissolved and head-space, samples were analyzed by means of Gas Chromatography using an Electron Capture Detector (ECD) in order to assess the N_2O concentration. Furthermore, a hot wire anemometer allowed the air velocity measurement within the funnel of each reactor and thus the flux of nitrous oxide emitted from the liquid surface of each reactor was assessed. The nitrous oxide emission was assessed also in terms of Emission Factor (EF) evaluated in accordance with method proposed by (Tsuneda et al. 2005). Moreover, the abundance of measured N_2O concentrations, dissolved and emitted, coupled with the detailed knowledge of the liquid fluxes passing through each reactor allowed the calculation of nitrous oxide mass balance that highlighted the production or the consumption of N_2O within each reactor.

3   Results

Data collected over almost two years underline the huge variability of N_2O concentration measured; indeed, the nitrous oxide concentrations ranged within 7 orders of magnitude (from 10^{-1}µg N_2O-N L^{-1} up to 10^5 µg N_2O-N L^{-1}).

Such extreme variability in N_2O concentrations resulted also in a wide range of emission factor measured during the experimentation. In Fig. 3 the average value of emission factors measured for each experimental ley out are depicted.

Data depicted in Fig. 2 highlight the influence exerted by the layout on the nitrous oxide emission. In details, the DN-MBR scheme result as featured by the highest emission factor (16% of influent nitrogen on average). It is worth noticing that also the influent wastewater composition played a significant role in increasing the N_2O emission. Indeed the DN-SBR scheme treated an influent wastewater composed also by salt and diesel fuel. With regard to the UCT-MBR and UCT-MB-MBR configuration, the scarcity of carbon availability imposed during the lowest values of C/N ratio resulted in an increase of N_2O emission likely due to a limitation of denitrification process. To summarize, the configuration that yielded the lowest EF was the UCT-MB-MBR that was featured by a mean emission equal to 0.5% of influent nitrogen. Actually, the operational condition influenced the emission also during this period. As an example, when an SRT = 30 d was imposed to the pilot plant, the mean emission factor resulted equal to 7.57%.
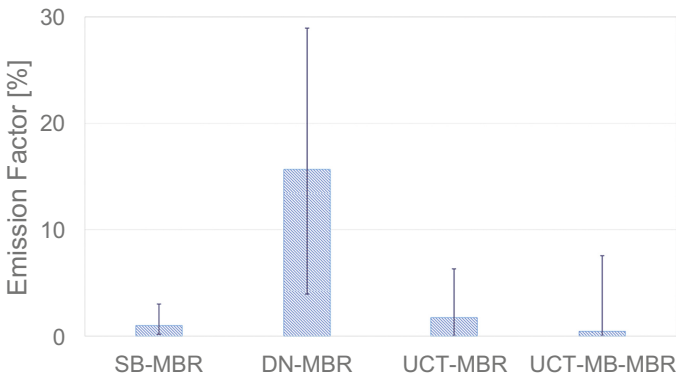
Fig. 2. Nitrous oxide concentration measured in the Head space and in the liquid bulk of Aerobic (a) and Anoxic (b) reactors over the experimentation

In order to describe also the role played by each reactor in contributing to the total emission, in Fig. 3 is depicted a comparison of mean EF assessed for each reactor during UCT-MBR and UCT-MB-MBR configuration.

Data depicted in Fig. 3 highlight the strong reduction in EF during the UCT-MB-MBR layout. Such result is likely due to an improvement in biological performances exerted by the co presence of both suspended and attached biomass. The
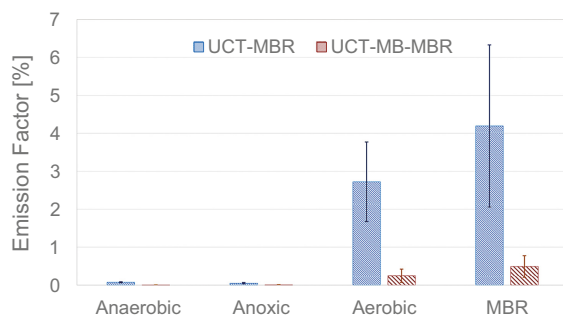
Fig. 3. Comparison of mean EF measured in each biological reactor during the UCT-MBR and UCT-MB-MBR layout

biofilm presence improved the nitrogen removal efficiency thus leading to a lower N_2O emission.

In order to compare direct and indirect emission, in Fig. 4 data related to the relationship between the air flow versus, indirect (Fig. 4a) and direct emissions (Fig. 4b) obtained are reported.
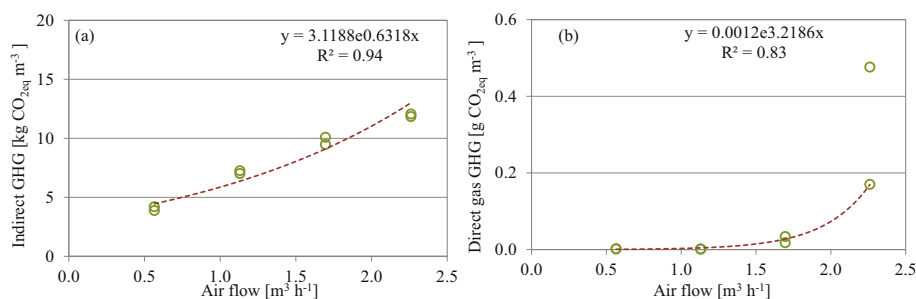
Fig. 4. Relationship between the air flow and indirect GHG emissions (a); correlation between the air flow rate direct GHG emissions (b)

An exponential relationship ($R^2 = 0.83$) between the air flow and the indirect (Fig. 4a) and direct (Fig. 4b) GHG emissions was found.

In terms of GHG emissions (both direct and indirect) the lowest air flow ($0.6 \ m^3 h^{-1}$) seems to be more adequate than the others. Such result highlights the interlinkages between different involved phenomena. Indeed, a "multiple trade-off" has to be performed for identifying the best value of the air flow to mitigate GHG emissions and to reduce the EQI and OCs value.

4   Conclusions

The understanding of processes that enhance GHG emission as well as the knowledge of operational varibles and conditions that favour their production represent key challenges investigated by the scientific community in the last years. Indeed, many efforts have been recently evoted in experimental activities with the aim to: i. assessing the main mechanisms of GHG formation, ii. evaluating the operational conditions that favour their production.

In this context, some aspects related to GHG production/emission are still poorly understood and deserve further investigations. For instance, despite many studies revealed that N_2O formation mostly derives from AOB activity, the conditions that trigger its formation are still not clear. Moreover, from a management point of view, literature studies highlighted the need to focus on GHG emission from WWTPs. Indeed, if the target is only represented by the liquid effluent quality coupled to the minimization of the operational cost, the GHG emission might be significant. As an example, the decrease of the dissolved oxygen set-point inside the nitrification reactor could promote the increase of N_2O production due to incomplete nitrification, despite the reduction of the operational costs.

In this light, a plant wide mathematical modelling could represent a useful tool for the comparison of different scenarios (in terms of either design or management) for the evaluation of the best system performance, referring to both quality of the liquid effluent, reduction of gaseous emissions and operational costs reduction.

In this light, the aim of the scientific community should be the build-up of simplified mathematical tools, derived by complex dynamic mathematical models, to be used as decision support systems able to simulate the quality of gaseous and liquid emissions from WWTPs and to provide useful indications for the optimization of the system management.

References

Ekama GA, Siebritz IP, Marais GR (1983) Considerations in the process design of nutrient removal activated sludge processes. Water Sci Technol 15:285–318

Flores-Alsina X, Arnell M, Amerlinck Y, Corominas L, Gernaey KV, Guo L, Lindblom E, Nopens I, Porro J, Shaw A, Vanrolleghem PA, Jeppsson U (2011a) A dynamic modelling approach to evaluate GHG emissions from wastewater treatment plants. In: Proceedings of World Congress on Water, Climate and Energy

GWRC-Global Water Research Coalition (2011) N_2O and CH_4 emission from wastewater collection and treatment systems — state of the science report, 2011–29, London, UK

IPCC (2007) Changes in atmospheric constituents and in radiative forcing. In: Solomon S et al. (eds.) Climate change 2007: the physical science basis. Contribution of working group I to the fourth assessment report of the intergovernmental panel on climate change. Cambridge University Press, Cambridge, pp 114–143

IPCC, Climate Change (2013) The physical science basis. In: Contribution of working group I to the fifth assessment report of the intergovernmental panel on climate change. Cambridge University Press, Cambridge, New York, p 1535

Kampschreur MJ, Temmink H, Kleerebezem R, Jetten MSM, van Loosdrecht MCM (2009) Nitrous oxide emission during wastewater treatment. Water Res 43:4093–4103

Kimochi Y, Inamori Y, Mizuochi M, Xu K-Q, Matsumura M (1998) Nitrogen removal and N_2O emission in a full-scale domestic wastewater treatment plant with intermittent aeration. J Ferment Bioeng 86(2):202–206

Mannina G, Morici C, Cosenza A, Di Trapani D, Ødegaard H (2016a) Greenhouse gases from sequential batch membrane bioreactors: a pilot plant case study. Biochem Eng J 112:114–122

Mannina G, Cosenza A, Di Trapani D, Laudicina VA, Morici C, Ødegaard H (2016b) Nitrous oxide emissions in a membrane bioreactor treating saline wastewater contaminated by hydrocarbons. Bioresour Technol 219:289–297

Mannina G, Cosenza A, Di Trapani D, Capodici M, Viviani G (2016c) Membrane bioreactors for treatment of saline wastewater contaminated by hydrocarbons (diesel fuel): an experimental pilot plant case study. Chem Eng J 291:269–278

Mannina G, Capodici M, Cosenza A, Di Trapani D, Laudicina VA, Ødegaard H (2017a) Nitrous oxide from moving bed based integrated fixed film activated sludge membrane bioreactors. J Environ Manage 187:96–102

Mannina G, Capodici M, Cosenza A, Di Trapani D, van Loosdrecht MCM (2017b) Nitrous oxide emission in a University of Cape Town membrane bioreactor: the effect of carbon to nitrogen ratio. J Cleaner Prod 149:180–190

Tsuneda S, Mikami M, Kimochi Y (2005) Effect of salinity on nitrous oxide emission in the biological nitrogen removal process for industrial wastewater. J Hazard Mater 119:93–98

Environmental Assessment of Anammox Process in Mainstream with WWTP Modeling Coupled to Life Cycle Assessment

M. Besson[1,2,3(✉)], L. Tiruta-Barna[1,2,3], and M. Spérandio[1,2,3]

[1] Université de Toulouse; INSA, UPS, INP, LISBP,
135 Avenue de Rangueil, 31077 Toulouse, France
[2] INRA, UMR792 Ingénierie des Systèmes Biologiques et des Procédés,
31400 Toulouse, France
[3] CNRS, UMR5504, 31400 Toulouse, France

Abstract. This work aims to assess the environmental balance of this process by an integrated approach consisting in modeling the WWTP and life cycle assessment. In this way two models were developed to represent HRAS and PN/A in one single stage with oxygen limitation. These models have been calibrated with literature data, and validated by modeling Strass WWTP (Austria). Finally, the models were used to compare the mainstream application to a reference WWTP. The LCA have been conducted at Endpoint and Midpoint level with different emission factors of nitrous oxide. In this way the threshold value of emission factor until the process is still interesting, from an environmental point of view, can be determined.

Keywords: Partial Nitritation/Anammox · Mainstream · Wastewater treatment plant · Process modeling · Life cycle assessment

1 Introduction

Nowadays replacing the nitrification/denitrification step in wastewater treatment plant (WWTP) by partial Nitritation/Anammox (PN/A) is considered as an opportunity to meet the energy self-sufficiency of the WWTP (Kartal et al. 2010). PN/A consists of the combination of ammonium oxidizing bacteria (AOB) and Anammox bacteria. The first oxides ammonium to nitrite and the second will convert ammonium and nitrite into nitrate and dinitrogen gas. In this way, the aeration demand is decreased (only half of the ammonia needs to be converted into nitrite) and no organic matter is needed for denitrification allowing converting more organic matter into methane. This last can be done with Enhanced Primary Clarification (EPC) and/or High-Rate Activated Sludge (HRAS) to produce more primary sludge.

PN/A application on the mainstream is currently actively investigated, tackling progressively the technological barriers (microbial competition, a low growth rate at ambient temperature…) (Laureni et al. 2015). However, as the emission of greenhouse gases and especially nitrous oxide is still under estimation, the environmental sustainability is not well evaluated. Until now, the few study of environmental assessment used only lab-scale results or rough calculation for energy balance (Kuenen et al. 2011; Schaubroeck et al. 2015).

2   Material and Method

Six scenarios have been compared (Figs. 1 and 2): (i) the *Reference* WWTP performing both nitrogen and phosphorus removal and anaerobic digestion of the sludge, (ii) the *Reference EPC*; (iii) the same configuration as the *Reference* with a single-stage reactor of PN/A as sidestream treatment (*SideStream*); (iv) the reference with EPC scenario and with sidestream (*SideStream EPC*); (v) an AB system consisting of a primary sedimentation tank, an HRAS followed by a single-stage reactor of PN/A with polishing treatment (aerobic stage, denitrification stage and post aerated tank) (*Main-Stream*); (vi) the MainStream scenario with EPC (*MainStream EPC*).
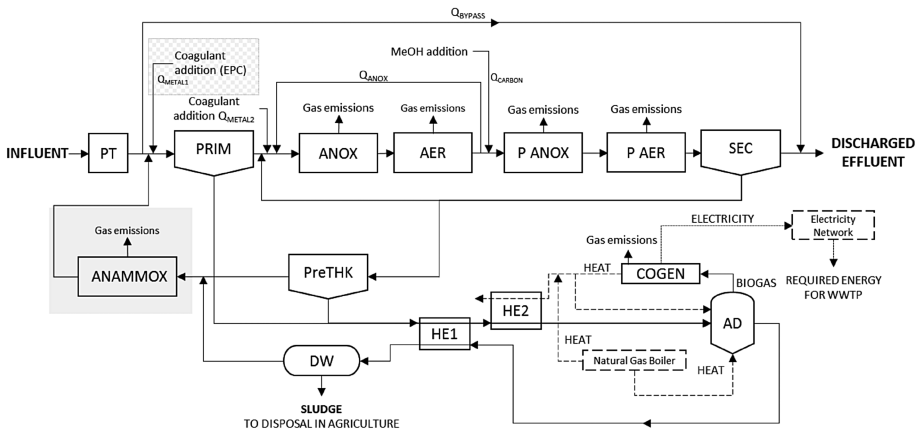

Fig. 1. Plant configuration for the Reference scenario and for SideStream in grey box and with EPC in checkerboard pattern. (Solid lines: liquid, solid and gas flows, dashed lines: energy flows)
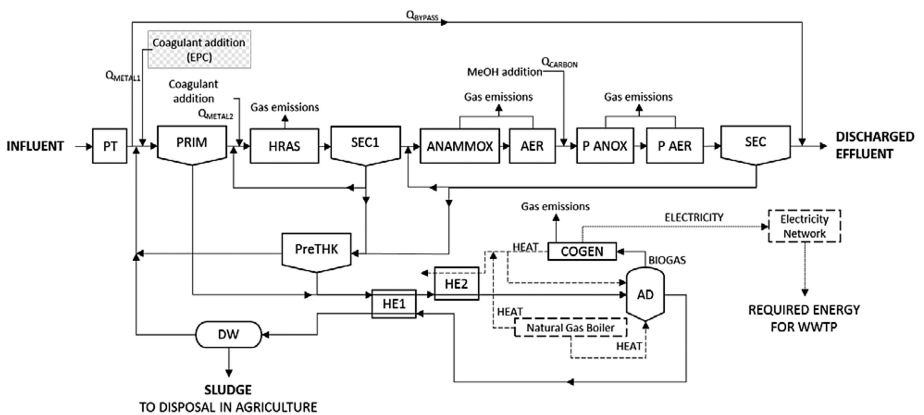

Fig. 2. Plant configuration for MainStream and MainStream EPC (in checkerboard pattern). (Solid lines: liquid, solid and gas flows, dashed lines: energy flows)

The WWTP in *Reference* scenario, is an adaptation of the benchmark simulation model n°2 (BSM2) from (Jeppsson et al. 2006), in order to comply stricter discharge standard (TN < 10 mgN/L; TP < 1 mgP/L; NH_4-N < 4 mgN/L).

The comparison was based on the integrated Dynamic Modeling-Life Cycle Assessment (DM-LCA) framework developed by (Bisinella de Faria et al. 2015) adapted to this case study. This tool makes the interface (by using Python) between the software SUMO version 15beta69.1 for WWTP simulation and the software Umberto® with Ecoinvent 2.2 for LCA. The platform calculates the energy production and consumption and more generally the inventory for the life cycle assessment of modeling results.

The High Rate Activated Sludge can remove 70–80% of total COD (Zhao et al. 2000), by the combination of adsorption, coagulation, and flocculation. The adsorption is achieved in very short time in the order of minutes (Guellil et al. 2001) leading to a SRT around 1 day and HRT around 30 min (Jimenez et al. 2015). The modeling approach chosen in this study, is the one detailed by (Wett et al. 2015). This simplified model applied only in the HRAS reactor, mimicked absorption and storage by increasing the heterotrophic growth rate and achieved incomplete readily biodegradable COD removal by increasing the substrate half-saturation coefficient of heterotrophs. The parameters of flocculation of colloidal matter have been also modified. The modeling of single-stage PN/A can be done in two different ways: (i) by considering the transfer from the bulk phase in aggregates/biofilm; (ii) the simulation of the biofilm/aggregates can be neglected but the kinetic parameters need to be apparent. Despite the induced simplifications, this last approach was chosen.

To validate the entire platform with the different models, the framework DM-LCA has been used to model the WWTP from Strass. The Strass WWTP is composed of two stages biological treatment (A/B plant) with anaerobic digestion of the sludge and sidestream treatment composed of partial nitritation and anammox process (Nowak et al. 2011). Moreover, the WWTP of Strass in Austria has achieved energy self-sufficiency since 2005.

3   Results

The model of HRAS was calibrated with the data from (Nogaj et al. 2015) and (Jimenez et al. 2015). The two models of HRAS and PN/A were used to model Strass WWTP, which is one of the first WWTP achieving electricity self-sufficiency (Nowak et al. 2011). Both consumption and production of electricity showed an error around 10% (Table 1), which leads to 2% of error regarding electricity return on investment.

Concerning the PN/A in mainstream application the energy balance and LCA results (respectively Figs. 3 and 5) presents that unlike the scenario *ReferenceEPC* and *SideStreamEPC*, the electricity self-sufficiency, was achieved without using more chemicals (methanol). The main gain comes from the decrease in aeration. By the electricity production avoided, the last scenario *MainStreamEPC* can reduce climate change impact by 26%, if we consider the same emission factor for nitrous oxide for both (0.5% of N-nitrified). A first analysis on the effect of emission factor in the PN/A

Table 1. Comparison of electricity consumption and production for Strass WWTP (from (Wett et al. 2007), reference year: 2005)

	Electricity consumption	Pumping station	Mechanical treatment	A stage	SBR reject water	B stage	Sludge treatment	Off gas treatment	Lighting and buildings	Electricity production	Electricity Return on Investment
Unit	kWh/d										Ratio
Real WWTP	**7,869**	710	318	758	196	3,530	1,000	800	557	**8,600**	**1.09**
Simulated	**8,769**	642	517	928	134	4,165	1,054	800	526	**9,359**	**1.07**
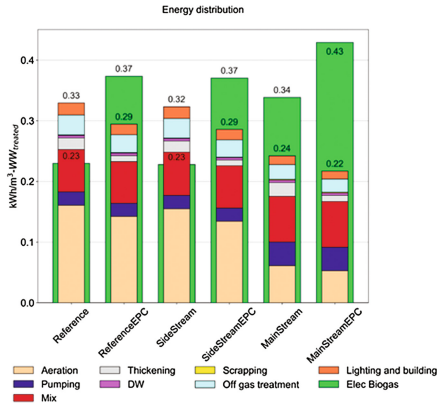
Fig. 3. Energy balance for the 6 scenarios
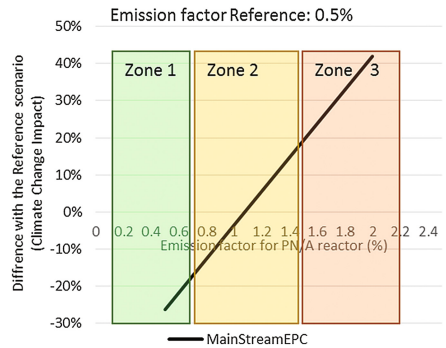
Fig. 4. Effect of emission factor on climate change midpoint impact

reactor (see Fig. 4) showed that it must stay below 0.7% to limit climate change (Zone 1). In the other way, upper 1.4% the process will increase climate change without doubt (Zone 3). Between these two values, the difference is not statistically significant from a LCA point of view (Zone 2). In the extended article, impacts contribution will be discussed in detail.

Moreover, the scenario *MainStream* and *MainStreamEPC* will be compared regarding the efficiency of the first treatment (HRAS alone or coupled with EPC). The influence of the separation efficiency of the first stage (colloidal matter, suspended solid loss), will be discussed regarding several consequences as a flux of COD to PN/A stage, energy balance, Anammox performance, residual nitrogen concentration and polishing denitrification unit.
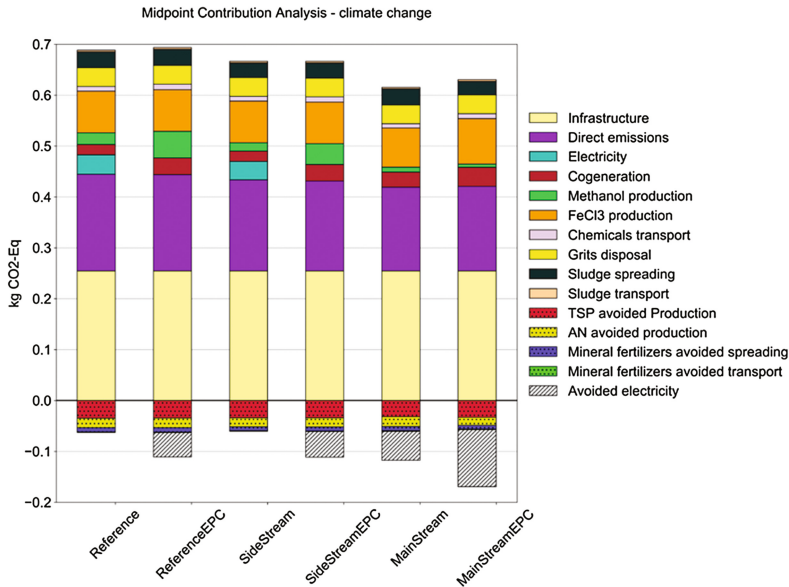
Fig. 5. Climate change impact for the 6 scenarios

4   Conclusion

This study gives some perspective and recommendations to develop PN/A application in the mainstream. LCA gives the boundaries of N_2O emission factor to reach in the PN/A process and hierarchize the contribution of each treatment step to the overall impacts. The energy gain may be significant with an electricity return on investment from 1.3 to 1.9, depending on the strategy chosen for organic matter capture and conversion to methane.

References

de Faria ABB, Spérandio M, Ahmadi A, Tiruta-Barna L (2015) Evaluation of new alternatives in wastewater treatment plants based on dynamic modelling and life cycle assessment (DM-LCA). Water Res 84:99–111. doi:10.1016/j.watres.2015.06.048

Guellil A, Thomas F, Block J-C, Bersillon J-L, Ginestet P (2001) Transfer of organic matter between wastewater and activated sludge flocs. Water Res 35:143–150. doi:10.1016/S0043-1354(00)00240-2

Jeppsson U, Rosen C, Alex J, Copp J, Gernaey KV, Pons M-N, Vanrolleghem PA (2006) Towards a benchmark simulation model for plant-wide control strategy performance evaluation of WWTPs. Water Sci Technol 53:287–295. doi:10.2166/wst.2006.031

Jimenez J, Miller M, Bott C, Murthy S, De Clippeleir H, Wett B (2015) High-rate activated sludge system for carbon management – Evaluation of crucial process mechanisms and design parameters. Water Res 87:476–482. doi:10.1016/j.watres.2015.07.032

Kartal B, Kuenen JG, van Loosdrecht MCM (2010) Sewage treatment with anammox. Science 328:702–703. doi:10.1126/science.1185941

Kuenen J, Kartal B, van Loosdrecht M (2011) Application of anammox for N-removal can turn sewage treatment plant into biofuel factory. Biofuels 2:237–241. doi:10.4155/bfs.11.10

Laureni M, Weissbrodt DG, Szivák I, Robin O, Nielsen JL, Morgenroth E, Joss A (2015) Activity and growth of anammox biomass on aerobically pre-treated municipal wastewater. Water Res 80:325–336. doi:10.1016/j.watres.2015.04.026

Nogaj T, Randall A, Jimenez J, Takacs I, Bott C, Miller M, Murthy S, Wett B (2015) Modeling of organic substrate transformation in the high-rate activated sludge process. Water Sci Technol 71:971. doi:10.2166/wst.2015.051

Nowak O, Keil S, Fimml C (2011) Examples of energy self-sufficient municipal nutrient removal plants. Water Sci Technol 64:1. doi:10.2166/wst.2011.625

Schaubroeck T, De Clippeleir H, Weissenbacher N, Dewulf J, Boeckx P, Vlaeminck SE, Wett B (2015) Environmental sustainability of an energy self-sufficient sewage treatment plant: improvements through DEMON and co-digestion. Water Res 74:166–179. doi:10.1016/j.watres.2015.02.013

Wett B, Al-Omari A, Bowden G, Stinson B, Szilagyi N, Takacs I, Jimenez J, De Clippeleir H, De Bardadillo C, Murthy S, Bailey W (2015) How short should the SRT be? – Investigation of parallel vs series C- and N-removal processes at the Blue Plains AWTP. Presented at the WEFTEC water environment federation technical exhibition and conference, Chicago, USA

Wett B, Buchauer K, Fimml C (2007) Energy self-sufficiency as a feasible concept for wastewater treatment systems. In: IWA leading edge technology conference. Asian Water, Singapore, pp 21–24

Zhao W, Ting YP, Chen JP, Xing CH, Shi SQ (2000) Advanced primary treatment of waste water using a bio-flocculation-adsorption sedimentation process. Acta Biotechnol 20:53–64. doi:10.1002/abio.370200109

Multi-point Monitoring of Nitrous Oxide Emissions and Aeration Efficiency in a Full-Scale Conventional Activated Sludge Tank

G. Bellandi[1,2(✉)], C. Caretti[1], S. Caffaz[3], I. Nopens[2], and R. Gori[1]

[1] Department of Civil and Environmental Engineering,
University of Florence, via di S. Marta 3, 50139 Florence, Italy
[2] BIOMATH, Department of Mathematical Modelling,
Statistics and Bioinformatics, Ghent University,
Coupure Links 653, 9000 Ghent, Belgium
[3] Publiacqua SpA, Via Romania snc, 50055 Lastra a Signa, Firenze, Italy

Abstract. In this work the biological tank of a WRRF in Italy was monitored placing five floating hoods on a plug-flow-like biological aerated tank surface in order to capture emission dynamics in both time and space domains. The five hoods report which location is more responsible for N_2O production at a certain moment of the day. Moreover, with this experimental investigation, a spatial shift in N_2O production towards the end of the biological tank could be detected. This provides important insights in the changes in biological dynamics especially with varying incoming load.

Keywords: GHG · Aeration · Off-gas

1 Introduction

Biological processes for water recovery in wastewater treatment sensibly contribute to global warming through direct emission sources that can be found throughout the whole plant area. Indirect emissions are also considerable for conventional water resource recovery facilities (WRRFs). However, direct emissions can have a major importance on the overall carbon footprint of the plant due to the biological generation of nitrous oxide (N_2O). Among the greenhouse gases (GHGs) known to be heavily contributing to the carbon footprint of a treatment plant, to date N_2O is globally recognized as a primary target to be reduced due to its very high global warming potential, i.e. about 300 times the one of CO_2 (Ravishankara 2009). N_2O can be produced during biological nitrogen (N) removal in WRRFs using activated sludge (AS) technology and can represent by itself 78% of the plant carbon footprint (Daelman et al. 2013). Hence, the increasing concern regarding N_2O in the water sector over the past few years and the efforts concentrated in understanding the specific bio-chemical processes responsible for N_2O production (Schreiber et al. 2012) and the WRRF design and operational factors impacting its emission (Guo et al. 2013; Kampschreur et al. 2009; Monteith et al. 2005).

The biological formation of N_2O can mainly take place from the activity of heterotrophic bacteria (heterotrophic denitrification) and from the activity of ammonia oxidizing bacteria (AOB). In particular, AOBs seem to be the most effective contributors in N_2O production due to their double production pathway and their ability to shift between them depending on the local conditions in the tank (Kim et al. 2010; Wunderlin et al. 2012). As a matter of fact, these production pathways are favored by different operational conditions, which strongly depend on the technology used, the wastewater treated and the control strategy applied to the biological process (Ahn et al. 2010; Kampschreur et al. 2008). Dissolved oxygen (DO) and NO_2^- concentrations along with COD/N ratio appear to be the key influencing factors for N_2O production pathways (Aboobakar et al. 2013; Kampschreur et al. 2009).

2   Materials and Methods

San Colombano WRRF (Lastra a Signa, Florence, Italy), treats urban wastewater coming from Florence and surrounding municipalities with a capacity of 600,000 PE and a flowrate of approximately 60 Mm^3/y. It is a municipal CAS WRRF (managed by Publiacqua S.p.A.) with a modified Ludzak-Ettinger denitrification-nitrification configuration. The biological treatment is carried out in 12 identical plug flow tanks working in parallel and grouped in 3 lanes among which the influent is equally divided. Aeration is provided by fine-bubble diffusers (ABS, PIK300 with an area of 0.06 m^2) with EPDM membranes disposed in three zones along the aerated area with decreasing density of aerators towards the tank outlet: 14.3%, 10.1% and 8.5%. The age of diffusers differs between the lanes but not within the same lane. Air flow from blowers is equally partitioned between the three lanes.

Grab samples were taken hourly by means of an automatic sampler just before the entrance in the denitrification tank and analysis of NH_4^+ were made with standard kits (Hach). The samples were filtered with paper filter and 0.45 μm filters before refrigerated storage.

Five floating hoods were distributed over the area of one of the aeration tanks as reported in Fig. 1. The first four hoods had an area of 0.35 m^2, while the fifth hood covered 0.7 m^2 of the tank surface. The hoods were connected via a Teflon tube (4 mm in diameter) to a gas analyser (Innova, Pollution, Italy) for CO_2, N_2O and water vapour measurements. The sample from each hood was directed to the analyser by means of a multiplex sampler allowing measurements from each location every 5 min. Only the fifth hood was connected also to an off-gas analyser equipped with a zirconium oxide fuel cell (AMI Model 65, Advanced Micro Instruments, USA) for measuring oxygen partial pressure in the gas flow leaving the aerated tank, an absorption column (h = 0.255 m, d = 0.025 m) for removing CO_2 and moisture from the off-gas, a hot wire anemometer for measuring the off-gas flow rate captured by the hood and a data acquisition card (National Instruments, sbRIO-9632). Dissolved oxygen readings were also logged via an oximeter (LDO, Hach).
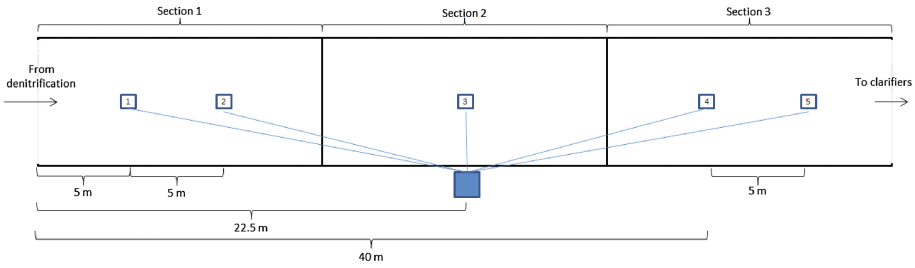
Fig. 1. Sampling locations at the aerated biological tank of San Colombano WRRF

3   Results and Discussion

From the measurements of the off-gas collected from the different hoods (Fig. 2) it is possible to notice that locations 4 and 5 appear to be more biologically active (in terms of CO_2 production) for the first half of the measurements. However, it must be pointed out that the low concentration in the off-gas for both CO_2 and N_2O is probably related to the typical diluted character of the plant influent. Despite this, the consistent and recursive sinusoidal shape of the time series suggests that both the microbial respiration (for which the CO_2 concentration in the off-gas can be assumed to be a valuable indicator) and the N_2O production find a maximum point source in location 4 until the incoming ammonia (measured before entering the biological treatment) starts to increase (Fig. 2, at 13:00). This suggests that the biomass activity in location 4 was at the maximum rate experienced in the biological tank for that part of the day.
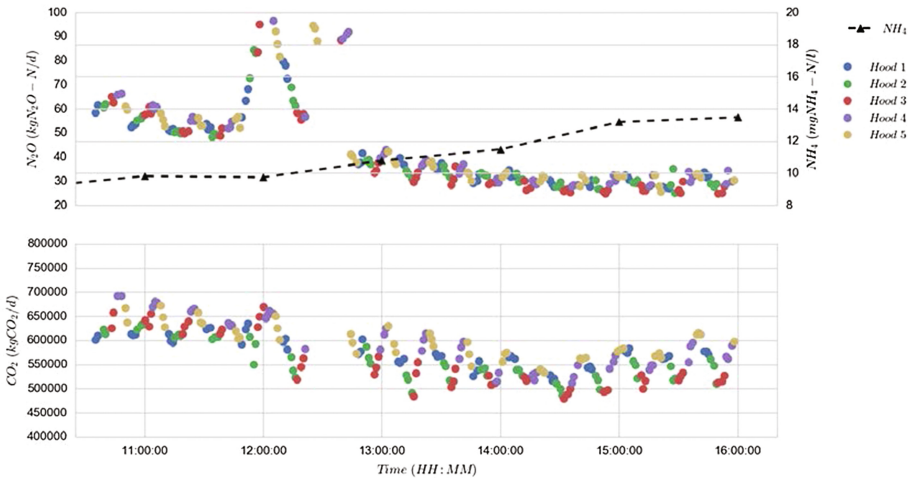
Fig. 2. N_2O and CO_2 emissions calculated for the whole surface of the aeration tank from the 5 hoods

The peak in N_2O concentration visible around 12:00 is most probably due to an increase in aeration over the whole tank which causes more efficient N_2O stripping from the liquid (available in the full paper). Interestingly, this increase in airflow did not influence the measurements of CO_2, however, allowing the same conclusions for location 4 at that time of the day.

As soon as the incoming ammonia concentration starts to increase in the afternoon, this trend is slowly shifted making location 5 as the most active for the last part of the day. This conclusion is again consistent for both CO_2 and N_2O concentrations.

In Fig. 3 concentrations of CO_2 are reported and compared to the relative N_2O concentration in the off-gas from all the different hoods. A relation between the biological activity and the N_2O emission could be drawn for the different positions on the tank. In general, low N_2O emissions relate to low bacterial activity (low CO_2 emissions due to low respiration) and high variability in N_2O values when the biomass works at regime. This confirms an expectable behavior of the data but it also suggests that locations 4 and 5 considerably remain present in the high N_2O emission part.
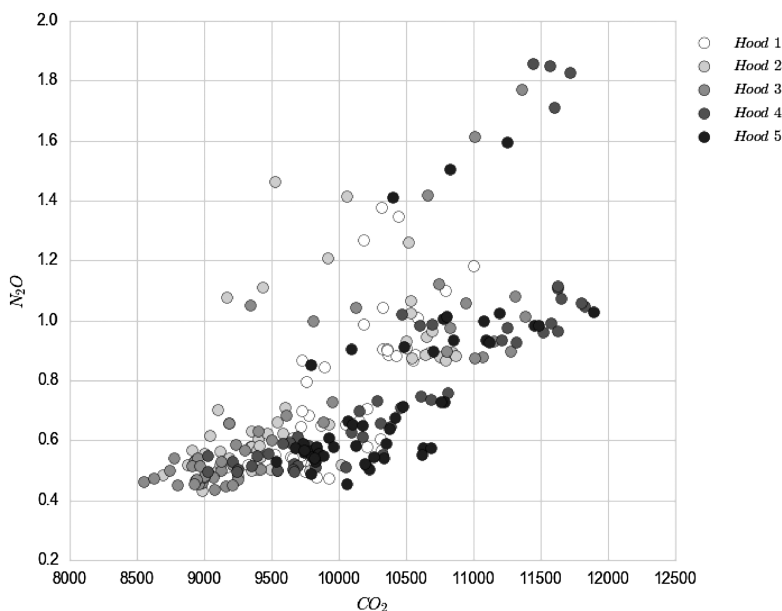
Fig. 3. Scatterplot of N_2O against CO_2 concentrations in the off-gas for each hood

A statistical overview of emission factors reported (Table 1) confirms the observations on location 4, while not showing the same for location 5. However, in the data shown in Fig. 2, location 5 gives maximum contribution to N_2O emission when the overall emissions are decreasing from all locations. The predominance of location 5 only in the second part of the day and, most importantly, when the overall emissions tend to decrease makes location 5 stats appear lower than the rest of the locations. As for location 1, 2 and 3, they show normally a tendency to be the lowest emitting

Table 1. Stats of emission factors for each hood (expressed in kg NH_4^+-N/kg N_2O-N)

Hood number	1	2	3	4	5
Mean	0.297	0.287	0.265	0.306	0.276
Standard deviation	0.185	0.165	0.148	0.153	0.118
Min	0.164	0.152	0.151	0.170	0.155
Max	0.976	0.863	0.839	0.633	0.571

location in comparison with 4 and 5, from their mean values (Table 1) and their behavior in the dataset (Fig. 2). However, these initial locations also show the highest variability (up to 0.976 kgNH_4^+-N/kgN_2O-N) and unsuitability for assessment of emission factors from a sampling campaign shorter than a full day.

4   Conclusions

The experimental method used allowed to simultaneously monitor different locations of a full-scale aeration tank and highlights differences in the biomass activity and its emissions.

Results give important insights in the variability of N_2O emission for both the temporal and spatial domain relative to influent dynamics. Measurement locations closer to the outlet of the bioreactor showed the highest contributions to N_2O emission, while locations at the beginning of the reactor showed the highest variability in emission factors.

Data confirm the unsuitability of the use of a general emission factor for estimating N_2O production, again especially for the locations closer to the inlet which, in some cases, even triplicated with respect to their average emission.

To our knowledge, this is the first time that spatial resolution of N_2O emissions is made visible at this resolution. Upcoming work will focus on acquiring more data in WRRFs having stronger influent loads.

References

Aboobakar A, Cartmell E, Stephenson T, Jones M, Vale P, Dotro G (2013) Nitrous oxide emissions and dissolved oxygen profiling in a full-scale nitrifying activated sludge treatment plant. Water Res 47:524–534

Ahn JH, Kim S, Park H, Katehis D, Pagilla K, Chandran K (2010) Spatial and temporal variability in atmospheric nitrous oxide generation and emission from full-scale biological nitrogen removal and non-BNR processes. Water Environ Res 82:2362–2372

Daelman MRJ, van Voorthuizen EM, van Dongen LGJM, Volcke EIP, van Loosdrecht MCM (2013) Methane and nitrous oxide emissions from municipal wastewater treatment – results from a long-term study. Water Sci Technol 67:2350

Guo LS, Lamaire-chad C, Bellandi G, Daelman MRJ, Maere T, Nous J, Flameling T, Weijers S, Mark CM, Loosdrecht V, Volcke EIP, Nopens I, Vanrolleghem PA (2013) High frequency

field measurements of nitrous oxyde (N2O) gas emissions and influencing factors at WWTPs under dry and wet weather conditions. In: WEF/IWA Nutrient Removal and Recovery

Kampschreur MJ, Tan NCG, Kleerebezem R, Picioreanu C, Jetten MSM, Van Loosdrecht MCM (2008) Effect of dynamic process conditions on nitrogen oxides emission from a nitrifying culture. Environ Sci Technol 42:429–435

Kampschreur MJ, Temmink H, Kleerebezem R, Jetten MSM, van Loosdrecht MCM (2009) Nitrous oxide emission during wastewater treatment. Water Res 43:4093–4103

Kim SW, Miyahara M, Fushinobu S, Wakagi T, Shoun H (2010) Nitrous oxide emission from nitrifying activated sludge dependent on denitrification by ammonia-oxidizing bacteria. Bioresour Technol 101:3958–3963

Monteith HD, Sahely HR, MacLean HL, Bagley DM (2005) A rational procedure for estimation of greenhouse-gas emissions from municipal wastewater treatment plants. Water Environ Res 77:390–403

Ravishankara AR (2009) Nitrous oxyde (N2O): the dominant ozone-depleting substance emitted in the 21st century. Science 326:123–125 (80-.)

Schreiber F, Wunderlin P, Udert KM, Wells GF (2012) Nitric oxide and nitrous oxide turnover in natural and engineered microbial communities: biological pathways, chemical reactions, and novel technologies. Front Microbiol 3:372

Wunderlin P, Mohn J, Joss A, Emmenegger L, Siegrist H (2012) Mechanisms of N2O production in biological wastewater treatment under nitrifying and denitrifying conditions. Water Res 46:1027–1037

Measuring Energy Demand and Efficiency at WWTPs: An Econometric Approach

S. Longo[(✉)], J.M. Lema, M. Mauricio-Iglesias, and A. Hospido

Department of Chemical Engineering, Institute of Technology,
Universidade de Santiago de Compostela, 15782 Santiago de Compostela, Spain

Abstract. As the number of wastewater treatment plants (WWTPs) increases worldwide and the effluent quality requirements become more demanding, the issue of energy efficiency has been attracting increasing attention from an environmental and economic point of view. However, defining and measuring energy efficiency in WWTPs is still a challenge. Energy efficiency is typically approximated by energy intensity, i.e. kWh/m^3. However WWTPs can perform different functions (i.e. removing of COD, removing of N and/or P, resource recovery, producing an effluent free of pathogens), or perform the same function with different technologies, making the comparison of WWTPs a challenging task. Thus, common energy intensity indicators have limited value, as they do not provide enough information of the WWTPs operation. Furthermore, changes in energy intensity are just approximate indicators for changes in energy efficiency since they are affected by external (exogenous) factors.

This study describes how linear regression analysis can be used as a means to estimate energy efficiency in WWTPs, by accounting for the impact of external factors and the diversity of treatment functions. Likewise, based on the analysis of a relatively large sample of WWTPs, the effect of some important variables on energy efficiency is discussed, which open possibilities for improving benchmarking comparability of WWTPs.

Keywords: Energy efficiency · Wastewater · Regression analysis

1 Introduction

Modern wastewater treatment plants (WWTPs) count with a number of on- and offline sensors that provide data on the performance of the plant. However, plant management does not always take full advantage of the analysis of process data. One of the potential uses of plant operation data is the evaluation of energy efficiency, which can be carried out by benchmarking. However, defining and measuring energy efficiency in WWTPs is still a challenge. Energy efficiency is typically approximated by energy intensity, despite several shortcomings related to this measure (Longo et al. 2016). Energy intensity is defined as the amount of energy use per unit of activity (e.g. volume of treated wastewater). Changes in energy intensity are just approximate indicators for changes in energy efficiency since they are affected by external (exogenous) factors such as the influent characteristics, climate factors, scale effect of plant size and other construction parameters. Furthermore, considering that WWTPs perform different

functions, i.e. removing of COD, removing of N and/or P, resource recovery, producing an effluent free of pathogens, general energy intensity indicators (i.e. kWh/m^3 or kWh/PE) have limited value, as they do not provide enough information of the WWTPs operation.

This abstract has two goals. We will describe how linear regression models can be used as a means to determine energy efficiency in WWTPs, while accounting for the impact of external factors. Likewise, based on the analysis of a relatively large sample of WWTPs, we will discuss the effect of some important variables on energy efficiency. Based on these indicators, it is then possible to identify the saving potential that can be reached with improvement in the level of energy efficiency (Chung 2011).

Literature that attempts to analyse the impact of operational variables on the energy efficiency is relatively scarce and sometimes contradictory (Longo et al. 2016). Hence, the analysis undertaken here explicitly takes into account energy consumption, and allows identifying the variables in the process that are drivers for energy consumption and, thus can be used to draw better comparisons among plants.

2 Materials and Methods

2.1 Data Collection

The data about energy consumption and operation of WWTP were gathered (i) by web-search engines with keywords: 'wastewater', 'WWTP', 'energy', 'energy consumption', 'energy performance', 'energy efficiency assessment', 'energy benchmarking', 'life cycle assessment', and (ii) collecting energy data from regional water agencies (in particular from Germany, Spain and Switzerland) by private communications. A total of 415 WWTPs from different countries were inventoried. The data included and calculated for the analysis are summarized in Table 1.

SecTreat and *TertTreat* are categorical variables for technology employed for secondary treatment and presence or not of tertiary treatment, respectively. *SIZE* is plant actual capacity expressed as person equivalent (PE). *FLOW* is average influent flowrate expressed in m^3/day. *PLF* and *DIL* are two indices defined as plant load factor and dilution factor, calculated as follow:

$$PLF = \frac{served\,PE}{design\,PE}100[\%] \tag{1}$$

$$DIL = \frac{daily\,influent\,flowrate}{served\,PE}[L/PE \cdot d] \tag{2}$$

CODinf, *CODeff*, *Ninf*, *Neff*, *Pinf* and *Peff* are respectively chemical oxygen demand, nitrogen and phosphorus concentration in the influent and effluent of the plant. Temp is outdoor temperature. Finally Y_1, Y_2 and Y_3 are total energy demand, volumetric and load basis energy intensity.

Table 1. Summary of variables considered for the exploratory analysis

Variable	Variable name	Abbreviation	Range	Units
X_1	Secondary treatment	*SecTreat*	'BNR'; 'MBR'; 'CAS'; 'Extended Aeration'; 'M/H-rate AS'; 'Oxidation Ditch'; 'Trickling filter'	–
X_2	Tertiary treatment	*TerTreat*	YES - NO	–
X_3	Plant size	*SIZE*	19–500,118	PE
X_4	Average flowrate	*FLOW*	6–126,082	m³/d
X_5	Plant load factor	*PLF*	1–512	%
X_6	Dilution factor	*DIL*	69–1,565	L/(PE·d)
X_7	Influent COD concentration	*CODinf*	96–1,820	mgCOD/L
X_8	Effluent COD concentration	*CODeff*	5–1,009	mgCOD/L
X_9	Influent N concentration	*Ninf*	6–151	mgN/L
X_{10}	Effluent N concentration	*Neff*	0–76	mgN/L
X_{11}	Influent P concentration	*Pinf*	0.5–27.6	mgP/L
X_{12}	Effluent P concentration	*Peff*	0–8	mgP/L
X_{11}	Outdoor Temperature	*Temp*	9.5–19.5	°C
Y_1	Energy consumption	*E*	10–36,563	kWh/day
Y_2	Volumetric based energy intensity	*EUI_Vol*	0.05–6.43	kWh/m³
Y_3	Load based energy intensity	*EUI_PE*	9.41–546	kWh/PE·year

3 Methodology

In this study, a linear regression approach is used to control for aspects that systematically influence the energy use at WWTPs. Regression models describe the relationship between a *depended variable, Y,* and *independent variables*, *X*. The dependent variable is also called the *response variable*. Independent variables are also called *explanatory* or *predictor variables*. Preliminary data analysis has shown that energy efficiency has a nonlinear dependency of operational variables (Longo et al. 2016). Therefore, using a

log-log functional form it is possible to determine a linear model describing the energy use in function of the explanatory variables. The log-log estimated equation is given by:

$$lnY = \beta_o + lnX\,\beta + \varepsilon \tag{3}$$

After estimating the log-log model, the β coefficients can be used to determine the impact of independent variables (X) on dependent variable (Y). In fact the coefficients in a log-log model represent the elasticity of Y variable with respect to X variable. In other words, the coefficient is the estimated percent change in your dependent variable for a percent change in the independent variables. The sign of the coefficient gives the direction of the effect. Moreover, ε, which represents the difference between actual and predicted average energy use, defines the relative energy inefficiency versus an equivalent plant with average performance.

Three different response variables, Y, were modelled here (as reported in Table 1) in order to study impact of external factors on total energy consumption (Y_1) and on two common energy intensity indicators (Y_2 and Y_3), which are commonly used as proxy of energy efficiency when comparing WWTPs performance. The models obtained were refined and checked for outliers, variegate multicollinearity, leverage and whether improper functional forms were used.

4   Results and Discussion

4.1   Estimated Energy Use Models

Following the previously described procedures three regression models were tested in order to describe the relationship between energy consumption and operational parameters in the following way:

$$lnY_i = \beta_o + \beta_{SecTreat}SecTreat + \beta_{TerTreat}TerTreat + \beta_{Temp}lnTemp + \beta_{PE}lnPE$$
$$+ \beta_{PLF}lnPLF + \beta_{DIL}lnDIL + \beta_{Nout}lnNout + \varepsilon, \tag{4}$$

where Y_i is one of the three dependent variables modelled as reported in Table 1.

The estimation results of the WWTPs energy demand model using different dependent variables are given in Table 2. The estimated coefficients are statistically significant in all models and show that the effect of the covariates on the dependent variable has the expected sign. For easier interpretation, the plots of estimated effects of predictors in the fitted models are presented in Fig. 1.

4.2   Impact of Operational Conditions on Energy Consumption

Plant size. It has been reported that the size of WWTPs influences its energy efficiency (Longo et al. 2016), which is confirmed by this study. Plant size has the largest effect in M1, and its elasticity found was 0.91 (Table 2), thus it results that on average 1 percent increase in plant size is associated with 0.91 percent increase in total energy

Table 2. Estimated WWTPs energy demand function

Parameter	M1 (Y = kWh/day)		M2 (Y = kWh/m³)		M3 (Y = kWh/PE)	
Intercept	−0.403***	(0.059)	−0.835***	(0.122)	−1.051***	(0.153)
SecTreat (Trickling filter)						
BNR	0.430***	(0.063)	0.893***	(0.131)	1.123***	(0.165)
Extended aeration	0.420***	(0.066)	0.871***	(0.136)	1.096***	(0.172)
M/H-rate AS	0.317***	(0.078)	0.659***	(0.162)	0.829***	(0.204)
Trickling filter-AS	0.330***	(0.125)	0.684***	(0.259)	0.860***	(0.326)
MBR	0.548***	(0.112)	1.138***	(0.233)	1.431***	(0.293)
Oxidation ditch	0.316***	(0.090)	0.655***	(0.188)	0.824***	(0.236)
CAS	0.370***	(0.119)	0.768***	(0.247)	0.966***	(0.310)
TerTreat (NO)						
YES	0.132**	(0.051)	0.275**	(0.107)	0.346**	(0.135)
lnTemp	0.084***	(0.021)	0.174***	(0.043)	0.219***	(0.055)
lnSIZE	0.912***	(0.018)	−0.348***	(0.037)	−0.438***	(0.047)
lnPLF	−0.114***	(0.015)	−0.237***	(0.031)	−0.299***	(0.039)
lnDIL	0.038**	(0.018)	−0.599***	(0.038)	0.100**	(0.048)
lnNout	0.095***	(0.015)	−0.197***	(0.032)	−0.248***	(0.041)
Root mean squared error	0.273		0.565		0.711	
Adjusted R-Squared	0.926		0.681		0.496	

*** Significant at 1% level; ** Significant at 5% level; * Significant at 10% level.
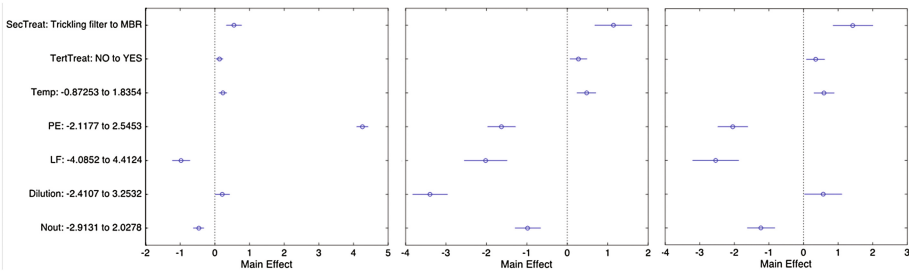
Fig. 1. Plot effect of estimated models M1 (left), M2 (centre) and M3 (right). This plot shows the estimated effect on the response variable from changing each predictor vales from one value to another. The two values are chosen to produce a relatively large effect on the response. The circles show the magnitude of the effect and the lines show the upper and the lower confidence limits for the main effect

consumption. Moreover, considering the used econometric specification (log-log), a positive coefficient included in the range $0 < \beta_i < 1$ indicates that the impact of the independent variable becomes smaller as it increases, which is consistent with previous studies reporting that larger plants are normally more energy efficient. Likewise, Fig. 1 shows how, as size increases energy efficiency decreases, leading to an improvement of energy efficiency as measured by these indicators.

Type of treatment. Different technologies, which tend to have different costs and operational characteristics, are used worldwide. Designers choose specific treatment type based on environmental standards and socio-economic factors in order to maximize the effectiveness of WWTPs. As WWTPs usually operate in different conditions, comparing the performance of WWTPs using different technologies is not trivial. Our analysis confirms that the type of treatment plays an important role in determining energy performance and the results are reported in Fig. 2. MBR are characterized by the higher energy consumption for the three models, due to their intensive membrane aeration rate. In contrast, the less energy intensive technology was found to be tricking filtration. The rest of technologies, correlated with higher energy consumption than tricking filter but lower than MBR, do not present significant differences when compared among themselves (results not shown). On the contrary plant carrying out additional tertiary treatment were found on average to have a 13% higher energy consumption with comparison to plant carrying out only secondary treatment (Table 2, M1).
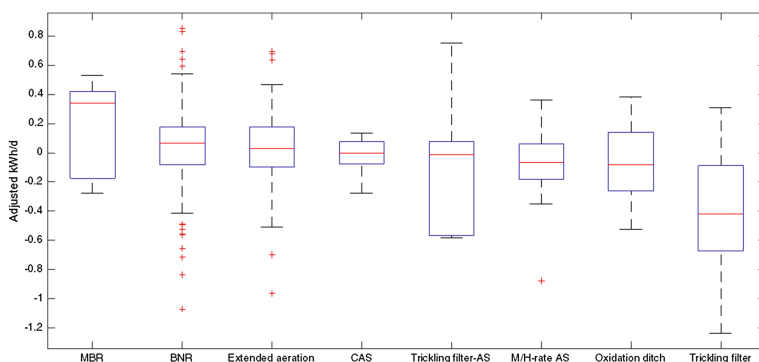
Fig. 2. Adjusted plot of energy use (M1) for type of secondary treatment. This plot shows the fitted response as function of variable secondary treatment type, with other predictors averaged out by averaging the fitted values over the data used in the fit. Adjusted points are computed by adding the residual to the adjusted fitted values for each observation.

Under-over capacity. The estimated *PLF* elasticity is positive and highly significant in all three models. Plants receiving lower loads compared to design values present a significantly worse energy performance, since energy consumption decreases when approaching values of 100% and keeps decreasing for overloaded plants. The results suggest that plant oversize should be as much as possible reduced the design phase and/or by revamping operation with division in two or more treatment lines in order to adapt process operation to seasonal variation of pollution load.

Influent characteristics. Another factor that impact negatively energy use at WWTPs is influent dilution. Influent characteristics are critical factors of WWTP performance greatly impacting several key parameters for operation (such as C/N ratio, aeration requirement, sludge production etc....). From the analysis of our dataset energy

consumption increases when increasing the *DIL*. Thus, keeping the rest of variables constant, (i.e. size, load factor and nitrogen concentration in the effluent) a plant receiving a more diluted wastewater has higher energy consumption. This effect it is clearer in M3 (Fig. 1) where energy consumption is normalized on the load entering the plant (Y_3(kWh/PE)). In this case increasing *DIL* has a strong negative effect on energy efficiency due to additional energy consumption for influent pumping. Moreover, the coefficient for *DIL* is found to be negative and very high in M2, confirming that kWh/m^3 is a poor proxy for the energy efficiency as it is highly influenced by the degree of dilution of the wastewater.

Nitrogen removal treatment intensity. Nitrogen effluent concentration is expected to be positively correlated with energy consumption. In fact when controlling for influent dilution, lower nitrogen concentration in the effluent is supposed to cause higher energy consumption for aeration. As expected, Nout is positively and significantly associated with higher energy consumption at WWTPs in all three models.

Temperature. Temperature has a complex effect on a WWTP operation. On the one hand increasing the temperature increases the biological activity, both the substrate uptake rate as the endogenous respiration. On the other hand, oxygen solubility decreases sharply when increasing temperature, leading to a higher energy demand for aeration. It is difficult to conclude which of these effects prevail. Table 2 shows that an increase of outdoor temperature (taken as a proxy of water temperature) is related to an increase of energy consumption suggesting that, in the analysed range, the higher aeration energy demand may be more significant.

5   Conclusion

This study describes how linear regression analysis can be used as a means to determine energy efficiency in WWTPs, by accounting for the impact of external factors. Likewise, based on the analysis of a relatively large sample of WWTPs, the effect of some important variables on energy efficiency is discussed, which open possibilities for improving benchmarking comparability for WWTPs. This analysis confirms that energy intensity indicator (i.e. kWh/m^3) is not an accurate proxy for energy efficiency given that changes in energy intensity are a function of changes in several factors. Based on these findings, it is then possible to identify the saving potential that can be reached with improvement in the level of energy efficiency. Finally, due to its relative simplicity, the analysis here discussed can be easily reproduced by engineers, auditors or water utilities, helping them with the decision-making process when investing on energy efficiency measures.

References

Chung W (2011) Review of building energy-use performance benchmarking methodologies. Appl Energy 88(5):1470–1479

Longo S, d'Antoni BM, Bongards M, Chaparro A, Cronrath A, Fatone F, Hospido A (2016) Monitoring and diagnosis of energy consumption in wastewater treatment plants. A state of the art and proposals for improvement. Appl Energy 179:1251–1268

N_2O and CO_2 Emissions from Secondary Settlers in WWTPs: Experimental Results on Full and Pilot Scale Plants

M. Caivano[1(✉)], R. Pascale[1], G. Mazzone[1], A. Buchicchio[1], S. Masi[1], G. Bianco[2], and D. Caniani[1]

[1] Scuola di Ingegneria, Università della Basilicata,
viale dell'Ateneo Lucano n. 10, Potenza, Italy
[2] Dipartimento di Scienze, Università della Basilicata,
viale dell'Ateneo Lucano n. 10, Potenza, Italy

Abstract. Data about Greenhouse Gas (GHG) emissions from settling units in wastewater treatment plants (WWTPs) are limited, probably because of the increased difficulties in evaluating direct emissions when there is absence of an induced air stream through the liquid volume (Caivano et al. 2016). Particularly, gas samples collection is not immediate and easy due to the low off-gas flow leaving the liquid surface.

In this study, a modified off-gas apparatus is proposed, to avoid these experimental problems. A floating hood was connected to a blower to simulate the wind action and encourage the gas stripping. The incoming air flow rates were fixed to 4, 9, and 16 Nl min^{-1}, simulating a wind velocity of 1.05, 2.36, and 4.19 m/s, respectively, in order to measure GHG emissions from a full-scale plant in several conditions. The same experimental conditions and a reproducible sampling apparatus were employed to measure GHG emissions also from a pilot plant. The monitoring of the full-scale plant shows that the concentrations of N_2O and CO_2 in the off-gas change rapidly, demonstrating the stripping effect induced by the blower air flow. A peak is reached and then a rapidly decrease is observed, proving a gradual decrease of mass transfer phenomena. As expected, the peak value increases with increasing the wind speed, whereas the time at which the peak is observed decreases. Regarding the pilot-scale plant, the results show the slow diffusion phenomena occurring in a closed system, preventing the mass transfer from the liquid to the gaseous phase.

Keywords: Non-aerated tanks · Settling · GHG emissions

1 Introduction

In the last decades, the assessment of GHG emissions from WWTPs is an increased concern. The GHG Protocol Corporate Standard recommends to group emissions into three "scopes" (WBCSD and WRI 2004). Particularly, Scope I emissions, including carbon dioxide (CO_2), nitrous oxide (N_2O) and methane (CH_4) emissions due to wastewater and sludge treatment processes (LGOP 2010), are usually distinguished in volumetric and surface emissions, respectively. The first are due to the diffusivity from

the liquid to the air bubbles during aeration periods, and the latter are due to the evaporation phenomena involving the liquid surface (Schneider et al. 2015; Beaulieu et al. 2012). The importance of wind velocity in evaluating the surface emissions is clear. The wind speed improves the gas evaporation rates because of growing eddies, even though this aspect is not always considered in emissions evaluation.

The research mainly focuses on volumetric emissions coming from aerated compartments (i.e. oxidation tanks) because of the large amount of stripped gases due to aeration devices. Indeed, to our knowledge, data about GHG emissions from settlers and thickeners are limited, probably because of the increased difficulties in evaluating direct emissions when there is absence of an induced air stream through the liquid phase (Caivano et al. 2016). Particularly, gas samples could not be immediately collected due to the insignificant off-gas flow leaving the liquid surface. Moreover, the positioning of the floating hood on non-aerated basins could lead to a changing in gas partial pressure, modifying consequently the natural equilibrium between the gas and the liquid phase.

In this study, a monitoring campaign on settler units is presented, suggesting an innovative approach to measure N$_2$O and CO$_2$ emissions coming from non-aerated basins. The secondary settler in a medium-sized municipal WWTP was monitored and interesting results were found in determining N$_2$O and CO$_2$ concentrations versus sampling time. A modified off-gas apparatus equipped with a blower was used for collecting gases from the liquid surface. Moreover, in order to deepen the influence of chemical/physical/biological phenomena on the production/emission of GHG from settlers, a pilot scale plant was built and operated by the Sanitary and Environmental Engineering Department of School of Engineering of University of Basilicata (Italy).

Data gathered from experimental activities are useful to develop a database in order to increase knowledge concerning the influence of management parameters on GHG emissions from non-aerated treatment of sludge (Caniani et al. 2015).

2 Materials and Methods

2.1 Full-Scale Settler Monitoring

The monitored secondary settler (43 m in diameter) is the sludge treatment unit of a municipal WWTP located in Basilicata (Southern Italy), serving 160,000 population equivalents and receiving an average wastewater flow of 1,734 m^{3}h^{-1}.

The off-gas test campaigns were conducted using a specific apparatus developed by the Civil and Environmental Engineering Department of the University of Basilicata, as described below. A stainless steel floating hood (1 × 0.7 × 0.4 m, L × W × H) with a cross sectional area of 0.7 m^2 and a volume of 280 L was used to capture the gas fluxes from the liquid surface of the settler.

The hood was connected to a flow analyzer (Fig. 1) and the gas flow rates were measured using a mass flowmeter for compressed air. A perforated Teflon tube placed along the internal perimeter of the floating hood was connected to a blower to simulate a radial wind velocity and encourage the gas stripping.
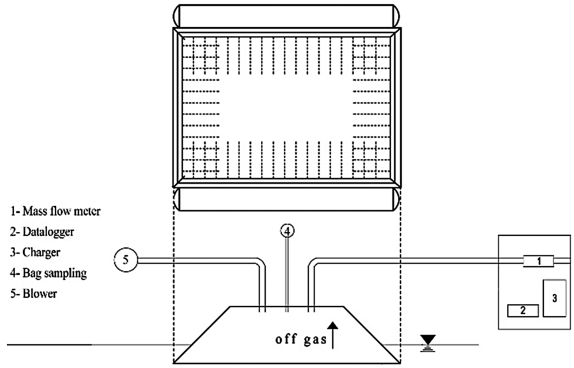
Fig. 1. Layout of the off-gas apparatus

The incoming air flow rates ($Q_{air,in}$) were fixed to 4, 9, and 16 Nl min^{-1}, simulating a wind velocity of 1.05, 2.36, and 4.19 m/s, respectively. In order to evaluate the temporal variability of gas concentrations in the off-gas exiting from the settler liquid surface, ten off-gas samples were collected in Tedlar bags (Zefon International, Ocala, USA) via a Gilian GilAir Sampling Pump (Sensidyne, St. Petersburg, USA) for each $Q_{air,in}$ at 0, 5, 10, 15, 20, 25, 30, 40, 50 and 60 min after the hood positioning.

Three sampling points were chosen on the settler surface to monitor gas fluxes, one for each influent air flow rate.

In order to ensure more considerations on GHG production and emission, the concentrations of dissolved CO_2, N_2O, and hydroxylamine (NH_2OH) in the sludge were evaluated (Table 1) by GC-BID method (Pascale et al. 2017). Each concentration value was averaged for three replicates in order to obtain reliable results.

Table 1. Concentration of dissolved N_2O (ppbv), NH_2OH (ppbv), and CO_2 (ppmv) in the liquid phase

	N_2O (ppb$_v$)	NH_2OH as N_2O (ppb$_v$)	CO_2 (ppm$_v$)
Liquid sample	352.63	211.38	6466.92

2.2 Pilot-Plant Monitoring

Figure 2a shows a simplified drawing of the pilot apparatus used for the lab experimentations, designed by the Civil and Environmental Engineering Department of the University of Basilicata.

The settler (unit 4 in Fig. 2a) was equipped with an off-gas apparatus to collect and conveying the off-gas into a flow meter (Fig. 2b). A stainless steel hood with a cross sectional area equal to the column area was used to close tightly the column and capture the gas fluxes from the sludge surface, ensuring no air contaminations. In order to assess the effects of the sludge settling on the GHG production and making a comparison with the results on the full-scale plant, the pilot plant was fed with sludge
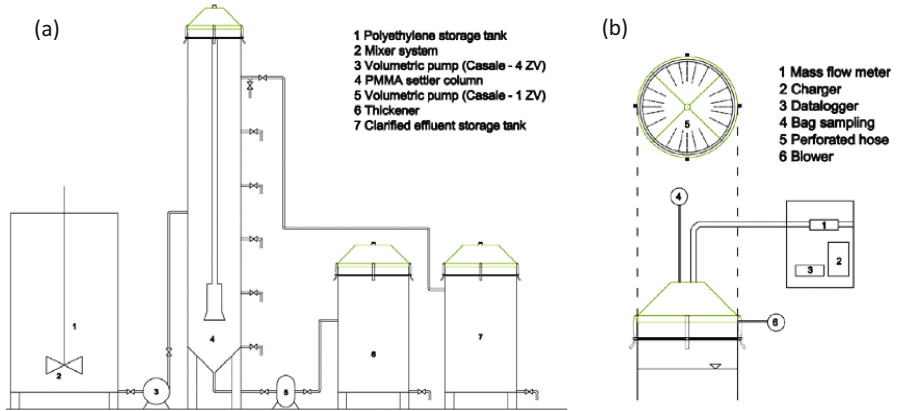
Fig. 2. Simplified drawing of the pilot plant (a) and simplified configuration of the pilot off-gas apparatus (b)

coming from the secondary settler underflow of the municipal WWTP previously described. Off-gas samples collection was performed as for full-scale settler.

3 Results and Discussions

3.1 Full-Scale Results

Regarding the monitoring of the real-scale settler, Fig. 3 presents the trend of N$_2$O (a) and CO$_2$ (b) concentrations in the off-gas versus sampling time. The trend for a Q$_{air, in}$ of 9 l/min shows the rapidly increase of N$_2$O and CO$_2$ in the exhaust gas exiting from the liquid surface, demonstrating the stripping effect induced by the blower air flow. After 10 min sampling, a peak is reached and then a rapidly decrease is observed, proving a gradual decrease of the stripping effect.

The peak of the trend for a Q$_{air,in}$ of 16 l/min is not visible but a maximum in emissions is reached immediately after few seconds sampling. That means that in case of strong wind (e.g. 4.19 m/s) the dissolved gases at the liquid surface are immediately stripped. Then, to observe another significant mass transfer, the diffusion from the liquid deep layers have to occur.

The trend for a Q$_{air,in}$ of 4 l/min shows a peak of emissions after 15 min sampling. Therefore, as expected, the peak value increases with increasing the Q$_{air,in}$, whereas the time at which the peak is observed decreases, confirming that at high wind velocity more N$_2$O and CO$_2$ are stripped and the peaks occur faster. These trends occur, probably, because the diffusion phenomena in non-aerated basins are very slow and a surface aeration is not enough to guarantee the mass transfer from the bottom layers to the top ones, in the period under study.
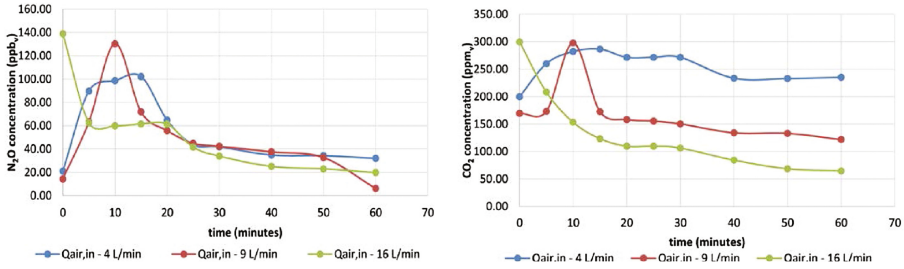
Fig. 3. N_2O (a) and CO_2 (b) concentrations versus sampling time – full scale plant

3.2 Pilot-Scale Results

Regarding the monitoring of the pilot-scale settler, Fig. 4 presents the trend of N_2O (a) and CO_2 (b) concentrations in the gaseous phase versus sampling time.
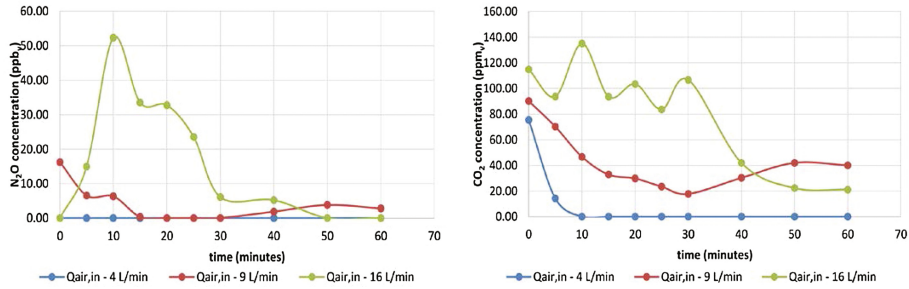

Fig. 4. N_2O (a) and CO_2 (b) concentrations versus sampling time – pilot scale plant

The amount of emitted N_2O and CO_2 is lower in comparison to the full-scale unit, probably because the diffusion phenomena are slower, thus hindering the mass transfer process. Under a simulated wind speed of 1.05 m/s, N_2O in the off-gas is absent, that is the concentration is not significantly higher than atmospheric ones, probably because of the low mass transfer associated with a very low dissolved gas concentration. The N_2O trend shows that for the highest air flow rate the N_2O concentration in the off-gas rapidly increases reaching the peak after 10 min sampling. Therefore, the dissolved gas at the liquid surface is completely stripped and the N_2O concentration decreases because of the slow diffusion rate, until the induced air stream is no longer enough to favor mass transfer.

The CO_2 trend shows that for low air flow rates the stripping is faster and then a decrease of CO_2 concentration in the exhaust gas is observed, proving that the induced air is not able to favor the diffusion from the bottom to the top of the tank. The CO_2 trend at highest air flow rate shows several peaks and a rapid decrease in CO_2 concentration in the exhaust gas after 30 min of sampling. The peaks prove the capacity of high simulated wind speed in promoting diffusion phenomena from down to upper

sludge layers, favoring mass transfer from the liquid to the gaseous phase. As expected, the highest measured concentrations increase with increasing the $Q_{air,in}$ for both N$_2$O and CO$_2$.

4   Conclusions

The present work could be considered a valid support tool in monitoring non-aerated basins in wastewater treatment plants. A novel methodology is suggested in order to assess GHG emissions from non-aerated tanks with the main aim to improve the plant performance and reduce the total CFP. Experimental results are conducted on secondary settlers, because of the poor literature knowledge on these system even though they can be strong contributors on emissions from WWTPs. Radial wind speeds are simulated through the floating hood headspace, by means the fixing of the air flow rate of the blower in order to find a possible correlation between the air flows and the GHG concentrations in the off-gas. Different operating conditions are investigated, giving attention to how the wind velocity can affect the gas evaporation on the liquid surface, as well the mass transfer from the liquid to the gaseous phase. The experimental activities on lab and real-scale plants give significant results in terms of N$_2$O and CO$_2$ concentrations in the exhaust gas leaving the surface layers of the settling sludge. Working at known air flow rates inside the hood headspace has allowed to find a correlation between the simulated wind velocity and the gas stripping.

The obtained results allowed us to investigate on the increasing gas concentrations during the time and during stronger wind conditions. The achieved results could help in assessing the performance of the secondary settler, quantifying its contribution to the total Carbon Footprint (CFP) of the monitored plant. Innovative configurations could be proposed for settlers in order to reduce the wind effects on emissions, mostly in windy areas. Furthermore, the presented methodology could be the starting point for a standard protocol for gas sampling and measurement in non-aerated tanks.

Surely, more investigation are need to better understand the behavior of non-aerated tanks and enlarge the available decision support system to guarantee a suitable wastewater cycle.

References

Beaulieu JJ, Shuster WD, Rebholz JA (2012) Controls on gas transfer velocities in a large river. J Geophys Res Biogeosci 2012:117

Caniani D, Esposito G, Gori R, Mannina G (2015) Towards a new decision support system for design, management and operation of wastewater treatment plants for the reduction of greenhouse gases emission. Water 7:5599–5616. doi:10.3390/w7105599

Caivano M, Bellandi G, Mancini IM, Masi S, Brienza R, Panariello S, Gori R, Caniani D (2016) Monitoring the aeration efficiency and carbon footprint of a medium-sized WWTP: experimental results on oxidation tank and aerobic digester. Environ Technol. doi:10.1080/09593330.2016.1205150

California Air Resources Board, California Climate Action Registry ICLEI - Local Governments for Sustainability, The Climate Registry, Local Government Operations Protocol (LGOP) (2010) For the quantification and reporting of greenhouse gas emissions inventories Version 1.1

Pascale R, Caivano M, Buchicchio A, Mancini IM, Bianco G, Caniani D (2017) Validation of an analytical method for simultaneous high-precision measurements of greenhouse gas emissions from wastewater treatment plants using a gas chromatography-barrier discharge detector system. J Chromatogr A 1480:62–69

Schneider AG, Townsend-Small A, Rosso D (2015) Impact of direct greenhouse gas emissions on the carbon footprint of water reclamation processes employing nitrification denitrification. Sci Total Environ 505:1166–1173

World Business Council for Sustainable Development (WBCSD) and the World Resources Institute (WRI) (2004), Measuring to manage: a guide to designing GHG accounting and reporting programs. World Resources Institute, November 2007. ISBN 978-1-56973-671-5

Effect of Temperature on N$_2$O and NO Emission in a Partial Nitrification SBR Treating Reject Wastewater

Z. Bao[1,2], S. Midulla[1,3], A. Ribera-Guarida[1], G. Mannina[3], D. Sun[2], and M. Pijuan[1(✉)]

[1] Catalan Institute for Water Research (ICRA),
Scientific and Technological Park of the University of Girona, Girona, Spain
[2] Beijing Key Lab for Source Control Technology of Water Pollution,
Beijing Forestry University, Beijing, China
[3] Dipartimento di Ingegneria Civile, Ambientale,
Aerospaziale, dei Materiali, Università di Palermo,
Viale delle Scienze, Ed. 8, 90128 Palermo, Italy

Abstract. Temperature is a very important parameter during nitritation, having a direct effect on ammonia oxidation rate (AOR) and enzymatic activities which relate to both N$_2$O and NO emission. This study aims at investigating the effect of temperature on AOR, N$_2$O and NO production in an enriched ammonia oxidizing bacteria (AOB) sequencing batch reactor (SBR) performing partial nitrification (PN) of synthetic reject wastewater. To achieve that, a SBR was subject to several shifts in temperature (in the range of 30 to 15 °C, 5 °C for each decrease). Cycle studies, which contain two aeration phases, were conducted under each temperature. The results showed that AOR specific exponentially correlates with the temperature during the temperature decreasing experiments. With the decrease of the temperature, N$_2$O firstly increased and then dropped to very low levels along with the decrease of the AOR, unlike NO that did not show any apparent connection with the temperature.

Keywords: Ammonia oxidation rate · Nitrous oxide · Nitric oxide · Reject wastewater · Temperature

1 Introduction

Nitrous oxide (N$_2$O), a potent greenhouse gas, can be produced during biological removal of nitrogen through the processes of nitrification and denitrification (Mannina et al. 2016; Foley et al. 2010; Kampschreur et al. 2009). Also, Nitric Oxide (NO) can be produced during these processes, and although it has received less attention by the research community, it is a detrimental gas toxic for many microorganisms and also involved in the depletion of the ozone layer (Rodríguez-Caballero and Pijuan 2013). Nitrification occurs during aerobic conditions and therefore N$_2$O and NO production during this process is of special concern since the gases produced are directly emitted. The production of N$_2$O and NO during nitrification occurs during the conversion of ammonia to nitrite, a process called PN or nitritation which is conducted by AOB. This

process is becoming more attractive for wastewater treatment plants due to its aeration savings and is widely implemented for reject wastewater treatment and lately also for domestic wastewater treatment.

N_2O and NO are produced through two different pathways during nitrification: (*i*) the hydroxylamine (NH_2OH) oxidation pathway, and (*ii*) the nitrifier denitrification pathway. There have been several studies reporting the factors affecting N_2O production in enriched AOB cultures. The effect of pH (Law et al. 2011), DO (Pijuan et al. 2014) and both DO and NO_2^- (Peng et al. 2015) have been explored and linked to N_2O production. On the other hand, less information is available regarding the combined behaviour of N_2O and NO under different conditions. N_2O and NO emissions were studied in the same reactor enriched with AOB bacteria (Rodríguez-Caballero and Pijuan 2013). These authors found that SBR cycle configurations reducing N_2O emissions resulted in an increase of NO, highlighting the importance of monitoring both gases simultaneously. Also, the relationships between the ammonia oxidation rate and the NO and N_2O production rates have been reported, being linear (Stüven and Bock 2001) and exponential (Law et al. 2012), respectively.

Temperature is a very important parameter during nitritation having a direct effect on ammonia oxidation rate (AOR) (Guo et al. 2010, Kim et al. 2008) and enzymatic activities (i.e. NirK and NoR), which can be related to N_2O and NO emission. Nevertheless, little is known about the effect that temperature shifts have on these emissions during partial nitrification.

This study aims at investigating the effect of temperature on AOR, N_2O and NO production in an enriched AOB sequencing batch reactor (SBR) performing partial nitrification of synthetic reject wastewater. To achieve that, an SBR was subject to several shifts in temperature (in the range of 30 to 15 °C), and cycle studies were conducted under each temperature.

2   Methods and Materials

A cylindrical SBR with a working volume of 8L treating synthetic reject wastewater was used for this study. Before starting the experiments the temperature in the reactor was controlled at 30 °C, mimicking the temperature conditions of reactors treating reject wastewater. The cycle configuration consisted in: feed-1 (1'15"), aeration-1 (105'), feed-2 (1'15"), aeration-2 (103'), purge (2') settling (132'30") and decanting (15'). 1L of synthetic reject wastewater (NH_4HCO_3, 1 g NH_4^+-N/L) was added into the reactor during each feeding phase resulting in a hydraulic retention time (HRT) of 24 h. DO was controlled within the range of 1.5–2.0 mg O_2/L and pH was only controlled when reaching values below 7.0 by adding $NaHCO_3$ 1 M. At the time of the study, the SBR had been under stable operation for more than 2 years, with 98% conversion of NH_4^+ to NO_2^- and no NO_3^- detected in the effluent. The percentage of AOBs analysed by FISH was around 80% of the total bacterial population.

The effect of temperature shifts on N_2O and NO emissions was assessed in the same SBR. Four different temperatures were tested: 30 °C (normal temperature of the reactor), 25 °C, 20 °C and 15 °C. The reactor was operated for 1 week under each temperature
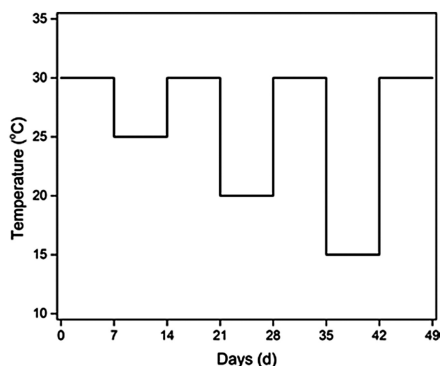
Fig. 1. Schematic representation of the changes of temperature applied in the reactor.

and then it was returned to 30 °C for another week before changing the temperature again. A schematic representation of the experimental approach is presented in Fig. 1.

Two cycle studies were conducted under each temperature with samples for NH$_4^+$, NO$_2^-$ and NO$_3^-$ being taken at the first 10 min, as well as the half and the end of each aeration phases. Online off-gas measurements of N$_2$O and NO emissions were carried out with commercially available online gas analysers (Servomex 4900 and ECO physics CLD60, respectively).

The equations used to calculate N$_2$O (Eq. 1), NO (Eq. 2) and AOR (Eq. 3) are detailed below. AOR$_{sp}$ was calculated as the slope of the straight line interpolating the concentration of ammonia found in the reactor, the time and the concentration of the biomass.

$$N_2O = \sum_{t=15}^{t} C_{N_2O} \times Q_{gas} \times t \tag{1}$$

$$NO = \sum_{t=15}^{t} C_{NO} \times Q_{gas} \times t \tag{2}$$

$$AOR_{sp} = \frac{dC_{NH_4^+ - consumed}}{dt \times MLVSS} \tag{3}$$

Where the C_{N_2O} and C_{NO} are

C_{N_2O} (g N$_2$O − N/L) = C_{N_2O} (ppmv)*10^{-6}*N$_2$O molar volume (0.0423 at 15 °C, 0.0416 at 20 °C, 0.0409 at 25 °C, 0.0402 at 30 °C) *28.

C_{NO} (g N$_2$O-N/L) = C_{NO} (ppmv)*10^{-6}*NO molar volume (same as the N$_2$O molar volume) *14.

t is the time (min) and Q_{gas} is the aeration rate (L/min).

3   Results and Discussion

3.1   PN-SBR Performance

The biomass was able to oxidise all the ammonium to nitrite when operating at 30 °C and 25 °C. However, some accumulation of ammonium was observed at the end of aeration 2 during 20 °C and 15 °C due to the low AOR. This is because the ammonia oxidation rate was affected by the temperature and decreased when temperature decreased. Figure 2 shows the effect of temperature on ammonia oxidation rate in the SBR. The relationship between specific AOR and temperature has been found to be exponential (Fig. 2), similar to some previous studies (Guo et al. 2010). In any of the temperatures, the concentrations of nitrate were negligible in the effluent which indicated that the partial nitrification performance of the system was not disturbed.
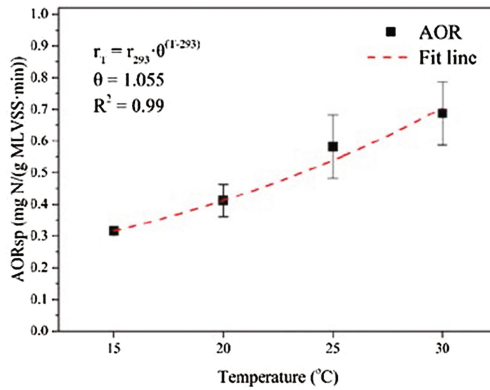
Fig. 2. Specific AOR at different temperatures.

3.2   N$_2$O and NO Emissions

Both N$_2$O (Fig. 3a) and NO (Fig. 3b) were emitted during the two aeration phases. In the first aeration, a big N$_2$O peak was detected and attributed to the stripping of N$_2$O produced during settling (Rodríguez-Caballero and Pijuan 2013). A second peak of N$_2$O was found at the beginning of feed-2, being much lower than the first one. During the rest of the aeration periods, the emissions were very low and remained constant. The behavior of NO was different from the one of N$_2$O. No peak was observed at the beginning of the cycle and its profile was very similar between both aeration phases (as shown in Fig. 3b).

N$_2$O and NO emissions were calculated using data from the whole cycle, excluding the data from the first 15 min (in order to eliminate the N$_2$O and NO produced during the settling) and only calculating the emissions during the second aerobic phase (including feed-2 period) (Fig. 4). In the case of N$_2$O, the majority of emissions were obtained during the first 15 min and attributed to the N$_2$O produced during settling. Similar emissions were observed in the temperature range from 30 to 20 °C,
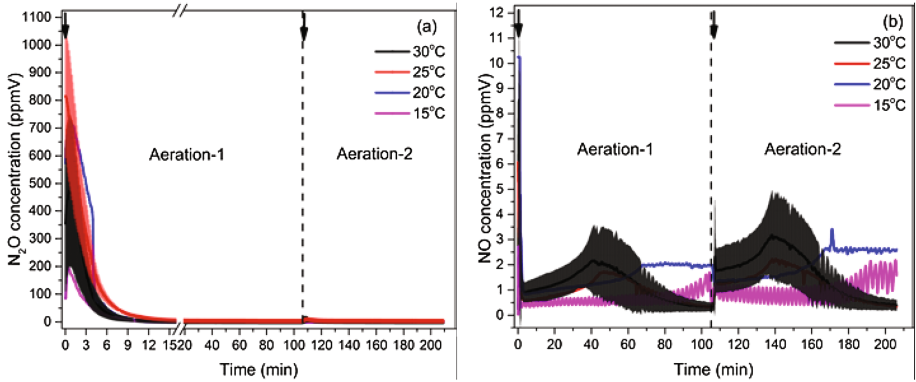
Fig. 3. N$_2$O and NO emission patterns at different temperatures (Arrows represent the feeding period).
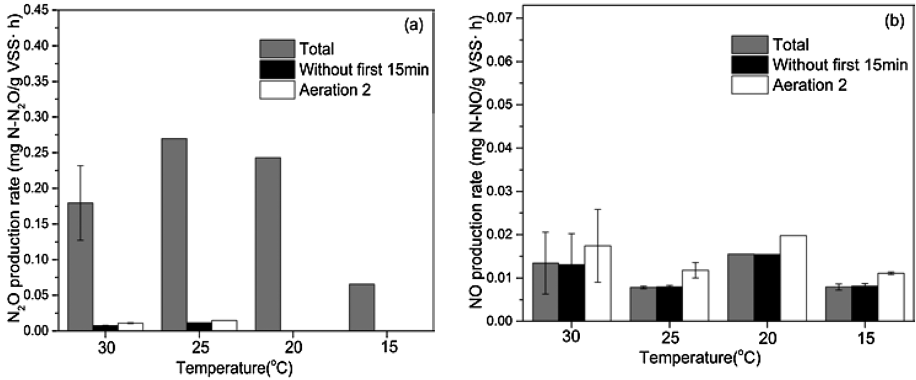
Fig. 4. N$_2$O and NO production rate with and without cut of the first peak

decreasing when the reactor was operating at 15 °C. Also interesting is the fact that no N$_2$O emissions were detected under 20 and 15 °C apart for those ones coming from the settling. In the case of NO emissions, these ones occurred along all the aeration phases, being the emissions from the second aeration always higher. No correlation was found with the temperature.

The N$_2$O and NO emission rates and ratios were calculated subtracting the first 15 min of aeration at different temperatures (Table 1). N$_2$O production rate firstly increased when decreasing the temperature to 25 °C and then decreased with the decrease of the temperature. However, no apparent connection was found between NO and temperature, being the NO emissions of the same order of magnitude as the N$_2$O emissions.

Table 1. N_2O and NO emission rates and ratios at different temperatures

Temperature	N_2O production rate		NO production rate	
(°C)	(mg N/g VSS·h)	(N-N$_2$O/N-NH$_4^+$)%	(mg N/g VSS·h)	(N-NO/N-NH$_4^+$)%
30	0.007	0.018%	0.015	0.037%
25	0.011	0.033%	0.008	0.029%
20	0.000	0.000%	0.018	0.072%
15	0.000	0.000%	0.010	0.051%

4   Conclusions

- AOR_{sp} exponentially correlates with the temperature during the temperature decreasing experiments.
- With the decrease of the temperature, N_2O firstly increased and then dropped to very low levels along with the decrease of the AOR, unlike NO that did not show any apparent connection with the temperature.

References

Foley J, De Haas D, Yuan Z, Lant P (2010) Nitrous oxide generation in full-scale biological nutrient removal wastewater treatment plants. Water Res 44(3):831–844

Guo J, Peng Y, Huang H, Wang S, Ge S, Zhang J, Wang Z (2010) Short-and long-term effects of temperature on partial nitrification in a sequencing batch reactor treating domestic wastewater. J Hazard Mater 179(1):471–479

Kampschreur MJ, Temmink H, Kleerebezem R, Jetten MS, van Loosdrecht MC (2009) Nitrous oxide emission during wastewater treatment. Water Res 43(17):4093–4103

Kim J-H, Guo X, Park H-S (2008) Comparison study of the effects of temperature and free ammonia concentration on nitrification and nitrite accumulation. Process Biochem 43(2):154–160

Law Y, Lant P, Yuan Z (2011) The effect of pH on N_2O production under aerobic conditions in a partial nitritation system. Water Res 45(18):5934–5944

Law Y, Ni B-J, Lant P, Yuan Z (2012) N_2O production rate of an enriched ammonia-oxidising bacteria culture exponentially correlates to its ammonia oxidation rate. Water Res 46 (10):3409–3419

Mannina G, Ekama G, Caniani D, Cosenza A, Esposito G, Gori R, Garrido-Baserba M, Rosso D, Olsson G (2016) Greenhouse gases from wastewater treatment — a review of modelling tools. Scie Tot Env 551:254–270

Peng L, Ni B-J, Ye L, Yuan Z (2015) The combined effect of dissolved oxygen and nitrite on N_2O production by ammonia oxidizing bacteria in an enriched nitrifying sludge. Water Res 73:29–36

Pijuan M, Tora J, Rodríguez-Caballero A, César E, Carrera J, Pérez J (2014) Effect of process parameters and operational mode on nitrous oxide emissions from a nitritation reactor treating reject wastewater. Water Res 49:23–33

Rodríguez-Caballero A, Pijuan M (2013) N$_2$O and NO emissions from a partial nitrification sequencing batch reactor: exploring dynamics, sources and minimization mechanisms. Water Res 47(9):3131–3140

Stüven R, Bock E (2001) Nitrification and denitrification as a source for NO and NO$_2$ production in high-strength wastewater. Water Res 35(8):1905–1914

Production of Greenhouse Gases from Biological Activated Sludge Processes: N$_2$O Emission Factors and Influences of the Sampling Methodology

A.L. Eusebi[✉], D. Cingolani, M. Spinelli, and F. Fatone

SIMAU Department, Università Politecnica delle Marche,
Via Brecce Bianche, 12, 60100 Ancona, Italy
a.l.eusebi@univpm.it

Abstract. The biological activated sludge reactors for the treatment of urban wastewater influence the environmental impact in terms of N$_2$O production. The quantification of this impact highly depends both by reactors configurations, gases sampling points and analysis methodologies. In this paper the predinitrification-nitrification configuration was studied in real plant (80,000 PE). The N$_2$O production was monitored by using fixed and floating samplers and by changing the sampling point at the head and at the end of the reactor. The monitored emitted concentrations were found in the range of 0.05–1.6 mgN$_2$O/m^3. The data were affected by the used sampling method. Higher concentrations resulted for fixed sampler when the sampling ratio of the head space volume and the air flowrate was lower than 0.05 l/m^3/h. The N$_2$O mass balance showed percentages of N$_2$O for influent TN in the range of 0.004–0.0004% N$_2$O/TN on the basis of the sampling position.

Keywords: Activated sludge · Green house gases · Sampling methods · Dinitrogen oxide · Emission factor

1 Introduction

The production of gaseous dinitrogen oxide (N$_2$O) is actually one of the more important scientific topics to minimize the environmental impact of the biological processes for urban wastewater. In fact, the produced N$_2$O from wastewater treatment plants was quantified as 3.2% of the global N$_2$O production (IPCC 2001). The concentrations, the mass loads and the emission factors are often variable depending both by e scale of the monitored plants, by e instruments used for the N$_2$O analysis and by the sampling methodologies. In fact, for full scale applications by treating urban wastewater the percentages of emission varied in the range of 0.04 to 0.800% in terms of N$_2$O produced for influent total nitrogen (TN) (Yan et al. 2014). The N$_2$O analysis is often realized in different points of the full scale reactors and in many cases the sampling phase is carried out by grab samples collected by using the bag technique and gas chromatograph instrument (Rodriguez-Caballero et al. 2014).

In this scenario, this paper shows the results of 2 months of monitoring and experimental tests for N_2O quantification.

2   Materials and Methods

The activity was realized in full scale plant for urban wastewater treatment (design capacity of 80,000 PE and nominal influent flow of 30,000 m^3/d). The activated sludge process (13700 m^3) applied conventional predenitrification and nitrification process. All the influent, effluent and biomass flows were analysed in terms of main macro-pollutants concentrations and kinetic rates according to the standard methods (APHA 2005). In the nitrification reactor was monitored the N_2O emissions in continuous modality. The monitoring of the gaseous compounds was achieved with the MIR9000CLD analyser (Environment Italia S.p.A.) that combined the measurements of the N_2O through infrared spectroscopy with the NO and NO2 analysed by chemiluminescence. One calibration every week by standard gas cylinders was executed to assure the correct measurements. One external pump ensured the aspiration of the gaseous sample (4 L/h).The gaseous flow sampled was filtered for dust removal and cooled at 4 °C before the analysis. Software for the acquisition of the data allowed the recording of the emission values every minute. The sampling point was changed at the head (at 5 m of the total length) and at the end (at 30 m of the total length) of the reactor. Moreover, both fixed (n° 3 samplers) and floating (n° 3 samplers) samplers were used for the monitoring phase. The six samplers were structured by providing the cover of each sampler with open tube (same diameter of 10 cm and length of 1 m) and placing the probe for the gas suction at a height of 50 cm. The head space of the samplers was designed and constructed equal to 200 l, 150 l and 70 l both for the fixed and for the floating samplers. The nitrogen mass balance was realized and the cumulative emission factors (EF) (gN2O/kgTNinfluent; gN2O/kgMLVSS/d) were calculated. Moreover, the emission data was compared with the results of continuous biological process via nitrite realized in demonstrative scale (2.88 m^3 of total volume) by treating the same influent urban wastewater of the main full scale plant.

3   Results and Discussions

The influent characterization, both average and standard deviation data, was reported in Table 1 at temperature of 17.7 ± 1.5 °C. Limiting condition in COD/TN ratio was present with possible problems in the denitrification phase. Also the average data and the standard deviations of the nitrification and denitrification rates were shown. The reactor worked at 10 days of SRT and the MLVSS concentration was 3485 ± 0.636.

The monitoring of concentrations and loads of N_2O emission was reported in Fig. 1 highlighting also the different position of the samplers. The monitored concentrations were in the range of 0.05–1.6 mg/m^3. Notwithstanding the low values detected, the effect of the sampling position seems appreciable. In fact, the average N_2O concentration was equal to 0.399 mg/m^3 at the head of the reactor and equal to 0.057 mg/m^3 at the end of the biological unit.

Table 1. Influent characterization and kinetic rates

	pH	COD	CODs	TKN	NH$_4$-N	NO$_2$-N	NO$_3$-N	kn	real kd	max kd
		mg/l	mg/l	mg/l	mg/l	mg/l	mg/l	kg/kgMLVSS/d		
Aver.	7.4	88.7	41.6	28.6	25.1	0.0	0.93	0.114	0.021	0.054
St. Dev.	0.1	33.5	20.5	10.5	3.2	0.0	0.76	0.027	0.009	0.008

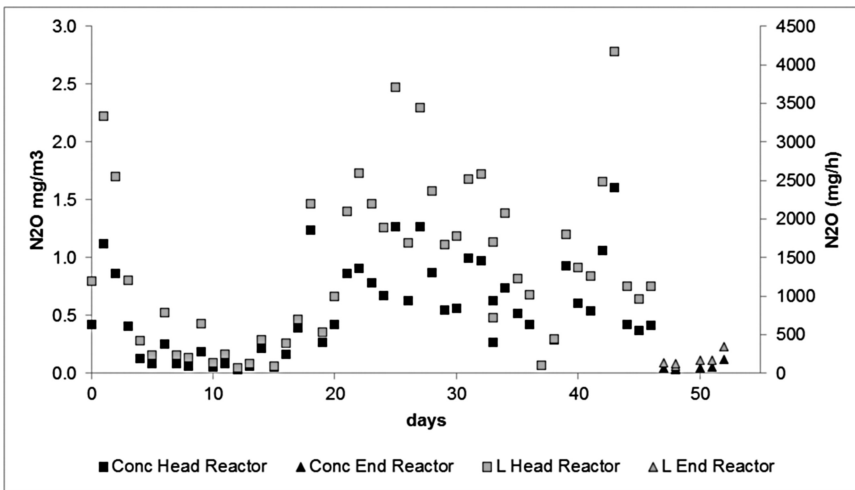**Fig. 1.** N$_2$O loads and concentrations at the head and at the end of the reactor

Moreover, the concentrations of the head of the reactor were elaborated considering the different head space of the sampler. According to the Fig. 2 a and b, the N$_2$O values, as expected, increment at higher air flows for more elevated stripping phenomena. Notwithstanding this correlation was more evident in the floating samplers (Fig. 2b) more than the fixed ones (Fig. 2a). Therefore, other specific parameters were evaluated. In fact, the N$_2$O concentrations were related to the sampling ratio expressed in terms of litres of sampling head space applied compared to influent gaseous air flow.

According to the data of Fig. 2c, the N$_2$O emissions were higher in the fixed sampler when the sampling ratio was lower than 0.05 l/m^3/h. This aspect could be linked to compression phenomena in the head space when the hydraulic level changed in the fixed sampling chamber. This phenomenon was not evaluated for the floating samplers (Fig. 2d).

The full scale emission factors were calculated according to the reference sampling value of 0.05 l/m^3/h and deleting the concentrations data obtained with lower sampling ratio. In the full scale reactor the N$_2$O percentages emitted for influent TN were 0.0039% N$_2$O/TN and 0.00039% N$_2$O/TN respectively at the head and at the end of the reactor. Lower percentages in full scale plants for urban wastewater were found in the literature scenario and equal to 0.116% N$_2$O/TN for plug flow reactor (Rodriguez-Caballero et al.
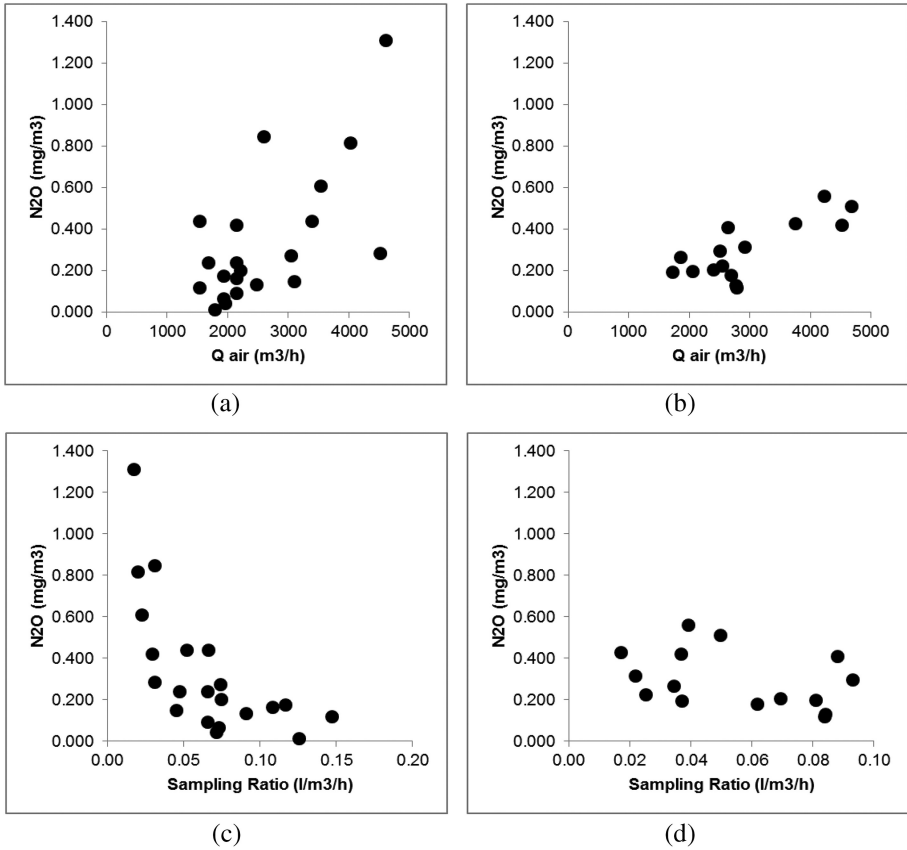
Fig. 2. (a) Fixed sampler N_2O-Gaseous air flow (b) Floating sampler N_2O-Gaseous air flow (c) Fixed sampler N_2O-Gaseous air flow (d) Floating sampler N_2O-Gaseous air flow

2014) and in the range of 0.04–0.1% N_2O/TN for A2O (Anaerobic-Anoxic-Oxic) configuration (Yan et al. 2014).

Moreover, EF was calculated equal to 3.56 ± 0.05 (Head Reactor) and 0.53 ± 0.01 (End Reactor) mgN_2O/kgMLVSS/d for the two positions. The average value (2.04 mgN_2O/kgMLVSS/d) was compared with emission factor of biological process applying via nitrite approach. In the demonstrative biological reactor via nitrite, the average EF was calculated equal to 0.16 ± 0.12 and 0.05 ± 0.05 gN_2O/kgMLVSS/d, respectively, for Phases A and B. The denitritation velocity was limiting during Phase A (0.046 ± 0.01 kgNOx-N/kgMLVSS/d) and incremented up to 0.093 ± 0.03 kgNOx-N/kgMLVSS/d after dosing external carbon (Phase B). The factors of conventional process and via nitrite biological reactor were different for one order of magnitude.

4 Conclusions

In the studied real plant (80,000 PE) negligible concentrations of N_2O were found as emitted by nitrification section. The data concentrations were affected by the sampling method. The effect of the sampling position seems appreciable. In fact, the average N_2O concentration was equal to 0.399 mg/m^3 and to 0.057 mg/m^3 respectively at the head and at the end of the biological unit by changing also the final Emission Factors. Moreover the N_2O emissions were higher in the fixed sampler when the sampling ratio was lower than 0.05 l/m^3/h. Therefore the floating samplers represent the optimized modality to minimize the compression phenomena. Finally, the N_2O percentages were lower than the literature and in the range of 0.0039–0.00039% N_2O/TN. In terms of activated biomass, the Emission Factors resulted equal to 3.56 ± 0.05 (Head Reactor) and 0.53 ± 0.01 (End Reactor) mgN$_2$O/kgMLVSS/d for the two sampling positions.

References

APHA (2005) Standard methods for the examination of water and wastewater 2005, 21st edn. APHA, AWWA and WEF, Washington, DC

IPCC (2001) Guidelines for National Greenhouse Gas Inventories, vol. 5, Waste, pp. 6.24–6.26. IGES, Kanagawa

Rodriguez-Caballero A, Poch P (2014) Evaluation of process conditions triggering emissions of green-house gases from a biological wastewater treatment system. Sci Total Environ 15 (493):384

Yan X, Li L, Liu J (2014) Characteristics of greenhouse gas emission in three full-scale wastewater treatment processes. J Environ Sci 26(2):256–263

Analysis and Optimization of Energy Consumption in Relation to GHG Management: The Case Study of Medio Sarno Wastewater Treatment Plant

A. Falcone[1]([✉]), L. Pucci[1], S. Guadagnuolo[1], R. De Rosa[1],
A. Giuliani[1], B.M. d'Antoni[2], G. Lofrano[3], G. Libralato[4],
F. Fatone[5], and M. Carotenuto[3]

[1] Consorzio Nocera Ambiente, Via S. Maria delle Grazie 562,
84015 Nocera Superiore, SA, Italy
[2] Department of Biotechnology, University of Verona,
Strada Le Grazie 15, 37134 Verona, Italy
[3] Department of Chemistry and Biology, Salerno University,
via Giovanni Paolo II, 132, 84084 Fisciano, SA, Italy
[4] Department of Biology, University of Naples Federico II,
via Cinthia ed. 7, 80126 Naples, Italy
[5] Department of Materials and Environmental Science and Urban Planning,
Università Politecnica delle Marche, Ancona, Italy

Abstract. A multistep methodology for the evaluation of the energetic behaviour of a wastewater treatment plant has been carried out, in according to Horizon2020 Enerwater methodology. The study took into account each phase of the process scheme, in order to obtain specific electricity consumption values for all the electro-mechanic devices. Data from both tele-control system and direct measurements in field have been acquired in order to perform a critical analysis for improving energy efficiency.

Keywords: Energy efficiency · Greenhouse gases · Wastewater treatment · Benchmarking

1 Introduction

Most direct emissions resulting from wastewater treatment plants (WWTPs) based on biological processes are greenhouse gases (GHG) such as carbon dioxide (CO_2), methane (CH_4), and nitrous oxide (N_2O), while other indirect emissions are released by on site energy generation from biogas combustion (De Haas and Foley 2009; Campos et al. 2016). The CO_2 emitted in relation to energy demand can be directly reduced enhancing the energy efficiency of WWTPs (Libralato et al. 2012). In this way, both the reduction of environmental impacts and the decrease of treatment costs, increasing energy savings, can be accomplished simultaneously. In terms of costs, the main efficient way to reduce GHG emissions is to modify the operational conditions of WWTP units even if this is could not be always possible due to the operational limitations of the installed units (Panepinto et al. 2016).

In this study, we monitored for one year the energy consumption in all treatment units (pre-treatment and pumping stations; primary treatment rainwater and aerated storage; secondary treatment; tertiary treatment; sludge treatment; return liquor treatment; and odour treatment) of Medio Sarno WWTP (Nocera Superiore, Campania, Southern Italy) (300.000 p.e.) managed by Consorzio Nocera Ambiente. Moreover, GHG emissions were evaluated in order to support their minimization.

2   Materials and Methods

To estimate the overall electric energy consumption of Medio Sarno WWTP, the calculated power values (P) were multiplied for the operating time of each device. During the survey of the devices operating in the WTTP, the electro-mechanic equipment was later grouped and classified in homogeneous categories according to ENERWATER methodology.

3   Results and Discussion

Results were summarised in Table 1 and showed that the phase requiring the highest amount of electricity was the biological oxidation (> 50%) followed by pre-treatment and pumping stations.

Table 1. Electric energy consumption for each stage according to ENERWATER methodology

Stage description	kWh/d	%
Stage 1: Pre-treatment and pumping stations	3,430	25
Stage 2: Primary treatment rainwater and aerated storage	1,007	7
Stage 3: Secondary treatment	409	46
Stage 4: Tertiary treatment	802	6
Stage 5: Sludge treatment	700	5
Stage 6: Return liquor treatment		0
Stage 7: Odour treatment	1,497	11
Total	**13,844**	

The values of key performance indicators (KPIs) on the base of the estimated energy consumption were reported in Table 2. The comparison of KPIs of Medio Sarno WWTP with other WWTPs outlined a general equivalency in their values. The main deviations involved the indexes related to total nitrogen removal, while the values of the index connected to wastewater volume and COD removal were more similar (Panepinto et al. 2016).

Table 2. Critical evaluation of electric energy demand of Medio Sarno WWTP; EEC = electric energy consumption

SPECIFIC ENERGY PERFORMANCE INDICATORS (daily values average)		
EEC/volume of treated wastewater	kWh/m^3	0.38
EEC/BOD$_5$ load removed	kWh/kg BOD$_5$	2.50
EEC/COD removed	kWh/kg COD	1.00
EEC/TSS removed	kWh/kg TSS	3.18
EEC/TN removed	kWh/kg N	46.50
EEC/NH$_4$ removed	kWh/kg NH$_4$	38.40
EEC/P removed	kWh/kg P	209.06

In order to estimate GHG emissions, we referred to the "Methodology Guide for Evaluating Greenhouse gas emissions by water and sanitation services" (2013) prepared by ASTEE and based on IPCC Guidelines for National Greenhouse Gas Inventories (2006) and the GHG Protocol prepared by WBSCD and WRI. WWTP operational data were summarized in Table 3.

Table 3. Operational data for GHG emissions calculations

Scope	Operational data	Units	Value
1	TKN removed	ton/yr	118
1	COD removed	ton/yr	5,476
1	TKN discharged	kg/yr	69,275
1	Ton of COD discharged	ton/yr	455
2	Electricity consumption	MWh/yr	5,021
3	Peracetic acid consumption	l/yr	59,205
3	Poly consumption	kg/yr	16,863
3	Sludge landfilled	ton TSS/yr	3,049
3	Screenings landfilled	ton TSS/yr	45
3	Grit landfilled	ton TSS/yr	215
3	Annual transport for biosolids	t*km/year	1,798,245
3	Annual transport for grit	t*km/year	167,850
3	Annual transport for screen	t*km/year	35,157

GHG emissions (Table 4), as required by the GHG Protocol, were quantified in the following order: Scope (1) direct emissions from the sewage process and discharge into surface water; Scope (2) indirect emissions associated with the consumption of electricity, steam or gas; Scope (3) other indirect emissions related to production and transport of chemicals, transport and treatment of sludge and by-products.

As shown in Fig. 1, energy consumption provided the greatest contribution to carbon footprint (39%) followed by sewage process (31%), biosolids, screening and grits (24%), effluent (5%) and others (1%).

Table 4. GHG estimates (ton CO_2-eq/yr), with breakdown according to scope (IPCC, 2007)

| Scope	Description of emission	Total (tCO_2eq/yr)
1	Emissions linked to the sewage process	2599.7
1	Discharges into surface water	447.5
	Direct emissions (SCOPE 1) Subtotal	**3047.2**
2	Indirect emissions linked to energy consumption	3263.9
	Indirect emissions associated with energy (SCOPE 2) Subtotal	**3263.9**
3	Indirect emissions (reagents and consumables)	93
3	Indirect emissions (biosolids, screenings&grit)	1997.3
	Other indirect emissions (SCOPE 3) Subtotal	**2090.3**
	Operational Carbon Footprint	**8401.5**
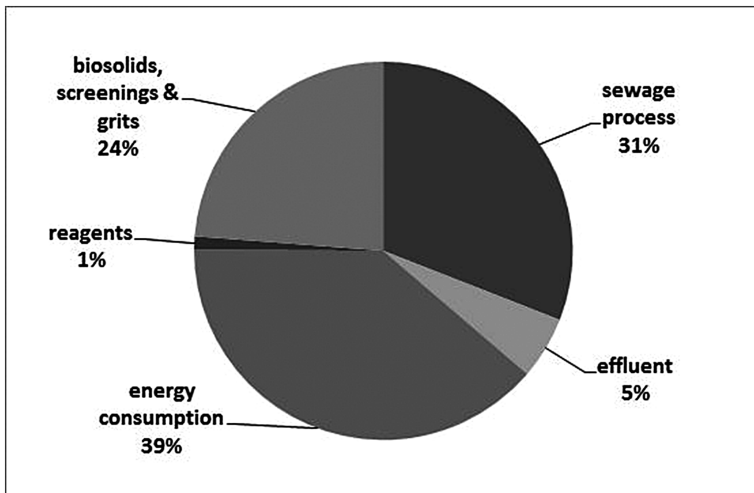
Fig. 1. Carbon Footprint (%) breakdown at Medio Sarno WWTP

4   Conclusions

This study evidenced that:

- The phase requiring the highest fraction of the electricity consumption is the biological oxidation (> 50%) followed by pre-treatment and pumping stations;
- The energy consumption associated to the oxidation tank and pumping stations can be greatly reduced thought optimization;
- Energy consumption provided the greatest contribution to the carbon footprint (39%) followed by sewage process (31%), biosolids, screening and grits (24%), effluent (5%) and others (1%).

Our next goal will be to set the best operational condition to keep the WWTP efficient as well as to minimize its carbon footprint.

References

Campos JL, Valenzuela-Heredia D, Pedrouso A, Val del Río A, Belmonte M, Mosquera-Corral A (2016) Greenhouse gases emissions from wastewater treatment plants: minimization, treatment, and prevention. J Chem 2016:1–12

De Haas D, Foley J (2009) Energy and green house footprints of wastewater treatment plants in South east Queensland. AWA Ozwater Conference, 16–19 March 2009, Melbourne Australia

Libralato G, Ghirardini AV, Avezzù F (2012) To centralise or to decentralise: an overview of the most recent trends in wastewater treatment management. J Environ Manage 94(1):61–68

Panepinto D, Fiore S, Zappone M, Genon G, Meucci L (2016) Evaluation of the energy efficiency of a large wastewater treatment plant in Italy. Appl Energy 161:404–411

Application of Event-Based Real-Time Analysis for Long-Term N$_2$O Monitoring in Full-Scale WWTPs

V. Vasilaki[1], M. Danishvar[2], Z. Huang[2], A. Mousavi[2],
and E. Katsou[1(✉)]

[1] Department of Mechanical, Aerospace and Civil Engineering;
Institute of Environment, Health and Societies, Brunel University London,
Uxbridge Campus, Middlesex, Uxbridge UB8 3PH, UK
`Vasileia.Vasilaki.l@my.brunel.ac.uk`,
`Evina.Katsou@brunel.ac.uk`
[2] Systems Engineering Research Group,
Department of Electronic and Computer Engineering,
Brunel University London, Middlesex, Uxbridge UB8 3PH, UK
`{Morad.Danishvar,Zhengwen.Huang,`
`Ali.Mousavi}@brunel.ac.uk`

Abstract. Nitrous oxide (N$_2$O) emissions from wastewater treatment plants (WWTPs) are gaining increased attention globally. Several operating parameters, the configuration, environmental conditions and microbiological diversity of the biological processes affect significantly nitrous oxide (N$_2$O) formation in WWTPs. However there are still uncertainties regarding the exact triggering mechanisms and the dependancies between the N$_2$O emissions and main performance parameters of the plant. The aim of this work is to apply an event-based sensitivity analysis (EventTracker) to investigate dependencies and potential patterns between the operating parameters monitored online in wastewater treatment processes and N$_2$O emissions. The complete dataset from long-term N$_2$O monitoring in a full-scale plug-flow and two Carrousel reactors published by Daelman et al. (2015) was used for the analysis. The event-based sensitivity analysis indicated significant dependencies between the system parameters (i.e. nitrite, nitrate, ammonia) and N$_2$O emissions. Spearman's rank correlation coefficient was applied using monthly datasets indicating significant correlations between nitrite and nitrate sensor signals with the N$_2$O emissions. The latter was mainly observed in cases characterised by high N$_2$O emission fluxes supporting the event-based sensitivity analysis. The examined method enabled the grouping of the system parameters based on the identified dependencies. The results indicated that N$_2$O emissions can provide information for the state of the examined biological processes.

Keywords: N$_2$O emissions · Full-scale WWTPs · Sensitivity analysis · Real-time control

1 Introduction

The wastewater treatment sector is responsible for 6% of the anthropogenic nitrous oxide (N_2O) emissions, according to the intergovernmental panel on climate change (IPCC) estimates (Palut and Canziani 2007). N_2O is generated during nitrification and it is an intermediate during denitrification; however the exact triggering mechanisms, operational and environmental conditions for its formation are still under investigation. Several N_2O monitoring studies in the past years have led to (i) a better understanding of N_2O generation pathways, (ii) the development of strategies for site-specific N_2O emissions mitigation and (iii) the development of mechanistic process-based models that aim to integrate GHG emissions generation in the design, operation and optimization of biological processes. However, the monitoring and control of the N_2O emissions in full-scale wastewater treatment processes remains a challenge. This is mainly attributed to the complexity of interacting biological processes that consume or produce N_2O (Todt and Dörsch 2016). Statistical analysis has been widely used in the literature to identify correlations in N_2O dynamics with target operating parameters (i.e. dissolved oxygen, ammonia, nitrite) in full-scale plants. However, regression analyses seem to provide inconclusive evidence of dependencies of N_2O generation with specific triggering process parameters (Ahn et al. 2010; Abookabar et al. 2013). The aim of this study is to apply an event-based sensitivity analysis based on cause-effect relationships to evaluate potential relationships between the parameters monitored online and the N_2O emissions in the plug-flow and two Carrousel reactors applied in the work of Daelman et al. (2015). The introduction of un-biased event-based real-time data pattern recognition will evaluate whether an alternative to classical statistical method can be used to: (i) track and register the real-time data generated by the monitoring and control system, (ii) find the interrelationship between system parameters and identify patterns, (iii) evaluate the efficacy of event-based data analysis to potentially control and optimize the performance of the WTTPs regarding N_2O emissions.

2 Materials and Methods

2.1 Process Description and Data Origin

The description of the studied configurations of the plug-flow reactor and of the two Carrousel reactors, influent concentrations, efficiency of the system, as well as the complete dataset used for the analysis is included in the study of Daelman et al. (2015). The plant treats $80.000 \ m^3d^{-1}$ domestic wastewater. Secondary treatment consists of an anoxic-oxic plug-flow reactor with subsurface aerators followed by a primary settler and anaerobic selector connected with two parallel Carrousel reactors. The applied scheme includes alternation of anoxic/oxic zones in the Carrousel reactors that are equipped with surface aerators and controlled by the ammonia level. The overall efficiency of the system in terms of total nitrogen (TN) removal during the monitoring campaign was 81%.

The analysis has been focused on one of the Carrousel reactors (Carrousel 2) equipped with ammonia (NH_4), nitrate (NO_3), total suspended solids (TSS), temperature and three dissolved oxygen (DO) probes as shown in Fig. 1 (Daelman et al. 2015).
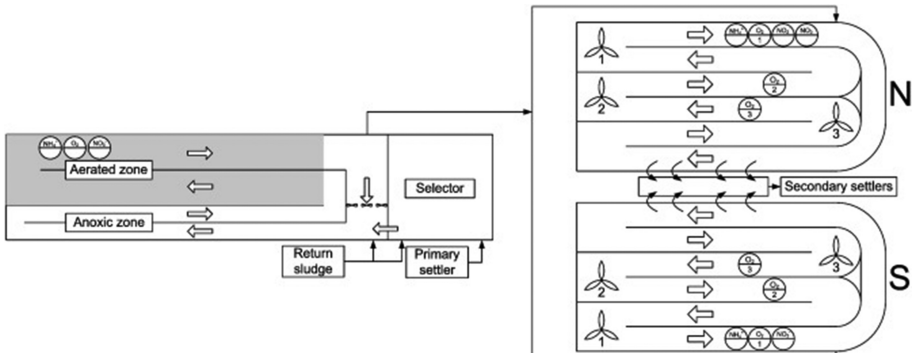
Fig. 1. Plug-flow and Carrousel reactors (Carrousel bottom: Carrousel 1, Carrousel top: Carrousel 2) (Daelman et al. 2015)

2.2   Event-Based Real-Time Analysis for N2O Monitoring

A novel event-based learning mechanism is deployed to better understand the relationship between N_2O emissions and other parameters monitored online in the WWTP. The steps are: (i) implementation of the unbiased EventTracker (Tavakoli et al. 2013) technique to identify relationships between observed and latent variables of the system (ii) validation of patterns (strength of relations) found by EventTracker with spearman's rank correlation coefficient, (iii) implementation of the EventiC (Danishvar et al. 2017) method to group the system input-output and control parameters, resulting in a simple scenario builder as a look up table, (iv) identification of cases (in the time series) that the system has low or high N_2O emissions.

In this context, events are the tangible and reasonable changes to a specific signal (from sensors, machines, actuators, and other sources of data) that coincide with one another. Event tracking identifies such relationships in real-time. In order to track events in a sensor signal the standard deviation of the signal fluctuation for all the time period is calculated. Threshold for registering an event is taken if the difference between two consecutive values is $\geq 10\%$ of this standard deviation. By implementing the algorithm using the data from the database of Daelman et al. (2015) the un-biased event tracker detects and defines the most relevant input parameters of the system with the outputs. Thus, the sensitivity of the system output (i.e. N_2O and NOx) for all the potential influential parameters of the system emerges. The application of EventiC showed which group of system parameters are highly coupled and potentially influence each other during the process. A false negative test was conducted as described by Danishvar et al. (2017) to validate the results of eventTracker and EventiC.

3   Results and Discussion

3.1   Monitored Parameters

Table 1 shows the average values and standard deviations of the parameters monitored online in the Carrousel reactor 2. There is significant variation of N_2O emissions and NO_3 concentration (see Daelman et al. 2015).

Table 1. Parameters monitored in the Carrousel reactor 2

	N_2O (kg/h)	NH_4 (mg/l)	NO_3 (mg/l)	NO_2 (mg/l)	DO1 (mg/l)	DO2 (mg/l)	DO3 (mg/l)	Temperature (°C)
Average	1.40	1.63	5.8	1.2	0.6	0.8	1.9	16
Standard deviation	2.1	2.2	4	1.1	0.9	0.9	0.6	3.5

3.2   EventTracker and EventiC

Table 2 compares the results of EventTracker with Spearman's rank correlation coefficient ($p < 0.01$) for 295 days of hourly aggregated data. EventTracker identified significant dependencies between the N_2O emissions and ammonia, nitrate and DO1 (dissolved oxygen probe 1) in the Carrousel reactor 2. Similar trends were also observed

Table 2. Eventracker algorithm and linear regression analysis of N_2O emissions in Carrousel reactor 1

Output parameter (location)	Input parameters (location)	Level of sensitivity (this study)	Pearson's correlation and coefficient of determination
N_2O emissions Carrousel 2 (kg N_2O/h)	N_2O plug-flow	High	Low
	N_2O Carrousel 1	High	Low
	NH_4-N Carrousel 2	High	Low
	NO_3-N Carrousel 2	High	Low
	DO1 Carrousel 2	High	Low
	DO2 Carrousel 2	Low	Low
	DO3 Carrousel 2	Medium	Low
	TSS Carrousel 2	Low	Low
	Temperature Carrousel 2	Low	Low

in the two Carrousel reactors treating the effluent of the plug-flow reactor and operating at the same set-points DO. Therefore, similar emission dynamics are expected.

Moreover, changes in the NH_4, DO and NO_3 concentrations in the Carrousel reactor 2 seem to coincide with changes in N_2O emissions load. Spearman's correlation coefficient for the whole dataset indicated that there is no significant relationship between these variables and N_2O emissions. The application of Spearman's correlation coefficient to the hourly sensor signals taken at different months indicated that there is a variation in the relationship between N_2O emissions and operating parameters in Carrousel 2. More specifically, in cases of increased and variable N_2O emissions, significant dependencies between nitrate and nitrite concentrations and N_2O emissions were observed. On the other hand, at low N_2O emission levels with not significant variability, we didn't identify dependencies. However, as shown in Fig. 2 Spearman's rank correlation results in less sensitivity of N_2O emissions to the DO probes in the reactor the respective one indicated by the EventTracker. Rodriguez-Caballero et al. (2014) demonstrated that N2O dynamics were not significantly affected by changes in DO (1.5–2 mg/l) or aeration flow rate; the latter is attributed to the constant nitrification efficiency.
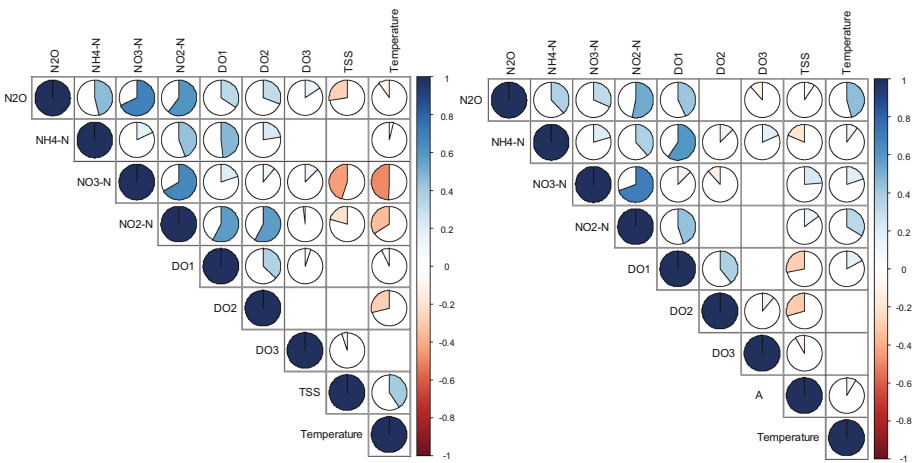

Fig. 2. Spearman's rank correlation coefficient (left): month 6/2011 (right): month: 9/2011 for sensor signals in Carrousel reactor 2 (only results with p-value < 0.01 are shown)

Observed data from operation (Fig. 3) show that the profile of N_2O emissions in Carrousel reactor 2 follows the same pattern with NO_3-N concentration profile, confirming the results of EventTracker. Significant correlation between N_2O fluxes and NO_3-N concentration have been also identified in soils (Cowan et al. 2015). However, NO_3-N is not directly involved in the known pathways for N_2O formation; thus there are limited studies that examine potential relationship interconnections and further analysis is required.
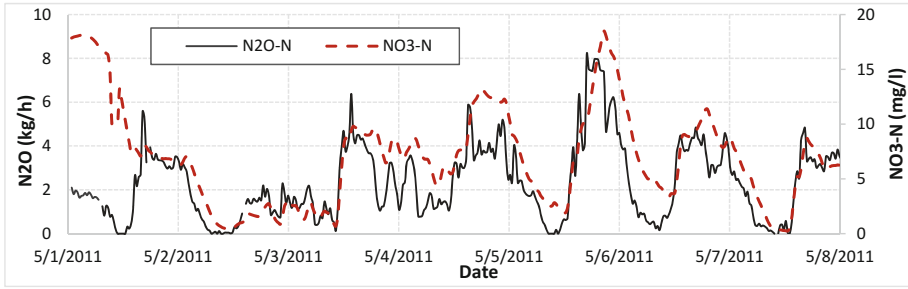
Fig. 3. N$_2$O emissions and NO$_3$ concentration data for Carrousel reactor 1

EventiC was applied to the hourly aggregated data in order to identify the group of system parameters that influences each other during the process (Fig. 4). Two different groups were identified; one is consisting of the TSS and temperature variables in the two Carrousel reactors, while the other with all the other monitored parameters. It can

Fig. 4. Eventic algorithm grouping the system parameters with interelations (dark green: high impact, light green:moderate impact) (Color figure online)

be concluded that the system is less sensitive to changes in the DO2 and DO3 probes in both Carrousel reactors.

The data fed to the EventiC algorithm indicated that N$_2$O emissions can potentially be used as an additional parameter for process monitoring. Figure 5, shows the box-plots of NO$_2$-N concentration in the Carrousel reactor 2 for all the periods with (i) low N$_2$O emissions (ranging from 0 to 0.05 kg/h)), (ii) high N$_2$O emissions (emissions higher than 4.5 kg/h representing 10% of the highest values), (iii) complete dataset. High N$_2$O emissions present similar trends with higher than average NO$_2$-N concentration in the reactor.
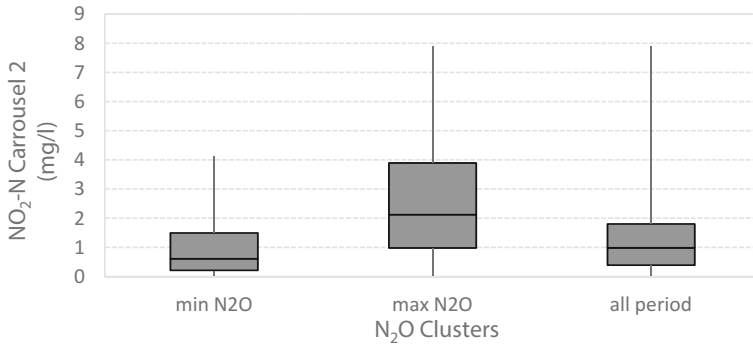
Fig. 5. Boxplots of the NO_2-N concentration (mg/l) in the Carrousel reactor 2 for different clusters of N_2O emissions

4   Conclusions

The unbiased real-time event based sensitivity analysis has provided useful information on the dependencies of N_2O emissions with specific operating variables monitored online (nitrite, nitrate, ammonium) in a full-scale Carrousel reactor. Spearman's rank correlation analysis for the whole dataset was unable to identify correlations between system parameters and N_2O emissions, mainly due to the fact that the relationship of the examined parameters was highly variable during the system operation (considering monthly data). EventiC grouping of relevant system parameters in order of importance and relevance can potentially filter abundant sensor signals and lead to an improved mathematical formulization of complex biological processes.

References

Aboobakar A, Cartmell E, Stephenson T, Jones M, Vale P, Dotro G (2013) Nitrous oxide emissions and dissolved oxygen profiling in a full-scale nitrifying activated sludge treatment plant. Water Res 47:524–534. doi:10.1016/j.watres.2012.10.004

Ahn JH, Kim S, Park H, Rahm B, Pagilla K, Chandran K (2010) N2O emissions from activated sludge processes, 2008–2009: results of a national monitoring survey in the United States. Environ Sci Technol 44:4505–4511. doi:10.1021/es903845y

Cowan NJ, Norman P, Famulari D, Levy PE, Reay DS, Skiba UM (2015) Spatial variability and hotspots of soil N2O fluxes from intensively grazed grassland. Biogeosciences 12(5):1585–1596

Daelman MRJ, van Voorthuizen EM, van Dongen UG, Volcke EIP, van Loosdrecht MCM (2015) Seasonal and diurnal variability of N2O emissions from a full-scale municipal wastewater treatment plant. Sci Total Environ 536:1–11

Danishvar M, Mousavi A, Broomhead P (2017, accepted) Modelling the eco-system of causality: the real-time unaware event-data clustering (EventiC). IEEE Trans Syst Man Cybern

Palut MPJ, Canziani OF (2007) Contribution of working group II to the fourth assessment report of the intergovernmental panel on climate change. Cambridge University Press, Cambridge

Tavakoli S, Mousavi A, Broomhead Peter (2013) Event tracking for real-time unaware sensitivity analysis (EvenTracker). IEEE Trans Knowl Data Eng 25(2):348–359. doi:10.1109/TKDE.2011.240

Todt D, Dörsch P (2016) Mechanism leading to N2O production in wastewater treating biofilm systems. Rev Environ Sci Bio/Technol 15(3):355–378

Rodriguez-Caballero A, Aymerich I, Poch M, Pijuan M (2014) Evaluation of process conditions triggering emissions of green-house gases from a biological wastewater treatment system. Sci Total Environ 493:384–391. doi:10.1016/j.scitotenv.2014.06.015

Disinfection Unit of Water Resource Recovery Facilities: Critical Issue for N_2O Emission

M. Caivano[1(✉)], R. Pascale[1], G. Mazzone[1], S. Masi[1],
S. Panariello[2], and D. Caniani[1]

[1] Scuola di Ingegneria, Università della Basilicata, Potenza, Italy
[2] Acquedotto Lucano S.p.A., Potenza, Italy

Abstract. In this study, the floating hood technique for gas collection has been coupled with the off-gas method to monitor greenhouse gas emissions from the chlorination unit in a municipal water resource recovery facility located in Italy. Experimental measurements of direct nitrous oxide (N_2O) from chlorination step were performed in order to investigate the contribution of this unit on the net carbon footprint. Interesting results were found on the chlorination unit which proved to be the major contributor to direct N_2O emissions, due to the chemical interaction between hydroxylamine and the disinfectant agent (i.e. hypochlorite). For the first time, we measured for the chlorination unit a specific emission factor of 0.008 $kg_{CO2,eq}\ kg_{bCOD}^{-1}$, proving the innovativeness of our findings.

Keywords: Disinfection · Greenhouse gas · Emission · Nitrous oxide

1 Introduction

Water resource recovery facilities (WRRFs) are responsible for the emission of greenhouse gases (GHGs). Efforts for monitoring and accounting for GHG emissions from WRRFs are of increasing interest (Caivano et al. 2016) and increasing attention is also given to the assessment of N_2O emission due to its high global warming potential (GWP), 300 times stronger than CO_2 over an atmospheric residence time of 100–120 years (Caniani et al. 2015).

Several studies have been performed to monitor full-scale plants in terms of GHG emission. Many of these studies concern the aerated tanks (i.e. activated sludge tanks) for ease of sampling methods and accuracy of analyses (Redmon et al. 1983), however the other treatment units remain poorly investigated (Caivano et al. 2016).

Indeed, to our knowledge no experimental results are available yet on disinfection unit, although it could be a potentially source of N_2O. It could be reasonable to think that in disinfection unit could occur significant levels of nitrogen compounds, NH_2OH for example, as intermediates of nitrification process (Ni et al. 2014; Pocquet et al. 2016), due to not complete processes and not suitable operational conditions. The simultaneous use of strong oxidants as disinfection agents could lead the production of great amount of N_2O.

Indeed, Seike et al. (2004) used an oxidation step for the determination of NH_2OH concentration in the water by means of sodium hypochlorite (NaClO) as oxidizing

agent. It should be considered that NH_2OH could have a crucial role in the production of N_2O. N_2O can be produced both during nitrification and denitrification processes. Indeed, during nitrification, N_2O is formed during the chemical decomposition of intermediates, such as hydroxylamine (NH_2OH) and nitrite. N_2O is also produced during the incomplete oxidation of NH_2OH because of formation of nitrosyl radical (NOH) (Caniani et al. 2015). Thus, if NaClO is used as disinfectant agent, the NH_2OH accumulated in the liquid phase during activated sludge processes could be certainly oxidized to N_2O in the disinfection unit.

In this study, a first attempt to measure N_2O emissions from the chlorination unit is reported. N_2O emission fraction was estimated as percentage of the influent load of nitrogen (N) and a qualitative mass balance of N_2O was performed to investigate the fate of N_2O during disinfection with NaClO.

2 Materials and Methods

2.1 Plant Understudy

The chlorination unit of a medium-sized municipal WRRF located in Potenza (Italy) was monitored by means of the off-gas method. The WRRF monitored serves 160,000 populations equivalents and treats organic matter and nitrogen with a Modified Ludzak-Ettinger (MLE) configuration. As shown in Fig. 1, the treated effluent is directed to the disinfection unit, the last treatment before releasing into a small neighbouring stream.
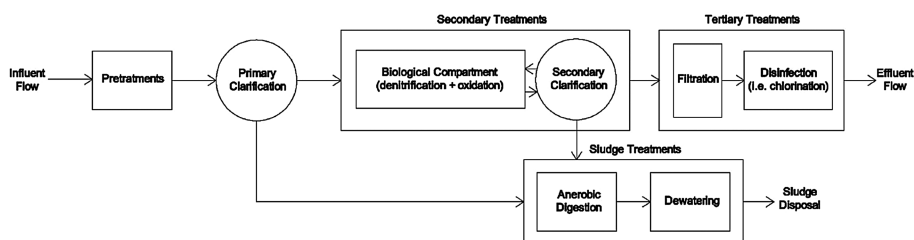

Fig. 1. Flow-chart of the WRRF under study

In particular, the chlorination is powered by 27 lh^{-1} of pure sodium hypochlorite (NaClO 12%).

The off-gas measurements were performed in the month of June, during a monitoring campaign that lasted 4 days.

2.2 Off-Gas Apparatus

Chlorination unit was monitored using the off-gas technique in order to evaluate direct N_2O emission using a specific method developed by the Civil and Environmental Engineering Department of the University of Basilicata.

A stainless steel floating hood ($1 \times 0.7 \times 0.4$ m, L $\times$ W $\times$ H) with a cross sectional area of 0.7 m^2 and a volume of 280 l (Fig. 2) was used to capture the gas fluxes from the liquid surface at the post-chlorination unit (Fig. 3) where a considerable turbulence affected the stripping of dissolved N_2O (sN_2O).
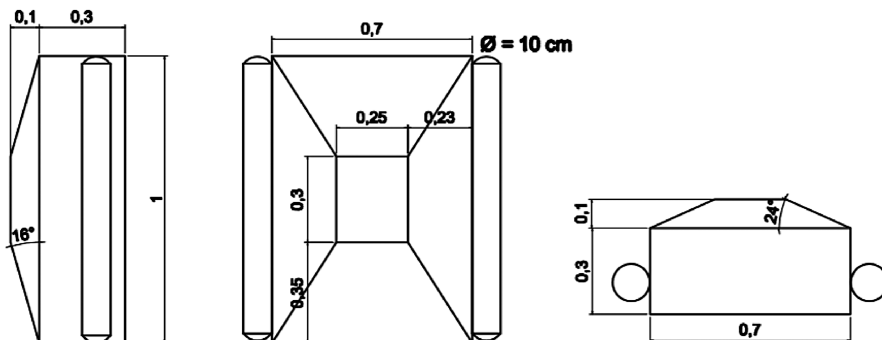

Fig. 2. Floating hood design (the measurements are in meters)

The hood headspace was connected to an analyzer through a hose of 16 mm in diameter and the gas flow rates were measured using a mass flow meter for compressed air (MISDA DN15 – SATEMA S.a.S). The hood was also equipped with a valve for gas sampling in order to connect suitable sampling bags through a hose of 4 mm in diameter. The gas samples, collected by means of Tedlar bags equipped with a vacuum pump, were analysed by an optimized method based on gas chromatograph equipped with a barrier ionization discharge detector (GC-BID) (Pascale et al. 2017).

2.3 Sampling Procedure

In order to collect an off-gas sample from the chlorination, the floating hood was positioned on the post-chlorination unit (Fig. 3) where a considerable turbulence affected the stripping of sN_2O.

The hood was manually positioned and tightly fixed with ropes in order to minimize the effect of turbulence, and it was immersed in the liquid about 10 cm to ensure no air contaminations.

The flow meter recorded a value every thirty seconds for fifteen minutes and the average value was $1.04 \ 10^{-2}$ Nm^3 min^{-1}.

Since the gas sampling plan depends on the geometry of the tank, one point was chosen as representative in the post-chlorination well.
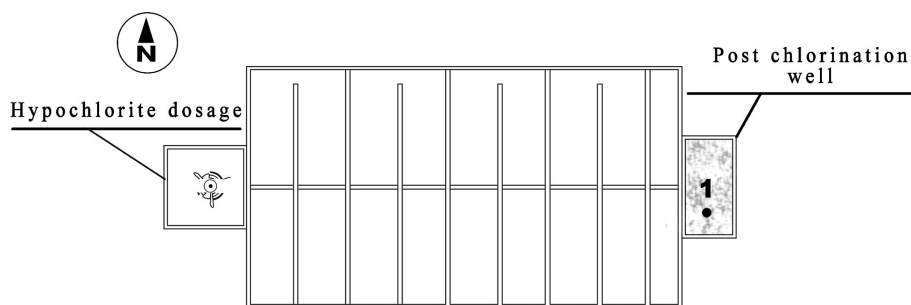
Fig. 3. Layout of the sampling position in the disinfection unit

3   Results and Discussions

The result, expressed as N_2O emission factor (EF), was computed by normalizing the flux to the daily influent TKN, as reported by Chandran (2011), according to Eq. 1:

$$EF_{N2O} = \frac{\overline{N_2O}}{\text{NH}_4 - \text{N}_{in}} \cdot \bar{Q}_{off-gas} \tag{1}$$

Interesting results were found confirming our predictions. Indeed, as expected, the chlorination unit shows an important contribution to N_2O emissions, estimating an EF value of 0.00022 $kg_{N2O\text{-}N}$ kg_{NH4-N}^{-1} or 0.022%, ten times higher than biological unit. This can be explained as the NH_2OH produced during the nitrification processes, in the previous biological compartment, reaches the disinfection unit as dissolved compound. Therefore, the chemical reaction with the disinfecting agent (i.e., NaClO) could promote its transformation in N_2O during the chlorination step. Indeed, as shown in the Table 1, the concentration of dissolved N_2O and NH_2OH in the influent and in the effluent of chlorination step have an inverse trend.

Table 1. Concentration of dissolved N_2O (sN_2O in ppbv), NH_2OH (ppbv), and CO2 (ppmv) along chlorination line (*)

	sN_2O (ppb_v)	NH_2OH (as N_2O) (ppb_v)
Chlorination influent	130.55 ± 1.39	212.61 ± 2.78
Chlorination effluent	346.90 ± 1.39	1.04 ± 2.78

(*) Each concentration value was averaged of three replicates.

The induced chemical reaction causes the increase in dissolved N_2O, consequently incrementing the emissions in the post-chlorination well where the stripping is promoted due to the presence of turbulence. This is one of the key novelties of this work, suggesting that more attention should be given to the chlorination that to date has been neglected as a potential source of N_2O in WRRFs.

Important novelties emerge when looking at Fig. 4, which allows us to investigate the fate of N_2O after the wastewater treatments and interesting considerations are possible on the chlorination unit.
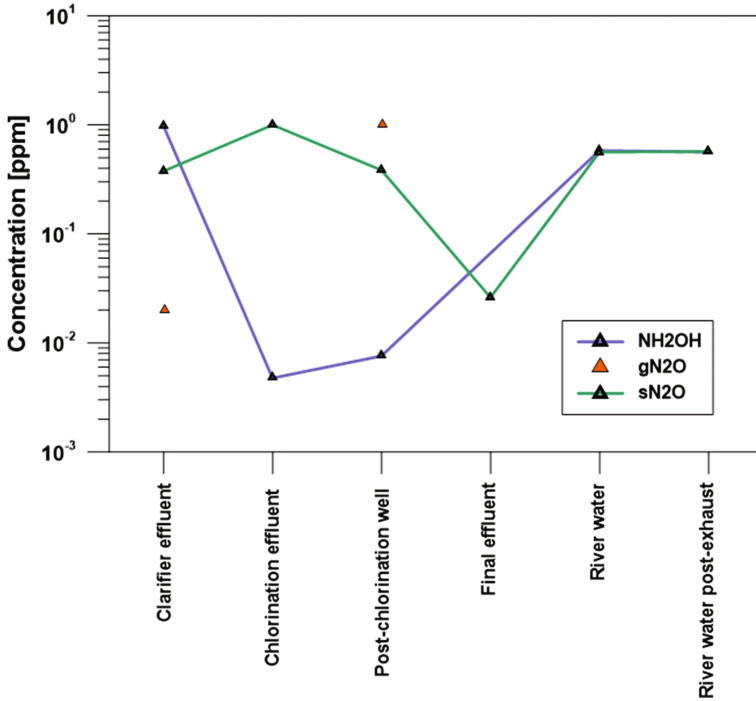
Fig. 4. A comparison of N2O liquid and gas, and of NH2OH

Almost all NH_2OH in the clarifier effluent is transformed into N_2O in the chlorination unit, thus the N_2O concentration in the liquid phase increased from 0.131 ppmv to 0.347 ppmv. The considerable increase of sN_2O due to the chemical reaction between NH_2OH and $NaClO$ is followed by an abrupt decrease because of turbulence in the post-chlorination well, favoring N_2O stripping.

These results confirm the chemical interaction between NH_2OH and $NaClO$, strengthening the hypothesis that the chlorination unit can be a significant contributor to the N_2O emissions.

4   Conclusions

In this study, the N_2O fate at the chlorination step in a medium sized plant (serving a population equivalent of 160000) was evaluated to support the development of innovative tools to monitor GHG emissions, as well as promote control strategies to improve the performance of WRRFs). The off-gas technique allowed the evaluation of

N_2O emissions from chlorination, since its large global warming potential., a first attempt to measure N_2O emissions from the chlorination unit is reported. The off-gas testing performed during the monitoring campaign proved that the chlorination unit is the major contributor to N_2O emissions due to the chemical reaction between the NH_2OH and disinfectant agent (i.e. NaClO). This reaction causes the increase in dissolved N_2O, incrementing consequently the emissions in the post-chlorination well, where the stripping is promoted due to the presence of turbulence.

Further research regards lab tests that will be performed to confirm the contribution of the chlorination unit to the net carbon footprint (CFP) of the monitored plant. Liquid samples from the secondary clarification effluent will be treated with different concentrations of NaClO and other disinfectant agents in order to optimize the chemical processes inside the chlorination step, taking into account the possible interferences (i.e. nitrate and nitrite). The results could be useful to regulate the disinfection unit in real WRRFs, minimizing the emissions from the chlorination unit by means of the right amount of the suitable disinfectant. Data gathered in this study, as well as the analytical methods implemented in GC analysis, are the key novelties of this work. The obtained results suggest to give more attention to the chlorination that, to date, has been neglected as a potential source of N_2O in WRRFs.

References

Caivano M, Bellandi G, Mancini IM, Masi S, Brienza R, Panariello S, Gori R, Caniani D (2016) Monitoring the aeration efficiency and carbon footprint of a medium-sized WWTP: experimental results on oxidation tank and aerobic digester. Environ Technol 11(6):1–10

Caniani D, Esposito G, Gori R, Mannina G (2015) Towards a new decision support system for design, management and operation of wastewater treatment plants for the reduction of greenhouse gases emission. Water 7(10):5599–5616

Chandran K (2011) Protocol for the measurement of nitrous oxide fluxes from biological wastewater treatment plants. Methods Enzymol 486:369–385 Chap. 16

Ni B, Peng L, Law Y, Guo J, Yuan Z (2014) Modeling of nitrous oxide production by autotrophic ammonia- oxidizing bacteria with multiple production pathways. Environ Sci Technol 48(7):3916–3924

Pascale R, Caivano M, Buchicchio A, Mancini IM, Bianco G, Caniani D (2017) Validation of an analytical method for simultaneous high-precision measurements of greenhouse gas emissions from wastewater treatment plants using a gas chromatography-barrier discharge detector system. J Chromatogr A 1480:62–69

Pocquet M, Wu Z, Queinnec I, Spérandio M (2016) A two pathway model for N2O emissions by ammonium oxidizing bacteria supported by the NO/N2O variation. Water Res 88(1):948–959

Redmon D, Boyle WC, Ewing L (1983) Oxygen transfer efficiency measurements in mixed liquor using off-gas techniques. Water Pollut Control Fed 55(11):1338–1347

Seike Y, Fukumori R, Senga Y, Oka H, Fujinaga K, Okumura M (2004) A simple and sensitive method for the determination of hydroxylamine in fresh-water samples using hypochlorite followed by gas chromatography. Anal Sci 20(1):139–142

CO$_2$ Removal from Biogas as Product of Waste-Water-Treatments

M. Oliva[1(✉)], C. Costa[1], and R. Di Felice[2]

[1] Dipartimento di Chimica e Chimica Industriale,
Università degli Studi di Genova, Genoa, Italy
[2] Dipartimento di Ingegneria Civile Chimica ed Ambientale,
Università degli Studi di Genova, Genoa, Italy

Abstract. In order to satisfy the future energy demands, the development of alternative sources of energy is currently object of interest. Among all the possibilities, biogas is a renewable methane-based fuel obtainable by anaerobic digestion of different types of raw materials, including waste-waters. This gas product contains relevant amounts of methane (CH$_4$), carbon dioxide (CO$_2$) with traces of other compounds and, to be used, it needs to be purified from the components responsible of a decreasing in the combustion efficiency. On the upgrading process, the CO$_2$ removal is necessary to respect the Wobbe Index specification and it can be realized by various technologies in different devices. Among all the current techniques, CO$_2$-absorption into physical or chemical solvents in packed towers is commonly applied, but the use of gas-liquid membrane contactors represents an innovative alternative. In particular the second ones are characterized by various operational advantages, such as independent gas/liquid control, optimal load of the absorbent, no entrainment, flooding or foaming and modular and very compact devices. In this work a polypropylene hollow fiber membrane contactor was used to investigate the CO$_2$-absorption from a model gas mixture into aqueous solutions of monoethanolamine (MEA), piperazine (PZ), methyildiethanolamine (MDEA) and their mixtures. The effect of reagent type and concentration was studied as well as the influence of temperature and gas composition. Experimental results show the high reactivity of MEA and PZ, capable of increasing the absorption rate in MDEA-based solvents, characterized by large loading capacity and easiness of regeneration.

Keywords: Biogas · Biomethane · CO$_2$ absorption · Membrane contactor

1 Introduction

Biogas is a non-petroleum-based fuel composed of methane (CH$_4$), carbon dioxide (CO$_2$) and traces of other compounds (H$_2$O, H$_2$S, NH$_3$, CO, O$_2$, N$_2$, syloxanes, hydrocarbons), seen as a potential solution in the current energetic-environmental scenario. This gas mixture represents a renewable resource obtainable from different types of organic materials, such as sewage sludges, agricultural and municipal wastes, by the action of various groups of microorganisms in absence of air. Anaerobic digestion is a complex biological process capable of converting an organic substrate to methane through three major steps: hydrolysis, acetogenesis and methanogenesis.

The composition of the final system depends on the nature of the initial substrate. For example, levels of methane are different in the decomposition of fat (about 70%), protein (about 63%) and cellulose (about 50%). Moreover the global process can include pretreatments and co-digestion technologies to enhance the production of methane (Andriani et al. 2014).

The application of biogas from waste-water-treatments are various, but its utilization as an alternative source of energy attracts the main part of the public attention. To be transported and used, the fuel needs to be purified from the components harmful to natural gas grid, appliances or end-users and to be upgraded to enhance the combustion efficiency. In the second case, carbon dioxide is removed to optimize calorific value and relative density, in order to respect the Wobbe Index specification. The final product, the so-called biomethane, is a gaseous fuel typically containing methane (95–97%) and small amounts of carbon dioxide (1–3%). The biogas upgrading can be realized by different techniques, based on CO_2-adsorption on solid substrates, CO_2-absorption into physical or chemical solvents, cryogenic and membrane separation or on CH_4-enrichment by biological processes (Rickebosch et al. 2011; Tippayawong and Thanompongchart 2010).

Among all these technologies, carbon dioxide scrubbing with water or basic solvents is commonly applied. The gas absorption using membrane gas–liquid contactors is regarded as a promising alternative to the conventional technologies for the removal and recovery of CO_2 from various feed streams (Gabelman and Hwang 1999). This process can offer operational and economic advantages over spray towers or packed columns. Operational advantages include independent gas/liquid control, flexible operation, optimal load of the absorption liquid, no entrainment, flooding or foaming and modular and very compact equipment.

In this work a polypropylene hollow fiber membrane contactor was utilized to absorb CO_2 from a model gas mixture into an aqueous solution. Three different reagents were selected and studied to this end: two well-known reagents, monoethanolamine (MEA) and methyldiethanolamine (MDEA), and two less common alternatives, piperazine (PZ) and PZ/MDEA mixtures. Important criteria for the selection of liquid absorbents are high reactivity with CO_2, large loading capacity, easiness of regeneration, nontoxicity, chemical compatibility with the membrane material, low vapor pressure, good thermal stability. For the various options mentioned above, the effect of reagent type and concentration has been investigated as well as the influence of temperature and gas composition.

2   Materials and Methods

Carbon dioxide and methane of more than 99.9% purity (procured by Air Liquid Italia) were used as feed gases. The absorbing reagents employed during the tests are monoethanolamine (MEA) $\geq$ 99%, piperazine (PZ) $\geq$ 99%, methyl-diethanolamine (MDEA) $\geq$ 99%, all obtained from Aldrich.

Figure 1 shows a schematic drawing of the experimental equipment. The system is continuous in the gas phase, with the gas flowing into the lumen of the hollow fibers, and discontinuous in the liquid phase.
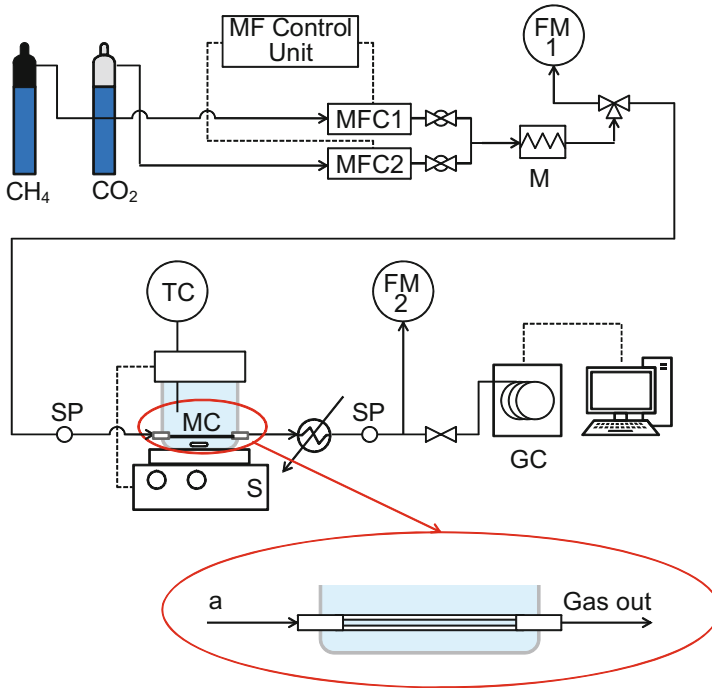
Fig. 1. Experimental setup for absorption of CO$_2$ in aqueous solutions. MC: membrane contactor; MFC: mass flow controller; M: mixer; SP: sampling point; FM: flow meter; TC: temperature controller; S: magnetic stirrer; GC: gas chromatograph

The absorbent aqueous solution is contained into a glass vessel that can be thermally insulated. A magnetic stirrer ensures the continuous mixing of the liquid. The liquid temperature is monitored and maintained at the desired value (within $\pm 1°$ C) by a temperature controller. Two side openings at the bottom of the vessel, sealed by rubber o-rings, enable the module housing. The membrane modules are built in-house and are composed of four polypropylene hollow fibers (Accurel S6/2 from Membrana, Germany),

In a typical experiment, a liquid solution at known concentration is charged into the stirred vessel, and then the gas stream is fed from compressed gas cylinders to the module at a selected flow rate. The flow rate and the composition are adjusted by means of mass flow controllers (Brooks Instrument MFC SLA 5850) that send the pure gases to a mixer and then to the module. The gas volume flow rates at the inlet and at the outlet of the contactor are measured by digital bubble meters while the compositions are continuously analyzed using an Agilent 490 microGC equipped with a capillary column PoraPLOT U and a thermal conductivity detector. The carbon dioxide absorption flux Q (mol/m^{2}s) is estimated by performing a mass balance over the contactor, based on the measured change in CO$_2$ flow rate between the inlet and the outlet of the membrane module, at any time:

$$Q_{CO2} = \frac{v\left(C_{CO2,in} - C_{CO2,out}\right)}{A} \qquad (1)$$

where v is the gas flow rate (m^3/s), C_{CO2} is the CO$_2$ concentration (mol/m^3) in the gas phase (at the inlet and outlet of the contactor), A is the interfacial area useful for the mass transfer.

3 Results and Discussions

MEA is commonly used as benchmark reagent as abundant literature data are available. PZ has been identified recently as a promising new reagent for CO$_2$ capture owing to its significant advantages: PZ-based aqueous solutions are resistant to thermal and oxidative degradation, have less volatility than MEA solutions, are not corrosive to stainless steel, are less toxic; moreover, the rate constant for the reaction of PZ with CO$_2$ is very high. On the contrary, MDEA reaction rate with CO$_2$ is lower than that of many other alkanolamines; notwithstanding MDEA has found widespread use because of its great loading capacity and its very low heat of reaction.

The mixtures of PZ and MDEA are expected to retain the high rate of the reaction of PZ with CO$_2$ and the low enthalpy of the reaction of MDEA with CO$_2$, leading to high absorption rates and low stripper reboiler duty, a factor that usually constitutes the main cost in CO$_2$ removal units and is principally dependent on the heat of reaction.

As an example, a selection of the many obtained results is shown here. Figure 2 illustrates the results of the various experimental tests carried out to study the effect of single reagent concentration. CO$_2$ absorption flux is plotted as a function of MEA, PZ or MDEA concentration in the aqueous solution. In all cases a rise in concentration gradually increases CO$_2$ transfer rate. PZ behaves qualitatively like MEA, showing however a higher performance. For MDEA solutions the fluxes are one order of magnitude lower.

Fig. 2. Effect of single reagent concentration on the absorption flux from a biogas containing 15% v/v of CO$_2$ with the balance being CH$_4$. T = 25° C, P = 1 atm

The effect of reagent type on CO$_2$ absorption rate can be appreciated in Fig. 3. The PZ-based absorbents show the best CO$_2$ uptake efficiency. The solutions containing both MDEA and PZ achieve slightly lower performance, that get worse if the PZ percentage is reduced. These trends can be qualitatively explained if the physico-chemical parameters governing the process are taken into consideration.
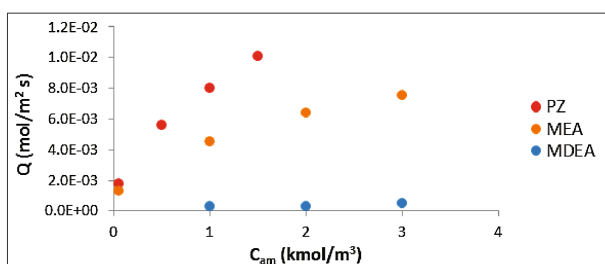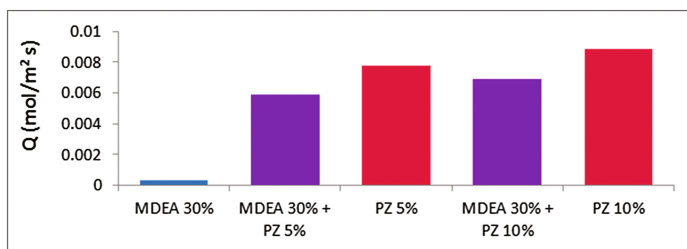
Fig. 3. Effect of liquid composition on the absorption flux from a biogas containing 15% v/v of CO_2 with the balance being CH_4. T = 25° C, P = 1 atm

The reaction rate of CO_2 with PZ may explain the higher removal efficiency of this reagent. From literature data, at T = 25° C k_{PZ} = 58000 m³/(kmol s) (Samanta and Bandyopadhyay 2007), whereas k_{MDEA} = 4 m³/(kmol s) (Versteeg and van Swaaij 1988), 4 orders of magnitude lower. Comparing PZ solutions and MDEA/PZ solutions, an appreciable reduction in the absorption flux can be observed for the latter, also when the two systems retain the same PZ concentration. This fact can be ascribed to the higher viscosity resulting from the MDEA addition in the PZ aqueous solution, which hinders molecular diffusion in the liquid phase. However it is not convenient to enhance overly the PZ content, because the heat of absorption for the mixed absorbent is significantly increased by adding PZ as an activator: for comparison, heats of absorption at 120° C (desorber conditions) and loading 0.4 mol-CO_2/mol-amine are ∼55 kJ/mol CO_2 for MDEA and ∼100 kJ/mol CO_2 for PZ (Kim and Svendsen 2011).

4   Conclusions

Amine based absorbents are particularly efficient in CO_2 removal from biogas and allow, by suitably varying the ratio between liquid and gas flow rates, to obtain bio-methane of high purity (CO_2 capture efficiency can reach 100%). Nevertheless each reagent has its own advantages and drawbacks, associated with different reaction mechanisms and different physicochemical properties. An aqueous mixture of 30 wt% MDEA and 5 wt% PZ seems a convenient option that maintains acceptable absorption rate, very high loading capacity, low heat of absorption.

References

Andriani D, Wresta A, Atmaja TD, Saepudin A (2014) A review on optimization production and upgrading biogas through CO_2 removal using various techniques. Appl Biochem Biotechnol 172:1909–1928

Gabelman A, Hwang S (1999) Hollow fiber membrane contactors. J Membr Sci 159:61–106

Kim I, Svendsen HF (2011) Comparative study of the heats of absorption of post-combustion CO_2 absorbents. Int J Greenh Gas Control 5:390–395

Rickebosch E, Drouillon M, Vervaeren H (2011) Techniques for transformation of biogas to biomethane. Biomass Bioenerg 35:1633–1645

Samanta A, Bandyopadhyay SS (2007) Kinetics and modeling of carbon dioxide absorption into aqueous solutions of piperazine. Chem Eng Sci 62:7312–7319

Tippayawong N, Thanompongchart P (2010) Biogas quality upgrade by simultaneous removal of CO_2 and H_2S in a packed column reactor. Energy 35:4531–4535

Versteeg GF, van Swaaij WPM (1988) On the kinetics between CO_2 and alkanolamines both in aqueous and non-aqueous solutions – II. Tertiary amines. Chem Eng Sci 43:587–591

Quantification of CO$_2$ and N$_2$O Emissions from a Pilot-Scale Aerobic Digester, Towards the Validation and Calibration of the First Activated Sludge Model for Aerobic Digestion (AeDM1)

M. Caivano[✉], S. Masi, G. Mazzone, I.M. Mancini, and D. Caniani

Scuola di Ingegneria, Università della Basilicata, Potenza, Italy

Abstract. In this study, a pilot aerobic digester was developed and operated to monitor N$_2$O and CO$_2$ emissions using the off-gas technique. A 30-days monitoring campaign was carried out to evaluate the impact of aerobic digestion (AeD) in Greenhouse Gas (GHG) estimation. After the achievement of the equilibrium conditions for a conventional AeD, a monitoring campaign was performed assuming 20 days as sludge retention time. The N$_2$O gas flux was found equal to 71.7 mg$_{N2O}$ m^{-2}min^{-1} against 16914 mg$_{CO2}$ m^{-2}min^{-1} calculated for CO$_2$, demonstrating that strong aerobic oxidation processes occur inside the digester. In terms of equivalent CO$_{2,}$ N$_2$O covers the 55% of the total CO$_{2,eq}$ emissions and CO$_2$ the 45%. The experimental campaigns were coupled with the development of a mathematical model for AeD, named Aerobic Digestion Model No. 1 (AeDM1). The Morris Method allowed us to carry out a sensitivity analysis on the main kinetic parameters, resulting that the maximum specific growth rate of heterotrophs is the more sensitive parameter. After the model calibration, the experimental results on the pilot digester were used to validate the model, inserting the data collected during the experimental tests as model inputs.

Keywords: Aerobic digestion · Nitrous oxide · Modelling

1 Introduction

The increased interest towards GHG emissions brings the researchers to spend their forces into the evaluation of carbon footprint (CFP) of wastewater treatment plants (WWTPs). The scientific community turns the attention mainly to on-site emissions because knowledge on how biological pathways produce gases has to be amplified and many solutions regarding the control of operational parameters are proposed in order to minimize gases production and emissions (Caniani et al. 2015).

Even though the knowledge about sampling and measuring methods of gas is wide (*inter alia*, Law et al. 2012; Aboobakar et al. 2013; Ye et al. 2014; Caivano et al. 2016), experimental measurements of gas emissions from AeD are actually absent in literature, although these units are popular in Italy as excess sludge treatment in small/medium-sized WWTPs (i.e. 20,000–50,000 inhabitants equivalent).

In this work, a pilot-scale aerobic digester was realized in order to quantify CO_2 and N_2O emissions during sludge treatment. After the achievement of the equilibrium conditions for a conventional AeD, a monitoring campaign was performed assuming 20 days as sludge retention time (SRT). The principles of the off-gas technique were applied to collect and conveying gases into a flow meter in order to evaluate the off-gas flow rates. Furthermore, the gas bag technique was used to collect gas samples and perform off-line measurements of N_2O and CO_2 concentrations in the off-gas.

Since the mathematical modelling is the most important tool for developing control strategies and designing WWTPs, the experimental results were accompanied with the development of the first model for AeD (AeDM1).

Include the AeDM1 in the simulation platform of a WWTP is of important concern because of the possibility to investigate on the AeD contribution in the estimation of the plant CFP.

2 Materials and Methods

2.1 Pilot Plant Configuration

Figure 1 shows a simplified drawing of the pilot apparatus used for AeD experimentation. A cylindrical aerated tank with a diameter of 30 cm, a cross sectional area of 0.07 m², and 70 cm deep (Fig. 1a), was connected to the off-gas apparatus (Fig. 1b). This 10 L reinforced polyethylene tank was equipped with an aeration system
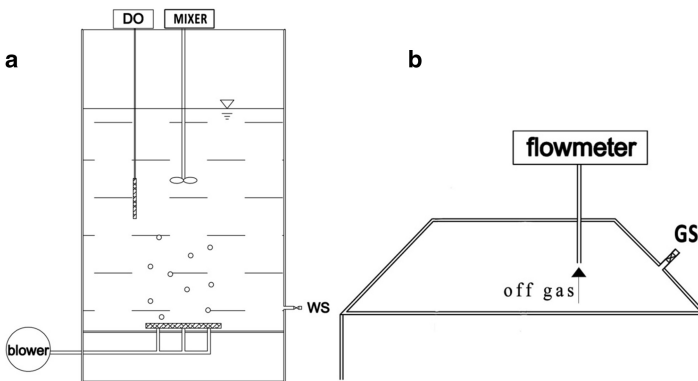
Fig. 1. Simplified drawing of the pilot digester (a) and focus on the Off-gas apparatus (b)

consisting in four suitable porous ceramic stones connected to a blower, supplying an air flow rate of 0.05 m^3h^{-1}. The tank was equipped with a DO probe for online DO monitoring to allow the oxygen control over the sludge volume and ensure an average DO concentration of 1–2 mg/l (Metcalf and Eddy 2003). The digester was fed with sludge coming from the secondary settler underflow of a full-scale WWTP located in Basilicata Region and designed to serve 160,000 EI. The pilot digester was firstly fed

with 6L of sludge and, subsequently, 0.06L of fresh sludge were introduced for each testing day to compensate the same discharged amount.

A 30-days monitoring campaign was carried in the month of July 2015, in which the first ten days were dedicated to reaching the equilibrium conditions for a conventional AeD and the remained days to complete the process, assuming 20 days as SRT. After 20 days the performance of the pilot plant were evaluated. 38.9% decreasing in TSS concentration and 51% decreasing in VSS concentration were observed, respectively, which are values closer to the literature range for well performed systems (Metcalf and Eddy 2003).

A simplified off-gas apparatus was used during the experimental campaign to collect and conveying the exhaust gas into a flow meter (Fig. 1b). A reinforced polyethylene hood with a cross sectional area equal to the reactor area was used to close tightly the reactor and capture the gas fluxes from the sludge surface.

The hood headspace was connected to the flowmeter through and gas flow rates were measured by a hot wire anemometer. However, difficulties in measuring the off-gas flow rates were found due to the insignificant off-gas flow leaving the liquid surface. Therefore, the off-gas flow rate was assumed equal to the air flow rate (0.05 m^{3}h^{-1}).

The hood was also equipped with a valve for gas sampling (GS in Fig. 1b) to connect 2L Super-Inert Multi Foil gas bags, equipped with a vacuum pump. In view to obtain a homogeneous representation of gas emissions, a gas sampling plan was fixed, consisting in the collection of eight sampling bags per day every 15 min for 13 testing days.

2.2 Model for Aerobic Digestion

The experimental results on the pilot digester were coupled with the development of a mathematical model for AeD, named Aerobic Digestion Model No. 1 (AeDM1).

The AeDM1 consists of an aerobic AS unit (ASU) working in discontinuous feeding of sludge, in which the mass balances on each state variables are performed as suggested. The biological phenomena taking place in AeD are described by a modified ASMN model (Hiatt and Grady 2008), as proposed by Pocquet et al. (2016), suggesting an integrated approach to better simulate the biological nitrogen removal processes (BNR), as well as their influence on N$_2$O production. Therefore, 18 state variables and 19 dynamic processes were modelled.

The model needed to be calibrated using the data collected during the experimental tests.

By means of the Morris Method (Morris 1991), a sensitivity analysis was performed on the AeDM1 to asses which parameters influence the BNR processes inside the reactor. The sensitivity analysis allowed us to individuate which ones have a strong influence (on a scale from I as small/negligible influence to IV as very high influence) on the model output, ensuring the model calibration. The output variables analyzed in this work are represented by the NH$_4^+$, NO$_2^-$, NO$_3^-$, NH$_2$OH, and N$_2$O.

Twelve kinetic parameters were involved in the Morris Method (Table 1), whereas default values suggested by Hiatt and Grady (2008) were used for the other parameters.

Table 1. Parameters involved in the sensitivity analysis

Parameters	Unit	Lower bound	Upper bound
μ_H	1/d	3	3.12
μ_{AOB}	1/d	0.2	0.9
μ_{NOB}	1/d	0.2	0.9
b_H	1/d	0.06	0.2
b_{AOB}	1/d	0.05	0.15
b_{NOB}	1/d	0.05	0.15
Y_H	g biomass/g COD	0.3	0.7
Y_{AOB}	g biomass/g COD	0.10	0.15
Y_{NOB}	g biomass/g COD	0.10	0.15
$i_{N/XD}$	gN/g COD	0.01	0.06
η_{AOB_ND}	dimensionless	0.239	0.27
η_{AOB_NN}	dimensionless	0.001	0.002

3 Results and Discussions

3.1 N_2O and CO_2 Emissions from the Pilot AeD

The N_2O emission factor (EF) was computed by normalizing the flux to the daily influent NH_4^+, as reported by Chandran (2011). A mean value of the N_2O concentration during the test period was calculated and found equal to 6.023 ppm_v. Thus, on average the calculated N_2O EF (kg_{N2O-N}/kg_{NH4-N}) for the pilot digester was $6 \cdot 10^{-5}$ $kg_{N2O-N}\ kg_{NH4-N}^{-1}$ or 0.006%, resulting lower than the range proposed by Chandran (2011) for AS (from 0.01% to 1.8%).

Moreover, the N_2O gas flux was 71.7 $mg_{N2O}m^{-2}min^{-1}$ against 16914 $mg_{CO2}m^{-2}min^{-1}$ calculated for CO_2, demonstrating that strong aerobic oxidation processes occur inside the digester. However, the N_2O flux can be considered negligible than that of CO_2.

Assuming a conversion factor of 0.74 $kg_{bCOD}\ kg_{COD}^{-1}$ (Henze et al. 2000), the specific amount of equivalent CO_2 ($CO_{2,eq}$) emitted from AeD, due to the direct transformation of biodegradable organic matter and nutrients, was also calculated as mass of $CO_{2,eq}$ per mass of influent biodegradable COD (bCOD). Using the N_2O GWP of 289 kg_{CO2}/kg_{NO2} (IPCC 2006), average CO_2 and N_2O emissions fractions were 0.00028 $kgCO_{2,eq}/kg_{bCOD}$ and 0.00034 $kgCO_{2,eq}/kg_{bCOD}$, respectively, contributing to a total $CO_{2,eq}$ emission of 0.00062 $kgCO_{2,eq}/kg_{bCOD}$. Particularly, N_2O covers the 55% of the total $CO_{2,eq}$ emissions and CO_2 the 45%.

As expected, the emissions from AeD are lower than those from conventional AS systems mainly because of the discontinuous feeding of organic matter, although the SRT is higher.

3.2   Model Calibration

Table 2 shows the corresponding class of sensitivity, obtained from the normalized average elementary effect for each input parameter.

Table 2. Sensitivity classification

	NH$_4^+$	NO$_3^-$	NO$_2^-$	N$_2$O	NH$_2$OH
μ_H	IV	III	IV	IV	IV
μ_{AOB}	III	I	III	III	III
μ_{NOB}	III	II	III	III	III
b_H	II	I	II	II	I
b_{AOB}	II	I	II	II	I
b_{NOB}	II	I	I	II	I
Y_H	II	I	III	III	II
Y_{AOB}	I	I	I	II	I
Y_{NOB}	II	I	II	II	I
$i_{N/XD}$	I	I	I	I	I
η_{AOB_ND}	II	I	II	II	I
η_{AOB_NN}	I	I	I	I	I

The maximum specific growth rate of heterotrophs (mu_H) is the more sensitive parameter for all the model outputs. Therefore, the variation, as well as its interaction with the parameters kept fixed at their baseline value, determines a variation of NO$_2^-$, NO$_3^-$, NH$_2$OH, and N$_2$O.

3.3   Model Validation

A comparison between the model output and the lab-measurements was performed in order to assess the reliability of the constructed model, including the estimation of the N$_2$O emissions. The results are reported in Fig. 2.

Generally, R^2 values greater than 0.7 are considered suitable for the best data fitting, however the obtained values have been also admitted in this study because of the use of experimental data on pilot scale as model inputs. The regression analysis proves that the model values of COD, TSS, and VSS are closed than those recorded during experimental tests, admitting R^2 values in the range 35–40%. More experimental tests on both pilot scale and full scale aerobic digesters are needed to improve the model in simulating nitrogen compounds.
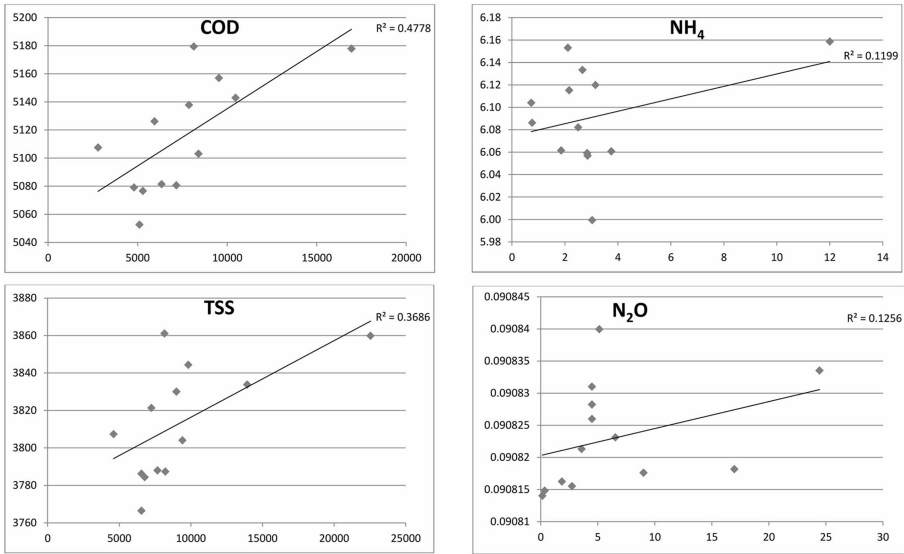
Fig. 2. Model validation

4   Conclusions

The increasing interest in GHG emissions from WWTPs has been leading to new tools for their designing and managing.

However, limited experimental measurements of direct GHG emissions from AeD are available in the literature, giving attention only to AD and their capability in recovering the biogas.

Therefore, a pilot AeD was realized in order to quantify N_2O and CO_2 emissions during aerobic sludge treatments. The interest towards AeD is also justified by the lack in literature of a wide knowledge on these systems, even though they are commonly used in Italy as excess sludge treatment in medium/small-sized WWTPs (20,000–50,000 EI). The experimental results show that N_2O cover the most of CO_2 equivalent emissions (55%) because of its higher GWP than that CO_2. However, in terms of flux, N_2O emissions can be considered negligible. Furthermore, the trend on N_2O emissions during the testing days is influenced by BNR processes and a comparison with NH_4 loads in the incoming sludge was performed.

The experimental measurements were correlated with a mathematical model, that is able to evaluate the interactive effects of several operating conditions on the treatment unit and GHG emissions. Since the mathematical modelling is still a valid aid to develop control strategies and design WWTPs, the Aerobic Digestion Model no. 1 (AeDM1) is proposed in this work to simulate the AeD processes, including N_2O estimation.

These findings represent important novelties to assess the performance of small/medium- sized plants, especially regarding the estimation of both the carbon and the energy footprint, contributing to broaden the available dataset on GHG emissions from WWTPs. Moreover, the new model is a valid tool to assess the influence of AeD

units on the functionality of the whole plant, also in terms of direct and indirect emissions. AeDM1 contributes in developing a valid decision support tool to the practitioners, providing a robust base on which design and manage the excess sludge treatment and disposal.

References

Aboobakar A, Cartmell E, Stephenson T, Jones M, Vale P, Dotro G (2013) Nitrous oxide emissions and dissolved oxygen profiling in a full-scale nitrifying activated sludge treatment plant. Water Res 47(2013):524–534

Caivano M, Bellandi G, Mancini IM, Masi S, Brienza R, Panariello S, Gori R, Caniani D (2016) Monitoring the aeration efficiency and carbon footprint of a medium-sized WWTP: experimental results on oxidation tank and aerobic digester. Environ Technol. doi:10.1080/09593330.2016.1205150

Caniani D, Esposito G, Gori R, Mannina G (2015) Towards a new decision support system for design, management and operation of wastewater treatment plants for the reduction of greenhouse gases emission. Water 7:5599–5616. doi:10.3390/w7105599

Chandran K (2011) Protocol for the measurement of nitrous oxide fluxes from biological wastewater treatment plants. Methods Enzymol 486:369–385 1st edn. Elsevier Inc

Henze M, Gujer W, Mino T, van Loosdrecht MCM (2000) Activated sludge models ASM1, ASM2, ASM2d, ASM3. IWA scientific and technical report no. 9. IWA, London

Hiatt WC, Grady CPL Jr (2008) An updated process model for carbon oxidation, nitrification, and denitrification. Water Environ Res 80(11):2145–2156

Intergovernmental Panel on Climate Change (IPCC) (2006) Wastewater treatment and discharge. In: Eggleston HS, Buendia L, Miwa K, Ngara T, Tanabe K (eds) Guidelines for national greenhouse gas inventories, institute for global environmental strategies (IGES), Japan, pp 1–28

Law Y, Ye L, Pan Y, Yuan Z (2012) Nitrous oxide emissions from wastewater treatment processes. Philos Trans Roy Soc B 367:1265–1277

Metcalf & Eddy (2003) Wastewater engineering. McGraw-Hill, Boston

Morris MD (1991) Factorial sapling plan for preliminary computational experiments. Technometrics 33(2):161–174

Pocquet M, Wu Z, Queinnec I, Spérandio M (2016) A two pathway model for N2O emissions by ammonium oxidizing bacteria supported by the NO/N2O variation. Water Res 88:948–959

Ye L, Ni B, Law Y, Byers C, Yuan Z (2014) A novel methodology to quantify nitrous oxide emissions from full-scale wastewater treatment systems with surface aerators. Water Res 48:257–268

Seasonal and Diurnal Variations of GHG Emissions Measured Continuously at the Viikinmäki Underground WWTP

A. Kuokkanen[1(✉)], A. Mikola[2], and M. Heinonen[1]

[1] Helsinki Region Environmental Services Authority, 00066 Helsinki, Finland
[2] Department of Built Environment, Aalto University, 00076 Aalto, Finland

Abstract. The gaseous emissions of an underground activated sludge treatment plant with total nitrogen removal have been measured on-line since 2012. The continuous Fourier transform infrared (FT-IR) measurement of CO_2, NO, NO_2, N_2O, NH_3 and CH_4 is situated in the single exhaust air pipe, thus covering the whole wastewater treatment process. The measurement data from 2015 showed that the seasonal and diurnal variations of N_2O and CH_4 are considerable. When comparing N_2O and CH_4 emissions as CO_2 equivalents to CO_2 formed in the activated sludge process, the impact of N_2O was dominant. The CH_4 emission was considerably smaller, and the emissions of NOx and NH_3 from biological treatment were small. The long term variations of N_2O or CH_4 production were not linked directly to load variations or other "apparent" factors such as temperature, nitrogen load, nitrogen reduction or anoxic volume. There was neither a clear seasonal pattern. The short interval variations of N_2O were similar to but not identical with CO_2 variations.

Keywords: GHG · N_2O · WWTP · FTIR

1 Introduction

The Viikinmäki wastewater treatment plant (WWTP) is a pre-denitrifying activated sludge (AS) plant with post-denitrification filters, treating the wastewaters of app. 800 000 persons and local industry. The average wastewater inflow in 2015 was 280 000 m^3/d and the average COD and total nitrogen loads to the treatment plant were 151 000 kg COD/d and 13 200 kg N/d. The total nitrogen removal in AS varies depending of season but due to post-treatment with denitrifying filters and methanol addition the total nitrogen removal is over 90% with little seasonal variation. The number of anoxic and aerated zones in AS is controlled automatically based on effluent on-line NH_4-N measurements on each of the nine treatment lines. The total sludge age is controlled according to seasonal changes of wastewater temperature and it varies in the range of 7 to 12 days. The average mixed liquor suspended solids concentration in 2015 was mainly between 2.5 and 4.5 g/L.

The treatment plant is situated underground and all ventilation exhaust air passes through one single pipe which has been equipped with a continuous FT-IR measurement of gaseous emissions since 2012. The measurement gives an insight on the level and variations of total emissions of several gaseous compounds throughout several years.

Kosonen et al. ([2016](#)) studied N_2O production and variations in Viikinmäki based on a one-year data period during 2012–2013. Here, N_2O data from 2015 is presented, together with other gaseous compounds.

2 Materials and Methods

The concentrations of CO_2, NO, NO_2, N_2O, NH_3 and CH_4 are measured from the exhaust air vent of the Viikinmäki underground WWTP using Gasmet CEMS II Fourier transform infrared (FTIR).

The measurement is situated at the sole exhaust air pipe where air from all wastewater treatment process steps is included: screening, sand removal, pre-aeration, pre-sedimentation, aeration, post-sedimentation and post denitrifying filters as well as treatment of screenings, sand and reject water from sludge drying. The treatment process is presented in Fig. [1](#).
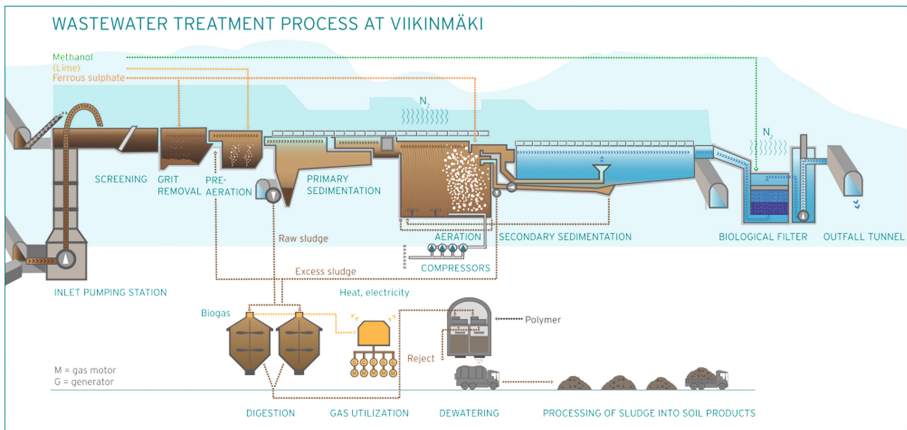

Fig. 1. The Viikinmäki WWTP. The dark background represents the underground parts of the process

The total exhaust air flow from the underground treatment plant is app. 110 ± 10 m^3/s. The air flow variations are small and the variations of concentrations are equivalent to variations in emissions.

3 Results and Discussion

Daily averages of measured values of gaseous compounds in 2015 are presented in Fig. [2](#). All measured values varied during the year. N_2O was particularly high in December and CH_4 and NO_2 in March–April. The highest daily average of N_2O was 250% of the yearly average and the lowest one only 20% of average. For CH_4 the maximum and minimum were 160% and 40%, respectively. The large variations
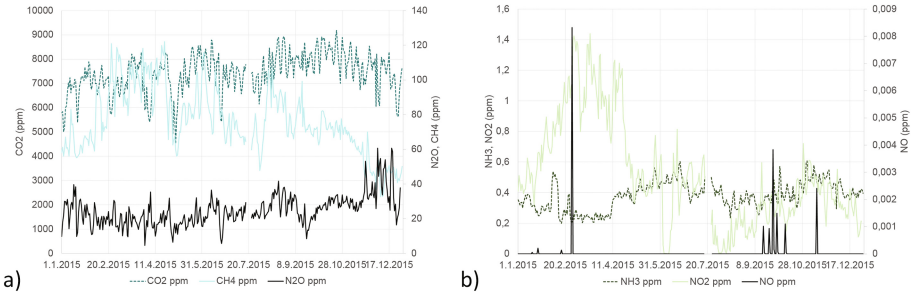
Fig. 2. (a) N_2O, CH_4 and CO_2 and (b) NH_3, NO and NO_2 concentrations in ventilation exhaust air

indicate that short term measurement campaigns can be unrepresentative in estimating total emissions of activated sludge plants, as has been observed also by Daelman et al. (2013) in a long term study of a covered wastewater treatment plant in the Netherlands.

The indirect greenhouse gases NO and NO_2 as well as NH_3 are also included in the gas measurement (Fig. 2b). Their concentrations in the ventilation exhaust air were low compared to CO_2, N_2O and CH_4. NO_2 was present in highest concentrations and also the variations were considerable. Some similarity in the occurrence of peak values of CH_4 and NO_2 could be observed. NO was basically negligible.

When expressed as CO_2 equivalents, (Fig. 3) the impact of N_2O on total emissions was clearly significant, even when compared to the large, direct CO_2 production from wastewater treatment.
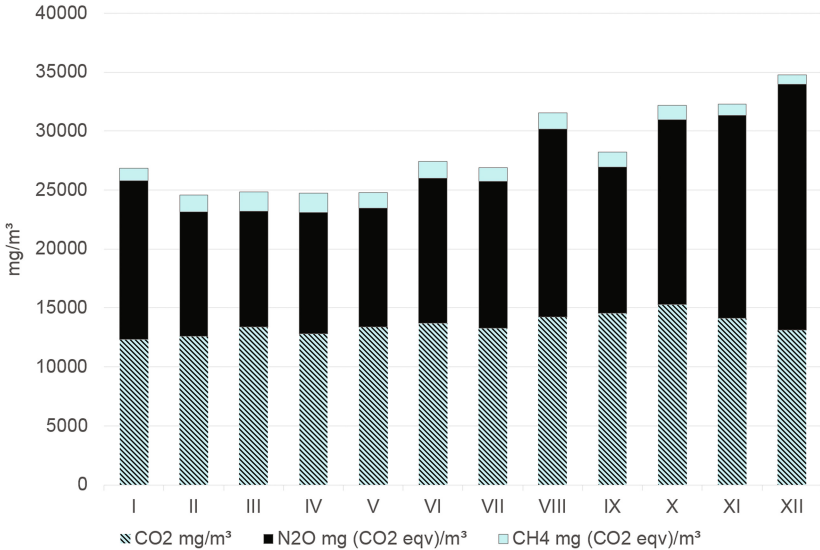

Fig. 3. Monthly averages of N_2O, CH_4 and CO_2 in 2015 as CO_2 equivalents (factor of 298 for N_2O and 25 for CH_4)

The CO_2 measured at Viikinmäki WWTP correlated well with total aeration air consumption during short periods but not as much during longer periods (Fig. 4). Both the air consumption and CO_2 production are strongly dependent of organic load, but there are several factors influencing them differently such as wastewater temperature, sludge age, anoxic volume, wastewater flow changes and in the case of Viikinmäki also variations of nitrogen load and subsequently methanol addition to denitrifying filters. The yield of bacterial mass in aerobic conditions is app. 0,67 as COD and in anoxic conditions it is assumed to be the same or smaller (Barked and Dold 1997). Thus a considerable CO_2 emission is formed in both anoxic and aerobic treatment steps. It is generally assumed that CO_2 formed in wastewater treatment is not fossil and thus not a part of GHG-emissions. However, according to Tseng et al. (2016) wastewater COD and consequently the CO_2 emissions originate partially from fossil sources.
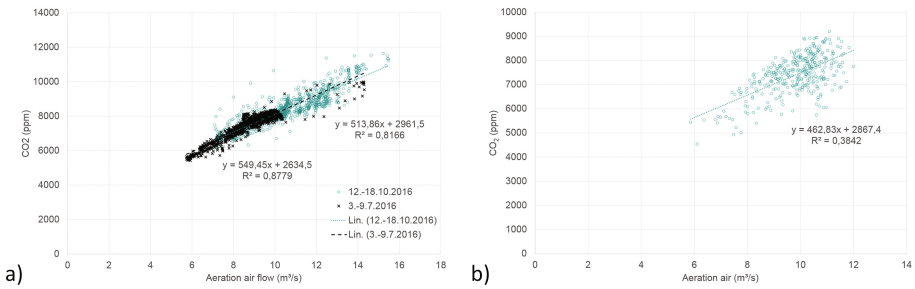

Fig. 4. The correlations of CO_2 in ventilation exhaust air and aeration air in (a) 10 min averages during two separate one-week periods and (b) 24 h averages during the year 2015

Unlike long term variations (Fig. 2a) the short interval variations of N_2O were similar to but not identical with CO_2 variations (Fig. 5). This was possibly linked to changes in air flow and thus consequently due to changes in stripping. The variations were larger when the anoxic volume varied, which can in the case of N_2O also be due to changes in denitrification and possible N_2O consumption. The influence of the changes of anoxic volume on N_2O emissions in short interval data was observed by both Kosonen et al. (2016) and Blomberg et al. (submitted).
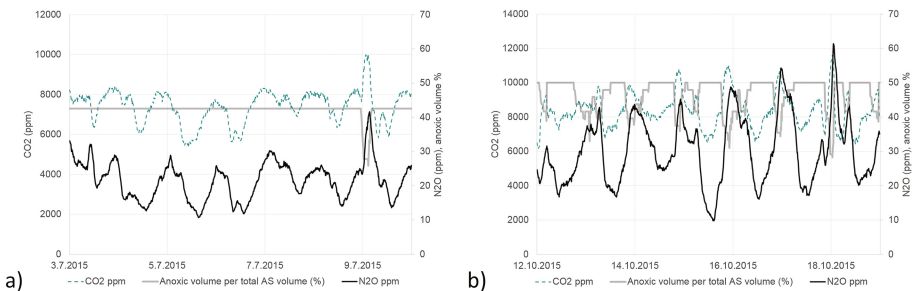

Fig. 5. CO_2 and N_2O concentration variations during two separate weeks: (a) in July with a mainly steady anoxic volume and (b) in October with daily variations in anoxic volume

The changes in N_2O production were not linked directly to load variations or other "apparent" factors such as temperature, nitrogen load, nitrogen reduction or anoxic volume (Fig. 6). There was neither a clear seasonal pattern. The highest monthly average of N_2O was observed in December and the lowest in March (Fig. 2a), while Kosonen et al. (2016) had observed the highest values in June 2013 and the lowest in July 2012. As the studies have thus presented no distinct ways of mitigating N_2O emissions without compromising nitrogen removal, dynamic modeling work based on Viikinmäki data (Blomberg et al. submitted) has been started.
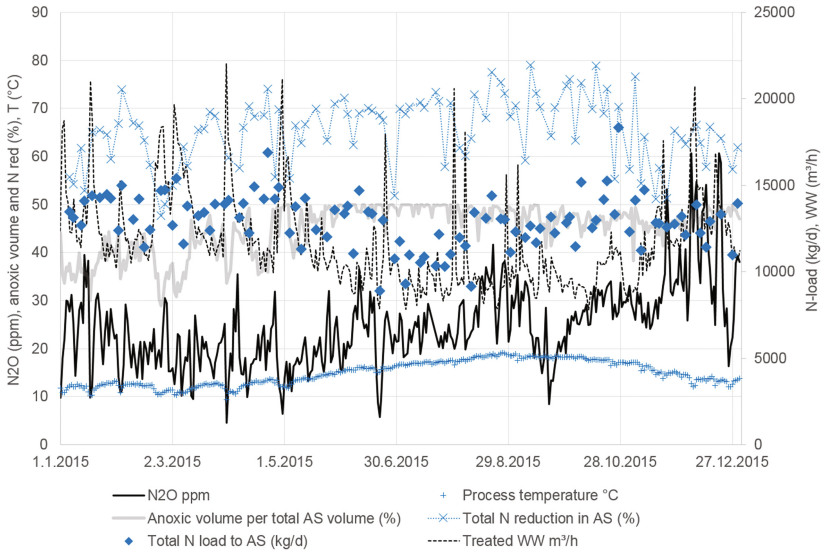

Fig. 6. N_2O emissions (ppm), process temperature (°C), anoxic volume (%), total nitrogen load to AS (kg/d), nitrogen reduction in the activated sludge process (%) and treated wastewater (m^3/d)

4   Conclusions

An underground WWTP with only one ventilation exhaust air pipe offers a rare opportunity for measuring total gas emissions from a wastewater treatment process, revealing the total yearly loads and the extent of concentration variations throughout long periods – that could possibly also be used as additional reference measurements in calibrating process models.

When comparing measured emissions and calculating N_2O and CH_4 as CO_2 equivalents, the impact of N_2O was dominant. The CH_4 emission was considerably smaller, and the emissions of NOx and NH_3 from biological treatment were small.

The yearly variations of the production of greenhouse gases N_2O and CH_4 production could not be directly linked to variations in temperature, load or process conditions.

References

Barker PS, Dold PL (1997) General model for biological nutrient removal activated-sludge systems: model presentation. Water Environ Res 69(5):969–984

Blomberg K, Kosse P, Mikola A, Kuokkanen A, Fred T, Heinonen M, Mulas M, Lübken M, Wichern M, Vahala R (submitted) Modelling nitrous oxide production in a full-scale wastewater treatment plant: a calibrated and validated extension of ASM3. Environ Sci Technol

Daelman MRJ, van Voorthuizen EM, van Dongen LGJM, Volcke EIP, van Loosdrecht MCM (2013) Methane and nitrous oxide emissions from municipal wastewater treatment – results from a long-term study. Water Sci Technol 67(10):2350–2355

Kosonen H, Heinonen M, Mikola A, Haimi H, Mulas M, Corona F, Vahala R (2016) Nitrous oxide production at a fully covered wastewater treatment plant: results of a long-term online monitoring campaign. Environ Sci Technol 50(11):5547–5554

Tseng LY, Robinson AK, Zhang X, Xu X, Southon J, Hamilton AJ, Sobhani R, Stenstrom MK, Rosso D (2016) Identification of preferential paths of fossil carbon within water resource recovery facilities via radiocarbon analysis. Environ Sci Technol 50(22):12166–12178

The Relationship Between Gene Activity and Nitrous Oxide Production During Nitrification in Activated Sludge Systems

P. Kowal[✉] and J. Mąkinia

Faculty of Civil and Environmental Engineering,
Gdansk University of Technology,
Narutowicza Street 11/12, 80-233 Gdansk, Poland
{przkowal, jmakinia}@pg.gda.pl

Abstract. The aim of this study was to identify the dominant pathways involved in the nitrogen removal processes at different DO concentrations. The analysis was performed based on the activity control of selected functional genes and N_2O production measurements. In particular, a relationship between the gene activity and N_2O production was investigated in the presence of NO_2-N. A series of laboratory experiments were carried out in a batch scale reactor with a working volume of 10 dm^3. The duplicate nitrification tests were run at different DO set points: 0.4; 0.7 and 1.0 g O_2/m^3. In the first scenario, ammonium constituted sole nitrogen source, whereas ammonium and nitrite were added to the reactor at the ratio 1:1 in the second scenario. During tests with ammonium only N_2O production increased with the decrease of aeration intensity. The maximum N_2O concentration (0.06 g N-N_2O/dm^3), observed at the DO concentration = 0.4 g O_2/m^3, was almost two times higher compared to the experiment carried out at the DO concentration = 1.0 g O_2/m^3. In contrary, different patterns were obtained when a mixture of ammonium and nitrite- was added. Values of the indicators that characterize N_2O emission were at least 6 time higher contrary to tests with only ammonium. NO_2- presence during nitrification stimulated N_2O production regardless of the DO concentration. Gen activity measurements showed that in case of nitrifying bacteria, hydroxylamine oxidation, rather than autotrophic denitrification, is the main contributor to N_2O production under the DO-limited conditions.

Keywords: N_2O production · Nitrification · Oxygenation level · *nirS, nirK* and *hao* gene activity · Real-time PCR

1 Introduction

Reduction of greenhouse gas (GHG) emissions is one of the most important challenges faced by the operators of modern wastewater treatment plants (WWTPs). A special interest has been paid to nitrous oxide (N_2O) due to its very high global warming potential ($\sim$320 times higher than CO_2). In the case of WWTPs, N_2O has been identified as an important intermediate or end product of several pathways related to nitrogen removal. Biological processes which take place in the aerobic compartments are implicitly the main contributors to the overall N_2O emission from WWTPs (Fig. 1).
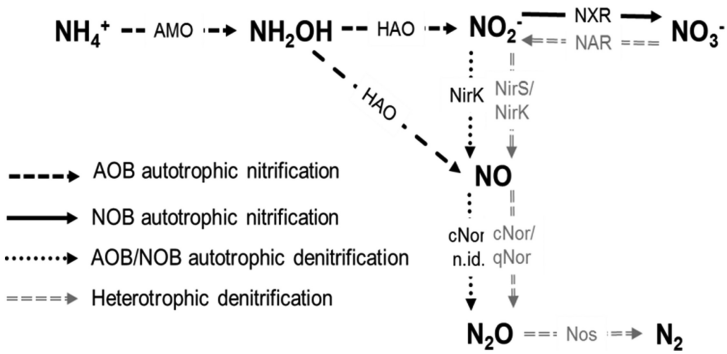
Fig. 1. Main biochemical pathways involved in N_2O production under DO-limited conditions, and mediated by ammonium oxidizing bacteria (AOB), nitrite oxidizing bacteria (NOB) and heterotrophic denitrifiers. (Other abbreviations: AMO – ammonium monooxygenase; HAO - hydroxylamine oxidase, NXR - nitrite oxidoreductase; NAR – nitrate reductase, NirK/NirS nitrite reductases, cNor – cytochrome nitric oxide reductase, Nos - nitrous oxide reductase; n. id. – not identified)

The effect of dissolved oxygen (DO) concentration, nitrogen load or nitrite (NO_2-N) accumulation on N_2O production has widely been recognized and described (e.g. Peng et al. 2014, 2015). However, mentioned investigations do not clarify which biochemical mechanism i.e. autotrophic nitrification, heterotrophic or autotrophic denitrification is the main contributor to N_2O production under DO-limited conditions.

The aim of this study was to identify the dominant pathways involved in the nitrogen removal processes at different DO concentrations. The analysis was performed based on the activity control of selected functional genes and N_2O production measurements. In particular, a relationship between the gene activity and N_2O production was investigated in the presence of NO_2-N.

2   Materials and the Methods

Experimental Set-up and Measurements of N_2O Production
A series of laboratory experiments were carried out in a batch reactor with a working volume of 10 dm^3. The reactor was equipped with the systems for continuous monitoring and control of pH, temperature and DO concentration. On-line measurements of N_2O were conducted using a clark-type N_2O-R microsensor (Unisense, Aarhus, Denmark).

Activated sludge used in the experiments originated from the local large biological nutrient removal (BNR) facility (440,000 PE) located in the city of Gdynia. The concentration of the biomass ranged from 2.5 to 3.0 g_{MLVSS}/m^3. The duplicate nitrification tests were run at different DO set points: 0.4; 0.7 and 1.0 g O_2/m^3. In the first scenario, ammonium constituted sole nitrogen source, whereas ammonium and nitrite were added to the reactor at the ratio 1:1 in the second scenario. At the beginning of the tests with the ammonium only, its concentration was increased to approximately 25 g N/m^3. After finishing the test with ammonium, the sludge was kept in the reactor

overnight at the same DO level. On the next day, a new test was run with the addition of a mixture of ammonium and nitrite. The total inorganic nitrogen concentration in the feed solution was ensured at approximately 25.0 g N/m^3. During each experiment, the process temperature set point was kept at 20° C, pH remained in the range of 7.5 to 8.0, and the mixing intensity was set to approximately 80 rev/min. The adequate amount of alkalinity was ensured by addition of 2 mol NaHCO$_3$ per each gram of nitrogen. In order to control the process performance, mixed liquor samples were withdrawn from the batch reactor with a set frequency, and then filtered under vacuum pressure on the Whatman GF/C. Concentrations of NH$_4$-N, NO$_3$-N, NO$_2$-N were determined using Xion 500 spectrophotometer (Dr Lange GmbH, Germany). The total nitrogen concentration was determined in Total Nitrogen Measuring Unit TNM-1 (Shimadzu, Japan). Mixed liquor suspended solids (MLSS) and mixed liquor volatile suspended solids (MLVSS) in the reactor were determined by the gravimetric method according to the Polish Standards (PN-72/C-04559).

Microbiological Analyses

In order to assess the distribution of nitrifying/denitrifying genes in the total microbial population, mixed liquor samples were collected at the beginning of each test, whereas samples for the gene activity monitoring were collected in parallel to the samples for chemical measurements. The gene activity was estimated by real-time polymerase chain reaction (PCR) based on the mRNA transcripts levels measure. Activities of the following genes were analysed: gene *hao* which encodes hydroxylamine oxidase to control the activity of the conventional nitrification pathway; *nirS* and *nirK* genes encoding the alternative forms of nitrite reductase which may participate in autotrophic denitrification as well heterotrophic denitrification.

The real-time PCR with specific primer sets were applied for both DNA and RNA analyses (Table 1).

Table 1. List of the analyzed genes with specific primer sets used for the real-time PCR

Gene name	Encoded product	Primer name
nirS	cd-cytochrome Nitrite Reductase (cdNIR)	nirS 1f/nirS 3r
nirK	Copper Nitrite Reductases (CuNIR)	nirK876/nirK1040
hao	Hydroxylamine Oxidase (HAO)	Haof1/Hzocl1F1R
16S rRNA	16S rRNA	1055F/1392R

Evaluation of the activity of each gene was performed by the relative quantification method (formula $2^{\Delta Ct}$) with respect to the level of the 16S rRNA, which is continuously synthesized in bacterial cells.

3   Results and Discussion

Effect of Oxygenation on AUR and N₂O Production Rate

The ammonium utilization rate (AUR) reached the highest value (= 1.76 mg N-NH$_4$/g$_{MLVSS}$.h) during the batch experiment at the DO concentration = 1.0 g O$_2$/m^3 and ammonium as sole nitrogen source. Along with the decrease of DO during the subsequent experiments, lower AURs were observed, i.e. 1.56 and 1.30 mg N-NH$_4$/g$_{MLVSS}$.h, respectively, for the DO concentration of 0.7 and 0.4 g O$_2$/m^3. In the case of the test with nitrite at the DO concentration = 1.0 g O$_2$/m^3, the AUR was comparable to the corresponding experiment with only ammonium. However, nitrite was implicitly an important factor inhibiting the first stage of the nitrification at the lower DO concentrations. The opposite trends, compared to the AURs in the experiments with only ammonium, were observed for N$_2$O production, which increased with the decrease of aeration intensity. The maximum N$_2$O concentration (0.06 g N-N$_2$O/dm^3), observed at the DO concentration = 0.4 g O$_2$/m^3, was almost two times higher compared to the experiment carried out at the DO concentration = 1.0 g O$_2$/m^3. In contrary, different patterns were obtained when a mixture of ammonium and nitrite$^-$ was added. What is crucial values of the indicators that characterize N$_2$O emission were at least 6 time higher contrary to tests with only ammonium. Another important aspect related to NO$_2^-$ presence during nitrification is that it stimulates N$_2$O production regardless of the DO concentration. N$_2$O emissions parameters were comparable for all applied aeration variants when nitrite was dosed. The obtained results are summarized in Table 2.

Table 2. Summary of N$_2$O production measurements at different DO concentrations

Nitrogen source	Indicator	DO (g O$_2$/m^3)		
		0.4	0.7	1.0
Only ammonium (NH$_4$-N)	Max. N$_2$O concentration [mg N/dm^3]	0.06	0.051	0.034
	N$_2$O production rate compared to initial NH$_4$-N concentration [%]	1.74	1.46	0.96
	N$_2$O production rate [mg N/(g$_{MLVSS}$.h)]	0.017	0.015	0.011
	Ammonium utilization rate [mg N/(g$_{MLVSS}$.h)]	1.30	1.56	1.76
Ammonium + nitrite (NH$_4$-N i NO$_2$-N)	Max. N$_2$O concentration [g N-N$_2$O/dm^3]	0.35	0.35	0.37
	N$_2$O-N production rate compare to initial NH$_4$-N and NO$_2$-N concentrations [%]	4.0	4.3	3.9
	N-N$_2$O production rate [mg N-N$_2$O)/(g$_{MLVSS}$.h)]	0.23	0.20	0.19
	Ammonium utilization rate [(mg N-NH$_4$)/(g$_{MLVSS}$.h)]	0.60	1.01	1.75

Observed N$_2$O production was inversely correlated with the AURs, whereas the DO decrease and NO$_2$-N presence stimulated N$_2$O production. A potential explanation of the observed patterns may be related to HNO$_2$ formation, which takes place at high NO$_2$-N concentrations along with decreasing pH and inhibits AOB. N$_2$O emission induction, with which NO$_2$-N presence accompanies, may be a consequence of detoxification reactions launched in bacterial cells. It has been reported (e.g. Kozlowski et al. 2014) that denitrifying genes, such as *nirK*, may participate in autotrophic denitrification. Applied condition may also triggering conventional denitrification pathway which is basically controlled by *nirS* gene. In order to verify which pathway promote N$_2$O production, the activities of particular genes were investigated.

Gene distribution analysis results revealed that *nirS* and *nirK* genes were present in the microbial community at a similar level, i.e. approximately 0.14–0.15 gene copy per single copy of 16S rDNA. This finding is in contradiction to the data reported by Pang et al. (2016) who noted that *nirS* gene would usually be present more frequently in comparison with *nirK*. This explicitly confirms that the gene distribution is specific for a particular wastewater treatment system. In the case of *hao* gene, its distribution was lower at several orders of magnitude ($\sim$0,004 per 1 copy of 16S rDNA). This means that the metabolic potential of the denitrification pathway was significantly higher in comparison with the nitrification pathway. This finding may be related to the fact that the denitrifying genes are widely distributed among heterotrophs, which constitute the major component of the microbial community. It should also be emphasized that nitrifiers may also possess some of the denitrifying genes which also increase their contribution in the overall gene pool.

Figure 2 shows a sample behaviour of the nitrogen compounds (including N$_2$O), pH, and gene activities during the experiment with a mixture of ammonium and nitrite at the DO concentration = 1.0 g O$_2$/m^3.
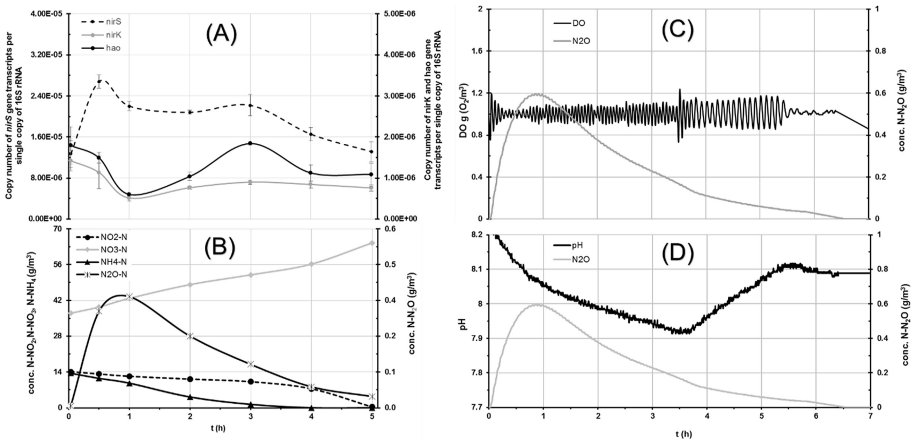

Fig. 2. Gene activity (A); nitrogen forms concentration (B); DO (C); pH and N$_2$O production changes (D) during the nitrification experiment with ammonium and nitrite addition at DO = 1.0 g O$_2$/m^3

Before ammonium consumption was completed, a stepwise pH decrease was observed, whereas the pH tended to rise from the moment when only nitrite was present in the reactor. The N_2O production began immediately after the addition of nitrogen compounds and reached the maximum value after approximately one hour later. From that moment, N_2O production was continuously decreasing along with the depletion of the substrates (ammonia and nitrite). Shifts over pH and concentrations of particular nitrogen compounds confirm that N_2O production under the DO-limited conditions depends on the cumulative activity of different biochemical pathways and substrate concentrations. The activity levels of *nirK* and *hao* genes were significantly lower compared to *nirS* gene. However initial gene copy number should be taken into account. While the initial gen copy number of *hao* was lower over few orders of magnitude compared to *nirK* the number of RNA transcripts produced by those genes were comparable. This observation supports the hypothesis with regard to the nitrifying bacteria, that hydroxylamine oxidation, rather than autotrophic denitrification, is the main contributor to N_2O production under the DO-limited conditions.

4 Conclusions

The significant *nirS* gene induction, observed especially during the experiments with the nitrite addition, confirmed that limited aeration would induce heterotrophic denitrification simultaneously to nitrification. The obtained results revealed that the gene activity control may be a useful tool for recognizing the different biochemical pathways of N_2O production and developing strategies for N_2O control in bioreactors.

References

Peng L, Ni B-J, Ye L, Yuan Z (2015) The combined effect of dissolved oxygen and nitrite on N_2O production by ammonia oxidizing bacteria in an enriched nitrifying sludge. Water Res 73:29–36

Kozlowski JA, Price J, Stein LY (2014) Revision of N_2O-producing pathways in the ammonia-oxidizing bacterium, *Nitrosomonas europaea* ATCC 19718. Appl Environ Microbiol 80:4930–4935

Pang J, Matsuda M, Kuroda M, Inoue D, Sei K, Nishida K, Ike M (2016) Characterization of the genes involved in nitrogen cycling in wastewater treatment plants using DNA microarray and most probable number-PCR. Front Environ Sci Eng 10(4):07

Peng L, Ni BJ, Erler D, Ye L, Yuan Z (2014) N_2O production by ammonia oxidizing bacteria in an enriched nitrifying sludge linearly depends on inorganic carbon concentration. Water Res. 66:12–21 https://www.ncbi.nlm.nih.gov/pubmed/25706224

Greenhouse Gases from Wastewater Treatment Plants

A Graphical User Interface as a DSS Tool for GHG Emission Estimation from Water Resource Recovery Facilities

L. Frunzo[1(✉)], G. Esposito[2], R. Gori[3], D. Caniani[4], M. Caivano[4,5], A. Cosenza[6], and G. Mannina[6]

[1] Department of Mathematics and Applications "R. Caccioppoli",
University of Naples "Federico II",
Via Cintia 1 Complesso Montesantangelo, 80126 Napoli, Italia
`luigi.frunzo@unina.it`
[2] Department of Civil and Mechanical Engineering,
University of Cassino and Southern Lazio,
Via Di Biasio 43, 03043 Cassino (FR), Italy
[3] Department of Civil and Environmental Engineering (DICEA),
University of Florence, Via Santa Marta 3, 50139 Firenze, Italia
`riccardo.gori@dicea.unifi.it`
[4] School of Engineering, University of Basilicata,
Viale dell'ateneo Lucano 10, 85100 Potenza, Italy
[5] Department of Civil and Environmental Engineering,
University of California, Irvine, CA 92697-2175, USA
[6] Department of Civil, Environmental, Aerospace, Materials Engineering,
University of Palermo, Viale delle Scienze, 90128 Palermo, Italy

Abstract. A Grafical User Interface (GUI) for the greenhouse gas (GHG) emissions from WWTPs based on four models aimed at quantifying the gas emissions from the aerated tanks (i.e. CAS and MBR reactor), aerobic digesters, secondary clarifiers and anaerobic digesters have been englobed in a GUI in order to provide a valid decision support system (DSS) to the practitioners. The GUI allows to estimate such emissions for the different WWTP phases considered. The GUI has been developed on MATLAB platform and provides as output the GHG emissions in terms of CO_2 and N_2O fluxes.

Keywords: Graphical user interface · DSS · Greenhouse gas · Urban wastewater treatment plant

1 Introduction

For most of engineering applications, mathematical models can represent valuable support tools as they provide useful information for the decisional process without the time, cost and risk of an experimental activity. For instance, in the environmental applications, mathematical models can be used to estimate (GHG) emissions from the different sections of a wastewater treatment plant (WWTP) (Flores-Alsina et al. 2011; Corominas et al. 2012). However, in most of the cases mathematical models come in complex form and thus are not accessible to practical users. In this work, four models aimed at quantifying
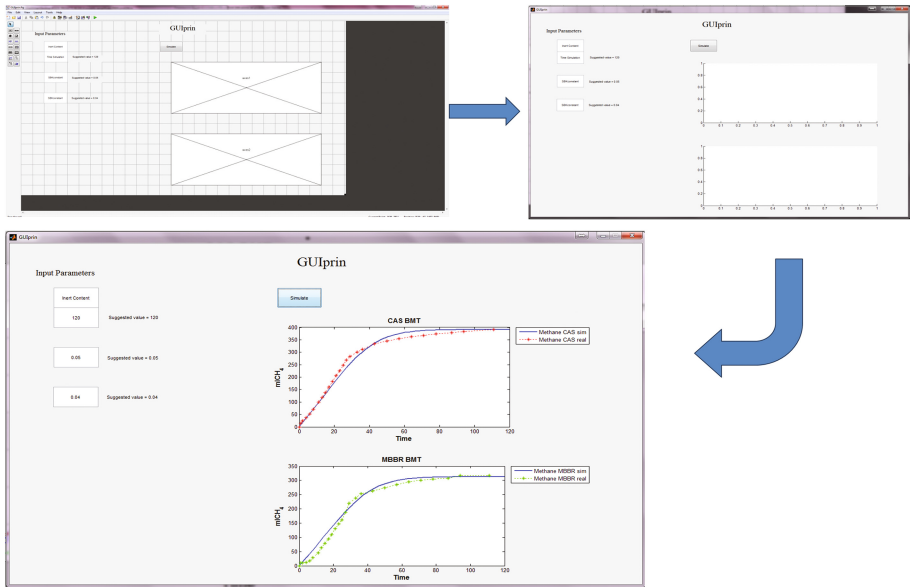
Fig. 1. Procedure for GUI development

the gas emissions from the aerated tanks (i.e. CAS and MBR reactor), aerobic digesters, secondary clarifiers and anaerobic digesters are englobed in a GUI in order to provide a valid decision support system (DSS) to the practitioners (Fig. 1).

2 Mathematical Models Implemented in the GUI

2.1 *Aerated Tanks*

Estimation of indirect internal GHG emissions

The contribution of aeration systems in the indirect internal emission of CO_2 per day ($kgCO_{2,eq}/d$) for an urban wastewater treatment plants (WWTPs) can be evaluated from (Redmon et al. 1983):

$$\left[\frac{kgCO_{2,eq}}{d}\right] = k \int P_w dt \tag{1}$$

where:

P_w is the P_w is the blower break horsepower (kW),

In cases of a WWTP where the power demand, energy consumption and air flow-rate of aeration systems are not monitored (very frequent situation on the Italian territory), the off-gas method was observed to be a valid tool for estimating indirect internal emissions. The total air flow (Q_{tot}) blown through the tank surface, given by the weighted average of the different measurements over tank surface, allows to derive the actual power (P_w) used by blowers with the adiabatic compression formula (Eq. 2).

$$P_w(kW) = \frac{Q_{tot} \cdot P_1}{17.4 \cdot e_M \cdot e_B} \cdot \left[\left(\frac{P_2}{P_1} \right)^{0.283} - 1 \right] \tag{2}$$

where:

Q_{tot} is the total air flow rate (m^3/min),
e_M is the motor efficiency (dimensionless),
e_B is the blower efficiency (dimensionless),
P_1 and P_2 are the inlet and outlet absolute pressure (kPa), respectively

Specifications of the blower P_2 can be derived from the relative characteristic curve (P1 is always ~ 0.95 of the atmospheric pressure due to the inlet suction).

Estimation of direct emissions due to bacterial respiration

In the calculation of the CO_2 direct emission due to microbial respiration in ASP, it is important to highlight the carbon emission intensity of COD (i.e. the amount of CO2 emitted per unit of COD oxidised, or kCOD). If wastewater organic compounds could be represented through the formula $C_{10}H_{19}O_3N$ (widely used for the case of domestic wastewater) we obtain that $k_{COD} = 0.99$ kg_{CO2eq}/kg_{COD}. Analogously, in case of activated sludge biomass, we obtain that kBIOMASS = 1.03 kg_{CO2eq}/kg_{COD}.

Estimation of N_2O emissions with MBR technology

N_2O flux due to the MBR ($N_2O,_{MBR}$) [$mgN_2O-Nm^2h^{-1}$] has been quantified on the basis of the membrane Fouling Rate (FR) according to (Mannina et al. 2015):

$$N_2O,_{MBR} = 0.02FR^{\wedge}1.93 \tag{3}$$

2.2   Aerobic digesters (AeD) and secondary clarifiers

The relationships for both N_2O and CO_2 produced and emitted in aerobic digesters (AeD) and secondary clarifiers in WWTPs and the available measured data of wastewater and sludge characteristics has been determinated through multiregression analysis. Two different types of correlation analysis have been carried out, i.e. a simple linear regression analysis and a complex regression analysis. The simple regression method consists of testing the simple linear equation to find a relationship between the dependent variable (Y) and the independent variable (X), as in Eq. 1:

$$Y = c_1 \cdot X + c_2 \tag{4}$$

where c_1 and c_2 are the regression coefficients. The coefficient of determination (R^2) has been also evaluated to provide a measure of how well observed outcomes are fitted by the empirical model.

Estimation of emission from aerobic digesters (AeD)

Regarding the aerobic digestion, the simple regression method has been performed by considering, as dependent variables (Y): N_2O and CO_2 (ppm) emissions from the pilot digester. The independent variables (X) taken into account are summarized in Table 1.

Table 1. Independent variables taken into account during the simple regression analysis on AeD data

Symbol	Definition	Unit
NH_{4in}	Influent concentration of ammonia	mg/l
NO_{3in}	Influent concentration of nitrate	mg/l
COD_{in}	Influent concentration of COD	mg/l
$NH_{4in,AeD}$	Ammonia concentration in AeD influent	mg/l
$NO_{3in,AeD}$	Nitrate concentration in AeD influent	mg/l
$COD_{in,AeD}$	COD concentration in AeD influent	mg/l
$NH_{4out,AeD}$	Ammonia concentration in AeD effluent	mg/l
$NO_{3out,AeD}$	Nitrate concentration in AeD effluent	mg/l
$COD_{out,AeD}$	COD concentration in AeD effluent	mg/l
DO	Dissolved oxygen in AeD	mg/l

The regression analysis has been carried out by considering the data recorded during experimental campaigns on the pilot digester developed by the Research Group of the Engineering School at the University of Basilicata, using the secondary settler underflow of a full-scale WWTP as digester feeding (Caniani et al. 2015; Caivano et al. 2017a).

Estimation of emission from secondary clarifiers
Regarding the secondary clarifier, the simple regression method has been performed by considering the following dependent variables (Y): N_2O and CO_2 (ppm) emissions from settler tank ($N_2O_{(g)}$ and $CO_{2(g)}$), and N_2O and CO_2 (mg/l) dissolved in the liquid effluent of the settler ($N_2O_{(l)}$ and $CO_{2(l)}$). The independent variables (X) summarized in Table 2 have been taken into account.

Table 2. Independent variables taken into account during the simple regression analysis on clarifier data

Symbol	Definition	Unit
$NH_{4in,se}$	Ammonia concentration in clarifier influent	mg/l
$NO_{3in,se}$	Nitrate concentration in clarifier influent	mg/l
$NO_{2in,se}$	Nitrite concentration in clarifier influent	mg/l
TSS	Total suspended solid in the clarifier	mg/l
NH_2OH	Hydroxylamine concentration in clarifier influent	mg/l
Wind speed	Simulated wind speed on the tank liquid surface	m/s

The regression analysis has been carried out by considering the data recorded during experimental campaigns on the pilot clarifier developed by the Research Group of the Engineering School at the University of Basilicata, using the secondary settler underflow of a full-scale WWTP as pilot tank feeding, as well as the data recorded on the full scale-settler itself (Caivano et al. 2017b).

2.3   Anaerobic digesters

Estimation of emission from Anaerobic digester

Emission from Anaerobic digestion has been evaluated through a mathematical model based on differential mass balance equations for the substrates and the products of the process. A single substrate has been taken into account (Organic matter, considered as COD), the overall velocity of the whole anaerobic digestion process has been hypothesized to be equal to hydrolysis velocity of the complex macromolecules. In particular, a modified version of surfaced based kinetic (SBK) approach has been used.

The mathematical model is constituted by the following system of ordinary differential equation:

$$\frac{dS}{dt} = -K_{sbk}a^* \frac{S}{K_s + S} \tag{5}$$

$$\frac{dP}{dt} = \sigma K_{sbk}a^* \frac{S}{K_s + S} \tag{6}$$

$$\frac{dX}{dt} = \sigma K_{sbk}a^* \frac{S}{K_s + S} \tag{7}$$

where:

S is the complex organic substrate mass [M];
P is the products [L^3];
X is the microbial biomass [M];
K_{sbk} = disintegration kinetic constant [M L^{-2} T^{-1}];
K = like half saturation constant [M]
N = order of the reaction
σ = stoichiometric coefficient
a^* = mass-specific disintegration surface area [L^2];

Assuming that all organic solid particles have the same spherical shape and initial size and they are progressively and uniformly degraded in all directions from the outside towards the inside, the a* can be determined as follows:

$$a^* = \frac{3}{\mu R} \tag{8}$$

where:

μ is the density, while R is the organic solid particles radius, assumed time dependent in according with the following expression

$$R = R_0 - K_{sbk}\frac{t}{\mu} \tag{9}$$

The final CO_2 emission has been evaluated considering the complete combustion of the CH_4 produced and adding the CO_2 produced during the anaerobic digestion process.

2.4   Graphic user interface (GUI)

A GUI for the GHG emissions from WWTPs based on the models proposed in the previous sections has been developed. The GUI allows to estimate such emissions for the different WWTP phases considered. The input parameters to the GUI are represented by independent variables characterising the single models and default input values of input parameters are set. The GUI has been developed on MATLAB platform and provides as output the GHG emissions in terms of CO_2 and N_2O fluxes.

3   Conclusions

A GUI for the evaluation of GHGs emissions from WWTP has been developed. For each phase of the WWTP a suitable mathematical model, has been selected and implemented in MATLAB platform. The GUI is able to provide the GHG emissions (dependent variables) by varying the input operational parameters (independent variables).

References

Caniani D, Esposito G, Gori R, Mannina G (2015) Towards a new decision support system for design, 7 management and operation of wastewater treatment plants for the reduction of greenhouse gases emission. Water (Basel) 7:5599–5616

Caivano M, Masi S, Mancini IM, Caniani D (2017a) Quantification of CO2 and N2O emissions from a pilot-scale aerobic digester, towards the validation and calibration of the first Activated Sludge Model for aerobic digestion (AeDM1). Submitted to FICWTM

Caivano M, Pascale R, Buchicchio A, Mazzone G, Masi S, Mancini IM, Caniani D (2017b) N_2O and CO_2 emissions from secondary settlers in WWTPs: experimental results on full- and pilot scale plants. Submitted to FICWTM

Corominas L, Flores-Alsina X, Snip L, Vanrolleghem PA (2012) Comparison of different modeling approaches to better evaluate greenhouse gas emissions from whole wastewater treatment plants. Biotechnol Bioeng 109(11):2854–2863

Flores-Alsina X, Corominas L, Snip L, Vanrolleghem PA (2011) Including greenhouse gas emissions during benchmarking of wastewater treatment plant control strategies. Water Res. 45(16):4700–4710

Mannina G, Cosenza A (2015) Quantifying sensitivity and uncertainty analysis of a new mathematical model for the evaluation of greenhouse gas emissions from membrane bioreactors. J Membr Sci 475:80–90

Redmon DT, Boyle WC, Ewing L (1983) Oxygen transfer efficiency measurements in mixed liquor using off-gas techniques. Water Pollut Control Fed 55:1338–1347

A Novel Comprehensive Procedure for Estimating Greenhouse Gas Emissions from Water Resource Recovery Facilities

R. Gori[1]([✉]), G. Bellandi[1], C. Caretti[1], S. Dugheri[2], A. Cosenza[3],
V.A. Laudicina[4], G. Esposito[5], L. Pontoni[5], D. Caniani[6],
M. Caivano[6,7], D. Rosso[7,8], and G. Mannina[3]

[1] Department of Civil and Environmental Engineering (DICEA),
University of Florence, Via Santa Marta 3, 50139 Firenze, Italia
`riccardo.gori@dicea.unifi.it`
[2] Occupational Health Division, Careggi Hospital,
Largo P. Palagi 1, 50139 Firenze, Italia
[3] Department of Civil, Environmental, Aerospace, Materials Engineering,
University of Palermo, Viale delle Scienze, 90128 Palermo, Italy
[4] Department of Agricultural and Forest Sciences, University of Palermo,
Viale Delle Scienze Edificio 4, 90128 Palermo, Italy
[5] Department of Civil and Mechanical Engineering,
University of Cassino and Southern Lazio,
Via Di Biasio 43, 03043 Cassino (FR), Italy
[6] School of Engineering, University of Basilicata,
Viale Dell'Ateneo Lucano 10, 85100 Potenza, Italy
[7] Department of Civil and Environmental Engineering,
University of California, Irvine, CA 92697-2175, USA
[8] Water-Energy Nexus Center, University of California,
Irvine, CA 92697-2175, USA

Abstract. The emissions of the major greenhouse gases (GHGs), i.e. carbon dioxide (CO_2), methane (CH_4), and nitrous oxide (N_2O) from water resource recovery facilities (WRRFs) are of increasing concern in the water industry. In order to produce useful and comparable information for monitoring, assessing, and reporting GHG emissions from WRRFs, there is a need for a generally accepted methodology for their quantification. This paper aims at proposing the first protocol for monitoring and accounting for GHG emissions from WRRFs, taking into account both direct and indirect internal emissions and focusing the attention on plant sections known to be primarily responsible for GHG emissions (i.e. oxidation tanks and sludge digestors). The main novelties of the proposed protocol are: (i) measurement of direct internal emissions ascribed to aeration devices; (ii) estimation of indirect internal emissions derived from field measurement; (iii) GHG emission offset due to biogas energy recovery quantified by monitoring biogas composition in case of anaerobic digestion. Finally, the proposed methodology enables and allows the gathering of useful information on plants (e.g. energetic efficiency of the aeration device system and composition of biogas produced in anaerobic digestion) to address potential strategies for improving the plants' performance.

1   Introduction

The emissions of the major greenhouse gases (GHGs), i.e. carbon dioxide(CO_2), methane (CH_4), and nitrous oxide (N_2O) from water resource recovery facilities (WRRFs) are of increasing concern in the water industry (Caivano et al. 2016; Caniani et al. 2016; Kampschreur et al. 2008). In order to produce useful and comparable information for monitoring, assessing, and reporting GHG emissions from WRRFs, there is a need for a generally accepted methodology for their quantification.

CO_2 is directly produced in aerobic biological processes by the oxidation of organic compounds accompanied by cell growth. CO_2 derived from wastewater treatment is assumed to originate from short-lived biogenic material (IPCC 2006), however, fossil organic carbon was found in the incoming wastewater of WRRFs and related to direct fossil CO_2 emissions from oxidation by activated sludge (AS), depending in the extent, on wastewater composition and treatment configuration (Law et al. 2013). N_2O is currently the single most important ozone-depleting gas (Ravishankara 2009). N_2O emissions occurring in aerated zones are lined to nitrogen load, volumetric stripping, and the role of ammonia-oxidizing bacteria (Daelman et al. 2015; Guo et al. 2013). Stenström et al. (2014) have found that N_2O formed in liquid phase during denitrification accumulates mainly in the water volume until aeration starts and thereafter it is quickly stripped off to the atmosphere. Similarly, this can happen for CH_4. Although methanogenic activity in AS tanks is deemed to be insignificant (Gray et al. 2002), dissolved CH_4 can enter aerobic AS reactors, where is stripped or biologically oxidized (Daelman et al. 2012), from sewers (Guisasola et al. 2008) or sections of the WWTPs where anaerobic conditions occur, e.g. in anaerobic selectors (Techobanoglous et al. 2014; Wentzel et al. 2008). Therefore, beside the actual GHG production occurring in aeration tanks, stripping induced by aeration is one of the main causes making this compartment one of the major contributors to WRRF direct emissions.

This paper aims at proposing the first protocol for monitoring and accounting for GHG emissions from WRRFs, taking into account both *direct* and *indirect internal* emissions and focusing the attention on plant sections known to be primarily responsible for GHG emissions (i.e. oxidation tanks and sludge digestors). The main novelties of the proposed protocol are: (i) measurement of *direct internal* emissions ascribed to aeration devices; (ii) estimation of *indirect internal* emissions derived from field measurement; (iii) GHG emission offset due to biogas energy recovery quantified by monitoring biogas composition in case of anaerobic digestion.

Finally, the proposed methodology enables and allows the gathering of useful information on plants (e.g. energetic efficiency of the aeration device system and composition of biogas produced in anaerobic digestion) to address potential strategies for improving the plants' performance.

2 Estimation of Indirect Emission from Aerated Tanks

The off-gas technique (Redmon et al. 1983) is proposed as a method for estimating indirect GHG emissions from aerated tanks (oxidation tanks and aerobic stabilization tanks) from plants using diffused air aeration systems. The layout of the proposed device is represented in Fig. 1.
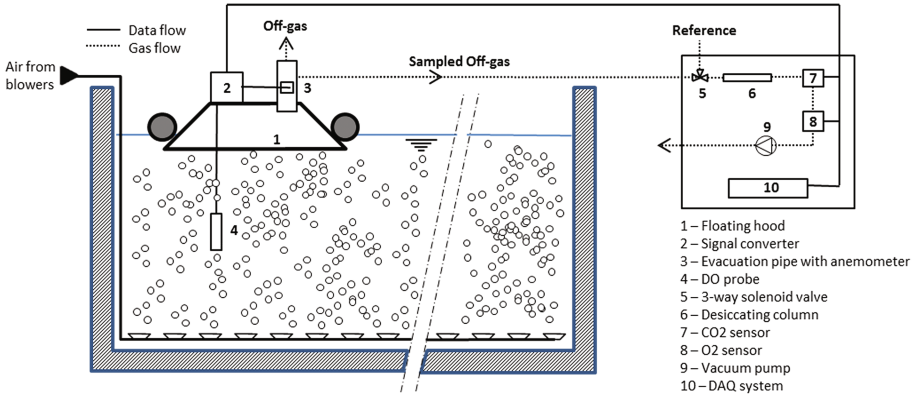

Fig. 1. Schematic layout of the off-gas analyzer for measuring OTE in aerated tanks

The methodology also has the potential for:

- monitoring the trend of fouling and scaling of diffusers which can affect their operation and efficiency and, therefore, energy consumption and indirect GHG emissions;
- investigating the relationship between air flow-rate and OTE.

A floating hood captures the off-gas leaving the tank surface and the flow rate is measured by a hot wire anemometer. The system is also equipped with a probe for measuring DO in the liquid phase, required for correcting the OTE to standard conditions (i.e. αSOTE). The captured stream is sent to an off-gas analyzer for analysis of O_2 and CO_2.

In cases of aeration systems that use blowers, it is possible to derive the actual power (P_w) used by blowers with the adiabatic compression formula (Eq. 1).

$$P_w(kW) = \frac{Q_{tot} \cdot P_1}{17.4 \cdot e_M \cdot e_B} \cdot \left[\left(\frac{P_2}{P_1} \right)^{0.283} - 1 \right] \tag{1}$$

Q_{tot} is the total air flow rate (m^3/min), e_M is the motor efficiency (dimensionless), e_B is the blower efficiency (dimensionless), P_1 and P_2 are the inlet and outlet absolute pressure (kPa), respectively. Specifications of the blower P_2 can be derived from the relative characteristic curve (P_1 is always ~ 0.95 of the atmospheric pressure due to the inlet suction). Energy consumption is calculated by integrating P_w over time (Eq. 2),

and can thus be used to calculate and account for the blowers contribution to indirect internal emissions:

$$Internal\ indirect\ GHG\ emission\ (IIE) \left[\frac{kgCO_{2,eq}}{d}\right] = \int k \cdot P_w dt \qquad (2)$$

In the case of static power generation portfolios, or due to unavailability of data, the carbon emission intensity for power generation (k, kgCO2, eq/kWh) can be taken out of the integral and which converts to the cumulative energy consumption. The measured air flow can be normalized for the area covered by the hood and extended in the proximity of each measurement point so that the whole tank surface is virtually covered.

3   Estimation of Direct Emission from Aerated Tanks

The estimation of direct emission from aerated tanks (i.e. AS and aerobic digesters) requires the monitoring of both off-gas flow rate and GHG concentration in the off-gas of aerated tanks. Because operating conditions (e.g. DO, COD/N ratio, ammonium concentration) are variable both in time and space, direct emission of GHGs are expected to be variable as well. For this reason, unless aerated tanks are covered, the procedure suggests a simultaneous multi-point monitoring of aerated tanks using floating hoods. The procedure proposed here suggests to carry out from 2 to 4 campaigns per year in order to cover the entire possible temperature range and appreciate seasonal variations of phenomena affecting the GHG emissions. In order to appreciate the diurnal variations within a single campaign, online and high-frequency devices should be adopted. Measurements should be done every 10–20 min by monitoring GHG concentration in the off-gas for a minimum of 24 h up to one week. In the case of multiple day monitoring, it is preferable to also include weekend samples, which significantly contribute to increase the GHG emissions estimation accuracy (Daelman et al. 2015).

The procedure suggests the use of the IR analyzer due to its measurement accuracy and the ease of operation. The instrument should compensate for temperature fluctuations and water vapor interference, and other gases known to potentially bias the measurements. An alternative to IR for online monitoring of CO_2, N_2O, and CH_4 is the micro-Gas Chromatograph (GC) equipped with two columns, divided in two parallel channels, using He as carrier gas. Channel 1, equipped with a PoraPlotQ (PPQ) and Channel 2, with a divinylbenzene-ethyleneglycol-dimethacrylate polymer column. The analytical performance is ensured by the chromatographic technology allowing for components' separation and, therefore, for very accurate measurements. Although it is not yet as popular as IR based tools, this instrument is characterized by a compact design that makes it as portable as other online monitoring equipment.

4   Estimation of GHG's Direct Emission from Biogas Combustion

One of the main concerns in anaerobic digestion (AD) is acidification of the medium which can also lead to, amongst other problems, an increase in H_2 production in the biogas due the inhibition of the hydrogenotrophic methanogenesis. With regards to GHG emissions, the presence of H_2 in the biogas is known to be responsible for a higher NOx production in the exhaust fumes from the process of biogas conversion to energy. It is strongly suggested to monitor H_2 levels in the biogas, not only to control the state of the anaerobic reactors, but also to prevent potential GHG emissions.

In order to estimate direct GHG emissions due to biogas combustion, the procedure suggests to measure:

– BMP of the sludge;
– percent composition of the biogas to optimize the power production with particular reference to the CH_4/CO_2 ratio;
– percentage of H_2 in the biogas.

Table 1. Summary of existing protocols for GHG emissions from WRRFs derived from literature

Reference	Type of sample	Gas flux measurement	Use Emission Factor	Quantified GHG	Remarks
Monteith et al. 2005	–	No	No	CO_2, CH_4	Carbon mass balance and energy balance of sections for liquid and solids treatment.
IPCC 2006	–	No	Yes	N_2O, CH_4	GHG emissions estimate based on EFs associated with specific populations and type of WRRFs.
USEPA 2007	–	No	Yes	N_2O, CH_4	Based on the procedure proposed by IPCC (2006).
CEC 2006	–	No	Yes	N_2O, CH_4	Simplified version of the IPCC protocol (IPCC 2006).
GWRC 2011	Gas and liquid	Yes	No	N_2O, CH_4	Based on full-scale data to establish new emission factors than the IPCC ones.
Chandran 2011	Gas and liquid	Yes	No	N_2O	Combines real-time measurement of gas with discrete measurements of liquid.

Monitoring of the biogas composition also allows the calculation of a reliable CO_2, $_{eq}$ offset due to energy recovery from biogas which is proportional to the biogas produced and biogas composition. The combustion gas can be analyzed in order to assess the real CH4 oxidation efficiency during combustion Table 1.

5   Total GHG Emission and CFP

To determine the total CFP, all sources must be converted to $CO_{2,eq}$ multiplying emission of N_2O and CH_4 times their respective GWP (i.e. 298 end 25 respectively, IPCC 2006). For space reason, details will be provided in the full paper.

6   Conclusions

The protocol presented in this paper contains a selection of available measurements methods for GHG detection and CFP assessment for different applications. This selection was based on field measurements and laboratory tests to validate the capabilities of each analytical and theoretical technique. The main novelties of the proposed protocol are: (i) measurement of direct internal emissions ascribed to aeration devices, generally reported as the most important contributors to WRRF CFP; (ii) estimation of indirect internal emissions derived from field measurement, which are not always easy to assess as it depends on the grade at which the plant is monitored and online data are logged; (iii) monitoring the biogas composition for considering a GHG emission offset due to energy recovery in case of the presence of an anaerobic digester, as an alternative method for a double purpose (i.e. biogas quality monitoring and GHG emission limitation).

GHG emissions from aerated AS tanks are the major contributors to direct emissions of a WRRF. Literature studies highlight the potential of this compartment in emitting GHG generated already in the sewer or in other plant compartments (e.g. primary settlers, pre-denitrification tanks). In this view, this paper focuses on direct GHG emissions at the aeration tank considering a valuable assumption for regular plant design. In those cases where the wastewater flow would be extensively agitated before entering the aeration tank a dedicated assessment of this particular section should be considered.

Existing measurement techniques and conversion methods were selected in order to define the best combination of solutions in the framework of quantifying the overall CFP of WRRFs.

References

Caivano M, Bellandi G, Mancini IM, Masi S, Brienza R, Panariello S, Gori R, Caniani D (2016) Monitoring the aeration efficiency and carbon footprint of a medium-sized WWTP: experimental results on oxidation tank and aerobic digester. Environ Technol, 1–10

Caniani D, Esposito G, Gori R, Caivano M, Masi S, Cosenza A, Abuissa A, Mannina G (2016) Towards a reduction of Greenhouse Gas emission from wastewater treatment plants: a new plant wide experimental and modelling approach. In: SIDISA 2016, X International Symposium on Sanitary and Environmental Engineering, Rome, 19–23 June 2016

CEC (2006) Inventory of California Greenhouse Gas Emissions and Sinks: 1990 to 2004. Sacramento, CA

Chandran K (2011) Protocol for the Measurement of Nitrous Oxide Fluxes from Biological Wastewater Treatment Plants. In: Methods in Enzymology. Elsevier Inc., pp. 369–385

Daelman MRJ, van Voorthuizen EM, van Dongen UGJM, Volcke EIP, van Loosdrecht MCM (2012) Methane emission during municipal wastewater treatment. Water Res 46:57–70

Daelman MRJ, van Voorthuizen EM, van Dongen UGJM, Volcke EIP, van Loosdrecht MCM (2015) Seasonal and diurnal variability of N2O emissions from a full-scale municipal wastewater treatment plant. Sci Total Environ 536:1–11

Gray ND, Miskin IP, Korniova O, Curtis TP, Head IM (2002) Occurrence and activity of Archaea in aerated activated sludge wastewater treatment plants. Environ Microbiol 4:158–168

Guisasola A, de Haas D, Keller J, Yuan Z (2008) Methane formation in sewer systems. Water Res 42:21–30

Guo L.S, Lamaire-chad C, Bellandi G, Daelman MRJ, Maere T, Nous J, Flameling T, Weijers S, Mark CM, Loosdrecht V, Volcke EIP, Nopens I, Vanrolleghem PA (2013) High frequency field measurements of Nitrous oxyde (N2O) Gas Emissions and Influencing Factors at WWTPs under Dry and Wet Weather Conditions. In: WEF/IWA Nutrient Removal and Recovery 2013

GWRC, 2011. N2O and CH4 emission from wastewater collection and treatment systems, London

IPCC (2006) Guidelines for National Greenhouse Gas Inventories. Prepared by the National Greenhouse Gas Inventories Programme, Kanagawa

Kampschreur MJ, van der Star WRL, Wielders HA, Mulder JW, Jetten MSM, van Loosdrecht MCM (2008) Dynamics of nitric oxide and nitrous oxide emission during full-scale reject water treatment. Water Res 42:812–826

Law Y, Jacobsen GE, Smith AM, Yuan Z, Lant P (2013) Fossil organic carbon in wastewater and its fate in treatment plants. Water Res 47:5270–5281

Monteith HD, Sahely HR, MacLean HL, Bagley DM (2005) A rational procedure for estimation of greenhouse-gas emissions from municipal wastewater treatment plants. Water Environ Res 77:390–403

Ravishankara AR (2009) Nitrous Oxyde (N2O): The Dominant Ozone-Depleting Substance Emitted in the 21st Century. Science 326(80):123–125

Redmon DT, Boyle WC, Ewing L (1983) Oxygen transfer efficiency measurements in mixed liquor using off-gas techniques. Water Pollut Control Fed 55:1338–1347

Stenström F, Tjus K, La Cour Jansen J (2014) Oxygen-induced dynamics of nitrous oxide in water and off-gas during the treatment of digester supernatant. Water Sci Technol 69:84–91

Techobanoglous G, Burton FL, Stensel HD (2014) Wastewater Engineering: Treatment and Reuse, 5th edn. Metcalf and Eddy, McGraw-Hill series in civil and environmental engineering. McGraw-Hill, New York

USEPA (2007) Inventory of U.S. Greenhouse Gas Emissions and Sinks: 1990–2005. US Environmental Protection Agency, Washington DC

Wentzel MC, Comeau Y, Ekama GA, van Loosdrecht MCM, Brdjanovic D (2008) Enhanced biological phosphorus removal, Biological waste water treatment. Principles, Model Des, 155–170. IWA Publ.

A New Plant Wide Modelling Approach for the Reduction of Greenhouse Gas Emission from Wastewater Treatment Plants

D. Caniani[1(✉)], A. Cosenza[2], G. Esposito[3], L. Frunzo[3], R. Gori[4],
G. Bellandi[4], M. Caivano[1], and G. Mannina[2]

[1] University of Basilicata, School of Engineering,
Viale dell'Ateneo Lucano N.10, Potenza, Italy
[2] University of Palermo, Department of Civil, Environmental,
Aerospace and Materials Engineering, Viale delle Scienze, 90128 Palermo, Italy
[3] University of Cassino and the Southern Lazio,
Department of Civil and Mechanical Engineering,
Via Di Biasio, 43, 03043 Cassino, FR, Italy
[4] University of Florence, Department of Civil and Environmental Engineering,
Via S. Marta 3, 50139 Florence, Italy

Abstract. Recent studies about greenhouse gas (GHG) emissions show that sewer collection systems and wastewater treatment plants (WWTPs) are anthropogenic GHG potential sources. Therefore, they contribute to the climate change and air pollution. This increasing interest towards climate change has led to the development of new tools for WWTP design and management. This paper presents the first results of a research project aiming at setting-up an innovative mathematical model platform for the design and management of WWTPs. More specifically, the study presents the project's strategy aimed at setting-up a plant-wide mathematical model which can be used as a tool for reducing/controlling GHG from WWTP. Such tool is derived from real data and mechanicistic detailed models (namely, Activated Sludge Model's family). These latter, although are a must in WWTP modelling, hamper a comprehensive and easy application due to complexity, computational time burdens and data demanding for a robust calibration/application. This study presents a summary of the results derived from detailed mechanistic models which have been applied to both water and sludge line of a WWTP: primary treatment, biological reactor, secondary settler, membrane bioreactor, sludge digester etc. The project is organized in overall four research units (RUs) which focus each on precise WWTP units.

Keywords: GHG emissions · Mathematical modelling · Wastewater treatment plants

1 Introduction

Wastewater treatment plants (WWTPs) are responsible for the emission of greenhouse gases (GHGs), such as nitrous oxide (N_2O), methane (CH_4), and carbon dioxide (CO_2). Efforts for monitoring and accounting for GHG emissions from WWTPs are of

increasing interest (Daelman et al. 2013; Caniani et al. 2015; Caivano et al. 2016; Mannina et al. 2016c).

The mathematical modelling of activated sludge (AS) treatment is the most important tool for developing control strategies and designing WWTPs. In 1982, the International Association on Water Pollution Research and Control (IAWPRC) established a Task Group on Mathematical Modelling for Design and Operation of Activated Sludge Processes. From 1982 at now, mathematical modelling has widely developed, evolved and combined with the control systems (Olsson 2012). However, there is still work to be done to link this knowledge acquired and integrate it at system-wide framework level.

Moreover, N_2O emission from WWTP represents a frontier of Research that still requires to be crossed. N_2O emissions primarily occur in aerated zones owing to the fact that the main contributors are active stripping and ammonia-oxidizing bacteria, rather than heterotrophic denitrifiers. Indeed, despite during the last years efforts have been done to better understand the key elements on the N_2O production/modelling, several questions remain scarcely understood (Caniani et al. 2015; Mannina et al. 2016c).

In this work, we present the key methodological features and some of the results of a research project aiming at developing an innovative simulation platform for the design and management of WWTPs. Such a platform is aimed at reducing the energy consumption and pollutant/residue emissions (namely, residual pollutants in the effluent, sludge and GHGs) from WWTPs. Overall, the project is constituted by four research units (RUs): University of Palermo (RU1), University of Basilicata (RU2), University of Cassino and Southern Lazio (RU3) and University of Florence (RU4).

2   Materials and Methods

2.1   Research Unit 1

The objective of RU1 is the study of the chemical/physical/biological phenomena of advanced wastewater treatment systems, through designing, building and operating an MBR plant at pilot scale aimed at removing nutrients (Mannina et al. 2016b). Three mechanistic integrated membrane bioreactor (MBR) mathematical models (namely, Model I, Model II and Model III) all of the Activated Sludge Model (ASM) family (Henze et al. 2000) have been implemented, including the simulation of N_2O and CO_2 emissions

Model I has been applied to a pilot plant having a pre-denitrification scheme (anoxic and aerobic reactors in series) and equipped with an hollow fiber membrane for the solid – liquid separation (20 L h^{-1} of saline industrial wastewater were considered as influent) (Mannina et al. 2016a). Model II and III have been applied to a pilot plant with a University Cape Town (UCT) (anaerobic, anoxic and reactors in series) MBR scheme (20 L h^{-1} of real wastewater were considered as influent) (Mannina et al. 2016b). Each model has been calibrated as in Mannina et al. 2011. By comparing measured and simulated data the efficiency of each model output (E_i) and the total model efficiency (E_{MOD}) have been evaluated as proposed by Mannina et al. (2011).

2.2   Research Unit 2

The aim of RU2 was the deepening of the chemical/physical/biological phenomena of and aerobic digestion (AeD) more effectively. To this end, RU2 has designed, built and operated a pilot scale plant for aerobic digestion in order to investigate the GHG emissions in different operating conditions. Moreover, a new Aerobic Digestion Model 1, AeDM1, has been developed (Caivano et al. 2015) to simulate the aerobic digestion processes including also GHG emissions. The biological phenomena taking place in AeD are described by a modified ASMN model (Hiatt and Grady 2008), as proposed by Pocquet et al. (2016).

The AeDM1 model has been calibrated and validated using the data collected during the lab-experimental tests on a pilot-scale aerobic digester performed on June-August 2015. The influent and effluent sludge characteristics (e.g. COD, TSS, NH_4^+, NO_2^- and NO_3^-) and the kinetic parameters, evaluated by means of the respirometric tests (in collaboration with RU3), were used as input data. The sensitivity analysis (Caivano 2017), carried out by applying the Morris screening method (Morris 1991), on the main kinetic parameters allowed us to individuate the parameters that have a high influence on the model output, ensuring the model calibration.

2.3   Research Unit 3

RU3 has linked the operative conditions of the anaerobic digestion (sludge age, sludge concentration, retention time) and the quality of the reactors feed, to the biogas production, energy recovery and GHGs emission. Activities of the RU3 are carried through both experimental and modeling approaches. Data gathered from experimental activities are collected for setting up a database in order to increase knowledge and develop detailed models able to properly predict the observed phenomena. The proposed mathematical model is a modified version of the ADM1 model (Batstone et al. 2002) and it is based on differential mass balance equations for substrates, products and biomasses involved in the anaerobic digestion process. The main novelty of the proposed model consists in applying a surface based kinetics approach (Esposito et al. 2011a) for the hydrolysis process, which is useful when hydrolysis is the rate limiting step of the anaerobic digestion. The model simulates the dynamics of 32 state variables and includes more than 70 parameters.

2.4   Research Unit 4

The applicability of available kinetic models to the case of a full-scale WWTP in Italy was investigated by RU4. One of the most advanced kinetic models was selected as the test model seen its recent application to another full scale scenario (Guo and Vanrolleghem 2014). The model of the plant was already implemented by the plant manager in WEST (DHI) currently in use for normal plant optimization operation. The selected model describes the production of N_2O through a single pathway approach (i.e. AOB denitrification) based on Mampaey et al. (2013) with the addition of terms for oxygen limitation and inhibition, and terms for free ammonia (FA) and free nitrous acid (FNA) inhibition.

The use of Principal Component Analysis (PCA) was chosen as an alternative method for approaching N_2O emission modelling to investigate for an alternative to the current kinetic models. Indeed, the large quantity of available data makes possible to look for hidden relations between operational variables and N_2O emission. Therefore, a dataset from a field measurement campaign and SCADA data available from a WWTP were used to build a PCA-based statistical model.

3   Results and Discussion

3.1   Research Unit 1

Findings showed a general improvement of the model output efficiency between Model II and Model III. This result is mainly evident for the aerated reactors thus demonstrating that detailing the N_2O formation process during nitrification has led to the improvement of the model results. Data of Fig. 1 show a good agreement between measured and modelled value. However, an overestimation of simulated data occurred for the three models, excepting two cases, both for dissolved and off-gas N_2O. This result is likely debited to the discrete sampling. Continuous sampling would improve the results
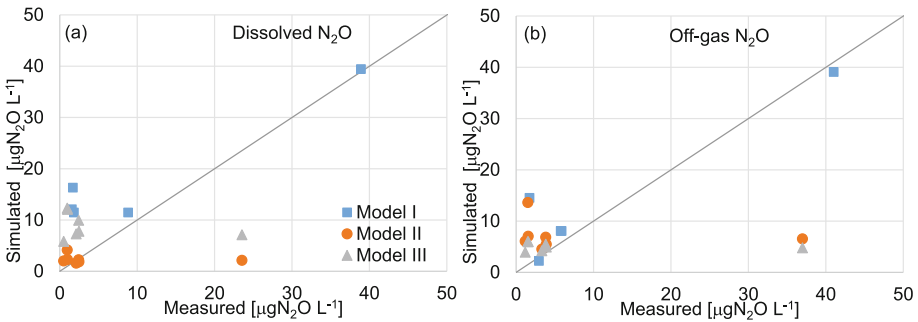
Fig. 1. Measured versus simulated data for each model of the dissolved N_2O (a) and off-gas N_2O (b) concentration

3.2   Research Unit 2

The maximum specific growth rate of heterotrophs (mu_H) is the more sensitive parameter for all the model outputs. Therefore, the variation, as well as its interaction with the parameters kept fixed at their baseline value, determines a variation of NO_2^-, NO_3^-, NH_2OH, and N_2O (Caivano 2017).

The comparison between the model output and the lab-measurements (Fig. 2) showed the reliability of the constructed model, including the estimation of the N_2O emissions.
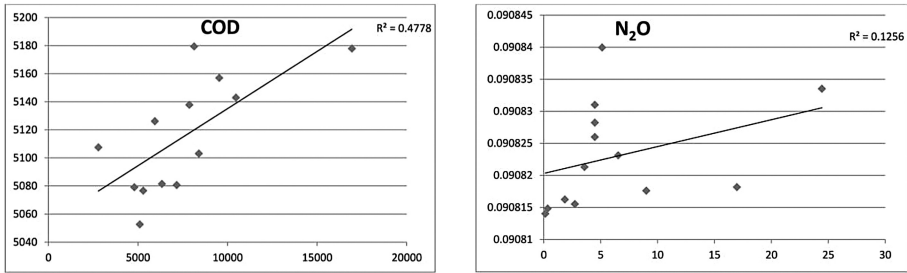
Fig. 2. Example of the model validation

3.3   Research Unit 3

A sensitivity analysis for 75 model parameters has been performed by using a derivative method in order to investigate their effects on simulation outputs. Model calibration was used to estimate the surface based kinetic constant, K_{sbk}, by adopting the protocol introduced by Esposito et al. (2011b) and comparing model results with experimental measurements of methane production from sewage sludge of different WWTP technologies (e.g. MBR and CAS). Comparison between experimental data and modelling results after calibration is reported in Fig. 3.
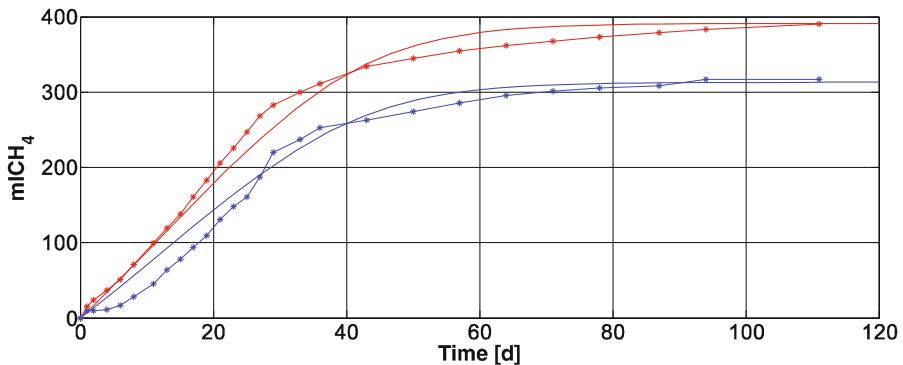
Fig. 3. Comparison between experimental data and modelling results after calibration: red-continuous line is modelled CAS biogas production, red-starred line is experimental CAS biogas production; blue-continuous line is modelled MBR biogas production, blue-starred line is experimental MBR biogas production

3.4   Research Unit 4

Results of the measurement campaign were used for developing a stochastic model based on PCA that could be implemented to estimate and mitigate N_2O emissions. Long datasets of different parameters recorded during the measurement campaigns and other plant data acquired, in parallel, by the WWTP SCADA system, were used to

mine hidden information about N_2O production. This information was unravelled using a combination of data processing methods and mathematical tools available in literature.

Results show that even only DO, NH_4 and NO_3 (known to be the most meaningful variables for N_2O emissions among the ones normally monitored in a SCADA system) could manage to cluster high N_2O emissions data (Fig. 4).
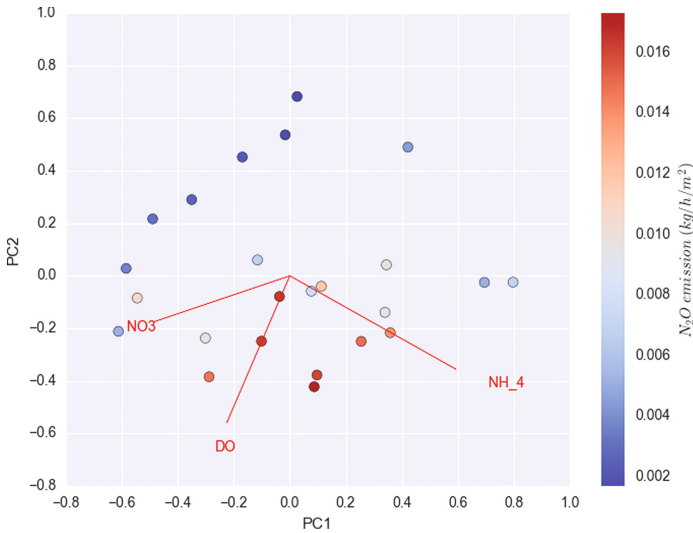

Fig. 4. Example of the application of the statistical PCA model to a full scale dataset

4   Conclusion

Traditionally, WWTPs have had the aim of meeting the quality standards of effluent, ensuring a high quality of water bodies and sustainable management costs. However, in recent years, the wastewater treatment objectives have been expanded and include the reduction of greenhouse gas emissions, as a result of the growing concern about climate change and environmental protection. Therefore, it is necessary to develop innovative approaches for an integrated WWTP management system. The collected database of measurements allowed us to develop and apply models of biological processes occurring in the water line and the sludge line of conventional and advanced treatment systems.

The main preliminary conclusions are summarises in the following:

- Concerning the modelling of the MBR treatment, N_2O formation process during nitrification has led to the improvement of the model results.
- N_2O emission from AeD mainly depends on the maximum specific growth rates of heterotrophs, ammonia-oxidizing bacteria and nitrite-oxidizing bacteria and on the growth yield of heterotrophs.

- The mathematical model for anaerobic digestion is useful when hydrolysis is the rate limiting step of the anaerobic digestion.
- The obtained findings derived for full-scale modelling application, highlight the capabilities of online data when combined to full-scale measurements..

References

Batstone DJ, Keller J, Angelidaki I, Kalyuzhnyi SV, Pavlostathis SV, Rozzi A et al (2002) Anaerobic digestion model no.1, Rep. No. 13. IWA Publishing, London, p 74

Caivano M, Saluzzi F, Caniani D, Masi S, Mannina G (2015) Development of an aerobic digestion model for the assessment of greenhouse gases production (AeDMG1): Calibration and validation. In: EuroMed 2015 Desalination for Clean Water and Energy Cooperation among Mediterranean Countries of Europe and the MENA Region, Palermo

Caivano M, Masi S, Mazzone G, Mancini IM, Caniani D (2017) Quantification of CO2 and N2O emissions from a pilot-scale aerobic digester, towards the validation and calibration of the first Activated Sludge Model for aerobic digestion (AeDM1). In FICWTM 2017: Frontiers International Conference on Wastewater Treatment, 21–24 May 2017, Palermo, Italy

Caniani D, Esposito G, Gori R, Mannina G (2015) Towards a new decision support system for design, management and operation of wastewater treatment plants for the reduction of greenhouse gases emission. Water 7:5599–5616, doi:10.3390/w7105599

Daelman MRJ, van Voorthuizen EM, van Dongen LGJM, Volcke EIP, van Loosdrecht MCM (2013) Methane and nitrous oxide emissions from municipal wastewater treatment – results from a long-term study. Water Sci Technol 67:2350

Esposito G, Frunzo L, Panico A, Pirozzi F (2011a) Modelling the effect of the OLR and OFMSW particle size on the performances of an anaerobic co-digestion reactor. Process Biochem 46 (2):557–565

Esposito G, Frunzo L, Panico A, Pirozzi F (2011b) Model calibration and validation for OFMSW and sewage sludge co-digestion reactors. Waste Manag 31(12):2527–2535

Guo LS, Vanrolleghem PA (2014) Calibration and validation of an activated sludge model for greenhouse gases no. 1 (ASMG1): prediction of temperature-dependent N2O emission dynamics. Bioprocess Biosyst Eng 37:151–163

Henze M, Gujer W, Mino T, Van Loosdrecht MCM (2000) Activated sludge models ASM1, ASM2, ASM2d and ASM3. In: IWA Task Group on Mathematical Modelling for Design and Operation of Biological Wastewater Treatment. IWA Publishing, London, UK

Hiatt WC, Grady Jr CPL (2008) An updated process model for carbon oxidation, nitrification, and denitrification. Water Environ Res 80:2145–2156

Mampaey KE, Beuckels B, Kampschreur MJ, Kleerebezem R, van Loosdrecht MCM, Volcke EIP (2013) Modelling nitrous and nitric oxide emissions by autotrophic ammonia-oxidizing bacteria. Environ Technol 34(12):1555–1566

Mannina G, Ekama G, Caniani D, Cosenza A, Esposito G, Gori R, Garrido-Baserba M, Rosso D, Olsson G (2016a) Greenhouse gases from wastewater treatment — A review of modelling tools. Sci Total Environ 551–552:254–270

Mannina G, Capodici M, Cosenza A, Di Trapani D (2016b) Carbon and nutrient biological removal in a University of Cape Town membrane bioreactor: Analysis of a pilot plant operated under two different C/N ratios. Chem Eng J 296:289–299

Mannina G, Capodici M, Cosenza A, Di Trapani D, Viviani G (2016c) Sequential batch membrane bioreactor for wastewater treatment: effect of salinity increase. Bioresour Technol 209:205–212

Mannina G, Cosenza A, Vanrolleghem PA, Viviani G (2011) A practical protocol for calibration of nutrient removal wastewater treatment models. J Hydroinformatics 13(4):575–595

Morris MD (1991) Factorial sampling plans for preliminary computational experiments. Technometrics 33(2):161e174

Olsson G (2012) ICA and me - A subjective review. Water Res 46:1585–1624

Pocquet M, Wu Z, Queinnec I, Spérandio M (2016) A two pathway model for N_2O emissions by ammonium oxidizing bacteria supported by the NO/N_2O variation. Water Res 88:948–959

Moving Bed Biofilm Reactors and Hybrid Systems

New Applications for MBBR and IFAS Systems

H. Ødegaard[(✉)]

Scandinavian Environmental Technology AS,
Hellemsveien 421, N-7165 Oksvoll, Trondheim, Norway

Abstract. In this extended abstract some of the advances that have been made in MBBR and IFAS systems over the last 10 years are discussed. It is focused on new applications such as MBBR-based processes for nitrogen removal by de-ammonification, biological phosphate removal and MBBR-based membrane bioreactors.

Keywords: De-ammonification · Bio-P removal · MBBR-based MBR

1 Introduction

The MBBR is a pure biofilm flow-through reactor, i.e. there is no recycle of biomass from the downstream separation reactor and back to the MBBR. The biofilm (or attached biomass) is growing on carriers that are suspended in the reactor and moving freely around with the currents set up by aeration (in oxic reactors) and mixing (in anoxic reactors). Since there is no recycle, the biomass concentration entering the separation reactor is low (equal to the biomass production), and the use of any separation reactor alternative is possible. When combined with compact separation reactors MBBR systems are extremely compact (Ødegaard et al. 1994).

The Integrated Fixed Film Activated Sludge System (IFAS for short) is a hybrid activated sludge/MBBR system – where biofilm carriers are included in the activated sludge tank. In an IFAS system, nitrification can be achieved at a much lower SRT_{MLSS} than in a CAS system, and nitrogen removal is obtained at a much lower reactor volume (Ødegaard et al. 2014).

The paper, on which this extended abstract is based, focuses on advances in MBBR-based processes for de-ammonification, biological phosphate removal and membrane bioreactors.

2 Nitrogen Removal by de-Ammonification in MBBR-Based Plants

Over the last 10 years, research focus has been on de-ammonification as an alternative process to nitrification/denitrification. MBBR-based systems have proven themselves particularly suitable for de-ammonification in the side-stream as well as in mainstream.

In a biofilm it is possible carry out both nitritation by aerobic ammonia-oxidizing bacteria (AeAOB) and de-nitritation by anaerobic ammonia-oxidizing bacteria (AnAOB) in the same biofilm. Partial nitrification to nitrite and autotrophic N-removal (i.e. anammox) may occur simultaneously within the biofilm, where aerobic and anoxic zones results from oxygen mass transfer limitation under limited dissolved oxygen (DO) conditions. In a MBBR the ammonium oxidizing bacteria (AeAOB) as well as the anammox (AnAOB) bacteria are maintained in the attached biofilm on the suspended carriers retained in the reactor by the sieves, with no risk of biomass washout. AeAOB oxidize NH_4 to NO_2 in the aerobic zone of the biofilm (i.e. outer part) while AnAOB bacteria located in the anoxic zone of the biofilm (i.e. inner part) consume NO_2 produced by AeAOB together with the excess NH_4-N. The main challenge of such single-stage de-ammonification is to prevent further oxidation of nitrite to nitrate by nitrite oxidizing bacteria (NOB) (Trela et al. 2014).

Since de-ammonification is easiest implemented when the temperature is high (preferably $> \sim 25$ °C), the ammonium concentration is high (>500 mg NH_4-N/l) and the C/N-ratio is low, the process has been successfully implemented for sludge reject water (in side-stream), that normally represents about 25% of the nitrogen load on a typical BNR plant. It is not yet established as a proven process for nitrogen removal in the mainstream.

3   De-ammonification in the Sidestream

ANITA^{TM}Mox is a single-stage MBBR de-ammonification process. In the ANITA^{TM}MOX system a DO control system is used to prevent nitrite oxidation in the aerobic zone of the biofilm while maximizing the amount of nitrite available for the anammox bacteria. The DO set-point is automatically adjusted based on online inlet and outlet concentrations of NH_4 and NO_3 to control the NO_3 production below 11% of NH_4–N removed (i.e. stoichiometric NO_3 production by anammox) while at the same time keeping high NH_4-oxidation performance in the reactor. This real-time DO control strategy reduces the need of mechanical mixer in the MBBR due to the continuous aeration pattern (Christensson et al. 2013).

When comparing the pure 1-stage MBBR version with the 1-stage IFAS version, it was demonstrated in lab-scale that the nitrogen removal capacity in side-stream treatment was almost 4 times higher in the IFAS version. Full-scale experiences with ANITA^{TM}Mox from the demonstration plant at Sjölunda WWTP in Sweden, in pure biofilm as well as in IFAS mode, confirm the findings in the lab- and pilot-scale tests (Veuillet et al. 2014).

When comparing 2-stage MBBR and 1-stage MBBR on sludge reject water Cema et al. (2010) found excellent nitritation in the 2-stage system, but that it was more difficult to control the anammox stage. Inhibition was experienced in a 2-stage pilot-plant, while the nitrites produced by AOB were consumed immediately by anammox in the 1-stage process.

4   De-ammonification in the Main Stream

The challenges of mastering mainstream de-ammonification are: (a) the dominance of NOB growth at lower temperatures that makes the selection of AOB over NOB challenging, (b) stimulation of AOB growth and suppression of NOB growth, (c) effective retention of the anammox biomass in a reactor; (d) low transformation rates because of low temperature in main-stream (Trela et al. 2014).

At this time most developers and researchers work with MBBR-based IFAS systems for mainstream de-ammonification (Veuillet et al. 2014; Malovanyy et al. 2015). IFAS-based ANITA^{TM}Mox is, for instance, proposed to be used in two strategies – one is to move carriers from to the less robust main-stream process from the more robust side-stream process and the other is to the feed alternate between the mainstream COD-treated effluent and the side-stream reject water to a multi-celled IFAS (Lemaire et al. 2015).

The development of the MBBR system over the years has demonstrated, however, that better control and operability has been achieved when dividing the bacterial cultures in separate stages – making it possible to optimize process conditions for exactly this stage. The single-stage, pure MBBR seems to be inferior to the single-stage MBBR-based IFAS for de-ammonification. However, a two-stage pure MBBR-process, where nitritation and anammox is separated in two different stages, may be competitive in a mainstream process if NOB control can be secured through an extended BOD-removal in the C-stage and bio-augmentation from the side-stream to the mainstream. Indeed Piculell et al. (2016) demonstrated that stable nitritation and anammox was achievable in a lab-study when exposing the biomass periodically to high concentration reject water and using a special saddle-shaped carrier for biofilm thickness control, in order to favour AOB activity and suppress NOB growth.

5   Biological P-Removal

When conditions are favorable (sufficiently high concentration of easily biodegradable COD in incoming water), biological P-removal may be implemented in IFAS plants in the same way as in conventional activated sludge bio-P plants. It is more challenging to achieve bio-P removal in a pure MBBR plant. Two strategies have been demonstrated.

6   Bio-P in a Discontinuously Operated (SBR) MBBR

Through experiments in small pilot scale, Helness (2007) demonstrated that biological phosphorus and nitrogen removal could be achieved in a MBBR operated as a SBR (Helness and Ødegaard, 2005). It was found that the SBR cycle should be tuned to achieve near complete removal of easily biodegradable soluble COD in the anaerobic phase and complete nitrification in the aerobic phase. For a SBR MBBR process like this, the design criteria as in Table 1 was recommended for a wastewater with COD:N: P ∼ 100:10:2 (Helness, 2007).

Table 1. Proposed design values for a SBR MBBR for a wastewater with COD:N:P $\sim$ 100:10:2 (Helness 2007)

Parameter	Design value
Total COD-loading rate, (g COD m^{-2}d^{-1})	< 5
Anaerobic BSCOD[a]-loading rate, (g BSCOD m^{-2}d^{-1})	< 5
Aerobic ammonia loading rate, (g NH$_4$-N m^{-2}d^{-1})	< 0.4
Required influent BSCOD/PO$_4$-P	20

[a]BSCOD – biodegradable soluble COD

7   Bio-P in Continuously Operated MBBR

Saltnes et al. (2016) presented an alternative continuous, pure MBBR bio-P process where the carriers are moved physically from the aerobic to the anaerobic zone by a conveyer belt. The MBBR is partitioned in several anaerobic and aerobic zones – all containing carries. There are no sieves between the zones, and the carriers are flowing, together with the water, through openings in the partition walls between the zones, first through the mechanically mixed, anaerobic zones and thereafter through the aerated zones. From the last aerobic zone the carriers are transported mechanically by a conveyer that also separate the carriers from the wastewater, back to the first anaerobic zone, while the wastewater leaves the bioreactor from the last aerobic zone. Based on pilot plant experiments at HIAS WWTP in Norway, Saltnes et al. (2016) concluded that an effluent concentration of 0.4 g P m^{-3} (the full-scale plant standard) could be reached in the full-scale plant (at a HRT of 5–10 h), provided that a particulate P- concentration of less than 0.2 mg g P m^{-3} could be maintained after biomass separation.

Simultaneous nitrification/denitrification (SND) is studied in on-going experiments. So far the average ammonia load, the nitrification rate and the denitrification rate have been 0,86 g N m$^{-2\cdot}$d^{-1}, 0,54 g N m$^{-2\cdot}$d^{-1} and 0,33 g N m$^{-2\cdot}$d^{-1} respectively (Saltnes et al. 2016).

8   MBBR-Based Membrane Bioreactor (MBR) Systems

When very strict effluent standards are to me met (typically in re-use situations), membrane bioreactors (MBR) are being favored. Traditional MBR's are based on activated sludge with biomass separation by UF membranes (typical pore size: 40 µm) designed for a reasonably high MLSS concentration (7–10 g MLSS m^{-3}) and a membrane flux of around 20 l m$^{-2\cdot}$h^{-1}. The main drawback of the traditional MBR process is the high energy consumption caused by the extra air that is used for keeping the membranes from fouling and clogging too fast. The higher energy also results in comparatively high operation cost. An interesting alternative is a MBBR-based MBR system that may be based on a pure MBBR or an IFAS-based MBR see Fig. 1. The nomenclature has been confusing in literature and it is recommended that the expression MBBR-MBR is reserved for systems like the one in Fig. 1a while IFAS–MBR should be used for the systems in Fig. 1b and c.
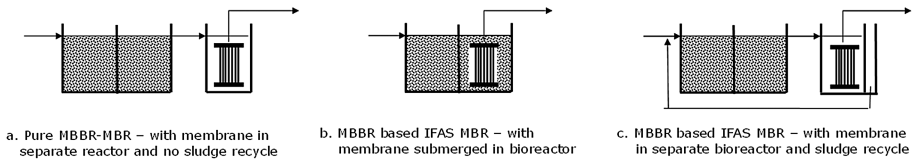
a. Pure MBBR-MBR – with membrane in separate reactor and no sludge recycle

b. MBBR based IFAS MBR – with membrane submerged in bioreactor

c. MBBR based IFAS MBR – with membrane in separate bioreactor and sludge recycle

Fig. 1. The various MBBR-based MBR systems

9 Pure MBBR + Membrane (MBBR-MBR)

In the combination of pure MBBR and membrane separation, the membrane unit may be placed directly after the MBBR as an immersed membrane or as a separate, contained membrane unit. Most of the studies on MBBR with UF separation reported so far, have been based on immersed membranes (Leiknes and Ødegaard 2006; Ivanovic and Leiknes 2012). These studies have shown that the concentration of biomass as well as the particle size distribution of the MLSS adjacent to the membrane, is influencing the fouling of the membrane and several measures has been proposed in order to minimize this particle caused fouling.

The alternative to immerged membranes, would be contained membranes placed directly after the MBBR. Since the biomass concentration introduced to the contained membrane reactor will be in the range of 200–300 mg SS/l, this is, however, a difficult approach. Ødegaard et al. (2012) investigated in pilot-scale, therefore, the use of an intermediate, high-rate biomass separation step (Disc filter of DAF) between the MBBR and the membrane unit. It was found that the solution based on MBBR – coagulation/flocculation – DAF – UF was the one with the lowest fouling, the highest possible operating flux, the lowest backwash water consumption and the lowest membrane cleaning chemicals consumption.

Even though a fair amount of R&D has been executed and some few plants have been built, plants for pure MBBR-MBR is not yet common. Most of the studies that compare the pure MBBR-MBR and the IFAS-MBR go in the favour of IFAS-MBR (Leyva-Díaz et al. 2016).

10 MBBR Based Hybrid MBR (IFAS MBR)

Most of the studies that compare the traditional MBR and the IFAS-MBR go in the favour of IFAS-MBR. The IFAS-MBR is claimed to have the advantage of operating at higher fluxes, being more compact, having better energetic efficiencies and better membrane fouling control than the traditional MBR. Many research studies have been performed in lab-scale in a system with the membrane immersed in the bioreactor (Duan et al. 2015; Leyva-Díaz et al. 2016). Most new full-scale MBR plants today, however, use separate membrane tanks and sludge.

In many studies the SRT and HRT in the IFAS-MBR has been about the same as in conventional MBRs (i.e. SRT: 15-30 d, HRT: 10–24 h). In this author's opinion, this does not utilize the full potential of IFAS-MBR in the practical scale where size and

cost matters. The benefit of IFAS is that nitrification can be obtained at less than half of the SRT_{MLSS} than what is required in CAS plants (Ødegaard et al. 2014). Moreover, at a lower SRT_{MLSS} more carbon will be available for denitrification through hydrolysis of the MLSS. Several studies (Rusten et al. 2003; Onnis-Hayden et al. 2011) have shown that the specific denitrification rate in IFAS systems is around twice as high as in CAS systems. Hence the IFAS MBR-system may have a much more compact bioreactor than the conventional MBR, since the nitrification zone as well as the denitrification zone both may be smaller.

11 A Comparison Between MBBR, MBR and MBBR-Based MBR Processes

In order to evaluate the practical full-scale potentials of the MBBR-based MBR processes for advanced wastewater treatment, a comparative analysis between MBBR, MBR and MBBR-based MBR processes has been carried out. The study is based on data for an existing, large wastewater treatment plant ($Q_d = 190.000$ m^3/d) that is to be upgraded within very limited space, and with very strict effluent standard (Tot N < 4 g m^{-3}, Tot P < 0.3 g m^{-3}). Three alternative processes (with sub-alternatives) were analysed at 18 °C as well as at 10 °C (only the at 18 °C alternative is discussed here):

- MBBR (with subsequent advanced particle separation based on DAF + Disc filter (DF))
- MBR (activated sludge-based MBR with UF-membranes for biomass separation)
- IFAS-MBR (IFAS with MBBR-carriers in aerobic reactors only and with UF-membranes for biomass separation)

The alternatives were based on combined pre-and post-denitrification and chemical P-removal. The MBR alternatives were analysed with and without external carbon source, and with one alternative based on biological P-removal. The three basic processes were analyzed with three different pre-treatment alternatives; (a) no primary (fine screen only), (b) primary treatment (based on settling) and (c) chemically enhanced primary treatment (CEPT).

When dimensioning the bioreactor in MBR systems, one may include (or not) the biomass in the membrane tank when designing for the nitrification tank volume. Membrane fouling is, however, very dependent upon the extent of organic matter degradation in the water that is to be membrane separated, which again is dependent upon the SRT_{MLSS}. Because the SRT_{MLSS} is lower in the IFAS MBR, and in order to be able to compare on as equal basis as possible, the biomass of the membrane tank is not included in the sizing of the nitrification tank. It was included, however, in the calculation of the aerobic SRT_{MLSS}. Because of the relatively low C/N-ratio, external carbon source would have to be used in the MBBR-alternative. In the MBR- and IFAS MBR alternatives, hydrolysis would be more extensive and it would be possible to meet the required standard without external carbon source if an extra post-anoxic volume for endogenous denitrification was included. The analysis was also carried out at 10 °C, but the results from this is not included in this extended abstract.

The Disc filter station (in the MBBR alternative) is placed above ground and no volume is calculated, but rather the surface space required. The MBR alternatives need a fine sieve between the bioreactor and the membrane reactor to prevent hair etc., to clog the membrane. The size the DF in the MBBR alternative and the fine sieve in the MBR alternatives are about equally large both in volume and foot-print.

In Table 1 the required process volumes for the most probable process alternatives are compared for three alternatives of primary treatment at 18°C. The volumes are given relative to the volume for the MBR without external carbon source.

Table 2 shows that the bioreactor volumes needed, as well as the construction foot-print for the whole plant, of the MBBR alternative and the MBR alternative are quite similar. Carbon source has to be used in the MBBR-alternative while the MBR alternative may be without, but then to the cost of a larger volume. The MBR alternative has a bit lower bioreactor volume ($\sim$9%) than the MBBR when external C-source is used, but a bit higher volume than the MBBR ($\sim$9%) when external C-source is not used in the MBR alternative. The difference on full plant footprint between the two is slightly less than the difference in bioreactor volumes.

Table 2. Relative bioreactor volumes and construction foot-print at different primary treatments (18°C)

Treatment system	Bioreactor volume required (m³)[a]			Construction foot-print (m²)[b]		
	Primary	No Primary	CEPT[f]	Primary	No Primary	CEPT[f]
MBBR + DAF + DF[c]	0.91	1.14	0.82	0.96	1.06	0.92
MBR[d]	1.00 (0.81)	1.33	0.71	1.00 (0.91)	1.1.15	0.87
IFAS-MBR[e]	0.57	0.65	0.34	0.80	0.84	0.69

[a] Proces volume for bioreactor. Primary tanks (when used), separation reactors (DAF and UF) as well as sieves
(disc filter and membrane sieve) have the same volume in each category – hence excluded from comparison
[b] Primary tank, flocculation (in CEPT) as well as sieves (DF and membrane sieve) included in foot-print calculation
[c] With Fe-addition for P-precipitation and with external carbon source
[d] With Fe-addition for P-precipitation and without external carbon source (with external C-source in brackets)
[e] With Fe-addition for P-precipitation and without external carbon source
[f] P-precipitation carried out in CEPT. All alternatives with CEPT have external carbon source added

It is interesting to note, tough, that even if external carbon is not used, the IFAS MBR alternative is by far the process that requires the smallest process volume as well as the smallest foot-print. To this author's knowledge, the IFAS-MBR is not used in full-scale plants yet. This analysis proves that it has the potential of becoming a very competitive alternative.

References

Cema G, Trela J, Plaza E, Surmacz-Górska J (2010) Partial nitration/Anammox process – from two-step towards one-step process. In: Proceedings of IWA World Water Congress, Montreal, 19–24 September 2010

Christensson M, Ekström S, Andersson Chan A, Le Vaillant E, Lemaire R (2013) Experience from start-ups of the first ANITA Mox plants. Water Sci Tech 67(12):2677–2684

Duan L, Li S, Han L, Song Y, Zhou B, Zhang J (2015) Comparison between moving bed-membrane bioreactor and conventional membrane bioreactor systems. part I: bacterial community. Environ Earth Sci 73(9):4891–4902

Helness H (2007) Biological phosphorous removal in a moving bed biofilm reactor. PhD-thesis, 2007:177 Norwegian University of Science and Technology (NTNU), Trondheim, Norway

Helness H, Ødegaard H (2005) Biological phosphorus and nitrogen removal from municipal wastewater with a moving bed biofilm reactor. In: Proceedings of IWA Specialized Conference Nutrient Management in Wastewater Treatment Processes and Recycle Streams, Krakow, 19–21 September 2005, pp 435–444. ISBN 83-921140-1-9

Ivanovic I, Leiknes T (2012) The biofilm membrane bioreactor (BF-MBR)—a review. Desalination Water Treat. 37(1–3):288–295

Leiknes T, Ødegaard H (2006) The development of a biofilm membrane bioreactor. Desalination 202:135–143

Lemaire R, Veuillet F, Zozor P, Stefansdottir D, Christensson M, Skonieczny T, Ochoa J (2015) Mainstream deammonification using ANITA™Mox Process. In: Proceedings of IWA Conference on Nutrient Removal and Recovery, Gdansk, Poland, 17–21 May 2015

Leyva-Díaz JC, Martin-Pacual J, Poyatos JM (2016) Moving bed biofilm reactor to treat wastewater. Int J Environ Sci Technol. doi:10.1007/s13762-016

Malovanyy A, Yang J, Trela J, Plaza E (2015) Combination of UASB reactor and partial nitritation/Anammox MBBR for municipal wastewater treatment. Biores Technol 180:144–153

Onnis-Hayden A, Majed N, Schramm A, Gu AZ (2011) Process optimization by decoupled control of key microbial populations: Distribution of activity and abundance of polyphosphate-accumulating organisms and nitrifying populations in a full-scale IFAS-EBPR plant. Water Res 45(2011):3845–3854

Piculell M, Christensson M, Jönsson K, Welander T (2016) Partial nitrification in MBBRs for mainstream deammonification with thin biofilms and alternating feed supply. Wat Sci Tech 73(5):1253–1260

Rusten B, Nielsen M, Welander T, Rasmussen V (2003) Increasing the capacity of activated sludge plants by using AS/MBBR hybrid process with Kaldnes biofilm carriers. In: Proceedings of the 5th IWA Conference on Biofilms Systems Cape Town, South Africa

Saltnes T, Sørensen G, Eikås S (2016) Biological nutrient removal in a continuous biofilm process. In: Presented at IWA Biennial Congress, Brisbane, Australia, October 2016

Trela J, Malovanyy A, Yang J, Plaza E, Trojanowicz K, Sultana R, Wilén B-M, Persson F, Baresel C (2014) De-Ammonification. Synthesis report 2014 R&D at Hammarby Sjöstadsverk. IVL-report no B 2210 October 2014. http://www.ivl.se/download/18.1acdfdc8146d949da6d43f9/1413294579949/B2210+Synthesis+report+2014.pdf

Veuillet F, Bausseron A, Gonidec E, Chastrusse S, Christensson M, Lemaire R, Ochoa J (2014) ANITA™Mox deammonification process: possibility to handle high COD level using the IFAS configuration. In: Proceedings of IWA Water Congress & Exhibition; Lisbon, Portugal, September 21–26, 2014

Ødegaard H, Rusten B, Westrum T (1994) A new moving bed biofilm reactor - Applications and results. Wat Sci Tech 29(10–11):157–165

Ødegaard H, Mende U, Skjerping EO, Simonsen S, Strube R, Bundgaard E (2012) Compact tertiary treatment based on the combination of MBBR and contained hollow fibre UF-membranes. Desalination Water Treat 42(1–3):80–86. http://dx.doi.org/10.1080/19443994.2012.683145

Ødegaard H, Christensson M, Sørensen K (2014) Hybrid Systems. In: Jenkins. D, Wanner, J (eds) Activated Sludge 100 years – and counting. Chap 15. IWA Publishing, London

Applications of Mobile Carrier Biofilm Modelling for Wastewater Treatment Processes

F. Sabba[1], J. Calhoun[1(✉)], B.R. Johnson[2], G.T. Daigger[3],
R. Kovács[4], I. Takács[5], and J. Boltz[6]

[1] RF WasteWater, Raleigh, NC, USA
`{fab,jason}@rfwastewater.com`
[2] CH2M HILL, Englewood, CO, USA
`bruce.johnson2@ch2m.com`
[3] University of Michigan, Ann Arbor, MI, USA
`gdaigger@umich.edu`
[4] Dynamita, SARL, Budapest, Hungary
`robert@dynamita.com`
[5] Dynamita, SARL, Nyons, France
`imre@dynamita.com`
[6] Volkert, Mobile, AL, USA
`jboltz@volkert.com`

Abstract. One-dimensional (1-D) biofilm models have been demonstrated reliable for specific types of biofilm reactor design. Limitations using mechanistic biofilm models for engineering design do not rely on improved biofilm models, but rely on improved biofilm reactor models. This is important when considering that biofilm reactors containing submerged, free-moving biofilm carriers are the most widely applied biofilm system(s) for municipal wastewater treatment. This paper presents a new biofilm reactor model that considers the impact of submerged free-moving biofilm carrier (Xcarrier) movement on system performance. The model accounts for a hydrodynamic condition characterized as plug flow with back mixing (to model axial dispersion). The relevance of this new biofilm reactor model to engineering situations is evaluated by applying it to relevant scenarios and comparing model results.

Keywords: ASM · Water quality · Simulators

1 Introduction

The intentional use of biofilms in wastewater treatment systems is becoming increasingly more common with the advent of such processes as Integrated Fixed Film Activated Sludge (IFAS), Moving Bed Biofilm Reactors (MBBR), and Biological Aerated Filters (BAFs) to name a few. At the same time the use of sophisticated simulation tools to size and design wastewater treatment systems is becoming increasingly more common (WEF MOP 31). The current generation of commercial wastewater simulation tools mostly provide methods of simulating biofilm based

systems, but each simulator has its advantages and disadvantages with respect to biofilm modeling, (Boltz et al. 2011). However, all these currently available simulators have some inherent limitations that may not be immediately apparent to the normal user of these tools.

This paper examines the use of simulators in evaluating a new biofilm modelling approach where the carrier is allowed to flow within the entire secondary treatment system, i.e. a Mobile Carrier (MC) system. A model based comparison of a Modified Ludzack-Ettinger (MLE) bioreactor has been completed. The comparison is based upon the operation of a conventional activated sludge, an IFAS and a Mobile Carrier (MC) system.

2   Materials and Methods

The authors have collaborated to develop an approach, currently implemented in Sumo™, (Dynamita, France), that provides a switch whereby biofilm carriers are allowed to transfer between the various components that make up a bioreactor system. The biofilm carriers are handled as a separate phase in the model structure (similar to liquids, gases, and solids) and will flow through any unit processes if allowed. This approach is shown graphically in Fig. 1. The biofilm model used for this simulation is the base MBBR module in Sumo™ (Kovács et al. 2013). For purposes of this simulation, it was assumed that there was no loss of the biofilm carrier in either the waste activated sludge (WAS) or in the secondary clarifier effluent.

Old method (bulk only):

Components	Bulk
Biomass	√
Substrate	√
Oxygen	√
etc...	√

New method (carrier and bulk):

| Components | Media (if switched on) | | | | Liquid |
	Carrier surface	Biofilm bottom	Biofilm layers	Biofilm top	Bulk
Biomass	√	√	√	√	√
Substrate	√	√	√	√	√
Oxygen	√	√	√	√	√
etc...	√	√	√	√	√
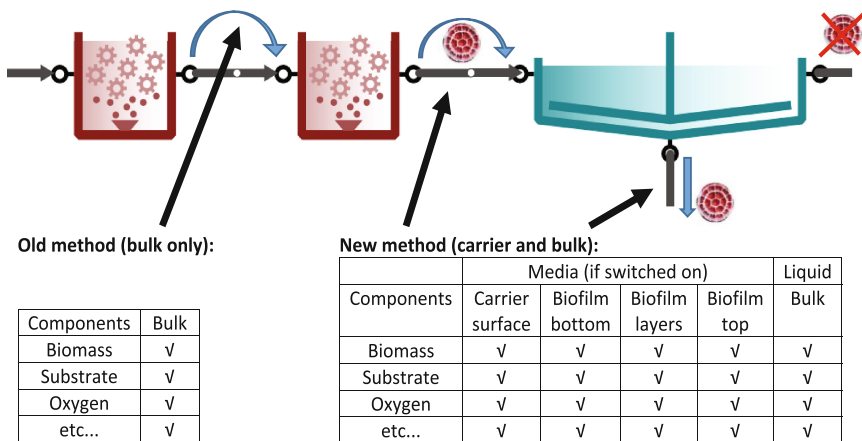
Fig. 1. Conceptual approach to biofilm transfer between unit processes

Another modification from standard biofilm modelling was in the use of standard half saturation values (i.e. K values in the Monod terms) for the suspended phase and an estimate of the intrinsic half-saturation values in the biofilm phase. It has been recognized for some time (Grady et al. 2011), and recently reiterated (Shaw et al. 2013),
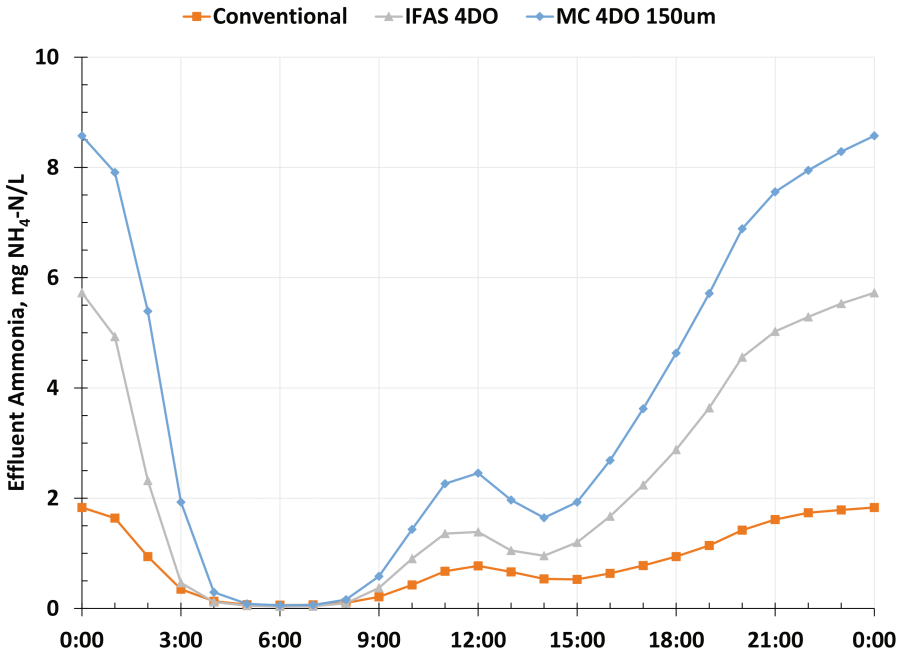
Fig. 2. Ammonia Diurnal profile for systems
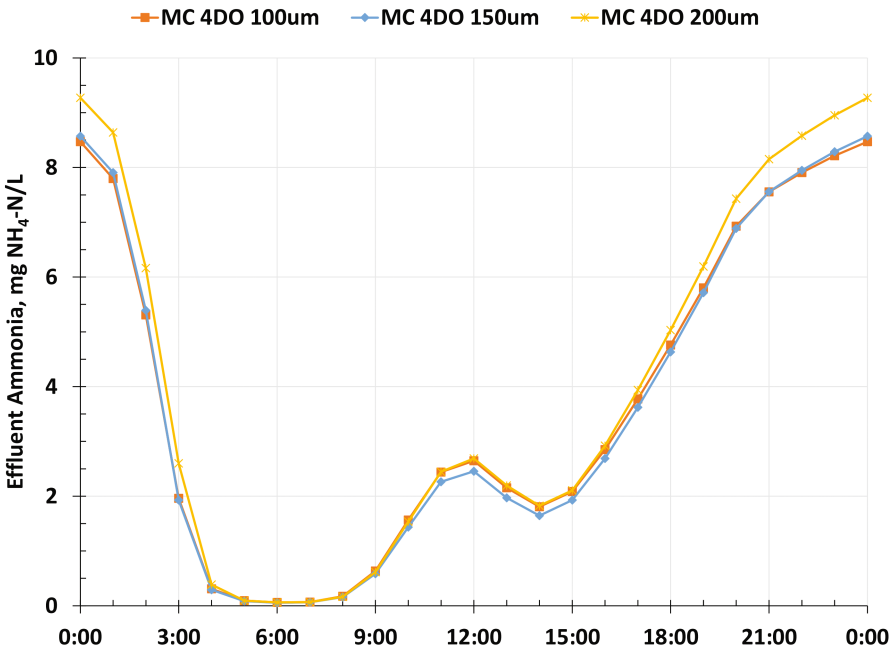
Fig. 3. Effect of biofilm thickness on MC System

Table 1. Average daily effluent nutrient from different MLE bioreactor systems

	Conventional	IFAS	MC
Ammonia, $mgNH_4\text{-}N\ L^{-1}$	0.9	2.6	4.1
Nitrate, $mgNO_3\text{-}N\ L^{-1}$	10.9	14.2	13.3
Phosphate, $mgPO_4\text{-}P\ L^{-1}$	4.6	3.6	4.0

that the half-saturation values typically applied in suspended growth (activated sludge) systems are actually "lumped" parameters that approximate the net effect of the mass transfer limitations into the activated sludge flocs, and the true, or intrinsic, half saturation values for the components in question. This lumping of effects is necessary to properly characterize overall suspended growth performance, as mass transfer effects are often an order of magnitude or more greater than the true half-saturation values (absent mass transfer/diffusional limitations). Should a simulation user keep the typical activated sludge default half-saturation values in a biofilm simulation, where diffusion is explicitly accounted for, the net impact is to significantly underestimate biofilm performance because, effectively, the impact of mass transport limitations on performance is overly estimated.

The biofilm half saturation values used in this simulation work were assumed to be $1/10^{th}$ the values of the suspended growth half saturation values. Setting half saturation values separate within a single CSTR zone is currently not possible in the commercially available simulators. However, CH2 M's $Pro2D^2$ simulation platform has been designed to allow this separation of values (Boltz et al. 2009). $Pro2D^2$ is based upon the IWA ASM2d model, modified to include methanol degraders and endogenous decay products.

A steady state simulation of the MLE system was first completed in $Pro2D^2$. The system design was based on achieving an effluent ammonia level of 0.5 mg NH_4-N L^{-1}. This same system was then converted to a IFAS based reactor system with a 50% fill in all the reactors and achieving the same effluent ammonia, with the differentiated half saturation values as previously described. Lastly, an identical steady state run was done with the half saturation values identical, and adjusted by the same fraction until the ammonia removal performance of that system matched the differentiated run. This estimate of the combined half saturation values was then used in dynamic simulations of the conventional, IFAS, and MC systems which investigated the impacts of dissolved oxygen and biofilm thickness on the MC process.

3 Results and Conclusions

The effluent diurnal ammonia profiles of the three different bioreactor systems are shown in Fig. 2. It can be seen that the biofilm systems were more heavily impacted by the diurnal load, with the MC system apparently being more susceptible. It would be expected that the biofilm thickness in an MC system would be lower than in conventional IFAS or MBBR systems as a result of the additional shear of recycle pumping. Figure 3 examines the impact of different biofilm thicknesses on the effluent ammonia from the MC system running at a 4 mg L^{-1} DO in the aerobic zones. The results show, somewhat counter-intuitively, that the effluent ammonia decreases in the

thinner biofilm systems. Table 1 summarizes the average daily nutrient discharge concentrations for the three bioreactor systems shown in Fig. 2. The increased susceptibility to diurnal changes of the biofilm systems shown in Fig. 2 is reflected in the higher effluent nutrients from biofilm systems.

A simulator based investigation of mobile biofilm carriers showed significant differences in performance. These results are applicable to such systems as granular activated sludge in flow through systems, and indicate that just modelling these systems as suspended growth processes can result in erroneous performance predictions. The full paper will go into more detail about the biofilm performance, morphology and applications to full scale systems, such as main-stream Anammox.

References

Boltz JP, Morgenroth E, Brockmann D, Bott C, Gellner WJ, Vanrolleghem PA (2011) Systematic evaluation of biofilm models for engineering practice: components and critical assumptions. Water Sci Technol 64, 4(1):930–952

Boltz JP, Johnson BR, Daigger GT, Sandino J (2009) Modeling integrated fixed-film activated sludge and moving bed biofilm reactor systems 1: mathematical treatment and model development. Water Environ Res 81(6):555–575

Grady CPL Jr, Daigger GT, Love NG, Filipe CDM (2011) Biological Wastewater Treatment, 3rd edn. CRC Press, Boca Raton

Kovács R, Takács I, Benke JD (2013) Facilitating biofilm reactor modelling with an easy-to-use spreadsheet-based tool designed for process engineers. In: IWA Biofilm Conference, Paris, France

Shaw A, Takács I, Pagilla KR, Murthy S (2013) A new approach to assess the dependency of extant half-saturation coefficients on maximum process rates and estimate intrinsic coefficients. Water Res 47(16):5986–5994

Application of the MBBR Technology
to Achieve Nitrification Below 1° C:
Biofilm and Microbiome Analysis

R. Delatolla[1(✉)], Bradley Young[2], and A. Stintzi[3]

[1] Department of Civil Engineering, University of Ottawa, Ottawa, Canada
[2] Veolia Water Technology Canada, Montreal, Canada
[3] Department of Biochemistry, Microbiology and Immunology,
University of Ottawa, Ottawa, Canada

Abstract. The regulatory framework throughout the world is becoming increasingly stringent with respect to ammonia discharge from municipal wastewater treatment plants. Meeting these regulations are challenging in northern and cold climate regions due to the well characterized significant temperature effects on nitrification in conventional biological treatment systems. The aim of this research is to investigate the effects of ammonia loading rates on ammonia removal rates at 1° C and determine the impact on the microbial communities at low temperatures through the application of variable pressure scanning electron microscopy (VPSEM), confocal laser scanning microscopy (CLSM) and next generation sequencing. Investigating the microbial community during long exposure to 1° C will provide necessary information to understand the potential and design constraints of nitrifying MBBR systems in northern and cold climate regions.

Keywords: MBBR · Biofilm · Nitrification · Next generation sequencing · Confocal microscopy

1 Introduction

The regulatory framework throughout the world is becoming increasingly stringent with respect to ammonia discharge from municipal wastewater treatment plants (EEC 1991; Canada Gazette 2012; USEPA 2014). Meeting these regulations are challenging in northern and cold climate regions due to the well characterized significant temperature effects on nitrification in conventional biological treatment systems (EEC 1991; Canada Gazette 2012; USEPA 2014).

The biologically mediated process of nitrification is conventionally sensitive to low temperatures, with nitrification rates declining substantially or becoming completely impeded below 8° C (Hurse and Connor 1999; Randall and Buth 1984; Shammas 1986). This temperature effect is exacerbated in northern passive biological systems where the temperature of the final effluent decreases to 1° C and lower for extended operation resulting in numerous systems discharging elevated ammonia concentrations during winter operation.

The MBBR technology has been recently implemented at different locations within the treatment train of passive treatment systems to achieve nitrification below 8° C.

Installing the MBBR technology after the first lagoon in multi-lagoon systems has demonstrated the potential for long term operation of low temperature MBBR nitrification at 4° C. However, it should be noted that implementation of a nitrifying MBBR unit after the first lagoon also demonstrated that nitrification rates were significantly impeded by heterotrophic overgrowth (Houweling et al. 2007; Delatolla et al. 2010). More recently, lab and field scale nitrifying MBBR systems have been studied after the last lagoon of multi-lagoon systems. Installation after the last lagoon, with operation at conservative hydraulic and substrate loading rates, has shown that nitrifying MBBR units are able to achieve significant nitrification kinetics at 1° C (Almomani et al. 2014; Hoang et al. 2014). However, recent pilot work has indicated that long term operation at high ammonia loading rates and elevated bulk phase total ammonia concentrations can reduce the kinetic performance of low temperature nitrification (Young et al. 2016; Young et al. 2017 *in press*).

2   Materials and Methods

Four pilot nitrifying MBBR reactors were installed after the last lagoon of the Masson Angers lagoon wastewater treatment plant in Quebec, Canada and were operated across an entire winter season (Fig. 1). The pilot MBBR reactors were operated at various
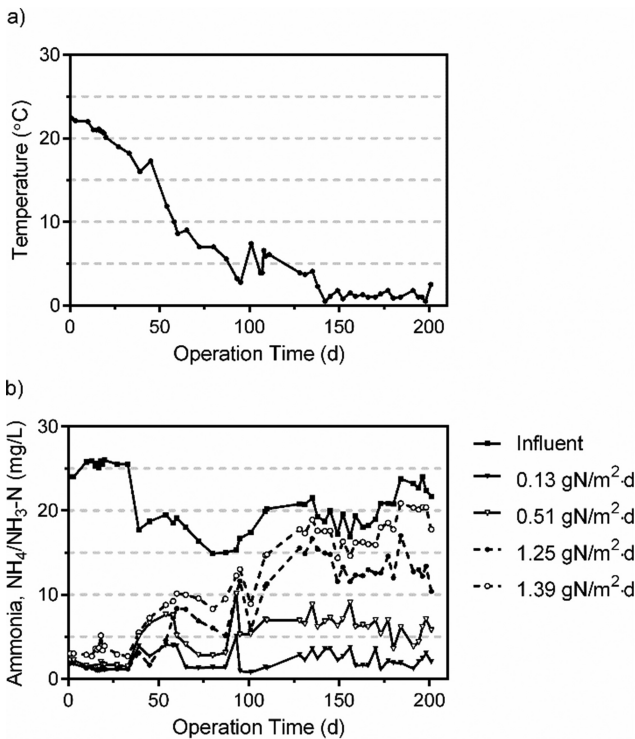
Fig. 1. MBBR nitrification at various SALRs across time of operation, (a) temperature, (b) ammonia concentration (Young et al. 2017)

Table 1. Kinetics and effluent ammonia concentrations (Young et al. 2017)

SALR (gN/m^2•d)	Temperature (° C)	SARR (gN/m^2•d)	Effluent ammonia (mgN/L)
2.36 ± 0.05	20.6 ± 0.5	2.0 ± 0.06	3.9 ± 0.4
0.13 ± 0.05	1.0 ± 0.1	0.09 ± 0.01	2.1 ± 0.7
0.51 ± 0.02	1.0 ± 0.1	0.32 ± 0.03	5.8 ± 1.2
1.25 ± 0.01	1.0 ± 0.1	0.35 ± 0.05	12.4 ± 1.2
1.43 ± 0.05	1.0 ± 0.1	0.22 ± 0.03	20.3 ± 0.2

ammonia surface area loading rates (SALRs) to investigate the operation and optimization of attached growth treatment systems for ammonia removal at very low temperatures over extended periods of operation (Table 1). The transition from 20° C (summer operation) to 1° C (winter operation) and during long term operation at 1° C were modelled using Arrhenius temperature correction coefficients.
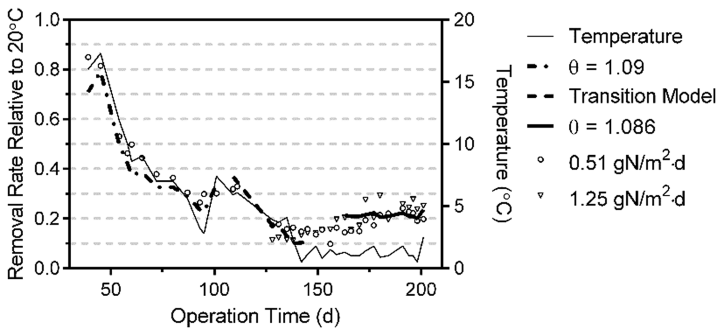
Fig. 2. Removal rates relative to 20° C across time of operation showing Arrhenius correction coefficient models applied to low temperature operation at SALR of 0.51 and 1.25 gN/m2·d (Young et al. 2017)
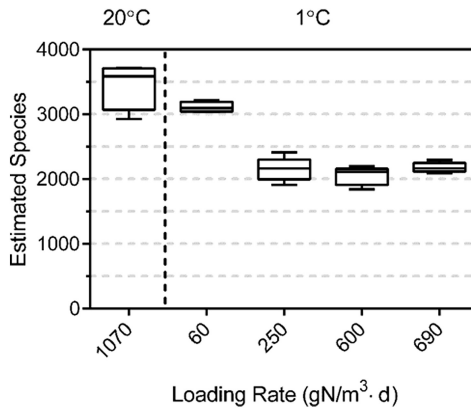
Fig. 3. Alpha diversity of microbial communities across SALRs at 20° C and 1° C (Young et al. 2017)
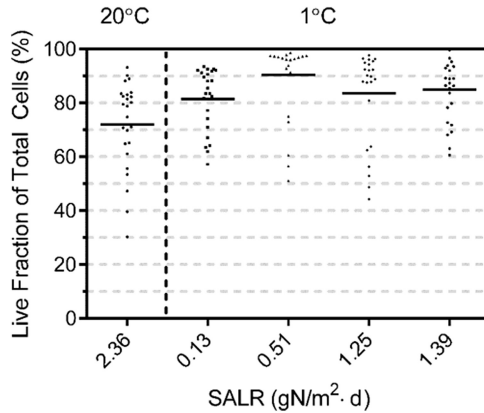
Fig. 4. Live fraction of total cells across SALRs at 20° C and 1° C (Young et al. 2017)

3   Results and Conclusions

The steady state ammonia surface area removal rates (SARRs) at 1° C on average were 22.8% of the maximum ammonia removal rate at 20° C (Table 1), which corresponds to an Arrhenius temperature correction of 1.086 during steady operation at 1° C (Fig. 2). The microbial communities of the nitrifying MBBR biofilm were shown to be significantly more diverse at 20° C as compared to 1° C operation (Fig. 3). Although less diverse at 1° C, 2,000 species of bacteria were identified in the nitrifying biofilm during operation at this low temperature. Nitrosomonads were shown to be the dominant ammonia oxidizing bacteria (AOB) and Nitrospira was shown to be the dominant nitrite oxidizing bacteria (NOB) in all the pilot MBBR reactors at all temperatures. Operation at the highest loading conditions tested in this study at 1° C were shown to reduce the ammonia removal rate compared to lower loading conditions at 1° C. The lower performance at higher loading conditions at 1° C demonstrated an enrichment in the stress response metagenomics pathways of the system, which demonstrates that a maximum loading rate should be observed for design at temperatures of 1° C. Overall, however at appropriate loading conditions the performance of the post carbon removal nitrifying MBBR systems were shown to be enhanced at 1° C by an increase in the viable embedded biomass as well as thicker biofilm (Fig. 4). This effectively increases the number of viable cell present during low temperature operation, which partially compensates for the significant decrease in rate of ammonia removal per nitrifying cell and enabled the technology to achieve long term, robust and efficient nitrification at 1° C.

References

Almomani FA, Delatolla R, Örmeci B (2014) Field study of moving bed biofilm reactor technology for post-treatment of wastewater lagoon effluent at 1° C. Environ Technol 35 (13):1596–1604

Canada Gazette (2012) Wastewater systems effluent regulations. Part II, 146(15), 18 July 2012

Delatolla R, Tufenkji N, Comeau Y, Gadbois A, Lamarre D, Berk D (2010) Investigation of laboratory-scale and pilot-scale attached growth ammonia removal kinetics at cold temperatures and low influent carbon. Water Qual Res J Can 45(4):427–436

EEC (1991) Council directive concerning urban waste-water treatment. OJEC 134(40)

Hoang V, Delatolla R, Abujamel T, Mottawea W, Gadbois A, Laflamme E, Stintzi A (2014) Nitrifying moving bed biofilm reactor (MBBR) biofilm and biomass response to long term exposure to 1° C. Water Res 49:215–224

Houweling D, Monette F, Millette L, Comeau Y (2007) Modelling nitrification of a lagoon effluent in moving-bed biofilm reactors. Water Qual Res J Can 42(4):284–294

Hurse TJ, Connor MA (1999) Nitrogen removal from wastewater treatment lagoons. Water Sci Technol 39:191–198

Randall CW, Buth D (1984) Nitrite build-up in activated sludge resulting from temperature effects. J Water Pollut Control Fed 56:1039–1044

Shammas NK (1986) Interactions of temperature, pH, and biomass on the nitrification process. J Water Pollut Control Fed 58:52–59

U.S. Environmental Protection Agency (USEPA) (2014) State development for nitrogen and phosphorus pollution

Young B, Delatolla R, Ren B, Kennedy K, Laflamme E, Stintzi A (2016) Pilot scale tertiary MBBR nitrification at 1° C: characterization of ammonia removal rate, solids settleability and biofilm characteristics. Environ Technol 37(16):2124–2132

Young B, Delatolla R, Kennedy K, Laflamme E, Stintzi A (2017) Low temperature MBBR nitrification: microbiome analysis. Water Res. doi:10.1016/j.watres.2016.12.050 (in press)

Proof of Concept of Removal of Carbon and Nitrogen from Wastewater Through a Novel Process of Biofilm SND

M.I. Hossain[1(✉)], L. Cheng[2], R.M.G. Flavigny[1],
and R. Cord-Ruwisch[1]

[1] School of Engineering and Information Technology,
Murdoch University, Murdoch, Perth 6150, Australia
{Md.Hossain,R.Cord-Ruwich}@murdoch.edu.au
[2] School of Civil and Environmental Engineering,
Nanyang Technological University, Singapore, Singapore
Lcheng@ntu.edu.sg

Abstract. A novel biofilm reactor is invented to remove carbon and nitrogen from wastewater with low energy consumption. This biofilm reactor contains glycogen accumulating organism (GAO) biofilm, zeolite powder and ammonium oxidizing bacteria (AOB) biofilm. Under anaerobic condition for 24 h, this unique biofilm structure enabled a removal of carbon and nitrogen from wastewater via PHBs/PHAs microbial synthetic pathway and ammonium physical adsorption on zeolite. After draining out the wastewater, the biofilm reactor was subjected to passive aeration for 24 h so that the adsorbed ammonium was oxidised by the AOB biofilm and the produced nitrite and nitrate were reduced by the GAO biofilm through denitrification using the stored PHBs/PHAs as electron donor. This simultaneous nitrification and denitrification, which was evident by a net production of nitrogen gas, led to regeneration of zeolite and GAO. Removal efficiencies were >99% for C and >80% for N. SND in air can be explained to be due to an oxygen gradient formed in the biofilm.

Keywords: Glycogen accumulating organism (GAO) · Biofilm · Simultaneous nitrification and denitrification

1 Introduction

Conventional wastewater treatment process using activated sludge has been reliably and extensively used to remove organic matter and nutrients from wastewater since its introduction 100 years ago. However, this treatment technology suffers from disadvantages such as high operational costs and dependency on a continuous energy supply. About one-third of the total operating cost of a wastewater treatment plant is attributed to energy requirements, and approximately 60–65% of the total energy consumption is used for aeration (Foley et al. 2010). This high energy costs is due to poor solubility of oxygen in bulk wastewater.

As one of the key wastewater components, removal of ammonium requires both nitrification and denitrification processes, which occur under different conditions. The

most common design to enable nitrification and denitrification is using two different reactors: one catering to the autotrophic bacteria and the second to the heterotrophic bacteria. However, simultaneous nitrification and denitrification (SND) can also accommodate to one reactor with strict control of dissolved oxygen. This has been achieved in an approach of producing bio-flocs with oxygen gradient inside. However, regardless of two separated reactors or single reactor, the key disadvantage of these system is the oxygen supply normally induces simultaneous oxidation of biological oxygen demand (BOD) partially, which usually results in an incomplete denitrification. Therefore, minimise the waste of BOD due to the oxidation with oxygen during nitrification phase is crucial to achieve more economical wastewater treatment process.

To address the aformentioned two major disadvantages of conventional wastewater treatment process, a novel engineered biofilm reactor was invented to evaluate the efficiency of carbon and nitrogen removal. The stability of the system was also tested by repeated cycles of treatment.

2 Materials and Method

2.1 Zeolite Amended Biofilms

Packing materials (AMB^{TM} Biomedia Bioballs) packed in a tubular container with an inner diameter of about 60 mm and a height of 75 mm. The bioreactor had a bed volume of about 250 mL and a void volume of about 100 mL. The packing materials were used as carrier for the BOD storage biomass biofilm formation (GAO) (Flavigny and Cord-Ruwisch 2003). Once the GAO biofilm was established, ammonium selective ion changer of zeolite (grain size of <0.3 mm) was coated on the surface of GAO biofilm and formed a zeolite coating layer. This zeolite coating layer was then used as carrier for ammonium oxidizing biomass (AOB) biofilm formation. 2 L of AOB culture with OD_{600} value of 1.2 was continuously flushed through the tubular column for 12 h until the OD_{600} value decreased to about 0.1, indicating more than 90% of AOB was attached to the zeolite layer. The dry weight ratio of GAO to AOB to zeolite was about 3.5:5:1. The structure of biofilm is illustrated in Fig. 1. The temperature of the reactor was kept at around 25°C and the pH value of the reactor was monitored.
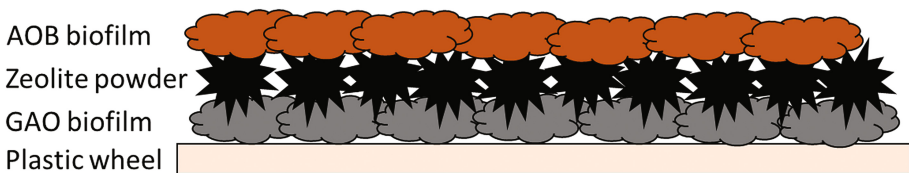
Fig. 1. Schematic diagram of zeolite modified biofilm

3   Experimental Setup and Operation

The wastewater treatment process was carried out using synthetic wastewater (Third et al. 2003) via two-stage operation mode (Fig. 2) At the stage one, a load of synthetic wastewater (350 mL) was up-flushed into the reactor and the biofilm was given 24 h anaerobic conditions to remove organic carbon and zeolite to adsorb ammonium. At the stage two, the introduced liquid was drained out mostly due to the gravity. Only a minimum amount of residual liquid (less than 50 mL) was remained and slowly circulated through the column so that the evolution of different components in the residual wastewater could be monitored. The top of the tubular container was open to enable oxygen passively venting through the porous packing materials. The biofilm coated on the carrier was exposed to air for 24 h. Repeated cycles of stage one and stage two treatment were carried out for the evaluation of system stability.
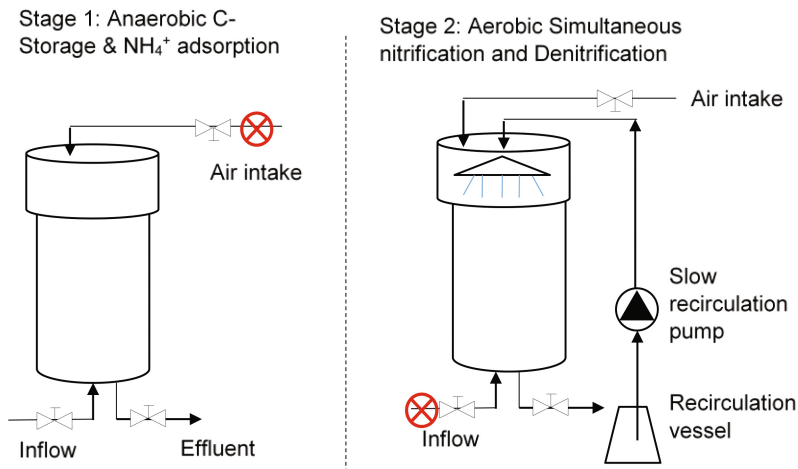
Fig. 2. Schematic diagram of the reactor operation including anaerobic phase of stage 1 and aerobic phase of stage 2

4   Results and Discussion

During the anaerobic phase (stage one), almost 100% organic carbon removal and more than 80% ammonium removal were achieved. (Figure 3). At stage two, a large fraction of the liquid (85%) was drained out to enable oxygen supply to the biomass. The remaining liquid (15%, 50 mL) was recirculated for 24 h. As expected, the introduction of oxygen through porous packing materials via passive aeration allowed nitrification of ammonium, which was then converted to nitrite and nitrate (Fig. 4). The total accumulative amount of nitrite and nitrate was larger than the amount of ammonium in the remained liquid, suggesting that ammonium adsorbed by zeolite was also nitrified and the produced end products (nitrite and nitrate) were released into the liquid phase. At later stage of stage two, the accumulative nitrite and nitrate decreased dramatically,
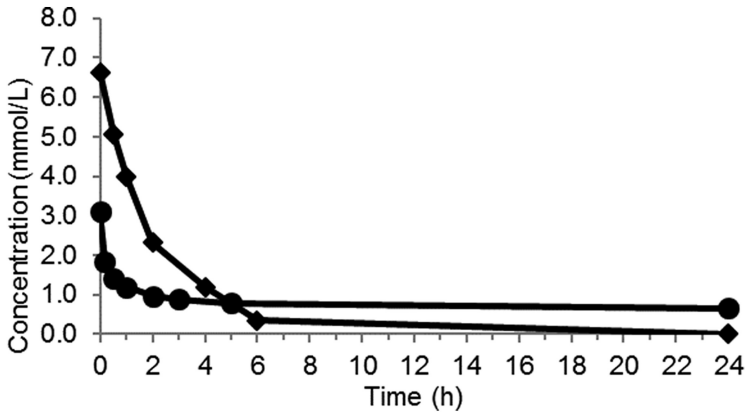
Fig. 3. Removal of acetate (♦) and ammonium (●) from three-void volume of wastewater during anaerobic phase (stage 1)
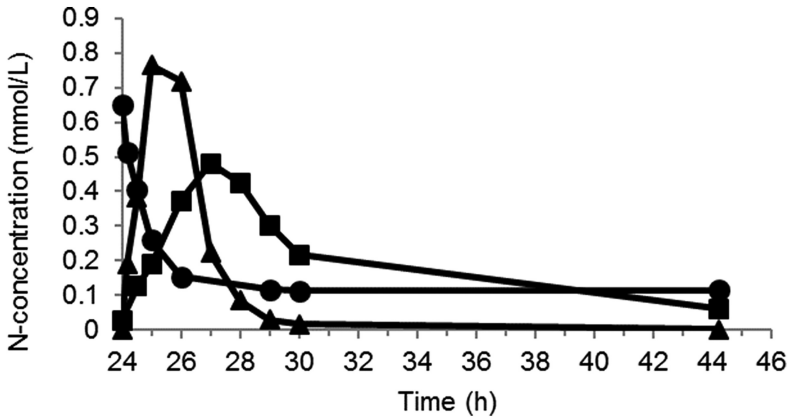
Fig. 4. Evolution of nitrogen components (ammonium (●), nitrite (▲) and nitrate (■)) during the aerobic phase (Stage 2)

indicating denitrification reaction occurred even under aerobic condition. This was also evident by nitrogen gas production (data not shown). At the stage two, the occurrence of SND reaction in full atmospheric oxygen condition is probably due to oxygen gradient in the biofilm.

The performance stability was evaluated by running 7 cycles of wastewater treatment continuously. It shows that a constant ammonium removal was achieved through ammonium adsorption on zeolite. It should be noted that a constant acetate removal efficiency higher than 99% was also achieved during the anaerobic stage (stage 1). It is interesting to note that the cumulative ammonium added to the reactor (100 mg-N or 7.1 mmol-N) was about twice higher than the total theoretical adsorption capacity of the zeolite (54 mg-N or 3.8 mmol-N) (Fig. 5), indicating a successful biological regeneration of zeolite.
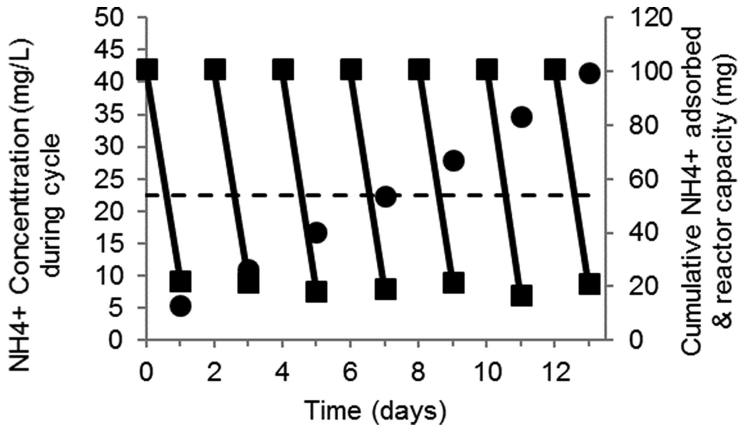
Fig. 5. Constant ammonium removal during repeated cycles of treatment. NH_4^+ concentration in individual cycles (■), cumulative ammonium added to the reactor (●) and theoretical zeolite adsorption capacity (- -)

5   Conclusions

Overall, the system developed in this work is a novel combination of biological and physical steps for carbon and nitrogen removal from wastewater. In the zeolite amended biofilm reactor, removal of organic carbon and ammonium was achieved at stage one by GAO and zeolite under anaerobic conditions. At stage two, the SND reaction under full atmospheric oxygen conditions was achieved, resulting in zeolite bio-regeneration as well as GAO regeneration through PHBs/PHAs oxidation. Over a medium-term operation, this novel biofilm reactor repeatedly removed soluble carbon and total nitrogen at a constant rate without need of bubbling oxygen. The findings from the current study indicate a sustainable atmospheric SND process, leading to a high-energy efficient wastewater treatment process since the technology avoids the high energy-consuming transfer of oxygen to the bulk wastewater.

References

Flavigny R, Cord-Ruwisch R (2003) Organic carbon removal from wastewater by a PHA storing biofilm using direct atmospheric air contact as oxygen supply. Biores Technol 187:182–188

Foley J, de Haas D, Hartley K, Lant P (2010) Comprehensive life cycle inventories of alternative wastewater treatment systems. Water Res 44(5):1654–1666

Third KA, Burnett N, Cord-Ruwisch R (2003) Simultaneous nitrification and denitrification using stored substrate (PHB) as the electron donor in an SBR. Biotechnol Bioeng 83(6):706–720

Effect of Salinity Variation on the Autotrophic Kinetics of the Start-up of Membrane Bioreactor and Hybrid Moving Bed Biofilm Reactor-Membrane Bioreactor at Low Hydraulic Retention Time

J.C. Leyva-Díaz[1,2(✉)], A. Rodríguez-Sánchez[1,2], J. González-López[3], and J.M. Poyatos[1,2]

[1] Department of Civil Engineering, University of Granada, Granada, Spain
[2] Institute of Water Research, University of Granada, Granada, Spain
[3] Department of Microbiology, University of Granada, Granada, Spain

Abstract. A membrane bioreactor (MBR) and a hybrid moving bed biofilm reactor-membrane bioreactor (hybrid MBBR-MBR) for municipal wastewater treatment were studied to determine the effect of salinity on the nitrogen removal and autotrophic kinetics. The biological systems were analyzed during the start-up phase under regular and variable salinities, with a hydraulic retention time (HRT) of 6 h. The variable salinity affected the autotrophic biomass, which caused a reduction of the nitrogen degradation rate and an increase of time to remove ammonium from municipal wastewater.

Keywords: Moving bed biofilm reactor · Autotrophic kinetics · Salinity

1 Introduction

The growing awareness of environmental protection has led to more stringent legislation regarding the treatment of saline wastewater before discharge. This aspect is especially important for activities such as the fish canning, petroleum, petrochemical and tannery industries, as well as the wastewater produced during shipboard activities that is characterized by high saline concentrations (Sun et al. 2010; Abdollahzadeh Sharghi et al. 2014).

In recent years, membrane bioreactor (MBR) systems have been applied to treat saline wastewater (Di Bella et al. 2013). To improve the performance of MBR regarding the pollutant removal and membrane filtration, the hybrid moving bed biofilm reactor-membrane bioreactor (hybrid MBBR-MBR) systems have been developed during the last years (Leyva-Díaz et al. 2014).

The analysis of available scientific literature shows a lack of knowledge in terms of autotrophic biomass respiratory activity in MBR and hybrid MBBR-MBR used to treat municipal wastewater under salinity variation. In light of this, kinetic modeling can be an important tool for design and operation of MBR and hybrid MBBR-MBR plants (Leyva-Díaz et al. 2014).

The aim of this study was to assess the effect of salinity on the autotrophic bacteria kinetics during the start-up of MBR and hybrid MBBR-MBR working at low hydraulic retention time (HRT) (6 h).

2 Materials and Methods

An MBR (Fig. 1a) and a hybrid MBBR-MBR (Fig. 1b), working in parallel, were fed with municipal wastewater containing regular (1.05 mS cm^{-1}) and variable salinity (1.2–6.5 mS cm^{-1}). These systems included a bioreactor divided into four zones: one anoxic zone and three aerobic ones, as well as a membrane tank. There was a biomass recycling from the membrane tank to the bioreactor to get the working mixed liquor suspended solids (MLSS) concentration and the nitrogen removal. The total biomass concentration for the steady state was 2,500 mg L^{-1}. Wastewater treatment plants (WWTPs) operated at HRT of 6 h. The working volumes of the bioreactor and the membrane tank were 24 L and 4.32 L, respectively, and the anoxic zone of the bioreactor had a volume of 6 L. Regarding the hybrid MBBR-MBR, the K1 media filling-fraction had a value of 35% in the aerobic zone and the anoxic zone did not
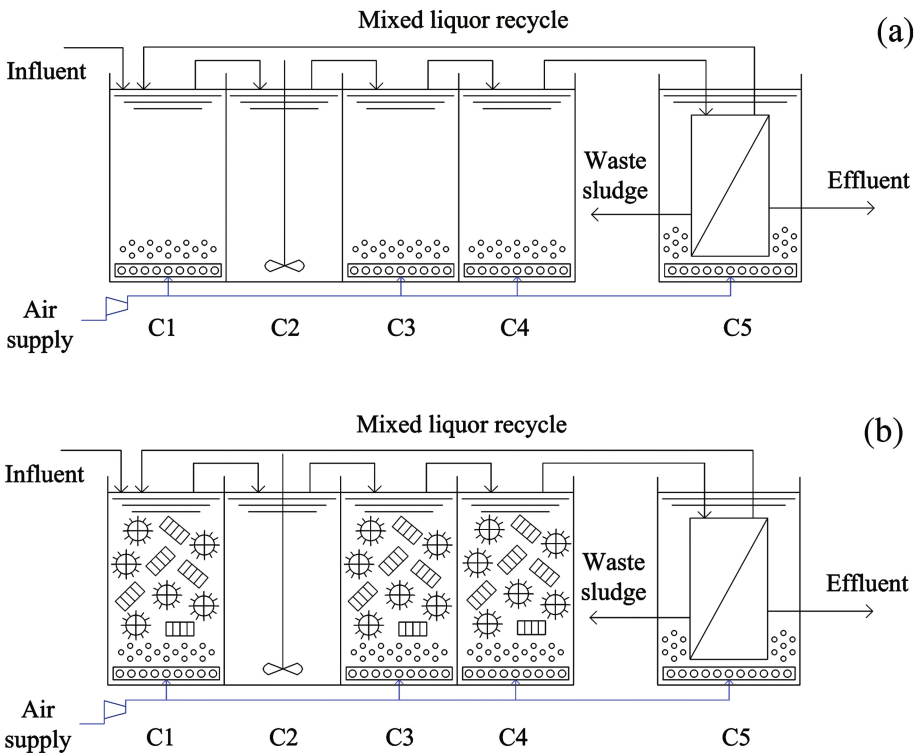
Fig. 1. Diagram of the experimental plants used in the study. (a) Membrane bioreactor (MBR). (b) Hybrid moving bed biofilm reactor-membrane bioreactor (hybrid MBBR-MBR).

contain carriers. Furthermore, the dissolved oxygen (DO) in the aerobic zone varied between 2.0 and 2.5 mg O_2 L^{-1} and DO in the anoxic zone fluctuated between 0.2 and 0.4 mg O_2 L^{-1}.

Respirometric tests were carried out on suspended biomass for the MBR. In order to evaluate the effect of biomass adhered to carriers, respirometric assays were performed on total biomass, suspended and attached, for the hybrid MBBR-MBR. Kinetic parameters for autotrophic bacteria and the total nitrogen (TN) degradation rate ($r_{su,A}$) were evaluated through respirometric techniques according to Leyva-Díaz et al. (2013). The evolution of the dynamic oxygen uptake rate (R_s) was registered from the respirograms obtained (Leyva-Díaz et al. 2013).

The concentrations of MLSS and mixed liquor volatile suspended solids (MLVSS) were calculated from standard methods (APHA 2012). The concentrations of autotrophic biomass (X_A) were determined by supposing the percentages of autotrophic bacteria that were obtained by Leyva-Díaz et al. (2015) for the same MBR and hybrid MBBR-MBR under similar operation conditions.

Thus, respirometric tests allowed for assessing the maximum specific growth rate ($\mu_{m,A}$), substrate half-saturation coefficient ($K_{M,A}$) and yield coefficient (Y_A) for autotrophic biomass. The assessment of these parameters was carried out in six steps:

(1) Determination of the oxygen consumption (OC) through the integration of R_s, as shown in Eq. (1):

$$OC = \int_{t_0}^{t} R_s dt \quad (mgO_2 \ L^{-1}) \tag{1}$$

(2) Estimation of Y_A according to Eq. (2) described by Helle (1999):

$$Y_A = \frac{S - OC}{S_{NH} \cdot f_{cv}} \quad (mgVSS \ mgTN^{-1}) \tag{2}$$

where S is the ammonium concentration expressed as oxygen (mgO$_2$ L^{-1}), S_{NH} is the ammonium concentration expressed as total nitrogen (mgTN L^{-1}) and f_{cv} is a conversion factor (1.42 mgO$_2$ mgVSS^{-1}).

(3) Evaluation of the substrate degradation rate (r_{su}) from R_s:

$$r_{su} = \frac{R_s}{1 - \frac{Y_A \cdot S_{NH} \cdot f_{cv}}{S}} \quad (mgO_2 L^{-1} h^{-1}) \tag{3}$$

(4) Assessment of the empirical specific growth rate (μ_{emp}) from the relation between the cell growth rate and r_{su}:

$$\mu_{emp} = \frac{\frac{1}{f_{cv}} \cdot R_s}{\left(1 - \frac{Y_A \cdot S_{NH} \cdot f_{cv}}{S}\right) \cdot X_A} \quad (h^{-1}) \tag{4}$$

where X_A is the concentration of autotrophic biomass (mgVSS L^{-1})

(5) Estimation of $\mu_{m,A}$ and $K_{M,A}$ through the linearization of the Monod model (Monod 1949):

$$\frac{1}{\mu_{emp}} = \frac{1}{\mu_{m,A}} + \frac{K_{M,A}}{\mu_{m,A}} \cdot \frac{1}{S_{NH}} \quad (h)$$
(5)

Therefore, the $r_{su,A}$ can be expressed as a function of the autotrophic kinetic parameters, as well as the substrate and biomass concentrations, as indicated in Eq. (6):

$$r_{su,A} = \frac{\mu_{m,A} \cdot S_{NH} \cdot X_A}{Y_A \cdot (K_{M,A} + S_{NH})}$$
(6)

3   Results and Discussion

Table 1 shows the autotrophic kinetic parameters for MBR and hybrid MBBR-MBR working at regular and variable salinities. It should be noted that the values of $\mu_{m,A}$ were higher for the systems operating under regular salinity than those obtained for the technologies working under variable salinity, which favored the substrate degradation rate. Moreover, the values of $K_{M,A}$ were higher for the systems working under variable salinity, which could be due to the inability of autotrophic biomass to use the whole substrate.

Table 1. Autotrophic kinetic parameters, $\mu_{m,A}$, $K_{M,A}$, Y_A, for the start-up of MBR and hybrid MBBR-MBR working under regular and variable salinity. Y_A (yield coefficient for autotrophic biomass), $\mu_{m,A}$ (maximum specific growth rate for autotrophic biomass), $K_{M,A}$ (half-saturation coefficient for ammonium nitrogen).

Salinity condition	Wastewater treatment plant	Y_A (mgVSS mgTN^{-1})	$\mu_{m,A}$ (h^{-1})	$K_{M,A}$ (mgTN L^{-1})
Regular (1.05 mS cm^{-1})	MBR	1.2684 ± 0.1522	0.1607 ± 0.0144	0.3887 ± 0.0390
	Hybrid MBBR-MBR	1.5681 ± 0.1725	0.3579 ± 0.0376	3.9188 ± 0.4311
Variable (1.2–6.5 mS cm^{-1})	MBR	1.5193 ± 0.2279	0.0145 ± 0.0017	15.5913 ± 1.8710
	Hybrid MBBR-MBR	1.6424 ± 0.2628	0.0128 ± 0.0013	35.7900 ± 3.7580

The multivariate analysis linking the operational conditions of the MBR and hybrid MBBR-MBR systems working with municipal wastewater under regular and variable salinity with the Monod growth model parameters clearly showed the influence of salinity and dissolved oxygen concentration in the autotrophic kinetics of the systems (Fig. 2). The yield coefficient for autotrophic biomass (Y_A) (purple triangle) and the half-saturation coefficient for ammonium nitrogen ($K_{M,A}$) (red triangle) had a positive correlation with conductivity and dissolved oxygen concentration in the aerobic zone.
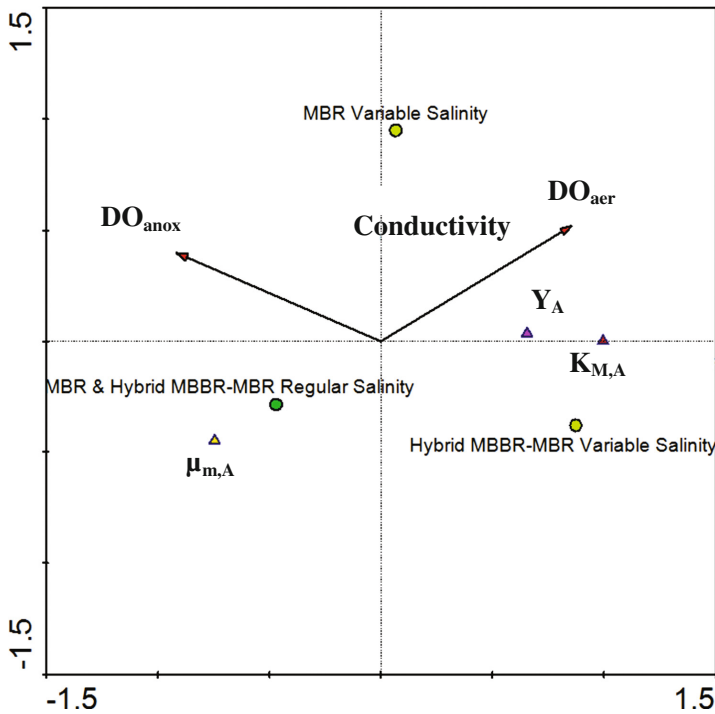
Fig. 2. Multivariate redundancy analysis triplot linking the autotrophic kinetics of MBR and hybrid MBBR-MBR systems working under regular and variable salinity wastewater with the conductivity and dissolved oxygen in the anoxic and aerobic chambers, DO_{anox} and DO_{aer}, respectively, of the bioreactors. (Color figure online)

On the other hand, the maximum specific growth rate for autotrophic biomass ($\mu_{m,A}$) (yellow triangle) was negatively correlated with electric conductivity and dissolved oxygen concentration in the aerobic zone.

In light of this, it was clearly shown that high variations of electric conductivity led to the lowest $r_{su,A}$ values concerning total nitrogen removal during the start-up of MBR and hybrid MBBR-MBR under variable salinity (Fig. 3). Therefore, the autotrophic kinetics was slower for the systems working under variable salinity. Johir et al. (2013) demonstrated an inhibitory effect of salinity on ammonium removal efficiency for an MBR system.

In this regard, it should be highlighted that autotrophic biomass required less time for ammonium oxidation during the start-up of MBR and hybrid MBBR-MBR working under regular salinity due to their higher $r_{su,A}$ (Fig. 3). Thus, a longer time would be required to accomplish the steady state for the systems working under variable salinity (Fig. 3).
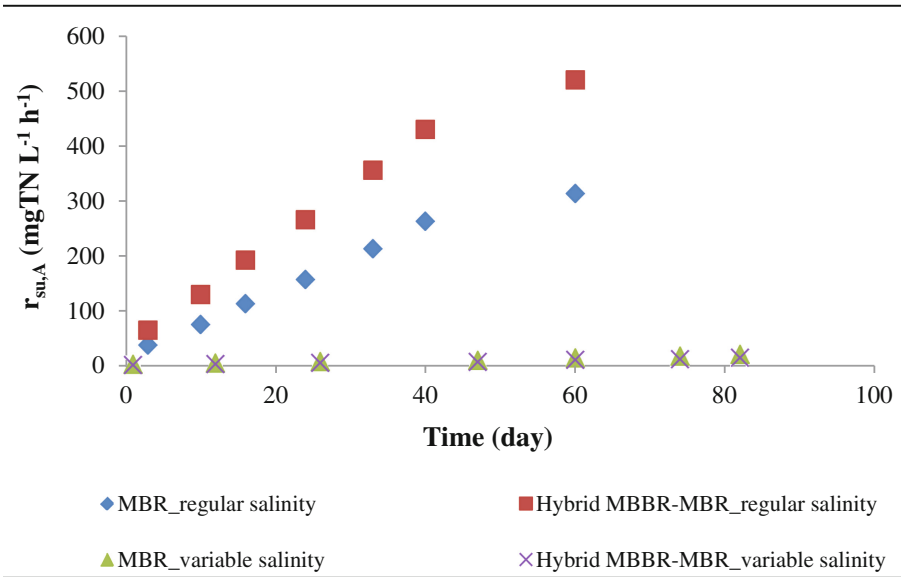
Fig. 3. Evolution of total nitrogen degradation rate ($r_{su,A}$) obtained in the autotrophic kinetic study for the MBR and hybrid MBBR-MBR under regular and variable salinity.

4   Conclusions

Variable salinity slowed down the total nitrogen degradation rate as a consequence of the reduction of the maximum specific growth rate for autotrophic biomass and the increase of the half-saturation coefficient for ammonium nitrogen. Thus, the autotrophic biomass could be inhibited by salinity, implying the inability of this kind of biomass to degrade ammonium substrate.

The MBR and hybrid MBBR-MBR systems that operated at regular salinity showed the highest values for total nitrogen degradation rate, which involved less time to oxidize ammonium during the start-up phase.

References

Abdollahzadeh Sharghi E, Bonakdarpour B, Pakzadeh M (2014) Treatment of hypersaline produced water employing a moderately halophilic bacterial consortium in a membrane bioreactor: effect of salt concentration on organic removal performance, mixed liquor characteristics and membrane fouling. Bioresour Technol 164:203–213

APHA (2012) Standard methods for the examination of water and wastewater, 22nd edn. American Public Health Association, Washington DC

Di Bella G, Di Trapani D, Torregrossa M, Viviani G (2013) Performance of a MBR pilot plant treating high strength wastewater subject to salinity increase: analysis of biomass activity and fouling behaviour. Bioresour Technol 147:614–618

Helle S (1999) A respirometric investigation of the activated sludge treatment of BKME during steady state and transient operating conditions. Thesis, University of British Columbia

Johir MAH, Vigneswaran S, Kandasamy J, BenAim R, Grasmick A (2013) Effect of salt concentration on membrane bioreactor (MBR) performances: detailed organic characterization. Desalination 322:13–20

Leyva-Díaz JC, Calderón K, Rodríguez FA, González-López J, Hontoria E, Poyatos JM (2013) Comparative kinetic study between moving bed biofilm reactor-membrane bioreactor and membrane bioreactor systems and their influence on organic matter and nutrients removal. Biochem Eng J 77:28–40

Leyva-Díaz JC, Martín-Pascual J, Muñío MM, González-López J, Hontoria E, Poyatos JM (2014) Comparative kinetics of hybrid and pure moving bed reactor-membrane bioreactors. Ecol Eng 70:227–234

Leyva-Díaz JC, González-Martínez A, González-López J, Muñío MM, Poyatos JM (2015) Kinetic modeling and microbiological study of two-step nitrification in a membrane bioreactor and hybrid moving bed biofilm reactor-membrane bioreactor for wastewater treatment. Chem Eng J 259:692–702

Monod J (1949) The growth of bacterial cultures. Annu Rev Microbiol 3:371–394

Sun C, Leiknes T, Weitzenbock J, Thorstensen B (2010) Development of a biofilm-MBR for shipboard wastewater treatment: the effect of process configuration. Desalination 250:745–750

Fish-Canning Wastewater Treatment by Means of Aerobic Granular Sludge for C, N and P Removal

R. Campo[1(✉)], P. Carrera-Fernández[2], G. Di Bella[1],
A. Mosquera-Corral[2], and A. Val del Río[2]

[1] Faculty of Engineering and Architecture, Università di Enna "Kore",
Cittadella Universitaria, 94100 Enna, Italy
[2] Department of Chemical Engineering, Institute of Technology,
Universidade de Santiago de Compostela, 15782 Santiago de Compostela, Spain

Abstract. This research work analyses the development of aerobic granular sludge to simultaneously remove organic matter (COD), nitrogen (N) and phosphorous (P), from saline fish-canning wastewater. A 1.6 L sequencing batch reactor (SBR) with volumetric exchange ratio (VER) of 50% and a hydraulic retention time (HRT) of 0.25 d, was used. The SBR was operated in 3-hours cycles comprising: 60 min anaerobic feeding, 112 min aeration, 7–1 min settling and 1–7 min effluent discharge. The salt concentration was approximately 10.4 ± 0.8 g NaCl/L, and the applied organic loading rate (OLR) of 5.4 ± 1.9 kg COD/(m^3·d). Under these working conditions, aerobic granules were observed after 34 days of operation, although some filamentous bacteria were present on the surface of the aggregates. The granular biomass had a concentration of volatile suspended solids (VSS) of 1.34 g VSS/L, a mean diameter of 1.35 mm and a density next to 11.5 g VSS/L$_{granule}$. However, after 41 days of operation a fluffy-flocculent suspension was formed, together with granules, probably due to the salinity and the fraction of slowly biodegradable COD of the feeding ($\approx 35\%$ of total COD). Good removal efficiencies of soluble COD were observed ($\approx 80\%$), while ammonium and phosphorous were mainly removed to cover the minimum metabolic demand of heterotrophic strains. In fact, the enrichment of the biomass with slow growing autotrophic and phosphorous accumulating bacteria, especially in a saline environment, require a longer time of operation.

Keywords: Aerobic granules · Nitrogen · Phosphorous · Saline wastewater

1 Introduction

The fish-canning sector constitutes often the main source of benefits for the local economy especially in coastal regions of the world. During the fish processing, huge amounts of wastewater are produced, mainly characterized by high salinity and high organic matter (COD) and nutrients content, mainly nitrogen (N) and phosphorous (P). Moreover, this wastewater presents a great variability of composition, which depends on the production period and the type of product and process used (Cristóvão et al. 2015).

The treatment of the fish-canning wastewater via biological processes is desirable since this is mainly constituted by organic biodegradable substances. However, wastewaters as those from the fish canneries, with high salt content, are known to be significantly difficult to treat by conventional biological methods hindering the appropriated performance of the biological processes and providing bad settling properties of the biomass (Zhao et al. 2016). So, the use of halophilic bacteria to attain high removal efficiencies, or the application of new technologies able to retain large biomass concentrations, are suggested as possible solutions. In this sense, aerobic granular sludge (AGS) based technologies are being under consideration, since they accumulate larger amounts of sludge, so resulting more compact than the conventional activated sludge (CAS) systems. This lower footprint of a AGS systems is due to the dense and compact self-aggregated microorganisms, which have high settleability, allow for high solids retention and treat high loading rates (Beun et al. 2002). Furthermore, the simultaneous removal of COD, N and P can be achieved in a single reactor due to the stratification of microbial populations inside the biomass granules (De Kreuk et al. 2005). For these reasons, the application of AGS is interesting for the treatment of fish-canning wastewater, since these factories are normally located in coastal areas with limited surface availability.

Among the biological processes occurring in the AGS the activity of the autotrophic bacteria, in special the nitrite-oxidizing bacteria (NOB), is known to be inhibited by the salt, while the ammonia-oxidizing bacteria (AOB) could not be affected at a salinity of 33 g NaCl/L (Bassin et al. 2011). However, the treatment of high saline fish canning wastewater (15 g NaCl/L) did not exert a detrimental effect on the operation of an AGS reactor removing only COD and N, although the granules formation was delayed (Figueroa et al. 2008). Moreover, an inhibition of phosphorous accumulating organisms (PAO) could be observed, caused by the salt or the accumulation of nitrite concentrations due to NOB loss of activity (Welles et al. 2014). On the other hand, Pronk et al. (2014), showed that the structure of granules remained stable, despite an increase in nitrite and reduction in PAO activity up to 33 g NaCl/L. This indicates the lack of precise information about the effects of the salt in these systems. The aim of this study is to evaluate the possibility to grow aerobic granular sludge, to simultaneously remove COD, N and P, from saline fish-canning wastewater.

2 Materials and Methods

A sequencing batch reactor (SBR) with a total volume of 2 L, a working volume of 1.6 L and a H/D ratio of 5.6 was used. The reactor was operated in 3-hours cycles comprising: 60 min anaerobic feeding from the bottom of the reactor, 112 min aeration, 7–1 min settling and 1–7 min effluent discharge. The volumetric exchange ratio (VER) was fixed at 50% and the hydraulic retention time (HRT) was kept at 0.25 d. The wastewater fed to the SBR was collected from a fish-canning factory located in the south of Galicia (Spain) with the composition described in Table 1. The SBR was inoculated with 0.8 L of activated sludge from the biological reactor in operation in the fish cannery, characterized by a sludge volumetric index (SVI) of 300 mL/(g TSS) and a concentration of volatile suspended solids (VSS) of 2.27 g VSS/L. The reactor was

Table 1. Composition of the fish canning wastewater fed to the SBR

	Stages (days of operation)			
	S-I (0–15)	S-II (16–22)	S-III (23–43)	S-IV (44–51)
Settling time (min)	7	4	1	7
COD_T (mg/L)	2075 ± 113	2162 ± 312	2045 ± 457	1273 ± 292
COD_S (mg/L)	1710 ± 231	1655 ± 282	1620 ± 459	900 ± 62
TSS (mg/L)	253 ± 74	288 ± 5	252 ± 128	275 ± 5
VSS (mg/L)	186 ± 30	220 ± 5	165 ± 61	210 ± 5
NH_4^+-N (mg/L)	104 ± 4	99 ± 4	104 ± 10	110 ± 4
PO_4^{3-}-P (mg/L)	21 ± 3	24 ± 8	19 ± 13	8 ± 1

operated for 51 days in four stages (S-I to S-IV) depending on the imposed settling time. Indeed, to avoid an initial excessive biomass washout and to favour the selection of microorganisms with the best settling properties, the settling time was gradually decreased from 7 to 1 min (S-I to S-III), and subsequently it was temporarily increased to 7 min to favour a higher retention of slower growing microorganisms. The salt concentration was approximately 10.4 ± 0.8 g NaCl/L, and the applied organic loading rate (OLR) of 5.4 ± 1.9 kg COD/(m^3·d).

The pH, conductivity, chemical oxygen demand (COD), ammonia, nitrate, nitrite, phosphate, total suspended solids (TSS), VSS concentrations and the SVI were determined according to the Standard Methods (APHA 2005). Total COD (COD_T) was measured directly in the sample and the soluble COD (COD_S) from the sample filtered through 0.45 μm pore size filters. The morphology and size distribution of the granules were measured regularly by using an Image Analysis procedure with a stereomicroscope (Stemi 2000-C, Zeiss). Biomass density, in terms of g VSS per litre of granules, was determined with dextran blue and following the methodology proposed by Beun et al. (2002).

3   Results and Discussions

3.1   Granulation Process

First small aggregates, average diameter of 450 μm, were observed after 6 days of operation (Fig. 1). The biomass concentration in the reactor was of 0.8 g VSS/L, with a density of 5.2 g VSS/L$_{granule}$ and the SVI after 5 min of settling (SVI$_5$) around 63 mL/g TSS. After 15 days of operation, the biomass increased up to 3.6 g VSS/L due to the accumulation of flocculent biomass which worsened the settling capacity (SVI$_5$ of 148 mL/g TSS). Therefore, in order to enhance the hydraulic selection of the heaviest granules, on day 16 the settling time was reduced to 4 min (Stage II). Then a significant biomass washout took place and the biomass decreased to 1.73 g VSS/L on the day 22. The SVI$_5$ further increased to 283.5 mL/g TSS caused by the flocculent biomass which hampered the biomass settling process. At this point, the settling time was further reduced to 1 min (Stage III). On day 34 of operation, only granules were
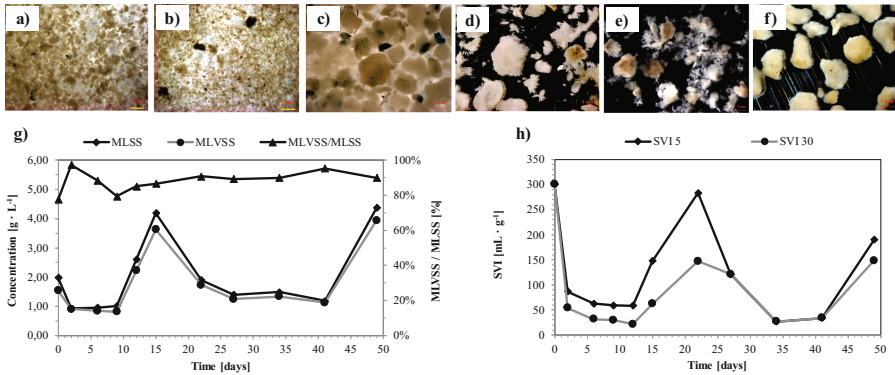
Fig. 1. Steps of granulation (magnification 6.5X, bar size 1 mm): (a) 6th day; (b) 15th day; (c) 22nd day; (d) 34th day; (e) 41st day; (f) 51th day; (g) evolution of mixed liquor total and volatile suspended solids concentrations; (h) evolution of sludge volume index

observed, at a concentration of 1.34 g VSS/L and with a mean diameter of 1.35 mm. The density was approximately 11.5 g $VSS/L_{granule}$ and the SVI_5 sharply decreased to 26.8 mL/g TSS, equal to the SVI after 30 min of settling (SVI_{30}). Then after 34 days of operation, the biomass inside the SBR was granular, although some filamentous bacteria were present on the surface of the aggregates.

On day 41, the shape of the granules became round. A *fluffy* suspension probably linked to the high salinity (Zhao et al. 2016) and the slowly biodegradable COD of the feeding (Pronk et al. 2015) was observed. This COD fraction represented approximately 35% of the total fed COD. The granules at this point had a mean diameter of 1.68 mm, a VSS concentration of 1.13 g VSS/L, a density of 18.6 g $VSS/L_{granule}$ and a $SVI_5 \approx SVI_{30}$ equal to 33.8 mL/g TSS. To favour the accumulation of slow-growing bacteria, on day 43 the settling time was temporary increased to 7 min. So, on the day 51 a mixture of both compact rounded granules and a fraction of flocculent biomass was present inside the reactor. Granules reached a mean diameter of 1.72 mm, a concentration of 3.12 g VSS/L, a density of 34.3 g $VSS/L_{granule}$, but also a high SVI_5 of 189.7 mL/g TSS.

3.2 C, N and P Removal Efficiencies

During the four operational stages, good removal efficiencies of COD_S were observed (Table 2). To date, ammonium and phosphorous were mainly removed to cover the minimum metabolic demand of heterotrophic strains. Indeed, the enrichment of the system with slow growing autotrophic and PAO, especially in a saline environment, require a longer time.

Table 2. Removal efficiencies in percentage (%) during the operational stages of the SBR

Parameter	S-I	S-II	S-III	S-IV
COD_S	62 ± 20	84 ± 10	79 ± 10	83 ± 9
NH_4^+-N	24 ± 14	29 ± 19	46 ± 15	12 ± 11
PO_4^{3}-P	36 ± 31	60 ± 15	81 ± 17	67 ± 30

4   Conclusions

Aerobic granular biomass was developed after 34 days from start up, treating fish-canning wastewater characterized by a high salinity (approximately 10.4 g NaCl/L) and slowly biodegradable COD fraction (about 35%). Simultaneous proliferation of flocculent biomass was observed subsequently, probably due to the salinity and/or the recalcitrant COD fraction of the feeding. Good removal efficiencies between 80–90% of soluble COD were observed. However, in a saline environment, a longer time is required for the microbial selection of slow-growing microorganisms able to remove ammonium and phosphorous.

References

APHA (2005) Standard methods for the examination of water and wastewater. American Water Works Association/American Public Works Association/Water Environment Federation

Bassin JP, Pronk M, Muyzer G, Kleerebezem R, Dezotti M, van Loosdrecht MCM (2011) Effect of elevated salt concentrations on the aerobic granular sludge process: linking microbial activity with microbial community structure. Appl Environ Microbiol 77:7942–7953

Beun JJ, Van Loosdrecht MCM, Heijnen JJ (2002) Aerobic granulation in a sequencing batch airlift reactor. Water Res 36:702–712

Cristóvão RO, Botelho CM, Martins RJE, Loureiro JM, Boaventura RAR (2015) Fish canning industry wastewater treatment for water reuse – a case study. J Clean Prod 87:603–612

De Kreuk MK, Heijnen JJ, Van Loosdrecht MCM (2005) Simultaneous COD, nitrogen, and phosphate removal by aerobic granular sludge. Biotechnol Bioeng 90:761–769

Figueroa M, Mosquera-Corral A, Campos JL, Méndez R (2008) Treatment of saline wastewater in SBR aerobic granular reactors. Water Sci, Technol

Pronk M, Abbas B, Al-zuhairy SHK, Kraan R, Kleerebezem R, van Loosdrecht MCM (2015) Effect and behaviour of different substrates in relation to the formation of aerobic granular sludge. Appl Microbiol Biotechnol 99:5257–5268

Pronk M, Bassin JP, De Kreuk MK, Kleerebezem R, Van Loosdrecht MCM (2014) Evaluating the main and side effects of high salinity on aerobic granular sludge. Appl Microbiol Biotechnol 98:1339–1348

Welles L, Lopez-Vazquez CM, Hooijmans CM, Van Loosdrecht MCM, Brdjanovic D (2014) Impact of salinity on the anaerobic metabolism of phosphate-accumulating organisms (PAO) and glycogen-accumulating organisms (GAO). Appl Microbiol Biotechnol 98:7609–7622

Zhao Y, Park H-D, Park J-H, Zhang F, Chen C, Li X, Zhao D, Zhao F (2016) Effect of different salinity adaptation on the performance and microbial community in a sequencing batch reactor. Bioresour Technol 216:808–816

Preliminary Evaluation of Sharon-Anammox Process Feasibility to Treat Ammonium-Rich Effluents Produced by Double-Stage Anaerobic Digestion of Food Waste

S. Milia[1]([✉]), G. Tocco[2], G. Erby[1], G. De Gioannis[2], and A. Carucci[2]

[1] National Research Council, Institute of Environmental Geology
and Geoengineering (IGAG-CNR), Rome, Italy
[2] Department of Civil-Environmental Engineering and Architecture,
University of Cagliari, Cagliari, Italy

Abstract. In this study, a Sharon-Anammox system was started up and fed with an ammonium-rich (1,500 $mgNH_4$-N L^{-1}) synthetic medium simulating the effluent produced by double-stage anaerobic digestion of food waste (AD-FW). The effects of different process parameters (e.g., hydraulic retention time, nitrogen loading rate, etc.) and influent characteristics (e.g., influent alkalinity) on reactors performance were thoroughly evaluated. As to the Sharon reactor, reducing the hydraulic retention time did not cause any detrimental effect on overall process performance (the observed NH_4-N removal efficiency and effluent NO_2-N/NH_4-N molar ratio were $60.8 \pm 4.5\%$ and 1.58 ± 0.27, respectively), although a slightly longer time was required to achieve process stability. The Anammox reactor was able to withstand the same nitrogen loading rates applied to the Sharon unit, and the observed nitrogen removal rate was high ($89.9 \pm 0.5\%$), indicating good process performance. The information gathered in this preliminary study will be useful for the treatment of real AD-FW wastewater.

Keywords: Anaerobic digestion · Anammox · Autotrophic nitrogen removal · Partial nitritation

1 Introduction

Due to its increasing production observed in recent years, the eco-sustainable management of food waste (FW) has become a challenging environmental priority. The attractive possibility to modify the anaerobic digestion (AD) process of such wastes in order to achieve the recovery of energy as a mixture of H_2 and CH_4 (biohythane), rather than only CH_4, is currently under investigation (Roy and Das 2016). However, since AD has no significant effect on nitrogen, its liquid effluents are characterized by high ammonium concentrations (>1,000 $mgNH_4$-N L^{-1}) and represent, if not properly managed, a threat to the environment. In order to develop a truly eco-sustainable approach, maximization of energy recovery from FW by anaerobic digestion (AD-FW) must be considered as important as the minimization of its potential environmental impacts.

   Within this framework, a double-stage system based on Sharon (Single reactor for High activity Ammonia Removal Over Nitrite) and granular sludge Anammox (ANaerobic AMMonium OXidation) was started up in this study, and fed with a synthetic influent simulating the NH_4-N content and alkalinity of real wastewater produced by an AD-FW system aimed at the recovery of H_2 and CH_4. In order to determine the best operating conditions, different hydraulic retention times (HRT) and nitrogen loading rates (NLR) were tested for both reactors, and the effects of other process parameters and influent characteristics on reactors performance were thoroughly evaluated. Moreover, acute toxicity assessments and prolonged exposure tests were carried out to evaluate the response of unacclimated biomass to the real AD-FW wastewater.

   A comprehensive set of information was gathered, which will be helpful for the progressive replacement of the synthetic influent with real AD-FW wastewater.

2   Materials and Methods

The Sharon unit consisted in a 2 L continuous flow stirred tank reactor operated as a chemostat (without biomass recirculation) at controlled temperature (35 ± 0.5 °C). The reactor was inoculated with activated sludge drawn from the municipal wastewater treatment plant of Cagliari (Italy). The plan of the experimental activity for the Sharon unit is summarised in Table 1. For each HRT tested, the reactor was started-up with fresh activated sludge.

Table 1. Plan of the experimental activity and main operating conditions for the Sharon unit

Phase	Duration (d)	NH_4-N inf. (g L^{-1})	NLR (gN L^{-1} d^{-1})	HRT (d)	Alkalinity/NH_4-N molar ratio (-)	Dissolved Oxygen (DO) (mg L^{-1})
S1	59	1.5	1.0	1.5	1.0[a]	$\sim$ sat.
S2	54	1.5	1.2	1.25	1.0	$\sim$ sat.
S3	60	1.5	1.5	1.0	1.0	$\sim$ sat.
S4	30	1.5	1.5	1.0	1.0	2.0
S5	21	1.5	1.5	1.0	1.3[b]	2.0
S6	21	1.5	1.5	1.0	1.3	1.5
S7	6	1.5	1.5	1.0	1.3	1.0

[a] typical value reported in literature for synthetic influents of partial nitrition reactors.
[b] average value observed in real AD-FW wastewater.

   As to the Anammox unit, a 2 L sequencing batch reactor (SBR) was operated at controlled temperature (35 ± 0.5 °C) and pH (7.0 ± 0.1), and inoculated with granular Anammox biomass originating from a previous experimental campaign. The 6-hour cycle configuration consisted of 200–267 min feeding, 83–150 min reaction, 5 min settling and 5 min effluent withdrawal. Table 2 shows the plan of the experimental activity for the Anammox unit.

Table 2. Plan of the experimental activity and main operating conditions for the Anammox unit

Phase	Duration (d)	NH_4-N inf. (g L^{-1})	NO_2-N inf. (g L^{-1})	Influent NO_2-N/NH_4-N molar ratio (-)	NLR (gN L^{-1} d^{-1})	HRT (d)
A1	35	0.70	0.80	1.15	1.0	1.5
A2	43	0.70	0.80	1.15	1.2	1.25
A3	176	0.70	0.80	1.15	1.5	1.0
A4	96	0.65	0.85	1.30	1.5	1.0

Both the Sharon and the Anammox reactors were fed with a synthetic influent. As to the Sharon reactor, the composition of the synthetic medium was: NH_4HCO_3 8,466 mg L^{-1}, KH_2PO_4 1,000 mg L^{-1}, $MgSO_4 \cdot 7H_2O$ 100 mg L^{-1}, $NaHCO_3$ 0–2,700 mg L^{-1}, and trace elements solution (Milia et al. 2015) 10 mL L^{-1}. As to the Anammox reactor, the composition of the synthetic medium was: NH_4HCO_3 3,848–3,938 mg L^{-1}, $NaNO_2$ 3,952–4,030 mg L^{-1}, $MgSO_4 \cdot 7H_2O$ 200 mg L^{-1}, KH_2PO_4 6.25 mg L^{-1}, $CaCl_2$ 300 mg L^{-1}, $FeSO_4 \cdot 7H2O$ 12.5 mg L^{-1} and trace elements solution (Van de Graaf et al. 1996) 1.25 mL L^{-1}.

Acute toxicity batch assessments were carried out as described by Ficara and Rozzi (2001) on unacclimated biomass drawn from the Sharon reactor, using real AD-FW wastewater produced by a two-stage anaerobic digestion process aimed at the recovery of H_2 and CH_4 from food waste. Prolonged exposure tests were carried out on the Sharon reactor by temporarily replacing the synthetic influent with real AD-FW wastewater, using different exposure times. Specific Anammox activity (SAA) was determined as described by Lotti et al. (2014).

Microbiological characterization was performed by fluorescence in situ hybridization (FISH) on representative biomass samples, according to Amann et al. (1990). Hybridizations with group specific probes for ammonium oxidizing bacteria (NSO1225, NSO190), nitrite oxidizing bacteria (NTSPA and NIT3), and Anammox bacteria (AMX820, AMX368 and PLA46) were carried out simultaneously with probes EUB338, EUB338-II and EUB338-III combined in a mixture (EUB338mix) for the detection of most bacteria, and with DAPI staining for quantifying the total number of cells. All probes were purchased from MWG-Biotech (Germany), and synthesized with 5'-FITC (green) and 5'-Cy3 (red) labels. Details on oligonucleotide probes are available at ProbeBase (Loy et al. 2007). Slides were examined with an epifluorescence microscope (Olympus BX51) at different magnifications (100, 400 and 1000x); images were captured with an Olympus XM10 camera using Cell-F software (Olympus, Germany). DAIME software (Daims et al. 2006) was used for FISH quantification of hybridized cells.

3   Results and Discussion

As to the Sharon reactor, partial nitrition was successfully achieved at each applied HRT (Fig. 1), and NO_3-N production remained always below 3% of total influent nitrogen, indicating the successful washout of nitrite oxidizing bacteria (NOB). However, a slightly longer period was required to achieve stable NH_4-N removal efficiencies at the lowest
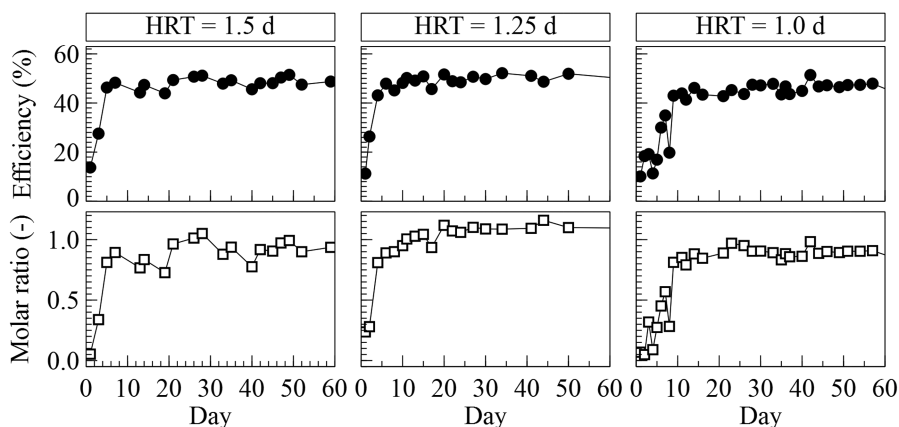
Fig. 1. Time profiles of ammonium removal efficiency (●) and effluent NO_2-N/NH_4-N molar ratio (□) during Phases S1, S2 and S3 of the Sharon reactor

HRT tested (it took 6, 5 and 11 days for HRT of 1.5, 1.25 and 1 d, respectively), due to the combined effect of low solids retention time and increased NLR.

According to FISH analysis (Fig. 2a and b), ammonium oxidizing bacteria were found to be dominant in the system (74% of total bacteria), and confirmed the almost complete washout of NOB (3% of total bacteria).

Overall process performance did not change substantially, as summarised in Table 3. In particular, both NH_4-N removal efficiency and effluent NO_2-N/NH_4-N molar ratio were lower than the stoichiometric values (i.e. 50% and 1.0, respectively), given the influent Alkalinity/NH_4-N molar ratio of 1 and irrespective of the DO concentrations tested.

During Phase S5, increasing the Alk/NH_4-N molar ratio up to the average value observed in real AD-FW wastewater (i.e., 1.3) led to a corresponding increase in both NH_4-N removal efficiency (from 47.0 ± 2.3 to $60.8 \pm 4.5\%$) and effluent NO_2-N/NH_4-N molar ratio (from 0.89 ± 0.09 to 1.58 ± 0.27), compared to Phase S4. Surprisingly, good process performance was maintained even when DO concentration was reduced to 1.5 ppm (Phase S6), which is lower than DO levels usually adopted in conventional wastewater treatment plants; however, such interesting behavior must be confirmed with real AD-FW wastewater, where organics are also present. Further decrease in DO concentration (Phase S7) led to irreversible worsening of process performance (Fig. 3).

Acute toxicity assessments carried out on unacclimated biomass drawn from the Sharon reactor showed the strong toxicity of real AD-FW even at low concentrations (IC50 dosages ranged from 11 to 47 mL L^{-1}, with a strong positive correlation with VSS concentration). On the contrary, prolonged exposure tests (exposure times of 1 h, 2 h, 4 h and 8 h) showed an increase in process performance, which was directly proportional to exposure time. During the 8 h-long test, NH_4-N removal efficiency and effluent NO_2-N increased from 47% to 56%, and from 726 to 848 mg L^{-1}, respectively: this positive effect progressively decreased after switching back to the synthetic
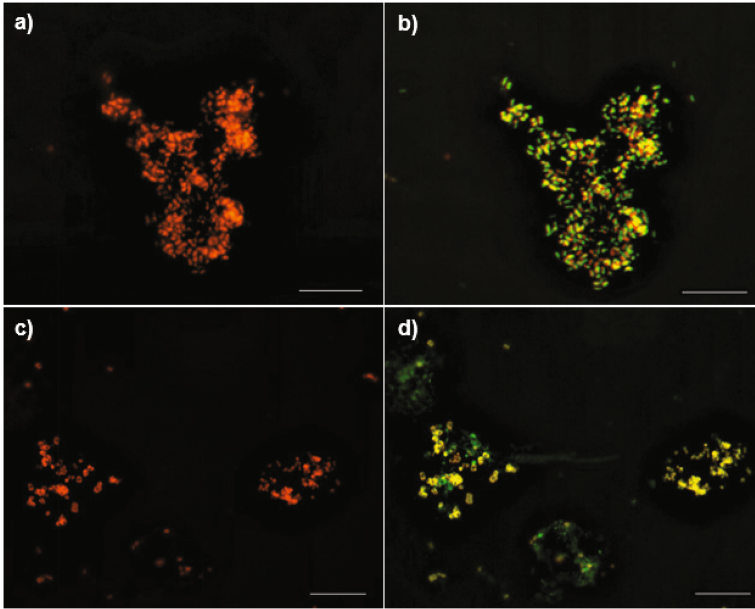
Fig. 2. FISH micrographs of Sharon biomass samples drawn at the end of Phase S3: (a) Cy3-labeled ammonium oxidizing bacteria (NSO1225 probe); (b) overlapping of FITC-labeled EUBmix and Cy3-labeled NSO1225 probes, resulting in yellow AOB cells. FISH micrographs of Anammox biomass samples drawn at the end of Phase A4: (c) Cy3-labeled anammox bacteria (AMX820 probe); (d) overlapping of FITC-labeled EUBmix and Cy3-labeled AMX820 probes, resulting in yellow anammox cells. Scale bar is 20 μm (Color figure online)

Table 3. Average Sharon performances during Phases S1 to S4

Phase	Effluent NH$_4$-N (mg L^{-1})	Effluent NO$_2$-N (mg L^{-1})	Effluent NO$_3$-N (mg L^{-1})	Effluent NO$_2$-N/NH$_4$-N molar ratio (-)	NH$_4$-N removal efficiency (%)
S1	787 ± 52	627 ± 66	7.7 ± 3.4	0.90 ± 0.09	48.2 ± 2.2
S2	756 ± 33	781 ± 42	19.6 ± 1.9	1.04 ± 0.08	49.2 ± 2.0
S3	799 ± 30	721 ± 20	10.3 ± 3.3	0.90 ± 0.05	46.4 ± 2.2
S4	802 ± 41	714 ± 43	10.8 ± 3.5	0.89 ± 0.09	47.0 ± 2.3

feeding, and it was related to the combination of AD-FW wastewater high alkalinity and dilution rate in the chemostat, which avoided inhibition.

As to the Anammox reactor, a fairly stable behaviour was observed throughout the whole experiment (Fig. 4): nitrite discharge rate (NitDR) was negligible (mostly zero), the NRR (nitrogen removal rate) to NLR ratio (NRR/NLR) was 97 ± 4%, and the total nitrogen removal efficiency (NRE) was 89 ± 4%, indicating good process performance. The observed removed NH$_4$-N/removed NO$_2$-N/produced NO$_3$-N ratio was 1/1.24 ± 0.10/0.19 ± 0.02 during Phases A1 through A3. During Phase A4, a higher influent NO$_2$-N/NH$_4$-N ratio was applied, mainly resulting in a slight increase in
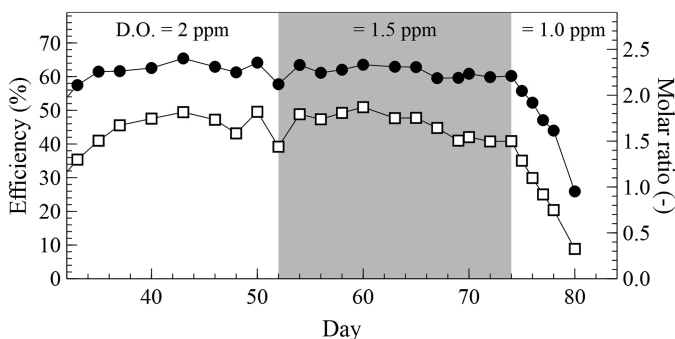
Fig. 3. Time profiles of ammonium removal efficiency (●) and effluent NO_2-N/NH_4-N molar ratio (□) during Phase S5 (D.O., 2 ppm), S6 (D.O., 1.5 ppm) and S7 (D.O., 1 ppm) of the Sharon reactor
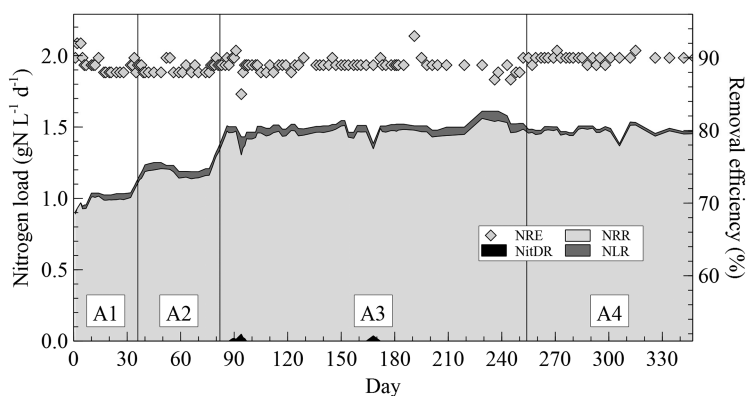
Fig. 4. Time profiles of NLR, NRR, NitDR and NRE in the Anammox unit

overall performance (NRR/NLR ratio and NRE increased to $98.5 \pm 0.5\%$ and $89.9 \pm 0.5\%$, respectively).

SAA showed an increasing trend as the applied NLR was increased (Phases A1–A3), while no substantial differences were observed between Phases A3 and A4 (Fig. 5).

As expected, FISH analysis confirmed the abundance of Anammox bacteria (Fig. 2c and d), which accounted for $66 \pm 1.8\%$ of total bacteria (Phase A4), in agreement with previously reported studies (Van der Star et al. 2007).
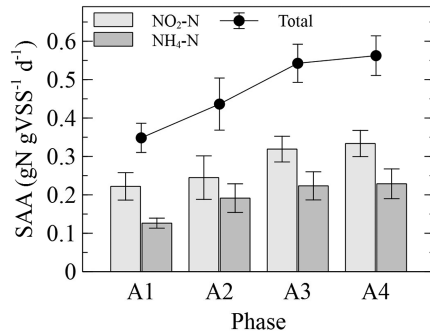
Fig. 5. Average specific Anammox activity (SAA) observed during Phases A1, A2, A3 and A4

4   Conclusions

Based on the results observed, the following main conclusions can be drawn:

- reducing the HRT in the Sharon reactor did not cause any significant effect on process performance, although a slightly longer time was required to achieve process stability;
- increasing synthetic influent alkalinity up to typical values of real AD-FW wastewater led to an improvement of Sharon reactor performance, which produced an effluent suitable to be treated by Anammox even at low DO concentrations (1.5 ppm);
- although acute toxicity batch assessments showed a potential toxicity of real AD-FW wastewater, prolonged exposure tests (continuous operation) showed an improvement of process performance, suggesting the combination of AD-FW wastewater high alkalinity and dilution rate in the chemostat as a possible key factor to avoid inhibition and process failure when switching to real AD-FW wastewater;
- granular Anammox SBR was able to withstand the same NLRs applied to the Sharon unit, and the increase of influent NO_2-N/NH_4-N molar ratio (corresponding to higher NH_4-N removal rates in the Sharon reactor) led to an increase in NRE.

The information gathered in this study will be useful for the treatment of real AD-FW wastewater.

References

Amann R, Krumholz L, Stahl DA (1990) Fluorescent-oligonucleotide probing of whole cells for determinative, phylogenetic, and environmental studies in microbiology. J Bacteriol 172 (2):762–770

Daims H, Lücker S, Wagner M (2006) Daime, a novel image analysis program for microbial ecology and biofilm research. Environ Microbiol 8:200–213

Ficara E, Rozzi A (2001) pH-stat titration to assess nitrification inhibition. J Environ Eng 127:698–704

Loy A, Maixner F, Wagner M, Horn M (2007) ProbeBase - an online resource for rRNA-targeted Oligonucleotide probes: new features. Nucleic Acids Res 35:800–804

Lotti T, Kleerebezem R, Lubello C, Van Loosdrecht MCM (2014) Physiological and kinetic characterization of a suspended cell anammox culture. Water Res 60:1–14

Milia S, Perra M, Cappai G, Carucci A (2015) SHARON process as preliminary treatment of refinery wastewater with high organic carbon-to nitrogen ratio. Desalin Water Treat 57:17935–17943

Roy S, Das D (2016) Biohythane production from organic wastes: present state of art. Environ Sci Pollut Res 23:9391–9410

Van de Graaf AA, De Bruijn P, Robertson LA, Jetten MSM, Kuenen JG (1996) Autotrophic growth of anaerobic ammonium-oxidizing microorganisms in a fluidized bed reactor. Microbiology+ 142:2187–2196

Van der Star WRL, Abma W, Blommers D, Mulder J-W, Tokutomi T, Strous M, Picioreanu C, Van Loosdrecht MCM (2007) Startup of reactors for anoxic ammonium oxidation: experiences from the first full-scale anammox reactor in Rotterdam. Water Res 41:4149–4163

Shipboard Slop Treatment by Means of Aerobic Granular Sludge: Strategy Proposal for Granulation and Hydrocarbons Removal

R. Campo$^{(\boxtimes)}$ and G. Di Bella

Faculty of Engineering and Architecture, Università di Enna "Kore",
Cittadella Universitaria, 94100 Enna, Italy

Abstract. This study investigates the possibility to achieve aerobic granulation for the treatment of saline shipboard slop wastewater to remove hydrocarbons. Two sequencing batch reactors (SBR) with a working volume of 3.5 L, were used. In the first reactor (R1), granules were previously cultivated with a step-wise increase of salinity and, subsequently, they were gradually adapted to hydrocarbons. In the second reactor (R2), granules were simultaneously adapted to a gradual increase of salinity and hydrocarbons. Both the reactors were operated with an organic loading rate (OLR) of 1.6 KgCOD·m^{-3}·d^{-1}, by setting a 6-hours cycle. The volumetric exchange ratio (VER) was fixed at 50% and the hydraulic retention time (HRT) was kept at 0.5 days. Five parallel phases of 30 days-duration were studied. When only slop was fed to reactor, in R1 the total suspended solids (TSS) and granules dimension decreased till about 4.7 g·L^{-1} and 1.25 mm respectively, probably due to a metabolic inhibition and a breakage of granules. In R2 the TSS concentration stabilized on a value next to 4.4 g·L^{-1} and no degranulation was observed (mean diameter $\approx$ 1 mm), probable due to a biological adaptation and a biodegradation of the adsorbed recalcitrant fraction. In R1, the reduction of total petroleum hydrocarbons (TPH) in liquid phase and the increase of TPH on granules, confirmed that a physical bioadsorption effect was dominant. In R2 a decreasing trend of TPH bioadsorbed on granules, together with a contextual depletion in liquid phase, suggested a probable occurrence of hydrolysis and biodegradation of the bioadsorbed hydrocarbons.

Keywords: Aerobic granular sludge · Saline wastewater · Hydrocarbons

1 Introduction

Sea pollution due to the direct discharge of shipboard wastewater is a question of relevant environmental impact. Slop wastewaters are produced from the washing of oil tankers with sea water and their direct discharge to the sea is strictly prohibited by IMO-Marpol 73/78 regulation. This kind of shipboard wastewater is characterized by high salinity and high recalcitrant fraction mainly made of hydrocarbons. The treatment of slops is not easy to achieve mainly due to their heterogeneous composition, and the presence of emulsified oils. Chemical processes are commonly used to treat industrial wastewater, ensuring high removal efficiencies but they imply high operational costs,
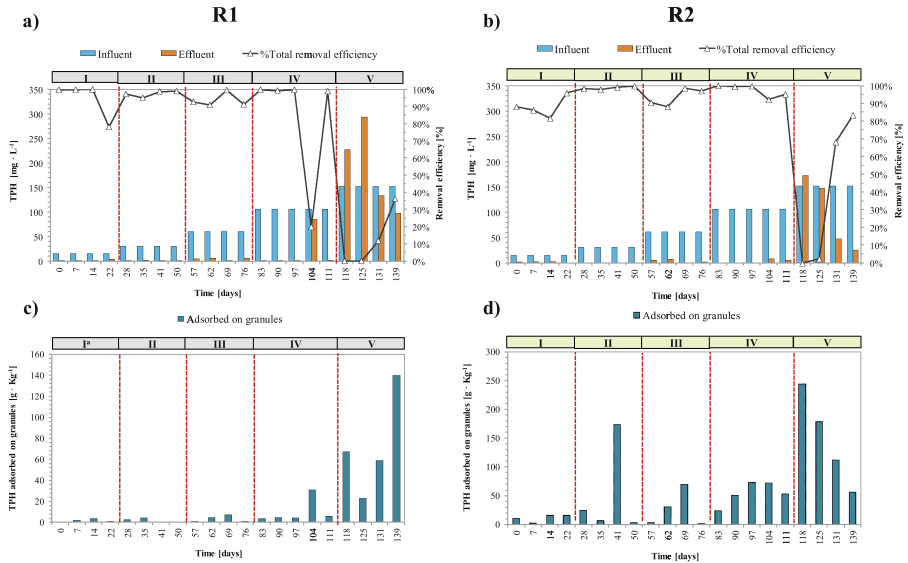
Fig. 1. TPH in liquid and in solid phase in R1 ((a) and (c)) and in R2 ((b) and (d)), respectively

related to the use of chemicals, and a considerable environmental impact. On the other hand, biological processes are environmental-friendly but, at the same time, they are more delicate to face the biodegradation of recalcitrant substrate in high salinity operational conditions. So, it is necessary to adapt microorganisms to hard environment conditions like the presence of salt and/or of slowly biodegradable substrates, to achieve good removal efficiencies. One of the most promising biological technologies based on the self-aggregation of microorganisms is represented by the aerobic granular sludge (AGS) reactors (De Kreuk et al. 2005). Aerobic granules are generated under sequential batch operational conditions and ensure the possibility to simultaneously remove carbon, nitrogen and phosphorous by means of their stratified structure in more layers with aerobic, anoxic and anaerobic microenvironments. Recently, an emerging research topic relating the AGS technology is the ability of granules to bio-adsorb the particulate fractions of industrial wastewater, so increasing the contact time between the substrates and the microorganisms and promoting the hydrolysis and biodegradation of the more recalcitrant fractions. Previously, it was studied the possibility to cultivate granular sludge with slop wastewater (Corsino et al. 2015). However, it has not been investigated the single effect of salinity and hydrocarbons, as well as the bioadsorption of recalcitrant substrate on granules' surface when a 100% volume of real slop wastewater is fed to reactor. The aim of this study is to evaluate the best granulation strategy for hydrocarbons removal in a high saline environment. In particular, a comparison between the treatment with mature granules previously adapted to salinity and with granules simultaneously cultivated with salinity and hydrocarbons, was assessed.

2 Materials and Methods

Two sequencing batch reactors (SBRs), hereinafter called R1 and R2, with a working volume of 3.5 L and a H/D ratio of 10, were used. The reactors were operated in 6-hours cycles comprising: 20 min feeding, 320–333 min aeration, 2–15 min settling and 5 min effluent discharge. The volumetric exchange ratio (VER) was fixed at 50% and the hydraulic retention time (HRT) was kept at about 0.5 d. Shipboard slops were collected from barges located in an oil costal deposit in the Augusta harbour in Sicily (Italy) and they were fed to reactors after a preliminary step of de-oiling to remove a high portion of floating oil & greases. Slops were mainly characterized by a total chemical oxygen demand (COD_T) of 816 ± 94 mg•L^{-1}, a soluble chemical oxygen demand (COD_S) of 530 ± 32 mg•L^{-1}, a total organic carbon (TOC) of 390 ± 3 mg•L^{-1}, total petroleum hydrocarbons (TPHs) of 151 ± 3 mg•L^{-1}, chlorides concentration next to 24 ± 0.12 g Cl^{-}•L^{-1} and a pH of 7.78 ± 0.62. In order to better understand the best way to treat this kind of recalcitrant wastewater, granules in R1 were previously cultivated with a stepwise increase of salinity and, in this study, they were gradually adapted to hydrocarbons. On the other hand, in R2 granules were simultaneously adapted to a gradual increase of salinity and hydrocarbons. In both reactors, five parallel phases of 30 days-duration were studied (Table 1). In order to ensure a stepwise increase of salt and hydrocarbons and to obtain an almost constant OLR next to 1,6 KgCOD•m^{-3}•d^{-1} throughout all the experimental period, a mixture of synthetic wastewater and a real slop wastewater was prepared. The synthetic wastewater was characterized by the following stoichiometric proportions (Beun et al. 2002): $C_2H_3NaO_2$ 97.7 mM, $MgSO_4$ • $7H_2O$ 3.7 mM, K_2HPO_4 20 mM, KH_2PO_4 10 mM, KCl 4.8 mM, NH_4Cl 30 mM. From Phase I to Phase V, a progressive reduction of synthetic wastewater and a simultaneous increase of slop volume fraction, implied a gradual increase of salt (for R2) and hydrocarbons (for R1 and R2), till treating a 100% of volume of real slop wastewater. Since slop wastewater is devoid of minimal nitrogen and phosphorous concentrations for heterotrophic metabolisms, K_2HPO_4, KH_2PO_4 and NH_4Cl were continuously added during the experimentation in order to ensure a minimum ratio of C:N:P next to 100:5:1. The dissolved oxygen, pH and conductivity, were measured by means of an on-line probe. The COD, ammonia, nitrate, nitrite, total suspended solids (TSS), volatile suspended solids (VSS) concentrations and the sludge volume index (SVI) were determined according to the Standard Methods (APHA 2005). COD_T was directly measured in the sample while the COD_S from the sample filtered through 0.45 μm pore size filters. TPHs were extracted from liquid phase and solid phase according to EPA 3510c and EPA 3545a, respectively. The extracted volumes were analysed by means of Gas Chromatography – Flame Ionization Detector (GC-FID). The morphology and size distribution of granules were measured regularly by using an Image Analysis procedure with a stereomicroscope. Biomass density, in terms of g VSS per litre of granules, was determined with dextran blue and following the methodology proposed by Beun et al. (2002).

Table 1. Main operational conditions

Phase	Parameter							
	Settling time (min)		OLR (KgCOD•m3d-1)		Salinity (gCl-•L-1)		TPH (mg•L-1)	
	R1	R2	R1	R2	R1	R2	R1	R2
I	2	2	1.6	1.6	24	1	15	15
II	2	2	1.6	1.6	24	3	30	30
III	2	2	1.6	1.6	24	7	60	60
IV	2	2	1.6	1.6	24	15	106	106
V	2	2	1.6	1.6	24	24	151	151

3 Results and Discussions

3.1 Granules Properties

In R1, mature and salt-adapted granules maintained the TSS concentration around 8 $g•L^{-1}$ until the end of Phase IV, while in Phase V a decrease till about 4.7 $g•L^{-1}$ was probably due to a metabolic inhibition without a net growth of biomass. This was confirmed by observing the time course of the mean diameter which noticeably decreased from about 2 mm to about 1.25 mm in Phase V, suggesting that the inhibition of microorganisms was reflected on the cleavage and dimensions reduction of granules, even though they maintained a high density ($\approx$97 gTSS/L). Observing R2 data, granules were cultivated and simultaneously adapted to salt and hydrocarbons. During the granulation period, it was registered an almost constant increase of TSS till about 3.9 $g•L^{-1}$ at the end of Phase III. Subsequently, in Phase IV it was observed a rapid increase of TSS concentration till about 7.8 $g•L^{-1}$ probably due to a high biosorption effect of hydrocarbons on granules surface and porosity. In the last Phase V no degranulation was observed, and the TSS concentration stabilized on a value next to 4.4 $g•L^{-1}$ probable due to the biological adaptation and biodegradation of the bioadsorbed recalcitrant fraction. Regarding the granules dimensions, the mean diameter of granules rapidly increased in Phase II up to 1.25 mm and slightly decreased to around 1 mm at the end of the experimentation. Granules appeared structurally strong, with a density of about 72 gTSS/L. The mean diameter of granules in R2 always was lower than R1 and this conferred a higher specific surface area available for bioadsorption phenomena.

3.2 Removal Efficiencies

Regarding the total COD removal efficiency, it always was next to 90% for both the reactors until the end of Phase IV. However, in Phase V, fed with only slop wastewater, a noticeable decrease of the performance was observed, especially in R1 than in R2, where the removal efficiency collapsed down to about 30% and 67% respectively. Since the soluble COD was always removed with high efficiency ($\approx$80%) throughout all the experimental period, these trends could be related to a probable granules saturation of the recalcitrant particulate fraction of slop and to a following desorption in

the bulk which is discharged with the effluent. The difference between the two reactors suggested a biological removal of the recalcitrant substrate bioadsorbed in R2. In order to better understand the effect of the process on the hydrocarbons removal, TPH were extracted and analysed both in liquid phase and in solid phase bioadsorbed on granules, as shown in Fig. 1. Discussing about the Phase V, in which only slop was fed to the systems, in R1 it was initially registered an outlet concentration in liquid phase higher than in the inlet, confirming granules saturation and release of adsorbed hydrocarbons. Then the TPH concentration in liquid phase fall down, but by observing the always increasing concentration in the solid phase, it was mainly due to a new bioadsorption effect more than a biological effect of biodegradation. Looking at R2, initially it was registered a slight outflow of TPH, due to a probable saturation of aerobic granules, followed by a high depletion of TPH in the outlet liquid phase. The evaluation of the bioadsorbed fraction on granules surface was assessed by means of the extraction and the analysis of TPH from solid phase. The bioadsorbed fraction in R1, increased in Phase V, confirming the main role of biosorption of granules. On the other hand, in R2 it was noticed a decreasing trend of the bioadsorbed quantity that, together with the contextual TPH depletion in liquid phase, was likely due to hydrolysis and biodegradation of the hydrocarbons bioadsorbed previously. This suggested a biological activity of microorganisms aggregated inside the granules and, therefore, a biological adaptation to TPH. Moreover, it could be observed that the concentration of adsorbed TPH in R2 is higher than R1. This is probably due to the slight dimensions of granules in R2 that implied a higher specific surface area which could promote the adsorption of more hydrocarbons.

4   Conclusions

Two strategies for the treatment of shipboard slop characterized by high salinity and hydrocarbons, were studied: the first one by means of mature granules adapted to salinity, the second one regarded the granulation with slop, directly. By comparing the results, it could be asserted that the second line is better for a biological adaptation of microorganisms to TPHs. Indeed, it is more difficult to adapt mature granules to an industrial recalcitrant substrate, while it is easier to simultaneously granulate and acclimate the new forming granules to an industrial wastewater. During granulation, the biosorption of slowly biodegradable particulate substrate is enhanced by the aggregation phenomena, thus increasing the contact time with microorganisms and promoting the biological adaptation.

References

APHA (2005). Standard methods for the examination of water and wastewater. American Water Works Association/American Public Works Association/Water Environment Federation

Beun JJ, Van Loosdrecht MCM, Heijnen JJ (2002) Aerobic granulation in a sequencing batch airlift reactor. Water Res 36:702–712. doi:10.1016/S0043-1354(01)00250-0

Corsino SF, Campo R, Di Bella G, Torregrossa M, Viviani G (2015) Cultivation of granular sludge with hypersaline oily wastewater. Int Biodeterior Biodegrad 105:192–202. doi:10. 1016/j.ibiod.2015.09.009

De Kreuk MK, Heijnen JJ, Van Loosdrecht MCM (2005) Simultaneous COD, nitrogen, and phosphate removal by aerobic granular sludge. Biotechnol Bioeng 90:761–769

IMO-MARPOL 73/78 International Maritime Organizations regulation Prevention of Air Pollution from Ships

Bacterial Community Structure of an IFAS-MBRs Wastewater Treatment Plant

P. Cinà[1]([✉]), G. Bacci[2], G. Gallo[1], M. Capodici[3], A. Cosenza[3],
D. Di Trapani[3], R. Fani[2], G. Mannina[3], and A.M. Puglia[1]

[1] Laboratory of Molecular Microbiology and Biotechnology,
STEBICEF Department, University of Palermo,
Viale delle Scienze Ed. 16, 90128 Palermo, Italy
[2] Laboratory of Microbial and Molecular Evolution,
Department of Biology, University of Florence, Florence, Italy
[3] Dipartimento di Ingegneria Civile, Ambientale, Aerospaziale, dei Materiali,
Università di Palermo, Viale delle Scienze, Ed. 8, 90100 Palermo, Italy

Abstract. In this work, the bacterial community putatively involved in BNR events of a UCT-MBMBR pilot plant was elucidated by both culture-dependent and metagenomics DNA analyses. The presence of bacterial isolates belonging to Bacillus (in the anoxic compartment) and to Acinetobacter, Stenotrophomonas, Rhodococcus, Escherichia and Aeromonas (in the aerobic compartment) is in agreement with the nitrification/denitrification processes observed in the plant. Moreover, the study of bacterial community structure by NGS revealed a microbial diversity suggesting a biochemical complexity which can be further explored and exploited to improve UCT-MBMBR plant performance.

Keywords: Bacterial communities · NGS · Biological nutrient removal · Wastewater treatment plant · Membrane bioreactors · MBBR · Enhanced biological phosphorus removal · IFAS-MBR

1 Introduction

The principal objective of domestic or industrial wastewater treatment is generally to make effluents less hazardous to human or environment health. It is well known that nutrients (particularly, nitrogen and phosphorus compounds) may have adverse environmental impacts (e.g., eutrophication, toxicity towards the aquatic organisms, etc.…) (Wang et al. 2006). Biological nutrient removal (BNR) from domestic wastewater has been extensively investigated and developed in the last years. In systems aimed at the BNR in-series anaerobic, anoxic and aerobic reactors are required (Wanner et al. 1992; Mannina et al. 2016) where nitrogen (N) and phosphorus (P) removal is accomplished by heterotrophic denitrifying bacteria and polyphosphate-accumulating organisms (PAOs), requiring a carbon source (Naessens et al. 2012). In particular, the biological phosphorus removal is usually achieved through the growth of PAOs, able to accumulate P and to store it as intracellular polyphosphate (poly-P) under alternating anaerobic/aerobic conditions (Li et al. 2013). Thus, knowledge of bacterial communities

that take root in wastewater treatment plant is indispensable for a better understanding of the biological processes that allow the nutrient removal and perspectively for improving plant BNR performance. In this study bacterial communities of an Integrated Fixed Film Activated Sludge (IFAS) University Cape Town (UCT) membrane bioreactor (MBR) was investigated.

2 Methods

2.1 Plant Design

The IFAS-UCT-MBR pilot plant was characterized by three in-series reactors: one anaerobic (volume 62 L), one anoxic (volume 102 L) and one aerobic (volume 211 L) compartment according to the UCT scheme (Fig. 1).
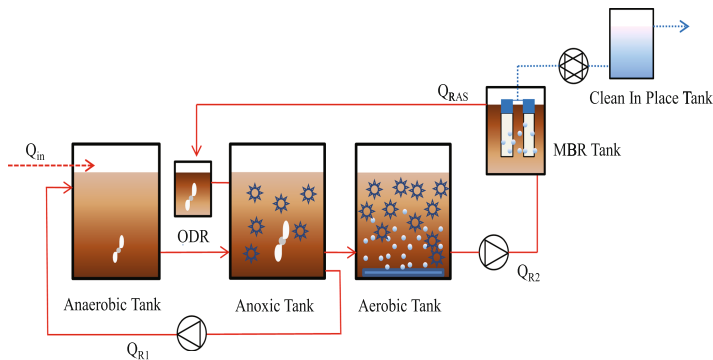
Fig. 1. Schematic lay-out of IFAS-UCT-MBR pilot plant

The IFAS-UCT-MBR pilot plant was operated for 60 days and was fed with a mixture of real wastewater (deriving from the University buildings and characterized by higher ammonia content compared to typical domestic wastewater) and synthetic wastewater. In particular, MBBR processes rely on the use of small plastic carriers elements (courtesy of amitec Co. Ltd., carriers density = 0.95 g cm^3) that are kept in constant motion throughout the entire volume of the reactor, for biofilm growth. The plastic carriers were a 15 and 40% filling fraction, corresponding to a net surface area of 75 and 200 m^2 m^{-3} 120 in the anoxic and aerobic reactor, respectively.

2.2 Identification of Bacterial Isolates

Wastewater aliquots of 100 µL r from the aerobic and anoxic tanks were collected, serially diluted and, then, plated on Luria Bertami (LB), Mannitol Soya flour (MS) and R2YE agar-media (Kieser et al. 2000). The plates were incubated at 30°C until appearance of microbial colonies (2–5 days). The bacterial colonies, selected on the basis of pigmentation and morphology, were repeatedly plated on agar-media to obtain

pure cultures. The bacterial isolates were characterized on the base of their 16S rDNA sequence using the universal bacterial primers 27F and 1492R (Frank et al. 2008) for 16S rDNA amplification by colony PCR as previously described (Gallo et al. 2012; Milanesi et al. 2015). The PCR products were purified by using NucleoSpin Gel and PCR Clean-up (MACHERY-NAGEL, Germany). Sequencing was performed by BMR Genomics srl. Phylogenetic relationships to known species were inferred by neighbour–joining, using the software Mega6 (Tamura et al. 2013).

2.3   Metagenomic Analysis Based on 16S rDNA Sequencing

Metagenomic DNA was extracted from 50 mL aliquots of wastewater from aerobic, anoxic and anaerobic compartment, respectively. In addition, two colonized carriers from aerobic and anoxic compartments were used to obtain Metagenomic DNA. Since CTAB performed better in reducing humic contamination, it was used in the buffer for sodium dodecyl sulfate (SDS)-based DNA extraction. The metagenomic analysis was performed through new generation sequencing (NGS) by Illumina platform (BMR Genomics srl).

3   Results and Discussion

After 2–5 days of incubation, bacterial colonies appeared on the surface of agar-medium plates inoculated with serially diluted wastewater aliquots. The colonies showed different phenotypes: most had a white translucent pigmentation, someone white with a matt pigmentation and one showed orange pigmentation. A total of 14 isolates (8 and 6 from aerobic and anoxic tank, respectively) were selected and obtained as pure cultures. From all the 14 isolates, a 16S rDNA sequence was obtained to carry out phylogenetic analysis. As all the isolates from anoxic tank belonged to *Bacillus* genus, the isolates from aerobic tank belonged to five different bacterial genera: *Acinetobacter* (2 isolates), *Stenotrophomonas* (2 isolates), *Rhodococcus* (2 isolates), *Escherichia* (1 isolates) and *Aeromonas* (1 isolates). Interestingly, they are all implied in nitrification/denitrification processes (Di Bonaventura et al. 2004).

The 16S rDNA-based metagenomic analysis revealed 12 (Operational taxonomic unit) OTU. In general, the bacterial community composition of anaerobic, anoxic and aerobic compartments are quite similar; indeed, the most relevant differences are quantitatively observed for the less represented OTUs. In particular, the most representative OTUs were: Saprospiraceae (27.30%), Rhodocyclaceae (26.61%), Sphingobacteriales (12.96%) in aerobic compartment (Fig. 2a); Rhodocyclaceae (22.69%), Saprospiraceae (19.99%), and Sphingobacteriales (10.54%) in anoxic compartment (Fig. 2b); Rhodocyclaceae (21.60%), Saprospiraceae (19.20%), and Sphingobacteriales (10.29%) in anaerobic compartment (Fig. 2e). Concerning the colonized carriers, the bacterial community composition almost paralleled that one of the corresponding compartment, with Saprospiraceae and Rhodocyclaceae the most abundant OTUs in both cases. However, the less abundant OTUs Rhodanobacter, in aerobic and anoxic conditions, and Thermomonas and Clostridium sensu strictu, in aerobic condition, were observed only in the carries.
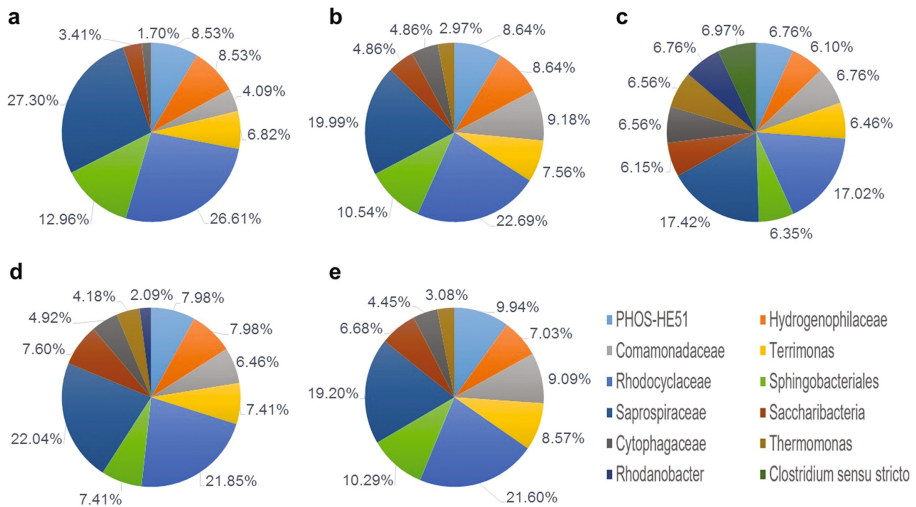
Fig. 2. Bacterial OTU relative abundance in (a) aerobic tank, (b) anoxic tank, (c) aerobic tank carriers, (d) anoxic tank carriers (e) anaerobic tank

4   Conclusions

The bacterial community putatively involved in BNR events of a IFAS-UCT-MBR pilot plant was elucidated by both culture-dependent and metagenomics DNA analyses. The presence of bacterial isolates in the anoxic and aerobic compartments is in agreement with the nitrification/denitrification processes observed in the plant (Mannina et al. unpublished results). Moreover, the study of microbial community structure by NGS revealed a microbial diversity and suggests a biochemical complexity which has to be further explored and exploited to improve IFAS-UCT-MBR plant performance.

References

Di Bonaventura G, Spedicato G, D'Antonio D, Robuffo I, Piccolomini R (2004) Biofilm formation by *Stenotrophomonas maltophilia:* modulation by Quinolones, Trimethoprim-Sulfamethoxazole, and Ceftazidime. Antimicrob Agents Chemother 48(8):151–160

Frank JA, Reich CI, Sharma S, Weisbaum JS, Wilson BA, Olsen GJ (2008) Critical evaluation of two primers commonly used for amplification of bacterial 16S rRNA genes. Appl Environ Microbiol 74:2461–2470

Gallo G, Baldi F, Renzone G, Gallo M, Cordaro A, Scaloni A, Puglia AM (2012) Adaptative biochemical pathways and regulatory networks in Klebsiella oxytoca BAS-10 producing a biotechnologically relevant exopolysaccharide during Fe (III)-citrate fermentation. Microb Cell Fact 11:152

Kieser Y, Bibb MJ, Buttner MJ, Chater KF, Hopwood DA (2000) Practical Streptomyces genetics. The John Innes Foundation, Norwich

Li C, Wang T, Zheng N, Zhang J, Ngo HH, Guo W, Liang S (2013) Influence of organic shock loads on the production of N2O in denitrifying phosphorus removal process. Bioresour Technol 141:160–166

Mannina G, Capodici M, Cosenza A, Di Trapani D (2016) Carbon and nutrient biological removal in a University of Cape Town membrane bioreactor: analysis of a pilot plant operated under two different C/N ratios. Chem Eng J 296:289–299

Milanesi C, Cresti M, Costantini L, Gallo M, Gallo G, Crognale S, Faleri C, Gradi A, Baldi F (2015) Spoilage of oat bran by sporogenic microorganisms revived from soil buried 4000 years ago in Iranian archaeological site. Int Biodeter Biodegr 104:83–91

Naessens W, Maere T, Nopens I (2012) Critical review of membrane bioreactor models Part 1: biokinetic and filtration models. Bioresour Technol 122:95–106

Tamura K, Stecher G, Peterson D, Filipski A, Kumar S (2013) MEGA6: molecular evolutionary genetics analysis version 6.0. Mol Biol Evol 30:2725–2729

Wang XJ, Xia SQ, Chen L, Zhao JF, Renault NJ, Chovelon JM (2006) Nutrients removal from municipal wastewater by chemical precipitation in a moving bed biofilm reactor. Process Biochem 41(4):824–828

Wanner J, Cech JS, Kos M (1992) New process design for biological nutrient removal. Water Sci Technol 25(4–5):445–448

Removal Performance of Organic Matter of MBR and Hybrid MBBR-MBR Systems During Start-up and Stabilization Phases Treating Variable Salinity Urban Wastewater

A. Rodriguez-Sanchez[1,2(✉)], J.C. Leyva-Diaz[1,2], J. Gonzalez-Lopez[1], and J.M. Poyatos[1,2]

[1] Institute of Water Research, University of Granada, Granada, Spain
[2] Department of Civil Engineering, University of Granada, Granada, Spain

Abstract. A MBR and two hybrid MBBR-MBR with different configurations were used for the treatment of variable salinity wastewater. The systems were started-up and operated until stabilization conditions while being fed with salinity-amended urban wastewater. The salinity-amended urban wastewater was generated by the mixture of urban wastewater and salinity-amended tap water to obtain a feeding with salinity in the range of 1–6.5 mS cm^{-1}. The three bioreactors were subjected to cyclical salinity variations with a cycle consisting of 6 h at 6.5 mS cm^{-1} salinity and 6 h at regular wastewater salinity. The system was evaluated for its performance in organic matter removal by COD and BOD$_5$ measurements. Also, the kinetics of its heterotrophic biomass was characterized by the means of respirometric tests. The results showed a very good removal of COD and BOD$_5$, with the MBBR-MBRanox showing the highest performances. The heterotrophic kinetics were higher at lower total solids concentrations with the MBR system having the fastest kinetics during the start-up. These results will be of use for the future application of MBR and hybrid MBBR-MBR systems to the treatment of variable salinity wastewater.

Keywords: MBR · Hybrid MBBR-MBR · Variable salinity wastewater

1 Introduction

Saline effluents can be found in both industrial and urban wastewater. In the case of urban wastewater, the most common case is found in coastal or island cities, which face infiltration of seawater in the sewage system during certain tidal periods of even permanently. Therefore, biological wastewater treatment systems in these placements need to handle loads of variable salinity influents, which could seriously affect the microbial metabolisms on which these treatment processes depend. In this sense, salinity causes reduction of bioavailability of nutrients, higher osmotic pressures that lead to higher cell mortality rates, and inhibition of biodegradation processes, among others (Rodriguez-Sanchez et al. 2017).

The MBR and MBBR-MBR technologies present several advantages over more traditional activated sludge systems (Rodriguez-Sanchez et al. 2017) and therefore

could be a proper technological approach for the treatment of variable salinity urban wastewater.

Thus, a membrane bioreactor (MBR) and two hybrid moving bed biofilm reactor-membrane bioreactor (MBBR-MBR) with different configurations at lab-scale were started up and operated for the treatment of variable salinity urban wastewater. To our knowledge, this is the first attempt to monitor the organic matter removal and heterotrophic kinetics in MBR and hybrid MBBR-MBR systems subjected to cyclical salinity variations. The performance of the three systems in terms of BOD_5 and COD removal was analysed during the start-up. The kinetic characterization of the heterotrophic biomass in the systems was also done by the means of respirometric tests. Heterotrophic kinetics, BOD_5 and COD removal efficiency, and operational parameters of the systems were linked to analyze the relationships among these variables.

2   Materials and Methods

The three systems were designed as a four-chambers bioreactor with a subsequent membrane tank. Each chamber had an operation volume of 6 L and the membrane tank had an operation volume of 4.32 L. The first, third and fourth chambers in each of the bioreactors were aerated using fine bubble diffusers to provide a complete mix in their volumes. The membrane tank was aerated using a coarse bubble diffuser to prevent biomass growth over the membrane module. The second chamber was not aerated to achieve anoxic conditions in the systems, and thus its content was completely mixed by the means of mechanical stirring. The membrane module was composed of polyvinylidene hollow fibers with 0.04 µm pore diameter, providing a total membrane area of 0.20 m^2. The influent wastewater was introduced in the first chamber and forced to flow through the second, third and fourth chambers before being discharged into the membrane tank, from which the effluent flow was extracted through the membrane using a cyclical operation of 9-minute permeation and 1-minute backwash. The hydraulic retention time (HRT) was of 6 h and the solids retention time was of 91.17 days. A recycling flow was forced from the membrane tank to the first chamber of each of the systems in a 500% of the influent flow. The three systems were configured as different technologies. One was set up as an MBR system. The other two were set up as hybrid MBBR-MBR systems with the filling of K1 carriers. The carriers were used to fill the 35% of: (i) all chambers in the configuration hybrid MBBR-MBRanox; (ii) the three aerobic chambers in the configuration hybrid MBBR-MBRn/anox.

This study used a salinity-amended urban wastewater influent. This was made using a mixture of real urban wastewater and NaCl-amended tap water. The urban wastewater was collected from the Los Vados WWTP, located in Granada, Spain. Tap water was amended with NaCl to achieve an electric conductivity of about 50 mS cm^{-1}. The urban wastewater and salinity-amended tap water were mixed in a mixing tank prior to being fed to the bioreactors. The mixing was controlled electronically to achieve a cycle of: 6 h of urban wastewater only; 6 h of a mixture of urban wastewater and NaCl amended tap water with a final electric conductivity of 6.5 mS cm^{-1} (around 3.5 g-NaCl L^{-1}).

The operational parameters of dissolved oxygen, pH, electric conductivity and temperature were measured using a multimeter. The influent and effluent BOD_5, COD and TSS were measured according to the established standard protocols (APHA 2012).

The biofilm density of the carriers was measured following the method described by (Leyva-Diaz et al. 2015). In this way, 10 carriers were collected from the system, introduced in Tween 80 solution and sonicated during 3 min for detachment of biomass, the centrifuged at 3500 rpm during 10 min at room temperature and finally filtered in 0.45 µm pore diameter filter. Biofilm density was measured in the dehydrated filter and extrapolated to the total volume of the bioreactor given that the volume occupied by carriers was known.

The respirometric tests and the microbial kinetics characterization was done following the methods defined by (Leyva-Diaz et al. 2013). These were conducted in a gas flux/static liquid respirometer. For the purpose of respirometry, a sample of 1 L was extracted from the bioreactors (including carriers for the hybrid MBBR-MBR systems) and aerated during 18–24 h at 20°C before the respirometric test. During the respirometric test, the temperature was controlled at 20°C and the pH in the range of 7.5 ± 0.75. The sample was continuously stirred by a mechanical agitator and completely mixed by a recirculating pump. The aeration of the sample was provided by an aeration pump. The characterization of the heterotrophic kinetics of the biomass was done by using sodium acetate as substrate in a 500 mg L^{-1} concentration at three different dilutions of 50%, 80% and 100%. The data recorded during the respirometric test was then processed for the calculation of kinetics parameters for the heterotrophic biomass following the procedure described by (Leyva-Diaz et al. 2013).

The data collected for the performance in organic matter removal, operational parameters and kinetic parameters was treated to conform multivariate redundancy analyses linking these variables. One of these linked the removal of BOD_5 and COD with the rate of substrate utilization (r_{su}) of the MBR and hybrid MBBR-MBRs at different substrate concentrations (30, 60, 90, 120, 150, 180, 210, 240, 270 and 300 mg L^{-1} COD). The other linked the operational parameters (TSS, SRT, HRT, Salinity, DO, pH and temperature) with the rates of substrate utilization mentioned above. The calculation of the multivariate redundancy analyses was done using the Canoco 4.5 for Windows using a full permutation model under 499 unconstrained Monte-Carlo simulations.

3   Results and Discussion

The performance data in terms of BOD_5 showed a very good removal efficiency, with values in the range of 93–98% when MLSS reached 1800 mg L^{-1}, 97–98.5% at 2100 mg L^{-1} MLSS and 97–99.6% at 2500 mg L^{-1} MLSS. In terms of COD, the performances at the same operational times were of 63–80%, 75–82% and 88–94%. Overall, the hybrid MBBR-MBRanox showed the best performance in BOD_5 and COD removal efficiency at these operation times, even though the results showed not statistically significant differences between the systems at the same operation time. These results were lower than those found for the start-up and stable operation of a MBR and hybrid MBBR-MBR systems under constant 6.5 mS cm-1 salinity feeding, where the
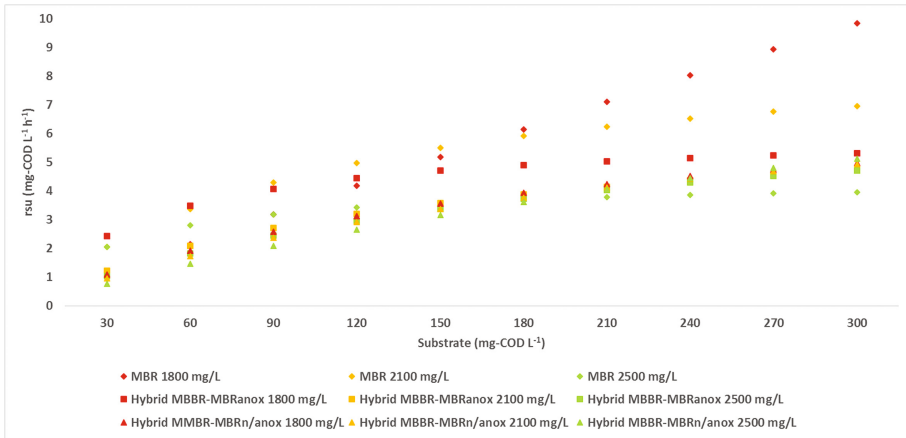
Fig. 1. Rates of substrate utilization for the MBR (diamond), hybrid MBBR-MBRanox (square) and hybrid MBBR-MBRn/anox (triangle) at MLSS concentrations of 1800 (red), 2100 (orange) and 2500 (green) mg L^{-1} MLSS concentration (Color figure online)

values oscillated in the range of 80–90% for COD removal and 95–98% for BOD$_5$ removal (Rodriguez-Sanchez et al. 2017).

The rates of substrate utilization (r_{su}) of the heterotrophic biomass in a range of substrate of 30-300 mg-COD L^{-1} for the three systems at the operation times of 1800,
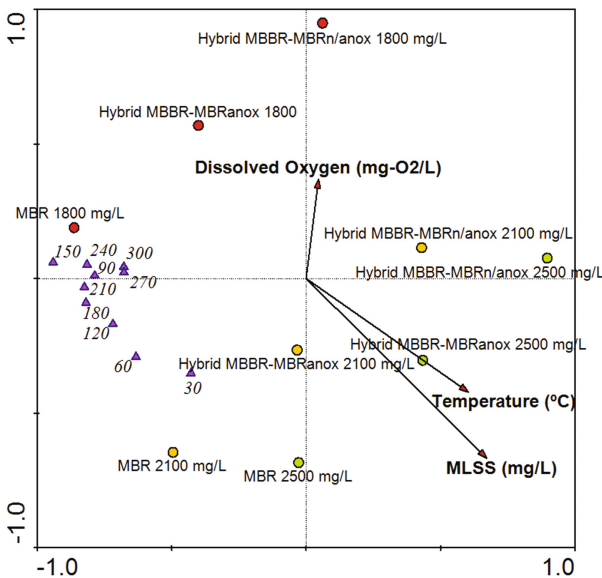
Fig. 2. Multivariate redundancy analysis triplot linking the operational parameters of the system (arrows) with the rates of substrate utilization of the MBR, hybrid MBBR-MBRanox and hybrid MBBR-MBRn/anox at 1800, 2100 and 2500 mg L^{-1} MLSS. The rates of substrate utilization used corresponded to 30, 60, 90, 120, 150, 180, 210, 240, 270 and 300 mg-COD L^{-1} and were represented as purple triangles. The systems were depicted as circles (Color figure online)

2100 and 2500 mg L^{-1} MLSS are shown in Fig. 1. Overall, each of the systems showed higher r_{su} values at lower MLSS concentrations, as has been shown for the start-up of MBR and hybrid MBBR-MBR under regular salinity wastewater and constant 6.5 mS cm^{-1} salinity wastewater (Leyva-Diaz and Poyatos 2015; Rodriguez-Sanchez et al. 2017). In terms of heterotrophic kinetics the MBR was the fastest during the start-up. At 2500 mg L^{-1} MLSS concentrations all systems had similar r_{su} values. In this sense, the three systems showed a progression to stability in their microbial kinetics, which were denoted by a reduction in the r_{su} and the differences among the systems. This was related to the reduction in differences in the BOD$_5$ and COD removal performances, with a 5% and 17% difference in BOD$_5$ and COD at 1800 mg L^{-1} MLSS, 1.5% and 7% at 2100 mg L^{-1}, and 1.6% and 6% at 2500 mg L^{-1}. The kinetic behaviour found for the systems working under variable salinity conditions were similar to that observed in these systems under regular and constant salinity wastewater (Leyva-Diaz and Poyatos 2015; Rodriguez-Sanchez et al. 2017).

Two multivariate redundancy analyses were developed to link the heterotrophic kinetics of the systems at different substrate rates with the operational parameters and the BOD$_5$ and COD removal efficiencies. Dissolved oxygen concentration, temperature and MLSS were the operational parameters that ordinated the samples analysed, and among those MLSS was the one with higher correspondence (Fig. 2). The heterotrophic kinetics were positively correlated with dissolved oxygen at higher substrate concentrations and negatively correlated at lower substrate concentrations. The r_{su} values were
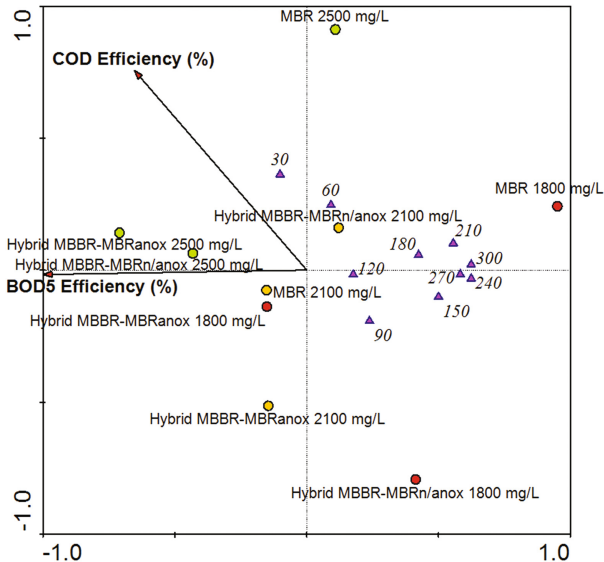
Fig. 3. Multivariate redundancy analysis triplot linking the BOD$_5$ and COD removal efficiencies (arrows) with the rates of substrate utilization of the MBR, hybrid MBBR-MBRanox and hybrid MBBR-MBRn/anox at 1800, 2100 and 2500 mg L^{-1} MLSS. The rates of substrate utilization used corresponded to 30, 60, 90, 120, 150, 180, 210, 240, 270 and 300 mg-COD L^{-1} and were represented as purple triangles. The systems were depicted as circles (Color figure online)

negatively correlated with the MLSS, as showed by the kinetics parameter analysis (Fig. 1). With respect to removal performances, the samples were more correlated with COD performance than BOD_5 performance (Fig. 3). Heterotrophic kinetics showed a negative correlation with COD and BOD_5 removal efficiencies.

4 Conclusions

The heterotrophic kinetics during the start-up of the MBR and the two hybrid MBBR-MBR systems under variable salinity influent wastewater was similar to that of the regular salinity conditions in terms of evolution patterns. Lower MLSS concentrations were correlated with higher heterotrophic kinetics.

References

APHA (2012) Standard methods for the examination of water and wastewater, 22nd edn. American Public Health Association, Washington DC

Leyva-Diaz JC, Calderon K, Rodriguez FA, Gonzalez-Lopez J, Hontoira E, Poyatos JM (2013) Comparative kinetic study between moving bed biofilm reactor-membrane bioreactor and membrane bioreactor systems and their influence on organic matter and nutrients removal. Biochem Eng J 77:28–40

Leyva-Diaz JC, Gonzalez-Martinez A, Gonzalez-Lopez J, Munio MM, Poyatos JM (2015) Kinetic modeling and microbiological study of two-step nitrification in a membrane bioreactor and hybrid moving bed biofilm reactor–membrane bioreactor for wastewater treatment. Chem Eng J 259:692–702

Leyva-Diaz JC, Poyatos JM (2015) Start-up of membrane bioreactor and hybrid moving bed biofilm reactor-membrane bioreactor: kinetic study. Water Sci Technol 72:1948–1953

Rodriguez-Sanchez A, Leyva-Diaz JC, Gonzalez-Lopez J, Poyatos JM (2017) Performance and kinetics of membrane and hybrid moving-bed biofilm-membrane bioreactors treating salinity wastewater. AIChE J. doi:10.1002/aic.15694

Impact of Hydraulic Retention Time on MBR and Hybrid MBBR-MBR Systems Through Microbiological Approach: TGGE and Enzyme Activities

A. Rodriguez-Sanchez[1,2(✉)], J.C. Leyva-Diaz[1,2], K. Calderon[3],
J.M. Poyatos[1,2], and J. Gonzalez-Lopez[1]

[1] Institute of Water Research, University of Granada, Granada, Spain
[2] Department of Civil Engineering, University of Granada, Granada, Spain
[3] Department of Microbiology, Faculty of Sciences,
Universidad Autónoma de México, Mexico DF, Mexico

Abstract. The microbial community structure and the enzyme activities of a MBR and two hybrid MBBR-MBR systems were analyzed at two different hydraulic retention times. The TGGE fingerprinting showed that the microbial community structure was deeply dependent on the operational HRT. The activities of acid phosphatase, basic phosphatase and α-glucosidase enzyme activities also were affected by the different HRT. A multivariate redundancy analysis showed that the first of these was positively correlated with the HRT, while the other two were negatively correlated. In this sense, the microbiological approach could successfully explain the influence of the HRT over the bacterial communities and activities in the MBR and hybrid MBBR-MBR systems analyzed.

Keywords: Temperature gradient gel electrophoresis · Scanning electron microscopy · Enzyme activities

1 Introduction

Wastewater discharge to the environment is still today a challenging environmental problem worldwide. The treatment of wastewater therefore has become a decisive parameter in the mitigation of pollution caused by polluted water discharges in the last century. In the light of this, activated sludge systems have become the dominant technology for the treatment of urban wastewater. Nevertheless, more novel technologies offer advantages over activated sludge systems, such as the MBR and the MBBR. In this sense, these advantages concern operation at higher total solids concentrations, more efficient biomass retention, lower footprint required for implementation, longer solids retention times during operation, among others (Rodriguez-Sanchez et al. 2017). Also, the combination of a MBBR and a MBR creates the MBBR-MBR, which have similar advantages over the traditional activated sludge systems and over separate MBR and MBBR technologies, such as lower membrane fouling with respect to the MBR and improved settleability of suspended biomass with regard to the MBBR

(Rodriguez-Sanchez et al. 2017). MBBR-MBR systems could be of pure configuration when no recycling flow from the membrane tank to the MBBR is set, and are name as hybrid when such recycling exists. The usage of MBR and hybrid MBBR-MBR for the treatment of urban wastewater needs to be evaluated, giving special attention to the parameters under which they can be operated. One of the most important of them is the hydraulic retention time (HRT), which drives the amount of time that wastewater resides in the bioreactor.

A MBR and two hybrid MBBR-MBR systems were operated for the treatment of urban wastewater under two different HRTs of 30.40 and 26.47 h. The changes in the microbial communities were monitored by the means of TGGE, while the changes in microbial activity were observed through enzyme activities.

2   Materials and Methods

The three bioreactors were composed by four 6 L chambers and a 4.32 L membrane tank with a 0.04 µm pore diameter membrane module. The influent was forced to pass through all the chambers and then discharged into the membrane tank from which was withdrawn through the membrane module by the means of a peristaltic pump. The first (C1), third (C3) and fourth (C4) chambers, as well as the membrane tank, were aerated, which also provided complete mixing. The second chamber (C2) was anoxic and mixing was ensured by mechanical stirring. The MBR (P1) configuration showed no carriers and the hybrid MBBR-MBR systems had 35% chamber volume of carriers: (i) in all chambers for the MBBR-MBRanox (P2); (ii) in the aerobic chambers for the MBBR-MBRn/anox (P3). The bioreactors were operated for the treatment of urban wastewater collected from the Los Vados WWTP, located in Granada, Spain.

During operation time, mixed liquor samples were collected from the three pilot scale systems. Attached biomass from carriers was collected following the methodology described by Reboleiro-Rivas et al. (2013). Briefly, 50 carriers were collected from the bioreactors, then submerged into 0.9% NaCl saline solution, vortexed for 1 min, sonicated for 3 min for biomass detachment, and then detached biomass was collected from saline solution by centrifugation at 3500 rpm during 10 min at room temperature.

The DNA extraction procedure, nested PCR and TGGE procedure of suspended and attached biomass in each of the chambers of the MBR and the two hybrid MBBR-MBR systems were done in accordance with (Molina-Muñoz et al. 2009). In this case, the extracted DNA was first subjected to a PCR amplification of the 16S rRNA gene using the primer pair fD1-rD1. The amplicons obtained were then subjected to another PCR amplification of the V3 hypervariable of the 16D rRNA gene region. The PCR conditions of both amplifications were derived from (Molina-Muñoz et al. 2007). The temperature gradient used for the separation of the V3 amplicons was of 43–63°C, and the electrophoresis was done at 125 V for 8 h. The TGGE fingerprinting analysis was done using Gel Compar II software.

The enzyme activities for α-glucosidase, acid phosphatase and alkaline phosphatase were measured following (Reboleiro-Rivas et al. 2013). The determination of the enzyme activities was done for the attached biomass and the suspended biomass. Acid and basic phosphatase were done using 1% p-nitrophenyl phosphate as substrate,

and α-glucosidase was done using 1% *p*-nitrophenyl α-glucopyranoside. The reactions were developed in pH 4.8 acetic-acetate buffer, pH 9.6 bicarbonate-carbonate buffer, and pH 7.6 Tris-HCl buffer for the acid phosphate, basic phosphatase and α-glucosidase, respectively. The incubation was done using 1 mL of biomass, 2 mL of buffer and 1 mL of substrate and at 37°C. Phosphatases were incubated for 30 min and α-glucosidase for 60 min. The reaction was stopped using 2 mL of 0.2M NaOH for the phosphatases and by boiling water bath for 5 min for the α-glucosidase. The samples were then centrifuged at 3000 rpm during 15 min and the supernatant was measured by the means of an spectrophotometer. The measurements were done in triplicate.

3   Results and Discussion

The TGGE fingerprinting for the 30.4 and 26.47 h HRT are shown in Figs. 1 and 2, respectively. For the HRT of 30.40 h, the samples could be divided into five different groups at 60% difference threshold. One group was represented by chambers C1, C2 and C3 of P1; chambers C3 and C4 of P2, both fixed biofilm and planktonic biomass, with addition of fixed biomass of chamber C2 of P2, conform another group; samples from P3 were grouped in two different groups; the remaining samples were clustered into another group. For the 26.47 h HRT, five different groups could be formed after clustering of samples at 60% difference threshold, with two of them composed by samples from P3; other containing six samples from P2; another had C1, C2 and C4 from P1; the other samples were contained in the last group. There were clear differences in the bacterial community structure of P1, P2 and P3 at both HRTs, while it existed a very close similarity between suspended biomass and attached biomass in each of the chambers containing carriers.

The acid phosphatase, alkaline phosphatase and α-glucosidase activities for the HRT of 30.4 h had the highest values at P2. Trends in these three enzyme activities between different chambers were not clear. The differences in the bacterial community
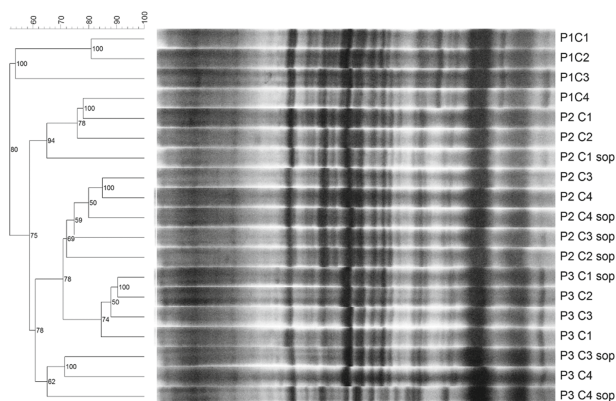
Fig. 1. TGGE fingerprinting of all biomass samples of the MBR and the two hybrid MBR-MBR systems at 30.4 h HRT. The fixed biomass is noted as "sop"
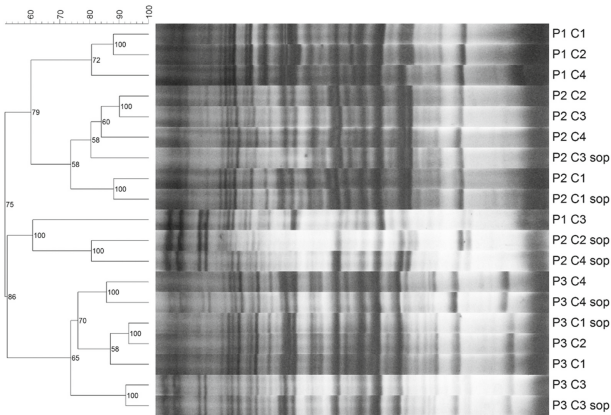
Fig. 2. TGGE fingerprinting of all biomass samples of the MBR and the two hybrid MBR-MBR systems at 26.47 h HRT. The fixed biomass is noted as "sop"

activities differed from P2, with fixed biomass presenting higher activity values, to P3, where suspended biomass showed higher activities. On the other hand, for the HRT of 26.47 h, the P3 had the highest α-glucosidase, acid phosphatase and alkaline phosphatase activities. The suspended biomass had higher activity values than the fixed biofilm in all bioreactors. Also, no differences were clear among chambers within the same bioreactor.

The main difference between the two cycles of operation resided in the different HRT – 30.40 h and 26.47 h – and the values of MLSS and BD in the system. Mean values for α-glucosidase, acid phosphatase and alkaline phosphatase activities present higher values at 30.40 h HRT than at 26.47 h HRT. In this sense, enzyme activity could be related to HRT in such a way that higher HRT leads to higher enzyme activity. It was observed that HRT is one of the parameters that best capture variability of enzyme activity in MBR systems (Reboleiro-Rivas et al. 2013). On the other hand, both cycles offered a similar pattern in the values at fixed biofilm and suspended biomass. In both cases, enzyme activities for α-glucosidase and phosphatase were higher for the fixed biomass. It has been thought that extracellular polymeric substances generated for the conformation of fixed bacterial biofilm impedes the release of extracellular enzymes such as α-glucosidase and phosphatase, which reduces its activity (Reboleiro-Rivas et al. 2013).

A multivariate redundancy analysis was done in order to link the three enzyme activities with the different operational parameters between the two cycles of operation, mainly the MLSS, the BD and the HRT (Fig. 3). The results showed that the alkaline phosphatase had a strong positive correlation with the HRT, while the acid phosphatase activity had a strong negative correlation with this variable. In this sense, the results demonstrated that the HRT defined the activities of the phosphatase enzyme for the MBR and MBBR-MBR systems operated. On the other hand, the α-glucosidase activity had a timid, positive correlation with the HRT. With respect to the MLSS and BD, the alkaline phosphatase activity had a strong negative correlation with the BD and

Code	Bioreactor and Chamber	HRT (h)
1	P1C1	30.40
2	P1C2	30.40
3	P1C3	30.40
4	P1C4	30.40
5	P2C1	30.40
6	P2C1 sop	30.40
7	P2C2	30.40
8	P2C2 sop	30.40
9	P2C3	30.40
10	P2C3 sop	30.40
11	P2C4	30.40
12	P2C4 sop	30.40
13	P3C1	30.40
14	P3C1 sop	30.40
15	P3C2	30.40
16	P3C3	30.40
17	P3C3 sop	30.40
18	P3C4	30.40
19	P3C4 sop	30.40
20	P1C1	26.47
21	P1C2	26.47
22	P1C3	26.47
23	P1C4	26.47
24	P2C1	26.47
25	P2C1 sop	26.47
26	P2C2	26.47
27	P2C2 sop	26.47
28	P2C3	26.47
29	P2C3 sop	26.47
30	P2C4	26.47
31	P2C4 sop	26.47
32	P3C1	26.47
33	P3C1 sop	26.47
34	P3C2	26.47
35	P3C3	26.47
36	P3C3 sop	26.47
37	P3C4	26.47
38	P3C4 sop	26.47
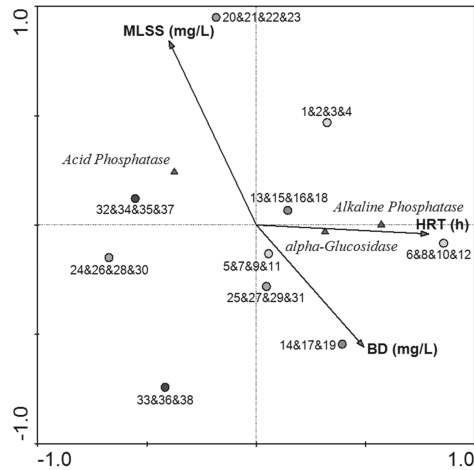
Fig. 3. Multivariate redundancy analysis linking the acid phosphatase, alkaline phosphatase and α-glucosidase activities with the operational conditions MLSS, BD and HRT. The enzyme activities are depicted as purple triangles. The operational conditions are depicted as arrows. The samples are depicted as circles (Color figure online)

a strong positive correlation with the MLSS. On the contrary, the acid phosphatase and the α-glucosidase activities had a slight positive correlation with the BD and a slight negative correlation with the MLSS. These results point out that fixed biofilms in the hybrid MBBR-MBR systems are responsible for the acid phosphatase activity, while the alkaline phosphatase activity is dominant within the suspended biomass. Thus, the configuration of the biomass in the MBR and the hybrid MBBR-MBR systems studied defined the dominance of acid or alkaline phosphatase activities.

4   Conclusions

The TGGE fingerprinting showed that operational conditions, specially the HRT, affected severely the microbial community structure of the bioreactors, showing big differences among the different HRT scenarios. Also, for all of the HRTs, there was a remarkable similarity between the attached and suspended biomass in chambers with carriers. Enzyme activities showed no clear trends among the chambers in the same bioreactor, but showed an influence of the operational conditions, including the HRT, in the enzyme activities of the biomass. The enzyme activities analyzed were always

higher for the suspended biomass than for the attached biomass. The multivariate redundancy analysis demonstrated that the acid phosphatase was positively correlated with the HRT, while the basic phosphatase and the α-glucosidase were negatively correlated with it.

References

Reboleiro-Rivas P, Martin-Pascual J, Juarez-Jimenez B, Poyatos JM, Hontoria E, Rodelas B, Gonzalez-Lopez J (2013) Enzymatic activities in a moving bed membrane bioreactor for real urban wastewater treatment: effect of operational conditions. Ecol Eng 61:23–33

Molina-Muñoz M, Poyatos JM, Vilchez R, Hontoria E, Rodelas B, Gonzalez-Lopez J (2007) Effect of the concentration of suspended solids on the enzymatic activities and biodiversity of a submerged membrane bioreactor for aerobic treatment of domestic wastewater. Appl Microbiol Biotechnol 73:1441–1451

Molina-Muñoz M, Poyatos JM, Sánchez-Peinado MM, Hontoria E, González-López J, Rodelas B (2009) Microbial community structure and dynamics in a pilot-scale submerged membrane bioreactor aerobically treating domestic wastewater under real operation conditions. Sci Total Environ 407:3994–4003

Rodriguez-Sanchez A, Leyva-Diaz JC, Gonzalez-Lopez J, Poyatos JM (2017) Performance and kinetics of membrane and hybrid moving-bed biofilm-membrane bioreactors treating salinity wastewater. AIChE J. doi:10.1002/aic.15694

UCT-MBR vs IFAS-UCT-MBR
for Wastewater Treatment: A Comprehensive
Comparison Including N_2O Emission

G. Mannina[1]([✉]), M. Capodici[1], A. Cosenza[1], D. Di Trapani[1],
G.A. Ekama[2], and H. Ødegaard[3]

[1] Dipartimento di Ingegneria Civile, Ambientale, Aerospaziale, dei Materiali,
Università di Palermo, Viale delle Scienze, Ed. 8, 90100 Palermo, Italy
{giorgio.mannina,marco.capodici,alida.cosenza,
daniele.ditrapani}@unipa.it
[2] Water Research Group, Department of Civil Engineering,
University of Cape Town, Rondebosch, Cape Town 7700, South Africa
george.ekama@uct.ac.za
[3] Department of Hydraulic and Environmental Engineering,
NTNU - Norwegian University of Science and Technology,
7491 Trondheim, Norway
hallvard.odegaard@ntnu.no

Abstract. In this study the performance (in terms of carbon and nutrient removal) and N_2O emission of two plant configurations adopting innovative technologies were investigated. With this regards, an University Cape Town (UCT) membrane bioreactor (MBR) plant and an Integrated Fixed Film Activated Sludge (IFAS) -UCT-MBR plant were monitored. Both plants treat real wastewater under two different values of the influent carbon nitrogen ratio (C/N = 5 mgCOD/mgN and C/N = 10 mgCOD/mgN). Results have shown the highest carbon and nutrients removal efficiencies for the IFAS-UCT-MBR configuration during both the two investigated C/N values. Furthermore, the lowest N_2O emission occurred for the IFAS-UCT-MBR.

Keywords: WWTP · Nutrient removal · Greenhouse gases · Global warming · Biofilm

1 Introduction

Nitrogen (N) and phosphorus (P) compounds (nutrients), discharged with wastewater, could seriously affect the quality of receiving water bodies, since their presence favours eutrophication and can be toxic for the aquatic organisms (Wang et al. 2006). Therefore, their removal from wastewater is an imperative requirement. With this regards, biological nutrient removal (BNR) processes have been largely explored, since they have the advantage of avoiding the use of chemicals compared with chemical processes. Despite conventional activated sludge (CAS) processes are effective for removal of organic and nutrients compounds, the overall efficiency is strictly depending on the final settler operation (Wanner 2002). Therefore, in the last years new and

innovative technologies have been investigated in order to overcome the main drawbacks of the CAS systems and meet stricter water quality effluent limits. In this context, membrane bioreactor (MBR) technology guarantees higher effluent standard and has also the advantage of making the efficiency of the biological processes independent from the biomass settling properties.

Among the new technologies, it is notwithstanding to mention the moving bed biofilm reactors (MBBR), where biomass grows as biofilm on small plastic carrier elements, and MBBR-based Integrated Fixed Film Activated Sludge (IFAS) reactors, where biomass grows both as suspended flocs and as biofilm. When IFAS systems are combined with a MBR (realizing an IFAS-MBR) there is the potential to gain the best characteristics of both biofilm processes and membrane separation. IFAS - MBR reactors are especially useful when slowly growing organisms as nitrifiers have to be maintained inside a WWTP limiting the required reactor volumes due to the coexistence of both suspended biomass and biofilm and membrane separation. Although MBR and IFAS-MBR systems have several advantages with respect to CAS, they are characterized by specific peculiarities, which would strongly influence greenhouse gas (GHG) production/emission (mainly nitrous oxide, N_2O produced during the BNR processes). For example, the intensive aeration for fouling mitigation in MBR can promote the N_2O stripping. However, very few studies have been performed with this concern in biofilm and MBR systems (Todt and Dörsch 2016; Mannina et al. 2017). Therefore, further investigations are required in order to identify the key operating factors affecting the N_2O emission from plants where advanced technologies are adopted. With this regards the main goal of this work is to investigate the performance (in terms of carbon and nutrient removal) and N_2O emission of two plant configurations adopting innovative technologies: i. University Cape Town (UCT) MBR plant; ii. IFAS-UCT-MBR plant. Both plants treat real wastewater under two different values of the influent carbon nitrogen ratio (C/N = 5 mgCOD/mgN and C/N = 10 mgCOD/mgN).

2 Materials and Methods

2.1 Pilot Plants

Two pilot plants were built at the Laboratory of Sanitary and Environmental Engineering of Palermo University. In particular, a University Cape Town (UCT) Membrane Bioreactor (MBR) and an Integrated Fixed Film Activated Sludge (IFAS) UCT-MBR were studied under two different values of the influent C/N ratio. Both plants were characterized by identical reactors dimensions and lay-out. In particular, both pilot plants consisted of a 62 L stirred anaerobic reactor, a 102 L stirred anoxic reactor and a 221 L aerobic reactor, provided with fine bubble diffusers. In the membrane compartment was placed an ultrafiltration hollow fiber membrane module (Koch Puron® 3 bundle) characterized by a pore size of 0.03 μm and membrane net area of 1.4 m^2. In the IFAS-UCT-MBR plant, suspended plastic carriers (Amitech®, 0.95 g·cm^{-3} and 500 m^2m^{-3} density and specific surface respectively) were placed into aerobic and anoxic reactor in order to reach a filling ratio equal to 40% and 15%

corresponding to a net surface area equal to 200 $m^2 \cdot m^{-3}$ and 75 $m^2 m^{-3}$ respectively. The anaerobic, anoxic, aerobic and MBR reactors were equipped with specific covers that made it possible to collect and sample the overall gas in the headspace from each compartment of the pilot plant.

2.2 Influent Wastewater

The pilot plant was fed with municipal wastewater mixed with a synthetic wastewater in order to control the C/N ratio. The experimental campaign was divided into two phases, each characterized by a different C/N value. The UCT-MBR plant was operated at the sludge retention time (SRT) value of 50 days (for C/N = 5 mgCOD/mgN) and 40 days (for C/N = 10 mgCOD/mgN). The IFAS-UCT-MBR plant was operated at the SRT value of 65 days (for C/N = 5 mgCOD/mgN) and 40 days (for C/N = 10 mgCOD/mgN).

2.3 Sampling and Monitoring Campaign

The influent wastewater, the different reactors and the effluent permeate were sampled and analyzed for chemical oxygen demand (COD), biochemical oxygen demand (BOD), total nitrogen (TN), ammonium nitrogen (NH_4-N), nitrate nitrogen (NO_3-N), nitrite nitrogen (NO_2-N), orthophosphate (PO_4-P). All analyses were performed according to the APHA (2005).

The respirometric batch experiments were carried out on a "flowing gas/static-liquid" respirometer, according to the procedure described in literature (Mannina et al. 2017). Extracellular polymeric substances (EPSs) were extracted according to the procedure reported in literature (Cosenza et al. 2013; Mannina et al. 2016). The membrane fouling has been analysed according to the procedure reported in literature (Mannina et al. 2016).

Gas samples were collected from the funnel shape cover of the anaerobic, anoxic, aerobic and MBR reactors and transferred into glass vials and analysed with a gas chromatograph (GC). Air velocity was assessed by using a TMA 21HW Hot Wire anemometer in order to evaluate the gas flux. Liquid samples were collected from the anaerobic, anoxic, aerobic and MBR reactors and the dissolved N_2O concentration was extracted by adopting the procedure proposed by Kimochi et al. (1998). The measured N_2O concentrations were used to assess the N_2O emission factor according to the procedure proposed by Tsuneda et al. (2005).

3 Results and Discussion

3.1 Removal Performance

Table 1 summarizes the average values of COD, N and P removal efficiencies. In terms of COD removal, data of Table 1 show that the solid liquid separation through the membrane allowed to maintain high total COD removal efficiency during each phase and for each plant configuration. However, the biological COD removal (η_{BIO}) was

Table 1. Average removal efficiency values for each pollutant, plant configuration and experimental phase (C/N = 5 and C/N = 10)

Symbol	Description	UCT-MBR		IFAS-UCT-MBR	
		C/N = 5	C/N = 10	C/N = 5	C/N = 10
η_{TOT}	Total COD removal efficiency	98.47	98.31	98.06	98.59
η_{BIO}	Biological COD removal efficiency	73.58	83.03	79.50	84.01
η_{PHYS}	Physical COD removal efficiency	24.89	15.28	18.55	14.58
ηN_{tot}	Total N removal efficiency	39.00	69.24	53.14	69.36
η_{nitr}	Nitrification efficiency	80.61	95.40	81.08	90.93
η_{denit}	Denitrification efficiency	32.27	56.25	42.78	52.02
η_{PO4}	PO_4-P removal efficiency	-	71.82	67.16	87.50

affected by the influent both by the plant configuration and influent C/N value. Indeed, η_{BIO} increased with the increase of influent C/N. However, for the same C/N value the highest η_{BIO} was obtained for the IFAS-UCT-MBR configuration. This result is mainly debited to the adding role in carbon removal due to the biofilm.

Similar results were found for the nitrogen removal; indeed, the simultaneous growth of biofilm in the aerobic and anoxic reactors was able to enhance the total nitrogen removal in the IFAS-UCT-MBR configuration even at the lowest C/N value (at C/N = 5 ηN_{tot} was equal to 39% and 53.14% for UCT-MBR and IFAS-UCT-MBR configuration, respectively).

The attached biomass in the anoxic reactor has had a key role for the improvement of phosphorus removal under the lowest C/N value. Indeed, as reported in Table 1 during the Phase at C/N = 5 the phosphorus removal failed for the UCT-MBR configuration. This result was due to the COD limitation during denitrification, which caused that a great mass of NO_3-N was pumped back from the anoxic to the anaerobic tank in the UCT-MBR scheme, thus disturbing the biological phosphorus removal mechanisms. Conversely, the contribution of biofilm (which does not compete for carbon with the suspended biomass) in the IFAS-UCT-MBR configuration allowed to improve phosphorus removal.

3.2   Membrane Fouling

Figure 1 shows the results of the total membrane resistance (R_T). Data of Fig. 1 show an higher tendency of membrane to be fouled in the IFAS-UCT-MBR (Fig. 1b) configuration than UCT-MBR one (Fig. 1a). Indeed, five physical cleanings were required during the UCT-MBR configuration to maintain the R_T value under the value suggested from manufactures. Conversely, nine physical and four chemical cleanings (adopting sodium hypochlorite) cleanings were required for the IFAS-UCT-MBR configuration. This result is likely debited to the increased sludge viscosity due to the biofilm.
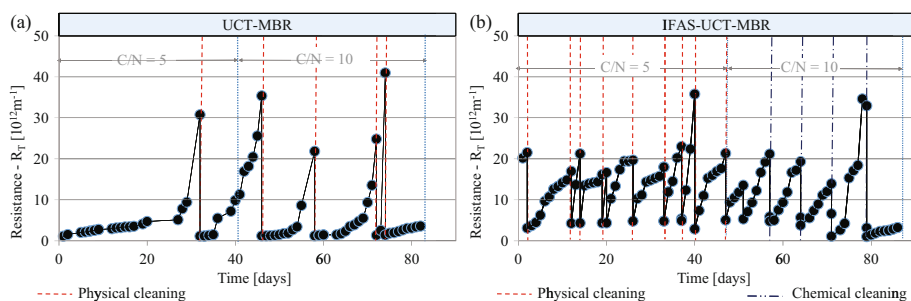
Fig. 1. Total membrane resistance (R_T) for the UCT-MBR (a) and IFAS-UCT-MBR (b) configuration

3.3   N₂O Emissions

The average of the N_2O emission factors (percentage of the influent nitrogen emitted as N_2O) for both plant configurations and influent C/N values are depicted in Fig. 2.
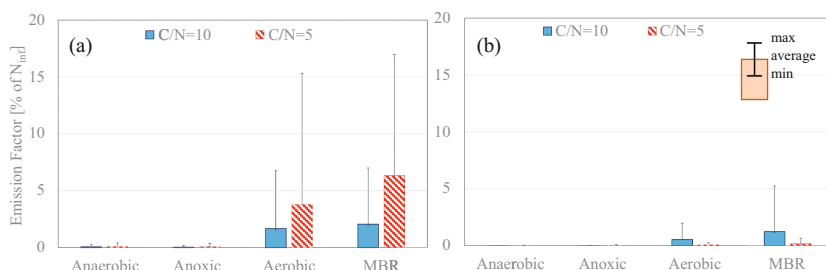
Fig. 2. Average Nitrous oxide Emission factors assessed during UCT-MBR (a) and during IFAS-UCT-MBR (b) for both investigated C/N values.

For both configurations, the largest part of emission occurred from the aerated reactors (Fig. 2). However, the aerated reactors of the UCT-MBR configuration emitted much more than that of the IFAS-UCT-MBR configuration. Specifically, on average 3.5% of the influent nitrogen was emitted as N_2O from the UCT-MBR plant and 0.5% (of the influent nitrogen) from IFAS-UCT-MBR plant. The presence of biofilm and suspended biomass in the IFAS-UCT-MBR plant has improved the nitrogen removal processes efficiency resulting in a sharp reduction of the N_2O emission factor.

4   Conclusions

The comparison of two plant configurations (UCT-MBR and IFAS-UCT-MBR) under two different influent C/N ratio (5 and 10 mgCOD/mgN) has been performed. The IFAS-UCT-MBR configuration provided the best results in terms of pollutants removal

performance during both the two investigated C/N values. Furthermore, the lowest N_2O emission (with respect to the influent nitrogen) occurred for the IFAS-UCT-MBR. However, the IFAS-UCT-MBR showed a greater tendency of being fouled respect to the UCT-MBR configuration. This result could have serious effects in terms of indirect GHG emissions due to the increase of the energy requirement for permeate extraction with the increase of membrane fouling.

References

APHA (2005) Standard Methods for the Examination of Water and Wastewater. APHA, AWWA and WPCF, Washington DC, USA

Cosenza A, Di Bella G, Mannina G, Torregrossa M (2013) The role of EPS in fouling and foaming phenomena for a membrane bioreactor. Bioresour Technol 147:184–192

Kimochi Y, Inamori Y, Mizuochi M, Xu K-Q, Matsumura M (1998) Nitrogen removal and N_2O emission in a full-scale domestic wastewater treatment plant with intermittent aeration. J Ferment Bioeng 86:202–206

Mannina G, Capodici M, Cosenza A, Di Trapani D (2016) Carbon and nutrient biological removal in a University of Cape Town membrane bioreactor: analysis of a pilot plant operated under two different C/N ratios. Chem Eng J 296:289–299

Mannina G, Capodici M, Cosenza A, Di Trapani D, van Loosdrecht MCM (2017) Nitrous oxide emission in a University of Cape Town membrane bioreactor: the effect of carbon to nitrogen ratio. J Cleaner Prod 149:180–190

Todt D, Dörsch P (2016) Mechanism leading to N_2O production in wastewater treating biofilm systems. Rev Environ Sci Biotechnol 15(3):355–378

Tsuneda S, Mikami M, Kimochi Y (2005) Effect of salinity on nitrous oxide emission in the biological nitrogen removal process for industrial wastewater. J Hazard Mater 119:93–98

Wang XJ, Xia SQ, Chen L, Zhao JF, Renault NJ, Chovelon JM (2006) Nutrients removal from municipal wastewater by chemical precipitation in a moving bed biofilm reactor. Process Biochem 41(4):824–828

Wanner J (2002) Control of filamentous bulking in activated sludge. In: Bitton G (ed) Encyclopedia of environmental microbiology. John Wiley & Sons Inc., New York, pp 1306–1315

Anaerobic Digestion and Modelling

Exploring the Feasibility of a Novel Municipal Wastewater Treatment System via Dynamic Plant-Wide Simulation

E. Bozileva[1,2(✉)], R. Khiewwijit[3], H. Temmink[1], H.H. Rijnaarts[1], and K.J. Keesman[2]

[1] Sub-department of Environmental Technology,
Wageningen University and Research Centre, Wageningen, The Netherlands
[2] Biobased Chemistry and Technology,
Wageningen University and Research Centre, Wageningen, The Netherlands
[3] Wetsus European Centre of Excellence for Sustainable Water Technology,
Leeuwarden, The Netherlands

Abstract. A plant-wide simulation study is presented in which we investigated the feasibility of a novel centralized municipal wastewater treatment system design as previously proposed by Khiewwijit et al. (2015). This design includes processes as bioflocculation (BF), anaerobic digestion (AD), partial nitritation (PN) and Anammox (ANA). We specifically investigate the effects of operational conditions (SRT, HRT, dissolved oxygen set point and temperature) on carbon recovery potential and ability to meet N discharge criteria according to European legislation. The results suggest that BF-AD can be a promising technology combination for carbon recovery. However, PN-ANA is as yet not suitable for European conditions within the context of studied design at the current state of technology development.

Keywords: Plant-wide simulation · Bioflocculation · Anaerobic digestion · Partial nitritation · Anammox

1 Introduction

Municipal wastewater is commonly treated in conventional activated sludge (CAS) systems. The CAS process is very robust and provides high quality effluent in terms of COD and nutrient concentrations (Metcalf et al. 1991). However, the concept of CAS is far from being sustainable due to considerable energy requirements and low potential for energy and nutrient recovery.

To address these shortcomings, Khiewwijit et al. (2015) proposed an alternative system (similar to that shown in Fig. 1), consisting of bioflocculation (BF), anaerobic digestion (AD), partial nitritation (PN) and Anammox (ANA). BF acts as a compact pre-concentration step, performed at extremely short sludge and hydraulic retention times to avoid mineralisation of organic matter. AD recovers this pre-concentrated organic matter in the form of methane or volatile fatty acids. The PN-ANA combination performs nitrogen removal at considerably lower oxygen requirements compared to the conventional nitrification-denitrification practices. Furthermore, it does not
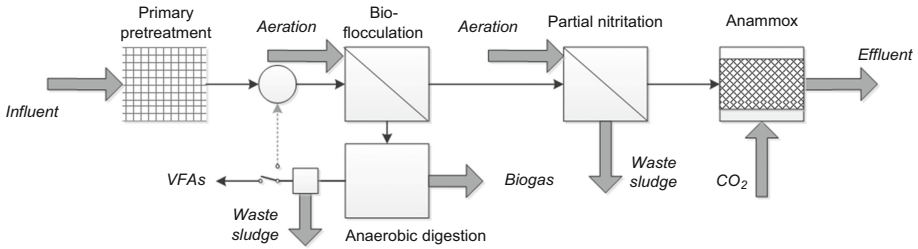
Fig. 1. Wastewater treatment process configuration investigated in this study. Two alternative operating modes are shown (with the focus on energy recovery and VFA production)

require organic matter, which can therefore be recovered. The results of lab-scale experiments and steady-state calculations, carried out by Khiewwijit et al. (2015), indicated that the proposed system would outperform CAS in terms of net energy yield and carbon emissions. However, to determine whether such performance can also be expected for a full-scale system a more elaborate analysis is needed that takes into account complex microorganism interactions. In this work we performed such an analysis, with focus on carbon recovery and effluent quality, by carrying out dynamic plant-wide simulations at different operational conditions (HRT, SRT, dissolved oxygen level, temperature) for fixed hydraulic, organic and nutrient loads.

2   Materials and Methods

The configuration investigated in this study is given in Fig. 1. System influent is defined by average values of dry weather influent available at http://www.benchmarkWWTP. org/.

The BF was assumed to be taking place in MBR and was modelled with biomass kinetic model. The model assumes that biomass dynamics is characterized by ASM1 (Henze et al. 2000) calibrated for an MBR by Baek et al. (2009). Alternatively BF was simulated with the aforementioned model extended for slowly biodegradable substrate adsorption onto floc, as in Dold et al. (1980) (further referred to as ASM1+), and with the ASM1SMP model calibrated for an MBR by Mannina et al. (2011). The AD was modelled with ADM1 (Batstone et al. 2002) assuming that the reactor is represented by a CSTR. The PN-ANA was modelled as SHARON/Anammox process, with PN taking place in CSTR and ANA in granular sludge reactor. PN and ANA were modelled with ASM1 extended for two-step nitrification (Wyffels et al. 2004) and the presence of Anammox bacteria (Ni et al. 2009), respectively. Mass transfer within the granules was modelled with a 1D continuum biofilm model (Wanner and Gujer 1986), assuming constant granule dimensions (1 mm diameter).

For model integration we used the ASM-ADM interface as suggested by Nopens et al. (2009). The integrated system simulations were performed for a sufficient period of time to allow reaching of steady-state in the reactors (minimum of 100 days for individual BF simulation and maximum of four years for ANA).

3   Results and Discussion

The system shown in Fig. 1 was virtually split into two compartments that were analysed separately. The first compartment consisting of BF and AD was analysed in terms of carbon recovery efficiency. Carbon was recovered either in the form of methane or in the form of volatile fatty acids (VFAs). The second compartment consisting of PN-ANA was analysed in terms of final nitrogen concentration in the effluent. The operational conditions, that were varied to study the performance of each compartment, are shown in Table 1.

Table 1. The ranges of operational conditions considered in this study

	Carbon recovery compartment		Nitrogen removal compartment	
	BF	AD	PN	ANA
SRT (d)	0.5–2	–	–	–
HRT (h)	0.5–2	120–480	24–720	5
Temperature (°C)	20	35	20–30	20–30
Dissolved oxygen (gO_2/m^3)	2	–	0.1–2	–

The first unit operation of the carbon recovery compartment is BF unit. BF represents simple activated sludge process performed at extremely short $HRT < 1$ h and $SRT < 1$ day to avoid excessive sludge formation and mineralisation, while allowing organic matter pre-concentration via adsorption onto sludge flocs. Nevertheless, to the best of our knowledge, there is no model available at the moment that would explicitly take into account the process of flocculation/adsorption. Consequently the simulation results that follow are subject to model structure and parameter uncertainty and are mainly used only to approximately assess the degree of COD loss due to mineralisation. Whereas developing a BF model to reduce the uncertainty is out of scope of this study, in what follows we attempt to assess the uncertainty associated with model structure and (sensitive) parameter values.

To assess the uncertainty associated with model structure we evaluated the BF model output in terms of COD loss due to mineralisation and total COD concentration at the steady state for three candidate models: ASM1, ASM1+, and ASM1SMP. Figure 2 shows how the outputs are affected by operational conditions in BF (each point represents the model output after 100 days of simulation time at a constant load). Whereas all three models agree on total steady state COD concentration, discrepancies can be observed in predictions regarding the degree of mineralisation. Specifically, ASM1SMP predicts lower CO_2 loss at low SRT_{BF} (15% at $SRT_{BF} = 0.5$ days) and higher CO_2 loss at high SRT_{BF} (27% at $SRT_{BF} = 2$ days) compared to ASM1 and ASM1+. The differences between the latter two at the studied conditions are negligible. Consequently in what follows we use ASM1 to simulate BF, as its predicted outcome in terms of CO_2 loss at preferable operational conditions is "less optimistic" (20% at $SRT_{BF} = 0.5$ days) compared to ASM1SMP.
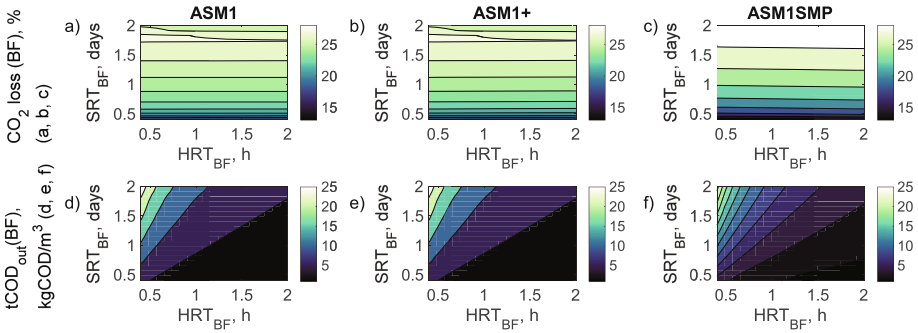
Fig. 2. The effect of operational conditions (HRT_{BF} and SRT_{BF}) on BF model outputs (COD loss associated with CO_2 production and total final COD concentration) for three models: ASM1, ASM1+, and ASM1SMP

To assess the uncertainty associated with parameter values we performed Monte Carlo simulations of BF with random sampling of parameters characterising heterotrophic yield (Y_H), heterotrophic growth rate (μ_{mH}), half saturation coefficient for S_s (K_S), and hydrolysis rate constant (k_H). The choice of parameters was based on previous research (Fenu et al. 2010), which identified those as the most influential for COD uptake. The range for parameter sampling was based on values reported in the literature (Baek et al. 2009; Henze et al. 2000; Jiang et al. 2005; Mannina et al. 2011). It can be seen (Fig. 3) that varying the parameter values within the specified ranges resulted in varying CO_2 loss percentage in a range from 16% to 23%, with most of the variance being attributed to Y_H and K_S. Whereas the established value range for CO_2 loss percentage cannot be considered final, it can be used as a rough measure of uncertainty that would propagate to downstream AD process.
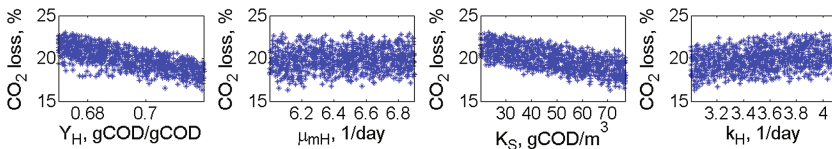
Fig. 3. Projections of variance in COD loss due to mineralisation as a result of variance in Y_H, μ_{mH}, K_S and k_H

Figure 4 shows how operational conditions in BF affect the output of AD in terms of methane or VFA recovery (each point represents the model output after 200 days of simulation time at a constant load). The results indicate that the methane recovery potential of the system is practically insensitive to the operational conditions in BF if AD is operated at *SRT* of 20 days. Figure 2b shows that operating BF at shorter *HRT* and *SRT* mildly improves methane recovery from 26% (at $HRT_{BF} = 2$ h and $SRT_{BF} = 2$ days) to 29% (at $HRT_{BF} = 0.5$ h and $SRT_{BF} = 0.5$ days), with respect to total influent COD. This result is comparable to 35% methane recovery (with respect to
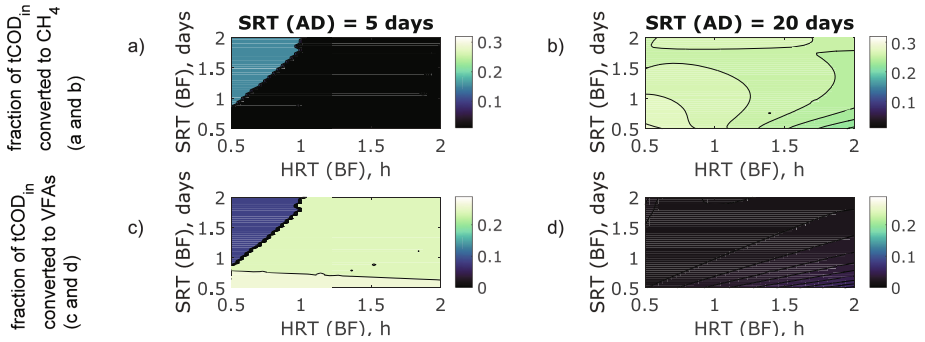
Fig. 4. Fraction of total influent COD converted to methane and to VFAs as a function of HRT and SRT in BF reactor for different SRTs in AD reactor

total influent COD) reported by Akanyeti et al. (2010) for a lab-scale BF-AD set-up. Such a low conversion was attributed by Akanyeti et al. (2010) to COD loss in BF due to mineralisation, which is especially prominent at high SRT. Indeed, Fig. 2 shows that even at the lowest considered HRT_{BF} and SRT_{BF} mineralisation is accountable for up to 21% of total COD loss.

The system can be alternatively operated in VFA recovery mode at short SRT_{AD} of 5 days. Figure 4c shows that for such system up to 27% of total COD_{in} can be recovered in the form of VFAs if BF is operated at $HRT_{BF} = 0.5$ h and $SRT_{BF} = 0.5$ days. The COD balances in carbon recovery compartment for two modes of operation are shown in Fig. 5.
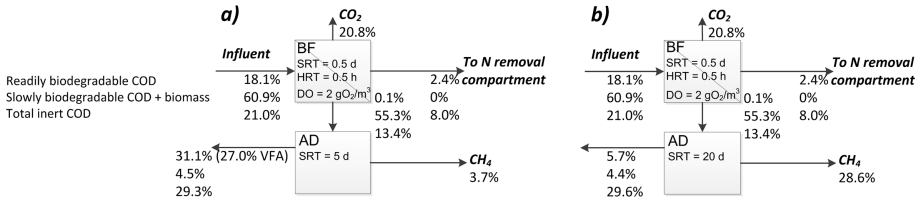
Fig. 5. Steady-state COD balances in carbon recovery compartment at the most beneficial conditions for VFA (a) and methane (b) recovery (within the ranges considered in this study)

The fact that bacteria that support N removal in PN-ANA are autotrophs, suggests that it is possible to decouple optimisation of carbon recovery and N removal compartments. Consequently, the analysis of N removal efficiency is performed for fixed $HRT_{BF} = 0.5$ h and $SRT_{BF} = 0.5$ days. The capacity of Anammox bacteria to convert nitrogenous compounds into dinitrogen gas relies on capacity of bacteria community in upstream PN reactor to ensure stoichiometric ratio of $NO_2^-:NH_3 = 1.32:1$, while avoiding the formation of nitrate. The latter can be achieved by regulating temperature (T), retention time, DO, pH and bicarbonate-to-ammonia ratio. Figure 6 shows how T_{PN-ANA}, HRT_{PN}, and DO_{PN} affect the steady-state $NO_2^-:NH_3$ ratio in PN and how it
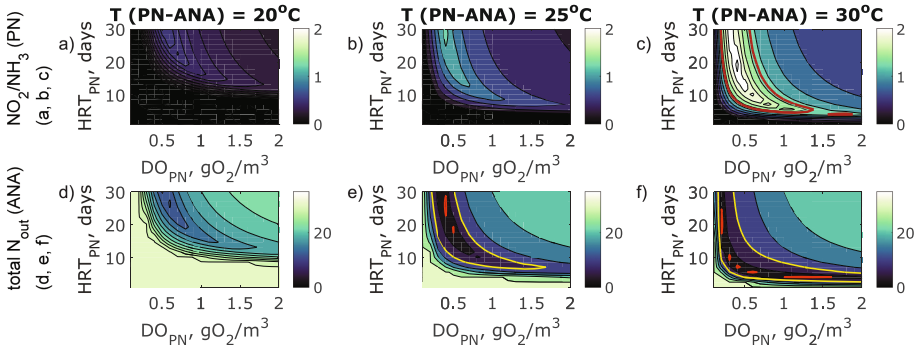
Fig. 6. Nitrite-to-ammonia ratio in PN reactor (a, b, c) and concentration of total effluent N (d, e, f) as a function of DO_{PN}, HRT_{PN}, and T_{PN-ANA}. Red line in a, b, and c corresponds to NO_2^-/NH_3 = 1.32. Yellow line in d, e, and f borders the area corresponding to total effluent N < 10 g/m^3. Orange line in d, e, and f borders the area corresponding to total effluent N < 2.2 g/m^3 (Color figure online)

translates into total steady-state N concentration in the effluent of ANA. It can be seen that there exist multiple combinations of HRT_{PN} and DO_{PN} that ensure meeting the old EU N discharge standard of 10 gN/m^3. Nevertheless, this standard can only be met for temperatures in PN-ANA above 25 °C. New EU N discharge standard of 2.2 gN/m^3 cannot be met at any of the studied conditions. This makes PN-ANA part of the system not very well suitable for European conditions at the current stage of technology development.

It should be noted, nevertheless, that the precise quantitative aspect of the simulation study should be taken with caution, and the work should be interpreted mainly in terms of the qualitative representations of the potentials, bottlenecks and shortcomings of the nonconventional wastewater treatment concepts considered from a perspective of an integrated system.

4   Conclusions

In this simulation study we discussed the feasibility of a novel municipal wastewater treatment system previously proposed by Khiewwijit et al. (2015). We specifically focused on assessing the effects of model assumptions and changes in operational conditions in BF on performance of AD in terms of methane and VFA recovery potential. We showed that operating the BF reactor at low *HRT* (around 0.5 h) and *SRT* (around 0.5 days) is beneficial for both methane and VFA recovery. Furthermore, we quantified the extent to which the methane and VFA recovery are affected by the abovementioned operational conditions in BF and selected operational conditions in AD. The results indicate that BF-AD can be a promising technology combination for carbon recovery. We additionally investigated the effect of operational conditions in PN-ANA on final effluent N concentration and showed that in the context of the studied system PN-ANA might not yet be suitable for European conditions at the current state

of technology development. It should be noted, however, that the precise quantitative aspect of the study should be treated with care, mainly due to high uncertainty associated with model output for BF unit. Nevertheless, we believe that the study provides valuable information on potentials and shortcomings of nonconventional wastewater treatment concepts, when viewed from an integrated system perspective.

References

Akanyeti I, Temmink H, Remy M, Zwijnenburg A (2010) Feasibility of bioflocculation in a high-loaded membrane bioreactor for improved energy recovery from sewage. Water Sci Technol 61(6):1433–1439. doi:10.2166/wst.2010.032

Baek SH, Jeon SK, Pagilla K (2009) Mathematical modeling of aerobic membrane bioreactor (MBR) using activated sludge model no. 1 (ASM1). J Ind Eng Chem 15(6):835–840. doi:10.1016/j.jiec.2009.09.009

Batstone DJ, Keller J, Angelidaki I, Kalyuzhny S, Pavlostathis S, Rozzi A, Sanders W, Siegrist H, Vavilin V (2002) The IWA anaerobic digestion model no 1 (ADM1). Water Sci Technol 45(10). doi:http://dx.doi.org/10.2166/9781780403052

Dold P, Ekama G, Marais G (1980) A general model for the activated sludge process. Prog Water Technol 12(6):47–77

Fenu A, Guglielmi G, Jimenez J, Spèrandio M, Saroj D, Lesjean B, Brepols C, Thoeye C, Nopens I (2010) Activated sludge model (ASM) based modelling of membrane bioreactor (MBR) processes: a critical review with special regard to MBR specificities. Water Res 44 (15):4272–4294. doi:10.1016/j.watres.2010.06.007

Henze M, Gujer W, Mino T, van Loosdrecht M (2000) Activated sludge models ASM1, ASM2, ASM2d and ASM3. IWA publishing. doi:http://dx.doi.org/10.2166/9781780402369

Jiang T, Liu X, Kennedy MD, Schippers JC, Vanrolleghem PA (2005) Calibrating a side-stream membrane bioreactor using Activated Sludge Model No. 1. Water Sci Technol 52(10–11):359–367

Khiewwijit R, Temmink H, Rijnaarts H, Keesman KJ (2015) Energy and nutrient recovery for municipal wastewater treatment: how to design a feasible plant layout? Environ Model Softw 68:156–165. doi:10.1016/j.envsoft.2015.02.011

Mannina G, Di Bella G, Viviani G (2011) An integrated model for biological and physical process simulation in membrane bioreactors (MBRs). J Membr Sci 376(1–2):56–69. doi:10.1016/j.memsci.2011.04.003

Metcalf L, Eddy HP, Tchobanoglous G (1991) Wastewater engineering: treatment, disposal, and reuse. McGraw-Hill, New York

Ni B-J, Chen Y-P, Liu S-Y, Fang F, Xie W-M, Yu H-Q (2009) Modeling a granule-based anaerobic ammonium oxidizing (ANAMMOX) process. Biotechnol Bioeng 103(3):490–499. doi:10.1002/bit.22279

Nopens I, Batstone DJ, Copp JB, Jeppsson U, Volcke E, Alex J, Vanrolleghem PA (2009) An ASM/ADM model interface for dynamic plant-wide simulation. Water Res 43(7):1913–1923. doi:10.1016/j.watres.2009.01.012

Wanner O, Gujer W (1986) A multispecies biofilm model. Biotechnol Bioeng 28(3):314–328. doi:10.1002/bit.260280304

Wyffels S, Van Hulle SWH, Boeckx P, Volcke EIP, Cleemput OV, Vanrolleghem PA, Verstraete W (2004) Modeling and simulation of oxygen-limited partial nitritation in a membrane-assisted bioreactor (MBR). Biotechnol Bioeng 86(5):531–542. doi:10.1002/bit.20008

Reshaping the Activated Sludge Model ASM2d for Better Manageability and Higher Integration Potential

H.H. Pham[1(✉)], Y. Wouters[1], M. Dalmau[2], J. Comas[2], and I. Smets[1]

[1] Chemical Engineering Department, KU Leuven, Celestijnenlaan 200F,
Bus 2424, 3001 Heverlee, Belgium
[2] LEQUIA, University of Girona, Campus de Montilivi, 17071 Girona,
Catalonia, Spain

Abstract. The European Water Framework Directive has pointed out that the best model for water management is management by river basin. However, to obtain an overview of the water quality in a river basin system, one has to look at the individual components of the system such as the sewer network, the wastewater treatment plant and the receiving water bodies and the interaction between them. Within this study, we develop an adjusted model from the original state-of-the-art activated sludge ASM2d model with as main focus to maximize the compatibility with the sewage and river water quality models while still assuring a sufficient prediction capacity of the activated sludge system. To this end, and to avoid the commonly required fractionation into the classic activated sludge model state variables, the latter are directly derived from the outputs of the sewage model (e.g., BOD5, COD, TN or TP) for the adjusted model. Furthermore, the modified ASM2d model is made more realistic and can be more broadly applied due to the re-introduction of organic nitrogen and phosphorus component state variables. While developed on the basis of the data of a wastewater treatment plant in Belgium, the validation of the adjusted model on a data set of a wastewater treatment plant in Girona (Spain) is highly promising.

Keywords: Wastewater treatment modeling · ASM2d · Model integration

1 Introduction

Worldwide, researchers are commonly using activated sludge models (Henze et al. 2000) to study and optimize all the biochemical processes in wastewater treatment plants (WWTPs). If we look at the whole picture of a (waste)water management system, WWTPs play a central role by receiving wastewater from sewage systems, and by treating and finally discharging the safe effluent to the environment such as rivers and lakes. To make sound decisions, engineers and/or managers have to look at the whole system although the availability of a straightforward integrated monitoring tool is, unfortunately, still limited. This lack results from the fact that the incompatibilities of the input/output between the sub-models (sewage and river water quality models) thus far remain unresolved.

Although over the last decades, integrated modeling has been on the research agenda (e.g., Vanrolleghem et al. 2005; Benedetti et al. 2004, 2007; Sharma et al. 2012), with the integrated modeling practice recently reviewed by Benedetti et al. (2013), a fully compatible and easy manageable framework is still missing. To link WWTP ASM models with other sewer and river sub-systems, efforts have predominantly focused on the development of *interfacing models* as can be seen in, e.g., Vanrolleghem et al. (2005).

However, the structure and associated state variables of the ASM models have not received much attention to improve the integration potential. Furthermore, to obtain a representative model, quite some experiments need to be performed, not only for the calibration and validation of the model but also for a proper fractionation of the input (Roeleveld and van Loosdrecht 2002; Hulsbeek et al. 2002).

Therefore, this work presents an adjusted activated sludge model which is better manageable when using it for either calibration or integration practice. The state-of-the-art activated sludge model ASM2d is selected as the starting model (structure), to establish a reference model, based on the data from a wastewater treatment in Belgium. On the basis of this reference model an adjusted model is developed. *The rationale of this adjusted ASM2d model is that the state variables of the model should be all directly derived from available wastewater measurement concentrations*. In this way, the outlet sewer measurements can be the direct input measurements for the WWTP model and its effluent variables can directly be translated in input variables for the river model. Finally, the adjusted model is validated by exploiting extra data for the Belgian WWTP and external data, i.e., from a pilot plant located in Girona, Spain.

2 Methodology and Results

To comply with the modeling rationale of exploiting as much as possible the already available measurements like COD, Total Nitrogen, Total Phosphorus etc., three main adaptations to the ASM2d model and its corresponding state variables are implemented, being:

– no fractionation of soluble organic biodegradable material but working with just one lumped BOD based state variable;
– no fractionation of particulate organic material but working with one lumped state variable;
– the re-introduction of organic nitrogen and phosphorus as state variables (as in former activated sludge models).

The new model is summarized by an adjusted Peterson matrix with 20 components and 24 processes.

The measurement campaign for the calibration of the adjusted model is summarized in Fig. 1. As can be seen, the newly (re-)introduced state variables (brown boxes in the middle) can be derived from filtered (denoted with 's' from soluble) and unfiltered COD, ammonium (NH_4-N), nitrite and nitrate (NOx-N), Total Nitrogen (TN), Total Phosphorus (TP), phosphate (PO4-P), BOD_5 and Total Suspended Solids measurements.
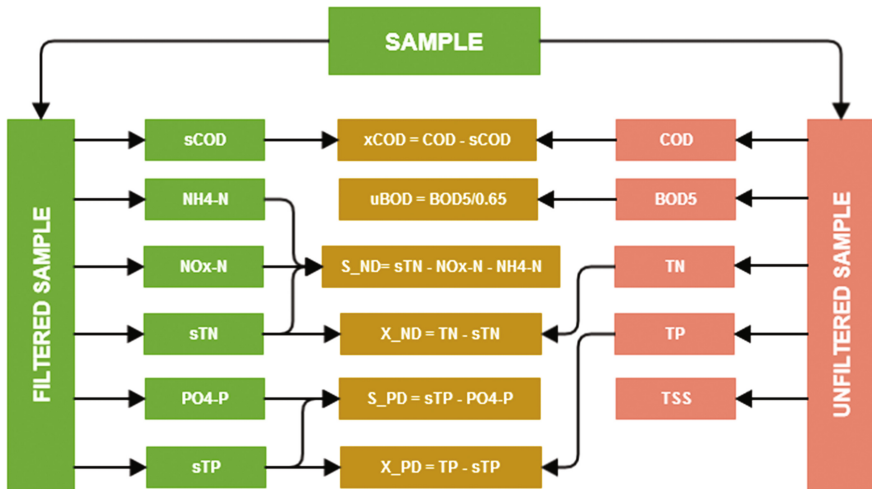
Fig. 1. Measurements required to initialize and calibrate the adjusted model. The newly (re-) introduced state variables (brown boxes in the middle) can be derived from filtered (denoted with 's' from soluble) and unfiltered COD, ammonium (NH$_4$-N), nitrite and nitrate (NOx-N), Total Nitrogen (TN), Total Phosphorus (TP), phosphate (PO4-P), BOD$_5$ and Total Suspended Solids measurements (Color figure online)
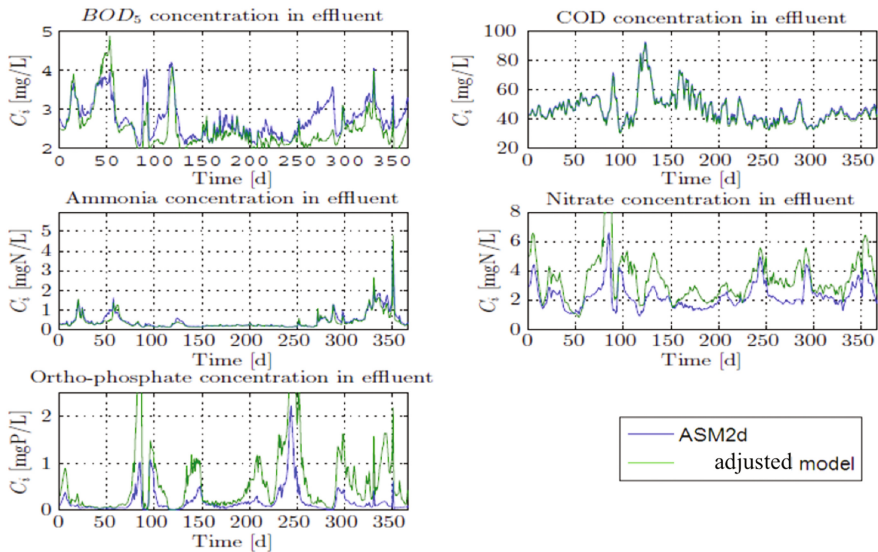
Fig. 2. Validation 1. Comparison of the BOD$_5$, COD, ammonium, nitrate, and phosphate concentration in the effluent as simulated by the ASM2d (blue line) and by the adjusted model (green line) for the Belgian WWTP data set (other year than for the calibration) (Color figure online)
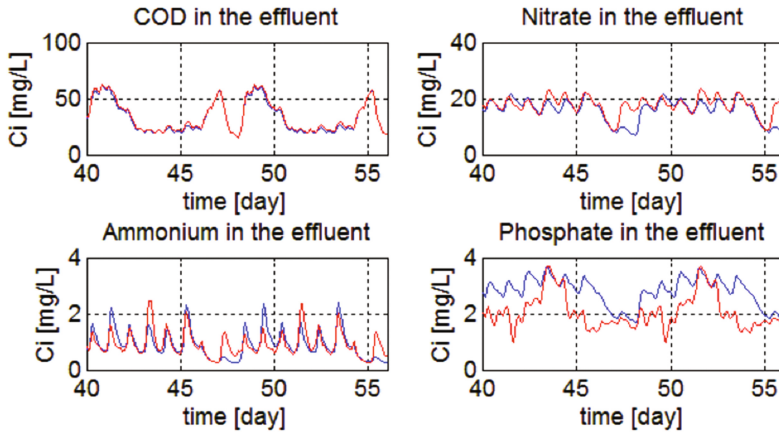
Fig. 3. Validation 2. Comparison of the COD, nitrate, ammonium and phosphate concentration in the effluent as simulated by the ASM2d (blue line) and by the adjusted model (red line) for the Girona WWTP data set (Color figure online)

Validation results of the adjusted model on the basis of the data of the wastewater treatment plant in Belgium (other data set than used for the calibration) and in Girona are depicted in Figs. 2 and 3. More specifically, the effluent profiles simulated by the adjusted model and by the calibrated ASM2d model are shown. In general, a slightly higher nitrate concentration can be observed. This is due to the re-introduction of organic nitrogen leading to a higher availability of ammonium through the ammonification process. Thus more nitrates will be formed from the increased availability of ammonium. The phosphate concentration obtained by the adjusted model is slightly higher but still acceptable for the Belgian case. For the Girona case, the values are lower than the ones simulated by the original model. This lower level comes from the fact that data of total phosphorus in the influent is not available for this plant. Therefore, we set the value of organic phosphorus (particulate and soluble) equal to zero in the influent file. Nevertheless, it is clear from the results that the adjusted model has been successfully implemented with new data sets and positive outcomes have been obtained.

3   Conclusions

–   An adjusted model based on the ASM2d model has been developed and validated with different data sets.
–   The fractionation step can be minimized with the adjusted model, via which uncertainty can avoided. Thanks to the incorporation of organic nitrogen and phosphorus, the adjusted model can be applied to a wider range of influents.
–   By using and producing directly measured concentrations, the integration of the modified model with sewer and river water quality models can be easily implemented.

References

Benedetti L, Meirlaen J, Vanrolleghem PA (2004) Model connectors for integrated simulations of urban wastewater systems. In: Bertrand-Krajewski J-L, Almeida M, Matos J, Abdul-Talib S (eds) Sewer networks and processes within urban water systems, pp 13–20. ISBN 1 84339 506 1

Benedetti L, Meirlaen J, Sforzi F, Facchi A, Gandolfi C, Vanrolleghem PA (2007) Dynamic integrated water quality modelling: a case study of the Lambro River, Northern Italy. Water SA 33(5):627–632

Benedetti L, Langeveld J, Comeau A, Corominas L, Daigger G, Martin C, Mikkelsen PS, Vezzaro L, Weijers S, Vanrolleghem PA (2013) Modelling and monitoring of integrated urban wastewater systems: review on status and perspectives. Water Sci Tech 68(6):1203–1215

Henze M, Gujer W, Mino T, van Loosdrecht M (2000) Activated sludge models: ASM1, ASM2, ASM2d and ASM3. IWA Publishing

Hulsbeek JJW, Kruit J, Roeleveld PJ, van Loosdrecht MCM (2002) A practical protocol for dynamic modelling of activated sludge systems. Water Sci Tech 45(6):127–136

Roeleveld PJ, van Loosdrecht MCM (2002) Experience with guidelines for wastewater characterisation in The Netherlands. Water Sci Tech 45(6):77–87

Sharma KR, Corrie S, Yuan Z (2012) Integrated modelling of sewer system and wastewater treatment plant for investigating the impacts of chemical dosing in sewers. Water Sci Tech 65 (8):399–405

Vanrolleghem PA, Rosen C, Zaher U, Copp J, Benedetti L, Ayesa E, Jeppsson U (2005) Continuity-based interfacing of models for wastewater systems described by Petersen matrices. Water Sci Tech 52(1–2):493–500

Population Dynamic of Microbial Consortia in a Granular Activated Carbon-Assisted Biofilm Reactor: Lessons from Modelling

M. Azari[✉], A.V. Le, and M. Denecke

Department of Urban Water and Waste Management,
University of Duisburg-Essen, Universitätsstraße 15, 45141 Essen, Germany
mohammad.azari-najaf-abad@uni-due.de

Abstract. In this work, experimental and long-term mathematical modelling approaches were combined to investigate mechanisms and drivers influencing on microbial consortia dynamics in an anaerobic granular biofilm reactor whereby dominantly anaerobic ammonium oxidation (anammox) and heterotrophic denitrifying bacteria can attach and grow on granular activated carbon (GAC). For this mean, a novel biofilm model including soluble microbial products (SMP) and extracellular polymeric substance (EPS) was developed to explain kinetics and abundance of independent microbial groups in terms of relative biovolume fraction and the spatial localization of bacteria in biofilm layers. The model was calibrated, validated and the model accuracy was checked using measured total nitrogen concentration and microbial biovolume fractions. For estimation of biovolume fraction an innovative enhanced protocol for quantitative fluorescence in-situ hybridization (qFISH), in-situ microscopy and digital image analysis for the cultivation-independent microorganisms was established. The model with EPS kinetics fits better for the bacteria groups of anammox bacteria, AOB and NOB compared to the model without EPS. Real-time producing BAP and UAP is simulated and it was presumed that he growth and existence of heterotrophs in anammox biofilm systems increase due to considering the autotrophic production of SMP.

Keywords: Granular biofilm · Population dynamics modelling · Microbial soluble products · Quantitative fluorescence in situ hybridization, anaerobic ammonium oxidation (anammox) · Denitrification

1 Introduction

Dynamic modelling of microbial interactions is of great significance in population ecology. In biological wastewater treatment modelling, simulation of microbial population helps to develop computational tools explaining the plausible mutualistic interactions between the microorganisms. This is essential to improve and optimize the bioreactor performance in terms of carbon and nutrient removal. The complex dynamic of microbial biofilm system in a wastewater treatment reactor is an example of an engineered environment requiring further symbiosis insights with using a mathematical model. Current implications from the mathematical modelling of biofilm reactors

mainly focus on simulation of the substrates fate but giving less insights into microbial population regarding to dominance, abundance and biocoenosis. In terms of real-time dynamic modelling of extracellular polymeric substances (EPS) and soluble microbial products (SMP) with focus on nitrogen converting bacteria only few studies are available (Ni et al. 2012; Liu et al. 2016) while the production of EPS components is linked to granule formation and the stability of biofilm reactor (Tan et al. 2017). In this work, the anaerobic ammonium oxidation (anammox), nitrification and denitrification were simulated in a full-scale biofilm reactor assisted by granular activated carbon (GAC) particles under anoxic conditions. The main aim of the work is to develop a comprehensive and novel model structure including SMP and EPS definitions to explain the abundance of major microbial groups in terms of relative biovolume fraction and to describe spatial localization of bacteria through biofilm layers. The specific objectives are: (1) to rank the sensitive parameters, calibrate, validate and check the accuracy and uncertainty of the model performance for simulation of carbon, nutrients and microbial biovolume fractions and (2) to predict the time-dependent concentration of SMP and EPS.

2 Materials and Methods

2.1 Operation of Anaerobic Biofilm Reactor and Chemical Measurements

The case study is a full scale anammox plant which has four main stages including feeding, biological treatment with activated sludge, ultrafiltration and activated carbon biofilm process before the main outflow. This study focused on the last part of the plant before the outflow consisting of granular activated carbon or GAC modules. Daily concentration of NH_4-N, NO_2-N and NO_3-N were recorded photo-metrically using German standards (Hach, Germany).

2.2 Model Structure and Evaluation

Due to high range of parameters in comprehensive biofilm models and based on the sensitivity analysis of our previous work (Azari et al. 2016), the model output results of biofilm models are significantly prone to changes in kinetic, stoichiometric and initial parameters, and hence these values and the ranges must be chosen and identified carefully and in a systematic way. Therefore, this work formulated a robust modeling protocol adapted from Zhu et al., 2016 for experimental design, data collection, sensitivity analysis, parameter identifiability analysis and model verification and evaluation procedure using activated Sludge Model No. 1 (ASM1) and the biofilm modelling platform in AQUASIM 2.1 (EAWAG, Switzerland). The model verification and evaluation procedure included the calibration, validation, model accuracy check and uncertainty analysis. An additional definition of soluble microbial products (SMP) and EPS was added to the model structure to compare the model performance with and without this definition. This structure can illustrate SMP production, EPS production and EPS hydrolysis rates due to Liu et al. (2016). SMPs were classified into two
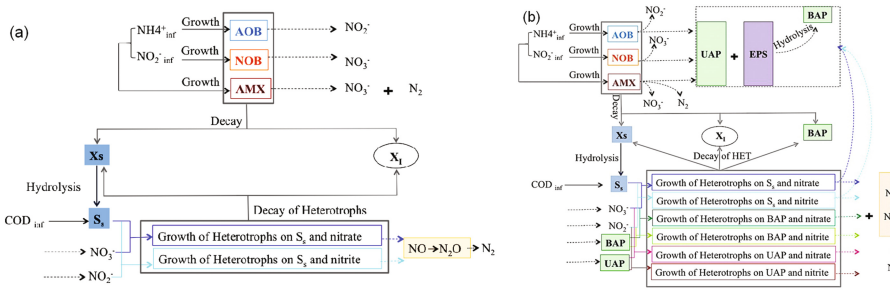
Fig. 1. The model structure without (a) and with considering the EPS kinetics and dynamics of SMP release (b) for anaerobic biofilm systems containing four groups of bacteria as anammox, AOB, NOB and heterotrophic denitrifiers. (UAP: utilization-associated products and BAP: biomass-associated products)

groups, utilization - associate products (UAP) from natural product of bacterial growth and biomass – associate products (BAP) from hydrolysis process of the active biomass. Figure 1a and b illustrate how two model structures with and without EPS kinetics were achieved. Since GAC is potential to adsorb natural organic compounds and ammonia, a simple adsorption isotherm equation (K_d approach) and a linear form of Freundlich equation was used to define adsorption kinetics (Ranjbar and Jalali 2015). The schematic algorithm for the proposed protocol is in Fig. 2.
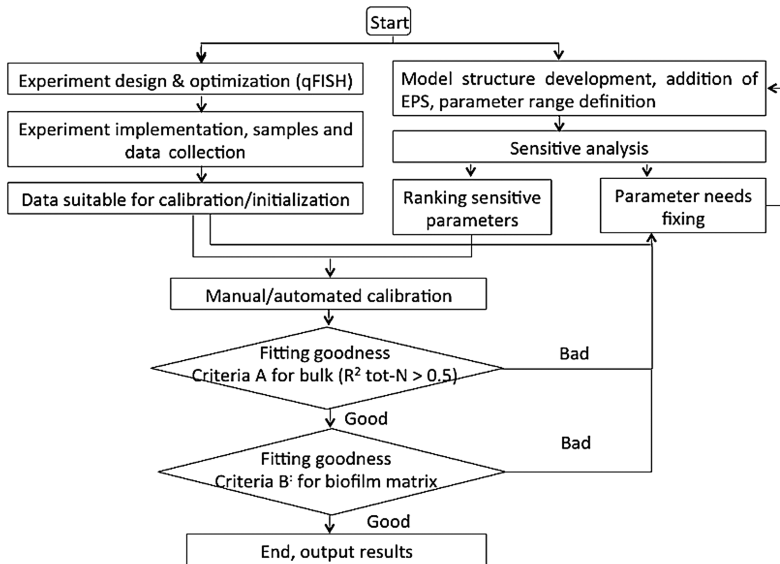
Fig. 2. The scheme of modelling protocol used for and model development and parametrization

2.3 Quantitative Fluorescence in Situ Hybridization (QFISH) and Digital Image Analysis

A novel protocol for optimized quantitative fluorescence in-situ hybridization (qFISH), in-situ microscopy and image analysis for the cultivation-independent quantification of biovolume fraction was established. The biomass was taken from the steady state operation of the anaerobic GAC biofilm reactor in five monthly timeframes. For each sample, qFISH adapted from Azari et al. (2017) using five oligonucleotide probes (AMX820 and Sca1309 for anammox fraction, Nso190 for AOB fraction, Ntspa662 and NIT3 for NOB fraction) was done in duplicate (Table 1). 20 FISH images from randomized field of observations (FOVs) were obtained and the quantification of biovolume fractions was done by calculating the area taken up by fluorescence targeted cells from specific probes compared to the area complimentary to the EUB 338 probe in ImageJ and daime software v2.1

Table 1. List of FISH probes applied in this research

Oligonucleotide probe for FISH	Corresponding genera/species	Formamide [%]
AMX 820 – Cy3	Candidatus Brocadia, Candidatus Kuenia	40%
Sca 1309 – Cy3	Genus Candidatus Scalindua	5%
Ntspa 662 – Cy3	Genus Nitrospira	35%
NIT 3 – Cy3	Nitrobacter spp.	40%
Nso 190 – Cy3	β-proteobacterialammonium oxidizing bacteria	55%
EUB 338mix – FITC	Most Eubacteria	5–55%

3 Results and Discussion

The sensitivity analysis (Fig. 3) remarked the remarkable sensitivity of the modeled results to heterotrophic biomass yield and maximum specific growth. The general behavior of the granular biofilm bioreactor after activated sludge process is characterized by a wastewater input with significant fluctuations in ammonia and COD with a COD:TN ratio from 4.61 to 19.87. Figure 4 represents the simulated concentration of total nitrogen in the bulk liquid for two model with and without EPS definition. The regression analysis implies a higher R-squared for total nitrogen for the model with EPS and SMP. This analysis implies a R-squared for total nitrogen equal to 0.66 for the model with EPS and 0.64 for the model without EPS kinetics. The relative abundances of anammox bacteria, AOB and NOB were visualized and estimated by qFISH with specific probes in five various timeframes. Due to Fig. 5 the mean percentage of anammox bacteria as dominant species to the total domain bacteria throughout one year was 52.2% ± 5.4 of total microbial groups while the simulated results give the relative abundance of 45.8% for the model without EPS and 53.7% for the model with EPS. For a better illustration, FISH micrographs with AMX820 specific probe and Sca1309 specific probe are illustrated in Fig. 6. For AOBs, the observed mean percentage of
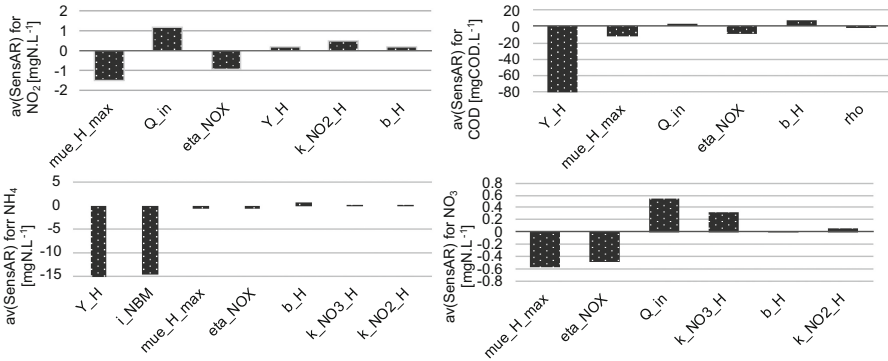
Fig. 3. Sensitivity ranking for ammonium, nitrite and nitrite nitrogen and COD for the model with EPS and SMP

bacteria to the total domain bacteria throughout the simulation was 5.7% of total microbial groups while the simulated results give the relative abundance of 15.8% for the model without EPS and 8.5% for the model with EPS (Fig. 5). However, the models better fit for anammox bacteria and AOBs rather than NOB as shown in Fig. 5. The model with EPS mimics the fluctuations in relative anammox abundance in a more realistic way compared to the simplified model without EPS. The model without EPS kinetics also overestimates the AOB fractions which can be due to the underestimation in heterotrophic growth rates due to the neglect of the heterotrophic synthesis from utilization of UAP and BAP. Producing BAP and UAP is simulated and presented in Fig. 7. The growth and existence of heterotrophs in anammox biofilm systems increase due to considering the autotrophic production of SMP (Laspidou and Rittmann 2002).
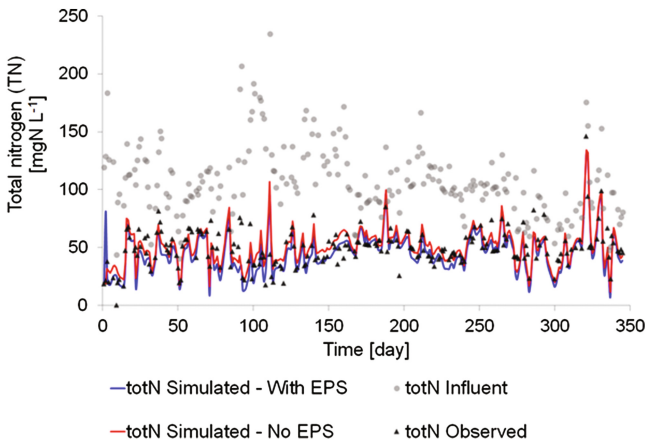
Fig. 4. Model evaluation for total nitrogen (TN) in the bulk liquid: simulation and observation
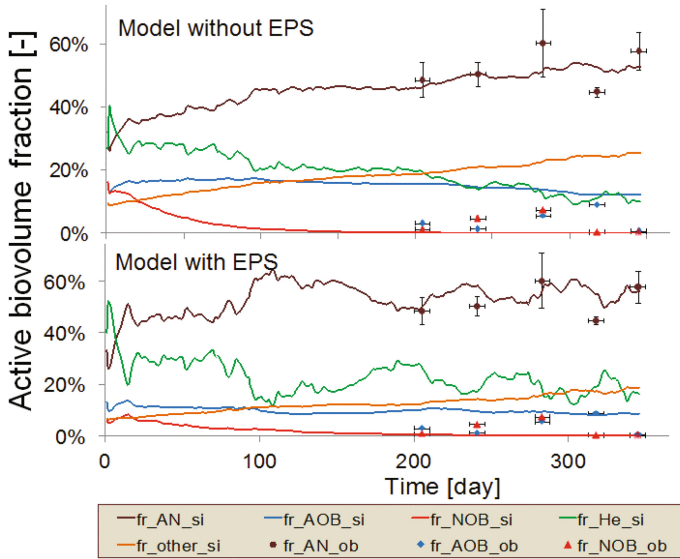
Fig. 5. Model evaluation results for relative abundance of three groups of bacteria (anammox bacteria, AOB and NOB). Continuous lines show the simulation while the scattered points are calculated values based on qFISH
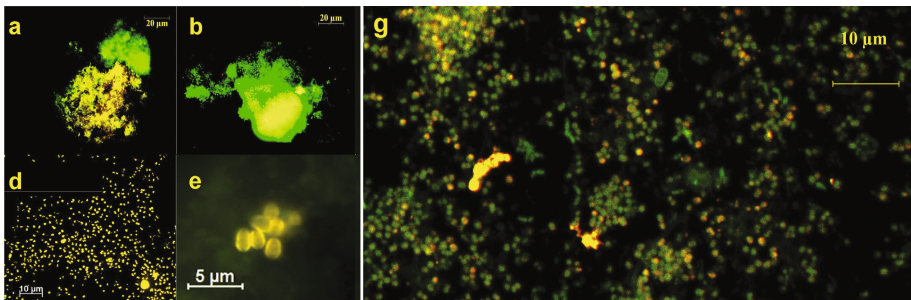
Fig. 6. Selected FISH micrographs with AMX820 specific probe (a, d, g) in Cy3 dye (yellow) and Sca1309 specific probe (b, e) in Cy3 dye (yellow). EUB mix 338 probe in FITC dye (green) was used to target for most of domain bacteria in granular biofilm samples (Color figure online)

Production and degradation of EPS and SMPs may be affected by changes in solid retention time which are not considered in this model and hence, they could impact on behavior of the model (Chen et al. 2012).
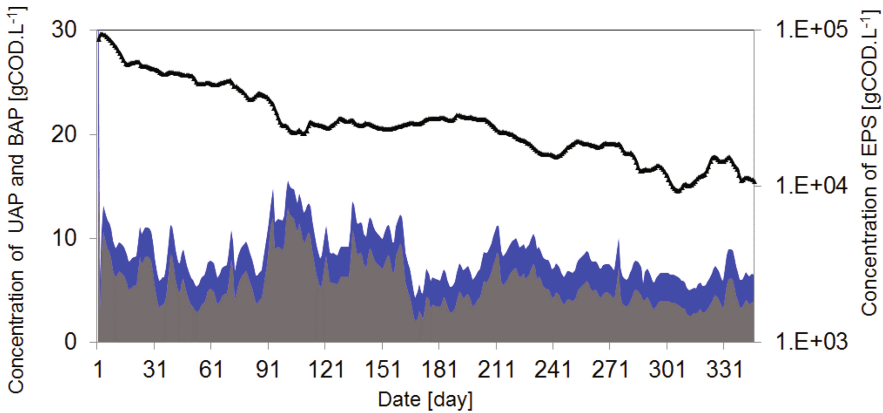
Fig. 7. Model-based analysis of SMP dynamics in the anammox process. (SMP = UAP + BAP), Grey color indicates BAP concentration and blue color is for UAP concentration. The black line is the prediction of the model for EPS concentration in the biofilm matrix (Color figure online)

4   Conclusions

The work dealt with the developing of a comprehensive model including SMP and EPS definitions to explain the abundance of independent microbial groups in a granular activated carbon-assisted biofilm reactor. The developed biofilm model can simulate with sufficient accuracy for inorganic nitrogen components in the bulk liquid and the targeted microbial biovolume fractions in the biofilm matrix. The model was statistically improved after the addition of EPS and SMP kinetics and the real-time production of EPS and SMP can be predicted. The model can simulate the fate of substrate and biomass biovolume fraction although a range of fails in predicting some peaks were simulated. Nevertheless, the model satisfactorily simulated the dynamic behavior at different operational timelines albeit various feeding characteristics and high fluctuations in input nitrogen loading rate and organic loading rates. An efficient production of SMP by autotrophs can control soluble organic carbon and inorganic nitrogen components in the effluent of WWTPs. The results of this work also highlighted the role of SMP and how SMP release can affect the performance of an anammox-based reactor. But the mathematical descriptions of the EPS and SMP kinetics parameters and the adsorption kinetics for simultaneous GAC process in the reactor can be further improved to describe more realistically the mechanisms of the production and degradation Besides, this model needs to be validated for one further data point for active biovolume fractions of AOB, NOB and anammox bacteria and for inactive estimated quantifiable EPS biovolume fraction in the biofilm matrix. Besides the microbial spatial localization can be further validated using a two-dimensional representation of simulated results of microbial population through biofilm layers compared with the direct image obtained from FISH-CLSM in thin layered biofilm samples.

References

Azari M, Lübken M, Denecke M (2016) Multispecies granular biofilm modelling for simultaneous anammox and denitrification processes in batch systems. In: Sauvage S, Sanchez-Perez JM, Rizzoli AE (eds) Proceedings of the 8th international congress on environmental modelling and software (IEMSs 2016), Toulouse, France. ISBN 978-88-9035-745-9

Azari M, Walter U, Rekers V, Gu JD, Denecke M (2017) More than a decade of experience of landfill leachate treatment with a full-scale anammox plant combining activated sludge and activated carbon biofilm. Chemosphere 174:117–126

Chen L, Tian Y, Cao C, Zhang S, Zhang S (2012) Sensitivity and uncertainty analyses of an extended ASM3-SMP model describing membrane bioreactor operation. J Membr Sci 389:99–109

Laspidou CS, Rittmann BE (2002) A unified theory for extracellular polymeric substances, soluble microbial products, and active and inert biomass. Water Res 36(11):2711–2720

Liu Y, Sun J, Peng L, Wang D, Dai X, Ni BJ (2016) Assessment of heterotrophic growth supported by soluble microbial products in anammox biofilm using multidimensional modeling. Sci Rep 6:27576

Ni BJ, Ruscalleda M, Smets BF (2012) Evaluation on the microbial interactions of anaerobic ammonium oxidizers and heterotrophs in anammox biofilm. Water Res 46(15):4645–4652

Ranjbar F, Jalali M (2015) The effect of chemical and organic amendments on sodium exchange equilibria in a calcareous sodic soil. Environ Monit Assess 187(11):1–21

Tan CH, Lee KWK, Burmølle M, Kjelleberg S, Rice SA (2017) All together now: experimental multispecies biofilm model systems. Environ Microbiol 19(1):42–53

Zhu A, Guo J, Ni BJ, Wang S, Yang Q, Peng Y (2016) A novel protocol for model calibration in biological wastewater treatment. In: Environmental engineering and activated sludge processes: models, methodologies, and applications. Apple Academic Press, pp 23–47

A Model for Continuous Sedimentation
with Reactions for Wastewater Treatment

R. Bürger[1]([✉]), S. Diehl[2], and C. Mejías[1]

[1] Departamento de Ingeniería Matemática and CI2MA,
Universidad de Concepción, Concepción, Chile
[2] Centre for Mathematical Sciences, Lund University, Lund, Sweden

Abstract. Continuously operated settling tanks are used for the gravity separation of solid-liquid suspensions in several industries. Mathematical models of these units form a topic for well-posedness and numerical analysis even in one space dimension due to the spatially discontinuous coefficients of the underlying strongly degenerate parabolic, nonlinear model partial differential equation (PDE). Such a model is extended to describe the sedimentation of multi-component particles that react with several soluble constituents of the liquid phase. The fundamental balance equations contain the mass percentages of the components of the solid and liquid phases. The equations are reformulated as a system of nonlinear PDEs that can be solved consecutively in each time step by an explicit numerical scheme. This scheme combines a difference scheme for conservation laws with discontinuous flux with an approach of numerical percentage propagation for multi-component flows. The main result is an invariant-region property, which implies that physically relevant numerical solutions are produced. Simulations of denitrification in secondary settling tanks in wastewater treatment illustrate the model and its discretization.

Keywords: Secondary settling tank · Multi-Component flow · Percentage propagation · Wastewater treatment

1 Introduction

This contribution is focused on models of secondary settling tanks (SSTs) in water resource recovery facilities. Such a model is extended herein to describe the sedimentation of multicomponent particles that react with several soluble constituents of the liquid phase. The model is developed, in part analyzed and simulated by (Bürger et al. 2016b). The governing model can be expressed as a system of nonlinear partial differential equations (PDEs) that can be solved consecutively in each time step by an explicit numerical scheme. Simulations of denitrification in SSTs illustrate the model and its discretization.

The new numerical method (not given in detail here) is based on theory for the system of model PDEs and can be seen as an extension of the Bürger-Diehl simulation model (Bürger et al. 2013) that includes biological reactions of an AMSx model. The approach is therefore different from previous investigations on reactive settling (Gernaey et al. 2006; Flores-Alsina et al. 2012; Ostace et al. 2012; Guerrero et al. 2013).

2 Materials and Methods

2.1 Mathematical Model and Numerical Method

The one-dimensional SST setup is outlined in Fig. 1. The model describes the evolution of the concentrations of the solids and liquid phases, $X = X(z,t)$ and $L = L(z,t)$, as functions of depth z and time t. The solid and fluid densities, ρ_X and ρ_L, are assumed to be constant. Moreover, the model keeps track of k_X particulate and k_L liquid components ($k_L - 1$ substrates and water), whose concentrations are collected in vectors $\boldsymbol{C} = \boldsymbol{C}(z,t)$, $\boldsymbol{S} = \boldsymbol{S}(z,t)$ and $\boldsymbol{W} = \boldsymbol{W}(z,t)$ or equivalently, percentage vectors $\boldsymbol{p}_X$ and $\boldsymbol{p}_L$:

$$\boldsymbol{C} = \boldsymbol{p}_X X = \begin{pmatrix} p_X^{(1)} \\ \vdots \\ p_X^{(k_X)} \end{pmatrix} X, \sum_{i=1}^{k_X} p_X^{(i)} = 1,$$
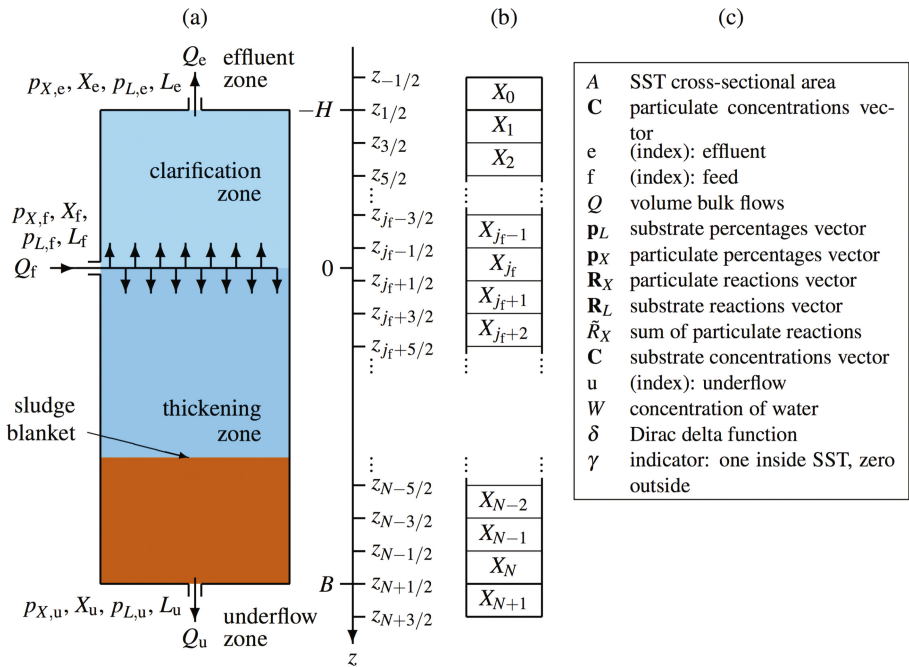
Fig. 1. (a) An ideal secondary settling tank (SST) with variables of the feed inlet, effluent and underflow indexed with f, e and u, respectively. The effluent, clarification, thickening, and underflow zones correspond to the respective intervals $< -H$, $-H < z < 0$, $0 < z < B$, and $z > B$. The sludge blanket (concentration discontinuity) separates the hindered settling zone and the compression zone. (b) Aligned illustration of the subdivision of the SST into internal computational cells, or layers (c) Nomenclature for PDE model

$$\boldsymbol{p}_L L = \begin{pmatrix} p_L^{(1)} \\ \vdots \\ p_L^{(k_L)} \end{pmatrix} \quad L = \begin{pmatrix} \boldsymbol{S} \\ W \end{pmatrix} = \begin{pmatrix} S^{(1)} \\ \vdots \\ S^{(k_L-1)} \\ W \end{pmatrix}, \quad \sum_{i=1}^{k_L} p_L^{(i)} = 1.$$

The governing model may include a full biokinetic ASMx at every depth z, and is based on the idea that hindered and compressive settling depend on the total particulate concentration (flocculated biomass) X. The governing system of equations are given as follows:

$$\frac{\partial X}{\partial t} + \frac{\partial F_X}{\partial z} = \delta(z)\frac{X_{\mathrm{f}}Q_{\mathrm{f}}}{A} + \gamma(z)\tilde{R}_X, \quad \text{where} \quad F_X = Xq + \gamma(z)\left(f_{\mathrm{b}}(X) - \frac{\partial D(X)}{\partial z}\right)$$

$$\frac{\partial(\boldsymbol{p}_X X)}{\partial t} + \frac{\partial(\boldsymbol{p}_X F_X)}{\partial z} = \delta(z)\frac{\boldsymbol{p}_{X,\mathrm{f}}X_{\mathrm{f}}Q_{\mathrm{f}}}{A} + \gamma(z)\boldsymbol{R}_X,$$

$$L = \rho_L\left(1 - \frac{X}{\rho_X}\right),$$

$$\frac{\partial(\bar{\boldsymbol{p}}_L L)}{\partial t} + \frac{\partial(\bar{\boldsymbol{p}}_L F_L)}{\partial z} = \delta(z)\frac{\bar{\boldsymbol{p}}_{L,\mathrm{f}}L_{\mathrm{f}}Q_{\mathrm{f}}}{A} + \gamma(z)\bar{\boldsymbol{R}}_L, \quad \text{where} \quad F_L = \rho_L\left(q - \frac{F_X}{\rho_X}\right),$$

$$p_L^{(k_L)} = 1 - \left(p_L^{(1)} + \ldots + p_L^{(k_L-1)}\right),$$

where the variables are explained in Fig. 1c. The unknowns are $X, L, \boldsymbol{p}_X$ and $\boldsymbol{p}_L$ as functions of z and t. Moreover $\bar{\boldsymbol{p}}_L$ contains the first $k_L - 1$ components of $\boldsymbol{p}_L$. Here we define $f_{\mathrm{b}}(X) = Xv_{\mathrm{hs}}(X)$, where v_{hs} is the given hindered settling velocity function, and D is a function that describes the sediment compressibility and satisfies $D(X) = 0$ for $X \leq X_{\mathrm{c}}$ and $D(X) > 0$ for $X > X_{\mathrm{c}}$, where X_{c} is a critical concentration. The bulk velocity q is defined in terms of the given bulk flows as $q(z,t) = \frac{Q_{\mathrm{e}}(t)}{A} = (Q_{\mathrm{f}}(t) - Q_{\mathrm{u}}(t))/A$ for $z < 0$ and $q(z,t) = \frac{Q_{\mathrm{u}}(t)}{A}$ for $z > 0$.

Mathematical models of SSTs form a topic for well-posedness and numerical analysis even in one space dimension due to the spatially discontinuous coefficients of the underlying strongly degenerate parabolic, nonlinear model PDE. The authors' research concentrates on the development and analysis of a numerical scheme for the approximate solution of the model (Bürger et al. 2016b). The main difficulties are its coupled nature, the discontinuous dependence of F_X on spatial position z, and the strongly degenerate behaviour that comes from the fact that $D(X) = 0$ on an X-interval of positive length. This scheme combines a difference scheme for conservation laws with discontinuous flux (Bürger et al. 2005) with an approach of numerical percentage propagation for multi-component flows (Diehl 1997). The main result is an invariant-region property, which implies that physically relevant numerical solutions are produced.

3   Numerical Example

To illustrate the model and its predictions, we consider the model functions

$$v_{hs}(X) = \frac{v_0}{1 + (X/\bar{X})^{\bar{r}}},$$

$$\sigma_e(X) = \begin{cases} 0 & \text{for } X < X_c, \\ \alpha(X - X_c) & \text{for } X > X_c, \end{cases} \quad D(X) = \int_{X_c}^{X} \frac{\rho_X v_{hs}(s)\sigma_e'(s)}{g(\rho_X - \rho_L)}\,ds.$$

We use a reduced biological model of denitrification, distinguishing $k_X = 2$ particulate components with concentrations X_{OHO} (ordinary heterotrophic organisms) and X_U (undegradable organics), and $k_L = 4$ liquid components, namely the substrates S_{N_3} (nitrate), S_S (readily biodegradable substrate) and S_{N_2} (nitrogen), and water, such that $\boldsymbol{p}_X X = \boldsymbol{C} = (X_{OHO}, X_U)^T$ and $\boldsymbol{S} = (S_{N_3}, S_S, S_{N_2})^T$. The reaction terms are then given by

$$\boldsymbol{R}_X = X_{OHO}\begin{pmatrix} \mu(\boldsymbol{S}) - b \\ f_P b \end{pmatrix},$$

$$\boldsymbol{R}_X = X_{OHO}\begin{pmatrix} -\frac{1-Y}{2.86Y}\mu(\boldsymbol{S}) \\ (1 - f_P)b - \frac{1}{Y}\mu(\boldsymbol{S}) \\ \frac{1-Y}{2.86Y}\mu(\boldsymbol{S}) \\ 0 \end{pmatrix} \Rightarrow \begin{cases} \tilde{R} = (\mu(\boldsymbol{S}) - (1 - f_P)b)X_{OHO} \\ \tilde{R} = \left((1 - f_P)b - \frac{\mu(\boldsymbol{S})}{Y}\right)X_{OHO} \end{cases},$$

with the growth rate function $\mu(\boldsymbol{S}) := \mu_{max}(S_{N_3}/(K_{NO_3} + S_{N_3}))(S_S/(K_S + S_S))$,. where values of all constant are given in the caption of Fig. 3. We choose the volumetric flows Q_f and Q_u and the feed concentration X_f as piecewise constant functions of t (see Fig. 2), and let $\boldsymbol{p}_{X,f}$ and $\boldsymbol{p}_{L,f}$ be constant.

The whole simulation is shown in Fig. 3. The initial steady state is kept during the first hour of the simulation. There is a sludge blanket, i.e., a discontinuity from a low
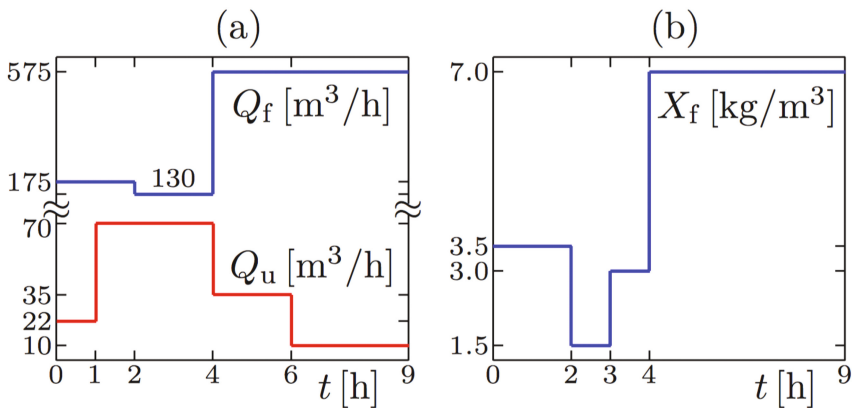
Fig. 2. Numerical example: Time dependence of (a) volumetric flows and (b) feed concentration
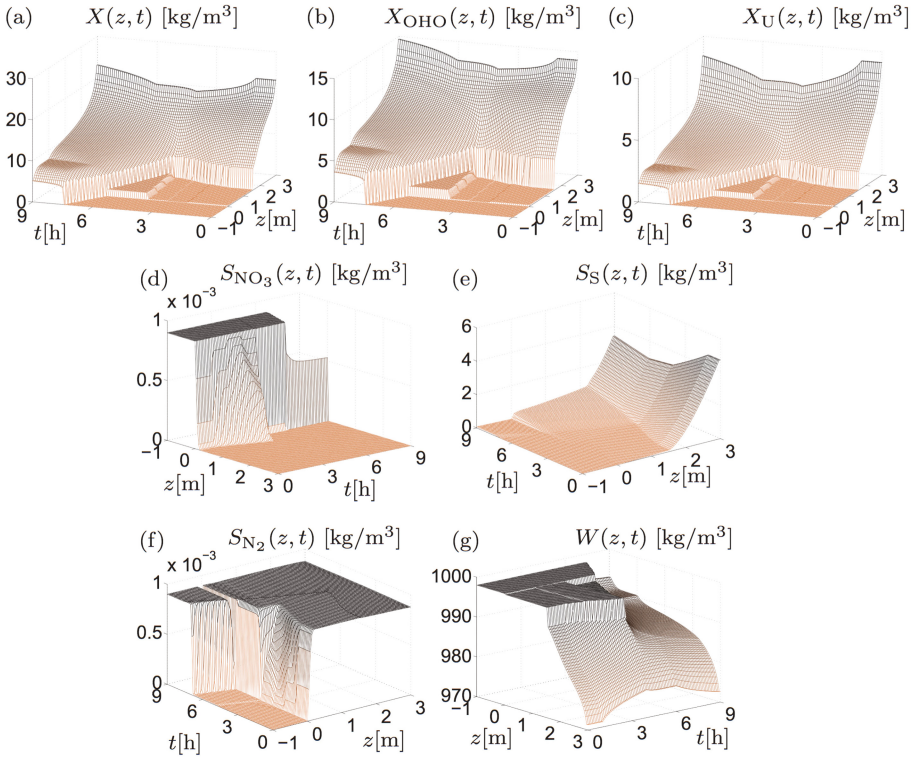
Fig. 3. Simulation of reactive settling (denitrification) in an SST starting from a stationary state followed by variations of the volumetric flows Q_u and Q_f and of the solids feed concentration X_f. Some of the constants involved are standard in ASM1 (Henze et al. 1987) while others have been modified since this is a strongly reduced model (Bürger et al., 2016a): $b = 6.94 \times 10^{-6}\,\text{s}^{-1}$, $f_p = 0.2$, $K_{NO_3} = 5 \times 10^{-4}\text{kgm}^{-3}$, $K_S = 0.02\text{kgm}^{-3}$, $X_{max} = 30\text{kgm}^{-3}$ (the maximum solids concentration), $\mu_{max} = 5.56 \times 10^{-5}\text{s}^{-1}$, $v_0 = 1.76 \times 10^{-3}\text{ms}^{-1}$, $\bar{X} = 3.87\text{kgm}^{-3}$, $\bar{r} = 3.58$, $\alpha = 0.2m^2\text{s}^{-2}$, $X_c = 5.0\text{kgm}^{-3}$, $\rho_X = 1050\text{kgm}^{-3}$, $\rho_L = 998\text{kgm}^{-3}$ (solid/fluid densities), $g = 9.8\text{ms}^{-2}$ (acceleration of gravity) and $Y = 0.67$ (yield factor)

concentration up to $X = X_c$. At $t = 4\,$h, the step change of control functions causes a rapidly rising sludge blanket that reaches the top of the SST around $t = 7\,$h, which means that the SST becomes overloaded with solids leaving also through the effluent. The fast reaction imply that the soluble (NO_3) is quickly converted to N_2 in regions where the bacteria OHO are present, which is below the sludge blanket.

4   Conclusions

The new model and numerical method for reactive settling, presented in detail by (Bürger et al. 2016b), includes hindered settling, compression and reactions according any chosen biokinetic model. Dispersion effects near the feed inlet of the SST have not been included; however, this can be done without any complications. An advantage of the numerical method is that it produces stable solutions in the sense that negative concentrations never appear, values of percentages lie always between zero and one, and the sum of all percentages of the solid (of liquid) components is always equal to one. Future developments include faster time-stepping of the numerical method.

References

Bürger R, Careaga J, Diehl S, Mejías C, Nopens I, Vanrolleghem PA (2016a) Simulations of reactive settling of activated sludge with a reduced biokinetic model. Comp Chem Eng 92:216–229

Bürger R, Diehl S, Farås S, Nopens I, Torfs E (2013) A consistent modelling methodology for secondary settling tanks: a reliable numerical method. Water Sci Tech 68:102–208

Bürger R, Diehl S, Mejías C (2016b) A difference scheme for a degenerating convection-diffusion-reaction system modelling continuous sedimentation. Submitted

Bürger R, Karlsen KH, Towers JD (2005) A model of continuous sedimentation of flocculated suspensions in clarifier-thickener units. SIAM J Appl Math 65:882–940

Diehl S (1997) Continuous sedimentation of multi-component particles. Math Meth Appl Sci 20:1345–1364

Flores-Alsina X, Gernaey KV, Jeppsson U (2012) Benchmarking biological nutrient removal in wastewater treatment plants: influence of mathematical model assumptions. Water Sci Tech 65:1496–1505

Gernaey KV, Jeppsson U, Batstone DJ, Ingildesen O (2006) Impact of reactive settler models on simulated WWTP performance. Water Sci Tech 53(1):159–167

Guerrero J, Flores-Alsina X, Guisasola A, Baeza JA, Gernaey KV (2013) Effect of nitrite, limited reactive settler and plant design configuration on the predicted performance of simultaneous C/N/P removal WWTPs. Bioresour Tech 136:680–688

Henze M, Grady CPL, Gujer W, Marais GVR, Matsuo T (1987) Activated sludge model no. 1. Science technical report no. 1. IAWQ, London

Ostace GS, Cristea VM, Agachi PS (2012) Evaluation of different control strategies of the waste water treatment plant based on a modified activated sludge model no. 3. Environ Eng Manage J 11:147–164

A Dynamic Model for Microalgae-Bacteria Aggregates Used for Wastewater Treatment

A. Vargas[✉], S. Escobar Alonso, J.S. Arcila, and G. Buitrón

Unidad Académica Juriquilla, Instituto de Ingeniería,
Universidad Nacional Autónoma de México, Querétaro, Mexico

Abstract. A dynamic model based on the activated sludge model 1 (ASM1) of IWA, complemented with a microalgal population and its associated processes, is proposed. The critical parameters of the model are fitted to experimental data from batch experiments inoculated with microalgae-bacteria aggregates from a stable high-rate algal pond laboratory bioreactor and fed with real wastewater from a nearby WWTP. The results show a good fit with experimental data, when the model uses a Contois law for the COD uptake rate and Monod kinetics for the other rates. The model considers bacterial nitrification and denitrification, as well as ammonia and nitrate uptake by the microalgae.

Keywords: Microalgae-bacteria aggregates · ASM1 · Wastewater treatment

1 Introduction

Microalgal-bacterial (MAB) systems used for wastewater treatment have been gaining attention in recent years because of their capability of simultaneous treatment and resource recovery from a waste stream. On one hand, the fact that microalgae produce oxygen and consume carbon dioxide (CO_2), while bacteria use the former and produce the latter, leads to a virtuous interaction that could avoid the need for external aeration, while mitigating CO_2 emissions (Muñoz and Guyiesse 2006). Additionally, the energy needed for operation is harvested from (sun)light, making it a low-energy solution to wastewater treatment. Recent research has shown that under adequate operating conditions, microalgae and bacteria can form aggregates that sediment easily (Arcila and Buitrón 2016), thus opening the possibility for harvesting this biomass and using it as feedstock for other energy-producing (bio)processes. Thus, MAB systems have a promising future as zero- or even negative-energy systems.

Although several experimental studies have shown the potential of MAB systems to treat several types of wastewater without supplying any external oxygen (Manser et al. 2016), to form microalgal-bacterial aggregates (MABA) in a sustained manner, and to operate correctly for prolonged periods of time, the systems are not yet completely understood and may not be resilient enough to withstand the unavoidable variations in feed flow and composition, as well as changes in environmental conditions that could collapse the system. After all, they are biological (i.e. living) systems and are subject to population dynamics.

One way to counter the effects of changing environmental or external perturbations, as well as our ignorance of the biology involved, is to use feedback control strategies to maintain the proper operating conditions, or even to optimize the system operation with respect to some criteria, e.g. cost, biomass productivity, treatment efficiency, etc. However, feedback control design usually requires a mathematical model of the system dynamics, either to design the controller, or simply to have a proper numerical simulation platform. Of course, models are also useful for other analytical purposes, since they also help us understand better the system and sometimes even "discover" properties otherwise hidden by experimental data.

We propose here a mathematical model that describes the dynamics in a simplified MAB system and support it with experimental data. The model is based on the Activated Sludge Model 1 (ASM1) of the IWA (Henze et al. 2000), adding the effect of inorganic carbon production and consumption (modelled as dissolved CO_2) by also considering a generic microalgae population which consumes nitrogen as ammonia (NH_4) under aerobic conditions and nitrate (NO_3) under anoxic conditions, as originally proposed by Zambrano et al. (2016). In fact, the model proposed is a modification of the latter.

2   Materials and Methods

Three batch experiments were performed. For each experiment, MABA were collected from a 50 L laboratory high-rate algal pond (HRAP), described by Arcila and Buitrón (2016), operating with a HRT of 10 d. The volatile suspended solids (VSS) were measured according to Standard Methods. On the other hand, wastewater entering a nearby WWTP was also collected and supplemented with ammonia at different concentrations; its COD was also determined. The HRAP had been operated for more than one year so the MABA were stable with very good settling properties, e.g. a settling velocity of 1.4 ± 0.2 m/h and an almost granular morphology.

Each experiment consisted of four batch cultivations in 0.5 L bioreactors under the same initial COD concentration (same wastewater), but different initial biomass concentrations achieved through dilutions. This lead to four S_0/X_0 ratios of 0.25, 0.5, 1 and 2 gCOD/gVSS. The three experiments had fixed illumination for approximately 13 h, provided by LED lamps, alternating with approximately 11 h of darkness, coinciding with the lighting conditions at the lab during each day. Temperature was not controlled, but remained at 20 ± 3°C throughout the experiment, with slight decreases during the night.

For the first two experiments, the bioreactors were sparged with CO_2–enriched air (35% CO_2 content) during the illumination periods, but not during darkness; anoxic conditions thus occurred during darkness and DO rose to mean saturation values of 7.53 mg/L during the day (the altitude at the laboratory is close to 1900 m). For the third experiment this enriched air was sparged continuously (no anoxic conditions). Samples for COD, ammonia, nitrite and nitrate were taken for off-line measurements whenever the illumination conditions were changed. The data was afterwards analysed using the *Scilab* numerical simulation platform, setting some parameters to values obtained from literature (mainly the stoichiometric coefficients) and fitting only the

specific reaction rates using a Nelder-Mead numerical optimization algorithm to minimise the weighted squared sum of residuals.

3   Results and Discussion

An important observation from the experimental data was that the NH_4 consumption rate was seemingly proportional to the biomass concentration, but the COD consumption rate seemed little affected by it. This indicated that the bacterial portion of biomass follows different kinetics than the algal counterpart. As expected, COD was consumed faster under aerobic conditions, while ammonia was not consumed during anoxia. There was nitrification and denitrification and when all the NH_4 had been consumed and COD was no longer present, the microalgae seemed to consume nitrate at a slower rate.

With these observations we propose a simple model that considers only two populations, microalgae and bacteria, and at least five reactions: growth of bacteria by consumption of COD under aerobic conditions (heterotrophs), growth of bacteria by consumption of COD and nitrate under anoxic conditions (heterotrophic denitrifiers), growth of bacteria by consumption of nitrate under aerobic conditions (autotrophic nitrifiers), growth of microalgae under illumination by consumption of ammonia, and growth of microalgae by consumption of nitrate under illumination and ammonia limitation. Furthermore, we add decay/maintenance reactions for both bacteria and microalgae. The kinetic expressions are all Monod, expect for the growth of bacteria on COD, which is of Contois type to take into account the phenomenon observed. The Gujer matrix for the model is presented on Table 1.

The results showed good correspondence between the experimental data and the model after fitting the parameters. Figure 1 shows the experimental results for COD, NH4 and NO3 for the second set of experiments, together with the results obtained after fitting the model.

Table 1. Gujer matrix for the proposed model (the CO_2 and DO columns are omitted)

Process	Variables					Rate equation
	X_{alg}	X_{bac}	S_{COD}	S_{NH}	S_{NO}	
Microalgal growth on NH_4	1			$-\frac{1}{Y_{NH}}$		$\mu_{alg}^{NH} X_{alg} \frac{S_{NH}}{K_{NH}+S_{NH}} \frac{S_{CO2}}{K_{CO2}+S_{CO2}} \frac{I_{hv}}{K_{hv}+I_{hv}}$
Microalgal growth on NO_3	1				$-\frac{1}{Y_{NO}}$	$\mu_{alg}^{NO} X_{alg} \frac{S_{NO}}{K_{NO}+S_{NO}} \frac{K_{NH}}{K_{NH}+S_{NH}} \frac{S_{CO2}}{K_{CO2}+S_{CO2}} \frac{I_{hv}}{K_{hv}+I_{hv}}$
Microalgae decay	-1			f_N^{alg}		$b_{alg}X_{alg}$
Aerobic growth on bacteria		1	$-\frac{1}{Y_H}$	$-f_N^{bac}$		$\mu_{bac}^{COD} X_{bac} \frac{S_{COD}}{K_{COD}X_{bac}+S_{COD}} \frac{S_{O2}}{K_{O2}+S_{O2}}$
Denitrification		1	$-\frac{1}{Y_H}$	$-f_N^{bac}$	$-\frac{1-Y_H}{2.86Y_H}$	$\mu_{bac}^{NO} X_{bac} \frac{S_{COD}}{K_{COD}X_{bac}+S_{COD}} \frac{S_{NO}}{K_{NO}+S_{NO}} \frac{K_{O2}}{K_{O2}+S_{O2}}$
Nitrification		1		$-\frac{1}{Y_A}-f_N^{bac}$	$\frac{1}{Y_A}$	$\mu_{bac}^{NH} X_{bac} \frac{S_{NH}}{K_{NH}+S_{NH}} \frac{S_{O2}}{K_{O2}+S_{O2}}$
Bacteria decay		-1		f_N^{bac}		$b_{bac}X_{bac}$
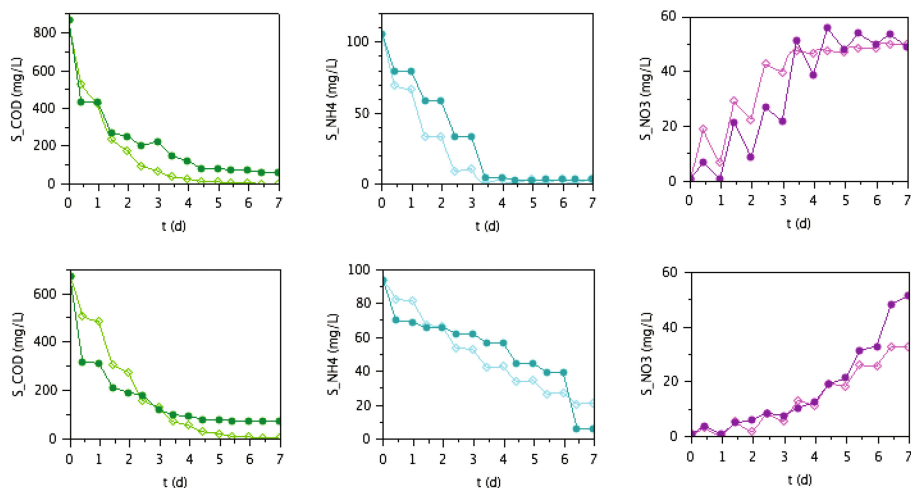
Fig. 1. Simulation results for the second experiment showing a good fit with the data (dark colours) for COD, NH_4 and NO_3. Top figure corresponds to the experimental conditions with $S_0/X_0 = 0.25$, while the bottom figures correspond to $S_0/X_0 = 2$

As can be appreciated, the proposed model fits the data well, and the parameter variation is within the expectations. The rate of microalgae growth on NH_4 is much larger than the one on NO_3. Bacterial nitrification does occur, but at a slower rate than the uptake of NH_4 by microalgae, whereas there is a clear denitrification process during the anoxic phases.

4   Conclusions

A simple model for microalgae-bacterial aggregates dynamics for wastewater treatment has been proposed. It is a based on ASM1, adding the microalgal population and its processes. A novelty is the use of Contois kinetics for the COD uptake process rate. Further studies will test the model prediction capabilities for a continuous regime in an HRAP.

References

Arcila JS, Buitrón G (2016) Microalgae-bacteria aggregates: effect of the hydraulic retention time on the municipal wastewater treatment, biomass settleability and methane potential. J Chem Technol Biotechnol 91(11):2862–2870

Henze M, Gujer W, Mino T, van Loosdrecht M (2000) Activated sludge models ASM1, AMS2, ASM2d and ASM3, scientific and technical report No. 9. IWA Publishing, London

Manser ND, Wang M, Ergas SJ, Mihelcic JR, Mulder A, van de Vossenberg J, van Lier JB, van der Steen P (2016) Biological nitrogen removal in a photosequencing batch reactor with an algal-nitrifying bacterial consortium and anammox granules. Environ Tech Lett 3(4):175–179

Muñoz R, Guyiesse B (2006) Algal-bacterial processes for the treatment of hazardous contaminants: a review. Wat Res 40(15):2799–2815

Zambrano J, Krustok I, Nehrenheim E, Carlsson B (2016) A simple model for algae-bacteria interaction in photo-bioreactors. Algal Res Biomass Biofuels Bioprod 19:155–161

Developing Process Models to Accurately Assess Global and Energy Performances of a WWTP Sludge Line: A Case Study in France

G. Baquerizo$^{(\boxtimes)}$, R. Samso, J. Fiat, J.-P. Canler, and S. Gillot

Irstea, UR MALY, Centre de Lyon-Villeurbanne, 69626 Villeurbanne, France
{guillermo.baquerizo,roger.samso,justine.fiat,
jean-pierre.canler,sylvie.gillot}@irstea.fr

Abstract. Mathematical models for the sludge line of a full-scale WWTP were developed with the aim of being integrated in a whole-plant model. A model describing the primary clarifier was also included. Reconciled data from plant routine sampling over a 2-year period together with data from dedicated campaigns were used to develop and calibrate the models. Different empirical correlations were identified to describe solids removal in primary settler, primary and activated sludge thickening, dewatering and drying, avoiding the assumption of constant removal efficiency. Analyses showed that characteristic particulate ratios (COD_P/TSS, P_{org}/TSS, N_{org}/TSS, VSS/TSS) remain constant during thickening, dewatering and drying processes. Therefore, in the implemented model these ratios were used for predicting concentrations of particulate compound in the process outputs. Mass balances of COD, N and P were completed by assuming that concentrations of soluble compounds are conserved. An extended version of ADM1 was implemented to simulate the full-scale digester fed with primary and activated sludge. A complete influent characterisation including Biochemical methane potential (BMP) tests was performed to provide an ADM1 compatible substrate fractionation Additionally, energy models for each unit process were determined through regression analyses to fit energy consumption with operating parameters. An energy audit of the plant was conducted to assess the energy consumption of each process. Electric energy, the consumed biogas as well as other energy sources were considered in the analyses. Single models were assembled to build the sludge line model that will be used to obtain reliable predictions for reject water composition, biogas production, dry sludge and energy consumption.

Keywords: Plant-wide modelling · Data analyses and reconciliation · Sludge treatment modelling · Energy modelling

1 Introduction

Most of the published works aiming at modelling the operation of full-scale wastewater treatment plants have been limited to separately describe each unit process or to only focus on wastewater treatment line ignoring the effect of the sludge processes.

However this approach is increasingly showing limitations in the view of the new challenges that facilities must face including optimization of energy balance, decrease of GHG emissions, nutrients recovery, and reduction of the carbon footprint, among others. In that sense the plant operation and performance is being progressively described using an integral approach through plant-wide modelling (Ekama 2009; Barat et al. 2013; Lizarralde et al. 2015). This holistic approach is recognised as a reliable tool for plant design, performance evaluation and optimization, since the different interactions across the plant are properly captured (Kazadi Mbamba et al. 2016). Nevertheless up to now plant-wide modelling has been mainly focused on steady-state studies, using average plant data. Furthermore, simple models assuming constant solids removal efficiencies and ideal processes have been usually used for simulation of the sludge treatment distorting predictions of the reject water composition. In addition, modelling of energy consumption in plant-wide models is restricted to the use of simple equations predicting the energy consumption of a limited number of equipment.

In particular, the improvement of energy balance in full-scale WWTPs by reducing the total energy consumption together with the optimization of the energy produced on-site, typically through anaerobic digestion, appears as one of the major driver in the wastewater industry. Different strategies have been reported to improve the digester performance in order to increase the biogas production including supply of external organic substrate carbon or increasing the COD removal by primary sedimentation (Svardal and Kroiss 2011). However a consistent analyse of the impacts generated under new operation conditions over the plant performances is strongly linked to reliably modelling both primary clarifiers and the sludge processes of the plant.

The objective of this work is to prepare the development of a plant-wide model able to accurately simulate the global performances of a full-scale plant under different operation conditions, including the energy balance. A comprehensive discussion of plant data analyses to develop reliable models for the sludge line describing mass balances and energy consumption of each individual unit process is provided.

2   Materials and Methods

2.1   Full-Scale WWTP

The modelled full-scale plant is located in the southeast of France and was designed for organic matter and nitrogen removal from domestic wastewater of approximately 300,000 p.e. A simplified layout of the plant is showed in Fig. 1. The incoming wastewater is initially treated in preliminary and primary stages (grit chamber, grease removal tank and conventional primary settler) followed by three parallel biological treatment lines. Each biological line consists in anoxic and aerobic basins (3670 m^3 and 7800 m^3, respectively) and two secondary clarifiers. The plant was designed to perform sequenced aeration. Primary sludge is thickened using a conventional gravitational thickener while activated sludge is thickened by centrifugation. The full-scale digester has a total volume of 4,000 m^3 with a working volume of 3,800 m^3. The digested sludge is dewatered in centrifuges and afterwards dried up to 85–90% dry solids, before being transported offsite. Over the studied period (2014 and 2015) the
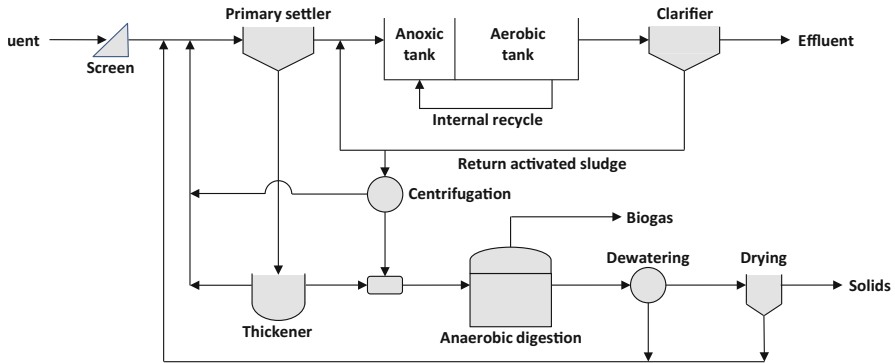
Fig. 1. Overall schematic flow diagram of the studied full-scale WWTP

average influent flow rate was 38980 m^3 d^{-1} and the average inlet loads were 18530 kg COD d^{-1}, 7540 kg BOD_5 d^{-1}, 1740 kg N d^{-1}, 228 kg P d^{-1}, representing 40% of the organic plant design load.

3 Historical-Plant Data

Plant data were obtained from both supervisory control and data acquisition system (SCADA) and routine sampling performed by the plant. Data from SCADA included flow rates of influent, effluent, internal recycle, return and extraction of waste activated sludge, thickened primary and activated sludge feeding digester, digested and dewatered sludge, and biogas. Operation times of electro-mechanic devices and the percentage of methane in biogas was also recorded from the supervisory system.

Routine sampling comprised daily measurements on composite samples from flow-proportional auto-samplers located at the influent and effluent. Primary effluent was measured weekly using samples obtained from a time-proportional sampler. Analyses included COD, BOD_5, TSS, VSS, NH_4-N, NO_2-N, NO_3-N, TKN, P_{tot}, PO_4-P. Additional weekly measurements of TSS and VSS from primary and activated sludge, thickened primary and activated sludge and digested sludge were also provided together with TS and VS in dewatered and dried sludge.

4 Measuring Campaigns

Additional sampling and analyses were carried in order to obtain supplementary data to developed unit process models. Three flow-proportional auto-samplers were located to characterise primary effluent, reject flows from thickened sludge (thickener + centrifugation), and reject flows from dewatering and drying. Weekly analyses of soluble and total COD, TSS, TKN, NH_4-N, P_{tot}, PO_4-P from composite samples were performed over 3 months according to standard methods.

A comprehensive analytical characterisation of the thickened primary and activated sludge was performed based on weekly composite samples over 4 months. Soluble and total COD, TSS, VSS, TKN, NH_4-N, P_{tot}, PO_4-P, lipids and VFAs were determined according to standard methods. The methane potential and biodegradability of both sludge were assessed using BMP tests following the procedure reported by Buffiere et al. (2008).

An energy audit of the plant was also conducted over the studied period. Electric energy, the consumed biogas as well as other energy sources produced/recovered during the treatment process were added to assess the total energy consumption of the plant. The daily electrical energy consumed by an electro-mechanic device (in kWh) was obtained by multiplying its active power (kW) by its operation time (h/d). Absorbed power of key electro-mechanic devices (i.e. pumping station, recirculating pumps, blowers) was measured on-site in order to enhance the energy consuming estimations. The thermal energy usage is associated to the energy consumption in the different boilers utilised for heating: digester, dryers and buildings. Daily thermal energy consumption (in kWh) was assessed by multiplying the boiler efficiency, daily volume of the fuel being combusted (biogas or natural gas) and the lower heating value (kWh/Nm^3).

5   Results and Discussion

5.1   Developing Unit Process Models Towards Sludge Line Simulation

The real plant data was analysed following the methodology proposed by Rieger et al. (2012). Reconciled data was then used to develop and/or calibrate models for single unit processes, briefly described in Table 1. Primary clarifier was modelled using a correlation between the TSS removal efficiency and the incoming concentration as reported in Silva et al. (2014). The parameters of the proposed removal efficiency curve were estimated using a linear regression (Fig. 2a). The settleability of particulate compounds (COD_P, N_{org} and P_{org}) was adjusted in order to fit measured values of primary effluent, in accordance with the primary clarifier model used in the Benchmark Simulation Model N°2 (BSM2, Jeppsson et al. 2006). Concentration of soluble compounds (COD_S, NH_4, NOx, PO_4) were assumed to be conserved, guarantying that total COD, N, and P mass balances are closed during primary sedimentation.

Different empirical correlations were found to describe solids removal in each sludge treatment processes of the plant. TSS removal efficiency was correlated with the hydraulic retention time and the inlet TSS in primary sludge and biological sludge thickeners, respectively. For digestate dewatering, a correlation between TSS in dewatered sludge and VSS/TSS ratio in digestate was found as depicted in Fig. 2b. A constant TS value in dry sludge was set according to plant measurements. Taking into account the observed values from measurement campaigns, it was assumed that particulate ratios (COD_P/TSS, N_{org}/TSS, P_{org}/TSS, VSS/TSS) and soluble concentrations remain constant during physical separation process. For processes involving centrifugation, output concentrations of soluble compounds were corrected by considering flow rates of both polymer and centrifuge wash.

Table 1. List of the models used in the plant-wide model

Process	Physical/Biological model	Energy model[a]
Primary settler	Non-reactive settler with variable solid removal efficiency	Primary sludge flow rate
Primary sludge thickener	Empirical correlation between TSS removal and hydraulic retention time	Constant
Activated sludge thickener	Empirical correlation between TSS removal and inlet solids load	Inlet TSS load
Anaerobic digester	Modified ADM1 including two composite fractions representing both types of thickened sludge	Inlet flow rate, average ambient temperature
Dewatering	Empirical correlation between TS in dewatered sludge and inlet VSS/TSS ratio	Inlet TSS load
Thermal sludge drying	Constant TS value in dry sludge	Inlet TS load

[a] Operating parameter(s) used to develop energy equations
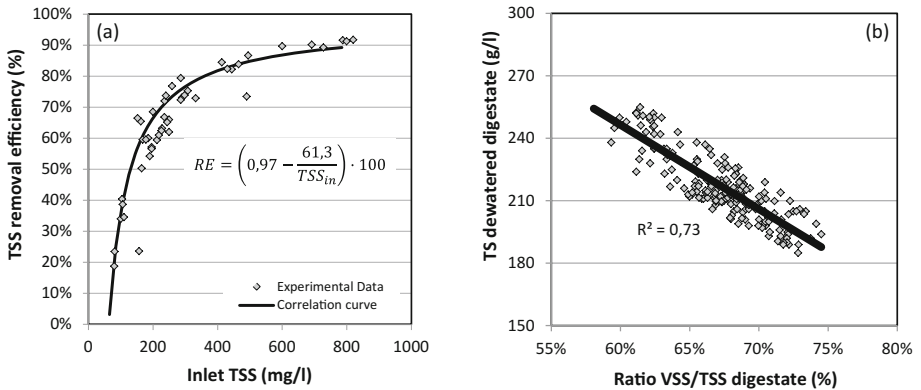
Fig. 2. Empirical correlation fitted to describe (a) TSS removal efficiency in primary clarifier and; (b) TS in dewatered digestate

For the extended ADM1 model, kinetic parameters were kept at default values except for the disintegration constant of both composites and hydrolysis constant (proteins, carbohydrates and lipids). The results of measurement campaign and BMP tests were used to perform COD fractionation of the digester fed (primary and secondary sludge) according to ADM1 input variables and also to estimate the stoichiometric fractions related to inert, lipids and proteins content in both composite fractions. Experimental biogas flow rate, CH_4 content, TSS, VSS, NH_4-N and VFAs in the digestate were looked at to calibrate kinetic parameters.

Energy models were determined through regression analyses to fit energy consumption with operating parameters. Equations were obtained for each unit process of
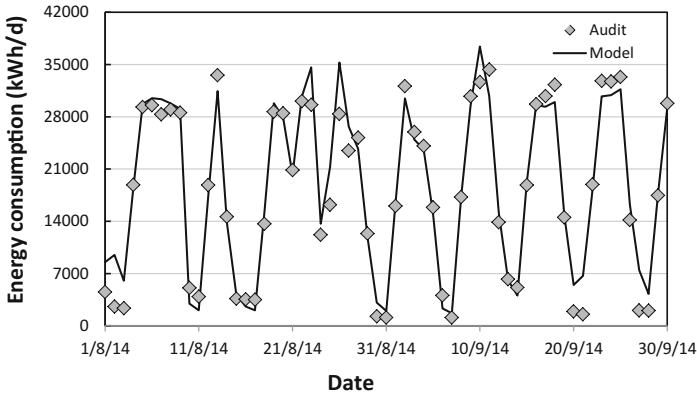
Fig. 3. Comparison between energy consumption calculated from the energy audit and predicted from energy models for the whole sludge treatment line (August and September 2014)

the plant. In Fig. 3 the total predicted energy consumed in the sludge line is shown. Contribution of sludge line can reach up to 70% of the total energy consumption of the plant mainly due to energy demand of the thermal sludge drying.

6   Conclusions

Reliable mathematical models for each unit process present in the sludge line of a full-scale WWTP were developed, including a primary clarifier model. Both reconciled plant-data and data from measured campaigns were used to obtain empirical correlations describing solids removal and output compositions (in terms of total and soluble COD, TKN, NH_4-N, P_{tot}, PO_4-P) of each physicochemical process of the plant. The full-scale digester was simulated using an extended version of ADM1 comprising two composite fractions representing thickened primary and activated sludge. A complete characterisation of both influents was performed to provide an ADM1 compatible substrate fractionation. The inherent properties of ADM1 together with a comprehensive characterisation of the digestate allowed obtaining a consistent description of the dewatering feed. Energy consumption models of each unit process were also obtained by combining operating parameters and results from the plant energy audit.

Different unit process and energy models developed here were integrated to build a whole-sludge line model that will be used to predict the key outputs of the sludge treatment line: reject water composition, biogas flow rate, dry sludge production and energy consumption.

References

Barat R, Serralta J, Ruano MV, Jimenez E, Ribes J, Seco A, Ferrer J (2013) Biological nutrient removal model Nº 2 (BNRM2): a general model for wastewater treatment plants. Water Sci Tech 67(7):1481–1489

Buffiere P, Frederic S, Marty B, Delgenes J-P (2008) A comprehensive method for organic matter characterization in solid wastes in view of assessing their anaerobic biodegradability. Water Sci Tech 58(9):1783–1788

Ekama GA (2009) Using bioprocess stoichiometry to build a plant-wide mass balance based steady-state WWTP model. Water Res 43(8):2101–2120

Jeppsson U, Rosen C, Alex J, Copp J, Gernaey KV, Pons M-N, Vanrolleghem PA (2006) Towards a benchmark simulation model for plant-wide control strategy performance evaluation of WWTPs. Water Sci Tech 53(1):287–295

Kazadi Mbamba C, Flores-Alsina X, Batstone DJ, Tait S (2016) Validation of a plant-wide phosphorus modelling approach with minerals precipitation in a full-scale WWTP. Water Res 100:169–183

Lizarralde I, Fernandez-Arevalo T, Brouckaert C, Vanrolleghem P, Ikumi DS, Ekama GA, Ayesa E, Grau P (2015) A new general methodology for incorporating physico-chemical transformations into multi-phase wastewater treatment process models. Water Res 74:239–256

Rieger L, Gillot S, Langergraber G, Shaw A (2012) Good modelling practice: guidelines for use of activated sludge models. IWA Publishing, London

Silva C, Quadros S, Ramalho P, Alegre H, Rosa MJ (2014) Translating removal efficiencies into operational performance indices of wastewater treatment plants. Water Res 57:202–214

Svardal K, Kroiss H (2011) Energy requirements for waste water treatment. Water Sci Tech 64 (6):1355–1361

Sensitivity Analysis and Calibration with Bayesian Inference of a Mass-Based Discretized Population Balance Model for Struvite Precipitation

B. Elduayen-Echave[✉], A. Ochoa de Eribe, I. Lizarralde,
G. Sánchez, E. Ayesa, and P. Grau

CEIT and Tecnun (University of Navarra),
Manuel de Lardizabal 15, 20018 San Sebastián, Spain

Abstract. Struvite precipitation has raised as a promising solution to recover phosphorous in wastewater treatment plants (WWTP). Struvite is a fertilizer that varies its performance depending on its size. This shows the need to upgrade one-step classic kinetic precipitation models by new frameworks as the Population Balance Model (PBM). In this abstract a mass-based Discretized Population Balance Model (DPBM) used to predict struvite precipitation is presented. The model includes primary nucleation, growth and aggregation mechanisms as a function of supersaturation index and kinetic parameters. Main advantage of the mass-based definition is that mass continuity is guaranteed and that it is fully compatible with other chemical and physicochemical reactions. A sensitivity analysis performed reveals exponents of nucleation and growth as the most relevant parameters in the pH evolution during precipitation and final Particle Size Distribution (PSD). Experimental data was used to calibrate the model employing Bayesian Inference. Selected values of the parameters showed good agreement with reality.

Keywords: PBM · Struvite · Bayesian inference

1 Introduction

Different technological solutions have been proposed during the last years in order to remove salts from wastewater and in some cases, obtaining them as a resource value. Among others, struvite ($MgNH_4PO_4 \cdot 6H_2O$) recovery from wastewater by crystallization has raised in the last years as a promising solution because it: (1) reduces operational costs associated with the maintenance of reactors and pipes due to blockage of phosphorous (P) salts, (2) fights global P scarcity and (3) reduces eutrophication problems in receiving waterways.

Struvite is a fertilizer that varies its performance depending on the size of the obtained granules (Tarragó et al. 2016). Therefore, it has to fulfill size specifications in order to be placed in the market. Thus, new salt-recovery technologies must consider the effect of operational and design variables on crystal formation and growth.

Mathematical modelling and simulation has been proved as a useful tool in design and operation of wastewater treatment plants (WWTP). Considering new challenges in the design and operation of technologies for salts removal and recovery, classical one-step kinetic models which only describe precipitation by the total mass obtained (Ikumi et al. 2013) should be upgraded by mathematical modelling frameworks as the PBM. Specifically, PBM has been used to define struvite precipitation using particle number distribution in Galbraith et al. (2014). However, dealing with models based on mass continuity seems more convenient in order to (1) avoid mass discontinuities (Hounslow et al. 1988; Galbraith and Schneider 2014) and (2), combine precipitation mechanisms with other phenomena taking place into the reactor, such as liquid-gas transfer, other salt precipitation or acid-base and ion pairing reactions.

Taking all this into account, the aim of this research is to build a mass based PBM to predict salt crystallization in wastewater considering PSD and other chemical and physicochemical reactions. To achieve this, objectives are to perform a sensitivity analysis of the developed model and calibrate it for the specific case of struvite precipitation using Bayesian Inference.

2 Materials and Methods

2.1 Precipitation Model

The mathematical model presented here predicts struvite precipitation. Included precipitation mechanisms are: primary nucleation, growth and aggregation. Precipitation mechanisms are defined as a function of supersaturation index and kinetic rates and exponents. Model parameters and variables, stoichiometry and kinetics are shown in Tables 1, 2 and 3, respectively.

The precipitation model for struvite is based on the DPBM presented in Hounslow et al. (1988). Struvite size range has been partitioned in 30 bins, which correspond to spherical particles sized between 0.001 and 0.812 mm of radius. The size of spheres of each bin is twice the previous one. Common wastewater equilibrium reactions as ion pairing and acid-base reactions are also included following guidelines and equations proposed in Lizarralde et al. (2015). As the PBM is mass based, the model could be further extended with other reactions as: liquid-gas transfer, other salts precipitation or other chemical reactions in a systematic and simple way. Finally, the model is constructed in WEST (www.mikebydhi.com) platform.

2.2 Experimental Data

Experimental data was obtained from a precipitation batch test. 650 mL of dissolution were prepared where initial concentration of P was 0.1 mol·l^{-1} and molar relationship between P, nitrogen (N) and magnesium (Mg) ions was 1:1.5:2. pH was measured every half second for the 20 min that the experiment lasted. The precipitated solid was filtered and dried at 50°C for 96 h. Final PSD was obtained by laser diffraction using SYMPATEC H820 equip and it was proved that composition of the sample was struvite by X-Ray diffraction with a Philips PW 1825 diffractometer.

Table 1. Variables and Parameters used in the model and their ranges for the sensitivity analysis and calibration

Name	Description	Unit	Maximum value	Minimum value
CwXSTRUi	Concentration of i sized struvite	g/m^3	–	–
IAP	Ion Activity Product: product of free ion species activities	$(Mol/l)^3$	–	–
Kr_Agg	Kinetic rate of aggregation	l/d	1E–12	5E–11
Kr_Growth	Kinetic rate of growth	mm/d	5E+05	1E+06
Kr_Nucl	Kinetic rate of nucleation	Nucleus/d·m^3	5E+16	9E+17
K_{sp} Stru	Solubility product of struvite	$(Mol/l)^3$	–	–
Li	Radious of i sized struvite	Mm	–	–
mXSTRUi	Mass of struvite contained in an sphere of i size	g/sphere	–	–
Min_dis_A	Kinetic inhibitor	g/m^3	0.005	0.1
Min_dis_G	Kinetic inhibitor	g/m^3	0.05	0.8
Mol_esf_i	Number of struvite moles in a sphere of i size	mol/sphere	–	–
Mw_i	Molecular weight of i	g/mol	–	–
Agg_Exp	Aggregation exponent	–	1	6
Nucl_Exp	Nucleation exponent	–	1	6
Growth_Exp	Growth exponent	–	1	8
Vw	Reactor volume	m^3	–	–

Table 2. Stoichiometry Matrix for Nucleation, Growth and Aggregation. Negative species are reactants in the reaction and positive ones, the products. Struvite$_i$ refers to i sized struvite. In nucleation, j refers to the smallest size. Growth_i_i+1 is the growth reaction from i to i+1 size. Aggregation_j_i is the aggregation of i and j sized particles

Species reaction	PO$_4$	Mg	NH$_3$	H$_2$O	Struvite$_j$	Struvite$_i$	Struvite$_{i+1}$
Nucleation	−Mol_esf_1* MW_PO$_4$	−Mol_esf_1* MW_Mg	−Mol_esf_1* MW_NH$_3$	−Mol_esf_1*6* MW_H$_2$O	Mol_esf_1* MW_STRU		
Growth_i_i+1	−Mol_esf_i* MW_PO$_4$	−Mol_esf_i* MW_Mg	−Mol_esf_i* MW_NH$_3$	−Mol_esf_i*6* MW_H$_2$O		−Mol_esf_i* MW_STRU	Mol_esf_i +1*MW_STRU
Aggregation_j_i					−Mol_esf_j* MW_STRU	−Mol_esf_i* MW_STRU*2^ (j−i)	−Mol_esf_i +1*MW_STRU*2^(j −i)

Table 3. Kinetic expressions used in the model. Growth_i_i+1 is the growth reaction from i to i+1 size. Aggregation_j_i is the aggregation of i and j sized particles

Reaction	Kinetic expression
Nucleation	$\mathrm{Kr\_Nucleation} * Vw * \log\left(\dfrac{IAP}{KspStru}\right)^{\mathrm{Nucl\_Exp}}$
Growth_i_i+1	$\mathrm{Kr\_Growth} * \dfrac{1\mathrm{sphere}}{(L_i+L_{i+1})/2} * \log\left(\dfrac{IAP}{KspStru}\right)^{\mathrm{Growth\_Exp}} * \left(\dfrac{CwXSTRUi}{CwXSTRUi + 2^{i}*\mathrm{Min\_dis\_G}}\right)$
Aggregation_j_i	$\mathrm{Kr\_Aggregation} * \dfrac{CwXSTRUi*CwXSTRUj}{m_{XSTRUi}*m_{XSTRUj}} * 0.001 * Vw * \log\left(\dfrac{IAP}{KspStru}\right)^{\mathrm{Agg\_Exp}}$

2.3   Sensitivity Analysis

A sensitivity analysis to quantify the partial effect of each parameter in each variable was done combining Matlab and WEST. The outputs were pH values and PSD at the end of the experiment. pH values were considered every 10 s for the first 2 min of experiment because that was the most critical period and every minute for the next 18 min.

Experimental conditions were reproduced s*(n + 1) times in WEST (s is the number of initial simulations and n the number of parameters which effect is computed) with random sets of parameters chosen by Latin Hypercube (LH) scheme. The influence of the eight kinetic parameters used in the model was quantified for 3,000 initial simulations, giving a total of 27,000 runs. Range of the parameters are included in Table 1.

Sensitivities were calculated using the one factor at a time method, based on van Griensven et al. (2006). From the initial simulation little changes are done in each parameter to see how chosen variables vary for that change:

$$S_{i,j} = \left| \frac{100 * \left(\frac{M(e_1,...,e_i*(1+f_i),...,e_p) - M(e_1,...,e_i,...,e_p)}{\frac{[M(e_1,...,e_i*(1+f_i),...,e_p) + M(e_1,...,e_i,...,e_p)]}{2}} \right)}{f_i} \right| \tag{1}$$

Where $S_{i,j}$ is the partial effect of the e_i parameter in each j point in the LH. M $(\cdot)$ refers to each considered variable and f_i is how much the parameter e_i changes. Total influence of the parameter (δ^{msqr}) in each output variable was calculated as proposed in Brun et al. (2001):

$$\delta_j^{msqr} = \sqrt{\frac{1}{s} \sum_{i=1}^{s} S_{i,j}^2} \tag{2}$$

2.4   Calibration

Calibration of the model was done employing Bayesian Inference. Experimental conditions were reproduced 10,000 times with parameter sets chosen by LH. Parameter ranges were those of the sensitivity analysis. Value of the output variables of each simulation were compared with the experimental results and the posterior density was calculated as follows:

$$p(\theta|y) \propto [M(\theta)]^{-N/2} \tag{3}$$

$$M(\theta) = \sum_{j=1}^{Nobs} |e_j(\theta)|^2 \tag{4}$$

$p(\theta|y)$ is the posterior density of the parameter set θ for the experimental data y. *Nobs* is the number of observed variables and $e_j(\theta)$ the normalized error in each

variable. N is the number of outputs considered, in this case 2. Errors have been normalized with the standard deviation: 0.1 for pH and 10 for PSD percentage. The discretization in the SYMPATEC H820 did not follow the same criteria as the model. Therefore, linear interpolation was done to compare the results.

3   Results and Discussion

3.1   Sensitivity Analysis

Results of the sensitivity analysis for PSD and pH are presented in Fig. 1. The total effect of the change in each parameter (δ_j^{msqr}) for each size of struvite and each pH time has been normalized with the highest effect. Therefore, the biggest value of the effect in each variable for a parameter is 1 and the rest of the parameters are compared to it.
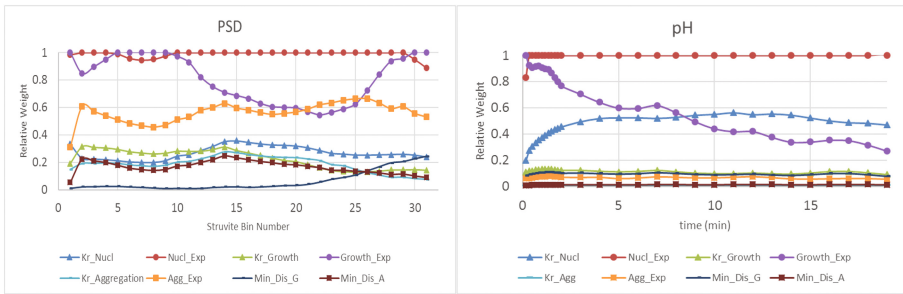
Fig. 1. δ^{msqr} values for the eight parameters to be calibrated for each size of struvite (a) and for the pH (b)

For final PSD, Nucl_Exp and Growth_Exp are the parameters with the highest influence in the output. Agg_Exp has a significant effect too, especially in the range of diameters between 105–435 µm, corresponding to bins 19-27. Kr_Nucl, Kr_Growth, and Kr_Aggregation should be also considered, while min_dis_G and min_dis_A have a very little effect in the final PSD.

Nucl_Exp is the parameter with the highest influence in the pH evolution. Growth_exp presents a relative influence between 0.8 and 1 for the first 2 min of the experiment. After that, its effect decays. Kr_Nucl has an average relative weight of 0.46, so it should be considered. The effect of the rest of the parameters is clearly below these three for the whole experiment. Considering both outputs, the most important parameters for the calibration of the model are: Nucl_Exp, Growth_Exp, Agg_Exp and Kr_Nucl.

3.2   Test Results

Experimental pH evolution is shown in Fig. 2(a). The pH decays sharply for the first two minutes and then remains almost constant for the rest of the experiment.
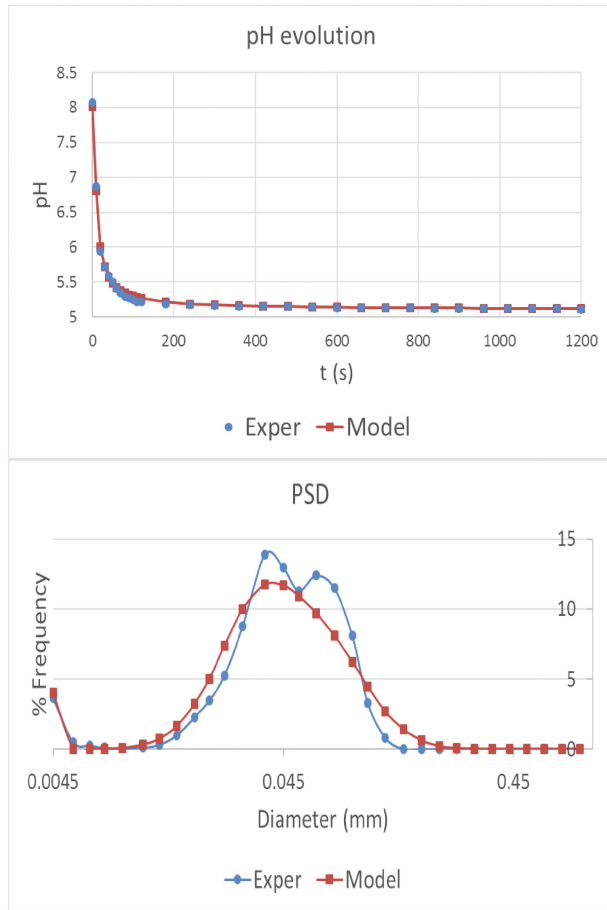
Fig. 2. Comparison between modelling results and experimental data

The experimental result of final PSD is shown in Fig. 2(b). PSD was measured three times from the obtained struvite and the average value is shown. The final PSD shows an accumulation in the volume of the smallest particles. This is an expected result, as the supersaturation was high in the experiment and therefore, primary nucleation is favored.

3.3   Calibration

The histogram with the posterior density distribution for Nucl_Exp and Growth_Exp is shown in Fig. 3. These parameters and Kr_Nucl (histogram not included) have peaked posterior densities. Agg_Exp presented a more diffuse distribution because the effect of the pH has more weight than the effect of the final PSD in the posterior density calculation. The rest of the parameters present a diffuse distribution too, which means
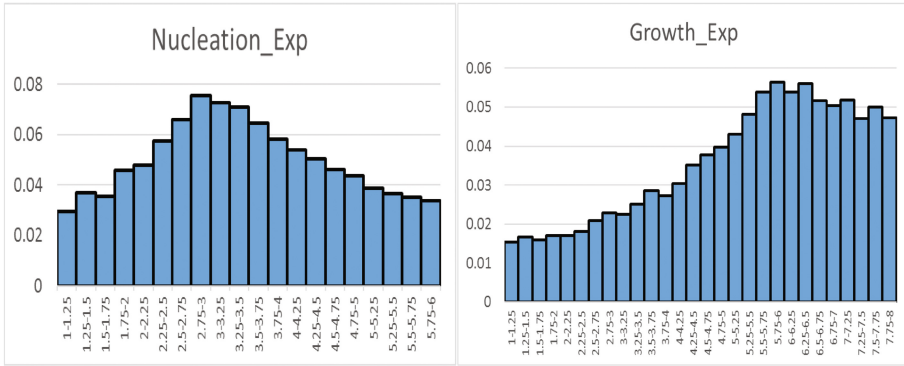
Fig. 3. Histograms of Posterior densities for Nucl_Exp (a), Growth_Exp (b)

that their value has not a big impact in the final result. This was something expected from the Sensitivity Analysis.

Parameter values of the parameter set with the highest posterior density are recorded in Table 4. A simulation in WEST-DHI with the same case study used for the calibration has been performed with these values and compared with experimental data in Fig. 2.

Table 4. Parameter values with the highest posterior density

Kr_Nucl	Nucl_Exp	Kr_Growth	Growth_Exp	Kr_Agg	Agg_Exp	Min_Dis_G	Min_Dis_A
1.82E +17	2.92	5.26E+06	5.88	1.33E– 12	1.84	3.74E–01	5.04E–02

For the pH evolution, maximum relative error in the measurements is 0.011. For the PSD, maximum relative error is 2.23. It was expected the PSD to be less exact than the pH in the calibration because as pointed out in Hanhoun et al. (2013) the uncertainty in the measurements using laser diffraction for non-spherical particles is big. However this is not a crucial issue because the model is capable to predict the shape of the PSD. Bearing in mind these uncertainties in the experimental measurements, it is considered that the model fulfilled the objective to predict both pH evolution and final PSD in a successful way.

4   Conclusions

A mass based DPBM has been constructed for struvite precipitation. Its main advantages are that size of precipitated material is considered, mass continuity is guaranteed and it is fully compatible with other chemical and physicochemical reactions. A sensitivity analysis has shown that exponents of nucleation and growth are the most important parameters. Calibration of these parameters using experimental data of pH evolution and final PSD and employing Bayesian Inference has been presented. From

the results obtained in this paper it can be said that the model proposed is valid in its structure and scope for the description of struvite formation and growth. Consequently, this model constitutes a valuable tool for the design and optimization of new technologies for resources recovery based on crystallization phenomena.

References

Brun R, Reichert P, Ku HR (2001) Practical identifiability analysis of large environmental simulation models. Water Resour Res 37(4):1015–1030

Galbraith SC, Schneider PA (2014) Modelling and simulation of inorganic precipitation with nucleation, crystal growth and aggregation: a new approach to an old method. Chem Eng J 240:124–132. Available at: http://linkinghub.elsevier.com/retrieve/pii/S1385894713015477. Accessed 27 May 2015

Galbraith SC, Schneider PA, Flood AE (2014) Model-driven experimental evaluation of struvite nucleation, growth and aggregation kinetics. Water Res 56:122–132. Available at: http://www.ncbi.nlm.nih.gov/pubmed/24662095. Accessed 27 May 2015

van Griensven A et al (2006) A global sensitivity analysis tool for the parameters of multi-variable catchment models. J Hydrol 324(1–4):10–23

Hanhoun M et al (2013) Simultaneous determination of nucleation and crystal growth kinetics of struvite using a thermodynamic modeling approach. Chem Eng J 215–216:903–912. Available at: http://linkinghub.elsevier.com/retrieve/pii/S1385894712013757. Accessed 18 Dec 2014

Hounslow J, Ryall RL, Marshall VR (1988) A discretized population balance for nucleation. Growth Aggregation 34(11):1821–1832

Ikumi DS, Harding TH, Brouckaert CJ, Ekama GA (2013) Plant-wide integrated biological, chemical and physical processes modelling of wastewater treatment plants in 3 phases (aqueous-gas-solid). Research Report, 138

Lizarralde I et al (2015) A new general methodology for incorporating physico-chemical transformations into multi-phase wastewater treatment process models. Water Res 74:239–256

Tarragó E et al (2016) Controlling struvite particles' size using the up-flow velocity. Chem Eng J 302:819–827

New Individual-Based Model Links Microbial Growth to the Energy Available in the Environment

R. González-Cabaleiro[1(✉)], T.P. Curtis[2], and I.D. Ofiţeru[1]

[1] School of Chemical Engineering and Advanced Materials,
Newcastle University, Merz Court, Newcastle upon Tyne NE1 7RU, UK
{rebeca.gonzalez-cabaleiro,dana.ofiteru}@ncl.ac.uk
[2] School of Civil Engineering and Geosciences, Newcastle University,
Cassie Building, Newcastle upon Tyne NE1 7RU, UK
tom.curtis@ncl.ac.uk

Abstract. A new individual-based model is presented in which we aim to describe microbial growth constrained by the environmental conditions at each point of a 2D space. The model is characterized for a full description of the physico-chemistry of the system and uses thermodynamics to approximate the microbial growth. The growth parameters are estimated using the information of the surroundings and it employs only first principles instead of relying on measurements at the population level. This allows ab initio approximation of the growth parameters, and therefore directly links microbial growth and environmental conditions. For this reason, the model is characterised for its flexibility. We test the model in three very different scenarios: anaerobic digestion, aerobic heterotrophic growth and nitrification. Due to its flexibility, rigorous thermodynamic calculations and the possibility to estimate the parameters ab initio, the model will be further used to hypothesize the presence of new functional groups or microbial species not yet discovered and to model complex microbial populations not well understood. Moreover, it can be used to study the rules that control microbial evolution or/and immigration.

Keywords: Individual-based model · Bacterial growth · Thermodynamics · Diffusion · pH

1 Introduction

Individual-based models are receiving increasing interest due to their capacity to describe microbial growth and spatial distribution of cells in a biofilm or floc. However, they are computational intensive and, most often than not, they use growth parameters inferred from measurements made at the population level. This can generate misleading results when analysing microbial growth at microscale (Hellweger et al. 2016).

In this work, we propose a comprehensive individual-based model (2D) that describes the microbial growth as a function of the energy available in the surroundings. It includes a detailed sub-model of the physico-chemistry of the system: gas-liquid and acid-base equilibriums are considered with the aim of understanding

how environmental changes affect the growth of the different microorganisms in a population (Batstone et al. 2012). This allows *ab initio* approximation of the growth parameters, and therefore directly links microbial growth and environmental conditions. The main advantage of this approach is that it reduces the necessity of parameter calibration, which makes testing new theories on microbial ecology a less daunting task. This will allow better understanding of microbial growth in complex communities and will implicitly increase our capacity to manipulate it in our favour.

2   Materials and Methods

Energetic calculations implicitly consider all the environmental variables that constrain the chemical reactions catalysed by microbial species. This further allows the approximation of the energy available to generate new biomass. Using this approach, we calculate the maximum growth yield (Y_{XS}^{max}) with the Energy Dissipation Method (Kleerebezem and van Loosdrecht 2010) and we consider Monod kinetics (q_S and Ks parameters) to describe the kinetics of any of the microbial species in the system. We assume that the bacteria will only be able to grow (Eq. 1) if they harvest extra energy besides the energy necessary for microbial maintenance (m_S). Otherwise, bacteria maintain (Eq. 2) or decay linearly with a constant k_d (Eq. 3) (Gonzalez-Cabaleiro et al. 2015).

$$\mu = Y_{XS}^{max} \cdot \left(q_S^{met} - m_S^{req} \right) \quad if \quad q_S^{cat} > m_S \tag{1}$$

$$\mu = 0 \quad if \quad q_S^{cat} = m_S \tag{2}$$

$$\mu = -k_d \cdot \frac{m_S^{req} - q_S^{cat}}{m_S^{req}} \quad if \quad q_S^{cat} < m_S \tag{3}$$

In some cases, the carbon source or other anabolic substrate limiting the growth can be different than the substrates needed for the catabolism. For this reason, two different substrate uptake rates are considered: (i) q_S^{cat} which accounts only for substrates limitation of the catabolic process; and (ii) q_S^{met} that considers all the substrates of the metabolism (including anabolism) and is used only when the bacteria grows (Eq. 1).

Two spatial configurations are studied: the biofilm and the floc. In the biofilm, the microbes are attached to a surface and diffusion of substrates occurs only from the top of the biofilm (Kreft et al. 2001). In the floc, the biofilm grows in the centre of the computational space and the diffusion of substrates occurs from the four frontiers of the 2D space (Ofiţeru et al. 2014).

The diffusion equation is solved in 2D for each of the substrates and products of the microbial activity using an implicit Crank-Nicolson scheme. Then, the concentration of all solvents is known in each node of the simulation space (Kreft et al. 2001). Once the concentrations are known, acid-base and liquid-gas equilibriums, pH and thermodynamics of all the chemical reactions occurring can be calculated in each node:

- *Acid-base equilibriums and pH*: The concentration of all the forms of the liquid components are calculated algebraically. A Newton-Raphson scheme finds the root

of the balance of charges and estimates the pH of each of the nodes. Then, the matrix of all the forms of the liquid components is calculated (hydrated and non-hydrated forms and until the 3rd deprotonation) (González-Cabaleiro et al. 2015).

- *Liquid-gas equilibrium*: The liquid - gas transfer is calculated using mass transfer coefficients corresponding to each of the components that move to the gas phase. Two configurations are implemented: (i) air-open system in which the variation of the partial pressures of the different gasses in the atmosphere is considered negligible; (ii) a close system in which a gas flow is produced when the accumulation of gasses in the head space exceeds the total atmospheric pressure fixed at the beginning of the operation.

- *Thermodynamics*: Gibbs free energy is calculated for all the biological reactions occurring in the system: the metabolisms of each of the microbial functional groups considered are described in terms of catabolism and anabolism (González-Cabaleiro et al. 2015). The energy of each of them is calculated which later allows the estimation of the growth yield of the bacteria in each position of the simulation space.

This model was coded in MATLAB® (2016) and uses an Excel interface in which the user can easily define new systems (aerobic, anaerobic, floc, biofilm, etc.).

Results and Discussion

We present three different scenarios (Fig. 1). All simulations were occur in a space of 200×200 μm, considering an average diameter of bacterial size of 1 μm and all the simulations occur at pH 7.

(a) Anaerobic digestion of glucose with intermediate production of butyric and acetic acids: In this case the reactor is assumed closed and the biogas produced is calculated. The competition of four bacteria with their growth limited by the energy available is analysed.

(b) Aerobic heterotrophic growth and competition of two bacteria with different growth strategies: The growth parameters are the same as in Kreft 2004. In this case, only oxygen limitation is considered and the growth yields are assumed constants as in Kreft 2004.

(c) Nitrification process analysing the competition of complete nitrifiers and ammonia-oxidizers: The competition for ammonia of both microorganisms is studied. The nitrite-oxidizers growth depends on the NO_2^- produced by the ammonia-oxidizers.

The model calculates the Gibbs free energy for each catabolism and anabolism of each functional group in each point of the system (Fig. 2). This permits the calculation of the metabolic stoichiometry coefficients and the growth yield of each of the microorganisms.
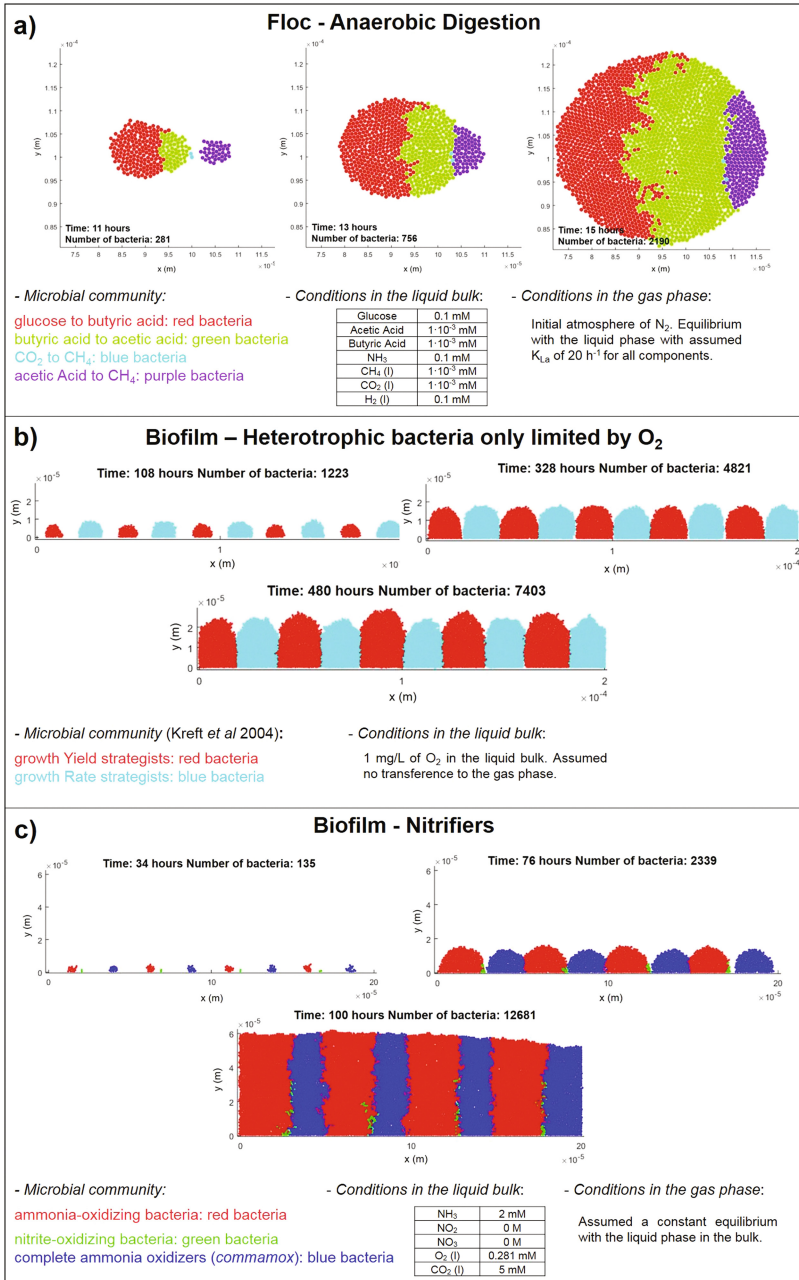
Fig. 1. Model simulations for different scenarios, with biofilm or floc geometry. Growth parameters are estimated or obtained from literature values. Diffusion coefficients of chemical components in water are obtained from Haynes 2016
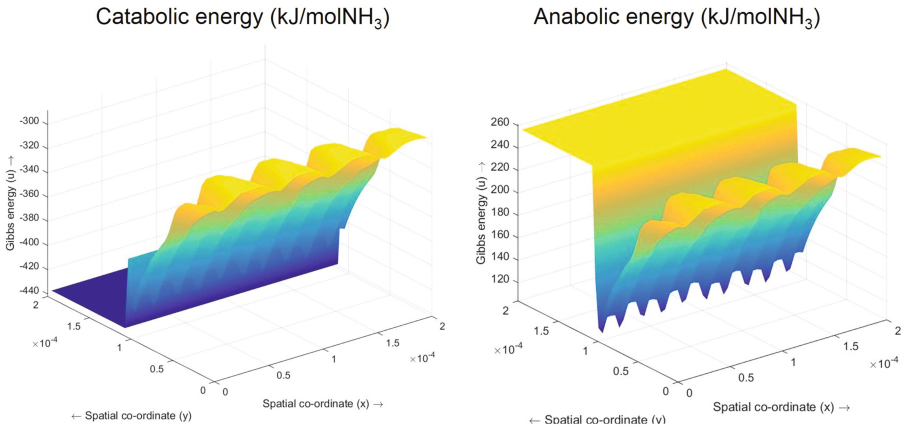
Fig. 2. Catabolic and anabolic energy of AOB at the end of the simulation

3   Conclusions

This individual-based model is the first one able to describe comprehensively the physico-chemistry of the system and how it affects the microbial growth. The growth parameters are estimated using the information of the surroundings and it employs only first principles like thermodynamic calculations, instead of relying on measurements at the population level. In the current realization of the model, we simulated three different cases, generating results that show an expected trend (anaerobic digestion and nitrifiers) or in accordance with published literature (heterotrophs) (Kreft 2004).

Due to its flexibility, rigorous thermodynamic calculations and the possibility to estimate the parameters *ab initio*, the model will be further used to hypothesize the presence of new functional groups or microbial species not yet discovered. Moreover, it can be used to study the rules that control microbial evolution and immigration.

References

Batstone DJ, Amerlinck Y, Ekama G, Goel R, Grau P, Johnson B et al (2012) Towards a generalized physicochemical framework. Water Sci Technol 66:1147–1161

Gonzalez-Cabaleiro R, Ofiteru ID, Lema JM, Rodriguez J (2015) Microbial catabolic activities are naturally selected by metabolic energy harvest rate. ISME J 9:2630–2641

González-Cabaleiro R, Lema JM, Rodríguez J (2015) Metabolic energy-based modelling explains product yielding in anaerobic mixed culture fermentations. PLoS ONE 10:e0126739

Haynes WM (2016) CRC Handbook of Chemistry and Physics, 97th edn

Hellweger FL, Clegg RJ, Clark JR, Plugge CM, Kreft J-U (2016) Advancing microbial sciences by individual-based modelling. Nat Rev Micro 14:461–471

Kleerebezem R, van Loosdrecht MCM (2010) A generalized method for thermodynamic state analysis of environmental systems. Crit Rev Env Sci 40:1–54

Kreft JU (2004) Biofilms promote altruism. Microbiology 150:2751–2760

Kreft J-U, Picioreanu C, Wimpenny JWT, van Loosdrecht MCM (2001) Individual-based modelling of biofilms. Microbiology 147:2897–2912

Ofiţeru ID, Bellucci M, Picioreanu C, Lavric V, Curtis TP (2014) Multi-scale modelling of bioreactor-separator system for wastewater treatment with two-dimensional activated sludge floc dynamics. Water Res 50:382–395

Improved Biological Nutrient Removal and Reduced Energy Consumption at a Retrofitted Wastewater Treatment Plant

C. Brepols[(⊠)], T. Engels, and H. Schäfer

Erftverband, Am Erftverband 6, 50126 Bergheim, Germany

Abstract. A case-study of a retrofit of an existing wastewater treatment plant with full biological nutrient removal is described. During the planning process dynamic modelling was used, to evaluate effluent quality and to design a process control strategy for intermittent denitrification. Finally a 30% increase in treatment capacity could be achieved while lowering the energy consumption and improving the actual effluent quality without building new bioreactors in the main treatment line.

Keywords: Biological nutrient removal · Modelling · Plant retrofit · Energy efficiency

1 Introduction

In 1988 the German Federal Government issued a plan to massively reduce nutrient loads to the north-sea by improving the wastewater treatment standard in all contributing river systems. As a consequence since 1989 Erftverband, being in charge of many municipal wastewater treatment plants (WWTP) in the Erft river catchment upgraded all WWTPs for biological nutrient removal.

One of the first WWTPs which was not only retrofitted but newly built and originally designed for biological nutrient removal was the WWTP of Bedburg-Kaster. The WWTP collects wastewaters from a number of small WWTPs, which have been decommissioned after new large sewers have been completed. The catchment area of the WWTP consists mainly of mixed-sewer-systems in two urban areas of the municipalities Bergheim and Bedburg and a number of smaller rural settlements in a lowland region. Operations of the new WWTP started in 1993 with a capacity of 50000 population equivalents (PE). The WWTP featured biological nutrient removal in a two line bioreactor with a sequence of pre-anoxic, anaerobic, anoxic and aerobic tanks, a sand-filtration for additional phosphorous precipitation and an anaerobic sludge digestion.

After almost 20 years of operation the WWTP required a retrofit: Over the years, the plant had almost reached its design capacity and ongoing municipal development demanded for a higher treatment capacity. Raw wastewater composition had also changed. The actual average C/N ratio in the influent was much lower than the original design values with sludge liquor contributing 20% of the ammonia load. Fresh-water saving and sewer rehabilitation in the catchment lowered the actual dry-weather inflow (Table 1). Pronounced shock-loadings and first-flush phenomena during storm weather

Table 1. Inflow conditions of the Bedburg-Kaster WWTP

Parameter	Unit	Design values 1990	Design values 2013
Design capacity	PE	50500	66000
Average dry weather inflow	m^3/d	15314	10560
Maximum storm weather inflow	L/s	520	520
COD load	kg COD/d	6060	5532
Total Nitrogen load	kg TNb/d	556	805
Total Phosporous load	kg P/d	152	136

conditions were thus observed. Flow distribution between the two bioreactor lines was uneven. The aeration system was aged and inefficient. Altogether, effluent concentrations for ammonia and nitrate were no longer satisfactory.

2 Materials and Methods

The actual design conditions were determined from operational data on flow, COD, nitrogen and phosphorous concentrations in influent 24-hour-mixed samples from a three-year period. Additional 2-hour mixed samples were taken to asses the diurnal variations of influent components.

A static model was used to calculate the design of the primary settling, bioreactor and secondary clarifier (ATV 2000; Design2Treat 2010), based on new design inflow conditions. Influence of reactor design and control strategy on effluent concentration and energy consumption were further assessed by using activated sludge model no. 1 (ASM1) in the Simba/Matlab software package (SIMBA, Release 6.0). Flow distribution between the bioreactor lines and flow conditions inside the newly equipped final aeration basin of the bioreactor were assessed using computational fluid dynamics (CFD) models (Hunze 2012).

Results and Discussion

The existing bioreactor consisted of two lines with a sequence of different compartments and an overall volume of 11922 m^3 (Table 2), with the final aerobic tank equipped as a 'race-track' basin (see also Fig. 1).

Table 2. Bioreactor compartments and volumes

Bioreactor compartment	Design 1990	Design 2013
2 pre-anoxic tanks	2 × 235 m^3	2 × 235 m^3
2 anaerobic tanks	2 × 1176 m^3	2 × 5726 m^3 intermittent aeration
2 anoxic tanks	2 × 1050 m^3	
2 anoxic/aerobic tanks	2 × 700 m^3	
2 aerobic tanks	2 × 2800 m^3	
Total volume	11922 m^3	11922
Anoxic volume/total volume	0,33	0,50
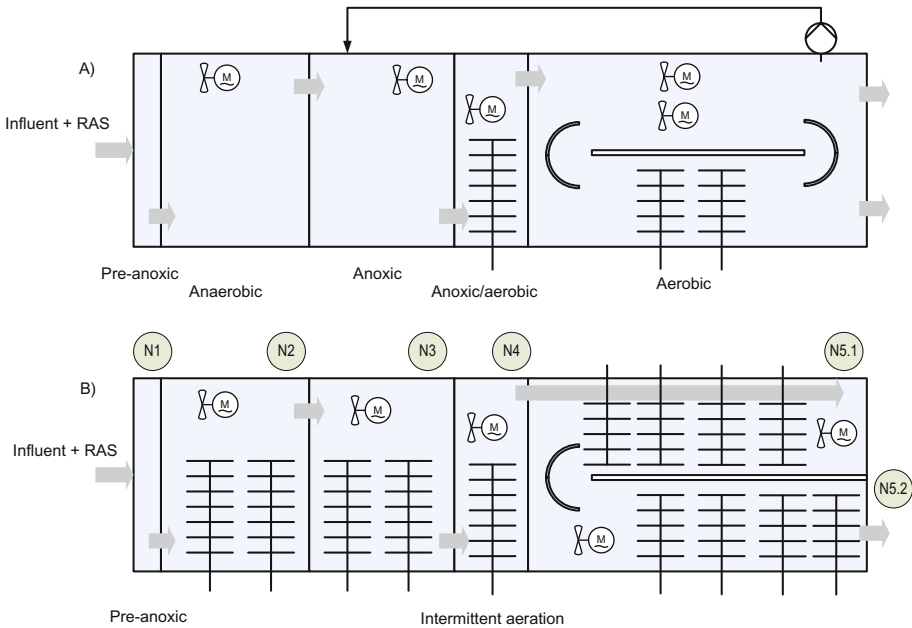
Fig. 1. Schematic floorplan of a bioreactor line (A) before and (B) after the plant retrofit and sampling spots of the simulation model (N1 to N5.2)

The static model of the WWTP showed that the given ratio of anoxic to total volume was not sufficient to achieve required degree of denitrification under the actual loading conditions. However, the overall bioreactor volume still was sufficient if ammonia loads coming from on-site sludge dewatering of digested sludge could be reduced significantly. As a consequence an anaerobic ammonia oxidation was planned, using the existing sludge liquor storage and two new sequencing batch reactors (SBR) for sludge liquor treatment. Optional acetic acid dosage to the main treatment line was foreseen as a backup in case of operational disturbances in sludge liquor treatment. The bioreactor was retrofitted with intermittent denitrification to improve operational flexibility and to increase the denitrification portion to an average of 50%. The race-track design of the final aeration basin raised questions on potential short circuits and insufficient aeration. Taking into account results from the CFD simulation (Hunze 2012) it was finally decided to convert the reactor to a plug-flow like design.

The dynamic model helped in designing an appropriate control strategy for intermittent aeration. Ammonia and nitrate online sensors inside the bioreactor and effluent function as feed-back signals for a cascade which controls the duration of the denitrification and nitrification phases as well as oxygen concentrations during the nitrification phase. Later a feed-forward signal of inflow was also used to start aeration pre-emptively, so that long lag times in the bioreactor and from the measurements could be compensated (Fig. 2). The model also helped to assess operations during the construction phase, when bioreactor lines were taken out of operation subsequently.
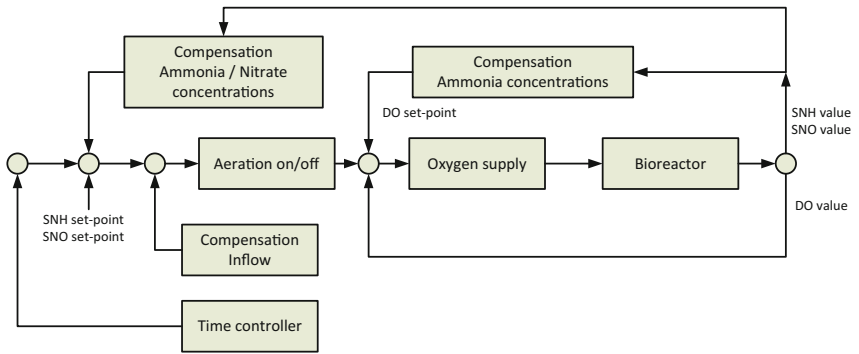
Fig. 2. Block-scheme of the aeration-time/oxygen-supply controller with feed-back and feed-forward compensation
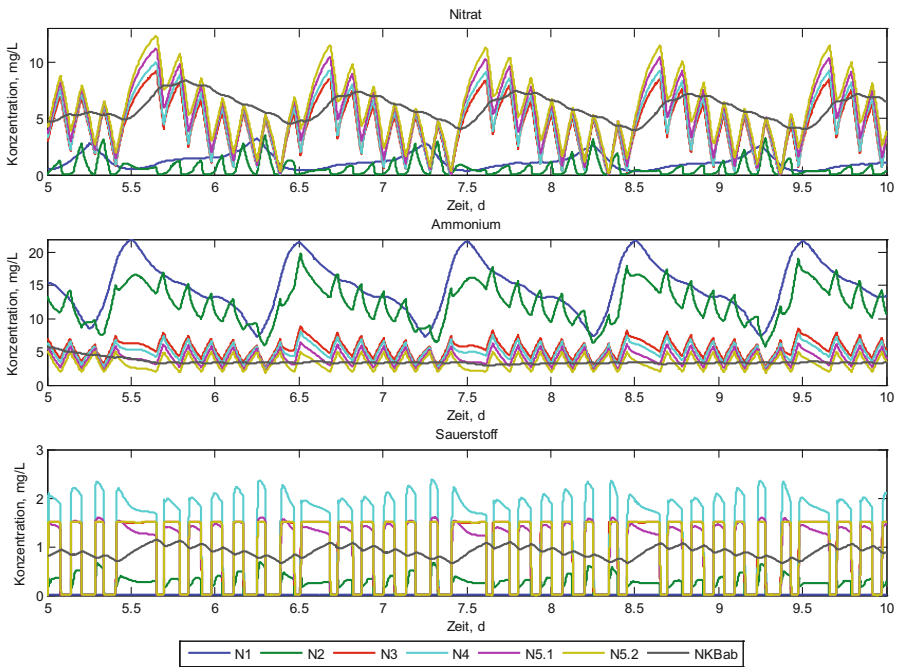
Fig. 3. Modelled concentrations of nitrate (above), ammonia (centre) and oxygen (below) during the construction phase at different sampling spots in the bioreactor (N1 to N5.2) and secondary clarifier effluent (NKBab)

Simulation results in Fig. 3 show how the controller sustains aerobic phases during the midday peak in order to maintain the required ammonia peak effluent concentration.

Actual operational data show that the WWTP was generally capable to achieve the predicted low nitrogen effluent concentrations. After the retrofit, average energy consumption of the entire WWTP was reduced from 8 MWh/d to nearly 6 MWh/d (Fig. 4).
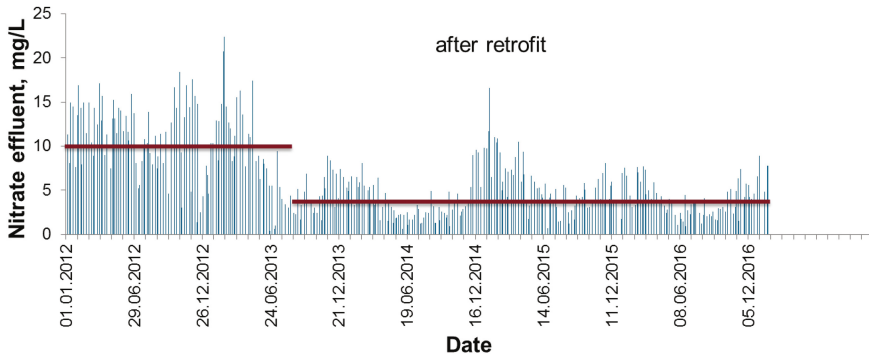
Fig. 4. Nitrate effluent concentrations before and after the retrofit, daily average values (blue) and long-term average (red)

Soon after its completion the side-stream anaerobic ammonia oxidation started working sufficiently but then suffered badly under low temperature conditions in winter. As a reaction the SBRs are now equipped with additional heat exchangers to maintain temperatures of more than 20° C throughout year. Heat exchangers are run on excess thermal energy form the WWTPs co-generation unit.

3   Conclusion

The capacity of the municipal WWTP could be increased from 50000 to 66000 PE. Building new bioreactor volume in the main treatment lines could be avoided, by changing the process from pre-denitrification to intermittent denitrification and building an additional sludge liquor treatment. Energy efficiency and the Effluent quality of the WWTP were significantly improved. The concept at Bedburg-Kaster WWTP thus serves as a role-model for other WWTP retrofits at the Erftverband.

References

ATV DVWK, ed (2000) Bemessung von einstufigen Belebungsanlagen. GFA, Verl. für Abwasser, Abfall und Gewässerschutz, Hennef

Design2Treat (2010) Version 5.0, Software tool for dimensioning of conventional activated sludge plants with suspended biomass, Gesellschaft zur Förderung der Abwassertechnik an der RWTH Aachen, e.V., Aachen

Hunze M (2012) Untersuchung der Strömungsverhältnisse in einem Verteilerbauwerk sowie in einem Belebungsbecken des GKW Kaster, Report to Erftverband, Hannover

Influence of the Sludge Concentration
on Oxygen Transfer and Energy Consumption
in Activated Sludge Systems

S.L. dos Santos[1(✉)], Y.C. Catunda[2], and A.C. van Haandel[3]

[1] Paraiba State University, Environmental Engineering Department,
Campina Grande, Brazil
[2] Federal University of Rio Grande do Norte,
Electrical Engineering Department, Natal, Brazil
[3] Federal University of Campina Grande,
Civil Engineering Department Campina Grande, Campina Grande, Brazil

Abstract. When auxiliary equipment like MBR or MBBR or granular sludge is used to reduce the reactor volume of activated sludge systems, the sludge concentration increases and this will affect the oxygen transfer capacity of the aeration system, so that for a given oxygen demand the required energy and hence the operational costs will increase. An experimental method is presented to determine the influence of sludge concentration on the oxygenation capacity. An investigation was carried out, in which the influence of the oxygenation capacity was measured as a function of sludge concentration, by applying respirometry. The results show that the sludge concentration affects severely the oxygen transfer coefficient. Flocculent sludge is much more affected than granular sludge: at 25° C.

Keywords: Activated sludge concentration · Respirometry · Oxygenation capacity

1   Introduction

The oxygenation capacity or of an aerator is determined by the critical concentration that is required to maintain enough dissolved oxygen in the system for proper performance and is expressed as the product of the transfer coefficient (K_{la}) and the difference between the saturation concentration (DO_s) and the critical concentration (DO_c) of dissolved oxygen (DO) (Van Haandel and Van de Lubbe 2012):

$$OC_m = K_{la}(DO_s - DO_c) \tag{1}$$

From Eq. (1) it can be seen that the oxygenation depends on three factors: the transfer coefficient, the saturation concentration for DO and the critical concentration. In principle each of these three factors can be affected by the sludge concentration. In this paper the influence of the sludge concentration on each factor is determined by respirometry. The result of our experimental investigation is that a high e sludge concentration reduces considerably the value of the transfer coefficient but has relatively little influence on the saturation concentration and the critical concentration of DO.

Some variants of the activated sludge process, have been applied as alternatives to operate the activated sludge systems at much higher than conventional sludge concentrations and thus reduce the required reactor volume. (Odegaard et al. 2000) These can be operated at a sludge concentration of 10-15 $g.L^{-1}$, as against 3-6 $g.L^{-1}$ in conventional systems. However the consequential higher sludge concentration is detrimental for oxygen transfer from the atmosphere to the mixed liquor.

The experimental results in this paper show that purely from the economic point of view, these high concentrations are counterproductive: The reduction of the investment costs due to the smaller volume does not compensate the increase of operational costs due to the large energy consumption for aeration. The results also show that the reduction of the transfer coefficient is much smaller for granular sludge than for flocculent sludge. Thus the optimal sludge concentration for granular sludge is higher than for flocculent sludge.

2   Materials and Methods

In this paper a method is presented to determine the influence of the sludge concentration on the oxygen transfer rate by using respirometry for the determination of K_{la}, DO_s and DO_c at different sludge concentrations. This method makes use of an automated respirometer, which is an apparatus that determines the oxygen uptake rate (OUR) in an activated sludge reactor. Figure 1 shows the respirometer with the auxiliary equipment: a DO electrode for acquisition of the DO concentration in the reactor vessel equipped with a stirrer and a computer to store data of DO and OUR as functions of time, also allowing to view the values of these parameters on line. The reactor may either be a lab scale or a full scale unit.
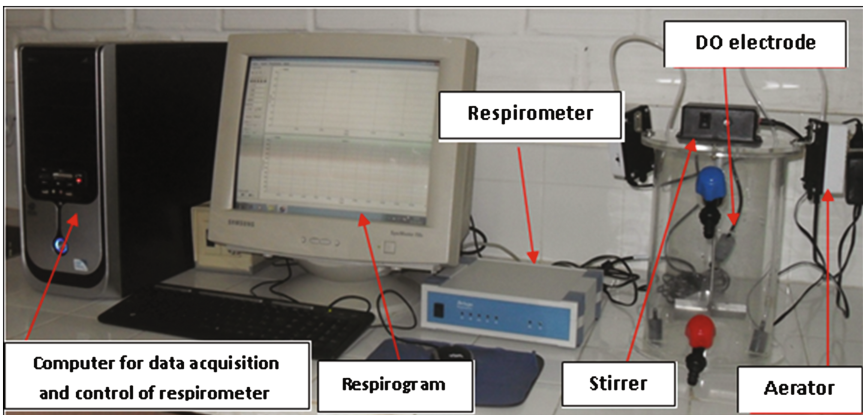
Fig. 1. Photo of the respirometer and the basic auxiliary equipment

A convenient method to determine the OUR is to fix an upper and a lower limit for the DO concentration and alternate periods of aeration until the upper set point and then switch off the aeration system till the lower set point is reached while to reactor continues to be stirred to ensure a uniform sludge concentration and substrate availability. Without aeration the decrease of the DO concentration in good approximation is linear with time until a critical concentration is reached, where DO becomes limiting and OUR decreases. Aeration is resumed when the lower set point is reached and a new cycle is initiated. The OUR is determined as the ratio between the decrease of the DO concentration from the upper to the lower set point and the time for the microbial sludge mass to consume the oxygen:

$$OUR = (DO_{max} - DO_{min})/(t_2 - t_1) \tag{2}$$

Where:

$DO_{max} - DO_{min}$ = setpoint for the maximum and minimum DO concentration
t_1, t_2 = beginning and end of a period without aeration

The software of the respirometer automatically calculates and plots both the variation of the measured DO concentration and the calculated OUR values as functions of time, so that the OUR variation with time can be seen on the monitor. Figure 2 is an example of such a respirogram: The top section of the figure shows the variation of the DO concentration with time and the bottom section shows the corresponding OUR values.
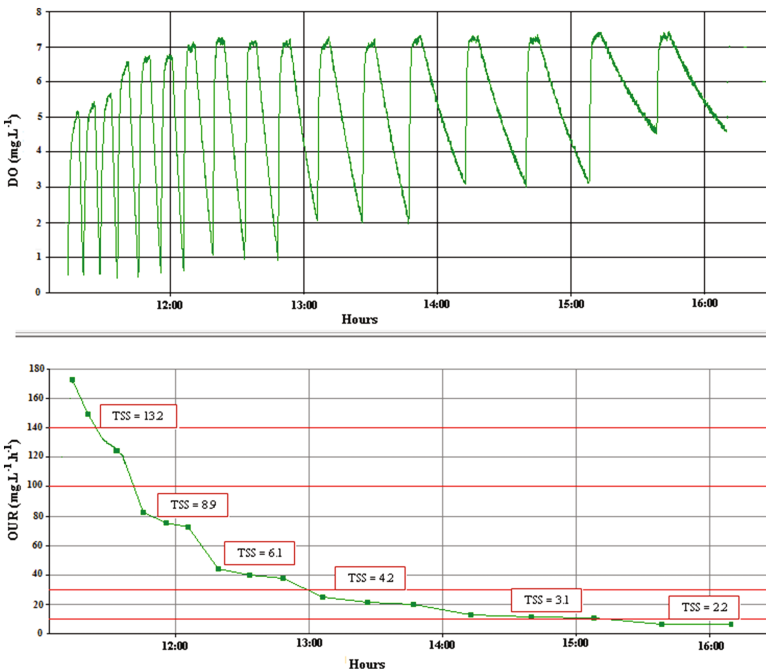
Fig. 2. Respirogram generated by the software of the respirometer with DO concentration (upper graph) and OUR (lower graph) as a functions of time for different concentrations of flocculent sludge

Figure 2 was obtained by measurements of DO and OUR of a sludge batch while periods of aeration were alternated with periods of non-aeration. As indicated the tests were carried out for different concentration of the sludge, thus obtaining OUR values for sludge concentrations from 13,2 to 2,2 gTSS.L^{-1}.

The experimental OUR data thus obtained were used to calculate the values for K_{la}, and DO_s by considering that during the period of aeration the rate of change of the DO concentration is expressed as the difference between the aeration rate (r_a) and OUR or: $dDO_l/dt = r_a -$ OUR $= K_{la}(DO_s\text{-}DO_l)$ – OUR, whereas during the period of non-aeration the rate of change is equal to OUR. By solving the differential equation one gets:

$$DO_l = (DO_s - \text{OUR}/K_{la}) * (1 - \exp(-K_{la}t)) + DO_o\exp(-K_{la}t) \qquad (2)$$

Where:

DO_o = the DO concentration at the beginning of the aeration period.

Equation (2) can be used to simulate the value of DO_l as a function of time for any value of K_{la} and DO_s and for any sludge concentration. The simulated DO_l curve can be compared to experimental DO_l values (Fig. 2) and those K_{la} and DOs values that generate a simulated DO_l profile with the closest correlation to the experimental values will be chosen as the true values for the different sludge concentrations. Then by estimating DO_c value from observed DO profiles the elements to calculate the oxygenation capacity in Eq. (2) are available. Table 1 is an example. The OC_{max} value for TSS = 0 is an extrapolation.

Table 1. Calculated values of K_{la}, DO_s and DO_c and the oxygenation capacity and relative energy consumption as functions of the sludge concentration

TSS (g.L^{-1})	OUR (mg.L^{-1}.min^{-1})	K_{la} (h^{-1})	DO_s (mg.L^{-1})	DO_c (mg.L^{-1})	OC (mg.L^{-1}.min^{-1})	En. cons. (kWh.kgO^{-1})
13.2	151	1.0	7.5	1.3	6.0	2.4
8.9	76	1.4	7.5	1.2	8.8	1.6
6.1	41	1.6	7.6	1.1	10.4	1.4
4.2	20	1.7	7.6	1.0	11.3	1.3
3.1	11	1.9	7.6	1.0	12.5	1.1
2.2	6	2.0	7.5	1.0	13.0	1.1
0	0	2.2	7.5	1.0	14.3	1

The results in Table 2 clearly show that the K_{la} value is very heavily influenced by the sludge concentration; the effect of DO_s and DO_c is only minor. Figure 3 shows the relationship between the sludge concentration and the oxygenation capacity for flocculent and for granular sludge. In both cases the experimental points indicate that there is a tendency of a linear relationship, but the OC value for granular sludge is much less affected by the sludge concentration. From the results the following empirical expressions was derived:
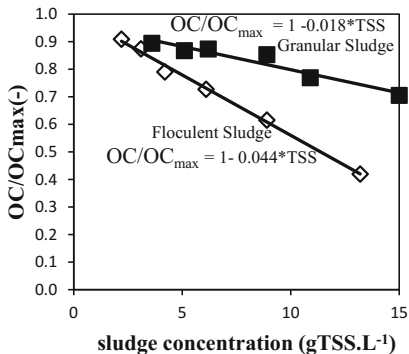
Fig. 3. Decrease of the oxygenation capacity of the aerator as function of the sludge concentration for flocculent (and for granular sludge
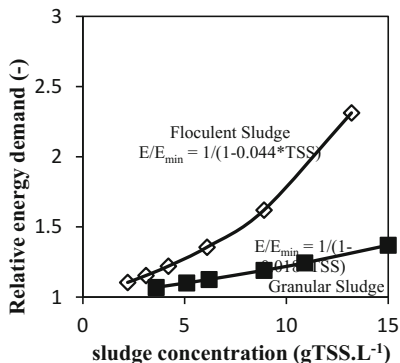
Fig. 4. Relative energy consumption for aeration as a function of the sludge concentration for flocculent and for granular sludge

$$\text{For flocculent sludge}: OC_m/OC_{max} = 1 - 0.044\text{TSS} \tag{3a}$$

$$\text{For granular sludge}: OC_m/OC_{max} = 1 - 0.018\text{TSS} \tag{3b}$$

The relative energy consumption can be correlated to the oxygenation capacity:

$$\text{For flocculent sludge}: E_x/E_{min} = OC_{max}/OC_m = 1/(1 - 0.044 * \text{TSS}) \tag{4a}$$

$$\text{For granular sludge}: E_x/E_{min} = OC_{max}/OC_m = 1/(1 - 0.018 * \text{TSS}) \tag{4b}$$

Where:

E_{min} = minimum energy required when $OC = OC_{max}$

E_x = Energy required when the sludge concentration has a value X_t

In Fig. 4 the points based on experimental observations and the curves of Eqs. 4a and 4b are plotted. The plot of the empirical relationships in Fig. 4 shows the strong effect of sludge concentration on energy consumption, especially in the case of flocculent sludge. For example for a sludge concentration of $X_t = 10$ g.L^{-1} the energy consumption is 79% larger than the minimum value when the sludge is flocculent, whereas in the case of granular sludge the increase is only 22%. The large difference in energy consumption at high sludge concentration can be a decisive factor of the operational costs.

3 Conclusions

(1) The oxygenation capacity of aerators (OC) in activated sludge systems is very heavily dependent on the sludge concentration: Experiments showed that OC decreases by 4.4% in the case of flocculent sludge and 1.8% for granular sludge per gram of total suspended solids.
(2) The decrease of the oxygenation capacity at increasing sludge concentrations is mainly due to a decrease of the oxygen transfer coefficient of the aerator equipment.
(3) The smaller reduction of the transfer coefficient for granular sludge is a very important factor for reduction of energy costs for aeration.
(4) At very high sludge concentrations the oxygen uptake rate may become so high the aeration equipment itself may require an upgrade. This represents additional investment and/or operational costs.

References

Odegaard H, Gisvold B, Strickland J (2000) The influence of carrier size and shape in the moving bed biofilm process. Water Sci Technol 41(5):383–392
Van Haandel AC, Van Der Lubbe J (2012) Handbook Biological Waste Water Treatment - Second edition: Design and Optimisation of Activated Sludge System. IWA Publishing of Alliance House, London, p 816

Ultrafiltration of Saline Waters in Geothermal Fields Hot Water Discharge

Y.I. Tosun[✉]

Şırnak University, Engineering Faculty,
Mining Engineering Department, Şırnak, Turkey
yildirimismailtosun@gmail.com

Abstract. Southeastern Anatolia contains sulphide ore deposits, sulfur-containing complexes containing 2–4% Fe and ferric acidic solutions and geothermal Billoris hot streams near field. Siirt and Hakkari regions contained showed wide distribution of metallic ions such as copper, lead, zinc in Fe sulphide deposits, even hot streams such as alkali brines of potassium and sodium in Billoris region. Siirt copper concentrator is produced at least 100 thousand tons of processed and several million tons of ore tailings in the pond as slurry. Every year about 1 million tonnes of saline waters fill the lakes and streams in the Mesopotamian. Geographical Water sources and produced ore tailings in Siirt was 300 thousand tons of ferric slurries. For this reason, the common waste slurry muds and effluents of ponds in the region becomes critical for nature and fish fauna and agricultural crops. It may be advantageous to assess the extent of these slurry mud and precipitates occurring in a particle size, usually below 10 microns. In our country, the evaluation of pyrite Fe silicate wastes in the Siirt and Hakkari region of 15 m thickness spread over a wide area outside of this ore production has been discussed as chemical production in this study. This research has proved to be advantageous in producing easily filtered and ultra-filtered in bands and pressure vessels and pond filtration of brine waste slurries and compared with their evaluation in terms of basic geo-permeability and hydraulical conductivity properties.

Keywords: Ultrafiltration · Saline waters · Brine solution · Brine filtration · Hot brines · Waste streams

1 Introduction

Most of solid matter and waste contaminants or substances of municipal slurry or AMD origin and wastewater treatment plant (WWTP) effluents are important point discharges for the presence of toxic compounds and residuals of industrial waste waters in rivers, streams and surface waters. The elimination of heavy metal matter of AMD within the WWTP or their retention is of primary concern in neutralization and saline waters in conventional sludge plants (CSP) the neutralization aeration tank and the final clarifier form one process unit. The separation of treated sewage and sludge occurs in the clarifier via sedimentation. Therefore the ability to sediment is an important selection criterion. The salt concentration in the mixed liquor is limited by the capacity of the clarifier. In membrane reactors this parameter is ofminor influence, as separation is

achieved via membrane filtration. Thus, the plant can be operated at higher colloids concentrations resulting in smaller plant sizes.

The most important advantage of MBRs is the complete retention of suspended solids, thus reducing emissions to the dissolved fractions. Higher costs and higher requirements in operation and maintenance as well as power consumption compared to conventional systems are well-known disadvantages. The particle size for capture in ultrafiltration are given in Table 1.

Table 1. Brine solution metal and alkali contents in mud and effluent

Filtration	Pond/Belt area	Mud		Effluent	
	(m2)	(mg/l)	(permeability, mD)	(mg/l)	(permeability, mD)
Pond	250	297	0,069	29,7	0,069
Belt	3	25	0.027	2,5	0.027
Pressure belt	1	10	0.007	1,0	0.007
Left/right margin	–	20	0.8	23	0.9

Typically, X-Flow UF membrane modules are specifically developed for the effective removal of these compounds like bacteria, viruses and solids to protect the downstream (spiral wound) NF/RO. the X-Flow membrane portfolio includes innovative hollow fiber NF. This technology does not require the pretreatment that a spiral wound NF would need due to two of its unique features: backwash ability and high chlorine resistance (Fig. 1).
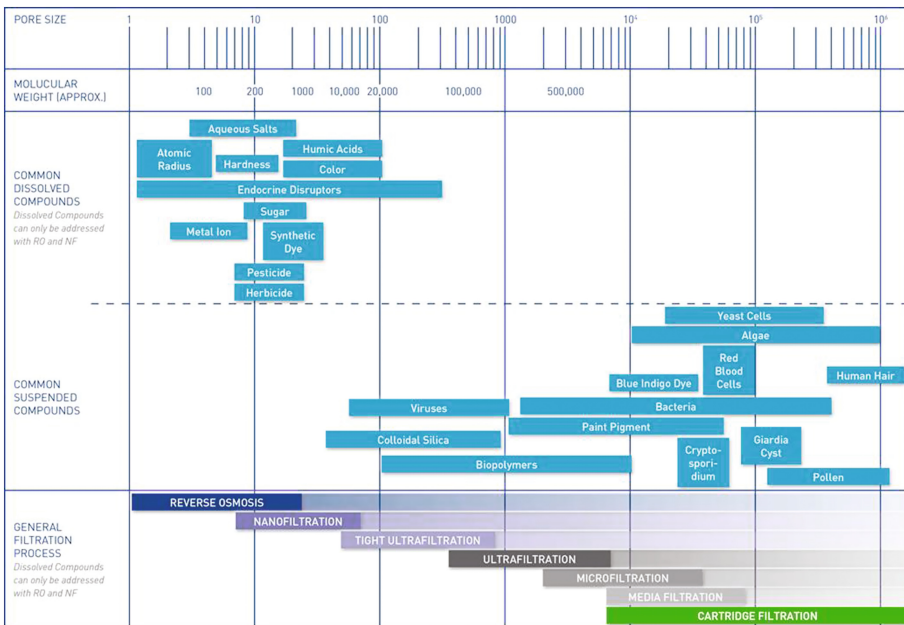
Fig. 1. The general filtration spectrum for ultra-filtration technique

Main advantages are described as follows;

- Removal of colloidal matter: 99.8% removal of colloidal silica
- High membrane packing density: the industry's smallest free volume in a membrane module
- 100% integrity testing on individual fibers
- Individual fiber repair
- Very good antifouling behavior
- Typical permeate quality:
  - SDI < 3
  - Turbidity < 0.1NTU

- Excellent chemical resistance with a wide pH range (1–12) and high chlorine stability (maximum free chlorine 250 mg/l)
- Typical high permeability: low energy consumption

CROSSFLOW
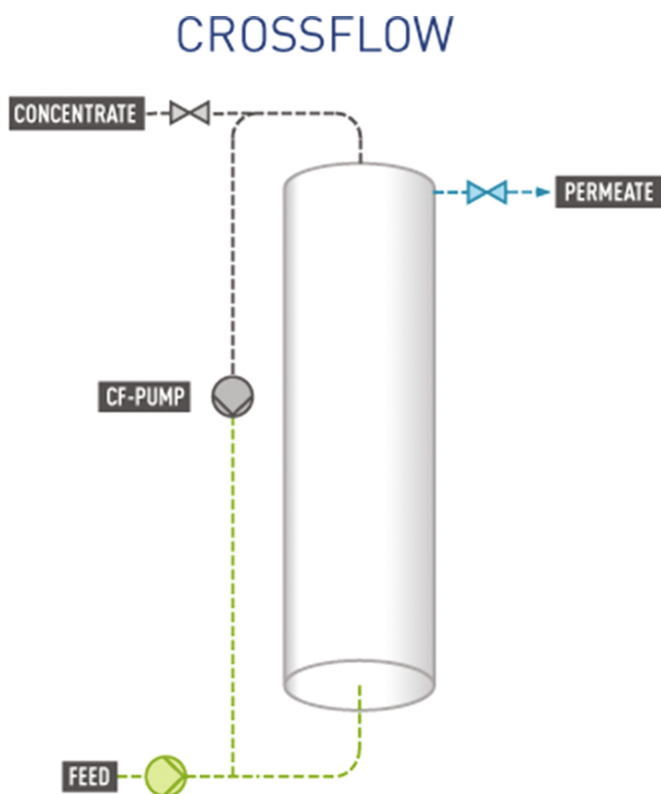
Fig. 2. Ultrafiltration hollow membrane experimentation model for saline hot waters

2   Methods

Ultrafiltration modules are usually racked in a skid (standard unit) of 6 modules. The permeate flow ranges between 1200–2400 L per hour per module, which amounts to 7.5–15 m^3 per hour per skid. The mode of operation is typically batch-wise, but continuous operation by alternation between two sets, or cascade systems, are also possible (Fig. 2).

3   Results and Discussion

The hydraulic resistivity of specific geo layers of clay and clay-bituminous geomembrane composites could be practiced over geo filtration and conductivity changed by the equation.

The hydraulic resistivity of specific geo layer could be explained by the equation

$$R = \int_0^t \left[n_j k_{ijkl} h_l + \int_0^i \left(\frac{\lambda k}{\rho} \right)^2 \delta_{ik} \right] h_k / dt \tag{1}$$

Density, porosity and time changed by time in the layer (Fig. 3).
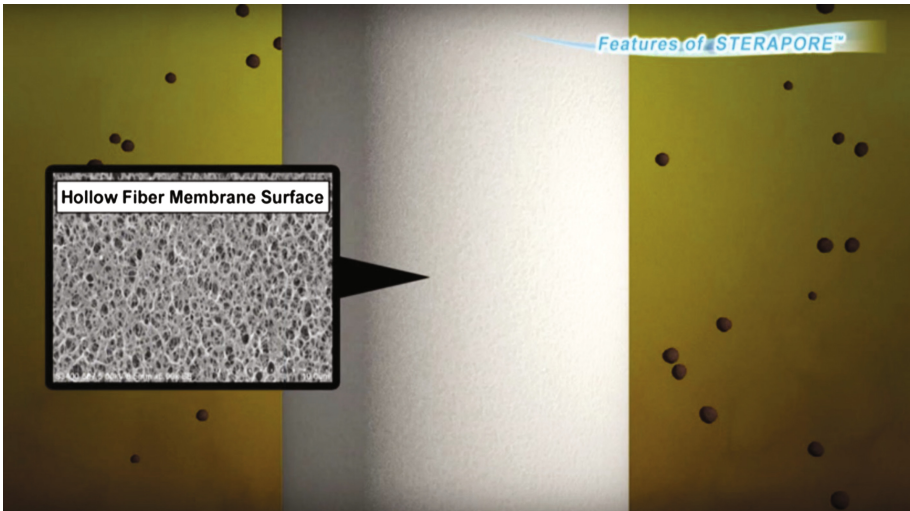
Fig. 3. Ultrafiltration hollow membrane structure and saline waste waters and hot waters

References

Andrews JF (1993) Modeling and simulation of wastewater treatment processes. Wat. Sci. Tech. 28(11/12):141–150

Ahel M, Giger W, Koch M (1994) Behaviour of alkylphenol polyethoxylate surfactants in the aquatic environment—I. Occurrence and transformation in sewage treatment. Water Res 28 (5):1131–1142

Brunner PH, Capri S, Marcomini A, Giger W (1988) Occurrence and behaviour of linear alkylbenenesulphonates, nonylphenol, nonylphenol mono- and nonylphenoldiethoxylats in sewage and sewage sludge treatment. Water Res 22(12):1465–1472

Clara M, Strenn B, Saracevic E, Kreuzinger N (2004) Adsorption of bisphenol-A, 17b-estradiole and 17a-ethinylestradiole to sewage sludge. Chemosphere 56(9):843–851

Clara M, Kreuzinger N, Strenn B, Gans O, Kroiss H (2005) The solids retention time—a suitable design parameter to evaluate the capacity of wastewater treatment plants to remove micropollutants. Water Res 39(1):97–106

Heberer T (2002a) Occurrence, fate and removal of pharmaceutical residues in the aquatic environment: a review of recent research data. Toxicol Lett 131(1–2):5–17

Heberer T (2002b) Tracking persistent pharmaceutical residues from municipal sewage to drinking water. J Hydrol 266(2–3):175–189

Joss A, Keller E, Alder AC, Göbel A, McArdell CS, Ternes T, Siegrist HR (2005) Removal of pharmaceuticals and fragrances in biological wastewater treatment. Water Res 39(14): 3139–3152

Martínez E, Gans O, Weber H, Scharf S (2004) Analysis of nonylphenol polyethoxylates and their metabolites in water samples by high-performance liquid chromatography with electrospray mass spectrometry detection. Water Sci Technol 50(5): 157–163

Nowak O, Franz A, Svardal K, Müller V, Kühn V (1999) Parameter estimation for activated sludge models with the help of mass balances. Water Sci Technol 39(4): 113–120

Rogers HR (1996) Sources, behaviour and fate of organic contaminants during sewage treatment and in sewage sludges. Sci Total Environ 185(1–3):3–26

Billing AE, Dold PL (1988a) Modelling techniques for biological reaction systems. 1. Mathematic description and model representation. Wat SA 14(4): 185–192

Modelling and Simulation of a Novel Pilot-Scale Microwave Assisted Catalytic Reactor for Continuous Flow Treatment of Wastewaters

K. Huddersman[✉] and A.V. Palitsin

Leicester School of Pharmacy, De Montfort University, Leicester, UK

Abstract. A design of a novel pilot-scale microwave (MW) assisted catalytic reactor for continuous flow treatment of wastewaters is proposed. In CFD and MW numerical simulations we have shown that the novel design of the MW assisted catalytic reactor can effectively address a problem of poor penetration of microwaves in bulk wastewater. The layered structure of the rotating catalyst discs provides effective distribution of microwaves along the surface of the catalyst and consequently ensures a strong absorption of MW radiation by the catalyst. The increase of MW reactor's dimensions up to full scale required by wastewater treatment industry is straightforward with the approach proposed in the report.

Keywords: Continuous flow treatment · Scale-Up problem · MW-Fenton · Microwave and CFD simulations

1 Introduction

In recent years, applications of microwave (MW) irradiation in wastewater treatment have been widely explored (Remya and Lin 2011). Although MW irradiation technique coupled with Fenton oxidation process have been shown to be very effective in the removal of contaminants from waste streams in laboratory scale systems, the application of them in pilot (Wang et al. 2014) and industrial scale systems remains in its infancy. In our opinion, there are two major reasons for this situation: (i) homogeneous catalytic processes require post-treatment removal of iron present as iron oxide sludge contaminated with non-degraded pollutant; and (ii) a lack of appropriate reactor designs suitable for scale-up, which is mainly limited by pour penetration depth of MW into the bulk wastewater or fluid streams. The modified polyacrylonitrile PAN catalysts developed at De Montfort University (Huddersman and Ischtchenko 2013) has eliminated the need for iron removal post treatment and broadened the pH range of application (Chi et al. 2013), whilst enabling continuous flow processes favoured by industry. The design for a novel MW assisted catalytic reactor addressing scale up constraints is presented in a patent application (Huddersman and Chi 2016).

2   Materials and Methods

2.1   Modified PAN Catalyst

The modified PAN catalyst (Huddersman and Ischtchenko 2013) contains immobilized Fe^{3+} and its reaction with hydrogen peroxide generates reactive hydroxyl radicals according to Fenton's reactions:

$$Fe^{2+} + H_2O_2 \rightarrow Fe^{3+} + HO^\bullet + HO^- \tag{1}$$

$$Fe^{3+} + H_2O_2 \rightarrow Fe^{2+} + HO_2^\bullet + H^+. \tag{2}$$
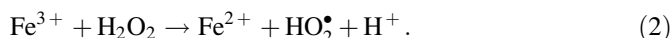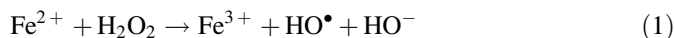
It has been demonstrated that Fenton advanced oxidation process (AOP) is able to decompose a wide variety of pollutants in waste waters such as herbicides, pharmaceutical and personal care products, etc. However, some reaction rates are very slow, thereby limiting the scope of applications Fenton's systems. The use of microwaves in Fenton AOP can stimulate the generation of hydroxyl radicals (Homem et al. 2013) and significantly increase the rate of pollutants removal.

2.2   Scheme of the Reactor

The scheme of the reactor is shown in Fig. 1. Metal wastewater tank (2) and rotating discs (3), covered with the catalyst, are both placed in MW cavity (1) which shields MW radiation from ambient space. MW radiation is produced by magnetrons (6) and
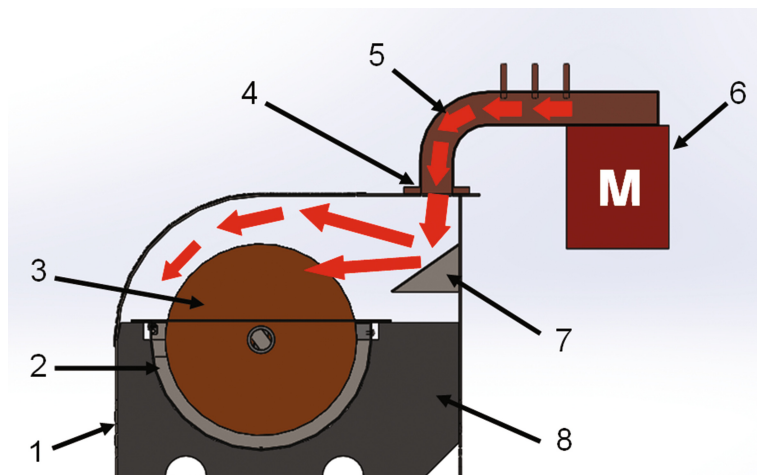
Fig. 1. Scheme of the proposed pilot-scale MW assisted catalytic reactor. 1 - microwave cavity, 2 - wastewater tank, 3 - catalyst rotating wheels, 4 - MW port, 5 - MW transmission line, 6 - MW source (magnetron), 7 - deflector of MW radiation, 8 - tank support

delivered to the cavity by waveguide transmission lines (5). Dimensions and positions of all reactor's elements have been optimized during numerical simulations in order to maximize MW absorption in the volume of the catalyst and consequently minimize a reflection of MW radiation from the cavity.

3   Results and Discussion

In the report we present the results for the pilot scale reactor with basic parameters shown in Table 1. 3D numerical simulation of the reactor have been performed in COMSOL Multiphysics® software, RF and CFD modules have been used. Simulations have shown that the proposed design is highly appropriate for scale-up because it efficiently overcomes the major restriction in MW systems - poor penetration depth of the microwaves into the water. The increase of wheel's diameter does not lead to huge reduction of MW absorption in the catalyst as long as the thickness of each disc remains less than a few centimeters and the distance between them exceeds 3–4 cm. These dimensions are valid if 2.45 GHz MW sources are used (for the other MW frequencies all dimensions can be changed approximately proportional to wavelength).

Table 1.   Basic parameters of pilot scale reactor

Parameter	Value
Length	0.8 m
Wheel's diameter	0.28 m
MW power	50–2000 W
Flow rate	0–1 l/min

Results of 3D simulations of electromagnetic fields are presented in Fig. 2; electric field distributions are shown in two planes: plane 1 goes through the catalyst disc and plane 2 is placed between the discs. Electric field is suppressed in the volume of catalyst discs (see plane 1) due to relatively high dielectric permittivity and loss factor of wetted catalyst. However, intensity of electric field between discs (see plane 2) is relatively high. It means that microwaves can easily propagate between the discs and consequently MW power can be delivered to the inner regions of each catalyst disc. Therefore the multilayer structure formed by separated catalyst rotating discs is highly favorable for designs of MW assisted reactors with large cross-sections. Rotation of the discs also performs physical averaging of absorbed MW power without an influence of moving parts on important electrodynamic characteristics of the cavity such as reflection coefficients and electric field pattern.

The power loss data obtained in microwave simulations have been used in CFD modelling of wastewater heating and flow streams distribution. The reactor's tank is divided into three sections by baffles which sufficiently restricts water flow between the sections. This allows us to conduct an optimisation of reactor's parameters by simulating each section independently, as it is shown in Figs. 3 and 4. For the reactor with parameters presented in Table 1 a computer with two Intel® Xeon® Quad Core 3.5
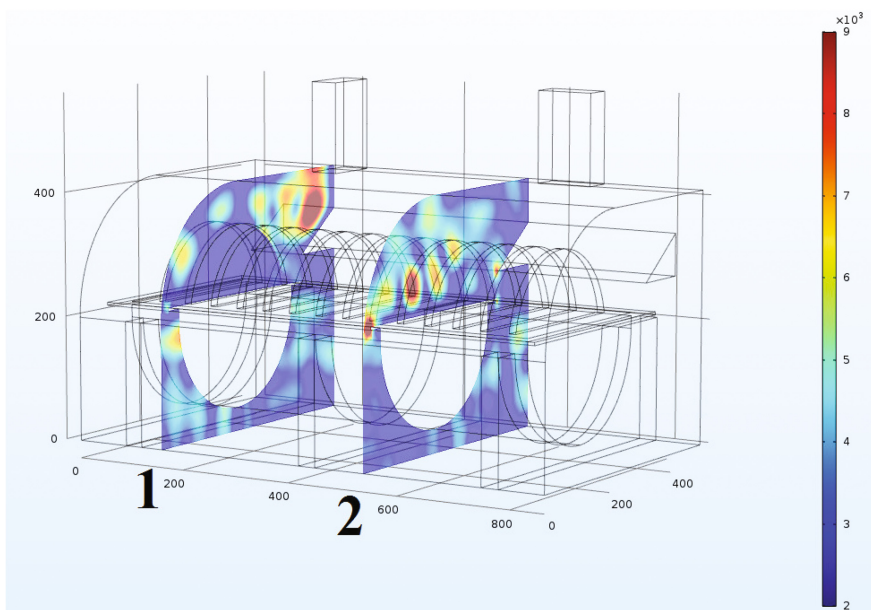
Fig. 2. 3D distribution of electric field in the reactor's cavity shown in two planes: plane 1 is placed in the catalyst disc; and plane 2 - between the discs
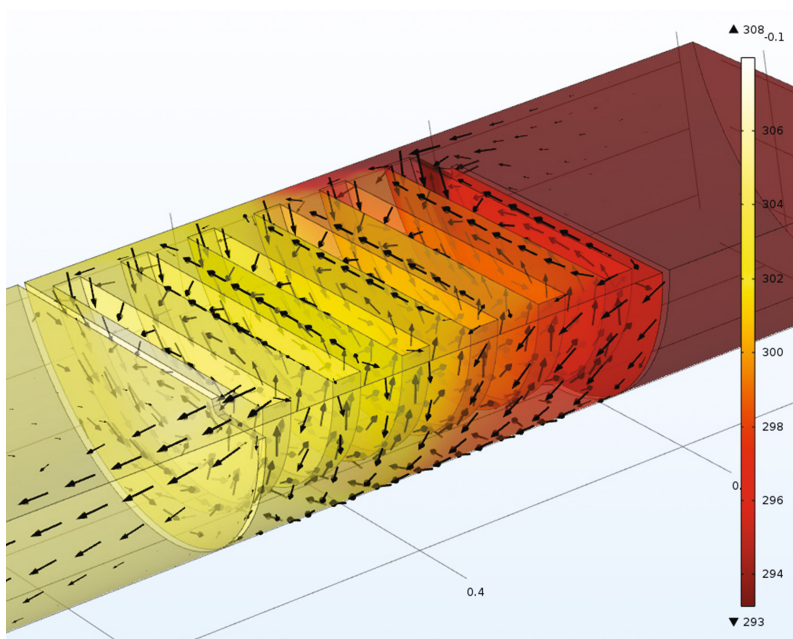
Fig. 3. Temperature distribution inside the middle section of the reactor - results of CFD simulation. Arrows are attributed to water flow
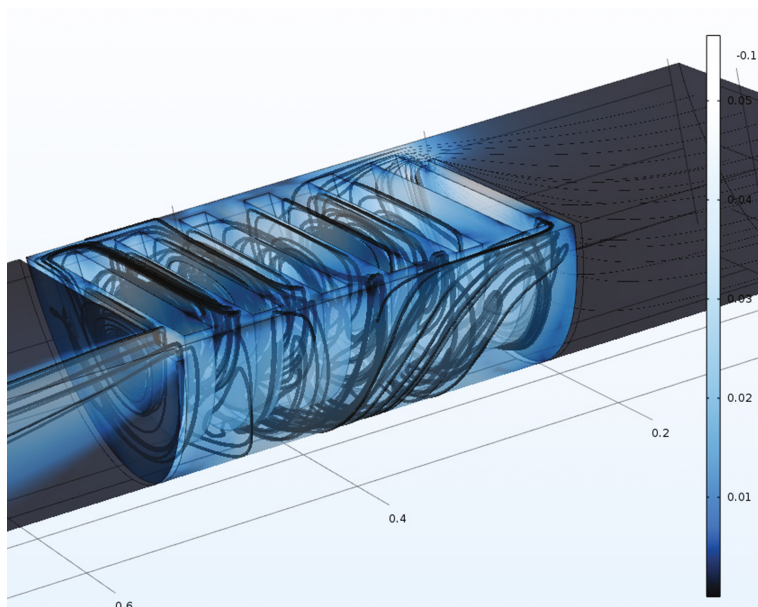
Fig. 4. Fluid streams inside the middle section of the reactor - results of 3D CFD simulation

GHz processors and 128 GB memory completes CFD simulation in 30 min; one section is simulated in less than 10 min. RF simulation of the whole reactor's cavity takes about 45 min for a single frequency.

4   Conclusion

In numerical simulation we have shown that the proposed novel design of the MW assisted catalytic reactor can effectively address a problem of poor penetration of microwaves in bulk wastewater. The layered structure of the rotating catalyst discs provides effective distribution of microwaves along the surface of the catalyst and consequently ensures a strong absorption of MW radiation by the catalyst. The increase of MW reactor's dimensions up to full scale required by wastewater treatment industry is straightforward with the approach proposed in the report. Correct energy and cost estimations depend on the achievable rate of pollutants removal which will be will available after the testing of the proposed pilot scale reactor.

References

Chi GT, Churchley J, Huddersman K (2013) Pilot-scale removal of trace steroid hormones and pharmaceuticals and personal care products from municipal wastewater using a heterogeneous fenton's catalytic process. Int J Chem Eng 2013:1–10 Article ID 760915

Homem V, Alves A, Santos L (2013) Microwave-assisted Fenton's oxidation of amoxicillin. Chem Eng J 220:35–44

Huddersman K, Ischtchenko V (2013) Fibrous catalyst, its preparation and use thereof. Patent 8410011

Huddersman K, Chi TG (2016) Rotating chemical contactor. Patent application No: PCT/GB22016/052849

Remya N, Lin JG (2011) Current status of microwave application in wastewater treatment — a review. Chem Eng J 166(3):797–813

Wang N, Zheng T, Jiang J, Lung W, Miao X, Wang P (2014) Pilot-scale treatment of p-Nitrophenol wastewater by microwave-enhanced Fenton oxidation process: effects of system parameters and kinetics study. Chem Eng J 239:351–359

Fouling Analysis for Different UF Membranes in Reactive Dyeing Wastewater Treatment

R.D. Zaf[1(✉)], B. Kocer Oruc[1], M. Erkanli[1], L. Yilmaz[2],
U. Yetis[1], and Z. Culfaz-Emecen[2]

[1] Department of Environmental Engineering,
Middle East Technical University, Ankara, Turkey
[2] Department of Chemical Engineering,
Middle East Technical University, Ankara, Turkey

Abstract. In this study, different ultrafiltration (UF) membranes are analyzed by means of their fouling characteristics. The aim of the work is pointing the most suitable membrane type for reactive-dying wastewater. Five different UF membranes (5 kDa PES (polyethersulfone), 5 kDa and 1 kDa RC (regenerated cellulose), 2 kDa TFC (thin film composite) and 3,5 kDa polypiperazine-amide) were compared based on color (as absorbance at wavelengths of 436, 525 and 620 nm) and TOC treatment efficiency, permeate flux and fouling reversibility. As a concurrent execution, in order to correlate membrane surface and fouling characteristics, the contact angle and roughness of these five different UF membranes are investigated. The overall results achieved indicated that composite membranes (TFC and polypiperazine-amide) are the best membranes among the tested ones, providing the highest color and TOC removals along with an acceptable fouling reversibility.

Keywords: Textile wastewater · Ultrafiltration · Membrane fouling

1 Introduction

Textile industry produces wastewater that is often very rich in salt and color, containing residues of dyes and other chemicals. Treating this wastewater to exceptionally high quality standards, typically for reuse purposes necessitates advanced treatment methods among which membrane technology is the leading one. However, membrane fouling which can be caused by dissolved and particulate solids appears as the major limitation with the use of membranes in wastewater reclamation that leads to reduced efficiency and a shorter membrane life. Other major design and operational challenge is the complexity of the concentrate disposal issue from high-pressure membranes.

In this study, membrane fouling problem in the reclamation of reactive dyeing wastewater from textile industry is addressed. UF is generally used as a pre-treatment method for nanofiltration (NF) or reverse osmosis (RO) applications [1, 2]. These applications are used also for the removal of salt content. However, in this study, a direct treatment by UF membrane is applied in order to recover salt for reactive-dyeing process. As UF is intended to be used for the reclamation of the wastewater as the water and the mineral salts, while leaving the spent dyes in the reject stream; a set of UF

membranes available in the market were considered and their fouling behaviours were investigated with the aim of proposing the most suitable membrane type for the UF of reactive-dyeing wastewater.

2 Materials and Methods

Batch UF tests were carried out using Amicon stirred cells (dead-end filtration). Textile wastewater samples (Table 1) taken from a textile dyeing plant located in Denizli, Turkey were used and five different UF membranes (5 kDa PES, 5 kDa and 1 kDa RC, 2 kDa TFC and 3.5 kDa polypiperazine-amide) were compared based on color (as absorbance at wavelengths of 436, 525 and 620 nm) and TOC treatment efficiency, permeate flux and fouling reversibility.

Table 1. Characteristics of dyeing bath wastewater

Wastewater	TOC mg/L	Absorbance (Color)			Turbidity NTU	Conductivity mS/cm
		436 nm	525 nm	620 nm		
Dyeing Bath	500	3,81	3,26	0,42	277,3	83

In the previous steps of filtration; compaction, chemical cleaning of membranes and permeance analysis are conducted, respectively. Following the filtration process, flux measurements both before and after cleaning are operated. The details of mentioned operations can be find in Table 2.

Table 2. Operational conditions of conducted filtration experiments

Stages in order	Pressure (bar)	Feed	Duration (min)	Stirring velocity (rpm)
Compaction	3	UPW[a]	Until flux steady-state is reached	–
Chemical cleaning	–	HNO$_3$ soln. (pH 3,0 ± 0,1)	15	–
		UPW	15	–
		NaOH (pH 10,0 ± 0,1)	15	–
		UPW	15	–
Permeance	1–2	UPW	–	–
Filtration	2	Wastewater	Until VRF[b] is 2,5	150 rpm
Flux after filtration	2	UPW	–	–
Physical cleaning	–	UPW	15	250 rpm
	2	UPW	–	–

(*continued*)

Table 2. (*continued*)

Stages in order	Pressure (bar)	Feed	Duration (min)	Stirring velocity (rpm)
Flux after physical cleaning				
Chemical cleaning	–	HNO3 soln. (pH 3,0 ± 0,1)	15	–
		UPW	15	–
		NaOH (pH 10,0 ± 0,1)	15	–
		UPW	15	–
Flux after chemical cleaning	2	UPW	–	–

[a]UPW: Ultra pure water, [b]VRF: Volume reduction factor

3   Results and Discussion

Flux analysis

In Fig. 1, the flux changes of five different membranes during filtration are represented. Flux decline observed for both 5 kDa PES and 3.5 kDa polypiperazine-amide membranes is apparently spectacular. However, as it can be seen from Table 3, 3.5 kDa polypiperazine-amide membrane has 100% flux recovery after cleaning processes. Despite the fact that the other membranes could be cleaned relatively well by physical and chemical cleaning, 5 kDa PES generally showed incomplete fouling reversibility
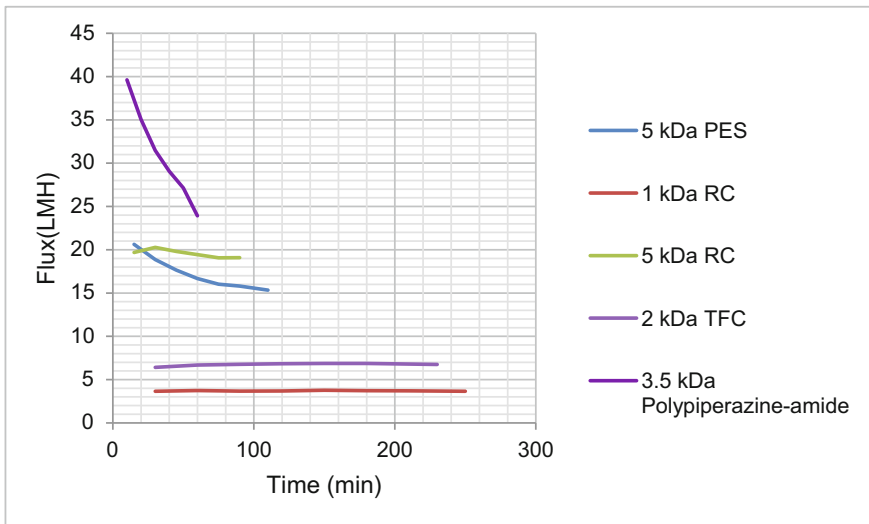
Fig. 1. Filtration flux vs time graph for different membranes

after further chemical cleaning (Table 3). Total resistance coming from concentration polarization (R_{cp}) and fouling (R_f) has increased during filtration period as a result of continuous increase on concentration polarization. It is not possible to show R_{cp} and R_f separately against the time because they are interconnected during filtration. However as concentration polarization is known as a reversible phenomenon, it can be said that while the R_{cp} is the main reason for flux decline during filtration, the R_f value, which is the resistance calculated by clean water permeance test (right after filtration), can be defined as fouling that causes the irreversible flux decline for 5 kDa PES membrane. This means 5 kDa PES membrane has much more fully retained material than other membranes even after further cleaning processes.

Table 3. Comparison of different membranes by the means of their fouling resistance and flux recovery

Membrane	Resistance due to fouling × 10–13 (m−1)	Clean water permeance (LMH/bar)	Flux recovery after physical cleaning (%)	Flux recovery after chemical cleaning (%)
5 kDa PES	0.8 ± 0.2	20.00 ± 0.0	82–92	84–90
5 kDa RC	0.2 ± 0.0	13.15 ± 0.15	96	100
3.5 kDa Polypiperazine-amide	0.0 ± 0.0	16.85 ± 0.45	100	100
2 kDa TFC	0.9 ± 0.9	4.35 ± 1.05	92–100	97–100
1 kDa RC	2.0 ± 2.0	3.25 ± 0.25	90–100	92–100
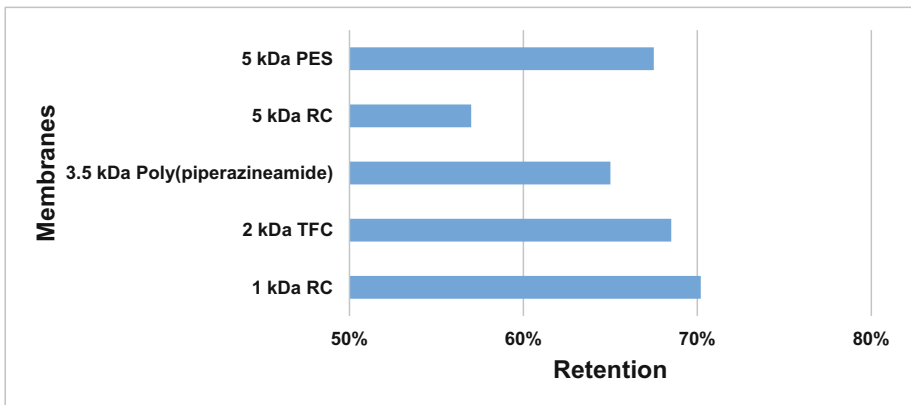
Fig. 2. TOC retentions of different membranes

Treatment efficiencies

Apart from flux analysis, retentions in color and total organic carbon (TOC) are investigated. Although there was not a remarkable difference among five membranes in terms of TOC retention (Fig. 2), TFC and polypiperazine-amide membranes showed better performances in color removal than the other membranes (Fig. 3).
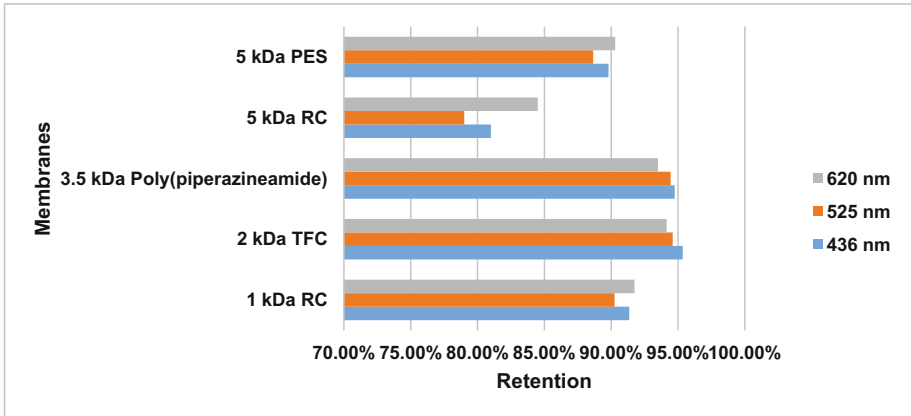
Fig. 3. Color retentions of different membranes

When surface characteristics (i.e. contact angle and roughness of the five membranes) were investigated, it was seen that TFC membrane which can be designated as having the lowest tendency for fouling, has also the lowest contact angle (Fig. 4). Contact angle of RC membranes could not been measured because of their very high hydrophilicity.
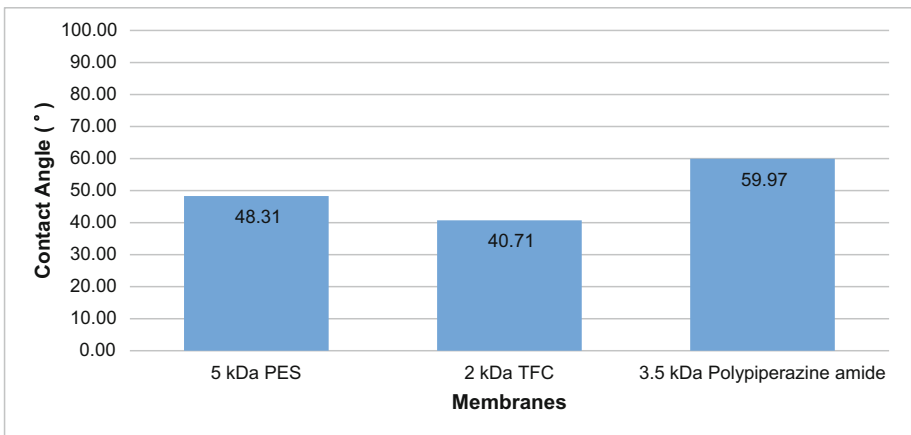
Fig. 4. Contact angle values of PES, TFC and Polypiperazine-amide membranes

Additionally, PES and RC membranes were found to have higher roughness than the membranes with composite materials (TFC and polypiperazine-amide). This finding was thought to be a cause of less fouling resistance observed with the composite membranes.

4   Conclusion

While membrane technology is an efficient alternative for textile industry wastewater treatment, membrane fouling is the major limitation in the economic and practical point of view. By comparing their flux recovery capacities after physical and chemical cleaning, the cleanability of PES membrane was observed as the lowest among these four different materials (PES, TFC, RC and polypiperazine-amide). TFC and polypiperazine-amide membranes showed better performances also in color removal than the other membranes Additionally, PES and RC membranes were found to have higher roughness than the membranes with composite materials (TFC and polypiperazine-amide). The overall results achieved indicated that composite membranes (TFC and polypiperazine-amide) are the best membranes among the tested ones, providing the highest color and TOC removals along with an acceptable fouling reversibility.

References

1. Fersi C, Dhahbi M (2008) Treatment of textile plant effluent by ultrafiltration and/or nanofiltration for water reuse. Desalination 222:263–271
2. Ciardelli G, Corsi L, Marcucci M (2000) Membrane separation for wastewater reuse in the textile industry. Res Conserv Recycl 31:189–197

Preliminary Study of Electrodialysis with Model Salt Solutions and Industrial Wastewater

K.V. Shestakov[1,2(✉)], R. Firpo[2], A. Bottino[2], and A. Comite[2]

[1] Department of Applied Geometry and Computer Graphics,
Tambov State Technical University, Tambov, Russia
`kostyanshestakov@mail.ru`
[2] Department of Chemistry and Industrial Chemistry,
University of Genoa, Genoa, Italy

Abstract. Electrodialysis (ED) is applied in different fields of industry (Strathmann 2010). It has found wide application in water and wastewater treatment, stabilization of wine, whey demineralization and also for recovery of valuable components associated with the depuration of wastewater. New treatment processes can be designed by integration with other membrane processes as well as nanofiltration an reverse osmosis. Aim of the work is the study of electrodialysis process with some model salt solutions and the attempt to apply it to some industrial wastewater. Electrodialysis tests were mainly performed using model solutions containing nitrates, ammonia or metals. Few tests have been carried out on some real effluents as coke oven wastewater or olive mill wastewater, which were treated in the electrodialysis plant after reverse osmosis concentration. In the present paper some results about the ED treatment of solution containing high copper concentration will be shown.

Keywords: Electrodialysis · Wastewater · Ion-exchange membranes

1 Introduction

Electrodialysis (ED) is an electrochemical separation process in which ions are transferred through ion-exchange membranes by means of a direct current (Xu and Huang 2008; Valero et al. 2011).

Usually the ED plant includes ED stack, power supply and several independent lines: electrodes rinsing, concentrate and dilute streams. Each line is constituted by: a pump, a tank, some valves and connections able to guide each stream toward the membrane stack. In the ED stack membranes are separated by spacers in the active area filled with the electrolyte. The spacer net prevents the membranes from touching each other. The stacked spacers have holes, which are arranged in a way to build two different channel systems. By this way, the concentrate streams and diluate stream circuit is built (Valero et al. 2011).

During a typical ED process an initial salt solution is fed to each of the sections, which are separated by ion selective membranes. In the extreme sections of the ED cell there are the electrodes that are needed to create the electric field in the electrolyte.

When applying the electric field, the ions of the electrolyte and the products of water dissociation of (H^+ and OH^-) come in orderly movement. Cations move toward the cathode and anions, respectively, to the anode. Moving of ions through the ion exchange membranes leads to two concentrated solutions and a desalted solution. In some configurations, bipolar membranes are used in addition to the cation and anion exchange membranes. Desalted and concentrated solutions are collected and separately discharged from the apparatus (Xu and Huang 2008; Valero et al. 2011).

Electrodialysis is applied in different fields of industry. It has found wide application in water and wastewater treatment, stabilization of wine, whey demineralization. The necessary degree of demineralization is achieved by a multistage water desalination. Due to the fact that the electrodialysis process does not require additional reagents, purified water also does not need additional purification. Also, one of applying fields is the recovery of valuable components associated with the depuration of wastewater (Oztekin and Altin 2016).

Using electrodialysis for the regeneration of solutions gives the possibility to obtain acid and alkali, which will reduce the consumption of reagents for the plants as a whole.

Usually the feed of ED can work without particular problems even with a Silt Density Index (SDI) of about 10 and therefore efficient pre-treatments of the feed to remove colloidal particles is not a strict requirement differently from the reverse osmosis usually needs a SDI < 3.

On the other hand the integration of ED with other membrane processes as well as nanofiltration and reverse osmosis can result in very efficient depuration processes with no or very little waste streams and the recovery of valuable products.

We have investigated the application of ED with some model solutions and with some industrial wastewater previously treated by nanofiltration or reverse osmosis. Hereafter the performance of ED in the treatment of high ionic strength copper solution will be described.

2 Materials and Methods

All experiments were carried out in a ED pilot plant (Fig. 1), which includes an ED stack cell and four independent lines. Each line consists of a jacketed tank with capacity of about 10 L, a pump and valves to set the working pressure at 0.5 bar, cartridge filter with porosity 5 μm, manometer (0–5 bar), flow meter (15–150 L/h), flow rate gauge valve and 2 taps for rinsing and discharge operations.

The ED stack cell (Fig. 2) has an active area of 10 cm × 10 cm. It was assembled with anionic exchange membranes type PC Acid 60 and cationic exchange membranes type CMX supplied by PCCell GmbH (Germany). A TDK – Lambda power supply (mod Genesys) able to work in constant voltage mode (0–80 V) or constant current mode (0–20 A) has been used. Electrodialysis tests were usually performed using a current density of about 1000–1500 A/m^2.

The electrodialysis tests aimed at the recovery of copper were mainly performed using model solutions containing nitrates ethylenediaminetetraacetic acid (EDTA), ammonia and additional metals. Few tests have been carried out on some real effluents

Fig. 1. ED pilot plant
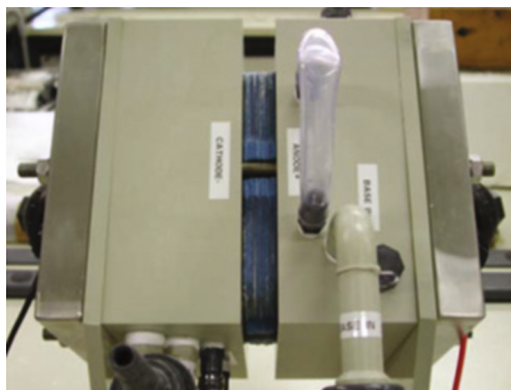
Fig. 2. ED cell

as an exhausted palladium rich plating solution. Moreover some runs were carried out on a coke oven wastewater and an olive mill wastewater previously concentrated by reverse osmosis.

According to scheme of ED plant in one independent line took place salt decomposition (diluate section), in two another was concentration of salt components (concentrate 1 and 2). Last fourth section was used for rinsing of electrodes.

A sample for each solution (conc. 1, diluate, conc. 2) was taken every 15, 30 or 60 min, depending on the applied voltage value, which affects the velocity of salt decomposition. For each sample, pH and conductivity values were measured. Also each 60 min samples were taken for ion chromatography and atomic absorption analysis.

3   Results and Discussion

Some preliminary tests with model solutions were performed to find the best power supply parameters. Further aim of these tests was to understand the velocity of salt decomposition, in order to set a proper sampling frequency, appropriate salt and metal ions concentrations and solutions volume.

It was established that optimal voltage for investigated model solutions is 21 V. It allows to get stable and not sharp increasing of direct current value during electrodialysis process, that confirms active salt decomposition and ion exchange. The values of direct current are presented in Table 1.

The current value difference between the two model solutions is related to the effect of copper which is complexed with EDTA.

Table 1. Direct current values during electrodialysis tests on a $NaNO_3$ (170 g/L) solution and on a $NaNO_3$ (170 g/L) containing $CuSO_4$ (157 mg/L) and EDTA (234 mg/L)

Time (min)	$NaNO_3$		$NaNO_3$ + EDTA + $CuSO_4$	
	(V)	(A)	(V)	(A)
0	21	10,79	21	7,93
15	21	11,76	21	9,81
30	21	12,75	21	12,19
45	21	13,59	21	13,23
60	21	14,35	21	14,25
75	21	15,05	21	15,19
90	21	15,57	21	15,69
105	21	16,05	21	16,33
120	21	16,59	21	16,83
135	21	16,47	21	17,15
150	21	15,8	21	17,78
165	21	10,79	21	17,93
180	21	11,76	21	17,22

In Figs. 3 and 4 it is reported the conductivity behaviour in both the concentrate and diluate sections during desalination process for 2 model solutions, containing only $NaNO_3$ or $NaNO_3$, EDTA, $CuSO_4$ respectively.

During the ED test it was not observed copper precipitation in any of the ED compartments due to the presence of EDTA. In fact on some test carried out y varying the pH on similar solution in a beaker without EDTA addition the precipitation can be
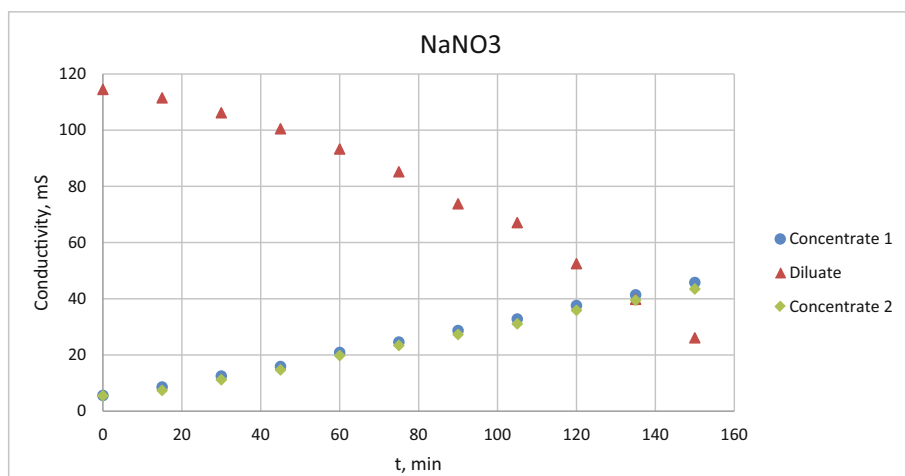
Fig. 3. Changing of samples conductivity during time for a model solution, containing $NaNO_3$ (170 g/L)
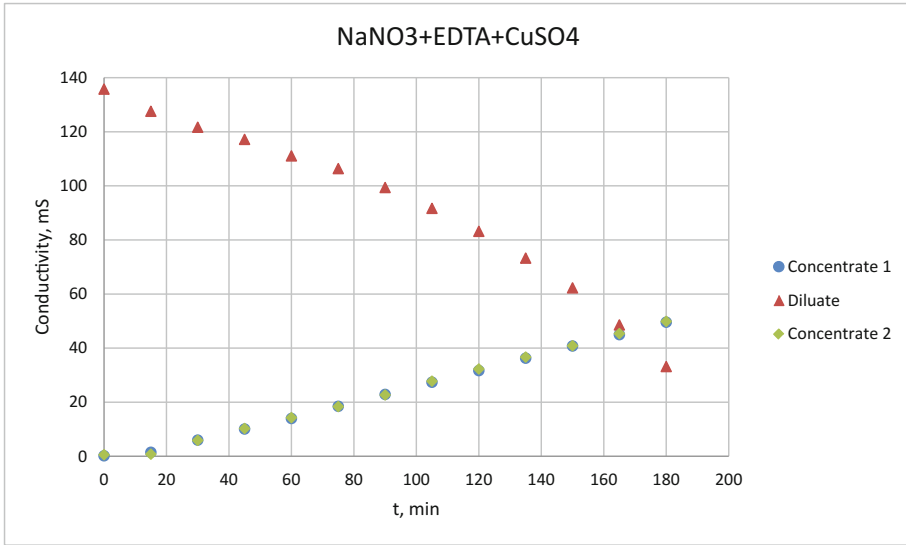
Fig. 4. Changing of samples conductivity during time for a model solution, containing $NaNO_3$ (170 g/L), EDTA (0,234 g/L), $CuSO_4$ (0,157 g/L)

Table 2. Nitrate concentration measured on the different ED compartments before and after the ED test on the model solution containing $NaNO_3$, EDTA and $CuSO_4$

Section	In the beginning of the test (g/L)	In the end of the test (g/L)
Concentrate 1	0.833	70.45
Dilute	176.4	39.71
Concentrate 2	1.402	69.07

observed at about pH 5,5. The slower decrease in the diluate conductivity can be again related to the size of the cupper-EDTA complex.

Table 2 shows the nitrate concentration measured on the different ED compartments before and after the ED test on the model solution containing $NaNO_3$, EDTA and $CuSO_4$. These data show right selection of power supply parameters.

Tests carried out with model solutions enlightened also some limits of the plant. The cooling system (coolant: tap water at about 13 °C) did not prove to be efficient enough to control temperature. All tests were characterized by a remarkable solution temperature rise (depending on current density) and by a significant water flux (electro-osmosis phenomenon). In spite of this fact, tests allowed to produce a satisfactory reduction of the salinity of the model wastewater.

The preliminary tests on the real industrial wastewater showed that the decrease of the salinity of the treated water was remarkable but that the high organic load can foul dramatically the membranes. In these non-optimal operating conditions, energy consumption need to be evaluated carefully, but the use of renewable energy systems can

improve the economic sustainability of the process. The integration of ED with RO is under evaluation.

4   Conclusions

The best power supply parameters was determined for ED processes with model solutions and industrial wastewater. Interesting results were obtained on the ED for the recovery of copper on high ionic strength model solutions where EDTA was used as chelating agent.

References

Oztekin E, Altin S (2016) Wastewater treatment by electrodialysis system and fouling problems. Online J Sci Technol 6(1):91–99

Strathmann H (2010) Electrodialysis, a mature technology with a multitude of new applications. Desalination 264:268–288

Valero F, Barceló A, Arbós R (2011) Electrodialysis technology: theory and applications. In: Schorr M (ed.) Desalination, Trends and Technologies, pp. 3–20

Xu T, Huang C (2008) Electrodialysis-based separation technologies: a critical review. AIChE J 54:3147–3159

Comparison of Two Mathematical Models for Greenhouse Gas Emission from Membrane Bioreactors

G. Mannina[✉] and A. Cosenza

Dipartimento di Ingegneria Civile, Ambientale Aerospaziale dei Materiali,
Università di Palermo, Viale delle Scienze, Ed. 8, 90100 Palermo, Italy
{giorgio.mannina, alida.cosenza}@unipa.it

Abstract. In this study two mathematical models (Model I and Model II), able to predict the nitrous oxide (N_2O) and carbon dioxide (CO_2) emission from an University Cape Town (UCT) – membrane bioreactor (MBR) plant, have been compared. Model I considers the N_2O production only during the denitrification. Model II takes into account the two ammonia-oxidizing bacteria (AOB) formation pathways for N_2O. Both models were calibrated adopting real data. Results highlight that Model II had a better capability of reproducing the measured data especially in terms of N_2O model outputs. Indeed, the average efficiency related to the N_2O model outputs was equal to 0.3 and 0.38 for Model I and Model II respectively.

Keywords: WWTP · N_2O modelling · Nutrient removal · Greenhouse gases

1 Introduction

During the last years, the attention on wastewater treatment plants (WWTPs) as sources of greenhouse gases (GHGs) (e.g., carbon dioxide, CO_2, nitrous oxide, N_2O, and methane, CH_4) has considerably increased. Among the GHGs produced by WWTPs, N_2O is the most environmentally hazardous due to its strong global warming potential (GWP) (298 higher that CO_2) and its capacity to deplete the stratospheric ozone layer (IPCC 2007).

An accurate quantification and mitigation of N_2O emissions is imperative for an environmental protection. With this regard, the adoption of mathematical models allows to select designing or operating choices aimed at reducing the total amount of GHG emissions from WWTPs.

Several efforts have been performed in literature for establishing the best tool to predict/quantify GHG (Mannina et al. 2016; Spérandio et al. 2016; Pocquet et al. 2016). However, the N_2O estimation is still the major crucial aspect in GHG modelling since its formation mechanisms are still under review (Ni et al. 2015). Current knowledge on N_2O emissions suggests that it can be produced both during nitrification and denitrification processes (Kampschreur et al. 2011). Furthermore, autotrophic ammonia-oxidizing bacteria (AOB) can contributes to N_2O production by means of two pathways: i. the nitrifier denitrification (ND) pathway, where N_2O represents the terminal product

of nitrite reduction (Law et al. 2012); ii. the incomplete hydroxylamine (NH_2OH) oxidation (NN) pathway, where N_2O is an intermediate product during the NH_2OH oxidation (Pocquet et al. 2016). With this regard, literature suggests that mathematical models that include both AOB contribution pathways reproduce well the measured data (Peng et al. 2015). However, this knowledge has been acquired on conventional activated sludge systems (CAS) often using short-term data (Ni et al. 2013b). Very few studies have been performed for integrated membrane bioreactor (MBR) models where physical separation processes and biological processes affecting the membrane fouling (e.g., soluble microbial products – SMP – formation/degradation) have to be included jointly. Specifically, Mannina and Cosenza (2015) have proposed an integrated ASM2d–SMP–GHG model (Model I) able to predict the N_2O and CO_2 emission from an University Cape Town (UCT) – MBR plant. Mannina and Cosenza (2015) consider the N_2O production only during the denitrification according to the approach of Hiatt and Grady (2008). A new integrated MBR model including the two AOB formation pathways for N_2O has been recently proposed by Mannina and Cosenza (2017) (namely, ASM2d-SMP-GHG-2P-AOB) (Model II). The purpose of this study was to compare the two models (i.e., Model I and Model II) for GHG emissions from MBR.

2 Materials and Methods

2.1 Mathematical Models Description

Both Model I and Model II are divided in two sub-models (physical and biological). The physical sub-model describes the key processes occurring during membrane physical separation, including membrane fouling (involving 6 model factors and 2 state variables). Regarding, the biological sub-models they are based both on the ASM2d and they include the SMP formation/degradation processes (Jiang et al. 2008; Henze et al. 2000). Furthermore, both models take into account CO_2 as state variable according to the continuity-based model interface as proposed by Vanrolleghem et al. (2005). Despite the aforementioned similarities, the biological sub-models are deeply different. Indeed, Model I employs the Hiatt and Grady (2008) approach for N_2O. Consequently, Model I considers the two-step nitrification process (involving AOB and nitrite oxidizing bacteria, NOB) and the four step denitrification process. Furthermore, the N_2O is modelled as an intermediate product during the heterotrophic denitrification (see further details in Mannina and Cosenza 2015). Conversely, Model II considers the N_2O formation due both to heterotrophic and autotrophic biomass. In particular, regarding the autotrophic, Model II describes N_2O formation during nitrification combining the two major AOB formation pathways, according to the approach presented by Pocquet et al. (2016). In Model II, N_2O formation during the heterotrophic denitrification is described as in Model I.

Finally, regarding the stripping of N_2O and CO_2 gas both Model I and II employ an algorithm based on the diffusion coefficients (Mannina and Cosenza 2015).

Model I involves 24 state variables and 109 model factors (stoichiometric, kinetic, fractionation and physical factors). While, Model II involves 25 state variables and 116 model factors.

2.2 Models Application and Calibration

Each model has been applied to a pilot plant with a UCT- MBR scheme treating $20\,L\,h^{-1}$ of real wastewater. For the models calibration an innovative calibration protocol was employed (Mannina et al. 2011). This innovative calibration protocol is based on a step wise calibration with respect to a group of model outputs. With this regard, model calibration has been carried out considering a long term monitoring data set. The selection of the model factors to be calibrated has been performed by applying the Standardized Regression Coefficient (SRC) method (Saltelli et al. 2004).

2.3 Criteria for Comparison

Both models were compared by calculating model efficiencies on the basis of measured and simulated data. Specifically, it has been calculated the efficiency of each model output (E_i) (exponential equation, E_{exp}) and the total model efficiency (E_{MOD}) (Mannina et al. 2011). Four coefficients have been adopted to quantify the goodness of model response: E_{exp}, the root mean squared error (RMSE), the Nash and Sutcliffe efficiency (N&S) (Nash and Sutcliffe 1970) and the determination coefficient, R^2.

3 Results and Discussion

For sake of conciseness, only the results related to the N_2O model outputs (both dissolved and off-gas concentration within each reactor of the UCT-MBR pilot plant) will be here presented and discussed.

Figure 1a shows the results of the average, maximum and minimum efficiency (calculated adopting the exponential expression) obtained during the calibration process for the dissolved and off-gas N_2O model outputs and for each model.
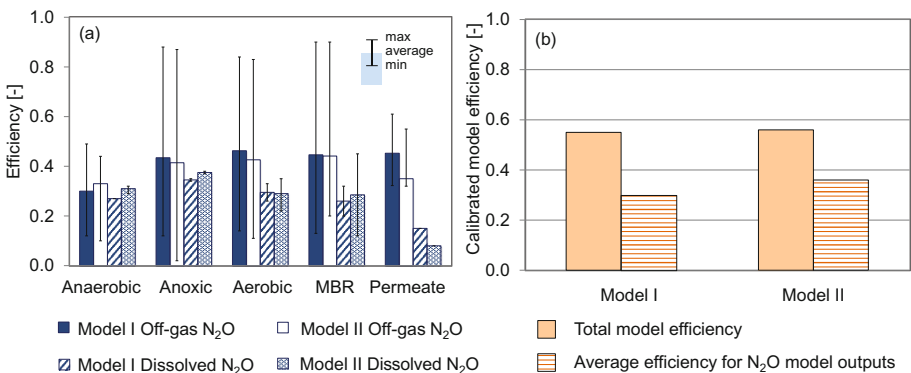
Fig. 1. Average, maximum and minimum efficiency (exponential expression) for dissolved and off-gas N_2O model outputs for each reactor and model (a); total model efficiency and average efficiency (exponential expression) for dissolved and off-gas N_2O model outputs related to the calibrated model (b)
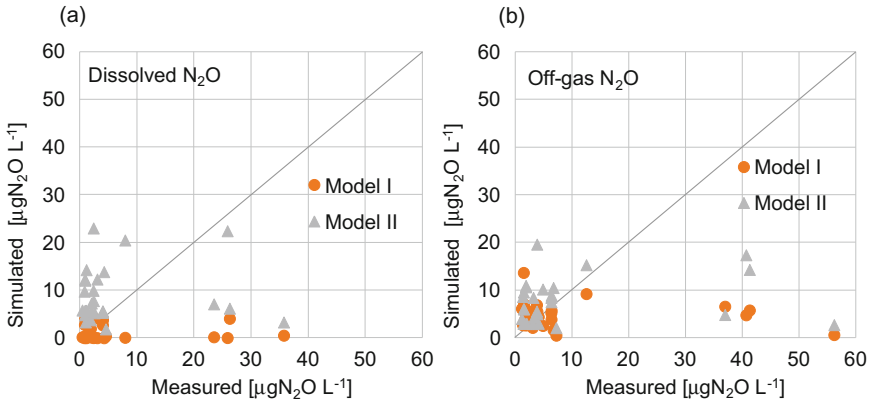
Fig. 2. Measured versus simulated data for calibrated Model I and Model II related to the dissolved (a) and Off-gas N_2O (b)

Figure 1b shows the total model efficiency (E_{MOD}) and the average efficiency for both models in terms of N_2O. A general improvement of the efficiency of the dissolved N_2O model outputs for non-aerated reactors (anaerobic and anoxic) and MBR has been obtained for the Model II (Fig. 1a). While, similar results were obtained in terms of Off-gas N_2O model outputs (Fig. 1a). Data of Fig. 1b confirm the general improvement of the calibrated Model II (respect to Model I) in terms of N_2O model outputs. Indeed, the average model efficiency of the N_2O model outputs increased from 0.3 (Model I) to 0.38 (Model II) (Fig. 1b).

For sake of completeness in Fig. 2 the measured versus simulated data for both dissolved (Fig. 2a) and off-gas N_2O (Fig. 2b) in each reactor of the pilot plant are shown. A slight overestimation of simulated data occurred for the two models, expecting some cases, both for dissolved and off-gas N_2O. This result is likely debited to the discrete sampling. Continuous sampling would likely improve the results.

Table 1. Values of the coefficients adopted for comparison between Model I and Model II

Model	Coefficient	Dissolved N_2O					Off-gas N_2O				E_{MOD}
		Anaer	Anoxic	Aerobic	MBR	Perm	Anaer	Anoxic	Aerobic	MBR	
I	E_{exp}	0.37	0.38	0.36	0.3	0.29	0.27	0.39	0.39	0.35	0.55
	N&S	−0.3	−0.06	−0.34	0.63	−1.17	−0.3	−0.09	−0.11	−0.15	
	R^2	0.37	0.02	0.02	0.12	0.39	0.08	0.02	0.02	0.012	
	RSME	0.013	0.009	0.009	0.01	0.013	0.021	0.014	0.013	0.014	
II	E_{exp}	0.32	0.43	0.32	0.4	0.27	0.29	0.4	0.39	0.45	0.56
	N&S	−0.13	0.04	−0.59	−1.16	−1.54	−0.16	0.26	−0.06	0.2	
	R^2	0.08	0.57	0.1	0.34	0.15	0.04	0.71	0.02	0.25	
	RSME	0.013	0.008	0.01	0.012	0.014	0.02	0.011	0.012	0.012	

Table 1 summarizes the results of the four coefficients adopted for evaluating the two models. Data of Table 1 confirm the general improvement of the results for Model II (respect to Model I) for N_2O state variables for each estimated coefficient.

4   Conclusions

Two integrated MBR models which include GHGs as state variables have been compared. The two models mainly differ for the description of N_2O production processes: Model I considers the N_2O production only during denitrification; Model II, more detailed than Model I, considers the contribution of autotrophic biomass during N_2O production considering both the ND and NN pathway. Model results showed a better capability of Model II in reproducing the measured data.

References

Henze M, Gujer W, Mino T, Van Loosdrecht M (2000) Activated sludge models ASM1, ASM2, ASM2d and ASM3. In: IWA task group on mathematical modelling for design and operation of biological wastewater treatment. IWA Publishing, London

Hiatt WC, Grady CPL Jr (2008) An updated process model for carbon oxidation, nitrification, and denitrification. Water Environ Res 80:2145–2156

IPCC (2007) Changes in atmospheric constituents and in radiative forcing. In: Solomon S et al (eds.), Climate Change 2007: The physical science basis. contribution of working group I to the fourth assessment report of the intergovernmental panel on climate change. Cambridge University Press, Cambridge, pp 114–143

Jiang T, Myngheer S, De Pauw DJW, Spanjers H, Nopens I, Kennedy MD, Kennedy MD, Amy G, Vanrolleghem PA (2008) Modelling the production and degradation of soluble microbial products (SMP) in membrane bioreactors (MBR). Water Res 42(20):4955–4964

Kampschreur MJ, Kleerebezem R, de Vet WWJM, van Loosdrecht MCM (2011) Reduced iron induced nitric oxide and nitrous oxide emission. Water Res 45:5945–5952

Law Y, Ni B-J, Lant P, Yuan Z (2012) N_2O production rate of an enriched ammonia-oxidising bacteria culture exponentially correlates to its ammonia oxidation rate. Water Res 46: 3409–3419

Mannina G, Cosenza A (2017) A new integrated MBR model including GHG emissions. Submitted to Environmental Science and Technology

Mannina G, Ekama G, Caniani D, Cosenza A, Esposito G, Gori R, Garrido-Baserba M, Rosso D, Olsson G (2016) Greenhouse gases from wastewater treatment — A review of modelling tools. Sci Total Environ 551–552:254–270

Mannina G, Cosenza A (2015) Quantifying sensitivity and uncertainty analysis of a new mathematical model for the evaluation of greenhouse gas emissions from membrane bioreactors. J Membr Sci 475:80–90

Mannina G, Cosenza A, Vanrolleghem PA, Viviani G (2011) A practical protocol for calibration of nutrient removal wastewater treatment models. J Hydroinformatics 13(4):575–595

Nash JE, Sutcliff JV (1970) River flow forecasting through the conceptual model, Part 1: a discussion of principles. J Hydro 10(3):282–290

Ni B-J, Pan Y, van den Akker B, Ye L, Yuan Z (2015) Full-scale modeling explaining large spatial variations of nitrous oxide fluxes in a step-feed plug-flow wastewater treatment reactor. Environ Sci Technol 49:9176–9184

Ni BJ, Ye L, Law Y, Byers C, Yuan Z (2013) Mathematical modeling of nitrous oxide (N2O) emissions from full-scale waste water treatment plants. Environ Sci Technol 47(14):7795–7803

Peng L, Ni B-J, Ye L, Yuan Z (2015) Selection of mathematical models for N2O production by ammonia oxidizing bacteria under varying dissolved oxygen and nitrite concentrations. Chem Eng J 281:661–668

Pocquet M, Wu Z, Queinnec I, Spérandio M (2016) A two pathway model for N_2O emissions by ammonium oxidizing bacteria supported by the NO/N2O variation. Water Res 88:948–959

Saltelli A, Tarantola S, Campolongo F, Ratto M (2004) Sensitivity analysis in practice. A guide to assessing scientific models, probability and statistics series. Wiley, Chichester

Spérandio M, Pocquet M, Guo L, Ni B-J, Vanrolleghem PA, Yuan Z (2016) Evaluation of different nitrous oxide production models with four continuous long-term wastewater treatment process data series. Bioprocess Biosyst Eng 39:493–510

Vanrolleghem PA, Rosen C, Zaher U, Copp J, Benedetti L, Ayesa E, Jeppsson U (2005) Continuity-based interfacing of models for wastewater systems described by Petersen matrices. Water Sci Technol 52:493–500

Determination of Kinetic Parameters in a Biological Aerated Filter (BAF) for Wastewater Treatment

A.I. Higuera-Rivera[✉] and S. González-Martínez

Environmental Engineering Department, Institute of Engineering,
National University of Mexico (Universidad Nacional Autónoma de México),
Mexico City, Mexico
AHigueraRi@iingen.unam.mx

Abstract. A laboratory scale biological aerated filter, upflow, the organic loading rates were adjusted to 0.9, 1.5, 2.1 and 3.0 kgDQO/m^3 d using synthetic wastewater. In this study the kinetic parameters of the simultaneous removal of organic matter and ammoniacal nitrogen were determined. The removal of total and dissolved COD increases inversely with the organic load from 74% to 80% and from 81% to 86%, respectively. Ammoniacal nitrogen is removed, from 72% to 87%. The hydraulic retention time was 2 h. The kinetic model used corresponds to the Monod model. The kinetic parameters obtained are the following values, Y of 0.55 mgTSS/mgCOD, k_d of 0.09 d^{-1}, μ_{max} of 0.24 d^{-1} and K_s of 7.2 mgCOD/L. The hydraulic behavior of the reactor was determined, using the Wolf and Resnick models and the axial dispersion, resulting mainly in completely mixed behavior.

Keywords: Kinetic models · Monod model · Biological aerated filter

1 Introduction

Biological aerated filters have been extensively studied and applied in the last 2 decades because of their advantages of removing solids, organic matter and nutrients in the same reactor, they can also work with high pollutant loads and reduce the space requirements (Wang et al. 2015).

Determining kinetic parameters in biological systems provides basic information for process analysis, control, design and optimization by reducing complex experimental data to mathematical expression. On the other hand, the kinetics also describes the operating or environmental factors that affect the rates of substrate consumption (Bhunia and Ghangrekar 2008).

To reach the reactor's maximum performance, the kinetic parameters should be taken into consideration at the process of engineering design instead of using only empirical methods. Various kinetic equations reported for biological processes generally relied on Monod's equation. The values of kinetic parameters are to be estimated by means of regression analysis of experimental data, generated from lab scale (Kaewsuk et al. 2010). The fundamental factor in the use of any kinetic expression is a

mass balance that depends on the type of reactor and its hydraulic behavior (Hidaka and Tsuno 2004).

The main objective of this work is to evaluate the kinetic parameters of the simultaneous removal of organic matter and ammoniacal nitrogen from residual synthetic water with composition similar to the municipal, using different values of organic load, in a biological aerated filter.

2 Materials and Methods

The BAF used (Fig. 1) is constructed of PVC, is of up flow with a useful volume of 8.4 L, it measures 0.15 m in diameter and 1.90 m in height of which 1 m is packed with lava stones, particles with a mean diameter of 9.5 mm, specific surface area of 391 m2/m3 and apparent porosity of 47%. Ojeda and Buitrón (2001) tested the growth velocity of biofilms and concluded that lava stones have the fastest colonization rates.

The reactor has point sampling valves and peristaltic pumps were used to take the composite samples of the influent and effluent.

The filter was operated continuously with a hydraulic retention time of 2 h. The BAF as part of the operation was backwash daily to remove the excess biomass to prevent the reactor from clogging, thereby maintaining biofilm activity. Air was supplied from the bottom of the filter, fed with 5 L/min. The

Fig. 1. BAF laboratory scale

wastewater was synthetically prepared with maltodextrin and hydrolyzed protein as organic matter.

According to APHA (2012), the following parameters were measured: COD total and dissolved, ammoniacal nitrogen, nitrate, orthophosphates, total and volatile suspended solids, to determine the performance of the reactor in the removal of contaminants and additionally Kjeldahl nitrogen to determine the amount of biomass within the reactor and the cell retention time.

To determine the hydraulic behavior, tracing tests were performed, with and without aeration. As a tracer, sodium chloride was injected continuously through the bottom of the filter and simultaneously the conductivity in the filter effluent was recorded at defined time intervals. For the analysis of the curves obtained from the tracing tests the method of evaluation of the flow patterns will be used by adjusting the curves using the model of Wolf and Resnick (1963) and the one of axial dispersion (Levenspiel 2004).

To obtain the kinetic parameters, a mass balance was used for microorganisms (Eq. 1) and another for substrate (Eq. 2) using Monod kinetics, where X is the

concentration of microorganisms within the reactor, X_0 is the initial concentration of microorganisms, X_e is the concentration of microorganisms in the effluent, S is the substrate concentration, Y is the yield coefficient, k_d is the decay constant, V is the effective volume of the reactor, Q is the flow rate of the wastewater, μ is the specific growth rate of microorganisms (Hasan et al. 2014).

$$\frac{dX}{dt} = \frac{QX_0}{V} - \frac{QX_e}{V} + (\mu - k_d)X \tag{1}$$

$$\frac{dS}{dt} = \frac{QS_0}{V} - \frac{QS}{V} - \frac{\mu X}{Y} \tag{2}$$

In steady state, X_0 was assumed as zero, the resultant linear equations are 3 and 4, where CRT is the cellular retention time, HRT is the hydraulic retention time, μ_{max} is the maximum specific growth rate of microorganisms and K_s is the saturation constant.

$$\frac{1}{CRT} = \frac{S_0 - S}{XHRT}Y - k_d \tag{3}$$

$$\frac{CRT}{1 + CRTk_d} = \frac{k_s}{\mu_{max}s} + \frac{1}{\mu_{max}} \tag{4}$$

The substrate removal rate, k, was calculated by dividing μ_{max} by the Y values of biomass.

3   Results and Discussion

For start-up, the mixed culture of sludge from a sequencing batch reactor was acclimatised for 26 days to develop active biomass attachment onto the lava stones.

For organic volumetric loads of 0.9, 1.5, 2.1 and 3.0 kgDQO/m^3·d (corresponding organic surface loads of 2.3, 3.8, 5.4 and 7.7 gDQO/m^2·d), the removal of total and dissolved COD increases inversely with the organic load from 74% to 80% and from 81% to 86%, respectively. Ammoniacal nitrogen is removed, like COD, in an inverse way with the organic load from 72% to 87%.

The cellular retention time increased when the load decreased, obtaining 10.7 days for the lowest load, 9.2 days for 3.8 gDQO/m^2·d, 8.3 days for 5.4 gDQO/m^2·d and 6.9 for the highest load used.

Of the pollutant removal profiles it was observed that between a sampling point and the other the difference is minimal, from which it is deduced that the reactor is mostly completely mixed, to support this observation, the tracing tests were carried out in the reactor.

With the model of Wolf and Resnick, it was obtained that the volume of the BAF for the tests with aeration, behaves predominantly as a complete mixture reactor, 70%, 10% as piston flow and 20% dead spaces, Fig. 2 shows that to a TRH (t/t0 = 1) for the experimental data 63% of the tracer had already left the reactor, in the case of the model came out 72%. When the test was performed without aeration, 75% of piston flow,
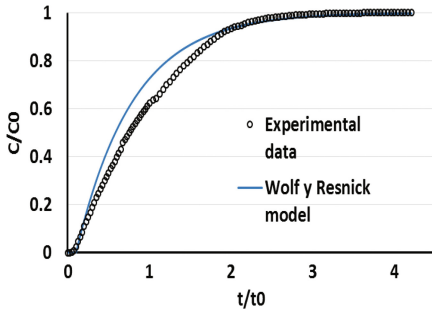
Fig. 2. Wolf and Resnick model with aeration
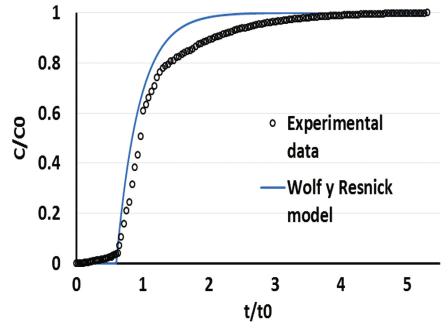
Fig. 3. Wolf and Resnick model without aeration

20% of fully mixed and 5% of dead spaces were obtained. Figure 3 shows that in a TRH, 61% of the tracer left the reactor during the experiment and the value corresponding to the model is 69%. Also a good adjustment of the experimental data to the model is observed.

From the Axial Dispersion model for aeration tests, a value of 0.287 was obtained for the dispersion modulus (d) and 0.078 for the non-aeration tests. Taking the criterion of piston flow $0.001 < d < 0.20$, dispersed flow $0.20 < d < 2.5$ and complete mixture $2.5 < d < 5.0$ (Pérez et al. 2010), the filter with aeration corresponds to a dispersed flow and the filter without aeration a Piston flow. Figure 4 shows that for the model 50% of the tracer left the reactor in a TRH and in Fig. 5 this value corresponds to 51%. A good adjustment of data to the model is observed in the case of BAF without aeration.

Of the linear equation resulting from Fig. 6 was obtained yiel coefficient (Y) with a value of 0.55 mgTSS/mgCOD (for activated sludge the reported range goes from 0.3 a 0.6 mgTSS/mgCOD) and the decay constant (k_d) whose value resulted from 0.09 d^{-1} (for activated sludge the reported range goes from 0.02 a 0.1 d^{-1}). Figure 7 presents the
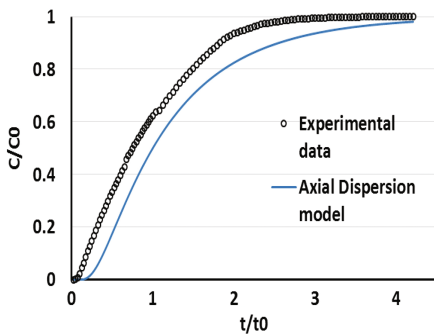
Fig. 4. Axial Dispersion model with aeration
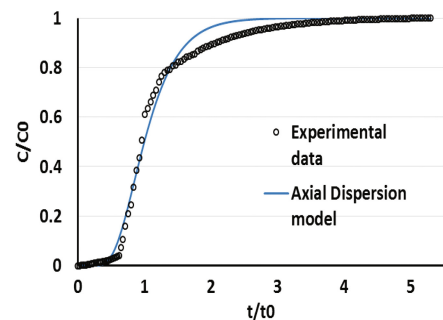
Fig. 5. Axial Dispersion model without aeration
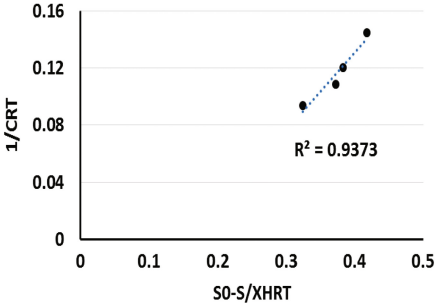
Fig. 6. Determination of Y y k_d
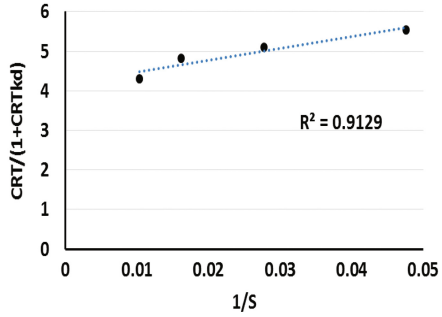
Fig. 7. Determination of μ_{max} y K_s

maximum specific growth rate of microorganisms (μ_{max}) corresponding to 0.24 d^{-1} and the saturation constant (K_s) with a value of 7.2 mgCOD/L, typical values reported range from 10 to 180 mg/L (Grady et al. 1999). The value corresponding to k is 0.44 mgCOD/d*mgTSS.

Figure 8 shows the Monod model and is compared with the experimental data to validate the obtained kinetic parameters, obtaining a value of 0.93 for the correlation coefficient. The difference may be due to the fact that the measured biomass included all the microorganisms inside the reactor and the substrate that was considered only
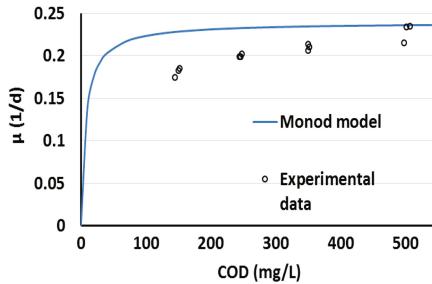
Fig. 8. Validation of kinetic parameters

corresponds to organic material.

4   Conclusions

The hydraulic behavior of the BAF is predominantly of complete mixing due to the turbulence produced by air fed with 20% dead spaces and only 10% of piston flow.

The correlation coefficients (R2) resulting from determining the kinetic parameters are greater than 0.9, which indicates a good fit of experimental data to the model used.

Because the saturation constant value is 7.2 mg/L, less than 10 mg/L, the microorganisms are considered to have high affinity for the substrate.

9% of the biomass in the reactor is consumed by endogenous respiration.

References

APHA, AWWA (2012). Standard methods for the examination of water and wastewater, 22 edn. American Public Health Association/America Water Works Association

Bhunia P, Ghangrekar MM (2008) Analysis, evaluation, and optimization of kinetic parameters for performance appraisal and design of UASB reactors. Bioresour Technol 99(7):2132–2140

Grady CPL, Daigger GT, Lim HC (1999) Biological wastewater treatment, vol 2. Marcel Dekker, New York

Hasan HA, Abdullah SRS, Kamarudin SK, Kofli NT, Anuar N (2014) Kinetic evaluation of simultaneous COD, ammonia and manganese removal from drinking water using a biological aerated filter system. Sep Purif Technol 130:56–64

Hidaka T, Tsuno H (2004) Development of a biological filtration model applied for advanced treatment of sewage. Water Res 38(2):335–346

Kaewsuk J, Thorasampan W, Thanuttamavong M, Seo GT (2010) Kinetic development and evaluation of membrane sequencing batch reactor (MSBR) with mixed cultures photosynthetic bacteria for dairy wastewater treatment. J Environ Manage 91(5):1161–1168

Levenspiel O (2004) Ingeniería de las reacciones químicas, vol 3. Limusa Wiley, México

Ojeda RL, Buitrón MG (2001) Support media selection for an anaerobi/aerobic SBR (original in Spanish) (Seleccio´n del medio de soporte para un reactor SBR anaerobio/aerobio). In: IX national congress on biotechnology and bioengineering. Veracruz, Mexico

Pérez J, Aldana G, Useche M, Rincón N, Bracho N, Mesa J (2010) Axial dispersion model performance a reactor of up flow anaerobic sludge blanket (UASB) under laboratory scale. Rev Téc Ing Univ Zulia 33(3):213–222

Wang H, Dong W, Li T, Liu T (2015) A modified BAF system configuring synergistic denitrification and chemical phosphorus precipitation: examination on pollutants removal and clogging development. Bioresour Technol 189:44–45

Wolf D, Resnick W (1963) Residence time distribution in real systems. I&EC Fundam 2:287–293

Computational Fluid Dynamic (CFD) in Wastewater Treatment

To Mix, or Not to Mix, That Is the Question

I. Nopens[1(✉)], R. Samstag[2], J. Wicks[3], J. Laurent[4], U. Rehman[1,5],
and O. Potier[6]

[1] BIOMATH, Department of Mathematical Modelling,
Statistics and Bio-Informatics, Ghent University, Ghent, Belgium
[2] Randal W. Samstag Civil and Sanitary Engineer, Bainbridge Island, WA, USA
[3] The Fluid Group, The Magdalen Centre, The Oxford Science Park,
Oxford OX4 4GA, UK
[4] Icube, UMR 7357, ENGEES, CNRS, Université de Strasbourg,
2 Rue Boussingault, 67000 Strasbourg, France
[5] AM-TEAM, Advanced Modelling for Process Optimisation,
Hulstbaan 63, 9112 Sint-Niklaas, Belgium
[6] Laboratoire Réactions et Génie des Procédés,
CNRS, Université de Lorraine, Nancy, France

Abstract. The use of Computational Fluid Dynamics (CFD) in the wastewater field has long been limited to troubleshooting of design flaws. Research-wise, this has recently opened up to the potential usage of CFD in the reactor design phase. Another noticeable shift is the one from only considering plain hydrodynamics to the coupling to kinetic models and population balance models (PBM). This vastly assists in design optimisation problems that are either driven by kinetics or physical processes such as flocculation or crystallisation which lead to different optimal solutions as the goal is quite different. This contribution provides some examples of the above and discusses how the know-how should be used to develop new design methods, hereby questioning how ideal mixing should be defined.

Keywords: Mixing · Computational fluid dynamics · Compartmental modelling · Reactor design

1 Introduction

Computational fluid dynamics (CFD) has become an accepted method for process analysis of fluid flows inmany industries. It recently has become widely used for analysis of hydraulic problems in water and wastewater treatment (WWT) but still needs to find wider acceptance for analysis of physical, chemical and biological processes in WWT. There are substantial financial and risk drivers to conduct CFD for better wastewater design (Wicklein et al. 2016).

Recently, a working group was formed under the wings of the IWA Specialist Group "Modelling and Integrated Assessment" (MIA) that brings together the community active in this field. Laurent et al. (2014) described an alternative way of using CFD as a supplement to using simpler models, whereas Wicklein et al. (2016) focused on good modelling practice for CFD modelling of WWT and Samstag et al. (2016)

provided an overview of CFD applications in the unit process of a wastewater treatment train. Nowhere (except possibly disinfection) is CFD used in a widespread or routine way as a design or risk-management tool. This offers clear opportunities to further develop the value of CFD in wastewater process evaluation.

This contribution provides some examples of (novel) ways of using CFD and its outcomes to benefit the wastewater sector.

2   Materials and Methods

Plain CFD examples solve the Navier-Stokes equations either in one or two phase. Mostly, turbulent conditions prevail and a set of turbulence equations are solved alongside.

When coupling to kinetics is required, scalar equations are defined for all species present in the kinetic model. Dissolved species follow the fluid flow and get additional source and sink terms according to the reactions they take part in. These terms can easily be derived from the Gujer matrix of an ASM model. Technically, they are implemented by means of user defined functions (UDF) when the commercial tool Fluent (Ansys) is used.

3   Results and Discussions

This section is structured as follows: first, a couple of example studies on mixing behaviour of bioreactors are shown, after which a general discussion is provided as to how CFD can aid in cost savings and more cost-effective reactor design.

A fully integrated CFD-kinetic model was developed for the outer ring (partly oxic and partly anoxic) of a concentric plant design (Eindhoven Water and Resource Recovery Plant (WRRF)) as shown in Fig. 1 (Rehman 2016). It was found that
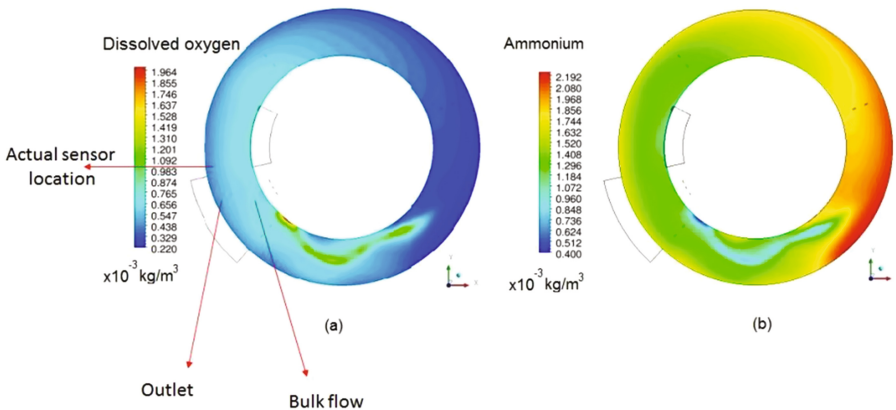
Fig. 1. Dissolved oxygen (a) and ammonium (b) concentrations at 3.45 m depth in the outer ring of the Eindhoven WRRF

significant deviations from complete mixed conditions prevailed due to the specific design (circular) and placement of inlets, outlets, propellers and recirculation flows. A key issue related to the circular design is the fact that the mixed liquor that is internally recycled is pushed to the outer wall when it hits the wall of air bubbles in the bottom aerated zones. This pushes the air plume to the inner wall and results in a significant heterogeneity of species concentrations and, hence, the local activity of micro-organisms. The heterogeneity can be quantified by introducing cumulative species distributions (CSD) (Fig. 2) which can further be adopted to develop a compartmental model that can be used instead of a tanks-in-series (TIS) approach (Fig. 3). The latter should reduce uncertainty in the mixing model and, hence, unnecessary calibration efforts. Furthermore, this analysis has clearly shown that the design can be improved. In a follow-up study, the obtained knowledge can now be used to test virtual scenarios that cure the major downsides of this process behaviour.
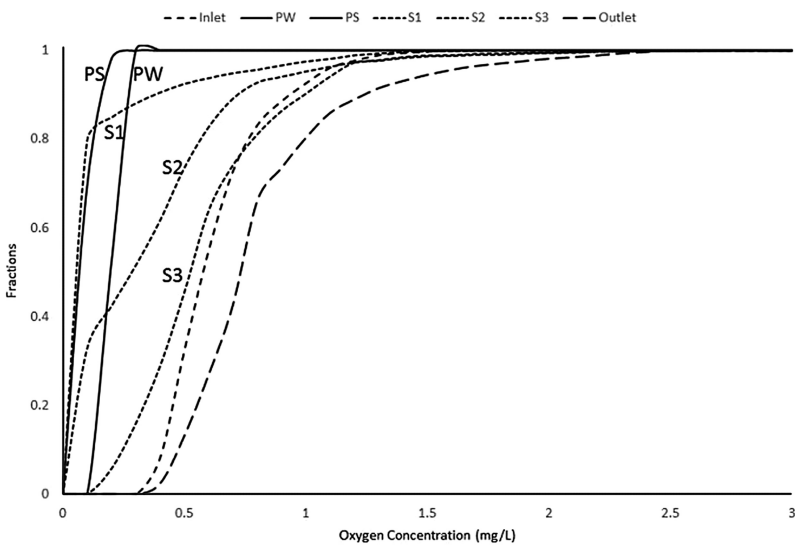
Fig. 2. Cumulative species distributions of dissolved oxygen at different locations in the outer ring of the Eindhoven WRRF. Steep curves reveal less heterogeneity and vice versa
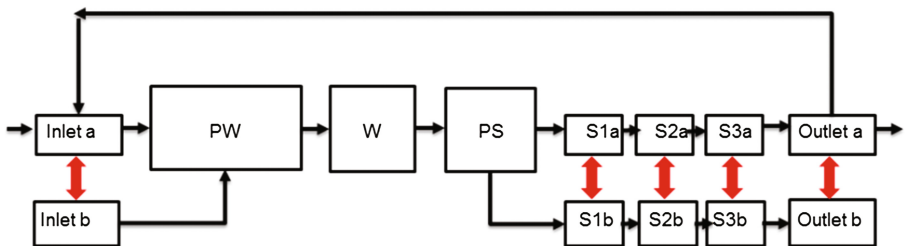
Fig. 3. Compartmental model of the outer ring of the Eindhoven WRRF

There are many other examples where the behaviour of a system cannot be described by a systemic model combined with a kinetic model. Some designs seem to behave better than expected, whereas others are underperforming. Kimura et al. (2008) found better performance behaviour of a baffled membrane bioreactor (BMBR) that could not be explained by a CSTR combined with an activated sludge (ASM) model. The unexpected appearance of bio-P removal in systems not designed for it is another example (Barnard et al. 2012; Verrecht et al. 2010). However, few authors link this to the specific mixing behaviour in a reactor and try to explain it through other complex theories or calibrating kinetics. Surface aerated oxidation ditch plants are yet another example of this as demonstrated by Rehman (2016). Recently, a lot of attention is going to the mixing behaviour of anaerobic digesters which is pretty much still a black box at full-scale mainly due to the difficulty to measure inside the system. Given the elevated viscosity and the typical limited amount of energy input for mixing, it cannot be expected to behave as completely mixed. Gas bubble production will only locally contribute to mixing, but not to a large extent. But it might as well be that this way of operation (i.e. not complete mix) is the key to make the process work. However, it becomes cumbersome to optimise the process without understanding the specifics as to why this is the case. In a sense it seems that reactor design in general is pretty much either business as usual (based on rules of thumb) or trial and error. Time has come to introduce model-based design. It is noteworthy that this in now common practice in e.g. chemical engineering where reactor design is a very hot topic at the moment.

Even at a small scale one can demonstrate that complete mixing can be problematic. Figure 4 shows a CFD-ASM simulation of unaerated 2L continuous flow-through respirometer at different flow rates. As can be seen, a high flow rate is needed to achieve almost complete mixed conditions. Compared to an ASM-CSTR model, affinity indices had to be recalibrated significantly. This emphasises that operating reactors under complete mixed conditions is something we might not want to pursue as this will come at a significant cost. It might be wiser to understand the consequences of incomplete mixing and turn this into a benefit of the system operation.
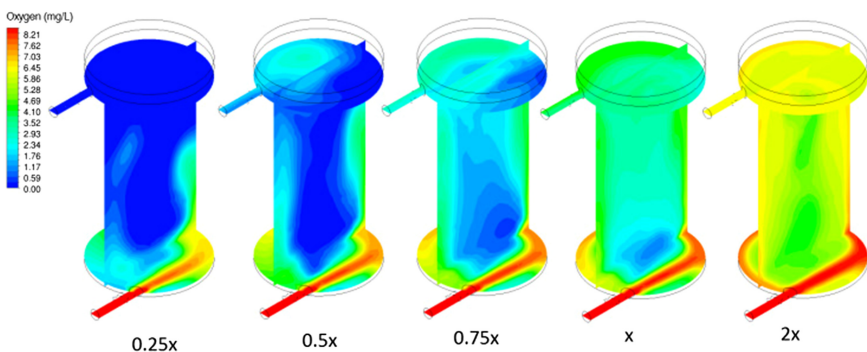
Fig. 4. Distribution of dissolved oxygen concentration in an unaerated continuous flow-through respiromter.

Thus far focus was on process kinetics. However, all the above also holds for physical process behaviour. Let us take the example of shear-induced coagulation or flocculation. Here, often the assumption of an average shear (G) is adopted in reactor design. However, pursuing this behaviour is similar to pursuing complete mix in terms of concentrations. It will be very costly to achieve and the question is whether it is really needed. Coagulation systems are actually designed as merely scaled up jar tests by means of some rules of thumb based on energy input. However, the energy dissipation will be different on different scales and one actually needs to think again in terms of distributions. Similar to the CSD discussed before, reactors will exhibit a shear distribution. Depending on the location of a floc or granule it will either be exposed to low shear or high shear. The former will promote flocculation, whereas the latter will promote breakage (depending on floc strength). Obviously, the pattern at which a floc is exposed to different shear environments will be of key importance. This pattern is entirely governed by the mixing pattern and, hence, location of inlet, outlet, inlet flow rate and position and speed of stirring devices. Hence, when scaling up, one should try to achieve a similar shear distribution and recirculation pattern in the reactor. The latter is, however, not straightforward. Again, many studies try to understand why a certain system is not behaving similar as their small scale counterparts. The issue is the scale-up rules that are not accounting for the important aspects of mixing. Also here, model-based design based on CFD models coupled with flocculation models is the way to go. Another observable trend is the scale-down of such processes (e.g. tube flocculators) which makes sense as they have a much better controllability. Hence, it might be smarter to design smaller reactors and use numbering-up instead of scaling up. Again, in chemical engineering this is an observable trend in order to enhance reactor performance.

A system that actually combines both impact of kinetics and a physical precipitation process is crystallisation. Indeed, local concentrations are important with respect to supersaturation to promote crystal growth. On the other hand, shear levels promote aggregation and breakage phenomena which drive the crystal size distribution. The latter is important when thinking in a Quality-by-Design (QbD) fashion with respect to reuse of the product. Current reactor designs are definitely not optimal in this respect. Tarrago et al. (2016) demonstrated that the CSD could be altered by simply changing the upflow velocity in struvite crystalliser. However, building knowledge is still required to improve the design in a targeted way. Hence, this is another field where advanced CFD modelling can lead to a large leap in process understanding and optimisation.

3.1   Discussion

It is clear from the above that mixing behaviour of bioreactors is vastly overlooked and needs more attention. This is important in terms of troubleshooting, which is the classical application of CFD in the wastewater field nowadays. However, the know-how that is built should also be adopted in model-based design. We need to build in the performance of a reactor in its design. We should leave the "era of averaging" as we have the tools at hand to do a much better job in engineering reactors.

When using models for reactor design, there are two new research problems that arise: (1) which method should we use and (2) how do we define optimal mixing.

The former is actually not so straightforward. One would immediately have the reflex of using CFD for this purpose. However, there are a myriad of different design subtleties that one can think of and, hence, the degrees of freedom are enormous. Given the vast computational load of CFD, especially when combined with kinetic and physical models, it is likely not the way to go, at least not in the decades to come. An alternative is to further develop the powerful concept of compartmental models as they are more computationally tractable and, hence, allow to simulate many more scenarios. A strategy could be to use CMs for optimisation and then link this optimal behaviour to reactor design. Obviously, this is a process that will take time. But is for sure the most promising route at this point.

The latter is another interesting point of discussion. Currently, ideal mixing patterns are either CSTR or plug flow. However, mostly we are somewhere in between. But that does not mean that these conditions cannot be "ideal" or optimal. We should probably adapt our terminology here and connect optimal mixing behaviour to the goal of the system. Optimal mixing can then be very different for different technologies. Striving for complete mixing is most likely not even what is required in many cases. We should use advanced models combining CFD, kinetics and physical processes to pinpoint what degree of mixing is optimal for a certain process and design reactors accordingly.

Finally, a question that often arises: Do all reactor operational and design optimisation projects need a CFD study? Well, at first it will be required for a certain amount of cases in order to build up knowledge. However, once sufficient know-how has been acquired, it can be turned into new and better design rules, not requiring a separate CFD study for every case.

4   Conclusions

This contribution clearly indicates that there is much more beyond the traditional way of using CFD for troubleshooting design flaws in wastewater treatment systems. When used in a smart way, it can lead to significant cost savings for existing plants and a higher level of cost-effectiveness for plants to be designed, hereby justifying the minor cost of a CFD modelling study in the overall project cost. The methodologies shown are generic and can be extended to different unit processes.

References

Barnard J, Houweling D, Analla H, Steichen M (2012) Saving phosphorus removal at the Henderson NV plant. Wat Sci Technol 65(7):1318–1322

Kimura K, Nishisako R, Miyoshi T, Shimada R, Watanabe Y (2008) Baffled membrane bioreactor (BMBR) for efficient nutrient removal from municipal wastewater. Water Res 42:625–632

Laurent J, Samstag R, Ducoste J, Griborio A, Nopens I, Batstone D, Wicks J, Saunders S, Potier O (2014) A protocol for the use of computational fluid dynamics as a supportive tool for wastewater treatment plant modelling. Wat Sci Technol 70(10):1575–1584

Rehman U (2016) Next generation bioreactor models for wastewater treatment systems by means of detailed combined modelling of mixing and biokinetics PhD thesis, Ghent University, Belgium

Samstag R, Ducoste J, Griborio A, Nopens I, Batstone D, Wicks J, Saunders S, Wicklien E, Kenny G, Laurent J (2016) CFD for wastewater treatment: an overview. Wat Sci Technol 74 (3):549–563

Tarrago E, Puig S, Ruscalleda M, Balaguer M, Colprim J (2016) Controlling struvite particles' size using the up-flow velocity. Chem Eng J 302:819–827

Verrecht B, Maere T, Benedetti L, Nopens I, Judd S (2010) Model-based energy optimisation of a small-scale decentralised membrane bioreactor for urban reuse. Water Res 44(14): 4047–4056

Wicklein E, Batstone DJ, Ducoste J, Laurent J, Griborio A, Wicks J, Saunders S, Samstag R, Potier O, Nopens I (2016) Good modelling practice in applying computational fluid dynamics for WWTP modelling. Wat Sci Technol 73(5):969–982

CFD Simulations of Fluid Dynamics Inside a Fixed-Bed Bioreactor for Sugarcane Vinasse Treatment

D.C.G. Okiyama[1(✉)], J.A. Rabi[1], R. Ribeiro[1], A.D.N. Ferraz Jr.[2], and M. Zaiat[2]

[1] Faculty of Animal Science and Food Engineering, University of São Paulo, Av. Duque de Caxias Norte 225, Pirassununga, SP 13635-900, Brazil
[2] São Carlos School of Engineering, University of São Paulo, Av. Trabalhador Sãocarlense 400, CP 359, São Carlos, SP 13566-590, Brazil

Abstract. Vinasse is a by-product from ethanol industry which can be exploited in ferti-irrigation after its treatment via APBR (anaerobic packed bed reactor). Comprehensive understanding of fluid dynamics within APBR is fundamental for its design and the goal of this work was to perform CFD (computational fluid dynamics) simulations of a laboratory-scale APBR by the use of commercial software. Tracer concentration patterns deviated from plain plug flow behaviour.

Keywords: Computational fluid dynamics · Agroindustrial effluent · Anaerobic packed bed reactor

1 Introduction

Resulting from the distillation of sugarcane juice, vinasse is a by-product of the sugar-ethanol industry. Large-scale exploitation of aforesaid agroindustrial effluent has long pointed to ferti-irrigation in sugarcane crops (Robertiello 1982). Nevertheless, due to high levels of organic matter, salt and nutrients usually found in vinasse, environmental issues have been raised towards its direct (i.e., untreated) long-term deposition onto crop soil (Madejón et al. 2001).

Anaerobic treatment of vinasse has been claimed as suitable practice prior to ferti-irrigation (Vlissidis and Zouboulis 1993) to mitigate both ground-water contamination and greenhouse effect gases emission (España-Gamboa et al. 2011). Anaerobic treatment can preserve the fertilising qualities (Moraes et al. 2014) while biogas can be recovered (Grisi et al. 2012).

Among anaerobic systems for high removal of biological oxygen demand (BOD), anaerobic packed bed reactor (APBR) is an attractive alternative thanks to its relatively simpler design and operation allied to its low cost and process stability (Ferraz Jr. 2013). Those engineering features are related to APBR ability to render higher solids retention time (SRT) with shorter hydraulic residence time (HRT) and toxicity tolerance (Satyawali and Balakrishnan 2008).

Fluid dynamics in APBR has been studied by relying on ideal operation assumptions such as plug-flow or perfectly-mixed reactor (Levenspiel 1999) and single-parameter models have then been invoked such as longitudinal dispersion and continuous-flow stirred-tank reactor (CSTR) in series (Fazolo et al. 2006; Méndez-Romero et al. 2011; Fernandes et al. 2013). While helpful to identify eventual departure from ideal operation, aforesaid models might be relatively simple in view of current computer resources. In other words, APBR fluid dynamics can be more complex than CSTR in series so that computational fluid dynamics (CFD) may identify either dead zones or short-circuiting flows.

Comprehensive description of fluid patterns in APBR is vital for its design and performance analysis. By relying on fundamental conservation principles, the application scope of physics-based (also known as white-box) models is broader than data-driven (or black-box) models (Datta and Sablani 2007). All-inclusive APBR models are prone to be complex inasmuch as fluid flow and convective-diffusive species transport in porous medium must be concurrently combined with biochemical processes (e.g. acidogenesis, acetogenesis, methanogenesis, and hydrolysis). CFD indeed arises as helpful engineering tool to study fixed-bed systems for effluent treatment (Parco et al. 2007; Brannock et al. 2010; Głuszcz et al. 2011).

In the present work, time-dependent (i.e. dynamic) two-dimensional (2-D) CFD simulations were performed concerning the fluid dynamics inside an existing laboratory-scale cylindrical APBR for sugarcane vinasse treatment (Ferraz Jr. 2013). Specifically, the objective was to numerically simulate the upward flow of a tracer solution within a 2-D vertical cross-section of the APBR during three times the theoretical HRT (Okiyama 2014).

2 Materials and Methods

While the main objective of the present work was to perform CFD simulations, this section outlines some information about the experimental bioreactors for vinasse treatment, which are depicted in Fig. 1(a). Each laboratory-scale cylindrical APBR was assembled in acrylic tubes by comprising feeding module (FM), bed section (BS), effluent collection module (EC), and biogas collection module (BC), as sketched in Fig. 1(b).

Low-density polyethylene small cylinders were used as the supporting medium in BS as a compromise between organic matter removal, APBR stability and biogas production (Ferraz 2013). Figure 1(c) shows samples of aforesaid cylinders, whose approximate dimensions are 5.0 mm of length and 4.5 mm of diameter. Cylinders randomly filled up BS volume so that its packed-bed porosity ranged from 0.47 to 0.54 at start-up. Table 1 summarises the length, the inner diameter, the geometric volume and the volume occupied by the liquid phase at each APBR compartment. Biogas collection module (BC) is solely occupied by the gas phase.

In view of values in Table 1, the total APBR volume occupied by the liquid phase ranged from 2.1865 L for lower BS porosity up to 2.3625 L for higher BS porosity. The bioreactor was initially filled up with water and tracer solution was subsequently fed at
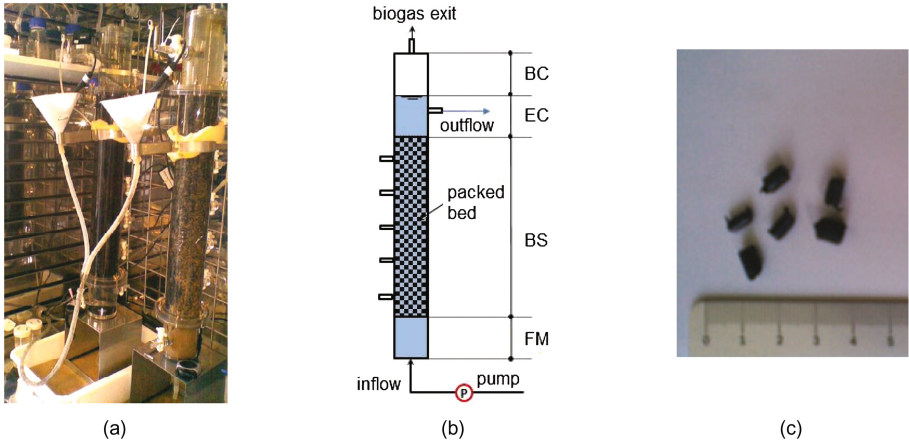
Fig. 1. Laboratory-scale cylindrical APBR for vinasse treatment: (a) picture of experimental bioreactors; (b) sketch depicting feeding module (FM), bed section (BS), effluent collection module (EC) and biogas collection module (BC); (c) picture of low-density polyethylene cylinders employed as supporting medium within BS

Table 1. Length, diameter, geometric volume and volume occupied by liquid phase of each APBR compartment

Compartment dimension	FM	BS		EC	BC
		Porosity = 0.47	Porosity = 0.54		
Length (m)	0.1	0.5	0.5	0.1	0.05
Diameter (m)	0.08	0.08	0.08	0.08	0.08
Geometric volume (10^{-3} m^3 = L)	0.5027	2.5133	2.5133	0.5027	0.2513
Volume with liquid (10^{-3} m^3 = L)	0.5027	1.1812	1.3572	0.5027	–

stepwise flow of 4.6 L/day, thereby yielding a theoretical HRT of approximately 12 h, namely 11.4 h for lower BS porosity and 12.3 h for higher BS porosity.

This work performed two sets of CFD simulations, one for each extreme porosity value at start-up (0.47 and 0.54) whose corresponding permeability was assessed through Kozeny-Carman correlation (Nield and Bejan 1992). For each numerically tested porosity (assumed to be uniform throughout BS compartment), Table 2 shows

Table 2. Porosity-dependent parameters used in CFD simulations of the laboratory-scale APBR

APBR porosity-dependent parameter	BS porosity = 0.47	BS porosity = 0.54
Bed total surface-to-volume ratio	683 m^{-1}	541 m^{-1}
Hydraulic radius	6.88×10^{-4} m	8.49×10^{-4} m
BS particle equivalent diameter	0.00275 m	0.0034
BS permeability	5.34×10^{-8} m^2	1.08×10^{-7} m^2

porosity-dependent parameters used in CFD simulations of the existing laboratory-scale APBR. Conversely, pipe-like flow (i.e. flow without porous medium) was assumed in both FM and EC compartments.

CFD simulations of the fluid dynamics in APBR were carried out with the help of COMSOL Multiphysics® by using the Chemical Species Transport module within the Chemical Reactor Engineering package. Specifically, transient 2-D (i.e. time-dependent two-dimensional) CFD simulations invoked the Transport of Diluted Species model in the Reacting Flow in Porous Media framework of the aforesaid commercial software.

The idea was to simulate upward fluid flow coupled with tracer (namely NaCl) transport in APBR compartments where tracer solution actually flows through, namely FM, BS and EC in Fig. 1(b). APBR was assumed to be initially filled up with clean water and stepwise tracer solution flow was fed in at FM inlet where Dirichlet boundary condition was imposed. Tracer concentration was assumed to remain constant at the experimental feeding value at FM inlet.

3   Results and Discussions

In order to set the number of finite elements for simulations, mesh-independence analysis was carried out by using 0.47 as BS porosity. Figure 2 depicts the finite-element meshes automatically generated by COMSOL Multiphysics® to APBR vertical cross-section. Used in subsequent simulations, normal mesh (with 12.352 elements) provided suitable compromise between computational effort and accuracy of numerical results. It is interesting to note that meshes are locally refined in transitions between APBR compartments as well as near walls, i.e. where steeper gradients (of tracer concentration and fluid velocity) are prone to occur.

For lower BS porosity (= 0.47), Fig. 3 shows tracer concentrations simulated in FM, BS and EC compartments for increasing time instants. CFD simulations pointed to plug-flow with some wall effects, which are noted (to some extent) along all vertical walls. Thereby, higher concentrations are observed around APBR centreline while lower concentrations occur near vertical walls. A somewhat parabolic profile prevails in the upward high concentration front, which deviates from plain plug flow behaviour. Relatively small dead zones are observed in the bottom of FM compartment. Simulations for higher BS porosity (= 0.54) yielded similar patterns, which are not shown here for the sake of brevity.

While tracer concentration at BS exit was numerically simulated as a function of BS radius, the experimental APBR actually referred to a single collection funnel at EC centroid. In view of that, two probing concentration profiles were screened: one at BS centreline and the other at BS half-radius. When compared to experimental data, the former yielded better results. Average concentration profile was evaluated through line-integral over the exiting fluid flow so that APBR features were assessed from both experimental and numerical concentration profiles. Experimental average HRT resulted as 11.6 h while CFD simulations rendered 10.6 to 11.4 h. As no preferential paths or relatively large dead zones were evidenced in CFD simulations, one may justify differences between average HRT values in terms of local variations in BS porosity, which was allegedly uniform in CFD simulations.
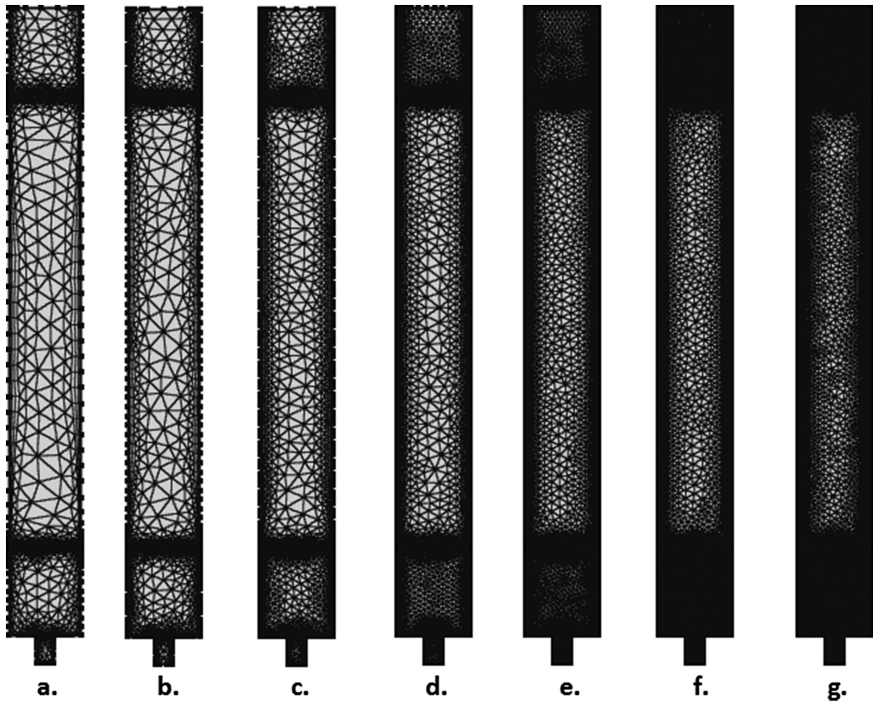
Fig. 2. Finite-element meshes automatically generated by COMSOL Multiphysics® for APBR vertical cross-section: (a) extremely coarse (4146 elements), (b) extra coarse (4.989 elements); (c) coarser (5.972 elements), (d) coarse (9.299 elements), (e) normal (12.352 elements), (f) fine (16.494 elements), (g) finer (27.811 elements)
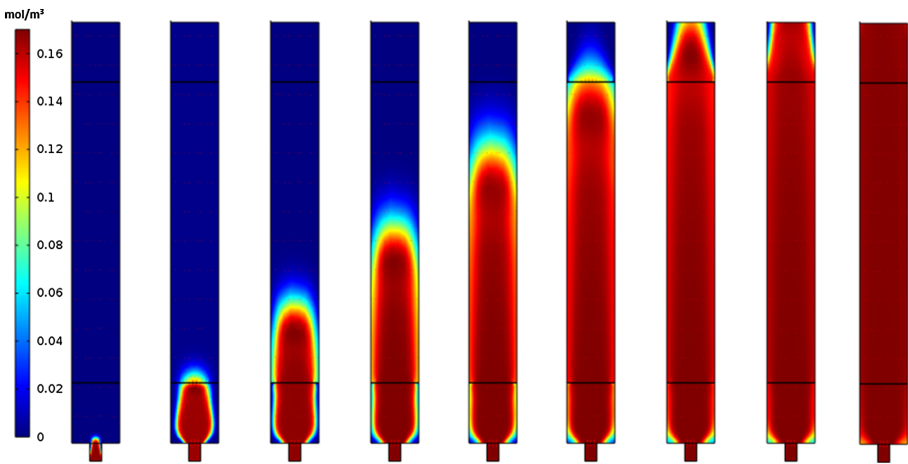
Fig. 3. Tracer concentrations simulated in FM, BS (porosity = 0.47) and EC compartments at increasing time instants (from left to right): 702 s (= 0.195 h), 7020 s (= 1.95 h), 10044 s (= 2.79 h), 21060 s (= 5.85 h), 28080 s (= 7.8 h), 35100 s (= 9.75 h), 42606 s (= 11.835 h), 50130 s (= 13.925 h), and 84330 s (= 23.425 h)

Care should then be exercised when performing CFD simulations while assuming constant porosity. User-defined routines, for instance, should be added to the simulator to account for biofilm on the carriers as well as suspended solids in the medium. Accordingly, as part of our ongoing research to develop in-house simulators of bioreactors for wastewater treatment, lattice Boltzmann method (LBM) has been considered as alternative route (van der Sman 2007). Known to yield relatively simpler computational codes (Mohamad 2011), LBM may numerically simulate either suspended solids in multiphase flow (Ladd and Verberg 2001) or biofilm formation and detachment (Picioreanu et al. 2001), in addition to biogas bubbles generation and transport (Chen 2010).

4   Conclusions

If compared to long-standing models for non-ideal bioreactors for wastewater treatment, CFD can be an efficient engineering tool as it is able to thoroughly depict the APBR in terms of its internal fluid dynamics as well as species concentration profiles. As far as design of up-flow APBR for sugarcane vinasse treatment is concerned, such comprehensive knowledge is strategic for not only scale-up procedures but also operation under distinct scenarios. Future developments may point to surrogate computational methods such as LBM so as to simulate biofilm on the carriers as well as suspended solids and/or biogas in the medium.

References

Brannock M, Leslie G, Wang Y, Buetehorn S (2010) Optimising mixing and nutrient removal in membrane bioreactors: CFD modelling and experimental validation. Desalination 250 (2):815–818

Chen X (2010) Simulation of 2D cavitation bubble growth under shear flow by lattice Boltzmann model. Commun Comput Phys 7(1):212–223

Datta AK, Sablani SS (2007) Mathematical modeling techniques in food and bioprocess: an overview. In: Sablani SS, Rahman MS, Datta AK, Mujumdar AR (eds) Handbook of food and bioprocess modeling techniques. CRC Press, Boca Raton, pp 1–11

España-Gamboa E, Mijangos-Cortes J, Barahona-Perez L, Dominguez-Maldonado J, Hernández-Zarate G, Alzate-Gaviria L (2011) Vinasses: characterization and treatments. Waste Manag Res 29(12):1235–1250

Fazolo A, Pasotto MB, Foresti E, Zaiat M (2006) Kinetics, mass transfer and hydrodynamics in a packed bed aerobic reactor fed with anaerobically treated domestic sewage. Environ Technol 27(10):1125–1135

Fernandes BS, Saavedra NK, Maintinguer SI, Sette LD, Oliveira VM, Varesche MBA, Zaiat M (2013) The effect of biomass immobilization support material and bed porosity on hydrogen production in an upflow anaerobic packed-bed bioreactor. Appl Biochem Biotechnol 170 (6):1348–1366

Ferraz ADN Jr (2013) Anaerobic digestion of sugar cane vinasse in acidogenic fixed bed reactor followed by methanogenic reactor sludge blanket type. Ph.D. thesis (in Portuguese), São Carlos School of Engineering, University of São Paulo, São Carlos, Brazil

Głuszcz P, Petera J, Ledakowicz S (2011) Mathematical modeling of the integrated process of mercury bioremediation in the industrial bioreactor. Bioproc Biosyst Eng 34(3):275–285

Grisi EF, Yusta JM, Dufo-López R (2012) Opportunity costs for bioelectricity sales in Brazilian sucro-energetic industries. Appl Energ 92:860–867

Ladd AJC, Verbeg R (2001) Lattice-Boltzmann simulations of particle-fluid suspensions. J Stat Phys 104(5):1191–1251

Levenspiel O (1999) Chemical reaction engineering, 3rd edn. Wiley, New York

Madejón E, López R, Murillo JM, Cabrera F (2001) Agricultural use of three (sugarbeet) vinasse composts: effect on crops and chemical properties of a Cambisol soil in the Guadalquivir river valley (SW Spain). Agric Ecosyst Environ 84(1):55–65

Méndez-Romero DC, López-López A, Vallejo-Rodríguez R, León-Becerril E (2011) Hydrodynamic and kinetic assessment of an anaerobic fixed-bed reactor for slaughterhouse wastewater treatment. Chem Eng Process 50(3):273–280

Mohamad AA (2011) Lattice Boltzmann method: fundamentals and engineering applications with computer codes. Springer, London

Moraes BS, Junqueira T, Pavanello LG, Cavalett O, Mantelatto PE, Bonomi A, Zaiat M (2014) Anaerobic digestion of vinasse from sugarcane biorefineries in Brazil from energy, environmental, and economic perspectives: profit or expense? Appl Energ 113:825–835

Nield DA, Bejan A (1992) Convection in porous media. Springer, New York

Okiyama DCG (2014) Numerical simulation of hydrodynamics within fixed-bed biorreactor for vinasse treatment. M.Sc. thesis (in Portuguese), Faculty of Animal Science & Food Engineering, University of São Paulo, Pirassununga, Brazil

Parco V, Du Toit G, Wentzel M, Ekama G (2007) Biological nutrient removal in membrane bioreactors: denitrification and phosphorus removal kinetics. Water Sci Technol 56(6):125–134

Picioreanu C, van Loosdrecht MCM, Heijnen JJ (2001) Two-dimensional model of biofilm detachment caused by internal stress from liquid flow. Biotech Bioeng 72(2):205–218

Robertiello A (1982) Upgrading of agricultural and agroindustrial wastes: the treatment of distillery effluents (vinasses). Agric Wastes 4(5):387–395

Satyawali Y, Balakrishnan M (2008) Wastewater treatment in molasses-based alcohol distilleries for COD and color removal: a review. J Environ Manag 86(3):481–497

van der Sman RGM (2007) Lattice Boltzmann simulation of microstructures. In: Sablani SS, Rahman MS, Datta AK, Mujumdar AR (eds) Handbook of food and bioprocess modeling techniques. CRC Press, Boca Raton, pp 15–39

Vlissidis A, Zouboulis AI (1993) Themophilic anaerobic digestion of alcohol distillery wastewaters. Biores Technol 43(2):131–140

Startup of Aerobic Granulation Technology: Troubleshooting Scale-up Issue

R. Pishgar[1]([⊠]), A. Kanda[1], G.R. Gress[2], H. Gong[1], and J.H. Tay[1]

[1] Department of Civil Engineering, University of Calgary,
2500 University Drive NW, Calgary, AB T2N 1N4, Canada
[2] Department of Mechanical Engineering, University of Calgary,
2500 University Drive NW, Calgary, AB T2N 1N4, Canada

Abstract. Numerous laboratory-scale studies confirmed the effectiveness of aerobic granulation technology for diverse treatment purposes. However, few pilot scale investigations have been conducted so far, and these studies revealed that a large-scale module could frustrate the microbial granulation process. In this study, the effect of scale-up on granule formation was investigated. Upflow air velocity, a function of the aeration rate, is normally deemed to be the main source of hydrodynamic shear force in bubble column reactors. Shear force is known as one of the important inducers of aerobic granulation. Superficial upflow air velocity (SUAV) is defined as aeration rate per cross-section area of the reactor. However, the findings of this study proved that maintaining SUAV was not sufficient for successful granulation. In addition, the parameter SUAV could not well represent the hydrodynamics of bubble column reactors, especially during the scale-up procedure. This study proved that air bubble distribution was of greater importance, as opposed to the effect of aeration rate. Mean distance between bubbles should be maintained constant regardless of the size of reactor. This provided similar shearing activity in different reactors with different scales, which appeared to be the critical requirement for successful granulation process in a larger module. To ensure similar bubble distances in bioreactors of different sizes, diffusers with the same porosity should be used, and their surface areas and the aeration rate should be increased by the scale-up ratio. Air bubble distribution dictated the gas holdup which was eventually determined to be the crucial factor for the scale-up of aerobic granular bubble column reactors.

Keywords: Aerobic granulation · Aeration rate · Drag force · Granule formation · Startup · Scale-up

1 Introduction

Aerobic granulation is a recent technology with a promising future. The technology involves agglomeration of activated sludge into dense and multispecies microbial aggregate, renowned as aerobic granules. Enhanced settling ability of aerobic granules retains high population of biomass in the reactor, turning it into a highly-effective wastewater treatment technique.

Numerous laboratory-scale studies (2–10 L bioreactors) confirmed the effectiveness of the aerobic granulation technique for diverse treatment purposes, including removal

of high organic loads (Moy et al. 2002), nutrients (Yilmaz et al. 2008; de Kreuk et al. 2005), and toxic compounds (Yi et al. 2006; Zhang et al. 1997; Zhang and Tay 2012). However, lack of in-depth knowledge on process scale-up has prevented widespread application of the technology in practice. So far, only a handful of studies have been dedicated to pilot scale investigation (Isanta et al. 2012; Long et al. 2014; Ni et al. 2009; Rocktäschel et al. 2015; Tay et al. 2005) which is a crucial step prior to full-scale implementation. Yet, the previous studies revealed some important but discouraging facts; a large-scale module could frustrate the microbial granulation process. In addition, aerobic granules were potentially subject to higher risk of disintegration in a large-scale bioreactor (Tay et al. 2005).

This study aimed at covering one of the aspects of the scale-up process; the objective was to investigate the effect of scale-up on granule formation. Granule formation in two reactors were compared: a 5-L lab-scale sequencing batch reactor (SBR) and a 24-L pilot-scale SBR; the issues in pilot module were identified, discussed, and the solutions were experimentally explored.

2 Materials and Methods

Two bubble column reactors were used to evaluate the effect of scale-up on the startup of aerobic granulation (Fig. 1); lab-scale reactor (R1) had internal diameter (ID) of 8 cm, and height of 80 cm. Pilot-scale reactor (R2) had an internal diameter (ID) of 13.7 cm, and was 15.3 cm in height. Working volume of R1 and R2 were 4.6, and 15.8 L individually. Full capacities of the reactors were not used to avoid biomass washout from the overflow ports (see Fig. 1). Washout was an individual or a combined consequence of three phenomena: (1) drastic surge of water at the beginning of aeration phase due to air pressure; (2) significant expansion of mixed liquor due to air hold up; (3) foaming due to high phosphate concentration and/or excess secretion of extracellular proteins.

1. Influent sampling port
2. Influent pump
3. Influent pump timer(s)
4. Feed tank
5. Air diffuser
6. Air compressor
7. Air pump timer
8. Gas venting
9. Overflow port
10. Sludge & effluent sampling port
11. Decanting valve timer(s)
12. Effluent tank
13. Microbial aggregates
14. Air bubbles
15. foaming
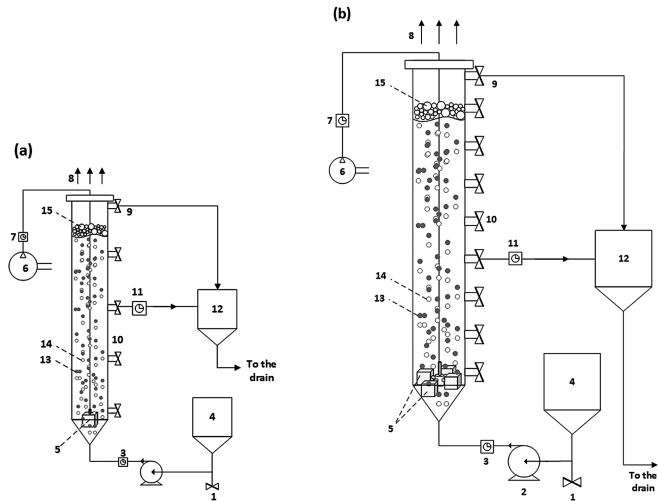
Fig. 1. Experimental setup; (a) 5-L lab-scale reactor, R1; (b) 24-L pilot reactor, R2

The bioreactors were inoculated with return activated sludge [50% (v/v)] from biological nutrient removal (BNR) process, collected from the Pine Creek Wastewater Treatment Plant, Calgary, Canada. The characteristics of seed sludge and SBR cycles are summarized in Tables 1 and 2 respectively. Volumetric exchange ratio (VER) was 50% in R1, and 43% in R2. Synthetic wastewater was composed of (mg/L): sodium acetate, 2440 (chemical oxygen demand, COD of 2000); NH_4Cl, 390 (NH_4-N, 100); K_2HPO_4, 89.7; KH_2PO_4, 17.3 (P-PO_4, 15); $CaCl_2.2H_2O$, 30; $MgSO_4.7H_2O$, 25; $FeSO_4.7H_2O$, 20; and 1 mL/L trace elements. Trace element solution contained $ZnCl_2$, $CuCl_2$, $MnSO_4.H2O$, $(NH_4)_6.Mo_7O_{24}.4H_2O$, $AlCl_3$, $CoCl_2.6H_2O$, and $NiCl_2$ (50 mg/L individually). The volumetric organic loading rate (OLR) was (in kg COD/m^3.d): 6.92 in R1, and 5.4 in R2. The OLR values were dictated by the VER and cycle time.

Table 1. Seed sludge characteristics

Seed sludge characteristics	R1	R2
MLSS (mg/L)	7782	8233 ± 48 (4)
MLVSS (mg/L)	5240	6963 ± 120 (4)
MLVSS/MLSS	0.67	0.85 ± 0.010 (4)
SVI_{30} (mL/g)	125	119
Mean particle size (μm)	139.48	147.18

Table 2. SBR cycle of bioreactors

Phase description	R1	R2
	Duration	Duration
Fill	8 min	7 min
Aeration	2.55 → 2.87 h	3.33 → 3.63 h
Settle	18 → 6 min	30 → 12 min
Decant	8 min	3 min
Total cycle	3.12 h	4.00 h

The influent and effluent characteristics were monitored for pH and temperature (YSI MultiLab IDS 4010-3). Soluble COD (sCOD), ammonia nitrogen (NH_3-N), phosphate (P-PO_4) concentrations were analyzed based on Standard Methods using relevant Hach kits (APHA 2012). Since sodium acetate was the sole carbon source, volatile fatty acids (VFAs) concentration as acetic acid was monitored by Hach kit (TNT872). Nitrate nitrogen (NO_3-N) concentration was analyzed by ion chromatography (Metrohm 930 Compact IC Flex). Nan-particulate organic content (NPOC) was determined by Shimadzu TOC-L CPH. A constant ratio was established between NPOC and sCOD concentrations of the influent and the effluent, and was continuously controlled. Then after, sCOD analysis was replaced by fast and convenient NPOC measurement. Sludge properties, including mixed liquid suspended solids (MLSS), mixed liquor volatile suspended solids (MLVSS), sludge volume index (SVI) were analyzed in accordance with Standard Methods (APHA 2012). Particle size distribution (PSD) was measured with a Malvern Mastersizer 2000 (detection limit ≤ 2000 μm).

3   Results and Discussion

3.1   *Granulation Process*

Although aerobic granules could be easily cultivated in 2 to 3 weeks in the lab-scale bioreactor (R1), aerobic granulation failed in the pilot reactor (R2). Many strategies were applied in the pilot reactor (R2) to resolve the problem (data not shown): mixed seed culture (30% v/v inactive sludge, 70% activated sludge) (Ni et al. 2010),

high phosphate concentration (Juang et al. 2010), step feeding (Wan et al. 2009; Chen et al. 2013), and anaerobic/aerobic SBR cycle (Bao et al. 2009).

Eventually, the issue was identified as an improper aeration pattern in the pilot reactor (R2). Aeration rate, or in other words, upflow air velocity, was deemed to be the main source of hydrodynamic shear force in bubble column reactors. Shear force is known as one of the important inducers of aerobic granulation. Increase in aeration rate leads to increase in particle-gas-liquid interactions, and thus increases attrition on the surface of microbial particles. However, the findings of this study proved that air bubble distribution was of prior importance, as opposed to the effect of aeration rate.

Aerobic granulation was not achieved in R2 unless diffuser configuration was modified. The modification included replacing the single cube diffuser with four of identical size. The modified air diffuser configuration led to a well-distributed air bubble pattern that could completely cover the cross-sectional area of the pilot reactor (R2) at different heights. It was supposed that granulation did not occur in the pilot reactor (R2) with a lower number of diffusers due to dominance of low-turbulence local zones although identical superficial upflow air velocity (SUAV) of 3.0 cm/s was maintained under both conditions. Likewise, granules could not form in the lab-scale column (R1) when the aeration system was defective, and the air bubble distribution was not uniform.

Figure 2 shows changes in particle size distribution in the bioreactors during the granulation process. Median particle size reached 200 µm in 7 days in R1, and 16 days in R2 with modified diffuser configuration; corresponding 90th percentiles were 600 µm in R1, and 623 µm in R2. According to de Kreuk et al. (2007), aerobic granules are particles with size equal to or beyond 200 µm. Profiles of particles size analysis were identical to those reported by Coma et al. (2012) during aerobic granulation. Such trends of particle size distribution suggested that granulation occurred in 1 week in R1, and in 2 weeks in R2. Figure 3 shows the granules formed in R1 and R2.
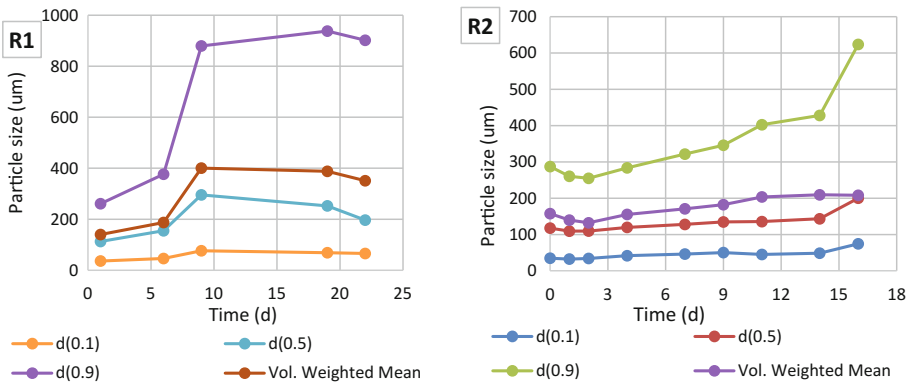
Fig. 2. Particle size distribution in small reactor (R1) and pilot reactor (R2) during the startup
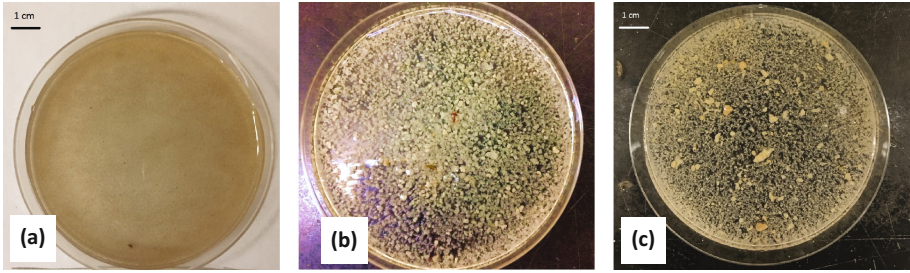
Fig. 3. Sludge morphology (a) in pilot reactor (R2) at day 1st; (b) in small reactor (R1) at day 18th; (c) in pilot reactor (R2) at day 23rd

Figure 4 depicts the alteration of feast/famine condition in a SBR cycle in R2 at day 3rd. Initial concentration of sCOD was 730 mg/L at the beginning of the SBR cycle. Considering the VER of 43% in R2, initial sCOD concentration of 820 mg/L could be predicted. Carbon source was depleted rapidly within 40 min of the cycle, which was distinguishable by sCOD and VFAs profiles. Thus, the biomass was subject to a long famine condition (over 2.8 h).
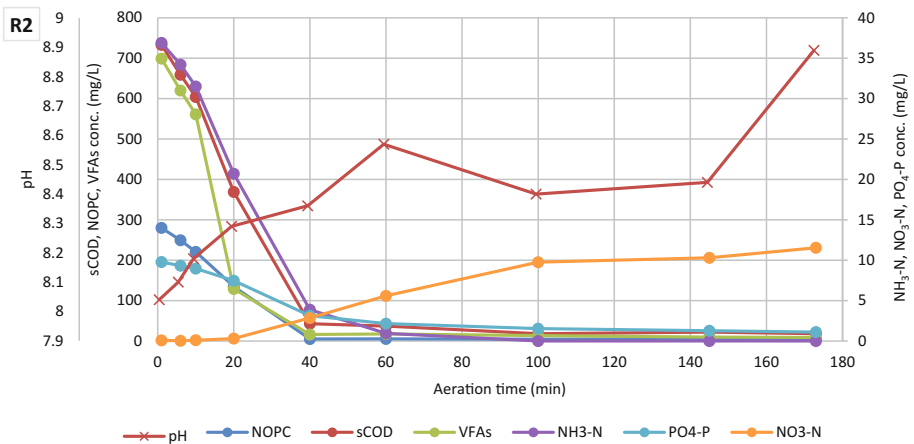
Fig. 4. Feast/famine regime in a cycle of R2 at day 3rd of startup

3.2 Crucial Effect of Air Bubble Distribution on Aerobic Granulation

A ratio was proposed for scale-up procedure (Eq. 1):

$$S = \frac{A_{R2}}{A_{R1}} \tag{1}$$

where S was scale-up ratio, and A_{R2} and A_{R1} were respective cross-sectional areas of pilot-reactor (R2) and lab-scale reactor (R1). In the current study, S = 3. Initially,

only the aeration rate was increased based on the scale-up ratio, from 9.1 L/min in R1 to 26 L/min in R2. Thus, equal SUAV of 3.0 cm/s was kept in both reactors. The SUAV has been defined as aeration rate per cross-sectional area of the reactor. Nevertheless, only one cube diffuser was mounted in the pilot reactor. When the diffuser surface area was increased based on the scale-up ratio as well, granulation occurred within 3–4 weeks in the pilot reactor (R2). The surface area was increased by replacing the single cube diffuser with four of identical size in R2 (see Fig. 1).

Based on the continuity equation, the aeration rate Q_A ($L^3.T^{-1}$) could be written in terms of both the SUAV and the actual upflow air velocity (AUAV):

$$Q_A = A_R\, U_{Sg} = A_b U_{Ag} \tag{2}$$

where U_{Sg} and U_{Ag} represented SUAV ($L.T^{-1}$), and AUAV ($L.T^{-1}$), and A_R and A_b stood for cross-sectional area of the reactor (L^2), and overall projected area of air bubble on the cross section of the reactor (L^2), respectively. If it was assumed that U_{Ag} must be the same for the two systems, and that the aeration rate should be scaled by S, then Eqs. 1 and 2 could give:

$$\frac{A_{b2}}{A_{R2}} = \frac{A_{b1}}{A_{R1}} \tag{3}$$

It was noted that if Eq. 3 was satisfied, then from Eqs. 1 and 2, the superficial velocity U_{SA} would also be the same for the two systems. The bubble area A_b could be defined as:

$$A_b = n_b.a_b \tag{4}$$

where n_b was the number of bubbles at a given cross section of the reactor, and a_b was the projected area (to the cross section) of a single air bubble (L^2). Assuming that bubble size and hence bubble area a_b was the same for the two reactors, Eqs. 3 and 4 produced:

$$\frac{n_{b2}}{A_{R2}} = \frac{n_{b1}}{A_{R1}} \tag{5}$$

which stated that the number of bubbles per *unit* cross-sectional area (L^{-2}) was the same for both reactors. This implied that the mean distance between bubbles would be identical for the two systems, which helped to ensure that the shearing activity was similar in small and pilot reactors. It appeared to be the critical requirement for successful granulation regardless of reactor size.

If diffusers of the same porosity were used, then producing more of the same bubbles by a factor of S (per Eqs. 1 and 5) was guaranteed by increasing the diffuser surface area by the same factor. That was,

$$\frac{A_{d2}}{A_{d1}} = S = \frac{A_{R2}}{A_{R1}} \tag{6}$$

where A_d was the overall surface area of the diffuser (L^2).

Equation 6 should be valid for any reactor design. It was assumed that air pressure was not controlled, thus, air pressure was increased proportionately along with increment in aeration rate. Based on Eq. 6, for successful scale-up, the porous area of the diffuser should be proportionally increased with the scale-up ratio S as well; if multiples of the same diffuser are used, the ratio S should only be applied to the surface area of the diffuser as the porosity stays constant. Accordingly, the number of the diffusers was increased in the current study. The proposed scale-up equation was valid until the wastewater composition and SBR cycle were kept constant. Under dissimilar circumstances, other parameters such as growth rate of organisms, air pressure, and OLR should be considered as well.

3.3 Mathematical Evaluation of the Theory

As discussed earlier, Eq. 6 was obtained based on the fact that shear force should be maintained constant, regardless of the scale of the reactor. However, increase in the aeration rate by the scale-up factor could not guarantee the similar shear activity unless a well-distributed aeration pattern was ensured and maintained as well. The shear force can be related to the drag force (F') that can be determined in SBR bubble column reactors as follows (Zhou et al. 2013):

$$F' = \frac{1}{2} C_D \rho_g \frac{\pi d_p^2}{4} u_{ng}^2 \tag{7}$$

where ρ_g is gas (or air) density ($M.L^{-3}$), d_p is particle diameter (L^3), and u_{ng} is net gas velocity ($L.T^{-1}$) which was equal to U_{Sg} over gas holdup, ε_g. In this study, $u_{ng} = U_{Ag}$. Gas hold, ε_g, has been defined as the ratio of gas phase volume to the total volume (Eq. 8). It could be measured by displacement method (Ramesh and Murugesan 2002). Drag coefficient, C_D, could be calculated using Eq. 9 that was valid over a complete range of Reynolds numbers (Zhou et al. 2013).

$$\varepsilon_g = (H_g - H)/H_g \tag{8}$$

$$C_D = \frac{24}{(Re)_p} \left[1 + 0.173(Re)_p^{0.657} \right] + \frac{0.413}{1 + 16.3(Re)_p^{-1.09}} \tag{9}$$

$$Re_p = \frac{d_p \rho_g u_g}{\mu_g} \tag{10}$$

where H and H_g were liquid heights (here, slurry or the mixed liquor) before and after aeration (L), Re_p was Reynolds number of the particles (dimensionless), μ_g was gas

viscosity ($M.L^{-1}.T^{-1}$), and u_g was the relative velocity between gas and a single particle which could be obtained as follows.

$$u_g = \left| U_{Ag} - u_p \right| \tag{11}$$

Number of diffusers could alter the drag force, regardless of the constant aeration rate. Supposedly, the drag force was affected by two means. First, increase in the number of diffusers led to a uniform bubble size distribution which could increase the gas holdup, ε_g. Large coalesced bubbles tended to rise faster, and thus, reduction in gas residence time decreased the gas holdup (Moshtari et al. 2009). Net gas velocity or actual upflow air velocity (U_{Ag}) had an inverse relation with the gas holdup (see Eq. 9). Thus, U_{Ag} decreases with an increase in ε_g although superficial air velocity (U_{Sg}) was kept constant. Decrease in U_{Ag} could decrease the drag force correspondingly (see Eq. 7). Second, decrease in U_{Ag} could reduce relative gas-particle velocity (see Eq. 11), which could decrease the drag coefficient, and thus, the drag force (see Eq. 8).

Gas holdup seemed to be the most important parameter in bubble column reactors that could define the prevailing hydrodynamic regime. Gas holdup regulated interfacial area, mass diffusion rate, and mean residence time of the gas phase (Moshtari et al. 2009; Saravanan et al. 2009). The results of this study suggested the effect of average air bubble size, air bubble density, and air bubble velocity on gas holdup. Many researchers investigated gas holdup in bubble column reactors in the field of chemical engineering (Hikita et al. 1980; Moshtari et al. 2009; Strasser and Wonders 2012; Ramesh and Murugesan 2002). Moshtari et al. (2009) discussed that developing an appropriate relation between superficial gas velocity, gas holdup, and the type of gas sparger played a key role in scaling up slurry bubble column reactors; the investigator demonstrated that different bubble size and gas holdup could be achieved using porous and perforated sparger although both spargers had identical porosities. However, there is a lack of proper communication between the two fields, i.e. chemical engineering and environmental engineering. Although aerobic granules have been mainly cultivated in bubble column reactors, there is a lack of knowledge about the relation between the gas holdup and the shear force in aerobic granular bioreactors. While the shear force has been properly identified as the crucial inducer of aerobic granulation, it has always been related to SUAV. However, the findings of this study proved that the SUAV parameter could not well represent the hydrodynamics of bubble column reactor, especially during the scale-up procedure.

4   Conclusion and Perspective

This study suggested that gas hold up was the most crucial factor for the scale-up of aerobic granular bubble column reactors. The gas holdup was dictated by air bubble distribution rather than the aeration rate. This study proved that the superficial upflow air velocity (SUAV) which has been defined as aeration rate per cross-section area of the reactor could not well represent the hydrodynamics of bubble column reactor, especially during the scale-up procedure. However, the results of this study should be further investigated and validated:

- A scale-up equation was proposed which was valid until the wastewater composition and SBR cycle were kept constant. Under dissimilar circumstances, other parameters such as growth rate of organisms, air pressure, and OLR should be considered as well.
- Air bubble distribution in terms of size and density, gas holdup, and net gas velocity (actual upflow air velocity) should be experimentally verified in the same pilot reactor with different diffuser configurations.

References

APHA (2012) Standard methods for the examination of water and wastewater. book, 22nd edn. American Public Health Association/American Water Works Association/Water Environment Federation, Washington, DC

Bao R, Yu S, Shi W, Zhang X, Wang Y (2009) Aerobic granules formation and nutrients removal characteristics in sequencing batch airlift reactor (SBAR) at low temperature. J Hazard Mater 168(2):1334–1340

Chen FY, Liu YQ, Tay JH, Ning P (2013) Alternating anoxic/oxic condition combined with step-feeding mode for nitrogen removal in granular sequencing batch reactors (GSBRs). Sep Purif Technol 105:63–68

Coma M, Verawaty M, Pijuan M, Yuan Z, Bond PL (2012) Enhancing aerobic granulation for biological nutrient removal from domestic wastewater. Bioresour Technol 103(1):101–108

Hikita H, Asai S, Tanigawa K, Segawa K, Kitao M (1980) Gas hold-up in bubble columns. Chem Eng J 20:59–67

Isanta E, Suárez-Ojeda ME, Val del Río A, Morales N, Pérez J, Carrera J (2012) Long-term operation of a granular sequencing batch reactor at pilot scale treating a low-strength wastewater. Chem Eng J 198–199:163–170

Juang YC, Adav SS, Lee DJ, Tay JH (2010) Stable aerobic granules for continuous-flow reactors: precipitating calcium and iron salts in granular interiors. Biores Technol 101 (21):8051–8057

de Kreuk MK, Kishida N, van Loosdrecht MCM (2007) Aerobic granular sludge–state of the art. Water Sci Technol 55(8–9):75–81

de Kreuk MK, Heijnen JJ, van Loosdrecht MCM (2005) Simultaneous COD, nitrogen, and phosphate removal by aerobic granular sludge. Biotechnol Bioeng 90(6):761–769

Long B, Yang CZ, Pu WH, Yang JK, Jiang GS, Dan JF, Li CY, Liu FB (2014) Rapid cultivation of aerobic granular sludge in a pilot scale sequencing batch reactor. Biores Technol 166:57–63

Moshtari B, Babakhani EG, Moghaddas JS (2009) Experimental study of gas hold-up and bubble behavior in gas–liquid bubble column. Pet Coal 51(1):27–32

Moy BYP, Tay JH, Toh SK, Liu Y, Tay STL (2002) High organic loading influences the physical characteristics of aerobic sludge granules. Lett Appl Microbiol 34(6):407–412

Ni BJ, Xie WM, Liu SG, Yu HQ, Wang YZ, Wang G, Dai XL (2009) Granulation of activated sludge in a pilot-scale sequencing batch reactor for the treatment of low-strength municipal wastewater. Water Res 43(3):751–761

Ni SQ, Fessehaie A, Lee PH, Gao BY, Xu X, Sung S (2010) Interaction of anammox bacteria and inactive methanogenic granules under high nitrogen selective pressure. Biores Technol 101(18):6910–6915

Rocktäschel T, Klarmann C, Ochoa J, Boisson P, Sørensen K, Horn H (2015) Influence of the granulation grade on the concentration of suspended solids in the effluent of a pilot scale sequencing batch reactor operated with aerobic granular sludge. Sep Purif Technol 142:234–241

Saravanan K, Ramamurthy V, Chandramohan K (2009) Gas hold up in multiple impeller agitated vessels. Mod Appl Sci 3(2):49–59

Strasser W, Wonders A (2012) Hydrokinetic optimization of commercial scale slurry bubble column reactor. AIChE J 58(3):946–956

Tay JH, Liu QS, Liu Y, Show KY, Ivanov V, Tay STL (2005) A comparative study of aerobic granulation in pilot-and laboratory-scale SBRs. In: Bathe S, de Kreuk M, McSwain B, Schwarzenbeck N (eds) Aerobic granular sludge. Book. IWA publishing, London

Wan J, Bessière Y, Spérandio M (2009) Alternating anoxic feast/aerobic famine condition for improving granular sludge formation in sequencing batch airlift reactor at reduced aeration rate. Water Res 43(20):5097–5108

Yi S, Zhuang WQ, Wu B, Tay STL, Tay JH (2006) Biodegradation of P-Nitrophenol by aerobic granules in a sequencing batch reactor. Environ Sci Technol 40(7):2396–2401

Yilmaz G, Lemaire R, Keller J, Yuan Z (2008) Simultaneous nitrification, denitrification, and phosphorus removal from nutrient-rich industrial wastewater using granular sludge. Biotechnol Bioeng 100(3):529–541

Zhang M, Tay JH, Qian Y, Gu XS (1997) Comparison between anaerobic-anoxic-oxic and anoxic-oxic systems for coke plant wastewater treatment. J Environ Eng 123(9):876–883

Zhang Y, Tay JH (2012) Co-metabolic degradation activities of trichloroethylene by phenol-grown aerobic granules. J Biotechnol 162(2–3):274–282

Zhou D, Liu M, Wang J, Dong S, Cui N, Gao L (2013) Granulation of activated sludge in a continuous flow airlift reactor by strong drag force. Biotechnol Bioprocess Eng 18(2):289–299

Coupling Multiphase Hydrodynamic Simulations and Biological Modelling of an Anammox Reactor

A. Vilà-Rovira[✉], M. Ruscalleda, M.D. Balaguer, and J. Colprim

LEQUIA, Institute of the Environment, University of Girona, Campus Montilivi,
Carrer Maria Aurèlia Capmany, 69, 17003 Girona, Catalonia, Spain
albert.vila@lequia.udg.cat

Abstract. This study integrated Computational Fluid Dynamics (CFD) and biological modeling (Activated Sludge Models) for the description of a novel anammox reactor configuration. This results in a full description of the hydrodynamics, the mixing degree of the system and biological performance within the overall reactor domain. The large recirculation of the system and the internal plates favored the correct mixing of the overall system, despite a particular point of preferable way of flow in the inlet stream of the reactor. From the removal rates distributions calculated with CFD and biomodel, it was feasible to demonstrate that the 45% of the domain had a zero reaction order in respect with the ammonium substrate (nitrite was in excess). The use of CFD and biomodels was demonstrated to be a powerful tool for the design and optimization of novel biological reactors, and especially for the Anammox process.

Keywords: Anammox · Computational fluid dynamics · Biological models · Multiphase simulations

1 Introduction

Autotrophic nitrogen removal by the anaerobic ammonium oxidation (anammox) process is a cost-efficient technology for the treatment of wastewater with low C/N ratio. The number of full-scale anammox reactors is still limited but continuously increasing over the world (Lackner et al. 2014). Anammox biomass is characterized by a slow growing rate (one of the main barriers for new full-scale implementations) and its capacity to form granules or biofilms. Despite several authors formulated bio-kinetic models for describing anammox process (Ni et al. 2009), hydraulic parameters play and important role in the granulation/biofilm formation and substrate distribution, among others, but have never been considered so far in modelling. The inclusion of Computational Fluid Dynamics (CFD) in wastewater treatment processes modelling is starting to be used as step forward in reactor design and optimization (Samstag et al. 2016). The aim of this study is the development of the first modelling approach integrating an anammox biological model with multiphase hydrodynamic model, as a new tool for anammox reactor design assessment.

2   Materials and Methods

CFD simulations were developed using Euler-Euler multiphase model (Versteeg and Malalasekera 1995). It included a water based primary phase (as a mixture of nitrogenous dissolved species) and nitrogen gas as a secondary dispersed phase. The flow conditions of the system involved turbulent conditions, which were accounted considering a realizable k-ε turbulent model (Andersson 2012). Boundary conditions were formulated with velocity inlet and degassing (gas escaping at the liquid interphase) profiles. The mesh size used in this study was of 850717 elements. Simulations were performed with an Intel Xenon CPU, with a processor of 2.27 GHz and 23.9 GB of RAM. The biokinetic model was formulated with an extension of ASM1 for describing the Anammox growth process rate (Takács et al. 2007). The stoichiometric and kinetic parameters values were obtained from the literature (Ni et al. 2009). A constant concentration of Anammox biomass within the overall domain was assumed in simulations. Influent was assumed to contain only dissolved nitrogen species (ammonium and nitrite, as well as the dissolved nitrogen gas and nitrate from the recirculation, once both flows were mixed).

The reactor design used in this work to test the model was a 430 L cylindrical anammox reactor, with an internal diameter of 0.502 m and 2.6 m of height (Fig. 1). A recirculation stream (QR) was implemented from the top to the bottom column to promote substrate distribution and kept the biomass suspended. The reactor was continuously fed from the bottom part (Q_{in}^0) and the outlet stream (Q_{out}) was derived from the recirculation. A set of internal plates was equally distributed along the reactor height (with alternate orientation) to ensure turbulence and granular sludge retention. Nitrogen gas, generated by anammox bacteria, was accumulated at the head space of
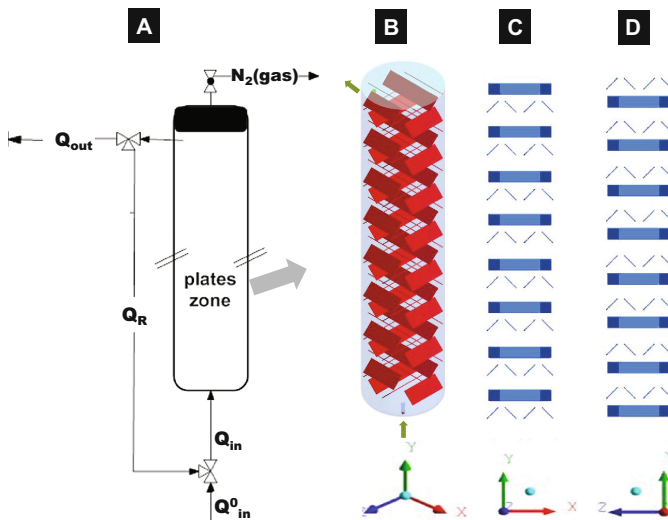
Fig. 1. Schematic representation of the model

the top of the column until the overpressure valve was opened. Operating temperature and pressure were set at 308.15 K and 1 atm, respectively.

3   Results and Discussion

The use of CFD permitted to determine the internal flux distribution in the anammox reactor, which determines the substrate distribution as well the solids suspension within the reactor domain. This is in advantage on conventional assumptions of ideal mixing conditions, since preferable ways of flow or death zones, among other conditions, can be identified within the reactor domain. The system modelled in this study had a large recirculation ratio (1:100) to ensure maximum homogenization, with daily inflow of 0.34 m^3·d^{-1}. The streamlines obtained from CFD simulation revealed the formation of internal recirculation streams, due the presence of the plates, and the generation of death zones at the lowest part of the reactor. The fluid was circulating upwards between the plates and downwards near the reactor wall and at the center of the reactor. Based on this, CFD provides the ratio of positive (upwards) and negative (downwards) velocities: 53% and 43%, respectively. This produces an overall mixing effect that ensures system homogenization between plates.

Moreover, CFD permitted also determining the reactor Residence Time Distribution (RTD) Function (E), which offered a description about the mixing conditions (Fig. 2-B/C). Parameters describing the RTD are presented in Table 1, the space time
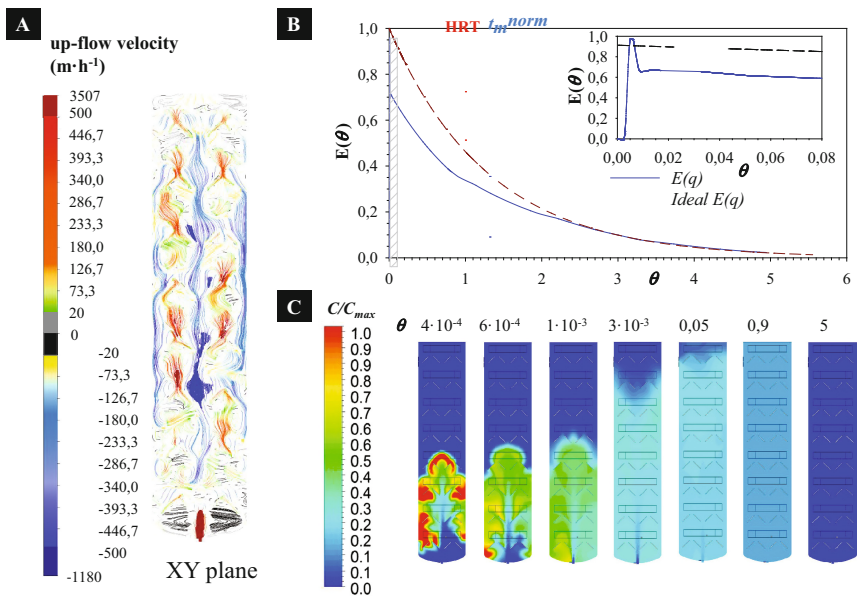
Fig. 2. Results from hydrodynamic simulation: (A) up flow velocity streamlines. (B) Residence Time Distribution (system and ideal conditions). (C) Contours of tracer concentration at different time of the distribution

Table 1. Results obtained from the Residence Time Distribution

Parameter	Value	Unit
t_m	1.72	d
σ^2	2.1	d^2
n (tanks in series)	0.9	–
α (quality number)	0.72	–

(1.3 d) was close to the mean residence time (tm = 1.7 d), indicating the closeness of the studied system to ideal mixing conditions. Additionally, the variance of the distribution (σ^2 = 2.1 d^2) indicated a spread distribution for residence time, mainly produced by the large recirculation as well as the presence of internal plates. Considering the model of Tanks in Series (n = 0.9; Fogler 2006), and the quality number obtained (0,72 in front of 0,625 for ideal conditions), it is reasonable to assume that the flow inside the column was practically perfectly mixed.

The distribution of substrate is also determining whether the biomass has the proper local conditions to be active in each zone along the reactor. In this sense, the use of CFD provides the advantage of obtaining a full description of the species distribution and the cell-specific removal rates of the system. For the case analysed in this study, the maximum removal rates are close to the reactor's loading rate (0.4 kg N·m^{-3}·d^{-1} at the bottom part of the reactor). Additionally, the use of CFD made possible knowing the reaction order at the different parts of the domain (Fig. 3C): a 45% of the liquid domain ha a maximum removal rate (zero order) with respect to the ammonium specie concentration. The nitrogen gas generation by anammox bacteria adds complexity to the model development by CFD. The model developed in this study considered that liquid was totally saturated of nitrogen gas (because of the large recirculation ratio) and the generated gas was directly released to the gas phase. Additionally, the system considered the upper boundary of the system as a free surface, from which gas scapped and the liquid was kept in the reactor (degassing boundary condition). For this reason the nitrogen gas volume fraction circulating within the liquid domain was quite low (volume fraction order of 1·10^{-3}) (Fig. 3E).
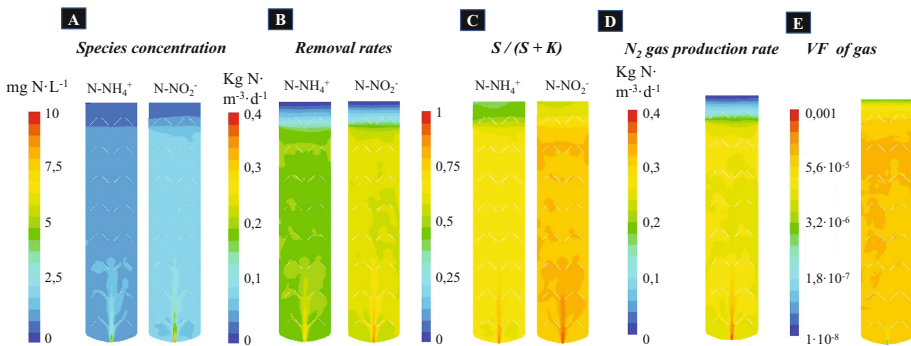
Fig. 3. Results from the biokinetic model: (A) Species concentration, (B) removal rates, (C) Monod terms ($S_x/(S_x + K_x)$), (D) Nitrogen gas generation rate, (E) VF_{gas}

4 Conclusions

The first modelling approach for an anammox reactor combining CFD and biokinetic model was developed. From this model, detailed information about species, phases and reaction rates were obtained allowing the optimization of process performance based on hydraulic parameters.

References

Andersson BEA (2012) Computational fluid dynamics for engineers

Fogler HS (2006) Elements of chemical reaction engineering. Prentice Hall PTR international series in the physical and chemical engineering sciences. doi:10.1016/0009-2509(87)80130-6

Lackner S, Gilbert EM, Vlaeminck SE, Joss A, Horn H, van Loosdrecht MCM (2014) Full-scale partial nitritation/anammox experiences - an application survey. Water Res 55:292–303. doi:10.1016/j.watres.2014.02.032

Ni B-J, Chen Y-P, Liu S-Y, Fang F, Xie W-M, Yu H-Q (2009) Modeling a granule-based anaerobic ammonium oxidizing (ANAMMOX) process. Biotechnol Bioeng 103:490–9. doi:10.1002/bit.22279

Samstag RW, Ducoste JJ, Griborio A, Nopens I, Batstone DJ, Wicks JD, Saunders S, Wicklein EA, Kenny G, Laurent J (2016) CFD for wastewater treatment: an overview. Water Sci Technol 74:549–563. doi:10.2166/wst.2016.249

Takács I, Vanrolleghem P, Wett B, Murthy S (2007) Elemental balance based methodology to establish reaction stoichiometry in environmental modeling. Water Sci Technol 56:37–41. doi:10.2166/wst.2007.606

Versteeg H, Malalasekera W (1995) An introduction to computational fluid dynamics the finite volume method

Understanding and Optimizing Peracetic Acid Disinfection Processes Using Computational Fluid Dynamics: The Case Study of Nocera (Italy) Wastewater Treatment Plant

R. Maffettone[1]([⊠]), F. Crapulli[2], S. Sarathy[4], L. Pucci[4], L. Rizzo[5], G. Lofrano[6], G. Raspa[7], S. Guadagnuolo[4], R. De Rosa[4], A. Giuliani[4], M. Carotenuto[8], S. Luise[8], and D. Santoro[3]

[1] Department of Civil Engineering, McGill University, Montreal, Canada
[2] Department of Chemical and Biochemical Engineering, Western University, London, ON, Canada
[3] Trojan Technologies, London, ON, Canada
[4] CONSORZIO NOCERA AMBIENTE, Nocera Superiore, SA, Italy
[5] Department of Civil Engineering, University of Salerno, Fisciano, SA, Italy
[6] Department of Chemistry and Biology, University of Salerno, Fisciano, SA, Italy
[7] Department of Chemical Engineering Material and Environment, La Sapienza University, Rome, Italy
[8] Hach Lange, Milan, Italy

Abstract. In this paper, a modeling study focused on optimizing the PAA disinfection performance in a full-scale contact tank currently operated at the Nocera (Italy) Wastewater Treatment Plant is presented. The disinfection process was monitored for over 2 weeks by collecting full-scale data on plant variability in flow, disinfectant demand/decay and microbial concentrations. A computational fluid dynamics (CFD) model of the contact tank describing the PAA disinfection process was developed. Four disinfection scenarios were analysed using an Eulerian-Lagrangian approach: (a) PAA disinfection under the existing conditions; (b) PAA disinfection with PAA pre-mixed prior to the contact tank; (c) PAA disinfection with PAA dosed with 8 injection points distributed over the entire length of the inlet weir; (d) PAA disinfection in an optimized plug-flow contact tank. All these scenarios were analysed for the same operating conditions, i.e. fixed flow, PAA demand/decay and inactivation kinetics. The model-based analysis clearly revealed that the optimized contact tank (scenario d) was able to achieve a much higher contact and extended between microorganisms and disinfectant thus resulting into a five-fold increase in microbial inactivation.

Keywords: Peracetic acid · Wastewater disinfection · Computational fluid dynamics

1   Introduction

Disinfection process plays a central role in wastewater treatment as it controls the release of pathogens in the environment. Peracetic Acid (PAA) is a widely used disinfectant in wastewater treatment that is substituting the use of chlorine, which is related to a concern of the disinfection by-products. The number of PAA disinfection installations is increasing in municipal wastewaters worldwide as well as in Italy. Advanced disinfection modelling strategies are required in order to achieve such complex balance among all the involved variables. In this work, a modeling study focused on optimizing the PAA disinfection performance of a full-scale contact tank currently operated at the Nocera (Italy) Wastewater Treatment Plant is presented. As a first step, the disinfection process was monitored for 2 weeks to collect full-scale real data on plant variability in flow, disinfectant demand and decay, and inlet/outlet microbial concentrations. These data have been used to develop an influent model able to track microbial dynamics (*Escherichia coli* used as indicator) as a function of the incoming flowrate and other water quality parameters. Such influent model was subsequently used as the input to a Computational Fluid Dynamics (CFD) model to comprehensively describe the disinfection process occurring in the contact tank in terms of reactor hydrodynamics, disinfectant decay and microbial inactivation in Eulerian and Lagrangian frameworks. Four scenarios were simulated and compared: (a) PAA disinfection under the existing conditions (scenario a); (b) PAA disinfection where PAA pre-mixed prior to the contact tank (scenario b); (c) PAA disinfection with PAA dosed with 8 injection points distributed over the entire length of the inlet weir (scenario c); (d) PAA disinfection in an optimized plug-flow contact tank (scenario d).

2   Materials and Methods

Relevant plant data were collected from the Nocera WWTP (Italy) for over two weeks. Viable *E.coli* concentration was enumerated in samples collected using two auto-samplers installed at the inlet and outlet of the contact tank. Each sample collector was set to collect 1 L sample every 20 min. Sodium thiosulphate (0.1 N) was added into the samples at the outlet to quench the residual PAA. Microbial counts were conducted in all collected samples using the membrane filtration method (Standard method 9222). PAA concentration in the contact tank was measured using the DPD method. PAA demand decay test were conducted at bench scale measuring the PAA residuals and *E.coli* inactivation at different contact times. Microbial data were modelled in order to estimate the dose-response of *E.coli* as a function of the PAA dose. The geometries of the existing contact tank in Nocera as well as the optimized baffled tank were reproduced and discretized in control elements using ANSYS Gambit v.2.4.6 (Ansys Inc., Canonsburg, USA) resulting in 5,100,000 total elements. The Nocera contact tank and the optimized one have identical volume with dimensions of 28 m 29.5 m $\times$ 3.5 m. Due to the high gradients of fluid velocity and PAA concentration at the top region of the tank, the entire volume was discretized into two parts: an upper region with depth of 0.3 m divided into 2,250,000 quad elements and the lower region divided in the remain 2,850,000 elements. CFD simulations were carried out using
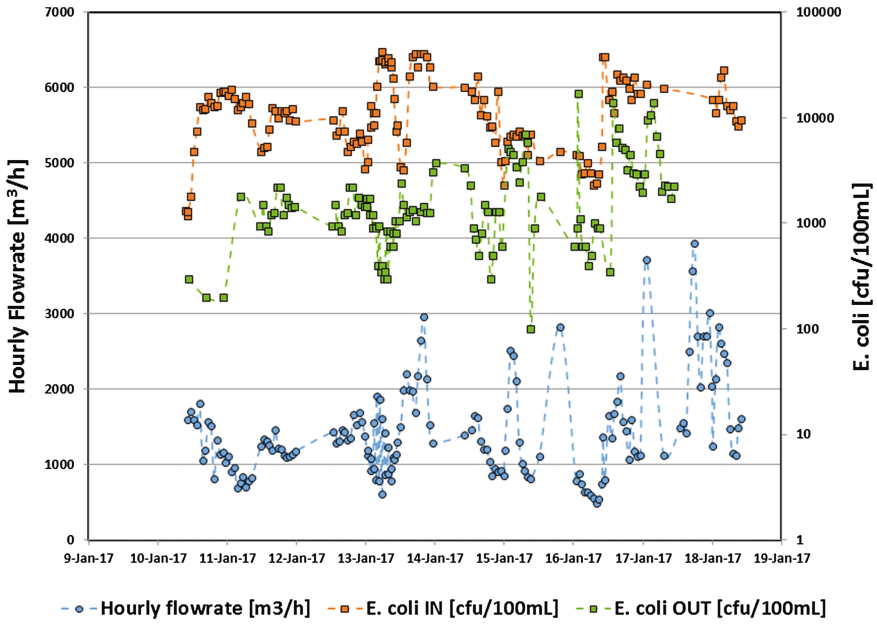
Fig. 1. Hourly flow rate and *E. coli* variability at inlet and outlet
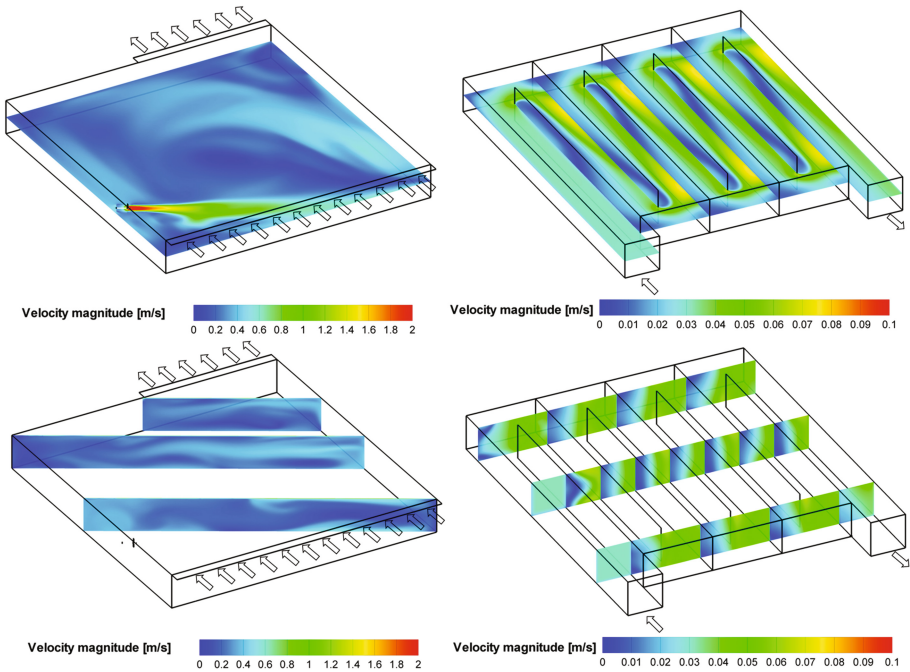
Fig. 2. Comparison between the existing (Nocera) vs. optimized baffle tanks for velocity magnitude [m/s]

Ansys Fluent v.12.1. A mass-flow boundary condition was set to specify the operating flowrate (1,356 m³/h) at the reactor inlet. The velocity pattern was defined by solving the continuity and Navier-Stokes equations for incompressible fluids. Reynolds number was below 2,000 therefore a laminar model was chosen in these simulations. A user-define-function (UDF) was implemented to calculate the PAA decay and CT dose delivered by the contact tank assuming 0.02793 1/min as first-order kinetic constant decay. In order to compare in a Eulerian-Lagrangian framework the disinfection performance of several reactor tank configurations, 5,000 massless and neutrally-buoyant particles were injected from the inlet and the PAA dose-per-particle was calculated.

3   Results and Discussions

Figure 1 shows the experimental data collected during the plant survey with the intent of characterizing the plant variability both in terms of microbial concentration entering/exiting the disinfection system and contact chamber flowrate. As the plot clearly shows, temporal structures are present in all the time series collected during the
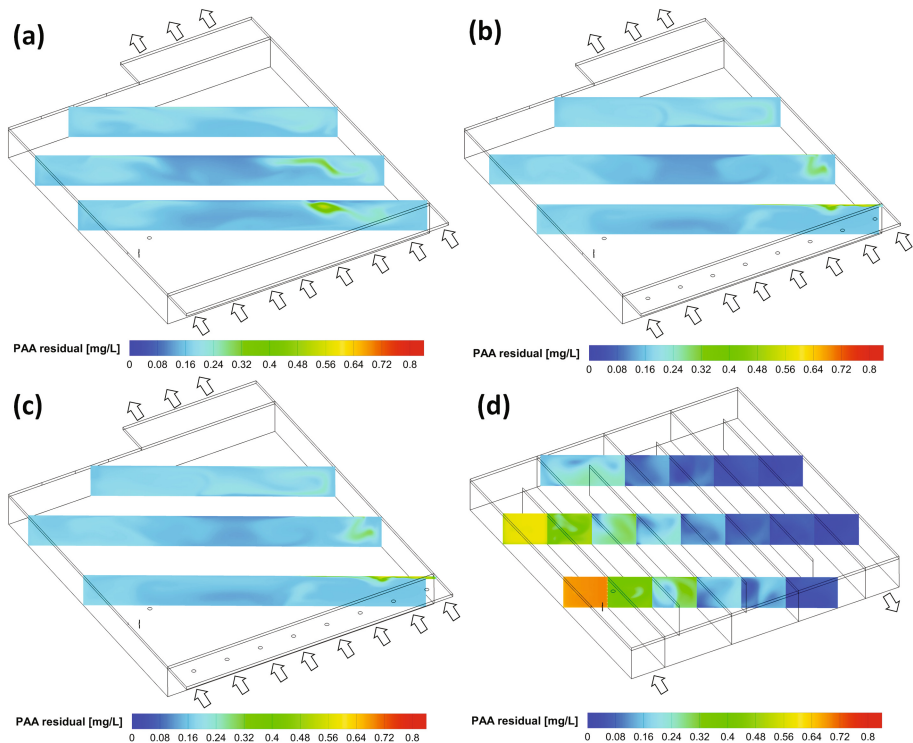
Fig. 3. Comparison between four process configurations: (a) scenario a; (b) scenario b; (c) scenario c; (d) scenario d

plant survey, confirming the importance of an influent model to take into account the water quality dynamics at play.

Figure 2 shows the contour of velocity magnitude along the horizontal middle-plane. It can be noticed that the existing contact tank currently operated at the Nocera plant is strongly affected by partial mixing and severe hydraulic short-circuiting, while the optimized baffled contact tank behaves like an almost ideal plug-flow reactor. In Fig. 3, the contours of PAA residual are shown for the four different scenarios. The contour plots confirm the hydraulic inefficiencies existing in the contact tank of Nocera (scenario a) as compared to the optimized baffled tank leading to a wide dose distribution (scenario d). The opposite is true for the optimized scenario as a consequence of more ideal hydraulic and disinfectant distribution in the tank (Fig. 4). In order to determine the extent of microbial inactivation, a segregated flow model was assumed and the experimental disinfection kinetics were mathematically convoluted with the Lagrangian dose distributions. Figure 5 shows that the CFD-optimized baffled tank performs much better in terms of microbial disinfection compared to the existing contact tank in Nocera.
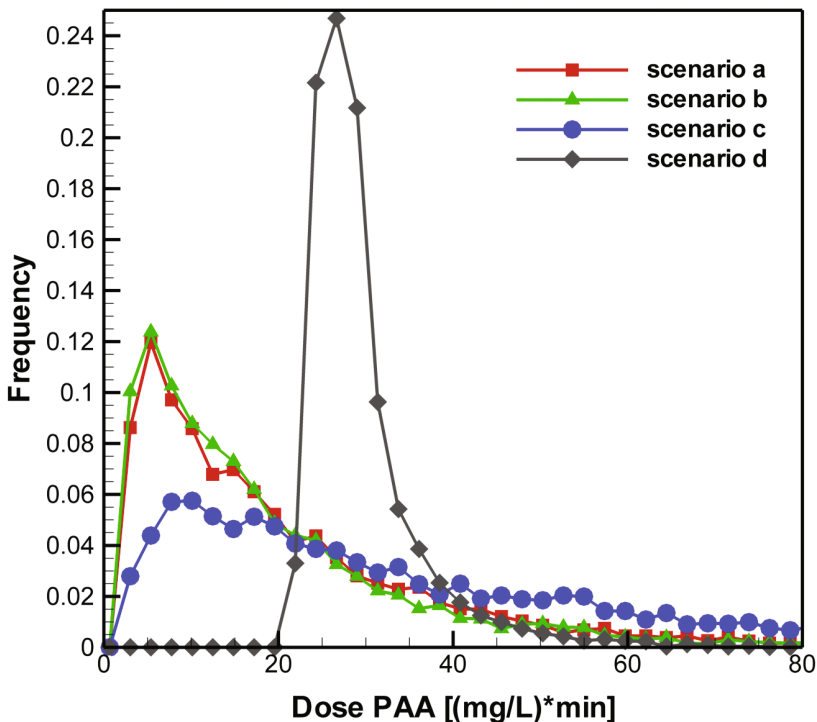
Fig. 4. PAA dose-per-particle distributions. Comparison among different scenarios: scenario a (red square), scenario b (green triangle), scenario c (blue circle), scenario d (black diamond)
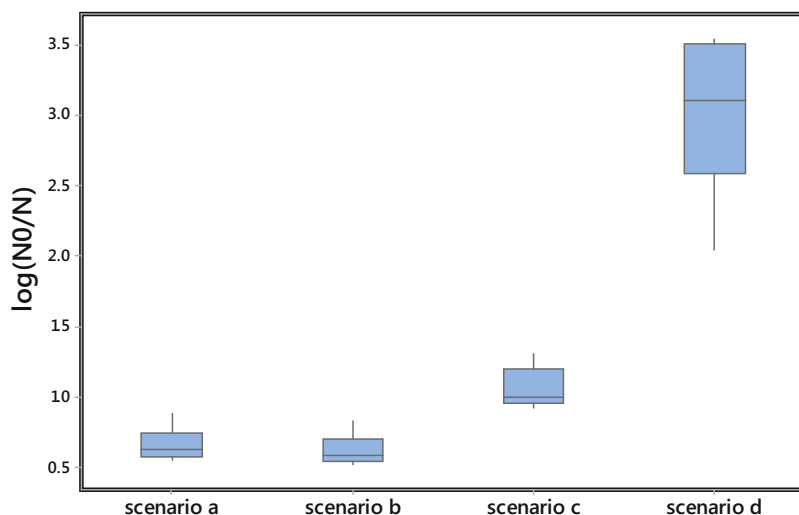
Fig. 5. Microbial inactivation (log scale) for the four investigated process scenarios

4 Conclusions

In this paper, the usefulness of a CFD-based analysis of disinfection processes occurring in a contact tankis reported. Numerical simulations were used to optimize disinfection performance of a full-scale contact tank currently operated at the Nocera (Italy) Wastewater Treatment Plant. Four scenarios were simulated and compared: (a) PAA disinfection under the existing conditions; (b) PAA disinfection with PAA pre-mixed prior to the contact tank; (c) PAA disinfection with PAA dosed with 8 injection points distributed over the entire length of the inlet weir; (d) PAA disinfection in an optimized plug-flow contact tank. Results showed how the optimized baffled contact tank was able to deliver a five-fold improvement in terms of log inactivation when compared against the existing scenario.

References

Dell'Erba A, Falsanisi D, Liberti L, Notarnicola M, Santoro D (2007) Disinfection by-products formation during wastewater disinfection with peracetic acid. Desalination 215(1–3):177–186

Koivunen J, Heinonen-Tanski H (2005) Peracetic acid (PAA) disinfection of primary, secondary and tertiary treated municipal wastewaters. Water Res 39(18):4445–4453

Lazarova V, Janex ML, Fiksdal L, Oberg C, Barcina I, Pommepuy M (1998) Advanced wastewater disinfection technologies: Short and long term efficiency. Water Sci Technol 38 (12):109–117

Santoro D, Gehr R, Bartrand TA, Liberti L, Notarnicola M, Dell'Erba A, Falsanisi D, Haas CN (2007) Wastewater disinfection by peracetic acid: Assessment of models for tracking residual measurements and inactivation. Water Env Res 79(7):775–787

Santoro D, Crapulli F, Raisee M, Raspa G, Haas CN (2015) Nondeterministic Computational Fluid Dynamics Modeling of Escherichia coli Inactivation by Peracetic Acid in Municipal Wastewater Contact Tanks. Environ Sci Technol 49(12):7265–7275

Modelling a Multiple Reference Frame Approach in an Oxidation Ditch of Activated Sludge Wastewater Treatment

Hossein Norouzi Firouz[(✉)], Mohammad-Hossein Sarrafzadeh, and Reza Zarghami

UNESCO Chair on Water Reuse, School of Chemical Engineering, College of Engineering, University of Tehran, Tehran, Iran
{h.norouzi7, sarrafzah, rzarghami}@ut.ac.ir

Abstract. Oxidation ditches (OD) are one of the most common aeration units or bioreactors in the activated sludge process. Flow and hydrodynamic characteristics play an important role in successful operation of an OD. It is difficult to study the rheology in a detailed way because it's time-consuming and expensive. However, due to the development of computational fluid dynamics (CFD), such a study has become easier and less expensive. CFD is a powerful tool to simulate the hydrodynamics. Since in mixing operations, the generation of fluid flow is due to the input of mechanical energy in form of rotation of the impeller, the one of very important consideration is the choice of a model that describes impeller rotation. The flow features associated with multiple rotating parts can be analyzed using the multiple reference frame (MRF) capability. Based on previous studies on OD in the field of wastewater treatment (few numbers has been done) there is no direct mention of the size of rotating zone for the simulation so a fundamental analysis is required and can be helpful for further studies in this field. In this study the effect of rotating zone dimensions on the accuracy of oxidation ditch simulation has been analyzed and four model of moving frame have been set and simulated. Based on the analysis the bigger the radius of rotating zone is the higher the accuracy of modelling is. Moreover, the rotating zone in multiple reference approach cannot be semi-circle.

Keywords: CFD · Wastewater treatment · Oxidation ditch · Multiple reference frame (MRF)

1 Introduction

In urban wastewater treatment, the main process to treat nitrogen and organic components of wastewater is the activated sludge one. Aeration in this process can represent up to 70% of the total energy expenditure of the plant (Yannick Fayolle 2007). Hence, optimization and design of the aeration is crucial and necessary because it reduces not only the cost of treatment but also improves the quality of desirable outputs. Oxidation ditches (OD) are one of the most common aeration units or bioreactors in the activated sludge process. The popularity of the OD is mainly due to its reliability, simplicity of operation and good treatment performance. Several types of

OD are used in the wastewater treatment plants however a three-dimensional solid–liquid two phase flow field in an oxidation ditch aerated with surface aerators was the main objective of this paper.

Flow and hydrodynamic characteristics play an important role in successful operation of an OD. It is difficult to study the rheology in a detailed way because it's time-consuming and expensive. However, due to the development of computational fluid dynamics (CFD), such a study has become easier and less expensive. CFD is a powerful tool to simulate the hydrodynamics and it has become increasingly popular in optimizing design and operation of waste water treatment plants (WWTPs). Since in mixing operations, the generation of fluid flow is due to the input of mechanical energy in form of rotation of the impeller, the one of very important consideration is the choice of a model that describes impeller rotation. The flow features associated with multiple rotating parts can be analysed using the multiple reference frame (MRF) capability.

Within this approach, the region in the vicinity of the impeller is solved using rotating frame of reference and the rest of the computational domain is solved in stationary frame of reference. It is obvious that the rotating region must embed the impeller geometry, the selection of the outer diameter of this region is however left to the skill of the user. Since the flow field, especially viscous stresses, in the vicinity of the blades is of primary importance in dispersion processes, the width and height of the rotating region can influence the quality of computational results (Zadravec 2007). Based on previous studies on OD in the field of wastewater treatment (few numbers has been done) there is no direct mention of the size of rotating zone for the simulation so a fundamental analysis is required and can be helpful for further studies in this field. In this study the effect of rotating zone dimensions on the accuracy of oxidation ditch simulation has been analysed.

2   Materials and Methods

For the validation of simulation, the experimental data of a study by Fan et al. (2010) has been used which are performed in a lab-scale oxidation ditch with a height of 120 mm which is designed according to that in a wastewater treatment plant (Long Fan 2010). The three-dimensional flow field in the oxidation ditch aerated with surface aerators like inverse umbrella is simulated. In Figs. 1 and 2 the geometry of oxidation ditch and the prepared mesh are shown, respectively.
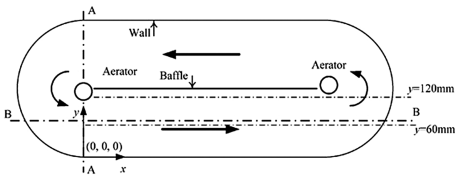
Fig. 1. The geometry of OD
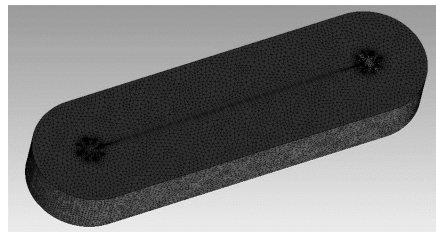
Fig. 2. The prepared mesh

The solid–liquid two-phase flow is modelled in the same oxidation ditch as in experiments. The simulation is limited to three-dimensional, steady state in a turbulent flow regime and turbulent effects are modelled by the standard k–ε model. All meshes are unstructured and composed of tetrahedrons. The number of grids is 564584.

The MRF method is used to simulate the flow field in the oxidation ditch. There are three reference frames in the whole flow field. One is inertial stationary reference and two are non-inertial rotating references. The domains circulating two aerators are calculated in the non inertial reference frames and the other domains are calculated in the inertial reference frame. The axes of two rotating references are the centreline of each aerator.

In order to analyse the influence of different dimensions of rotating zone, four model of moving frame have been set and simulated which can be seen in Table 1. In Fig. 3 the shape of the models are shown.

Table 1. Dimensionsof proposed rotating zones

Model No.	Diameter (mm)	Detail
1	32	Min.R
2	144	Mid R
3	288	Max.R
4	288	Semi circle
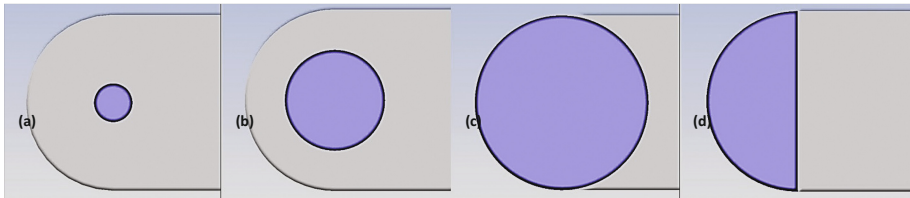
Fig. 3. Models of rotating zone: (a) minimum R- (b) middle R- (c) maximum R- (d) semi circle

3 Results and Discussions

Results of simulation have been illustrated in Fig. 4. As the diagram shows, the rotating zone with maximum radius has the closest result to the experimental data. Furthermore, as expected, the semi-circle model is far from the real circumstances and cannot be chosen.

On the other hand and also based on Fig. 5, it can be concluded that when the radius become bigger, the results are coming in to reality and are getting so close to the experimental results. In the full paper version, it will be shown that without regarding to the water quality or the number of phases, this result is valid, in general.
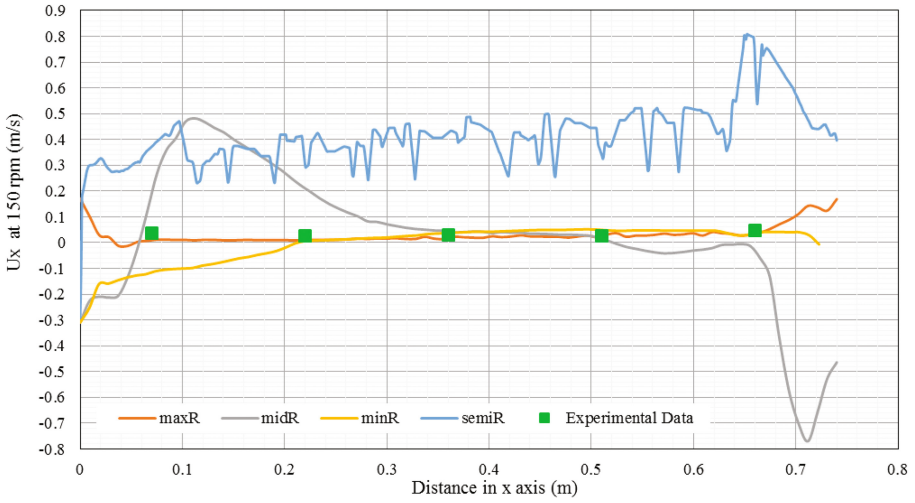
Fig. 4. U_x of proposed models at 150 (rpm) and experimental data
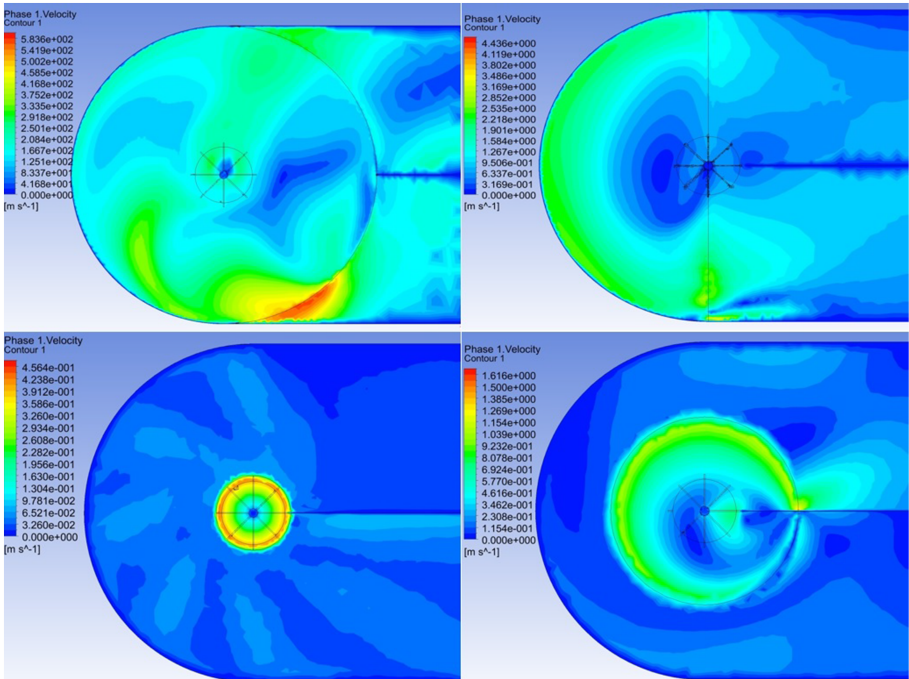
Fig. 5. Velocity contours of phase 1 of 4 proposed models: (a) max R- (b) semi R- (c) min R- (d) mid R

4   Conclusion

In addition to the knowledge of mathematical modelling and bioengineering, the skill of the one who models and simulate is undeniably significant. Hence, it has been shown in this study that the dimension of rotating zone is crucial for getting to reasonable results. Based on the analysis the bigger the radius of rotating zone is, the higher the accuracy of modelling is. Moreover, the rotating zone in multiple reference approach cannot be semi-circle.

References

Long Fan NX (2010) PDA experiments and CFD simulation of a lab-scale oxidation ditch with surface aerators. Chem Eng Res Des 88:23–33

Yannick Fayolle AC (2007) Oxygen transfer prediction in aeration tanks using CFD. Chem Eng Sci 62:7163–7171

Zadravec SB (2007) The influence of rotating domain size in a rotating frame of reference approach for simulation of rotating impeller in a mixing vessel. J Eng Sci Technol 2:126–138

HYDRODECA: CFD Modelling Platform
for Full-Scale Secondary Clarifiers of WWTPs

L. Basiero[2(✉)], C. Peña-Monferrer[1], J. Climent[1], P. Carratalá[1],
R. Martínez[1], J.G. Berlanga[2], and S. Chiva[1]

[1] Universitat Jaume I, Castellón, Spain
schiva@uji.es
[2] Sociedad de Fomento Agrícola Castellonense, S.A., Castellón, Spain
lbasiero@facsa.com

Abstract. This work describes the development of a Computational Fluid Dynamics (CFD) simulation platform focused on secondary clarifiers modelling. This tool allows reproducing in detail the fluid behaviour inside secondary settling tanks (SSTs), with the objective to improve the process in Wastewater Treatment Plants (WWTPs) by means of a better control, design and operation of those SST. Moreover, additional well-known SST models (empirical and lumped models) have been implemented to supplement the understanding of process operation. The most frequent types of full-scale secondary settling tanks have been studied, focusing both hydrodynamics and sludge settling performance. Several CFD models have been performed according to different configurations, being validated through experimental data. HYDRODECA is a simulation platform based on OpenFoam, developed as a tool for operators, researchers and technicians non-experts in CFD. An intuitive graphical user interface has been introduced, including specific tools to process operational data from the plant and an analysis assistant to understand the simulation results.

Keywords: CFD · Modelling · Secondary clarifier · Settling

1 Introduction

SSTs have been widely studied by means of different modelling approaches because they are one of the most hydraulically sensitive unit operations in the biological process of WWTPs. Performance of SSTs influences the solids inventory in the activated sludge unit and consequently have an impact in the biological treatment efficiency. On one hand, SSTs limit the maximum permissible flow rate entering the WWTPs; therefore, modelling the dynamics in the SSTs is an essential part to optimize and control WWTPs performance (Water Environmental Federation (WEF) 2005). On the other hand, settling process is considered one of the main stages in activated sludge processes, which has a great interest of the plant performance due to its critical operation and complexity. Ineffective separation of the sludge in the SST can impact the sludge retention time in the system, thus deteriorating the performance of the biological processes and, in consequence, the effluent water quality. Basically, settling process should accomplish two main aims: thickening function to recycle biomass, and retaining the solids to provide the biological activity in the system (Bürger et al. 2011).

SST empirical models and lumped parameter SST model are available in commercial simulators, and its use depends on the final purpose of the simulation. Thus, ideal clarifier models are sufficient for most of the objectives, whilst layered clarifier models are suitable to predict rising sludge blanket, indicating operation failures such as wash-out of solids. Subsequently, CFD models can reproduce fluid behaviour in detail, being the most advanced models in literature. It consists of two parts: a flow model providing the velocity and turbulent viscosity field, and a suspended solids transport model to determine sludge concentration field. In order to develop CFD models, exhaustive measuring campaign in the SSTs is needed. These models are not quite often applied in WWTPs operation, but rather they are mainly used in research at the moment. This is due to CFD models are more limited in use, because of their associated costs and the unfamiliarity with the mathematical models.

2   Materials and Methods

2.1   Platform Development

The development of this specific CFD modelling platform of secondary clarifiers has been performed by means of Open Source Software. This tool allows creating a complete CFD model, including geometry, mesh, setup, solver and analysis tool of the results. From this CFD simulation platform, HYDRODECA, you can reproduce hydrodynamics in detail and sludge settling process within different types of SST, evaluating the design through geometrical modifications on the configuration of their internal elements such us deflector feedwell and baffles. Moreover, SST modelling platform contains the traditional SST modelling tools (State Point and Lumped models) to support CFD user in terms of quick assessment of main operational parameters, and also with statistical and data processing tools to support the analysis process.

2.2   CFD Model Performance

3D CFD models have been performed defining a continuous phase and a solid dispersed phase transient simulations. The model is mainly based on the Drift Flux model to reproduce the relative motion between phases. From an essay column, a CFD model was performed to test hindered settling velocity equations and compression model, which were subsequently implemented in full-scale CFD models. Either stationary or transient analysis can be performed, introducing a dynamic influent flow in order to calculate the evolution of the Sludge Blanket Height (SBH) and the Sludge Concentration Distribution within the SST. A non-newtonian flow and complex rheological model can be considered.

2.3   Experimental Measurements for CFD Model Validation

Experimental measurements were conducted in different types of full-scale SSTs by means of different probes, in order to verify CFD models. Thus, SONATAX® probe

Fig. 1. Sonatax®, Solitax® and Vectrino® probes installed in a full-scale SST

was used to measure SBH in the tank, SOLITAX® probe was used to measure total suspended solids inside the blanket, and Vectrino® Nortek high-resolution acoustic velocimeter was used to measure fluid velocity at different radial profiles inside the settler (Fig. 1).

Previously, sedimentation column essays were carried out in order to characterise hindered settling velocity and compression model following the column test designed by (Ramin et al. 2014). Moreover, BOHLIN CVO 120 HG (High resolution) double concentric rheometer was used to obtain the characterization of the sludge viscosity (Eshtiaghi et al. 2013).

3 Results and Discussion

An overview of the SST specific CFD modelling platform is shown by means of the following screenshots. Figure 2 exhibits the meshing setup wizard, whereas Fig. 3 shows the setup to define the configuration process by means of the main operational parameters being evaluated through the State Point analysis tool.

CFD full-scale models were performed through the CFD platform. Simulation results of a Hopper SST (Fig. 4) and a Circular SST (Fig. 5) are shown. They were successfully used to reproduce daily operation in WWTPs being the distribution of
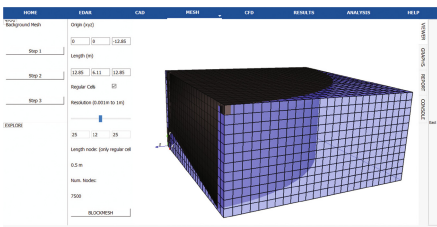
Fig. 2. Overview of meshing setup wizard
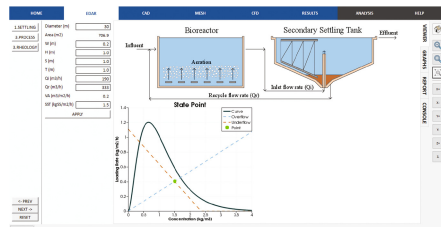
Fig. 3. Overview process parameters definition
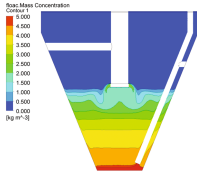
Fig. 4. Hopper SST CFD. Total suspended solids distribution.
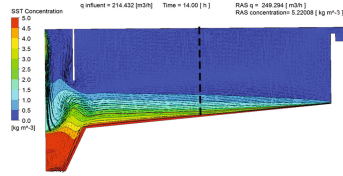
Fig. 5. Circular SST CFD model. Total suspended solids distribution. Vertical line to evaluate velocity.
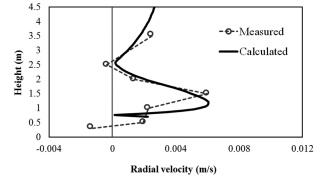
Fig. 6. Radial velocity profile for CFD validation measured in vertical line of Fig. 5.

suspended solids concentration and SBH the main parameters of interest. As said, CFD models have been validated experimentally; as an example, Fig. 6 shows good prediction in velocity profile.

4 Conclusions

Empirical models are still used to predict effluent characteristics and global sludge features, whereas CFD models are more used in research projects. This work suggests the importance of implementing CFD modelling practice in WWTP operation combined with lumped models in a unique platform. On one hand, CFD allows obtaining a detailed hydrodynamics performance of full-scale SST, reproducing the flow pattern to study defects on the fluid behaviour; new geometries and configurations can be performed. On the other hand, settling control, such us solids distribution within the tank can be easily predicted by lumped models and, therefore, properly calculated by means of CFD.

References

Bürger R, Diehl S, Nopens I (2011) A consistent modelling methodology for secondary settling tanks in wastewater treatment. Water Res 45:2247–2260

Eshtiaghi N, Markis F, Yap SD, Baudez JC, Slatter P (2013) Rheological characterisation of municipal sludge: a review. In: Clarifier Design, 2nd edn., Water

Water Environmental Federation (WEF) (2005) Clarifier Design. 2nd edn., Manual of Practice No. FD-8

Ramin E, Wágner DS, Yde L, Binning PJ, Rasmussen MR, Mikkelsen PS, Plósz BG (2014) A new settling velocity model to describe secondary sedimentation. Water Res 66:447–458

Hydro-Swapping: An Innovative CFD Approach Applied to a Real Bioreactor

J. Climent[1]([✉]), R. Martínez-Cuenca[1], L. Basiero[2], J.G. Berlanga[2],
and B.S. Chiva[1]

[1] Department of Mechanical Engineering and Construction, UNIVERSITAT
JAUME I, Av. Vicent Sos Baynat, s/n, 12071 Castellón, Spain
{jcliment,raul.martinez,schiva}@uji.es
[2] SOCIEDAD FOMENTO AGRÍCOLA CASTELLONENSE, S.A (FACSA),
C/Mayor, 82-84, 12001 Castellón, Spain
lbasiero@facsa.com, jgberlanga@grupogimeno.com

Abstract. This work shows the maximum potential of Computational Fluid Dynamics (CFD) tools applied to wastewater treatment plant (WWTP) operation by means of a novel full-scale ASM-CFD biological reactor model, which reproduces kinetics by means of two-phase flow simulations. The main aim is to perform the aeration cycles carrying out the actual control strategy in a real plant. For that, an innovative methodology of calculus has been defined; it consisted on a new approach based on swapping different hydrodynamics in the same tank depending on both the aeration cycles and the internal recycling rate. Subsequently, ASM1 can be successfully solved in transient state.

Keywords: Computational Fluid Dynamics · ASM1 · Two-phase flow

1 Introduction

The Modified Lutzack Ettinger (MLE) biological reactor is a commonly used nutrient removal configuration, typical of municipal WWTP and composed of anoxic and aerobic tanks. As known, this system represents one of the simplest within both nitrification-denitrification occur with greater efficiency (Water Environment Federation 2007). The adjustment of the internal recycling rate is often based on rules of thumb, which is a critical operational parameter providing nitrate to the anoxic zone. Moreover, supplying aeration in cycles, set by the ammonia concentration at the effluent, is a rather satisfactory manner to operate this bioreactor configuration. CFD techniques are well known and widely used in different fields related with hydrodynamics. Since hydraulic model can be enriched incorporating kinetic model, numerous two-phase flow CFD-ASM models have been performed mainly focused on turbulence and aeration modelling (Fayolle et al. 2007); (Karpinska and Bridgeman 2016). In this work, hydrodynamics in a biological reactor (with and without aeration) has been calculated by means of CFD simulation taking into account two different internal recycling rates with the purpose to analyse the nutrient removal efficiency by means of the ASM1 implementation.

2 Materials and Methods

A real full-scale biological reactor divided in two lanes of 2300 m^3 has been chosen for this study. Each WWT lane is divided into 3 tanks in a row (Fig. 1). The influent flow (about 10000 m^3/day), the external and internal sidestreams (about 110% and 400% of the influent flow, respectively), arrive continuously to the first tank. The two first compartments operated in anoxic whilst the third one in aerobic conditions. Mixing was provided by three stirrers and aeration fine bubble diffuser system. It is noticeable that the third stirrer, located in the aerobic tank, switches off when aeration is supplied, changing hydrodynamics significantly in the third tank.
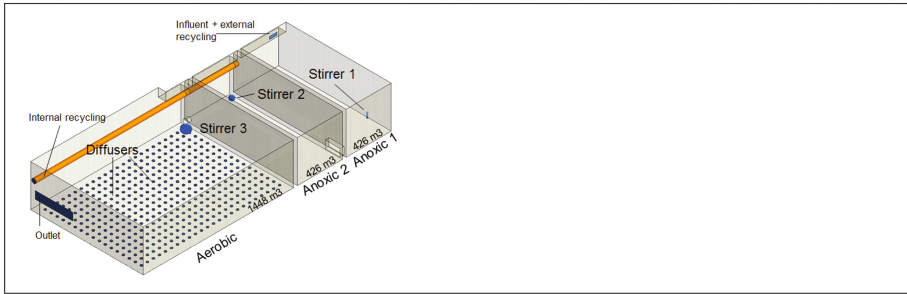
Fig. 1. 3D model of biological reactor LEM configuration

With respect to the hydrodynamics, the CFD model has been defined within a two-phase Eulerian-Eulerian framework to account for the effects of gas injection from the diffusers. The simulation of these flows is generally quite complex as it involves the interaction between the two phases and the self-interaction between them, i.e. collisions and breakage of bubbles (Liao and Lucas 2009; 2010). For the interface forces between gas-liquid, it has been considered the Ishii-Zuber drag correlation, the Favre Averaged turbulent dispersion, and the Sato correlation for bubble induced turbulence (Rzehak et al. 2015). The population balance model (PBM) was defined by the polydispersed multiple size group model (MUSIG) (Lo 1996), with Prince & Blanch model for bubble coalescence, and Luo & Svendsen model for the break-up. SST model was used for the turbulent field of the liquid phase, and a zero-equation turbulence model for the gas phase. With respect to the biokinetics, the ASM1 has been coupled with the hydrodynamics by considering a transport equation for the mass concentration of each state variable, φ_i:

$$\frac{\partial(\alpha_l \varphi_i)}{\partial t} + \mathbf{v_l} \cdot \nabla(\alpha_l \varphi_i \mathbf{v_l}) = S_{\varphi_i} \tag{1}$$

being v_l the velocity of the liquid phase, α_l the gas volume fraction of the liquid phase, and S_φ the source term for the i-th state variable. ASM1 equations have been taken from the model defined by (Henze et al. 2000). Input conditions were selected following experimental data measurements. Thus, the mass transfer is caused by the

oxygen transfer from the bubbles to the liquid being defined a k_L fixed whilst the interfacial area was calculated by the code using the PBM:

$$\frac{dm_b}{dt} = k_L a_i (C^* - C) \tag{2}$$

being m_b the mass of a single bubble, k_L the transfer coefficient, a_i the interfacial area concentration, C the oxygen concentration in the bubble and C* the saturation concentration of oxygen in the liquid.

Hydrodynamics have been calculated in steady state considering these 4 combinations with and without aeration; 200% and 400% internal recycling ratio of the influent flow (Ri). As other authors suggested (Le Moullec et al. 2008), simulations in this work have been run in two steps, maintaining hydrodynamics and ASM separately. Following this, assuming that hydrodynamics in the tanks can be considered constant during the aerobic and the anoxic periods, the innovative swapping approach, which changes hydrodynamics among these 4 combinations by means of swapping the transport equations, allows calculating kinetics reproducing accurately the fluid behaviour.

3   Results and Conclusions

Results show the hydrodynamics performance in detail inside the tanks (Fig. 2). It allows analysing fluid behaviour in two-phase flow under aerobic and anoxic conditions (Fig. 3). It must be emphasized the challenge in CFD modelling to develop multiphase flow systems to reproduce phenomena in detail reducing time computing by calculating separately hydrodynamics and kinetics. The innovative switching approach allows combining different hydrodynamics maintaining the transient evolution of state variables. It resulted useful when aeration was provided by means of cycles (Fig. 4) in order to maintain nitrogen compounds under control being the ammonia concentration at outlet set by [1–4,5] (mg/L) (Fig. 5).
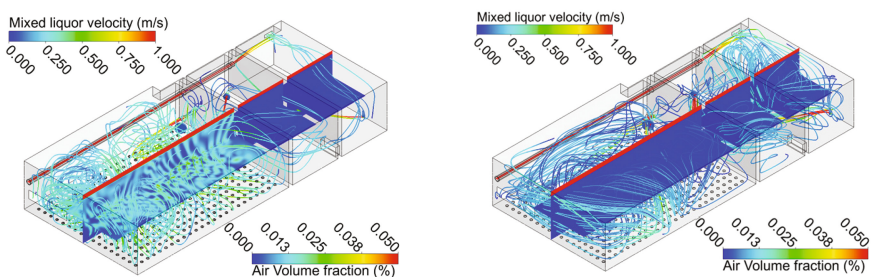
Fig. 2. Streamlines velocity and void fraction. Configuration of Ri = 400% with aeration (a) and without aeration (b)
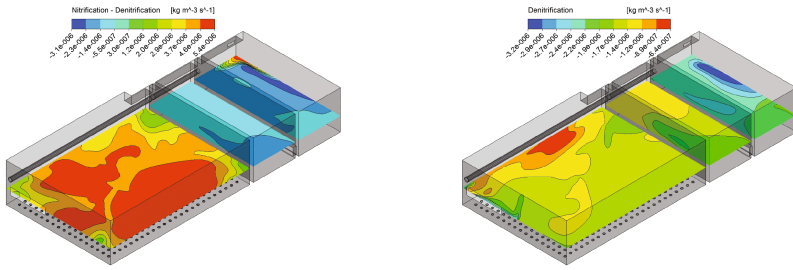
Fig. 3. Nitrification-denitrification rate with aeration (a), and denitrification rate without aeration (b)
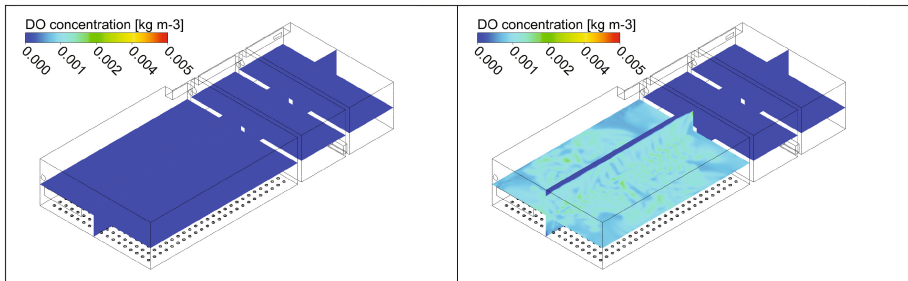
Fig. 4. DO concentration at t = 0 s (a) and at t = 10 s (b)
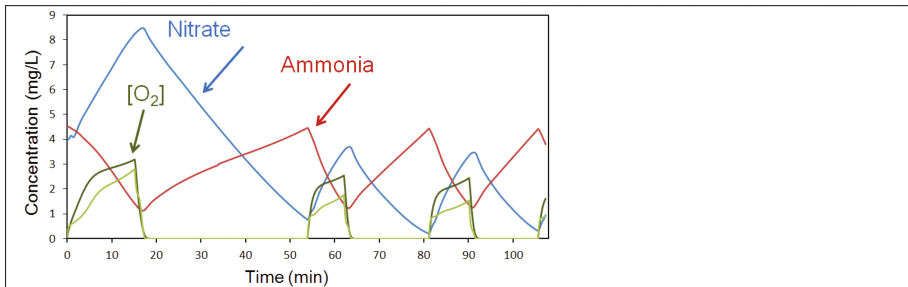
Fig. 5. Concentration of different state variables at the outlet. Aeration system was set by complying Ammonia concentration range of [1–4, 5] ppm

This paper presents a successful case study based on CFD modelling applied to real WWTP unit process. It shows the CFD as a decision-making tool to support the adjustment of essential control parameters such us the internal recycling ratio.

References

Fayolle Y, Cockx A, Gillot S, Roustan M, Héduit A (2007) Oxygen transfer prediction in aeration tanks using CFD. Chem Eng Sci 62:7163–7171. doi:10.1016/j.ces.2007.08.082

Henze M, Gujer W, Mino T, van Loosdrecht MCM (2000) Activated sludge models ASM1, ASM2, ASM2d and ASM3, vol. 121. IWA Publication. doi:10.1007/s13398-014-0173-7.2

Karpinska AM, Bridgeman J (2016) CFD-aided modelling of activated sludge systems – a critical review standard method of moments. Water Res 88:861–879. doi:10.1016/j.watres.2015.11.008

Liao Y, Lucas D (2009) A literature review of theoretical models for drop and bubble breakup in turbulent dispersions. Chem Eng Sci 64:3389–3406

Liao Y, Lucas D (2010) A literature review on mechanisms and models for the coalescence process of fluid particles. Chem Eng Sci 65(2010):2851–2864

Le Moullec Y, Potier O, Gentric C, Leclerc JP (2008) Flowfield and residence time distribution simulation of a cross-flow gas–liquid wastewater treatment reactor using CFD. Chem Eng Sci 63:2436–2449

Lo SM (1996) Application of population balance to cfd modelling of bubbly flow via the MUSIG model. AEA Technology, AEAT-1096

Rzehak R, Krepper E, Liao Y, Ziegenhein T, Kriebitzsch S, Lucas D (2015) Baseline model for the simulation of bubbly flows. Chem Eng Sci 38:1972–1978

Water Environment Federation (2007) Biological nutrient removal processes. Oper Municipal Wastewater Treat Plants 22(1):22–65

Mathematical Modelling in Diagnosis of Wastewater Treatment Plant

J. Drewnowski[1(✉)] and M. Zmarzły[2]

[1] Faculty of Civil and Environmental Engineering,
Gdansk University of Technology,
ul. Narutowicza 11/12, 80-233 Gdansk, Poland
`jdrewnow@pg.gda.pl`
[2] ZAPSOFT Ltd., ul. al. Kasztanowa 3A, 51-125 Wrocław, Poland
`m.zmarzly@zapsoft.pl`

Abstract. The paper reports the development of mathematical modelling in the diagnosis of the wastewater treatment plant (WWTP). Diagnosis of technical objects and/or biochemical processes control such as activated sludge systems in WWTP could be realized in many ways. One of the divisions of the diagnostic methods include modeling with or without a model of the object. The first of these is the analysis of the symptoms for which, based on the parameter values, the abnormality in the diagnosed objects are sought. Another way is to use models of objects undergoing diagnosis. In this case, the diagnosis comes down to a comparison of information from the response object model or the estimated parameters of the model with data from the real object. The aim of this study was to evaluate an innovative concept of the possible use the mathematical model and computer simulation in the diagnosis and control of activated sludge systems in WWTP. The first phase of this project involves creation and calibration of mathematical model of existing WWTP. By using MATLAB software the diagnosis software was created. The algorithm is based on a comparison of data from the mathematical model and measurements of the real date from WWTP, until it will detect any malfunction of the sensors in the case study. After detection of such abnormalities next step is to send information to the SCADA system, where the received data will decide, whether it is necessary to start further action related to the diagnosed sensor in WWTP.

Keywords: WWTP · Process control · ASM · Computer simulation · Diagnosis

1 Introduction

The description of the biochemical process through its mathematical representation, constitutes the first steps to model-based process control. Generally, the objective of a control system is to make the process output behave in a desired way by manipulating the plant inputs by actuators, such as valves and pumps. This leads to favourable process conditions for the demanded results and cost effective process operation. In modern WWTPs processes such as aeration, chemical feeds and sludge pumping are usually controlled by on-line sensor measurements. The proper estimation of these parameters in model has strong influence on the results of mathematical modelling and

computer simulation in controlling biochemical processes of WWTP - especially a biological part (e.g. nitrification zone/aeration system), where the costs of operation could be extremely high. Diagnosis of technical objects can be realized in many ways. One of the divisions of the diagnostic methods include modelling with or without a model of the object. The first of these is the analysis of the symptoms for which, based on the parameter values, the abnormality in the diagnosed objects are sought. Another way is to use models of objects undergoing diagnosis. In this case, the diagnosis comes down to a comparison of information from the response object model or the estimated parameters of the model with data from the real object. The aim of this study was to evaluate an innovative concept of the possible use the mathematical model and computer simulation in the diagnosis and control of WWTP.

2   Materials and Methods

2.1   Study Side

The "Klimzowiec" WWTP is a mechanical and biological treatment plant based on the use of active sludge in the Bardenpho system. The WWTP is managed by the Chorzow-Swietochłowice Water and Wastewater Utility. The studied plant consists of pre denitrification/dephosphatation zones as well as three denitrification and five nitrification bioreactors. Each of the nitrification bioreactors has three independent aeration zones. The average effluent flow is approximately 25,900 m^3/d which is equivalent around 200,000 RLM. The "Klimzowiec" WWTP also has six secondary settlers, of which only four are used at the same time.

2.2   Process of WWTP Model Evaluation

The experimental part was carried out to present the process of model evaluation and calibration according to laboratory study and on-line measurements in order to better integrate computer model to the conditions prevailing in the local parameters of individual biological part of bioreactor for aeration system at WWTP. The existing model of WWTP created in the WEST software is presented in Fig. 1. Whole automation system was made using the task scheduler and scripts. Each few minutes runs a script that first runs the applications that retrieves data from the SCADA system, processes them and then appends the relevant mathematical model input files. Next, the script runs with the relevant parameters of a mathematical model. After the end of the simulation result data from the model are prescribed to an archive file containing the output data model, where the current values of the measurements are saved corresponding to the values simulated.

Using MATLAB software the new solution in program was created, which is based on a comparison of simulation data results from the mathematical model and measurements from the real WWTP, which can detect any malfunction of the sensors in the modelled object. After detection of such abnormalities next step is to send information to the SCADA system, where the received data will decide, whether it is necessary to start further action related to the diagnosed sensor. Each of the measuring points can be
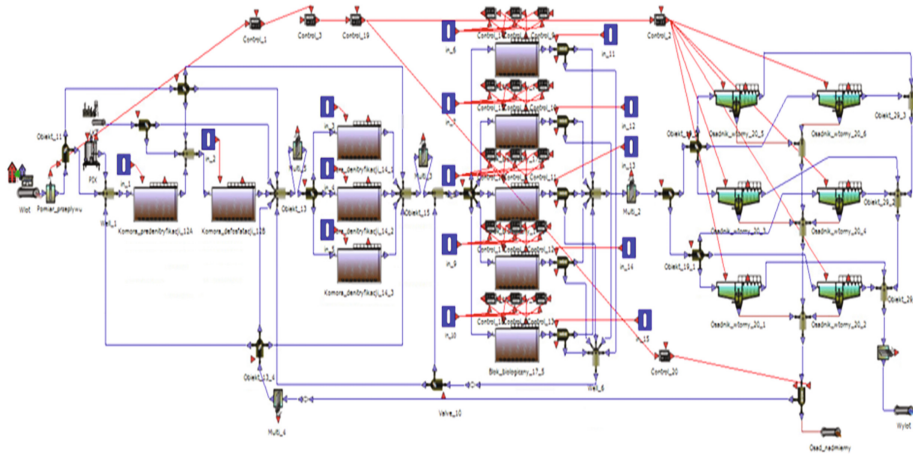
Fig. 1. The existing model of "Klimzowiec" WWTP created in the WEST software

diagnosed on the basis of individual rules. During the diagnosis of the sensor, the rate of measured values change should also be taken into account or changes in the measured value according to the daily cycle.

In case of measurements which are subjected to rapid fluctuations of the measured values or large changes in the diurnal cycle, the information of the occurrence of irregularities in the operation of the sensor will be generated by changing the parameter during the long term measurement. In contrast, when the measurement is not subjected to fluctuations in the daily cycle and the changes are not too dynamic, the first measurement value significantly different from the expected value can cause the program will notify of the anomalies occurrence in the sensor operation.

The standard model library in WEST software did not have the relevant elements to reflect all individual parts of WWTP. For this reason, new element corresponding to the regulation of the total suspended solids (TSS) concentration in the effluent was added. Moreover, the control system was based on regulating the amount of waste activated sludge (WAS) discharged from the system. In addition to that system following on-line measurements such as: concentration of NO_3-N, NH_4-N, PO_4-P in the WWTP effluent were implemented and used for continuously tuning of complex WWTP mathematical model (Fig. 1).

Modelling techniques include statistical methods, computer simulation, system identification, and sensitivity analysis, however, each one of these steps was important to understand the underlying dynamics of a complex system. In order to make a more accurate calibration of the hydraulic model in the WWTP tracer test with lithium chloride (LiCl) as a neutral agent in the denitrification tanks was conducted (Table 1). LiCl agent has been added just behind the recirculation zone, and samples were taken directly at the outlet of the denitrification tank. The results showed a difference in the wastewater flow rate between denitrification tanks no. 14/1, 14/2, 14/3 and were included into the model.

Table 1. Sample results of tracer test between denitrification tanks in WWTP

Tracer test in WWTP	Time	Denitrification tanks		
	[h:min]	14/1	14/2	14/3
Lithium chloride concentration [mg/l]	09:10	<0.03	<0.03	<0.03
	09:45	0.036	0.038	0.055
	10:20	0.076	0.075	0.091
	10:55	0.106	0.103	0.114
	12:25	0.13	0.128	0.131

2.3   Implementation of PreviSys System at WWTP

In this study the communication system called PreviSys device and appropriate software for communicating with SCADA, based on advanced algorithms in industrial automation were used. The PreviSys as a system with the monitoring/controlling process technology, mainly contained equation based on ASM as well as another advanced algorithms, including Model Predictive Control (MPC), which allowed to supply mathematical model in the current operating parameters of monitored/controlled object. The system also included an industrial PC for advanced process control of WWTP in order to carry out the modeling process in PreviSys: both a general purpose (MATLAB), as well as specialized software (WEST, GPS-x etc.) could be used to simulate the operation of WWTP (Fig. 2).
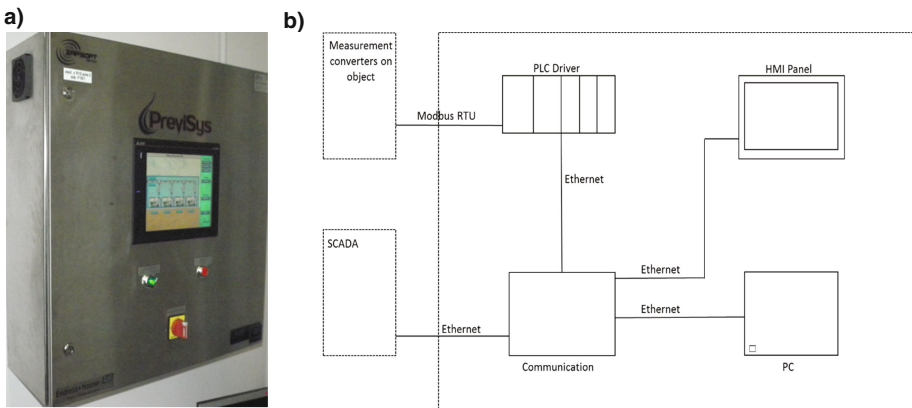
Fig. 2. The PreviSys communication system (a) real photo (b) scheme with the monitoring/controlling process technology

3   Results and Discussion

The task of diagnostic systems is the earliest and most accurate detection of irregularities in the operation of diagnosed object. Such a system allows the operator to unload the object because it causes that it does not need to monitor operating

parameters of the object in order to diagnose abnormal process. WEST (Wastewater Treatment Plant Engine for Simulation and Training) provides the modeller with a user friendly platform to use existing models or to implement and test new models. Basically, WEST is a modelling and simulation environment for any kind of process that can be described as a structured collection of Differential Algebraic Equations (DAE's). Currently, WEST is mainly applied to the modelling and simulation of WWTP (Vangheluwe et al. 1998, Vanhooren et al. 2003 and Mike by DHI 2012).

The WEST software ver. 2014 SP3, based on ASM2d (Activated Sludge Model No.2d) with extension ModTemp was used to create WWTP model fed with on-line data such as:

– inflow of wastewater from sewer system and truck dropping of wastewater with temporary portion (COD, TSS, TP and TKN)
– temperature in the pre-denitrification, phosphorus removal, denitrification zones
– oxygen concentration in each of the three nitrification bioreactors
– external and internal recirculation.

The Fig. 3 presents the value of the ammonia nitrogen concentration measured in the period between the 20th of May, and the 2nd of June 2016. It could be noticed that the measurement was gradually increasing with the passage of time. At the end of the measuring period, a decrease of the measured value was also noted, which was caused by carrying out the long term measurement and maintenance of the probe.
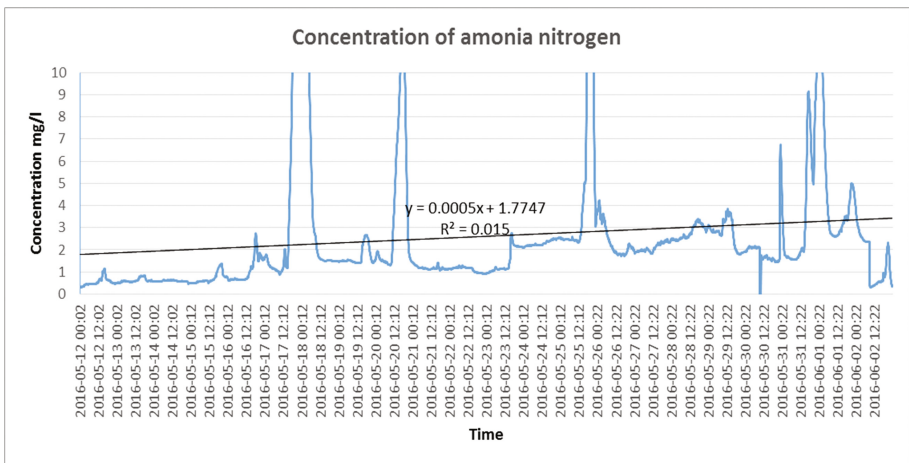
Fig. 3. The value of the ammonia nitrogen concentration measured

The process industry communications at WWTP developed in the last four decades, from 70's in several aeras. Each area introduced more detailed control to the field devices in many tasks of the control and/or supervisory systems. Introduction mathematical model and computer simulation to WWTP diagnostic allows to substantial early detection of deviations in the sensors operation, that play a major role in the modern industry automation development. In order to meet increasingly stringent nitrogen

limits, a variety of aeration control strategies are being implemented at Water Resource Recovery Facilities (WRRFs), which require increasing levels of instrumentation, control, and automation (ICA). The recent availability of reliable e.g. oxygen, ammonia, nitrate, and nitrite sensors have led to more advanced aeration control strategies such as ammonia based aeration control (ABAC) or ammonia vs. NOx (nitrate + nitrite) control (AVN). Following the implementation of ordinary DO control, a WRRF can further optimize the aeration system by including ABAC, which provides aeration and alkalinity savings by oxidizing the minimum amount of ammonia. This assists in meeting a target effluent concentration leading to an increased capacity for denitrification (through simultaneous nitrification denitrification and less oxygen transfer to anoxic zones) and potential supplemental carbon savings (Åmand et al. 2013; Reiger et al. 2014). The foregoing discussion demonstrates that there are many potentially successful strategies for advanced WWTP control, depended on properly functionated sensors. It is not possible to identify a single problem in WWTP in early stage, that will affect all utilities, because there is great diversity in wastewater characteristics, the construction and operation of activated sludge systems. Therefore, the proper solution such as mathematical modelling in diagnosis of WWTP for a studied object in Klimzowiec, undoubtedly have unique features and could be recommended.

4   Conclusions

The innovative idea to use mathematical modelling in diagnosis of WWTP is an important development. A commercial software WEST was used to model the WWTP configuration and for the dynamic simulation of the biochemical process, but the reason of greatest interest is the implementation of a special system and an appropriate communication software with SCADA as a development of mathematical model for the diagnosis of the plant. The task of diagnostic systems is the earliest and most accurate detection of irregularities in the operation of diagnosed object. Such a system allows the operator of WWTP to unload the object because it does not need to monitor operating parameters of the object in order to diagnose abnormal process. Each of the measuring points could be diagnosed on the basis of individual rules. During the diagnosis of the sensor, the rate of measured values change in the measured value according to the daily cycle and should also be taken into account. However, there is not a such device in existence that does not require an informed and properly-trained technician. This technology is still developing and should continue to improve as a part of future "Smart Control System" at WWTP. The important point is that wastewater utilities can be heroes instead of burdens by working towards a goal of biochemical process improvement and control for energy neutrality at WWTP.

References

Åmand L, Olsson G, Carlsson B (2013) Aeration control - a review. Water Sci Technol J Int Assoc Water Pollut Res 67(11):2374–2398

Mike by DHI (2012) WEST, Modelling Wastewater Treatment Plants, Short Description, pp 1–14

Rieger L, Jones RM, Dold PL, Bott CB (2014) Ammonia-based feedforward and feedback aeration control in activated sludge processes. Water Environ Res Res Publ. Water Environ Fed 86(1):63–73

Vangheluwe HL, Claeys F, Vansteenkiste GC (1998) The WEST++ wastewater treatment plant modelling and simulation environment. In: Bergiela A, Kerckhoffs E (eds) 10th European simulation symposium. Society for Computer Simulation (SCS), Nottingham

Vanhooren H, Meirlaen J, Amerlinck Y, Claeys F, Vangheluwe H, Vanrolleghem PA (2003) WEST: modelling biological wastewater treatment. J Hydroinformatics 5(1):27–50

A Different Approach for Steady-state Activated Sludge Modelling

A. Lahdhiri[1(✉)], M. Heran[2], and A. Hannachi[1]

[1] Laboratory of Process Engineering and Industrial Systems,
Chemical and Process Engineering Department,
Gabes National Engineering School, Gabes University, Gabes, Tunisia
[2] Department of Membrane Process Engineering,
European Membrane Institute, Montpellier University, Montpellier, France

Abstract. The complexity of the Activated Sludge Model no. 1 (ASM1) is one of the main obstacles hindering its use, particularly among wastewater treatment plant (WWTP) professionals. In this paper, a simplification procedure, based on steady-state mass balances, is proposed for the basic activated sludge process (ASP) configuration, consisting of an aerated bioreactor and a settler. Only organic carbon removal and nitrification were investigated. The proposed approach was applied to ASM1. It allowed having simple analytical expressions of the state variables. Expressions were then validated by comparison to simulation results given by the software GPS-X. As a result, they may be useful for different applications such as optimization, control or design.

Keywords: Activated sludge process · Activated sludge model no. 1 (ASM1) · Steady-state modelling

1 Introduction

Modelling of activated sludge processes (ASP) for domestic wastewater treatment has gained a lot of importance during the last decades particularly with the advent of the widely accepted activated sludge models (ASM) (Naessens et al. 2012). ASM have shown quite good predictive results, but this was at the expense of complex process models. Even with the use of the continuously stirred tank reactor (CSTR) assumption, a highly non-linear system of ordinary differential equations is obtained. This complexity is one of the main obstacles holding up the ASM widespread, particularly among WWTP professionals asking for model simplification (Hauduc et al. 2009). Since a full model is not always necessary for all users and all applications, various ASM simplification researches, that were application-motivated, are reported in literature. All of them dealt only with ASM1 (Henze et al. 2000). Different strategies were adopted such as model dimension reduction (Jeppsson and Olsson 1993; Queinnec and Gómez-Quintero 2009), linearization of the reaction rates (Anderson et al. 2000; Benhalla et al. 2010) or the whole mass balance equations (Smets et al. 2003).

In this paper, another simplification procedure, based on steady-state mass balances, is proposed. It allows having the analytical expressions of the state variables once the stabilized operation is reached. The impact of each kinetic, stoichiometric or

operating parameter on a state variable is directly given, with no need to carry out the time-consuming sensitivity analysis. These expressions can be used mainly as tools for new plant design or existing plant retrofitting studies.

2   Materials and Methods

In this study case, ASM1 was chosen and its default parameter values were utilized (Henze 2000). The basic ASP configuration is considered (Fig. 1). It is consisted of a single aerated continuously-stirred bioreactor followed by a settling tank. Both organic carbon and nitrogen removal are taken into account.
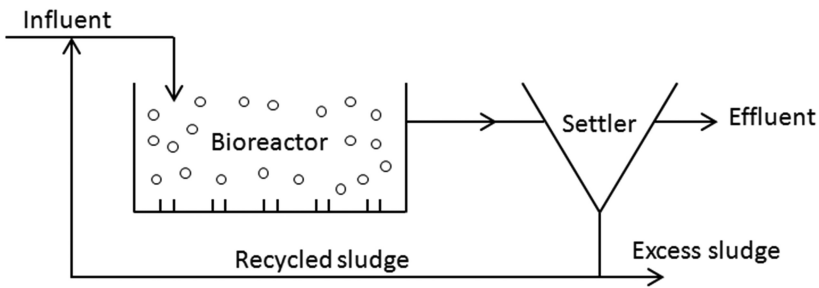
Fig. 1. The basic ASP configuration

Assumptions often used in previous studies are required: (i) no limitations in the dissolved oxygen and alkalinity, and (ii) a complete retention of the active biomass in the settling tank. In addition, it is assumed that all particulate compounds are entirely retained by the settler, which means that these compounds are totally recycled to the bioreactor. For this reason, mass balances of state variables were applied only for the bioreactor assuming that there are no particulate compounds in the effluent.

Obtained expressions were validated based on simulations using the GPS-X®Hydromantis software that were conducted in order to generate realistic data.

3   Steady-state Modelling

According to mass balances written in steady-state conditions, simple analytical expressions for all state variables are obtained.

For example, the heterotrophic biomass concentration (X_{BH}) is given by the Eq. (1):

$$X_{BH} = \frac{Y_H \, S_{Si} \, SRT/HRT}{1 + b_H \, SRT \, (1 - Y_H(1 - f_P))} \tag{1}$$

where HRT is the hydraulic retention time (d), SRT is the solid retention time (d), S_{Si} is the readily biodegradable organic substrate in the influent, b_H is the heterotrophic decay

rate (1/d), f_P is the fraction of biomass leading to particulate material (−) and Y_H is the heterotrophic yield (g cell COD formed/g COD oxidized).

4   Results and Discussion

To validate the expressions of the state variables, simulation results according to these expressions were compared to those given by GPS-X. Simulation operating conditions are presented in Table 1.

Table 1. Simulation operating conditions

SRT (d)	HRT (d)	Q (L/hr)	V (L)	$S_{NH4,i}$ (mg N/L)	COD/N	$S_{S,i}$ (mg COD/L)
20; 40; 60	0.5	5.75	60	70	4.5; 5	315; 350

With COD/N is the amount of organic substrate to ammonia in the influent.

An acceptable match was obtained between both results for all state variables, as shown in Figs. 2, 3, 4, 5 and 6 for the main sludge compounds: heterotrophic and the autotrophic biomass concentrations, COD concentration along with ammonia and nitrate and nitrite concentrations. Consequently, analytical expressions of state variables were validated, so they can be used for identification of optimum operating conditions.
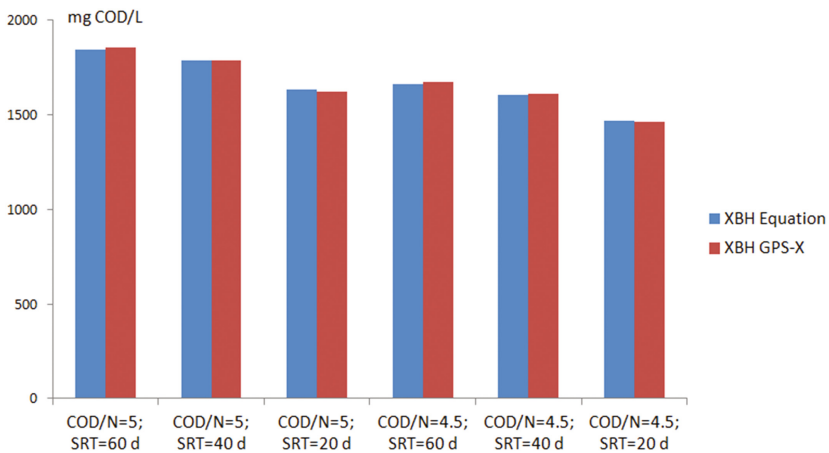
Fig. 2. Comparison of heterotrophic biomass concentrations (XB_H) given by simulations using steady-state equations (in blue) and using GPS-X software (in red) (Color figure online)
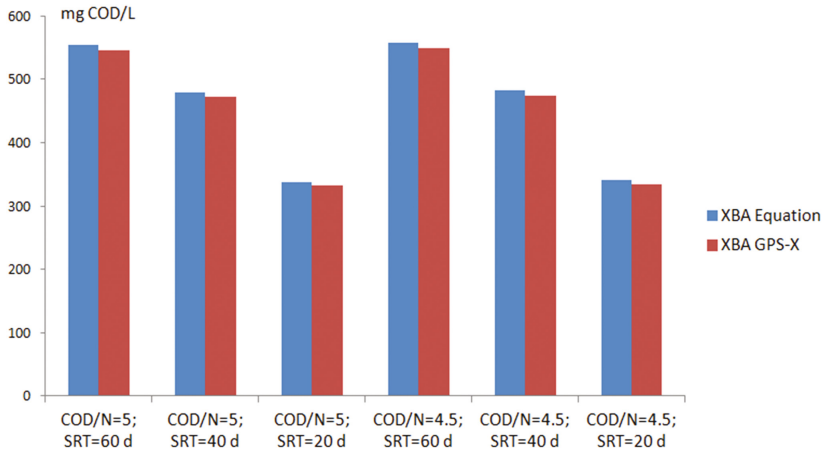
Fig. 3. Comparison of autotrophic biomass concentrations (XB$_A$) given by simulations using steady-state equations (in blue) and using GPS-X software (in red) (Color figure online)
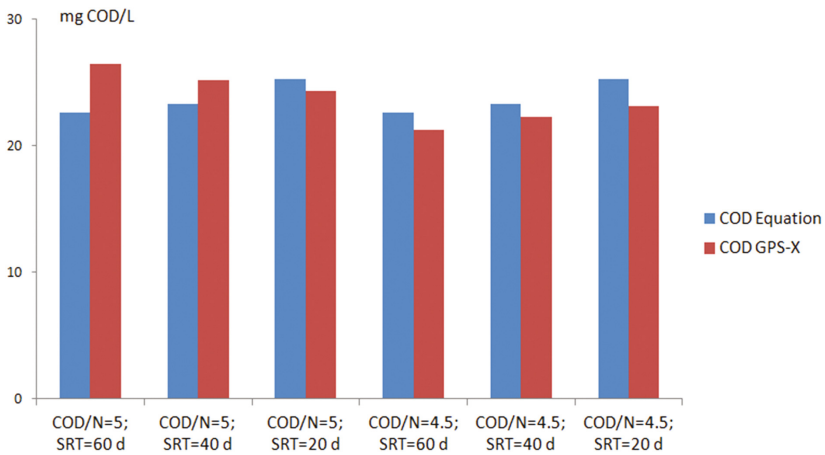
Fig. 4. Comparison of the amount of the biodegradable organic carbon (COD) given by simulations using steady-state equations (in blue) and using GPS-X software (in red) (Color figure online)
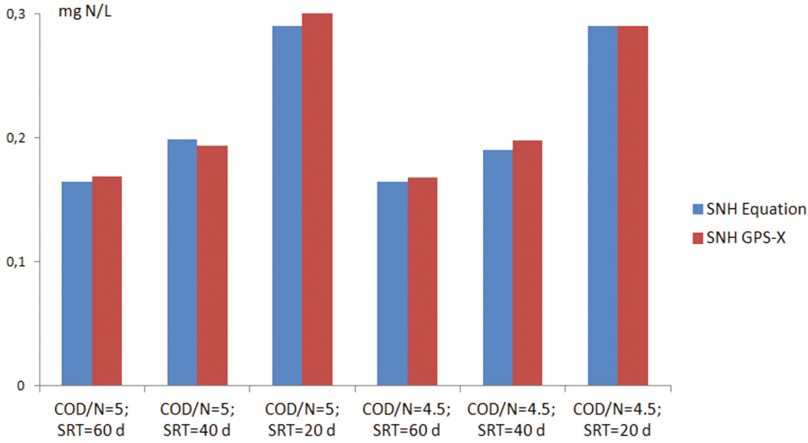
Fig. 5. Comparison of the free and ionized ammonia concentration (S_{NH}) given by simulations using steady-state equations (in blue) and using GPS-X software (in red) (Color figure online)
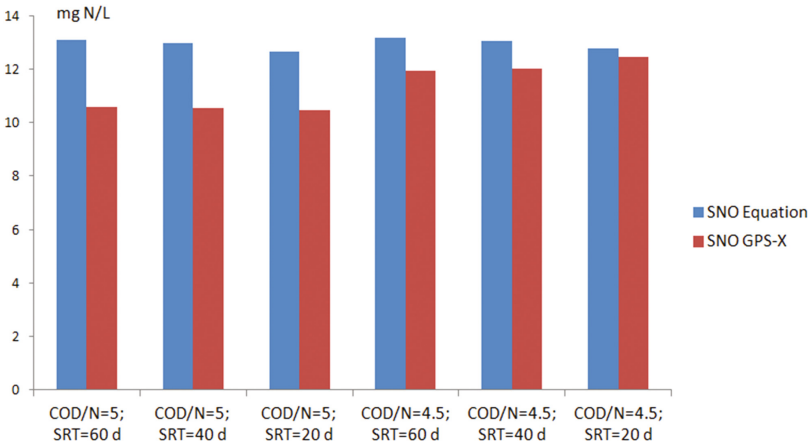
Fig. 6. Comparison of nitrate and nitrite concentration (S_{NO}) given by simulations using steady-state equations (in blue) and using GPS-X software (in red) (Color figure online)

5   Conclusion

An approach based on steady-state ASM1 mass balances was presented. Only a few assumptions were made to keep the model accuracy. After development, the obtained state variable expressions were validated by means of data generated using software simulations. The steady-state expressions showed satisfying predictions of the state variable concentrations. So, these relatively simple expressions may be useful for different applications such as optimization, control or design.

References

Anderson JS, Kim H, Mc Avoy JT, Hao OJ (2000) Control of an alternating aerobic-anoxic activated sludge system – Part 1: development of a linearization-based modeling approach. Contr Eng Pract 8:271–278

Benhalla A, Houssou M, Charif M (2010) Linearization of the full activated sludge model No 1 for interaction analysis. Bioprocess Biosyst Eng 33:759–771

Hauduc H, Gillot S, Rieger L, Ohtsuki T, Shaw A, Takács I, Winkler S (2009) Activated sludge modelling in practice: an international survey. Wat Sci Technol 60(8):1943–1951

Henze M, Gujer W, Mino T, van Loosdrecht M (2000) Activated sludge models ASM1, ASM2, ASM2d and ASM3. IWA scientific and technical report No. 9, London (GB)

Jeppsson U, Olsson G (1993) Reduced order models for on-line parameter identification of the activated sludge process. Water Sci Technol 28(11–12):173–183

Naessens W, Maere T, Nopens I (2012) Critical review of membrane bioreactor models – Part 1: Biokinetic and filtration models. Bioresour Technol 122:95–106

Queinnec I, Gómez-Quintero CS (2009) Reduced modeling and state observation of an activated sludge process. Biotechnol Prog 25(3):654–666

Smets IY, Haegebaert JV, Carrette R, Van Impe JF (2003) Linearization of the activated sludge model ASM1 for fast and reliable predictions. Water Res 37:1831–1851

Erratum to: Energy Recovery from Immobilised Cells of *Scenedesmus obliquus* after Wastewater Treatment

M. Gomez San Juan[1], F. Ometto[2], R. Whitton[1], M. Pidou[1,2], B. Jefferson[1], and R. Villa[1(✉)]

[1] Cranfield University, CWSI, Cranfield, UK
[2] Scandinavian Biogas Fuels AB, Linköping, SE, Sweden

Erratum to:
Chapter "Energy Recovery from Immobilised Cells
of *Scenedesmus obliquus* after Wastewater Treatment" in:
G. Mannina (ed.), *Frontiers in Wastewater Treatment*
***and Modelling*, Lecture Notes in Civil Engineering,**
DOI 10.1007/978-3-319-58421-8_42

The original version of the book was inadvertently published with misspelt author name "M. Gomes San Juan" in Chapter 'Energy Recovery from Immobilised Cells of *Scenedesmus obliquus* after Wastewater Treatment' which has to be corrected to read as "M. Gomez San Juan". The erratum chapter and the book have been updated with the change.

The updated online version of this chapter can be found at
http://dx.doi.org/10.1007/978-3-319-58421-8_42

Author Index

A

Abellán, M., 193
Adlin, N., 43
Alouache, A., 368
Amerlinck, Y., 92
Andreasen, P., 127
Araki, N., 218
Arcila, J.S., 602
Arena, F., 349
Arzate-Martínez, G., 343
Ávila, C., 313
Ayesa, E., 614
Azari, M., 588

B

Bacci, G., 550
Baeza, J.A., 98
Balaguer, M.D., 701
Bao, Z., 419
Baquerizo, G., 607
Barillon, B., 50
Basiero, L., 193, 718, 722
Basitere, M., 225
Behera, Chitta Ranjan, 30
Belanger, A., 182
Belgiorno, V., 159
Bellandi, G., 398, 482, 489
Ben Amar, N., 239
Benyahia, B., 253
Berardi, G., 178
Berlanga, J.G., 718, 722
Bessiere, Y., 50
Besson, M., 392
Beyerle, L., 149
Bianco, G., 412
Bignozzi, C.A., 337
Blandin, Gaetan, 188
Boczkaj, G., 331
Boltz, J., 508

Bonari, A., 308
Bordes, M.C., 193
Borea, L., 159
Borzooei, S., 138
Bossi, C., 308
Bottino, A., 656
Bozileva, E., 575
Brepols, C., 149, 628
Buchicchio, A., 412
Buitrón, G., 602
Bürger, R., 596

C

Caffaz, S., 308, 398
Caivano, M., 412, 444, 457, 476, 482, 489
Calderon, K., 561
Calero-Díaz, G., 165
Calhoun, J., 508
Caligaris, M., 50
Camera Roda, G., 318
Campo, R., 530, 544
Caneppele, F.L., 113
Caniani, D., 412, 444, 457, 476, 482, 489
Canler, J.-P., 607
Capodici, M., 73, 197, 385, 550, 567
Caramori, S., 337
Caretti, C., 121, 398, 482
Carotenuto, M., 431, 706
Carratalá, P., 718
Carrera-Fernández, P., 530
Carucci, A., 536
Catunda, Y.C., 633
Cauduro, G.P., 68
Chen, X.M., 18
Cheng, L., 518
Chiva, B.S., 722
Chiva, S., 718
Christensen, J., 127
Cinà, P., 550